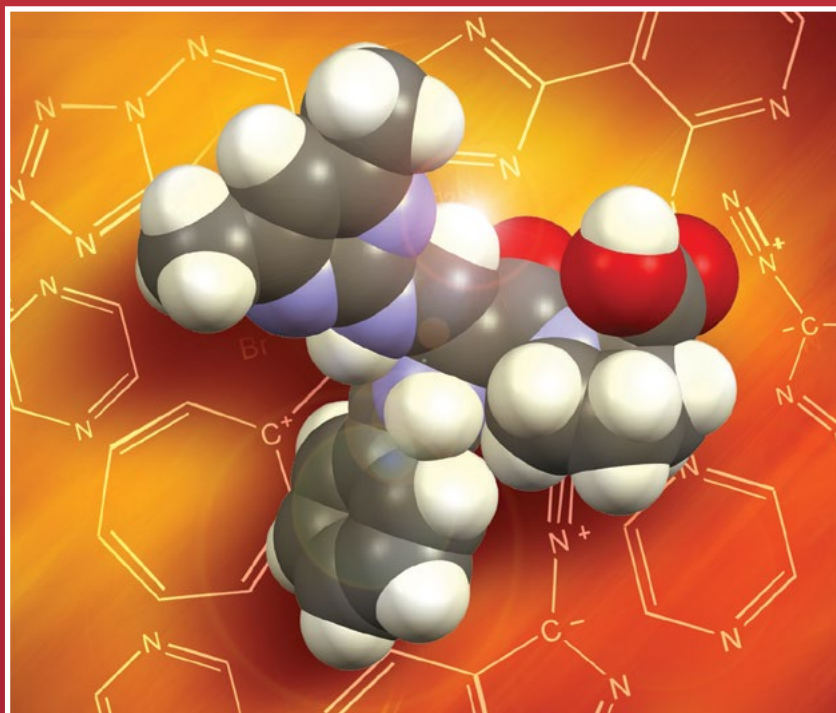


# Acta Chimica Slo

# Acta Chimica Slo

# Slovenica Acta C

4



64/2017

Dedicated to Professor and Academician Miha Tišler at the occasion of his 90<sup>th</sup> birthday

Selected titles: Synthesis of Novel 3D-Rich  $\alpha$ -Amino Acid-Derived 3-Pyrazolidinones ■ Synthesis and X-ray Structural Analysis of the Ruthenium(III) Complex Na[trans-RuCl<sub>4</sub>(DMSO)(PyrDiaz)], the Diazene Derivative of Antitumor NAMI-Pyr ■ Discrimination Between *Synechocystis* Members (Cyanobacteria) Based on Heterogeneity of Their 16S rRNA and ITS Regions ■ Geographical Origin Characterization of Slovenian Garlic Using Stable Isotope and Elemental Composition Analyses

<http://acta.chem-soc.si>

---

## EDITOR-IN-CHIEF

ALEKSANDER PAVKO

Slovenian Chemical Society, Hajdrihova 19, SI-1000 Ljubljana, Slovenija,  
E-mail: ACSi@fkt.uni-lj.si, Telephone: (+386)-1-476-0252; Fax: (+386)-1-1-476-0300

## ASSOCIATE EDITORS

Marija Bešter-Rogač, *University of Ljubljana, Slovenia*  
Janez Cerkovnik, *University of Ljubljana, Slovenia*  
Krištof Kranjc, *University of Ljubljana, Slovenia*  
Franc Perdih, *University of Ljubljana, Slovenia*  
Helena Prosen, *University of Ljubljana, Slovenia*  
Damjana Rozman, *University of Ljubljana, Slovenia*  
Melita Tramšek, *Jožef Stefan Institute, Slovenia*  
Irena Vovk, *National Institute of Chemistry, Slovenia*

## GUEST-EDITOR

Janez Cerkovnik, *University of Ljubljana, Slovenia*

## ADMINISTRATIVE ASSISTANT

Marjana Gantar Albreht, *National Institute of Chemistry, Slovenia*

---

## EDITORIAL BOARD

Wolfgang Buchberger, *Johannes Kepler University, Austria*  
Alojz Demšar, *University of Ljubljana, Slovenia*  
Stanislav Gobec, *University of Ljubljana, Slovenia*  
Marko Goličnik, *University of Ljubljana, Slovenia*  
Günter Grampp, *Graz University of Technology, Austria*  
Wojciech Grochala, *University of Warsaw, Poland*  
Danijel Kikelj, *Faculty of Pharmacy, Slovenia*  
Ksenija Kogej, *University of Ljubljana, Slovenia*  
Janez Košmrlj, *University of Ljubljana, Slovenia*  
Blaž Likozar, *National Institute of Chemistry, Slovenia*

Mahesh K. Lakshman, *The City College and  
The City University of New York, USA*  
Janez Mavri, *National Institute of Chemistry, Slovenia*  
Friedrich Sreinc, *University of Minnesota, USA*  
Walter Steiner, *Graz University of Technology, Austria*  
Jurij Svete, *University of Ljubljana, Slovenia*  
Ivan Švancara, *University of Pardubice, Czech Republic*  
Jiri Pinkas, *Masaryk University Brno, Czech Republic*  
Gašper Tavčar, *Jožef Stefan Institute, Slovenia*  
Christine Wandrey, *EPFL Lausanne, Switzerland*  
Ennio Zangrando, *University of Trieste, Italy*

---

## ADVISORY EDITORIAL BOARD

### Chairman

Branko Stanovnik, *Slovenia*

### Members

Josef Barthel, *Germany*  
Udo A. Th. Brinkman, *The Netherlands*  
Attilio Cesaro, *Italy*  
Dušan Hadži, *Slovenia*  
Vida Hudnik, *Slovenia*  
Venčeslav Kaučič, *Slovenia*

Željko Knez, *Slovenia*

Radovan Komel, *Slovenia*

Janez Levec, *Slovenia*

Stane Pejovnik, *Slovenia*

Anton Perdih, *Slovenia*

Slavko Pečar, *Slovenia*

Andrej Petrič, *Slovenia*

Boris Pihlar, *Slovenia*

Milan Randić, *Des Moines, USA*

Jože Škerjanc, *Slovenia*

Miha Tišler, *Slovenia*

Đurđa Vasić-Rački, *Croatia*

Marjan Veber, *Slovenia*

Gorazd Vesnaver, *Slovenia*


Jure Zupan, *Slovenia*

Boris Žemva, *Slovenia*

Majda Žigon, *Slovenia*

---

*Acta Chimica Slovenica* is indexed in: *Chemical Abstracts Plus*, *Current Contents (Physical, Chemical and Earth Sciences)*, *PubMed*, *Science Citation Index Expanded* and *Scopus*. Impact factor for 2016 is IF = 0.983.

Articles in this journal are published under Creative Commons Attribution 3.0 License  
 <http://creativecommons.org/licenses/by/3.0/>

### Izdaja – Published by:

SLOVENSKO KEMIJSKO DRUŠTVO – SLOVENIAN CHEMICAL SOCIETY

Naslov redakcije in uprave – Address of the Editorial Board and Administration

Hajdrihova 19, SI-1000 Ljubljana, Slovenija

Tel.: (+386)-1-476-0252; Fax: (+386)-1-476-0300; E-mail: chem.soc@ki.si

### Izdajanje sofinancirajo – Financially supported by:

Slovenian Research Agency, Ljubljana, Slovenia

National Institute of Chemistry, Ljubljana, Slovenia

Jožef Stefan Institute, Ljubljana, Slovenia

Faculty of Chemistry and Chemical Technology at University of Ljubljana, Slovenia

Faculty of Chemistry and Chemical Engineering at University of Maribor, Slovenia

Faculty of Pharmacy at University of Ljubljana, Slovenia

University of Nova Gorica, Nova Gorica, Slovenia

Chamber of Commerce and Industry of Slovenia – Chemical and Rubber Industry Association, Slovenia

Slovensko kemijsko društvo  
Slovenian Chemical Society



Članom je revija na voljo brezplačno. Za nečlane in pravne osebe znaša letna naročnina 50 EUR, za inozemstvo 110 EUR vključno s poštnino.

Annual subscription: 110 EUR including postage.

Transakcijski račun: 02053-0013322846

Bank Account No.: SI56020530013322846-Nova Ljubljanska banka d. d., Trg republike 2, SI-1520 Ljubljana, Slovenia, SWIFT Code: LJBA SI 2X

Na podlagi Zakona o davku na dodano vrednost sodi revija *Acta Chimica Slovenica* med proizvode, od katerih se obračunava DDV po stopnji 9,5 %.

*Acta Chimica Slovenica* izhaja štirikrat letno v 200 izvodih – *Acta Chimica Slovenica* appears quarterly in 200 copies

Oblikovanje ovitka – Design cover: KULT, oblikovalski studio, Simon KAJTNA, s. p. Grafična priprava za tisk: Majanafin, d. o. o. Tisk – Printed by: Tiskarna Skušek, Ljubljana

© Copyright by Slovenian Chemical Society



### Professor Miha Tišler

Writing a tribute to Professor Emeritus Dr. Miha Tišler on the occasion of his 90<sup>th</sup> birthday fills me with great honor. He was born in Ljubljana on September 18<sup>th</sup>, 1926. He graduated in chemistry at the Faculty of Natural Sciences and at the Faculty of Chemistry and Chemical Engineering in Ljubljana, Slovenia. With a scholarship from the British Council he was a postgraduate researcher in the laboratories of Lord Todd in Cambridge, England (1953–1955). There he prepared his PhD which he then defended in Ljubljana to obtain subsequently a PhD in chemistry on the basis of his thesis entitled „Syntheses in the Cycloheptatrienone Series“ (1955). In Cambridge he investigated 3-hydroxytropones and, among other compounds, he prepared at that time an unusual compound, the aromatic carboxycycloheptatrienylium (carboxyropylium) bromide.

His first appointment was as assistant in the Laboratory of Organic Chemistry at the University of Ljubljana and with time he gradually advanced to the position of Lecturer (Docent), Associate Professor (1961) and Full Professor (1964) as a permanent position. During 1971–1984 he served as Head of the Laboratory of Organic Chemistry and in 1995 he retired. He was a British Council Visiting Scientist (1966), Visiting Professor at the Universities of Freiburg, Germany (1962), Trieste, Italy (1985, 1986), Brigham Young University, Provo, Utah (1986), and under an exchange program with the National Academy of Sciences, Washington, he lectured at several universities in the USA (1968, 1979). He also spent two months as Visit-

ing Professor in Japan at the invitation of the Japan Society for Promotion of Science, Tokyo (1975), as well as in Australia (1982). He was plenary speaker at about 20 International Symposia or Congresses and at the Gordon Research Conference.

Professor Tišler is author or co-author of over 50 books, textbooks of organic and heterocyclic chemistry, monographs or review articles and over 500 published scientific papers. Of the many organic chemists who obtained the PhD degree by accomplishing their thesis under his guidance, nine were later elected and appointed at several faculties at the universities of Ljubljana and Maribor. The Organic Chemistry laboratory in Ljubljana has become internationally known as the school for heterocyclic chemistry.

His research was mainly devoted to the field of heterocyclic chemistry, syntheses of new heterocyclic systems and their transformations, development of new reagents, structural studies, tautomerism, elucidation of reaction mechanisms, *etc.*

New and interesting results were obtained from extensive investigation on azidotetrazolo isomerization. Target compounds were in the series of tetrazoloazines, and related tri- or polycyclic systems with an annelated tetrazole ring, such as azasteroids. Heterocyclic diazo compounds, in contrast to the corresponding diazonium salts, were practically unknown. Their synthesis was developed and it was possible to obtain for the first time an X-ray structure of 3-diazo-3*H*-indazole.

---

Many years of research were devoted to investigations of azoloazines and azaindolizines, *i.e.* bicyclic 10  $\pi$ -electron aromatic systems with bridgehead nitrogen atom which are, for example, isoelectronic with indole. Many new synthetic approaches towards bicyclic, tricyclic or polycyclic heterocyclic systems containing the azaindolizine unit (the six-membered ring being a pyridine, pyridazine, pyrazine or pyrimidine ring) were developed and their reactivity was investigated, such as the site of protonation and quaternization, hemolytic phenylation, *etc.*

An enormous synthetic potential was opened up with the introduction of *N,N*-dimethylaminoformamide (or acetamide) dialkyl acetals for the construction of new heterocyclic rings. The formamidines themselves or hydroxyiminomethyleneamino derivatives derived from them could be widely used for annelation reactions, for the formation of [2+2] cycloadducts with phenyl isocyanate, *etc.* Unsaturated *N,N*-dimethylamidine synthons, prepared from enamino amides, thioamides or esters and even activated methylene groups of pyridines, proved to be reactive with these acetals.

A fruitful collaboration with research possibilities was provided in the form of an exchange programme with the participation of Professors Jerald S. Bradshaw (BYU University Provo, Utah), Ronald J. Pugmire and David M. Grant (University of Utah, Salt Lake City), Gordon B. Barlin and Desmond J. Brown (John Curtin School of Medical Research, Canberra, Australia). Last but not least one should mention and acknowledge that Professor Tišler had great pleasure in a long-standing friendship, collaboration and support from Professors Jerald S. Bradshaw and Alan R. Katritzky (University of Florida, Gainesville), dating from the time when the latter was professor at the University of East Anglia in Norwich. He has also many friends at universities and institutes throughout the world.

Professor Tišler was Dean of the Faculty of Natural Sciences and Technology (1973–1976) and he was the first elected rector at the University of Ljubljana in the independent Slovenia (1991–1995). He served as Vice-President, President and Past-President of the International Society of Heterocyclic Chemistry (1973–1980). He is member of the ACS, MRSC, International Standing Committee of the International Association „Ius Primi Viri“ in Rome, Italy, and member of the Governing Council of the European Science Foundation (Strasbourg). He was also a member of the Permanent Committee of the European Rectors Conference and the State Council of Republic of Slovenia (1992–1997). He served as the National Representative in Organic Chemistry Division, Commission on Physical Organic Chemistry of IUPAC (1986–1997). He was elected to membership of the Slovenian Academy of Sciences and Arts (1970), Serbian Academy of Sciences and Arts (1978), Croatian Academy of Sciences and Arts (1979), New York Academy of Sciences (1980) and Academia Scientiarum et Artium Europaea, Salzburg (1995). He was decorated as Knight of the Order of St. Gregorius the Great (1995).

He received the Award for Science from Slovenia (1977), Plaque from the International Society of Heterocyclic Chemistry (1979), Honorary Medal and Diploma of the Slovak Technical University, Bratislava (1981), Diploma of the Tohoku University, Sendai (1975) and Hoshi University, Tokio (1986); he received documents of recognition from the Faculty of Pharmacy (1982) and Faculty of Natural Sciences and Technology, University of Ljubljana (1989) and the award Ambassador of the Republic of Slovenia (1995). He is an Inaugurated Honorary Member of the Florida Center for Heterocyclic Compounds, Gainesville, Florida. In 2000 he received the Honorary Degree (Doctor *honoris causa*) of the University of Ljubljana.

He served or is still serving at the Editorial or Advisory Board of the following scientific journals: Journal of Heterocyclic Chemistry, Heterocycles, Advances in Heterocyclic Chemistry, Heterocyclic Communications, Organic Preparations and Procedures International, Duga (Turkish Journal of Chemistry), Croatica Chemica Acta, Acta Chimica Slovenica (formerly Vestnik Slovenskega kemijskega društva).

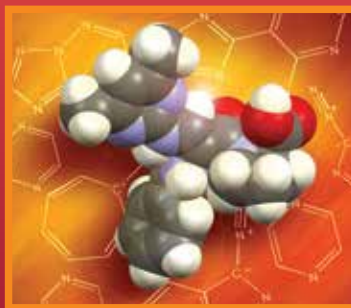
Professor Tišler (alone or with colleagues) organized several National or International Symposia or Congresses: 5<sup>th</sup> International Congress of Heterocyclic Chemistry (1975), 5<sup>th</sup> International Symposium on the Chemistry of Organic Sulfur Compounds (1978), 3<sup>rd</sup> Yugoslav Symposium of Organic Chemistry (1983) and TRISOC Symposium (symposium of the universities of Graz, Trieste and Ljubljana)(1985).

Since his retirement he has remained active in preparing some review articles (on pyridazines, which was first published in 1968, and thereafter in 1979, 1990, 2000, on heterocyclic quinones in 1989, and on heterocyclic amino acids (1995), all in Advances in Heterocyclic Chemistry).

Recently he published two books, *Molecules and their Messages*, and *Reminiscences and Reflections*, both in the Slovene language. Professor Tišler has always been an excellent supervisor to his students and friendly and helpful to his associates and acquaintances. I, as one of them, have been extremely fortunate in having him first as a supervisor during my PhD studies then later becoming one of his coworkers and colleagues; the result has been fruitful collaboration and friendship for almost sixty years.

Please join me in this celebration of Professor Miha Tišler commemorating the 90<sup>th</sup> anniversary and a distinguished career in chemistry. We wish him good health in the years ahead.

Branko Stanovnik  
Faculty of Chemistry and Chemical Technology  
University of Ljubljana



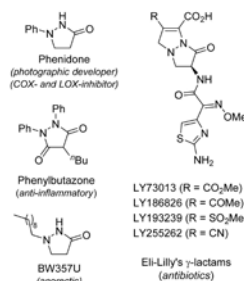
## SCIENTIFIC PAPER

715–726

Organic chemistry

### Synthesis of Novel 3D-Rich $\alpha$ -Amino Acid-Derived 3-Pyrazolidinones

Jaka Glavač, Georg Dahmann, Franc Požgan, Sebastijan Ričko, Bogdan Štefane, Jurij Svete and Uroš Grošelj

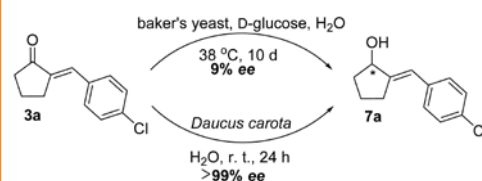


727–736

Organic chemistry

### Asymmetric Bio- and Chemoreduction of 2-Benzylidenecyclopentanone Derivatives

Bogdan Štefane, Uroš Grošelj, Jurij Svete and Franc Požgan

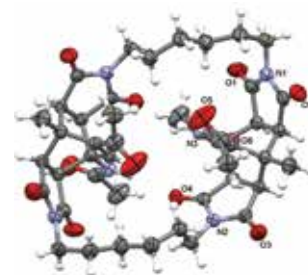


737–746

Organic chemistry

### A 26-Membered Macrocycle Obtained by a Double Diels–Alder Cycloaddition Between Two 2H-Pyran-2-one Rings and Two 1,1'-(Hexane-1,6-diyl)bis(1H-pyrrole-2,5-dione)s

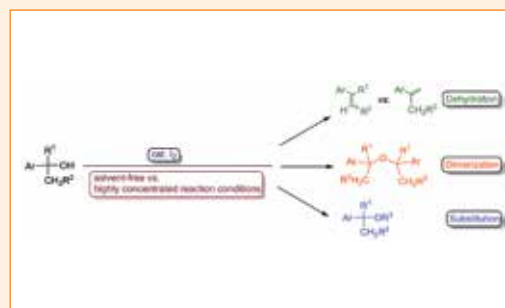
Bor Lucijan Turek, Marijan Kočevar, Krištof Kranjc and Franc Perdih



747–762 Organic chemistry

## Iodine-catalyzed Transformation of Aryl-substituted Alcohols Under Solvent-free and Highly Concentrated Reaction Conditions

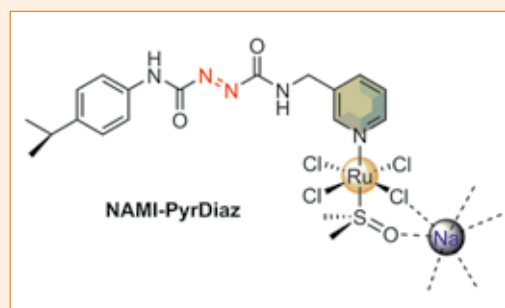
Marjan Jereb and Dejan Vražič



763–770 Organic chemistry

## Synthesis and X-ray Structural Analysis of the Ruthenium(III) Complex Na[*trans*-RuCl<sub>4</sub>(DMSO)(PyrDiaz)], the Diazene Derivative of Antitumor NAMI-Pyr

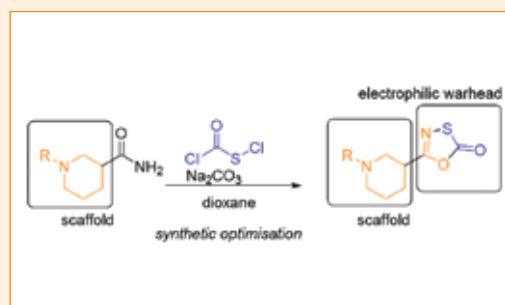
Jure Vajs, Andrej Pevec, Martin Gazvoda, Damijana Urankar, Evgeny Goreshnik, Slovenko Polanc and Janez Košmrlj



771–781 Biomedical applications

## Chlorocarbonylsulfenyl Chloride Cyclizations Towards Piperidin-3-yl-oxathiazol-2-ones as Potential Covalent Inhibitors of Threonine Proteases

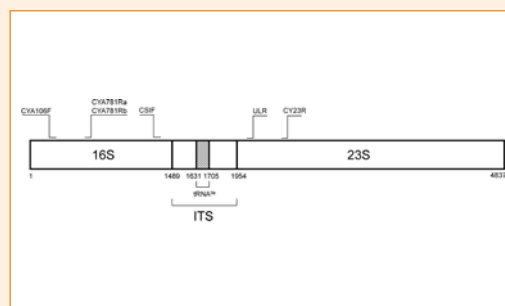
Marko Jukič, Katarina Grabrijan, Selmir Kadić, Fernando Juan de Lera Garrido, Izidor Sosič, Stanislav Gobec and Aleš Obreza



804–817 Biochemistry and molecular biology

## Discrimination Between *Synechocystis* Members (Cyanobacteria) Based on Heterogeneity of Their 16S rRNA and ITS Regions

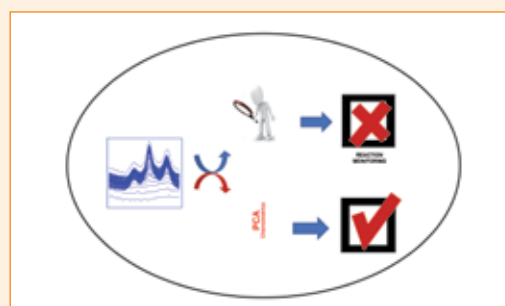
Mojca Juteršek, Marina Klemenčič and Marko Dolinar



818–824 General chemistry

## Reaction Monitoring by Means of Multivariate Data Analysis of Near-Infrared and Raman Spectra

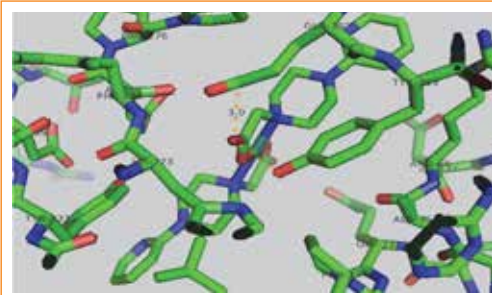
Dardan Hetemi and Steve Janagap



825–831 Inorganic chemistry

## Synthesis, Crystal Structures, Molecular Docking and MAO-B Inhibitory Activity of Transition Metal Complexes Derived from 2-(4-(Pyridin-2-yl)piperazin-1-yl)acetic Acid

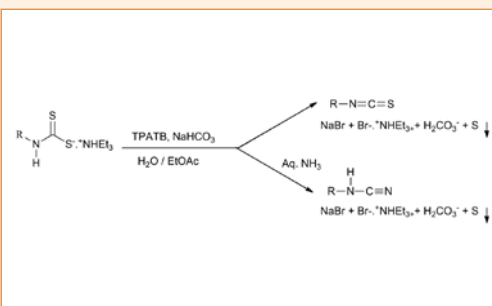
Yan-Jie Ren, Jin-Long Zhu, Li-Xin Zhang, Yin-Xiang Xu and Shao-Song Qian



832–841 Organic chemistry

## A Novel One-pot Synthesis of Isothiocyanates and Cyanamides from Dithiocarbamate Salts Using Environmentally Benign Reagent Tetrapropylammonium Tribromide

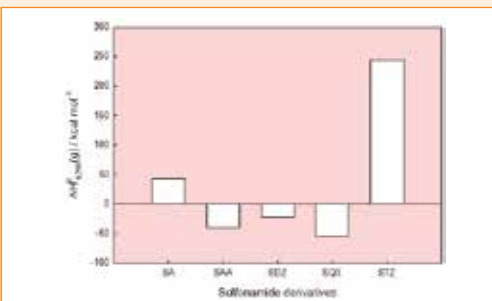
Neivotsonuo Bernadette Kuotsu, Latonglila Jamir, Tovishe Phucho and Upasana Bora Sinha



842–848 Physical chemistry

## Prediction of Physico-chemical Properties of Bacteriostatic N<sup>1</sup>-Substituted Sulfonamides: Theoretical and Experimental Studies

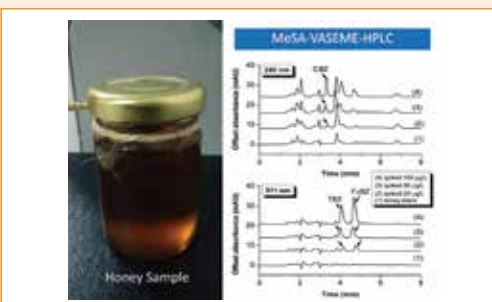
Hossein Nikoofard, Mohsen Sargolzaei and Farnosh Faridbod



849–857 Analytical chemistry

## Methyl Salicylate-Based Vortex-Assisted Surfactant-Enhanced Emulsification Microextraction and HPLC for Determination of Fungicides in Honey Samples

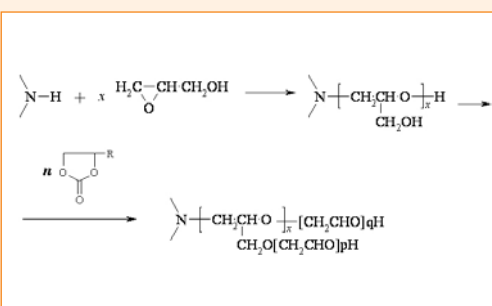
Yanawath Santaladchaiyakit, Jutamas Bunchamnan, Darunee Tongsa and Supalax Srijaranai



858–864 Applied chemistry

## A One-pot Multicomponent Reaction for the Synthesis of Oligoetherols with Azacyclic Rings

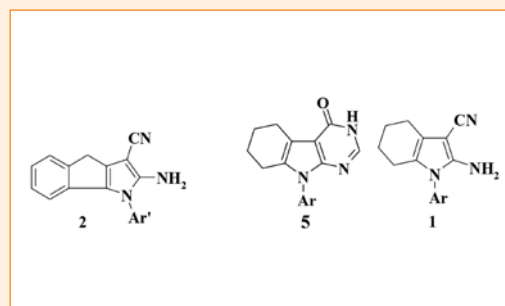
Jacek Lubczak, Renata Lubczak and Iwona Zarzyka



865–876 Organic chemistry

## Synthesis and Structure Activity Relationship of Some Indole Derivatives as Potential Anti-inflammatory Agents

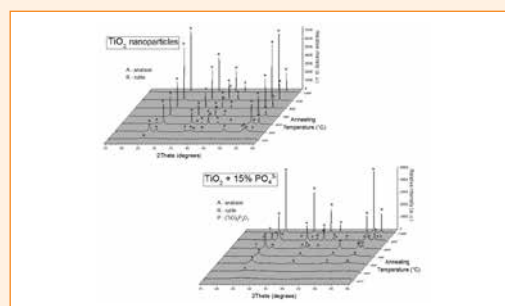
Samar S. Fatahala, Mohammed A. Khedr and Mossad S. Mohamed



877–887 Materials science

## Preparation and Investigation of the Thermal Stability of Phosphate-modified TiO<sub>2</sub> Anatase Powders and Thin Films

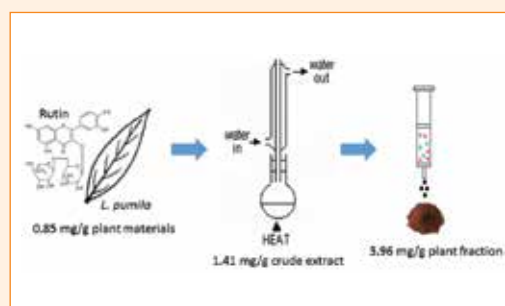
Uroš Prah and Irena Kozjek Škofic



888–894 Applied chemistry

## Recovery of Rutin from *Labisia pumila* Extract Using Solid Phase Extraction

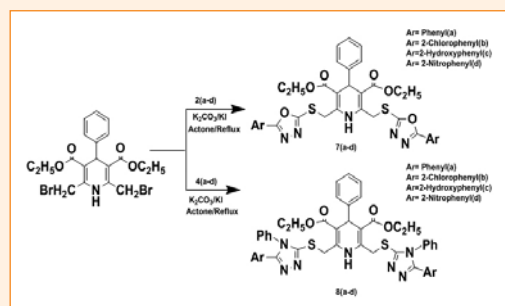
Lee Suan Chua, Nur Nabihah Ruzlan and Mohamad Roji Sarmidi



895–901 Organic chemistry

## Synthesis and Biological Evaluation of 1,2,4-Triazoles and 1,3,4-Oxadiazoles Derivatives Linked to 1,4-Dihydropyridines Scaffold

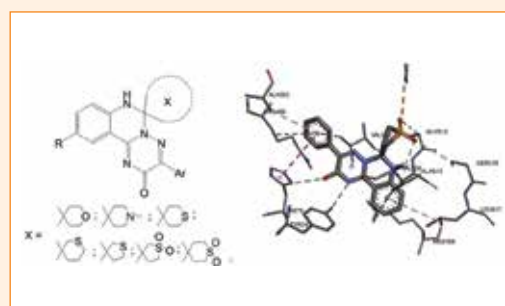
Maghsoud Ziaie, Karim Akbari Dilmaghani and Amir Tukmechi



902–910 Organic chemistry

## Design, Synthesis and Anti-inflammatory Activity of Derivatives 10-R-3-Aryl-6,7-dihydro-2H-[1,2,4]triazino [2,3-c]quinazolin-2-ones of Spiro-fused Cyclic Frameworks

Oleksandra Kolomoets, Oleksii Voskoboynik, Oleksii Antypenko, Galyna Berest, Inna Nosulenko, Vitaliy Palchikov, Olexandr Karpenko and Sergiy Kovalenko

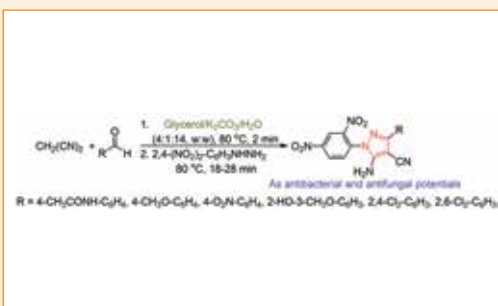




911-918 Organic chemistry

## Green One-pot Synthesis of Novel Polysubstituted Pyrazole Derivatives as Potential Antimicrobial Agents

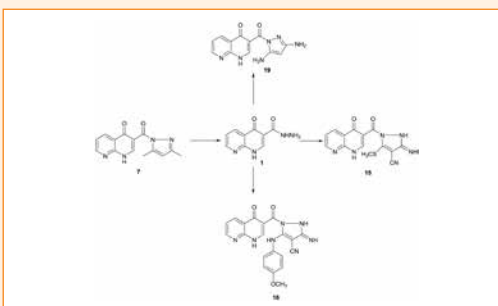
Hamid Beyzaei, Zahra Motraghi, Reza Aryan, Mohammad Mehdi Zahedi and Alireza Samzadeh-Kermani



919-930 Organic chemistry

## Synthesis and Biological Evaluation of Some Novel 1,8-Naphthyridine Derivatives

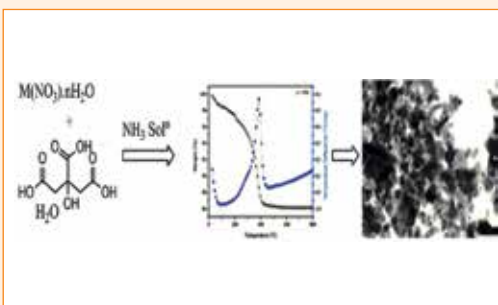
Sraa Abu-Melha



931-937 Materials science

## Preparation and Characterization of Chromium Doped Ni-Cu-Zn Nano Ferrites

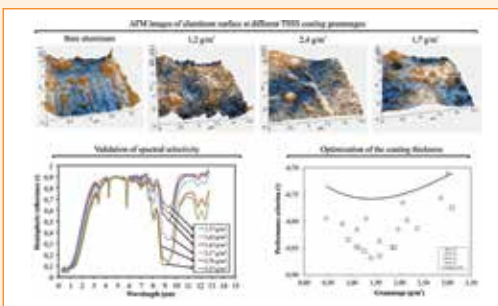
Bajarang Laxman Shinde, Laxman Appa Dhale, Venkat S. Suryavanshi and Kishan Shankarrao Lohar



938-944 Materials science

## The Impact of a Silane Pigment Treatment on the Properties of Thickness-sensitive Spectrally Selective Paints

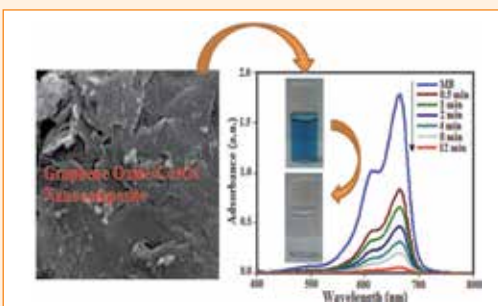
Miha Steinbücher, Peter Venturini, Jože Hafner, Matevž Zupančič, Peter Gregorčič and Iztok Golobič



945-958 Materials science

## Graphene Oxide/Co<sub>3</sub>O<sub>4</sub> Nanocomposite: Synthesis, Characterization, and Its Adsorption Capacity for the Removal of Organic Dye Pollutants from Water

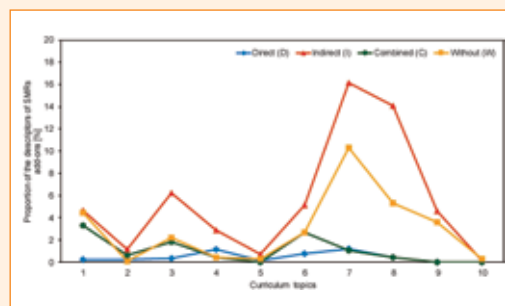
Kolsoum Pourzare, Saeed Farhadi and Yaghoub Mansourpanah



959–967 Chemical education

## The Integration of Submicroscopic Representations Used in Chemistry Textbook Sets into Curriculum Topics

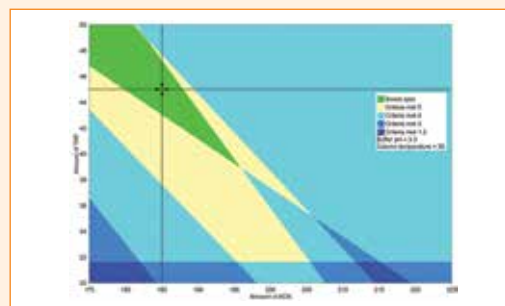
Špela Hrast and Vesna Ferik Savec



968–979 Analytical chemistry

## Optimization of UPLC Method for Simultaneous Determination of Rosuvastatin and Rosuvastatin Degradation Products

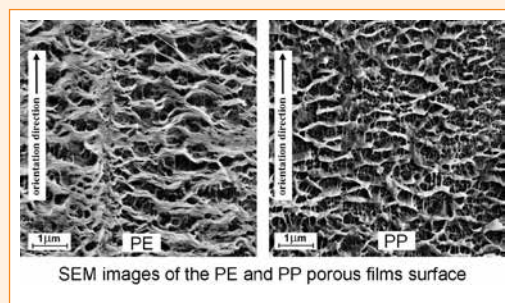
Jure Zakrajšek, Katarina Bevc-Černilec, Simona Bohanec and Uroš Urleb



980–987 Materials science

## Ordering Effects and Percolation in the Structure Formation Process of the Oriented Polyolefin Porous Films

Galina Kazimirovna Elyashevich, Dmitrii Vladimirovich Novikov, Ivan Sergeevich Kuryndin, Andreja Jelen and Vili Bukošek



988–1004 Organic chemistry

## Microwave-assisted One-pot Efficient Synthesis of Functionalized 2-Oxo-2-phenylethylenes-linked 2-Oxobenzo[1,4]oxazines and 2-Oxoquino[1,4]oxalines: ...

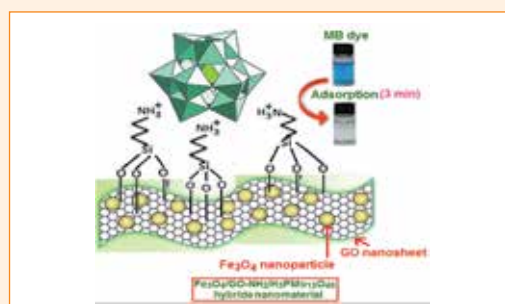
Vashundhra Sharma, Pradeep K. Jaiswal, Dharmendra K. Yadav, Mukesh Saran, Jaroslav Prikhodko, Manas Mathur, Ajit K. Swami, Irina V. Mashevskaya and Sandeep Chaudhary



1005–1019 Materials science

## Magnetically Recyclable Fe<sub>3</sub>O<sub>4</sub>/GO-NH<sub>2</sub>/H<sub>3</sub>PMo<sub>12</sub>O<sub>40</sub> Nanocomposite: Synthesis, Characterization, and Application in Selective Adsorption of Cationic Dyes from Water

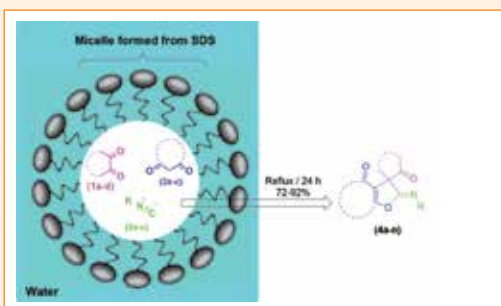
Saeed Farhadi, Mohammad Hakimi and Mansoureh Maleki



1020–1029 Organic chemistry

## Eco-Friendly Multi-Component Synthesis of $\gamma$ -Spiroiminolactones in Water

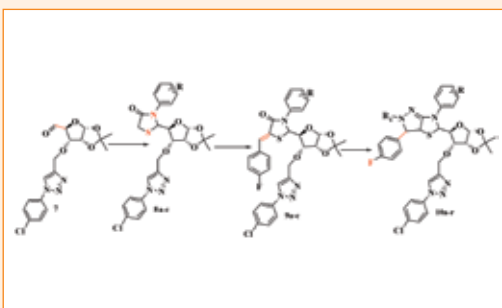
Hamid Reza Safaei and Mohsen Shekouhy



1030–1041 Organic chemistry

## Synthesis, Nematicidal and Antifungal Properties of Hybrid Heterocyclics

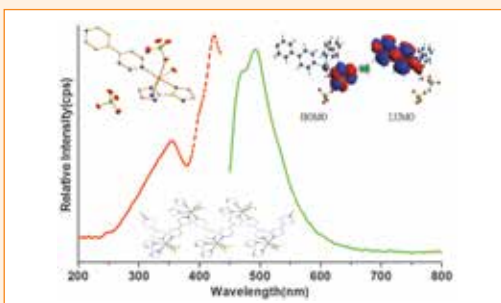
Avula Srinivas, Malladi Sunitha, Pulluri Karthik and K. Vasumathi Reddy



1042–1047 Inorganic chemistry

## Preparation, Structure, Photoluminescent and Semiconductive Properties, and Theoretical Calculation of a Novel Cadmium Complex with Mixed Ligands

Xiu-Guang Yi, Wen-Tong Chen, Jian-Gen Huang, Ding-Wa Zhang and Yin-Feng Wang

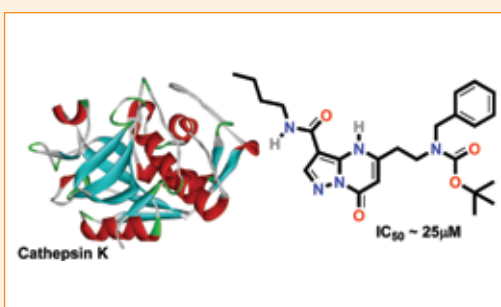


## SHORT COMMUNICATION

782–789 Organic chemistry

## Synthesis of Novel 5-(*N*-Boc-*N*-Benzyl-2-aminoethyl)-7-oxo-4,7-dihydropyrazolo[1,5-*a*]pyrimidin-3-carboxamides and Their Inhibition of Cathepsins B and K

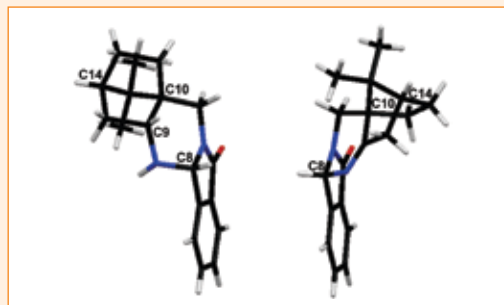
Branislav Lukić, Uroš Grošelj, Marko Novinec, and Jurij Svete



790–797 Organic chemistry

## Synthesis and Reduction of 10-Phthalimidocamphor Oxime

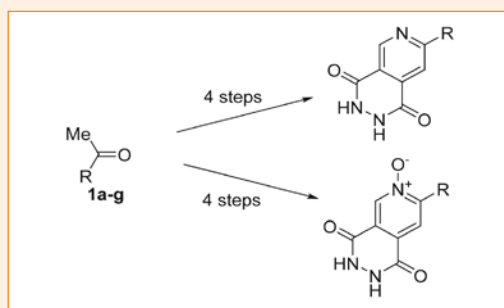
Uroš Grošelj, Amalija Golobič, Jurij Svete and Sebastijan Ričko



798–803 Organic chemistry

## The Synthesis of 7-Substituted-2,3-dihydropyrido [4,3-*d*]pyridazine-1,4-diones and 1,4-Dioxo-7-substituted-1,2,3,4-tetrahydropyrido[4,3-*d*]pyridazine 6-Oxides from Methyl Ketones

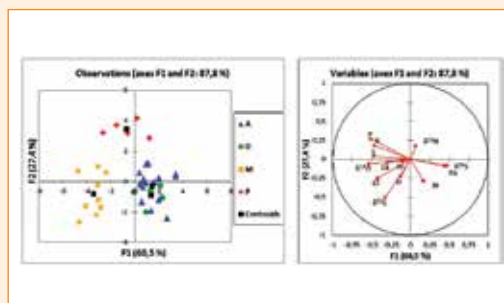
Benjamin Prek and Branko Stanovnik



1048–1055 Applied chemistry

## Geographical Origin Characterization of Slovenian Organic Garlic Using Stable Isotope and Elemental Composition Analyses

Anja Mahne Opatič, Marijan Nečemer, David Kocman and Sonja Lojen



Scientific paper

# Synthesis of Novel 3D-Rich $\alpha$ -Amino Acid-Derived 3-Pyrazolidinones

Jaka Glavač,<sup>1</sup> Georg Dahmann,<sup>2</sup> Franc Požgan,<sup>1</sup> Sebastijan Ričko,<sup>1</sup> Bogdan Štefane,<sup>1</sup> Jurij Svete,<sup>1</sup> and Uroš Grošelj<sup>1\*</sup>

<sup>1</sup> Faculty of Chemistry and Chemical Technology, University of Ljubljana, Večna pot 113, SI – 1000 Ljubljana, Slovenia.

<sup>2</sup> Medicinal Chemistry, Boehringer-Ingelheim Pharma GmbH&Co. KG, 88397 Biberach, Germany

\* Corresponding author: E-mail: uros.groselj@fkkt.uni-lj.si

Received: 12-04-2017

Dedicated to Professor Emeritus Miha Tišler, University of Ljubljana, on the occasion of his 90<sup>th</sup> birthday.

## Abstract

Synthetic approaches towards novel 3-pyrazolidinone derivatives functionalized at positions N(1) and/or C(5) were studied. 5-Aminoalkyl-3-pyrazolidinones were prepared in four steps from *N*-protected glycines via *Masamune-Claisen* homologation, reduction, *O*-mesylation, and cyclisation with a hydrazine derivative. The free amines were prepared by acidolytic deprotection. Title compound was also prepared by 'ring switching' transformation of *N*-Boc-pyrrolin-2(5*H*)-one with hydrazine hydrate. Hydrogenolytic deprotection of 5-(*N*-alkyl-*N*-Cbz-aminomethyl)pyrazolidine-3-ones followed by cyclisation with 1,1'-carbonyldiimidazole (CDI) gave two novel representatives of perhydroimidazo[1,5-*b*]pyrazole, which is an almost unexplored heterocyclic system. Amidation of 3-oxopyrazolidine-5-carboxylic acid gave the corresponding carboxamides in moderate yields. Diastereomeric non-racemic carboxamides obtained from (*S*)-AlaOMe and (*S*)-ProOMe were separated by MPLC.

**Keywords:** 3-Pyrazolidinones, amino acids, cyclization, heterocycles, synthesis

## 1. Introduction

Hetero(bi)cycles are commonly used building blocks for applications in medicinal chemistry, catalysis, and materials science.<sup>1,2</sup> In this context, 3-pyrazolidinones and their bicyclic analogues are attractive targets due to their easy availability from  $\alpha,\beta$ -unsaturated esters and because of their applicability and biological activity.<sup>3–6</sup> Pyrazolidinone derivatives have been employed as dyes and photographic developers<sup>3,5</sup> and as inhibitors of cyclooxygenase, lipoxygenase,<sup>7</sup> and  $\gamma$ -aminobutyrate aminotransferase<sup>8</sup> exhibiting analgesic, antipyretic, anti-inflammatory, and anorectic activity. Among bicyclic analogues, perhydropyrazolo[1,2-*a*]pyrazolones belong to azabicycloalkane amino acids, which are U-shaped conformationally constrained heterocyclic analogues of peptides that simulate  $\beta$ -turn structures.<sup>9,10</sup> Consequently, bicyclic pyrazolidinones are used as drugs to relieve Alzheimer's disease<sup>11</sup> and as antibacterial (Eli-Lilly's  $\gamma$ -lactam antibiotics),<sup>12</sup> and antitrypanosomal agents.<sup>13</sup> Synthetic applications of 3-pyrazolidi-

nones comprise their use as chiral auxiliaries,<sup>14–19</sup> as templates in asymmetric Diels-Alder cycloadditions,<sup>20–22</sup> and as a new scaffold in organocatalysis.<sup>23–30</sup> Typical examples of important 3-pyrazolidinone derivatives are depicted in Figure 1.

However, in spite of easy availability of simple pyrazolidinones from  $\alpha,\beta$ -unsaturated esters and hydrazine derivatives,<sup>3–6,31,32</sup> the synthesis of functionalized polysubstituted pyrazolidinones remains challenging. Consequently, a majority of saturated bi- and tricyclic 3-pyrazolidinones are either unknown or unexplored heterocyclic systems.

In the context of our ongoing work on the synthesis of chiral heterocycles with emphasis on pyrazole<sup>33,34</sup> and pyrazolidinone derivatives,<sup>31,32</sup> we reported the synthesis of tetrahydropyrazolo[1,5-*c*]pyrimidine-2,7-diones as the first representatives of a novel saturated heterocyclic system,<sup>35,36</sup> followed by preparation of closely related tetrahydropyrazolo[1,5-*c*]pyrimidine-3-carboxamides<sup>37</sup> and tetrahydro-1*H*-imidazo[1,5-*b*]pyrazole-2,6-diones.<sup>38</sup> In ex-

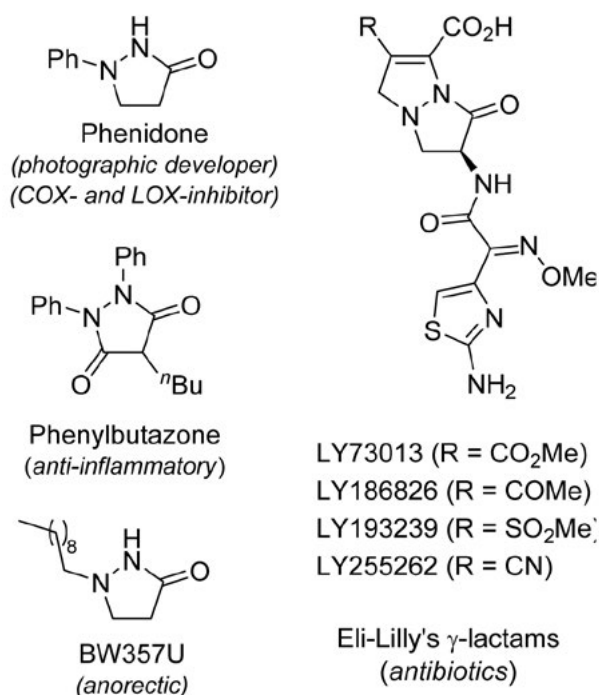
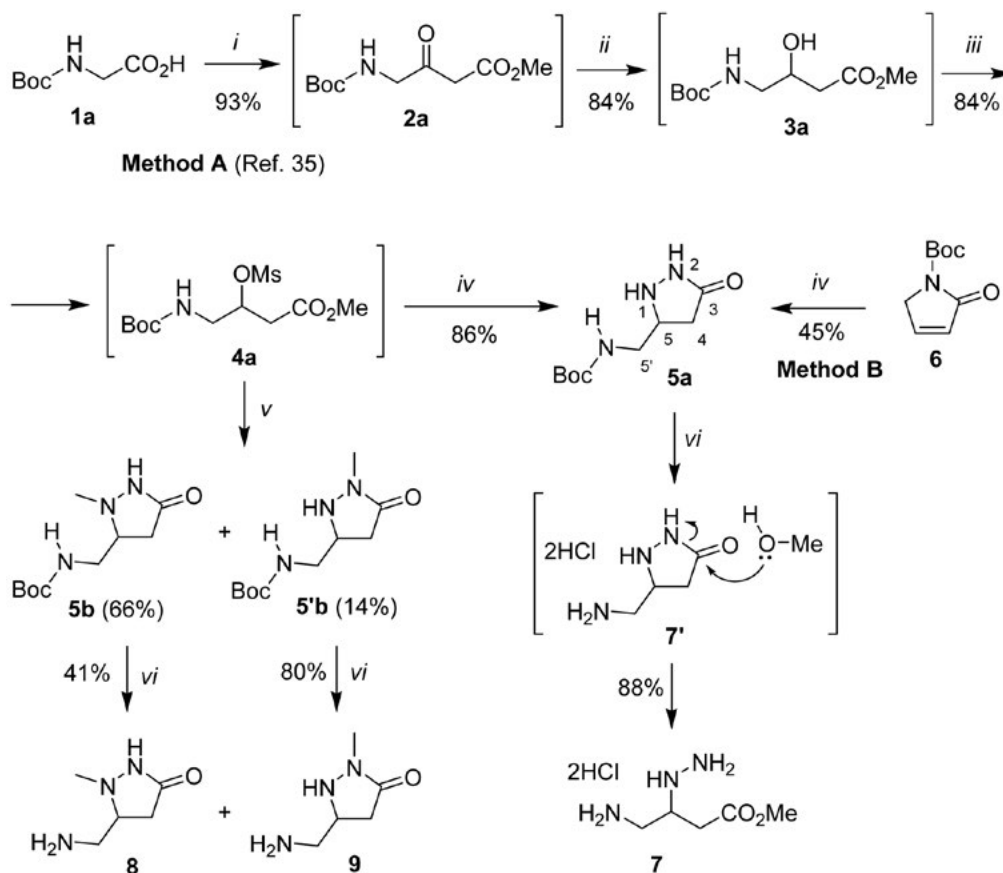


Figure 1. Examples of important 3-pyrazolidinone derivatives.

tension, the first representatives of octahydro-2*H*-2a,2a'-diazacyclopenta[*cd*]inden-2-one as a novel tricyclic pyrazolidinone-based system were also prepared.<sup>39</sup> Crucial for all of the above syntheses was the preparation of a pyrazolidinone key-intermediate with suitably functionalized substituent at position 5 allowing for cyclization to position 1. The 5-substituted pyrazolidinone was obtained by cyclization of the corresponding  $\beta$ -mesyloxy ester, which in turn was obtained in three steps from a suitably functionalized carboxylic acid.<sup>31</sup> Pyrazolidinones with 2-hydroxyethyl<sup>36</sup> and 2-aminoethyl<sup>35,37</sup> functional groups at position 5 were used as key intermediates in the synthesis of novel saturated heterocyclic systems, while 5-[(*S*)-1-aminoalkyl] derivatives prepared from *N*-protected  $\alpha$ -amino acids were used as scaffolds for potential organocatalysts<sup>38</sup> and as key-intermediates in the synthesis of 3-pyrrolinones.<sup>40</sup>

In addition to previously published 5-aminoethyl and 5-hydroxymethyl-3-pyrazolidinones, we also tried to prepare the 5-aminomethyl analogues, because they could be useful intermediates in the synthesis of novel saturated heterocycles in the imidazo[1,5-*b*]pyrazole and pyrazolo[1,5-*a*]pyrazine series. In this paper, we report the preparation and some follow-up transformations of 5-ami-



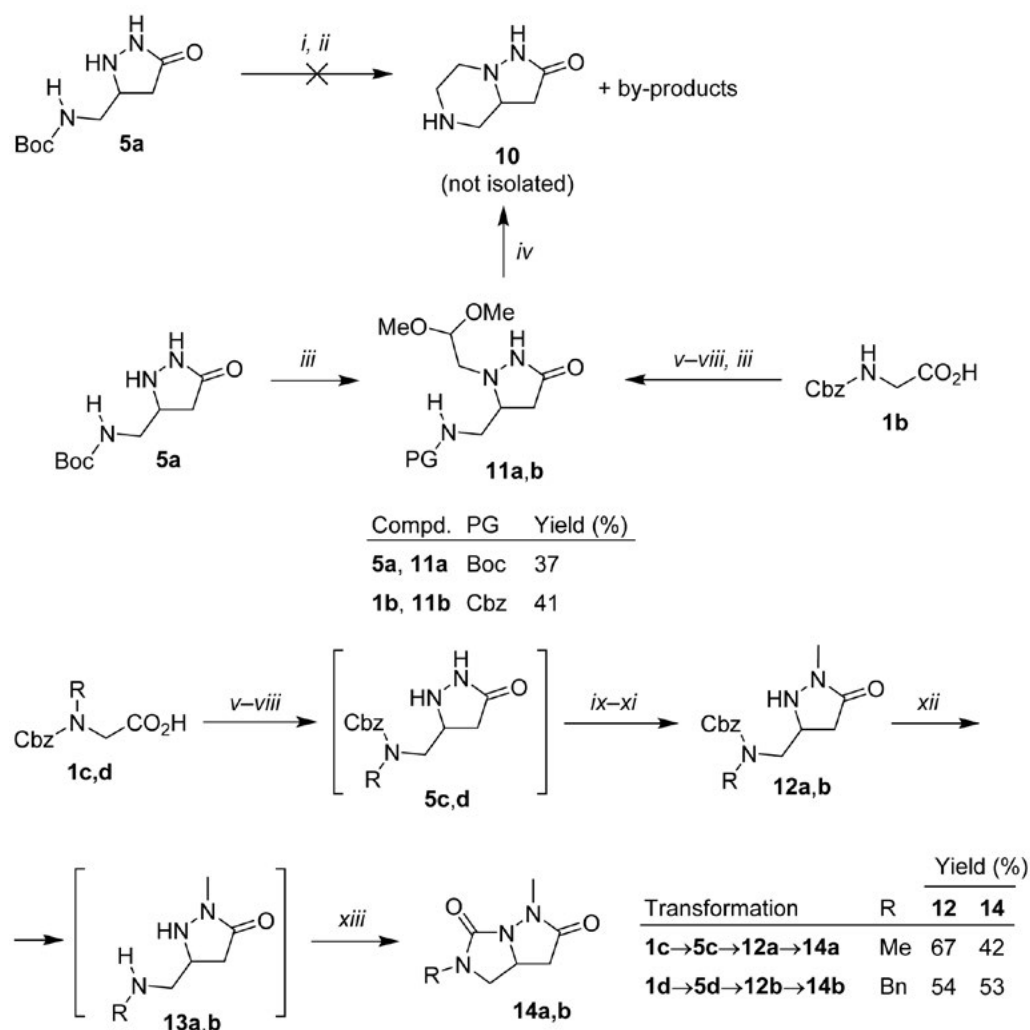
Scheme 1. Synthesis of the 5-aminomethyl-3-pyrazolidinones **5a**, **5b**, **5'b**, and **7–9**. Reaction conditions: *i*) CDI, THF, r.t. 2 h, then MeO<sub>2</sub>CCH<sub>2</sub>CO<sub>2</sub>K, MgCl<sub>2</sub>, r.t.; *ii*) NaBH<sub>4</sub>, MeOH, 0–20 °C; *iii*) MsCl, pyridine, CH<sub>2</sub>Cl<sub>2</sub>, 0 °C; *iv*) N<sub>2</sub>H<sub>4</sub>·H<sub>2</sub>O, MeOH, r.t.; *v*) MeNHNH<sub>2</sub>, MeOH, r.t., then chromatographic separation (MPLC); *vi*) HCl-EtOAc, MeOH, r.t.

nomethyl and 5-carboxy substituted 3-pyrazolidinones available from glycine derivatives and from dimethyl maleate, respectively. These novel pyrazolidinone derivatives are interesting intermediates in the synthesis of chiral saturated pyrazolidine-based heterocyclic systems.

## 2. Results and Discussion

First, 5-*tert*-butoxycarbonylaminoethyl-3-pyrazolidinones **5a**, **5b**, and **5'b** were prepared in four steps from commercially available *N*-Boc-glycine (**1a**) following a well-established literature protocol.<sup>35–39</sup> Masamune-Claisen condensation of amino acid **1a**, *i.e.* activation of **1a** with 1,1'-carbonyldiimidazole (CDI) followed by treatment of the intermediate imidazolide with a mixture of potassium monomethyl malonate and magnesium chloride gave the corresponding  $\beta$ -keto ester **2a** in 93% yield. Reduction of

**2a** with NaBH<sub>4</sub> in methanol followed by *O*-mesylation of the so formed alcohol **3a** afforded the  $\beta$ -mesyloxy ester **4a** in 71% yield over two steps. The mesylate **4a** was then cyclized with hydrazine hydrate or methylhydrazine to furnish the *N*(5')-protected 5-aminomethyl-3-pyrazolidinones **5a**, **5b**, and **5'b**. Cyclisation of the mesylate **4a** with methylhydrazine was regioselective to give a ~5:1 mixture of the major 1-methyl regioisomer **5b** and the minor 2-methyl isomer **5'b**. Upon chromatographic separation (MPLC), the pure regioisomers **5b** and **5'b** were obtained in 66% and 14% yields, respectively. To shorten the synthetic procedure for the preparation of **5a**, commercially available *tert*-butyl 2-oxo-2,5-dihydro-1*H*-pyrrole-1-carboxylate (**6**) was treated with hydrazine hydrate in methanol at room temperature to afford the pyrazolidinone **5a** in 45% yield. However, in spite of its greater simplicity, the latter procedure was less effective in terms of product yield. Finally, the respective free amines **7–9** were prepared



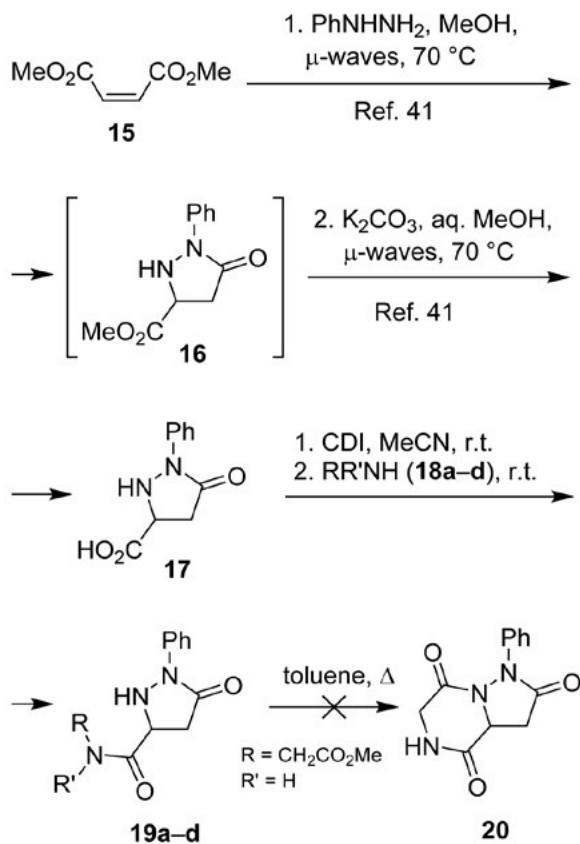
**Scheme 2.** Reaction conditions: *i*) TFA, CH<sub>2</sub>Cl<sub>2</sub>, r.t.; *ii*) 50% aq. glyoxal or (MeO)<sub>2</sub>CH<sub>2</sub>CHO, H<sub>2</sub>, Pd-C, MeOH, r.t.; *iii*) 50% aq. (MeO)<sub>2</sub>CH<sub>2</sub>CHO, NaBH<sub>4</sub>, MeOH, r.t.; *iv*) aq. HCl, MeOH, H<sub>2</sub>, Pd-C, r.t.; *v*) CDI, THF, r.t. 2 h, then MeO<sub>2</sub>CCH<sub>2</sub>CO<sub>2</sub>K, MgCl<sub>2</sub>, r.t.; *vi*) NaBH<sub>4</sub>, MeOH, 0–20 °C; *vii*) MsCl, pyridine, CH<sub>2</sub>Cl<sub>2</sub>, 0 °C; *viii*) N<sub>2</sub>H<sub>4</sub>·H<sub>2</sub>O, MeOH, r.t.; *ix*) Boc<sub>2</sub>O, r.t.; *x*) MeI, DMF, K<sub>2</sub>CO<sub>3</sub>, r.t.; *xi*) TFA-CH<sub>2</sub>Cl<sub>2</sub>, r.t.; *xii*) H<sub>2</sub>, Pd-C, MeOH, r.t.; *xiii*) CDI, DMF, r.t.

by acidolytic *N*-deprotection of **5a**, **5b**, and **5'b**. Quite unexpectedly, treatment of **5a** with HCl–MeOH gave the open-chain diamine **7**, which is explainable by acid-catalyzed ring-opening of the initially formed intermediate **7'** with methanol (Scheme 1).

Next, cyclisation of the pyrazolidinone **5a** was studied. Our initial goal was to prepare hexahydropyrazolo[1,5-*a*]pyrazin-2(1*H*)-one (**10**) by concomitant *N*-deprotection and reductive alkylation of **5a** with glyoxal or with dimethoxyacetaldehyde. Unfortunately, this approach did not work and furnished mixtures of products regardless of the variation of the reaction conditions. Nevertheless, we were able to detect the presence of the desired compound **10** in the crude reaction mixture by HRMS ( $m/z = 142.0974$ ,  $MH^+$ ). Attempted isolation and purification of this highly polar compound **10** failed. On the other hand, reductive alkylation of **5a** with dimethoxyacetaldehyde and  $NaBH_3CN$  in methanol at room temperature gave the corresponding 1-(2,2-dimethoxyethyl) derivative **11a** in 37% yield. In the same way, the Cbz-analogue **11b** was prepared in five steps from *N*-Cbz-glycine (**1b**). Finally, two novel 1,5-dialkyltetrahydro-1*H*-imidazo[1,5-*b*]pyrazole-2,6-diones **14a** and **14b** were synthesized. Following the established one-pot protocol (*cf.* Scheme 1), *N*-Cbz-sarcosine (**1c**) and *N*-benzyl-*N*-Cbz-glycine (**1d**) were transformed in four steps into the corresponding pyrazolidinones **5c** and **5d**. In a subsequent one-pot procedure,<sup>35</sup> compounds **5c** and **5d** were Boc-protected at N(1), methylated at N(2), and Boc-deprotected to give the N(1)-unsubstituted intermediates **12a** and **12b** in good yields over seven steps. Somewhat expectedly,<sup>38</sup> cyclizations of **12a,b** into imidazo[1,5-*b*]pyrazole derivatives **14a,b** proceeded well. Hydrogenolytic deprotection of the pyrazolidinones **12a** and **12b** followed by cyclisation of the intermediate free amines **13** with CDI furnished the expected 1,5-dimethyltetrahydro-1*H*-imidazo[1,5-*b*]pyrazole-2,6-diones **14a** and **14b** in 42% and 53% yield, respectively (Scheme 2).

In continuation, the amidation of 5-oxo-1-phenylpyrazolidine-3-carboxylic acid (**17**) was studied. Compound **17** was obtained in three steps from dimethyl maleate (**15**) following the literature procedure.<sup>41</sup> Activation of the carboxylic acid **17** with CDI followed by treatment with primary amines **18a–c** gave the corresponding carboxamides **19a–c** in moderate yields. Somewhat surprisingly, amidation proceeded equally well with secondary diethylamine (**18d**) to afford the tertiary carboxamide **19d** in 49% yield. Attempted cyclisation of the glycine derivative **19a** into 1-phenyltetrahydropyrazolo[1,5-*a*]pyrazine-2,4,7(1*H*)-trione (**20**) in refluxing toluene failed (Scheme 3).

Finally, amidation of racemic carboxylic acid was also performed with the non-racemic  $\alpha$ -amino esters, (*S*)-AlaOMe (**18e**) and (*S*)-ProOMe (**18f**). These amidations afforded mixtures of non-racemic diastereomers **19e/19'e** and **19f/19'f**. Subsequent separation of diastereomeric mixtures by medium pressure liquid chromatography furnished the non-racemic diastereomerically pure carboxamides



Compd.	R	R'	Yield (%)
<b>18a, 19a</b>	CH <sub>2</sub> CO <sub>2</sub> Me	H	45
<b>18b, 19b</b>	CH <sub>2</sub> CH <sub>2</sub> CO <sub>2</sub> Me	H	45
<b>18c, 19c</b>	CH <sub>2</sub> CH <sub>2</sub> Ph	H	50
<b>18d, 19d</b>	Et	Et	49

Scheme 3. Synthesis of 3-pyrazolidinone-5-carboxamides **19a–d**.

**19e, 19'e, 19f, and 19'f** in 13–23% yields. Unfortunately, all products **19e, 19'e, 19f, and 19'f** were obtained as oils and their absolute configuration could not be determined by X-ray diffraction. Therefore, the configurations of the products **19e, 19'e, 19f, and 19'f** are arbitrary (Scheme 4).

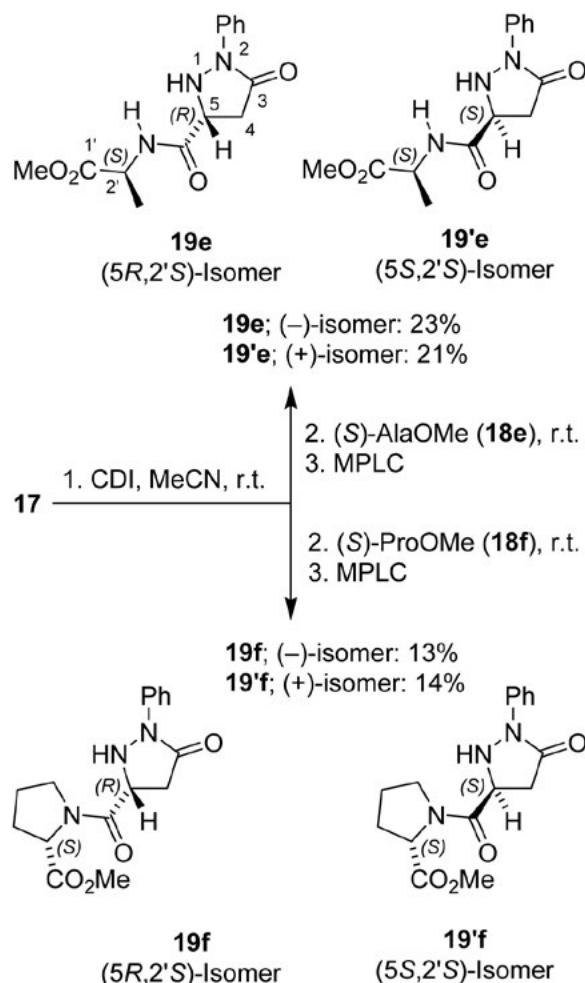
The structures of novel compounds **5a,b, 5'b, 7–9, 11a,b, 14a,b, 19a–f, and 19'e,f** were determined by spectroscopic methods (<sup>1</sup>H NMR, <sup>13</sup>C NMR, IR, MS, HRMS) and by elemental analyses for C, H, and N. Compounds **5b, 5'b, 8, 9, 11a,b, 14a,b, 19e,f, and 19'e,f** were not obtained in analytically pure form. Their identities were confirmed by <sup>13</sup>C NMR and HRMS.

## 3. Experimental

### 3.1. General Methods

Melting points were determined on a Stanford Research Systems MPA100 OptiMelt automated melting





**Scheme 4.** Synthesis of non-racemic 3-pyrazolidinones **19e,f** and **19'e,f**.

point system. The NMR spectra were obtained on a Bruker Avance III UltraShield 500 plus at 500 MHz for  $^1\text{H}$  and 126 MHz for  $^{13}\text{C}$ , using  $\text{CDCl}_3$  and  $\text{DMSO}-d_6$  (with TMS as the internal standard) as solvents. Mass spectra were recorded on an Agilent 6224 Accurate Mass TOF LC/MS spectrometer, IR spectra on a Bruker FTIR Alpha Platinum ATR spectrophotometer. Microanalyses were performed on a Perkin-Elmer CHN analyser 2400 II. Column chromatography (CC) was performed on silica gel (Fluka, Silica gel 60, particle size 35–70  $\mu\text{m}$ ). Medium performance liquid chromatography (MPLC) was performed on a Büchi Flash Chromatography System (Büchi Fraction Collector C-660, Büchi Pump Module C-605, Büchi Control Unit C-620) on silica gel (LiChroprep<sup>®</sup> Si 60, 15–25  $\mu\text{m}$ ), column dimensions: 23  $\times$  460 mm, backpressure: 10 Bar, detection: UV (254 nm). Catalytic hydrogenation was performed on a Parr Pressure Reaction Hydrogenation apparatus (500 mL). Optical rotation of chiral nonracemic compounds was measured on a Perkin-Elmer 241MC polarimeter.

*N*-Boc-Glycine (**1a**), *N*-Cbz-glycine (**1b**), *N*-Cbz-sarcosine (**1c**), *N*-benzyl-*N*-Cbz-glycine (**1d**), CDI, potassium

monomethyl malonate, anhydrous magnesium chloride, sodium borohydride, mesyl chloride, *tert*-butyl 2-oxo-2,5-dihydro-1*H*-pyrrole-1-carboxylate (**6**), glyoxal, dimethoxyacetaldehyde, sodium cyanoborohydride, sodium triacetoxyborohydride, tetrabutylammonium borohydride, trifluoroacetic acid (TFA), methyl glycinate hydrochloride (**18a**), methyl  $\beta$ -alaninate (**18b**), 2-phenylethylamine (**18c**), diethylamine (**18d**), (*S*)-*N*-Boc-alaninate (**18e**), and (*S*)-*N*-Boc-prolinate (**18f**) are commercially available. Methyl 4-*tert*-butoxycarbonylamino-3-oxobutanoate (**2a**),<sup>40</sup> methyl 4-benzyloxycarbonylamino-3-oxobutanoate (**2b**),<sup>42</sup> and 5-oxo-1-phenylpyrazolidine-3-carboxylic acid (**17**)<sup>41</sup> were prepared following the literature procedures.

### 3. 2. General Procedure for the Synthesis of *N*-protected 5-aminomethyl-3-pyrazolidinones **5a**, **5b**, and **5'b**

**Method A.** Compounds **5a**, **5b**, and **5'b** were prepared in a one-pot procedure following the combined slightly modified general literature procedures for the preparation of analogous compounds.<sup>35,38,39</sup>

#### 3. 2. 1. Methyl 4-*tert*-butoxycarbonylamino-3-oxobutanoate (**2a**)<sup>42</sup>

Under argon, CDI (1.94 g, 12 mmol) was added to a solution of Boc-glycine (**1a**) (1.75 g, 10 mmol) in anhydrous THF (20 mL) and the mixture was stirred at room temperature for 2 h. Then a solid mixture of anhydrous  $\text{MgCl}_2$  (0.893 g, 9.5 mmol) and potassium mono-methyl malonate (2.184 g, 14 mmol) was added under Ar in one portion via a powder funnel, which was rinsed with anhydrous THF (5 mL) and the mixture was stirred under Ar at r.t. for 20 h. Volatile components were evaporated *in vacuo* and the residue was triturated with EtOAc (80 mL). The resulting suspension was washed with 1 M aq.  $\text{NaHSO}_4$  (2  $\times$  20 mL) and brine (20 mL). The organic phase was dried over anhydrous  $\text{Na}_2\text{SO}_4$ , filtered, and the filtrate was evaporated *in vacuo* to give **2a**, which was used in the next step without purification. Yield: 2.15 g (93%) of yellow oil. Spectral data were in agreement with the literature data.<sup>42</sup>

#### 3. 2. 2. Methyl 4-*tert*-butoxycarbonylamino-3-hydroxybutanoate (**3a**)<sup>43</sup>

Finely powdered  $\text{NaBH}_4$  (650 mg, 17.2 mmol) was slowly added to a cooled (0  $^\circ\text{C}$ ) stirred solution of  $\beta$ -keto ester **2a** (6.94 g, 30 mmol) in MeOH (100 mL) and the resulting mixture was stirred at 0  $^\circ\text{C}$  for 1 h and then quenched at 0  $^\circ\text{C}$  by the addition of  $\text{H}_2\text{O}$  (150 mL) followed by the addition of 1 M aq. HCl (30 mL, 30 mmol). The product was extracted with dichloromethane (3  $\times$  150 mL) and the combined organic phase was washed with brine (150 mL). The organic phase was dried over anhydrous  $\text{Na}_2\text{SO}_4$ , filtered, and the filtrate was evaporated *in vacuo*.

The residue was dissolved in anh. toluene (30 mL) and the solution was evaporated *in vacuo* at 40 °C/2 mbar to give anhydrous crude **3a**, which was used in the next step without further purification. Yield: 5.93 g (84%) of yellowish oil. Spectral data were consistent with the literature data.<sup>43</sup>

### 3. 2. 3. Methyl 4-*tert*-butoxycarbonylamino-3-mesyloxybutanoate (**4a**)

MsCl (2.25 mL, 29 mmol) was added to a cooled (0 °C) solution of  $\beta$ -hydroxy ester **3** (5.83 g, 25 mmol) in anh. pyridine (30 mL) and the resulting mixture was stirred at 0 °C for 1 h and then at room temperature for 2 h. The reaction mixture was poured into cooled (0 °C) toluene (350 mL) and the toluene solution was washed thoroughly with 1 M aq. HCl (200 mL) and brine (2 × 200 mL). The organic phase was dried over anhydrous Na<sub>2</sub>SO<sub>4</sub>, filtered, and volatile components evaporated *in vacuo* to give crude **4a**, which was used in the next step without purification. Yield: 6.58 g (84%) of yellowish oil. <sup>1</sup>H-NMR (500 MHz, DMSO-*d*<sub>6</sub>):  $\delta$  1.37 (s, *t*-Bu); 2.20 (dd, *J* = 9.0; 15.1 Hz, 1H of CH<sub>2</sub>); 2.44 (dd, *J* = 3.8; 15.1 Hz, 1H of CH<sub>2</sub>); 2.86–2.98 (m, CH<sub>2</sub>); 3.82–3.90 (m, CH); 4.94 (d, *J* = 5.6 Hz, OH); 6.77 (t, *J* = 5.8 Hz, NH). <sup>13</sup>C-NMR (126 MHz, DMSO-*d*<sub>6</sub>):  $\delta$  28.2, 37.0, 37.9, 43.0, 51.7, 77.4, 78.2, 155.8, 169.8.

### 3. 2. 4. Preparation of 3-pyrazolidinones **5a**, **5b**, and **5'b**

**Method A.** Hydrazine monohydrate (0.75 mL, 15 mmol) or methylhydrazine (789  $\mu$ L, 15 mmol) was added to a solution of the mesylate **4a** (3 mmol) in CH<sub>2</sub>Cl<sub>2</sub> (25 mL) and the mixture was stirred at room temperature for 24–72 h. Volatile components were evaporated *in vacuo* and the residue was purified by CC. First, the non-polar impurities and starting material **4a** were eluted (EtOAc–hexane, 1:1), followed by elution of the products **5** and **5'** (EtOAc–MeOH, 10:1). Fractions containing the product were combined and volatile components evaporated *in vacuo* to give **5a** or **5b/5'b**. A mixture of regioisomers **5b** and **5'b** was separated by MPLC (EtOAc–MeOH, 20:1). Fractions containing the products were combined and volatile components were evaporated *in vacuo* to give **5b** and **5'b**, respectively.

#### *tert*-Butyl [(5-oxopyrazolidin-3-yl)methyl]carbamate (**5a**)

Prepared from **4a** (1.87 g, 6 mmol) and hydrazine hydrate (685  $\mu$ L, 13.8 mmol), stirring for 24 h. Yield: 1.12 g (86%) of white solid; m.p. 103–110 °C. <sup>1</sup>H-NMR (500 MHz, DMSO-*d*<sub>6</sub>):  $\delta$  1.38 (9H, s, *t*-Bu), 2.00 (1H, dd, *J* = 4.9; 16.4 Hz, 4-Ha), 2.36 (1H, dd, *J* = 7.9; 16.1 Hz, 4-Hb), 2.88–3.06 (2H, m, 3'-CH<sub>2</sub>), 3.48 (1H, br s, 3-H), 5.29 (1H, br s, 2-H), 6.88 (1H, t, *J* = 5.8 Hz, NHCH<sub>2</sub>), 8.98 (1H, s, 1-H). <sup>13</sup>C-NMR (126 MHz, DMSO-*d*<sub>6</sub>):  $\delta$  28.2, 35.0, 42.4, 56.4, 77.8, 155.9, 175.0. *m/z* (ESI) = 216 (MH<sup>+</sup>). HRMS–

ESI (*m/z*): [MH<sup>+</sup>] calcd for C<sub>9</sub>H<sub>18</sub>N<sub>3</sub>O<sub>3</sub>, 216.1343; found, 216.1339. Anal. Calcd for C<sub>9</sub>H<sub>17</sub>N<sub>3</sub>O<sub>3</sub>: C 50.22, H 7.96, N 19.52. Found: C 50.09, H 8.09, N 19.13. IR (ATR)  $\nu$  3344, 2970, 1692, 1649, 1522, 1445, 1392, 1365, 1277, 1252, 1175, 1124, 1081, 1053, 1000, 964, 901, 874, 782, 732, 638 cm<sup>-1</sup>.

#### *Tert*-Butyl [(2-methyl-5-oxopyrazolidin-3-yl)methyl]carbamate (**5b**) and *tert*-butyl [(1-methyl-5-oxopyrazolidin-3-yl)methyl]carbamate (**5'b**)

Prepared from **4a** (1.38 g, 4.43 mmol) and methylhydrazine (557  $\mu$ L, 10.37 mmol), stirring for 72 h.

#### *tert*-Butyl [(2-methyl-5-oxopyrazolidin-3-yl)methyl]carbamate (**5b**)

Yield: 670 mg (66%) of yellow oil. <sup>1</sup>H-NMR (500 MHz, DMSO-*d*<sub>6</sub>):  $\delta$  1.38 (9H, s, *t*-Bu), 1.95 (1H, dd, *J* = 4.2, 16.8 Hz, 4-Ha), 2.46 (3H, s, 2-Me), 2.70 (1H, dd, *J* = 8.1, 16.7 Hz, 4-Hb), 2.82–2.90 (1H, m, 3'-Ha), 2.99–3.08 (2H, m, 3'-Hb and 3-H), 6.89 (1H, t, *J* = 5.3 Hz, NHCH<sub>2</sub>), 9.30 (1H, s, 1-H). <sup>13</sup>C-NMR (126 MHz, DMSO-*d*<sub>6</sub>):  $\delta$  28.2, 32.5, 42.7, 46.6, 63.5, 77.8, 155.8, 172.1. *m/z* (ESI) = 230 (MH<sup>+</sup>). HRMS–ESI (*m/z*): [MH<sup>+</sup>] calcd for C<sub>10</sub>H<sub>20</sub>N<sub>3</sub>O<sub>3</sub>, 230.1499; found, 230.1496. IR (ATR)  $\nu$  3301, 2975, 2931, 1692, 1520, 1455, 1392, 1366, 1278, 1253, 1168, 1094, 1044 cm<sup>-1</sup>.

#### *tert*-Butyl [(1-methyl-5-oxopyrazolidin-3-yl)methyl]carbamate (**5'b**)

Yield: 150 mg (14%) of yellow oil. <sup>1</sup>H-NMR (500 MHz, DMSO-*d*<sub>6</sub>):  $\delta$  1.38 (9H, s, *t*-Bu), 2.09 (1H, dd, *J* = 5.1, 16.3 Hz, 4-Ha), 2.45 (1H, dd, *J* = 8.2, 16.2 Hz, 4-Hb), 2.81 (3H, s, 1-Me), 2.86–2.94 (1H, m 3'-Ha); 2.96–3.03 (1H, m, 3'-Ha), 3.41 (1H, br s, 3-H), 5.67 (1H, br s, 2-H), 6.89 (1H, t, *J* = 5.8 Hz, NHCH<sub>2</sub>). <sup>13</sup>C-NMR (126 MHz, DMSO-*d*<sub>6</sub>):  $\delta$  28.2, 30.6, 35.2, 42.6, 53.0, 77.8, 155.8, 170.5. *m/z* (ESI) = 230 (MH<sup>+</sup>). HRMS–ESI (*m/z*): [MH<sup>+</sup>] calcd for C<sub>10</sub>H<sub>20</sub>N<sub>3</sub>O<sub>3</sub>, 230.1499; found, 230.1503. IR (ATR)  $\nu$  3332, 2977, 2933, 1694, 1520, 1455, 1394, 1367, 1277, 1253, 1169, 1060, 957 cm<sup>-1</sup>.

**Method B.** Hydrazine hydrate (729  $\mu$ L, 15 mmol) was added to a solution of **6** (0.916 g, 5 mmol) in methanol (15 mL) and the mixture was stirred at r.t. for 48 h. Volatile components were evaporated *in vacuo* and the residue was purified by CC (EtOAc–MeOH, 10:1). Fractions containing the products were combined and volatile components were evaporated *in vacuo* to give **5a**. Yield: 481 mg (45%) of a yellow resin. Characterisation data for **5a** are given above in Section 3.2.4.1.

## 3. 3. General Procedure for Acidolytic Deprotection of Compounds **5a**, **5b**, and **5'b**. Synthesis of Free Amines **7–9**

2 M HCl in ethyl acetate (10 mL, 20 mmol) was added to a stirred solution of **5a**, **5b**, or **5'b** (4 mmol) in methanol (20 mL) and the mixture was stirred at r.t. for 72 h.

The precipitate was collected by filtration, washed with anh. Et<sub>2</sub>O (50 mL) and dried *in vacuo* to give 7–9.

### 3. 3. 1. 2-(1-Ammonio-4-methoxy-4-oxobutan-2-yl)hydrazin-1-ium chloride (7)

Prepared from **5a** (861 mg, 4 mmol). Yield: 778 mg (88%) of white solid; mp 187–191 °C. <sup>1</sup>H-NMR (500 MHz, DMSO-*d*<sub>6</sub>): δ 2.75 (1H, dd, *J* = 6.9, 17.0 Hz, 3-Ha), 2.83 (1H, dd, *J* = 6.3, 17.0 Hz, 3-Hb), 3.06 (2H, br s, 1-CH<sub>2</sub>); 3.64 (4H, br s, CO<sub>2</sub>Me, 2-H), 5.75 (1H, br s, NH), 8.34 (3H, br s, NH<sub>3</sub><sup>+</sup>), 9.65 (3H, br s, NH<sub>3</sub><sup>+</sup>). <sup>13</sup>C-NMR (126 MHz, DMSO-*d*<sub>6</sub>): δ 34.7, 39.3, 51.8, 52.8, 170.9. Anal. Calcd for C<sub>5</sub>H<sub>15</sub>Cl<sub>2</sub>N<sub>3</sub>O<sub>2</sub>: C 27.28, H 6.87, N 19.09. Found: C 27.58, H 6.69, N 18.84. IR (ATR) ν 3437, 3198, 2987, 1727, 1598, 1523, 1471, 1442, 1376, 1301, 1232, 1189, 1054, 1000, 987, 942, 902, 869, 772 cm<sup>-1</sup>.

### 3. 3. 2. 5-(Ammoniomethyl)-1-methyl-3-oxopyrazolidin-1-ium chloride (8)

Prepared from **5b** (688 mg, 3 mmol). Yield: 250 mg (41%) of white solid; mp 170–183 °C. <sup>1</sup>H-NMR (500 MHz, DMSO-*d*<sub>6</sub>): δ 2.42 (1H, br d, *J* = 11.4 Hz, 4-Ha), 2.81 (3H, s, 1-Me), 2.98 (1H, br d, *J* = 13.3 Hz, 4-Hb), 3.09 (2H, br d, 3'-CH<sub>2</sub>), 3.89 (1H, br s, 3-H), 7.90 (2H, br s, 2-H and NH<sup>+</sup>), 8.50 (3H, br s, NH<sub>3</sub><sup>+</sup>). <sup>13</sup>C-NMR (126 MHz, DMSO-*d*<sub>6</sub>): δ 32.6, 39.2, 45.2, 62.3, 171.5. *m/z* (ESI) = 130 (MH<sup>+</sup>). HRMS-ESI (*m/z*): [MH<sup>+</sup>] calcd for C<sub>5</sub>H<sub>12</sub>N<sub>3</sub>O, 130.0975; found, 130.0974. IR (ATR) ν 3438, 3004, 2484, 1750, 1493, 1456, 1443, 1425, 1385, 1322, 1302, 1261, 1223, 1166, 1118, 1104, 1053, 1013, 919 cm<sup>-1</sup>.

### 3. 3. 3. 5-(Ammoniomethyl)-2-methyl-3-oxopyrazolidin-1-ium chloride (9)

Prepared from **5'e** (85 mg, 0.37 mmol). Yield: 60 mg (80%) of very hygroscopic white semi-solid. <sup>1</sup>H-NMR (500 MHz, DMSO-*d*<sub>6</sub>): δ 2.40 (1H, dd, *J* = 4.7, 16.8 Hz, 4-Ha), 2.75 (1H, dd, *J* = 8.7, 16.8 Hz, 4-Hb), 2.94 (3H, s, 2-Me), 2.97–3.07 (2H, m, 5'-CH<sub>2</sub>), 3.92–4.01 (1H, m, 5-H), 4.91 (2H, br s, NH<sub>2</sub><sup>+</sup>), 8.33 (3H, br s, NH<sub>3</sub><sup>+</sup>). <sup>13</sup>C-NMR (126 MHz, DMSO-*d*<sub>6</sub>): δ 30.7, 33.9, 39.9, 51.2, 169.9. *m/z* (ESI) = 130 (MH<sup>+</sup>). HRMS-ESI (*m/z*): [MH<sup>+</sup>] calcd for C<sub>5</sub>H<sub>12</sub>N<sub>3</sub>O, 130.0975; found, 130.0972.

### 3. 4. Tert-Butyl ((2-(2,2-dimethoxyethyl)-5-oxopyrazolidin-3-yl)methyl)carbamate (11a)

NaBH<sub>3</sub>CN (465 mg, 15 mmol) was added in small portions within 1 h to a stirred solution of **5** (3.23 g, 15 mmol) and dimethoxyacetaldehyde (50% in H<sub>2</sub>O, 4.5 mL, 30 mmol) in methanol (30 mL) and the mixture was stirred at r.t. for 48 h. Volatile components were evaporated *in vacuo* and the residue was purified by CC (EtOAc–MeOH,

10:1). Fractions containing the product were combined and evaporated *in vacuo* to give **7a**. Yield: 1.606 g (37%) of white foam. <sup>1</sup>H-NMR (500 MHz, DMSO-*d*<sub>6</sub>): δ 1.37 (9H, s, *t*-Bu), 1.89 (1H, dd, *J* = 2.3, 16.4 Hz, 4'-Ha), 2.70 (1H, dd, *J* = 4.5, 12.7 Hz, 1H of NCH<sub>2</sub>), 2.75 (1H, dd, *J* = 8.4, 16.8 Hz, 4'-Hb), 2.78–2.87 (1H, m, 1H of NCH<sub>2</sub>), 2.89 (1H, dd, *J* = 5.9, 12.7 Hz, 1H of NCH<sub>2</sub>), 3.00 (1H, m, 1H of NCH<sub>2</sub>), 3.25 and 3.26 (6H, 2s, 1:1, 2 × OMe), 3.23–3.29 (1H, m, 3'-H overlapped by the signal for H<sub>2</sub>O), 4.40 (1H, dd, *J* = 4.5, 5.9 Hz, CH(OMe)<sub>2</sub>), 6.82 (1H, t, *J* = 5.9 Hz, NHCH<sub>2</sub>), 9.34 (1H, s, 1'-H). <sup>13</sup>C-NMR (126 MHz, DMSO-*d*<sub>6</sub>): δ 28.2, 31.8, 43.0, 52.9, 53.2, 60.8, 61.9, 77.7, 101.8, 155.7, 172.2. *m/z* (ESI) = 304 (MH<sup>+</sup>). HRMS-ESI (*m/z*): [MH<sup>+</sup>] calcd for C<sub>13</sub>H<sub>25</sub>N<sub>3</sub>O<sub>5</sub>, 304.1867; found, 304.1866. IR (ATR) ν 3395, 3055, 2982, 2936, 2836, 2360, 2340, 1699, 1507, 1452, 1423, 1392, 1367, 1266, 1169, 1132, 1074, 974, 896, 866, 741, 705, 668 cm<sup>-1</sup>.

### 3. 5. Benzyl ((2-(2,2-dimethoxyethyl)-5-oxopyrazolidin-3-yl)methyl)carbamate (11b)

The crude pyrazolidinone **5b** was prepared in four steps from *N*-Cbz-glycine (**1b**) following a one-pot procedure for the preparation of its *N*-Boc analogue **5a** (*cf.* Section 3.2. and Scheme 1). Reductive alkylation of the intermediate pyrazolidinone **5b** (1.246 g, 5 mmol) was performed in the same way as described above for the preparation of **11a**. The crude product **11b** was additionally purified by MPLC (EtOAc–MeOH, 10:1). Yield: 700 mg (41%) of yellow oil. <sup>1</sup>H-NMR (500 MHz, DMSO-*d*<sub>6</sub>): δ 1.91 (1H, dd, *J* = 2.5, 16.9 Hz, 4'-Ha), 2.71 (1H, dd, *J* = 4.5, 12.8 Hz, 1H of NCH<sub>2</sub>), 2.78 (1H, dd, *J* = 8.3, 16.8 Hz, 4'-Hb), 2.89 (1H, dd, *J* = 3.2, 5.9 Hz, 1H of NCH<sub>2</sub>), 2.90 (1H, m, 1H of NCH<sub>2</sub>), 3.08 (1H, m, 1H of NCH<sub>2</sub>), 3.24 and 3.25 (6H, 2s, 1:1, 2 × OMe), 3.29–3.36 (1H, m, 3'-H), 4.40 (1H, dd, *J* = 4.5, 5.9 Hz, CH(OMe)<sub>2</sub>), 5.02 (2H, d, *J* = 4.3 Hz, PhCH<sub>2</sub>), 7.29–7.39 (6H, m, Ph and NHCH<sub>2</sub>), 9.36 (1H, s, 1'-H). <sup>13</sup>C-NMR (126 MHz, DMSO-*d*<sub>6</sub>): δ 31.8, 43.4, 53.0, 53.1, 60.8, 61.8, 65.3, 101.8, 127.7, 127.8, 128.3, 137.1, 156.3, 172.9. *m/z* (ESI) = 338 (MH<sup>+</sup>). HRMS-ESI (*m/z*): [MH<sup>+</sup>] calcd for C<sub>16</sub>H<sub>23</sub>N<sub>3</sub>O<sub>5</sub>, 338.1711; found, 338.1709. IR (ATR) ν 3336, 3058, 2938, 2836, 2360, 2342, 1698, 1519, 1455, 1266, 1134, 1073, 977, 918, 869, 830, 739, 701, 668 cm<sup>-1</sup>.

### 3. 6. General Procedure for the Synthesis of 5-alkyl-1-methyltetrahydro-1H-imidazo[1,5-*b*]pyrazole-2,6-diones 14a,b

Bicyclic compounds **14a** and **14b** were obtained in nine steps from *N*-Cbz-sarcosine (**1c**) and *N*-benzyl-*N*-Cbz-glycine (**1d**). First, 3-pyrazolidinones **5c** and **5d** were prepared following a one-pot procedure for the preparation of their *N*-Boc analogue **5a** (*cf.* Section 3.2. and Scheme 1).<sup>35</sup>

### 3. 6. 1. Preparation of the Free Diamines 12a,b

Boc<sub>2</sub>O (2.4 g, 11 mmol) was added to a stirred solution of **5c,d** (9 mmol) in a mixture of dioxane (12 mL), water (25 mL), and Na<sub>2</sub>CO<sub>3</sub> (1.1 g, 10 mmol) and the mixture was stirred at r.t. for 24 h. Most of the dioxane was removed by evaporation *in vacuo* at 35 °C/50 mbar. EtOAc (50 mL) and brine (25 mL) were added to the aqueous residue, the biphasic system was transferred into a separatory funnel, shaken, and the phases were separated. The organic phase was washed with brine (2 × 20 mL), dried over anh. Na<sub>2</sub>SO<sub>4</sub>, filtered, and the filtrate was evaporated *in vacuo*. The residue was purified by CC (EtOAc/hexane, 1:1). Fractions containing the product were combined and evaporated *in vacuo*. Under argon, the residue was dissolved in anh. DMF (25 mL), K<sub>2</sub>CO<sub>3</sub> (691 mg, 5 mmol) and methyl iodide (934 μL, 15 mmol) were added and the mixture was stirred at r.t. for 72 h. Volatile components were evaporated *in vacuo*, EtOAc (100 mL) was added to the residue, and the mixture was washed with brine (3 × 30 mL). The organic phase was dried over anh. Na<sub>2</sub>SO<sub>4</sub>, filtered, and the filtrate was evaporated *in vacuo*. The residue was purified by CC (EtOAc/hexane, 1:1). Fractions containing the product were combined and evaporated *in vacuo*. The residue was dissolved in dichloromethane (20 mL), TFA (5 mL) was added and the mixture was stirred at r.t. for 24 h. Volatile components were evaporated *in vacuo*, EtOAc (150 mL) and brine (50 mL) were added, and the biphasic system was made alkaline by slow addition of solid K<sub>2</sub>CO<sub>3</sub> until pH 8–9 was reached. The mixture was stirred vigorously at r.t. for 5 min and then stirring was stopped and the phases were allowed to separate. The organic phase was washed with brine (2 × 10 mL), dried over anh. Na<sub>2</sub>SO<sub>4</sub>, filtered, and the filtrate was evaporated *in vacuo*. The residue was purified by CC (EtOAc/MeOH, 10:1). Fractions containing the product were combined and evaporated *in vacuo* to give **12a,b**, which were used in the next step without further purification.

### 3. 6. 2. Preparation of tetrahydro-1H-imidazo[1,5-b]pyrazole-2,6-diones 14a,b

A mixture of crude **12c,d** (1.5 mmol), methanol (20 mL), and 10% Pd–C (80 mg) was hydrogenated under 3 bar of H<sub>2</sub> at room temperature for 1.5 h. The catalyst was removed by filtration through a short pad of Celite®, washed with methanol (3 × 10 mL), and the combined filtrate was evaporated *in vacuo*. The residue was dissolved in toluene (20 mL) and the solution was evaporated *in vacuo* again to give anhydrous free diamine **13a,b**. The crude diamine **13** (1.5 mmol) was dissolved in anh. DMF (5 mL), CDI (262 mg, 1.5 mmol) was added, and the mixture was stirred at room temperature for 12 h. Volatile components were evaporated *in vacuo* and the residue was purified by CC (EtOAc–MeOH, 10:1). Fractions containing the product were combined and evaporated *in vacuo*. The residue (a mixture of **14** and imidazole) was dissolved in EtOAc

(1 mL), 2 M HCl–Et<sub>2</sub>O (1 mL), was added and the precipitate (imidazole hydrochloride) was removed by filtration and washed with anh. Et<sub>2</sub>O (2 × 2 mL). The filtrate was evaporated *in vacuo* to give **14a,b**.

### 1,5-Dimethyltetrahydro-1H-imidazo[1,5-b]pyrazole-2,6-dione (14a).

Prepared from **12a** (222 mg, 1.55 mmol) and CDI (265 mg, 1.55 mmol). Yield: 110 mg (42%) of yellow oil. <sup>1</sup>H-NMR (500 MHz, DMSO-*d*<sub>6</sub>): δ 2.41 (1H, dd, *J* = 7.8, 16.0 Hz, 3'-Ha), 2.70 (1H, dd, *J* = 11.3, 16.4 Hz, 3'-Hb), 2.75 (3H, s, 5'-Me), 3.13 (3H, s, 1'-Me), 3.35 (1H, dd, *J* = 1.2, 9.7 Hz, 4'-H), 3.58 (1H, dd, *J* = 7.35, 9.82 Hz, 4'-H), 4.30 (1H, dtd, *J* = 1.20, 7.65, 7.61, 10.97 Hz, CH). <sup>13</sup>C-NMR (126 MHz, DMSO-*d*<sub>6</sub>): δ 30.1, 32.3, 35.3, 47.6, 53.4, 162.6, 170.1. *m/z* (ESI) = 130 (MH<sup>+</sup>). HRMS–ESI (*m/z*): [MH<sup>+</sup>] calcd for C<sub>7</sub>H<sub>11</sub>N<sub>3</sub>O<sub>2</sub>, 170.0924; found, 170.0926. IR (ATR) ν 3486, 2926, 2798, 1685, 1496, 1436, 1410, 1384, 1360, 1292, 1253, 1219, 1173, 1146, 1085, 1063, 1037, 1020, 974, 926, 891, 838, 790, 737, 675 cm<sup>-1</sup>.

### 5-Benzyl-1-methyltetrahydro-1H-imidazo[1,5-b]pyrazole-2,6-dione (14b).

Prepared from **5c** (340 mg, 1.55 mmol) and CDI (265 mg, 1.55 mmol). Yield: 201 mg (53%) of yellow oil. <sup>1</sup>H-NMR (500 MHz, DMSO-*d*<sub>6</sub>): δ 2.44 (1H, dd, *J* = 16.2, 7.7 Hz, 3-Ha), 2.59 (1H, ddd, *J* = 16.3, 11.2, 1.1 Hz, 3-Hb), 3.16 (1H, dd, *J* = 9.8, 1.1 Hz, 4-Ha), 3.34 (3H, s, 1-Me), 3.50 (1H, dd, *J* = 9.7, 7.3 Hz, 4-Hb), 4.25 (1H, dtd, *J* = 11.3, 7.5, 1.1 Hz, 3'-H), 4.34 (1H, d, *J* = 14.8 Hz, 1H of CH<sub>2</sub>Ph), 4.46 (1H, d, *J* = 14.9 Hz, 1H of CH<sub>2</sub>Ph), 7.18–7.26 (2H, m, 2H of Ph), 7.27–7.43 (3H, m, 3H of Ph). <sup>13</sup>C-NMR (126 MHz, DMSO-*d*<sub>6</sub>): δ 32.7, 36.0, 45.4, 47.6, 54.0, 128.1, 128.1, 129.0, 135.2, 162.8, 169.6. *m/z* (ESI) = 246 (MH<sup>+</sup>). HRMS–ESI (*m/z*): [MH<sup>+</sup>] calcd for C<sub>13</sub>H<sub>16</sub>N<sub>3</sub>O<sub>2</sub>, 246.1237; found, 246.1237.

### 3. 7. General Procedure for the Synthesis of 5-oxopyrazolidine-3-carboxamides 19a–d

Under argon, CDI (0.892 g, 5.5 mmol) was added to a stirred suspension of carboxylic acid **17** (1.031 g, 5 mmol) in anh. acetonitrile (20 mL), the mixture was stirred at r.t. for 1.5 h, followed by addition of amine **18** (5 mmol). When amine **18** hydrochloride was used, one equivalent of *N*-methylmorpholine (NMM, 600 μL, 5 mmol) was added as well. The mixture was stirred at r.t. for 12 h and volatile components were evaporated *in vacuo*. The residue was taken up in dichloromethane (30 mL) and the solution was washed with 1 M aq. NaHSO<sub>4</sub> (2 × 20 mL), saturated aq. NaHCO<sub>3</sub> (2 × 20 mL), and brine (2 × 20 mL). The organic phase was dried over anh. Na<sub>2</sub>SO<sub>4</sub>, filtered, and the filtrate was evaporated *in vacuo*. Volatile components were evaporated *in vacuo* and the residue was purified by CC (EtOAc). Fractions containing the product were combined and evaporated *in vacuo* to give **19a–d**.

### 3. 7. 1. Methyl *rac*-(5-oxo-1-phenylpyrazolidine-3-carbonyl)glycinate (19a)

Prepared from **17** (1.031 g, 5 mmol), CDI (0.892 g, 5.5 mmol), methyl glycinate hydrochloride (**18a**) (628 mg, 5 mmol), and NMM (600  $\mu$ L, 5 mmol). Yield: 653 mg (45%) of red crystals; m.p. 148–152 °C.  $^1\text{H-NMR}$  (500 MHz, DMSO- $d_6$ ):  $\delta$  2.79 (1H, dd,  $J = 1.3, 16.6$  Hz, 4'-Ha), 3.06 (1H, dd,  $J = 9.3, 16.6$  Hz, 4'-Hb), 3.60 (3H, s, OMe), 3.85–3.97 (2H, m,  $\text{CH}_2\text{CO}_2\text{Me}$ ), 4.16–4.22 (1H, m, 5'-H), 6.86 (1H, d,  $J = 6.8$  Hz, 1'-H), 7.12 (1H, t,  $J = 7.4$  Hz, 1H of Ph), 7.37 (2H, dd,  $J = 7.3, 8.6$  Hz, 2H of Ph), 7.86 (2H, td,  $J = 1.2, 7.5$  Hz, 2H of Ph), 8.57 (1H, t,  $J = 6.1$  Hz,  $\text{NHCH}_2$ ).  $^{13}\text{C-NMR}$  (126 MHz, DMSO- $d_6$ ):  $\delta$  36.8, 40.7, 51.7, 54.6, 118.1, 123.7, 128.4, 138.8, 169.8, 170.0, 171.2.  $m/z$  (ESI) = 278 (MH $^+$ ). HRMS–ESI ( $m/z$ ): [MH $^+$ ] calcd for  $\text{C}_{13}\text{H}_{15}\text{N}_3\text{O}_4$ , 278.1135; found, 278.1138. Anal. Calcd for  $\text{C}_{13}\text{H}_{15}\text{N}_3\text{O}_4$ : C 56.31, H 5.45, N 15.15. Found: C 56.05, H 5.53, N 14.87. IR (ATR)  $\nu$  3359, 3219, 3005, 2959, 2930, 1754, 1695, 1655, 1593, 1525, 1489, 1461, 1440, 1403, 1358, 1338, 1312, 1281, 1242, 1205, 1160, 1127, 1096, 1075, 1031, 1013, 983, 968, 956, 932, 909, 828, 764, 718, 692, 659, 617  $\text{cm}^{-1}$ .

### 3. 7. 2. Methyl *rac*-3-(5-oxo-1-phenylpyrazolidine-3-carboxamido)propanoate (19b)

Prepared from **17** (208 mg, 1 mmol), CDI (178 mg, 1.1 mmol), methyl  $\beta$ -alaninate hydrochloride (**18b**) (140 mg, 1 mmol), and NMM (120  $\mu$ L, 1 mmol). Yield: 131 mg (45%) of pale yellowish crystals; m.p. 88–91 °C.  $^1\text{H-NMR}$  (500 MHz, DMSO- $d_6$ ):  $\delta$  2.41–2.54 (2H, m,  $\text{CH}_2\text{NH}$ ), 3.07 (1H, dd,  $J = 17.2, 9.3$  Hz, 4'-Ha), 3.13 (1H, dd,  $J = 17.2, 3.5$  Hz, 4'-Hb), 3.47 (1H, ddt,  $J = 13.6, 7.3, 5.1$  Hz,  $\text{CH}_2\text{CO}_2\text{Me}$ ), 3.50–3.60 (4H, m, OMe and 1H of  $\text{CH}_2\text{CO}_2\text{Me}$ ), 4.09 (1H, ddd,  $J = 9.7, 6.6, 3.4$  Hz, 5'-H), 5.43 (1H, d,  $J = 6.6$  Hz, 1'-H), 7.14 (1H, t,  $J = 7.4$  Hz, 1H of Ph), 7.37 (2H, dd,  $J = 8.7, 7.3$  Hz, 2H of Ph), 7.78 (1H, s,  $\text{NHCO}$ ), 7.82 (2H, d,  $J = 7.6$  Hz, 2H of Ph).  $^{13}\text{C-NMR}$  (126 MHz, DMSO- $d_6$ ):  $\delta$  33.7, 34.8, 37.2, 51.8, 55.31, 118.0, 124.7, 128.9, 138.2, 169.5, 170.0, 172.6.  $m/z$  (ESI) = 292 (MH $^+$ ). HRMS–ESI ( $m/z$ ): [MH $^+$ ] calcd for  $\text{C}_{14}\text{H}_{17}\text{N}_3\text{O}_4$ , 292.1292; found, 292.1295. Anal. Calcd for  $\text{C}_{14}\text{H}_{17}\text{N}_3\text{O}_4$ : C, 57.72; H, 5.88; N, 14.42. Found: C, 57.89; H, 5.61; N, 14.20. IR (ATR)  $\nu$  3371, 3284, 3073, 3026, 2954, 2932, 2883, 2848, 1722, 1695, 1593, 1525, 1496, 1455, 1434, 1398, 1361, 1337, 1323, 1309, 1272, 1231, 1198, 1178, 1160, 1121, 1078, 1054, 1028, 1009, 967, 925, 894, 875, 817, 753, 713, 690, 667, 615  $\text{cm}^{-1}$ .

### 3. 7. 3. 5-Oxo-*N*-phenethyl-1-phenylpyrazolidine-3-carboxamide (19c)

Prepared from **17** (208 mg, 1 mmol), CDI (178 mg, 1.1 mmol), and 3-phenylethylamine (**18c**) (126  $\mu$ L, 1 mmol). Yield: 154 mg (50%) of white crystals; m.p. 131–133 °C.  $^1\text{H-NMR}$  (500 MHz, DMSO- $d_6$ ):  $\delta$  2.73 (2H, td,  $J = 4.5, 6.7, 6.9$  Hz,  $\text{NHCH}_2$ ), 3.02 (1H, dd,  $J = 9.6, 17.7$  Hz, 4'-Ha), 3.09 (1H, dd,  $J = 3.3, 17.3$  Hz, 4'-Hb), 3.45 (1H, qd,  $J = 6.4, 13.1$  Hz, 1H of  $\text{CH}_2\text{Ph}$ ), 3.58 (1H, qd,  $J = 6.5, 13.1$  Hz, 1H of  $\text{CH}_2\text{Ph}$ ),

4.02 (1H, ddd,  $J = 3.3, 6.6, 9.8$  Hz, 5'-H), 5.31 (1H, d,  $J = 6.7$  Hz, 1'-H), 7.01–7.08 (1H, m, 1H of Ph), 7.11–7.24 (5H, m, Ph), 7.30–7.38 (2H, m, 2H of Ph), 7.67 (2H, d,  $J = 7.8$  Hz, 2H of Ph).  $^{13}\text{C-NMR}$  (126 MHz, DMSO- $d_6$ ):  $\delta$  35.4, 37.3, 40.4, 55.2, 117.8, 124.7, 126.6, 128.6, 128.7, 129.0, 138.2, 138.3, 169.4, 169.9.  $m/z$  (ESI) = 310 (MH $^+$ ). HRMS–ESI ( $m/z$ ): [MH $^+$ ] calcd for  $\text{C}_{18}\text{H}_{20}\text{N}_3\text{O}_2$ , 310.1550; found, 310.1555. Anal. Calcd for  $\text{C}_{18}\text{H}_{20}\text{N}_3\text{O}_2$ : C, 69.88; H, 6.19; N, 13.58. Found: C, 69.78; H, 6.13; N, 13.53. IR (ATR)  $\nu$  3314, 3193, 3079, 3061, 3024, 2936, 2863, 1944, 1872, 1805, 1686, 1651, 1593, 1539, 1492, 1479, 1454, 1434, 1361, 1323, 1311, 1298, 1287, 1252, 1217, 1189, 1153, 1120, 1087, 1065, 1031, 1004, 982, 952, 932, 902, 868, 833, 747, 716, 688, 657, 614  $\text{cm}^{-1}$ .

### 3. 7. 4. *N,N*-Diethyl-5-oxo-1-phenylpyrazolidine-3-carboxamide (19d)

Prepared from **17** (208 mg, 1 mmol), CDI (178 mg, 1.1 mmol), and diethylamine (**18d**) (104  $\mu$ L, 1 mmol). Yield: 128 mg (49%) of pale greyish crystals; m.p. 77–79 °C.  $^1\text{H-NMR}$  (500 MHz, DMSO- $d_6$ ):  $\delta$  1.05 (3H, t,  $J = 7.1$  Hz, Me), 1.18 (3H, t,  $J = 7.0$  Hz, Me), 2.85 (2H, d,  $J = 15.7$  Hz, 4'- $\text{CH}_2$ ), 3.32 (2H, m,  $\text{CH}_2\text{Me}$ ), 3.42 (2H, m,  $\text{CH}_2\text{Me}$ ), 4.55 (1H, m, 5'-H), 6.39 (1H, d,  $J = 9.37$  Hz, 1'-H), 7.07 (1H, t,  $J = 7.4$  Hz, 1H of Ph), 7.33 (2H, t,  $J = 7.85$  Hz, 2H of Ph), 7.77 (2H, d,  $J = 8.10$  Hz, 2H of Ph).  $^{13}\text{C-NMR}$  (126 MHz, DMSO- $d_6$ ):  $\delta$  12.7, 14.4, 37.4, 39.6, 40.9, 53.2, 117.7, 123.4, 128.4, 139.1, 168.2, 170.5.  $m/z$  (ESI) = 262 (MH $^+$ ). HRMS–ESI ( $m/z$ ): [MH $^+$ ] calcd for  $\text{C}_{14}\text{H}_{20}\text{N}_3\text{O}_2$ , 262.1550; found, 262.1551. Anal. Calcd for  $\text{C}_{14}\text{H}_{20}\text{N}_3\text{O}_2$ : C, 64.35; H, 7.33; N, 16.08. Found: C, 64.44; H, 7.20; N, 15.93. IR (ATR)  $\nu$  3212, 3063, 2979, 2932, 2901, 2873, 2159, 1699, 1631, 1593, 1496, 1481, 1471, 1424, 1369, 1320, 1272, 1233, 1218, 1154, 1140, 1102, 1072, 1042, 1029, 997, 965, 938, 906, 878, 843, 815, 760, 720, 692, 671, 660  $\text{cm}^{-1}$ .

## 3. 8. General Procedure for the Synthesis of Non-racemic Carboxamides 19e,f and 19'e,f

Mixtures of diastereomeric carboxamides **19e/19'e** and **19f/19'f** were prepared from racemic carboxylic acid **17** and (*S*)-amino esters **18e** and **18f**, respectively, following the general procedure for the preparation of racemic carboxamides **19a–d**. Mixtures of diastereomers **19e/19'e** and **19f/19'f** were separated by MPLC (EtOAc–hexane). Fraction containing the products were combined and evaporated *in vacuo* to give the non-racemic diastereomerically pure carboxamides **19e**, **19'e**, **19f**, and **19'f**.

### 3. 8. 1. Methyl (5*R*,2'*S*)-(3-oxo-2-phenylpyrazolidine-5-carbonyl)alaninate (19e) and its (5*S*,2'*S*)-isomer 19'e

Prepared from **17** (0.208 g, 1 mmol), CDI (0.178 g, 1.1 mmol), methyl (*S*)-alaninate hydrochloride (**18e**) (140

mg, 1 mmol), and NMM (120  $\mu$ L, 1 mmol); MPLC (EtOAc–hexane, 1:1).

**Data for the (–)-isomer 19e.** Yield: 67 mg (23%) of yellow oil;  $[\alpha]_D^{22}$  –64.5 (*c* 0.365, CH<sub>2</sub>Cl<sub>2</sub>), MPLC:  $R_t$  = 67 min. <sup>1</sup>H NMR (500 MHz, CDCl<sub>3</sub>):  $\delta$  1.33 (3H, d, *J* = 7.2 Hz, Me), 3.13 (2H, d, *J* = 6.4 Hz, 4'-CH<sub>2</sub>), 3.75 (3H, s, CO<sub>2</sub>Me), 4.16 (1H, q, *J* = 6.6 Hz, 2-H), 4.54 (1H, m, 5'-H), 5.48 (1H, d, *J* = 6.7 Hz, 3-H), 7.16 (1H, t, *J* = 7.4 Hz, 1H of Ph), 7.38 (2H, dd, *J* = 7.4, 8.7 Hz, 2H of Ph), 7.73 (1H, s, 1'-H), 7.83 (2H, dd, *J* = 1.2, 8.8 Hz, 2H of Ph). <sup>13</sup>C NMR (126 MHz, CDCl<sub>3</sub>):  $\delta$  18.25, 37.22, 48.06, 52.63, 55.29, 117.97, 124.84, 129.04, 138.23, 169.39, 169.80, 173.12. *m/z* (ESI) = 292 (MH<sup>+</sup>). HRMS–ESI (*m/z*): [MH<sup>+</sup>] calcd for C<sub>14</sub>H<sub>17</sub>N<sub>3</sub>O<sub>4</sub>, 292.1292; found, 292.1292. IR (ATR)  $\nu$  3469, 3367, 3227, 3068, 2992, 2952, 2848, 1739, 1664, 1595, 1518, 1495, 1454, 1352, 1323, 1310, 1210, 1154, 1112, 1056, 1030, 979, 932, 894, 847, 827, 754, 691, 670, 629 cm<sup>-1</sup>.

**Data for the (+)-isomer 19e.** Yield: 60 mg (21%) of yellow oil;  $[\alpha]_D^{22}$  +82.2 (*c* 0.39, CH<sub>2</sub>Cl<sub>2</sub>), MPLC:  $R_t$  = 78 min. <sup>1</sup>H NMR (500 MHz, CDCl<sub>3</sub>):  $\delta$  1.43 (3H, d, *J* = 7.1 Hz, Me), 3.09 (1H, dd, *J* = 9.3, 17.2 Hz, 4'-Ha), 3.16 (1H, dd, *J* = 3.5, 17.2 Hz, 4'-Hb), 3.62 (3H, s, CO<sub>2</sub>Me), 4.14 (1H, ddd, *J* = 3.5, 6.6, 9.7 Hz, 2-H), 4.54 (1H, m, 5'-H), 5.44 (1H, d, *J* = 6.7 Hz, 3-H), 7.16 (1H, t, *J* = 7.4 Hz, 1H of Ph), 7.38 (2H, dd, *J* = 7.4, 8.7 Hz, 1H of Ph), 7.81–7.90 (3H, m, 1'-H and 2H of Ph). <sup>13</sup>C NMR (126 MHz, CDCl<sub>3</sub>):  $\delta$  18.4, 37.0, 48.2, 52.5, 55.4, 118.42, 124.9, 129.0, 138.2, 169.3, 169.6, 172.6. *m/z* (ESI) = 292 (MH<sup>+</sup>). HRMS–ESI (*m/z*): [MH<sup>+</sup>] calcd for C<sub>14</sub>H<sub>17</sub>N<sub>3</sub>O<sub>4</sub>, 292.1292; found, 292.1293. IR (ATR)  $\nu$  3486, 3369, 3226, 3066, 2992, 2952, 2848, 1739, 1665, 1595, 1518, 1495, 1453, 1353, 1325, 1310, 1211, 1154, 1110, 1061, 1030, 1019, 980, 933, 899, 846, 827, 754, 691, 670, 617 cm<sup>-1</sup>.

### 3. 8. 2. Methyl (5*R*,2'*S*)-(3-oxo-2-phenylpyrazolidine-5-carbonyl)prolinate (19f) and its (5*S*,2'*S*)-isomer 19f

Prepared from 17 (0.208 g, 1 mmol), CDI (0.178 g, 1.1 mmol), methyl (S)-prolinate hydrochloride (18f) (166 mg, 1 mmol), and NMM (120  $\mu$ L, 1 mmol); MPLC (EtOAc–hexane, 2:1).

**Data for the (–)-isomer 19f.** Yield: 40 mg (13%) of yellow oil;  $[\alpha]_D^{22}$  –98.1 (*c* 0.425, CH<sub>2</sub>Cl<sub>2</sub>), MPLC:  $R_t$  = 67 min. <sup>1</sup>H NMR (500 MHz, CDCl<sub>3</sub>):  $\delta$  2.03–2.10 (2H, m, 4'-CH<sub>2</sub>), 2.09–2.18 (1H, m, 3-CH<sub>2</sub>), 2.23–2.31 (1H, m, 3-CH<sub>2</sub>), 2.95 (1H, dd, *J* = 8.2, 16.5 Hz, 4'-CH<sub>2</sub>), 3.07 (1H, dd, *J* = 11.3, 16.5 Hz, 4'-CH<sub>2</sub>), 3.54–3.63 (1H, m, 5-CH<sub>2</sub>), 3.65–3.71 (1H, m, 5-CH<sub>2</sub>), 3.76 (3H, s, CO<sub>2</sub>Me), 4.51 (1H, dt, *J* = 8.2, 11.0 Hz, 5-H), 4.60 (1H, dd, *J* = 3.9, 8.8 Hz, 2'-H), 5.67 (1H, d, *J* = 10.8 Hz, NH), 7.13 (1H, t, *J* = 7.4 Hz, 1H of Ph), 7.36 (2H, dd, *J* = 7.3, 8.7 Hz, 2H of Ph), 7.84 (2H, d, *J* = 7.3 Hz, 2H of Ph). <sup>13</sup>C NMR (126 MHz, CDCl<sub>3</sub>):  $\delta$  24.7, 28.8, 37.5, 46.4, 52.5, 54.9, 59.0, 118.4, 124.5, 128.7, 138.4, 168.4, 168.6, 172.0. *m/z* (ESI) = 318 (MH<sup>+</sup>). HRMS–ESI (*m/z*): [MH<sup>+</sup>] calcd for C<sub>16</sub>H<sub>19</sub>N<sub>3</sub>O<sub>4</sub>, 318.1448; found, 318.1447. IR (ATR)  $\nu$  3496, 3210, 3066, 2953, 2881, 2248,

1740, 1695, 1645, 1595, 1496, 1456, 1434, 1418, 1357, 1323, 1311, 1280, 1196, 1173, 1094, 1030, 998, 984, 963, 910, 861, 834, 790, 755, 728, 691, 670, 647, 616 cm<sup>-1</sup>.

**Data for the (+)-isomer 19f.** Yield: 43 mg (14%) of yellow oil;  $[\alpha]_D^{22}$  +2.5 (*c* 0.43, CH<sub>2</sub>Cl<sub>2</sub>), MPLC:  $R_t$  = 84 min. <sup>1</sup>H NMR (500 MHz, CDCl<sub>3</sub>):  $\delta$  2.02–2.13 (2H, m, 4-CH<sub>2</sub>), 2.11–2.20 (1H, m, 3-CH<sub>2</sub>), 2.23–2.29 (1H, m, 3-CH<sub>2</sub>), 2.89 (1H, dd, *J* = 8.1, 16.1 Hz, 4'-CH<sub>2</sub>), 3.02 (1H, dd, *J* = 11.3, 16.2 Hz, 4'-CH<sub>2</sub>), 3.47 (1H, td, *J* = 7.1, 9.6, 5-CH<sub>2</sub>), 3.76 (3H, s, CO<sub>2</sub>Me), 3.85 (1H, ddd, *J* = 4.3, 8.0, 10.0 Hz, 5-CH<sub>2</sub>), 4.51–4.54 (1H, m, 5-H), 4.55–4.58 (1H, m, 2'-H), 5.59 (1H, d, *J* = 10.7 Hz, NH), 7.13 (1H, t, *J* = 7.4 Hz, 1H of Ph), 7.36 (2H, dd, *J* = 7.3, 8.7 Hz, 2H of Ph), 7.86 (2H, d, *J* = 7.6 Hz, 2H of Ph). <sup>13</sup>C NMR (126 MHz, CDCl<sub>3</sub>):  $\delta$  24.6, 29.0, 37.6, 46.6, 52.5, 55.1, 59.2, 118.4, 124.5, 128.7, 138.4, 168.3, 168.6, 172.0. *m/z* (ESI) = 318 (MH<sup>+</sup>). HRMS–ESI (*m/z*): [MH<sup>+</sup>] calcd for C<sub>16</sub>H<sub>19</sub>N<sub>3</sub>O<sub>4</sub>, 318.1448; found, 318.1447. IR (ATR)  $\nu$  3468, 3212, 3064, 2953, 2882, 2251, 1739, 1695, 1643, 1595, 1495, 1455, 1434, 1419, 1356, 1323, 1311, 1282, 1196, 1172, 1094, 1031, 996, 981, 911, 856, 836, 792, 755, 729, 691, 670, 646, 615 cm<sup>-1</sup>.

## 4. Conclusions

1,2-Unsubstituted 5-aminomethyl-3-pyrazolidinones are available in four steps from *N*-protected glycines and their *N*-alkylated analogues. Although the alternative one-step 'ring switching' synthesis of 5-aminomethyl-3-pyrazolidinones is definitely simpler and shorter, the high price or difficult availability of the starting *N*-protected pyrrolin-2(5*H*)-one, as well as lower yield and purity of the so obtained product are disadvantageous. Regioselective reductive alkylation 1,2-unsubstituted pyrazolidinones with dimethoxyacetaldehyde provided the 1-(2,2-dimethoxyethyl) substituted 3-pyrazolidinones, which, unfortunately could not be cyclized into the desired hexahydropyrazolo[1,5-*a*]pyrazin-2(1*H*)-ones. On the other hand, a three step selective methylation provided selectively the 2-methyl regioisomers as key-intermediates in the preparation of two novel 1,5-dialkyltetrahydro-1*H*-imidazo[1,5-*b*]pyrazole-2,6 -diones, as rare representatives of almost unexplored 3D-rich heterocyclic system. The number of synthetic steps in the above preparations may seem disadvantageous, nevertheless, this is compensated by performing up to five subsequent steps via a one-pot procedure. Amidation of easily available 3-oxopyrazolidine-5-carboxylic acid yielded the corresponding carboxamides in moderate yields. Diastereomeric non-racemic carboxamides obtained from (S)-AlaOMe and (S)-ProOMe are separable by MPLC.

## 5. Acknowledgement

The authors acknowledge the financial support from the Slovenian Research Agency (research core funding No.

P1-0179). The financial support from the Boehringer-Ingelheim Pharma, Biberach, Germany is gratefully acknowledged.

## 6. References

1. J. A. Joule, K. Mills, In: *Heterocyclic Chemistry*, 5<sup>th</sup> ed., Wiley-Blackwell, West Sussex, UK, **2010**.
2. G. L. Patrick, In: *An Introduction to Medicinal Chemistry*, 4<sup>th</sup> ed., Oxford University Press: Oxford, UK, **2009**.
3. G. Varvounis, Y. Fiamegos, G. Pilidis, *Adv. Heterocycl. Chem.* **2001**, *80*, 73–156.
4. J. Elguero, In: A. R. Katritzky, C. W. Rees, E. F. V. Scriven, (Eds.), *Pyrazoles*, Comprehensive Heterocyclic Chemistry II, Elsevier, Oxford, **1996**, Vol. 3, pp. 1–75.
5. R. M. Claramunt, J. Elguero, *Org. Proc. Prep. Int.* **1991**, *23*, 273–320.
6. H. Dorn, *Chem. Heterocycl. Compd. USSR* **1981**, 3–31.
7. C. Cucurou, J. P. Battioni, D. C. Thang, N. H. Nam, D. Mansuy, *Biochemistry* **1991**, *30*, 8964–8970.
8. H. L. White, J. L. Howard, B. R. Cooper, F. E. Soroko, J. D. McDermed, K. J. Ingold, R. A. Maxwell, *J. Neurochem.* **1982**, *39*, 271–273.
9. S. Hanessian, L. Auzzas, *Acc. Chem. Res.* **2008**, *41*, 1241–1251.
10. J. Cluzeau, W. D. Lubell, *Biopolymers* **2005**, *80*, 98–150.
11. E. M. Kosower, E. Hershkowitz, IL patent 1990–94658 94658. 1994 19900607.
12. R. J. Ternansky, S. E. Draheim, A. J. Pike, F. T. Counter, J. A. Eudaly, J. S. Kasher, *J. Med. Chem.* **1993**, *36*, 3224–3229.
13. E. M. Kosower, A. E. Radkowsky, A. H. Fairlamb, S. L. Croft, R. A. Neal, *Eur. J. Med. Chem.* **1995**, *30*, 659–671.
14. S.-G. Wang, H. R. Tsai, K. Chen, *Tetrahedron Lett.* **2004**, *45*, 6183–6185.
15. C. L. Fan, W.-D. Lee, N.-W. Teng, Y.-C. Sun, K. Chen, *J. Org. Chem.* **2003**, *68*, 9816–9818.
16. C. H. Lin, K. S. Yang, J. F. Pan, K. Chen, *Tetrahedron Lett.* **2000**, *41*, 6815–6819.
17. K.-S. Yang, K. Chen, *J. Org. Chem.* **2001**, *66*, 1676–1679.
18. K.-S. Yang, J.-C. Lain, C.-H. Lin, K. Chen, *Tetrahedron Lett.* **2000**, *41*, 1453–1456.
19. K.-S. Yang, K. Chen, *Org. Lett.* **2000**, *2*, 729–731.
20. M. P. Sibi, L. M. Stanley, X. Nie, L. Venkatraman, M. Liu, C. P. Jasperse, *J. Am. Chem. Soc.* **2007**, *129*, 395–405.
21. M. P. Sibi, S. Manyem, H. Palencia, *J. Am. Chem. Soc.* **2006**, *128*, 13660–13661.
22. M. P. Sibi, L. Venkatraman, M. Liu, C. P. Jasperse, *J. Am. Chem. Soc.* **2001**, *123*, 8444–8445.
23. M. Lemay, L. Aumand, W. W. Ogilvie, *Adv. Synth. Catal.* **2007**, *349*, 441–447.
24. M. Lemay, J. Trant, W. W. Ogilvie, *Tetrahedron* **2007**, *63*, 11644–11655.
25. M. Lemay, W. W. Ogilvie, *J. Org. Chem.* **2006**, *71*, 4663–4666.
26. M. Lemay, W. W. Ogilvie, *Org. Lett.* **2005**, *7*, 4141–4144.
27. E. Gould, T. Lebl, A. M. Z. Slawin, M. Reid, A. D. Smith, *Tetrahedron* **2010**, *66*, 8992–9008.
28. J. B. Brazier, J. L. Cavill, R. L. Elliott, G. Evans, T. J. K. Gibbs, I. L. Jones, J. A. Platts, N. C. O. Tomkinson, *Tetrahedron* **2009**, *65*, 9961–9966.
29. G. J. S. Evans, K. White, J. A. Platts, N. C. O. Tomkinson, *Org. Biomol. Chem.* **2006**, *4*, 2616–2627.
30. J. L. Cavill, R. L. Elliott, G. Evans, I. L. Jones, J. A. Platts, A. M. Ruda, N. C. O. Tomkinson, *Tetrahedron* **2005**, *62*, 410–421.
31. U. Grošelj, J. Svete, *ARKIVOC* **2015**, Part vi, 175–205.
32. J. Svete, In: (4R\*,5R\*)-4-Benzoylamino-5-phenyl-3-pyrazolidinone – A Useful Building Block in the Synthesis of Functionalized Pyrazoles in Stereochemistry Research Trends, M. A. Horvat, J. H. Golob, Eds.; Nova Science Publishers, Inc., New York. **2008**, p. 129–182.
33. L. Šenica, N. Petek, U. Grošelj, J. Svete, *Acta Chim. Slov.* **2015**, *62*, 60–71.
34. L. Šenica, K. Stopar, M. Friedrich, U. Grošelj, J. Plavec, M. Počkaj, Č. Podlipnik, J. Svete, *J. Org. Chem.* **2016**, *81*, 146–161.
35. U. Grošelj, A. Podlogar, A. Novak, G. Dahmann, A. Golobič, B. Stanovnik, J. Svete, *Synthesis* **2013**, *45*, 639–650.
36. J. Mirnik, U. Grošelj, A. Novak, G. Dahmann, A. Golobič, M. Kasunič, B. Stanovnik, J. Svete, *Synthesis* **2013**, *45*, 3404–3412.
37. K. Lombar, U. Grošelj, G. Dahmann, B. Stanovnik, J. Svete, *Synthesis* **2015**, *47*, 497–506.
38. U. Grošelj, A. Golobič, J. Svete, B. Stanovnik, *Chirality* **2013**, *25*, 541–555.
39. E. Pušavec Kirar, M. Drev, J. Mirnik, U. Grošelj, A. Golobič, G. Dahmann, F. Požgan, B. Štefane, J. Svete, *J. Org. Chem.* **2016**, *81*, 8920–8933.
40. U. Grošelj, M. Žorž, A. Golobič, B. Stanovnik, J. Svete, *Tetrahedron* **2013**, *69*, 11092–11108.
41. Y. Bandala, R. Melgar-Fernández, R. Guzmán-Mejía, J. L. Olivares-Romero, B. R. Díaz-Sánchez, R. González-Olvera, J. Vargas-Caporalí, E. Juaristi, *J. Mex. Chem. Soc.* **2009**, *53*, 147–154.
42. C. R. Theberge, C. K. Zercher, *Tetrahedron* **2003**, *59*, 1521–1527.
43. M. P. C. Mulder, F. El Oualid, J. ter Beek, H. Ovaa, *ChemBio* **2014**, *15*, 946–949.

## Povzetek

Študirali smo sintezne pristope za pripravo novih 3-pirazolidinonskih derivatov funkcionaliziranih na položajih N(1) in/ali C(5). 5-aminoalkil-3-pirazolidinone smo pripravili v štirih korakih iz *N*-zaščitenih glicinov preko *Masamune-Claisenove* homologacije, redukcije, *O*-meziliranja in ciklizacije z derivati hidrazina. Proste amine smo pripravili z odščito v kislem. Ciljno spojino smo pripravili tudi z 'ring switching' transformacijo *N*-Boc-pirolin-2(5*H*)-ona s hidrazin hidratom. S katalitskim hidrogeniranjem smo odščitili 5-(*N*-alkil-*N*-Cbz-aminometil)pirazolidine-3-one in s sledečo ciklizacijo z 1,1'-karbonildiimidazolom (CDI) pripravili dva nova predstavnika perhidroimidazo[1,5-*b*]pirazola, ki je skoraj popolnoma neraziskan heterociklični system. Pri amidiranju 3-oksopirazolidin-5-karbonsilne kisline smo dobili ustrezne karboksamide s srednjimi izkoristki. Diastereomerne neracemne karboksamide, pripravljene iz (*S*)-AlaOMe in (*S*)-ProOMe, smo ločili s pomočjo MPLC kromatografske tehnike.



Scientific paper

# Asymmetric Bio- and Chemoreduction of 2-Benzylidenecyclopentanone Derivatives

Bogdan Štefane, Uroš Grošelj, Jurij Svete and Franc Požgan\*

Faculty of Chemistry and Chemical Technology, University of Ljubljana, Večna pot 113, SI- 1000 Ljubljana, Slovenia

\* Corresponding author: E-mail: franc.pozgan@fkkt.uni-lj.si

Received: 16-05-2017

Dedicated to Professor Emeritus Miha Tišler, University of Ljubljana, on the occasion of his 90<sup>th</sup> birthday.

## Abstract

Highly efficient asymmetric reduction of 2-benzylidenecyclopentanone derivatives to give the respective exocyclic allylic alcohols in *ee*'s up to 96% was performed with chiral oxazaborolidine-based catalysts. Complete enantioselectivity furnishing (S)-configured alcohol product could be achieved by bioreduction of 2-(4-chlorobenzylidene)cyclopentanone with *Daucus carota* root. The synthesized compounds may be used as enantiomerically enriched standards for the monitoring of the enzyme-catalyzed redox processes.

**Keywords:** Enantioselective reduction, cyclopentanone, AKR1C inhibitors, oxazaborolidine, bioreduction

## 1. Introduction

Chiral alcohols are important building blocks and intermediates in the synthesis of pharmaceuticals, fine chemicals, agrochemicals, flavors and fragrances, as well as functional materials.<sup>1</sup> Since ketones represent one of the most common families of unsaturated compounds, their asymmetric reduction represents the simplest and most powerful method for the preparation of enantiomerically enriched alcohols. The stereospecific reduction of carbonyl groups to the corresponding alcohols is also a functionalization reaction involved in the metabolism of endogenous compounds and xenobiotics containing these groups. Thus, it is often catalyzed by enzymes belonging to either dehydrogenase/reductase superfamily or the aldo-keto reductase (AKR) superfamily.<sup>2</sup> The human members of the AKR subfamily 1C are involved in the biosynthesis and inactivation of steroid hormones, and also in the biosynthesis of neurosteroids and prostaglandins.<sup>3</sup> These enzymes reduce carbonyl containing substrates to alcohols and also function *in vivo* as ketosteroid reductases, and thus regulate the activity of androgens, estrogens and progesterone in target tissues, and ligand occupancy and transactivation of their corresponding receptors.<sup>4</sup> Aberrant expression and action of AKR1C enzymes may lead to an imbalance in the metabolism of steroid hormones, and to further development of different patho-

physiological conditions.<sup>5</sup> These enzymes thus represent promising therapeutic targets in the development of new drugs. In the literature, structurally different compounds have been evaluated as AKR1C inhibitors, for example dietary phytoestrogens,<sup>6</sup> benzodiazepines,<sup>7</sup> cinnamic acids,<sup>8</sup> benzofurans, and phenolphthalein derivatives,<sup>9</sup> Ru(II) complexes,<sup>10</sup> salicylic and aminobenzoic acids derivatives, as well as some nonsteroidal anti-inflammatory drugs and their analogues.<sup>11,12</sup> In spite of a plethora of potent inhibitors of steroid metabolizing enzymes that have emerged, the search for new and more selective ones is an important field of investigation. Štefane *et al.*<sup>13</sup> indentified compounds based on cyclopentane scaffold, which are AKR1C1 and AKR1C3 substrates active in the low micromolar range, and thus represent promising starting points in the development of potential agents for treatment of hormone-dependent forms of cancer and other diseases involving these enzymes. AKR1C inhibitors are not only interesting as potential agents for the treatment of diseases, but also as molecular tools in the study of the pathophysiological roles of these enzymes. In the recent study Beranič *et al.* introduced new enzymatic assays employing racemic 2-(4-chlorobenzylidene)cyclopentanol (CBCP-ol) and its ketone counterpart 2-(4-chlorobenzylidene)cyclopentanone that allow monitoring of AKR1C-catalyzed reactions in the reductive and oxidative directions.<sup>14</sup> Since enzymes perform highly stereoselective reactions, it seems

useful to know, which enantiomer of CBCP-ol is involved in the redox process. For this reason we present herein the synthesis of enantiomerically enriched cyclopentyl alcohols (CBCP-ol and its 4-methoxy analogue) via the asymmetric chemo- and bioreduction of substituted 2-benzylidenecyclopentanones, which can serve as standards in monitoring of AKR1C-catalyzed reactions. The reduction of the benzene-fused analogue, indanone-derived chalcone, to the corresponding secondary allylic alcohol is also included.

## 2. Results and Discussion

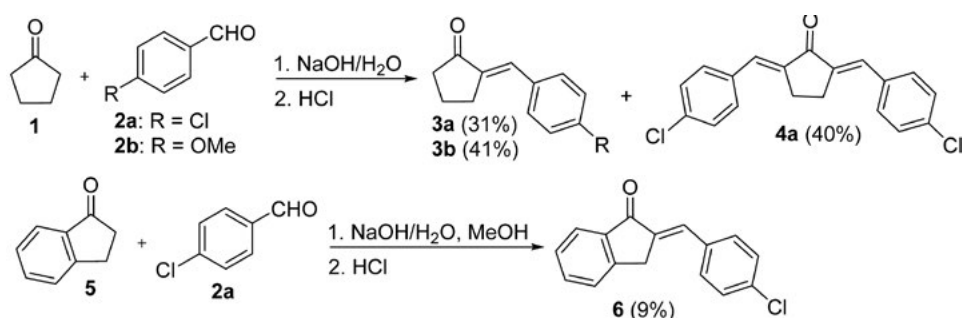
The starting compounds,  $\alpha$ -arylmethylene cyclic ketones **3** and **6** were synthesized in a base-induced aldol condensation from cyclopentanone (**1**) or 1-indanone (**5**) and the corresponding *p*-substituted benzaldehydes **2** following slightly modified literature procedure<sup>15</sup> (Scheme 1). The reaction of cyclopentanone with *p*-methoxybenzaldehyde (**2b**) towards benzylidenecyclopentanone **3b** proceeded smoothly, while using *p*-chlorobenzaldehyde (**2a**), besides the desired product **3a**, symmetrical abis(benzylidene) derivative **4a** was isolated as the by-product. 1-Indanone reacted with *p*-chlorobenzaldehyde leading to the product **6** in a very low 9% isolated yield. We were not,

however, interested in the optimization of these aldol condensation reactions.

With  $\alpha,\beta$ -unsaturated ketones **3** and **6** in hand, we investigated different methods for the selective carbonyl reduction to obtain the highest possible enantiomeric excess of the corresponding allylic alcohol products with exocyclic C=C double bond.

The most elegant method for the asymmetric reduction of prochiral ketones is either homogeneous or heterogeneous hydrogenation or transfer hydrogenation catalyzed by chiral metal catalysts.<sup>16</sup> Highly efficient asymmetric hydrogenation of  $\alpha$ -arylmethylene cyclopentanones was realized by chiral tailor-made iridium–spiroamino-phosphine catalysts;<sup>17</sup> for example, reduction of **3b** gave **7b** with 95% *ee* (enantiomeric excess). Unfortunately, in our case the use of some commercially available chiral rhodium and ruthenium catalysts **C1–C4** (Figure 1) in hydrogenation of cyclopentanone **3a** with molecular hydrogen (80 bars) led to very low yields and *ee* values of the secondary alcohol **7a**; the best *ee* of 12% (31% isolated yield) was obtained with Noyori's bifunctional ruthenium catalyst **C4**.

After report by Itsuno<sup>18</sup> that chiral aminoalcohols together with  $\text{BH}_3$  effected the enantioselective reduction of prochiral ketones, Corey<sup>19</sup> isolated the primarily formed oxazaborolidine derivative, and developed a powerful catalytic version of an original stoichiometric reduction. Con-



Scheme 1. Synthesis of  $\alpha$ -arylmethylene cyclic ketones **3**, **4** and **6**.

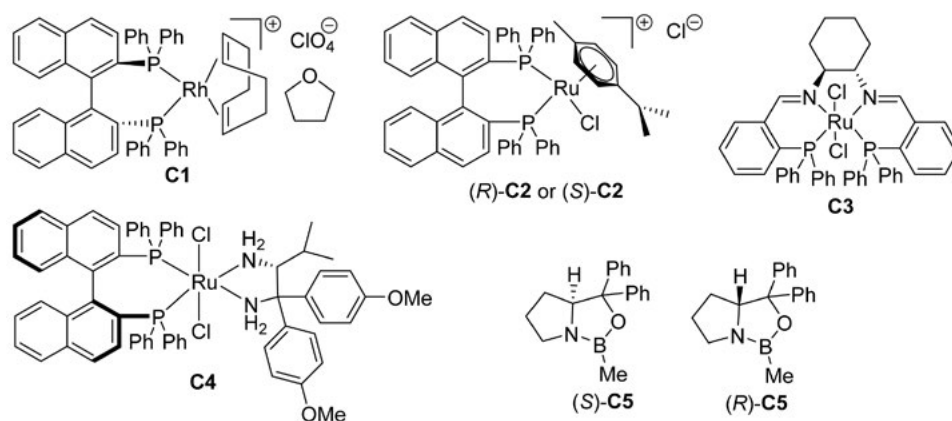


Figure 1. Chiral catalysts employed in the asymmetric reduction of cyclic ketones **3** and **6**.

sequently, enantioselective reduction of prochiral ketones with borane (or its derivatives) catalyzed by chiral oxazaborolidines has emerged as an excellent route to alcohols of high enantiomeric purity.<sup>20</sup> Since this method has many advantages such as predictable absolute configuration and high *ee* of chiral secondary alcohol products, it seemed logical to investigate whether oxazaborolidine-catalysed reduction of ketones **3** and **6** could afford the desired exocyclic allylic alcohols in high enantioselectivity. Indeed, the borane reduction of chlorobenzylidenecyclopentanone **3a** in the presence of 10 mol% of oxazaborolidine catalyst (*S*)-C5 at room temperature afforded the desired alcohol (*R*)-**7a** in 77% *ee* (as judged by chiral HPLC) (Table 1, entry 1). By varying different solvents, reaction temperatures, amount of reductant, and catalyst loading (Table 1, entries 2–8), the highest *ee* of 96% in reduction of **3a** was achieved with 1.88 equiv.  $\text{BH}_3 \times \text{Me}_2\text{S}$ , 20 mol% (*S*)-C5 in toluene at 0 °C. Typically, reduction was carried out by slow addition of a toluene solution of the ketone to an ice-cooled toluene solution of  $\text{BH}_3 \times \text{Me}_2\text{S}$  and catalyst (stirred for 10 min prior to adding the ketone). The same protocol was used in the reduction of the methoxy-substituted analogue **3b** giving (*R*)-**7b** but with significant loss of enantioselectivity (Table 1, entry 9). The opposite enantio-

mers, (*S*)-**7a** and (*S*)-**7b**, were obtained by the borane reduction with the oxazaborolidine catalyst (*R*)-C5 (Table 1, entries 10 and 11). Interestingly, chloro-substituted alcohols (*S*)-**7a** and (*R*)-**7a** were obtained with practically identical *ee* values (~95%), while catalyst (*R*)-C5 reduced methoxy-benzylidenecyclopentanone **3b** with increased enantioselectivity compared to catalyst (*S*)-C5 (90% vs. 82% *ee*). A dramatic drop in chemical yield and optical purity of the indanol alcohol **6** was observed in reduction of the indanone derivative **6** with either (*S*)-C5 or (*R*)-C5 catalyst. In spite of applying different reaction conditions (Table 1, entries 12–17), the corresponding alcohol **8** was not obtained in *ee* higher than 33%. Lower *ee* values associated with asymmetric reduction of indanone **6** as compared to cyclopentanone **3** may suggest that a fused benzene ring has a pronounced influence on the level of asymmetric induction with oxazaborolidine catalysts C5. Additionally, low isolated yield of indanol **8** might be due to its decomposition (or of parent ketone) under applied reaction conditions as was also established for reduction of analogous indanone-derived chalcones.<sup>21</sup>

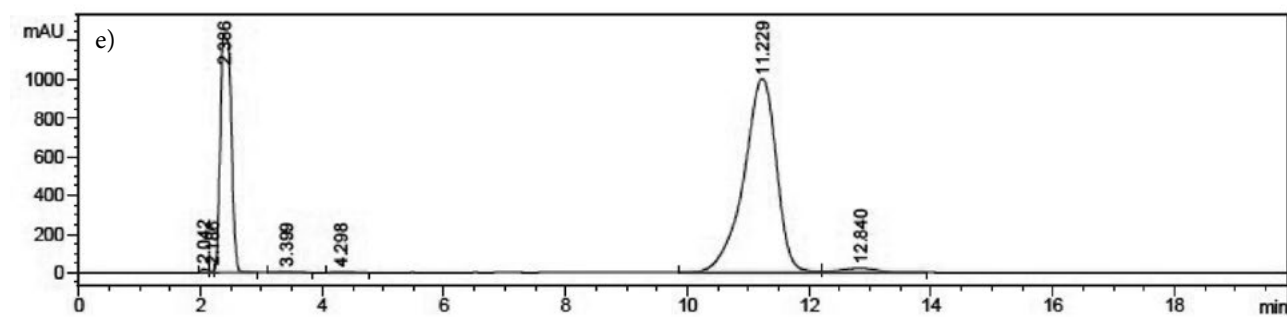
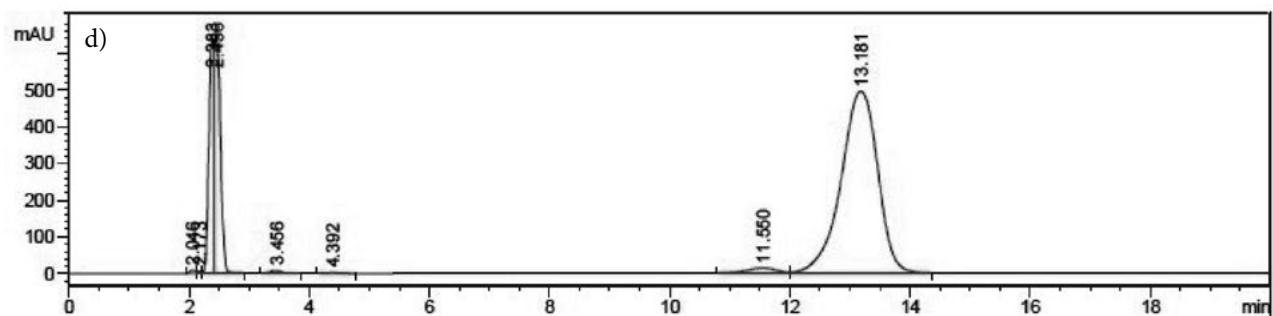
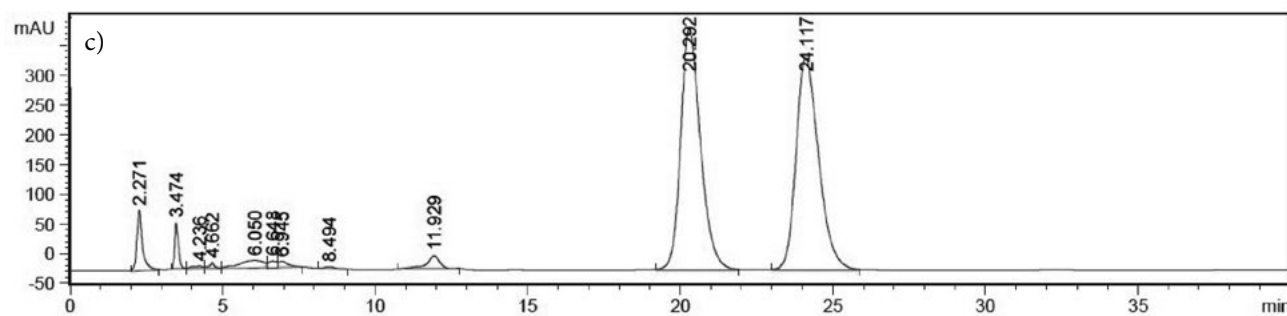
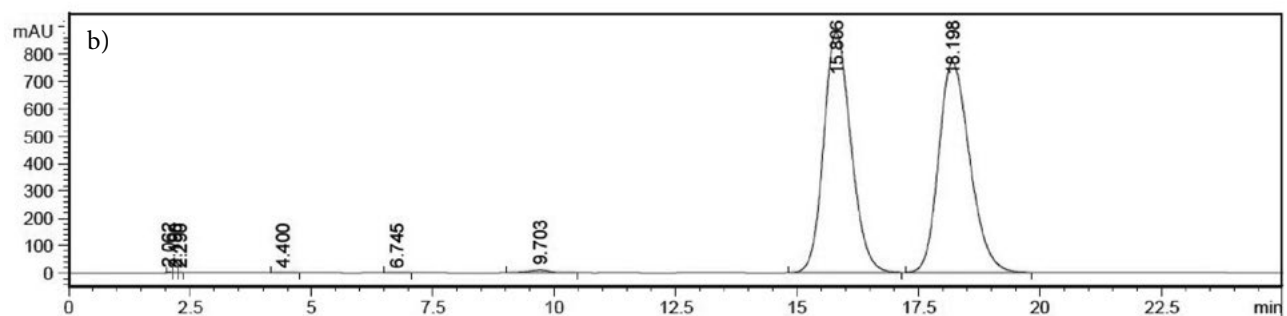
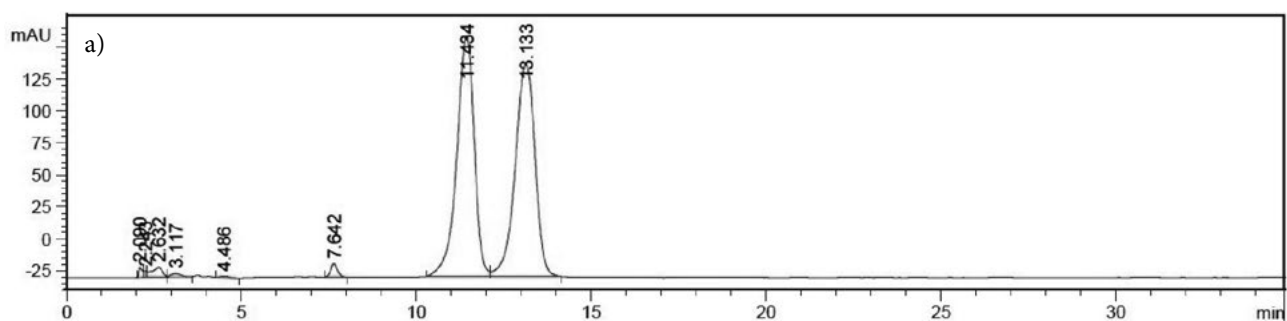
The enantiomeric excess of the allylic alcohols **7** and **8** was determined by chiral stationary phase HPLC. The corresponding racemic alcohols were synthesized by che-

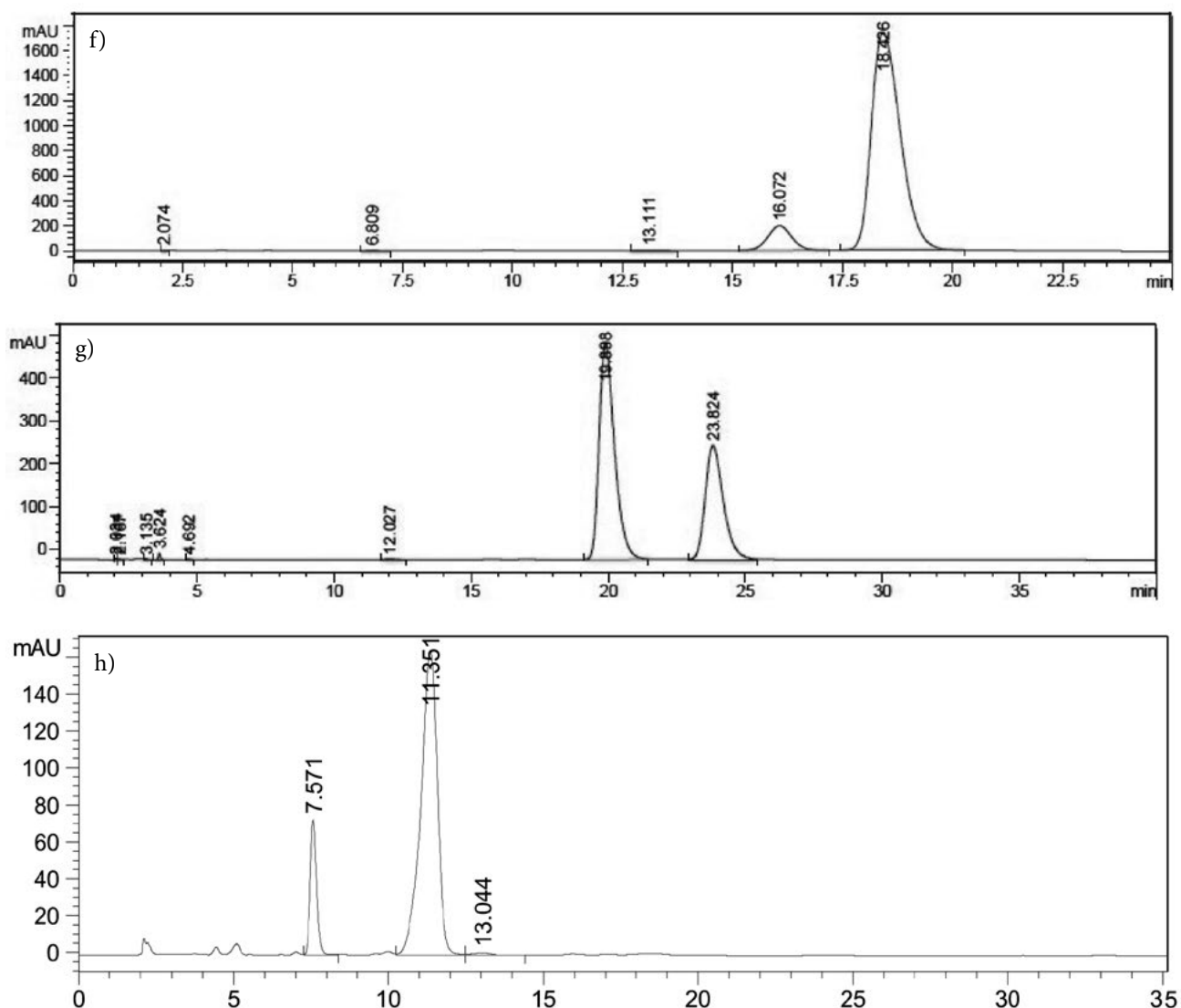
**Table 1:** Asymmetric reduction of cyclic ketones **3a,b** and **6** with oxazaborolidine catalysts C5.



entry	ketone	catalyst (mol%)	solvent	$\text{BH}_3 \times \text{Me}_2\text{S}$ (equiv.)	T (°C)	product	yield <sup>a</sup> (%)	<i>ee</i> <sup>b</sup> (%)
1	<b>3a</b>	( <i>S</i> )-C5, 10	THF	1.10	r. t.	<b>7a</b>	n.d.	77 ( <i>R</i> )
2	<b>3a</b>	( <i>S</i> )-C5, 10	THF	2.74	-20	<b>7a</b>	88	81 ( <i>R</i> )
3	<b>3a</b>	( <i>S</i> )-C5, 10	THF	1.70	-20	<b>7a</b>	67	32 ( <i>R</i> )
4	<b>3a</b>	( <i>S</i> )-C5, 10	THF	3.42	-20	<b>7a</b>	91	75 ( <i>R</i> )
5	<b>3a</b>	( <i>S</i> )-C5, 20	DCM	1.70	-6	<b>7a</b>	84	90 ( <i>R</i> )
6	<b>3a</b>	( <i>S</i> )-C5, 10	THF	2.74	0	<b>7a</b>	82	88 ( <i>R</i> )
7	<b>3a</b>	( <i>S</i> )-C5, 10	THF	1.70	0	<b>7a</b>	80	90 ( <i>R</i> )
8	<b>3a</b>	( <i>S</i> )-C5, 20	toluene	1.88	0	<b>7a</b>	77	96 ( <i>R</i> )
9	<b>3b</b>	( <i>S</i> )-C5, 20	toluene	1.88	0	<b>7b</b>	67	82 ( <i>R</i> )
10	<b>3a</b>	( <i>R</i> )-C5, 20	toluene	1.88	0	<b>7a</b>	70	95 ( <i>S</i> )
11	<b>3b</b>	( <i>R</i> )-C5, 20	toluene	1.88	0	<b>7b</b>	59	90 ( <i>S</i> )
12	<b>6</b>	( <i>R</i> )-C5, 20	toluene	1.88	0	<b>8</b>	15	23
13 <sup>c,d</sup>	<b>6</b>	( <i>R</i> )-C5, 20	toluene/ $\text{CH}_2\text{Cl}_2$	2.10	0	<b>8</b>	21	24
14 <sup>d</sup>	<b>6</b>	( <i>S</i> )-C5, 20	toluene/ $\text{CH}_2\text{Cl}_2$	1.27	0	<b>8</b>	20	33
15	<b>6</b>	( <i>S</i> )-C5, 20	$\text{CH}_2\text{Cl}_2$	1.27	0	<b>8</b>	19	21
16 <sup>e,f</sup>	<b>6</b>	( <i>S</i> )-C5, 20	THF	1.27	-30	–	–	–
17 <sup>e</sup>	<b>6</b>	( <i>S</i> )-C5, 20	$\text{CH}_2\text{Cl}_2$	1.27	-30	<b>8</b>	22	19

<sup>a</sup>Isolated yield is given. <sup>b</sup>Determined by chiral HPLC. <sup>c</sup>First solution of **6** added to a solution of (*R*)-C5, then  $\text{BH}_3 \times \text{Me}_2\text{S}$ . <sup>d</sup>Ketone dissolved in  $\text{CH}_2\text{Cl}_2$ , and catalyst in toluene. <sup>e</sup>Reaction quenched with MeOH. <sup>f</sup>The desired alcohol was not isolated.





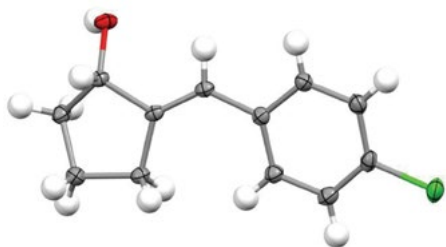
**Figure 2.** Chromatograms of (a) racemic alcohol **7a**, (b) racemic alcohol **7b**, (c) racemic alcohol **8**, (d) enantiomerically enriched (*R*)-**7a** obtained with (*S*)-**C5**, (e) enantiomerically enriched (*S*)-**7a** obtained with (*R*)-**C5**, (f) enantiomerically enriched (*R*)-**7b** obtained with (*S*)-**C5**, (g) alcohol **8** obtained with (*R*)-**C5**, (h) enantiomerically enriched (*R*)-**7a** obtained with *Daucus carota* root reduction.

moselective reduction with  $\text{NaBH}_4$  in the presence of  $\text{CeCl}_3 \times 6\text{H}_2\text{O}$ . They were used to find the optimal HPLC conditions for the separation of the pairs of the enantiomeric alcohols.

Although Corey's (*S*)-proline-derived or stereochemically related oxazaborolidines in general delivered *R*-configured allylic alcohols in reduction of enones,<sup>22</sup> the *R* absolute configuration of chlorobenzylidenecyclopentanol **7a** obtained from reduction with (*S*)-**C5** was unambiguously confirmed by X-ray crystallography (Figure 3). Additionally, this established also the configuration around the exocyclic C=C double bond as *E*. It should be made clear that stereochemical assignment for (*R*)-**7a** has not been previously made, although the absolute stereochemistry of related 2-benzylidenecyclopentanol obtained with Corey (*S*)-oxazaborolidine catalyst was determined to be

*R*.<sup>23</sup> Thus, formation of the alcohol (*R*)-**7a** from chloro-substituted cyclopentanone **3a** in the presence of oxazaborolidine catalyst (*S*)-**C5** is also consistent with the sense of asymmetric induction predicted by the Corey mechanistic model.<sup>24</sup> Consequently, we ascribed the *R* stereochemistry also to the methoxy-substituted alcohol **7b** provided by oxazaborolidine catalyst (*S*)-**C5**, while for alcohols **7a,b** arising from the borane reduction with catalyst (*R*)-**C5** the *S* configuration was concluded. This was further supported by comparison of the sense of optical rotation and HPLC elution sequence of the enantiomeric forms of the alcohols **7a** and **7b** obtained with catalysts (*S*)-**C5** and (*R*)-**C5**, respectively. Examination of the chromatogram (d) depicted in Figure 2 reveals, that for chloro-cyclopentanol **7a** delivered with catalyst (*S*)-**C5**, the (+)-(*R*)-form of the enantiomers separated on chiral column is eluted second.

Methoxy-cyclopentanol **7b** obtained with catalyst (*S*)-**C5** (Figure 2, chromatogram (f)) is also eluted second and returned a specific rotation of  $[\alpha]_D^{25} + 3.8$ , identical in sign to that of (*R*)-**7a**; consequently its configuration was proposed to be *R*. The opposite enantiomers of **7a** and **7b**, ob-



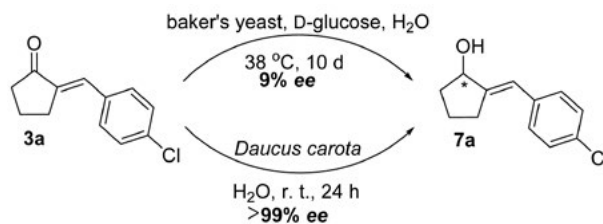
**Figure 3.** X-ray crystal structure of (*R*)-**7a**; thermal ellipsoids are set at 40% probability.

**Table 2** Crystallographic data, structure refinement summary, selected bond lengths, bond angles, and torsion angles for compound (*R*)-**7a**.

Property	Compound ( <i>R</i> )- <b>7a</b>
Empirical formula	C <sub>12</sub> H <sub>13</sub> ClO
Formula weight	208.67
Temperature	150(2)
Crystal system	orthorhombic
Space group	P2 <sub>1</sub> 2 <sub>1</sub> 2 <sub>1</sub>
<i>a</i> (Å)	4.99305(10)
<i>b</i> (Å)	9.3428(2)
<i>c</i> (Å)	22.2446(4)
$\alpha$ (°)	90.00
$\beta$ (°)	90.00
$\gamma$ (°)	90.00
Volume (Å <sup>3</sup> )	1037.69(4)
<i>Z</i>	4
<i>F</i> (000)	440
Crystal size (mm <sup>3</sup> )	0.08 × 0.25 × 0.60
$\mu$ (CuK $\alpha$ ) (/mm)	0.079
<i>N</i> <sub>ref</sub>	6371
<i>R</i>	0.0327
$R_w$	0.0876
<i>S</i>	1.08
<b>Bond length (Å)</b>	
C2(1) – Cl(1)	1.7440(16)
C(8) – C(9)	1.336(2)
O(1) – C(10)	1.4238(19)
<b>Bond angles (°)</b>	
C(5) – C(7) – C(8)	125.0(1)
C(8) – C(9) – C(11)	129.9(2)
C(8) – C(9) – C(10)	122.4(1)
C(9) – C(10) – O(1)	115.2(1)
<b>Torsion angles (°)</b>	
C(5) – C(7) – C(8) – C(9)	10.0(1)
C(7) – C(8) – C(9) – C(11)	–4.5(1)

tained with catalyst (*R*)-**C5**, both eluted on column first and the samples show levorotatory character. The dominant enantiomer of the indanol alcohol **8** obtained with (*R*)-**C5**, though in low excess, also eluted first on chiral column (Figure 2, chromatogram (g)), and the optical rotation of the sample was measured as  $[\alpha]_D^{25} - 13.4$ . On this basis it can be speculated that catalyst (*R*)-**C5** preferentially delivers the (*S*)-indanol **8** in the reduction of indanone **6**, while with catalyst (*S*)-**C5** the (*R*)-alcohol **8** is obtained as the major enantiomer.

Efficient asymmetric reduction of carbonyl compounds can also be achieved by means of bioreduction employing either isolated enzymes or whole cells system as mild and environmentally benign reduction systems. Fogliato *et al.* used baker's yeast<sup>25</sup> for the reduction of arylidene cyclopentanones and cyclohexanones reaching satisfactory enantioselectivity, while the secondary alcohols of excellent optical purity were obtained from *Daucus carota*<sup>26</sup> root reduction of structurally different prochiral ketones (up to 100% *ee*). Similarly, an  $\alpha,\beta$ -unsaturated ketone *trans*-4-phenylbut-3-en-2-one was regio- and stereoselectively reduced using carrot, celeriac, and beetroot enzyme systems to the corresponding (*S*)-allylic alcohol in *ee*'s 72–99%.<sup>27</sup> In our case, the baker's yeast reduction of chlorobenzylidenecyclopentanone **3a** gave very low isolated yield (5%) and optical purity (*ee* = 9%) of the corresponding alcohol **7a** even after incubating the reaction mixture at 38 °C for 10 days. On the contrary, the 24-hour-bioreduction with *Daucus carota* root (substrate/carrot, 1/134 (w/w)) delivered alcohol (*S*)-**7a** with >99% *ee* as determined in the crude product (Figure 2, chromatogram (h)), the amount of which was, however, very low after removal of the biomaterial (Scheme 2). Interestingly, asymmetric induction turned out to be time-dependent, namely *ee* value of (*S*)-**7a** reduced to 92% after incubating reaction mixture for four days at room temperature. It is noteworthy that isolation of the desired alcohol product from bioreduction is intrinsically messy, as the aqueous media contains the cellular mass, usual metabolites, nutrients, and the starting ketone.



**Scheme 2.** Bioreduction of benzylidenecyclopentanone **3a**.

### 3. Experimental

**General.** Toluene was dried with sodium and distilled. All other reagents and solvents were used as received from commercial suppliers. Melting points were deter-

mined on a Kofler micro hot stage. The NMR spectra were recorded at 302 K either on a Bruker Avance DPX 300 or Avance III 500 MHz spectrometer operating at 300 MHz or 500 MHz and 75.5 MHz or 126 MHz for  $^1\text{H}$  and  $^{13}\text{C}$  nuclei. The  $^1\text{H}$  NMR spectra in  $\text{CDCl}_3$  are referenced with respect to TMS as the internal standard. The  $^{13}\text{C}$  NMR spectra are referenced against the central line of the solvent signal ( $\text{CDCl}_3$  triplet at  $\delta = 77.0$  ppm). The coupling constants ( $J$ ) are given in Hz. The multiplicities are indicated as follows: s (singlet), d (doublet), t (triplet), q (quartet), qn (quintet), m (multiplet) and br (broad). IR spectra were obtained on a Bruker FTIR Alpha Platinum ATR spectrophotometer. MS spectra were recorded with an Agilent 6224 Accurate Mass TOF LC/MS instrument. Elemental analyses (C, H, N) were performed with a Perkin-Elmer 2400 Series II CHNS/O Analyzer. TLC was carried out on Fluka silica gel TLC-cards. Column chromatography was performed on 230–400-mesh silica gel. Merck silica gel 60 PF254 containing gypsum was used to prepare chromatotron plates. Radial chromatography was performed with Harrison Research, model 7924T chromatotron. HPLC analyses were performed with Agilent Technology 1260 Infinity HPLC instrument with UV detection. The known compounds were characterized by comparison of their physical or spectroscopic data with those in the literature.

**Synthesis of ketones 3a and 4a:** Cyclopentanone (**1**) (5.0 g, 59.4 mmol) and *p*-chlorobenzaldehyde (**2a**) (4.22 g, 30.02 mmol) were added into a 0.2 M aqueous NaOH solution (210 mL), and stirred at room temperature for 72 h. The reaction was quenched with water (210 mL), and the reaction mixture was acidified with 3.6% aqueous HCl solution (60 mL) to  $\text{pH} \sim 4$ . The product was extracted with  $\text{CH}_2\text{Cl}_2$  ( $3 \times 150$  mL), and combined organic layers were dried over anhydrous  $\text{Na}_2\text{SO}_4$ . The solvent was evaporated in vacuo, and the residue was purified by  $\text{SiO}_2$  column chromatography (petroleum ether : EtOAc = 20 : 1) to give 1.90 g (31%) of **3a** and 4.00 g (40%) of **4a**.

**2-(4-Chlorobenzylidene)cyclopentanone (3a):** mp 74–76 °C (lit.<sup>28</sup> 77–79 °C).

**2,5-Bis(4-chlorobenzylidene)cyclopentanone (4a):** mp 225–227 °C (lit.<sup>29</sup> 224–226 °C).

**Synthesis of 2-(4-methoxybenzylidene)cyclopentanone (3b):** Cyclopentanone (**1**) (1.0 g, 11.89 mmol) and *p*-methoxybenzaldehyde (**2b**) (896 mg, 6.58 mmol) were added into a 0.2 M aqueous NaOH solution (90 mL), and stirred at room temperature for 24 h, to which additional amount of cyclopentanone (298 mg, 3.54 mmol) was added, and stirred for further 12 h. The reaction was quenched with water (90 mL), and the reaction mixture was acidified with 3.6% aqueous HCl solution (20 mL) to  $\text{pH} \sim 4$ . The product was extracted with  $\text{CH}_2\text{Cl}_2$  ( $3 \times 100$  mL), and the combined organic layers were dried over anhydrous  $\text{Na}_2\text{SO}_4$ .

The solvent was evaporated in vacuo, and the residue was purified by  $\text{SiO}_2$  column chromatography (petroleum ether : EtOAc = 10 : 1) to give 843 mg (41%) of yellow crystalline product. Mp 65.4–66.3 °C (lit.<sup>28</sup> 68–69 °C).

**Synthesis of 2-(4-chlorobenzylidene)-2,3-dihydro-1H-inden-1-one (6):** To a solution of 1-indanone (**5**) (4.0 g, 30.27 mmol) and *p*-chlorobenzaldehyde (**2a**) (5.32 g, 37.85 mmol) in MeOH (20 mL), a 0.2 M aqueous NaOH solution (250 mL) was added and the reaction mixture was stirred at room temperature for 48 h. The reaction was quenched with water (200 mL), and the reaction mixture was acidified with 3.6% aqueous HCl solution (60 mL) to  $\text{pH} \sim 1$ . The product was extracted with  $\text{CH}_2\text{Cl}_2$  ( $3 \times 150$  mL) and combined organic layers were dried over anhydrous  $\text{Na}_2\text{SO}_4$ . The solvent was evaporated in vacuo and the residue was purified by  $\text{SiO}_2$  column chromatography (petroleum ether : EtOAc = 50 : 1; 20 : 1; 10 : 1; 5 : 1; 2 : 1) to give 732 mg (9%) of light yellow crystalline product. Mp 180.4–181.0 °C (lit.<sup>30</sup> 179 °C).

**Typical procedure for the synthesis of racemic alcohols – (±)-2-(4-chlorobenzylidene)cyclopentanol (±)-(7a):** 2-(4-Chlorobenzylidene)cyclopentanone (**3a**) (400 mg, 1.94 mmol) and  $\text{CeCl}_3 \times 6\text{H}_2\text{O}$  were dissolved in MeOH (20 mL), and stirred at room temperature for 30 min. Then solid  $\text{NaBH}_4$  (296 mg, 7.83 mmol) was added portion-wise. After 15 min additional amount of  $\text{NaBH}_4$  (140 mg, 3.70 mmol) was added, and stirred for further 1 h. The reaction was quenched with 1 M aqueous HCl solution (10 mL) and water (40 mL). The reaction mixture was stirred for 30 min and then extracted with EtOAc ( $3 \times 50$  mL). The combined organic layers were successively washed with 5% aqueous  $\text{NaHCO}_3$  solution (50 mL), water (30 mL), and brine (30 mL), and dried over anhydrous  $\text{Na}_2\text{SO}_4$ . The solvent was evaporated in a vacuo to give 360 mg (89%) of white crystalline product (±)-(7a), mp 76–77 °C. IR (ATR)  $\nu$  3358, 2964, 1911, 1705, 1620, 1493, 1405, 1325, 1243, 1166, 1143, 1090, 1027, 1009, 980, 940, 887, 823, 730  $\text{cm}^{-1}$ .  $^1\text{H}$  NMR (500 MHz,  $\text{CDCl}_3$ )  $\delta$  1.60 (br s, 1H, OH), 1.61–1.68 and 1.70–1.79 (2  $\times$  m, 2  $\times$  1H,  $\text{CH}_2$ ), 1.93–2.02 (m, 2H,  $\text{CH}_2$ ), 2.51–2.59 and 2.65–2.74 (2  $\times$  m, 2  $\times$  1H,  $\text{CH}_2$ ), 4.59 (m, 1H, OCH), 6.53 (br q,  $J$  2.5 Hz, 1H, C=CH), 7.28 (AA'BB',  $J$  8.8 Hz, 2H, Ar), 7.30 (AA'BB',  $J$  8.8 Hz, 2H, Ar).  $^{13}\text{C}$  NMR (125 MHz,  $\text{CDCl}_3$ )  $\delta$  22.3, 29.2, 34.7, 77.1, 122.4, 128.4, 129.5, 132.1, 136.2, 148.3. ESI–HRMS ( $m/z$ ):  $[\text{M}+\text{H}-\text{H}_2\text{O}]^+$  calcd for  $\text{C}_{12}\text{H}_{12}\text{Cl}$ , 191.0622; found, 191.0627.

**(±)-2-(4-Methoxybenzylidene)cyclopentanol (±)-(7b):** Prepared by the above procedure from **3b** (100 mg, 0.49 mmol). Yield 71%, mp 75.5–78.3 °C. IR (ATR)  $\nu$  3252, 2998, 2955, 2931, 2833, 1604, 1510, 1463, 1420, 1294, 1242, 1178, 1112, 1034, 973, 938, 886, 831, 753  $\text{cm}^{-1}$ .  $^1\text{H}$  NMR (500 MHz,  $\text{CDCl}_3$ )  $\delta$  1.50 (s, 1H, OH), 1.62–1.69 and 1.72–1.79 (2  $\times$  m, 2  $\times$  1H,  $\text{CH}_2$ ), 1.89–2.01 (m, 2H,  $\text{CH}_2$ ), 2.50–2.59 and 2.67–2.75 (2  $\times$  m, 2  $\times$  1H,  $\text{CH}_2$ ), 3.82 (s, 3H, Me),

4.58 (m, 1H, OCH), 6.52 (br q,  $J$  2.5 Hz, 1H, C=CH), 6.88 (AA'BB',  $J$  8.8 Hz, 2H, Ar), 7.30 (AA'BB',  $J$  8.8 Hz, 2H, Ar).  $^{13}\text{C}$  NMR (125 MHz,  $\text{CDCl}_3$ )  $\delta$  22.7, 29.3, 34.9, 55.2, 77.5, 113.7, 123.2, 129.6, 130.5, 145.5, 158.2. ESI-HRMS ( $m/z$ ):  $[\text{M}+\text{H}-\text{H}_2\text{O}]^+$  calcd for  $\text{C}_{13}\text{H}_{15}\text{O}$ , 187.1117; found, 187.1114. Analytical data are in agreement with the literature data.<sup>17</sup>

**(±)-2-(4-Chlorobenzylidene)-2,3-dihydro-1H-inden-1-ol (±)-(8):** Prepared by the above procedure from **6** (125 mg, 0.49 mmol). Yield 39%, mp 105.8–108.6 °C. IR (ATR)  $\nu$  3319, 3069, 3025, 2887, 2321, 2155, 2107, 1904, 1692, 1677, 1608, 1586, 1490, 1461, 1405, 1354, 1312, 1296, 1255, 1212, 1186, 1176, 1133, 1092, 1009, 954, 895, 866, 844, 823, 806, 745, 732  $\text{cm}^{-1}$ .  $^1\text{H}$  NMR (500 MHz,  $\text{CDCl}_3$ )  $\delta$  1.97 (br s, 1H, OH), 3.79–3.99 (m, 2H,  $\text{CH}_2$ ), 5.62 (br s, 1H, OCH), 6.86 (br q,  $J$  2.5 Hz, 1H, C=CH), 7.27–7.32 (m, 3H, Ar), 7.34–7.37 (m, 4H, Ar), 7.51–7.55 (m, 1H, Ar).  $^{13}\text{C}$  NMR (125 MHz,  $\text{CDCl}_3$ )  $\delta$  35.5, 78.3, 124.8, 124.9, 125.1, 127.3, 128.6, 128.8, 129.8, 132.7, 135.5, 140.7, 142.9, 145.5. ESI-HRMS ( $m/z$ ):  $[\text{M}+\text{H}-\text{H}_2\text{O}]^+$  calcd for  $\text{C}_{16}\text{H}_{12}\text{Cl}$ , 239.0622; found, 239.0612.

**Typical procedure for the asymmetric reduction with oxazaborolidines – synthesis of (R)-2-(4-chlorobenzylidene)cyclopentanol (R)-(7a).** To the ice-cooled (0 °C) solution of (S)-**C5** (0.1 mL, 0.1 mmol; 1 M in toluene) in dry toluene (1 mL),  $\text{BH}_3\cdot\text{Me}_2\text{S}$  (470  $\mu\text{L}$ , 0.94 mmol; 2 M in toluene) was added dropwise, and the mixture was stirred for 10 min. A solution of ketone **3a** (0.5 mmol) in dry toluene (1 mL) was slowly added to the previously prepared solution of reductant at 0 °C. After completion (judged by TLC) of the reaction, the mixture was evaporated, and the residue purified by  $\text{SiO}_2$  radial chromatography (petroleum ether : EtOAc = 5 : 1) to give 80 mg (77%) of enantiomerically enriched product. 96% ee;  $t_{\text{R}} = 11.6$  min (minor), 13.2 min (major), (chiracel OD-H chiral column, mobile phase: *i*-PrOH/hexane = 98/2, flow rate: 1.5 mL/min, wavelength: 240 nm),  $[\alpha]_{\text{D}}^{25} + 41.3$  (1.13,  $\text{CH}_2\text{Cl}_2$ ).

**(S)-2-(4-Chlorobenzylidene)cyclopentanol (S)-(7a):** for the synthesis details see Table 1, entry 10. Yield 70%, 95% ee;  $t_{\text{R}} = 11.2$  min (major), 12.8 min (minor) (chiracel OD-H chiral column, mobile phase: *i*-PrOH/hexane = 98/2, flow rate: 1.5 mL/min, wavelength: 240 nm),  $[\alpha]_{\text{D}}^{25} - 31.9$  (1.17,  $\text{CH}_2\text{Cl}_2$ ).

**(R)-2-(4-Methoxybenzylidene)cyclopentanol (R)-(7b):** for the synthesis details see Table 1, entry 9. Yield 67%, 82% ee;  $t_{\text{R}} = 16.1$  min (minor), 18.4 min (major), (chiracel OD-H chiral column, mobile phase: *i*-PrOH/hexane = 98/2, flow rate: 1.5 mL/min, wavelength: 240 nm),  $[\alpha]_{\text{D}}^{25} + 3.8$  (1.11,  $\text{CH}_2\text{Cl}_2$ ).

**(S)-2-(4-Methoxybenzylidene)cyclopentanol (S)-(7b):** for the synthesis details see Table 1, entry 11. Yield 59%,

90% ee;  $t_{\text{R}} = 16.0$  min (major), 18.7 min (minor) (chiracel OD-H), *i*-PrOH:heksan = 98:2, 1.5 mL/min,  $[\alpha]_{\text{D}}^{25} - 9.9$  (1.08,  $\text{CH}_2\text{Cl}_2$ ).

**2-(4-Chlorobenzylidene)-2,3-dihydro-1H-inden-1-ol (8):** for the synthesis details see Table 1, entry 13. Yield 21%, 24% ee;  $t_{\text{R}} = 19.9$  min (major),  $t_{\text{R}} = 23.8$  min (minor) (chiracel OD-H chiral column, mobile phase: *i*-PrOH/hexane = 98/2, flow rate: 1.5 mL/min, wavelength: 240 nm),  $[\alpha]_{\text{D}}^{25} - 13.4$  (0.96,  $\text{CH}_2\text{Cl}_2$ ).

**2-(4-Chlorobenzylidene)-2,3-dihydro-1H-inden-1-ol (6):** for the synthesis details see Table 1, entry 14. Yield 20%, 33% ee;  $t_{\text{R}} = 20.3$  min (minor),  $t_{\text{R}} = 24.1$  min (major) (chiracel OD-H chiral column, mobile phase: *i*-PrOH/hexane = 98/2, flow rate: 1.5 mL/min, wavelength: 240 nm).

**Hydrogenation of 3a with Noyori's catalyst C4:** 2-(4-Chlorobenzylidene)cyclopentanone (**3a**) (103 mg, 0.498 mmol), catalyst **C4** (6 mg, 4.9  $\mu\text{mol}$ ) and isopropanol (2 mL) were added to hydrogenation vessel under nitrogen atmosphere. Then  $\text{K}_2\text{CO}_3$  (10 mg, 0.072 mmol) was added, the autoclave was pressurized to 80 bars of  $\text{H}_2$ , and the reaction mixture was stirred at room temperature. After 2 days additional amount of **C4** (4.6 mg, 3.8  $\mu\text{mol}$ ) was added (ketone **3a** still present). Because the ketone **3a** was still not consumed after 7 days, additional amount of  $\text{K}_2\text{CO}_3$  (50 mg, 0.362 mmol) was added. After additional 5 days the reaction was still not complete, therefore  $\text{K}_2\text{CO}_3$  (10 mg, 0.072 mmol), catalyst **C4** (5 mg, 4.1  $\mu\text{mol}$ ) and isopropanol (1 mL) were added, and hydrogenated for further 4 days. The solvent was evaporated and the residue was purified by  $\text{SiO}_2$  column chromatography (petroleum ether : EtOAc = 5 : 1) to afford 32 mg (31%) of the product **7a**; ee = 12%.

**Reduction of 3a with baker's yeast:** To a stirred solution of D-glucose (10.0 g, 55.5 mmol) and baker's yeast (56.0 g) in water (200 mL) at 38 °C, 2-(4-chlorobenzylidene)cyclopentanone (**3a**) (1.0 g, 4.84 mmol) dissolved in the minimum amount of EtOH (5 mL) was added; the reaction mixture was stirred for 10 days. Then EtOAc (100 mL) was added and the crude reaction mixture was filtered through a pad of Celite. The filtrate was extracted with EtOAc (3  $\times$  100 mL), the organic phase was dried over anhydrous  $\text{Na}_2\text{SO}_4$ , and the solvent was evaporated under reduced pressure. The residue was purified by  $\text{SiO}_2$  column chromatography (petroleum ether : EtOAc = 5 : 1) to afford 45 mg (5%) of the product **7a** as a light yellow oil; ee = 9%.

**Reduction of 3a with Daucus carota root:** An ethanolic (5 mL) solution of 2-(4-chlorobenzylidene)cyclopentanone (**3a**) (100 mg, 0.484 mmol) was added to a suspension of freshly grated carrot root (13.4 g) in water (70 mL). The reaction mixture was stirred at room temperature for



24 h, then carrot root was filtered off and washed with water. Filtrate was extracted with EtOAc (3 × 50 mL). The organic phase was dried over anhydrous Na<sub>2</sub>SO<sub>4</sub> and the solvent was evaporated under reduced pressure to give 10 mg (10%) of crude red oily product **7a**; *ee* >99%.

## 4. Conclusion

In summary, we synthesized enantiomerically enriched exocyclic allylic alcohols by asymmetric reduction of cyclic  $\alpha$ -arylmethylene cyclic ketones. Highly enantioselective chemoreduction of 2-benzylidenecyclopentanone derivatives was achieved by applying chiral oxazaborolidine-derived catalysts under mild reaction conditions. The sense of asymmetric induction was in accordance with Corey mechanistic model, thus (*S*)-catalyst delivered (*R*)-alcohols, while (*R*)-catalyst gave (*S*)-alcohol products with *ee* values of up to 96%. The indanone-derived chalcone was much less efficiently reduced regarding the chemical yield and optical purity (33% *ee*). Bioreduction of 2-(4-chlorobenzylidene)cyclopentanone with baker's yeast gave very low *ee* of the corresponding allylic alcohol, while reduction with *Daucus carota* root turned out to be completely enantioselective. The synthesized allylic alcohols can serve as enantioenriched probes for the monitoring of oxidation-reduction processes catalyzed by AKR1C enzymes; these studies are currently under progress.

## 5. Acknowledgments

We acknowledge with thanks the financial support from the Slovenian Research Agency through grant P1-0179. We thank EN-FIST Centre of Excellence, Trg Osvoobodilne fronte 13, 1000 Ljubljana, Slovenia, for using SuperNova diffractometer and FTIR spectrophotometer. We also thank D. Potočnik for laboratory assistance.

## 6. References

- H.-U. Blaser, C. Malan, B. Pugin, F. Spindler, H. Steiner, M. Studer, *Adv. Synth. Catal.* **2003**, 345, 103–151. (a) T. M. Penning, *Chem. Biol. Interact.* **2015**, 234, 236–246; (b) Y. Jin, T. M. Penning, *Annu. Rev. Pharmacol. Toxicol.* **2007**, 47, 263–292; (c) U. Oppermann, *Annu. Rev. Pharmacol. Toxicol.* **2007**, 47, 293–322.
- (a) P. Brožič, S. Turk, T. L. Rižner, S. Gobec, *Curr. Med. Chem.* **2011**, 18, 2554–2565; DOI:10.2174/092986711795933713 (b) T. L. Rižner, T. M. Penning, *Steroids* **2014**, 79, 49–63. DOI:10.1016/j.steroids.2013.10.012
- (a) T. M. Penning, M. E. Burczynski, J. M. Jez, C.-F. Hung, H.-K. Lin, H. Ma, M. Moore, N. Palackal, K. Ratnam, *Biochem. J.* **2000**, 351, 67–77; (b) S. Steckelbroeck, Y. Jin, S. Gopishetty, B. Oyesanmi, T. M. Penning, *J. Biol. Chem.* **2004**, 279, 10784–10795; DOI:10.1074/jbc.M313308200 (c) O. A. Barski, S. M. Tipparaju, A. Bhatnagar, *Drug. Metab. Rev.*, **2008**, 40, 553–624. DOI:10.1080/03602530802431439
- (a) T. M. Penning, J. E. Drury, *Arch. Biochem. Biophys.* **2007**, 464, 241–250; DOI:10.1016/j.abb.2007.04.024 (b) T. M. Penning, M. C. Byrns, *Ann. N. Y. Acad. Sci.* **2009**, 1155, 33–42; DOI:10.1111/j.1749-6632.2009.03700.x (c) B. E. Henderson, H. S. Feigelson, *Carcinogenesis* **2000**, 21, 427–433; DOI:10.1093/carcin/21.3.427 (d) P. Brožič, S. Turk, T. L. Rižner, S. Gobec, *Curr. Med. Chem.* **2011**, 18, 2554–2565. DOI:10.2174/092986711795933713
- A. Krazeisen, R. Breitling, G. Möller, J. Adamski, *Mol. Cell. Endocrinol.* **2001**, 171, 151–162. DOI:10.1016/S0303-7207(00)00422-6
- N. Usami, T. Yamamoto, S. Shintani, Y. Higaki, S. Ishikura, Y. Katagiri, A. Hara, *Biol. Pharm. Bull.* **2002**, 25, 441–445. DOI:10.1248/bpb.25.441
- P. Brožič, B. Golob, N. Gomboc, T. L. Rižner, S. Gobec, *Mol. Cell. Endocrinol.* **2006**, 248, 233–235. DOI:10.1016/j.mce.2005.10.020
- Y. Higaki, N. Usami, S. Shintani, S. Ishikura, O. El-Kabbani, A. Hara, *Chem. Biol. Interact.* **2003**, 143, 503–513. DOI:10.1016/S0009-2797(02)00206-5
- K. Traven, M. Sinreih, J. Stojan, S. Seršen, J. Kljun, J. Bezenšek, B. Stanovnik, I. Turel, T. L. Rižner, *Chem. Biol. Interact.* **2015**, 234, 349–359. DOI:10.1016/j.cbi.2014.11.005
- P. Brožič, S. Turk, A. O. Adeniji, J. Konc, D. Janežič, T. M. Penning, T. L. Rižner, S. Gobec, *J. Med. Chem.* **2012**, 55, 7417–7424. DOI:10.1021/jm300841n
- S. Gobec, P. Brožič, T. L. Rižner, *Bioorg. Med. Chem. Lett.* **2005**, 15, 5170–5175. DOI:10.1016/j.bmcl.2005.08.063
- B. Štefane, P. Brožič, M. Vehovc, T. L. Rižner, S. Gobec, *Eur. J. Med. Chem.* **2009**, 44, 2563–2571. DOI:10.1016/j.ejmech.2009.01.028
- N. Beranič, B. Štefane, B. Brus, S. Gobec, T. L. Rižner, *Chem. Biol. Interact.* **2013**, 202, 204–209. DOI:10.1016/j.cbi.2012.12.003
- A. P. Phillips, J. Mentha, *J. Am. Chem. Soc.* **1956**, 78, 140–145. DOI:10.1021/ja01582a040
- (a) B. Štefane, F. Požgan, *Top. Curr. Chem.* **2016**, 374, 1–67; DOI:10.1007/s41061-015-0002-2 (b) B. Štefane, F. Požgan, *Cat. Rev. Sci. Eng.* **2014**, 56, 82–174; DOI:10.1080/01614940.2013.869461 (c) F. Požgan, B. Štefane in: I. Karamé (Ed.): Hydrogenation: Asymmetric hydrogenation and transfer hydrogenation of ketones, InTech, Rijeka, Croatia, **2012**, pp. 31–68.
- J.-B. Xie, J.-H. Xie, X.-Y. Liu, W.-L. Kong, S. Li, Q.-L. Zhou, *J. Am. Chem. Soc.* **2010**, 132, 4538–4539. DOI:10.1021/ja100652f
- A. Hirao, S. Itsuno, N. Nakahama, N. Yamazaki, *J. Chem. Soc., Chem. Commun* **1981**, 315–317. DOI:10.1039/c39810000315
- E. J. Corey, R. K. Bakshi, S. Shibata, *J. Am. Chem. Soc.* **1987**, 109, 5551–5553. DOI:10.1021/ja00252a056
- E. J. Corey, C. J. Helal, *Angew. Chem. Int. Ed.* **1998**, 37,

- 1986–2012. DOI:10.1002/(SICI)1521-3773(19980817)37:15<1986::AID-ANIE1986>3.0.CO;2-Z
21. T. Yildiz, *Tetrahedron: Asymmetry* **2015**, *26*, 497–504. DOI:10.1016/j.tetasy.2015.03.008
22. (a) E. J. Corey, R. K. Bakshi, S. Shibata, C.-P. Chen, V. K. Singh, *J. Am. Chem. Soc.* **1987**, *109*, 7925–7926. DOI:10.1021/ja00259a075
- (b) E. J. Corey, A. V. Gavai, *Tetrahedron Lett.* **1988**, *29*, 3201–3204; DOI:10.1016/0040-4039(88)85121-9
- (c) E. J. Corey, J. O. Link, *Tetrahedron Lett.* **1989**, *30*, 6275–6278; DOI:10.1016/S0040-4039(01)93871-7
- (d) E. J. Corey, R. K. Bakshi, *Tetrahedron Lett.* **1990**, *31*, 611–614; C. Y. Hong, N. Kado, L. E. Overman, *J. Am. Chem. Soc.* **1993**, *115*, 11028–11029.
23. A. F. Simpson, C. D. Bodkin, C. P. Butts, M. A. Armitage, T. Gallagher, *J. Chem. Soc., Perkin Trans 1* **2000**, 3047–3054. DOI:10.1039/b004540n
24. (a) D. A. Evans, *Science* **1988**, *240*, 420–426; DOI:10.1126/science.3358127
- (b) D. K. Jones, D. C. Liotta, *J. Org. Chem.* **1993**, *58*, 799–801; DOI:10.1021/jo00056a001
- (c) L. P. Linney, C. R. Self, I. H. Williams, *J. Chem. Soc., Chem. Commun.* **1994**, 1651–1652. DOI:10.1039/C39940001651
25. G. Fogliato, G. Fronza, C. Fuganti, S. Lanati, R. Rallo, R. Rigoni, S. Servi, *Tetrahedron* **1995**, *51*, 10231–10240. DOI:10.1016/0040-4020(95)00578-V
26. J. S. Yadav, S. Nanda, P. T. Reddy, A. B. Rao, *J. Org. Chem.* **2002**, *67*, 3900–3903. DOI:10.1021/jo010399p
27. E. Majewska, M. Kozłowska, *Tetrahedron Lett.* **2013**, *54*, 6331–6332. DOI:10.1016/j.tetlet.2013.09.041
28. M. Austin, O. J. Egan, R. Tully, A. C. Pratt, *Org. Biomol. Chem.* **2007**, *5*, 3778–3786. DOI:10.1039/b711620a
29. J.-X. Wang, L. Kang, Y. Hu, B. guo Wei, *Synth. Commun.* **2002**, *32*, 1691–1696. DOI:10.1081/SCC-120004261
30. N. P. Buu-Hoï, N. D. Xuong, *J. Chem. Soc.* **1952**, 2225–2228. DOI:10.1039/JR9520002225

## Povzetek

Učinkovita asimetrična redukcija 2-benzilidenciklopentanonskih derivatov s kiralnimi oksazaborolidinskimi katalizatorji vodi selektivno do nastanka eksocikličnih alilnih alkoholov z enantiomernimi presežki do 96 %. Popolno enantioselektivnost lahko dosežemo z bioredukcijo 2-(4-klorobenziliden)ciklopentanona s korenjem, pri čemer nastane ustrezen alkohol z S konfiguracijo. Sintetizirane spojine lahko služijo kot enantiomerno obogateni standardi pri spremljanju enantiomernosti kataliziranih

Scientific paper

# A 26-Membered Macrocyclic System Obtained by a Double Diels–Alder Cycloaddition Between Two 2*H*-Pyran-2-one Rings and Two 1,1'-(Hexane-1,6-diyl)bis(1*H*-pyrrole-2,5-dione)s

Bor Lucijan Turek, Marijan Kočevar, Krištof Kranjc\*  
and Franc Perdih\*

Faculty of Chemistry and Chemical Technology, University of Ljubljana, Večna pot 113, SI-1000 Ljubljana, Slovenia

\* Corresponding author: E-mail: franc.perdih@fkkt.uni-lj.si;  
kristof.kranjc@fkkt.uni-lj.si

Received: 19-05-2017

Dedicated to Professor Emeritus Miha Tišler, University of Ljubljana,  
on the occasion of his 90<sup>th</sup> birthday.

## Abstract

With the application of a double dienophile 1,1'-(hexane-1,6-diyl)bis(1*H*-pyrrole-2,5-dione) for a [4+2] cycloaddition with a substituted 2*H*-pyran-2-one a novel 26-membered tetraaza heteromacrocyclic system **3** was prepared via a direct method under solvent-free conditions with microwave irradiation. The macrocycle prepared is composed of two units of the dienophile and two of the diene. The structure of the macrocycle was characterized on the basis of IR, <sup>1</sup>H and <sup>13</sup>C NMR and mass spectroscopy, as well as by the elemental analysis and melting point determination. With X-ray diffraction of a single crystal of the macrocycle we have determined that the two acetyl groups (attached to the bridging double bond of the bicyclo[2.2.2]octene fragments) are oriented towards each other (and also towards the inside of the cavity of the macrocycle), therefore, mostly filling it completely.

**Keywords:** Macrocycles, 2*H*-Pyran-2-ones, [4+2] Cycloaddition, Crystal structure, Hydrogen bonds, Polymorphs

## 1. Introduction

Macrocycles are privileged molecule structures that are of paramount importance in many areas of chemistry, including drug development,<sup>1</sup> formation of coordination compounds and metal-organic frameworks.<sup>2</sup> Generally they possess properties (structural, chemical, physical and biological) that set them apart from their linear or small-ring analogues, the reason being that they can often provide sufficient flexibility for interactions with other molecules (e.g. for binding to an enzyme's active site or for a coordination to a guest ion during phase catalysis) combined with the advantages brought by the fact that they often contain more than one binding motif. This means that all of the interactions between the host (or enzyme) and the macrocycle are taking place between two molecules only and consequently the enthalpy of the interaction is not so unfavourable as would be in the case where

more (smaller) ligands interact simultaneously with the host.

Even though the synthesis of macrocycles has achieved some remarkable successes, there is still a lack of general approach towards them.<sup>3</sup> There were many successful attempts towards the preparation of macrocycles, one of the most-often used being dilution techniques triggering the macrocyclization via lactonization, lactamization, metathesis reaction etc. (that were recently used for the first asymmetric total synthesis of aspergillide D<sup>4</sup> or for the total synthesis of mandelalide A).<sup>5</sup> Other options include the template-induced cyclization (around the host ion)<sup>6</sup> and cyclization on a solid support (like Merrifield-based synthesis of cyclic peptides or such inspired by non-ribosomal peptide aldehydes).<sup>7</sup> More contemporary approaches are based on multi multicomponent macrocyclizations (MiBs)<sup>8</sup> that include various bifunctional building blocks. However, neither of the above mentioned ap-

proaches can be applied universally. So there is still place for new routes. Recently, a lot of effort was devoted to multicomponent reactions that efficiently offer access to various macrocycles, including the possibility to incorporate points of diversity, which are, nevertheless, generally introduced before or after the key cyclization step.<sup>9</sup> However, even this approach is generally applied just to obtain the requisite linear precursors that are latter assembled via a suitable ring-closing reaction into the final macrocyclic target.<sup>10–14</sup> Of interest are also preparations of calix[4]arene systems linked with 1,2,4-triazole and 1,3,4-oxadiazole derivatives,<sup>15</sup> as well as other tetraaza macrocycles applied as ligands in various coordination compounds.<sup>16</sup>

Herein we present another approach, where two double Diels–Alder cycloadditions between two molecules of the substituted 2*H*-pyran-2-ones (each acting as a “double” diene)<sup>17</sup> and two molecules of the double dienophile provide a 26-membered tetraaza macrocyclic system. This strategy can be termed a multicomponent reaction (as four molecules react to form the macrocycle) with four individual [4+2] pericyclic reactions representing the crucial ring-closing steps.

## 2. Experimental

### 2.1. Materials and Measurements

Melting points were determined on a micro hot stage apparatus and are uncorrected. <sup>1</sup>H NMR spectra were recorded at 29 °C with a Bruker Avance III 500 spectrometer at 500 MHz using Me<sub>4</sub>Si as an internal standard. <sup>13</sup>C NMR spectra were recorded at 29 °C with a Bruker Avance III 500 spectrometer at 125 MHz and were referenced against the central line of the solvent signal (CDCl<sub>3</sub> triplet at 77.0 ppm or DMSO-*d*<sub>6</sub> septet at 39.5 ppm). The coupling constants (*J*) are given in Hertz. IR spectra were obtained with a Bruker Alpha Platinum ATR FT-IR spectrometer on a solid support as microcrystalline powder. MS spectra were recorded with an Agilent 6624 Accurate Mass TOF LC/MS instrument (ESI ionization). Elemental analyses (C, H, N) were performed with a Perkin Elmer 2400 Series II CHNS/O Analyzer. TLC was carried out on Fluka silica-gel TLC-cards.

The starting 2*H*-pyran-2-one **1** was prepared by the method devised by Kepe, Kočever *et al.*<sup>18</sup> as follows: from acetylacetone, *N,N*-dimethylformamide dimethyl acetal (DMFDMA) and hippuric acid by heating in acetic anhydride according to the published procedure 5-acetyl-3-benzoylamino-6-methyl-2*H*-pyran-2-one was obtained; followed by the removal of the benzoyl group (in concentrated H<sub>2</sub>SO<sub>4</sub> upon heating) analogously as previously described<sup>19,20</sup> and subsequent derivatization of the free 3-amino group with acetyl chloride the 2*H*-pyran-2-one **1** was obtained.<sup>21</sup> Dienophile **2** was prepared by a modification of the procedures published by Cava *et al.*<sup>22</sup> All other reagents and solvents were used as received from commercial suppliers.

Microwave reactions were performed in air using a focused microwave unit (Discover by CEM Corporation, Matthews, NC, USA). The machine consists of a continuous, focused microwave power-delivery system with an operator-selectable power output ranging from 0 to 300 W. Reactions were conducted in darkness in glass vessels (capacity 10 mL) sealed with rubber septum. The pressure was controlled by a load cell connected to the vessel via the septum. The temperature of the reaction mixtures was monitored using a calibrated infrared temperature controller mounted below the reaction vessel and measuring the temperature of the outer surface of the reaction vessel. The mixtures were stirred with a Teflon-coated magnetic stirring bar in the vessel. Temperature, pressure, and power profiles were recorded using commercially available software provided by the manufacturer of the microwave unit.

### Synthesis of 1,1'-(Hexane-1,6-diyl)bis(1*H*-pyrrole-2,5-dione) (**2**)<sup>22</sup>

To a clear solution of maleic anhydride (2.03 g, 20 mmol) in diethyl ether (30 mL) a separately prepared mixture of hexane-1,6-diamine (2.07 g, 10 mmol) in diethyl ether (10 mL) is added dropwise at room temperature. The viscous suspension is further stirred at room temperature for 1 h and thereafter cooled on ice. Precipitated product is isolated by vacuum filtration and used in the next step without drying or additional purification.

The entire obtained solid is slowly added to a mixture of sodium acetate (0.66 g, 8 mmol) and acetic anhydride (8 mL) in an Erlenmeyer flask while vigorously stirring at room temperature. After the completion of the addition, the reaction mixture is heated on water bath (approx. 100 °C) for 1 h, cooled to room temperature and poured onto ice–water mixture (30 g). The precipitated product is isolated by vacuum filtration, rinsed 3 times with distilled water and once with a few mL of petroleum ether yielding crude **2** (0.56 g, 20%) that is further crystallized from ethanol.

M.p. 139–141 °C (EtOH), m.p. (lit.)<sup>23</sup> 139–141 °C (EtOH). IR (ATR) 3104, 3087, 2936, 2856, 1686, 1453, 1418, 1372, 1327, 1240, 1129 cm<sup>-1</sup>. <sup>1</sup>H NMR (500 MHz, CDCl<sub>3</sub>): δ 1.29 (m, 4H, 2 × NCH<sub>2</sub>CH<sub>2</sub>CH<sub>2</sub>), 1.59 (m, 4H, 2 × NCH<sub>2</sub>CH<sub>2</sub>CH<sub>2</sub>), 3.51 (t, 4H, 2 × NCH<sub>2</sub>CH<sub>2</sub>CH<sub>2</sub>), 6.69 (s, 4H, 4 × CH). <sup>13</sup>C NMR (125 MHz, CDCl<sub>3</sub>): δ 25.6, 27.8, 36.9, 124.4, 171.1. MS (ESI+) *m/z* 277 (MH<sup>+</sup>). HRMS (ESI+) calcd. for C<sub>14</sub>H<sub>17</sub>N<sub>2</sub>O<sub>4</sub> (MH<sup>+</sup>): 277.1183. Found: 277.1181. Anal. calcd. for C<sub>14</sub>H<sub>16</sub>N<sub>2</sub>O<sub>4</sub>·0.1 H<sub>2</sub>O: C, 60.47; H, 5.87; N, 10.07. Found: C, 60.43; H, 5.89; N, 9.95.

### Synthesis of the Macrocycle **3**

A 10 mL quartz microwave vessel is loaded with 2*H*-pyran-2-one **1** (105 mg, 0.5 mmol), dienophile **2** (152 mg, 0.55 mmol) and *n*-butanol (100 mg). A stirring bar is added and the vessel closed with the rubber septum. The reaction mixture is irradiated with microwaves (150 W) at

150 °C for 45 min. Thereafter, the reaction mixture is cooled to room temperature and diisopropyl ether is added (0.5 mL). The precipitated product is collected by vacuum filtration providing crude macrocycle **3** (150 mg, 34%) that is further crystallized from DMF.

M.p. 255–257 °C (DMF). IR (ATR) 3368, 2940, 2860, 1766, 1698, 1548, 1437, 1399, 1367 cm<sup>-1</sup>. <sup>1</sup>H NMR (500 MHz, DMSO-*d*<sub>6</sub>): δ 1.03 (m, 8H, 2 × NCH<sub>2</sub>CH<sub>2</sub>CH<sub>2</sub>CH<sub>2</sub>CH<sub>2</sub>N), 1.23 (m, 8H, 2 × NCH<sub>2</sub>CH<sub>2</sub>CH<sub>2</sub>CH<sub>2</sub>CH<sub>2</sub>CH<sub>2</sub>N), 1.85 (s, 6H, 2 × Me), 1.95 (s, 6H, 2 × NHCOCH<sub>3</sub>), 2.02 (s, 6H, 2 × COMe), 3.00 (d, *J* = 7.5 Hz, 4H, 2 × 3a-H, 4a-H), 3.18 (m, 8H, 2 × NCH<sub>2</sub>CH<sub>2</sub>CH<sub>2</sub>CH<sub>2</sub>CH<sub>2</sub>CH<sub>2</sub>N), 4.11 (d, *J* = 7.5 Hz, 4H, 2 × 7a-H, 8a-H), 6.82 (s, 2H, 2 × CH), 8.43 (s, 2H, 2 × NH). <sup>13</sup>C NMR (125 MHz, DMSO-*d*<sub>6</sub>): δ 18.2, 23.5, 25.8, 27.0, 27.4, 37.7, 41.2, 42.9, 48.8, 57.2, 138.2, 142.7, 170.3, 174.1, 175.3, 195.8. MS (ESI+) *m/z* 884 (MH<sup>+</sup>). HRMS (ESI+) calcd. for C<sub>46</sub>H<sub>55</sub>N<sub>6</sub>O<sub>12</sub> (MH<sup>+</sup>): 883.3872. Found: 883.3844. Anal. calcd. for C<sub>46</sub>H<sub>54</sub>N<sub>6</sub>O<sub>12</sub>·0.8 H<sub>2</sub>O: C, 61.57; H, 6.24; N, 9.37. Found: C, 61.57; H, 6.36; N, 9.27.

## 2. 2. Crystallography

Single-crystal X-ray diffraction data were collected at room temperature on a Nonius Kappa CCD diffractometer using graphite monochromated Mo-Kα radiation ( $\lambda =$

0.71073 Å). The data were processed using DENZO.<sup>24</sup> Structures were solved by direct methods implemented in SIR97<sup>25</sup> and refined by a full-matrix least-squares procedure based on  $F^2$  with SHELXL-2014.<sup>26</sup> All non-hydrogen atoms were refined anisotropically. Hydrogen atoms were readily located in a difference Fourier maps and were subsequently treated as riding atoms in geometrically idealized positions, with C–H = 0.93 (aromatic), 0.98 (methine), 0.97 (methylene) or 0.96 Å (CH<sub>3</sub>), N–H = 0.86 Å and with  $U_{\text{iso}}(\text{H}) = kU_{\text{eq}}(\text{C or N})$ , where  $k = 1.5$  for methyl groups, which were permitted to rotate but not to tilt, and 1.2 for all other H atoms. To improve the refinement results, two reflections in the case of **2a**, eleven reflections in the case of **2b** and twenty eight reflections in the case of **3-2DMF** with too high values of  $\delta(F^2)/\text{e.s.d.}$  and with  $F_o^2 < F_c^2$  were deleted from the refinement. In **2b** a proposed twin law has been applied according to Platon analysis and the  $R_1$  factor has improved from 8.13% to 7.75%, however, instead of estimated BASF 0.19 the refined BASF was found to be 0.00939. In the crystal structure of **3-2DMF** a solvate DMF molecule is disorder over two positions with refined ratio 0.82:0.18 and ISOR instruction was used for the refinement of C25B atom in DMF. Crystallographic data are listed in Table 1. X-Ray powder diffraction data were collected at room temperature using a PANalytical X'Pert PRO MPD diffractometer with  $\theta$ - $2\theta$  reflection geometry,

**Table 1.** Crystal data and refinement parameters for the compounds **2a**, **2b** and **3-2DMF**.

Compound	<b>2a</b>	<b>2b</b>	<b>3-2DMF</b>
CCDC	1547701	1547702	1547703
Molecular formula	C <sub>14</sub> H <sub>16</sub> N <sub>2</sub> O <sub>4</sub>	C <sub>14</sub> H <sub>16</sub> N <sub>2</sub> O <sub>4</sub>	C <sub>52</sub> H <sub>68</sub> N <sub>8</sub> O <sub>14</sub>
Molecular weight	276.29	276.29	1029.14
Crystal system	Triclinic	Monoclinic	Orthorhombic
Space group	<i>P</i> – 1	<i>P</i> 2 <sub>1</sub> / <i>a</i>	<i>P</i> <i>c</i> <i>a</i> <i>n</i>
<i>a</i> (Å)	4.5975(2)	8.4999(3)	10.4260(10)
<i>b</i> (Å)	5.5190(3)	6.6347(2)	17.5217(2)
<i>c</i> (Å)	14.1680(10)	12.6120(5)	27.8937(4)
$\alpha$ (°)	93.956(3)	90	90
$\beta$ (°)	97.222(4)	98.295(2)	90
$\gamma$ (°)	97.692(4)	90	90
<i>V</i> (Å <sup>3</sup> )	352.08(4)	703.80(4)	5095.7(5)
<i>Z</i>	1	2	4
<i>D</i> <sub>calc</sub> (g cm <sup>-3</sup> )	1.303	1.304	1.341
$\mu$ (mm <sup>-1</sup> )	0.097	0.097	0.098
<i>F</i> (000)	146	292	2192
Crystal dimensions (mm)	0.60 × 0.35 × 0.05	0.60 × 0.50 × 0.05	0.28 × 0.13 × 0.08
Reflections collected	2464	3070	11000
Data / restraints / parameters	1540 / 0 / 91	1566 / 0 / 93	5819 / 6 / 369
<i>R</i> <sub>int</sub>	0.0227	0.0204	0.0320
<i>R</i> <sub>1</sub> , <i>wR</i> <sub>2</sub> [ <i>I</i> > 2σ( <i>I</i> )] <sup>a</sup>	0.0444, 0.1231	0.0775, 0.2475	0.0486, 0.1157
<i>R</i> <sub>2</sub> , <i>wR</i> <sub>2</sub> (all data) <sup>b</sup>	0.0580, 0.1343	0.0854, 0.2540	0.0855, 0.1335
Goodness of fit on $F^2$ , <i>S</i> <sup>c</sup>	1.039	1.097	1.010
Extinction coefficient	–	0.62(15)	–
$\Delta\rho_{\text{max}}$ , $\Delta\rho_{\text{min}}$ (e Å <sup>-3</sup> )	0.128, –0.150	0.226, –0.229	0.263, –0.306

<sup>a</sup>  $R = \sum |F_o| - |F_c| / \sum |F_o|$ , <sup>b</sup>  $wR_2 = \{\sum [w(F_o^2 - F_c^2)^2] / \sum [w(F_o^2)^2]\}^{1/2}$ , <sup>c</sup>  $S = \{\sum [(F_o^2 - F_c^2)^2] / (n/p)\}^{1/2}$  where *n* is the number of reflections and *p* is the total number of parameters refined.

primary side Johansson type monochromator and Cu-K $\alpha$  radiation ( $\lambda = 1.54059 \text{ \AA}$ ).

### 3. Results and Discussion

#### 3.1. Synthesis

The strategy for the synthesis of the macrocycle **3** was based on our previous experiences with the [4+2] cycloadditions of variously substituted 2*H*-pyran-2-ones and appropriate dienophiles, including *N*-substituted maleimides.<sup>27–31</sup> Namely, it was already observed that 2*H*-pyran-2-ones can act as “double” dienes, reacting in two consecutive Diels–Alder reactions with two distinctive molecules of the dienophiles, yielding bicyclo[2.2.2]octenes.<sup>30</sup> The initial cycloaddition step leads to the formation of CO<sub>2</sub>-bridged oxabicyclo[2.2.2]octenes that in the next step eliminate a molecule of CO<sub>2</sub> (via a retro-hetero-Diels–Alder reaction) providing cyclohexadiene systems that act as new dienes for another molecule of dienophile finally providing the double cycloadducts. On the other hand, if the two molecules of the dienophile would be connected by a suitable tether, it would be possible to expect that the second cycloaddition step would take place intramolecularly. At least in theory, the smallest possible cyclic product would consist of just one bicyclo[2.2.2]octene fragment (formed out of one 2*H*-pyran-2-one ring) and one molecule of the double dienophile. Related examples were already described by the application of cycloocta-1,4-diene.<sup>32</sup> Of course, it could be also possible that larger cycles would be obtained, for example such that contain two bicyclo[2.2.2]octene moieties and two molecules of the double dienophile.

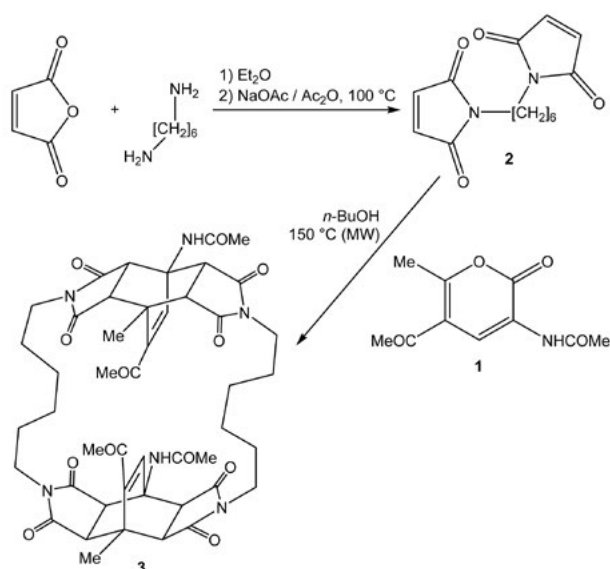
Here, we have focused our attention to a 3-acetyl-amino-6-methyl-2*H*-pyran-2-one (**1**) and 1,1'-(hexane-

1,6-diyl)bis(1*H*-pyrrole-2,5-dione) (**2**) as the double dienophile (Scheme 1). In this case one could expect the formation of various cyclic systems, the simplest one consisting of one bicyclo[2.2.2]octene fragment and one fragment stemming from **2**. The other possibility would be the formation of the macrocyclic ring from two dienes **1** and two molecules of **2**. Even larger systems that could form theoretically, however, were not expected (as their formation is entropically less likely); on the other hand, the formation of a linear polymer containing bicyclo[2.2.2]octene fragments (stemming from **1**) alternating with the dienophile parts (from **2**) could not be excluded.

The preparation of the double dienophile **2** was carried out according to the literature procedure<sup>22</sup> starting from the commercially available maleic anhydride and hexane-1,6-diamine in diethyl ether at room temperature. After the first reaction step (*i.e.* the formation of an opening intermediate consisting of a terminal carboxylic acid group-formed by the opening of the anhydride ring-and a new amide fragment arising from the reaction between the remaining carbonyl group and the amine group of the hexane-1,6-diamine. This intermediate is in the next reaction step mixed with the solution of sodium acetate in acetic anhydride and upon heating to 100 °C re-cyclized into the new maleimide ring. Of course, because the starting hexane-1,6-diamine is a bi-functional compound containing two suitable amine groups, the above described reaction sequence takes place on both sides of the diamine, therefore furnishing the desired double dienophile **2**.

2*H*-Pyran-2-one derivative **1**, applied in this synthetic approach, can be straightforwardly accessed *via* a one-pot synthesis starting from the simple commercially available precursors: a carbonyl compound containing an activated CH<sub>2</sub> group (*i.e.* acetylacetone), a C<sub>1</sub>-synthon such as *N,N*-dimethylformamide dimethyl acetal (DMFDMA) and hippuric acid (**2**) as an *N*-acylglycine derivative as previously described by Kepe, Kočevar and co-workers.<sup>18</sup> The synthesis takes place under heating (approx. 65–70 °C) in acetic anhydride (or in a mixture with acetic acid) as the solvent yielding the substituted 3-benzoylamino-2*H*-pyran-2-one. To convert this into the desired 3-acylamino derivative **1**, cleavage of the amide bond is executed (in conc. H<sub>2</sub>SO<sub>4</sub> at approx. 80 °C), the product containing a free NH<sub>2</sub> group is isolated by the extraction in CH<sub>2</sub>Cl<sub>2</sub> (after addition of water and neutralization with sodium hydrogen sulfate)<sup>19</sup> and further acetylated with acetyl chloride at room temperature in CH<sub>2</sub>Cl<sub>2</sub> with the addition of pyridine as the base.<sup>21</sup>

Compound **2** was in the next step applied as the double dienophile in the Diels–Alder reaction with 5-acetyl-3-acetylamino-6-methyl-2*H*-pyran-2-one (**1**) as the diene component. Because 2*H*-pyran-2-one skeletons can in general participate in two separate Diels–Alder reactions, the combination of the double dienophile **2** and the 2*H*-pyran-2-one derivative **1** was deemed appropriate for the preparation of a macrocyclic system. We assumed that



Scheme 1. Reaction sequence leading to the macrocycle **3**.

the most probable outcome would be the reaction of two molecules of the dienophile **2** with two molecules of *2H*-pyran-2-one **1**. In this way the former *2H*-pyran-2-one skeleton would be transformed into a new bicyclo[2.2.2]octene moiety (as described above), however due to the bifunctional nature of the dienophile **2**, both bicyclo[2.2.2]octenes would be connected with two  $-\text{[CH}_2\text{]}_6-$  tethers.

The cycloaddition between dienophile **2** and *2H*-pyran-2-one derivative **1** was carried out employing microwave irradiation<sup>33</sup> at 150 °C in closed vessel and under solvent-free conditions, just with a small addition of *n*-BuOH (100 mg for a 10 mL vessel). Its function was to prevent the deposition of the dienophile **2** on the upper (colder) parts of the reaction vessel as a consequence of its sublimation, as we have devised previously.<sup>34</sup>

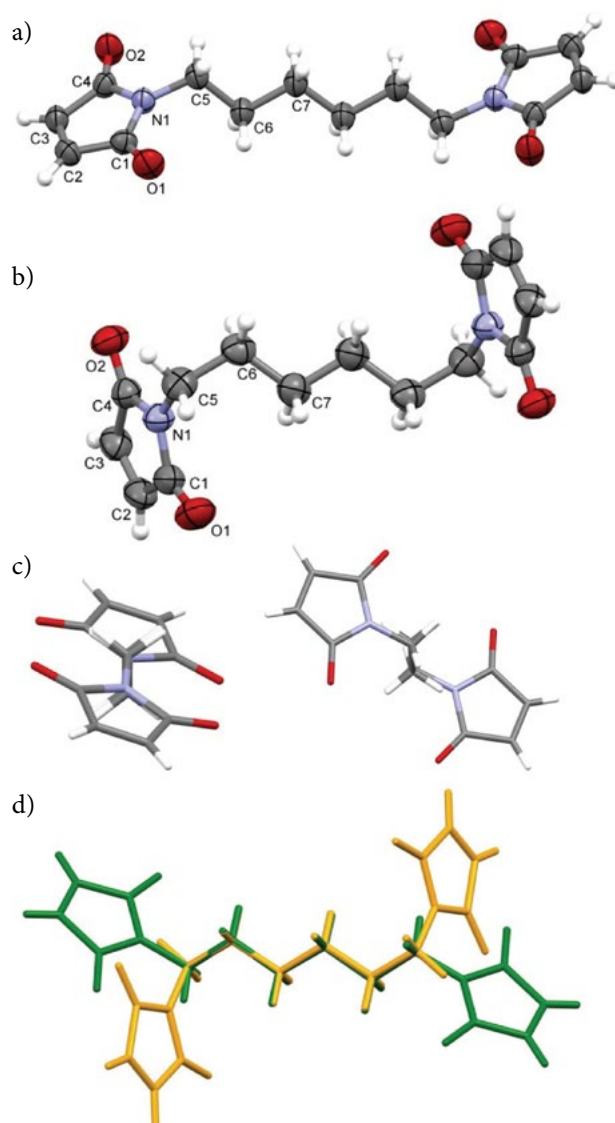
Indeed, after the cooling of the reaction mixture and addition of diisopropyl ether, product **3** was isolated and further crystallized from DMF. According to the <sup>1</sup>H NMR analysis of **3** it was clear that a macrocycle was obtained, composed of two  $-\text{[CH}_2\text{]}_6-$  chains (multiplets at  $\delta$  1.03, 1.23 and 3.18 ppm each integrated for 8H, belonging to the two central  $\gamma$ -CH<sub>2</sub> groups of the chain, to the two  $\beta$ -CH<sub>2</sub> units and to the two  $\alpha$ -CH<sub>2</sub> groups, respectively), two methyl groups (singlet at  $\delta$  1.85 ppm integrated for 6H), two acetylamino groups (singlet at  $\delta$  1.95 ppm integrated for 6H) and two acetyl groups (singlet at  $\delta$  2.02 ppm integrated for 6H). Furthermore, two most characteristic doublets (each for 4H) were observed at  $\delta$  3.00 and 4.11 ppm, each corresponding to the two sets of protons on the bicyclo[2.2.2]octene fragment. According to our experiences with NMR spectra of such systems, from the existence of only two doublets and from the coupling constant observed (*i.e.* 7.5 Hz), we can conclude that the bicyclo[2.2.2]octene fragment is of the symmetric *exo,exo* structure, also consistent with our previous results.<sup>30</sup> Furthermore, a singlet at  $\delta$  6.82 (for 2H) corresponding to both protons attached to the double bond of the bicyclo[2.2.2]octene fragments and a singlet at  $\delta$  8.43 (for 2H) for the two NH groups were also observed in <sup>1</sup>H NMR. In the IR spectrum of **3** bands corresponding to the NH group at 3368 cm<sup>-1</sup> and carbonyl group at 1698 cm<sup>-1</sup> were observed. These data were further corroborated by the <sup>13</sup>C NMR and mass spectroscopy, as well as elemental analysis, establishing the structure of **3** as a novel 26-membered tetraaza heteromacrocyclic system.

### 3.2. Crystal Structures

X-Ray crystal structures of **2** and **3** were determined, where two polymorphs of 1,1'-(hexane-1,6-diyl)bis(1*H*-pyrrole-2,5-dione) (**2**) were observed. All bond lengths of **2a**, **2b** and **3** are within normal ranges.<sup>35</sup> Conventional re-crystallization of **2** from ethanol, followed by cooling to 5 °C provided a crystalline form **2a**. On the other hand, slow precipitation of **2** from its mixture with starting **1** in toluene (*i.e.* a reaction mixture remaining after an unsuc-

cessful attempt to prepare **3**) upon evaporation of the solvent at 5 °C provided a different polymorph **2b**. Polymorph **2a** crystallizes in triclinic *P*-1 space group and polymorph **2b** in monoclinic *P*2<sub>1</sub>/*a* space group (Figure 1a,b). In both polymorphs asymmetric unit is composed of a half of molecule **2** due to the inversion center in the middle of C7–C7' bond.

In **2a** and **2b** the 1*H*-pyrrole-2,5-dione ring is planar. The maximum deviation from the mean plane described by the ring atoms is +0.004(1) and –0.004(1) Å for the C4 and N1 atoms in **2a** and a negligible deviation in the range +0.001(1) to –0.001(1) Å for the C1 and C3 and N1 and C2 atoms in **2b**. Such small deviations from planarity were observed also in two known polymorphs of 1*H*-pyrrole-2,5-dione (maleimides).<sup>36,37</sup> The main difference in



**Figure 1.** Molecular structure and atom numbering scheme for a) **2a** and b) **2b**. Probability ellipsoids are drawn at the 50% level. c) View along C<sub>6</sub> chain for **2a** (left) and **2b** (right). d) Molecular overlay of polymorphs **2a** (green) and **2b** (orange).

the molecular geometry between the polymorphs of **2** is in the N1–C5–C6–C7 torsion angle being  $-175.71(13)^\circ$  in the form **2a** (where CH<sub>2</sub> hydrogens are eclipsed over the succinimide ring) and  $68.4(3)^\circ$  in **2b** (where CH<sub>2</sub> hydrogens are eclipsed over themselves only and not over the succinimide ring) (Figure 1c,d).

In the crystal structure **2a** centrosymmetric hydrogen-bonded dimers formation is facilitated by C3–H3...O2

hydrogen bonding between adjacent pyrrole-2,5-dione moieties with the graph set motif<sup>f8</sup> R<sub>2</sub><sup>2</sup>(8) and centrosymmetric hydrogen-bonded tetramers are formed *via* C2–H2...O2 and C3–H3...O2 hydrogen bonding between adjacent pyrrole-2,5-dione moieties with the graph set motif R<sub>4</sub><sup>2</sup>(10) generating infinite 2D layer (Table 2, Figure 2). Wavy 2D layers are present also in **2b**, however, hydrogen-bonded trimers formation is facilitated by C2–H2...O2

Table 2. Hydrogen bond geometry of **2a**, **2b** and 3·2DMF (Å and °).

D–H...A	D–H (Å)	H...A (Å)	D...A (Å)	D–H...A (°)	Symmetry code
<b>2a</b>					
C2–H2...O2	0.93	2.38	3.2650(17)	159.0	$x - 1, y - 1, z$
C3–H3...O2	0.93	2.51	3.4057(17)	161.3	$-x + 1, -y, -z + 1$
<b>2b</b>					
C2–H2...O2	0.93	2.42	3.341(4)	172.9	$x, y - 1, z$
C3–H3...O2	0.93	2.45	3.369(4)	167.7	$-x - \frac{1}{2}, y - \frac{1}{2}, -z + 1$
<b>3·2DMF</b>					
N3–H3...O4	0.86	2.17	3.0207(18)	168.1	$x, -y, -z + \frac{1}{2}$
C1–H1...O6	0.98	2.44	2.982(2)	114.7	$x, y, z$
C2–H2...O7	0.98	2.60	3.384(2)	137.3	$x, y, z$
C4–H4...O7	0.98	2.44	3.317(3)	149.4	$x, y, z$
C5–H5...O3	0.98	2.54	3.374(2)	142.8	$x - \frac{1}{2}, -y + \frac{1}{2}, z$
C5–H5...O6	0.98	2.56	3.125(2)	116.8	$x, y, z$
C15–H15A...O6	0.96	2.53	3.382(2)	147.5	$x + 1, y, z$
C17–H17B...O4	0.96	2.60	3.443(3)	146.4	$x, -y, -z + \frac{1}{2}$
C17–H17C...O5	0.96	2.44	3.314(3)	150.8	$x - 1, y, z$

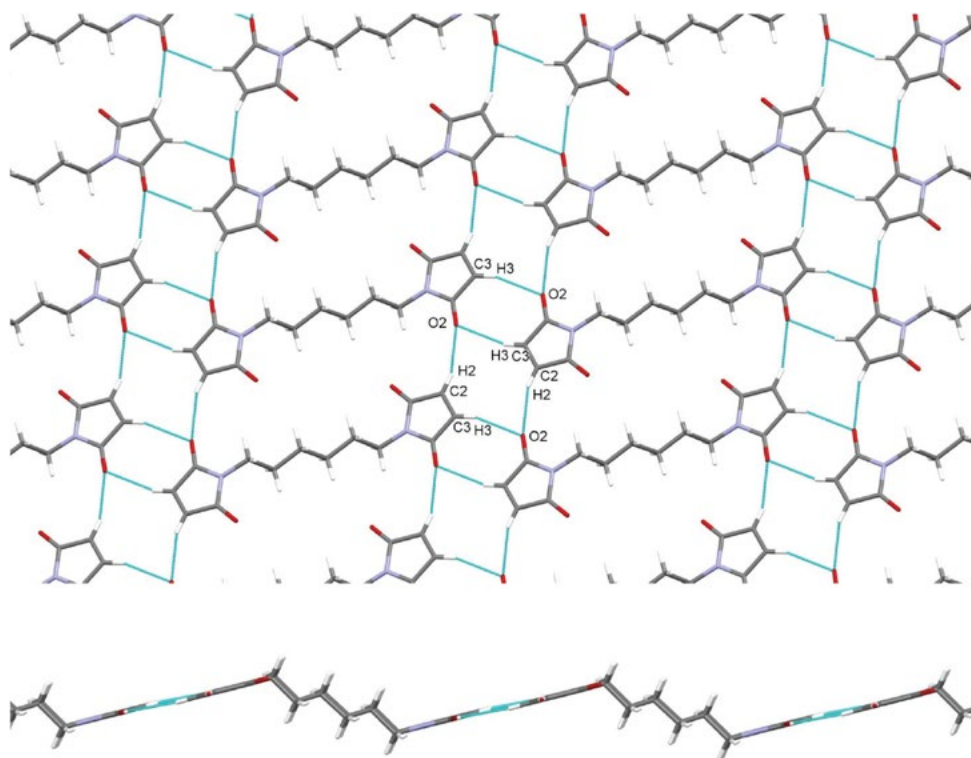
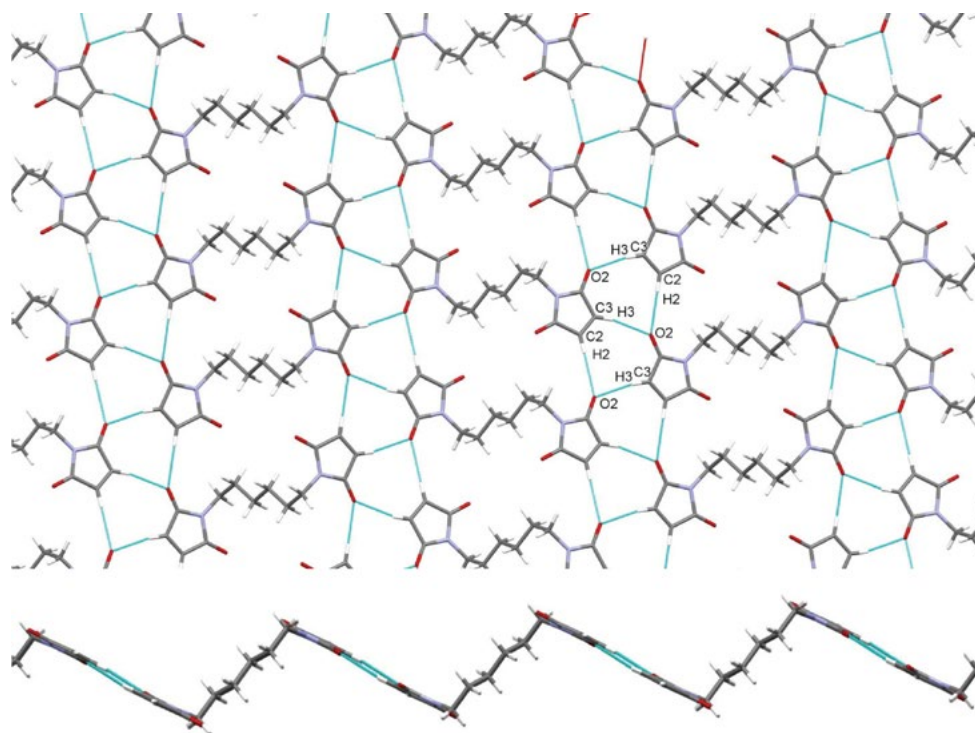
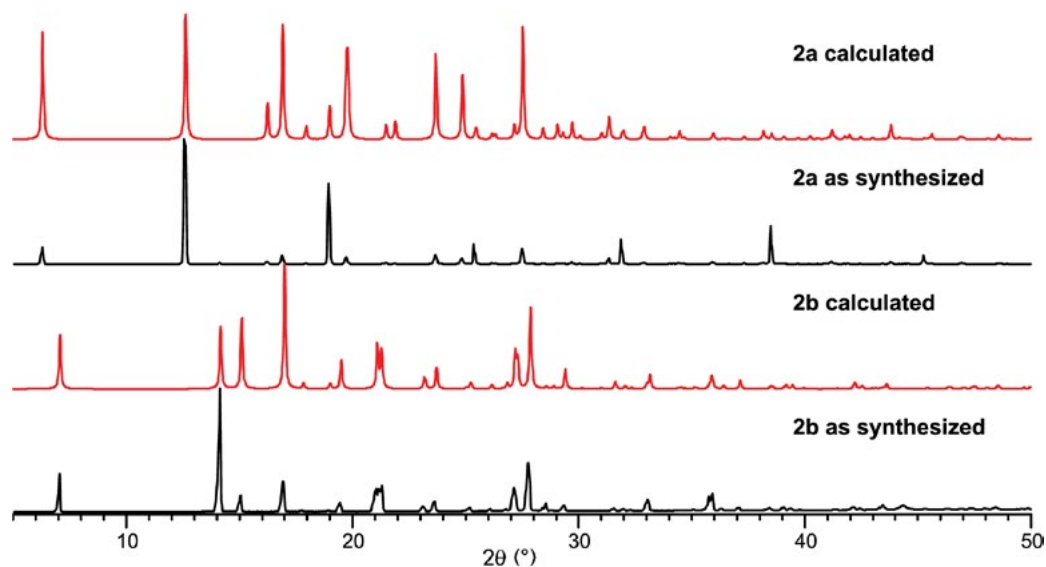


Figure 2. 2D layer formation in **2a** generated by C–H...O hydrogen bonding (blue dashed lines) with graph set motifs R<sub>2</sub><sup>2</sup>(8) and R<sub>4</sub><sup>2</sup>(10) (top). View along the layer (bottom).





**Figure 3.** 2D layer formation in **2b** generated by C–H...O hydrogen bonding (blue dashed lines) with graph set motif  $R^2_3(9)$ . (top). View along the layer (bottom).



**Figure 4.** Calculated and experimentally determined PXRD patterns of polymorphs **2a** and **2b**.

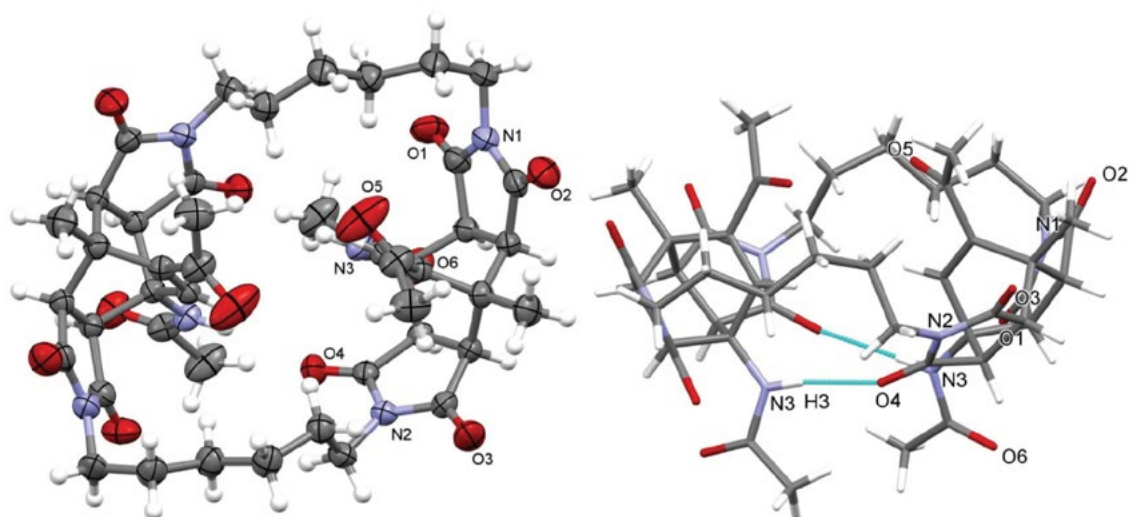
and C3–H3...O2 hydrogen bonding between adjacent pyrrole-2,5-dione moieties with the graph set motif  $R^2_3(9)$  (Table 2, Figure 3). The experimental PXRD patterns of **2a** and **2b** correspond well with the simulated data based on the single-crystal diffraction thereby supporting reasonable phase purities (Figure 4). Differences observed between experimental and simulated PXRD patterns are due to preferential orientations.

X-Ray analysis of the product **3** has confirmed the results of NMR analysis, namely that this is a 26-membered tetraaza macrocyclic system, being composed of two bicyclo[2.2.2]octene moieties, each of them fused with two succinimide rings; both these fragments are additionally connected with two  $-\text{[CH}_2\text{]}_6-$  tethers into the macrocyclic structure **3** (Figure 5). Macrocycle **3**·2DMF crystallizes in orthorhombic  $Pca n$  space group and the asymmetric unit

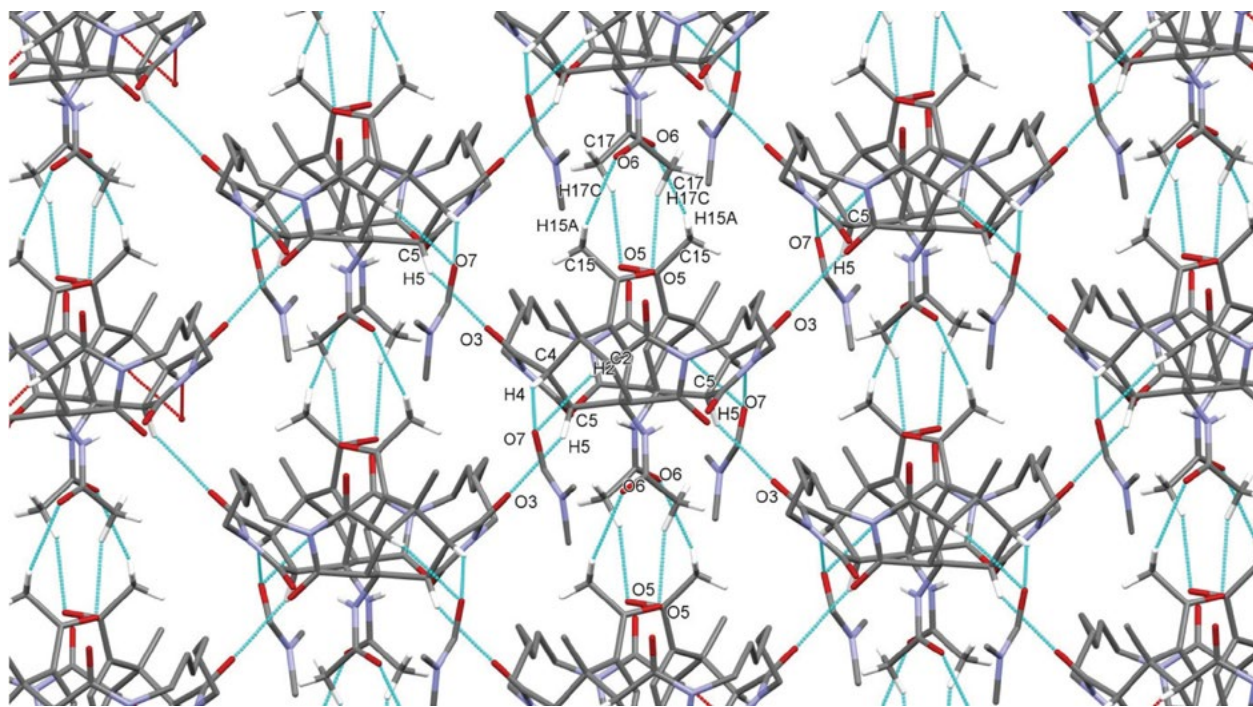
is composed of half of the macrocyclic molecule **3** (due to a 2-fold axis positioned in the middle of the macrocycle) and one solvate DMF molecule.

The two acetyl groups (attached to the bridging double bond of the bicyclo[2.2.2]octene fragments) are oriented towards each other (and also towards the interior of the cavity of the macrocycle **3**) therefore mostly filling it completely and thus presumably disabling the ability of **3** to be involved in the host–guest interactions. Furthermore, the

bowl-like shape macrocycle **3** is stabilized by two intramolecular N3–H3...O4 hydrogen bonds between the amide hydrogen of the acetylamino group attached to one bicyclo[2.2.2]octene fragment and one of the carbonyl groups of the succinimide ring fused to the other bicyclo[2.2.2]octene fragment with the graph set motif  $R_2^2(12)$ . Additionally, in the crystal structure **3**·DMF macrocyclic molecule is linked *via* C2–H2...O7 and C4–H4...O7 hydrogen bonding to DMF solvate molecule generating the graph set motif



**Figure 5.** Molecular structure of **3**. Probability ellipsoids are drawn at the 50% level (left). Solvate molecules have been removed for clarity. Intramolecular N–H...O hydrogen bonding indicated by blue dashed lines (right). Hydrogen atoms not involved in the motif shown have been omitted for clarity.



**Figure 6.** 2D layer formation in **3** generated by C–H...O hydrogen bonding (blue dashed lines). Hydrogen atoms not involved in the motif shown have been omitted for clarity.

$R_2^1(6)$ . Infinite 2D layer is formed due to C5–H5...O3, C15–H15A...O6 and C17–H17C...O5 hydrogen bonding with six adjacent macrocycle molecules generating the graph set motifs C(5), C(15),  $R_2^2(8)$  (Table 2, Figure 6).

## 4. Conclusion

Herein we describe a preparation of a novel 26-membered tetraaza heteromacrocyclic system **3** that was obtained *via* a direct method under solvent-free conditions with microwave irradiation starting from a substituted 5-acetyl-3-acetylamino-6-methyl-2*H*-pyran-2-one (**1**) and 1,1'-(hexane-1,6-diyl)bis(1*H*-pyrrole-2,5-dione) (**2**) acting as a double dienophile for the Diels–Alder cycloaddition. Single-crystal X-ray diffraction patterns of the dienophile **2** and macrocycle **3** were measured and have provided an important insight into their solid state structure. For compound **2** we have found two different polymorphic structures; for both the mode of packing and crystal architecture were determined. 2D layers are formed in both polymorphs facilitated by C2–H2...O2 and C3–H3...O2 hydrogen bonding between adjacent pyrrole-2,5-dione moieties with the graph set motifs  $R_2^2(8)$  and  $R_4^2(10)$  in **2a** and graph set motif  $R_3^2(9)$  in **2b**. Also for the macrocycle **3** we were able to confirm the other spectroscopic results therefore concluding that **3** is a 26-membered tetraaza macrocyclic system, composed of two bicyclo[2.2.2]octene fragments (each of them fused with two succinimide rings); both such units are connected into the heterocyclic ring via two  $-\text{[CH}_2\text{]}_6-$  tethers. Additionally, it was shown that both double-bond bridges of the two bicyclo[2.2.2]octene fragments are oriented towards the interior of the macrocycle's cavity, therefore presumably disabling the possibility for the host–guest interactions of **3**. The two bicyclo[2.2.2]octene parts of the bowl-like shaped macrocycle **3** are stabilized by two intramolecular N3–H3...O4 hydrogen bonds between the amide hydrogen of the acetylamino group attached to one bicyclo[2.2.2]octene fragment and one of the carbonyl groups of the succinimide ring fused to the other bicyclo[2.2.2]octene fragment. Infinite 2D layer is formed due to C5–H5...O3, C15–H15A...O6 and C17–H17C...O5 hydrogen bonding with six adjacent macrocycle molecules.

## 5. Supplementary Material

Crystallographic data of **2a**, **2b** and **3** were deposited in the Cambridge Crystallographic Data Center under the number CCDC 1547701–1547703. CIF files containing complete information on the studied structures may be obtained free of charge from the Director, CCDC, 12 Union Road, Cambridge, CB2 1EZ, UK, fax +44-1223-336033; e-mail: data\_request@ccdc.cam.ac.uk or from the following web site: www.ccdc.cam.ac.uk/data\_request/cif.

## 6. Acknowledgement

The authors thank the Ministry of Education, Science and Sport of the Republic of Slovenia and the Slovenian Research Agency for financial support (grant Nos. P1-0230-0103 and P1-0230-0175).

## 7. References

1. K. Josephson, A. Ricardo, J. W. Szostak, *Drug Discov. Today* **2014**, *19*, 388–399. DOI:10.1016/j.drudis.2013.10.011
2. H. Zhang, R. Zou, Y. Zhao, *Coord. Chem. Rev.* **2015**, *292*, 74–90. DOI:10.1016/j.ccr.2015.02.012
3. S. Collins, S. Bartlett, F. L. Nie, H. F. Sore, D. R. Spring, *Synthesis* **2016**, *48*, 1457–1473. DOI:10.1055/s-0035-1561414
4. B. K. Jena, G. S. Reddy, D. K. Mohapatra, *Org. Biomol. Chem.* **2017**, *15*, 1863–1871. DOI:10.1039/C6OB02435A
5. T. M. Brutsch, P. Bucher, K. H. Altmann, *Chem. Eur. J.* **2016**, *22*, 1292–1300. DOI:10.1002/chem.201504230
6. N. Uchida, R. X. Zhi, J. Kuwabara, T. Kanbara, *Tetrahedron Lett.* **2014**, *55*, 3070–3072. DOI:10.1016/j.tetlet.2014.03.126
7. L. R. Malins, J. N. deGruyter, K. J. Robbins, P. M. Scola, M. D. Eastgate, M. R. Ghadiri, P. S. Baran, *J. Am. Chem. Soc.* **2017**, *139*, 5233–5241.
8. L. A. Wessjohann, D. G. Rivera, O. E. Vercillo, *Chem. Rev.* **2009**, *109*, 796–814. DOI:10.1021/cr8003407
9. E. M. Driggers, S. P. Hale, J. Lee, N. K. Terrett, *Nat. Rev.* **2008**, *7*, 608–624.
10. B. Beck, G. Larbig, B. Mejat, M. Magnin-Lachaux, A. Picard, E. Herdtweck, A. Dömling, *Org. Lett.* **2003**, *5*, 1047–1050. DOI:10.1021/ol034077e
11. J. K. Sello, P. R. Andreatina, D. Lee, S. L. Schreiber, *Org. Lett.* **2003**, *5*, 4125–4127. DOI:10.1021/ol035773h
12. T. Pirali, G. C. Tron, J. Zhu, *Org. Lett.* **2006**, *8*, 4145–4148. DOI:10.1021/ol061782p
13. C. Hebach, U. Kazmaier, *Chem. Commun.* **2003**, 596–597. DOI:10.1039/b210952b
14. S. A. Dietrich, L. Banfi, A. Basso, G. Damonte, G. Guanti, R. Riva, *Org. Biomol. Chem.* **2005**, *3*, 97–106. DOI:10.1039/b414374d
15. Z. D. Ghezelbash, K. A. Dilmaghani, *Acta Chim. Slov.* **2016**, *63*, 790–797.
16. R. Vafazadeh, G. Zare-Sadrabadi, *Acta Chim. Slov.* **2015**, *62*, 889–894. DOI:10.17344/acsi.2015.1611
17. For a review on Diels–Alder reactions of 2*H*-pyran-2-one derivatives, see: K. Kranjc, M. Kočevar, *Arkivoc* **2013**, (*i*), 333–363.
18. V. Kepe, M. Kočevar, S. Polanc, B. Verček, M. Tišler, *Tetrahedron* **1990**, *46*, 2081–2088. DOI:10.1016/S0040-4020(01)89774-X
19. F. Požgan, K. Kranjc, V. Kepe, S. Polanc, M. Kočevar, *Arkivoc* **2007**, (*viii*), 97–111.

20. M. Kočevar, *Acta Chim. Slov.* **1996**, 43, 143–152 (*Chem. Abstr.* **1996**, 125, 576047).
21. F. Požgan, M. Krejan, S. Polanc, M. Kočevar, *Heterocycles* **2006**, 69, 123–132. DOI:10.3987/COM-05-S(O)1
22. M. P. Cava, A. A. Deana, K. Muth, M. J. Mitchell, *Org. Synth.* **1961**, 41, 93–95. DOI:10.15227/orgsyn.041.0093
23. S. Doi, Y. Takayanagi: Ion exchange resin catalysts for bismaleimide manufacture. JP 62221668 A, September 29, 1987.
24. Z. Otwinowski, W. Minor, *Methods Enzymol.* **1997**, 276, 307–326. DOI:10.1016/S0076-6879(97)76066-X
25. A. Altomare, M. C. Burla, M. Camalli, G. L. Casciarano, C. Giacovazzo, A. Guagliardi, A. G. G. Moliterni, G. Polidori, R. Spagna, *J. Appl. Cryst.* **1999**, 32, 115–119. DOI:10.1107/S0021889898007717
26. G. M. Sheldrick, *Acta Cryst.* **2015**, C71, 3–8.
27. L. Kukuljan, K. Kranjc, F. Perdih, *Acta Chim. Slov.* **2016**, 63, 905–913. DOI:10.17344/acsi.2016.2911
28. J. Suljagić, A. Juranovič, M. Krivec, K. Kranjc, M. Kočevar, *J. Heterocycl. Chem.* **2017**, 54, 457–464. DOI:10.1002/jhet.2603
29. M. Krivec, M. Gazvoda, K. Kranjc, S. Polanc, M. Kočevar, *J. Org. Chem.* **2012**, 77, 2857–2864. DOI:10.1021/jo3000783
30. K. Kranjc, F. Perdih, M. Kočevar, *J. Org. Chem.* **2009**, 74, 6303–6306. DOI:10.1021/jo9011199
31. K. Kranjc, M. Kočevar, F. Iosif, S. M. Coman, V. I. Parvulescu, E. Genin, J.-P. Genêt, V. Michelet, *Synlett* **2006**, 1075–1079.
32. M. Eto, K. Harano, T. Hisano, *J. Chem. Soc., Perkin Trans. 2* **1993**, 963–966. DOI:10.1039/P29930000963
33. K. Kranjc, M. Kočevar, *Curr. Org. Chem.* **2013**, 17, 448–456. DOI:10.2174/1385272811317050003
34. K. Kranjc, M. Kočevar, *Collect. Czech. Chem. Commun.* **2006**, 71, 667–678. DOI:10.1135/cccc20060667
35. F. H. Allen, O. Kennard, D. G. Watson, L. Brammer, A. G. Orpen, R. Taylor, *J. Chem. Soc., Perkin Trans. 2* **1987**, S1–S19. DOI:10.1039/p298700000s1
36. P. J. Cox, S. F. Parker, *Acta Cryst.* **1996**, C52, 2578–2580.
37. M. E. Light, I. E. D. Vega, P. A. Gale, CSD Communication (Private Communication), **2007**, refcode: TEKQAB01.
38. J. Bernstein, R. E. Davis, N. L. Shimoni, N.-L. Chang, *Angew. Chem., Int. Ed.* **1995**, 34, 1555–1573. DOI:10.1002/anie.199515551

## Povzetek

Z uporabo dvojnega dienofila 1,1'-(heksan-1,6-diil)bis(1*H*-pirol-2,5-diona) za [4+2] cikloadicijo s substituiranim 2*H*-pirol-2-onom smo z neposredno metodo brez uporabe topil pod pogoji obsevanja z mikrovalovi pripravili nov 26-členski tetraaza heteromakrociklični sistem **3**. Pripravljeni makrocikel je sestavljen iz dveh enot dienofila in dveh dienskih enot. Strukturo makrocikla smo ugotovili s pomočjo IR, <sup>1</sup>H in <sup>13</sup>C NMR ter masne spektroskopije, kot tudi z elementno analizo in določitvijo temperature tališča. Z rentgensko difrakcijo monokristala makrocikla smo ugotovili, da sta dve acetilni skupini (vezani na mostovno dvojno vez biciklo[2.2.2]oktenskoga fragmenta) v prostoru orientirani ena proti drugi (in hkrati tudi proti osrčju votline makrocikla) ter jo s tem bolj ali manj v celoti zapolnjujeta.

Scientific paper

# Iodine-catalyzed Transformation of Aryl-substituted Alcohols Under Solvent-free and Highly Concentrated Reaction Conditions

Marjan Jereb<sup>1,\*</sup> and Dejan Vražič<sup>2</sup><sup>1</sup> Chair of Organic Chemistry, Faculty of Chemistry and Chemical Technology, Večna pot 113, 1000 Ljubljana, Slovenia<sup>2</sup> Present address: Krka, d. d., Novo mesto, Šmarješka cesta 6, 8501 Novo mesto, Slovenia

\* Corresponding author: E-mail: marjan.jereb@fkkt.uni-lj.si

Tel.: (+386) 1 479 8577 Fax: (+386) 1 241 9144

Received: 18-09-2017

*Dedicated to Professor Emeritus Miha Tišler, University of Ljubljana, on the occasion of his 90<sup>th</sup> birthday.*

## Abstract

Iodine-catalyzed transformations of alcohols under solvent-free reaction conditions (SFRC) and under highly concentrated reaction conditions (HCRC) in the presence of various solvents were studied in order to gain insight into the behavior of the reaction intermediates under these conditions. Dimerization, dehydration and substitution were the three types of transformations observed with benzylic alcohols. Dimerization and substitution reactions were predominant in the case of primary- and secondary alcohols, whereas dehydration prevailed in the case of tertiary alcohols. The relative reactivity of substituted 1-phenylethanols in I<sub>2</sub>-catalyzed dimerization under SFRC provided a good Hammett plot  $\rho^+ = -2.8$  ( $r^2 = 0.98$ ), suggesting the presence of electron-deficient intermediates with a certain degree of developed charge in the rate-determining step.

**Keywords:** Alcohols, catalysis, green chemistry, Hammett correlation, iodine

## 1. Introduction

Green chemistry is currently a popular topic in chemistry. Numerous serious efforts have been made to improve and simplify existing methods and procedures, especially in terms of atom-economy, process-efficiency, health, risk and waste-minimization.<sup>1–3</sup> Transformations of neat reactants under solvent-free reaction conditions (SFRC) are one of the best solutions in this regard.<sup>4–7</sup> In the solid/solid system, a remarkable reaction rate enhancement was observed just by introducing small amounts of solvent vapor into the reaction mixture.<sup>8</sup> Moreover, the course of the reaction can be dramatically influenced under highly concentrated reaction conditions (HCRC).<sup>9</sup> It has been documented that water can remarkably affect the course of the reaction,<sup>10–12</sup> including enantioselectivity.<sup>13–15</sup> Water has become a reaction solvent of immense importance for the selectivity/reactivity studies of nucleophiles and electrophiles,<sup>16–18</sup> where carbocation intermediates play an important role.<sup>19–21</sup> Mixtures of water with organic

solvents have been employed to determine the geometry of the transition states,<sup>22</sup> with the hydrophobic effect attracting attention in studies of organic reactions in the presence of water.<sup>23–25</sup> In recent years, iodine<sup>26,27</sup> has emerged as remarkable catalyst exhibiting high water tolerance in diverse types of reactions. One of beneficial properties of iodine is its high affinity towards molecular oxygen as well as functional groups bearing at least one oxygen atom.<sup>28,29</sup> It has been established that iodine is an efficient catalyst for the transformation of alcohols under SFRC, with tertiary alcohols being dehydrated;<sup>30</sup> while primary and secondary transformed into ethers or esters.<sup>31–33</sup> This protocol has been already applied under various conditions<sup>34–36</sup> all indicating participation of the reaction intermediates having a partial positive charge. Recently, important mechanistic studies on the iodine-catalyzed reactions in solution have been published,<sup>37,38</sup> but the knowledge of the behavior of iodine under SFRC and HCRC remains largely undiscovered.<sup>39</sup>

The above reasons prompted us to investigate the reactivity of several model substrates in iodine-catalyzed transformations of alcohols under SFRC and HCRC. The alcohol substrates were selected to study different electronic effects and geometry. The role of the potentially present heteroatom and antiaromaticity of intermediates on transformations will be validated on sterically hindered dibenzo-substituted alcohols. Stereochemistry and regioselectivity of dehydration reactions and the role of the reaction medium polarity (protic *vs.* aprotic), nucleophilicity and  $pK_a$  under HCRC will be examined as well.

## 2. Experimental

### 2.1. General

1-Phenylethanol **1a**, 1,1-diphenylethanol **1d** and 4-methoxybenzyl alcohol **1m** are commercially available, the other alcohols were prepared by various methods. A) Modified Grignard procedure,<sup>40</sup> a typical experiment: under inert atmosphere, one crystal of iodine was added to magnesium turnings (60 mmol) in 5 mL of dry THF, and a few drops of the corresponding halogenide (PhCH<sub>2</sub>Cl, PhBr or EtI) (60 mmol). The rest of the halogenide was diluted with 25 mL of dry THF and slowly added at room temperature. The reaction mixture was refluxed for 90 minutes, then cooled to room temperature, diluted with 50 mL of dry THF and a solution of the appropriate carbonyl molecule (PhCOMe, Ph<sub>2</sub>CO, 4'-methoxyacetophenone, 2'-methoxyacetophenone, 4-methoxybenzaldehyde, 4,4'-dimethoxybenzophenone or 9-fluorenone) (20 mmol) in 50 mL of dry THF was slowly added and the reaction mixture was refluxed for two hours. After cooling, THF was evaporated and the reaction mixture diluted with Et<sub>2</sub>O and water. The organic phase was separated, washed with water, dried over anhydrous Na<sub>2</sub>SO<sub>4</sub>; the solvent evaporated and pure products were obtained after column chromatography or crystallization. Alcohols prepared by method A: 1,2-diphenyl-2-propanol<sup>41</sup> **1c**, 1,1-diphenyl-1-propanol<sup>42</sup> **1e**, 1-(4-methoxyphenyl)-2-phenylethanol<sup>43</sup> **1i**, 1-(4-methoxyphenyl)-1-phenylethanol<sup>44</sup> **1j**, 1-(2-methoxyphenyl)-1-phenylethanol<sup>45</sup> **1k**, 1,1-bis(4-methoxyphenyl)-2-phenylethanol<sup>46</sup> **1l**, 2-(4-methoxyphenyl)-1-phenyl-2-propanol<sup>47</sup> **1n**, 9-ethyl-9-fluorenone<sup>48</sup> **4a**, 9-benzyl-9-fluorenone<sup>49</sup> **4b** and 9-benzyl-9-xanthenol<sup>50</sup> **4f**. B) Na/RX/carbonyl molecule, a typical experiment: xanthone or dibenzosuberone (20 mmol) was dissolved in toluene (40 mL), followed by the addition of ethyl iodide or benzyl chloride (60 mmol) and sodium (120 mmol). The reaction mixture was refluxed for one hour, cooled to room temperature, diluted with toluene; water was added in small portions. The organic phase was separated, washed with water, dried over anhydrous Na<sub>2</sub>SO<sub>4</sub> and the solvent removed under reduced pressure. Alcohols prepared by method B: 5-ethyl-10,11-dihydro-5H-dibenzo[a,d]cyclohepten-5-ol **4c**, 9-ethyl-9-xanthenol<sup>51</sup> **4e**, and 5-benzyl-10,11-dihydro-5H-diben-

zo[a,d]cyclohepten-5-ol **4d**. C) By reduction of commercially available ketones with NaBH<sub>4</sub>: 1,2-diphenylethanol<sup>41</sup> **1b**, 1-(4-methoxyphenyl)ethanol<sup>52</sup> **1h**, 1-(4-fluorophenyl)ethanol<sup>52</sup> **1o**, 1-(3-methylphenyl)ethanol<sup>52</sup> **1p**, 1-(3-methoxyphenyl)ethanol<sup>52</sup> **1q**, 1-(4-chlorophenyl)ethanol<sup>52</sup> **1r**, 1-(4-bromophenyl)ethanol<sup>52</sup> **1s**. D) By reduction using Al-KOH:<sup>53</sup> Xanthydrol<sup>54</sup> **10**. E) By halohydroxylation:<sup>55,56</sup> 1,1-diphenyl-2-bromoethanol<sup>57</sup> **1f** and 1,1-diphenyl-2-fluoroethanol<sup>58</sup> **1g**. Pure products were usually obtained using column chromatography (CC) at given conditions using Fluka 60 silica gel (63–200 μm, 70–230 mesh ASTM). Reaction progress was monitored by thin-layer chromatography on Merck 60 F<sub>254</sub> TLC plates or by <sup>1</sup>H NMR spectroscopy. NMR spectra were recorded on Bruker Avance 300 DPX, and Bruker Avance III 500 Instrument (<sup>1</sup>H: 300 MHz, <sup>13</sup>C: 75.5 MHz and 125 MHz). The <sup>1</sup>H spectra were referred to an internal standard (0 ppm for TMS) or to the residual <sup>1</sup>H signal of CHCl<sub>3</sub> at 7.26 ppm. The <sup>13</sup>C spectra were referred to the central line of CDCl<sub>3</sub> (77.00 ppm). New compounds were characterized by <sup>1</sup>H NMR, <sup>13</sup>C NMR and IR spectroscopy, HRMS and/or elemental analysis, and also with the melting points when solid. Known products were characterized by <sup>1</sup>H NMR and IR spectroscopy, melting point when solid and by LRMS in most of the cases. Additionally, <sup>13</sup>C NMR spectra were recorded for those products, whose <sup>13</sup>C NMR data were not found in the literature. Melting points were determined on Büchi 535 apparatus and are not corrected. Mass spectra were obtained with the electron ionization (EI). Elemental combustion analyses were performed on Perkin-Elmer analyzer 2400 CHN.

### 2.2. General Procedure for Iodine-catalyzed Transformation of Alcohols Under SFRC

The procedure is the same for solid and liquid substrates. Alcohol (1 mmol) and iodine (3 mol%) were mixed together in a 5 mL conical reactor and the reaction mixture stirred at 25 °C or 55 °C for various times (5 min to 192 h), progress was monitored by TLC or by <sup>1</sup>H NMR spectroscopy. The crude reaction mixture was diluted with *tert*-butyl methyl ether, washed with an aqueous solution of Na<sub>2</sub>S<sub>2</sub>O<sub>3</sub>, water, dried over Na<sub>2</sub>SO<sub>4</sub> and the solvent evaporated under reduced pressure. The crude reaction mixture was subjected to column chromatography or preparative TLC using hexane or petroleum ether/*tert*-butyl methyl ether mixtures and pure product(s) were obtained. Conversions were determined by <sup>1</sup>H NMR spectroscopy. The effects of reaction variables on the type of transformation and conversions are stated in Tables and Figures. In order to obtain the information (role) of the reaction variables and structure of substrate, the data (reaction times with lower conversion) are presented in some Tables. In the experimental section, the best reaction conditions are named; 3 mol% of I<sub>2</sub> were used, giving the highest yield.

## 2. 3. General Procedure for Iodine-catalyzed Transformation of Alcohols Under HCRC

The procedure is the same for solid and liquid substrates. To the mixture of alcohol (1 mmol) and various amounts of solvent ( $\text{CH}_2\text{Cl}_2$ , MeOH, EtOH, *i*-PrOH, TFE, HFIP, HCOOH, AcOH and  $\text{H}_2\text{O}$  3–300 mmol) iodine (3 mol%) was added in 5 mL conical reactor and the reaction mixture stirred at 25 °C from five minutes to 360 hours. Isolation and purification procedure was the same as described above. Conversions were determined by  $^1\text{H}$  NMR spectroscopy. Results are presented in Tables, Figures and Schemes. Isolation procedure is given for the best yield.

## 2. 4. Determination of Hammett Reaction Constant $\rho^+$ for the $\text{I}_2$ -catalyzed Dimerization of 1-phenylethanols

1-phenylethanols (0.5 mmol) (**1a**, **1o**, **1p**, **1q**, **1r**, **1s**) were separately placed in the conical reactors, transformation was induced by iodine (0.015 mmol, 3.8 mg, 3 mol %) at 55 °C. Alcohols **1o** and **1p** were stirred for two hours, and alcohols **1q**, **1r** and **1s** were stirred for three hours. The transformation was stopped by cooling, the reaction mixture was analyzed by  $^1\text{H}$  NMR spectroscopy and relative rate constants calculated from the equation<sup>59</sup>  $k_r = k_A/k_B = \log((A - X)/A)/\log((B - Y)/B)$ , derived from the Ingold-Shaw relation<sup>60</sup> where *A* and *B* are the amounts of starting material and *X* and *Y* the amounts of products derived from them. The relative rate factors thus obtained, collected in Figure 1, are the averages of at least two measurements, giving a good reproducibility, deviation of  $k_{rel}$  ranged ( $\pm$  3%). The reaction of reference substrate 1-phenylethanol **1a** was quenched separately after 2 h and 3 h and relative rate constants were obtained by means of  $^1\text{H}$  NMR spectroscopy utilising internal standard 1,1-diphenylethane.

## 2. 5. Volumetric Determination of Iodine After the $\text{I}_2$ -catalyzed Reaction of **1n** Under HCRC in MeOH

To a mixture of 1-(4-methoxyphenyl)-2-phenylethanol-1-ol **1n** (1 mmol, 228 mg) and methanol (3 mmol, 96 mg) iodine (0.03 mmol, 7.6 mg) was added and the mixture stirred for 30 minutes at 25 °C. A reaction mixture was diluted with acetonitrile (5 mL) and titrated with a standard solution of  $\text{Na}_2\text{S}_2\text{O}_3$  ( $c = 0.1022$  mol/L,  $V = 0.58$  mL).

## 2. 6. Volumetric Determination of Iodine After the $\text{I}_2$ -catalyzed Reaction of **1n** Under HCRC in $\text{CH}_2\text{Cl}_2$

To a mixture of 1-(4-methoxyphenyl)-2-phenylethanol-1-ol **1n** (1 mmol, 228 mg) and dichloromethane (3

mmol, 255 mg) iodine (0.03 mmol, 7.6 mg) was added and the mixture stirred for 30 minutes at 25 °C. A reaction mixture was diluted with acetonitrile (5 mL) and titrated with a standard solution of  $\text{Na}_2\text{S}_2\text{O}_3$  ( $c = 0.1022$  mol/L,  $V = 0.57$  mL).

## 2. 7. Spectroscopic and Analytical Data of Novel Compounds

### Bis[1-(4-fluorophenyl)ethyl] ether **2o**

SFRC (r.t. = 4.5 h, 55 °C), CC ( $\text{SiO}_2$ , petroleum ether), colorless oil (90%), as a mixture of stereoisomers in ratio 1/0.39; IR (neat): 2976, 2930, 1604, 1508, 1371, 1224, 1156, 1091, 949, 836  $\text{cm}^{-1}$ ;  $^1\text{H}$  NMR (300 MHz,  $\text{CDCl}_3$ ):  $\delta$  7.23–7.12 (m, 8H), 7.05–6.87 (m, 8H), 4.42 (q,  $J = 6.4$  Hz, 2H), 4.13 (q,  $J = 6.5$  Hz, 2H, major), 1.41 (d,  $J = 6.4$  Hz, 6H), 1.32 (d,  $J = 6.5$  Hz, 6H, major);  $^{13}\text{C}$  NMR (75.5 MHz,  $\text{CDCl}_3$ ):  $\delta$  162.2 (d,  $J = 245$  Hz, 2C, major), 162.0 (d,  $J = 245$  Hz, 2C, minor), 139.8 (d,  $J = 3$  Hz, 2C, minor), 139.6 (d,  $J = 3$  Hz, 2C, major), 127.8 (d,  $J = 8$  Hz, 4C, major), 127.7 (d,  $J = 8$  Hz, 4C, minor), 115.3 (d,  $J = 22$  Hz, 4C, major), 115.0 (d,  $J = 22$  Hz, 4C, minor), 74.1 (minor), 73.9 (major), 24.7 (major), 23.1 (minor); MS  $m/z$  (EI): 262 ( $\text{M}^+$ , <1%), 247 (4), 123 (100), 103 (20); HRMS: Calcd for  $\text{C}_{16}\text{H}_{16}\text{F}_2\text{O}$  262.1169; found 262.1172.

### Bis[1-(3-methylphenyl)ethyl] ether **2p**

SFRC (r.t. = 4.5 h, 55 °C), CC ( $\text{SiO}_2$ , hexane/ $\text{CH}_2\text{Cl}_2$ ), colorless oil (87%), as a mixture of stereoisomers in ratio 1/0.37; IR (neat): 2973, 2924, 1607, 1487, 1447, 1368, 1160, 1092, 1034, 786, 705  $\text{cm}^{-1}$ ;  $^1\text{H}$  NMR (300 MHz,  $\text{CDCl}_3$ ):  $\delta$  7.22–6.93 (m, 16H), 4.42 (q,  $J = 6.4$  Hz, 2H), 4.14 (q,  $J = 6.5$  Hz, 2H, major), 2.36 (s, 6H, major), 2.30 (s, 6H, minor), 1.41 (d,  $J = 6.4$  Hz, 6H, minor), 1.32 (d,  $J = 6.5$  Hz, 6H, major);  $^{13}\text{C}$  NMR (75.5 MHz,  $\text{CDCl}_3$ ):  $\delta$  144.2, 144.2, 137.9, 137.7, 128.3, 128.1, 128.1, 127.8, 127.0, 126.9, 123.3, 123.3, 74.6 (major), 74.4 (minor), 24.7 (major), 22.9 (minor), 21.5 (major), 21.4 (minor); MS  $m/z$  (EI): 254 ( $\text{M}^+$ , <1%), 135 (23), 119 (100), 105 (13), 91 (16); HRMS: Calcd for  $\text{C}_{18}\text{H}_{22}\text{O}$  254.1671; found 254.1677. Anal. Calcd for  $\text{C}_{18}\text{H}_{22}\text{O}$ : C, 84.99; H, 8.72. Found: C, 84.65; H, 9.03.

### Bis[1-(4-bromophenyl)ethyl] ether **2s**

SFRC (r.t. = 18 h, 55 °C), CC ( $\text{SiO}_2$ , hexane), white solid (81%), as a mixture of stereoisomers in ratio 1/0.53; mp 68–74 °C; IR (neat):  $\text{cm}^{-1}$ ;  $^1\text{H}$  NMR (300 MHz,  $\text{CDCl}_3$ ):  $\delta$  7.45 (d,  $J = 8.4$  Hz, 4H), 7.38 (d,  $J = 8.4$  Hz, 4H), 7.11 (d,  $J = 8.4$  Hz, 4H), 7.09 (d,  $J = 8.4$  Hz, 4H), 4.42 (q,  $J = 6.4$  Hz, 2H, minor), 4.13 (q,  $J = 6.5$  Hz, 2H, major), 1.41 (d,  $J = 6.4$  Hz, 6H, minor), 1.32 (d,  $J = 6.5$  Hz, 6H, major);  $^{13}\text{C}$  NMR (75.5 MHz,  $\text{CDCl}_3$ ):  $\delta$  143.1, 142.9, 131.7, 131.4, 128.0, 127.9, 121.3, 121.0, 74.2, 74.2, 24.5 (major), 23.0 (minor); MS  $m/z$  (EI): 382 ( $\text{M}^+$ , 2%), 367 (5), 226 (6), 199 (21), 185 (100), 104 (35); HRMS: Calcd for  $\text{C}_{16}\text{H}_{16}\text{Br}_2\text{O}$  381.9568; found 381.9578.

**5-Ethyl-10,11-dihydro-5H-dibenzo[a,d]cyclohepten-5-ol 4c**

(20 mmol (4.17 g) dibenzosuberone, 120 mmol (2.76 g) Na, 60 mmol (9.36 g) EtI, 40 mL toluene, 1 h, reflux), CC (SiO<sub>2</sub>, CH<sub>2</sub>Cl<sub>2</sub>/petroleum ether, 1/4) and crystallization (petroleum ether), white solid (82%); mp 61.0–62.0 °C; IR (KBr): 3400, 2932, 1485, 1455, 1317, 1080, 1041, 965, 924, 889, 750 cm<sup>-1</sup>; <sup>1</sup>H NMR (300 MHz, CDCl<sub>3</sub>): δ 7.91–7.88 (m, 2H), 7.26–7.08 (m, 6H), 3.41–3.31 (m, 2H), 3.01–2.91 (m, 2H), 2.23 (q, *J* = 7.4 Hz, 2H), 2.14 (s, 1H), 0.69 (t, *J* = 7.4 Hz, 3H); <sup>13</sup>C NMR (75.5 MHz, CDCl<sub>3</sub>): δ 144.6, 138.8, 130.2, 127.2, 127.1, 126.1, 79.4, 38.2, 34.6, 8.8; MS *m/z* (EI): 237 (M<sup>+</sup> – H, 2%), 220 (1), 209 (100), 131 (26), 103 (26), 91 (15); Anal. Calcd for C<sub>17</sub>H<sub>18</sub>O: C, 85.67; H, 7.61. Found: C, 85.88; H, 7.83.

**5-Benzyl-10,11-dihydro-5H-dibenzo[a,d]cyclohepten-5-ol 4d**

(20 mmol (4.17 g) dibenzosuberone, 120 mmol (2.76 g) Na, 60 mmol (7.59 g) PhCH<sub>2</sub>Cl, 40 mL toluene, 1 h, reflux), CC (SiO<sub>2</sub>, CH<sub>2</sub>Cl<sub>2</sub>/petroleum ether, 1/4) and crystallization (petroleum ether), white solid (85%); mp 61.6–63.7 °C; IR (KBr): 3468, 2924, 1599, 1486, 1450, 1275, 1077, 1012, 766, 700, 673 cm<sup>-1</sup>; <sup>1</sup>H NMR (300 MHz, CDCl<sub>3</sub>): δ 7.73–7.70 (m, 2H), 7.19–7.04 (m, 9H), 6.73–6.70 (m, 2H), 3.47 (s, 2H), 3.46–3.37 (m, 2H), 3.07–2.97 (m, 2H), 2.32 (s, 1H); <sup>13</sup>C NMR (75.5 MHz, CDCl<sub>3</sub>): δ 143.9, 139.1, 136.2, 130.7, 130.0, 127.7, 127.6, 127.3, 126.5, 126.2, 79.1, 51.9, 35.1; MS *m/z* (EI): 300 (M<sup>+</sup> – H, 1%), 282 (<1), 209 (100), 131 (49), 103 (19), 91 (27); Anal. Calcd for C<sub>22</sub>H<sub>20</sub>O: C, 87.96; H, 6.71. Found: C, 87.84; H, 6.83.

**2-Methoxy-2-(4-methoxyphenyl)-1-phenylpropane 6na**

HCRC (MeOH, r.t. = 4 h, 25 °C), CC (SiO<sub>2</sub>, petroleum ether), colorless viscous oil (39%); IR (neat): 2937, 2824, 1610, 1510, 1455, 1371, 1299, 1249, 1088, 832, 701 cm<sup>-1</sup>; <sup>1</sup>H NMR (300 MHz, CDCl<sub>3</sub>): δ 7.18–7.13 (m, 5H), 6.87–6.82 (m, 4H), 3.81 (s, 3H), 3.08 (s, 3H), 3.02 (d, *J* = 13.1 Hz, 1H), 2.95 (d, *J* = 13.1 Hz, 1H), 1.46 (s, 3H); <sup>13</sup>C NMR (75.5 MHz, CDCl<sub>3</sub>): δ 158.5, 137.6, 136.2, 130.7, 127.9, 127.5, 126.0, 113.2, 79.5, 55.2, 50.7, 50.3, 21.3; MS *m/z* (EI): 224 (M<sup>+</sup> – MeOH, 88%), 209 (20), 165 (56), 133 (100), 128 (18). Anal. Calcd for C<sub>17</sub>H<sub>20</sub>O<sub>2</sub>: C, 79.65; H, 7.86. Found: C, 79.22; H, 7.87.

**2-Ethoxy-2-(4-methoxyphenyl)-1-phenylpropane 6nb**

(EtOH, 30 mmol, r.t. = 19 h, 25 °C), CC (SiO<sub>2</sub>, petroleum ether), viscous colorless oil (73%); IR (neat): 2975, 1609, 1510, 1454, 1300, 1250, 1179, 1091, 1034, 833, 702 cm<sup>-1</sup>; <sup>1</sup>H NMR (300 MHz, CDCl<sub>3</sub>): δ 7.13–7.07 (m, 5H), 6.83–6.80 (m, 2H), 6.75 (d, *J* = 8.8 Hz, 2H), 3.79 (s, 3H), 3.30 (dq, *J* = 14.2 Hz, *J* = 7.0 Hz, 1H), 3.09 (dq, *J* = 14.2 Hz, *J* = 7.0 Hz, 1H), 2.96 (d, *J* = 13.1 Hz, 1H), 2.87 (d, *J* = 13.1 Hz, 1H), 1.43 (s, 3H), 1.16 (t, *J* = 7.0 Hz, 3H); <sup>13</sup>C NMR (75.5 MHz, CDCl<sub>3</sub>): δ 158.4, 137.7, 137.0, 130.8, 127.7, 127.4, 126.0, 113.2, 79.1, 57.6, 55.2, 51.0, 21.8, 15.8; MS

*m/z* (EI): 225 (M<sup>+</sup> – OEt, 5%), 179 (100), 151 (41). Anal. Calcd for C<sub>18</sub>H<sub>22</sub>O<sub>2</sub>: C, 79.96; H, 8.20. Found: C, 79.75; H, 8.56.

**1,2-Diphenylethyl formate 7ba**

HCRC (HCOOH, without I<sub>2</sub>, r.t. = 23 h, 25 °C), CC (SiO<sub>2</sub>, petroleum ether), viscous colorless oil (81%); IR (neat): 3064, 3031, 2925, 1724, 1495, 1450, 1167, 755, 699 cm<sup>-1</sup>; <sup>1</sup>H NMR (300 MHz, CDCl<sub>3</sub>): δ 7.99 (s, 1H), 7.32–7.16 (m, 8H), 7.07–7.04 (m, 2H), 6.02 (dd, *J* = 7.7 Hz, *J* = 6.2 Hz, 1H), 3.21 (dd, *J* = 13.8 Hz, *J* = 7.7 Hz, 1H), 3.06 (dd, *J* = 13.8 Hz, *J* = 6.2 Hz, 1H); <sup>13</sup>C NMR (75.5 MHz, CDCl<sub>3</sub>): δ 160.1, 139.3, 136.6, 129.5, 128.4, 128.3, 128.2, 126.7, 126.6, 76.5, 42.8; MS *m/z* (EI): 180 (M<sup>+</sup> – HCOOH, 61%), 135 (50), 107 (100), 91 (44), 79 (86), 77 (50). Anal. Calcd for C<sub>15</sub>H<sub>14</sub>O<sub>2</sub>: C, 79.62; H, 6.24. Found: C, 79.66; H, 6.27.

**1-(4-Methoxyphenyl)-2-phenylethyl formate 7ia**

HCRC (HCOOH, without I<sub>2</sub>, r.t. = 30 min, 25 °C), preparative chromatography (SiO<sub>2</sub>, CH<sub>2</sub>Cl<sub>2</sub>), white solid (55%); mp 63.0–63.8 °C; IR (KBr): 2910, 2837, 1710, 1512, 1242, 1163, 1035, 977, 831, 734, 698 cm<sup>-1</sup>; <sup>1</sup>H NMR (300 MHz, CDCl<sub>3</sub>): δ 8.01 (s, 1H), 7.28–7.18 (m, 5H), 7.14–7.08 (m, 2H), 6.85 (d, *J* = 8.8 Hz, 2H), 6.02 (dd, *J* = 7.8 Hz, *J* = 6.2 Hz, 1H), 3.80 (s, 3H), 3.24 (dd, *J* = 13.8 Hz, *J* = 7.8 Hz, 1H), 2.82 (dd, *J* = 13.8 Hz, *J* = 6.2 Hz, 1H); <sup>13</sup>C NMR (75.5 MHz, CDCl<sub>3</sub>): δ 160.2, 159.5, 136.7, 131.4, 129.5, 128.3, 128.1, 126.6, 113.8, 76.3, 55.2, 42.6; MS *m/z* (EI): 256 (M<sup>+</sup>, 3%), 211 (10), 165 (91), 137 (100), 109 (20), 69 (27); HRMS: Calcd for C<sub>16</sub>H<sub>16</sub>O<sub>3</sub>: 256.1099; found 256.1102. Anal. Calcd for C<sub>16</sub>H<sub>16</sub>O<sub>3</sub>: C, 74.98; H, 6.29. Found: C, 74.71; H, 6.27.

**(E)-1,5-Diphenyl-4-methyl-2,4-di(4-methoxyphenyl)pent-1-ene 9a**

SFRC (r.t. = 30 min, 25 °C), CC and separation by preparative chromatography (SiO<sub>2</sub>, petroleum ether/*t*-butyl methyl ether = 97.5/2.5), white solid (23%), mp 92.7–94.6 °C; IR (KBr): 2932, 2834, 1607, 1510, 1454, 1290, 1248, 1180, 1034, 824, 699 cm<sup>-1</sup>; <sup>1</sup>H NMR (300 MHz, CDCl<sub>3</sub>): δ 7.31–7.19 (m, 3H), 7.16–7.10 (m, 4H), 7.05–6.97 (m, 3H), 6.87 (d, *J* = 8.8 Hz, 2H), 6.74 (d, *J* = 8.8 Hz, 2H), 6.67–6.57 (m, 4H), 6.54 (s, 1H), 3.78 (s, 3H), 3.75 (s, 3H), 3.24 (d, *J* = 13.9 Hz, 1H), 3.17 (d, *J* = 13.9 Hz, 1H), 2.83 (d, *J* = 13.1 Hz, 1H), 2.66 (d, *J* = 13.1 Hz, 1H), 0.92 (s, 3H); <sup>13</sup>C NMR (75.5 MHz, CDCl<sub>3</sub>): δ 158.4, 157.2, 141.0, 138.9, 138.6, 137.6, 131.4, 130.5, 128.9, 128.2, 128.1, 128.0, 127.3, 126.2, 125.7, 113.3, 112.8, 55.2, 55.1, 50.0, 43.0, 42.8, 23.3; MS *m/z* (EI): 448 (M<sup>+</sup>, <1%), 357 (<2), 225 (100), 91 (15). Anal. Calcd for C<sub>32</sub>H<sub>32</sub>O<sub>2</sub>: C, 85.68; H, 7.19. Found: C, 85.37; H, 7.38.

**(Z)-1,5-Diphenyl-4-methyl-2,4-di(4-methoxyphenyl)pent-1-ene 9b**

SFRC (r.t. = 30 min, 25 °C), CC and separation by preparative chromatography (SiO<sub>2</sub>, petroleum ether/*t*-



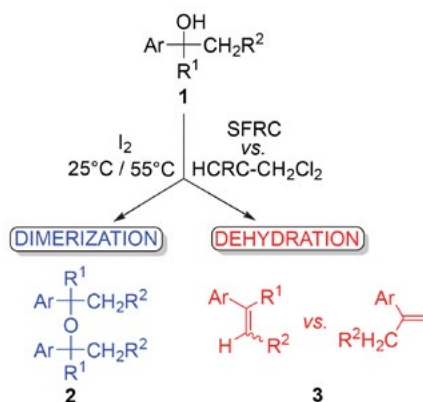
butyl methyl ether = 97.5/2.5), white solid (29%), mp 74.6–75.5 °C; IR (KBr): 2930, 2834, 1607, 1510, 1454, 1288, 1247, 1180, 1033, 826, 699  $\text{cm}^{-1}$ ;  $^1\text{H}$  NMR (300 MHz,  $\text{CDCl}_3$ ):  $\delta$  7.08–6.99 (m, 8H), 6.85–6.63 (m, 9H), 6.15 (s, 1H), 3.78 (s, 3H), 3.75 (s, 3H), 3.06 (d,  $J = 13.1$  Hz, 1H), 3.02 (d,  $J = 13.1$  Hz, 1H), 2.85 (d,  $J = 13.1$  Hz, 1H), 2.78 (d,  $J = 13.1$  Hz, 1H), 1.12 (s, 3H);  $^{13}\text{C}$  NMR (75.5 MHz,  $\text{CDCl}_3$ ):  $\delta$  158.1, 157.3, 139.6, 138.6, 138.4, 137.7, 134.3, 130.5, 130.0, 128.9, 128.2, 127.7, 127.3, 125.9, 125.8, 113.5, 112.9, 55.2, 55.1, 53.6, 50.4, 42.9, 23.3; MS  $m/z$  (EI): 448 ( $\text{M}^+$ , <1%), 357 (1), 225 (100), 91

(17). Anal. Calcd for  $\text{C}_{32}\text{H}_{32}\text{O}_2$ : C, 85.68; H, 7.19. Found: C, 85.52; H, 7.44.

### 3. Results and Discussion

Most of the published  $\text{I}_2$ -catalyzed transformations of alcohols were conducted in relatively diluted solution, in a concentration range of 23 mol to 157 mol of solvent per mol of alcohol.<sup>61,62</sup> In contrast, we examined the behavior of substituted benzylic alcohols in highly-concentrated

**Table 1.** The effect of the alcohol structure **1** and reaction conditions (SFRC vs. HCRC) on the type of iodine-induced transformation



Entry	Alcohol			Reaction conditions <sup>a</sup> and time	Conversion <sup>b</sup> [%]	Dimerization / Dehydration		
	Ar	R <sup>1</sup>	R <sup>2</sup>			2	3	
1	Ph	H	H	<b>a</b>	A, 165 h	38	100	
2					B, 165 h	90	100	
3	Ph	H	Ph	<b>b</b>	A, 67 h	88	81	19
4					B, 67 h	10	100	
5	Ph	CH <sub>3</sub>	Ph	<b>c</b>	A, 20 h	100		100 <sup>c</sup>
6					B, 48 h	100		100 <sup>d</sup>
7	Ph	Ph	H	<b>d</b>	A, 10 min	100		100
8					B, 1 h	97		100
9	Ph	Ph	CH <sub>3</sub>	<b>e</b>	A, 3 h <sup>e</sup>	100		100
10					B, 1 h	10		100
11	Ph	Ph	Br	<b>f</b>	A, 96 h <sup>e</sup>	98		100
12					B, 1 h	0		
13	Ph	Ph	F	<b>g</b>	A, 192 h <sup>e</sup>	57		100
14					B, 1 h	0		
15	<i>p</i> -An	H	H	<b>h</b>	A, 15 min	92	100	
16					B, 15 min	92	100	
17	<i>p</i> -An	H	Ph	<b>i</b>	A, 230 min	100	73	27
18					B, 1 h	95	100	
19	<i>p</i> -An	Ph	H	<b>j</b>	A, 5 min	100		100
20					B, 5 min	100		100
21	<i>o</i> -An	Ph	H	<b>k</b>	A, 15 min	100		100
22					B, 15 min	100		100
23	<i>p</i> -An	<i>p</i> -An	Ph	<b>l</b>	A, 200 min	31		100
24					B, 200 min	100		100

<sup>a</sup> A: SFRC; 1 mmol of **1** and 0.03 mmol of  $\text{I}_2$ ; B: HCRC; 1 mmol of **1**, 3 mmol of  $\text{CH}_2\text{Cl}_2$  and 0.03 mmol of  $\text{I}_2$ . <sup>b</sup> Conversion and product distribution determined by  $^1\text{H}$  NMR spectroscopy. <sup>c</sup> 4% of (*Z*)-isomer relatively to (*E*)-alkene, traces of the Hofmann alkene. <sup>d</sup> 5% of (*Z*)-isomer relatively to (*E*)-alkene, Zaitsev vs. Hofmann = 85/15. **1c** remained intact without iodine under conditions A and B. <sup>e</sup> Reaction temperature was 55 °C, in all other cases was 25 °C.

reaction medium, that contained only 3 mol of solvent per mol of the reactant. Various substituted secondary and tertiary benzylic alcohols **1a–l**, possessing different structural features were selected as substrates (Scheme 1). Groups Ar, R<sup>1</sup>, and R<sup>2</sup> having electron-releasing substituents should enhance the stability of electron-deficient intermediates, whereas β-halogen atom R<sup>2</sup> in **1f** and **1g** should increase the acidity of the methylene protons. The results of the iodine catalyzed transformation under SFRC and HCRC with alcohols **1a–l** are summarized in Table 1 indicating that tertiary alcohols underwent dehydration, while secondary alcohols predominantly dimerized into ether derivatives **2**. The aggregate state of alcohols played an important role; reaction mixtures in the case of solid alcohols **1** became pasty, which proved to be essential for the reaction progress. On the other hand, liquid alcohols were less challenging in terms of their aggregate state. 1-Phenylethanol **1a** yielded exclusively ether **2a** under both types of the reaction conditions (entries 1 and 2, A=SFRC, B=HCRC-CH<sub>2</sub>Cl<sub>2</sub>). Introduction of an additional phenyl group at C-2 (**1b**) increased the reactivity affording dimer **2b** as the major product (81%), and *trans*-stilbene (19%) as the sole dehydration product (entry 3). Enhanced reactivity of **1b** could be ascribed to the stabilizing effect of the additional phenyl group. A remarkable decrease in reactivity was observed for fluoro-substituted analogues of **1a**: 1-(2,3,4,5,6-pentafluorophenyl)ethanol and 1-phenyl-2,2,2-trifluoroethanol remained intact after three days at 85 °C under SFRC.

Tertiary alcohols **1c**, **1d** and **1e** only underwent dehydration into alkene **3** (Table 1, entries 5–10). A mixture of (*Z*)- and (*E*)-1,2-diphenylpropene was formed from **1c**,

with the latter being the major product. The transformation of **1c** was accompanied by the formation of 2,3-diphenyl-1-propene (entries 5 and 6). **1c** remained intact without iodine under conditions A and B, signifying the role of iodine. The role of acidity of the hydroxyl group and the C-2 hydrogen atom of C-2 halogenated tertiary alcohols **1f** and **1g** in I<sub>2</sub>-catalyzed transformation was examined (Table 1, entries 11–14).

Reactivity was diminished in both cases, but fluoro derivative **1g** (entry 13) reacted considerably more sluggishly than the bromo analogue **1f** (entry 11), suggesting the ease of the proton removal from C-2 not being the most crucial in the process of dehydration, but the electron-accepting properties of the halomethyl group on the stability of the electron-deficient reaction intermediates. The introduction of methoxy group to the aromatic ring did not alter the reaction pathway in the case of 1-(4-methoxyphenyl)ethanol **1h**, but dimerization was remarkably faster than with 1-phenylethanol **1a** (entries 15 and 16). A similar enhancement of reactivity, induced by methoxy group, was observed also in the case of 1-(4-methoxyphenyl)-2-phenylethanol **1i**; dimerization was the major process, the proportion of the dehydration grew to 27% (Table 1, entry 17) when compared with **1b** (entry 3) under SFRC. Interestingly, **1i** gave dimeric ether **2i** as the sole product under HCRC (entry 18). Tertiary alcohols **1j** and **1k** underwent dehydration, while position of the methoxy group (*p*-MeO vs. *o*-MeO) did not play a substantial role on the type of transformation and reaction rate (entries 19–22). The substantially lower reactivity of triaryl-substituted alcohol **1l** could be ascribed to the fact that substrate has the highest melting point and the lowest solubility

**Table 2.** The effects of geometry, ring size and substituents on the iodine-catalyzed dehydration of tertiary alcohols **4**



Entry	Alcohol		4	Reaction time <sup>a</sup>	Conversion [%] <sup>b</sup>
	Y	R			
1	/	CH <sub>3</sub>	<b>a</b>	15 min	3
2	/	Ph	<b>b</b>	23 h	100
3	/	Ph	<b>b</b>	15 min	0
4	/	Ph	<b>b</b>	96 h	0
5	CH <sub>2</sub> CH <sub>2</sub>	CH <sub>3</sub>	<b>c</b>	15 min	79
6	CH <sub>2</sub> CH <sub>2</sub>	CH <sub>3</sub>	<b>c</b>	154 min	100
7	CH <sub>2</sub> CH <sub>2</sub>	Ph	<b>d</b>	15 min	35
8	CH <sub>2</sub> CH <sub>2</sub>	Ph	<b>d</b>	154 min	100
9	O	CH <sub>3</sub>	<b>e</b>	15 min	67
10	O	CH <sub>3</sub>	<b>e</b>	60 min	100
11	O	Ph	<b>f</b>	15 min	65
12	O	Ph	<b>f</b>	30 min	100

<sup>a</sup> Reaction conditions: 1 mmol of **4**, 3 mmol of CH<sub>2</sub>Cl<sub>2</sub> and 0.03 mmol of I<sub>2</sub> stirred at 25 °C. <sup>b</sup> Determined by <sup>1</sup>H NMR spectroscopy.

among alcohols **1**, and the reaction mixture required a longer time to become pasty under SFRC (31% conversion, entry 23). In spite of the poor solubility of **11** in  $\text{CH}_2\text{Cl}_2$ , enhanced molecular migration was achieved, reflecting in a considerably higher degree of conversion under HCRC (entry 24). In general, the reactivity of the secondary and the tertiary alcohols differs drastically regardless on the conditions SFRC or HCRC. The secondary alcohols have a strong tendency of dimerization into ethers, while the tertiary alcohols underwent dehydration into alkenes. Such a clear-cut might be surprising; however, it could be somehow anticipated.<sup>31</sup> One of the reasons for smooth dehydration of the tertiary-, in comparison with the secondary alcohols, might be the formation of the thermodynamically more stable alkenes. In addition, dimerization of the sterically hindered tertiary alcohols is disfavored. It could be concluded that substantially higher reactivity of methoxy-substituted alcohols (Table 1, entries 15–24) is likely a consequence of stabilization of the intermediates involved – the electron deficient species. Furthermore, we examined the role of geometry, ring size and heteroatom on  $\text{I}_2$ -catalyzed transformation of the dibenzo-substituted tertiary alcohols **4** under HCRC- $\text{CH}_2\text{Cl}_2$ ; the results are collected in Table 2.

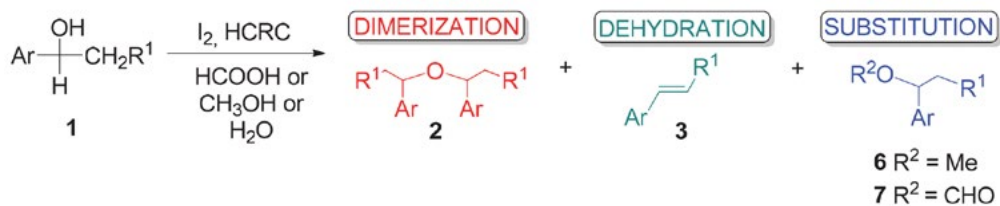
Fluorene derivative **4a** yielded 9-ethylidene fluorene **5a** (Table 2, entries 1 and 2) but phenyl-substituted derivative **4b** was not reactive under these conditions (entries 3 and 4). The low reactivity of **4a** and **4b** might be associated with the geometry and formation of the potential anti-aromatic fluorenyl carbocation.<sup>31,63,64</sup> Dibenzosuberan deriva-

tives **4c** and **4d** are not planar and were considerably more reactive than **4a** an additional phenyl group did not enhance the reactivity of **4d**. The substitution of a  $\text{CH}_2\text{CH}_2$  group in the dibenzosuberan derivative with an O-atom decreased the reactivity of 9-ethyl-xanthen-9-ol **4e**, while phenyl derivative **4f** was more reactive than **4e**. The results showed the importance of the geometry of the structure of the electron-deficient intermediates in dehydration reactions under HCRC.

Further, we examined the role of nucleophilic, protic solvents (possessing different acidity, ionizing power, hydrophobicity, and solubility of **1** and  $\text{I}_2$ ) on iodine-catalyzed transformations of secondary benzylic alcohols under HCRC (Table 3).

Three reaction pathways were operative: dimerization, dehydration and substitution. The important role of solvent added on the type of transformation was demonstrated on 1,2-diphenylethanol **1b** (entries 1–4). No reaction took place in MeOH, in the presence of HCOOH, only substitution occurred yielding **7ba** (entry 3); in contrast, in the presence of  $\text{H}_2\text{O}$ , dimerization was the dominant process (entry 4). Substrate **1b** is considerably hydrophobic and does not possess a strong electron-donating group, which is reflected in its relatively low reactivity. Introduction of methoxy group to the *para* position of the phenyl ring remarkably enhanced the reactivity and selectivity of reaction of 1-(4-methoxyphenyl)-2-phenylethanol **1i** under HCRC (entries 5–8); contrary to **1b**, in the case of MeOH, the methyl ether **6ia** was obtained. Another surprising difference was established in the presence of

**Table 3.** The effect of hydroxy-substituted solvent on the iodine-catalyzed transformations of alcohols **1** under HCRC



Entry	Alcohol		1	Reaction conditions <sup>a</sup>	Conversion [%] <sup>b</sup>	Product distribution <sup>c</sup>		
	Ar	R <sup>1</sup>				2	3	6/7
1	Ph	Ph	<b>b</b>	$\text{CH}_2\text{Cl}_2$ / 67 h	10	100		
2				MeOH / 67 h	0			
3				HCOOH / 23 h	89			100
4				$\text{H}_2\text{O}$ / 67 h	14	90	10	
5	<i>p</i> -An	Ph	<b>i</b>	$\text{CH}_2\text{Cl}_2$ / 60 min	97	100		
6				MeOH / 20 h	100		5	95
7				HCOOH / 30 min	100	87		13 <sup>d</sup>
8				$\text{H}_2\text{O}$ / 230 min	100	88	12	
9	<i>p</i> -An	H	<b>h</b>	$\text{CH}_2\text{Cl}_2$ / 15 min	92	100		
10				MeOH / 180 min	95	5		95
11				HCOOH / 30 min	98	8		92
12				$\text{H}_2\text{O}$ / 15 min	96	100		

<sup>a</sup> 1 mmol of **1**, 3 mmol of solvent and 0.03 mmol of  $\text{I}_2$  stirred at 25 °C. <sup>b</sup> Conversion and product distribution determined by <sup>1</sup>H NMR spectroscopy.

<sup>c</sup> Dimerization vs. Dehydration vs. Substitution. <sup>d</sup> A ratio 2/7 without  $\text{I}_2$  was 23/77.

HCOOH, where dimerization was the main process (entry 7), while transformation without  $I_2$  furnished a mixture of **2i** and **7ia** in reversed ratio (23/77). The contrasting result suggests that iodine activated **1i**. Results of reactivity of **1i** (entries 5–8) suggest that iodine activated **1i** which dimerized predominantly in the absence of good nucleophiles (entries 5, 7 and 8). In the presence of MeOH, a methoxy ether **6ia** was the major product (entry 6), while a small extent of dehydration was observed in the cases of 1,2-diaryl-substituted alcohols only. 1-(4-methoxyphenyl) ethanol **1h**, the least hydrophobic and sterically-hindered in this series, was the most reactive (entries 9–12), but with altered selectivity. In the presence of  $CH_2Cl_2$  and  $H_2O$ , dimerization took place (entries 9 and 12), while substitution was the main process in the presence of MeOH and HCOOH, giving **6ha** and **7ha**, respectively (entries 10 and 11). **1h** was esterified with HCOOH under SFRC without iodine,<sup>32</sup> thus signifying the role of  $pK_a$ , and iodine has little influence on reaction of **1h** with HCOOH (entry 11). The reactivity pattern of **1h** is similar to **1i**, where substitution predominantly took place in the presence of relatively good nucleophiles, whereas dimerization is prevalent in their absence.

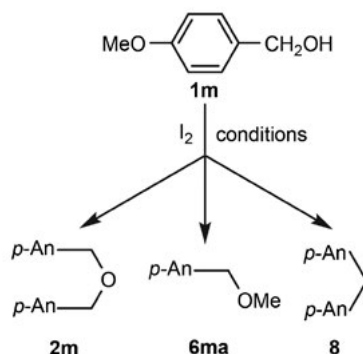
The alcohols and alkenes substituted with electron rich-aromatic groups might be sensitive to polymerization and are known to undergo different types of transformation. Indeed, 4-methoxybenzyl alcohol **1m** proved to be the right target in this regard (Table 4); under SFRC, dimerization giving **2m** was the main process (entry 1), *ipso*-substitution also took place, however polymerization completely prevailed after 200 minutes producing tar material only. Similar product distribution was obtained under HCRC- $CH_2Cl_2$  (entry 2). No other alkylation of the aromatic ring was noted.

The third reaction channel was substitution; it occurred in the presence of MeOH giving **6ma**, and a small proportion of dimer **2m** was also formed, but no polymerization was noted, even after 190 hours (entry 3). Dimerization was the main process in the absence of a nucleophile, and *ipso*-substitution appeared as minor, but additional reaction channel. Considering that *ipso*-substitution is often related with cationic intermediates,<sup>65</sup> it could be assumed that formation of **8** is another suggestion of involvement of electron-deficient intermediates.

Next, we studied the transformation of sterically hindered and hydrophobic tertiary alcohol with the electron-rich aromatic ring, 1-phenyl-2-(4-methoxyphenyl)-2-propanol **1n** in the presence of a catalytic amount of iodine (Table 5).

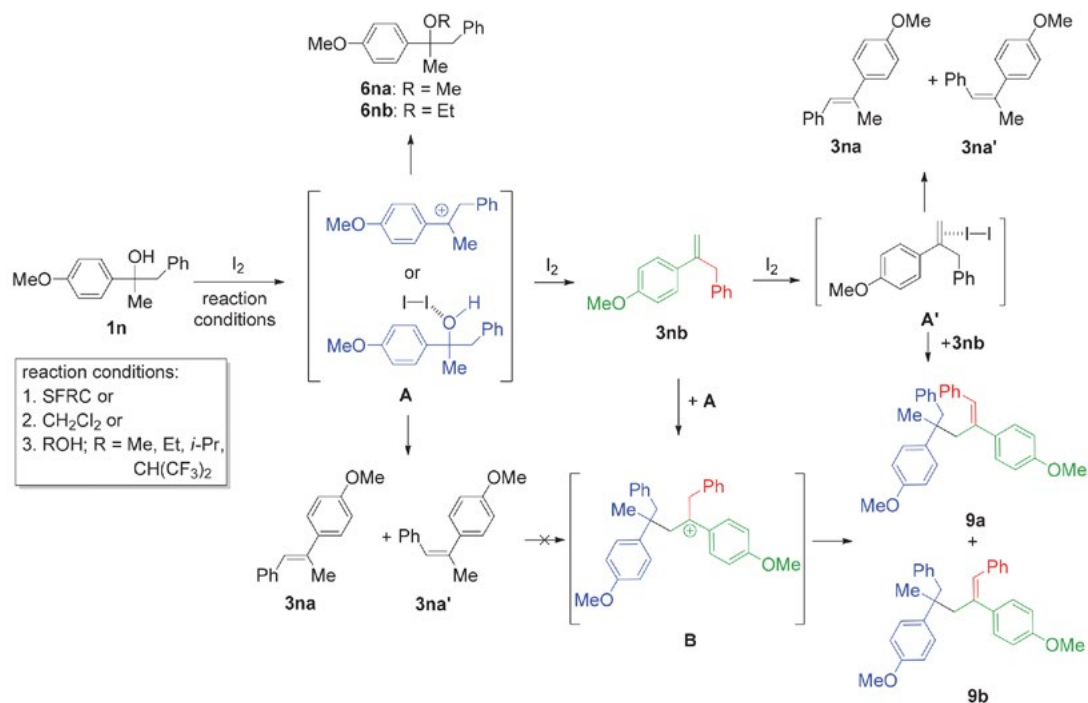
**1n** is a substrate of choice because it possesses an activated aromatic ring for good reactivity and it could form a well stable potential intermediate to study its fate under SFRC and HCRC. Reaction mixture after 30 minutes at room temperature under SFRC contained at least three products. The major product was easily identified as the Zaitsev-type product, (*E*)-2-(4-methoxyphenyl)-1-phenyl-1-propene **3na** (entry 1). However, the two other products had very similar physicochemical properties, reflecting in almost identical retention factors; the molecular mass of 448 indicated that dimerization occurred. The structures of these two alkenes were elucidated on the basis of 1D and 2D NMR spectra and identified as (*E*)-1,5-diphenyl-4-methyl-2,4-bis(4-methoxyphenyl)pent-1-ene **9a** and its (*Z*)-isomer **9b**. The explanation of the formation of these two alkenes is presented in Table 5. The results suggest that iodine likely induced the formation of tertiary electron-deficient intermediate or related species, probably similar to the intermediate **A**; its subsequent dehydra-

**Table 4.** The effect of the reaction conditions on the iodine-catalyzed transformation of 4-methoxybenzyl alcohol



Entry	Reaction conditions <sup>a</sup>	Conversion [%] <sup>b</sup>	Dimerization / Ipso / Substitution <sup>c</sup>		
			2m	/	8 / 6ma
1	SFRC / 150 min	54	82	/	8
2	HCRC- $CH_2Cl_2$ / 150 min	37	86	/	14
3	HCRC-MeOH / 190 h	91	10	/	90

<sup>a</sup>SFRC: 1 mmol of **1m** and 0.03 mmol of  $I_2$ , HCRC: 1 mmol of **1m**, 3 mmol of solvent and 0.03 mmol of  $I_2$  stirred at 25 °C. <sup>b</sup>Conversion and product distribution determined by  $^1H$  NMR spectroscopy. <sup>c</sup>Dimerization vs. *Ipso* substitution vs. Substitution.

Table 5. The effect of the reaction conditions on the iodine-catalyzed transformations of **1n**

Entry	Reaction conditions <sup>a</sup>	Conversion [%] <sup>b</sup>	3na'+3na <sup>c</sup>	3nb	Product distribution		
					9a	9b	6 <sup>d</sup>
1	SFRC	100	57		23	20	
2	CH <sub>2</sub> Cl <sub>2</sub> -3 mmol	100	58		21	21	
3	CH <sub>2</sub> Cl <sub>2</sub> -30 mmol	98	70	12	8	10	
4	CH <sub>2</sub> Cl <sub>2</sub> -300 mmol	0					
5	MeOH-3 mmol	78	30	15			55
6	MeOH-30 mmol	68					100
7	MeOH-300 mmol	0					
8	EtOH-3 mmol	61	44	23			33
9	(CH <sub>3</sub> ) <sub>2</sub> CHOH-3 mmol	77	67	33			
10	(CF <sub>3</sub> ) <sub>2</sub> CHOH-3 mmol	100	72		14	14	

<sup>a</sup> SFRC; 1 mmol of **1n** and 0.03 mmol of I<sub>2</sub>, HCRC; 1 mmol of **1n**, 3, 30 or 300 mmol of solvent and 0.03 mmol of I<sub>2</sub> stirred at 25 °C for 30 min.

<sup>b</sup> Conversion determined by <sup>1</sup>H NMR spectroscopy. <sup>c</sup> Data refer to the sum of **3na** and **3na'**, with (E)/(Z) = 95/5 (entries 1, 5, 8–10) and (E)/(Z) = 90/10 in entries 2 and 3. <sup>d</sup> Methoxy ether **6na** in the case of MeOH and ethoxy ether **6nb** in the case of EtOH were formed.

tion predominantly led to the mixture of (Z)- and (E)-2-(4-methoxyphenyl)-1-phenyl-1-propene **3na** and **3na'**, the Hofmann type dehydration furnished 2-(4-methoxyphenyl)-3-phenyl-1-propene **3nb**. However, the latter **3nb** was not stable under the studied conditions and further attacked primarily formed species **A**, resulting in a cationic-like intermediate **B** or a related species, and removal of the benzylic proton furnished the isomeric alkenes **9a** and **9b**. Continuing, we examined the effect of 3 mmol of CH<sub>2</sub>Cl<sub>2</sub> on the transformation of 1 mmol of **1n**. The added solvent had no significant impact on the type of transformation (entry 2). Alkene **3nb** was isolated and treated in an independent experiment with 3 mol% of I<sub>2</sub> in dichloromethane until the full consumption of **3nb**. Alkenes **3na**, **3na'**, **9a** and **9b** were formed in this process potentially via **A'**. **A** could furnish **3na** and **3na'** or it could add to

the rest of **3nb** producing **9a** and **9b**. In contrast, an independent transformation of a mixture of the isolated alkenes **3na** and **3na'** with 3 mol% of I<sub>2</sub> failed, since **3na** and **3na'** remained intact. Alkenes **3na** and **3na'** are thermodynamically more stable than **3nb** and were not be activated by iodine. In contrast, a larger amount (30 mmol) of CH<sub>2</sub>Cl<sub>2</sub> suppressed addition of the species **A** to alkene **3nb** and favored the formation of the Zaitsev type product **3na** (entry 3). Interestingly, **1n** remained unreacted in a highly diluted solution of 300 mmol of dichloromethane (entry 4). It is obvious that the vicinity of the reacting species is of the prime importance, demonstrating a crucial role of the concentration. In the presence of 3 mmol of MeOH, dehydration and substitution processes were observed, giving alkenes **3na**, **3na'** and **3nb** and methoxy ether **6na** (entry 5). Methanol blocked the addition of **A** to alkene **3nb**, the

selectivity Zaitsev vs. Hofmann decreased (entry 5) in comparison with the entries 1–3. Turnover in transformation occurred in the presence of a 10-fold higher amount of MeOH, and only ether **6na** was obtained (entry 6); no reaction took place in the presence of 300 mmol of methanol (entry 7). In the presence of 3 mmol of ethanol (entry 8), the same reaction pathways were observed as in the presence of methanol (entry 5). In the presence of *i*-PrOH and (CF<sub>3</sub>)<sub>2</sub>CHOH (HFIP), no substitution occurred (entries 9 and 10); the Zaitsev alkene was more favored than in EtOH (entry 8), and finally reached 72% in the presence of HFIP, where alkene **3nb** was further transformed to **9a** and **9b** (entry 10). It could be concluded that dehydration and further reaction of the formed intermediates took place under SFRC and HCRC in the presence of a non-nucleophilic solvent (CH<sub>2</sub>Cl<sub>2</sub>) and HFIP. The latter solvent is known to stabilize the carbocationic intermediates,<sup>66,67</sup> and this could be an indication that our intermediates may be similar. The competition between dehydration and substitution took place under HCRC (3 mmol of alcohol, entries 5 and 8) in a nucleophilic solvent (MeOH and EtOH), while in the presence of 30 mmol of methanol, substitution took place exclusively. It is noteworthy to say that certain processes take place under SFRC and HCRC, but not under classical diluted conditions in a solution – the formation of **9a** and **9b** is such an example.

4-methoxybenzyl alcohol **1m** proved to be very reactive substrate under the studied conditions, and it tended to yield insoluble, probably polymerized products after prolonged reaction time. Consequently, we decided to explore the reactivity of exceedingly acid sensitive 9*H*-xanthene-9-ol **10** in the presence of catalytic amount of I<sub>2</sub> (Table 6).

Alcohol **10** was found to be very reactive; the reaction under SFRC was accomplished in 15 minutes at room temperature in spite of a solid reactant and catalyst. To our surprise, disproportionation took place giving the product

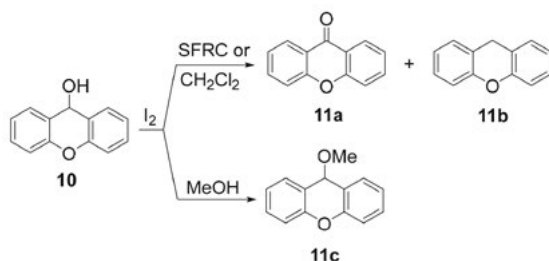
**11a** and **11b** as the only products (entry 1). Similar observation could be made in detritylation of ethers using I<sub>2</sub> in methanol.<sup>68</sup> We published a detailed iodine-catalyzed disproportionation of ethers under SFRC.<sup>39</sup> Disproportionation took place also in the presence of dichloromethane under HCRC, and it was even faster probably due to the higher migration of the reactants (entry 2). Transformation of **10** under HCRC in the presence of MeOH yielded the related methoxy ether **11c**, a very acid sensitive compound, too (entry 3).

In order to obtain information about the role of geometry (cyclic 9-xanthhydrol vs. acyclic diphenyl methanol) and substituents, the transformation of diphenyl methanol and bis(4-methoxyphenyl)methanol was studied under HCRC-CH<sub>2</sub>Cl<sub>2</sub>. Only dimerization took place, and no disproportionation was noted. Dimerization of bis(4-methoxyphenyl)methanol to bis[bis(4-methoxyphenyl)methyl] ether occurred in five minutes, while bis(diphenylmethyl) ether was obtained in 71% yield after two days at room temperature. In MeOH, substitution took place, and bis(4-methoxyphenyl)methyl methyl ether was formed in 77% yield. Diphenyl methanol yielded the corresponding methyl ether as the main product, and a small amount of bis(diphenylmethyl)ether. Bis(pentafluorophenyl)methanol was found inert in the I<sub>2</sub>-catalyzed reaction; no conversion was noted after two days at 85 °C under SFRC. It can be concluded that reactivity is essentially dependent on the structure and geometry of the alcohol; the electron-accepting groups tend to disfavor the transformation.

4-Methoxyphenyl-substituted alcohols **1m** and **1h** were proved very sensitive to the reaction conditions; for that reason, we investigated the role of *p*K<sub>a</sub> of alcohols added under HCRC, Table 7.

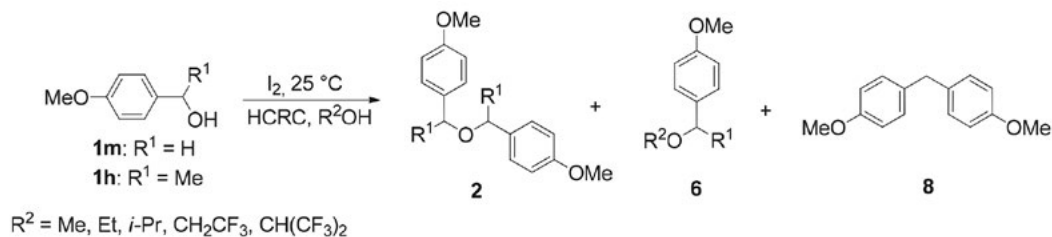
Dimerization of 4-methoxybenzyl alcohol **1m** was the main process in the absence of a good nucleophile (HCRC-CH<sub>2</sub>Cl<sub>2</sub>), while *ipso*-substitution took place as

Table 6. The effect of the reaction conditions on iodine-catalyzed transformation of **10**



Entry	Reaction conditions	Conversion (%) <sup>c</sup>	Distribution of products			
			11a	/	11b	/
1	SFRC <sup>a</sup> / 15 min	100	50	/	50	
2	CH <sub>2</sub> Cl <sub>2</sub> <sup>b</sup> / 5 min	100	50	/	50	
3	MeOH <sup>b</sup> / 5 min	100				100

<sup>a</sup> 1 mmol of **10**, 0.03 mmol of I<sub>2</sub>, T = 25 °C. <sup>b</sup> 1 mmol of **10**, 3 mmol of solvent, 0.03 mmol I<sub>2</sub>, T = 25 °C. <sup>c</sup> Conversion and product distribution determined by <sup>1</sup>H NMR spectroscopy.

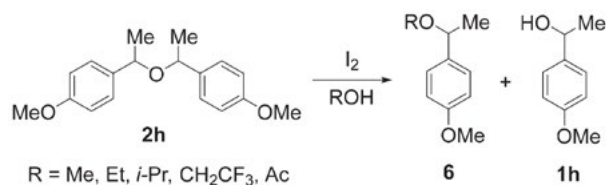
**Table 7.** The effect of the HCRC on the transformation of **1m** and **1h**

Entry	1	R <sup>2</sup> OH	Reaction time <sup>a</sup>	Conversion (%) <sup>b</sup>	Dimerization		Substitution		Ipso
					2	/	6	/	
1	<b>1m</b>	MeOH	190 h	91	10	/	90		
2	<b>1m</b>	EtOH	360 h	80	16	/	80	/	4
3	<b>1m</b>	<i>i</i> -PrOH	360 h	67	29	/	64	/	7
4	<b>1m</b>	CF <sub>3</sub> CH <sub>2</sub> OH	1 h	40	77	/	/		23
5	<b>1m</b>	(CF <sub>3</sub> ) <sub>2</sub> CHOH	1 h	30	65	/	/		35
6	<b>1h</b>	MeOH	15 min	43	14	/	86		
7	<b>1h</b>	MeOH	3 h	95	5	/	95		
8	<b>1h</b>	EtOH	15 min	49	61	/	39		
9	<b>1h</b>	EtOH	25 h	98	12	/	88		
10	<b>1h</b>	<i>i</i> -PrOH	15 min	37	80	/	20		
11	<b>1h</b>	<i>i</i> -PrOH	25 h	98	25	/	75		
12	<b>1h</b>	CF <sub>3</sub> CH <sub>2</sub> OH	15 min	83	20	/	80		
13	<b>1h</b>	CF <sub>3</sub> CH <sub>2</sub> OH	2.5 h	96	8	/	92		
14	<b>1h</b>	(CF <sub>3</sub> ) <sub>2</sub> CHOH	15 min	60	100				

<sup>a</sup>1 mmol of **1**, 3 mmol of R<sup>2</sup>OH, 0.03 mmol of I<sub>2</sub>, T = 25 °C. <sup>b</sup>Conversion and product distribution determined by <sup>1</sup>H NMR spectroscopy.

well (Table 4, entry 2). The addition of alcohols extensively retarded transformation of **1m** (Table 7, entries 1–3); the proportion of substitution is decreasing with the growing sterical hindrance and the reducing nucleophilicity of the solvent. A noteworthy modulation of the reactivity was noted in the case of more acidic and low nucleophilic 2,2,2-trifluoroethanol (TFE) and HFIP. Starting **1m** displayed a strong tendency of polymerization in the latter two alcohols, and after too long reaction time, the tar material was only isolated. The reaction time was consequently limited to one hour and dimerization and *ipso*-substitu-

tion were the only processes (entries 4 and 5). Both alcohols are poor nucleophiles, and no substitution took place. An additional methyl group contributed to the substantially higher reactivity of 1-(4-methoxyphenyl)ethanol **1h** in comparison with **1m**, dimerization and substitution became the only reaction channels. Dimerization was the exclusive transformation in the absence of a good nucleophile (HCRC-CH<sub>2</sub>Cl<sub>2</sub>) (Table 3, entry 9). In the presence of MeOH, EtOH and *i*-PrOH substitution and dimerization took place (Table 7, entries 7, 9 and 11), exhibiting a similar reactivity pattern as in the case of **1m**. It is evident that

**Table 8.** The effect of the hydroxy-substituted solvent on the conversion of **2h** under HCRC

Entry	ROH	Reaction time <sup>a</sup>	Conversion (%)	6		1h
				/		
1	MeOH	3 h	75	97	/	3
2	EtOH	15 h	74	97	/	3
3	<i>i</i> -PrOH	15 h	52	96	/	4
4	CF <sub>3</sub> CH <sub>2</sub> OH	1.5 h	91	95	/	5
5	CH <sub>3</sub> COOH	6 h	79	88 <sup>c</sup>	/	12

<sup>a</sup>Reaction conditions: 1 mmol of **2h**, 3 mmol ROH, 0.03 mmol of I<sub>2</sub>, T = 25 °C, R. t. (reaction time). <sup>b</sup>Conversion and product distribution determined by <sup>1</sup>H NMR spectroscopy. <sup>c</sup>The product is 1-(4-methoxyphenyl)ethyl acetate **6he**.

the dimeric ether **2** is a kinetically controlled product (entries 6–11), and iodine could catalyze its transesterification.<sup>69</sup> Transformations of **1h** were faster in presence of the fluorinated solvents; in the case of a better nucleophile TFE, substitution almost completely prevailed (entries 12 and 13), while in the presence of HFIP dimerization was the only process (entry 14). It could be concluded that reactivity patterns of **1m** and **1h** in the presence of iodine under SFRC and HCRC are similar. Dimerization of both alcohols is the key process in the absence of a good nucleophile, while substitution took place predominantly in the presence of a good nucleophile.

It is evident in the Table 7 that dimerization is followed by transesterification, and we decided to further investigate this rather unexplored process, Table 8.

Functionalization of **2h** in the presence of methanol under HCRC yielded the corresponding methyl ether **6ha** (97%) and 3% of the alcohol **1h** (entry 1). This is an indication that relation between **1h** and **2h** is reversible. The conversion roughly corresponds with the nucleophilicity of the alcohols (entries 1–3); in the case of the most sterically hindered and least nucleophilic *i*-PrOH the lowest conversion was achieved. A surprising turning point was observed in CF<sub>3</sub>CH<sub>2</sub>OH (entry 4). Although considerably more acidic and worse nucleophile than ethanol, the highest conversion was achieved in CF<sub>3</sub>CH<sub>2</sub>OH. The result reflects the much stronger stabilization of the reaction intermediates in comparison with the simple alkyl alcohols. Transformation of **2h** in the presence of acetic acid yielded the corresponding acetate ester **6he** (entry 5), demonstrating the carboxylic acids are suitable nucleophiles in this reaction. Products **6** were considerably more stable than **2h**, and remained intact in the presence of iodine.

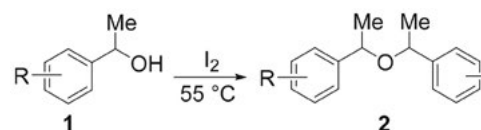
The Hammett correlation<sup>70,71</sup> is a convenient tool for the estimation of the nature of the reaction intermediates and the type of bond cleavage, and in the case of ionic in-

termediates, the degree of the charge developed. It is determined under homogenous conditions in diluted solution; however, we decided to examine the relative reactivity of the substituted 1-phenylethanols in I<sub>2</sub>-catalyzed dimerization under SFRC (Figure 1). The SFRC conditions are challenging, and therefore the Hammett correlation has been rarely studied.<sup>72</sup>

The relative reactivity of 1-phenylethanol **1a** toward its substituted 4-F **1o**, 3-Me **1p**, 3-MeO **1q**, 4-Cl **1r** and 4-Br **1s** derivatives was studied at 55 °C, all the alcohols are liquid at given temperature. In all cases, dimeric ethers **2a** and **2o-s** were formed and good Hammett correlation ( $r^2 = 0.98$ ) was obtained utilizing  $\sigma^+$  substituent constants. The slope  $\rho^+ = -2.8$  suggests the transition state involving electron-deficient intermediates with a partial developed charge in a rate-determining step. A similar value of  $\rho = -2.76$  was obtained in I<sub>2</sub>-catalyzed dihydroperoxidation of benzaldehydes in acetonitrile at 22 °C.<sup>73</sup> It can be summarized that iodine has a remarkable feature of generation of species that would normally require the use of a strong acid.

In order to demonstrate the role of iodine, reactivity of different catalytic systems were examined on an exceedingly acid-sensitive substrate 9*H*-xanthene-9-ol **10**, giving **11a** and **11b** smoothly,<sup>74</sup> Table 9.

Entries 1 and 2 were added from Table 6 for easier comparison. Transformation of **10** in the presence of phosphomolybdic acid hydrate under SFRC was much less effective in comparison with the I<sub>2</sub>-catalyzed reaction (entry 3), while reaction in the presence of methanol yielded the methoxy ether **11c** with 84% selectivity (entry 4). Expectedly, disproportionation of **10** in the presence of 57% aqueous solution of HI was the only process<sup>75</sup> (entry 5), whereas in the presence of methanol 80% of **11c** was formed (entry 6); displaying similar reactivity in the presence of heteropoly acid and HI (entries 3–6). Reaction of



Entry	R	1	$\sigma^+$	$\log k_{rel}$
1	4-F	<b>1o</b>	-0.07	0.30
2	3-Me	<b>1p</b>	-0.07	0.24
3	H	<b>1a</b>	0	0
4	3-OMe	<b>1q</b>	0.05	-0.10
5	4-Cl	<b>1r</b>	0.11	-0.24
6	4-Br	<b>1s</b>	0.15	-0.37

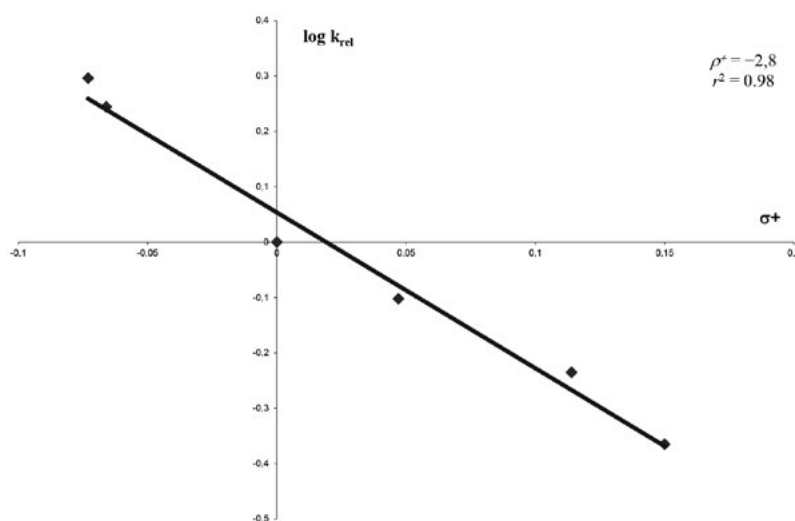
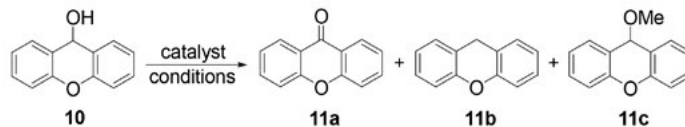


Figure 1. Hammett correlation analysis on I<sub>2</sub>-catalyzed dimerization of **1**.



**Table 9.** Comparison of activity of different catalysts on the transformation of **10**<sup>a</sup>

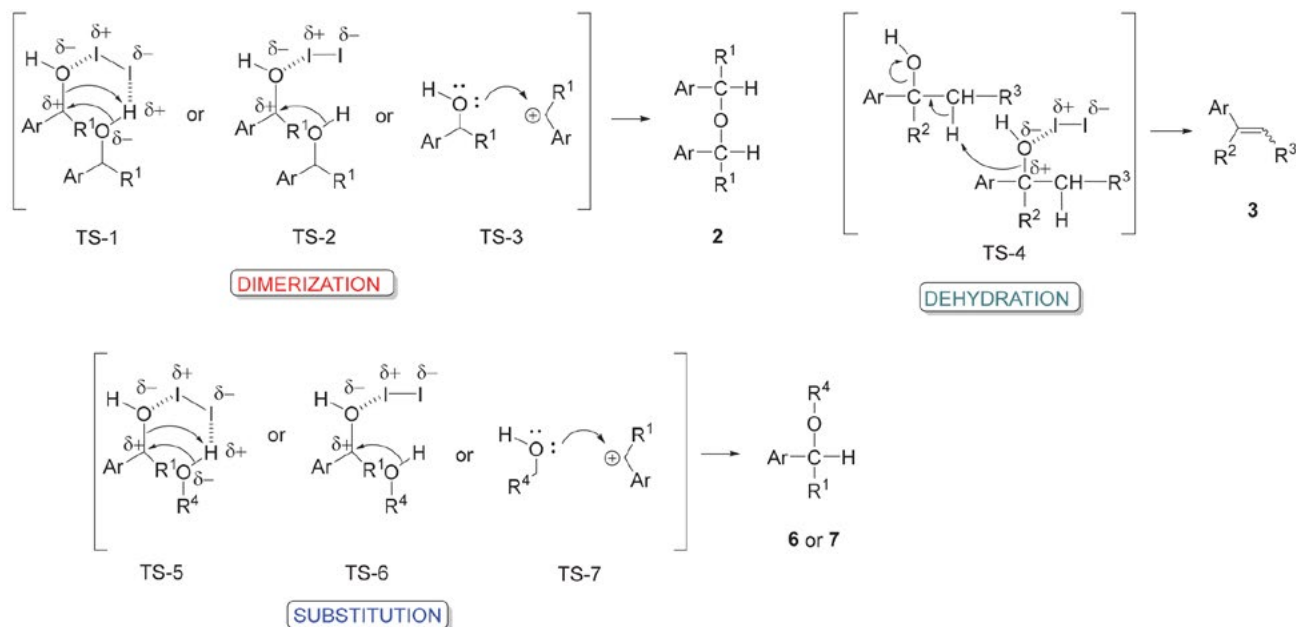
Entry	Catalyst	Reaction time, rt	Conversion (%) <sup>b</sup>	11a	11b	11c
1	3% I <sub>2</sub> /SFRC <sup>c</sup>	15 min	100	50	50	
2	3% I <sub>2</sub> /MeOH	5 min	100			100
3	PMA/SFRC <sup>d</sup>	15 min	29 <sup>e</sup>	7	7	
4	PMA/MeOH <sup>f</sup>	5 min	100	8	8	84
5	3% HI (57%) <sup>g</sup>	15 min	100	50	50	
6	3% HI (57%)/MeOH <sup>h</sup>	5 min	100	10	10	80
7	3% I <sub>2</sub> /3% H <sub>2</sub> O/MeOH <sup>i</sup>	5 min	100			100
8	3% I <sub>2</sub> /3% KI/SFRC <sup>j</sup>	15 min	100	50	50	
9	3% I <sub>2</sub> /3% KI/MeOH <sup>k</sup>	5 min	100			100
10	3% I <sub>2</sub> /3% Bu <sub>4</sub> Ni/SFRC <sup>l</sup>	15 min	40 <sup>m</sup>	2	2	
11	3% I <sub>2</sub> /3% Bu <sub>4</sub> Ni/MeOH <sup>n</sup>	5 min	95			100

<sup>a</sup> Reaction conditions: **10** (1 mmol, 198 mg) and various catalysts, rt. <sup>b</sup> Conversion and product distribution determined by <sup>1</sup>H NMR spectroscopy.

<sup>c</sup> Entries 1 and 2 from Table 6. <sup>d</sup> **10** (1 mmol, 198 mg) and phosphomolybdic acid hydrate (PMA, H<sub>3</sub>[P(Mo<sub>3</sub>O<sub>10</sub>)<sub>4</sub>] · xH<sub>2</sub>O), 60 mg. <sup>e</sup> 71% of unreacted **10** and 15% of a new, unidentified product presumably a ROR type dimer of **10**. <sup>f</sup> **10** (1 mmol, 198 mg), methanol (3 mmol, 96 mg) and PMA (60 mg). <sup>g</sup> **10** (1 mmol, 198 mg) and HI (57% aqueous solution, 0.03 mmol, 6.7 mg). <sup>h</sup> **10** (1 mmol, 198 mg), methanol (3 mmol, 96 mg) and HI (57% aqueous solution, 0.03 mmol, 6.7 mg). <sup>i</sup> **10** (1 mmol, 198 mg), H<sub>2</sub>O (0.03 mmol, 0.6 mg), methanol (3 mmol, 96 mg) and I<sub>2</sub> (0.03 mmol, 7.6 mg). <sup>j</sup> KI (0.03 mmol, 5 mg) and I<sub>2</sub> (0.03 mmol, 7.6 mg) were stirred for 20 minutes, **10** (1 mmol, 198 mg) was added. <sup>k</sup> KI (0.03 mmol, 5 mg), I<sub>2</sub> (0.03 mmol, 7.6 mg) were stirred for 20 minutes, **10** (1 mmol, 198 mg) and methanol (3 mmol, 96 mg) were added. <sup>l</sup> I<sub>2</sub> (0.03 mmol, 7.6 mg) and Bu<sub>4</sub>Ni (0.03 mmol, 11.1 mg) were stirred for 20 minutes, **10** (1 mmol, 198 mg) was added. <sup>m</sup> 60% of unreacted **10** and 36% of a new product, presumably a ROR type dimer of **10**. <sup>n</sup> I<sub>2</sub> (0.03 mmol, 7.6 mg), Bu<sub>4</sub>Ni (0.03 mmol, 11.1 mg) were stirred for 20 minutes, **10** (1 mmol, 198 mg) and methanol (3 mmol, 96 mg) were added.

**10** in a mixture of 3% of I<sub>2</sub>, 3 % of water and 3 mmol of methanol furnished **11c** as the only product (entry 7). The result indicates that iodine is relatively highly water tolerant<sup>76</sup> and retains its catalytic activity in contrast to the numerous other Lewis acids. Iodine and KI were stirred together before **10** were added in order to establish the effect

of iodine complexation. Disproportionation took place quantitatively, indicating at least two possible scenarios. Complexation of iodine and potassium iodide might be poor; on the other hand, triiodide could possibly catalyze the disproportionation (entry 8). Reaction of **10** with the system I<sub>2</sub>/KI/MeOH yielded the methoxy ether **11c** as a

**Scheme 1.** A suggested role of iodine in transformation of alcohols under SFRC and HCRC.

sole product (entry 9). Additional complexation of  $I_2$  with  $Bu_4NI$  almost completely suppressed disproportionation, suggesting that formation of triiodide was a key (entry 10). Reaction of **10** with  $I_2/Bu_4NI$  in the presence of methanol yielded the methoxy ether **11c** only, while no disproportionation took place (entry 11). In reactions in entries 3 and 10 an unidentified product appeared, seemingly a dimeric ether of **10**. There is often speculated, though not experimentally proven, that the *in-situ* formed HI is the actual catalyst in the iodine-catalyzed transformations.<sup>77</sup> A potential formation of HI would probably result in a loss of the reaction selectivity (comparison of entries 2 and 6). The results indicate that iodine was the active catalyst, where complexation changed the reaction pathway considerably. Additionally, iodine was titrated with a standard solution of  $Na_2S_2O_3$  after the end of the disproportionation of **10**. The entire amount of iodine was present at the end of the reaction. Similar observation was made in the case of dimerization of a secondary alcohol and substitution reaction with methanol, strongly indicating iodine as the active catalyst in these reactions.

A tentative explanation of the reaction pathways is presented on Scheme 2. The driving force in all cases is presumably polarization of the reactants by iodine. We proposed such halogen bond<sup>78</sup> activation in disproportionation of ethers under SFRC<sup>39</sup>, which is in agreement with recent computational<sup>37</sup> and experimental studies.<sup>38</sup> A simultaneous TS-1 or two separated activation processes TS-2, including carbenium ion TS-3 could be proposed as the key steps in the dimerization process. In the absence of a better nucleophile, the starting alcohol took over a role of an attacking nucleophile, affording the dimer **2**. The dehydration process of the tertiary alcohols might be initiated by polarization of the starting alcohol as shown in TS-4. The substitution step is suggested as a concomitant activation TS-5 or a divided activation TS-6 or by carbenium ion TS-7.

In the presence of added stronger nucleophile, substitution products **6** and **7** substantially prevailed over the dimerization products **2**.

## 4. Conclusions

To summarize, we have studied iodine-catalyzed transformations of aryl-substituted alcohols under SFRC and under HCRC, the concentration was proved to have an exceptional impact on the transformation. Achieving a pasty aggregate state of solid substrates in the presence of  $I_2$  was of vital importance for the reaction progress. Primary and secondary alcohols underwent two main transformations, depending on the reaction conditions. Dimerization took place in absence of the good nucleophiles under SFRC and HCRC, while substitution prevailed in presence of the good nucleophiles. The tertiary alcohols exhibited a strong tendency of dehydration into alkenes, which is in sharp contrast with the reactivity of primary and second-

ary alcohols. The difference in thermodynamic stability of the alkenes, derived from the tertiary and the secondary alcohols, is supposedly a driving force for the observed selectivity. Substitution was another process observed in the presence of the hydroxylic solvents; their acidity, nucleophilicity and hydrophobicity were important parameters for studying the reactivity of those alcohols. 4-Methoxyphenyl-substituted alcohols possessed higher reactivity than phenyl analogues; their pentafluorophenyl counterparts were unreactive under the studied conditions. The results indicated the electron-deficient intermediates to be likely involved in these processes, the geometries of the molecule and heteroatom share an important part in reactivity. 4-Methoxybenzyl alcohol yielded its dimeric ether and bis(4-methoxyphenyl)methane, a product derived *via* the  $I_2$ -catalyzed *ipso*-substitution. 4-Methoxybenzyl alcohol exhibited higher reactivity in TFE and HFIP than in EtOH and in *i*-PrOH under HCRC, thus indicating stronger stabilization of the reaction intermediates in the fluorinated alcohols. A tertiary benzylic alcohol **1n** was demonstrated to possess a special reactivity. It appears that upon its dehydration all three possible alkenes were obtained. The thermodynamically less stable alkene unexpectedly reacted with the initially formed intermediate, furnishing two dimeric alkenes. It is worth mentioning that certain processes take place under SFRC and HCRC, but not under the classical diluted conditions. This is an indication that reacting species have to be in close vicinity. Iodine catalyzed the disproportionation of 9*H*-xanthene-9-ol **10** under SFRC and HCRC, and in contrast, the substitution took place in the presence of MeOH. Iodine is a convenient catalyst for transesterification under mild conditions, it has a potential for interconversion of ether to ester. The Hammett correlation analysis of the  $I_2$ -catalyzed dimerization of substituted 1-phenylethanols under SFRC ( $T = 55\text{ }^\circ\text{C}$ ) furnished straight-line  $\rho^+ = -2.8$  ( $r^2 = 0.98$ ). This fact strongly suggests the involvement of the electron-deficient intermediates with a certain degree of the developed charge in the transition state.

## 5. Acknowledgement

We thank Prof. Marko Zupan for his initiative part of the research. We are grateful the Slovenian Research Agency for the financial support (P1-0134 and P1-0230), to Dr. D. Žigon at the Mass Spectroscopy Centre at the 'Jožef Stefan' Institute in Ljubljana, and to Mrs. T. Stipanovič and Prof. J. Svete for elemental combustion analysis.

## 6. References

1. J. Clark, D. Macquarrie, Eds. *Handbook of Green Chemistry & Technology*; Blackwell: Oxford, U. K. 2002.  
DOI:10.1002/9780470988305

2. M. Lancaster, *Green Chemistry: An Introductory Text*; Royal Society of Chemistry, Cambridge, U. K., **2002**.
3. P. Tundo, V. Esposito, V., (Eds.): *Green Chemical Reactions*; Springer, Dordrecht, Netherlands, **2008**.
4. K. Tanaka, (Ed.): *Solvent-Free Organic Synthesis*; Wiley-VCH: Weinheim, Germany, **2009**.
5. P. J. Walsh, H. Li, C. A. de Parrodi, *Chem. Rev.* **2007**, *107*, 2503–2545. DOI:10.1021/cr0509556
6. M. B. Gawande, V. D. B. Bonifácio, R. Luque, P. S. Branco, R. S. Varma, *ChemSusChem* **2014**, *7*, 24–44. DOI:10.1002/cssc.201300485
7. M. A. P. Martins, C. P. Frizzo, D. N. Moreira, L. Buriol, P. Machado, *Chem. Rev.* **2009**, *109*, 4140–4182. DOI:10.1021/cr9001098
8. S. Nakamatsu, S. Toyota, W. Jones, F. Toda, *Chem. Commun.* **2005**, 3808–3810. DOI:10.1039/b503922c
9. A. Orita, G. Uehara, K. Miwa, J. Otera, *Chem. Commun.* **2006**, 4729–4731. DOI:10.1039/b609567d
10. M. Feller, A. Karton, G. Leitus, J. M. L. Martin, D. Milstein, *J. Am. Chem. Soc.* **2006**, *128*, 12400–12401. DOI:10.1021/ja0641352
11. Z. Tang, Z.-H. Yang, L.-F. Cun, L.-Z. Gong, A.-Q. Mi, Y.-Z. Jiang, *Org. Lett.* **2004**, *6*, 2285–2287; DOI:10.1021/ol049141m
12. I. Pravst, M. Zupan, S. Stavber, *Tetrahedron Lett.* **2006**, *47*, 4707–4710. DOI:10.1016/j.tetlet.2006.04.119
13. G. Angelici, R. J. Corrêa, S. J. Garden, C. Tomasini, *Tetrahedron Lett.* **2009**, *50*, 814–817. DOI:10.1016/j.tetlet.2008.12.007
14. Y. Hayashi, T. Sumiya, J. Takahashi, H. Gotoh, T. Urushima, M. Shoji, *Angew. Chem. Int. Ed.* **2006**, *45*, 958–961. DOI:10.1002/anie.200502488
15. P. Dzedzic, W. Zou, J. Háfren, A. Córdova, *Org. Biomol. Chem.* **2006**, *4*, 38–40. DOI:10.1039/B515880J
16. S. Minegishi, S. Kobayashi, H. Mayr, *J. Am. Chem. Soc.* **2004**, *126*, 5174–5181. DOI:10.1021/ja031828z
17. T. Bug, H. Mayr, *J. Am. Chem. Soc.* **2003**, *125*, 12980–12986. DOI:10.1021/ja036838e
18. T. B. Phan, M. Breugst, H. Mayr, *Angew. Chem. Int. Ed.* **2006**, *45*, 3869–3874. DOI:10.1002/anie.200600542
19. H. Mayr, J. Ammer, M. Baidya, B. Maji, T. A. Nigst, A. R. Ofial, T. Singer, *J. Am. Chem. Soc.* **2015**, *137*, 2580–2599. DOI:10.1021/ja511639b
20. T. L. Amyes, I. W. Stevens, J. P. Richard, *J. Org. Chem.* **1993**, *58*, 6057–6066. DOI:10.1021/jo00074a036
21. H. F. Schaller, H. Mayr, *Angew. Chem. Int. Ed.* **2008**, *47*, 3958–3961. DOI:10.1002/anie.200800354
22. R. Breslow, *Acc. Chem. Res.* **2004**, *37*, 471–478. DOI:10.1021/ar040001m
23. R. Breslow, *Acc. Chem. Res.* **1991**, *24*, 159–164. DOI:10.1021/ar00006a001
24. H. Y. Bae, C. E. Song, *ACS Catal.* **2015**, *5*, 3613–3619. DOI:10.1021/acscatal.5b00685
25. R. N. Butler, A. G. Coyne, W. J. Cunningham, E. M. Moloney, *J. Org. Chem.* **2013**, *78*, 3276–3291. DOI:10.1021/jo400055g
26. F. C. Küpper, M. C. Feiters, B. Olofsson, T. Kaiho, S. Yanagida, M. B. Zimmermann, L. J. Carpenter, G. W. Luther III, Z. Lu, M. Jonsson, L. Kloo, L. *Angew. Chem. Int. Ed.* **2011**, *50*, 11598–11620.
27. Z. Jinjin, G. Wenchao, C. Honghong, L. Xing, L. Qiang, W. Wenlong, *Chin. J. Org. Chem.* **2014**, *34*, 1941–1957. DOI:10.6023/cjoc201405003
28. M. Jereb, D. Vražič, M. Zupan, *Tetrahedron* **2011**, *67*, 1355–1387. DOI:10.1016/j.tet.2010.11.086
29. Y.-M. Ren, C. Cai, R.-C. Yang, *RSC Adv.* **2013**, *3*, 7182–7204.
30. H. Hibbert, *J. Am. Chem. Soc.* **1915**, *37*, 1748–1763. DOI:10.1021/ja02172a015
31. G. Stavber, M. Zupan, S. Stavber, *Tetrahedron Lett.* **2006**, *47*, 8463–8466. DOI:10.1016/j.tetlet.2006.09.154
32. M. Jereb, D. Vražič, M. Zupan, *Tetrahedron Lett.* **2009**, *50*, 2347–2352. DOI:10.1016/j.tetlet.2009.02.224
33. M. Jereb, D. Vražič, M. Zupan, *Acta Chim. Slov.* **2009**, *56*, 652–658.
34. Y. Kasashima, A. Uzawa, T. Nishida, T. Mino, M. Sakamoto, T. Fujita, *J. Oleo Sci.* **2009**, *58*, 421–427. DOI:10.5650/jos.58.421
35. Y. Ide, Y. Hori, S. Kobayashi, M. D. Hossain, T. Kitamura, *Synthesis* **2010**, 3083–3086.
36. W. Rao, A. H. L. Tay, P. J. Goh, J. M. L. Choy, J. K. Ke, P. W. H. Chan, *Tetrahedron Lett.* **2008**, *49*, 122–126. DOI:10.1016/j.tetlet.2007.11.005
37. M. Breugst, E. Detmar, D. von der Heiden, *ACS Catal.* **2016**, *6*, 3203–3212. DOI:10.1021/acscatal.6b00447
38. D. von der Heiden, S. Bozkus, M. Klussmann, M. Breugst, *J. Org. Chem.* **2017**, *82*, 4037–4043. DOI:10.1021/acs.joc.7b00445
39. M. Jereb, D. Vražič, *Org. Biomol. Chem.* **2013**, *11*, 1978–1999. DOI:10.1039/c3ob27267b
40. *Vogel's Textbook of Practical Organic Chemistry*, Longman Group Limited: London, U. K., **1959**, pp 252.
41. Y. Suh, J.-s. Lee, S. H. Kim, R. D. Rieke, *J. Organomet. Chem.* **2003**, *684*, 20–36. DOI:10.1016/S0022-328X(03)00500-X
42. E. D. Bergmann, A. M. Meyer, *J. Org. Chem.* **1965**, *30*, 2840–2841. DOI:10.1021/jo01019a510
43. G. V. M. Sharma, K. L. Reddy, P. S. Lakshmi, R. Ravi, A. C. Kunwar, *J. Org. Chem.* **2006**, *71*, 3967–3969. DOI:10.1021/jo052418r
44. V. Dimitrov, S. Stanchev, B. Milenkov, T. Nikiforov, P. Demirev, *Synthesis* **1991**, 228–232.
45. R. Stoermer, O. Kippe, *Chem. Ber.* **1903**, *36*, 3992–4013. DOI:10.1002/cber.19030360459
46. C. F. Koelsch, *J. Am. Chem. Soc.* **1932**, *54*, 2487–2493. DOI:10.1021/ja01345a046
47. I. Ho, J. G. Smith, *Tetrahedron* **1970**, *26*, 4277–4286. DOI:10.1016/S0040-4020(01)93071-6
48. D. J. Cram, D. R. Wilson, *J. Am. Chem. Soc.* **1963**, *85*, 1249–1257. DOI:10.1021/ja00892a009
49. Y. Sprinzak, *J. Am. Chem. Soc.* **1958**, *80*, 5449–5455. DOI:10.1021/ja01553a033
50. W. Ried, J. Schönherr, *Chem. Ber.* **1960**, *93*, 1870–1877. DOI:10.1002/cber.19600930826

51. I. T. Badejo, R. Karaman, J. L. Fry, *J. Org. Chem.* **1989**, *54*, 4591–4596. DOI:10.1021/jo00280a026
52. G.-Q. Li, Z.-Y. Yan, Y.-N. Niu, L. Y. Wu, H.-L. Wei, Y.-M. Liang, *Tetrahedron: Asymmetry* **2008**, *19*, 816–821. DOI:10.1016/j.tetasy.2008.03.012
53. J. M. Khurana, A. Sehgal, A. Gogia, A. Manian, G. C. Maikap, *J. Chem. Soc. Perkin Trans 1*, **1996**, 2213–2215. DOI:10.1039/P19960002213
54. A. F. Holleman, *Org. Synth., Coll. Vol. 1*, **1941**, 554–555.
55. M. Zupan, P. Škulj, S. Stavber, *Arkivoc*, **2001**, *2*, 108–118.
56. M. Zupan, P. Škulj, S. Stavber, *Tetrahedron* **2001**, *57*, 10027–10031. DOI:10.1016/S0040-4020(01)01031-6
57. S. J. Cristol, J. R. Douglass, J. S. Meek, *J. Am. Chem. Soc.* **1951**, *73*, 816–818. DOI:10.1021/ja01146a094
58. G. Stavber, M. Zupan, M. Jereb, S. Stavber, *Org. Lett.* **2004**, *6*, 4973–4976. DOI:10.1021/ol047867c
59. R. E. Pearson, J. C. Martin, *J. Am. Chem. Soc.* **1963**, *85*, 3142–3146. DOI:10.1021/ja00903a021
60. C. K. Ingold, F. R. Shaw, *J. Chem. Soc.* **1927**, 2918–2926. DOI:10.1039/JR9270002918
61. X. Zhang, W. Rao, P. W. H. Chan, *Synlett* **2008**, 2204–2208.
62. J. S. Yadav, B. V. S. Reddy, N. Thirumurtulu, N. M. Reddy, A. R. Prasad, *Tetrahedron Lett.* **2008**, *49*, 2031–2033. DOI:10.1016/j.tetlet.2008.01.017
63. S. Ward, T. Messier, M. Lukeman, *Can. J. Chem.* **2010**, *88*, 493–499. DOI:10.1139/V10-032
64. X. Creary, A. Wolf, *J. Phys. Org. Chem.* **2000**, *13*, 337–343. DOI:10.1002/1099-1395(200006)13:6<337::AID-POC249>3.0.CO;2-T
65. S. M. Bonesi, M. Fagnoni, *Chem. Eur. J.* **2010**, *16*, 13572–13589. DOI:10.1002/chem.201001478
66. G. G. Gurzadyan, S. Steenken, *Chem. Eur. J.* **2001**, *7*, 1808–1815. DOI:10.1002/1521-3765(20010417)7:8<1808::AID-CHEM18080>3.0.CO;2-8
67. A. Berkessel, M. R. M. Andreae, H. Schmickler, *J. Lex, Angew. Chem. Int. Ed.* **2002**, *41*, 4481–4484. DOI:10.1002/1521-3773(20021202)41:23<4481::AID-ANIE4481>3.0.CO;2-7
68. J. L. Wahlstrom, R. C. Ronald, *J. Org. Chem.* **1998**, *63*, 6021–6022. DOI:10.1021/jo972222u
69. S. Das, R. Borah, R. R. Devi, A. J. Thakur, *Synlett*, **2008**, 2741–2762.
70. Hammett, L. P. *J. Am. Chem. Soc.* **1938**, *59*, 96–103. DOI:10.1021/ja01280a022
71. Hammett, L. P. *Chem. Rev.* **1935**, *17*, 125–136. DOI:10.1021/cr60056a010
72. M. Jereb, M. Zupan, S. Stavber, *Helv. Chim. Acta*, **2009**, *92*, 555–566. DOI:10.1002/hlca.200800308
73. K. Žmitek, M. Zupan, S. Stavber, J. Iskra, *J. Org. Chem.* **2007**, *72*, 6534–6540. DOI:10.1021/jo0708745
74. F. Goronwy Kny-Jones, A. Miles Ward, *J. Chem. Soc.* **1930**, 535–542. DOI:10.1039/JR9300000535
75. C. Waterlot, D. Couturier, M. De Backer, B. Rigo, B. *Can. J. Chem.* **2000**, *78*, 1242–1246. DOI:10.1139/v00-082
76. K. Ramalinga, P. Vijayalakshmi, T. N. B. Kaimal, *Tetrahedron Lett.* **2002**, *43*, 879–882. DOI:10.1016/S0040-4039(01)02235-3
77. K. M. Kim, D. J. Jeon, E. K. Ryu, *Synthesis* **1998**, 835–836.
78. G. Cavallo, P. Metrangolo, R. Milani, T. Pilati, A. Priimagi, G. Resnati, G. Terraneo, *Chem. Rev.* **2016**, *116*, 2478–2601. DOI:10.1021/acs.chemrev.5b00484

## Povzetek

Preučevali smo z jodom katalizirane pretvorbe alkoholov pri reakcijskih pogojih brez topil (RPBT) in pri visoko koncentriranih pogojih (VKP) v prisotnosti različnih topil, da bi dobili vpogled v obnašanje reakcijskih intermediatov pri takšnih pogojih. Ugotovili smo, da z benzilnimi alkoholi potečejo trije različni tipi pretvorb: dimerizacija, dehidracija in substitucija. Dimerizacija in substitucija pretežno potečeta v primeru primarnih in sekundarnih alkoholov, medtem, ko dehidracija prevladuje v primeru terciarnih alkoholov. Relativna reaktivnost substituiranih 1-feniletanolov pri z jodom katalizirani dimerizaciji pri RPBT daje dobro Hammettovo korelacijo  $\rho^+ = -2.8$  ( $r^2 = 0.98$ ), ki kaže na prisotnost elektronsko siromašnih intermediatov z določeno stopnjo razvitega naboja v prehodnem stanju.

Scientific paper

# Synthesis and X-ray Structural Analysis of the Ruthenium(III) Complex Na[*trans*-RuCl<sub>4</sub>(DMSO)(PyrDiaz)], the Diazene Derivative of Antitumor NAMI-Pyr

Jure Vajs,<sup>1</sup> Andrej Pevec,<sup>1</sup> Martin Gazvoda,<sup>1</sup> Damijana Urankar,<sup>1</sup>  
Evgeny Goreshnik,<sup>2</sup> Slovenko Polanc<sup>1</sup> and Janez Košmrlj<sup>1,\*</sup>

<sup>1</sup> Faculty of Chemistry and Chemical Technology, University of Ljubljana, Večna pot 113, SI-1000 Ljubljana, Slovenia

<sup>2</sup> Department of Inorganic Chemistry and Technology, Jožef Stefan Institute, Jamova 39, SI-1000 Ljubljana, Slovenia

\* Corresponding author: E-mail: janez.kosmrlj@fkkt.uni-lj.si

Received: 09-17-2017

Dedicated to Professor Emeritus Miha Tišler, University of Ljubljana, on the occasion of his 90<sup>th</sup> birthday.

## Abstract

Novel tetrachloridoruthenium(III) complex Na[*trans*-RuCl<sub>4</sub>(DMSO)(PyrDiaz)] (**3**) with pyridine-tethered diazenedicarboxamide **PyrDiaz** ligand (**PyrDiaz** = *N*<sup>1</sup>-(4-isopropylphenyl)-*N*<sup>2</sup>-(pyridin-2-ylmethyl)diazene-1,2-dicarboxamide) was synthesized by direct coupling of **PyrDiaz** with sodium *trans*-bis(dimethyl sulfoxide)tetrachloridoruthenate(III) (Na-[*trans*-Ru(DMSO)<sub>2</sub>Cl<sub>4</sub>]). Compound **3** is the analogue of the antimetastatic Ru(III) complex NAMI-A and NAMI-Pyr. Single crystal X-ray diffraction analysis revealed that the compound **3** is a polymeric complex with the ruthenium and sodium centres.

**Keywords:** Diazene, pyridine, ruthenium(III), sodium, polymeric complex

## 1. Introduction

Based on the WHO estimates, cancer is one of the leading causes of mortality worldwide accounting for 8.8 million deaths in 2015.<sup>1</sup> In addition to surgical removal of tumours and radiation therapy, chemotherapy is one of the most commonly applied treatments of cancer. Burden associated with chemotherapy, however, is intrinsic and acquired resistance,<sup>2</sup> and severe side-effects that are responsible for considerable morbidity, greatly reducing the effectiveness of the therapy. This, and the striking estimate that the global incidence of cancer continues to increase, urges for new strategies and chemical entities to be devised.<sup>3</sup>

Commenced with a group of platinum chemotherapeutic agents that has been in clinical use for half of a century,<sup>4–6</sup> other precious-metal-based alternatives lately enticed an army of chemists worldwide.<sup>7</sup> As a result, some ruthenium-based compounds of unique properties, sur-

passing cisplatin in activity, particularly on resistant tumours, and with reduced host toxicity at active doses have been discovered.<sup>8,9</sup>

In the treatment of a complex disease like cancer it is unlikely for a single drug to be effective. To increase the chemotherapeutic success, a combination of two or more active agents having separate targets is commonly administered at the therapy.<sup>10</sup> A promising alternative to these so-called cocktails are hybrid molecules that are composed of two or more covalently bound drugs; the compounds that can possess combined pharmacological properties of the individual drugs<sup>10,11</sup> yet superior synergistic effects.<sup>12,13</sup>

Over the past years, we have investigated redox-active<sup>14</sup> diazenedicarboxamides as potential anti-cancer agents.<sup>15</sup> The results of the *in vitro* experiments suggested that they likely target tumour cell redox mechanism by oxidation of glutathione into glutathione disulphide.<sup>16</sup> A synergistic effect was noted by treating some tumour cell lines with the combination of cisplatin and selected diazenedicar-

boxamides,<sup>16c</sup> prompting us to consider novel diazenecarboxamide-platinum conjugates (Figure 1).<sup>6,17</sup> This has led to complex **A**, possessing higher cytotoxicity against T24 bladder carcinoma cells as compared to the parent platinum precursor ( $[\text{PtCl}(\text{DMSO})(\text{en})]\text{Cl}$ ; en = ethylenediamine) and organic ligand, for example.<sup>18</sup> Redox-active diazenecarboxamides were also combined with organometallic  $[\text{Ru}(\text{II})\text{-Arene}]$  to generate complexes with interesting coordination modes and chemical reactivity (Figure 2).<sup>19,20</sup> In the context of our endeavour in the field of potential anti-cancer agents, complex **B** was identified as highly cytotoxic against tumour cell lines with  $\text{IC}_{50}$  values in the

low micro-molar range.<sup>19,21</sup> The activity of **B** was cell-type specific and comparable in both cancer cell lines and their drug-resistant subline. A tenfold increase in the sensitivity of tumour cervical carcinoma cell lines (HeLa) with depleted intracellular glutathione level in comparison to the untreated HeLa suggested glutathione as the molecular target of **B**.<sup>19</sup>

Encouraged by these results and inspired by ruthenium(III) complexes NAMI-A (imidazolium *trans*-[tetrachlorido(dimethyl sulfoxide)imidazole ruthenium(III)]),<sup>22</sup> KP1019 (indazolium *trans*-[tetrachloridobis(1*H*-indazole)ruthenium(III)]) and its sodium salt KP1339<sup>23</sup> (Fig-

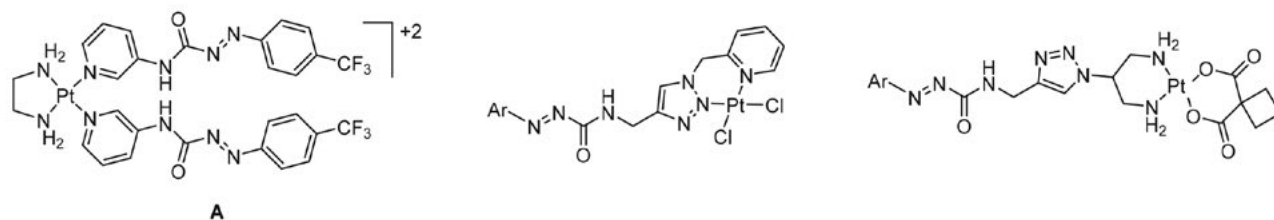


Figure 1. Selected diazenecarboxamide-platinum conjugates.

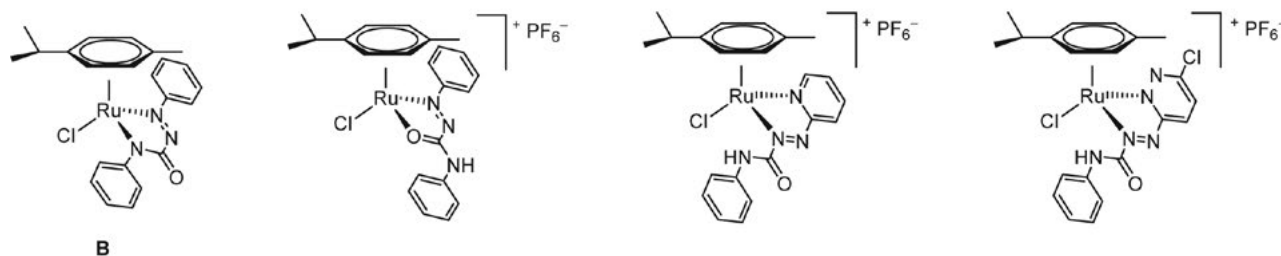


Figure 2. Selected organometallic  $[\text{Arene-Ru}^{\text{II}}\text{-Diazenecarboxamide}]$  compounds.

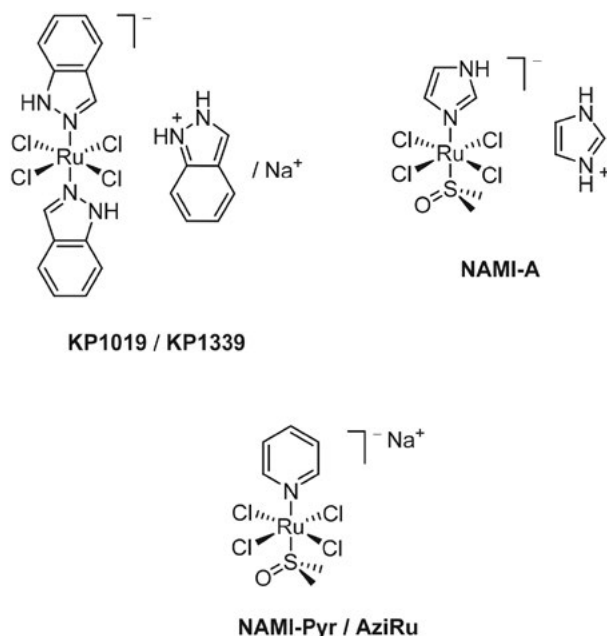


Figure 3. Selected  $\text{Ru}(\text{III})$  complexes having anti-cancer activity.

ure 3), we were prompted to examine the coordination ability of diazenedicarboxamide *N*<sup>1</sup>-(4-isopropylphenyl)-*N*<sup>2</sup>-(pyridin-2-ylmethyl)diazene-1,2-dicarboxamide (**1**) (Scheme 1). Compound **1** has been previously screened for anti-cancer activity.<sup>24</sup>

## 2. Experimental

Starting materials and solvents for the synthesis of the examined compounds were used as obtained, and without further purification, from Aldrich, Fluka and Alfa Aesar. IR spectrum was obtained with a Bruker ALPHA Platinum ATR spectrometer on a solid sample support (ATR). NMR spectra were recorded in  $\text{D}_2\text{O}$  with a Bruker Avance III 500 MHz instrument operating at 500 MHz, at 296 K, and referenced to the peak of HOD ( $\delta = 4.63$  ppm). An Agilent 6224 time-of-flight (TOF) mass spectrometer equipped with a double orthogonal electrospray source at atmospheric pressure ionization (ESI) coupled to an Agilent 1260 HPLC was used for recording HRMS spectra.

Mobile phase composed of two solvents: A was 0.1% formic acid in Milli-Q water, and B was 0.1% formic acid in acetonitrile mixed in the ratio of 1:1. Compound was prepared by dissolving the sample in acetonitrile and injected (0.1  $\mu$ L) into the LC-MS. Flow rate was 0.4 mL/min. Fragmentor voltage was 150 V. Capillary voltage 4000 V. Mass range 100–1100. Elemental analysis (C, H, N) was performed with Perkin Elmer 2400 Series II CHNS/O Analyser. Melting points were determined on the microscope hot stage.

## 2. 1. The Synthesis of Compound 3

$N^1$ -(4-Isopropylphenyl)- $N^2$ -(pyridin-2-ylmethyl)diazene-1,2-dicarboxamide<sup>24</sup> (**1**, 163 mg, 0.5 mmol) was added to a solution of sodium *trans*-bis(dimethyl sulfoxide)tetrachloridoruthenate(III) ( $\text{Na}[\text{trans-Ru}(\text{DMSO-S})_2\text{Cl}_4]$ )<sup>25</sup> (**2**, 106 mg, 0.25 mmol) in acetone (10 mL) and stirred at room temperature for 2 h. The solvent was removed under reduced pressure. Dry residue was re-suspended in dichloromethane and filtered off to remove unreacted ligand **1**. The precipitate was dried in air to give compound **3** (165 mg, 99%). Crystal suitable for X-ray structure determination was found in the crude product. Purple solid; mp >250 °C dec.; IR  $\nu$  3245, 3035, 2959, 1736, 1718, 1603, 1534, 1482, 1459, 1438  $\text{cm}^{-1}$ ; HRMS (ESI-)  $m/z$  for  $\text{C}_{19}\text{H}_{25}\text{Cl}_4\text{N}_5\text{O}_3\text{RuS}^-$  [ $\text{M} - \text{Na}$ ] $^-$ : calcd 646.9462, found 646.9467,  $m/z$  for  $\text{C}_{17}\text{H}_{18}\text{Cl}_3\text{N}_5\text{O}_2\text{Ru}^-$  [ $\text{M} - \text{Na} - \text{DMSO} - \text{HCl}$ ] $^-$ : calcd 532.9560, found 532.9554; Anal. calcd for  $\text{C}_{19}\text{H}_{25}\text{Cl}_4\text{N}_5\text{O}_3\text{NaRuS} \cdot 0.1 \text{H}_2\text{O}$ : C, 34.00; H, 3.78; N, 10.43; found: C, 34.48; H, 3.96; N, 10.60.

## 2. 2. X-ray Structure Determination

Crystal data and refinement parameters of **3** ( $[\text{NaRuCl}_4\text{I}(\text{DMSO})_n]$ ) are listed in Table 1. Single-crystal data were collected at 150 K on a Gemini A diffractometer

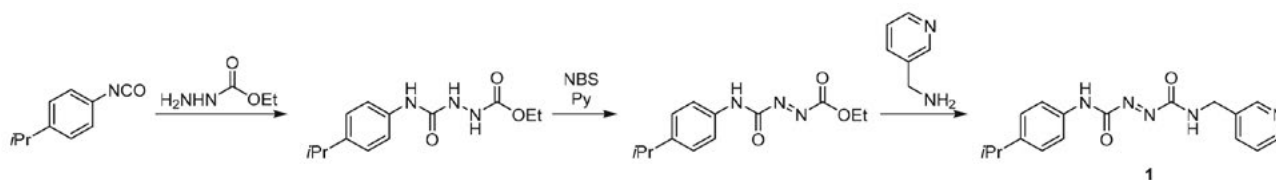
equipped with an Atlas CCD detector, using graphite monochromated CuK $\alpha$  radiation ( $\lambda = 1.54184 \text{ \AA}$ ). The data were treated using the CrysAlisPro software suite program package.<sup>26</sup> Analytical absorption correction was applied. Structure of compound **3** was solved using direct methods with SHELXS-97<sup>27</sup> and refined using the least-squares method on  $F^2$  with SHELXL-2014<sup>28</sup> and using the graphical interface of OLEX2.<sup>29</sup> Figures were prepared using Diamond software.<sup>30</sup> CCDC 1569486 contains the supplementary crystallographic data for **3**. These data can be obtained free of charge from The Cambridge Crystallographic Data Center via [www.ccdc.cam.ac.uk/data\\_request/cif](http://www.ccdc.cam.ac.uk/data_request/cif).

## 3. Results and Discussion

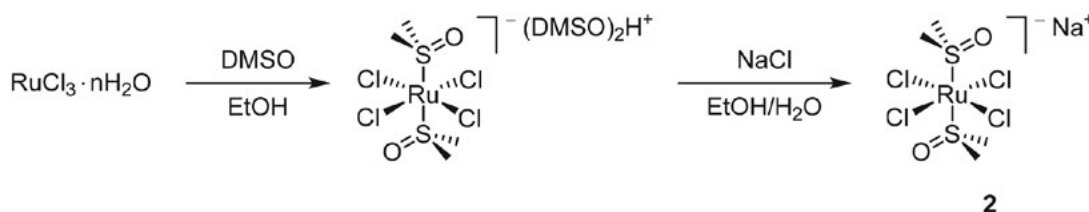
The pyridine-tethered diazenedicarboxamide,  $N^1$ -(4-isopropylphenyl)- $N^2$ -(pyridin-2-ylmethyl)diazene-1,2-dicarboxamide (**1**), was prepared in a three step reaction sequence starting from the commercial reactants as previously described by us (Scheme 1).<sup>24</sup> Thus, the addition of carbazate to 4-isopropylphenyl isocyanate gave ethyl 2-((4-isopropylphenyl)carbamoyl)hydrazine-1-carboxylate, which was oxidized with *N*-bromosuccinimide (NBS) into ethyl 2-((4-isopropylphenyl)carbamoyl)diazene-1-carboxylate. Subsequent nucleophilic displacement with 3-picolylamine afforded the target compound **1**.

Sodium *trans*-bis(dimethyl sulfoxide)tetrachloridoruthenate(III) ( $\text{Na}[\text{trans-Ru}(\text{DMSO-S})_2\text{Cl}_4]$ , **2**) was selected as the ruthenium(III) precursor. This compound was prepared by the literature procedure starting from the commercial hydrated  $\text{RuCl}_3$  via hydrogen *trans*-bis(dimethyl sulfoxide)tetrachloridoruthenate(III) ( $[(\text{DMSO})_2\text{H}][\text{trans-Ru}(\text{DMSO-S})_2\text{Cl}_4]$ ) as shown in Scheme 2.<sup>25</sup>

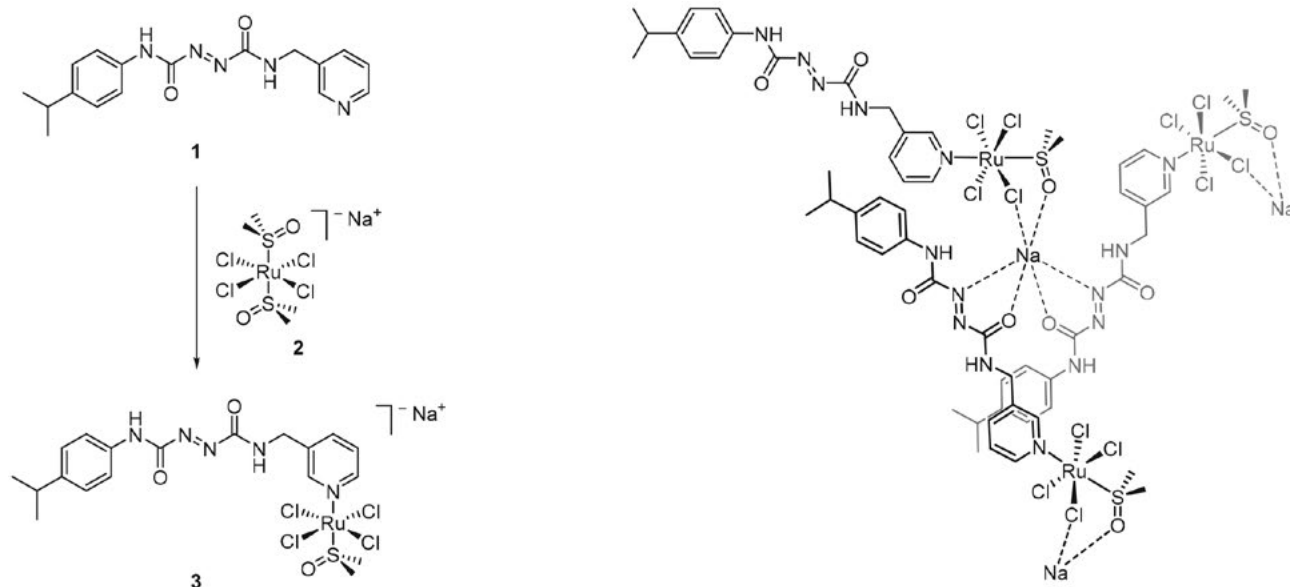
The coordination of ligand **1** to the ruthenium of **2** was performed using procedure based on that reported for



Scheme 1. Synthesis of pyridine-tethered diazenedicarboxamide ligand **1** (PyrDiaz).<sup>24</sup>



Scheme 2. Preparation of Ru(III) precursor **2**.<sup>25</sup>



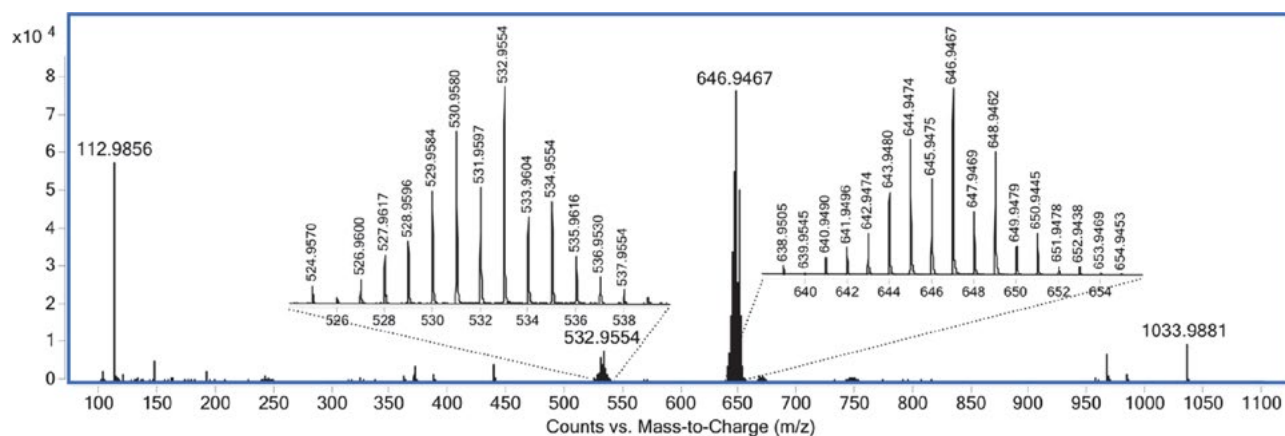
**Scheme 3.** Synthesis of Ru(III) complex 3 (left) and schematic presentation of sodium ion stabilized three-dimensional framework (right).

NAMI-A.<sup>31</sup> Combining complex 2 with an excess of ligand 1 in acetone solution resulted in displacement of one dimethyl sulfoxide ligand in the ruthenium coordination sphere and the formation of a new compound 3 shown in Scheme 3 (left). In contrast to our previous findings<sup>19,20</sup> for arene-ruthenium(II) compounds from Figure 2, in complex 3 diazene moiety did not participate in coordination to the metal centre. Instead, the pyridine part of the molecule replaced one axial dimethyl sulfoxide ligand. The charge compensation was provided by sodium ion. In solid state, the sodium ion interconnects the anionic ruthenium units into a three-dimensional framework, schematically presented in Scheme 3 (right).

The structure of the complex 3 was fully characterized by <sup>1</sup>H NMR, elemental analysis and ESI-HRMS. Complex 3 was analysed by high-resolution (HRMS) electrospray ionization mass spectrometry in negative ion

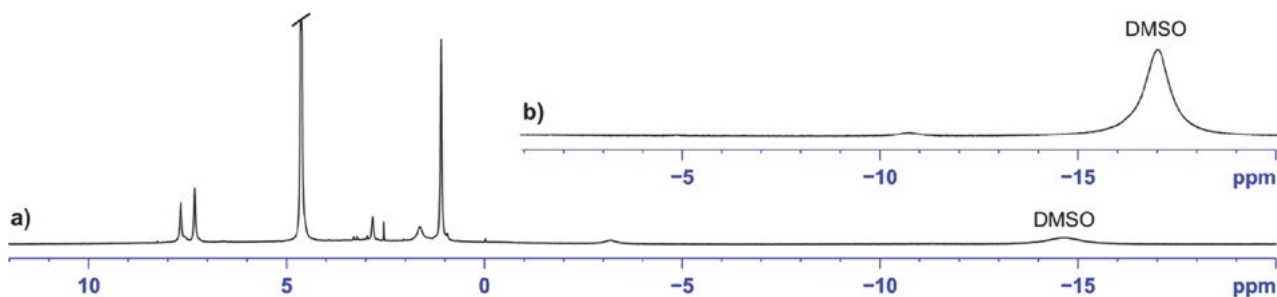
mode (ESI<sup>-</sup>). The spectrum, shown in Figure 4, was dominated by the parent  $[\text{Ru}^{\text{III}}\text{Cl}_2(\text{DMSO})(\text{PyrDiaz})]^-$  ion at  $m/z$  646.9467 (calcd for  $\text{C}_{19}\text{H}_{25}\text{Cl}_4\text{N}_5\text{O}_3\text{RuS}^-$ : 646.9462). Another peak at  $m/z$  532.9566 was interpreted as a result of in source collision-induced dissociation of the parent ion giving  $[\text{Ru}^{\text{III}}\text{Cl}_2(\text{PyrDiaz} - \text{H})]^-$  ion at  $m/z$  532.9554 (calcd for  $\text{C}_{17}\text{H}_{18}\text{Cl}_3\text{N}_5\text{O}_2\text{Ru}^-$  ( $[\text{M} - \text{Na} - \text{HCl}]^-$ : 532.9560). In positive mode (ESI<sup>+</sup>), the spectrum of compound 3 was featureless.

The paramagnetic ruthenium(III) ion severely broadened the NMR signals of coordinated ligands, not allowing the assignment procedure. The <sup>1</sup>H NMR spectra of freshly prepared D<sub>2</sub>O solutions of complexes 2 and 3 are shown in Figure 5. Chemical shifts of the coordinated DMSO ligand, peaks at ca. -15 ppm to -18 ppm, are in agreement with published data for the NAMI-type complexes.<sup>31,32</sup> Monitoring the D<sub>2</sub>O solution of 3 for 24 h at



**Figure 4.** ESI- HRMS spectrum of compound 3. Peaks at  $m/z$  112.9856 and  $m/z$  1033.9881 are due to calibrants.



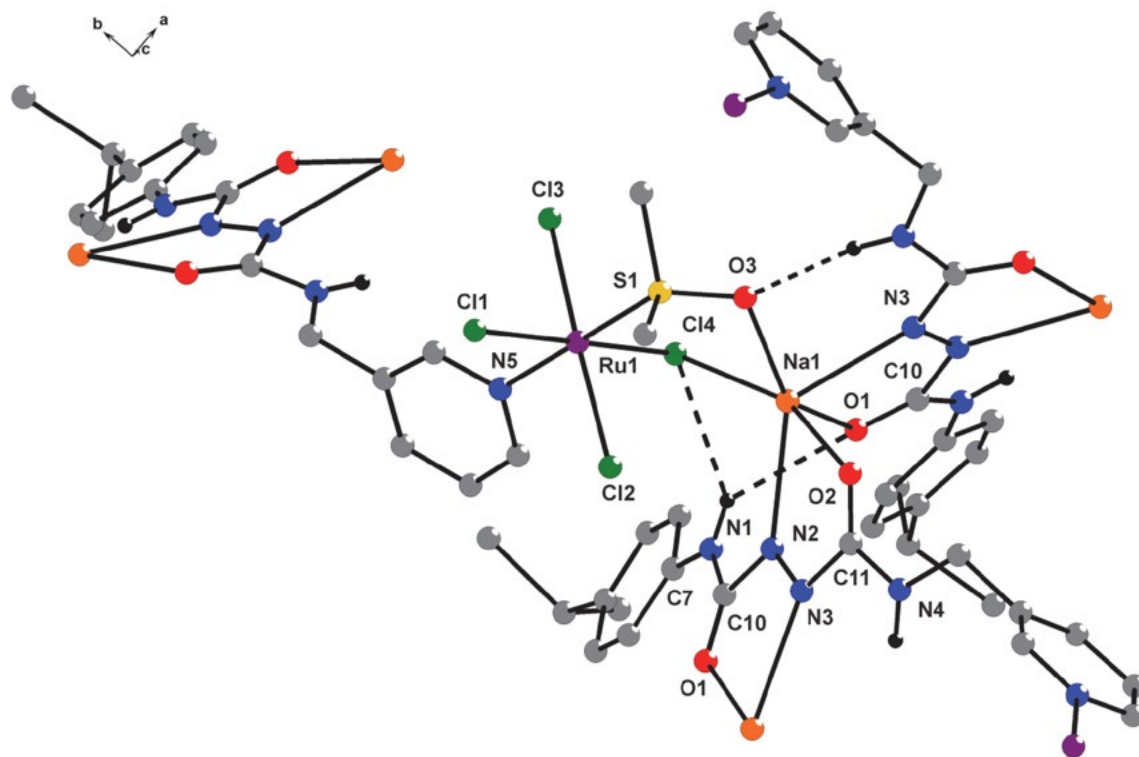


**Figure 5.**  $^1\text{H}$  NMR spectrum of a) complex **3**, and b) complex **2** as  $\text{D}_2\text{O}$  solutions. Relevant insets are only shown (spectra were recorded with spectral width of 60 ppm, number of scans = 128).

room temperature by  $^1\text{H}$  NMR indicated the formation of a complex mixture of products as seen by the appearance of several overlapping broad resonances in the spectra. The structures of these by-products could not be deduced from the spectra.

The structure of compound **3** could unambiguously be determined by a single crystal X-ray structure determination and is displayed in Figure 6. Selected bond lengths and angles are given in Table 2. Compound **3** is a polymeric complex with the ruthenium and sodium metallic atoms. Each of the  $\text{Ru}^{\text{III}}$  atoms are hexacoordinated by sulphur atom from DMSO molecule and the pyridine nitrogen of **1** in apical positions and four chlorido ligands in an equatorial plane. The sulphur-bound DMSO and ligand **1** are *trans* in nearly octahedral geometry of ruthenium cen-

tral atom. The Ru–N and Ru–S bond distances of 2.109(6) and 2.2924(17) Å, respectively, are very similar to those found in the related structures containing *trans*- $\text{RuNCl}_4\text{S}$  donor set.<sup>33–35,37</sup> Three of the chlorido ligands are terminal while Cl4 forms a bridge between the ruthenium and sodium atoms. The DMSO ligand also forms a bridge between a ruthenium centre (through its sulphur atom) and a sodium (through its oxygen) thus forming a five membered  $\text{RuClNaOS}$  ring in the crystal structure. The sodium has six atoms in its distorted octahedrally coordinated environment with the resulting  $\text{ClN}_2\text{O}_3$  donor set. Sodium atom is coordinated by two ligands **1**, each through one of the diazene nitrogen and one carbonyl oxygen atom. The coordination sphere of sodium atom in the structure of compound **3** is fulfilled by oxygen (bridging DMSO) and



**Figure 6.** Part of the crystal structure of the compound **3**, showing atom numbering scheme and hydrogen bonding interactions. The hydrogens on carbon atoms have been omitted for clarity.

**Table 1.** Crystal data and structure refinement details for **3**.

<b>3</b>	
formula	C <sub>19</sub> H <sub>25</sub> Cl <sub>4</sub> N <sub>5</sub> NaO <sub>3</sub> RuS
Fw (g mol <sup>-1</sup> )	669.36
crystal size (mm)	0.59 × 0.12 × 0.01
crystal color	Yellow
crystal system	Orthorhombic
space group	<i>P n a</i> 2 <sub>1</sub>
<i>a</i> (Å)	9.64914(19)
<i>b</i> (Å)	21.4978(6)
<i>c</i> (Å)	14.5013(3)
<i>V</i> (Å <sup>3</sup> )	3008.07(12)
<i>Z</i>	4
calcd density (g cm <sup>-3</sup> )	1.478
<i>F</i> (000)	1348
no. of collected reflns	9948
no. of independent reflns	4713
<i>R</i> <sub>int</sub>	0.0443
no. of reflns observed	4388
no. parameters	323
Flack parameter	-0.022(16)
<i>R</i> [ <i>I</i> > 2σ( <i>I</i> )] <sup>a</sup>	0.0415
<i>wR</i> <sub>2</sub> (all data) <sup>b</sup>	0.1113
<i>Goof</i> , <i>S</i> <sup>c</sup>	1.067
maximum/minimum residual electron density (e Å <sup>-3</sup> )	+0.909/-0.462

<sup>a</sup>  $R = \sum ||F_o| - |F_c|| / \sum |F_o|$ , <sup>b</sup>  $wR_2 = \{ \sum [w(F_o^2 - F_c^2)^2] / \sum [w(F_o^2)] \}^{1/2}$ .

<sup>c</sup>  $S = \{ \sum [(F_o^2 - F_c^2)^2] / (n/p) \}^{1/2}$  where *n* is the number of reflections and *p* is the total number of parameters refined.

**Table 2.** Selected bond lengths (Å) and angles (°) for **3**.

Ru1 – Cl1	2.3294(17)	Cl1 – Ru1 – Cl2	92.44(7)
Ru1 – Cl2	2.3624(18)	Cl1 – Ru1 – Cl3	90.27(7)
Ru1 – Cl3	2.3387(17)	Cl1 – Ru1 – Cl4	175.82(7)
Ru1 – Cl4	2.3797(17)	Cl1 – Ru1 – S1	89.86(7)
Na1 – O1	2.397(7)	Cl1 – Ru1 – N5	89.57(18)
Na1 – O2	2.290(6)	N5 – Ru1 – S1	179.32(18)
Na1 – O3	2.319(6)	Cl2 – Ru1 – Cl3	177.29(7)
Na1 – N2	2.558(6)	O1 – Na1 – O2	104.3(3)
Na1 – N3	2.542(7)	O1 – Na1 – O3	141.3(2)
Na1 – Cl4	2.683(3)	O1 – Na1 – N2	77.2(2)
N1 – C10	1.321(11)	O1 – Na1 – N3	64.0(2)
N2 – N3	1.228(9)	O1 – Na1 – Cl4	83.72(19)
N2 – C10	1.490(9)	N2 – N3 – C11	109.5(6)
N3 – C11	1.474(9)	N3 – C11 – N4	110.1(6)
N4 – C11	1.345(10)	N3 – N2 – C10	111.3(6)
O1 – C10	1.198(9)	C10 – N1 – C7	127.7(7)
O2 – C11	1.204(9)	C11 – N4 – C12	119.4(6)

**Table 3.** Hydrogen bonding geometry for **3**.

D – H ... A	<i>d</i> (D – H)/ Å	<i>d</i> (H ... A)/ Å	<i>d</i> (D ... A)/ Å	<(DHA)/ °
N1 – H1N1 ... Cl4	0.88	2.72	3.455(5)	141.9
N1 – H1N1 ... O1	0.88	2.53	3.236(7)	137.4
N4 – H1N4 ... O3	0.88	2.05	2.922(6)	169.9

bridging chlorido ligand. Both diazene nitrogen atoms and both carbonyl oxygen atoms of ligand **1** are involved in the coordination to sodium atoms in the polymeric structure of compound **3**. A similar coordination environment around sodium ion has been found in related tetrachloridoruthenium(III) complexes.<sup>33–36</sup> The crystal structure of **3** is further stabilized by three intramolecular hydrogen bonds of the type N–H...O and N–H...F (Table 3).

A pyridine-heterocycle unsubstituted analogue of **3**, called NAMI-Pyr<sup>37</sup> and AziRu<sup>38</sup> (Figure 3), has been reported to show interesting reactivity profiles towards biologically relevant targets.<sup>9</sup> Derivatives with functionalized pyridine ligand have also been investigated.<sup>32</sup> Unfortunately, no biological studies of **3** were possible due to its instability and decomposition in protic solvents (*vide supra*).

## 4. Conclusions

We have reported the synthesis of novel tetrachloridoruthenium(III) complex Na[*trans*-RuCl<sub>4</sub>(DMSO)(PyrDiaz)] (PyrDiaz = *N*<sup>1</sup>-(4-isopropylphenyl)-*N*<sup>2</sup>-(pyridin-2-ylmethyl)diazene-1,2-dicarboxamide), a pyridine-tethered derivative of NAMI-A that has a redox-active diazencarboxamide ligand (PyrDiaz) in the structure. It has been designed to target tumour cell-lines synergistically by means of known antiproliferative activity of NAMI-A and glutathione oxidation ability enacted by the diazene part of the molecule. Although in this particular case the instability and decomposition of Na[*trans*-RuCl<sub>4</sub>(DMSO)(PyrDiaz)] in protic solvents disabled biological studies, work is in progress to improve the physicochemical properties of such PyrDiaz-ruthenium(III) complexes.

## 5. Acknowledgments

The authors acknowledge the financial support from the Slovenian Research Agency (research core funding No. P1-0230, Young Researcher Grant to JV, and No. P1-0175).

## 6. References

1. <http://www.who.int/mediacentre/factsheets/fs297/en/> (accessed: July 29, 2017)
2. V. Brabec, J. Kasparkova, *Drug Resist. Updates* **2005**, *8*, 131–146. DOI:10.1016/j.drug.2005.04.006

3. B. A. Chabner, T. G. Roberts, Jr., *Nat. Rev. Cancer* **2005**, 5, 65–72. DOI:10.1038/nrc1529
4. B. Rosenberg, L. VanCamp, J. E. Trosko, V. H. Mansour, *Nature* **1969**, 222, 385–386. DOI:10.1038/222385a0
5. For selected informative reading, see: (a) M. Galanski, M. A. Jakupec, B. K. Keppler, *Curr. Med. Chem.* **2005**, 12, 2075–2094; DOI:10.2174/0929867054637626  
(b) A. V. Klein, T. W. Hambley, “Platinum-Based Anticancer Agents”, in: T. Storr (Ed.): *Ligand design in medicinal inorganic chemistry*, John Wiley & Sons, 2014; DOI:10.1002/9781118697191.ch2  
(c) T. C. Johnstone, K. Suntharalingam, S. J. Lippard, *Chem. Rev.* **2016**, 116, 3436–3486; DOI:10.1021/acs.chemrev.5b00597  
(d) D. M. Cheff, M. D. Hall, *J. Med. Chem.* **2017**, 60, 4517–4532. DOI:10.1021/acs.jmedchem.6b01351
6. J. D. White, M. M. Haley, V. J. DeRose *Acc. Chem. Res.* **2016**, 49, 56–66. DOI:10.1021/acs.accounts.5b00322
7. For selected informative reading, see: (a) S. P. Fricker, *Dalton Trans.* **2007**, 4903–4917; (b) P. C. A. Bruijninx, P. J. Sadler, *Curr. Opin. Chem. Biol.* **2008**, 12, 197–206; (c) I. Romero-Canelón, P. J. Sadler, *Inorg. Chem.* **2013**, 52, 12276–12291; (d) K. Dralle Mjos, C. Orvig, *Chem. Rev.* **2014**, 114, 4540–4563; (e) R. D. Teo, J. Y. Hwang, J. Termini, Z. Gross, H. B. Gray, *Chem. Rev.* **2017**, 117, 2711–2729; (f) T. Lazarević, A. Rilak, Ž. D. Bugarčić, *Eur. J. Med. Chem.* **2017**.  
<http://dx.doi.org/10.1016/j.ejmech.2017.04.007>.
8. For selected informative reading, see: (a) C. S. Allardyce, P. J. Dyson, *Platinum Metals Rev.* **2001**, 45, 62–69; (b) I. Kostova, *Curr. Med. Chem.* **2006**, 13, 1085–1107; DOI:10.2174/092986706776360941  
(c) W. H. Ang, P. J. Dyson, *Eur. J. Inorg. Chem.* **2006**, 4003–4018; DOI:10.1002/ejic.200600723  
(d) E. S. Antonarakis, A. Emadi, *Cancer Chemother Pharmacol.* **2010**, 66, 1–9; DOI:10.1007/s00280-010-1293-1  
(e) A. Bergamo, G. Sava, *Dalton Trans.* **2011**, 40, 7817–7823; DOI:10.1039/c0dt01816c  
(f) C. G. Hartinger, N. Metzler-Nolte, P. J. Dyson, *Organometallics* **2012**, 31, 5677–5685; DOI:10.1021/om300373t  
(g) A. Bergamo, C. Gaiddon, J. H. M. Schellens, J. H. Beijnen, G. Sava, *J. Inorg. Biochem.* **2012**, 106, 90–99; DOI:10.1016/j.jinorgbio.2011.09.030  
(h) C. Mu, C. J. Walsby, “Ruthenium Anticancer Compounds with Biologically-Derived Ligands”, in: T. Storr. (Ed.): *Ligand design in medicinal inorganic chemistry*, John Wiley & Sons, 2014; DOI:10.1002/9781118697191.ch15  
(i) M. J. Chow, W. H. Ang, “Organoruthenium(II)-Arene Complexes: Structural Building Blocks for Anticancer Drug Discovery”, in: K. Kam-Wing Lo (Ed.): *Inorganic and Organometallic Transition Metal Complexes with Biological Molecules and Living Cells*, Academic Press, 2016.
9. C. Riccardi, D. Musumeci, C. Irace, L. Paduano, D. Montesarchio, *Eur. J. Org. Chem.* **2017**, 1100–1119.
10. L. K. Gediya, V. C. O. Njar, *Expert Opinion on Drug Discovery* **2009**, 4, 1099–1111. DOI:10.1002/ejoc.201600943
11. B. Meunier, *Acc. Chem. Res.* **2008**, 41, 69–77. DOI:10.1021/ar7000843
12. A. Muller-Schiffmann, J. Marz-Berberich, A. Andreyeva, R. Ronicke, D. Bartnik, O. Brener, J. Kutzsche, A. H. C. Horn, M. Hellmert, J. Polkowska, K. Gottmann, K. G. Reymann, S. A. Funke, L. Nagel-Steger, C. Moriscot, G. Schoehn, H. Sticht, D. Willbold, T. Schrader, C. Korth, *Angew. Chem. Int. Ed.* **2010**, 49, 8743–8746. DOI:10.1002/anie.201004437
13. S. Patyar, A. Prakash, B. Medhi, *J. Pharm. Pharmacol.* **2011**, 63, 459–471. DOI:10.1111/j.2042-7158.2010.01236.x
14. J. Košmrlj, M. Kočevar, S. Polanc, *J. Chem. Soc., Perkin Trans. 1* **1998**, 3917–3920. DOI:10.1039/a808381i
15. For reviews, see: (a) J. Košmrlj, M. Kočevar, S. Polanc, *Synlett* **2009**, 2217–2235; (b) H. Kaur, S. Yadav, B. Narasimhan, *Anti-Cancer Agents in Medicinal Chemistry* **2016**, 16, 1240–1265. DOI:10.2174/1871520616666160607012042
16. (a) L. Pieters, J. Košmrlj, R. Lenaršič, M. Kočevar, S. Polanc, *Arhivoc* **2001**, 42–50.  
(b) T. Čimbora-Zovko, S. Bombek, J. Košmrlj, L. Kovačić, S. Polanc, A. Katalinić, M. Osmak, *Drug Dev. Res.* **2004**, 61, 95–100. DOI:10.1002/ddr.10336  
(c) I. Martin-Kleiner, S. Bombek, J. Košmrlj, B. Čupić, T. Čimbora-Zovko, S. Jakopec, S. Polanc, M. Osmak, J. Gabrilovac, *Toxicol. In Vitro* **2007**, 21, 1453–1459. DOI:10.1016/j.tiv.2007.06.005  
(d) S. Jakopec, K. Dubravcic, S. Polanc, J. Košmrlj, M. Osmak, *Toxicol. In Vitro* **2006**, 20, 217–226. DOI:10.1016/j.tiv.2005.06.008  
(e) S. Jakopec, K. Dubravcic, A. Brozovic, S. Polanc, M. Osmak, *Cell Biol. Toxicol.* **2006**, 22, 61–71. DOI:10.1007/s10565-006-0023-2
17. (a) D. Urankar, A. Pevec, J. Košmrlj, *Eur. J. Inorg. Chem.* **2011**, 1921–1929; DOI:10.1002/ejic.201001051  
(b) N. Stojanović, D. Urankar, A. Brozović, A. Ambrović-Ristov, M. Osmak, J. Košmrlj, *Acta Chim. Slov.* **2013**, 60, 368–374.
18. S. Grabner, J. Košmrlj, N. Bukovec, M. Čemažar, *J. Inorg. Biochem.* **2003**, 95, 105–112. DOI:10.1016/S0162-0134(03)00092-8
19. M. G. Sommer, P. Kureljak, D. Urankar, D. Schweinfurth, N. Stojanović, M. Bubrin, M. Gazvoda, M. Osmak, B. Sarkar, J. Košmrlj, *Chem. Eur. J.* **2014**, 20, 17296–17299. DOI:10.1002/chem.201404448
20. M. G. Sommer, S. Marinova, M. J. Krafft, D. Urankar, D. Schweinfurth, M. Bubrin, J. Košmrlj, B. Sarkar, *Organometallics* **2016**, 35, 2840–2849. DOI:10.1021/acs.organomet.6b00424
21. For reviews on organometallic anticancer drugs, see refs. 8f,h,i.
22. J. M. Rademaker-Lakhai, D. van den Bongard, D. Pluim, J. H. Beijnen, J. H. M. Schellens, *Clin. Cancer Res.* **2004**, 10, 3717–3727. DOI:10.1158/1078-0432.CCR-03-0746
23. C. G. Hartinger, M. A. Jakupec, S. Zorbas-Seifried, M. Groessl, A. Egger, W. Berger, H. Zorbas, P. J. Dyson, B. K. Keppler, *Chem. Biodivers.* **2008**, 5, 2140–2155. DOI:10.1002/cbdv.200890195

24. J. Vajs, S. Soviček, P. Kureljak, N. Stojanović, I. Steiner, D. Eljuga, D. Urankar, M. Kočevar, J. Košmrlj, S. Polanc, M. Osmak, *Acta Chim. Slov.* **2013**, *60*, 842–852.
25. E. Alessio, G. Balducci, M. Calligaris, G. Costa, W. M. Attia, G. Mestroni, *Inorg. Chem.* **1991**, *30*, 609–618.  
DOI:10.1021/ic00004a005
26. Rigaku Oxford Diffraction, CrysAlisPro Software System, Version 1.171.38.41, Rigaku Corporation, Oxford, UK, 2015.
27. G. M. Sheldrick, *Acta Crystallogr.* **2008**, *A64*, 112–122.  
DOI:10.1107/S0108767307043930
28. G. Sheldrick, *Acta Crystallogr. Sect.* **2015**, *C71*, 3–8.  
DOI:10.1107/S2053273314026370
29. O. V. Dolomanov, L. J. Bourhis, R. J. Gildea, J. A. K. Howard, H. Puschmann, *J. Appl. Crystallogr.* **2009**, *42*, 339–341.  
DOI:10.1107/S0021889808042726
30. Crystal Impact GbR, Bonn, Germany (2004–2005) DIAMOND v3.1.
31. E. Alessio, G. Balducci, A. Lutman, G. Mestroni, M. Calligaris, W. M. Attia, *Inorg. Chim. Acta* **1993**, *203*, 205–217.  
DOI:10.1016/S0020-1693(00)81659-X
32. For selected recent example, see: C. Mu, S. W. Chang, K. E. Prosser, A. W. Y. Leung, S. Santacruz, T. Jang, J. R. Thompson, D. T. T. Yapp, J. J. Warren, M. B. Bally, T. V. Beischlag, C. J. Walsby, *Inorg. Chem.* **2016**, *55*, 177–190.  
DOI:10.1021/acs.inorgchem.5b02109
33. C. M. Anderson, A. Herman, F. D. Rochon, *Polyhedron* **2007**, *26*, 3661–3668. DOI:10.1016/j.poly.2007.03.041
34. S. Ferrara, A. Kreider-Mueller, J. M. Tanski, C. M. Anderson, *Acta Crystallogr.* **2011**, *E67*, m756–m757.
35. C. M. Anderson, S. S. Jain, L. Silber, K. Chen, S. Guha, W. Zhang, E. C. McLaughlin, Y. Hu, J. M. Tanski, *J. Inorg. Biochem.* **2015**, *145*, 41–50.  
DOI:10.1016/j.jinorgbio.2014.12.017
36. Z. Trávníček, M. Matiková-Mařarová, *Acta Crystallogr.* **2010**, *E66*, m348–m349.
37. M. I. Webb, R. A. Chard, Y. M. Al-Jobory, M. R. Jones, E. W. Y. Wong, C. J. Walsby, *Inorg. Chem.* **2012**, *51*, 954–966.  
DOI:10.1021/ic202029e
38. G. Mangiapia, G. D'Errico, L. Simeone, C. Irace, A. Radulescu, A. Di Pascale, A. Colonna, D. Montesarchio, L. Paduano, *Biomaterials* **2012**, *33*, 3770–3782.  
DOI:10.1016/j.biomaterials.2012.01.057

## Povzetek

Z neposredno reakcijo med **PyrDiaz** ligandom (**PyrDiaz** =  $N^1$ -(4-izopropilfenil)- $N^2$ -(piridin-2-ilmetil) diazen-1,2-dikarboksamid) in natrijevim *trans*-bis(dimetil sulfoksid)tetrakloridorutenatom(III) ( $\text{Na}[\textit{trans}\text{-Ru}(\text{DMSO})_2\text{Cl}_4]$ ) smo sintetizirali nov tetrakloridorutenijev(III) kompleks  $\text{Na}[\textit{trans}\text{-RuCl}_4(\text{DMSO})(\text{PyrDiaz})]$  (**3**) s piridin-funkcionaliziranim diazenkarboksamidnim ligandom **PyrDiaz**. Spojina **3** je analog antimetastatičnega Ru(III) kompleksa NAMI-A in NAMI-Pyr. Rentgenska difrakcijska analiza monokristala je pokazala, da je spojina **3** polimeren kompleks z rutenijevimi in natrijevimi kovinskimi atomi.

Scientific paper

# Chlorocarbonylsulfenyl Chloride Cyclizations Towards Piperidin-3-yl-oxathiazol-2-ones as Potential Covalent Inhibitors of Threonine Proteases

Marko Jukič,<sup>1</sup> Katarina Grabrijan,<sup>1</sup> Selmir Kadić,<sup>1</sup>  
Fernando Juan de Lera Garrido,<sup>1,2</sup> Izidor Sosič,<sup>1</sup> Stanislav Gobec<sup>1</sup> and Aleš Obreza<sup>1,\*</sup>

<sup>1</sup> University of Ljubljana, Faculty of Pharmacy, Department of medicinal chemistry; Aškerčeva 7, SI-1000, Ljubljana, Slovenia

<sup>2</sup> Universidad de Castilla–La Mancha (Albacete); Universidad de Castilla–La Mancha, Altagracia, 50 13071 Ciudad Real, Spain

\* Corresponding author: E-mail: ales.obreza@ffa.uni-lj.si  
phone: +386 1 47 69 677; fax: +386 1 42 58 031

Received: 29-09-2017

*Dedicated to Professor Emeritus Miha Tišler, University of Ljubljana, on the occasion of his 90<sup>th</sup> birthday.*

## Abstract

Using rescaffolding approach, we designed piperidine compounds decorated with an electrophilic oxathiazol-2-one moiety that is known to confer selectivity towards threonine proteases. Our efforts to prepare products according to the published procedures were not successful. Furthermore we identified major side products containing nitrile functional group, resulting from carboxamide dehydration. We systematically optimized reaction conditions towards our desired products to identify heating of carboxamides with chlorocarbonylsulfenyl chloride and sodium carbonate as base in dioxane at 100 °C. Our efforts culminated in the preparation of a small series of piperidin-3-yl-oxathiazol-2-ones that are suitable for further biological evaluation.

**Keywords:** Cyclization, amide dehydration, oxathiazole-2-one, threonine protease, covalent inhibitors, irreversible inhibition

## 1. Introduction

Proteases play key roles in complex biological systems and in multiple structural and signalling pathways. They constitute a historically important field in medicinal chemistry and continue to represent a source of potential drug targets. They are involved in the pathology of hypertension, autoimmune and inflammatory diseases, reperfusion injury, blood clotting disorders, HIV and other viral infections, parasitic and bacterial infections, and last but not least, cancer.<sup>1</sup> Protease inhibitors are not valuable only as potential drugs but also as experimental tools for structural biology,<sup>2</sup> as they can be used as molecular probes in the elucidation of protease structures and protease pathway mechanisms.<sup>3</sup> Recently, databases of proteases (sometimes also termed peptidases, proteinases or proteolytic

enzymes) have been established as a resource in this immense research field; namely the *Merops* database with over 4000 individual entries.<sup>4</sup>

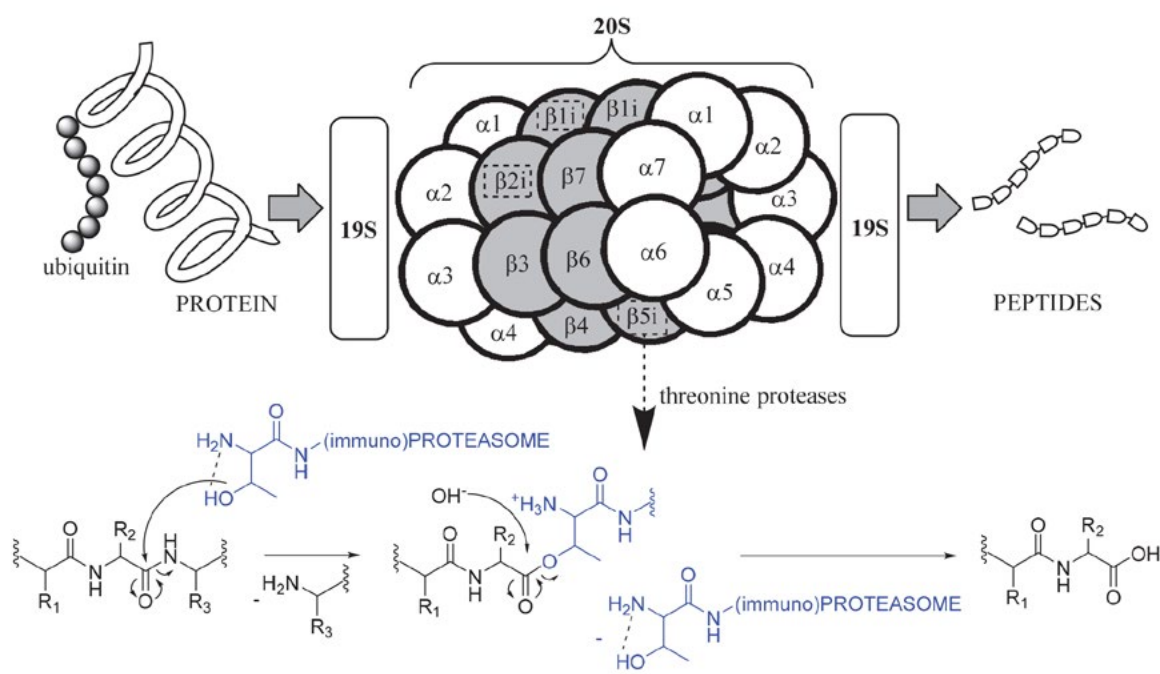
Our research efforts are mainly focused on the *N*-terminal threonine proteases that form stable covalent acyl-enzyme complexes and are subsequently hydrolyzed to afford product peptides. Threonine proteases constitute 99 entries in the *Merops* database, where we specifically study the threonine-type endopeptidases, such as the proteasomes.<sup>5</sup> The proteasomes consist of a central proteolytic unit, known as the 20S proteasome, and the 19S regulators, which together make up a 26S structure (Figure 1). The constitutive isoform of the proteasome is expressed in all eukaryotic cells while its immunomodulatory isoform, the immunoproteasome, is mainly expressed in cells associated with the immune system, such as lymphocytes and

monocytes.<sup>5,6</sup> The constitutive proteasome contains three enzymatically active subunits, namely the  $\beta 1c$  (caspase-like), the  $\beta 2c$  (trypsin-like), and the  $\beta 5c$  (chymotrypsin-like) that are embedded into a barrel-shaped structure consisting of four rings of  $\beta$ -subunits and  $\alpha$ -subunits in an abba order. The immunoproteasome has essentially the same overall structure, only the catalytically active subunits of cCP are replaced by their counterparts  $\beta 1i$ ,  $\beta 2i$ , and  $\beta 5i$  (Figure 1). The 20S proteasome core particle of both isoforms is a protease of 720 kDa and 28 individual subunits and is responsible for essential proteolytic degradation during cellular inflammatory and oxidative stress.<sup>7</sup> Immunoproteasome is also important for the generation of peptides for antigen presentation; moreover, recent studies also suggest a pleiotropic role in cellular function of the immunoproteasome.<sup>8–10</sup>

There is an amounting body of research on the small-molecule inhibitors of proteasomes.<sup>5,11</sup> Both marketed medicines, bortezomib and carfilzomib, equally inhibit the catalytically active  $\beta 5$  subunits of the constitutive proteasome and the immunoproteasome. The combined inhibition of both isoforms leads to cytotoxicity that limits the clinical application of these broad spectrum proteasome inhibitors.<sup>6</sup> In addition, many of the investigational compounds are peptide-like compounds and this represents a serious limitation to their metabolic stability and bioavailability.<sup>5</sup> To overcome these problems, multiple approaches can be found in literature: design of reversible proteasome inhibitors,<sup>12</sup> use of structural differences in the binding sites of both proteasomes in structure-based drug design,<sup>13,14</sup> design of highly selective and hydrolytically more

stable peptidic compounds,<sup>15</sup> design of highly selective non-peptidic compounds,<sup>16</sup> use of non-catalytic residues or allosteric sites in inhibitor design,<sup>17</sup> and the design of selective electrophilic warheads.<sup>18</sup> The majority of these compounds are covalent irreversible inhibitors bearing an electrophilic warhead that is capable of reacting with the *N*-terminal threonine residue in the catalytic active site of the examined protease.<sup>5,11</sup> Electrophilic warheads belong to structural classes of aldehydes,  $\alpha',\beta'$ -epoxyketones,  $\alpha$ -keto aldehydes,  $\beta$ -lactones, vinyl sulfones, Michael-acceptor systems, and boronates.<sup>19</sup> The active interest in this field is clearly represented by a very recent publication,<sup>19</sup> where a new mechanism for an existing warhead was reported, i.e. the formation of 1,4-oxazepane upon reaction of an  $\alpha',\beta'$ -epoxyketone warhead with the *N*-terminal threonine rather than the previously reported morpholine ring.<sup>14,19</sup> Such new developments provide invaluable data for the design of novel and selective irreversible inhibitors of threonine proteases.

In order to design targeted covalent inhibitors of threonine protease, we sought to examine the available electrophilic warheads.<sup>20</sup> We were in particular interested in compounds that could provide a suitable reactivity and selectivity towards threonine proteases. Recently, oxathiazol-2-one moiety was identified in a high-throughput screening campaign as a promising candidate.<sup>21</sup> The proposed mechanism of the covalent modification of *N*-terminal threonine induced by this electrophilic fragment is depicted in Figure 2 and proceeds through cyclocarbonylation.<sup>18,21</sup> In current paper we describe an optimized synthetic approach towards oxathiazol-2-one electrophilic war-



**Figure 1.** Proteasome (immunoproteasome) assembly with  $\beta 1i$  (caspase-like),  $\beta 2i$  (trypsin-like) and  $\beta 5i$  (chymotrypsin-like) *N*-terminal threonine proteases.

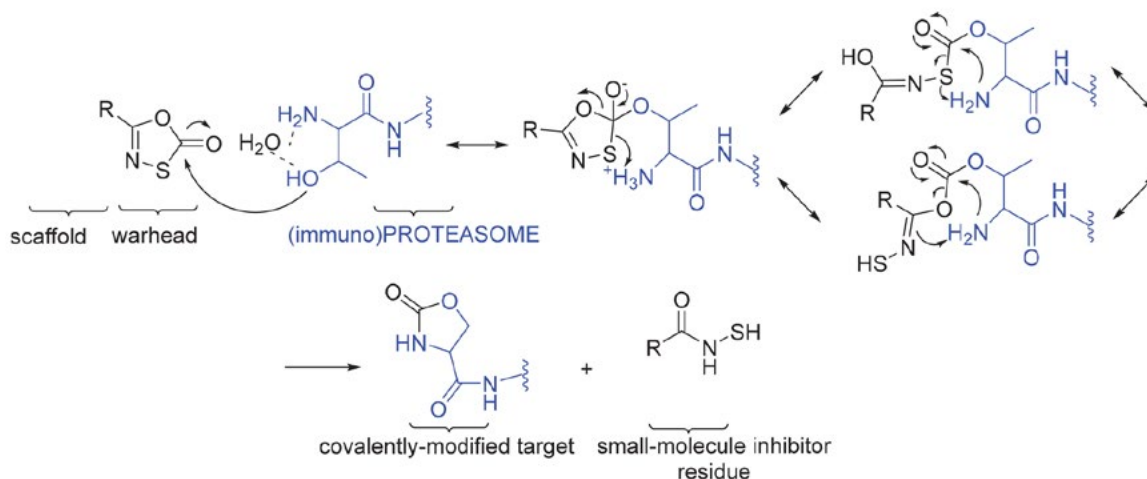


Figure 2. Oxathiazol-2-one electrophilic warhead and its interaction mechanism with the N-terminal threonine in the active site

head in compounds with basic nitrogen atom and the preparation of a focused library of piperidin-3-yl-oxathiazol-2-ones that are suitable for further biological evaluation.

## 2. Results and Discussion

We designed our compounds on the basis of their synthetic accessibility and their potential to be modified accordingly during further optimizations. Therefore, we selected a piperidine central core derivatized with an electrophilic oxathiazol-2-one warhead that could confer the selectivity towards threonine proteases as reported beforehand (Figure 3).<sup>18,21</sup>

We started the synthesis with the alkylation of nipecotamide employing a set of alkyl bromides in DMF as a solvent and  $\text{Na}_2\text{CO}_3$  as a base to obtain compounds **2a**, **2b** and **2c–e**. In the case of compound **2f**, alkylation with *p*-nitrobenzylbromide was followed by hydrogenation in MeOH with final acylation using benzyl chloride. The key step in the synthesis was the cyclization of suitably substituted nipecotamides **2a–f** into piperidin-3-yl-oxathiazol-2-ones **7–3e** using chlorocarbonylsulfonyl chloride as a reagent (Figure 4). This synthetic approach was reported by Gryder *et al.* when they described the synthesis of the oxathiazol-2-one analogue of bortezomib. The penultimate carboxamide dipeptide was successfully transformed

into the oxathiazol-2-one-bortezomib in high yield by using chlorocarbonylsulfonyl chloride in refluxing THF.<sup>22</sup>

Despite our numerous attempts to obtain the final oxathiazol-2-ones **3a–f** by following the original procedure no product could be isolated. Initial experiments in refluxing THF resulted in a complex mixture of products.<sup>23</sup> If the experiments were performed at lower temperature (0 °C, room temperature), no apparent conversion was observed. Our first modification of the original procedure was to use relatively nonpolar and system-inert toluene as a solvent that could provide an alternative reactant/intermediate stabilization pattern and would enable a broader temperature sweep. This system was also described by Gurjar *et al.* where they heated the mixture of amide and chlorocarbonylsulfonyl chloride in toluene from 60 to 90 °C until the settlement of HCl evolution, followed by 1 h of reflux; this yielded > 50% of isolated oxathiazol-2-one.<sup>23</sup> No conversion was observed in our case at lower temperatures (0 °C, room temperature) with a formation of complex mixture of products at 60 °C and reflux conditions. Further experiments using pyridine as solvent afforded similar results. Nevertheless, a difference in reaction scope can be observed as besides previously mentioned report by Gryder *et al.*,<sup>22</sup> literature only describes a relatively simple case of benzamide cyclization towards final 5-phenyl-1,3,4-oxathiazol-2-one. In our case, the reaction incorporated a piperidin-3-yl central scaffold (compounds **2a–e**) containing an additional basic centre. We also conducted a thor-

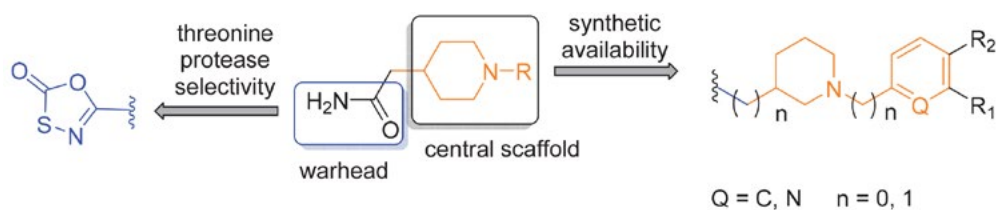
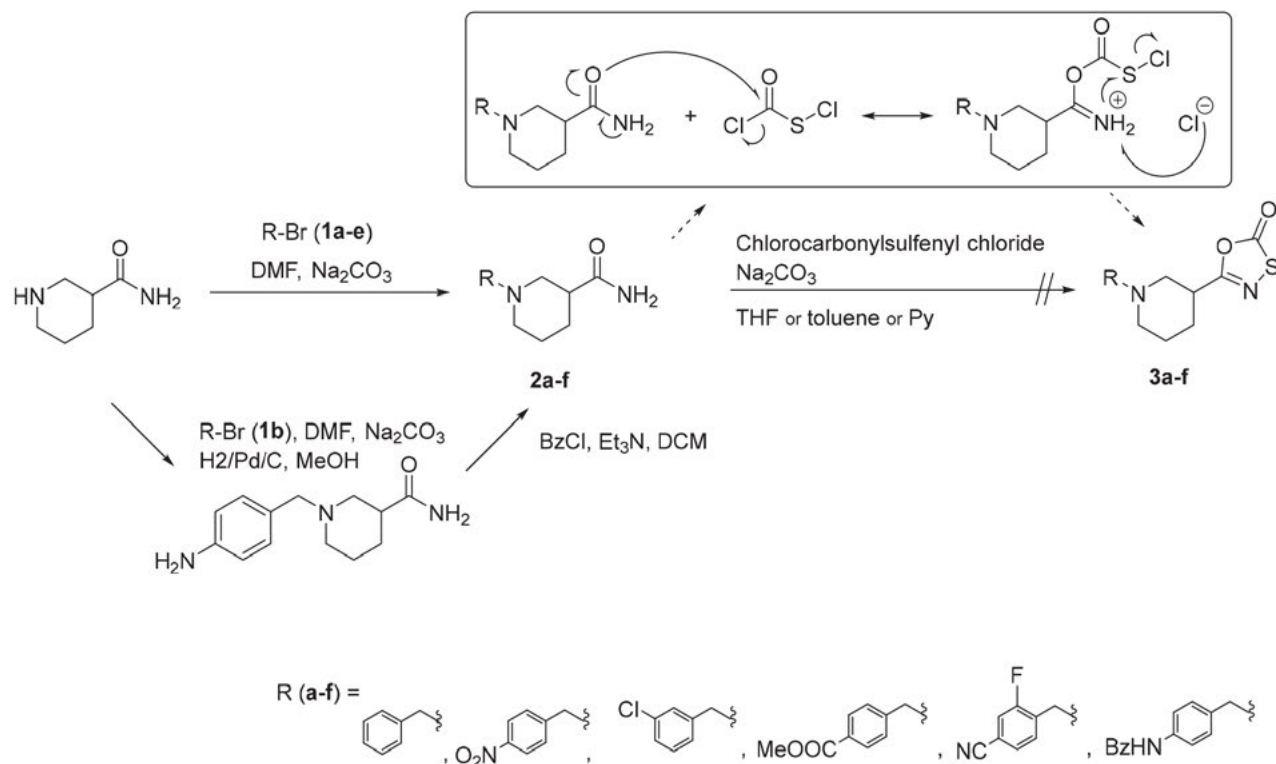


Figure 3. Design of piperidin-3-yl-oxathiazol-2-ones as potential covalent inhibitors of threonine proteases.

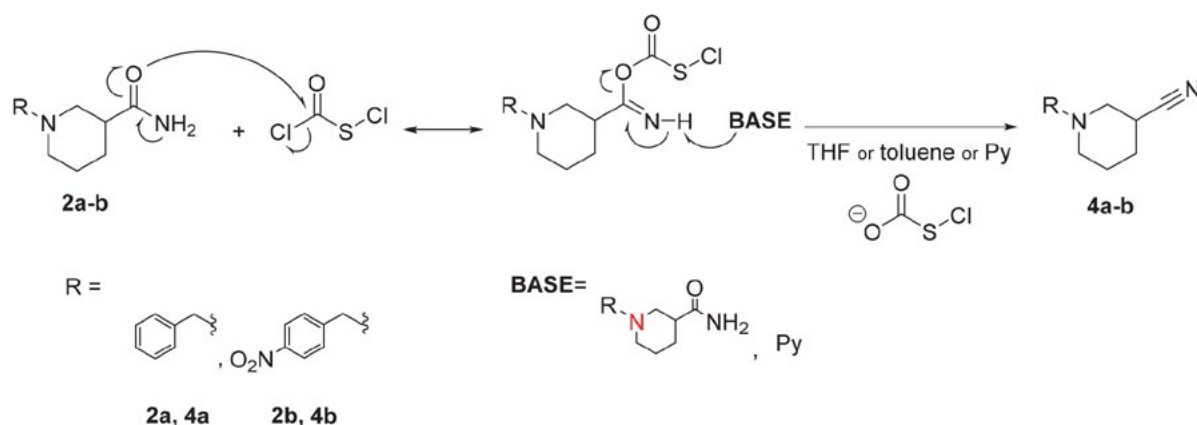


**Figure 4.** Cyclization of piperidine carboxamides towards final piperidin-3-yl-oxathiazol-2-ones.

ough separation of complex product mixtures in the case of cyclization of compound **2a** and identified a dominant side product (> 30% yield) flanked by a myriad of other chemical species that could not be obtained at a significant quantity. The dominant side product was identified when examining its  $^{13}\text{C}$  NMR spectrum. Namely, the carbon atom of the carboxamide **2a** can be found as expected at 178.3 ppm (400 MHz,  $\text{DMSO}-d_6$ ), whereas the carbon of the dominant side product species was found upfield at 121.8 ppm. When recording IR spectrum, a marked peak at  $2240\text{ cm}^{-1}$  was found indicating the presence of a nitrile functionality; the formation of the side product 1-benzylpiperidine-3-carbonitrile **4a** (Figure 5) was then further confirmed by

HRMS. The nature of this reaction outcome can be rationalized as presented in Figure 5.

In our reaction system, the dehydration process is facilitated by the primary amide **2a** (Figure 5) that readily couples with the chlorocarbonylsulfonyl chloride to form an active intermediate (Figure 5). The coupling is followed by rapid elimination that is catalyzed either with the starting substituted piperidine as a base or is assisted by other bases in the reaction system (such as pyridine) to form the corresponding nitrile **4a** (Figure 5). Indeed, similar dehydrations of primary carboxamides using an acidic reagent such as  $\text{POCl}_3$ ,  $\text{SOCl}_2$  are well documented in literature.<sup>24,25</sup> More recent, chemoselective and milder methods were



**Figure 5.** The proposed mechanism of dehydration of primary amides to nitriles using chlorocarbonylsulfonyl chloride.



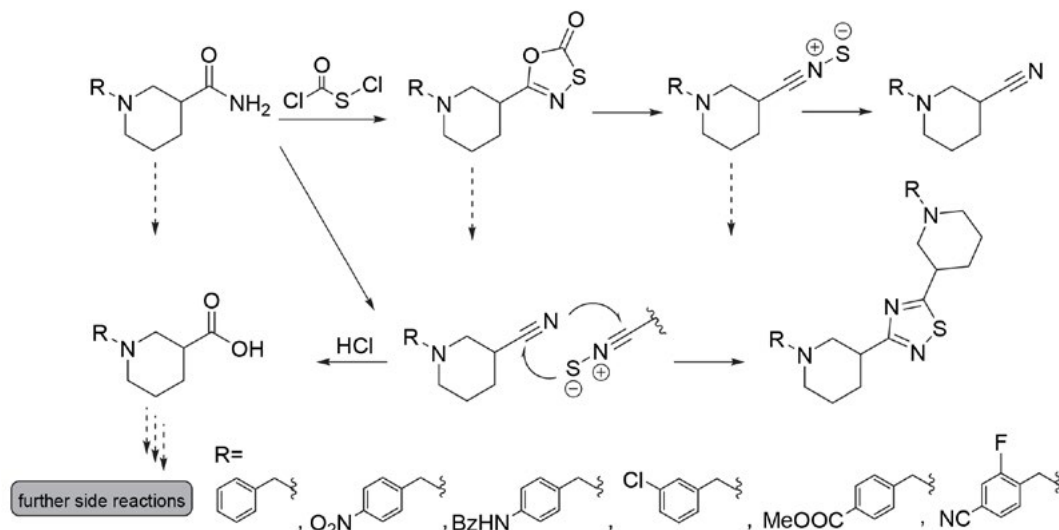


Figure 6. Possible side reaction pathways in the synthesis of piperidin-3-yl-oxathiazol-2-ones.

also reported, where ethyl dichlorophosphate/DBU system or methyl (carboxysulfamoyl)triethylammonium hydroxide (Burgess reagent) were used as the dehydrating reagents.<sup>26,27</sup> In addition, Vilsmeier reagents,<sup>28</sup> bromodimethylsulfonium bromide (BDMS),<sup>29</sup> PdCl<sub>2</sub> in aqueous acetonitrile,<sup>30</sup> Swern oxidation conditions and other catalytic or alternative methods using silanes, silazanes, chlorosilanes, alkoxy silanes, and aminosilanes were also de-

scribed.<sup>31–33</sup> The myriad of reaction side products that was observed is a consequence of multitude of side reactions that can occur during dehydration reactions, such as thermal decomposition of the formed oxathiazol-2-one and hydrolysis reactions (Figure 6). The formed oxathiazol-2-one can also take part in the 1,3-dipolar nitrile sulphide cycloaddition reaction with available nitrile to obtain thiadiazoles as side products.<sup>34</sup> The nitrile sulphide is

Table 1. Synthesis of piperidin-3-yl-oxathiazol-2-ones 3a–f.

Cpd. No	Product	Yield ( $\eta$ ) (%) <sup>a</sup>
3a		68
3b		22
3c		42
3d		33
3e		43
3f		16

<sup>a</sup> Yield after purification using column chromatography (SiO<sub>2</sub> support with *n*-hexane:EtOAc solvent system as an eluent).

generated *in situ* by thermal decomposition of oxathiazol-2-one.<sup>35</sup> Nitrile sulphides are short-lived species prone to fragmentation and can take part in further cycloadditions.<sup>36–38</sup>

After initial unsuccessful attempts to prepare the desired compounds **3a–f**, we turned our attention to microwave-assisted report on flow-chemistry synthesis of oxathiazol-2-one in dioxane at 200 °C and residence time of 1 min in a flow reactor reported by Öhrngren *et al.*<sup>39</sup> On this basis, we modified the reaction procedure and dissolved the carboxamides **2a–f** (Figure 4) in dry dioxane (27 mL/1 mmol carboxamide), used an excess of solid Na<sub>2</sub>CO<sub>3</sub> (5 eq) and chlorocarbonylsulfonyl chloride (2 eq), and stirred the reaction mixture at 100 °C for 16 h under argon to obtain the desired oxathiazol-2-ones **3a–f** (Figure 4) in 16 to 68% yields (Table 1).

### 3. Experimental

Chemicals from commercial sources were used without further purification. Anhydrous THF, DCM and Et<sub>3</sub>N were dried and purified by distillation over Na, K<sub>2</sub>CO<sub>3</sub> and KOH, respectively. Analytical thin-layer chromatography (TLC) was performed on Merck silica gel (60F<sub>254</sub>) plates (0.25 mm). Column chromatography was performed on silica gel 60 (Merck, particle size 0.040–0.063 mm). Melting points were determined on a Reichert hot stage microscope and are uncorrected. <sup>1</sup>H-, COSY-, HMQC- and <sup>13</sup>C-NMR spectra were recorded on a Bruker AVANCE DPX<sub>400</sub> spectrometer in CDCl<sub>3</sub> or DMSO-*d*<sub>6</sub> solution with TMS as internal standard. Chemical shifts are reported in ppm (δ) downfield from TMS. All the coupling constants (*J*) are in hertz. IR spectra were recorded on a PerkinElmer Spectrum BX System FT-IR spectrometer. Mass spectra were obtained with a VG-Analytical Autospec Q mass spectrometer with ESI ionization (MS Centre, Jožef Stefan Institute, Ljubljana). All reported yields are those of purified products.

#### 1-Benzylpiperidine-3-carboxamide (2a)

To a solution of piperidine-3-carboxamide (500 mg, 3.90 mmol) in 50 mL DMF, solid Na<sub>2</sub>CO<sub>3</sub> (460 mg, 4.33 mmol) and benzyl bromide (1.44 g, 8.42 mmol) were added. The reaction was stirred at 100 °C overnight. DMF was removed under reduced pressure, the residue dissolved in EtOAc (30 mL) and extracted with 0.5 M HCl (2 × 15 mL). The pH of combined aqueous phases was adjusted to 8 with NaHCO<sub>3</sub> and extracted with EtOAc (4 × 30 mL). Combined organic phases were washed with H<sub>2</sub>O (1 × 30 mL), brine (1 × 30 mL) and dried over Na<sub>2</sub>SO<sub>4</sub>. The volatiles were removed under reduced pressure to give compound **2a** as white solid. Yield = 56%; TLC (EtOAc:MeOH = 2:1), R<sub>f</sub> = 0.50; m.p. 108–110 °C; <sup>1</sup>H NMR (400 MHz, DMSO-*d*<sub>6</sub>) δ 1.34–1.48 (m, 2H, H-5), 1.58–1.74 (m, 2H, H-4), 1.85–1.99 (m, 2H, H-6), 2.27–2.32 (m, 1H, H-2),

2.68–2.78 (m, 2H, H-2 and H-3), 3.44 (dd, *J* 4.4, 13.2 Hz, 2H, CH<sub>2</sub>), 6.75 (br s, 1H, NH<sub>2</sub>), 7.22–7.34 (m, 6H, ArH and NH<sub>2</sub>); <sup>13</sup>C NMR (400 MHz, CDCl<sub>3</sub>) δ 22.8 (C-5), 26.9 (C-4), 41.8 (C-3), 53.8 (C-6), 55.0 (C-2), 63.5 (CH<sub>2</sub>), 127.4 (C-4'), 128.4 (C-3' and C-5'), 129.2 (C-2' and C-6'), 137.6 (C-1'), 178.0 (OCNH<sub>2</sub>); IR (ATR) ν 3333, 3148, 2932, 2758, 1632, 1429, 1368, 1356, 1337, 1253, 1100, 1070, 1002, 858, 734, 698, 666, 564, 518 cm<sup>-1</sup>; MS *m/z* (relative intensity): 240.95 (M+Na, 100), 219.03 (M+H, 30).

#### 1-(4-Nitrobenzyl)piperidine-3-carboxamide (2b)

To a solution of piperidine-3-carboxamide (500 mg, 3.90 mmol) in 50 mL DMF, solid Na<sub>2</sub>CO<sub>3</sub> (460 mg, 4.33 mmol) and 4-nitrobenzyl bromide (1.69 g, 7.82 mmol) were added. The reaction was stirred at 100 °C overnight. DMF was removed under reduced pressure, the residue dissolved in EtOAc (30 mL) and extracted with 0.5 M HCl (2 × 15 mL). The pH of combined aqueous phases was adjusted to 8 with NaHCO<sub>3</sub> and extracted with EtOAc (4 × 30 mL). Combined organic phases were washed with H<sub>2</sub>O (1 × 30 mL), brine (1 × 30 mL) and dried over Na<sub>2</sub>SO<sub>4</sub>. The volatiles were removed under reduced pressure to give compound **2b** as pale orange solid. Yield = 93%; TLC (EtOAc:MeOH = 2:1), R<sub>f</sub> = 0.63; m.p. 111–114 °C; <sup>1</sup>H NMR (400 MHz, DMSO-*d*<sub>6</sub>) δ 1.33–1.36 (m, 1H, H-5), 1.43–1.48 (m, 1H, H-4), 1.60–1.65 (m, 1H, H-5), 1.72–1.76 (m, 1H, H-4), 1.91–2.09 (m, 2H, H-6 and H-2), 2.30–2.33 (m, 1H, H-6), 2.69–2.78 (m, 2H, H-2 and H-3), 3.55–3.63 (m, 2H, CH<sub>2</sub>), 6.76 (br s, 1H, NH<sub>2</sub>), 7.27 (br s, 1H, NH<sub>2</sub>), 7.56–7.60 (m, 2H, H-2' and H-6'), 8.19 (dd, *J* 2.0, 4.8 Hz, 2H, H-3' and H-5'); <sup>13</sup>C NMR (400 MHz, DMSO-*d*<sub>6</sub>) δ 24.4 (C-5), 27.0 (C-4), 42.3 (C-3), 53.2 (C-6), 55.8 (C-2), 61.4 (CH<sub>2</sub>), 123.3 (C-3' and C-5'), 129.6 (C-2' and C-6'), 146.5 (C-1'), 146.9 (C-4'), 175.4 (OCNH<sub>2</sub>); IR (ATR) ν 3385, 3180, 2926, 2787, 1644, 1605, 1512, 1421, 1341, 1249, 1204, 1166, 1102, 1048, 989, 862, 797, 736, 720 cm<sup>-1</sup>; MS *m/z* (relative intensity): 261.97 (M-H, 100).

#### 1-(4-Chlorobenzyl)piperidine-3-carboxamide (2c)

To a solution of piperidine-3-carboxamide (500 mg, 3.90 mmol) in 50 mL DMF, solid Na<sub>2</sub>CO<sub>3</sub> (460 mg, 4.33 mmol) and 3-chlorobenzyl bromide (1.64 g, 7.99 mmol) were added. The reaction was stirred at 100 °C overnight. DMF was removed under reduced pressure, the residue dissolved in EtOAc (30 mL) and extracted with 0.5 M HCl (2 × 15 mL). The pH of combined aqueous phases was adjusted to 8 with NaHCO<sub>3</sub> and extracted with EtOAc (4 × 30 mL). Combined organic phases were washed with H<sub>2</sub>O (1 × 30 mL), brine (1 × 30 mL) and dried over Na<sub>2</sub>SO<sub>4</sub>. The volatiles were removed under reduced pressure to give compound **2c** as pale orange solid. Yield = 53%; TLC (EtOAc:MeOH = 2:1), R<sub>f</sub> = 0.60; <sup>1</sup>H NMR (400 MHz, CDCl<sub>3</sub>) δ 1.55–1.61 (m, 1H, H-5), 1.65–1.77 (m, 2H, H-4 and H-5), 1.82–1.84 (m, 1H, H-4), 2.26 (s, 1H, H-6), 2.44–2.53 (m, 2H, H-2 and H-6), 2.59 (s, 1H, H-2), 2.73

(s, 1H, H-3), 3.46 (s, 2H, CH<sub>2</sub>), 6.07 (br s, 1H, NH<sub>2</sub>), 7.14–7.16 (m, 1H, NH<sub>2</sub>), 7.24–7.26 (m, 4H, ArH); <sup>13</sup>C NMR (400 MHz, CDCl<sub>3</sub>) δ 22.9 (C-5), 26.9 (C-4), 41.9 (C-3), 53.7 (C-6), 55.1 (C-2), 62.9 (CH<sub>2</sub>), 127.2, 127.6 (C-3' and C-5'), 129.1, 129.7 (C-2' and C-6'), 134.3 (C-4'), 139.8 (C-1'), 177.8 (CONH<sub>2</sub>); IR (ATR) ν 3342, 3162, 2937, 2800, 2763, 1626, 1597, 1573, 1426, 1371, 1342, 1300, 1256, 1207, 1157, 1106, 1075, 1044, 996, 985, 930, 892, 875, 863, 808, 786, 776, 717, 682, 655, 569, 516 cm<sup>-1</sup>; MS *m/z* (relative intensity): 275.29 (M+Na, 100), 253.29 (M+H, 20).

#### Methyl 4-((3-carbamoylpiperidin-1-yl)methyl)benzoate (2d)

To a solution of piperidine-3-carboxamide (200 mg, 1.56 mmol) in 50 mL DMF, solid Na<sub>2</sub>CO<sub>3</sub> (320 mg, 3.02 mmol) and methyl 4-(bromomethyl)benzoate (540 mg, 2.36 mmol) were added. The reaction was stirred at 100 °C overnight. DMF was removed under reduced pressure, the residue dissolved in EtOAc (30 mL) and extracted with 0.5 M HCl (2 × 15 mL). The pH of combined aqueous phases was adjusted to 8 with NaHCO<sub>3</sub> and extracted with EtOAc (4 × 30 mL). Combined organic phases were washed with H<sub>2</sub>O (1 × 30 mL), brine (1 × 30 mL) and dried over Na<sub>2</sub>SO<sub>4</sub>. The volatiles were removed under reduced pressure to give compound **2d** as white solid. Yield = 91 %; TLC (EtOAc:MeOH = 2:1), R<sub>f</sub> = 0.62; <sup>1</sup>H NMR (400 MHz, DMSO-*d*<sub>6</sub>) δ 1.32–1.42 (m, 1H, H-5), 1.44–1.49 (m, 1H, H-4), 1.59–1.64 (m, 1H, H-5), 1.71–1.75 (m, 1H, H-4), 1.88–1.95 (m, 1H, H-6), 1.98–2.03 (m, 1H, H-2), 2.29–2.35 (m, 1H, H-6), 2.68–2.71 (m, 1H, H-2), 2.74–2.78 (m, 1H, H-3), 3.52 (d, *J* 2.8 Hz, 2H, CH<sub>2</sub>), 3.85 (s, 3H, CH<sub>3</sub>), 6.77 (br s, 1H, NH<sub>2</sub>), 7.27 (br s, 1H, NH<sub>2</sub>), 7.44 (d, *J* 8.4 Hz, 2H, H-2' and H-6'), 7.92 (dd, *J* 2.0, 4.8 Hz, 2H, H-3' and H-5'); IR (ATR) ν 3403, 3183, 2936, 2797, 1715, 1647, 1434, 1415, 1273, 1239, 1199, 1165, 1112, 1086, 1027, 995, 964, 860, 806, 760, 754, 706 cm<sup>-1</sup>.

#### 1-(4-Cyano-2-fluorobenzyl)piperidine-3-carboxamide (2e)

To a solution of piperidine-3-carboxamide (500 mg, 3.90 mmol) in 50 mL DMF, solid Na<sub>2</sub>CO<sub>3</sub> (460 mg, 4.33 mmol) and 4-(bromomethyl)-3-fluorobenzonitrile (1.75 g, 8.17 mmol) were added. The reaction was stirred at 100 °C overnight. DMF was removed under reduced pressure, the residue dissolved in EtOAc (30 mL) and extracted with 0.5 M HCl (2 × 15 mL). The pH of combined aqueous phases was adjusted to 8 with NaHCO<sub>3</sub> and extracted with EtOAc (4 × 30 mL). Combined organic phases were washed with H<sub>2</sub>O (1 × 30 mL), brine (1 × 30 mL) and dried over Na<sub>2</sub>SO<sub>4</sub>. The volatiles were removed under reduced pressure to give compound **2e** as pale yellow solid. Yield = 71 %; TLC (EtOAc:MeOH = 2:1), R<sub>f</sub> = 0.66; m.p. 126–128 °C; <sup>1</sup>H NMR (400 MHz, DMSO-*d*<sub>6</sub>) δ 1.30–1.31 (m, 1H, H-5), 1.42–1.45 (m, 1H, H-4), 1.59–1.64 (m, 1H, H-5), 1.69–1.73 (m, 1H, H-4), 1.93–1.99 (m, 1H, H-6), 2.02–2.08 (m, 1H, H-2), 2.28–2.33 (m, 1H, H-6), 2.67–2.70 (m,

1H, H-2), 2.74–2.78 (m, 1H, H-3), 3.58 (s, 2H, CH<sub>2</sub>), 6.77 (br s, 1H, NH<sub>2</sub>), 7.27 (br s, 1H, NH<sub>2</sub>), 7.61 (t, *J* 7.6 Hz, 1H, H-5'), 7.68 (dd, *J* 1.6, 6.4 Hz, 1H, H-2'), 7.82 (dd, *J* 1.6, 8.4 Hz, 1H, H-3'); <sup>13</sup>C NMR (400 MHz, CDCl<sub>3</sub>) δ 22.9 (C-5), 26.8 (C-4), 41.9 (C-3), 53.5 (C-6), 55.3 (C-2), 56.0 (CH<sub>2</sub>), 112.8 (C-4'), 117.5 (CN), 119.2 (C-5'), 128.1 (C-3'), 130.8 (C-1'), 132.3 (C-2'), 162.1 (C-6'), 177.5 (OCNH<sub>2</sub>); IR (ATR) ν 3364, 3187, 2929, 2811, 2227, 1646, 1611, 1569, 1486, 1411, 1350, 1298, 1246, 1201, 1166, 1089, 1002, 941, 849, 830, 731 cm<sup>-1</sup>; MS *m/z* (relative intensity): 283.71 (M+Na, 100), 261.78 (M+H, 20).

#### 1-(4-Benzamidobenzyl)piperidine-3-carboxamide (2f)

Argon was bubbled into a solution of **2b** (5.811 g, 17.6 mmol) in MeOH (70 mL) for 15 minutes. 10% Pd/C, unreduced, was then added and H<sub>2</sub> was bubbled into the stirred solution until the starting compound was no longer observed with TLC. Pd/C was filtered off and the solution concentrated *in vacuo* to yield crude product which was purified with column chromatography (EtOAc:MeOH = 2:1). Oily product was dissolved in DCM (30 mL). Et<sub>3</sub>N (250 mg, 2.47 mmol) and benzoyl chloride (265 mg, 2.36 mmol) were added and the reaction mixture was stirred at room temperature overnight. DCM was removed under reduced pressure, the residue dissolved in EtOAc (30 mL) and extracted with 0.5 M HCl (1 × 10 mL). The pH of combined aqueous phases was adjusted to 8 with NaHCO<sub>3</sub> and extracted with EtOAc (2 × 15 mL). Combined organic phases were washed with H<sub>2</sub>O (1 × 20 mL), brine (1 × 20 mL) and dried over Na<sub>2</sub>SO<sub>4</sub>. The volatiles were removed under reduced pressure to give compound **2f** as colourless oil. Yield = 16 %; TLC (EtOAc:MeOH = 2:1), R<sub>f</sub> = 0.36; <sup>1</sup>H NMR (400 MHz, DMSO-*d*<sub>6</sub>) δ 1.06–1.63 (m, 1H, H-5), 1.64–1.70 (m, 3H, H-4 and H-5), 1.89–1.99 (m, 1H, H-6), 2.29–2.34 (m, 2H, H-2 and H-6), 2.67–2.76 (m, 1H, H-2), 2.78–2.99 (m, 1H, H-3), 3.01–3.51 (m, 2H, CH<sub>2</sub>), 6.76 (br s, 1H, NH<sub>2</sub>), 7.24–7.29 (m, 3H, H-2' and H-6' and NH<sub>2</sub>), 7.52–7.62 (m, 3H, H-3" and H-4" and H-5"), 7.72–7.76 (m, 2H, H-3' and H-5'), 7.95–7.97 (m, 2H, H-2" and H-6"), 10.26 (d, *J* 4.4 Hz, 1H, NH).

#### 5-(1-Benzylpiperidin-3-yl)-1,3,4-oxathiazol-2-one (3a)

To a solution of 1-benzylpiperidine-3-carboxamide (**2a**, 240 mg, 1.10 mmol) in dioxane (30 mL) in a three-necked flask, solid Na<sub>2</sub>CO<sub>3</sub> (580 mg, 5.47 mmol) and chlorocarbonylsulfonyl chloride (288 mg, 2.20 mmol) were added under argon. The reaction mixture was stirred at 100 °C overnight, cooled to room temperature and after the addition of Et<sub>3</sub>N (0.75 mL) stirred for 15 minutes. The precipitate was filtered off and the residue concentrated *in vacuo*. Product was purified with column chromatography using hexane:EtOAc=3:1 as an eluent to give yellow oily product. Yield = 68%; TLC (hexane:EtOAc = 3:1), R<sub>f</sub> = 0.56; <sup>1</sup>H NMR (400 MHz, DMSO-*d*<sub>6</sub>) δ 1.50–1.56 (m, 2H, H-5 and H-4), 1.70–1.72 (m, 1H, H-5), 1.88–1.93 (m, 1H, H-4), 2.08–2.12 (m, 1H, H-6), 2.20–2.25 (m, 1H, H-2),

2.65–2.68 (m, 1H, H-6), 2.88–2.92 (m, 2H, H-2 and H-3), 3.50 (d, *J* 2.8 Hz, 2H, CH<sub>2</sub>), 7.23–7.34 (m, 5H, ArH); <sup>13</sup>C NMR (400 MHz, CDCl<sub>3</sub>) δ 24.2 (C-5), 27.0 (C-4), 38.6 (C-3), 53.5 (C-6), 55.1 (C-2), 63.1 (CH<sub>2</sub>), 127.2 (C-4'), 128.3 (C-3' and C-5'), 128.9 (C-2' and C-6'), 137.8 (C-1'), 162.9 (NCO), 174.3 (SCO); IR (ATR) ν 2942, 2800, 1758, 1666, 1599, 1493, 1467, 1450, 1350, 1320, 1287, 1188, 1152, 1097, 1071, 1049, 1025, 981, 926, 879, 791, 769, 738, 697, 664, 633, 599, 569, 522 cm<sup>-1</sup>; HRMS-ESI (*m/z*): [M+H]<sup>+</sup> calcd for C<sub>14</sub>H<sub>16</sub>N<sub>2</sub>O<sub>2</sub>S, 277.1015, found, 277.1011.

### 5-(1-(4-Nitrobenzyl)piperidin-3-yl)-1,3,4-oxathiazol-2-one (3b)

To a solution of 1-(4-nitrobenzyl)piperidine-3-carboxamide (**2b**, 100 mg, 0.380 mmol) in dioxane (20 mL) in a three-necked flask, solid Na<sub>2</sub>CO<sub>3</sub> (200 mg, 1.87 mmol) and chlorocarbonylsulfonyl chloride (100 mg, 0.760 mmol) were added under argon. The reaction mixture was stirred at 100 °C overnight, cooled to room temperature and after the addition of Et<sub>3</sub>N (0.27 mL) stirred for 15 minutes. The precipitate was filtered off and the residue concentrated *in vacuo*. Product was purified with column chromatography using hexane:EtOAc = 2:1 as an eluent to give yellow oily product. Yield = 22%; TLC (hexane:EtOAc = 2:1), R<sub>f</sub> = 0.38; <sup>1</sup>H NMR (400 MHz, DMSO-*d*<sub>6</sub>) δ 1.52–1.58 (m, 2H, H-4 and H-5), 1.71–1.74 (m, 1H, H-5), 1.91–1.94 (1H, H-4), 2.16 (s, 1H, H-6), 2.26 (d, *J* 9.6 Hz, H-2), 2.65–2.68 (m, 1H, H-6), 2.88–2.96 (m, 2H, H-2 and H-3), 3.65 (s, 2H, CH<sub>2</sub>), 7.58 (d, *J* 8.8 Hz, 2H, H-3' and H-5'), 8.18 (d, *J* 8.8 Hz, 2H, H-2' and H-6'); <sup>13</sup>C NMR (400 MHz, DMSO-*d*<sub>6</sub>) δ 24.1 (C-5), 26.6 (C-4), 38.3 (C-3), 53.5 (C-6), 54.9 (C-2), 61.5 (CH<sub>2</sub>), 123.8 (C-2' and 6'), 130.1 (C-3' and C-5'), 147.0 (C-1' and C-4'), 162.9 (NCO), 174.7 (SCO); IR (ATR) ν 2939, 2792, 1758, 1598, 1515, 1340, 1191, 1092, 926, 858, 802, 738, 650, 571 cm<sup>-1</sup>; HRMS-ESI (*m/z*): [M+H]<sup>+</sup> calcd for C<sub>14</sub>H<sub>15</sub>N<sub>3</sub>O<sub>4</sub>S, 322.0867, found, 322.0862.

### 5-(1-(4-Chlorobenzyl)piperidin-3-yl)-1,3,4-oxathiazol-2-one (3c)

To a solution of 1-(4-chlorobenzyl)piperidine-3-carboxamide (**2c**, 300 mg, 1.19 mmol) in dioxane (30 mL) in a three-necked flask, solid Na<sub>2</sub>CO<sub>3</sub> (630 mg, 5.94 mmol) and chlorocarbonylsulfonyl chloride (466 mg, 3.55 mmol) were added under argon. The reaction mixture was stirred at 100 °C overnight, cooled to room temperature and after the addition of Et<sub>3</sub>N (0.83 mL) stirred for 15 minutes. The precipitate was filtered off and the residue concentrated *in vacuo*. Product was purified with column chromatography using hexane:EtOAc = 3:1 as an eluent to give brown oily product. Yield = 33 %; TLC (H:EtOAc = 3:1), R<sub>f</sub> = 0.42; <sup>1</sup>H NMR (400 MHz, CDCl<sub>3</sub>) δ 1.57–1.69 (m, 2H, H-5 and H-4), 1.77–1.83 (m, 1H, H-5), 2.01–2.04 (m, 1H, H-4), 2.09–2.14 (m, H, H-6), 2.28–2.33 (m, 1H, H-2), 2.73–2.76 (m, 1H, H-6), 2.89–2.98 (m, 2H, H-2 and H-3), 3.50 (s, 2H, CH<sub>2</sub>), 7.16–7.31 (m, 4H, ArH); <sup>13</sup>C NMR (400 MHz,

CDCl<sub>3</sub>) δ 24.2 (C-5), 26.9 (C-4), 38.6 (C-3), 53.5 (C-6), 55.1 (C-2), 62.5 (CH<sub>2</sub>), 126.9, 127.4 (C-3' and C-5'), 128.9, 128.6 (C-2' and C-6'), 134.2 (C-4'), 140.2 (C-1'), 162.7 (NCO), 174.3 (SCO); IR (ATR) ν 3339, 3160, 2938, 2801, 2764, 1762, 1626, 1598, 1573, 1463, 1427, 1371, 1342, 1300, 1257, 1207, 1157, 1105, 1075, 1046, 997, 930, 892, 876, 863, 808, 776, 717, 705, 682, 655, 569, 536, 516 cm<sup>-1</sup>; HRMS-ESI (*m/z*): [M+H]<sup>+</sup> calcd for C<sub>14</sub>H<sub>15</sub>ClN<sub>2</sub>O<sub>2</sub>S, 311.0626, found, 311.0621.

### Methyl 4-((3-(2-oxo-1,3,4-oxathiazol-5-yl)piperidin-1-yl)methyl)benzoate (3d)

To a solution of methyl 4-((3-carbamoylpiperidin-1-yl)methyl)benzoate (**2d**, 300 mg, 1.09 mmol) in dioxane (30 mL) in a three-necked flask, solid Na<sub>2</sub>CO<sub>3</sub> (570 mg, 5.38 mmol) and chlorocarbonylsulfonyl chloride (285 mg, 2.16 mmol) were added under argon. The reaction mixture was stirred at 100 °C overnight, cooled to room temperature and after the addition of Et<sub>3</sub>N (0.75 mL) stirred for 15 minutes. The precipitate was filtered off and the residue concentrated *in vacuo*. Product was purified with column chromatography using hexane:EtOAc = 2:1 as an eluent to give yellow oily product. Yield = 43%; TLC (hexane:EtOAc = 2:1), R<sub>f</sub> = 0.29; <sup>1</sup>H NMR (400 MHz, DMSO-*d*<sub>6</sub>) δ 1.45–1.57 (m, 2H, H-5, H-4), 1.72–1.75 (m, 1H, H-5), 1.91–1.95 (m, 1H, H-4), 2.09–2.17 (m, 1H, H-6), 2.24–2.34 (m, 1H, H-2), 2.65–2.68 (m, 1H, H-6), 2.87–2.96 (m, 2H, H-2 and H-3), 3.59 (s, 2H, CH<sub>2</sub>), 3.85 (s, 3H, CH<sub>3</sub>), 7.45 (d, *J* 8.4 Hz, 2H, H-2' and H-6'), 7.93 (dd, *J* 2.0, 4.8 Hz, 2H, H-3' and H-5'); <sup>13</sup>C NMR (400 MHz, DMSO-*d*<sub>6</sub>) δ 23.5 (C-5), 26.1 (C-4), 37.5 (CH<sub>2</sub>), 52.0 (C-6), 53.0 (C-2), 54.5 (CH<sub>3</sub>), 61.5 (CH<sub>2</sub>), 128.3, 128.7, 128.8, 129.1, 129.1 (C-2',3',4',5',6'), 144.0 (C-1'), 162.4 (CO), 166.1 (NCO), 174.2 (SCO); IR (ATR) ν 2946, 2801, 1759, 1717, 1609, 1434, 1415, 1395, 1349, 1309, 1275, 1190, 1173, 1106, 1049, 980, 928, 885, 801, 758, 731, 701, 650, 572, 538 cm<sup>-1</sup>; HRMS-ESI (*m/z*): [M+H]<sup>+</sup> calcd for C<sub>16</sub>H<sub>18</sub>N<sub>2</sub>O<sub>4</sub>S, 335.1061, found, 335.1066.

### 3-Fluoro-4-((3-(2-oxo-1,3,4-oxathiazol-5-yl)piperidin-1-yl)methyl)benzotrile (3e)

To a solution of 1-(4-cyano-2-fluorobenzyl)piperidine-3-carboxamide (**2e**, 300 mg, 1.15 mmol) in dioxane (30 mL) in a three-necked flask, solid Na<sub>2</sub>CO<sub>3</sub> (608 mg, 5.74 mmol) and chlorocarbonylsulfonyl chloride (303 mg, 2.30 mmol) were added under argon. The reaction mixture was stirred at 100 °C overnight, cooled to room temperature and after the addition of Et<sub>3</sub>N (0.75 mL) stirred for 15 minutes. The precipitate was filtered off and the residue concentrated *in vacuo*. Product was purified with column chromatography using hexane:EtOAc = 3:1 as an eluent to give yellow oily product. Yield = 43%; TLC (hexane:EtOAc = 3:1), R<sub>f</sub> = 0.29; <sup>1</sup>H NMR (400 MHz, DMSO-*d*<sub>6</sub>) δ 1.51–1.56 (m, 2H, H-5 and H-4), 1.70–1.72 (m, 1H, H-5), 1.91–1.92 (m, 1H, H-4), 2.14–2.19 (m, 1H, H-6), 2.30–2.35 (m, 1H, H-2), 2.64–2.67 (m, 1H, H-6), 2.91–2.95 (m,

2H, H-3 and H-2), 3.65 (s, 2H, CH<sub>2</sub>), 7.62 (t, J 7.6 Hz, 1H, H-5'), 7.69 (dd, J 1.6, 6.4 Hz, 1H, H-2'), 7.83 (dd, J 1.2, 8.4 Hz, 1H, H-3'); <sup>13</sup>C NMR (400 MHz, DMSO-*d*<sub>6</sub>) δ 23.5 (C-5), 26.0 (C-4), 37.5 (C-3), 52.7 (C-6), 54.2 (C-2), 54.3 (CH<sub>2</sub>), 111.3 (C-4'), 117.7 (CN), 119.3 (C-5'), 128.5 (C-3'), 131.2 (C-1'), 132.2 (C-2'), 158.8 (C-6), 162.4 (NCO), 174.2 (SCO); IR (ATR) ν 2947, 2811, 2232, 1758, 1599, 1571, 1496, 1413, 1356, 1260, 1189, 1153, 1089, 1050, 1024, 981, 941, 925, 870, 835, 783, 711, 621, 569 cm<sup>-1</sup>; HRMS-ESI (*m/z*): [M+H]<sup>+</sup> calcd for C<sub>15</sub>H<sub>14</sub>FN<sub>3</sub>O<sub>2</sub>S, 320.0873, found, 320.0869.

#### N-(4-((3-(2-oxo-1,3,4-oxathiazol-5-yl)piperidin-1-yl)methyl)phenyl)benzamide (3f)

To a solution of 1-(4-benzamidobenzyl)piperidine-3-carboxamide (2f, 83 mg, 0.250 mmol) in dioxane (30 mL) in a three-necked flask, solid Na<sub>2</sub>CO<sub>3</sub> (130 mg, 1.23 mmol) and chlorocarbonylsulfonyl chloride (65 mg, 0.492 mmol) were added under argon. The reaction mixture was stirred at 100 °C overnight, cooled to room temperature and after the addition of Et<sub>3</sub>N (0.75 mL) stirred for 15 minutes. The precipitate was filtered off and the residue concentrated *in vacuo*. Product was purified with column chromatography using hexane:EtOAc = 3:1 as an eluent to give yellow oily product. Yield = 16%; TLC (hexane:EtOAc = 3:1), R<sub>f</sub> = 0.07; <sup>1</sup>H NMR (400 MHz, DMSO-*d*<sub>6</sub>) δ 1.02–1.24 (m, 2H, H-5 and H-4), 1.54–1.56 (m, 1H, H-5), 1.68 (s, 2H, H-4 and H-6), 2.28–2.30 (m, 1H, H-2), 2.46–2.47 (m, 1H, H-6), 2.58–2.60 (m, 1H, H-2), 3.02 (s, 1H, H-3), 3.44–3.55 (m, 2H, CH<sub>2</sub>), 7.28 (d, J 8.4 Hz, 2H, H-2' and H-6'), 7.52–7.60 (m, 3H, H-3'' and H-4'' and H-5''), 7.74 (d, J 8.4 Hz, 2H, H-3' and H-5'), 7.94–7.97 (m, 2H, H-2'' and H-6''), 10.26 (s, 1H, NH); <sup>13</sup>C NMR (400 MHz, CDCl<sub>3</sub>) δ 23.4 (C-5), 27.6 (C-4), 52.9 (C-3), 54.7 (C-6), 62.1 (C-2), 76.5 (CH<sub>2</sub>), 120.2 (C-3' and C-5'), 127.1 (C-2'' and C-6''), 128.8 (C-2', C-6', C-3'' and C-5''), 129.8 (C-4'), 131.9 (C-1' and C-1''), 134.9 (C-4'), 165.8 (NHCO); IR (ATR) ν 2950, 2916, 2868, 2837, 1655, 1601, 1523, 1458, 1410, 1376, 1319, 1258, 1167, 1098, 997, 973, 841, 809, 168, 694 cm<sup>-1</sup>; HRMS-ESI (*m/z*): [M+H]<sup>+</sup> calcd for C<sub>12</sub>H<sub>21</sub>N<sub>3</sub>O<sub>3</sub>S, 396.1377, found, 396.1382.

#### 1-Benzylpiperidine-3-carbonitrile (4a)

In a three-necked flask 1-benzyl piperidine-3-carboxamide (2a, 100 mg, 0.458 mmol) was dissolved in pyridine (5 mL). Solution was cooled on ice and chlorocarbonylsulfonyl chloride (120 mg, 0.916 mmol) was added dropwise under argon. The reaction mixture was stirred at 80 °C overnight, cooled to room temperature and after the addition of Et<sub>3</sub>N (0.32 mL) stirred for 15 minutes. The precipitate was filtered off and the residue concentrated *in vacuo*. Product was purified with column chromatography using DCM: MeOH = 9:1 as an eluent to give a pure brownish solid. Yield = 33 %; TLC (DCM:MeOH = 9:1), R<sub>f</sub> = 0.95; <sup>1</sup>H NMR (400 MHz, DMSO-*d*<sub>6</sub>) δ 1.54 (s, 1H, H-4), 1.67 (s, 3H, H-4 and H-5), 2.27–2.28 (m, 1H, H-6),

2.46–2.55 (m, 2H, H-2 and H-3), 2.59 (s, 1H, H-6), 3.01 (s, 1H, H-2), 3.50–3.57 (m, 2H, CH<sub>2</sub>), 7.26–7.36 (m, 5H, ArH); <sup>13</sup>C NMR (400 MHz, DMSO-*d*<sub>6</sub>) δ 22.8 (C-5), 26.6 (C-4), 42.3 (C), 53.1 (C-6), 55.8 (C-2), 61.5 (CH<sub>2</sub>), 121.8 (CN), 126.9 (C-4'), 128.1, 128.2, 128.4, 128.6 (C-2',3',5',6'), 137.8 (C-1'); IR (ATR) ν 2943, 2804, 2766, 2240, 1493, 1452, 1393, 1349, 1309, 1257, 1205, 1151, 1099, 1072, 1011, 985, 959, 911, 868, 773, 604, 565, 542, 510 cm<sup>-1</sup>; MS *m/z* (relative intensity): 201.1 (M+Na, 100); HRMS-ESI (*m/z*): [M+H]<sup>+</sup> calcd for C<sub>14</sub>H<sub>16</sub>N<sub>2</sub>O<sub>2</sub>S, 201.1397, found, 201.1392.

#### 1-(4-Nitrobenzyl)piperidine-3-carbonitrile (4b)

In a three-necked flask 1-(4-nitrobenzyl)piperidine-3-carboxamide (2b, 100 mg, 0.380 mmol) was dissolved in pyridine (10 mL). The solution was cooled on ice and chlorocarbonylsulfonyl chloride (100 mg, 0.760 mmol) was added under argon. The reaction mixture was stirred at 80 °C overnight, cooled to room temperature and after the addition of Et<sub>3</sub>N (0.32 mL) stirred for 15 minutes. The precipitate was filtered off and the residue concentrated *in vacuo*. Product was purified with column chromatography using DCM:MeOH = 9:1 as an eluent to give a brownish solid. Yield = 34 %; TLC (DCM:MeOH = 9:1) R<sub>f</sub> = 0.96; <sup>1</sup>H NMR (400 MHz, CDCl<sub>3</sub>) δ 1.64–1.65 (m, 1H, H-5), 1.79–1.85 (m, 3H, H-5 and H-4), 2.46 (s, 2H, H-6), 2.63 (s, 2H, H-2), 2.81–2.84 (m, 1H, H-3), 3.63 (dd, J 6.8, 14.4 Hz, 2H, CH<sub>2</sub>), 7.53 (d, 2H, H-2' and H-6'), 8.19 (dd, J 2.0, 4.8 Hz, 2H, H-3' and H-5'); <sup>13</sup>C NMR (400 MHz, CDCl<sub>3</sub>) δ 23.4 (C-5), 27.4 (C-4), 27.9 (C-3), 53.3 (C-6), 55.1 (C-2), 61.7 (CH<sub>2</sub>), 121.0 (CN), 123.7 (C-3' and C-5'), 129.2 (C-2' and C-6'), 145.8 (C-1'), 147.3 (C-4'); IR (ATR) ν 2945, 2802, 2240, 1599, 1467, 1439, 1154, 1093, 1033, 1012, 990, 955, 801, 773, 696, 651, 547 cm<sup>-1</sup>; MS *m/z* (relative intensity): 246.1 (M+Na, 100); HRMS-ESI (*m/z*): [M+H]<sup>+</sup> calcd for C<sub>14</sub>H<sub>15</sub>N<sub>3</sub>O<sub>4</sub>S, 246.1242, found, 246.1243.

## 4. Conclusion

Based on the previously reported oxathiazol-2-one-bearing and nonpeptidic inhibitors of the chymotrypsin-like (β5i) subunit of the immunoproteasome, we designed a novel series of piperidin-3-yl-oxathiazol-2-ones as potential covalent inhibitors of threonine proteases. Compounds were designed with a synthetically accessible piperidine central core derivatized with an oxathiazol-2-one electrophilic moiety. In lieu of previously reported synthetic approaches, we identified a synthetic protocol that enables the cyclization of carboxamides incorporating a basic centre into oxathiazol-2-ones. This straightforward protocol using chlorocarbonylsulfonyl chloride as a reagent in dioxane afforded the desired products in moderate to good yields. Thus, a vast chemical space of 5-substituted oxathiazol-2-ones can be explored and various chemical libraries of inhibitors of threonine proteases can be compiled.

## Abbreviations

ATR IR	attenuated total reflectance infrared spectroscopy
BDMS	bromodimethylsulfonium bromide
CDCl <sub>3</sub>	deuterated chloroform
DBU	1,8-diazabicyclo(5.4.0)undec-7-ene
DCM	dichloromethane
DMSO	dimethyl sulfoxide
DMF	dimethylformamide
EtOAc	ethyl acetate
MTB	<i>Mycobacterium tuberculosis</i>
Py	pyridine
THF	tetrahydrofuran
TLC	thin-layer chromatography

## Conflict of interest

The authors declare they have no conflict of interest.

## 5. Acknowledgments

The authors acknowledge the financial support from the Slovenian Research Agency (research core funding No. P1-0208). We thank Dr. Dušan Žigon (Mass Spectrometry Center, Jožef Stefan Institute, Ljubljana, Slovenia) for mass spectra.

## 6. References

1. M. Drag, G. S. Salvesen, *Nat. Rev. Drug Discov.* **2010**, *9*, 690–701. DOI:10.1038/nrd3053
2. D. H. Lee, A. L. Goldberg, *Trends Cell Biol.* **1998**, *8*, 397–403. DOI:10.1016/S0962-8924(98)01346-4
3. C. H. Arrowsmith, J. E. Audia, C. Austin, J. Baell, J. Bennett, J. Blagg, C. Bountra, P. E. Brennan, P. J. Brown, M. E. Bunnage, C. Buser-Doepner, R. M. Campbell, A. J. Carter, P. Cohen, R. A. Copeland, B. Cravatt, J. L. Dahlin, D. Dhanak, A. M. Edwards, M. Frederiksen, S. V. Frye, N. Gray, C. E. Grimshaw, D. Hepworth, T. Howe, K. V. M. Huber, J. Jin, S. Knapp, J. D. Kotz, R. G. Kruger, D. Lowe, M. M. Mader, B. Marsden, A. Mueller-Fahrnow, S. Müller, R. C. O'Hagan, J. P. Overington, D. R. Owen, S. H. Rosenberg, R. Ross, B. Roth, M. Schapira, S. L. Schreiber, B. Shoichet, M. Sundström, G. Superti-Furga, J. Taunton, L. Toledo-Sherman, C. Walpole, M. A. Walters, T. M. Willson, P. Workman, R. N. Young, W. J. Zuercher, *Nat. Chem. Biol.* **2015**, *11*, 536–541. DOI:10.1038/nchembio.1867
4. N. D. Rawlings, E. O'Brien, A. J. Barrett, *Nucleic Acids Res.* **2002**, *30*, 343–346. DOI:10.1093/nar/30.1.343
5. E. M. Huber, M. Groll, *Angew. Chem. Int. Ed.* **2012**, *51*, 8708–8720. DOI:10.1002/anie.201201616
6. L. R. Dick, P. E. Fleming, *Drug Discov. Today* **2010**, *15.5*, 243–249. DOI:10.1016/j.drudis.2010.01.008
7. D. A. Ferrington, D. S. Gregerson, *Prog. Mol. Biol. Transl. Sci.* **2012**, *109*, 75–112. DOI:10.1016/B978-0-12-397863-9.00003-1
8. A. Schweitzer, A. Aufderheide, T. Rudack, F. Beck, G. Pfeifer, J. M. Plitzko, E. Sakata, K. Schulten, F. Förster, W. Baumeister, *Proc. Natl. Acad. Sci.* **2016**, *113*, 7816–21. DOI:10.1073/pnas.1608050113
9. R. Raynes, L. C. D. Pomatto, K. Davies, J. A. Kelvin, *Mol. Aspects Med.* **2016**, *50*, 41–55. DOI:10.1016/j.mam.2016.05.001
10. M. Schmidt, D. Finley, *Biochim. Biophys. Acta – Molecular Cell Research* **2014**, *1843*, 13–25.
11. A. F. Kisselev, W. A. Van Der Linden, H. S. Overkleeft, *Chem. Biol.* **2012**, *19*, 99–115. DOI:10.1016/j.chembiol.2012.01.003
12. M. Groll, Y. Koguchi, R. Huber, J. Kohno, *J. Mol. Biol.* **2001**, *311*, 543–548. DOI:10.1006/jmbi.2001.4869
13. E. M. Huber, M. Basler, R. Schwab, W. Heinemeyer, C. J. Kirk, M. Groettrup, M. Groll, *Cell* **2012**, *148*, 727–738. DOI:10.1016/j.cell.2011.12.030
14. M. Groll, K. B. Kim, N. Kairies, R. Huber, C. M. Crews, *J. Am. Chem. Soc.* **2000**, *122*, 1237–1238. DOI:10.1021/ja993588m
15. H. W. B. Johnson, J. L. Anderi, E. K. Bradley, J. Bui, J. Jones, S. Arastu-Kapur, L. M. Kelly, E. Lowe, D. C. Moebius, T. Muchamuel, C. Kirk, Z. Wang, D. McMinn, *Med. Chem. Lett.* **2017**, *8*, 413–417. DOI:10.1021/acsmedchemlett.6b00496
16. I. Sosič, M. Gobec, B. Brus, D. Knez, M. Živec, J. Konc, S. Lešnik, M. Ogizek, A. Obreza, D. Žigon, D. Janežič, I. Mlinarič-Raščan, S. Gobec, *Angew. Chem. Int. Ed.* **2016**, *55*, 5745–5748. DOI:10.1002/anie.201600190
17. C. Dubiella, R. Baur, H. Cui, E. M. Huber, M. Groll, *Angew. Chem. Int. Ed.* **2015**, *54*, 15888–15891. DOI:10.1002/anie.201506631
18. G. Lin, D. Li, L. P. S. de Carvalho, H. Deng, H. Tao, G. Vogt, K. Wu, J. Schneider, T. Chidawanyika, J. D. Warren, H. Li, C. Nathan, *Nature* **2009**, *461*, 621–626. DOI:10.1038/nature08357
19. J. Schrader, F. Henneberg, R. A. Mata, K. Tittmann, T. R. Schneider, H. Stark, G. Bourenkov, A. Chari, *Science* **2016**, *353*, 594–598. DOI:10.1126/science.aaf8993
20. J. Singh, R. C. Petter, T. A. Bailie, A. Whitty, *Nat. Rev. Drug Discov.* **2011**, *10*, 307–317. DOI:10.1038/nrd3410
21. H. Fan, N. G. Angelo, J. D. Warren, C. F. Nathan, G. Lin, *Med. Chem. Lett.* **2014**, *5*, 405–410. DOI:10.1021/ml400531d
22. B. E. Gryder, W. Guerrant, C. H. Chen, A. K. Oyelere, *Med. Chem. Comm.* **2011**, *2*, 1083–1086. DOI:10.1039/c1md00208b
23. C. Kuo, J. Zhu, J. Wu, C. Chu, C. Yao, K. Shia, *Chem. Comm.* **2007**, *3*, 301–303. DOI:10.1039/B614061K
24. A. S. Gurjar, V. Andrisano, A. D. Simone, V. S. Velingkar, *Bioorg. Chem.* **2014**, *57*, 90–98. DOI:10.1016/j.bioorg.2014.09.002
25. B. Rickborn, F. R. Jensen, *J. Org. Chem.* **1962**, *27*, 4608–4610. DOI:10.1021/jo01059a114
26. K. Mai, G. Patil, *Tetrahedron Lett.* **1986**, *27*, 2203–2206. DOI:10.1016/S0040-4039(00)84487-1
27. D. A. Claremon, B. T. Phillips, *Tetrahedron Lett.* **1988**, *29*, 2155–2158. DOI:10.1016/S0040-4039(00)86697-6

28. T. M. Bargar, C. M. Riley, *Syn. Comm.* **1980**, *10*, 479–487.  
DOI:10.1080/00397918008064272
29. L. D. S. Yadav, V. P. Srivastava, R. Patel., *Tetrahedron Lett.* **2009**, *50*, 5532–5535. DOI:10.1016/j.tetlet.2009.07.100
30. S. I. Maffioli, E. Marzorati, A. Marazzi, *Org. Lett.* **2005**, *7*, 5237–5239. DOI:10.1021/ol052100l
31. N. Nakajima, M. Ubukata, *Tetrahedron Lett.* **1997**, *38*, 2099–2102. DOI:10.1016/S0040-4039(97)00316-X
32. W. E. Dennis, *J. Org. Chem.* **1970**, *35*, 3253–3255.  
DOI:10.1021/jo00835a016
33. S. Zhou, K. Junge, D. Addis, S. Das, M. Beller, *Org. Lett.* **2009**, *11*, 2461–2464. DOI:10.1021/ol900716q
34. A. Aitha, S. Yennam, M. Behera, J. S. Anireddy, *Tetrahedron Lett.* **2016**, *57*, 1507–1510.  
DOI:10.1016/j.tetlet.2016.02.082
35. P. C. Unangst, G. P. Shrum, D. T. Connor, *J. Heterocycl. Chem.* **1993**, *30*, 357–359. DOI:10.1002/jhet.5570300211
36. J. Crosby, M. C. McKie, M. Paton, J. F. Ross, *Arkivoc* **2000**, *1*, 720–734.
37. R. M. Paton, *Chem. Soc. Rev.* **1989**, *18*, 33–52.  
DOI:10.1039/cs9891800033
38. R. K. Howe, T. A. Gruner, L. G. Carter, L. L. Black, J. E. Franz, *J. Org. Chem.* **1978**, *43*, 3736–3742.  
DOI:10.1021/jo00413a024
39. P. Öhrngren, A. Fardost, F. Russo, J. S. Schanche, M. Fagrell, M. Larhed, *Org. Process Res. Dev.* **2012**, *16*, 1053–1063.

## Povzetek

Z zamenjavo molekulskega skeleta smo načrtovali spojine s piperidinskim jedrom, derivatiziranim z oksatiazol-2-on-skim elektrofilnim centrom, ki omogoča selektivno zaviranje treoninskih proteaz. Sinteza produktov po postopkih, opisanih v literaturi, ni bila uspešna, poleg tega smo identificirali nitrile kot glavne stranske produkte, ki nastanejo pri dehidraciji karboksamidne funkcionalne skupine. S sistematično optimizacijo reakcijskih pogojev, smo s segrevanjem karboksamidov, klorokarbonilsulfenil klorida in natrijevega karbonata kot baze v dioksanu pri 100 °C pripravili serijo piperidin-3-il-oksatiazol-2-onov, primerno za nadaljnje biološko vrednotenje.

Short communication

# Synthesis of Novel 5-(*N*-Boc-*N*-Benzyl-2-aminoethyl)-7-oxo-4,7-dihydropyrazolo[1,5-*a*]pyrimidin-3-carboxamides and Their Inhibition of Cathepsins B and K

Branislav Lukić, Uroš Grošelj, Marko Novinec\* and Jurij Svete\*

Faculty of Chemistry and Chemical Technology, University of Ljubljana, Večna pot 113, SI – 1000 Ljubljana, Slovenia.

\* Corresponding author: E-mail: marko.novinec@fkkt.uni-lj.si,  
jurij.svete@fkkt.uni-lj.si

Received: 10-04-2017

Dedicated to Professor Emeritus Miha Tišler, University of Ljubljana,  
on the occasion of his 90<sup>th</sup> birthday.

## Abstract

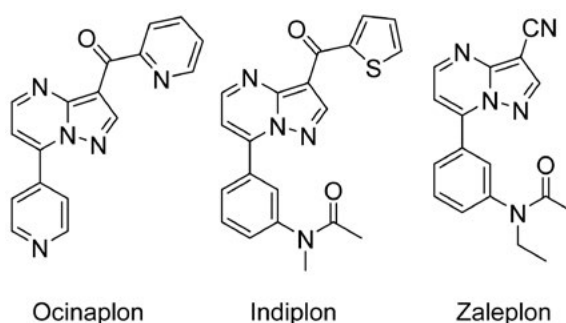
Eight novel 5-(*N*-Boc-*N*-benzyl-2-aminoethyl)-7-oxo-4,7-dihydropyrazolo[1,5-*a*]pyrimidin-3-carboxamides were prepared in three steps from methyl 3-amino-1*H*-pyrazole-4-carboxylate and methyl 5-(benzyl(*tert*-butoxycarbonyl)amino)-3-oxopentanoate. The synthetic procedure comprises cyclocondensation of the above starting compounds, hydrolysis of the ester, and bis(pentafluorophenyl) carbonate (BPC)-mediated amidation. Title carboxamides were tested for inhibition of cathepsins K and B. The *N*-butylcarboxamide **5a** exhibited appreciable inhibition of cathepsin K ( $IC_{50} \sim 25 \mu\text{M}$ ), while the strongest inhibition of cathepsin B was achieved with *N*-(2-picoly)carboxamide **5c** ( $IC_{50} \sim 45 \mu\text{M}$ ).

**Keywords:** Pyrazolo[1,5-*a*]pyrimidines, cathepsin inhibition, cyclization, synthesis

## 1. Introduction

Various 5–6 annulated heterocycles are important scaffolds for the preparation of compound libraries for medicinal and pharmaceutical applications.<sup>1,2</sup> Due to biological activity of many of its derivatives, pyrazolo[1,5-*a*]pyrimidine is an important heterocycle among 5–6-fused systems.<sup>3,4</sup> The importance of pyrazolo[1,5-*a*]pyrimidine is reflected in the results of a literature search<sup>5</sup> showing around 150,000 known pyrazolo[1,5-*a*]pyrimidine derivatives within 6,500 references and with preparation, biological study, and uses as the predominant substance roles. For 2016 alone, 74 references can be found for a term “pyrazolo[1,5-*a*]pyrimidines”. Among bioactive pyrazolo[1,5-*a*]pyrimidines there are hepatitis C virus inhibitors,<sup>6</sup> antagonists of serotonin 5-HT<sub>6</sub> receptors,<sup>7</sup> kinase inhibitors,<sup>8–10</sup> PET tumor imaging agents,<sup>11</sup> and inhibitors of amyloid  $\beta$ -peptide aggregation.<sup>12</sup> Sedative agents zaleplon and indiplon and the anxiolytic agent ocinaplon are approved drugs containing a pyrazolo[1,5-*a*]pyrimidine core (Figure 1).

Cathepsin K, a cysteine protease that is selectively and abundantly expressed within osteoclasts, is believed to



**Figure 1.** Approved drugs based on a pyrazolo[1,5-*a*]pyrimidine scaffold.

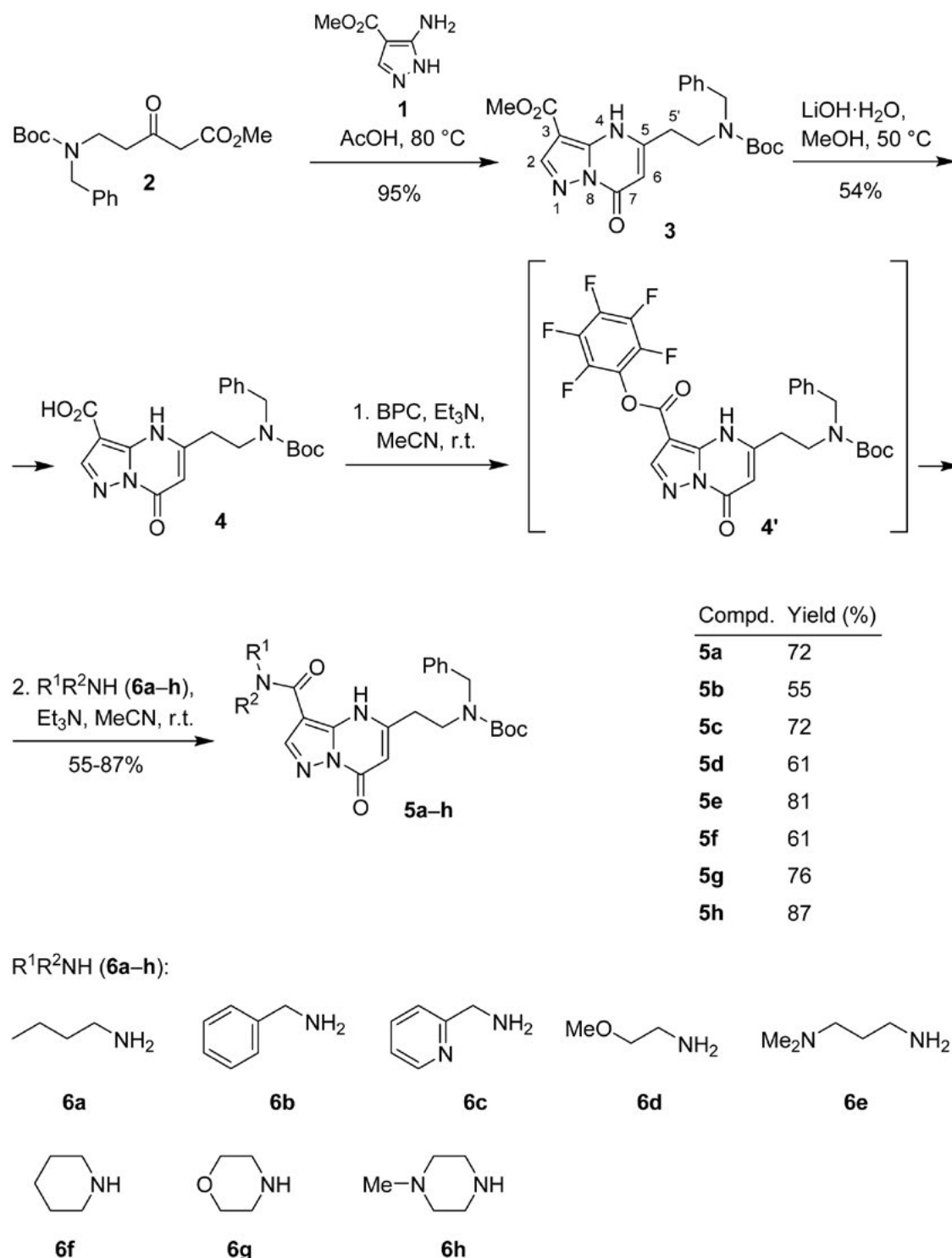
be crucial for the resorption of bone matrix.<sup>13–17</sup> The ability to degrade type I collagen allows cathepsin K to make a unique contribution to the balance between bone resorption and bone formation.<sup>18,19</sup> Inhibitors of cathepsin K could prevent bone resorption and may provide a promising approach for the treatment of osteoporosis, therefore inhibition of cathepsin K has been proposed as a promising strategy for the treatment of osteoporosis, cancer, and other diseases.<sup>13–15</sup> Several inhibitors have progressed into



clinical trials but there are, as yet, no inhibitors on the market.<sup>20</sup>

Pyrazolo[1,5-*a*]pyrimidines are commonly available by cyclocondensation of a 3-aminopyrazole derivative with a 1,3-dicarbonyl compound or its synthetic equivalent.<sup>3,21</sup> Due to this ease of access, a plethora of known

pyrazolo[1,5-*a*]pyrimidine derivatives is not surprising. Nevertheless, a more detailed literature search also reveals that 5-(2-aminoethyl) substituted pyrazolo[1,5-*a*]pyrimidines are much less known – 135 examples can be found by SciFinder<sup>3</sup>, however, without any literature reference available. Furthermore, the 5-(2-aminoethyl)pyrazolo



Scheme 1. Synthesis of title carboxamides **5a-h**.

[1,5-*a*]pyrimidine-3-carboxamides are, to the best of our knowledge, unknown. Recently, a substantial part of our studies were focused on the synthesis of novel pyrazolo[1,5-*a*]pyridine and pyrazolo[1,5-*c*]pyridine derivatives. In this connection, we reported (parallel) syntheses of libraries of novel 7-heteroarylpyrazolo[1,5-*a*]pyrimidine-3-carboxamides,<sup>22</sup> 7-oxopyrazolo[1,5-*a*]pyrimidine-3-carboxamides,<sup>23</sup> 7-(1-aminoethyl)pyrazolo[1,2-*a*]pyrimidines,<sup>24</sup> and tetrahydropyrazolo[1,5-*c*]pyrimidine-3-carboxamides.<sup>25</sup> In extension, we explored another synthetic approach based on direct cyclisation of methyl 5-amino-1*H*-pyrazole-4-carboxylate (**1**) with methyl 5-[benzyl(*tert*-butoxycarbonyl)amino]-3-oxopentanoate (**2**) to obtain a 5-(2-aminoethyl)pyrazolo[1,5-*a*]pyrimidine central building block for a late-stage derivatization at the carboxy function. Herein we report the results, the synthesis of 5-(*N*-Boc-*N*-benzyl-2-aminoethyl)-7-oxo-4,7-dihydropyrazolo[1,5-*a*]pyrimidin-3-carboxamides **5a–h** and their evaluation for inhibition of cathepsins B and K.

## 2. Results and Discussion

The starting  $\beta$ -keto ester, methyl 5-[benzyl(*tert*-butoxycarbonyl)amino]-3-oxopentanoate (**2**) was prepared in four steps from benzylamine (**6b**) and methyl acrylate following the literature procedures.<sup>23,26</sup> Subsequent cyclisation of **2** with methyl 5-amino-1*H*-pyrazole-4-carboxylate (**1**)<sup>27</sup> was performed in acetic acid at 80 °C for 24 h to afford methyl 5-(*N*-Boc-*N*-benzyl-2-aminoethyl)-7-oxo-4,7-dihydropyrazolo[1,5-*a*]pyrimidin-3-carboxylate (**3**) in 95% yield. Notably, heating at temperatures above 80 °C shortened the reaction times at the expense of the product yield due to partial acidolytic removal of the Boc group and concomitant formation of undesired by-products. Somewhat expectedly,<sup>23,25</sup> attempted hydrolysis of the ester function with aq. NaOH failed. Fortunately enough, hydrolysis of **3** into the desired carboxylic acid **4** could be performed upon prolonged treatment of the ester **3** with excess LiOH in aq. methanol to furnish the central intermediate **4** in 54% yield. For the final amidation step 1,1'-carbonyldiimidazole (CDI), 2-ethoxy-1-ethoxycar-

bonyl-1,2-dihydroquinoline (EEDQ), and bis(pentafluorophenyl) carbonate (BPC) were tested as the reagents for the activation of the carboxy group of **4**. As we already experienced previously in amidation of related hetarene-carboxylic acids,<sup>22–26</sup> BPC proved to be the most suitable reagent, because it gave the corresponding carboxamides **5** reproducibly and in good yields. Thus, upon activation of **4** with BPC to form the intermediate pentafluorophenyl ester **4'**, further treatment with 1:1 mixtures of amines and triethylamine for 12 h furnished the target carboxamides **5a–h** in 55–87% yields upon chromatographic workup (Scheme 1).

The structures of novel compounds **3**, **4**, and **5a–h** were determined by spectroscopic methods (<sup>1</sup>H NMR, <sup>13</sup>C NMR, IR, MS, HRMS). Spectral data for compounds **3**, **4**, and **5a–h** were in agreement with the data of closely related pyrazolo[1,5-*a*]pyrimidin-7(*4H*)-ones.<sup>1,3,4,21–23</sup>

Some physicochemical properties were calculated to estimate the drug-likeness of compounds **3**, **4**, and **5a–h**. The compounds have molecular weight (MW) between 412 and 503, number of atoms between 54 and 72, clogP between 1.3 and 3.6, number of hydrogen bond donors (HBD)  $\leq 2$ , number of hydrogen bond acceptors (HBA)  $\leq 5$ , and polar surface area (PSA) below 116 Å<sup>2</sup>. These calculated physicochemical properties are compliant with Lipinski's rule of five<sup>28–30</sup> indicating promising drug-likeness of the synthesized compounds **3**, **4**, and **5a–h** (Table 1).

The biological activity of compounds **3**, **4**, and **5a–h** was tested against the cysteine peptidases cathepsins B and K, which are both important drug targets.<sup>31</sup> All compounds were initially tested for their activity at a concentration of 100  $\mu$ M. As shown in Table 2, compound **5a** had the strongest inhibitory effect on cathepsin K, with an *IC*<sub>50</sub> value of 25  $\pm$  5  $\mu$ M under the experimental conditions used in the assay and complete (100%) inhibition was observed at concentrations of 600  $\mu$ M or higher. The effect of other compounds was significantly weaker and resulted in less than 50% inhibition. Cathepsin B was most strongly inhibited by compound **5c** (*IC*<sub>50</sub> value of 45  $\pm$  15  $\mu$ M) and to a lesser extent by compounds **5a** and **5d**. Altogether these results identify three compounds, **5a**, **5c** and **5d**, as potential lead compounds for further development (Table 2).

Table 1. Calculated physicochemical properties of compounds **3**, **4**, and **5a–h**.

Compd.	MW (g mol <sup>-1</sup> )	No. of atoms	ClogP	No. of HBD	No. of HBA	PSA (Å <sup>2</sup> )
<b>3</b>	426.47	57	2.62	1	4	100.5
<b>4</b>	412.45	54	2.41	2	4	111.5
<b>5a</b>	467.57	67	3.19	2	4	103.3
<b>5b</b>	501.59	68	3.57	2	4	103.3
<b>5c</b>	502.57	67	2.07	2	5	115.7
<b>5d</b>	469.54	65	1.81	2	5	112.6
<b>5e</b>	496.6	72	2.29	2	5	106.6
<b>5f</b>	479.58	68	2.34	1	4	94.6
<b>5g</b>	481.55	66	1.31	1	5	103.8
<b>5h</b>	494.60	70	1.87	1	5	97.8

Table 2: Effect of compounds 3, 4 and 5a–h on the activity of cathepsins K and B.<sup>a</sup>

Compound	Cathepsin K		Cathepsin B	
	RA (%) <sup>b</sup>	IC <sub>50</sub> (μM)	RA (%) <sup>b</sup>	IC <sub>50</sub> (μM)
control	100		100	
3	89		89	
4	84		84	
5a	29	25 ± 5	36	110 ± 30
5b <sup>c</sup>	–		–	
5c	94		20	45 ± 15
5d	95		23	150 ± 50
5e	69		104	
5f	60		–	
5g	74		61	
5h	112		101	

<sup>a</sup>) All experiments were performed in 50 mM sodium acetate buffer pH 5.5 containing 1 mM EDTA, 2.5 mM DTT and the fluorogenic substrate Z-Phe-Arg-AMC (5 μM final concentration). Final enzyme concentrations were 1 nM. IC<sub>50</sub> values were determined from titration curves. <sup>b</sup>) Residual activity at saturation. <sup>c</sup>) Activity of 5b could not be determined fluorometrically due to strong absorption of the compound at the excitation wavelength.

### 3. Experimental

#### 3.1. General Methods

Melting points were determined on a Stanford Research Systems MPA100 OptiMelt automated melting point system. The NMR spectra were obtained on a Bruker Avance III UltraShield 500 plus at 500 MHz for <sup>1</sup>H and 126 MHz for <sup>13</sup>C, using CDCl<sub>3</sub> and DMSO-d<sub>6</sub> (with TMS as the internal standard) as solvents. Mass spectra were recorded on an Agilent 6224 Accurate Mass TOF LC/MS spectrometer, IR spectra on a Bruker FTIR Alpha Platinum ATR spectrophotometer. Flash column chromatography (FC) was performed on silica gel (Fluka, Silica gel 60, particle size 35–70 μm).

Amines 6a–h, bis(pentafluorophenyl) carbonate (BPC), triethylamine, and LiOH · H<sub>2</sub>O are commercially available. Methyl 5-amino-1H-pyrazole-4-carboxylate (1)<sup>27</sup> and methyl 5-(benzyl(*tert*-butoxycarbonyl)amino)-3-oxopentanoate (2)<sup>26</sup> were prepared following the literature procedures.

#### 3.2. Synthesis of methyl 5-(*N*-Boc-*N*-benzyl-2-aminoethyl)-7-oxo-4,7-dihydropyrazolo[1,5-*a*]pyrimidin-3-carboxylate (3)

A mixture of 1 (1.413 g, 10 mmol), 2 (3.694 g, 10 mmol), and AcOH (20 mL) was stirred at 80 °C for 24 h. Volatile components were evaporated in vacuo and the residue was purified by FC (EtOAc). Fractions containing the product were combined and evaporated in vacuo to give 3. Yield: 4.059 g (95%) of pale beige solid; m.p. 161–165 °C. <sup>1</sup>H NMR (500 MHz, CDCl<sub>3</sub>): δ 1.30 (9H, s, *t*-Bu); 2.95 (2H, t, *J* = 10.0 Hz, CH<sub>2</sub>); 3.54 (2H, t, *J* = 10.0 Hz, CH<sub>2</sub>); 3.86 (3H, s, OMe); 4.45 (2H, s, CH<sub>2</sub>Ph); 5.72 (1H, s, 6-H); 7.29 (5H, m, Ph); 8.15 (1H, s, 2-H); 11.45 (1H, s,

NH). <sup>13</sup>C NMR (126 MHz, CDCl<sub>3</sub>): δ 27.6, 44.8, 48.3, 51.3, 59.7, 78.7, 96.5, 99.4, 127.1, 127.4, 128.3, 138.3, 143.0, 143.3, 154.4, 155.1, 162.0, 170.3. *m/z* (ESI) = 427 (MH<sup>+</sup>). HRMS–ESI (*m/z*): [MH<sup>+</sup>] calcd for C<sub>22</sub>H<sub>27</sub>N<sub>4</sub>O<sub>5</sub>, 427.1976; found, 427.1971. Anal. Calcd for C<sub>22</sub>H<sub>26</sub>N<sub>4</sub>O<sub>5</sub>: C 61.96, H 6.15, N 13.14. Found: C 61.90, H 6.29, N 13.17. IR (ATR) ν 3344, 2963, 1710, 1671, 1620, 1580, 1529, 1495, 1466, 1442, 1414, 1365, 1323, 1303, 1259, 1247, 1185, 1167, 1145, 1124, 1115, 1051, 1019, 963, 933, 887, 847, 791, 776, 729, 695, 683, 657, 632 cm<sup>-1</sup>.

#### 3.3. Synthesis of 5-(*N*-Boc-*N*-benzyl-2-aminoethyl)-7-oxo-4,7-dihydropyrazolo[1,5-*a*]pyrimidin-3-carboxylic acid (4)

A mixture of the ester 3 (3.408 g, 8 mmol), LiOH · H<sub>2</sub>O (2.016 g, 48 mmol), and methanol (30 mL) was stirred at 50 °C for 48 h. The reaction mixture was cooled to room temperature, and acidified to pH ~ 4 by careful addition of 1 M aq. NaHSO<sub>4</sub>. The precipitate was collected by filtration and washed with cold (0 °C) water (5 mL) to give 4. Yield: 2.215 g (54%) of white solid; m.p. 166–172 °C. <sup>1</sup>H NMR (500 MHz, CDCl<sub>3</sub>): δ 1.21 (9H, s, *t*-Bu); 2.90 (2H, t, *J* = 10.0 Hz, CH<sub>2</sub>); 3.36 (2H, t, *J* = 10.0 Hz, CH<sub>2</sub>); 4.45 (2H, s, CH<sub>2</sub>Ph); 5.68 (1H, s, 6-H); 7.29 (5H, m, Ph); 8.26 (1H, s, 2-H); 12.78 (1H, s, NH), CO<sub>2</sub>H exchanged. <sup>13</sup>C NMR (126 MHz, CDCl<sub>3</sub>): δ 27.5, 31.3, 44.9, 48.2, 78.7, 97.5, 98.7, 127.0, 127.4, 128.4, 138.3, 143.2, 144.2, 153.7, 154.8, 155.4, 163.3. *m/z* (ESI) = 413 (MH<sup>+</sup>). HRMS–ESI (*m/z*): [MH<sup>+</sup>] calcd for C<sub>21</sub>H<sub>25</sub>N<sub>4</sub>O<sub>5</sub>, 413.1806; found, 413.1812. Anal. Calcd for C<sub>21</sub>H<sub>24</sub>N<sub>4</sub>O<sub>5</sub> · H<sub>2</sub>O: C 58.60, H 6.09, N 13.02. Found: C 58.50, H 5.74, N 12.89. IR (ATR) ν 3648, 3368, 2977, 1682, 1635, 1575, 1495, 1464, 1446, 1404, 1366, 1345, 1302, 1281, 1252, 1218, 1200, 1160, 1131, 1073, 1047, 1015, 963, 940, 858, 841, 812, 780, 758, 725, 695, 669, 653 cm<sup>-1</sup>.

### 3. 4. Synthesis of 5-(*N*-Boc-*N*-benzyl-2-aminoethyl)-7-oxo-4,7-dihydropyrazolo[1,5-*a*]pyrimidin-3-carboxamides 5a–h

A mixture of carboxylic acid **4** (207 mg, 0.5 mmol), MeCN (5 mL), and Et<sub>3</sub>N (70 μL, 0.5 mmol) was stirred at room temperature for 5 minutes. Then, BPC (197 mg, 0.5 mmol) was added and the reaction mixture was stirred at r.t. for 2 h (activation of carboxylic acid **4** via formation of the pentafluorophenyl ester **4'**). Next, amine **6** (0.5 mmol) and Et<sub>3</sub>N (70 μL, 0.5 mmol) were added and stirring at room temperature was continued for 24 h. The reaction mixture was evaporated *in vacuo* (60 °C/2 mbar) and the crude semi-solid carboxamide **5** was purified by FC on silica gel (first EtOAc to elute the non-polar impurities, then CH<sub>2</sub>Cl<sub>2</sub>–MeOH, 10:1, to elute the product). Fractions containing the product were combined and evaporated *in vacuo* to give carboxamides **5a–h**.

#### 3. 4. 1. *tert*-Butyl benzyl{2-[3-(butylcarbamoyl)-7-oxo-4,7-dihydropyrazolo[1,5-*a*]pyrimidin-5-yl]ethyl}carbamate (**5a**)

Prepared from **4** (207 mg, 0.5 mmol) and butylamine (**6a**) (50 μL, 0.5 mmol). Yield: 167 mg (72%) of yellowish resin. <sup>1</sup>H NMR (500 MHz, CDCl<sub>3</sub>): δ 0.85 (3H, t, *J* = 7.0 Hz, CH<sub>2</sub>CH<sub>3</sub>); 1.27 (2H, m, CH<sub>2</sub>); 1.34 (9H, s, *t*-Bu); 1.42 (2H, m, CH<sub>2</sub>); 2.29 (2H, m, CH<sub>2</sub>); 3.23 (2H, m, CH<sub>2</sub>); 3.44 (2H, m, CH<sub>2</sub>); 4.38 (2H, s, CH<sub>2</sub>Ph); 5.41 (1H, s, 6-H); 7.28 (5H, m, Ph); 7.90 (1H, s, 2-H); 8.50 (1H, br s, NHBu); pyrimidone NH exchanged. <sup>13</sup>C NMR (126 MHz, CDCl<sub>3</sub>): δ 13.0, 13.7, 19.7, 28.2, 31.8, 38.5, 45.8, 51.0, 80.0, 101.1, 126.0, 127.2, 127.5, 127.9, 128.4, 128.7, 138.1, 155.7, 156.0, 159.0, 164.0. *m/z* (ESI) = 468 (MH<sup>+</sup>). HRMS–ESI (*m/z*): [MH<sup>+</sup>] calcd for C<sub>25</sub>H<sub>34</sub>N<sub>5</sub>O<sub>5</sub>, 468.2605; found, 468.2601. IR (ATR) ν 3300, 2930, 2175, 2110, 1985, 1960, 1684, 1619, 1537, 1512, 1494, 1451, 1413, 1364, 1245, 1157, 1115, 1047, 980, 885, 808, 775, 733, 697 cm<sup>-1</sup>.

#### 3. 4. 2. *tert*-Butyl benzyl{2-[3-(benzylcarbamoyl)-7-oxo-4,7-dihydropyrazolo[1,5-*a*]pyrimidin-5-yl]ethyl}carbamate (**5b**)

Prepared from **4** (207 mg, 0.5 mmol) and benzylamine (**6b**) (54 μL, 0.5 mmol). Yield: 137 mg (55%) of yellowish resin. <sup>1</sup>H NMR (500 MHz, CDCl<sub>3</sub>): δ 1.30 (9H, br s, *t*-Bu); 2.56 (2H, br s, CH<sub>2</sub>); 3.35 (2H, br s, CH<sub>2</sub>); 4.29 and 4.43 (4H, 2 br s, 3:1, 2 × CH<sub>2</sub>Ph); 5.57 (1H, br s, 6-H); 6.84–7.34 (10H, m, 2×Ph); 8.10 (1H, br s, 2-H); 8.76 (1H, br s, NH); pyrimidone NH exchanged. <sup>13</sup>C NMR (126 MHz, CDCl<sub>3</sub>): δ 28.1, 28.3, 36.5, 42.8, 46.1, 51.3, 51.9, 81.0, 100.7, 125.1, 127.3, 127.4, 128.5, 128.6, 136.7, 138.2, 138.9, 140.6, 142.7, 156.0, 159.6, 163.9. *m/z* (ESI) = 502 (MH<sup>+</sup>). HRMS–ESI (*m/z*): [MH<sup>+</sup>] calcd for C<sub>28</sub>H<sub>32</sub>N<sub>5</sub>O<sub>4</sub>, 502.2449; found, 502.2444. IR (ATR) ν 3278, 2975, 2114, 1618, 1535, 1494, 1451, 1413, 1364, 1244, 1207, 1156, 1115, 976, 884, 809, 774, 728, 696, 665, 630 cm<sup>-1</sup>.

#### 3. 4. 3. *tert*-Butyl benzyl(2-{7-oxo-3-[(pyridin-2-ylmethyl)carbamoyl]-4,7-dihydropyrazolo[1,5-*a*]pyrimidin-5-yl}ethyl)carbamate (**5c**)

Prepared from **4** (207 mg, 0.5 mmol) and 2-picolylamine (**6c**) (51 μL, 0.5 mmol). Yield: 190 mg (72%) of yellowish resin. <sup>1</sup>H NMR (500 MHz, DMSO-*d*<sub>6</sub>): δ 1.27 and 1.32 (9H, 2 br s, 2:1, *t*-Bu); 2.67–2.77 (2H, br s, CH<sub>2</sub>); 3.42–3.50 (2H, br s, CH<sub>2</sub>); 4.33 and 4.37 (2H, 2 br s, 1:2, CH<sub>2</sub>Ph); 4.60 (2H, d, *J* = 5.7 Hz, CH<sub>2</sub>Py); 5.48 and 5.50 (1H, 2 br s, 2:1, 6-H); 7.20–7.30 (5H, m, Ph); 7.30–7.37 (2H, m, 2H of Ph); 7.71 (1H, td, *J* = 7.7, 1.8 Hz, 1H of Py); 8.09 (1H, br s, 2-H); 8.47 (1H, br d, *J* = 4.2 Hz, 1H of Py); 9.16 (1H, br t, *J* = 6.0 Hz, NHCO); pyrimidone NH exchanged. <sup>13</sup>C NMR (126 MHz, DMSO-*d*<sub>6</sub>): δ 27.8, 43.8, 45.6, 45.8, 49.0, 78.8, 100.2, 120.9, 122.0, 127.0, 127.2, 127.4, 128.4, 136.7, 138.1, 138.5, 140.0, 141.5, 148.8, 155.0, 157.2, 159.0, 162.9. *m/z* (ESI) = 503 (MH<sup>+</sup>). HRMS–ESI (*m/z*): [MH<sup>+</sup>] calcd for C<sub>27</sub>H<sub>31</sub>N<sub>6</sub>O<sub>4</sub>, 503.2397; found, 503.2394. IR (ATR) ν 3679, 3607, 2926, 1730, 1624, 1537, 1497, 1393, 1368 cm<sup>-1</sup>.

#### 3. 4. 4. *tert*-Butyl benzyl(2-{3-[(2-methoxyethyl)carbamoyl]-7-oxo-4,7-dihydropyrazolo[1,5-*a*]pyrimidin-5-yl}ethyl)carbamate (**5d**)

Prepared from **4** (207 mg, 0.5 mmol) and 2-methoxyethylamine (**6d**) (63 μL, 0.5 mmol). Yield: 143 mg (61%) of yellowish resin. <sup>1</sup>H NMR (500 MHz, CDCl<sub>3</sub>): δ 1.45 (9H, s, *t*-Bu); 2.72–2.83 (2H, br s, CH<sub>2</sub>); 3.40 (3H, br s, OMe); 3.51–3.59 (4H, m, 2×CH<sub>2</sub>); 3.59–3.64 (2H, m, CH<sub>2</sub>); 4.44 (2H, br s, CH<sub>2</sub>Ph); 5.69 (1H, s, 6-H); 7.14–7.29 (6H, m, Ph and NHCO); 8.03 (1H, br s, 2-H); pyrimidone NH exchanged. <sup>13</sup>C NMR (126 MHz, CDCl<sub>3</sub>): δ 28.4, 39.2, 46.2, 51.8, 59.0, 71.1, 81.3, 99.2, 126.0, 127.8, 128.8, 132.2, 137.6, 139.0, 143.5, 151.0, 154.1, 155.8, 156.3, 163.1. *m/z* (ESI) = 470 (MH<sup>+</sup>). HRMS–ESI (*m/z*): [MH<sup>+</sup>] calcd for C<sub>24</sub>H<sub>32</sub>N<sub>5</sub>O<sub>5</sub>, 470.2398; found, 470.2393. IR (ATR) ν 3313, 2978, 2916, 1685, 1624, 1585, 1532, 1513, 1479, 1453, 1414, 1365, 1244, 1156, 1122, 1051, 1012, 993, 976, 858, 819, 774, 733, 698, 660 cm<sup>-1</sup>.

#### 3. 4. 5. *tert*-Butyl benzyl[2-(3-{[3-(dimethylamino)propyl]carbamoyl}-7-oxo-4,7-dihydropyrazolo[1,5-*a*]pyrimidin-5-yl)ethyl]carbamate (**5e**)

Prepared from **4** (207 mg, 0.5 mmol) and 3-dimethylaminopropylamine (**6e**) (63 μL, 0.5 mmol). Yield: 200 mg (81%) of yellowish resin. <sup>1</sup>H NMR (500 MHz, CDCl<sub>3</sub>): δ 1.40 (9H, s, *t*-Bu); 1.96–2.05 (2H, m, CH<sub>2</sub>); 2.71 (6H, br s, NMe<sub>2</sub>); 2.67–2.81 (2H, m, CH<sub>2</sub>); 3.03–3.12 (2H, m, CH<sub>2</sub>); 3.43–3.51 and 3.55–3.63 (4H, 2m, 3:1, 2 × CH<sub>2</sub>); 4.37 (2H, br s, CH<sub>2</sub>Ph); 5.70 (1H, s, 6-H); 7.16–7.34 (5H, m, Ph); 8.14 (1H, br s, 2-H); 8.65 (1H, br s, NHCO); pyrimidone NH exchanged. <sup>13</sup>C NMR (126 MHz, CDCl<sub>3</sub>): δ 25.9, 28.4, 28.5, 35.9, 43.4, 43.5, 45.7, 56.2, 79.7, 95.4,

101.1, 127.3, 127.7, 128.6, 137.3, 138.1, 139.1, 141.0, 156.0, 159.3, 165.0.  $m/z$  (ESI) = 497 (MH<sup>+</sup>). HRMS–ESI ( $m/z$ ): [MH<sup>+</sup>] calcd for C<sub>26</sub>H<sub>37</sub>N<sub>6</sub>O<sub>4</sub>, 497.2857; found, 497.2863. IR (ATR)  $\nu$  3285, 2937, 1995, 1690, 1619, 1537, 1493, 1450, 1411, 1364, 1243, 1158, 1112, 1020, 886, 806, 776, 735, 698, 665, 631 cm<sup>-1</sup>.

### 3. 4. 6. *tert*-Butyl benzyl{2-[7-oxo-3-(piperidine-1-carbonyl)-4,7-dihydropyrazolo[1,5-*a*]pyrimidin-5-yl]ethyl}carbamate (5f)

Prepared from **4** (207 mg, 0.5 mmol) and piperidine (**6f**) (37  $\mu$ L, 0.5 mmol). Yield: 128 mg (61%) of yellowish resin. <sup>1</sup>H NMR (500 MHz, CDCl<sub>3</sub>):  $\delta$  1.46 (9H, s, *t*-Bu); 1.68 (4H, br s, 2  $\times$  CH<sub>2</sub>); 1.74 (2H, br s, CH<sub>2</sub>); 2.76 (2H, br s, CH<sub>2</sub>); 3.53 (2H, br s, CH<sub>2</sub>); 3.73 (4H, br s, 2  $\times$  CH<sub>2</sub>); 4.41 (2H, br s, CH<sub>2</sub>Ph); 5.69 (1H, s, 6-H); 7.13–7.34 (5H, m, Ph); 7.96 (1H, br s, 2-H); pyrimidone NH exchanged. <sup>13</sup>C NMR (126 MHz, CDCl<sub>3</sub>):  $\delta$  24.6, 26.2, 28.5, 33.0, 46.0, 50.9, 52.1, 80.9, 99.1, 127.4, 127.7, 128.8, 137.8, 141.1, 141.1, 145.1, 150.7, 155.6, 156.3, 162.8.  $m/z$  (ESI) = 480 (MH<sup>+</sup>). HRMS–ESI ( $m/z$ ): [MH<sup>+</sup>] calcd for C<sub>26</sub>H<sub>34</sub>N<sub>5</sub>O<sub>4</sub>, 480.2605; found, 480.2599. IR (ATR)  $\nu$  2931, 2849, 1687, 1617, 1578, 1578, 1495, 1438, 1410, 1364, 1258, 1159, 1122, 1002, 970, 875, 851, 814, 764, 731, 698, 672, 629 cm<sup>-1</sup>.

### 3. 4. 7. *tert*-Butyl benzyl{2-[3-(morpholine-4-carbonyl)-7-oxo-4,7-dihydropyrazolo[1,5-*a*]pyrimidin-5-yl]ethyl}carbamate (5g)

Prepared from **4** (207 mg, 0.5 mmol) and morpholine (**6g**) (44  $\mu$ L, 0.5 mmol). Yield: 184 mg (76%) of yellowish resin. <sup>1</sup>H NMR (500 MHz, CDCl<sub>3</sub>):  $\delta$  1.46 (9H, s, *t*-Bu); 2.76 (2H, br s, CH<sub>2</sub>); 3.50–3.59 (2H, m, CH<sub>2</sub>); 3.79 (4H, br s, 2  $\times$  CH<sub>2</sub>); 3.81 (4H, br s, 2  $\times$  CH<sub>2</sub>); 4.44 (2H, br s, CH<sub>2</sub>Ph); 5.71 (1H, s, 6-H); 7.16–7.35 (5H, m, Ph); 7.97 (1H, br s, 2-H); pyrimidone NH exchanged. <sup>13</sup>C NMR (126 MHz, CDCl<sub>3</sub>):  $\delta$  28.5, 33.3, 45.9, 51.7, 60.6, 66.8, 81.4, 99.3, 127.8, 128.8, 133.6, 137.7, 140.9, 143.7, 145.3, 151.1, 155.7, 156.2, 163.2.  $m/z$  (ESI) = 482 (MH<sup>+</sup>). HRMS–ESI ( $m/z$ ): [MH<sup>+</sup>] calcd for C<sub>25</sub>H<sub>32</sub>N<sub>5</sub>O<sub>5</sub>, 482.2398; found, 482.2393. IR (ATR)  $\nu$  2974, 2922, 2843, 1685, 1619, 1580, 1532, 1513, 1453, 1434, 1412, 1365, 1245, 1157, 1114, 1065, 1051, 1010, 978, 935, 884, 817, 765, 733, 699, 630 cm<sup>-1</sup>.

### 3. 4. 8. *tert*-Butyl benzyl{2-[3-(4-methylpiperazine-1-carbonyl)-7-oxo-4,7-dihydro-pyrazolo[1,5-*a*]pyrimidin-5-yl]ethyl}carbamate (5h)

Prepared from **4** (207 mg, 0.5 mmol) and 4-methylpiperazine (**6h**) (56  $\mu$ L, 0.5 mmol). Yield: 215 mg (87%) of yellowish resin. <sup>1</sup>H NMR (500 MHz, CDCl<sub>3</sub>):  $\delta$  1.45 (9H, s, *t*-Bu); 2.40 (3H, br s, NCH<sub>3</sub>); 2.59 (4H, br t, *J* = 5.1 Hz, 2  $\times$  CH<sub>2</sub>); 2.70 and 2.76 (2H, 2br s, 1:1, CH<sub>2</sub>); 3.54 (2H, br s, CH<sub>2</sub>); 3.85 (4H, br s, 2  $\times$  CH<sub>2</sub>); 4.42 (2H, br s,

CH<sub>2</sub>Ph); 5.70 (1H, s, 6-H); 7.16–7.31 (5H, m, Ph); 7.96 (1H, br s, 2-H); pyrimidone NH exchanged. <sup>13</sup>C NMR (126 MHz, CDCl<sub>3</sub>):  $\delta$  28.5, 33.2, 43.8, 45.8, 46.1, 52.7, 54.8, 80.9, 98.9, 127.7, 128.8, 136.6, 137.2, 137.8, 138.9, 140.6, 141.3, 155.7, 156.6, 163.3.  $m/z$  (ESI) = 495 (MH<sup>+</sup>). HRMS–ESI ( $m/z$ ): [MH<sup>+</sup>] calcd for C<sub>26</sub>H<sub>35</sub>N<sub>6</sub>O, 495.2714; found, 495.2707. IR (ATR)  $\nu$  2977, 2958, 1685, 1621, 1583, 1531, 1495, 1414, 1364, 1243, 1155, 976, 879, 807, 767, 731, 698, 606 cm<sup>-1</sup>.

## 3. 5. Activity assays against cathepsins K and B

The activity of all compounds was tested against recombinant human cathepsins K and B produced in-house according to the known protocol.<sup>32</sup> All assays were performed in 50 mM sodium acetate buffer pH 5.5 containing 1  $\mu$ M EDTA and 2.5 mM DTT. The hydrolysis of the synthetic substrate Z-Phe-Arg-AMC (5  $\mu$ M final concentration) was followed fluorimetrically at an excitation wavelength of 370 nm and an emission wavelength of 455 nm. Final concentrations of the enzymes in the reaction mixtures were 1 nM. Experiments were first performed at a fixed compound concentration of 100  $\mu$ M. Compounds with significant inhibitory activity were re-tested by measuring residual enzyme activity in the presence of increasing concentrations of the compounds and IC<sub>50</sub> values were calculated from these titration curves.

## 4. Conclusions

Eight novel 5-(*N*-Boc-*N*-benzyl-2-aminoethyl)-7-oxo-4,7-dihydropyrazolo[1,5-*a*]pyrimidin-3-carboxamides **5a–h** were prepared in three synthetic steps from methyl 3-amino-1*H*-pyrazole-4-carboxylate (**1**) and methyl 5-(benzyl(*tert*-butoxycarbonyl)amino)-3-oxopentanoate (**2**). The synthetic procedure comprises cyclocondensation of the above starting compounds, hydrolysis of the ester function, and BPC-mediated amidation. This method offers a quick access to various 5-(2-aminoethyl) substituted pyrazolo[1,5-*a*]pyrimidin-3-carboxamides **5** from easily available starting materials. Testing of the intermediates **3** and **4** and title compounds **5a–h** for inhibition of cathepsins B and K revealed that most of them were weak inhibitors at 100 mM concentration. Carboxamide **5a** had the strongest inhibitory effect on cathepsin K, with an IC<sub>50</sub> value of 25  $\pm$  5  $\mu$ M. Cathepsin B was most strongly inhibited by compounds **5c** and **5d** with the respective IC<sub>50</sub> values of 45  $\pm$  15  $\mu$ M and 150  $\pm$  50  $\mu$ M and to a lesser extent by compound **5a** as well. Inhibitory activities of compounds **5a**, **5c**, and **5d** against cysteine peptidases cathepsins B and K identify them as potential leads for drug development. In summary, the synthetic method allows for a simple preparation of libraries of title compounds that could be useful for medicinal and pharmaceutical applications.

## 5. Acknowledgement

The authors acknowledge the financial support from the Slovenian Research Agency (research core funding No. P1-0179 and P1-0140). We thank to EN-FIST Centre of Excellence, Ljubljana, Slovenia, for using FTIR spectrophotometer.

## 6. References

- J. A. Joule, K. Mills, in: *Heterocyclic Chemistry*, 5th ed., Wiley-Blackwell, **2010**.
- G. L. Patrick, in: *An Introduction to Medicinal Chemistry*, 5th ed., Oxford University Press, Oxford, UK, **2013**.
- A. C. Regan, in: A. R. Katritzky, C. A. Ramsden, E. F. V. Scriven, R. J. K. Taylor (Ed.): *Pyrazolo[1,5-c]pyrimidine (73)* in *Comprehensive heterocyclic chemistry III*, Vol. 11, J. Cossy (Ed.), Elsevier Science Ltd., Oxford, **2008**, pp. 577–577; and references cited therein.
- M. H. Elnagdi, M. R. H. Elmoghayar, G. E. H. Elgemeie, *Adv. Heterocycl. Chem.* **1987**, *41*, 319–376.  
DOI:10.1016/S0065-2725(08)60164-6
- SciFinder® Scholar substructure search performed on February 25, 2017.
- J. Y. Hwang, M. P. Windisch, S. Jo, H. C. Kim, S. Kim, H. Kim, M. E. Lee, D.-S. Park, E. Park, S. Ahn, J. Cechetto, J. Kim, M. Liuzzi, Z. No, J. Lee, *Bioorg. Med. Chem. Lett.* **2012**, *22*, 7297–7301. DOI:10.1016/j.bmcl.2012.10.123
- A. V. Ivashchenko, E. S. Golovina, M. G. Kadieva, V. M. Kysil, O. D. Mitkin, I. M. Okun, *Pharm. Chem. J.* **2012**, *46*, 406–410. DOI:10.1007/s11094-012-0810-4
- E. J. Hanan, A. van Abbema, K. Barrett, W. S. Blair, J. Blaney, C. Chang, C. Eigenbrot, S. Flynn, P. Gibbons, C. A. Hurley, J. R. Kenny, J. Kulagowski, L. Lee, S. R. Magnuson, C. Morris, J. Murray, R. M. Pastor, T. Rawson, M. Siu, M. Ultsch, A. Zhou, D. Sampath, J. P. Lyssikatos, *J. Med. Chem.* **2012**, *55*, 10090–10107. DOI:10.1021/jm3012239
- T. Asano, H. Yamazaki, C. Kasahara, H. Kubota, T. Kontani, Y. Harayama, K. Ohno, H. Mizuhara, M. Yokomoto, K. Misumi, T. Kinoshita, M. Ohta, M. Takeuchi, *J. Med. Chem.* **2012**, *55*, 7772–7785. DOI:10.1021/jm3008008
- T. Kosugi, D. R. Mitchell, A. Fujino, M. Imai, M. Kambe, S. Kobayashi, H. Makino, Y. Matsueda, Y. Oue, K. Komatsu, K. Imaizumi, Y. Sakai, S. Sugiura, O. Takenouchi, G. Unoki, Y. Yamakoshi, V. Cunliffe, J. Frearson, R. Gordon, C. J. Harris, H. Kallou-Hosein, J. Le, G. Patel, D. J. Simpson, B. Sherborne, P. S. Thomas, N. Suzuki, M. Takimoto-Kamimura, *J. Med. Chem.* **2012**, *55*, 6700–6715. DOI:10.1021/jm300411k
- J. Xu, H. Liu, G. Li, Y. He, R. Ding, X. Wang, M. Feng, S. Zhang, Y. Chen, S. Li, M. Zhao, Y. Li, C. Qi, *Z. Naturforsch.* **2012**, *67B*, 827–834. DOI:10.5560/ZNB.2012-004
- L. C. Lopez, S. Dos-Reis, A. Espargaro, J. A. Carrodegua, M.-L. Maddelein, S. Ventura, J. Sancho, *J. Med. Chem.* **2012**, *55*, 9521–9530. DOI:10.1021/jm301186p
- T. Inaoka, G. Bilbe, O. Ishibashi, K. Tezuka, M. Kumegawa, T. Kokubo, *Biochem. Biophys. Res. Commun.* **1995**, *206*, 89–96. DOI:10.1006/bbrc.1995.1013
- A. G. Dossetter, H. Beeley, J. Bowyer, C. R. Cook, J. J. Crawford, J. E. Finlayson, N. M. Heron, C. Heyes, A. J. Highton, J. A. Hudson, A. Jestel, P. W. Kenny, S. Krapp, S. Martin, P. A. MacFaul, T. M. McGuire, P. M. Gutierrez, A. D. Morley, J. J. Morris, K. M. Page, L. R. Ribeiro, H. Sawney, S. Steinbacher, C. Smith, M. Vickers, *J. Med. Chem.* **2012**, *55*, 6363–6374. DOI:10.1021/jm3007257
- J. J. Crawford, P. W. Kenny, J. Bowyer, C. R. Cook, J. E. Finlayson, C. Heyes, A. J. Highton, J. A. Hudson, A. Jestel, S. Krapp, S. Martin, P. A. MacFaul, B. P. McDermott, T. M. McGuire, A. D. Morley, J. J. Morris, K. M. Page, L. R. Ribeiro, H. Sawney, S. Steinbacher, C. Smith, A. G. Dossetter, *J. Med. Chem.* **2012**, *55*, 8827–8837. DOI:10.1021/jm301119s
- J. Borišek, M. Vizovišek, P. Sosnowski, B. Turk, D. Turk, B. Mohar, M. Novič, *J. Med. Chem.* **2015**, *58*, 6928–6937. DOI:10.1021/acs.jmedchem.5b00746
- F. Lecaille, D. Bromme, G. Lalmanach, *Biochimie* **2008**, *90*, 208–226. DOI:10.1016/j.biochi.2007.08.011
- P. Garnero, O. Borel, I. Byrjalsen, M. Ferreras, F. H. Drake, M. S. McQueney, N. T. Foged, P. D. Delmas, J. M. Delaisse, *J. Biol. Chem.* **1998**, *273*, 32347–32352. DOI:10.1074/jbc.273.48.32347
- W. Kafienah, D. Bromme, D. J. Buttle, L. J. Croucher, A. P. Hollander, *Biochem. J.* **1998**, *331*, 727–732. DOI:10.1042/bj3310727
- Y. Wang, R. Li, Z. Zheng, H. Yia, Z. Li, *RSC Adv.* **2016**, *6*, 82961–82968. DOI:10.1039/C6RA14251F
- G. Hajos, Z. Riedl, in: R. Neier (Ed.): *Aza analogues of pyrazolo[1,5-a]pyridines containing additional nitrogen atoms in the sixmembered ring in Science of synthesis*, Houben-Weyl: methods of molecular transformations, Vol. 12, Thieme, Stuttgart, **2006**, pp. 667–678.
- S. Ahmetaj, N. Velikanje, U. Grošelj, I. Šterbal, B. Prek, A. Golobič, D. Kočar, G. Dahmann, B. Stanovnik, J. Svete, *Mol. Divers.* **2013**, *17*, 731–743. DOI:10.1007/s11030-013-9469-3
- M. Drev, U. Grošelj, Š. Mevec, E. Pušavec, J. Štrekelj, A. Golobič, G. Dahmann, B. Stanovnik, J. Svete, *Tetrahedron* **2014**, *70*, 8267–8279. DOI:10.1016/J.tet.2014.09.020
- L. Šenica, N. Petek, U. Grošelj, J. Svete, *Acta Chim. Slov.* **2015**, *62*, 60–71. DOI:10.17344/acsi.2014.712
- K. Lombar, U. Grošelj, G. Dahmann, B. Stanovnik, J. Svete, *Synthesis* **2015**, *47*, 497–506. DOI:10.17344/acsi.2014.712
- D. Žerovnik, U. Grošelj, D. Kralj, Č. Malavašič, J. Bezenšek, G. Dahmann, K. Stare, A. Meden, B. Stanovnik, J. Svete, *Synthesis*, **2010**, 3363–3373. DOI:10.1055/s-0030-1257864
- T. J. Nitz, K. Salzwedel, C. Finnegan, C. Wild, S. Brunton, S. Flanagan, C. Montalbetti, T. S. Coulter, M. Kimber, F. Magaraci, D. Johnston, WO 2008134035 A1 20081106, date of patent November 8, **2008**; *Chem. Abstr.* **2008**, *149*, 534234.
- C. A. Lipinski, F. Lombardo, B. W. Dominy, P. J. Feeney, *Adv. Drug. Del. Rev.* **2001**, *46*, 3–26. DOI:10.1016/S0169-409X(00)00129-0

29. A. K. Ghose, V. N. Viswandhan, J. J. Wendoloski, *J. Comb. Chem.* **1999**, *1*, 55–68. DOI:10.1021/cc9800071
30. A. Nadin, C. Hattotuwigama, I. Churcher, *Angew. Chem. Int. Ed.* **2012**, *51*, 1114–1122. DOI:10.1002/anie.201105840
31. M. Novinec, B. Lenarčič, *BioMol. Concepts* **2013**, *4*, 287–308. DOI:10.1515/bmc-2012-0054
32. M. Novinec, M. Pavšič, B. Lenarčič, *Prot. Expr. Purif.* **2012**, *82*, 1–5. DOI:10.1016/j.pep.2011.11.002

## Povzetek

Izhajajoč iz metil 3-amino-1*H*-pirazol-4-karboksilata in metil 5-(benzil(*tert*-butoksikarbonil)amino)-3-oksopentanoata (**2**) smo v treh sinteznih stopnjah pripravili osem novih 5-(*N*-Boc-*N*-benzil-2-aminoetil)-7-okso-4,7-dihidropirazololo[1,5-*a*]pirimidin-3-karboksamidov **5a-h**. Sintezni postopek sestavljajo ciklokondenzacija izhodnih spojin, hidroliza estra in amidiranje tako nastale karboksilne kisline z uporabo bis(pentafluorofenil) karbonata (BPC) kot aktivacijskega reagenta. Karboksamide **5a-h** smo testirali na inhibicijo katepsinov B in K. Najbolj aktiven inhibitor katepsina K (IC<sub>50</sub> ~ 25 μM) je bil *N*-butilkarboksamid **5a**, medtem ko smo najmočnejšo inhibicijo katepsina B izmerili z *N*-(2-pikolil) karboksamidom **5c** (IC<sub>50</sub> ~ 45 μM).

Short communication

# Synthesis and Reduction of 10-Phthalimidocamphor Oxime

Uroš Grošelj, Amalija Golobič, Jurij Svete and Sebastijan Ričko\*

Department of Organic Chemistry, Faculty of Chemistry and Chemical Technology, University of Ljubljana, Večna pot 113, SI – 1000 Ljubljana, Slovenia

\* Corresponding author: E-mail: sebastijan.ricko@fkkt.uni-lj.si  
Tel.: +386 1 479 8606

Received: 24-04-2017

Dedicated to Professor Emeritus Miha Tišler, University of Ljubljana, on the occasion of his 90<sup>th</sup> anniversary.

## Abstract

10-Phthalimidocamphor oxime was prepared from easily available 10-iodocamphor in two steps. Reduction of the oxime functionality resulted in the formation of two novel polycyclic isoindolinone heterocycles, the attempted preparation of the primary amine failed. The structures of novel heterocycles were unambiguously confirmed by single crystal X-ray diffraction as well as NMR techniques.

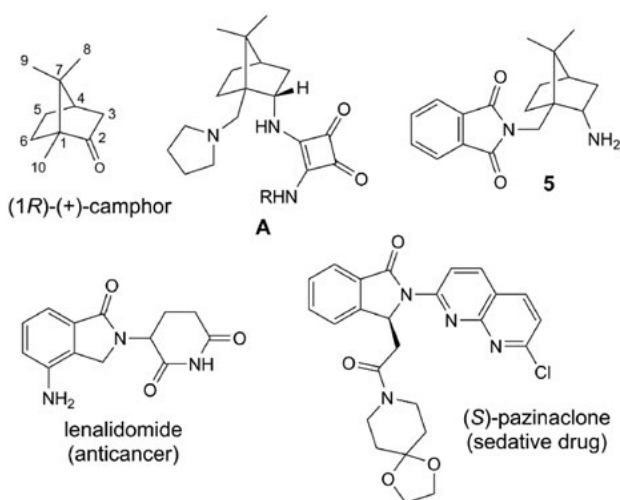
**Keywords:** 10-iodocamphor, 10-phthalimidocamphor oxime, camphor derived amines, reduction

## 1. Introduction

(1*R*)-(+)-Camphor and its enantiomer are renewable enantiomerically pure chiral pool starting materials. The unique reactivity of camphor enables its derivatization at positions 2, 3, 4, 5, 8-10, as well as selective cleavage of the C1-C2 and C2-C3 bonds (Figure 1).<sup>1,2</sup> All of the above makes camphor a very desirable starting compound for the preparation of a wide variety of products<sup>3</sup> ranging from natural products<sup>1,2</sup> to chiral auxiliaries,<sup>4,5</sup> ligands in asymmetric synthesis,<sup>6-10</sup> organocatalysts,<sup>11</sup> and NMR shift reagents.<sup>12</sup>

Within our continuing study on camphor-based diamines as potential organocatalyst scaffolds,<sup>13-15</sup> we recently reported on the synthesis of a novel type of 1,3-diamine-derived bifunctional squaramide organocatalysts **A** prepared from 10-iodocamphor and their application as highly efficient catalysts in Michael additions of 1,3-dicarbonyl nucleophiles to *trans*- $\beta$ -nitrostyrenes.<sup>16</sup> 10-Iodocamphor<sup>17</sup> has seen surprisingly limited application as the starting compound,<sup>18-24</sup> although, it can easily be prepared in sufficient quantities from (1*S*)-(+)-10-camphor-sulfonic acid.<sup>16</sup> Herein we report the results of the synthesis and reduction of 10-phthalimidocamphor oxime (**4**), which is a potential precursor for the preparation of mono-protected primary diamine camphor building block **5**.

Instead of the desired diamine **5**, isoindolinone heterocycles **6** and **7** were isolated. Isoindolinone/isoindole derivatives can be found in numerous natural and pharmaceutical compounds showing multiple biological activities (Figure 1).<sup>25</sup>



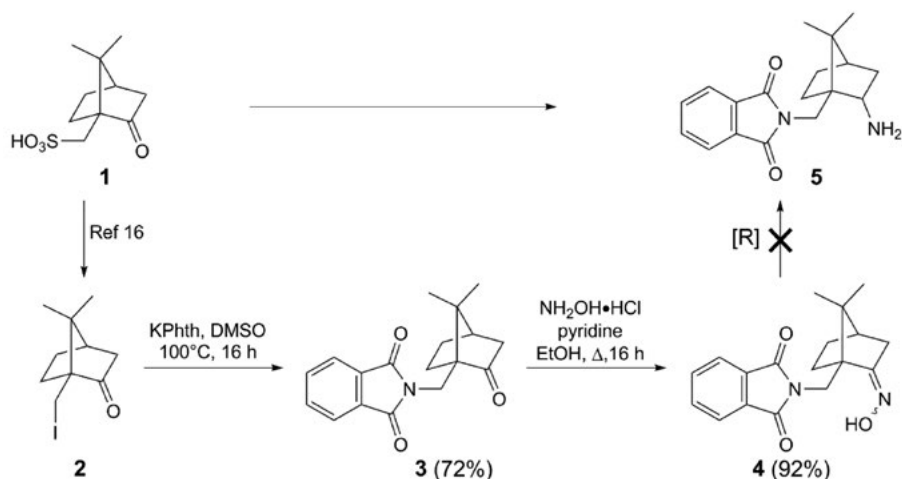


## 2. Results and Discussion

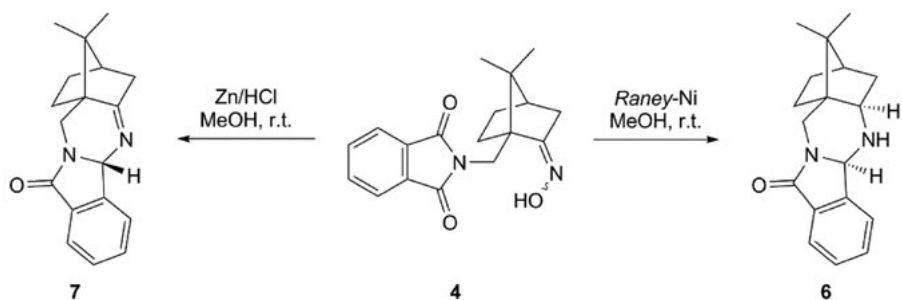
Following the literature procedure, (1S)-(+)-10-camphorsulfonic acid (**1**) was transformed into 10-iodocamphor (**2**).<sup>16</sup> The following reaction of **2** with potassium phthalimide gave the corresponding 10-phthalimidocamphor (**3**) in 72% yield. Finally, condensation of **3** with  $\text{NH}_2\text{OH}$  furnished in 92% yield the expected 10-phthalimidocamphor oxime (**4**). Next, reduction of the oxime **4** was studied with the aim of preparing mono-protected primary diamine camphor building block **5** (Scheme 1).

Thus, the results of the reduction of oxime **4** are summarized in Scheme 2 and Table 1. Catalytic hydrogena-

tion of **4** using Pd-C in MeOH with or without HCl yielded only the recovered starting material (Entries 1 and 2). On the other hand, reduction of **4** with Na in *n*-PrOH, as expected, gave a complex mixture of products (Entry 3). Catalytic hydrogenation using Raney-Ni gave the polycyclic secondary amine **6** in 37% isolated yield (Entry 4). Clearly, the reduction of oxime **4** was successful, though the reaction did not stop at the desired diamine level **5**. Therefore, the reduction with Raney-Ni was repeated in the presence of AcOH (Entry 5) and aqueous formaldehyde (Entry 6) in order to obtain either the amine **5** or a tertiary dimethylamine derivative. The former reaction again delivered compound **6** in 20% yield, while the later



Scheme 1. Attempted synthesis of monoprotected diamine **5**.



Scheme 2. Synthesis of amine **6** and imine **7** from oxime **4**.

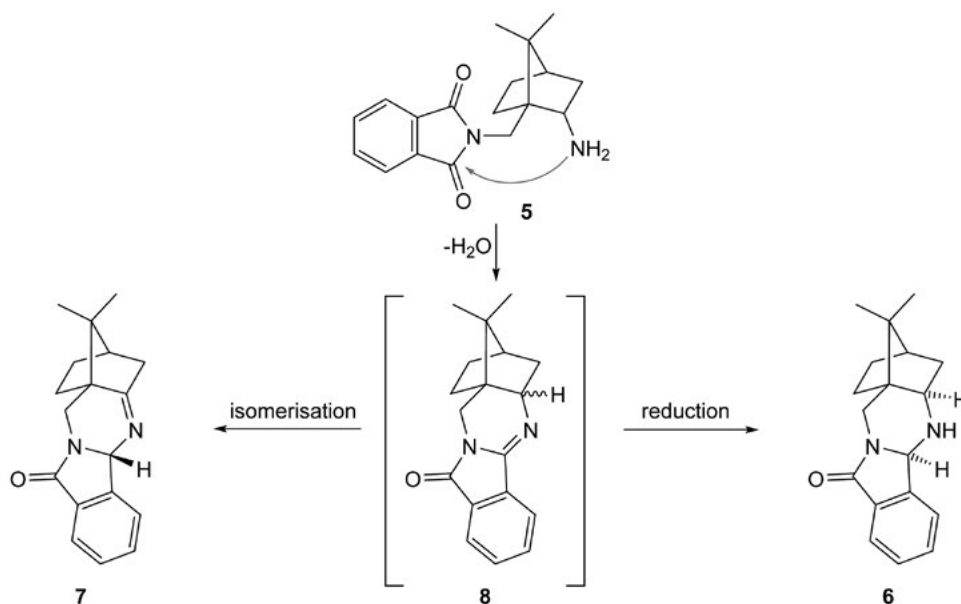
Table 1. Reduction of oxime **4** under various reaction conditions.

Entry	Reducing agent	Solvent	T (°C)	t (h)	Product/Yield (%)
1	Pd-C	MeOH	r.t.	8	no reaction
2	Pd-C/HCl	MeOH	r.t.	8	no reaction
3	Na	<i>n</i> -PrOH	90	2	complex mixture
4	Raney-Ni	MeOH	r.t.	8	<b>6</b> (37)
5	Raney-Ni/AcOH	MeOH	r.t.	8	<b>6</b> (20)
6	Raney-Ni/HCHO	MeOH	r.t.	8	complex mixture
7	Zn/HCl	MeOH	r.t.	a)	<b>7</b> (45)
8	Zn	AcOH	r.t.	a)	complex mixture
9	Zn/HCl	AcOH	r.t.	a)	complex mixture

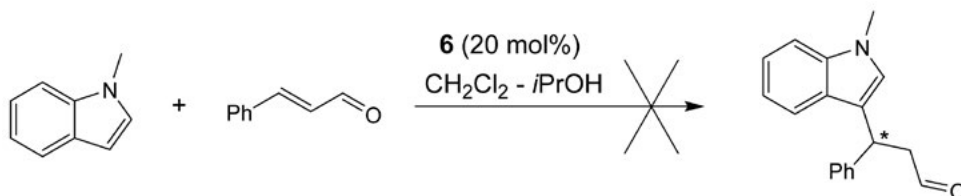
a) Till the disappearance of the starting material (TLC analysis).

yielded a complex mixture of products. Next, reduction of oxime **4** with Zn in MeOH in the presence of excess aqueous HCl was performed, furnishing imine **7** in 45% yield (*Entry 7*). Repeating the reduction of **4** with Zn in AcOH with or without aqueous HCl yielded complex mixtures of products (*Entries 8 and 9*).

The formation of the products **6** and **7** could be rationalized by the initial formation of the primary amine **5**, followed by the condensation with the proximal carbonyl group of the phthalimide functionality to give intermediate **8**. Isomerization of **8** to imine **7** is explained by a simple imine-imine tautomerisation, while reduction (or isomerization/reduction) of **8** would lead to amine **6** (*Scheme 3*). The configuration of the newly formed stereogenic centers seems to be dictated by the reducing agent applied.



**Scheme 3.** Rationalization of the formation of products **6** and **7**.



**Scheme 4.** Attempted addition of 1-methylindole to cinnamaldehyde catalyzed by **6**.

Compound **6** was tested as a potential covalent organocatalyst in the addition of 1-methylindole to cinnamaldehyde.<sup>26</sup> Amine **6** failed to catalyze the reaction (*Scheme 4*).

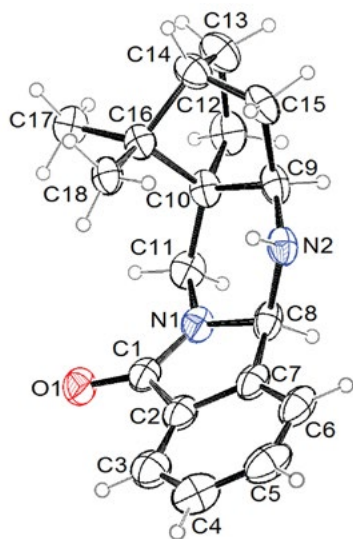
The structures of novel compounds **3**, **4**, **6**, and **7** were determined by spectroscopic methods (<sup>1</sup>H-NMR, <sup>13</sup>C-NMR, IR, HRMS).

## 2. 1. Crystal Structures of Compounds **6** and **7**

The asymmetric units of compounds **6** and **7** are depicted in *Figures 2* and *3*, respectively. In both structures there is one molecule in the asymmetric unit. Bond lengths are given in *Table 2*. Most of bond lengths are very similar both in **6** and **7**, with the exception of bonds including atoms N2 and C9. This is in accordance with their structural chemical formulas (as shown in *Scheme 2*) which differ only in the closeness of these two atoms. Bond N2-C9 in **6**, 1.463(3) Å, is significantly longer than 1.265(2) Å in **7**, which is in accordance with the fact that this is a single bond in **6** and a double bond in **7**. The average C(sp<sup>3</sup>)-N(3) single bond and C(sp<sup>2</sup>) = N(2) double bond in the literature<sup>1</sup> are 1.469(14) and 1.279(8) Å, respectively. Usually C(sp<sup>3</sup>)-C(sp<sup>3</sup>) bond distances are longer in comparison to C(sp<sup>3</sup>)-C(sp<sup>2</sup>). In accordance to this, C9-C10 and C9-C15 are longer in **6** than in **7**.

Molecules of **6** and **7** are asymmetric. In both structures, chiral carbon centres are C8, C10, and C14; in **6** C9 atom is also chiral. C10 and C14 from camphor part of the molecule have in both compounds absolute configuration (S) and (R), respectively. The absolute configuration of C8 atom from phthalimide ring is (R) in **6** and (S) in **7**, respec-

tively. Consequently, the conformation of molecules of **6** and **7** is different in a way how a camphor part is bonded to the remaining part of molecule which is shown in *Figure 4*. In accordance with their optical activity, both compounds crystallize in chiral space group. Compound **6** crystallizes in orthorhombic crystal system in  $P2_12_12_1$  and **7** in tetragonal  $P4_32_1$ , respectively. The packing of molecules is presented in *Figures 5* and *6*. In **6** molecules are connected via  $N2-H\cdots O1$  hydrogen bonds into chains parallel to  $b$  axis. Geometrical parameters of this H-bond are given in *Table 3*. The distance between the donor, N2,

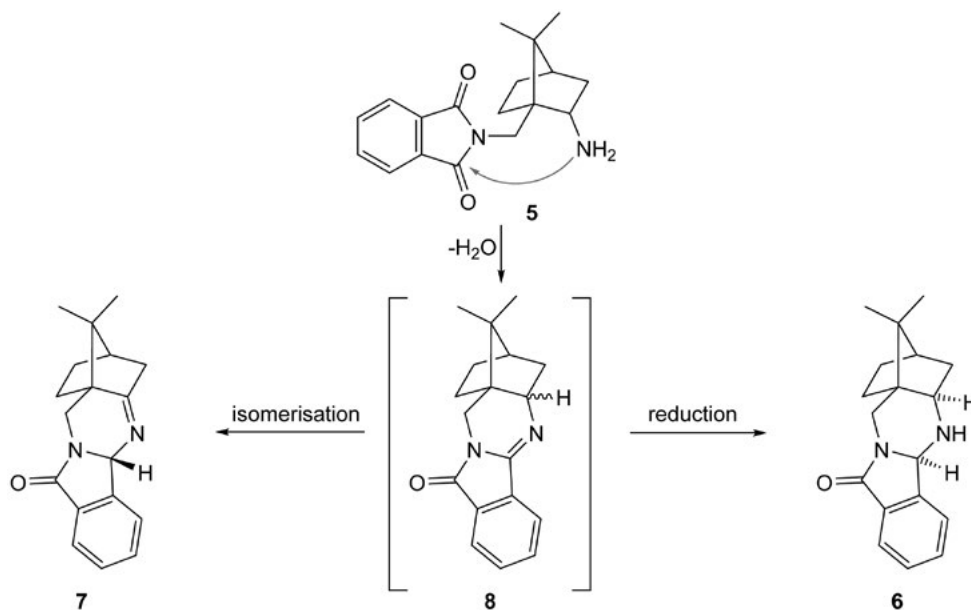


**Figure 2.** Ortep<sup>28</sup> drawing of asymmetric unit of compound **6**. Displacement ellipsoids are drawn with 25% probability level and the hydrogen atoms are shown as small spheres of arbitrary radii.

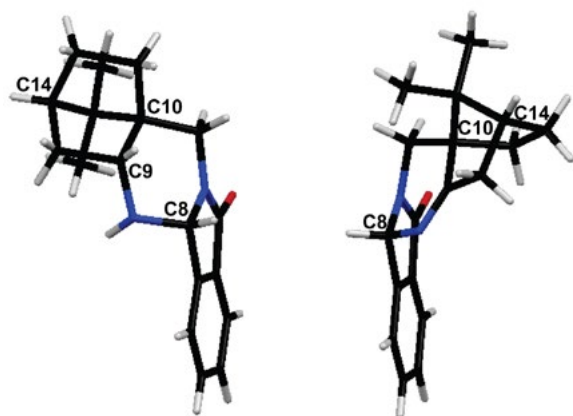
**Table 2.** Bond lengths in **6** and **7** (Å).

bond	6	7
O1-C1	1.230(2)	1.222(1)
N1-C1	1.347(3)	1.356(2)
N1-C8	1.466(3)	1.460(2)
N1-C11	1.453(3)	1.451(2)
<b>N2-C8</b>	<b>1.438(2)</b>	<b>1.464(2)</b>
<b>N2-C9</b>	<b>1.463(3)</b>	<b>1.265(2)</b>
C1-C2	1.490(3)	1.493(2)
C2-C7	1.381(3)	1.379(2)
C2-C3	1.377(3)	1.384(2)
C3-C4	1.375(4)	1.387(2)
C4-C5	1.373(5)	1.385(2)
C5-C6	1.389(4)	1.381(2)
C6-C7	1.387(3)	1.383(2)
C7-C8	1.504(3)	1.502(2)
<b>C9-C10</b>	<b>1.565(3)</b>	<b>1.519(2)</b>
<b>C9-C15</b>	<b>1.546(3)</b>	<b>1.522(2)</b>
C10-C11	1.521(3)	1.519(1)
C10-C12	1.551(3)	1.550(2)
C10-C16	1.557(3)	1.553(2)
C12-C13	1.540(3)	1.556(2)
C13-C14	1.531(3)	1.523(2)
C14-C15	1.532(3)	1.536(2)
C14-C16	1.551(3)	1.554(2)
C16-C17	1.538(3)	1.531(2)
C16-C18	1.526(3)	1.528(2)

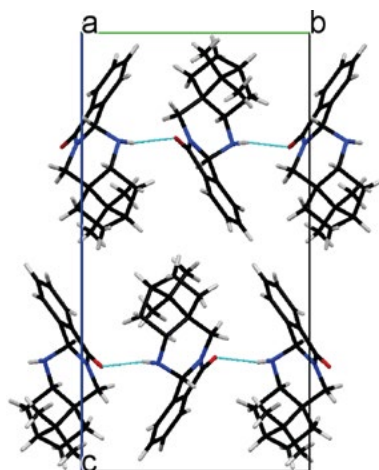
and acceptor, O1, is not short, which means that H-bond is weak. In **7** there are no N-H or O-H groups and consequently no classical intermolecular H-bonds. N and O atoms are acceptors of weak intermolecular H-bonds, donated by C-H moieties and presented in *Table 3*. In **6** and **7**



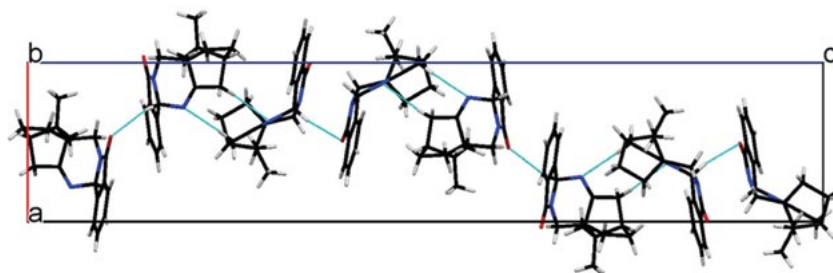
**Figure 3.** Ortep<sup>28</sup> drawing of asymmetric unit of compound **7**. Displacement ellipsoids are drawn with 25% probability level and the hydrogen atoms are shown as small spheres of arbitrary radii.



**Figure 4.** Mercury<sup>29</sup> drawing of compounds **6** (on left) and **7** (on right) with labelling of chiral carbon centers of the phthalimide part of the molecule.



**Figure 5.** Mercury<sup>29</sup> drawing of molecular packing in **6**. Light blue lines show intermolecular N-H...O hydrogen bonds.



**Figure 6.** Mercury<sup>29</sup> drawing of molecular packing in **7**. Light blue lines show weak intermolecular C-H...O and C-H...N hydrogen bonds.

**Table 3.** Hydrogen-bond geometry in **6** and **7** (Å, °).

D-H...A	D-H	H...A	D...A	D-H...A
N2-H2'...O1i	0.91(2)	2.25(2)	3.127(2)	161(2)
C8-H...O1ii	0.98	2.57	3.509(2)	162
C15-H...N2iii	0.97	2.69	3.654(2)	173

Symmetry codes: (i)  $-x, y+1/2, -z+1/2$ , (ii)  $1/2+x, 3/2-y, 1/4-z$ , (iii)  $y, x, -z$ .

there are no  $\pi\cdots\pi$  or  $\pi\cdots\sigma$  stacking interaction between aromatic rings.

### 3. Conclusion

The title 10-phthalimidocamphor oxime (**4**) was prepared as a precursor for the preparation of monoprotected camphor derived 1,3-diamine building block **5**. Reduction thereof under various reaction conditions could never be stopped at the diamine **5** level, instead polycyclic isoindolinone heterocycles **6** and **7** were isolated. The structures of **6** and **7** were confirmed by X-ray analysis of the corresponding monocrystals.

### 4. Experimental Section

Solvents for extractions and chromatography were of technical grade and were distilled prior to use. Extracts were dried over technical grade  $\text{Na}_2\text{SO}_4$ . Melting points were determined on a Kofler micro hot stage and on SRS OptiMelt MPA100 – Automated Melting Point System (Stanford Research Systems, Sunnyvale, California, United States). The NMR spectra were obtained on a Bruker UltraShield 500 plus (Bruker, Billerica, Massachusetts, United States) at 500 MHz for  $^1\text{H}$  and 126 MHz for  $^{13}\text{C}$  nucleus, using  $\text{DMSO}-d_6$  and  $\text{CDCl}_3$  with TMS as the internal standard, as solvents. Mass spectra were recorded on an Agilent 6224 Accurate Mass TOF LC/MS (Agilent Technologies, Santa Clara, California, United States), IR spectra on a Perkin-Elmer Spectrum BX FTIR spectrophotometer (PerkinElmer, Waltham, Massachusetts, United States). Catalytic hydrogenation was performed on a Parr Pressure Reaction Hydrogenation Apparatus (Moline, IL, USA).

Column chromatography (CC) was performed on silica gel (Silica gel 60, particle size: 0.035–0.070 mm (Sigma-Aldrich, St. Louis, Missouri, United States)).

#### Synthesis of 2-(((1*R*,4*R*)-7,7-dimethyl-2-oxobicyclo[2.2.1]heptan-1-yl)methyl)isoindoline-1,3-dione (**3**).

To a suspension of 10-iodocamphor (**2**) (420 mg, 1.51 mmol) in anhydrous DMSO (10 mL) under argon

potassium phthalimide (524 mg, 2.83 mmol) was added and the resulting reaction mixture was heated at 100 °C under argon for 16 h. Volatile components were evaporated *in vacuo*. The residue was suspended in H<sub>2</sub>O (20 mL) and extracted with EtOAc (3 × 40 mL). The combined organic phase was washed with H<sub>2</sub>O (20 mL) and NaCl (aq. sat., 20 mL), dried over anhydrous Na<sub>2</sub>SO<sub>4</sub>, filtered, and volatile components evaporated *in vacuo*. The residue was purified by column chromatography (EtOAc:petroleum ether = 1:2). Fractions containing the pure product **3** were combined and volatile components evaporated *in vacuo*. Yield: 320 mg (1.076 mmol, 72%) of white solid; mp 123–129 °C.  $[\alpha]_D^{25} = -2.4$  ( $c = 0.25$ , CH<sub>2</sub>Cl<sub>2</sub>). EI-HRMS:  $m/z = 298.1437$  (MH<sup>+</sup>); C<sub>18</sub>H<sub>20</sub>NO<sub>3</sub> requires:  $m/z = 298.1438$  (MH<sup>+</sup>);  $\nu_{\max}$  3469, 3189, 3066, 2959, 2888, 1773, 1731, 1712, 1604, 1466, 1426, 1398, 1373, 1361, 1309, 1295, 1191, 1157, 1142, 1106, 1089, 1053, 1031, 1008, 935, 872, 763, 712, 642, 625 cm<sup>-1</sup>. <sup>1</sup>H-NMR (500 MHz, CDCl<sub>3</sub>):  $\delta$  0.95 (s, 3H, Me); 1.10 (s, 3H, Me); 1.30–1.37 (m, 1H); 1.52–1.60 (m, 1H); 1.88 (d,  $J = 18.3$  Hz, 1H); 1.84–1.99 (m, 2H); 2.01 (t,  $J = 4.5$  Hz, 1H); 2.43 (ddd,  $J = 2.5$ ; 4.9; 18.4 Hz, 1H); 3.77 (d,  $J = 14.9$  Hz, 1H); 4.07 (d,  $J = 14.9$  Hz, 1H); 7.72 (dd,  $J = 3.0$ ; 5.5 Hz, 2H of Ar); 7.85 (dd,  $J = 3.1$ ; 5.4 Hz, 2H of Ar). <sup>13</sup>C-NMR (126 MHz, CDCl<sub>3</sub>):  $\delta$  19.5, 19.7, 26.7, 26.7, 34.7, 43.3, 43.5, 47.2, 61.1, 123.4, 132.2, 134.1, 168.9, 216.7.

#### Synthesis of 2-(((1R,4R)-2-(hydroxyimino)-7,7-dimethylbicyclo[2.2.1]heptan-1-yl)methyl)isoindoline-1,3-dione (**4**).

To a solution of ketone **3** (2.76 g, 9.28 mmol) in EtOH (45 mL) NH<sub>2</sub>OH·HCl (1.30 g, 18.7 mmol) and pyridine (1.10 g, 13.9 mmol) were added and the resulting reaction mixture was heated under reflux for 16 h. Volatile components were evaporated *in vacuo*, followed by the addition of H<sub>2</sub>O (25 mL) and finely powdered NaOH till the pH ~ 10–12. The resulting mixture was extracted with Et<sub>2</sub>O (5 × 40 mL). The combined organic phase was washed with H<sub>2</sub>O (5 mL) and NaCl (aq. sat., 5 mL), dried over anhydrous Na<sub>2</sub>SO<sub>4</sub>, filtered, and volatile components evaporated *in vacuo*. The residue was purified by column chromatography (EtOAc:petroleum ether = 1:2). Fractions containing the pure product **4** were combined and volatile components evaporated *in vacuo*. Yield: 2.67 g (8.54 mmol, 92%) of white solid; mp 151–155 °C.  $[\alpha]_D^{25} = -50.6$  ( $c = 0.33$ , CH<sub>2</sub>Cl<sub>2</sub>). EI-HRMS:  $m/z = 313.1547$  (MH<sup>+</sup>); C<sub>18</sub>H<sub>21</sub>N<sub>2</sub>O<sub>3</sub> requires:  $m/z = 313.1547$  (MH<sup>+</sup>);  $\nu_{\max}$  3469, 3280, 2945, 2881, 1774, 1713, 1612, 1467, 1427, 1395, 1387, 1362, 1338, 1312, 1297, 1245, 1197, 1158, 1104, 1028, 1015, 987, 962, 927, 913, 875, 855, 821, 800, 717, 611 cm<sup>-1</sup>. <sup>1</sup>H-NMR (500 MHz, CDCl<sub>3</sub>):  $\delta$  0.90 (s, 3H, Me); 1.07 (s, 3H, Me); 1.20–1.28 (m, 1H); 1.58–1.65 (m, 1H); 1.76–1.85 (m, 2H); 1.95–2.03 (m, 1H); 2.08 (d,  $J = 17.8$  Hz, 1H); 2.59 (dt,  $J = 3.8$ ; 17.9 Hz, 1H); 3.88 (d,  $J = 14.7$  Hz, 1H); 4.10 (d,  $J = 14.8$  Hz, 1H); 7.63 (br s, 1H); 7.72 (dd,  $J = 3.0$ ; 5.5 Hz, 2H of Ar); 7.85 (dd,  $J = 3.1$ ; 5.4 Hz, 2H of Ar). <sup>13</sup>C-NMR (126 MHz,

CDCl<sub>3</sub>):  $\delta$  19.2, 19.3, 27.0, 29.5, 32.9, 35.8, 44.6, 48.7, 55.5, 123.4, 132.2, 134.1, 168.5, 169.1.

#### Synthesis of (4bR,5aR,7R,9aS)-13,13-dimethyl-5,5a,6,7,8,9-hexahydro-10H-7,9a-methanoisoindolo[1,2-b]quinazolin-12(4bH)-one (**6**).

A mixture of compound **4** (246 g, 0.788 mmol), MeOH (50 mL), and Raney-Ni (100 mg) was hydrogenated (4 bar of H<sub>2</sub>) at room temperature for 8 h. The reaction mixture was filtered through a short pad of Celite®, washed with MeOH (20 mL), and the filtrate evaporated *in vacuo*. The residue was purified by column chromatography (1. *n*-hexane:Et<sub>2</sub>O = 1:3 to elute the nonpolar impurities; 2. Et<sub>3</sub>N:Et<sub>2</sub>O = 1:40 to elute the product **6**). Fractions containing the pure product **6** were combined and volatile components evaporated *in vacuo*. Yield: 83 mg (0.294 mmol, 37%) of white solid; mp 154–158 °C.  $[\alpha]_D^{25} = -163.0$  ( $c = 0.40$ , CH<sub>2</sub>Cl<sub>2</sub>). EI-HRMS:  $m/z = 283.1801$  (MH<sup>+</sup>); C<sub>18</sub>H<sub>23</sub>N<sub>2</sub>O requires:  $m/z = 283.1805$  (MH<sup>+</sup>);  $\nu_{\max}$  3326, 2941, 2881, 1672, 1485, 1460, 1431, 1388, 1368, 1356, 1331, 1300, 1276, 1263, 1243, 1192, 1153, 1130, 1112, 1087, 1053, 1013, 976, 948, 931, 898, 875, 846, 816, 793, 740, 708, 687, 675 cm<sup>-1</sup>. <sup>1</sup>H-NMR (500 MHz, CDCl<sub>3</sub>):  $\delta$  0.87 (s, 3H, Me); 0.99 (s, 3H, Me); 1.07–1.19 (m, 2H); 1.19–1.24 (m, 1H); 1.51–1.58 (m, 1H); 1.59–1.67 (m, 1H); 1.72–1.81 (m, 2H); 1.95 (dd,  $J = 8.9$ ; 13.5 Hz, 1H); 3.18 (d,  $J = 14.3$  Hz, 1H); 3.25 (dd,  $J = 4.6$ ; 8.9 Hz, 1H); 4.44 (d,  $J = 14.4$  Hz, 1H); 5.12 (s, 1H); 7.47–7.60 (m, 3H, 3H of Ar); 7.81–7.86 (m, 1H, 1H of Ar). <sup>13</sup>C-NMR (126 MHz, CDCl<sub>3</sub>):  $\delta$  21.2, 21.7, 26.9, 33.9, 37.9, 38.5, 44.1, 45.1, 46.4, 62.9, 70.6, 123.1, 123.8, 129.6, 131.7, 133.2, 142.8, 165.4.

#### Synthesis of (4bS,7R,9aS)-13,13-dimethyl-6,7,8,9-tetrahydro-10H-7,9a-methanoisoindolo[1,2-b]quinazolin-12(4bH)-one (**7**).

To a solution of **4** (113 mg, 0.362 mmol) in MeOH (10 mL) at room temperature HCl (aq. 12 M, 1 mL) was added. Next, at room temperature under vigorous stirring, Zn dust (100 mg, 1.53 mmol) was added. After the disappearance of the starting material (TLC analysis), the reaction mixture was filtered and the filtrate evaporated *in vacuo*. The residue was suspended in H<sub>2</sub>O (10 mL), finely powdered NaOH was added till the pH ~ 10–12 followed by extraction with Et<sub>2</sub>O (3 × 30 mL). The combined organic phase was washed with H<sub>2</sub>O (10 mL) and NaCl (aq. sat., 10 mL), dried over anhydrous Na<sub>2</sub>SO<sub>4</sub>, filtered, and volatile components evaporated *in vacuo*. The residue was purified by column chromatography (1. *n*-hexane:Et<sub>2</sub>O = 1:3 to elute the nonpolar impurities; 2. Et<sub>3</sub>N:Et<sub>2</sub>O = 1:25 to elute the product **7**). Fractions containing the pure product **7** were combined and volatile components evaporated *in vacuo*. Yield: 46 mg (0.163 mmol, 45%) of white solid; mp 164–172 °C.  $[\alpha]_D^{25} = +102.5$  ( $c = 0.33$ , CH<sub>2</sub>Cl<sub>2</sub>). EI-HRMS:  $m/z = 281.1646$  (MH<sup>+</sup>); C<sub>18</sub>H<sub>21</sub>N<sub>2</sub>O requires:  $m/z = 281.1648$  (MH<sup>+</sup>);  $\nu_{\max}$  2951, 2930, 2869, 1677, 1615, 1468, 1447, 1412, 1310, 1281, 1225, 1152, 1102, 1057, 1025, 975, 320, 795,

747, 709, 691, 621 cm<sup>-1</sup>. <sup>1</sup>H-NMR (500 MHz, CDCl<sub>3</sub>): δ 1.02 (s, 3H, Me); 1.04 (s, 3H, Me); 1.18–1.27 (m, 1H); 1.32–1.39 (m, 1H); 1.82–1.97 (m, 4H); 2.57–2.65 (m, 1H); 3.24 (d, J=13.3, 1H); 4.43 (d, J = 13.3 Hz, 1H); 5.83– 5.86 (m, 1H); 7.48–7.53 (m, 1H, 1H of Ar); 7.58–7.63 (m, 1H, 1H of Ar); 7.77–7.84 (m, 2H, 2H of Ar). <sup>13</sup>C-NMR (126 MHz, CDCl<sub>3</sub>): δ 18.6, 20.0, 26.9, 30.0, 38.3, 39.6, 43.3, 47.1, 53.0, 73.8, 123.4, 123.5, 129.1, 131.5, 132.1, 143.4, 167.6, 180.4.

#### 4. 1. Single Crystal X-ray Structure Analysis of Compounds 6 and 7

Single crystal X-ray diffraction data of compounds 6 and 7 have been collected on an Agilent SuperNova dual source diffractometer with an Atlas detector with CuKα radiation (1.54184 Å) at room temperature. The diffraction data were processed using CrysAlis PRO software.<sup>30</sup> Structure of both compounds was solved by direct methods, using SIR97.<sup>31</sup> A full-matrix least-squares refinement on F<sup>2</sup> was employed with anisotropic displacement parameters for all non-hydrogen atoms. H atoms were placed at calculated positions and treated as riding. For H atoms from methyl groups, torsion angles were calculated from electron density. Only H atom bonded to N2, was located from difference Fourier map and refined with isotropic displacement parameter. The absolute structure of both compounds was confirmed also by the refinement of Flack parameter. SHELXL97 software<sup>32</sup> was used for structure refinement and interpretation. Drawings of the structures were produced using ORTEP-3<sup>28</sup> and Mercury<sup>29</sup>. Structural and other crystallographic details on data collection and refinement have been deposited with the Cambridge Crystallographic Data Centre as supplementary publication numbers CCDC 1539864-1539865, for 6 and 7, respectively. These data can be obtained free of charge via www.ccdc.cam.ac.uk/conts/retrieving.html (or from the CCDC, 12 Union Road, Cambridge CB2 1EZ, UK; fax: 44 1223 336033; e-mail: deposit@ccdc.cam.ac.uk).

### 5. Acknowledgements

The authors acknowledge the financial support from the Slovenian Research Agency (research core funding No. P1-0179). We also thank to EN-FIST Centre of Excellence (Ljubljana, Slovenia) for using the SuperNova diffractometer.

### 6. References

1. T. Money, Remote functionalization of camphor: application to natural product synthesis. *Org. Synth.: Theory Appl.* **1996**, 3, 1–83.
2. T. Money, *Nat. Prod. Rep.* **1985**, 2, 253–289. DOI:10.1039/np9850200253
3. U. Grošelj, *Targets Heterocycl. Syst.* **2015**, 19, 62–100.
4. W. Oppolzer, *Tetrahedron* **1987**, 43, 1969–2004. DOI:10.1016/S0040-4020(01)86780-6
5. W. Oppolzer, *Pure Appl. Chem.* **1990**, 62, 1241–1250.
6. S. A. Matlin, W. J. Lough, L. Chan, D. M. H. Abram, Z. Zhou, *J. Chem. Soc., Chem. Commun.* **1984**, 1038–1040. DOI:10.1039/C39840001038
7. C. Chapuis, J. Jurczak, *Helv. Chim. Acta* **1987**, 70, 436–440. DOI:10.1002/hlca.19870700223
8. K. Tomioka, *Synthesis* **1990**, 541–549. DOI:10.1055/s-1990-26935
9. R. Noyori, M. Kitamura, *Angew. Chem. Int. Ed. Engl.* **1991**, 30, 49–69. DOI:10.1002/anie.199100491
10. H. C. Brown, P. V. Ramachandran, *Pure Appl. Chem.* **1991**, 63, 307–16. DOI:10.1351/pac199163030307
11. U. Grošelj, *Curr. Org. Chem.* **2015**, 19, 2048–2074. DOI:10.2174/1385272819666150713180204
12. H. L. Goering, J. N. Eikenberry, G. S. Koermer, *J. Chem. Soc.* **1971**, 93, 5913–5914. DOI:10.1021/ja00751a065
13. U. Grošelj, A. Golobič, K. Stare, J. Svete, B. Stanovnik, *Chirality* **2012**, 24, 307–317. DOI:10.1002/chir.21999
14. U. Grošelj, S. Ričko, J. Svete, B. Stanovnik, *Chirality* **2012**, 24, 412–419. DOI:10.1002/chir.22035
15. S. Ričko, A. Golobič, J. Svete, B. Stanovnik, U. Grošelj, *Chirality* **2015**, 27, 39–52. DOI:10.1002/chir.22386
16. S. Ričko, J. Svete, B. Štefane, A. Perdih, A. Golobič, A. Meden, U. Grošelj, *Adv. Synth. Catal.* **2016**, 358, 3786–3796. DOI:10.1002/adsc.201600498
17. J. D. Loudon, *J. Chem. Soc.* **1933**, 823–825. DOI:10.1039/jr9330000823
18. M. J. Spallek, G. Storch, O. Trapp, *Eur. J. Org. Chem.* **2012**, 2012, 3929–3945.
19. K. Bica, G. Gmeiner, C. Reichel, B. Lendl, P. Gaertner, *Synthesis* **2007**, 1333–1338.
20. S.-i. Watanabe, R. Hasebe, J. Ouchi, H. Nagasawa, T. Kataoka, *Tetrahedron Lett.* **2010**, 51, 5778–5780. DOI:10.1016/j.tetlet.2010.08.082
21. J. A. Gladysz, J. L. Hornby, J. E. Garbe, *J. Org. Chem.* **1978**, 43, 1204–1208. DOI:10.1021/jo00400a040
22. M. C. Galan, K. Jouvin, D. Alvarez-Dorta, *Carbohydr. Res.* **2010**, 345, 45–49. DOI:10.1016/j.carres.2009.09.034
23. J. E. H. Buston, I. Coldham, K. R. Mulholland, *J. Chem. Soc., Perkin Trans. 1* **1999**, 2327–2334. DOI:10.1039/a903050f
24. T. Sell, S. Laschat, I. Dix, P. G. Jones, *Eur. J. Org. Chem.* **2000**, 4119–4124. DOI:10.1002/1099-0690(200012)2000:24<4119::AID-EJOC4119>3.0.CO;2-X
25. K. Speck, T. Magauer, *Beilstein J. Org. Chem.* **2013**, 9, 2048–2078 and references cited therein. DOI:10.3762/bjoc.9.243
26. J. F. Austin, D. W. C. MacMillan, *J. Am. Chem. Soc.* **2002**, 124, 1172–1173. DOI:10.1021/ja017255c
27. F. H. Allen, D. G. Watson, L. Brammer, A. G. Orpen, R. Taylor, *International Tables for Crystallography* (2006). Vol. C, chapter 9.5, 790–811.
28. L. J. Farrugia, *J. Appl. Crystallogr.* **1997**, 30, 567–567. DOI:10.1107/S0021889897003117
29. C. F. Macrae, P. R. Edgington, P. McCabe, E. Pidcock, G. P.

- Shields, R. Taylor, M. Towler, J. van de Streek, *J. Appl. Cryst.* **2006**, 39, 453. DOI:10.1107/S002188980600731X
30. Agilent Technologies. CrysAlis PRO. Version 1.171.35.11; Agilent Technologies: Yarnton, Oxfordshire, England, (2011).
31. A. Altomare, M. C. Burla, M. Camalli, G. L. Cascarano, C. Giacovazzo, A. Guagliardi, A. G. G. Moliterni, G. Polidori, R. Spagna, *J. Appl. Crystallogr.* **1999**, 32, 115–119. DOI:10.1107/S0021889898007717
32. G. M. Sheldrick, *Acta Crystallogr., Sect. A* **2008**, A64, 112–122. DOI:10.1107/S0108767307043930

## Povzetek

10-Ftalimidokafra oksim smo pripravili iz enostavno dostopne 10-jodokafre v dveh korakih. Pri redukciji oksima ni prišlo do tvorbe primarnega amina ampak sta nastala dva nova policiklična izoindolidinska heterocikla. Njuni strukturo smo nedvoumno potrdili z rentgensko strukturo in NMR tehnikami.

Short communication

# The Synthesis of 7-Substituted-2,3-dihydropyrido [4,3-*d*]pyridazine-1,4-diones and 1,4-Dioxo-7-substituted-1,2,3,4-tetrahydropyrido[4,3-*d*]pyridazine 6-Oxides from Methyl Ketones

Benjamin Prek and Branko Stanovnik\*

Faculty of Chemistry and Chemical Technology, University of Ljubljana,  
Večna pot 113, P. O. Box 537, 1000 Ljubljana, Slovenia

\* Corresponding author: E-mail: branko.stanovnik@fkkt.uni-lj.si

Received: 12-07-2017

Dedicated to Professor Emeritus Miha Tišler, University of Ljubljana,  
on the occasion of his 90<sup>th</sup> birthday.

## Abstract

A general four-step transformation of alkyl, cycloalkyl, aryl, and heteroaryl methyl ketones via 3-(dimethylamino)-1-substituted-prop-2-en-1-ones, followed by microwave [2+2] cycloaddition of dimethyl acetylenedicarboxylate, cyclization of (2*E*,3*E*)-2-[(dimethylamino)methylene]-3-(2-substituted)succinates with ammonia or hydroxylamine hydrochloride into 2-substituted-pyridine-4,5-dicarboxylates and their *N*-oxides and final cyclization with hydrazine hydrate into of 7-substituted-2,3-dihydropyrido[3,4-*d*]pyridazine-1,4-diones and 1,4-dioxo-7-substituted-1,2,3,4-tetrahydropyrido[4,3-*d*]pyridazine 6-oxides is shown.

**Keywords:** methyl ketones, 7-substituted-2,3-dihydropyrido[4,3-*d*]pyridazine-1,4-diones, 1,4-dioxo-7-substituted-1,2,3,4-tetrahydropyrido[4,3-*d*]pyridazine 6-oxides

## 1. Introduction

There are several methods for the preparation of 2,3-dihydro[4,3-*d*]pyridazine-1,4-dione derivatives. They have been prepared by treatment of diethyl or dimethyl pyridine-3,4-dicarboxylate with hydrate of hydrazine in refluxing ethanol, and 6-aryl- and 6-aryl-2-methyl derivatives with hydrate of hydrazine in refluxing ethanol, which allow the formation of the corresponding 7-substituted and 5,7-disubstituted-2,3-dihydropyridazine[3,4-*d*]pyridazine-1,4-diones.<sup>1-4</sup> Cyclization of ethyl 3-cyanoisonicotinate with hydrazine proceeds at room temperature to give 4-aminopyrido[3,4-*d*]pyridazine-1(2*H*)-one,<sup>5,6</sup> while pyridine-3,4-dicarbonitriles give the corresponding pyrido[3,4-*d*]pyridazine-1,4-diones.<sup>7</sup> Other methods include cycloamination of 4-carbofunctional-5-vinylpyridazines,<sup>8,9</sup> condensation of 4,5-dicarbofunctional pyridazines with amines,<sup>9,10</sup> condensation of 4-(iminomethyl)pyridazines with enolates,<sup>10</sup> intramolecular cyclization of pyridinecarbohydrazides,<sup>1,11</sup> intramolecular cyclization of

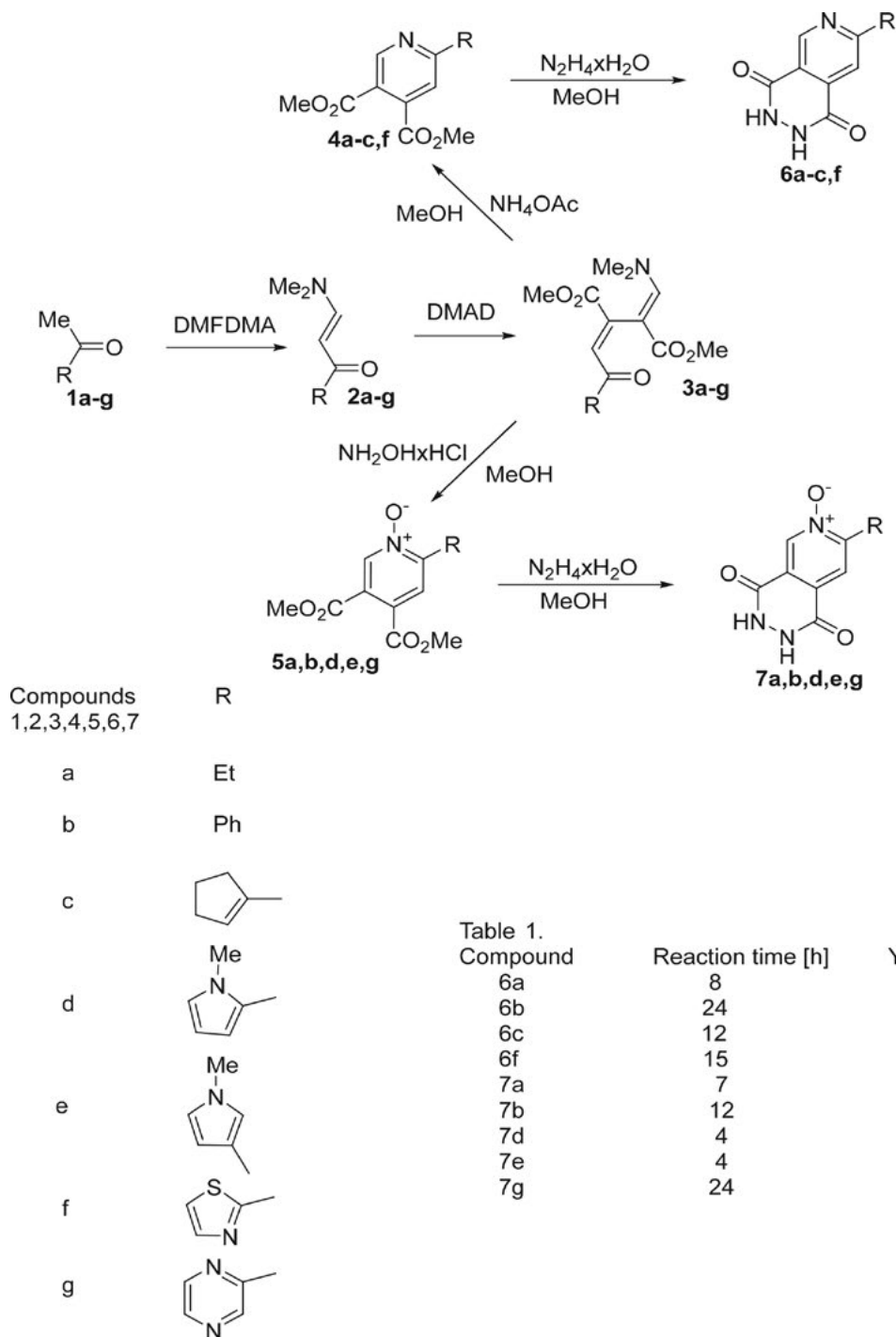
4-vinylpyridazine-5-carbonitriles,<sup>12,13</sup> by ring enlargement of furo[3,4-*c*]pyridine-1,3-diones,<sup>2,3,5,14,15</sup> 1*H*-pyrrolo[3,4-*c*]pyridine-1,3(2*H*)-diones with hydrazine,<sup>1,4,16,17</sup> by reaction of 5*H*-pyrano[3,4-*d*]pyridazines with amines,<sup>8</sup> intramolecular [4+2]cycloaddition of 1,2,4,5-tetrazines,<sup>18</sup> ring contraction of 2*H*-1,2,4-triazepines.<sup>14</sup> For a review see.<sup>19</sup>

Enaminones are well known starting compounds in the synthesis of heterocyclic systems. Their reactivity enables various transformations and functionalizations. Their synthetic value and broad applicability has also been demonstrated in the preparation of natural products and their analogues, such as aplysinopsins,<sup>20</sup> meridianines,<sup>21</sup> and dipodazines.<sup>22</sup> Besides the evident reactions with nucleophiles, they also exhibit reactivity with electrophiles as well, which only adds to their importance as building blocks in organic synthesis.<sup>23</sup> Reactions with electrophiles have been demonstrated in the synthesis of polysubstituted butadienes by microwave-assisted formal [2 + 2] cycloadditions of enaminones to electron-poor acetylenes.<sup>24</sup>



The functionalized buta-1,3-dienes as the basis of the synthetic route presented in this paper are prepared from simple and commercially available compounds such as alkyl, aryl, and heteroaryl methyl ketones. These are transformed by treatment with *N,N*-dimethylformamide dimethyl acetal (DMFDMA) or *tert*-butoxybis(dimethylamino)methane (Bredereck's reagent) into the corre-

sponding 3-(dimethylamino)-1-substituted-prop-2-enones, which are further transformed in a regioselective microwave assisted [2 + 2] cycloaddition with dimethyl acetylenedicarboxylate (DMAD)<sup>25</sup> to the before mentioned 1,3-butadienes. These highly functionalized buta-1,3-dienes proved to be useful and versatile reagents in the formation of highly substituted pyridine, pyridine *N*-oxides,



**Scheme 1.** Preparation of 7-substituted-2,3-dihydropyrido[3,4-d]pyridazine-1,4-diones **6a-c,f** and 1,4-dioxo-7-substituted-1,2,3,4-tetrahydropyrido[4,3-d]pyridazine 6-oxides **7a,b,d,e,g** from methyl ketones **1a-g**.

pyrrole, pyrido[3,4-*c*]pyridazine derivatives,<sup>25b</sup> 2-substituted pyridine-3,4-dicarboxylates and their *N*-oxides,<sup>10g</sup> and triazafulvalene derivatives.<sup>25d</sup>

Polysubstituted aminobutadienes, prepared by this procedure, are suitable for the preparation of polysubstituted pyridine derivatives. They also represent a group of isomeric intermediates in regard to the aminobutadienes prepared *via* the Michael addition in the Bohlmann-Rahtz synthesis of pyridine derivatives.<sup>26</sup> On this basis, a simple metal-free synthesis of 2-alkyl-, 2-cycloalkyl-, 2-aryl-, and 2-heteroaryl-substituted pyridine-3,4-dicarboxylates and their *N*-oxides has also been reported.<sup>25g</sup> Recently, we reported on a simple one-pot metal-free synthesis of 2,4,5-trisubstituted pyridine derivatives and their *N*-oxides by [2 + 2] cycloaddition of propyne iminium salts as electron-poor acetylenes to enamines as well.<sup>27</sup> We also reported a simple, metal-free synthesis of electron rich 2,4,6-trisubstituted pyridine derivatives<sup>28</sup> and the synthesis of polysubstituted benzene derivatives, where *N,N*-dimethylacetamide dimethyl acetal (DMADMA) served as the reagent and building block for generating aromatic final products.<sup>29,30</sup> Our existing knowledge of the enamines and 1,3-butadienes has been expanded to the synthesis of pyridines starting from Boc-protected amino acids, and the results of our research are presented in this paper.

## 2. Results and Discussion

In this communication we report a general and simple synthesis of 7-substituted-2,3-dihydropyrido[3,4-*d*]pyridazine-1,4-diones **6a-c,f** and 1,4-dioxo-7-substituted-1,2,3,4-tetrahydropyrido[4,3-*d*]pyridazine 6-oxides **7a, b,d,e,g** from methyl ketones **1a-g**. We have reported earlier a simple metal-free synthesis of dimethyl 2-substituted-pyridine-4,5-dicarboxylates **4a-c,f** and their *N*-oxides **5a,b,d,e,g** in the following manner: alkyl, aryl, and heteroaryl ketones **1a-g** have been converted by treatment with *N,N*-dimethylformamide dimethylacetal /DMFDMA or *t*-butoxybis(dimethylamino)methane (Bredereck's reagent) into the corresponding 3-(dimethylamino)-1-substituted-prop-2-en-ones **2a-g**, followed by microwave assisted [2 + 2] cycloaddition to dimethyl acetylenedicarboxylate to give dimethyl (2*E*,3*E*)-2-((dimethylamino)methylene)-3-(2-substituted)succinates **3a-g**. Compounds **3** gave by treatment with ammonium acetate or hydroxylamine hydrochloride the corresponding dimethyl 2-substituted-pyridine-4,5-dicarboxylates **4a-c,f** and dimethyl 2-substituted-4,5-bis(methoxycarbonyl)pyridine *N*-oxides **5a,b,d,e,g**.<sup>25c,f,g</sup> Treatment of compounds **4** and **5** with hydrazine hydrate afforded 7-substituted-2,3-dihydropyrido[3,4-*d*]pyridazine-1,4-diones **6a-c,f** and 1,4-dioxo-7-substituted-1,2,3,4-tetrahydropyrido[4,3-*d*]pyridazine 6-oxides **7a,b,d,e,g**, respectively. (Scheme 1, Table 1).

## 3. Experimental

### 3.1. General

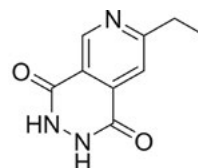
Melting points were determined on a Stanford Research Systems MPA100 OptiMelt automated melting point system. The NMR spectra were obtained on a Bruker Avance DPX 300 at 300 MHz for <sup>1</sup>H and 75.5 MHz for <sup>13</sup>C and on a Bruker Avance III UltraShield 500 plus at 500 MHz for <sup>1</sup>H and 126 MHz for <sup>13</sup>C, using acetone-*d*<sub>6</sub>, acetonitrile-*d*<sub>3</sub>, CDCl<sub>3</sub>, and DMSO-*d*<sub>6</sub> with Me<sub>4</sub>Si as the internal standard, as solvents. Mass spectra were recorded on a Agilent 6224 Accurate Mass TOF LC/MS spectrometer, IR spectra on a Perkin Elmer Spectrum BX FTIR spectrophotometer. Column chromatography (CC) was performed on silica gel (Fluka, Silica gel 60, particle size 35–70 μm).

The preparation of 2-substituted-pyridine-4,5-dicarboxylates **4a-c,f** and dimethyl 2-substituted-4,5-bis(methoxycarbonyl)pyridine *N*-oxides **5a,b,d,e,g** from alkyl, cycloalkyl, aryl and heteroaryl methyl ketones has been previously reported in our laboratory.<sup>25e,f,g</sup>

### 3.2. General procedure for the preparation of 7-substituted-2,3-dihydropyrido[3,4-*d*]pyridazine-1,4-diones and 1,4-dioxo-7-substituted-1,2,3,4-tetrahydropyrido[4,3-*d*]pyridazine 6-oxides

To a solution of 0.5 mmol of the starting compound (dimethyl 6-substituted pyridine-3,4-dicarboxylate or 2-substituted-4,5-bis(methoxycarbonyl)pyridine-*N*-oxide) in 2–3 mL of methanol, 1 mmol (2 equivalents) of hydrazine monohydrate was added, followed by the addition of 2–3 drops of concentrated hydrochloric acid. The reaction mixture was stirred vigorously and heated to reflux temperature for 4–24 h.

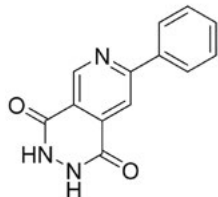
#### 3.2.1. 7-Ethyl-2,3-dihydropyrido[4,3-*d*]pyridazine-1,4-dione (**6a**)



The product was prepared from dimethyl 6-ethylpyridine-3,4-dicarboxylate (**4a**, 112 mg, 0.5 mmol), 90 °C, 8 h. The yellow product was collected by vacuum filtration and washed with Et<sub>2</sub>O. Yield: 57% (55 mg), yellow solid; mp = higher than 350 °C. <sup>1</sup>H NMR (500 MHz, DMSO-*d*<sub>6</sub>): δ 1.30 (3H, t, *J* = 7.5 Hz, CH<sub>3</sub>); 2.97 (2H, q, *J* = 7.6 Hz, CH<sub>2</sub>); 7.74 (1H, s, 8-CH); 9.25 (1H, s, 5-CH). <sup>13</sup>C NMR (125 MHz, DMSO-*d*<sub>6</sub>): δ 13.54, 30.77, 115.03, 148.30, 148.47, 164.77, 166.61, 166.74, 168.39. EI-HRMS: *m/z* = 192.0765 (MH<sup>+</sup>) found; C<sub>9</sub>H<sub>10</sub>N<sub>3</sub>O<sub>2</sub> calculated: *m/z*

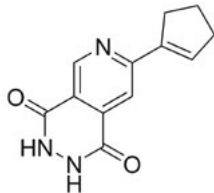
= 192.0768 (MH<sup>+</sup>); IR (ATR):  $\nu$  3426, 3302, 3250, 2960, 1664, 1612, 1575, 1476, 1364, 1207, 1077, 899 cm<sup>-1</sup>.

### 3. 2. 2. 7-Phenyl-2,3-dihydropyrido[4,3-d]pyridazine-1,4-dione (6b)



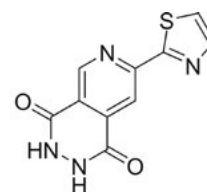
The product was prepared from dimethyl 6-phenylpyridine-3,4-dicarboxylate (**4b**, 261 mg, 096 mmol), 90 °C, 12 h. The yellow product was collected by vacuum filtration and washed by Et<sub>2</sub>O. Yield: 74% (170 mg), yellow solid; mp = 335–339 °C. <sup>1</sup>H NMR (500 MHz, DMSO-*d*<sub>6</sub>):  $\delta$  7.48–7.57 (3H, m, Ph); 8.19–8.23 (2H, m, Ph); 8.35 (1H, s, 8-CH); 9.36 (1H, s, 5-CH). <sup>13</sup>C NMR (125 MHz, DMSO-*d*<sub>6</sub>):  $\delta$  113.8, 121.9, 126.9, 128.9, 129.6, 135.4, 137.8, 149.1, 155.7, 156.2, 157.5. EI-HRMS:  $m/z$  = 240.0767 (MH<sup>+</sup>) found; C<sub>13</sub>H<sub>10</sub>N<sub>3</sub>O<sub>2</sub> calculated:  $m/z$  = 240.0768 (MH<sup>+</sup>); IR (ATR):  $\nu$  3289, 3178, 3034, 2978, 2920, 2798, 1898, 1648, 1559, 1454, 1112, 852 cm<sup>-1</sup>. LC-MS; 9.1 min;  $m/z$ : 240.1 (MH<sup>+</sup>).

### 3. 2. 3. 7-Cyclopentenyl-2,3-dihydropyrido[4,3-d]pyridazine-1,4-dione (6c)



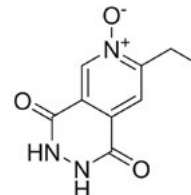
The product was prepared from dimethyl 6-cyclopentenylpyridine-3,4-dicarboxylate (**4c**, 150 mg, 0.56 mmol), 90 °C, 24 h. The solid product that was formed during the reaction was a mixture of the starting dicarboxylate and the product. The solid was collected by vacuum filtration, suspended in chloroform. The insoluble product was once more collected by vacuum filtration. Yield: 20% (26 mg), brown solid; mp = higher than 330 °C. <sup>1</sup>H NMR (500 MHz, DMSO-*d*<sub>6</sub>):  $\delta$  2.03 (2H, p,  $J$  = 7.5 Hz, 4-CH<sub>2</sub>); 2.54–2.60 (2H, m, 3-CH<sub>2</sub>); 2.76–2.82 (2H, m, 5-CH<sub>2</sub>); 6.87 (1H, s, 2-CH); 7.81 (1H, s, 8-CH); 9.23 (1H, s, CH). <sup>13</sup>C NMR (125 MHz, DMSO-*d*<sub>6</sub>):  $\delta$  22.8, 32.0, 33.2, 113.4, 121.0, 133.5, 134.5, 142.6, 148.6, 155.2, 155.8, 156.0. EI-HRMS:  $m/z$  = 230.0915 (MH<sup>+</sup>) found; C<sub>12</sub>H<sub>12</sub>N<sub>3</sub>O<sub>2</sub> calculated:  $m/z$  = 230.0924 (MH<sup>+</sup>). IR (ATR):  $\nu$  3163, 3016, 2947, 2892, 2839, 1649, 1598, 1553, 1434, 1368, 1325, 1291, 1232, 1101, 1036, 823 cm<sup>-1</sup>.

### 3. 2. 4. 7-(Thiazol-2-yl)-2,3-dihydropyrido[4,3-d]pyridazine-1,4-dione (6f)



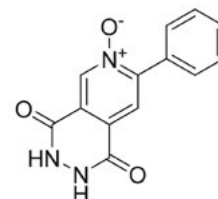
The product was prepared from dimethyl 6-(thiazol-2-yl)pyridine-3,4-dicarboxylate (**4f**, 89 mg, 0.32 mmol), 90 °C, 15 h. The yellow product was collected by vacuum filtration and washed with Et<sub>2</sub>O. Yield: 44% (35 mg), yellow solid; mp = the product decomposes at 250 °C. <sup>1</sup>H NMR (500 MHz, DMSO-*d*<sub>6</sub>):  $\delta$  7.97 (1H, d,  $J$  = 3.2 Hz, CH); 8.09 (1H, d,  $J$  = 3.2 Hz, CH); 8.54 (1H, d,  $J$  = 1.0 Hz, 8-CH); 9.29 (1H, d,  $J$  = 1.0 Hz, 5-CH). <sup>13</sup>C NMR (125 MHz, DMSO-*d*<sub>6</sub>):  $\delta$  113.3, 117.2, 123.6, 123.8, 144.9, 149.5, 151.8, 155.9, 165.8, 167.6. EI-HRMS:  $m/z$  = 245.015 (MH<sup>+</sup>) found; C<sub>10</sub>H<sub>5</sub>N<sub>4</sub>O<sub>2</sub>S calculated:  $m/z$  = 245.0139 (MH<sup>+</sup>); IR (ATR):  $\nu$  3420, 3260, 1741, 1721, 1661, 1654, 1602, 1569, 1465, 1438, 1298, 1242, 1134, 1085, 958 cm<sup>-1</sup>. LC-MS: 7.1 min;  $m/z$ : 247.3 (MH<sup>+</sup>).

### 3. 2. 5. 7-Ethyl-1,4-dioxo-1,2,3,4-tetrahydropyrido[4,3-d]pyridazine 6-oxide (7a)



The product was prepared from 2-ethyl-4,5-bis(methoxycarbonyl)pyridine 1-oxide (**5a**, 156 mg, 0.65 mmol), 90 °C, 7 h. The yellow solid was collected by vacuum filtration and washed with Et<sub>2</sub>O. Yield: 23% (31 mg), yellow solid; mp = 270–276 °C. <sup>1</sup>H NMR (500 MHz, DMSO-*d*<sub>6</sub>):  $\delta$  1.26 (3H, t,  $J$  = 7.4 Hz, CH<sub>3</sub>); 2.89 (2H, q,  $J$  = 7.4 Hz, CH<sub>2</sub>); 7.89 (1H, s, 8-CH); 8.61 (1H, s, 5-CH). <sup>13</sup>C NMR (125 MHz, DMSO-*d*<sub>6</sub>):  $\delta$  10.5, 23.3, 120.2, 123.5, 125.0, 134.8, 153.7, 154.3, 156.0. EI-HRMS:  $m/z$  = 208.0712 (MH<sup>+</sup>) found; C<sub>9</sub>H<sub>10</sub>N<sub>3</sub>O<sub>3</sub> calculated:  $m/z$  = 208.0717 (MH<sup>+</sup>). IR (ATR):  $\nu$  3203, 3047, 2974, 2810, 1626, 1549, 1454, 1432, 1366, 1317, 1268, 1043, 814 cm<sup>-1</sup>.

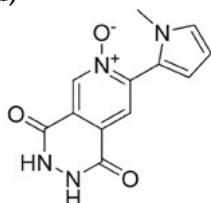
### 3. 2. 6. 1,4-Dioxo-7-phenyl-1,2,3,4-tetrahydropyrido[4,3-d]pyridazine 6-oxide (7b)



The product was prepared from 4,5-bis(methoxycarbonyl)-2-phenylpyridine 1-oxide (**5b**, 241 mg, 0.84 mmol), 90 °C, 12 h. The yellow solid was collected by vacuum filtration and washed with Et<sub>2</sub>O. Yield: 90% (190 mg), yellow

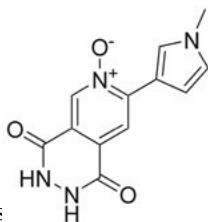
solid; mp = 275–285 °C.  $^1\text{H}$  NMR (500 MHz,  $\text{DMSO-}d_6$ ):  $\delta$  7.49–7.53 (3H, m, Ph); 7.82–7.85 (2H, m, Ph); 7.95 (1H, s, 8-CH); 8.65 (1H, s, 5-CH).  $^{13}\text{C}$  NMR (125 MHz,  $\text{DMSO-}d_6$ ):  $\delta$  123.1, 124.3, 126.1, 127.9, 129.3, 129.6, 131.9, 135.9, 150.4, 153.9, 154.7. EI-HRMS:  $m/z$  = 256.0716 ( $\text{MH}^+$ ) found;  $\text{C}_{13}\text{H}_{10}\text{N}_3\text{O}_3$  calculated:  $m/z$  = 256.0717 ( $\text{MH}^+$ ). IR (ATR):  $\nu$  3338, 3066, 2861, 1807, 1657, 155, 1466, 1448, 1269, 1096, 813  $\text{cm}^{-1}$ . LC-MS: 7.4 min;  $m/z$ : 256.1 ( $\text{MH}^+$ ).

### 3. 2. 7. 7-(1-Methyl-1H-pyrrol-2-yl)-1,4-dioxo-1,2,3,4-tetrahydropyrido[4,3-d]pyridazine 6-oxide (7d)



The product was prepared from 4,5-bis(methoxycarbonyl)-2-(1-methyl-1H-pyrrol-2-yl)pyridine 1-oxide (**5d**, 173 mg, 0.6 mmol), 90 °C, 4 h. The yellow product was collected by vacuum filtration and washed with  $\text{Et}_2\text{O}$ . Yield: 75% (115 mg), yellow solid; mp = 222–238 °C.  $^1\text{H}$  NMR (500 MHz,  $\text{DMSO-}d_6$ ):  $\delta$  3.58 (3H, s,  $\text{CH}_3$ ); 6.12 (1H, dd,  $J_1 = 3.7$  Hz,  $J_2 = 2.6$  Hz, 3'-CH); 6.40 (1H, dd,  $J_1 = 3.7$  Hz,  $J_2 = 1.8$  Hz, 5'-CH); 7.00 (1H, deg. dd,  $J = 2.2$  Hz, 4'-CH); 7.85 (1H, s, 8-CH); 8.64 (1H, s, 5-CH).  $^{13}\text{C}$  NMR (125 MHz,  $\text{DMSO-}d_6$ ):  $\delta$  40.5, 112.9, 118.3, 129.6, 129.8, 130.1, 131.0, 131.7, 141.1, 149.9, 159.9, 160.6. EI-HRMS:  $m/z$  = 259.0822 ( $\text{MH}^+$ ) found;  $\text{C}_{12}\text{H}_{11}\text{N}_4\text{O}_3$  calculated:  $m/z$  = 259.0826 ( $\text{MH}^+$ ); IR (ATR):  $\nu$  3424, 3301, 3078, 2953, 2929, 1664, 1651, 1558, 1485, 1471, 1308, 1255, 1103, 1072, 822  $\text{cm}^{-1}$ . LC-MS: 7.3 min;  $m/z$ : 259.2 ( $\text{MH}^+$ ).

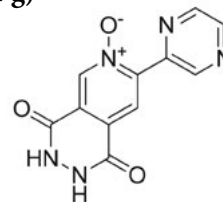
### 3. 2. 8. 7-(1-Methyl-1H-pyrrol-3-yl)-1,4-dioxo-1,2,3,4-tetrahydropyrido[4,3-d]pyridazine 6-oxide (7e)



The product was prepared from 4,5-bis(methoxycarbonyl)-2-(1-methyl-1H-pyrrol-3-yl)pyridine 1-oxide (**5e**, 340 mg, 1.17 mmol), 90 °C, 4 h. The yellow product was collected by vacuum filtration and washed with  $\text{Et}_2\text{O}$ . Yield: 89% (269 mg), yellow solid; mp = decomposes at 292 °C.  $^1\text{H}$  NMR (500 MHz,  $\text{DMSO-}d_6$ ):  $\delta$  3.72 (3H, s,  $\text{CH}_3$ ); 6.84 (1H, deg. dd,  $J = 1.2$ , 4'-CH); 6.91 (1H, deg. dd,  $J = 2.6$  Hz, 5'-CH); 8.18 (1H, s, 8-CH); 8.32 (1H, deg. dd,  $J = 2.0$  Hz, 2'-CH); 8.62 (1H, s, 5-CH).  $^{13}\text{C}$  NMR (125 MHz,  $\text{DMSO-}d_6$ ):  $\delta$  36.1, 108.0, 113.8, 117.5, 122.0, 123.3, 123.9, 126.8, 136.2, 146.8, 153.9, 154.7. EI-HRMS:  $m/z$  = 259.0823

( $\text{MH}^+$ ) found;  $\text{C}_{12}\text{H}_{11}\text{N}_4\text{O}_3$  calculated:  $m/z$  = 259.0826 ( $\text{MH}^+$ ); IR (ATR):  $\nu$  3416, 3295, 3199, 2992, 1653, 1614, 1571, 1535, 1487, 1442, 1366, 1250, 1171, 1091, 831  $\text{cm}^{-1}$ . LC-MS: 6.6 min;  $m/z$ : 259.2 ( $\text{MH}^+$ ).

### 3. 2. 9. 1,4-Dioxo-7-(pyrazin-2-yl)-1,2,3,4-tetrahydropyrido[4,3-d]pyridazine 6-oxide (7g)



The product was prepared from 4,5-bis(methoxycarbonyl)-2-(pyrazin-2-yl)pyridine 1-oxide (**5g**, 144 mg, 0.5 mmol), 90 °C, 24 h. The yellow product was collected by vacuum filtration and washed with  $\text{Et}_2\text{O}$ . Yield: 95% (125 mg), yellow solid; mp = higher than 350 °C.  $^1\text{H}$  NMR (500 MHz,  $\text{DMSO-}d_6$ ):  $\delta$  8.56 (1H, s, CH); 8.72 (s, 1H, CH); 8.78 (1H, d,  $J = 2.5$  Hz, CH); 8.87–8.91 (1H, m, CH); 9.87 (1H, d,  $J = 1.5$  Hz, CH).  $^{13}\text{C}$  NMR (125 MHz,  $\text{DMSO-}d_6$ ):  $\delta$  124.1, 136.5, 144.6, 144.9, 145.26, 145.29, 145.6, 146.9, 157.0, 158.1. EI-HRMS:  $m/z$  = 258.0624 ( $\text{MH}^+$ ) found;  $\text{C}_{11}\text{H}_8\text{N}_5\text{O}_3$  calculated:  $m/z$  = 258.0622 ( $\text{MH}^+$ ); IR (ATR):  $\nu$  3447, 3033, 2981, 1667, 1635, 1563, 1498, 1404, 1273, 1242, 1119, 827  $\text{cm}^{-1}$ . LC-MS: 5.9 min;  $m/z$ : 255.7 [(M-2H)].

## 4. Conclusion

A general four-step metal-free synthesis of a series of 7-substituted-2,3-dihydropyrido[3,4-d]pyridazine-1,4-diones and 1,4-dioxo-7-substituted-1,2,3,4-tetrahydropyrido[4,3-d]pyridazine 6-oxides was designed starting from alkyl, cycloalkyl, aryl or heteroaryl methyl ketones in good to excellent yields.

## 5. Acknowledgement

Financial support from the Slovenian Research Agency through grants P0-0502-0103, P1-0179 and J1-6689-0103-04 are gratefully acknowledged. We also thank the Krka d.d. (Novo mesto, Slovenia) for financial support.

## 6. Reference

1. Y. Oka, K. Omura, A. Miyake, K. Itoh, M. Tomimoto, N. Tada, S. Yurugi, *Chem. Pharm. Bull.* **1975**, *23*, 2239–2250.
2. R. G. Jones, *J. Am. Chem. Soc.* **1956**, *78*, 159–163.
3. D. B. Paul, *Aust. J. Chem.* **1984**, *37*, 87–93.
4. T. J. Van Bergen, R. M. Kellogg, *J. Amer. Chem. Soc.* **1972**, *94*, 8451–8471.

5. I. Matsuura, K. Okui, *Chem. Pharm. Bull.* **1969**, *17*, 2266–2272.
6. K. Yoshida, H. Otomasu, *Yakugaku Zasshi* **1976**, *96*, 33–36; *Chem. Abstr.* **1976**, *84*, 121754.
7. F. Ishikawa, S. Miyazaki, K. Ueno, JP 46029876 (1971); *Chem. Abst.* **1971**, *75*, 140875.
8. P. Y. Boamah, N. Haider, G. Heinisch, J. Moshuber, *J. Heterocycl. Chem.* **1988**, *25*, 879–883.
9. P. Y. Boamah, N. Haider, G. Heinisch, *J. Heterocycl. Chem.* **1989**, *26*, 933–939.
10. G. Heinisch, T. Langer, J. Tonnel, *J. Heterocycl. Chem.* **1996**, *33*, 1731–1735.
11. J. Barluenga, M. J. Iglesias, V. Gotor, *Synthesis* **1987**, 662–664.
12. H. Al-Awadhi, F. Al-Omran, M. H. Elnagdi, L. Infantes, C. Foces-Foces, N. Jagorevic, J. Elguero, *Tetrahedron* **1995**, *51*, 12745–12762.
13. F. M. Manhi, S. E. Zayed, F. A. Ali, M. H. Elnagdi, *Collect. Czech. Chem. Commun.* **1992**, *57*, 1770–1774.
14. A. Hasnaoui, M. El Messaoudi, J.-P. Lavergne, *J. Heterocycl. Chem.* **1985**, *22*, 25–27.
15. K. J. Gould, N. P. Hacker, J. F. W. McOmie, D. H. Perry, *J. Chem. Soc., Perkin Trans.1* **1980**, 1834–1840.
16. J. Z. Brzezinski, H. B. Bzowski, J. Epszajn, *Tetrahedron* **1996**, *52*, 3261–3272.
17. H. Śladowska, J. Potoczek, M. Sokowska, G. Rajtar, M. Sieklucka-Dziuba, T. Kocki, Z. Kleinrok, *Farmaco* **1998**, *53*, 468–474; *Chem. Abstr.* **1999**, *130*, 110222.
18. N. Heider, K. Mereiter, R. Wanko, *Heterocycles* **1994**, *38*, 1845–1858.
19. M. Sako, Product Class18: Product Subclass 5: Pyridopyridazines. In: Houben-Weyl, Science of Synthesis, Georg Thime Verlag, Stuttgart, New York 2006, vol 16, pp. 1137–1153.
20. (a) Selič, L.; Jakše, R.; Lampič, K.; Golič, L.; Golič-Grdadolnik, S.; Stanovnik, B. *Helv. Chim. Acta* **2000**, *83*, 2802–2811; (b) Selič, L.; Stanovnik, B. *Tetrahedron* **2001**, *57*, 3159–3164.
21. Jakše, R.; Svete, J.; Stanovnik, B.; Golobič, A. *Tetrahedron* **2004**, *60*, 4601–4608; (b) Časar, Z.; Bevk, D.; Svete, J.; Stanovnik, B. *Tetrahedron* **2005**, *61*, 7508–7519.
22. (a) Wagger, J.; Bevk, D.; Meden, A.; Svete, J.; Stanovnik, B. *Helv. Chim. Acta* **2006**, *89*, 240–248; (b) Wagger, J.; Golič-Grdadolnik, S.; Grošelj, U.; Meden, A.; Svete, J.; Stanovnik, B. *Tetrahedron: Asymmetry* **2007**, *18*, 464–475; (c) Wagger, J.; Grošelj, U.; Meden, A.; Svete, J.; Stanovnik, B. *Tetrahedron* **2008**, *64*, 2801–2815.
23. (a) Stanovnik, B. *J. Heterocycl. Chem.* **1999**, *36*, 1581–1593; (b) Stanovnik, B.; Svete, J. *Synlett* **2000** 1077–1091; (c) Stanovnik, B.; Svete, J. *Targets in Heterocyclic Systems, Synthesis, Reactions and Properties*, (Eds. O. A. Attanasi, D. Spinelli), Italian Society of Chemistry, Rome **2000**, Vol. 4, p. 105–137; (d) Stanovnik, B.; Svete, J. *Chem. Rev.* **2004**, *104*, 2433–2480.
24. (a) Bezenšek, J.; Koleša, T.; Grošelj, U.; Meden, A.; Stare, K.; Svete, J.; Stanovnik, B. *Curr. Org. Chem.* **2011**, *15*, 2530–2539; (b) Bezenšek, J.; Koleša, T.; Grošelj, U.; Wagger, J.; Stare, K.; Meden, A.; Svete, J.; Stanovnik, B. *Tetrahedron Lett.* **2010**, *51*, 3392–3397.
25. (a) Uršič, U.; Grošelj, U.; Meden, A.; Svete, J.; Stanovnik, B. *Tetrahedron Lett.* **2008**, *49*, 3775–3778; (b) Uršič, U.; Svete, J.; Stanovnik, B. *Tetrahedron* **2008**, *64*, 9937–9946; (c) Uršič, U.; Grošelj, U.; Meden, A.; Svete, J.; Stanovnik, B. *Helv. Chim. Acta* **2009**, *92*, 481–490; (d) Uršič, U.; Svete, J.; Stanovnik, B. *Tetrahedron* **2010**, *66*, 4346–4356; (e) Bezenšek, J.; Koleša, T.; Grošelj, U.; Meden, A.; Stare, K.; Svete, J.; Stanovnik, B. *Curr. Org. Chem.* **2011**, *15*, 2530–2539; (f) Bezenšek, J.; Koleša, T.; Grošelj, U.; Wagger, J.; Stare, K.; Meden, A.; Svete, J.; Stanovnik, B.; *Tetrahedron Lett.* **2010**, *51*, 3392–3397; (g) Bezenšek, J.; Prek, B.; Grošelj, U.; Kasunič, M.; Svete, J.; Stanovnik, B. *Tetrahedron* **2012**, *68*, 4719–4731.
26. (a) Bohlmann, F.; Rahtz, D. *Chem. Ber.* **1957**, *90*, 2265–2272; (b) Bagley, M. C.; Dale, J. W.; Bower, J. *Synlett* **2001**, 1149–1151.
27. Bezenšek, J.; Prek, B.; Grošelj, U.; Golobič, A.; Stare, K.; Svete, J.; Kantelehner, W.; Maas, G.; Stanovnik, B. *Z. Naturforsch.* **2014**, *69b*, 554–566.
28. Prek, B.; Grošelj, U.; Kasunič, M.; Zupančič, S.; Svete, J.; Stanovnik, B. *Aust. J. Chem.* **2015**, *68*, 184–195.
29. Prek, B.; Bezenšek, J.; Kasunič, M.; Grošelj, U.; Svete, J.; Stanovnik, B. *Tetrahedron* **2014**, *70*, 2359–2369.  
DOI:10.1016/j.tet.2014.02.039
30. For a review see: Stanovnik, B. *Org. Prep. Proc. Int.* **2014**, *46*, 24–65.

## Povzetek

V tem članku je opisana štiristopenjska pretvorba alkil, cikloalkil, aril in heteroaril metil ketonov, ki jih preko 3-(dimetilamino)-1-substituiranih-prop-2-en-1-onov z [2+2] cikloadicijo na dimetil acetilendikarboksilat pretvorimo v (2*E*,3*E*)-2-[(dimetilamino)metilen]-3-(2-substituirane)sukcinat in naprej z amoniakom ali hidroksilaminom v 2-substituirane piridin-4,5-dikarboksilate in njihove *N*-oksidi. Iz teh nastanejo pri cilizaciji s hidrazinovim hidratom 7-substituirani 2,3-dihidropirido[3,4-*d*]piridazin-1,4-dioni in 1,4-diokso-7-substituirani 1,2,3,4-tetrahidropirido[4,3-*d*]piridazin 6-oksidi.

Scientific paper

# Discrimination Between *Synechocystis* Members (Cyanobacteria) Based on Heterogeneity of Their 16S rRNA and ITS Regions

Mojca Juteršek, Marina Klemenčič and Marko Dolinar\*

Department of Chemistry and Biochemistry, Faculty of Chemistry and Chemical Technology, University of Ljubljana, Večna pot 113, SI-1000 Ljubljana, Slovenia

\* Corresponding author: E-mail: marko.dolinar@fkkt.uni-lj.si

Received: 06-02-2017

## Abstract

Cyanobacteria are an important group of microorganisms displaying a range of morphologies that enable phenotypic differentiation between the major lineages of cyanobacteria, often to the genus level, but rarely to species or strain level. We focused on the unicellular genus *Synechocystis* that includes the model cyanobacterial strain PCC 6803. For 11 *Synechocystis* members obtained from cell culture collections, we sequenced the variable part of the 16S rRNA-encoding region and the 16S - 23S internally transcribed spacer (ITS), both standardly used in taxonomy. In combination with microscopic examination we observed that 2 out of 11 strains from cell culture collections were clearly different from typical *Synechocystis* members. For the rest of the samples, we demonstrated that both sequenced genomic regions are useful for discrimination between investigated species and that the ITS region alone allows for a reliable differentiation between *Synechocystis* strains.

**Keywords:** *Synechocystis*; DNA barcoding; Cyanobacteria; rRNA; ITS region

## 1. Introduction

Cyanobacteria are Gram-negative prokaryotes characterized by their ability to execute oxygenic photosynthesis. They inhabit various environments, from oceans to freshwaters, but also including extreme locations such as deserts, hot springs and hypersaline habitats.<sup>1</sup> As a consequence, there is a considerable morphological diversity among these organisms, which was traditionally the key for taxonomic classification of cyanobacteria. However, improper growth conditions of wild strains when transferred to laboratory environment may result in the loss of morphological characteristics<sup>2,3</sup> which consequently leads to misidentification and false classification.

To overcome variable morphological criteria, DNA-based methods are becoming widely applied in the identification and cataloguing of cyanobacteria, either as the sole method of identification or in combination with phenotypic and ecological characterization.<sup>4</sup> Adherent to classification of other bacteria, DNA-based taxonomy in cyanobacteria is mostly based on similarity in their 16S rRNA sequences, with the assumption that individuals of the same species share greater sequence similarity than in-

dividuals of different species.<sup>5</sup> Although overall evolution of the 16S rRNA gene is rather slow, there are regions that are more variable, which allows for studying evolutionary relationships both between distant and closely related groups of organisms.<sup>6,7</sup>

Phylogenetic analysis based on 16S rRNA relies on the presumption that its gene only occurs in one copy per genome, or in case of multiple rRNA genes, that they are identical in sequence. Cyanobacteria commonly contain multiple ribosomal RNA operons and point-mutations can often be found in paralogous 16S rRNA gene copies. But since sequence heterogeneity is relatively low (mean = 0.2%), it is believed to have no significant impact on determining phylogenetic relationships.<sup>8</sup> Although the use of 16S rRNA gene sequences remains a common tool for identification of organisms to the species level, doubts were expressed whether there is sufficient variability in 16S rRNA gene sequences to allow for discrimination at the subgeneric level.<sup>9</sup>

Owing to increasing number of sequenced cyanobacterial genomes, which has already exceeded the number of 150,<sup>10</sup> the current phylogenetic studies that are in part based on 16S rRNA, also include a selection of more

variable sequences. In addition to sequences of protein-coding genes, e.g. *psbA*, *rbcl*, *rnpB*, *rpoC*, *gyrB*,<sup>11,12</sup> research has increasingly focused on the internal transcribed spacer of ribosomal RNA genes (16S–23S rRNA-ITS).<sup>13</sup> With its variable length and number,<sup>14</sup> rRNA ITS region is becoming a popular tool in identification and classification of cyanobacteria.<sup>15</sup> Three types of ITS regions were identified up to now in cyanobacteria, differing in the presence or absence of specific tRNA genes (reviewed by Sarma,<sup>16</sup>): the first type contains both tRNA<sup>Ile</sup> and tRNA<sup>Ala</sup> coding sequences (as found in *Anabaena* sp., *Nostoc* sp. or *Synechococcus* sp. PCC 6301), the second type contains only tRNA<sup>Ile</sup> (found e.g. in 47 strains of *Microcystis*, in *Synechocystis* sp. PCC 6803 and *Spirulina* sp. PCC 6313), while the third type has no identifiable tRNA-encoding sequence (as found in *Nodularia* sp. BCNO D9427). Restriction endonuclease digestion of amplified rRNA-ITS genomic segments has been used to delineate closely related cyanobacterial strains,<sup>17</sup> whereas sequencing has been shown to be successful in analysis of subgeneric relationships of *Microcystis*,<sup>18,19</sup> *Trichodesmium*,<sup>20</sup> *Synechococcus*,<sup>15,21</sup> *Prochlorococcus*,<sup>22</sup> *Aphanizomenon* and *Anabaena*<sup>3</sup> as well as various picocyanobacteria.<sup>23</sup>

Surprisingly, no in-depth taxonomic classification has been performed for the genus *Synechocystis*.<sup>24</sup> Although more than 20 species have been described and many more strains were deposited in culture collections, limited sequence data as well as lack of details at the sub-cellular level hinder adequate identification and classification. Several planktic species including *S. salina*, *S. limnetica*, *S. aquatilis*, and a few picoplanktic types are hardly morphologically distinguishable,<sup>25</sup> which calls for a molecular biological approach.

In our study, 11 different *Synechocystis* representatives were analysed for their 16S rRNA and ITS sequence properties. Up to now, 16S rRNA data were available only for a few strains, most of them not defined at the species level. ITS data were almost completely missing from databases. With our work we thus open ways for eventual ITS-based molecular discrimination between species and strains of the *Synechocystis* genus and present data that would be of equal interest for taxonomists, ecologists and evolution biologists investigating unicellular cyanobacteria.

## 2. Experimental

### 2.1. Cyanobacterial Strains

Cyanobacterial strains used in our study are listed in Table 1. They were all obtained from established culture collections specialized in maintaining microalgae, except for *S. nigrescens* that was obtained from a general supplier of teaching consumables. Strain collections and their acronyms that appear in strain codes were: Culture Collection

of Algae at Goettingen University (SAG), The Culture Collection of Algae and Protozoa (Scotland) (CCAP), Culture Collection of Autotrophic Organisms (Institute of Botany of the Academy of Sciences, Czech Republic) (CCALA), Pasteur Culture Collection of Cyanobacteria (PCC) and Carolina Biological Supply Company (Carolina). Most of the strains were catalogued with species names, except for three that were labelled with the genus and strain name/code. Although most of the strains were listed as non-axenic, microscopic inspection after several weeks of growth in our laboratory showed no or only minor contamination with other microorganisms.

All strains were cultured in liquid BG-11 medium (Sigma-Aldrich) with pH adjusted to 7.5 with 1 M HEPES, pH 8.6 (Calbiochem OmniPur grade) under constant cool white light (intensity of 25  $\mu\text{mol}/\text{m}^2\text{s}$   $\pm$  15%) and at room temperature (22 – 25°C). *Synechocystis nigrescens* was cultured in buffered BG-11 medium as above, with added NaCl to 500 mM final concentration.

**Table 1.** List of cyanobacterial strains used for morphological and sequence analyses

Species	Strain
<i>Synechocystis aquatilis</i>	SAG 90.79
<i>Synechocystis bourrellyi</i>	CCAP 1480/1
<i>Synechocystis fuscopigmentosa</i>	CCALA 810
<i>Synechocystis limnetica</i>	CCAP 1480/5
<i>Synechocystis minuscula</i>	SAG 258.80
<i>Synechocystis nigrescens</i>	Carolina
<i>Synechocystis pevalekii</i>	SAG 91.79
<i>Synechocystis salina</i>	CCALA 192
<i>Synechocystis</i> sp.	CCAP 1480/4
<i>Synechocystis</i> sp.	PCC 6714
<i>Synechocystis</i> sp.	PCC 6803

### 2.2. Polymerase Chain Reaction

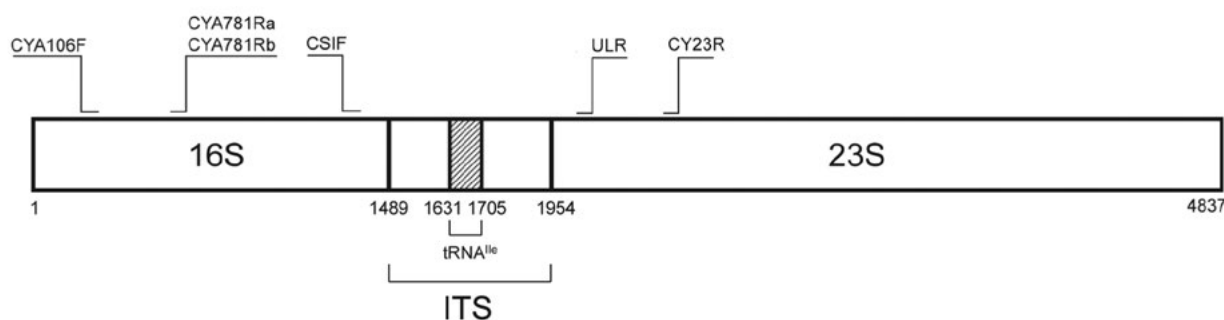
Cells from mid- to late exponential phase culture (1 ml) were pelleted by centrifugation. Supernatant was discarded and cells were resuspended in 40  $\mu\text{l}$  of sterile dH<sub>2</sub>O and heated for 10 min at 95°C. The lysed cells were used directly for PCR. Reactions were carried out in 20  $\mu\text{l}$  mixtures containing 1  $\mu\text{l}$  of boiled cell suspension, 1  $\times$  *Taq*-buffer with (NH<sub>4</sub>)<sub>2</sub>SO<sub>4</sub>, 2.5 mM MgCl<sub>2</sub>, 100  $\mu\text{M}$  of each dNTP, 0.5  $\mu\text{M}$  of each primer (Table 2) and 0.5 U of *Taq*-polymerase (Thermo Scientific), which was added to reaction mixtures after the initial denaturation. PCR reactions were carried out using the following programme: initial denaturation at 95 °C for 5 min, 30 cycles of 95 °C for 30 s, annealing at 55 °C (for ITS amplification) or 60 °C (for 16S rRNA gene amplification) for 30 s and elongation at 72 °C for 1 min (16S) or 2.5 min (ITS) with a final extension step at 72 °C for 7 min. PCR products were resolved on 1.2% or 1.5% agarose gels and visualized using ethidium bromide.

**Table 2.** List of specific primers used for amplification of 16S rDNA and ITS

Primer	Region	Primer sequence (5'-3')	Reference
CSIF	ITS	GTC ACG CCC GAA GTC GTT AC	18
ULR	ITS	CCT CTG TGT GCC TAG GTA TC	18
CY23R	ITS	CTC ATT CTT CAA CAG GCA C	This study
CYA106F	16S	CGG ACG GGT GAG TAA CGG TGA	2
CYA781Ra	16S	GAC TAC TGG GGT ATC TAA TCC CAT T	2
CYA781Rb	16S	GAC TAC AGG GGT ATC TAA TCC CTT T	2

We constructed the CY23R primer based on sequence alignment of 23S regions of 24 cyanobacterial species from 16 different genera found in sequence databases. A conserved region, identical in all aligned sequences (5' - GTGCCTGTTGAAGAATGAGCCGGCGA - 3') was used to design a primer with appropriate length and melting temperature to be used with the standard cyanobacteria-specific forward primer CSIF. Schematic representation of all the primers used is shown in Fig 1. CYA781Ra and CYA781Rb were always used as an equimolar mixture (0.5  $\mu$ M) of both, in combination with 0.5  $\mu$ M forward primer CYA106F.<sup>2</sup>

corresponds to nucleotide positions 90–751 (spanning variable regions V2-V4) in *Synechocystis* sp. PCC 6803 16S rRNA gene as it has proven to be useful for identification of cyanobacteria.<sup>2</sup> From ITS amplicons, the region spanning conserved domains D1 to D5 was analysed.<sup>26</sup> All the sequences were compared to the non-redundant dataset of the GenBank collection using BLASTN.<sup>27</sup> Individual pairwise alignments between sequences were performed using EMBOSS Water algorithm at the EMBL-EBI web server<sup>28</sup> and multiple sequence alignments using MUSCLE algorithm in MEGA version 6<sup>29</sup> for ITS regions or concatenated 16S and ITS. For multiple alignments of 16S sequences



**Figure 1:** Primer positions relative to the 16S and 23S coding regions. Nucleotide positions are labelled for reference as deduced from *Synechocystis* sp. PCC 6803 genome.

### 2. 3. Cloning and Sequencing

After electrophoresis, PCR products were excised from agarose gels and purified using GeneJet Gel Extraction Kit (Thermo Scientific). Purified products were ligated into pJET1.2 using CloneJET™ PCR Cloning Kit (Thermo Scientific). After transformation of competent *Escherichia coli* DH5 $\alpha$  cells and plating onto selective media, plasmid DNA was isolated from overnight cultures of one to several independent clones using Plasmid MiniPrep Kit (Thermo Scientific). Sequencing was performed by Macrogen Europe using compatible universal primers annealing to the plasmid backbone.

### 2. 4. Sequence Analyses

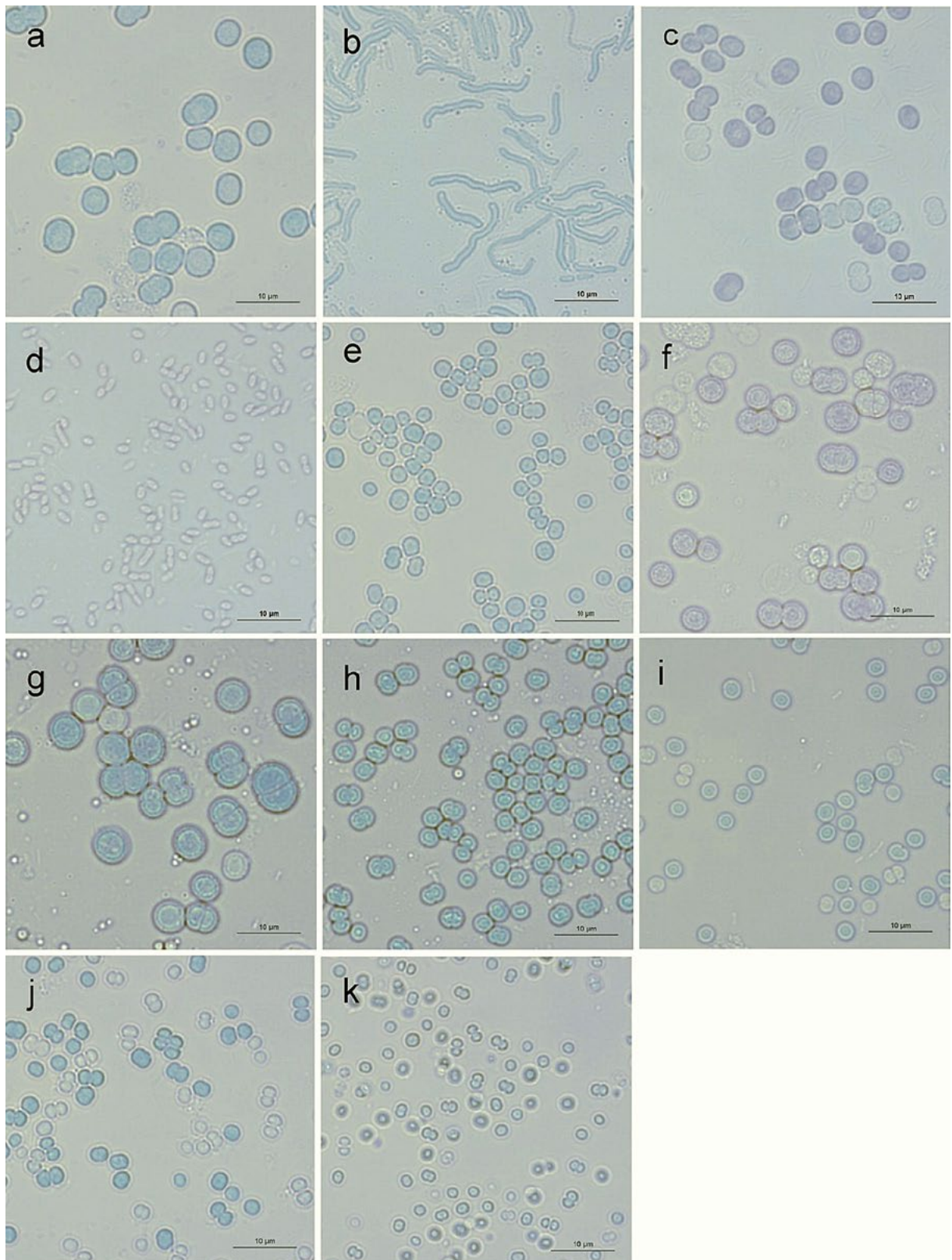
For sequence comparisons, only the polymorphic segment of the 16S rRNA gene or the ITS region were used. For 16S rRNA analyses we used the region which

we utilized RDP Aligner.<sup>30</sup> Analyses of tRNA composition in sequenced ITS regions were performed both manually, by finding the conserved segments of ITS in multiple alignments and comparing them to known consensus sequences for tRNA<sup>Ile</sup> and tRNA<sup>Ala</sup>, as well as with tRNAscan-SE v.1.21 program via the Lowe Lab Webserver Interface.<sup>31</sup>

In addition to cyanobacterial strains listed in Table 1, we investigated in detail the 16S rRNA coding and ITS regions of all three *Synechocystis* sp. strains whose complete genomes were sequenced up to now: PCC 6714, PCC 6803 and PCC 7509. These sequences are available in GenBank under ID codes CP007542.1, CP003265.1 and NZ\_ALVU02000001.1, respectively.

Maximum-likelihood trees were built using MEGA version 6<sup>29</sup> applying the Jukes-Cantor model. Bootstrap resampling using 1000 replicates was performed to test the robustness of the trees. We built 3 trees, based on 16S, ITS or concatenated 16S and ITS sequences using sequences





**Figure 2:** Microphotographs of *Synechocystis* strains at 1000× magnification. (a) *Synechocystis aquatilis* SAG 90.79, (b) *Synechocystis bourrellyi*\* CCAP 1480/1, (c) *Synechocystis fuscopigmentosa* CCALA 810, (d) *Synechocystis limnetica*\* CCAP 1480/5, (e) *Synechocystis minuscula* SAG 258.80, (f) *Synechocystis nigrescens*, (g) *Synechocystis pevalekii* SAG 91.79, (h) *Synechocystis salina* CCALA 192, (i) *Synechocystis* sp. CCAP 1480/4, (j) *Synechocystis* sp. PCC 6714, (k) *Synechocystis* sp. PCC 6803. Inverted microscope Nikon EclipseTE300 was used. Scale bar corresponds to 10 μm. \* denotes species samples with atypical morphology for *Synechocystis* members.

from strains analysed in this study (9 sequences for trees based on ITS and concatenated 16S and ITS sequences, and 10 for the tree based on 16S sequences, since from *Synechocystis nigrescens* we could only amplify 16S rRNA but not ITS region), sequences from two other *Synechocystis* strains with published whole genome sequence (*Synechocystis* sp. PCC 7509 and PCC 6714) and sequences from 4 fully sequenced non-*Synechocystis* strains, whose 16S or ITS regions showed high similarity to some of our analysed strains.

### 3. Results and Discussion

#### 3.1. Microscopic Investigation of the Strains

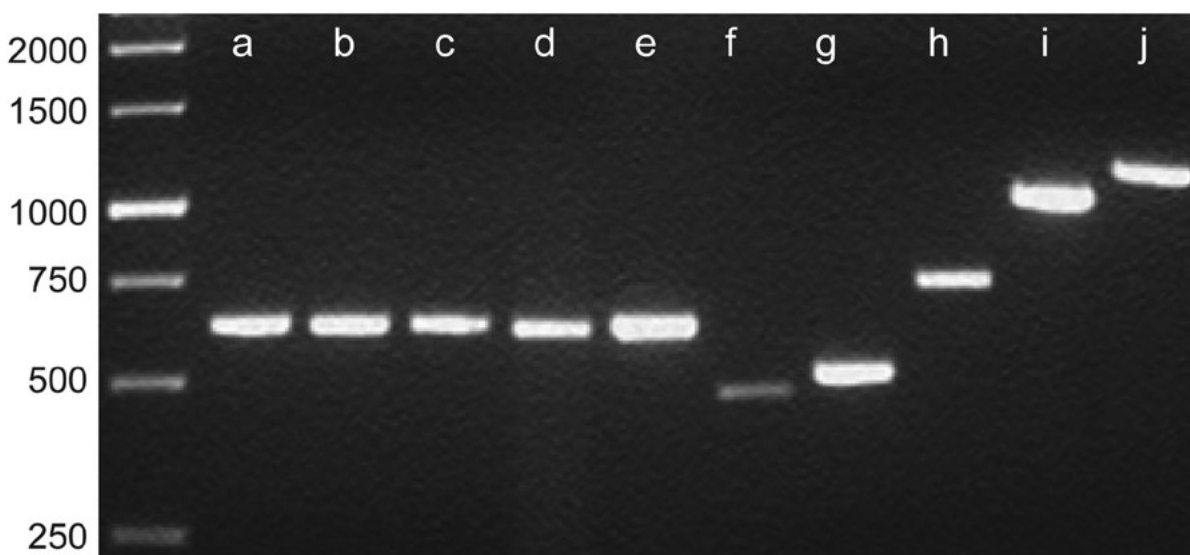
Microphotographs of *Synechocystis* strains at 1000× magnification are presented in Fig 2. Cells of strains that later proved to be phylogenetically closest to *Synechocystis* sp. PCC 6803 and PCC 6714 (*Synechocystis salina* CCALA 192, *Synechocystis* sp. CCAP 1480/4 and *Synechocystis minuscula*) were similar in shape and size (1–2.5 (5) μm) to the typical morphology<sup>32</sup> of *Synechocystis* members.

*Synechocystis limnetica* CCAP 1480/5 and *Synechocystis bourrellyi* CCAP 1480/1 resembled shape characteristics of *Synechococcus* genus members. Especially *Synechocystis bourrellyi* with cells several times longer than wide is evidently morphologically different from *Synechocystis* representatives and fits into description of *Synechococcus*-type cell shape: cells 1.5 up to more than 20 μm long and 0.4 to 6 μm wide, according to CyanoDB (<http://www.cyanodb.cz/Synechococcus>). We thus decided to interpret

sequence data obtained with these two strains with care and from here on we label both strains with an asterisk (\*) after the species name.

Three of the analysed strains showed cell diameters relatively large for the *Synechocystis* members. *Synechocystis pevalekii* SAG 91.79, *Synechocystis nigrescens* and *Synechocystis aquatilis* SAG 70.79 with diameters ranging from 3.5 to 5 μm represent this group. Although the typical diameter for *Synechocystis aquatilis* is expected to be 4.5 to 7 μm,<sup>33</sup> these cells are larger than typical<sup>32</sup> for *Synechocystis* members. According to their size, these three strains are similar to *Geminocystis* genus members (3–10 μm). Nevertheless we kept these strains for DNA analysis to find out the level of their relatedness to strains with the typical shape and size of *Synechocystis* members.

It has been observed before that cyanobacterial systematics that is based on morphology alone is problematic, as cells change morphology in varying growth conditions. This has for example been shown for the picobacterium *Cyanobacterium aponinum* that displays a very different habitus in salt water (elongated cells) as compared to freshwater.<sup>34</sup> In the literature, there are also reports that growth in laboratory conditions can alter cell phenotype as compared to natural growth conditions.<sup>35</sup> A DNA-based analysis has a clear advantage over microscopic analysis in that it is not affected by eventual changes in cell morphology. On the other hand, with PCR-based methods there is a risk of polymerase errors and cross-contamination, possibly leading to ambiguous results.<sup>36</sup> Furthermore, amplification of DNA from a minor population in non-axenic cultures can occur, especially when broad-specificity primers are used.<sup>2</sup> A microscopic check of the starting ma-



**Figure 3:** PCR amplification products of ITS regions for the 10 *Synechocystis* strains using CSIF and ULR primers, resolved on 1% agarose gel. (a) *Synechocystis* sp. PCC 6803, (b) *Synechocystis* sp. PCC 6714, (c) *Synechocystis* sp. CCAP 1480/4, (d) *Synechocystis salina* CCALA 192, (e) *Synechocystis minuscula* SAG 258.80, (f) *Synechocystis aquatilis* SAG 90.79, (g) *Synechocystis fuscopigmentosa* CCALA 810, (h) *Synechocystis pevalekii* SAG 91.79, (i) *Synechocystis limnetica*\* CCAP 1480/5, (j) *Synechocystis bourrellyi*\* CCAP 1480/1. Marker sizes are labelled to the left of the DNA ladder. \* denotes species that in microscopic analysis showed atypical morphology for *Synechocystis* members.

terial is thus always recommended. When we did so, we observed that two of the strains display a morphology that is atypical for *Synechocystis* members (consequently marked with an asterisk) and a few other strains had cells larger than typical for *Synechocystis*.

Without very good knowledge and long-standing expertise in microscopic investigation of unicellular cyanobacteria, cell morphologies might be inconclusive about the identity of the investigated species. The discrimination power of DNA is thus much higher and low-cost whole-genome sequencing might open doors to new approaches to strain identification. For the time being, DNA barcoding that is based on selected genomic regions seems to be a reasonable substitute. Even in the future, when polymorphic genomic regions are better understood, DNA barcoding will enable fast identification, possibly even of single cells.

### 3. 2. Amplification and Cloning of Genomic Regions

For cloning and sequencing of ITS regions, PCR products obtained with CSIF and either ULR or CY23R reverse primer were used (Figure 3). Only with *S. aquatilis*, two PCR products were obtained (only the larger product can be clearly seen in Fig. 3) and sequenced that differed in ITS length. All other samples resulted in one PCR product only. Amplicon lengths using CSIF/ULR primers and deduced ITS lengths as obtained by sequencing are given in Table 3.

**Table 3.** Summary of amplicon lengths using the combination of CSIF and ULR primers and deduced ITS lengths obtained for 10 *Synechocystis* representatives

Amplicon lengths were calculated from respective sequences after plasmid cloning of PCR products obtained with CSIF forward and CY23R or ULR reverse primer. ITS lengths correspond to the region spanning conserved domains D1 to D5.<sup>14</sup> *S. nigrescens* ITS region could not be amplified using any of the primers listed in Table 2.

Species	Amplicon length	ITS length
<i>Synechocystis aquatilis</i>	418 or 479	311 or 312
<i>Synechocystis bourrellyi</i> *	1185	1018
<i>Synechocystis fuscopigmentosa</i>	512	344
<i>Synechocystis limnetica</i> *	1056	888
<i>Synechocystis minuscula</i>	645	477
<i>Synechocystis pevalekii</i>	752	587
<i>Synechocystis salina</i>	632	466
<i>Synechocystis</i> sp. CCAP 1480/4	632	467
<i>Synechocystis</i> sp. PCC 6714	631	465
<i>Synechocystis</i> sp. PCC 6803	631	465

\* denotes species that in microscopic analysis showed atypical morphology for *Synechocystis* members.

According to ITS lengths (Table 3), *Synechocystis* members can roughly be divided into four groups. The

shortest ITS regions (310–350 bp) were found in *S. aquatilis* and *S. fuscopigmentosa* (group A). Most of the analysed representatives belong to the group B with ITS lengths of between 460 and 480 bp (including *S. minuscula*, *S. salina*, CCAP 1480/4, PCC 6714 and PCC6803). Group C with intermediate size ITS region (587 bp) was represented by *S. pevalekii*, while the eventual group D displayed very long ITS regions (*S. limnetica*\* 888 bp, *S. bourrellyi*\* 1018 bp – both were morphologically atypical for *Synechocystis* members as can be seen in Fig. 2). These differences in ITS lengths allow for a rapid PCR-based differentiation between some of the *Synechocystis* members without sequencing, although strain determination cannot be achieved by using universal ITS primers alone.

Iteman et al. reported that ITS regions of cyanobacteria vary in length from 283 to 545 bp,<sup>14</sup> which is with exclusion of *S. bourrellyi*\* and *S. limnetica*\* true also for the ITS regions of the analysed *Synechocystis* strains (Table 3). Interestingly, ITS lengths of the two atypical species samples (1018 bp for *S. bourrellyi*\* and 888 bp for *S. limnetica*\*) correspond to the lengths that were reported for *Synechococcus* representatives,<sup>37</sup> i.e. between 820 bp (WH 7803) and 1065 bp (PCC 7001). These results are in accordance with the morphological features of the two strains (Fig. 2), displaying characteristics of *Synechococcus* rather than *Synechocystis* species. Taken together, the great variety of the lengths of the ITS segments represents a good starting point for development of amplification-based approaches to differentiation between species and strains within the *Synechocystis* genus.

### 3. 3. Sequence Comparisons

Sequences of 16S rRNA gene variable regions were determined for products of PCR amplification using primers CYA106F and CYA781Ra/b. All the sequences obtained within this work are deposited in GenBank (KT354181–KT354212 and KT371491–KT371499). Respective ID codes are listed in the following sections for each of the strains analysed.

We compared variable segments of 16S rRNA genes and complete ITS sequences from our experiments with those available in GenBank using BLAST. The result of the comparison was a list of sequences with highest levels of identity. Below, we are summarizing our findings for individual species/strains.

In the text, the term ‘clone’ refers to sequences that we obtained on plasmid-cloned PCR products resulting from amplification of template DNA from individual cyanobacterial cell cultures.

#### 3. 3. 1. *Synechocystis Aquatilis*

*S. aquatilis* is the type species of the genus (Komárek, 2006) and there are several 16S rRNA encoding sequences deposited in the GenBank that enabled their easy align-

ment and analysis of inter-strain differences. We analysed two independent clones of the 16S rRNA region (IDs: KT354181, KT354182). Both our sequences displayed 99.5% identity to the database sequence KM020011.1 originating from the same strain and the same culture collection as ours. Three identical database sequences from 3 *Cyanobacterium aponinum* strains showed the second highest score (97% sequence identity to our sequence): KSU-WH-5 (ID: KT807478.1) collected in Saudi Arabia, lklSCC30 (ID: KM438201.1) collected in Greece and PCC 10605 (ID: CP003947.1), for which the complete genome<sup>38</sup> is available.

Up to now, partial or full 16S rRNA sequences of 8 other *Synechocystis aquatilis* strains have been deposited in GenBank. They did not appear among top-scored hits in our initial sequence comparison and were therefore separately aligned to our sequences using the multisequence alignment program Clustal W2. Comparison of 237 nucleotides shared by all the deposited sequences revealed close relation of our clones to sequences belonging to two different *S. aquatilis* strains (ISB32 and ISB33, isolated from hot springs in Iran) having 99.7% (1 polymorphic site) and 92.5% (18 polymorphic sites) sequence identity, respectively. Sequences of the 16S rRNA from other 6 *Synechocystis aquatilis* strains deposited in GeneBank differed substantially from our newly determined sequences and seem only distantly related to SAG 90.97. Either the strains are genetically substantially polymorphic or the depositors failed to properly determine the species.

BLASTN sequence similarity search comparing our 4 clones of the ITS region positioned *Cyanobacterium aponinum* PCC 10605 as the top match with 95% sequence identity. Except ours, there are no ITS sequences attributed to *Synechocystis aquatilis* currently deposited in GenBank.

### 3. 3. 2. *Synechocystis bourellyi*\*

Sequences of two 16S rRNA-coding clones (IDs: KT354187, KT354188) and of one ITS region clone (KT354189) were compared to the complete GenBank dataset. The highest score (99.5% identity, 3 mismatches for KT354187 and 99.7% identity or 2 mismatches for KT354188) was shared with various strains of the *Synechococcus* genus (*Synechococcus elongatus* CCAP 1479/1B (ID: KM020008.1), *Synechococcus* sp. CCAP 1479/10 (ID: HE975006.1), *Synechococcus* sp. PCC 7009 (ID: AM709628.1), *Synechococcus* sp. EW15 (ID: DQ275602.1) and *Synechococcus* sp. BO8806 (ID: AF317072.1)). Comparison with complete genome sequences showed *Cyanobium gracile* PCC 6307 (ID: CP003495.1) with 99.2% (5 mismatches with KT354187) or 99.4% sequence identity (4 mismatches with KT354188) as the highest scoring result.

The ITS region we have amplified was unexpectedly long (Table 3 and Fig. 3). BLASTN search identified *Synechococcus* sp. PCC 7009 (ID: AM709628.1) as the highest

score with only two mismatched nucleotides. As with 16S rRNA coding regions, complete genome sequence with the highest score was that of *Cyanobium gracile* PCC 6307 (ID: CP003495.1) with 92.9% sequence identity.

Both 16S rRNA encoding and ITS region sequences thus demonstrate highest identities with members of the *Synechococcus* genus, but also of other related genera. This is in line with the microscopic observations (Fig. 2). *Synechocystis* members did not appear as top scores in the sequence comparisons we have performed.

### 3. 3. 3. *Synechocystis fuscopigmentosa*

Two identical 16S rRNA-coding sequences were obtained (ID: KT371491) displaying 98.9% identity to the corresponding region of *Geminocystis* sp. NIES-3709 (ID: AP014821.1).

Next, we analysed two sequences of the ITS region and also found them identical (ID: KT371492). BLASTN search results showed sequence from *Cyanobacterium* sp. PAP1 (ID: EF555569.1) as the most similar one, but the coverage was not complete since the GenBank submission for PAP1 strain does not contain full ITS sequence. *Geminocystis* sp. NIES-3709 (ID: AP014821.1) displayed the highest overall score among available sequences with complete coverage (96.8% identity).

### 3. 3. 4. *Synechocystis limnetica*\*

Two 16S rRNA-coding clones were sequenced and analysed (IDs: KT354190, KT354191). Sequence alignment showed that among the cyanobacterial 16S rRNA sequences deposited in databases, *S. limnetica*\* has the highest similarity with *Synechococcus* sp. MA0607K (ID: FJ763779.1), having 8 or 9 mismatches (for the two clones) in the variable segment alone. Sequence of the ITS region (1 clone sequenced; KT354192) has the highest identity, 87.6%, with *Prochlorococcus marinus* MIT9313 (whole genome, ID: BX548175.1). BLASTN search resulted in sequences with higher identity to our clone (up to 98%), but they were assigned to uncultured and taxonomically undefined organisms. Although *Synechocystis limnetica*\* is highly related to *Synechocystis bourellyi*\* (97%) in the 16S variable region, it differs substantially in the ITS region (57%), as can be seen from Tables 4 and 5.

### 3. 3. 5. *Synechocystis minuscula*

Two clones of the 16S region were identical in sequence (ID: KT354193). The top search result after BLASTN sequence similarity analysis was a GenBank entry KM019989.1 from essentially the same strain, albeit 1 mismatch was detected. The second best results were *Synechocystis salina* LEGE 06155 (ID: HQ832911.1, isolated from the intertidal zone in Northern Portugal) and *Synechocystis* cf. *salina* LEGE 07073 (ID: HM217083.1, isolated

from an estuarine habitat, also in Northern Portugal), both with 97.4% identity.

In the GenBank database we found a 16S rRNA coding sequence of another *Synechocystis minuscula* strain (AICB 62; ID: KJ746516.1), but it displayed only low identity (86.8%) with the sequence of our analysed strain. The AICB 62 strain originated from the Algal and Cyanobacterial Collection (AICB) of the Institute of Biological Research from Cluj-Napoca, Romania.

The 4 clones of the ITS region differed only in the first nucleotide position so that pairs of sequences KT354195/KT354196 and KT354194/KT354197 were identical. They had the highest alignment score with the sequence of *Synechocystis* sp. PAK13 (ID: EF555571.1) and *Synechocystis* sp. PAK12 (ID: EF555570.1)<sup>32</sup> with 84.7% identity, but these PAK strains sequences had only 75% of the total ITS region length covered. The best result with the full coverage of the ITS region was with *Gloeothece* sp. PCC 6909 (CCAP 1480/4, ID: HE975009.1), having 80% identity.

### 3. 3. 5. *Synechocystis nigrescens*

Two 16S rRNA coding sequences were analysed (IDs: KT354198 and KT354199). They displayed one mismatch when compared to each other. BLASTN analysis identified *Synechocystis* sp. SAG 37.92 (ID: KM020010.1) as the highest score with only one mismatch. All other sequences with high similarity were assigned to genera *Geminocystis* or *Synechocystis*.

The ITS region could not be analysed because we were unable to amplify it using any of the primer combinations from Table 2. This might point to the fact that the 5' amplification primer was not hybridizing with the template despite the fact that the annealing region seems to be highly conserved<sup>2</sup> among different cyanobacteria.

### 3. 3. 6. *Synechocystis pevalekii*

Two 16S rRNA-coding sequences were analysed (IDs: KT354200 and KT354201). BLASTN analysis surprisingly showed *Chamaesiphon subglobosus* PCC 7430 (ID: AY170472.1) as the hit with the highest score with only 2 (ID: KT354200) or 3 (ID: KT354201) mismatches in the variable region of the 16S rRNA gene. Comparison with complete genome sequences showed 16S rRNA gene from *Chamaesiphon minutus* PCC 6605 (ID: CP003600.1) as the highest scoring sequence with 97.3% identity.

For the ITS region, we analysed 5 clones (IDs: KT354202 – KT354206). All of them displayed 90% sequence identity with *Chamaesiphon minutus* PCC 6605 (complete genome, ID: CP003600.1). All other hits were less related to the *S. pevalekii* sequence in this region.

Interestingly, microscopic observations of *Synechocystis pevalekii* SAG 70.79 showed almost no morphologic characteristics of the genus *Chamaesiphon* in contrast to our sequence alignment results.

### 3. 3. 7. *Synechocystis salina*

Two 16S rRNA-coding sequences were analysed (IDs: KT354209, KT354210). The highest alignment score obtained was that of *Gloeo capsa alpicola* FACH-400 (ID: JX872524.1; three mismatches with KT354209 and one with KT354210) and *Gloeothece* sp. PCC 6909 (CCAP 1480/4, ID: HE975009.1; three mismatches with both clones). *Gloeo capsa alpicola* has been reclassified among genera twice; first it has been assigned to *Synechocystis* genus and lately ordered<sup>32</sup> into a new genus as *Geminocystis herdmannii*. Complete genome sequence with the highest score was that of *Synechocystis* sp. PCC 6803 (ID: CP003265.1) with 98.2% identity in the variable part of the 16S rRNA coding region.

Two sequences of the ITS region (IDs: KT354211, KT354212) were found to contain two polymorphic sites. There was 99.8% (1 mismatch with KT354211) or 100% identity (KT354212) with *Gloeothece* sp. PCC 6909 (CCAP 1480/4, ID: HE975009.1). The next highest identity score was obtained with *Synechocystis* sp. PAK12 (ID: EF555570.1), displaying 93.2% identity.

### 3. 3. 8. *Synechocystis* sp. CCAP 1480/4

It should be noted that in the culture collection, CCAP 1480/4 strain is described as *Synechocystis* sp., while in GenBank this same strain is labelled as *Gloeothece* sp. PCC 6909. Two clones of 16S rRNA coding sequence were analysed. They were identical (ID: KT354207) and showed one mismatch when compared to 16S sequences of both *Gloeo capsa alpicola* FACHB-400 (ID: JX872524.1) and *Gloeothece* sp. PCC 6909 (CCAP1480/4, ID: HE975009.1). The closest complete genome sequence was that of *Synechocystis* sp. PCC 6803 (ID: CP003265.1) with 98.5% identity (10 mismatches across the variable part of the 16S rRNA sequence).

The ITS region (ID: KT354208) displayed 100% identity with *Gloeothece* sp. PCC 6909 (CCAP 1480/4, ID: HE975009.1). The next highest score was that of *Synechocystis* sp. PCC 6714 (complete genome, ID: CP007542.1) having 91.3% identity.

*Gloeothece* members are characterized by formation of small colonies which are enveloped in mucilaginous envelopes while *Synechocystis* does not form microcolonies. Our observations (Fig. 2) showed no characteristic envelopes in the strain analysed.

### 3. 3. 9. *Synechocystis* sp. PCC 6714

The genomic sequence of *Synechocystis* sp. PCC 6714 has previously been determined,<sup>39</sup> therefore only one clone of its ITS region (ID: KT371499) was sequenced. It showed 3 mismatches to the genomic sequence of this strain deposited in GenBank (ID: CP007542.1).

### 3. 3.10. *Synechocystis* sp. PCC 6803

Essentially, results with the *Synechocystis* sp. PCC 6803 strain were as expected from the genomic sequence,<sup>40</sup>

although 4 polymorphic sites were found in 16S rRNA coding sequences in our 4 clones (IDs: KT371493 – KT371496). None of our clones was identical to any other published sequence and all 4 had *Synechocystis* sp. LMECYA 68, a strain from Cyanobacteria Culture Collection Estela Sousa e Silva in Portugal (ID: EU078508.1), as the highest BLASTN hit, followed by three *Synechocystis* sp. strains: PUPCCC 62 (ID: KF475890.1), an isolate from India, and KSU-AQIQ-1 (ID: LN997853.1) and KSU-WH-2 (ID: KT807477.1), both discovered in Saudi Arabia. Sequences of these three strains were identical to that in the deposited genomic sequence of *Synechocystis* sp. PCC 6803. Sequence identities for LMECYA 68 strain ranged from 100% with one of our clones to 99.7% (2 mismatches) with another one. In the other three strains (and equally in the published PCC 6803 strain), sequences differed in 1 to 3 positions from our sequence.

Analysis of two clones of ITS sequences (IDs: KT371497, KT371498) showed 0 and 1 mismatches, respectively with the published genomic sequence<sup>40</sup> of *Synechocystis* sp. PCC 6803.

Although *Synechocystis* sp. PCC 6803 is of utmost importance for research on photosynthesis, evolution, as well as for biotechnology and synthetic biology, this strain has never been taxonomically defined to the species level.

Especially for environmental and biosafety investigations, it would be helpful to assign a species to this strain as well. From our sequence data, the PCC6803 strain is closely related to *Synechocystis salina*, but not identical. Our results show that PCC 6803 is a distinct taxonomic entity despite the fact that it was described as ‘corresponding to *S. aquatilis*<sup>32</sup> based mainly on its morphologic similarity to the type strain. We found out that the ITS regions of these two *Synechocystis* members are very different, sharing only 52% of the sequence, and that also the 16S rRNA coding variable regions are only 86% identical.

A summary of our findings is presented in Tables 4 and 5, showing identities among the variable segment of the 16S rRNA genes and the ITS sequences, respectively, for 11 *Synechocystis* species/strains (10 for the ITS region). Also included in the tables is *Synechocystis* sp. PCC 7509, the only strain with whole genome sequence available besides PCC 6803 and PCC 6714, both of which we analysed independently.

As evident from Table 4, there are three species that in their 16S rRNA gene sequences differ substantially from the remaining *Synechocystis* members in our study, namely *S. bourrellyi*\* (which only shows substantial similarity with *S. limnetica*\*), *S. nigrescens* (more closely related only to *S. aquatilis*) and *S. limnetica*\* (similar only to *S. bourrellyi*\*).

**Table 4.** Summary of 16S rRNA variable region sequence identities among *Synechocystis* members. Sequences used for comparison were obtained in our laboratory, only those of PCC 6714 and PCC 7509 were taken from GenBank. For PCC 6803 our data were in accordance with GenBank sequences. Shade intensity increases with higher values of sequence identity.

	<i>S. aquatilis</i> SAG 90.79	<i>S. bourrellyi</i> * CCAP 1480/1	<i>S. fuscopigmentosa</i> CCALA 810	<i>S. limnetica</i> * CCAP 1480/5	<i>S. minuscula</i> SAG 258.80	<i>S. nigrescens</i>	<i>S. pevalekii</i> SAG 91.79	<i>S. salina</i> CCALA 192	<i>Synechocystis</i> sp. CCAP 1480/4	<i>Synechocystis</i> sp. PCC 6714	<i>Synechocystis</i> sp. PCC 6803	<i>Synechocystis</i> sp. PCC 7509
<i>S. aquatilis</i> SAG 90.79												
<i>S. bourrellyi</i> * CCAP 1480/1	83											
<i>S. fuscopigmentosa</i> CCALA 810	95	85										
<i>S. limnetica</i> * CCAP 1480/5	83	97	85									
<i>S. minuscula</i> SAG 258.80	87	86	88	88								
<i>S. nigrescens</i>	94	84	87	83	88							
<i>S. pevalekii</i> SAG 91.79	88	88	90	88	90	89						
<i>S. salina</i> CCALA 192	88	86	89	87	96	89	91					
<i>Synechocystis</i> sp. CCAP 1480/4	88	87	89	87	96	90	91	99				
<i>Synechocystis</i> sp. PCC 6714	86	87	88	87	97	87	90	98	98			
<i>Synechocystis</i> sp. PCC 6803	86	86	88	87	97	87	90	98	98	99		
<i>Synechocystis</i> sp. PCC 7509	89	85	90	85	89	89	90	90	90	88	88	

\* denotes species that in microscopic analysis showed atypical morphology for *Synechocystis* members

Identities in the ITS region (Table 5) are far lower than in 16S-rRNA coding region and only a few strains clearly converge in a single group, namely PCC 6803, PCC 6714, CCAP 1480/4 and *S. salina*. For other species/strains identity was below 65% when compared to each other within the dataset.

We additionally compared the variable part of the 16S rRNA coding sequences that were determined in our laboratory with those known previously for members of all the major lineages of cyanobacteria (Appendix, Fig. B). *Synechocystis* members from our analysis appear distributed among Chroococciopsidales, Chroococcales, Os-

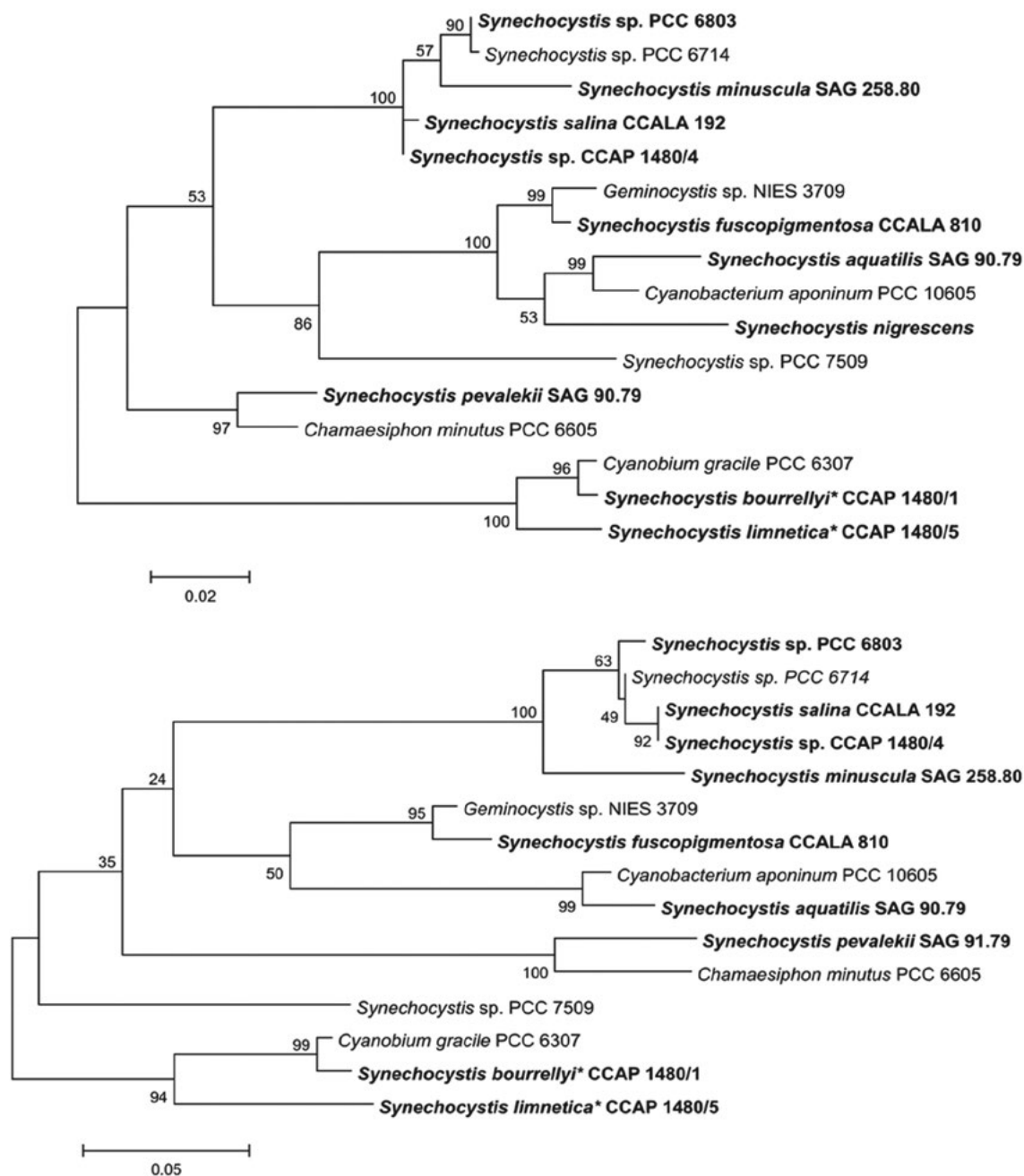
**Table 5.** Summary of ITS sequence identities among *Synechocystis* members  
Sequence data for PCC 6714 and PCC 7509 were taken from GenBank, all other were obtained in our laboratory. For PCC 6803 our sequences data were in accordance with GenBank sequences. Shade intensity increases with higher values of sequence identity.

	<i>S. aquatilis</i> SAG 90.79	<i>S. bourellyi</i> * CCAP 1480/1	<i>S. fuscopigmentosa</i> CCALA 810	<i>S. limnetica</i> * CCAP 1480/5	<i>S. minuscula</i> SAG 258.80	<i>S. pevalekii</i> SAG 91.79	<i>S. salina</i> CCALA 192	<i>Synechocystis</i> sp. CCAP 1480/4	<i>Synechocystis</i> sp. PCC 6714	<i>Synechocystis</i> sp. PCC 6803	<i>Synechocystis</i> sp. PCC 7509
<i>S. aquatilis</i> SAG 90.79											
<i>S. bourellyi</i> * CCAP 1480/1	45										
<i>S. fuscopigmentosa</i> CCALA 810	79	47									
<i>S. limnetica</i> * CCAP 1480/5	50	57	49								
<i>S. minuscula</i> SAG 258.80	50	37	55	38							
<i>S. pevalekii</i> SAG 91.79	52	42	53	48	48						
<i>S. salina</i> CCALA 192	52	36	55	41	78	48					
<i>Synechocystis</i> sp. CCAP 1480/4	52	36	55	42	78	49	99				
<i>Synechocystis</i> sp. PCC 6714	53	35	52	43	77	44	91	91			
<i>Synechocystis</i> sp. PCC 6803	52	35	51	41	77	43	91	91	91		
<i>Synechocystis</i> sp. PCC 7509	62	45	61	47	52	63	51	51	51	48	

\* denotes species that in microscopic analysis showed atypical morphology for *Synechocystis* members

Based on our sequence data, we prepared phylogenetic trees based on 16S rRNA coding region (Fig. 4 top), ITS region (Fig. 4 bottom) and concatenated 16S and ITS (see Appendix). Phylogenetic trees that are based on 16S rRNA-coding and ITS sequences alone do not differ substantially from each other. Nevertheless, they do differ slightly in positioning of *S. minuscula* in the cluster closely related to PCC 6803 (but in the 16S rRNA-based tree, its positioning is supported with low bootstrap. Also *Synechocystis* sp. PCC 7509 is positioned differently in 16S rRNA and ITS trees. Although topologies differ slightly, we do not believe that this influences interpretation of our results. Our intention was not to determine definite intrageneric phylogenetic positions of analysed strains but to illustrate that taxonomic positioning of some *Synechocystis* species is not in accordance with their phylogeny even on the genus level. Namely, they show higher sequence relatedness to representatives of genera other than *Synechocystis*, which is evident from both trees, as well as from the tree based on concatenated sequences (see Appendix, Fig. A).

cillatoriales, and eventually Synechococcales (only the two strains that were evidently different from others by appearance). This is in good accordance with the previously published phylogenetic tree based on 31 protein sequences from all the fully sequenced genomes of cyanobacteria known in 2014 (Fig. 1 in<sup>24</sup>), just that we additionally found *S. pevalekii* as a new member of the genus evading the Chroococcales order, showing relatedness to Oscillatoriales. *S. bourellyi*\* and *S. limnetica*\* stand even further apart from the rest of the analysed *Synechocystis* members, further corroborating the idea that they might have been either mislabelled before they came in our laboratory or were incorrectly taxonomically determined at deposition in the culture collection. Another possible explanation would be horizontal gene transfer, since it is known to be common among cyanobacteria, especially for protein-coding genes.<sup>41,42</sup> Further analyses of additional phenotypic and genotypic characteristics would provide unambiguous conclusions about the observed variability.



**Figure 4.** Phylogenetic trees for the analysed members of the *Synechocystis* genus based on our sequences (bolded strain names) of the variable segment in 16S rRNA coding region (top) and of ITS regions (bottom). For comparison, sequence data for PCC 6714 and PCC 7509 as deposited in GenBank were included.\* denotes strains that in microscopic analysis showed atypical morphology for *Synechocystis* members.

### 3. 4. tRNA coding Sequences Within ITS Regions

ITS regions in all the strains that we analysed contained tRNA<sup>Ile</sup> sequences. Only sequences of *S. aquatilis*, *S. bourrellyi*\*, *S. fuscopigmentosa*, *S. limnetica*\* and *S. pevalekii* additionally contained the tRNA<sup>Ala</sup> sequence, which was not observed in members of the *Synechocystis* genus

before. This could be considered an interesting example of the heterogeneity in *Synechocystis*. We found the first case of a two-tRNA ITS in *Synechocystis* in PCC 7509 genome<sup>38</sup> and we further expanded the number of known *Synechocystis* members harbouring 2 tRNA-coding sequences in their ITS to 5 additional species (*S. aquatilis*, *S. bourrellyi*\*, *S. pevalekii*, *S. fuscopigmentosa* and *S. limnetica*\*). It remains to be elucidated whether the addition of tRNA<sup>Ala</sup>



coding sequence could have happened through horizontal gene transfer. Alternatively, this could be a sign of a polyphyletic development or, even more likely, of erroneous taxonomic standing of some of the *Synechocystis* species. Again, it cannot be excluded that some strains in culture collections are mislabelled, as e.g. Rajaniemi-Wacklin et al.<sup>43</sup> reported loss of colony structure for cultured *Snowella* strains, upon which they could be easily misidentified as *Synechocystis*. However, *Snowella* (as well as *Woronichinia* and *Merismopedia*) strains from their study were phylogenetically related to *Synechocystis* members.

It has been noted before that more than a half of the strains in the culture collections are probably incorrectly identified.<sup>44</sup> Similarly, Garcia-Pichel et al. discovered that one of the *Microcoleus chthonoplastes* strains in a culture collection and one from a research laboratory were not closely related to fresh isolates and to a cultured strain from another microalgal collection.<sup>45</sup> More recently, Gkelis et al. presented evidence that a *Limnothrix* strain was previously misidentified as a *Planktothrix* strain.<sup>46</sup> DNA-analyses should therefore be used as an important identification factor for culture collections, similarly to what has recently been done<sup>47</sup> on a small scale with a green algae collection from Germany.

Identification of *Synechocystis* and related cyanobacteria in the environmental samples is important from the ecological, but also from the biosafety point of view. *Synechocystis* sp. PCC 6803 is probably the most important cyanobacterial strain in synthetic biology and modern biotechnology. We therefore wished to know whether there are any close relatives of this strain present in aquatic environments and planned to develop a DNA barcoding approach specifically for these unicellular cyanobacteria. In biosafety risk assessments, knowing wild-type relatives of the production strain can help better estimate the risk of e.g. horizontal gene transfer, especially as *Synechocystis* sp. PCC 6803 is known to be naturally competent for transformation.

An extensive review of the current status in cyanobacterial systematics was published by Komárek et al. in 2014.<sup>24</sup> We did not want to go into details of fundamental questions of cyanobacterial taxonomy but instead provide a range of new data that could help in better understanding of the *Synechocystis* genus through its genetic heterogeneity, and eventually contribute to a more precise taxonomic delineation of *Synechocystis* members. In addition, our data could serve as the basis for development of a rapid DNA-based discrimination approach.

The genus *Synechocystis* was listed as one of the polyphyletic genera that need a taxonomic revision.<sup>24</sup> Cyanodb database (<http://www.cyanodb.cz/Synechocystis>) catalogues as many as 23 *Synechocystis* species described between 1892 and 2006, and three additional species as 'unclear taxa'. Despite our efforts, we could obtain from culture collections around the world only 8 *Synechocystis* representatives that were clearly labelled with a species

name. Where several strains of the same species were available, we only analysed one arbitrary chosen strain.

Our search through nucleotide sequence databases revealed that there were relatively few data available for this group of cyanobacteria. Although *Synechocystis* sp. PCC 6803 was the first photosynthetic organism for which a complete genomic sequence was available,<sup>40</sup> there is a considerable gap in understanding genomes of related cyanobacteria. Only two other *Synechocystis* strains were fully sequenced up to now, PCC 6714<sup>39</sup> and PCC 7509.<sup>38</sup> To complement these datasets, there were some sequences of the 16S rRNA-coding regions available for other members of the genus in the sequence databases.

Up to now there has been little work done on comparative genomics of the *Synechocystis* genus. After the first attempt by Korelusová et al.<sup>32</sup> who did the initial comparisons of several strains (not assigned to species) on structural and genetic level, several new sequences were deposited into databases. A report of Kopf et al. focused on a recently sequenced *Synechocystis* sp. PCC 6714 that is closely related to PCC 6803.<sup>48</sup> They showed that the 16S rRNA-coding segment is 99.4% identical to that of PCC 6803, but that almost a quarter of protein-coding genes is unique to each strain.

A recent systematic overview of cyanobacterial genomes encompasses 54 very diverse taxa from across the cyanobacterial phylum that were newly sequenced.<sup>38</sup> Among these, there was the *Synechocystis* sp. strain PCC 7509 that in the phylogenetic tree appeared as only vaguely related to the PCC 6803 strain.

We inspected all three complete genomes of *Synechocystis* genus members for the number and heterogeneity of their rRNA operons. They all contained two identical operons each. In contrast, our sequence analyses show that some strains do display broader heterogeneity in their ITS regions, mostly as single-nucleotide polymorphisms, but also as segment insertions/deletions. Although we did not focus on intrastain heterogeneity, we provided a clear evidence of ITS polymorphism that is worth considering in developing DNA barcoding tools and elsewhere. It should be noted that cyanobacteria harbour multiple copies of their genome<sup>49</sup> and that there is no clear proof that these copies indeed are identical at the sequence level. Our finding that rRNA sequences are heterogeneous within single strains suggests that 'copies' might differ slightly from each other.

We observed a much greater variability among species in the ITS than 16S rRNA-coding regions, although even 16S rRNA variable sequences differed among several species of the same genus more than we initially expected (Table 4). There were only a few species/strains pairs within the genus that shared >90% identity in the variable segment of the 16S rRNA-coding region. ITS regions were either very similar among strains or quite varied, e.g. *S. minuscula* and *S. pevalekii* display only 48% identity, while *S. salina* and *S. minuscula* share 78% identity in the ITS region (Table 5). This is a good basis for development of

ITS-specific primers that could differentiate between species of the same genus.

Including genomic regions outside the rRNA operon in the analysis could contribute to fine-positioning of genus members into a system, but it was not essential for discrimination between strains, as our results clearly show.

Although our prime interest remains the development of a tool for easy determination of *Synechocystis* members in water bodies, our current results demonstrate the applicability of DNA-based approach in discriminating between species/strains belonging to the same cyanobacterial genus. Moreover, they represent a solid basis for taxonomic reconsideration of *Synechocystis* and related cyanobacterial genera.

## 4. Conclusions

ITS region sequences proved to discriminate among species and strains of *Synechocystis* members and thus represent a solid basis for DNA barcoding. The observed differences between genus members indicate the presence of several genetic clusters which might lead to a taxonomic reinvestigation of the genus. Interestingly, we observed that two out of 11 strains obtained from cell culture collection show morphological and genetic properties different from expected for *Synechocystis* genus members.

Our results greatly expand the range of *Synechocystis* representatives with available genomic sequence data and demonstrate that *Synechocystis* genus currently consists of members that are genetically too different to form one single genus. The need for reconsideration of the genus, previously suggested by Komárek et al.<sup>24</sup> is thus additionally substantiated.

## 5. Acknowledgements

We wish to thank Dr. Bojan Sedmak from the National Institute of Biology for access to the epifluorescence microscope. This project has received funding from the European Union's Seventh Programme for research, technological development and demonstration under grant agreement No 308518, CyanoFactory. Parts of this work have also been supported by the Slovenian Research Agency within the research programme P1-0048a.

## 6. References

1. J. Komárek, *Algae* **2006**, *21*, 349–375. DOI:10.4490/ALGAE.2006.21.4.349
2. U. Nübel, F. Garcia-Pichel, G. Muyzer, *Appl. Environ. Microbiol.* **1997**, *63*, 3327–3332.
3. M. Gugger, C. Lyra, P. Henriksen, A. Couté, J. F. Humbert, K. Sivonen, *Int. J. System. Evol. Microbiol.* **2002**, *52*, 1867–1880.
4. N. Engene, R. C. Coates, W. H. Gerwick, *J. Phycol.* **2010**, *46*, 591–601. DOI:10.1111/j.1529-8817.2010.00840.x
5. E. M. Eckert, D. Fontaneto, M. Coci, C. Callieri, *Life* **2015**, *5*, 50–64. DOI:10.3390/life5010050
6. C. R. Woese, *Microbiol. Rev.* **1987**, *51*, 221–271.
7. S. Smit, J. Widmann, R. Knight, *Nucl. Acids Res.* **2007**, *35*, 3339–3354. DOI:10.1093/nar/gkm101
8. N. Engene, H. W. Gerwick, *Fottea* **2011**, *1*, 17–24. DOI:10.5507/fot.2011.003
9. G. E. Fox, J. D. Wisotzkey, P. Jurtschuk, Jr., *Int. J. Syst. Evol. Microbiol.* **1992**, *42*, 166–170.
10. N. Walworth, U. Pfreundt, W. C. Nelson, T. Mincer, J. F. Heidelberg, F. Fu, J. B. Waterbury, T. Glavina del Rio, L. Lynne Goodwin, N. C. Kyrpides, M. L. Land, T. Woyke, D. A. Hutchins, W. R. Hess, E. A. Webb, *Proc. Natl. Acad. Sci. U.S.A.* **2015**, *112*, 4251–4256. DOI:10.1073/pnas.1422332112
11. D. Honda, A. Yokota, J. Sugiyama, *J. Mol. Evol.* **1999**, *48*, 723–739. DOI:10.1007/PL00006517
12. P. S. Seo, A. Yokota, *J. Gen. Appl. Microbiol.* **2003**, *49*, 191–203. DOI:10.2323/jgam.49.191
13. V. Piccin-Santos, M. Mendes Brandão, M. Do Carmo Bittencourt-Oliveira, *J. Phycol.* **2014**, *4*, 736–743. DOI:10.1111/jpy.12204
14. I. Iteman, R. Rippka, N. Tandeau de Marsac, M. Herdman, *Microbiol.* **2002**, *148*, 481–496. DOI:10.1099/00221287-148-2-481
15. G. Rocap, D. L. Distel, J. B. Waterbury, S. W. Chisholm, *Appl. Environ. Microbiol.* **2002**, *68*, 1180–1191. DOI:10.1128/AEM.68.3.1180-1191.2002
16. T. A. Sarma, *Handbook of cyanobacteria*. CRC Press, Boca Raton, USA, **2013**. Also available from: <http://www.crcnetbase.com/isbn/978-1-4665-5941-7>, (accessed January 19, 2017)
17. W. Lu, E. H. Evans, S. M. McColl, V. A. Saunders, *FEMS Microbiol. Lett.* **1997**, *153*, 141–149. DOI:10.1111/j.1574-6968.1997.tb10475.x
18. I. Janse, M. Meima, W. E. A. Kardinaal, G. Zwart, *Appl. Environ. Microbiol.* **2003**, *69*, 6634–6643. DOI:10.1128/AEM.69.11.6634-6643.2003
19. W. E. A. A. Kardinaal, I. Janse, M. Kamst-van Agterveld, M. Meima, J. Snoek, L. R. Mur, J. Huisman, G. Zwart, P. M. Vissler, *Aquat. Microb. Ecol.* **2007**, *48*, 1–12. DOI:10.3354/ame048001
20. K. M. Orcutt, U. Rasmussen, E. A. Webb, J. B. Waterbury, K. Gundersen, B. Bergman, *Appl. Environ. Microbiol.* **2002**, *68*, 2236–2245. DOI:10.1128/AEM.68.5.2236-2245.2002
21. S. Becker, M. Fahrbach, P. Böger, A. Ernst, *Appl. Environ. Microbiol.* **2002**, *68*, 4486–4494. DOI:10.1128/AEM.68.9.4486-4494.2002
22. A. A. Shibl, L. R. Thompson, D. K. Ngugi, U. Stingl, *FEMS Microbiol. Lett.* **2014**, *356*, 118–126. DOI:10.1111/1574-6968.12490
23. N. D. Crosbie, M. Pöckl, T. Weisse, *Appl. Environ. Microbiol.* **2003**, *69*, 5716–5721. DOI:10.1128/AEM.69.9.5716-5721.2003
24. J. Komárek, J. Kaštovský, J. Mareš, J. R. Johansen, *Preslia* **2014**, *86*, 295–335.

25. J. Komárek, *Hydrobiol.* **2016**, *764*, 259–270.  
DOI:10.1007/s10750-015-2242-0
26. I. Iteman, R. Rippka, N. Tandeau de Marsac, M. Herdman, *Microbiol.* **2000**, *146*, 1275–1286.  
DOI:10.1099/00221287-146-6-1275
27. S. F. Altschul, W. Gish, W. Miller, E. W. Myers, D. J. Lipman, *J. Mol. Biol.* **1990**, *215*, 403–410.  
DOI:10.1016/S0022-2836(05)80360-2
28. W. Li, A. Cowley, M. Uludag, T. Gur, H. McWilliam, S. Squizzato, Y. M. Park, N. Buso, R. Lopez, *Nucl. Acids Res.* **2015**, *43*(W1), W580–584. DOI:10.1093/nar/gkv279
29. K. Tamura, G. Stecher, D. Peterson, A. Filipski, S. Kumar, *Mol. Biol. Evol.* **2013**, *30*, 2725–2729.  
DOI:10.1093/molbev/mst197
30. J. R. Cole, Q. Wang, J. A. Fish, B. Chai, D. M. McGarrell, Y. Sun, C. T. Brown, A. Porras-Alfaro, C. R. Kuske, J. M. Tiedje, *Nucl. Acids Res.* **2014**, *42*(D1), 633–642.  
DOI:10.1093/nar/gkt1244
31. P. Schattner, A. N. Brooks, T. M. Lowe, *Nucl. Acids Res.* **2005**, *33*, W686–9. DOI:10.1093/nar/gki366
32. J. Korelusová, J. Kaštovský, J. Komárek, *J. Phycol.* **2009**, *45*, 928–937. DOI:10.1111/j.1529-8817.2009.00701.x
33. J. Komárek, K. Anagnostidis, in: H. Ettl, G. Gärtner, H. Heynig, D. Mollenhauer (Eds.), *Süßwasserflora von Mitteleuropa 19/1*, Gustav Fischer, Jena, Germany, **1998**.
34. I. Moro, N. Rascio, N. La Rocca, M. Di Bella, C. Andreoli, *Algal. Stud.* **2007**, *123*, 1–15.  
DOI:10.1127/1864-1318/2007/0123-0001
35. R. W. Castenholz, J. B. Waterbury, in: J. T. Staley, M. P. Bryant, N. Pfennig, J. G. Holt (Eds.): *Bergey's manual of systematic bacteriology*, Williams and Wilkins, Baltimore, USA, **1989**, pp. 1710–1789.
36. F. von Wintzingerode, U. B. Göbel, E. Stackebrandt, *FEMS Microbiol. Rev.* **1997**, *21*, 213–29.  
DOI:10.1111/j.1574-6976.1997.tb00351.x
37. W. Laloui, K. A. Palinska, R. Rippka, F. Partensky, N. Tandeau de Marsac, M. Herdman, I. Iteman, *Microbiol.* **2002**, *148*, 453–465. DOI:10.1099/00221287-148-2-453
38. P. M. Shih, D. Wu, A. Latifi, S. D. Axen, D. P. Fewer, E. Talla, A. Calteau, F. Cai, N. Tandeau de Marsac, R. Rippka, M. Herdman, K. Sivonen, T. Coursin, T. Laurent, L. Goodwin, M. Nolan, K. W. Davenport, C. S. Han, E. M. Rubin, J. A. Eisen, T. Woyke, M. Gugger, C. A. Kerfeld, *Proc. Natl. Acad. Sci. U.S.A.* **2013**, *110*, 1053–1058.  
DOI:10.1073/pnas.1217107110
39. M. Kopf, S. Klähn, B. Voss, K. Stuber, B. Huettel, R. Reinhardt, W. R. Hess, *Genome Announc.* **2014**, *2*, e00757–14.  
DOI:10.1128/genomeA.00757-14
40. T. Kaneko, S. Sato, H. Kotani, A. Tanaka, E. Asamizu, Y. Nakamura, N. Miyajima, M. Hirotsawa, M. Sugiura, S. Sasamoto, T. Kimura, T. Hosouchi, A. Matsuno, A. Muraki, N. Nakazaki, K. Naruo, S. Okumura, S. Shimpo, C. Takeuchi, T. Wada, A. Watanabe, M. Yamada, M. Yasuda, S. Tabata, *DNA Res.* **1996**, *3*, 109–136. DOI:10.1093/dnares/3.3.109
41. O. Zhaxybayeva, J. P. Gogarten, R. L. Charlebois, W. F. Doolittle, R. T. Papke, *Genome Res.* **2006**, *16*, 1099–1108.  
DOI:10.1101/gr.5322306
42. S. Yerrapraganda, J. L. Siefert, G. E. Fox, *Methods Mol. Biol.* **2009**, *532*, 339–366. DOI:10.1007/978-1-60327-853-9\_20
43. P. Rajaniemi-Wacklin, A. Rantala, M. A. Mugnai, S. Turichia, S. Ventura, J. Komárková, L. Lepistö, K. Sivonen, *J. Phycol.* **2006**, *42*, 226–232.  
DOI:10.1111/j.1529-8817.2006.00179.x
44. J. Komárek, K. Anagnostidis, *Algal. Stud.* **1989**, *56*, 247–345.
45. F. Garcia-Pichel, L. Prufert-Bebout, G. Muyzer, *Appl. Environ. Microbiol.* **1996**, *62*, 3284–3291.
46. S. Gkelis, P. Rajaniemi, E. Vardaka, M. Moustaka-Gouni, T. Tanaras, K. Sivonen, *Microb. Ecol.* **2005**, *49*, 176–182.  
DOI:10.1007/s00248-003-2030-7
47. R. Hoshina, *BMC Res. Notes* **2014**, *7*, 592.  
DOI:10.1186/1756-0500-7-592
48. M. Kopf, S. Klähn, N. Pade, C. Weingärtner, M. Hagemann, B. Voss, W. R. Hess, *DNA Res.* **2014**, *21*, 255–266.  
DOI:10.1093/dnares/dst055
49. K. Zerulla, K. Ludt, J. Soppa, *Microbiol.* **2016**, *162*, 730–739.  
DOI:10.1099/mic.0.000264

## Povzetek

Cianobakterije so pomembna skupina mikroorganizmov z zelo raznoliko morfolgijo, na podlagi katere lahko fenotipsko razlikujemo med taksonomskimi linijami cianobakterij. Vendar je morfološko razlikovanje zanesljivo predvsem na ravni rodu, na ravni vrste ali seva pa pogosto ne. Osredotočili smo se na rod enoceličnih cianobakterij *Synechocystis*, ki vključuje tudi modelni cianobakterijski sev PCC 6803. Določili smo zaporedja variabilnega dela genomske regije rRNA 16 S in regije ITS med zapisoma za rRNA 16 S in 23 S za 11 predstavnikov rodu *Synechocystis*. Zaporedja dveh od enajstih analiziranih sevov iz zbirke kultur so se pomembno razlikovala od zaporedij tipičnih predstavnikov rodu *Synechocystis*. Opaženo razlikovanje na molekularni ravni smo potrdili tudi z mikroskopijo. Za ostale seve smo ugotovili, da sta obe genomski regiji, ki se sicer že uporabljata v taksonomiji bakterij, ustrezni za razlikovanje med analiziranimi vrstami, pri čemer regija ITS omogoča tudi zanesljivo razlikovanje med sevi iz rodu *Synechocystis*.

Scientific paper

# Reaction Monitoring by Means of Multivariate Data Analysis of Near-Infrared and Raman Spectra

Dardan Hetemi<sup>1,2\*</sup> and Steve Janagap<sup>1,3</sup><sup>1</sup> Department of Chemistry, University of Bergen, Allégaten 41, N-5007 Bergen, Norway.<sup>2</sup> Pharmacy Department, Medical Faculty, University of Prishtina "Hasan Prishtina", Rr. "Dëshmorët e Kombit" p.n., 10000 Prishtina, Kosovo.<sup>3</sup> Department of Chemistry, College of Arts and Sciences, University of the Philippines Visayas, 5023 Miagao, Iloilo, Philippines.

\* Corresponding author: E-mail: dardan.hetemi@uni-pr.edu

Received: 06-02-2017

## Abstract

An efficient, versatile and non-destructive in situ method in reaction monitoring using vibrational spectroscopy is described. A Suzuki cross-coupling reaction was monitored in which the substrate 1-iodo-2-nitrobenzene reacted with the electrophile phenylboronic acid to form the product 2-nitrobiphenyl. To hasten the reaction, palladium(II) acetate and potassium carbonate were added to serve as catalyst and to promote transmetalation, respectively. This reaction was monitored using near-infrared and Raman spectroscopy. The recorded data was subjected to multivariate analysis such as principal component analysis in order to detect spectral changes due to the formation of the product. To confirm the presence of the desired product, offline analyses were performed using gas chromatography-mass spectrometry and nuclear magnetic resonance spectroscopy. The results demonstrate how Raman spectroscopy is able to detect the formation of the product in real time, whereas near-infrared spectroscopy fails to do so.

**Keywords:** Raman spectroscopy, near-infrared spectroscopy, reaction monitoring, Suzuki cross-coupling, multivariate data analysis

## 1. Introduction

Organic synthesis enables the creation of diverse chemical structures of complex architecture in the laboratory. New strategies to develop syntheses, optimize reaction outcomes, and investigate reaction mechanisms are important. One of the interesting reactions to synthesize substituted biphenyls<sup>1</sup> involves the Suzuki cross-coupling reaction, a protocol of which has been disclosed elsewhere.<sup>2</sup> The carbon-carbon bond construction method<sup>3,4,5,6</sup> in organic synthesis has allowed chemists to assemble complex molecular frameworks to prepare numerous natural products,<sup>7</sup> drug precursors,<sup>8</sup> biological compounds,<sup>9</sup> organic products<sup>10</sup> and herbicides.<sup>11</sup> Lately, the conditions developed for the cross-coupling reaction have many desirable features for large scale syntheses and are persuasively used in the industrial synthesis of pharmaceutical and chemical products. In daily laboratory work, time together with accuracy plays a crucial role in monitoring techniques particularly in in situ reactions.

Systems requiring long reaction times are frequently experienced in organic synthesis. For such reactions, in situ reaction monitoring techniques coupled with multivariate analysis serve as an excellent approach for determining reaction progress without interruption. Thus, on-line vibrational spectroscopy has become an increasingly useful tool for research and process development.<sup>12,13,14</sup>

Near-infrared (NIR) and Raman spectroscopy are suitable instrumental techniques in monitoring the formation of a desired product in real time. In comparison to gas chromatography-mass spectrometry (GC-MS) analysis which requires considerable time to provide a result, the NIR and Raman spectroscopic techniques provide an immediate response that considerably shortens analysis time. By these techniques, it is possible to obtain a huge amount of information about the reaction with minimum effort and time.<sup>15</sup> Another advantage of NIR and Raman spectroscopy in reaction monitoring is that they can provide information on the appearance of reaction intermediates.

They also give information about whether the reaction proceeds in the right direction. These advantages make NIR and Raman attractive techniques in pharmaceutical and industrial production.

The usefulness of the above-mentioned vibrational spectroscopic techniques in monitoring in situ reactions is much improved if they are coupled with proper data analysis. Chemometrics involves processing chemical data using mathematical and statistical methods in order to extract useful information. Principal components analysis (PCA)<sup>16</sup> is applied in order to extract chemical information from the spectra. Spectral data collected by NIR and Raman spectroscopy are complex and normally possesses broad overlapping absorption bands. A single NIR spectrum contains absorptions at many wavelengths that are measured at different times and the vast amount of spectrum generated by the instrument requires chemometric tools for analysis. Often, the measured absorbances at various wavelengths are highly correlated (they are not independent of each other) and this multicollinearity results to poor prediction. PCA is applied to significantly reduce the multidimensionality of the data while retaining most of the information where it decomposes the originally correlated variables to a new limited set of latent variables called principal components. These principal components represent the common variations in the data set where the first principal component accounts for most variations in the data; the second principal component explains the second greatest variations and so on. With PCA, data size is reduced and data overfitting is avoided.

In this study, a Suzuki cross-coupling reaction was investigated<sup>1</sup> and monitored using NIR and Raman spectroscopy. The model reaction involved the palladium-catalyzed Suzuki cross-coupling of 1-iodo-2-nitrobenzene and phenylboronic acid to produce 2-nitrobiphenyl. The reaction protocol involves addition of a catalyst (palladium(II)

acetate) and a base (potassium carbonate) to promote transmetalation. **Scheme 1** shows the synthesis of 2-nitrobiphenyl.

A review of literature revealed vast amount of materials concerning the Suzuki cross-coupling reaction<sup>4,5,17,18</sup> but only few reports<sup>19,20</sup> describe the use of NIR and Raman with the reaction. To the best of our knowledge, no report on combining NIR or Raman spectroscopy and multivariate analysis in monitoring Suzuki cross-coupling reactions have been published before. Thus, this study presents a novel monitoring of a Suzuki cross-coupling reaction through vibrational spectroscopic methods and multivariate data analysis.

As the Suzuki cross-coupling reactions lead to the formation of by-products as the reaction proceeds, the reaction time and other experimental conditions need to be monitored and controlled. Additionally, the monitoring should provide an immediate estimate of the progress of the ongoing reactions. This is important because Suzuki cross-coupling reactions give very low yield. The reaction of 2-chlorophenylboronic acid with 1-iodo-2-nitrobenzene has been reported as giving as little as 2% product yield<sup>1</sup> under some conditions.

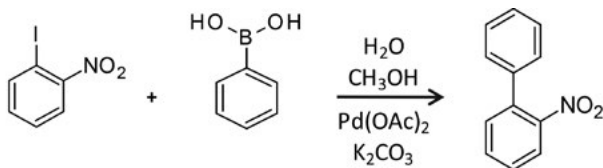
## 2. Experimental Section

### 2.1. Chemicals

1-Iodo-2-nitrobenzene ( $\geq 97\%$ ), phenylboronic acid ( $\geq 99\%$ ), methanol ( $\geq 99.9\%$ ), dichloromethane ( $\geq 99.9\%$ ) and potassium carbonate ( $\geq 99\%$ ) were purchased from Sigma-Aldrich (Missouri, USA). Palladium(II) acetate ( $\geq 98\%$ ) was purchased from Fluka (Buchs, Switzerland). All products were used as received without further purification.

### 2.2. Reaction Procedure

The first step of the boscalid synthesis was chosen as a model for the Suzuki cross-coupling reaction. Instead of using 1-chloro-2-nitrobenzene as substrate for the synthesis of boscalid, an organohalide compound 1-iodo-2-nitrobenzene was used. This is due to the higher activity of ArI compared with ArCl in oxidative addition ( $\text{ArI} \gg \text{ArCl}$ )



**Scheme 1.** Synthesis of 2-nitrobiphenyl.

**Table 1.** Temperature, concentration and sampling times at each experiment run.

No. exp.	T [°C]	C [mmol/mL]	Samples were withdrawn in specific time [min]						
			Sample 1	Sample 2	Sample 3	Sample 4	Sample 5	Sample 6	
1	23	0.167	60						
2	50	0.167	60						
3	60	0.167	5	10	15	30	45	60	
4	50	0.250	30	60					
1	60	0.250	5	10	15	30	45	60	
2	65	0.250	5	10	15	30	45	60	

Br>>ArCl).<sup>21,22</sup> The procedure for the synthesis of 2-nitrobiphenyl has been published elsewhere.<sup>1</sup> Briefly, methanol (5 mL) and water (1 mL) were mixed in a round-bottom flask. Potassium carbonate (0.414 g, 3 mmol), palladium(II) acetate (0.006 g, 0.03 mmol), 1-iodo-2-nitrobenzene (0.362 g, 1.5 mmol) and phenylboronic acid (0.177 g, 1.5 mmol) were then added to make the concentration 0.250 mmol/mL with respect to substrate (1-iodo-2-nitrobenzene). The solution was flashed with N<sub>2</sub> gas and covered with aluminum foil. The reaction mixture was heated at 50 or 60 °C under stirring. The reaction was monitored online with NIR and Raman methods. Samples were withdrawn at specific times without interrupting the reaction (as shown in **Table 1**), filtered through cotton and silica gel with dichloromethane and analyzed by GC-MS.

### 2. 3. Workup Procedure of Product

Water (30 mL) was added to a crude product obtained after evaporation of methanol under reduced pressure. The solution was extracted three times with dichloromethane using 30 mL every extraction. The resulting organic solution was washed with saturated aqueous solution of sodium chloride (30 mL). The organic solution was evaporated under reduced pressure and the target product 2-nitrobiphenyl was obtained as dark yellowish oil and analyzed by NMR.

### 2. 4. Instrumentation

A Perstorp NIR Systems 6500 (Maryland, USA) was used for recording the NIR spectra. The NIR spectra of the reaction mixture were obtained at specific time intervals using the fiber optic probe and were recorded from 1100–2500 nm range at 2 nm data interval and using 32 scans per spectrum. The path length was set to 0.5 mm using a 0.25 mm feeler gauge. An average of about 20 s was required to obtain one spectrum. Background and sample spectra were collected using the same parameter settings. The instrument control software used was Vision (FOSS NIRSystems, Inc., MD). The spectrum data was exported as an ASCII file. MATLAB 7.4 (The MathWorks Inc., Natick, MA) was used for multivariate analysis. The software was run on a Microsoft Windows 7 Professional 2009 operating system (Microsoft Corporation, WA, USA).

Raman scattering spectra were recorded on a RamanRxn1 analyzer (Kaiser Optical Systems, Inc., USA). Measurements were made with an immersion BallProbe<sup>®23</sup> connected to the instrument via a fiber optic bundle. The laser wavelength and power were set to 785 nm and 100 mW, respectively. The spectral range was from 0–3800 cm<sup>-1</sup> and spectral acquisition setting parameters were set (time of exposure was fixed to 2 s; number of accumulations was set to two).

HoloGram 4.1 (Kaiser Optical Systems Inc., Michigan, USA) was used as the instrument control software. The recorded spectra were exported using HoloReact 2.0 (Kaiser Optical Systems Inc., Michigan, USA) to MATLAB. The Raman spectra were combined into one data matrix ( $D_{i \times j}$ ) with dimensions  $i \times j$ , where ( $i$ ) represents spectra and ( $j$ ) represents frequencies.

The GC-MS used was HP 5890 II gas chromatograph coupled with HP 5971 mass spectrometer. The capillary column used was fused silica (30 m × 0.2 mm I.D.) coated with Chrompack, CP-Sil 8 CB low bleed/MS (0.25 μm film thickness). The GC oven temperature was programmed as follows: start temperature was 50 °C ramped to 70 °C at 5 °C/min then increased up to 300 °C at 25 °C/min. Direct on-column injection was used, and the injector port temperature was 250 °C. Helium was used as carrier gas. Xcalibur 1.2 (Thermo Fisher Scientific Inc.) was used for instrument control and data analysis.

NMR spectra were recorded on a Bruker BioSpin DPX400 (<sup>1</sup>H NMR: 400.13 MHz, <sup>13</sup>C NMR: 100.61 MHz) spectrometer. Deuterated chloroform (CDCl<sub>3</sub>) was used as solvent for the preparation of the samples and the internal standard. The chemical shifts were expressed in ppm values relative to tetramethylsilane (TMS). Multiplicities were reported using the following abbreviations: s (singlet), d (doublet), t (triplet), q (quartet), dd (double doublet) and m (multiplet). The spectra were recorded at room temperature and the data were processed with MestReNova 5.2 (Santiago de Compostela, Spain).

## 3. Results and Discussion

The reaction being monitored in this study is the synthesis of 2-nitrobiphenyl from 1-iodo-2-nitrobenzene and phenylboronic acid in the presence of palladium(II) acetate and potassium carbonate (see **Scheme 1**) via the Suzuki cross-coupling mechanism. To determine the best conditions that would give a high product yield, several factors were tested: amount of substrate (1-iodo-2-nitrobenzene), reaction temperature and time. It is therefore important to perform an optimization experiment by varying the levels of the variables and checking the yield at different time intervals as the reaction proceeds. In situ monitoring of the reaction was carried out by using NIR and Raman spectroscopy.

### 3. 1. Reaction Optimization

Similar results were obtained in the synthesis of 2-nitrobiphenyl following the protocol described in a previous study,<sup>1</sup> where 99% yield was achieved after 90 min reaction time at 20 °C. With the aim to shorten the reaction time (to 60 min) but still obtaining a high yield, temperatures higher than 20 °C were tested. Since reaction temperature and substrate concentration (1-iodo-2-nitrobenzene) are

**Table 2.** Experimental set-up employed in the optimization procedure.

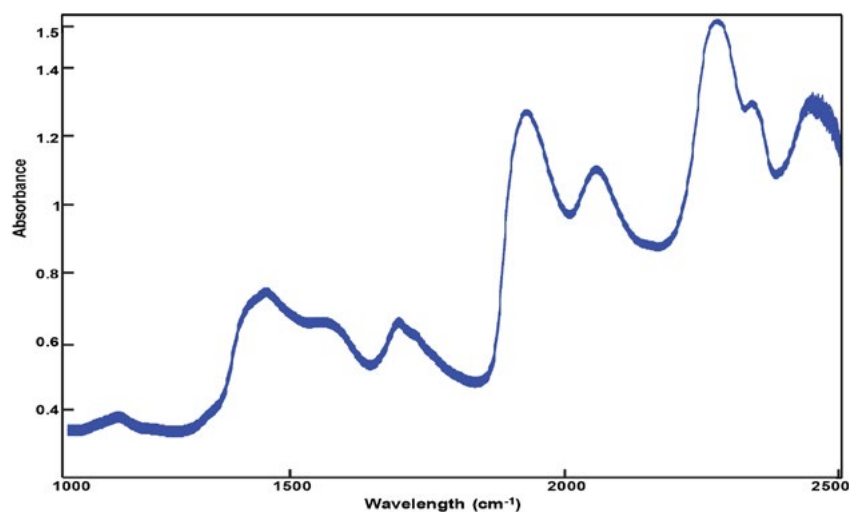
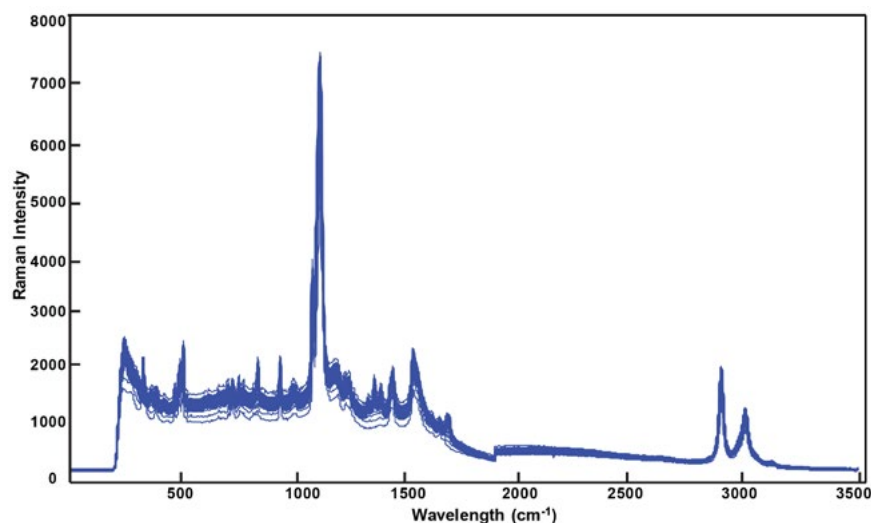
Exp. no.	T [°C]	C [mmol/mL]	Time [min]	Yield by GC-MS [%]
1	23	0.167	60	4.0
2	50	0.167	60	35.3
3	60	0.167	60	71.1
4	50	0.250	60	49.2
5	60	0.250	60	90.0
6	65	0.250	60	99.7

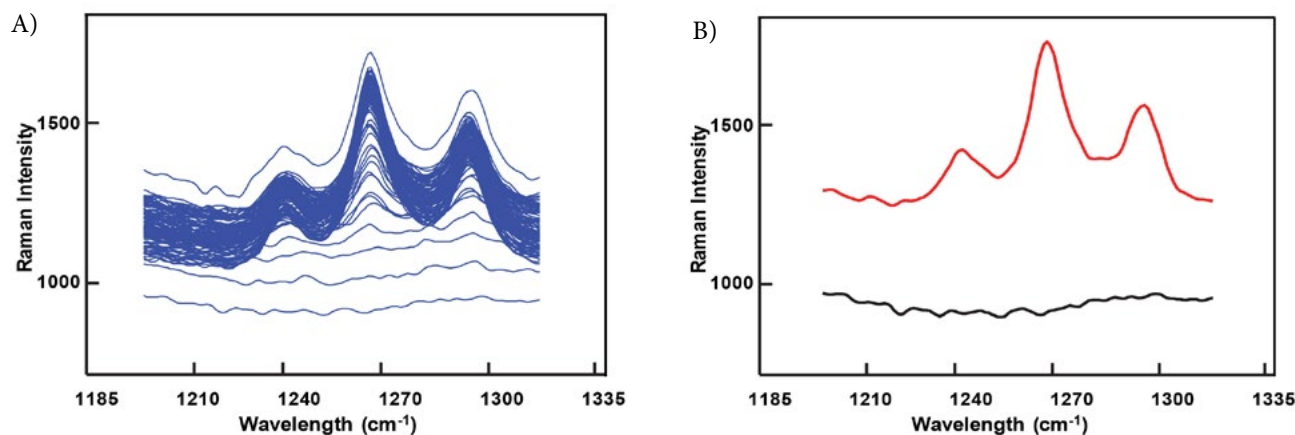
critical factors affecting the yield, several experiments were conducted by varying these factors, assigning low and high values. A summary of the optimization experiments is presented in **Table 2**. Results show consistently that the yield of the reaction increases as temperature is

increased. The higher the temperature, the higher is the yield. When the concentration of the substrate is increased from 0.167 to 0.250 mmol/mL, the same trend is observed: the greater the concentration of the substrate, the higher is the yield. This suggests that the substrate is stoichiometrically converted to the product, 2-nitrobiphenyl. The reaction carried out at 65 °C and 0.250 mmol/mL substrate concentration, afforded the highest reaction yield (99.7%). This optimized reaction was monitored by means of fiber optical NIR and Raman spectroscopy (**Figures 1** and **2**).

### 3. 2. In Situ Vibrational Spectroscopy Monitoring

Visual inspection of the NIR spectra (**Figure 1**) of the samples monitored from the start of the reaction until the end shows no noticeable spectrum profile changes to distinguish the appearance of the product 2-nitrobiphenyl.

**Figure 1.** A series of NIR spectra recorded of a Suzuki cross-coupling reaction that was conducted at reaction temperature of 65 °C.**Figure 2.** A series of Raman spectra recorded of a Suzuki cross-coupling reaction that was conducted at reaction temperature of 65 °C.



**Figure 3.** A) Magnified view of a specific region in the Raman spectra; B) The black and red spectra correspond to the first and last recorded spectra, respectively, as reaction proceeds.

By using principal component analysis (PCA), the data were pre-processed by mean-centering and first derivative method using 4<sup>th</sup> order polynomial fit.<sup>24</sup> Mean-centering and use of derivatives are pretreatment techniques to correct systematic variations in the NIR raw data between samples. The variations may be due to nonhomogeneous reaction mixing, sample density gradient, sample viscosity, and other factors that could affect the integrity of the samples during in situ sampling. These lead to light scattering effects and result in baseline shifts and scaling variations. Mean-centering and first derivative methods were selected as optimal pretreatments as they give the lowest statistical errors in preliminary data analysis. PCA was performed in the pretreated spectra to reduce the dimension of NIR spectra matrix for processing and handling multicollinearity. Emerged peak were analysed for the substrates and product (data not shown) and there were no significant profile changes in the spectra as reaction proceeds. This shows that NIR method is not sensitive in detecting formation of the product. On the other hand, the Raman spectra (**Figure 2**) show characteristic stretching vibrations of the biphenyl C-C bridge in the region 1200–1320  $\text{cm}^{-1}$ .<sup>25,26,27</sup> Spectral changes in this region signal conversion of the reactants (1-iodo-2-nitrobenzene and phenylboronic acid) into the desired product (2-nitrobiphenyl). To see more clearly, the region is magnified and presented in **Figure 3A**.

In **Figure 3B**, the black spectrum corresponds to the initial condition when the substrate was present in the reaction, while the red spectrum represents the final recorded spectrum, which shows the presence of the target molecule in the reaction mixture. The emergence of the peaks at the specific region (1200–1320  $\text{cm}^{-1}$ ) in the last spectrum shows the emergence of the desired product (C-C bridge stretch of biphenyl). Further offline analysis by GC-MS and NMR confirmed that the spectral changes could be attributed to the formation of the product 2-nitrobiphenyl via the Suzuki cross-coupling reaction. The GC-MS

chromatogram and NMR spectrum are presented in Supporting Information.

### 3. 3. Multivariate Data Analysis

Principal component analysis (PCA) is an exploratory technique that highlights the differences in the spectra collected and gives a simple visual idea as to the relationship between the spectra. By using PCA, we have analysed the emerged peak for the substrates and product (data not shown). No significant change that could be attributed to the formation of the product was observed. In the contrary, good results were obtained for the specific region (1200–1320  $\text{cm}^{-1}$ ) in the Raman spectra treated with PCA where the data matrix (120 × 120) was pre-processed using the same techniques as for NIR data. The first principal component (PC1) explains 87.91% of the total variance and from the sample and score plot (**Figure 4**), it is possible to establish a time-concentration profile.

**Figure 4** shows that the concentration of the product increases proportionally with time. This increase continues until the reaction is complete. During the course of the reaction, a series of spectra were recorded every 30 s so the sample 120 corresponds to the time of 60 min, the end of reaction monitoring (99.7% yield by GC-MS). The curve shows that the reaction has almost finished after 30 min (corresponding to sample 60). This is in full agreement with the offline measurements of GC-MS that shows the yield of 98.3% for 30 min (**Table 3**). Also, in the beginning of the reaction (blue circle in **Figure 4**) we do not have the product yet so the black curve is not increasing. All offline measurements for GC-MS can be seen in the **Table 3**.

As mentioned earlier, PCA was also performed in the NIR data and results show that no significant findings can be established from the collected data. NIR instrumentation is inadequate for monitoring the reaction due to low sensitivity of detection. This study shows that Ra-



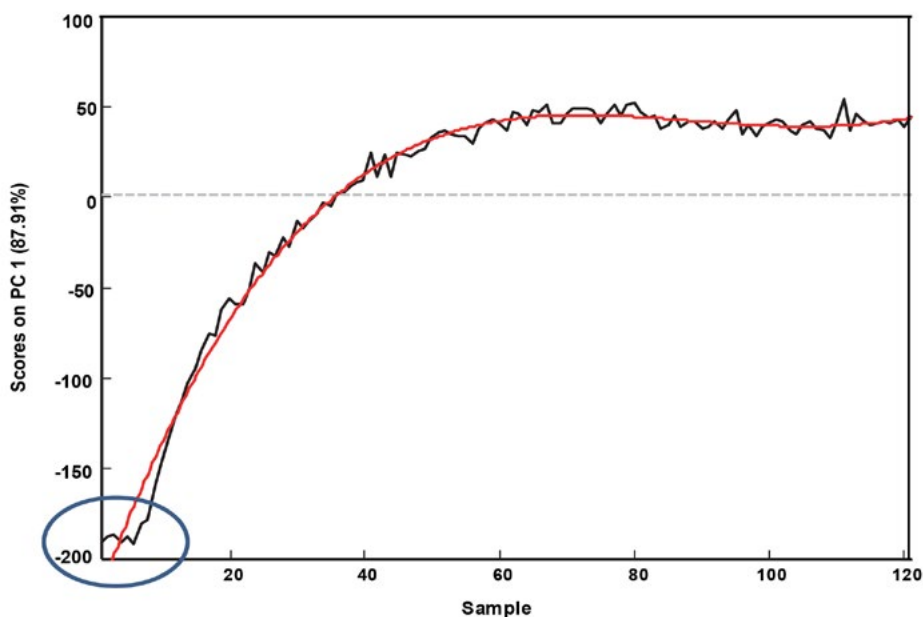


Figure 4. Samples and scores plot of the data in 1200–1320  $\text{cm}^{-1}$  region. The red line shows the 4<sup>th</sup> degree polynomial fit.

Table 3. The time of sample withdrawn and the yield measured by GC-MS.

Time [min]	Yield by GC-MS [%]
0	0
5	59.5
10	79.8
15	87.9
30	98.3
45	99.6
60	99.7

man spectroscopy is more sensitive and is the appropriate technique over NIR in reaction monitoring.

## 4. Conclusions

Monitoring of reactions using vibrational spectroscopy coupled with multivariate data analysis finds very important applications nowadays in pharmaceutical and chemical industries. The possibility of online detection of a desired product in an ongoing chemical reaction without system interruption is the main advantage why these techniques in combination with PCA have wide use in the industry. Monitoring of reactions in industry commonly uses the NIR method but this present paper demonstrated that the Raman method is more sensitive and effective and thus, suitable for reaction monitoring.

The power of multivariate technique such as PCA in combination with the Raman instrumentation has been shown. The Raman results have been validated by

offline techniques such as GC-MS and NMR. Results of online and offline techniques confirm the detection of the desired product making feasible the monitoring of a Suzuki cross-coupling reaction by real time Raman spectroscopy.

## 5. Acknowledgments

European Commission (Erasmus Mundus Scholarships) and University of Bergen are acknowledged for funding the project. The former is acknowledged for financial support.

## 6. Supporting Information

GC-MS of 2-nitrobiphenyl; <sup>1</sup>H NMR of 2-nitrobiphenyl.

## 7. References

1. R. R. Gonzale, L. Liguori, A. M. Carrillo, H.-R. Bjørsvik, *J. Org. Chem.* **2005**, 70, 9591–9594. DOI:10.1021/jo051589t
2. N. Miyura, K. Yamada, A. Suzuki, *Tetrahedron Lett.* **1979**, 20, 3437–3440. DOI:10.1016/S0040-4039(01)95429-2
3. E. Negishi, *Acc. Chem. Res.* **1982**, 15, 340–348. DOI:10.1021/ar00083a001
4. A. Suzuki, *J. Organomet. Chem.* **1999**, 576, 147–168. DOI:10.1016/S0022-328X(98)01055-9
5. N. Miyaura, *Chem. Rev.* **1995**, 95, 2457–2483. DOI:10.1021/cr00039a007

6. L. Zhao, F. Derridj, S. Djebbar, Ch. Bruneau, H. Doucet, *Tetrahedron Lett.* **2015**, 56, 4354–4358. DOI:10.1016/j.tetlet.2015.05.082
7. S. J. Danishefsky, J. J. Masters, W. B. Yound, J. T. Link, L. B. Snyder, Th. V. Magee, D. K. Jung, R. C. A. Isaacs, W. G. Bornmann, Ch. A. Alaimo, C. A. Coburn, M. J. Di Grandi, *J. Am. Chem. Soc.* **1996**, 118, 2843–2859. DOI:10.1021/ja952692a
8. H. A. Saader, I. M. Mosleh, M. M. El-Abadelah, *Molecules*, **2009**, 14, 2758–1767. DOI:10.3390/molecules14082758
9. X. Zheng, W. Meng, F. Qing, *Tetrahedron Lett.* **2004**, 45, 8083–8085. DOI:10.1016/j.tetlet.2004.08.180
10. A. Ganesan, *Drug Discovery Today*, **2002**, 7, 47–55. DOI:10.1016/S1359-6446(01)02087-6
11. H. H. Szmant, *Organic building blocks of the chemical industry*. Wiley: New York, **1989**, Chapter 4.
12. I. Marziano, D. C. A. Sharp, P. J. Dunn, P. A. Hailey, *Org. Process Res. Dev.* **2000**, 4, 357–361. DOI:10.1021/op000030m
13. K. Hossain, H. Y. Cho, K. J. Kim, J. W. Choi, *Biosens. Bioelectron.* **2015**, 71, 300–305. DOI:10.1016/j.bios.2015.04.053
14. Y. Wu, Y. Jin, Y. Li, D. Sun, X. Liu, Y. Chen, *Vib. Spectrosc.* **2012**, 58, 109–118. DOI:10.1016/j.vibspec.2011.10.006
15. W. L. Guo, Y. P. Du, Y. C. Zhou, S. Yang, J. H. Lu, H. Y. Zhao, Y. Wang, L. R. Teng, *World J. Microbiol. Biotechnol.* **2012**, 28, 993–1002. DOI:10.1007/s11274-011-0897-x
16. I. T. Jolliffe, *Principal Component Analysis*; Springer: New York, **2002**.
17. S. D. Dreher, S.-E. Lim, D. L. Sandrock, G. A. Molander, *J. Org. Chem.*, **2009**, 74, 3626–3631. DOI:10.1021/jo900152n
18. M. P. Lorenzo, *J. Phys. Chem. Lett.* **2012**, 3, 167–174. DOI:10.1021/jz2013984
19. G.; Rothenberg, S. C. Cruz, G. P. F. van Strijdonck, H. C. J. H. Hoefsloot, *Adv. Synth. Catal.* **2004**, 346, 347–473.
20. N. E. Leadbeater, R. J. Smith, *Org. Lett.* **2006**, 8, 4589–4591. DOI:10.1021/ol061803f
21. A. F. Littke, Ch. Dai, G. C. Fu, *J. Am. Chem. Soc.* **2000**, 122, 4020–4028. DOI:10.1021/ja0002058
22. H. Kurosawa, A. Yamamoto, (Ed.): *Fundamentals of Molecular Catalysis, Current Method in Inorganic Chemistry*; Vol.3; Elsevier Science, Tokyo, Japan **2003**, pp.115–123.
23. <http://ballprobe.com/index.html> (accessed: March 14, 2016).
24. A. Savitzky, M. J. E. Golay, *Anal. Chem.*, **1964**, 38, 1627–1639. DOI:10.1021/ac60214a047
25. J. S. Gromiuk, H. Gluchowska, B. Tarsiuk, L. Mazur, Z. Rzacynska, *J. Mol. Struct.* **2014**, 1070, 110–116. DOI:10.1016/j.molstruc.2014.04.030
25. K. C. Bantz, Ch. L. Haynes, *Vib. Spectrosc.* **2009**, 50, 29–35. DOI:10.1016/j.vibspec.2008.07.006
27. G. Socrates, *Infrared and Raman Characteristic Group Frequencies: Tables and Charts*, 3rd ed., Wiley: New York, **2001**.

## Povzetek

Opisujemo učinkovito, vsestransko in neporušno »in situ« metodo za spremljanje reakcij z uporabo vibracijske spektroskopije. Spremljali smo Suzukijevo reakcijo, pri kateri je substrat 1-jodo-2-nitrobenzen reagiral z elektrofilom fenilborovo kislino in tvoril produkt 2-nitrobifenil. Da bi pospešili reakcijo, smo dodali paladijev(II) acetat kot katalizator in kalijev karbonat, ki promovira reakcijo transmetalacije. To reakcijo smo spremljali z bližnjo infrardečo in z Ramansko spektroskopijo. Podatke smo obdelali z multivariantno analizo, kot je metoda glavnih osi (PCA), da bi ugotovili, do katerih sprememb v spektrih pride zaradi nastanka produkta. Za potrditev prisotnosti želenega produkta smo izvajali tudi »off-line« analizo s plinsko kromatografijo-masno spektrometrijo in z jedrsko magnetno resonančno spektroskopijo. Rezultati pokažejo, da z Ramansko spektroskopijo lahko zaznamo tvorbo produkta v realnem času, medtem ko z bližnjo infrardečo spektroskopijo to ni možno.

Scientific paper

# Synthesis, Crystal Structures, Molecular Docking and MAO-B Inhibitory Activity of Transition Metal Complexes Derived from 2-(4-(Pyridin-2-yl)piperazin-1-yl)acetic Acid

Yan-Jie Ren, Jin-Long Zhu, Li-Xin Zhang, Yin-Xiang Xu  
and Shao-Song Qian\*

School of Life Sciences, Shandong University of Technology, Zibo 255049, P. R. China

\* Corresponding author: E-mail: sdutqianss@163.com

Tel.: 0086-533-2780271; Fax: 0086-533-2781329.

Received: 22-02-2017

## Abstract

Three new complexes derived from 2-(4-(pyridin-2-yl)piperazin-1-yl)acetic acid (**HL**),  $[M(L)_2(H_2O)_2]$  where  $M = Cu^{II}$  (**1**),  $Zn^{II}$  (**2**) and  $Cd^{II}$  (**3**), have been synthesized and characterized by IR spectroscopy, elemental analysis and X-ray crystallography. The inhibitory activity of these three complexes against MAO-B was tested *in vitro*, and the molecular docking experiments were also carried out to rationalize their binding models. Both the experimental and docking simulation results indicated that complex **1** has the best inhibitory activity with  $IC_{50}$  value being  $6.5 \pm 0.31 \mu M$ .

**Keywords:** Metal complexes, Crystal Structure, MAO-B inhibitor; Molecular Docking

## 1. Introduction

Monoamine oxidases (MAOs, EC 1.4.3.4) are well known enzymes bound to the outer membrane of mitochondria through a C-terminal transmembrane helix and catalyze the oxidative deamination of monoamine neurotransmitters in the central nervous system.<sup>1–3</sup> MAOs occur in two forms designated as MAO-A and MAO-B, which have different substrate preference and inhibitor specificity.<sup>4,5</sup>

An increase of the dopamine levels as well as a neuroprotective effect can be observed following the inhibition of MAO-B.<sup>6</sup> Therefore, MAO-B inhibitors can be used to treat the neurodegenerative disorders such as Alzheimer's disease (AD) and Parkinson's disease (PD).<sup>7–9</sup> Kinds of heterocyclic scaffolds such as chalcone,<sup>10</sup> coumarin,<sup>11</sup> pyrazoline<sup>12</sup> and oxadiazole<sup>13</sup> derivatives have been demonstrated as MAO-B inhibitors. Recently, pyridoxine-resveratrol hybrids Mannich base derivatives have been reported as MAO-B inhibitors by Yang et al.<sup>14</sup>

As mentioned above, most reported MAO-B inhibitors are organic heterocyclic molecules while MAO-B inhibitors based on metal complexes are seldom discussed. In our earlier work, we investigated the urease inhibitors

and the MAO-B inhibitory activity of metal complexes.<sup>15,16</sup> The inhibitory activities of these bioactive complexes are affected by the central metal and the coordination modes of the ligand. As a continuation of our study, in this paper, three new complexes  $[M(L)_2(H_2O)_2]$  where  $M = Cu^{II}$  (**1**),  $Zn^{II}$  (**2**) and  $Cd^{II}$  (**3**), were obtained derived from 2-(4-(pyridin-2-yl)piperazin-1-yl)acetic acid (**HL**) and corresponding metal nitrates. Herein, the synthesis, characterization, MAO-B inhibitory activity and molecular docking are presented.

## 2. Experimental Section

### 2.1. Materials and Methods

All chemicals and solvents were analytical reagent grade and purchased from Aladdin Industrial Corporation (China). They were used without purification. Elemental analyses for C, H, and N were conducted using the Pregl-Dumas technique on a Thermo Fischer Flash EA1112. FT-IR spectra were recorded from 400–4000  $cm^{-1}$  on a Nicolet 750 Magna IR spectrometer using KBr pellets. The enzyme inhibitory activity was measured on a Bio-Tek Synergy™ HT Microplate reader.

## 2. 2. Synthesis of 2-(4-(pyridin-2-yl)piperazin-1-yl)acetic Acid (HL)

HL was prepared according to the method reported with suitable modification.<sup>17,18</sup> 1-(pyridin-2-yl)piperazine (1.00 g, 0.0060 mol), bromoacetic acid (2.50 g, 0.0179 mol), and potassium hydroxide (1.50 g, 0.267 mol) were dissolved in 30 mL absolute ethanol. The mixture was refluxed for 10 h. When the reaction was finished, the solution was cooled to room temperature and neutralized with 1 M HCl. White precipitate was filtered to give HL (1.01 g, 74%).

## 2. 3. General Procedure for the Synthesis of Complexes 1–3

Nitrate (0.040 mmol) was dissolved in 4 mL of methanol solution which was carefully layered on the top of 4 mL water solution of HL (8.84 mg, 0.040 mmol) and KOH (2.24 mg, 0.040 mmol). The solutions were left for a few days at room temperature and then the crystals were obtained.

[Cu(L)<sub>2</sub>(H<sub>2</sub>O)<sub>2</sub>] (1) Yield: 0.0372 g, (43% on the basis of HL). IR (KBr, cm<sup>-1</sup>): 3365; 2970; 1596; 1467; 1384; 845; 681. Anal. Calcd. for C<sub>22</sub>H<sub>32</sub>N<sub>6</sub>O<sub>6</sub>Cu: C, 48.97; H, 5.97; N, 15.56. Found: C, 49.09; H, 5.95; N, 15.56%.

[Zn(L)<sub>2</sub>(H<sub>2</sub>O)<sub>2</sub>] (2) Yield: 0.0442 g, (51% on the basis of HL). IR (KBr, cm<sup>-1</sup>): 3338; 2943; 1595; 1454; 1395; 831; 664. Anal. Calcd. for C<sub>22</sub>H<sub>32</sub>N<sub>6</sub>O<sub>6</sub>Zn: C, 48.76; H, 5.95; N, 15.51; Found: C, 48.91; H, 5.92; N, 15.56%.

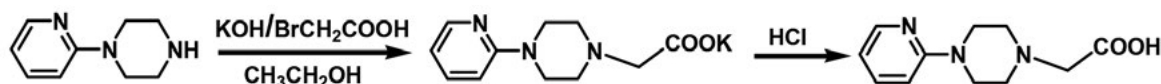
[Cd(L)<sub>2</sub>(H<sub>2</sub>O)<sub>2</sub>] (3) Yield: 0.0433 g, (46% on the basis of HL). IR (KBr, cm<sup>-1</sup>): 3359; 2995; 1594; 1458; 1394; 836; 671. Anal. Calcd. for C<sub>22</sub>H<sub>32</sub>N<sub>6</sub>O<sub>6</sub>Cd: C, 44.87; H, 5.48; N, 14.27; Found: C, 45.02; H, 5.46; N, 14.29%.

## 2. 4. X-ray Crystallography

Diffraction intensities for the complexes were collected at 298(2) K using a Bruker D8 VENTURE PHOTON diffractometer with Mo-Kα radiation (λ = 0.71073 Å). The structures were solved by direct methods and refined against F<sup>2</sup> by full-matrix least-squares methods using the SHELXTL-97.<sup>19,20</sup> All non-hydrogen atoms were refined anisotropically, the water H atoms in the complexes were located in difference Fourier maps and refined isotropically with O–H distances restrained to 0.85(1). All other H atoms were placed in idealized positions and constrained to ride on their parent atoms. Details of the crystal parameters, data collection, and refinement are listed in Table 1. The selected bond length and angle data are given in Table 2. The hydrogen bonding data are summarized in Table 3.

## 2. 5. Rat Brain MAO-B Inhibition Assay

MAO-B was obtained from wista mice with the method that was reported earlier.<sup>21</sup> The content of MAO-B was detected by MU30905 ELISA Kit (details in supplementary



Scheme 1 Synthesis of 2-(4-(pyridin-2-yl)piperazin-1-yl)acetic acid

Table 1. Crystallographic data for complex 1–3.

Empirical formula	1 C <sub>22</sub> H <sub>32</sub> CuN <sub>6</sub> O <sub>6</sub>	2 C <sub>22</sub> H <sub>32</sub> N <sub>6</sub> O <sub>6</sub> Zn	3 C <sub>22</sub> H <sub>32</sub> CdN <sub>6</sub> O <sub>6</sub>
<i>M<sub>r</sub></i>	540.09	541.93	588.95
Crystal system	triclinic	monoclinic	monoclinic
Space group	<i>P</i> -1	<i>P</i> 2 <sub>1</sub> / <i>c</i>	<i>P</i> 2 <sub>1</sub> / <i>c</i>
<i>a</i> (Å)	6.1916(6)	15.0279(13)	15.0305(14)
<i>b</i> (Å)	8.1504(8)	7.1943(6)	7.2772(6)
<i>c</i> (Å)	12.7804(13)	11.7348(9)	11.8887(10)
α (°)	95.079(3)	90	90
β (°)	103.019(3)	101.273(3)	101.986(3)
γ (°)	106.241(3)	90	90
<i>V</i> (Å <sup>3</sup> )	595.33(10)	1244.23(18)	1272.04(19)
<i>Z</i>	1	2	2
ρ <sub>c</sub> (g cm <sup>-3</sup> )	1.507	1.446	1.538
<i>F</i> (000)	283.0	568.0	604.0
Data / param. / restr.	2187 / 148 / 0	2202 / 161 / 4	2929 / 157 / 12
μ(Mo-Kα) / mm <sup>-1</sup>	0.968	1.036	0.907
GOF	1.108	1.110	1.090
<i>R</i> <sub>1</sub> <sup>a</sup> , <i>wR</i> <sub>2</sub> <sup>b</sup> ( <i>I</i> > 2σ( <i>I</i> ))	0.0663, 0.1684	0.0660, 0.2290	0.0370, 0.1085

<sup>a</sup> *R*<sub>1</sub> = Σ||*F*<sub>o</sub>| - |*F*<sub>c</sub>|| / Σ|*F*<sub>o</sub>|. <sup>b</sup> *wR*<sub>2</sub> = [Σ*w*(*F*<sub>o</sub><sup>2</sup> - *F*<sub>c</sub><sup>2</sup>)<sup>2</sup> / Σ*w*(*F*<sub>o</sub><sup>2</sup>)]<sup>1/2</sup>

materials).<sup>22</sup> The MAO-B inhibitory properties of complex 1–3 were carried out as it was reported previously.<sup>23</sup>

## 2. 6. Molecular Docking

Molecular docking of complexes 1–3 with the active site of human MAO-B (3LA4) was performed by the AUTODOCK 4.2 program suite. The graphical user interface AutoDockTools (ADT) was performed to setup every inhibitor enzyme interaction, where all hydrogen atoms were added, Gasteiger charges were calculated and non-polar hydrogen atoms were merged to carbon atoms. The result file was saved as pdbqt file. The 3D structures of ligand molecules were saved in Mol2 format with the aid of the program Mercury 3.0. The partial charges of Mol2 file were further modified by using the ADT package (version 1.5.4) so that the charges of the non-polar hydrogen atoms would be assigned to the atom to which the hydrogen is attached. The choice of the flexible bonds in the ligands was in accordance with SP3 hybridization. The nitrogen atoms of ligands in complexes 1–3 were assembled as non-protonated. The resulting file was saved as pdbqt file.

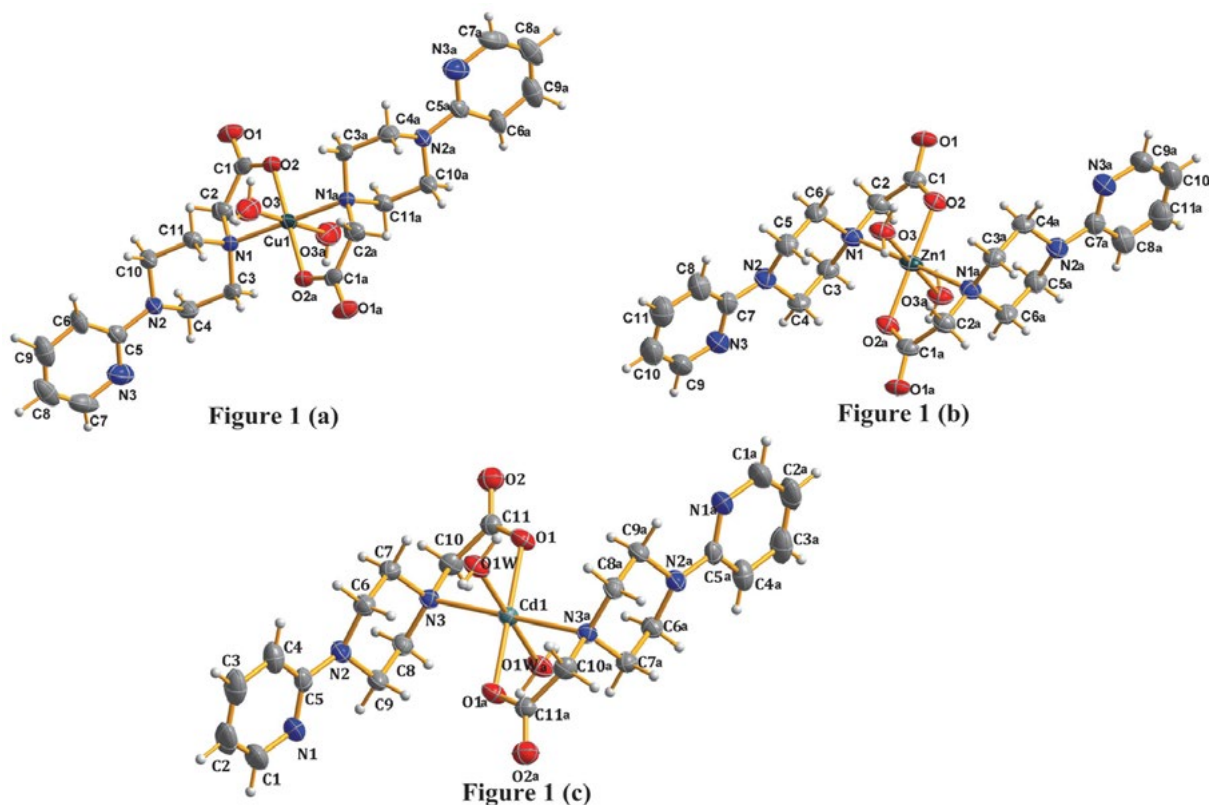
The AutoDock Vina docking procedure was used to generate the docking output files.<sup>24</sup> In all docking, a grid box size of  $60 \times 60 \times 60$  pointing in  $x$ ,  $y$  and  $z$  directions was built, the maps were centered on N5 atom of FAD600.<sup>25,26</sup> A grid spacing of  $0.375 \text{ \AA}$  and a distances-dependent function

of the dielectric constant were used for the calculation of the energetic map. Default parameters were used except num-modes, which was set to 10. The results of the most favorable free energy of binding were selected as the resultant complex structures. At the end of the docking, the result was analyzed using Pymol 2.5 program.

## 3. Results and Discussion

### 3. 1. IR Spectroscopy

The IR spectra of these complexes were similar. They all show broad band ranging from  $3500 \text{ cm}^{-1}$  to  $3300 \text{ cm}^{-1}$  indicating the O–H stretching of the water and methanol molecules. The asymmetric stretching mode  $\nu_{as}(\text{COO}^-)$  was located around  $1595 \text{ cm}^{-1}$  ( $1596 \text{ cm}^{-1}$  in 1,  $1595 \text{ cm}^{-1}$  in 2 and  $1594 \text{ cm}^{-1}$  in 3), while the strong symmetric stretching mode  $\nu_s(\text{COO}^-)$  for complexes 1–3 was clearly visible around  $1391 \text{ cm}^{-1}$  ( $1384 \text{ cm}^{-1}$  in 1,  $1395 \text{ cm}^{-1}$  in 2 and  $1394 \text{ cm}^{-1}$  in 3). The separation value  $\Delta\nu [\nu_{as}(\text{COO}^-) - \nu_s(\text{COO}^-)]$  of the carboxylic based complexes could be used to discriminate the coordination mode of the carboxyl group.  $\Delta\nu < 200 \text{ cm}^{-1}$  indicated the bidentate mode, whereas  $\Delta\nu > 200 \text{ cm}^{-1}$  indicated the monodentate mode.<sup>27,28</sup> Therefore, the  $\Delta\nu$  values  $[\nu_{as}(\text{COO}^-) - \nu_s(\text{COO}^-)]$  for complexes 1–3 is around  $204 \text{ cm}^{-1}$ , which means that the coordination mode of the carboxyl group in these complexes is monodentate.

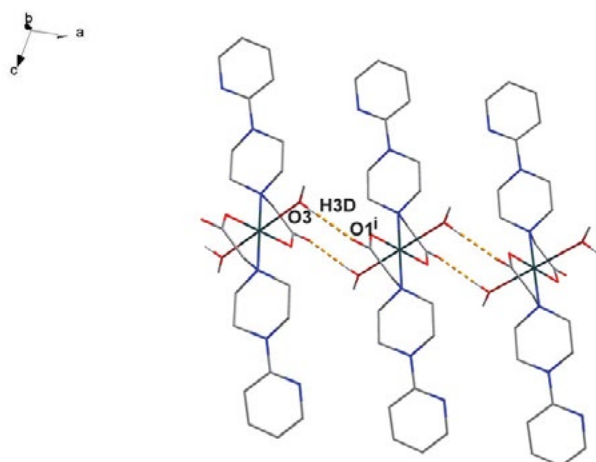


**Figure 1.** Molecular structure showing the atom-labelling scheme. Displacement spheres are drawn at the 50% probability level. The molecular diagram of (a) 1, (b) 2, (c) 3.

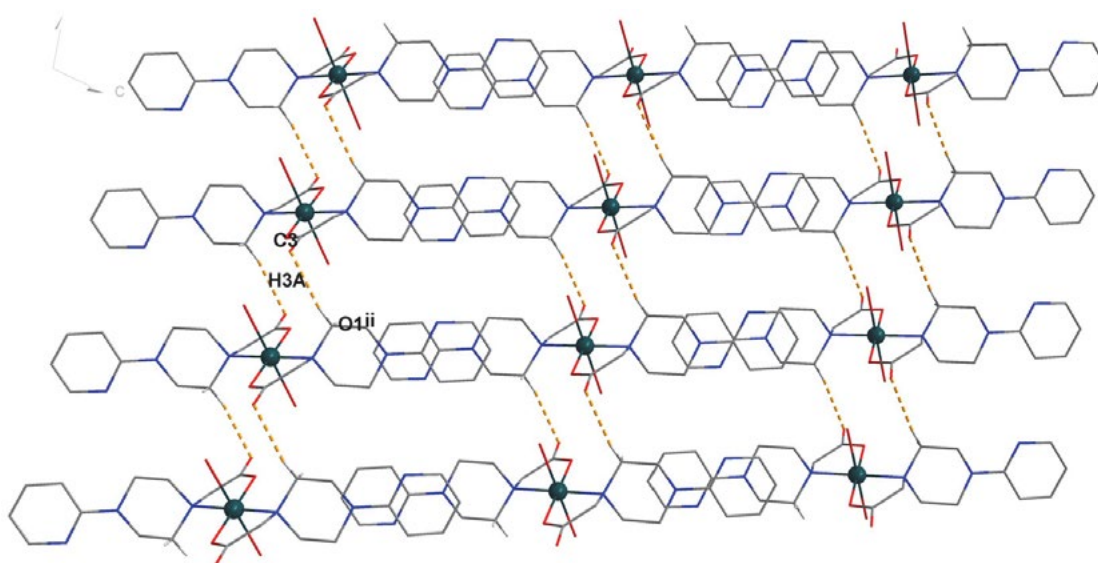
### 3. 2. Description of Crystal Structures

Complex **1** crystallizes in triclinic space group  $P\bar{1}$ , while complexes **2** and **3** crystallize in monoclinic space group  $P2_1/c$ . As shown in Figure 1, these three complexes possess very similar mononuclear structure, so only the structure of **1** is described here in detail. As shown in Figure 1(a), one asymmetric unit contained half of the complex molecule  $[\text{Cu}(\text{L})_2(\text{H}_2\text{O})_2]$ . Every mononuclear complex molecule included one copper ion, two ligand molecules and two coordinated water molecules. Ligand **L** behaves as a bidentate ligand resulting in the forming of a novel distorted five-membered heterocyclic ring around copper ion. These two five-membered rings are coplanar. The equatorial plane is surrounded by two O-atom donors (O2 and O2a) and two N-atom donors (N1 and N1a) from two **L** ligands, while the axial positions are occupied by

O-atom donors (O3 and O3a) from two coordinated water molecules. In addition, the sum of the equatorial angles  $\text{N1-Cu1-O2}$ ,  $\text{O2-Cu1-N1a}$ ,  $\text{N1a-Cu1-O2a}$  and  $\text{O2a-Cu1-N1}$  for complex **1** ( $= 360.00^\circ$ ) is equal to the ideal value ( $360.00^\circ$ ), which ensures the planarity of equatorial plane. The axial Cu–O average distance ( $2.866 \text{ \AA}$ ) is longer than the equatorial Cu–O average distance ( $2.048 \text{ \AA}$ ) and Cu–N average distance ( $1.922 \text{ \AA}$ ), showing the stretched tetrahedroid surrounding the Cu(II) center. Compared with the other piperazine-Cu(II) complexes, the Cu–O



**Figure 2.** 1-D zig-zag chain of complex **1**. Dashed lines denote hydrogen bonds. Symmetry code: (i)  $-x, 1-y, -z$ .



**Figure 3.** The hydrogen-bond-driven 2D sheet of **1** extended in  $bc$  plane. Symmetry code: (ii)  $1+x, y, z$

**Table 2.** Selected bond lengths ( $\text{\AA}$ ) and angles ( $^\circ$ ) for **1-3**

<b>1</b>			
Cu1–O2	1.922(4)	Cu1–O3	2.866(4)
Cu1–N1	2.048(3)		
O2–Cu1–O3	98.30(13)	O2–Cu1–N1	84.33(12)
O2–Cu1–O3a	81.70(13)	O2–Cu1–N1a	95.67(12)
O3–Cu1–N1	93.97(11)	O3–Cu1–N1a	86.03(11)
<b>2</b>			
Zn1–O2	2.006(4)	Zn1–O3	2.107(4)
Zn1–N1	2.362(4)		
O2–Zn1–O3	94.02(14)	O2–Zn1–N1	78.76(13)
O2–Zn1–O3a	85.98(14)	O2–Zn1–N1a	101.25(13)
O3–Zn1–N1	87.95(15)	O3–Zn1–N1a	92.05(15)
<b>3</b>			
Cd1–O1	2.213(2)	Cd1–O1W	2.3055(19)
Cd1–N3	2.456(3)		
O1–Cd1–O1W	94.92(7)	O1–Cd1–N3	74.32(8)
O1–Cd1–O1Wa	85.08(7)	O1–Cd1–N3a	105.68(8)
O1W–Cd1–N3	87.69(8)	O1W–Cd1–N3a	92.31(8)

Symmetry codes: (a)  $1-x, 1-y, -z$  for **1**;  $1-x, 2-y, 2-z$  for **2** and  $1-x, -y, 1-z$  for **3**.

**Table 3.** Geometrical parameters for hydrogen bonds for **1**

Hydrogen bonds	D–H (Å)	H...A (Å)	D...A (Å)	D–H...A(°)
O3–H3D...O1 <sup>i</sup>	0.85	1.96	2.788(5)	164
C3–H3A...O1 <sup>ii</sup>	0.97	2.53	3.476(6)	166

Symmetry codes: (i)  $-x, 1 - y, -z$ ; (ii)  $1 + x, y, z$ .

carboxyl bond (1.938 Å) is similar to the Cu–O carbonyl bond length (1.923 Å), and Cu–N bond length (2.033 Å) in complex **1** is also similar to the other piperazine-Cu(II) complexes. The bond distances and bond angles are normal compared to other reported Cu (II) complexes.<sup>29</sup>

Water acts a hydrogen bond donor. As shown in Figure 2, complex **1** presents enhanced hydrogen-bonding framework in the solid state (Table 3). Two coordinated water molecules (O3 and O3a) are involved in a chain formation through O3–H3D1...O1<sup>i</sup> hydrogen bonding (symmetry code: (i)  $-x, 1 - y, -z$ ).

As shown in Figure 3, these chains stack in a interleaved fashion in *bc* plane, the hydrogen bonds exist between the carboxyl group of ligand **L** and the carbon atom of other ligand **L** form intermolecular C3–H3A...O1<sup>ii</sup> (symmetry code: (ii)  $1 + x, y, z$ )

### 3. 3. Inhibitory Activity Against MAO-B

Statistical analyses of data were performed using SPSS 19.0 program. Data reported as means  $\pm$  SEM for three independent samples in duplicate. Statistical differences between the groups were considered significant if the *p* value was  $< 0.05$ . Specific results please see Table 4. It was found that compared with iproniazid phosphate as the positive control (IP,  $IC_{50} = 7.59 \pm 1.17 \mu\text{M}$ ),<sup>30</sup> complex **1** ( $IC_{50} = 6.52$

**Table 4.** Inhibition of rat brain MAO-B for **HL**, complexes **1–3**, and IP

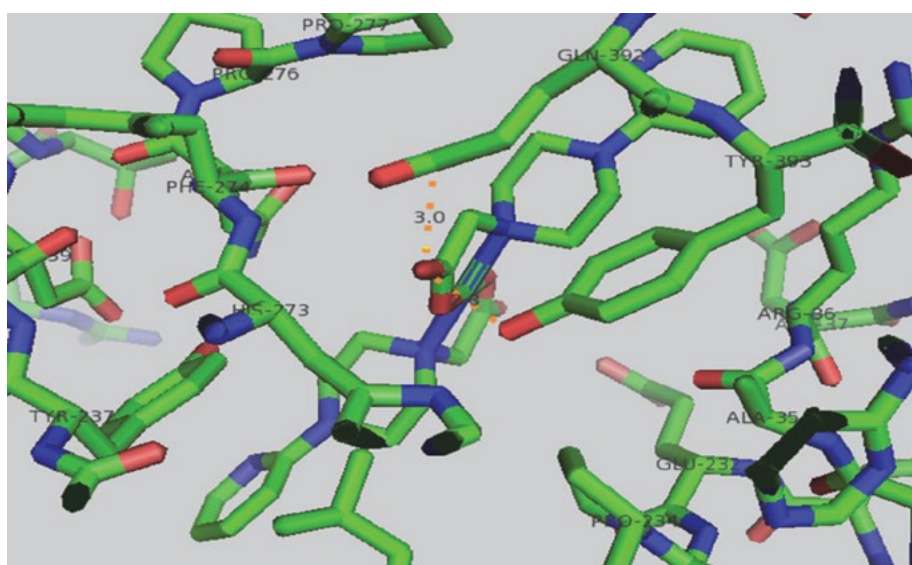
Test material	$IC_{50}$ ( $\mu\text{M}$ )
<b>1</b>	$6.52 \pm 0.31$
<b>2</b>	$>100$
<b>3</b>	$>100$
<b>HL</b>	$76.1 \pm 2.51$
Cu(NO <sub>3</sub> ) <sub>2</sub>	$12.31 \pm 1.06$
Zn(NO <sub>3</sub> ) <sub>2</sub>	$>100$
Cd(NO <sub>3</sub> ) <sub>2</sub>	$>100$
IP*	$7.59 \pm 1.17$

$\pm 0.31 \mu\text{M}$ ) had good inhibitory activity on MAO-B, while complexes **2** and **3** ( $IC_{50} > 100 \mu\text{M}$ ) showed no inhibitory activity. Both Cu(NO<sub>3</sub>)<sub>2</sub> and ligands have a certain inhibitory capacity for monoamine oxidase, after the two combine to form a complex **1**, complex **1** showed good inhibitory activity, therefore, they show certain synergistic effects.

### 3. 4. Molecular Docking

The binding models of complexes **1**, **2**, **3** with MAO-B (1S3E) were simulated using the AutoDock Vina docking program to validate their structure-activity relationships. The docking results show that only the complex **1** has good binding with the active site of MAO-B (1S3E).

The binding model of complex **1** and 1S3E is shown in Figure 4. All amino acid residues around complex **1** are shown. In the binding model, the main stabilizing factors that stabilize the Cu(L)<sub>2</sub>-1S3E complex are the hydrophobic contacts and hydrogen bonding interactions. The O1 atom in complex **1** serves as a hydrogen bond acceptor re-



**Figure 4.** Binding mode of complex **1** with human monoamineoxidase-B. The complex molecule and MAO-B were shown as stick, the hydrogen bonds were shown as yellow dash lines

ceived one strong hydrogen bonding interaction from Tyr393. The hydrogen-bonding distance of Tyr393 N–H...O2 is 2.8 Å. The results of the molecular docking indicate that the complex **1** could be well fitted in the active pocket of MAO-B.

## 4. Conclusion

This paper reports that synthesis, crystal structure, molecular docking, and monoamine oxidase B inhibitory activities of three transition metal complexes with 2-(4-(pyridin-2-yl)piperazin-1-yl)acetic acid ligand. Molecular docking assay showed the potential binding model of complex **1** with MAO-B. The complex **1** exhibits MAO-B inhibiting activity *in vitro* at micromole concentrations ( $IC_{50} = 6.5 \pm 0.31 \mu\text{M}$ ), whereas complex **2** and **3** exhibits no MAO-B inhibiting activity ( $IC_{50} > 100 \mu\text{M}$ ). Now, we are synthesizing specific compounds that inhibit the MAO-B based on the complex **1** structure.

## 5. Supplementary Information

CCDC files 1515965 (**1**), 1515778 (**2**) and 1515777(**3**) contain the supplementary crystallographic data for this paper. These data can be obtained free of charge from The Cambridge Crystallographic Data Centre via [www.ccdc.cam.ac.uk/data\\_request/cif](http://www.ccdc.cam.ac.uk/data_request/cif).

## 6. References

- M. B. Youdim, G. G. Gollins, M. Sandler, *J. Biochem.* **1971**, *121*, 34–36. DOI:10.1042/bj1210034P
- J. C. Shih, *Neuropsychopharmacol.* **1991**, *4*, 1–7.
- J. W. Greenawalt, C. Schnatiman, *J. Cell. Biol.* **1970**, *46*, 173–179. DOI:10.1083/jcb.46.1.173
- C. W. Abell, S. W. Kwan, *Prog. Nucleic. Acid. Res.* **2001**, *65*, 129–156. [http://dx.doi.org/10.1016/S0079-6603\(00\)65004-3](http://dx.doi.org/10.1016/S0079-6603(00)65004-3) DOI:10.1016/S0079-6603(00)65004-3
- O. Nakagawasai, Y. Arai, E. H. Satoh, N. Satoh, M. Neda, M. Hozumi, R. Oka, H. Hiraga, T. Tadano, *Neurotoxicology* **2004**, *25*, 223–232. DOI:10.1016/S0161-813X(03)00101-3
- H. P. Volz, C. H. Gleiter, *Drug. Aging* **1998**, *13*, 341–355. DOI:10.2165/00002512-199813050-00002
- J. C. Jean, *Neurotoxicology* **2004**, *25*, 21–30. DOI:10.1016/S0161-813X(03)00112-8
- M. B. Youdim, D. Edmondson, K. F. Tipton, *Nat. Rev. Neurosci.* **2006**, *7*, 295–309. DOI:10.1038/nrn1883
- S. S. Jossan, P. G. Gillberg, C. G. Gottfries, I. Karlsson, L. Orelund, *Nat. Rev. Neurosci.* **1997**, *45*, 1–12. [http://dx.doi.org/10.1016/0306-4522\(91\)90098-9](http://dx.doi.org/10.1016/0306-4522(91)90098-9) DOI:10.1016/0306-4522(91)90098-9
- T. Shigeo, Y. Kuwai, M. Tabata, *Planta Med.* **1987**, *53*, 5–8. DOI:10.1055/s-2006-962604
- J. Joubert, G. B. Foka, B. P. Repsold, D. W. Oliver, E. Kapp, S. F. Malan, *Eur. J. Med. Chem.* **2017**, *125*, 853–864. DOI:10.1016/j.ejmech.2016.09.041
- B. Evranos-Aksöz, S. Yabanoğlu-Çiftçi, G. Uçar, K. Yelekçi, R. Ertan, *Bioorg. Med. Chem. Lett.* **2014**, *24*, 3278–3284. DOI:10.1016/j.bmcl.2014.06.015
- S. Distinto, R. Meleddu, M. Yanez, R. Cirilli, G. Bianco, M. L. Sanna, A. Arridu, P. Cossu, F. Cottiglia, C. Faggi, F. Ortuso, S. Alcaro, E. Maccioni, *Eur. J. Med. Chem.* **2016**, *108*, 542–552. DOI:10.1016/j.ejmech.2015.12.026
- X. Yang, X. M. Qiang, Y. Li, L. Luo, R. Xu, Y. X. Z. Zheng, Z. C. Cao, Z. H. Tan, Y. Deng, *Bioorg. Chem.* **2017**, *71*, 305–314. DOI:10.1016/j.bioorg.2017.02.016
- J. Qin, Q. Yin, S. S. Zhao, J. Z. Wang, S. S. Qian, *Acta Chim. Slov.* **2016**, *63*, 55–61.
- D. D. Yang, R. Wang, J. L. Zhu, Q. Y. Cao, J. Qin, H. L. Zhu, S. S. Qian, *J. Mol. Struct.* **2017**, *1128*, 493–498. DOI:10.1016/j.molstruc.2016.08.037
- C. T. Sadashiva, S. C. J. N. Narendra, K. C. Ponnappa, G. T. Veerabasappa, K. S. Rangappa, *Bioorg. Med. Chem. Lett.* **2016**, *16*, 3932–3936. DOI:10.1016/j.bmcl.2006.05.030
- Z. J. Chen, C. N. Xu, J. L. Zhu, D. D. Yang, S. S. Zhao, Y. N. Chen, S. S. Qian, *Acta Chim. Slov.* **2016**, *63*, 165–172. DOI:10.17344/acsi.2015.2109
- G. M. Sheldrick, *Acta Crystallogr. A* **2008**, *64*, 112–122. DOI:10.1107/S0108767307043930
- Bruker, SMART (Version 5.63), SAINT (Version 6.02), SADABS (Version 2.03), Bruker AXS Inc. 2002, Madison, Wisconsin, USA.
- B. E. Yoon, J. Woo, Y. E. Chun, H. Chun, S. Jo, J. Y. Bae, H. An, J. O. Min, S. J. Oh, K. S. Han, H. Y. Kim, T. Kim, Y. S. Kim, Y. C. Bae, C. J. Lee, *J. Physiol.* **2014**, *592*, 4951–4968. DOI:10.1113/jphysiol.2014.278754
- A. Holt, D. F. Sharman, G. B. Baker, M. M. Palcic, *Anal. Biochem.* **1977**, *244*, 384–392. DOI:10.1006/abio.1996.9911
- M. O. Ogunrombi, S. F. Malan, G. T. Blanche, N. Castagnoli, J. J. Bergh, J. P. Petzer, *Bioorg. Med. Chem.* **2008**, *16*, 2463–2472. <http://dx.doi.org/10.1016/j.bmc.2007.11.059> DOI:10.1016/j.bmc.2007.11.059
- O. Trott, A. J. Olson, *J. Comput. Chem.* **2010**, *31*, 455–461. DOI:10.1002/jcc.21334
- M. B. Nunez, F. P. Maguna, N. B. Okulik, E. A. Castro, *Bioorg. Med. Chem. Lett.* **2004**, *14*, 5611–5617. DOI:10.1016/j.bmcl.2004.08.066
- L. Santana, H. Gonzalez-Diaz, E. Quezada, *J. Med. Chem.* **2008**, *51*, 6740–6751. DOI:10.1021/jm800656v
- C. T. Sadashiva, J. N. N. S. Chandra, K. C. Ponnappa, G. T. Veerabasappa, K. S. Rangappa, *J. Bioorg. Med. Chem. Lett.* **2006**, *16*, 3932–3936. DOI:10.1016/j.bmcl.2006.05.030
- I. Turel, J. Kljun, *J. Curr. Top. Med. Chem.* **2011**, *11*, 2661–2687. DOI:10.2174/156802611798040787
- H. Y. Luo, J. M. Lo, P. E. Fanwick, J. G. Stowell, M. A. Green, *J. Inorg. Chem.* **1999**, *38*, 2071–2078. DOI:10.1021/ic981324f
- S. S. Xie, X. Wang, N. Jiang, Y. W. Yu, D. G. K. Wang, J. S. Lan, Z. R. Li, L. Y. Kong, *Eur. J. Med. Chem.* **2015**, *95*, 153–165. DOI:10.1016/j.ejmech.2015.03.040



## Povzetek

Sintetizirali smo tri nove komplekse z 2-(4-(piridin-2-il)piperazin-1-il)ocetno kislino (**HL**),  $[M(L)_2(H_2O)_2]$ , kjer je  $M = Cu^{II}$  (**1**),  $Zn^{II}$  (**2**) in  $Cd^{II}$  (**3**), ter jih okarakterizirali z IR spektroskopijo, elementno analizo in rentgensko kristalografijo. *In vitro* smo določili inhibitorno aktivnost pripravljenih treh kompleksov proti MAO-B ter izvedli simulacijo molekularnega dockinga za razumevanje načina vezave. Eksperimentalni podatki in računalniške simulacije kažejo, da ima kompleks **1** največjo inhibitorno aktivnost z  $IC_{50}$  vrednostjo  $6.5 \pm 0.31 \mu M$ .

Scientific paper

# A Novel One-pot Synthesis of Isothiocyanates and Cyanamides from Dithiocarbamate Salts Using Environmentally Benign Reagent Tetrapropylammonium Tribromide

Neivotsonuo Bernadette Kuotsu,<sup>1,3</sup> Latonglila Jamir,<sup>2</sup> Tavishe Phucho<sup>3</sup>  
and Upasana Bora Sinha<sup>3,\*</sup>

<sup>1</sup> Department of chemistry, Kohima Science College (Autonomous), Jotsoma-797002, Nagaland, India

<sup>2</sup> Department of Environmental Science, Nagaland University, Lumami-798627, Nagaland, India

<sup>3</sup> Department of Chemistry, Nagaland University, Lumami-798627, Nagaland, India

\* Corresponding author: E-mail: upasanabsinha@gmail.com

Received: 06-03-2017

## Abstract

A highly efficient and simple protocol for the synthesis of isothiocyanates and cyanamides from their respective amines in the presence of a mild, efficient, and non-toxic reagent tetrapropylammonium tribromide is described. High environmental acceptability of the reagents, cost effectiveness and high yields are the important attributes of this methodology.

**Keywords:** TPATB, desulfurization, oxidation, isothiocyanates, sodium bicarbonate, cyanamide.

## 1. Introduction

Isothiocyanates are one of the most important synthetic intermediates for the preparation of both sulphur and nitrogen containing organic compounds especially for heterocycles.<sup>1</sup> The isothiocyanate functionality is frequently encountered in natural products, including sesquiterpenes.<sup>2</sup> Additionally, synthetic isothiocyanates have proven to have some biological activity, such as anti-proliferative<sup>3</sup> and enzyme inhibitory for the HIV virus.<sup>4</sup> Numerous methods for the preparation of isothiocyanates have been reported, starting from amines,<sup>5</sup> dithiocarbamates,<sup>6</sup> organic halides,<sup>7</sup> olefins<sup>8</sup> and aldoximes.<sup>9</sup> Among the literature methods, the most widely used procedure is the synthesis by the decomposition of dithiocarbamates using heavy metals,<sup>10</sup> thiophosgene, iodine, ethylchlorocarbamate and claycop.<sup>11</sup> Although many synthetic methods for the preparation of isothiocyanates have been reported to date,<sup>12–32</sup> most methods suffer from the employment of highly toxic reagents. Thus, there is still need for a commercially viable and environmentally acceptable protocol for the synthesis of isothiocyanates. We describe herein a modified, environmentally benign and cost-effective met-

hod for the synthesis of isothiocyanates via TPATB-mediated decomposition of dithiocarbamate salt in the presence of sodium bicarbonate in water/ethyl acetate biphasic solvent system at room temperature (Scheme 1).

Similarly, in continuation of our work we have synthesised cyanamides from the dithiocarbamate salt. Cyanamides have attracted considerable attention as a class of versatile organic molecules. They have a wide range of uses in organic synthetic chemistry<sup>33</sup> and coordination chemistry<sup>34</sup> as they can be used as building blocks for the construction of not only diverse N-containing compounds but also as metal ligands with their unique reactivity and structure of the cyanamide unit. Additionally, it has been found that some cyanamide based compounds show a diversity of interesting bioactivities, inhibition of spontaneous myogenic, and peptide activator activities.<sup>35</sup> It has also been proved that cyanamide is a natural product present in higher plants even though its distribution is limited.<sup>36</sup> The broad applications of cyanamides have resulted in the development of several methods for their synthesis over the years. The most common among these is the reaction of cyanogens chloride or bromide with amines or with imide salts.<sup>37</sup> However, this method involves the use of po-

tassium or sodium cyanide and bromine for the preparation of cyanogen halide (which is again highly toxic), making the protocol environmentally unacceptable. Literature reports on various other methods for the preparation of cyanamide using different synthetic strategies, such as cyanation of amines using  $\text{CN}^+$  equivalents as synthons,<sup>38–44</sup> Tiemann rearrangement of amidoximes,<sup>45</sup> coupling reactions involving Pd isocyanides, allyl carbonates and trimethylsilyl azide,<sup>46</sup> and sodium bis(trimethylsilyl)amide as deoxygenating or desulfurizing agents.<sup>47</sup> Yet another method for the preparation of cyanamides involves the reaction of hypervalent iodine(V) species with  $N,N'$ -disubstituted glycolamide.<sup>48</sup> However, all the procedures reported so far seem to have certain environmental concerns as they involve direct or indirect use of toxic and corrosive reagents, strong alkaline conditions, expensive reagents and catalysts, high reaction temperatures and tedious purification procedures. We have been interested to an extent in the synthesis of isothiocyanates and cyanamides, therefore, in this context we develop an alternative method involving the use of alkyl or aryl dithiocarbamate using tetrapropylammonium tribromide as a double desulfurizing agent.

## 2. Experimental

### 2.1. General Procedure for the Synthesis of Phenyl Isothiocyanate

To a stirred and ice cooled suspension of phenyl dithiocarbamate salt (Table 1, compound **1**) (540 mg, 2 mmol) in ethylacetate (5 mL), and water (5 mL) was added  $\text{NaHCO}_3$  (336 mg, 4 mmol). To this was added TPATB (0.852 g, 2 mmol) pinch wise over a period of 10–15 minutes to yield phenylisothiocyanate (Table 1, compound **1a**). During this period, precipitation of elemental sulfur was observed. Completion of the reaction was confirmed by TLC. Ethyl acetate (10 mL) was further added to the reaction mixture. The organic layer was washed with water (2–5 mL), dried over anhydrous  $\text{Na}_2\text{SO}_4$ , concentrated under reduced pressure and purified over a short column of silica gel while eluting it with hexane–ethyl acetate (97:3) to give the pure product (Table 1, compound **1a**) (216 mg, 80%).

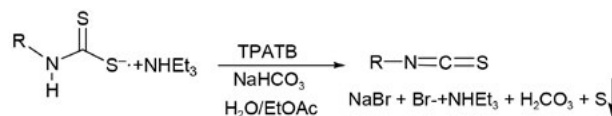
### 2.2. General Procedure for the Synthesis of Phenylcyanamide

To a stirred and ice cooled suspension of dithiocarbamate (Table 2, compound **1**) (540 mg, 2 mmol) in ethyl acetate (5 mL), was added  $\text{NaHCO}_3$  (336 mg, 4 mmol). To this was then added TPATB (0.852 g, 2 mmol) pinch wise over a period of 10–15 minutes to yield phenylisothiocyanate. During this period precipitation of elemental sulfur was observed. After complete addition of TPATB, 25%

aqueous  $\text{NH}_3$  (2.5 mL) was added drop wise to the stirred reaction mixture to give 1-phenylthiourea. After stirring for 10 minutes at room temperature, the excess of  $\text{NH}_3$  was removed in a rotary evaporator whereby the solvent ethyl acetate was also simultaneously removed leaving behind the aqueous layer. To the crude reaction mixture was then further added ethyl acetate (5 mL) and  $\text{NaHCO}_3$  (336 mg, 4 mmol). To the resultant solution, TPATB (0.852 g, 2 mmol) was added in small pinches, during which further precipitation of elemental sulfur was observed. The conversion of 1-phenylthiourea to phenylcyanamide (Table 2, compound **1b**) was observed within 5 minutes of the complete addition of TPATB. Completion of the reaction was confirmed by TLC. The precipitated sulfur was filtered, washed with ethyl acetate ( $2 \times 5$  mL). The organic layer was washed with water ( $2 \times 5$  mL) and dried over anhydrous  $\text{Na}_2\text{SO}_4$ , concentrated under reduced pressure and purified over a short column of silica gel eluting it with hexane–ethyl acetate (97:3) to give the pure product (Table 2, compound **1b**) (188 mg, 80%) as an oily liquid.

## 3. Results and Discussion

The dithiocarbamic acid salt is readily converted into the corresponding isothiocyanate (Table 1, compound **1a**), simply by treating it with TPATB in the presence of sodium bicarbonate in water/ethyl acetate biphasic medium in good to excellent yields in shorter time (15 minutes) as shown in Scheme 1.

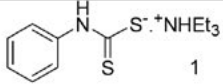
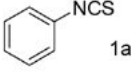
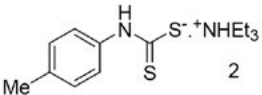
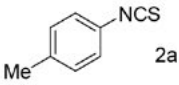
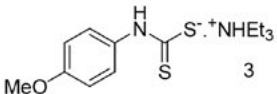
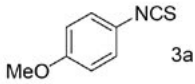
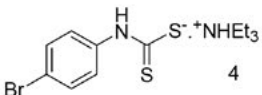
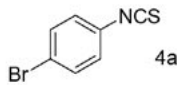
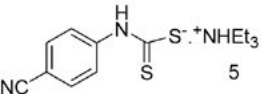
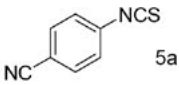
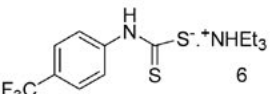
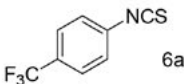
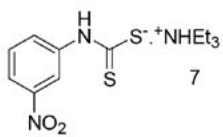
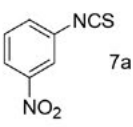
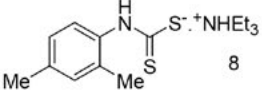
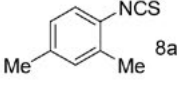
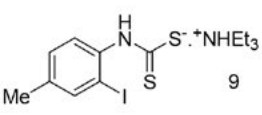
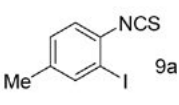
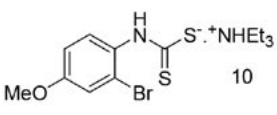
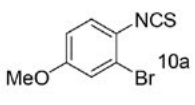
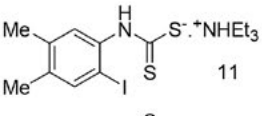
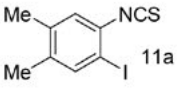
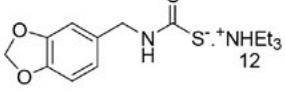
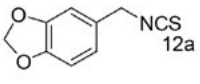
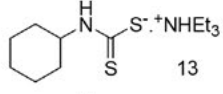
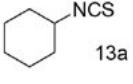
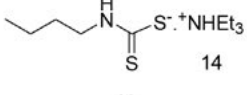
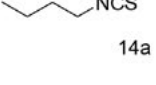
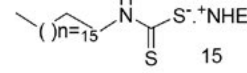
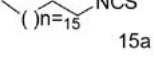


Scheme 1. Preparation of isothiocyanate from dithiocarbamate salt

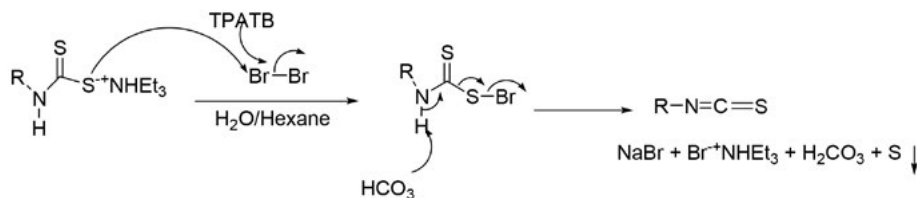
The use of water/ethyl acetate biphasic solvent system has several potential advantages. In addition to the benign character of both water and ethyl acetate, the coexistence of water with ethyl acetate helps in extracting the isothiocyanate to the organic layer leaving behind the impurities in the aqueous layer which in turn facilitates an easy workup. TPATB is soluble in ethyl acetate and on stirring dissolves, thus getting delivered to the water-ethyl acetate interphase for desulfurization. Moreover, the water phase dissolves the base sodium bicarbonate and retains the dithiocarbamic acid salt in aqueous layer. The use of sodium bicarbonate over organic bases offers a mild and effective green approach towards the synthesis of isothiocyanates. The mechanism of the present transformation is given below in Scheme 2.<sup>48</sup>

Thus, the method provides an ecologically and economically viable process for the preparation of isothiocyanates. The preparation of isothiocyanates was performed

Table 1. Preparation of Isothiocyanates from Dithiocarbamate Salt and TPATB<sup>a</sup>

Substrate	Product <sup>b</sup>	Yield (%) <sup>c</sup>
 1	 1a	80
 2	 2a	92
 3	 3a	81
 4	 4a	92
 5	 5a	92
 6	 6a	90
 7	 7a	77
 8	 8a	90
 9	 9a	85
 10	 10a	80
 11	 11a	92
 12	 12a	86
 13	 13a	90
 14	 14a	85
 15	 15a	88

<sup>a</sup> Reactions were monitored by TLC; <sup>b</sup> Confirmed by IR, <sup>1</sup>H NMR and <sup>13</sup>C NMR; <sup>c</sup> Isolated yield.



**Scheme 2.** Mechanism of the formation of isothiocyanate from dithiocarbamate salt

on freshly prepared dithiocarbamate salts synthesized from a variety of structurally different alkyl and aryl amines. The results are summarized in Table 1. Substrates containing activating substituents (Table 1, compounds 2–3) gave the expected products efficiently as also did substrates containing deactivating substituents (Table 1, compounds 4–7). Trisubstituted substrates (Table 1, compounds 8–10) as well as highly hindered substrates (Table 1, compound 11) gave the corresponding isothiocyanates in high yields. Benzylic substrate (Table 1, compound 12) and aliphatic substrates (Table 1, compounds 13–15) also gave their expected products (Table 1, compound 12a) and (Table 1, compounds 13a–15a) respectively in excellent yields.

Similarly, for the synthesis of cyanamides the methodology was based on: (i) formation of isothiocyanate from alkyl/aryl dithiocarbamate salt by desulfurization with TPATB in the presence of triethylamine as the base in ethyl acetate solvent, (ii) treating the *in situ* generated isothiocyanate with aqueous  $\text{NH}_3$  to afford alkyl/aryl thioamides and (iii) further oxidative desulfurization of thioamides to cyanamide with TPATB in the presence of triethylamine (Scheme 2). The mechanism of the present transformation is given below.<sup>49</sup> Based on these findings, we thus report herein a practical, environmentally benign, high yielding and one pot preparation of cyanamides from dithiocarbamate salts using cheap and non-toxic reagent TPATB (Scheme 3) in an innocuous solvent ethyl acetate.

Implementing this one pot method, a wide variety of aromatic and aliphatic cyanamides have been prepared from their parent dithiocarbamate salts. Phenyl cyanamide (Table 2, compound 1b) was obtained in excellent yield from its dithiocarbamate (Table 2, compound 1). Monosubstituted substrates bearing deactivating substituents (Table 2, compounds 2–6) readily underwent this reaction to produce the desired cyanamides (Table 2, compounds 2b–6b) in high yields. The method worked smoothly for substrates with electron donating substituents such as (Table 2, compounds 7–8) to afford the corre-

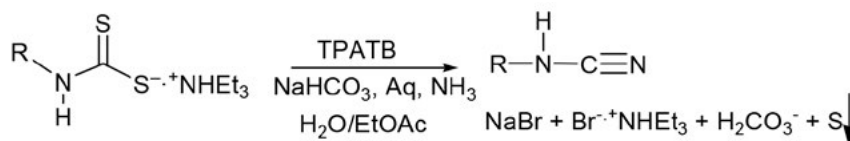
sponding cyanamides (Table 2, compounds 7b–8b) in high yields. A noteworthy aspect is that the present methodology can be applied to substrates containing sensitive substituents such as keto functionality (Table 2, compound 9b) as well as trisubstituted ones (Table 2, compound 10b). Cyclic and open chain aliphatic cyanamides (Table 2, compounds 11b–12b) were obtained from their corresponding dithiocarbamate salts (Table 2, compounds 11–12) under the same reaction conditions. We further investigated the efficacy of this method towards benzylic dithiocarbamate (Table 2, compounds 13–14) and dithiocarbamate salt of homoveratryl amine (Table 2, compound 15) which underwent the reaction smoothly to yield their respective corresponding cyanamide products (Table 2, compounds 13b–14b) and (Table 2, compound 15a) in good yields under the similar reaction conditions.

## 4. Spectroscopic and Analytical Data

**1-Isothiocyanato-benzene (1a).** Oily;  $^1\text{H}$  NMR (400 MHz,  $\text{CDCl}_3$ )  $\delta$  7.21–7.37 (m, 5H, ArH).  $^{13}\text{C}$  NMR (100 MHz,  $\text{CDCl}_3$ )  $\delta$  125.8, 127.4, 129.6, 131.3, 135.3. IR (KBr) 3064, 2164, 2063, 1591, 1489, 1474, 1451, 1070, 927, 905, 749, 684  $\text{cm}^{-1}$ . Anal. Calcd for  $\text{C}_7\text{H}_5\text{NS}$  (135.19): C, 62.19; H, 3.73; N, 10.36; S, 23.72. Found: C, 62.22; H, 3.71; N, 10.35; S, 23.73.

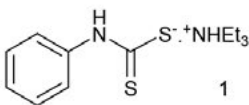
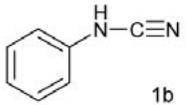
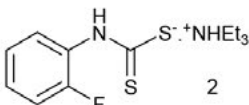
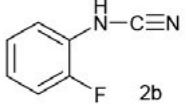
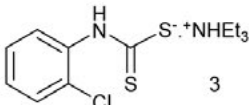
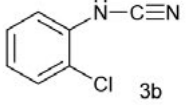
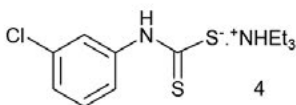
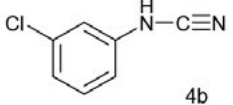
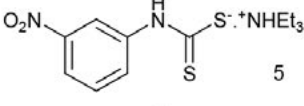
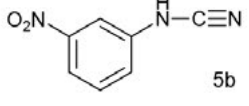
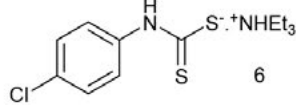
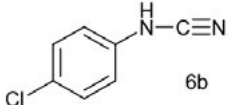
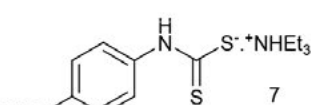
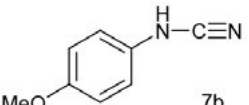
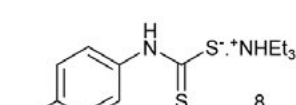
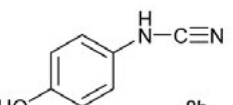
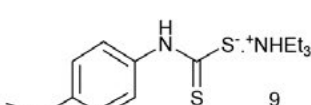
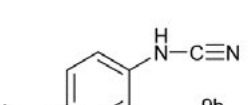
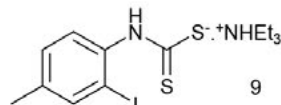
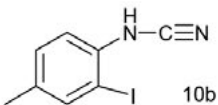
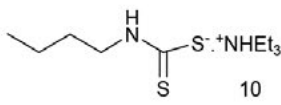
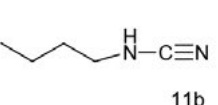
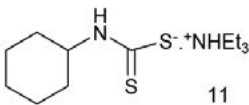
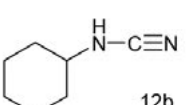
**1-Isothiocyanato-4-methyl-benzene (2a).** Oily;  $^1\text{H}$  NMR (400 MHz,  $\text{CDCl}_3$ )  $\delta$  2.33 (s, 3H,  $\text{CH}_3$ ), 7.06–7.13 (m, 4H, ArH).  $^{13}\text{C}$  NMR (100 MHz,  $\text{CDCl}_3$ )  $\delta$  21.2, 125.4, 128.2, 130.1, 134.4, 137.4. IR (KBr) 2920, 2094, 1503, 929, 812, 790, 497  $\text{cm}^{-1}$ . Anal. Calcd for  $\text{C}_8\text{H}_7\text{NS}$  (149.15): C, 64.36; H, 4.73; N, 9.39; S, 21.51. Found: C, 64.32; H, 4.75; N, 9.41; S, 21.56.

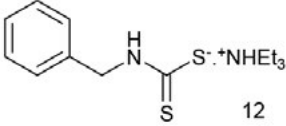
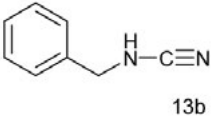
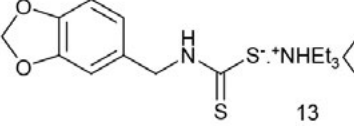
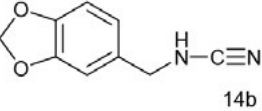
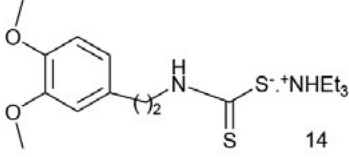
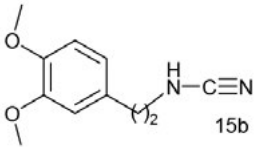
**1-Isothiocyanato-4-methoxy-benzene (3a).** Oily;  $^1\text{H}$  NMR (400 MHz,  $\text{CDCl}_3$ )  $\delta$  3.80 (s, 3H,  $\text{CH}_3$ ), 6.85 (d, 2H,  $J = 8.8$  Hz, ArH), 7.16 (d, 2H,  $J = 8.8$  Hz, ArH).  $^{13}\text{C}$  NMR



**Scheme 3.** Mechanism for the formation of cyanamide

Table 2. Preparation of cyanamides from dithiocarbamates and TPATB<sup>a</sup>

Substrate	Product <sup>b</sup>	Yield (%) <sup>c</sup>
 1	 1b	72
 2	 2b	70
 3	 3b	70
 4	 4b	75
 5	 5b	71
 6	 6b	77
 7	 7b	70
 8	 8b	68
 9	 9b	65
 9	 10b	78
 10	 11b	60
 11	 12b	62

Substrate	Product <sup>b</sup>	Yield (%) <sup>c</sup>
 12	 13b	64
 13	 14b	67
 14	 15b	66

<sup>a</sup> Reactions were monitored by TLC; <sup>b</sup> Confirmed by IR, <sup>1</sup>H NMR and <sup>13</sup>C NMR; <sup>c</sup> isolated yield

(100 MHz, CDCl<sub>3</sub>) δ 55.4, 114.6, 123.2, 126.8, 133.7, 158.4. IR (KBr) 3000, 2956, 2835, 2170, 2098, 1580, 1599, 1503, 1459, 1440, 1292, 1251, 1179, 1166, 1028, 927, 824, 614, 513 cm<sup>-1</sup>. Anal. Calcd for C<sub>8</sub>H<sub>7</sub>NOS (165.22): C, 58.16; H, 4.27; N, 8.48; S, 19.40. Found: C, 58.08; H, 4.23; N, 8.34; S, 19.34.

**1-Bromo-4-isothiocyano-benzene (4a).** White solid, m.p. 58 °C (lit.<sup>1a</sup> 58 °C), <sup>1</sup>H NMR (400 MHz, CDCl<sub>3</sub>) δ 7.09 (d, 2H, *J* = 8.8 Hz, *ArH*), 7.47 (d, 2H, *J* = 8.8 Hz, *ArH*). <sup>13</sup>C NMR (100 MHz, CDCl<sub>3</sub>) δ 120.8, 127.2, 130.5, 132.8, 136.9. IR (KBr) 3074, 2925, 2171, 2071, 1578, 1478, 1474, 1399, 1067, 1011, 923, 818, 490, 438 cm<sup>-1</sup>. Anal. Calcd for C<sub>7</sub>H<sub>4</sub>BrNS (214.03): C, 39.24; H, 1.88; N, 6.54; S, 14.99. Found: C, 39.21; H, 1.93; N, 6.50; S, 15.04.

**4-Isothiocyano-benzonitrile (5a).** White solid; m.p. 119–120 °C (lit.<sup>21</sup> 121 °C), <sup>1</sup>H NMR (CDCl<sub>3</sub>, 400 MHz) δ 7.31 (d, *J* = 8.8 Hz, 2H), 7.66 (d, *J* = 8.8 Hz, 2H); <sup>13</sup>C NMR (CDCl<sub>3</sub>, 100 MHz) δ 110.6, 117.9, 126.5, 133.6, 135.9, 139.4; IR (KBr) 3435, 2197, 2124, 2104, 1591, 1492, 1277, 933, 836, 544 cm<sup>-1</sup>. Anal. Calcd for C<sub>8</sub>H<sub>4</sub>N<sub>2</sub>S (166.13): C, 59.95; H, 2.51; N, 17.49; S, 20.03. Found: C, 59.98; H, 2.49; N, 17.45; S, 19.98.

**1-Isothiocyano-4-trifluoromethyl-benzene (6a).** White solid; m.p. 43 °C (lit.<sup>22</sup> bp 205–207 °C); <sup>1</sup>H NMR (CDCl<sub>3</sub>, 400 MHz) δ 7.32 (d, *J* = 8.4 Hz, 2H, *ArH*), 7.61 (d, *J* = 8.4 Hz, 2H, *ArH*); <sup>13</sup>C NMR (CDCl<sub>3</sub>, 100 MHz) δ 122.4, 125.1, 126.1, 126.9, 127.0, 129.0, 129.4, 135.15, 138.4; IR (KBr) 3427, 2081, 1613, 1413, 1325, 1137, 1106, 1066, 839, 590 cm<sup>-1</sup>. Anal. Calcd for C<sub>8</sub>H<sub>4</sub>F<sub>3</sub>NS (203.12): C, 47.26; H, 1.98; N, 6.89; S, 15.79. Found: C, 47.22; H, 1.96; N, 6.91; S, 15.75.

**1-Isothiocyano-3-nitro-benzene (7a).** Oily; <sup>1</sup>H NMR (400 MHz, CDCl<sub>3</sub>) δ 7.54 (s, 2H, *ArH*), 8.06 (s, 1H, *ArH*),

8.11–8.14 (m, 1H, *ArH*). <sup>13</sup>C NMR (100 MHz, CDCl<sub>3</sub>) δ 120.7, 121.9, 130.6, 131.6, 133.3, 139.6, 148.8. IR (KBr) 3091, 3074, 2227, 2161, 2106, 1526, 1470, 1348, 1302, 892, 809, 736, 665 cm<sup>-1</sup>. Anal. Calcd for C<sub>7</sub>H<sub>4</sub>N<sub>2</sub>O<sub>2</sub>S (180.13): C, 46.63; H, 2.23; N, 15.55; S, 17.81. Found: C, 46.65; H 2.26; N, 15.51; S, 17.78.

**1-Isothiocyano-2,4-dimethyl-benzene (8a).** Oily; <sup>1</sup>H NMR (400 MHz, CDCl<sub>3</sub>) δ 2.30 (s, 3H, CH<sub>3</sub>), 2.33 (s, 3H, CH<sub>3</sub>), 6.96 (d, 1H, *J* = 9.2 Hz, *ArH*), 7.01 (s, 1H, *ArH*), 7.07 (d, 1H, *J* = 8.0 Hz, *ArH*). <sup>13</sup>C NMR (100 MHz, CDCl<sub>3</sub>) δ 18.2, 21.1, 125.6, 127.4, 131.2, 134.6, 137.4. IR (KBr) 2920, 2131, 2085, 1490, 1455, 1379, 1229, 1036, 947, 901, 875, 812 cm<sup>-1</sup>. Anal. Calcd for C<sub>9</sub>H<sub>9</sub>NS (163.17): C, 66.19; H, 5.55; N, 8.58; S, 19.66. Found: C, 66.15; H, 5.52; N, 8.63; S, 19.64.

**2-Iodo-1-isothiocyano-4-methylbenzene (9a).** White solid; m.p. 62–65 °C; <sup>1</sup>H NMR (400 MHz, CDCl<sub>3</sub>) δ 2.30 (s, 3H, CH<sub>3</sub>), 7.13 (m, 2H, *ArH*), 7.62 (s, 1H, *ArH*). <sup>13</sup>C NMR (100 MHz, CDCl<sub>3</sub>) δ 20.9, 94.2, 126.7, 130.1, 132.3, 136.1, 139.1, 139.9. IR (KBr) 2916, 2134, 1633, 1474, 1042, 929, 811 cm<sup>-1</sup>.

**2-Bromo-1-isothiocyano-4-methoxy-benzene (10a).** White solid; m.p. 77 °C; <sup>1</sup>H NMR (400 MHz, CDCl<sub>3</sub>) δ 3.80 (s, 3H, CH<sub>3</sub>), 6.82 (m, 1H, *ArH*), 7.11 (m, 1H, *ArH*), 7.18 (d, 1H, *J* = 8.0 Hz, *ArH*); <sup>13</sup>C NMR (100 MHz, CDCl<sub>3</sub>) δ 56.0, 114.4, 118.5, 121.6, 124.1, 127.7, 136.7, 158.8; IR (KBr) 2972, 2125, 1594, 1560, 1483, 1296, 1263, 1220, 1039, 807, 617 cm<sup>-1</sup>. Anal. Calcd for C<sub>8</sub>H<sub>6</sub>BrNOS (244.05): C, 39.33; H, 2.47; N, 5.73; S, 3.14. Found: C, 39.29; H, 2.52; N, 5.70; S, 3.11.

**1-Iodo-2-isothiocyano-4,5-dimethyl-benzene (11a).** White solid; m.p. 54 °C; <sup>1</sup>H NMR (400 MHz, CDCl<sub>3</sub>) δ 2.18

(s, 3H, CH<sub>3</sub>), 2.22 (s, 3H, CH<sub>3</sub>), 6.99 (s, 1H, ArH), 7.30 (s, 1H, ArH); <sup>13</sup>C NMR (100 MHz, CDCl<sub>3</sub>) δ 19.4, 19.5, 117.2, 124.1, 127.8, 129.3, 133.8, 137.4, 137.9; IR (KBr) 2922, 2853, 2192, 2118, 1472, 1372, 1273, 1076, 1048, 933, 882, 824, 708 cm<sup>-1</sup>. Anal. Calcd for C<sub>9</sub>H<sub>8</sub>INS: C, 37.39; H, 2.79; N, 4.84; S, 11.09. Found: C, 37.42; H, 2.81; N, 4.81; S, 11.06. MS (AP<sup>+</sup>) Calcd for C<sub>9</sub>H<sub>8</sub>INS: 288.94. Found: 288.97 (M<sup>+</sup>).

**5-(Isothiocyanatomethyl)benzo[d][1,3]dioxole (12a).** Reddish oil. <sup>1</sup>H NMR (400 MHz, CDCl<sub>3</sub>) δ 4.59 (s, 2H, CH<sub>2</sub>), 5.98 (s, 2H, CH<sub>2</sub>), 6.74–6.80 (m, 3H, ArH). <sup>13</sup>C NMR (100 MHz, CDCl<sub>3</sub>) δ 48.7, 101.5, 107.7, 108.6, 120.7, 128.0, 132.1, 147.8, 148.2. IR (KBr) 2895, 2087, 1503, 1445, 1369, 1322, 1251, 1101, 1028, 924 cm<sup>-1</sup>.

**Isothiocyanato-cyclohexane (13a).** <sup>1</sup>H NMR (400 MHz, CDCl<sub>3</sub>) δ 1.28–1.96 (m, 10H, CH<sub>2</sub>), 3.67 (m, 1H, CH). <sup>13</sup>C NMR (100 MHz, CDCl<sub>3</sub>) δ 23.0, 24.9, 33.0, 55.2, 129.6. IR (KBr) 2937, 2858, 2175, 2102, 2060, 1450, 1361, 1320, 986, 891, 720, 702 cm<sup>-1</sup>. Anal. Calcd for C<sub>7</sub>H<sub>11</sub>NS (141.23): C, 59.53; H, 7.85; N, 9.92; S, 22.70. Found: C, 59.50; H, 7.81; N, 9.88; S, 22.74.

**1-Isothiocyanato-*n*-butane (14a).** Oily liquid. <sup>1</sup>H NMR (400 MHz, CDCl<sub>3</sub>) δ 0.92 (t, *J* = 7.4 Hz, 3H, CH<sub>3</sub>), 1.37–1.47 (m, 2H, CH<sub>2</sub>), 1.61–1.69 (m, 2H, CH<sub>2</sub>), 3.42 (t, *J* = 6.6 Hz, 2H, CH<sub>2</sub>). <sup>13</sup>C NMR (100 MHz, CDCl<sub>3</sub>) δ 13.2, 19.7, 31.9, 44.7, 129.4. IR (KBr) 2925, 2088, 1597, 1401, 1218, 1116, 753 cm<sup>-1</sup>.

**1-Isothiocyanato-octadecane (15a).** Gummy, <sup>1</sup>H NMR (CDCl<sub>3</sub>, 400 MHz) δ 0.879 (t, *J* = 6.8 Hz, 3H, CH<sub>3</sub>), 1.25 (m, 28H, CH<sub>2</sub>), 1.71–1.72 (m, 4H, CH<sub>2</sub>), 3.50 (t, *J* = 6.4 Hz, 2H, CH<sub>2</sub>); <sup>13</sup>C NMR (CDCl<sub>3</sub>, 100 MHz) δ 14.3, 22.8, 26.7, 29.0, 29.5, 29.7, 29.8, 30.1, 32.1, 45.2; IR (KBr) 2923, 2853, 2185, 2096, 1463, 1455, 1346, 721 cm<sup>-1</sup>. Anal. Calcd for C<sub>19</sub>H<sub>37</sub>NS: C, 73.24; H, 11.97; N, 4.50; S, 10.29. Found: C, 73.27; H, 12.01; N, 4.48; S, 10.25. MS (ES<sup>-</sup>) Calcd for C<sub>19</sub>H<sub>37</sub>NS: 311.26. Found: 311.19 (M<sup>+</sup>).

**Phenyl cyanamide (1b).** Gummy; <sup>1</sup>H NMR (CDCl<sub>3</sub>, 400 MHz) δ 7.02–7.07 (m, 3H, ArH), 7.28–7.33 (m, 2H, ArH), 7.64 (brs, 1H, NH). <sup>13</sup>C NMR (100 MHz, CDCl<sub>3</sub>) δ 112.2, 115.5, 123.6, 129.8, 137.4. IR (KBr) 3175, 2919, 2227, 1600, 1501, 1249, 748, 689 cm<sup>-1</sup>. Anal. Calcd for C<sub>7</sub>H<sub>6</sub>N<sub>2</sub> (118.13): C, 71.17; H, 5.12; N, 23.71. Found: C, 71.27; H, 5.09; N, 23.67.

**2-Fluorophenyl cyanamide (2b).** White solid; m.p. 95 °C; <sup>1</sup>H NMR (CDCl<sub>3</sub>, 400 MHz) δ 6.87 (brs, 1H, NH), 6.90–7.45 (m, 4H, ArH). <sup>13</sup>C NMR (100 MHz, CDCl<sub>3</sub>) δ 110.9, 115.7, 115.9, 116.8, 124.1, 124.1, 125.09, 125.12, 125.6, 125.8, 150.1, 152.5. IR (KBr) 3068, 2037, 1606, 1587, 1495, 1265, 1212, 1104, 941, 808, 752 cm<sup>-1</sup>. Anal. Calcd for C<sub>7</sub>H<sub>5</sub>FN<sub>2</sub> (136.13): C, 61.76; H, 3.70; N, 20.58. Found: C, 61.80; H, 3.73; N, 23.53.

**2-Chlorophenyl cyanamide (3b).** White solid; m.p. 101–103 °C; <sup>1</sup>H NMR (CDCl<sub>3</sub>, 400 MHz) δ 6.56 (brs, 1H, NH), 7.05 (m, 1H, ArH), 7.31 (m, 2H, ArH), 7.35 (m, 1H, ArH). <sup>13</sup>C NMR (100 MHz, CDCl<sub>3</sub>) δ 110.0, 116.2, 120.4, 124.5, 128.6, 129.9, 134.3. IR (KBr) 3163, 2921, 2243, 1598, 1500, 1426, 1295, 1049 cm<sup>-1</sup>. Anal. Calcd for C<sub>7</sub>H<sub>5</sub>ClN<sub>2</sub> (152.58): C, 55.10; H, 3.30; N, 18.36. Found: C, 55.11; H, 3.32; N, 18.29.

**3-Chlorophenyl cyanamide (4b).** White solid; m.p. 93–95 °C; <sup>1</sup>H NMR (CDCl<sub>3</sub>, 400 MHz) δ 6.92 (m, 1H, ArH), 7.03 (m, 2H, ArH), 7.26 (t, *J* = 8.0 Hz, 1H, ArH). <sup>13</sup>C NMR (100 MHz, CDCl<sub>3</sub>) δ 111.1, 113.8, 115.9, 124.0, 130.9, 135.7, 138.7. IR (KBr) 3154, 2910, 2237, 1602, 1513, 1423, 1256 cm<sup>-1</sup>. Anal. Calcd for C<sub>7</sub>H<sub>5</sub>ClN<sub>2</sub> (152.58): C, 55.10; H, 3.30; N, 18.36. Found: C, 55.10; H, 3.29; N, 18.29. MS (ESI): 152 (M<sup>+</sup>).

**3-Nitrophenyl cyanamide (5b).** Yellow solid; m.p. 133–135 °C; <sup>1</sup>H NMR (CDCl<sub>3</sub> + DMSO, 400 MHz) δ 7.38 (d, *J* = 8.4 Hz, 1H, ArH), 7.52 (t, *J* = 8.4 Hz, 1H, ArH), 7.85 (m, 2H, ArH). <sup>13</sup>C NMR (100 MHz, CDCl<sub>3</sub> + DMSO) δ 109.6, 110.7, 116.8, 120.8, 130.1, 139.9, 148.4. IR (KBr) 3147, 2919, 2241, 1621, 1531, 1354, 1260, 1071, 937, 871 cm<sup>-1</sup>. Anal. Calcd for C<sub>7</sub>H<sub>5</sub>N<sub>3</sub>O<sub>2</sub> (163.14): C, 51.54; H, 3.09; N, 25.76. Found: C, 51.58; H, 3.12; N, 25.71; MS (ESI): 163 (M<sup>+</sup>).

**4-Chlorophenyl cyanamide (6b).** White solid; m.p. 95 °C; <sup>1</sup>H NMR (CDCl<sub>3</sub>, 400 MHz) δ 6.91 (d, *J* = 8.0 Hz, 2H, ArH), 7.28 (d, *J* = 8.0 Hz, 2H, ArH). <sup>13</sup>C NMR (100 MHz, CDCl<sub>3</sub>) δ 111.4, 116.9, 128.9, 129.9, 136.2. IR (KBr) 3166, 2954, 2234, 1600, 1494, 1251, 1091 cm<sup>-1</sup>. Anal. Calcd for C<sub>7</sub>H<sub>5</sub>ClN<sub>2</sub> (152.58): C, 55.10; H, 3.30; N, 18.36. Found: C, 55.09; H, 3.33; N, 18.32.

**4-Methoxyphenyl cyanamide (7b).** White solid; m.p. 86–89 °C; <sup>1</sup>H NMR (CDCl<sub>3</sub>, 400 MHz) δ 3.78 (s, 3H, CH<sub>3</sub>), 6.87 (d, *J* = 8.8 Hz, 2H, ArH), 6.95 (d, *J* = 8.8 Hz, 2H, ArH). <sup>13</sup>C NMR (100 MHz, CDCl<sub>3</sub>) δ 55.8, 112.8, 115.2, 117.0, 130.6, 156.1. IR (KBr) 3180, 2926, 2218, 1456, 1295, 1238, 1105, 1037, 826 cm<sup>-1</sup>. Anal. Calcd for C<sub>7</sub>H<sub>6</sub>N<sub>2</sub>O (148.17): C, 64.85; H, 5.44; N, 18.91. Found: C, 64.91; H, 5.40; N, 18.93.

**4-Hydroxyphenyl cyanamide (8b).** White solid; m.p. 259–261 °C; <sup>1</sup>H NMR (CDCl<sub>3</sub> + DMSO, 400 MHz) δ 5.67 (brs, 1H, NH), 6.77 (d, *J* = 8.8 Hz, 2H, ArH), 6.83 (d, *J* = 8.8 Hz, 2H, ArH), 8.98 (brs, 1H, OH). <sup>13</sup>C NMR (100 MHz, CDCl<sub>3</sub> + DMSO) δ 112.8, 115.6, 115.8, 129.5, 152.2. IR (KBr) 3213, 2992, 2230, 1613, 1519, 1444, 1258, 1224 cm<sup>-1</sup>. Anal. Calcd for C<sub>7</sub>H<sub>6</sub>N<sub>2</sub>O (134.14): C, 62.68; H, 4.51; N, 20.88. Found: C, 62.72; H, 4.55; N, 20.83.

**4-Acetylphenyl cyanamide (9b).** White solid; m.p. 153–157 °C; <sup>1</sup>H NMR (CDCl<sub>3</sub> + DMSO, 400 MHz) δ 2.56 (s,



3H, CH<sub>3</sub>), 7.08 (d, *J* = 8.8 Hz, 2H, ArH), 7.91 (d, *J* = 8.8 Hz, 2H, ArH). <sup>13</sup>C NMR (100 MHz, CDCl<sub>3</sub> + DMSO) δ 25.9, 110.9, 114.5, 129.8, 131.2, 142.9, 196.2. IR (KBr) 3188, 2966, 2228, 1666, 1599, 1585, 1411, 1362, 1278, 1176, 962 cm<sup>-1</sup>. Anal. Calcd for C<sub>9</sub>H<sub>8</sub>N<sub>2</sub>O (160.18): C, 67.49; H, 5.03; N, 17.48. Found: C, 67.53; H, 5.08; N, 17.44. MS (ESI): 160 (M<sup>+</sup>).

**2-Iodo-4-methylphenyl cyanamide (10b).** White solid; m.p. 144 °C; <sup>1</sup>H NMR (CDCl<sub>3</sub>, 400 MHz) δ 2.29 (s, 3H, CH<sub>3</sub>), 6.17 (brs, 1H, NH), 7.17 (dd, *J* = 8.2 Hz, 2H, ArH), 7.56 (s, 1H, ArH). <sup>13</sup>C NMR (100 MHz, CDCl<sub>3</sub>) δ 20.4, 84.2, 110.7, 115.4, 130.9, 135.4, 139.6. IR (KBr) 3229, 2919, 2217, 1603, 1573, 1502, 1420, 1383, 1283, 1032, 866, 805 cm<sup>-1</sup>. Anal. Calcd for C<sub>8</sub>H<sub>8</sub>N<sub>2</sub> (258.06): C, 37.23; H, 2.73; N, 10.86. Found: C, 37.27; H, 2.75; N, 10.84.

***n*-Butyl cyanamide (11b).** Gummy; <sup>1</sup>H NMR (CDCl<sub>3</sub>, 400 MHz) δ 0.94 (t, *J* = 7.6 Hz, 3H, CH<sub>3</sub>), 1.40 (m, 2H, CH<sub>2</sub>), 1.58 (m, 2H, CH<sub>2</sub>), 3.06 (m, 2H, CH<sub>2</sub>), 4.61 (brs, 1H). <sup>13</sup>C NMR (100 MHz, CDCl<sub>3</sub>) δ 13.6, 19.5, 31.7, 45.7, 117.2. IR (KBr) 3207, 2961, 2875, 2221, 1614, 1463, 1373, 1171 cm<sup>-1</sup>. Anal. Calcd for C<sub>5</sub>H<sub>10</sub>N<sub>2</sub> (98.15): C, 61.19; H, 10.27; N, 28.54. Found: C, 61.22; H, 10.23; N, 28.48.

**Cyclohexyl cyanamide (12b).** Gummy; <sup>1</sup>H NMR (CDCl<sub>3</sub>, 400 MHz) δ 1.31 (m, 5H, CH<sub>2</sub>), 1.61 (m, 1H, CH<sub>2</sub>), 1.78 (m, 2H, CH<sub>2</sub>), 1.95 (m, 2H, CH<sub>2</sub>), 3.09 (m, 1H, CH<sub>2</sub>), 3.91 (brs, 1H, NH). <sup>13</sup>C NMR (100 MHz, CDCl<sub>3</sub>) δ 24.3, 25.1, 32.6, 54.3, 115.9. IR (KBr) 3196, 2933, 2857, 2217, 1453, 1367, 1167 cm<sup>-1</sup>. Anal. Calcd for C<sub>7</sub>H<sub>12</sub>N<sub>2</sub> (124.19): C, 67.70; H, 9.74; N, 22.56. Found: C, 67.67; H, 9.70; N, 22.50.

**Benzyl cyanamide (13b).** Gummy; <sup>1</sup>H NMR (CDCl<sub>3</sub>, 400 MHz) δ 4.11 (d, *J* = 5.2 Hz, 2H, CH<sub>2</sub> CH<sub>2</sub>), 4.66 (brs, 1H, NH), 7.27–7.37 (m, 5H, ArH). <sup>13</sup>C NMR (100 MHz, CDCl<sub>3</sub>) δ 49.9, 116.7, 127.9, 128.4, 128.9, 136.4. IR (KBr) 3207, 2925, 2220, 1455, 1359, 1155, 1014 cm<sup>-1</sup>. Anal. Calcd for C<sub>8</sub>H<sub>8</sub>N<sub>2</sub> (132.17): C, 72.70; H, 6.10; N, 21.19. Found: C, 72.66; H, 6.13; N, 21.11.

**Benzo[1,3]dioxol-5-ylmethyl cyanamide (14b).** White solid; m.p. 82–84 °C; <sup>1</sup>H NMR (CDCl<sub>3</sub>, 400 MHz) δ 4.05 (d, *J* = 5.2 Hz, 2H, CH<sub>2</sub>), 4.57 (brs, 1H, NH), 5.94 (s, 2H, OCH<sub>2</sub>), 6.77 (m, 3H). <sup>13</sup>C NMR (100 MHz, CDCl<sub>3</sub>) δ 49.9, 101.4, 108.46, 108.54, 116.5, 121.7, 130.1, 147.8, 148.2. IR (KBr) 3233, 2952, 2897, 2220, 1500, 1445, 1038, 925, 809 cm<sup>-1</sup>. Anal. Calcd for C<sub>9</sub>H<sub>8</sub>N<sub>2</sub>O<sub>2</sub> (176.18): C, 61.36; H, 4.58; N, 15.90. Found: C, 61.41; H, 4.61; N, 15.85.

**3,4-Dimethoxyphenylethyl cyanamide (15b).** Gummy; <sup>1</sup>H NMR (CDCl<sub>3</sub>, 400 MHz) δ 2.84 (t, 2H, CH<sub>2</sub>), 3.28 (q, *J* = 7.2 Hz, 2H, CH<sub>2</sub>), 3.83 (s, 3H, CH<sub>3</sub>), 3.84 (s, 3H, CH<sub>3</sub>), 4.37 (brs, 1H, NH), 6.76 (m, 3H, ArH). <sup>13</sup>C NMR (100 MHz, CDCl<sub>3</sub>) δ 35.5, 47.5, 55.92, 55.95, 111.4, 111.9, 116.5, 120.9, 130.0, 147.8, 148.9. IR (KBr) 3274, 2937, 2219, 1592,

1517, 1464, 1262, 1236, 1156, 1142, 1026, 913 cm<sup>-1</sup>. Anal. Calcd for C<sub>11</sub>H<sub>14</sub>N<sub>2</sub>O<sub>2</sub> (206.24): C, 64.06; H, 6.84; N, 13.58. Found: C, 64.12; H, 6.80; N, 13.54.

## 5. Conclusion

In conclusion, we have developed a general, economical and environmentally benign method for the preparation of isothiocyanates and cyanamides from their corresponding dithiocarbamic acid salts. The use of non-toxic and eco-friendly reagents and solvents without the formation of any side products makes this methodology potentially useful. The yield could in fact be considered as very good if not excellent.

**Acknowledgements** UBS acknowledges the financial support received from UGC (UGC/MRP 43-192/2014). N. B. Kuotsu acknowledges the support of this research from UGC (F.5.77/2014-15/MRP/NERO) Thanks are due to CIF/IIT Guwahati for NMR spectra

## 6. References

- (a) A. K. Mukerjee, R. Ashare, *Chem. Rev.* **1991**, *91*, 1–24. DOI:10.1021/cr00001a001  
(b) M. Dobosz, M. Wujec, *Heterocycles*, **2002**, *57*, 1135–1141. DOI:10.3987/COM-02-9461
- (a) N. Kuhnert, G. Williamson, B. Holst, *J. Labl. Comp. Radiopharm.* **2001**, *44*, 347–355. DOI:10.1002/jlcr.462  
(b) N. Kuhnert, Y. Lu, *Labl. Comp. Radiopharm.* **2004**, *47*, 501–507. DOI:10.1002/jlcr.833
- C. Nastruzzi, R. Cotesi, E. Eposito, E. Menegatti, O. Leoni, R. Ironi, S. J. Palmier, *Agric. Food. Chem.* **2000**, *48*, 3572–3575. DOI:10.1021/jf000191p
- K. Xu, P. Thornalley, *J. Biochem. Pharmacol.* **2000**, *6*, 221–231. DOI:10.1016/S0006-2952(00)00319-1
- C. X. Zhang, K. Y. Lee, A. J. Kelly, R. T. Burke, *J. Org. Chem.* **2000**, *65*, 6237–6240. DOI:10.1021/jo000139s
- (a) J. E. Hodgkins, W. P. Reeves, *J. Org. Chem.* **1956**, *21*, 404–405. DOI:10.1021/jo01110a006  
(b) J. E. Hodgkins, W. P. Reeves, *J. Org. Chem.* **1964**, *29*, 3098–3099. DOI:10.1021/jo01033a524
- C. G. Cho, G. H. Posne, *Tetrahedron Lett.* **1992**, *33*, 3599–3602. DOI:10.1016/S0040-4039(00)92512-7
- T. Kitamura, S. Kobayashi, H. Taniguchi, *J. Org. Chem.* **1990**, *55*, 1801–1805. DOI:10.1021/jo00293a025
- J. N. Kim, K. S. Jung, J. H. Lee, J. S. Son, *Tetrahedron Lett.* **1997**, *38*, 1597–1598. DOI:10.1016/S0040-4039(97)00121-4
- J. Goerdeler, C. Ho, *Chem. Ber.* **1984**, *117*, 1636–1639. DOI:10.1002/cber.19841170431
- H. M. Mesharam, S. Dale, J. S. Yadav, *Tetrahedron Lett.* **1997**, *38*, 8743–8744. DOI:10.1016/S0040-4039(97)10158-7
- A. Toshimitsu, S. Uemura, M. Okano, N. Watanabe, *J. Org. Chem.* **1983**, *48*, 5246–5251. DOI:10.1021/jo00174a018
- D. Albanese, M. Penso, *Synthesis* **1991**, 1001–1002.

- DOI:10.1055/s-1991-26629
14. W. G. Shan, G. F. Bian, W. K. Su, X. R. Liang, *Org. Prep. Proced. Int.* **2004**, *36*, 283–286.  
DOI:10.1080/00304940409355967
15. J. N. Kim, E. K. Ryu, *Tetrahedron Lett.* **1993**, *34*, 8283–8284.  
DOI:10.1016/S0040-4039(00)61411-9
16. J. N. Kim, K. S. Jung, H. J. Lee, J. S. Son, *Tetrahedron Lett.* **1997**, *38*, 1597–1598. DOI:10.1016/S0040-4039(97)00121-4
17. W. Adam, R. M. Bargon, S. G. Bosio, W. A. Schenk, D. Stalke, *J. Org. Chem.* **2002**, *67*, 7037–7041. DOI:10.1021/jo026042i
18. M. Arisawa, M. Ashikawa, A. Suwa, M. Yamaguchi, *Tetrahedron Lett.* **2005**, *46*, 1727–1729.  
DOI:10.1016/j.tetlet.2005.01.069
19. L. Valette, S. Poulain, X. Fernandez, L. Lizzani-Cuvelier, *J. Sulfur Chem.* **2005**, *26*, 155–161.  
DOI:10.1080/17415990500070144
20. T. Isoda, K. Hayashi, S. Tamai, T. Kumagai, Y. Nagao, *Chem. Pharm. Bull.* **2006**, *54*, 1616–1619. DOI:10.1248/cpb.54.1616
21. B. Zhong, R. S. Al-Awar, C. Shih, J. H. Grimes Jr., M. Vieth, C. Hamdouchi, *Tetrahedron Lett.* **2006**, *47*, 2161–2164.  
DOI:10.1016/j.tetlet.2006.01.119
22. W. J. Neely, *Aust. J. Chem.* **1960**, *13*, 341–346.  
DOI:10.1071/CH9600341
23. M. Bollini, J. J. Casal, D. E. Alvarez, L. Boiani, M. González, H. Cerecetto, A. M. Bruno, *Bioorg. Med. Chem.* **2009**, *17*, 1437–1444. DOI:10.1016/j.bmc.2009.01.011
24. E. Dyer, T. B. Johnson, *J. Am. Chem. Soc.* **1932**, *54*, 777–787.  
DOI:10.1021/ja01341a048
25. G. M. Dyson, T. Harrington, *J. Chem. Soc.* **1942**, 374–375.  
DOI:10.1039/JR9420000374
26. J. C. Jochims, A. Seeliger, *Tetrahedron* **1965**, *21*, 2611–2616.  
DOI:10.1016/S0040-4020(01)93917-1
27. R. Gottfried, *Angew. Chem., Int. Ed. Engl.* **1966**, *5*, 963–964.  
DOI:10.1002/anie.196609632
28. C. Larsen, K. Steliou, D. N. Harpp, *J. Org. Chem.* **1978**, *43*, 337–339. DOI:10.1021/jo00396a035
29. C. Larsen, D. N. Harpp, *J. Org. Chem.* **1981**, *46*, 2465–2466.  
DOI:10.1021/jo00325a007
30. S. Kim, K. Y. Yi, *J. Org. Chem.* **1986**, *51*, 2613–2615.  
DOI:10.1021/jo00363a046
31. S. Kim, K. Y. Yi, *Tetrahedron Lett.* **1985**, *26*, 1661–1664.  
DOI:10.1016/S0040-4039(00)98578-2
32. J. Grayson, *I. Org. Process Res. Dev.* **1997**, *1*, 240–246.  
DOI:10.1021/op970002c
33. (a) A. Servais, M. Azzouz, D. Lopes, C. Courillon, M. Malacria, *Angew. Chem. Int. Ed.* **2007**, *46*, 576–579.  
DOI:10.1002/anie.200602940  
(b) M. H. Larraufie, C. Ollivier, L. Fensterbank, M. Malacria, E. Laocte, *Angew. Chem. Int. Ed.* **2010**, *49*, 2178–2181.  
DOI:10.1002/anie.200907237  
(c) Z. Pan, S. M. Pound, N. R. Rondla, C. J. Douglas, *Angew. Chem., Int. Ed.* **2014**, *53*, 5170–5174.  
(d) H. Basavaprabhu, V. V. Sureshbabu, *Org. Biomol. Chem.* **2012**, *10*, 2528–2533. DOI:10.1039/c2ob06916d  
(e) V. Panduranga, H. Basavaprabhu, V. V. Sureshbabu, *Tetrahedron Lett.* **2013**, *54*, 975–979.  
DOI:10.1016/j.tetlet.2012.12.027
- (f) S. Kamijo, T. Jin, Y. Yamamoto, *Angew. Chem. Int. Ed.* **2002**, *41*, 1780–1782. DOI:10.1002/1521-3773(20020517)41:10<1780::AID-ANIE1780>3.0.CO;2-#
- (g) L. V. R. Bonaga, H. C. Zhang, B. E. Maryanoff, *Chem. Commun.* **2004**, 2394–2395. DOI:10.1039/B410012C
- (h) K. Fukumoto, T. Oya, M. Itazaki, H. Nakazawa, *J. Am. Chem. Soc.* **2009**, *131*, 38–39. DOI:10.1021/ja807896b
- (i) R. L. Giles, J. D. Sullivan, A. M. Steiner, R. E. Looper, *Angew. Chem., Int. Ed.* **2009**, *48*, 3116–3120.  
DOI:10.1002/anie.200900160
- (j) S. Guin, S. K. Rout, A. Gogoi, W. Ali, B. K. Patel, *Adv. Synth. Catal.* **2014**, *356*, 2559–2565.  
DOI:10.1002/adsc.201400011
- (k) T. K. Lane, B. R. D'Souza, J. Louie, *J. Org. Chem.* **2012**, *77*, 7555–7563. (l) V. Kumar, M. P. Kaushik, A. Mazumdar, *Eur. J. Org. Chem.* **2008**, 1910–1916. DOI:10.1021/jo3012418
34. (a) C. J. Adams, *J. Chem. Soc., Dalton Trans.* **1999**, 2059–2064.  
DOI:10.1039/a901959f  
(b) A. S. Smimov, E. S. Butukhanova, N. A. Bokach, G. L. Starova, V. V. Gurzhiy, M. L. Kuznetsov, V. Y. Kukushkin, *Dalton Trans.* **2014**, *43*, 15798–15811.  
DOI:10.1039/C4DT01812E  
(c) M. Yuan, S. Gao, H. L. Sun, G. Su, *Inorg. Chem.* **2004**, *43*, 8221–8223. DOI:10.1021/ic048547s
35. (a) D. G. Barret, D. N. Deaton, A. M. Hassell, R. B. McFadyen, A. B. Miller, L. R. Miller, J. A. Payne, L. M. Shewchuk, D. H. Willard, L. L. Wright, *Bioorg. Med. Chem. Lett.* **2005**, *15*, 3039–3043. DOI:10.1016/j.bmcl.2005.04.032  
(b) H. W. K. Bischofsheim, H. J. L. Hogheim, J. R. S. Kelkheim, A. W. Egelsbach, S. F. Idstein, H. W. J. Niedernhausen, S. P. Frankfurt, *US 6369069B1*, **2002**.  
(c) K. S. Atwal, G. J. Grover, S. Z. Ahmed, P. G. Sleph, S. Dzwonczyk, A. J. Baird, D. E. Normandin, *J. Med. Chem.* **1995**, *38*, 3236–3245. DOI:10.1021/jm00017a007  
(d) P. W. Manley, U. Quast, *J. Med. Chem.* **1992**, *35*, 2327–2340. DOI:10.1021/jm00090a025  
(e) G. Danger, A. Michaut, M. Bucchi, L. Boiteau, J. Canal, R. Plascal, *Angew. Chem. Int. Ed.* **2013**, *52*, 611–614.  
DOI:10.1002/anie.201207730
36. T. Kamo, M. Endo, M. Sato, R. Kasahara, H. Yamaya, S. Hiradate, Y. Fujii, N. Hirai, M. Hirota, *Phytochemistry* **2008**, *69*, 1166–1172. DOI:10.1016/j.phytochem.2007.11.004
37. (a) B. J. Von, *Ber. Dtsch. Chem. Ges.* **1900**, *33*, 1438–1452.  
DOI:10.1002/cber.19000330208  
(b) L. Y. Hu, J. Guo, S. S. Mager, J. B. Fischer, K. J. Burke-Howie, G. J. Durant, *Ber. Dtsch. Chem. Ges.* **1900**, *33*, 1438–1452.  
DOI:10.1002/cber.19000330208  
(c) G. Kaupp, J. Schmeyers, J. Boy, *Chem.–Eur. J.* **1998**, *4*, 2467–2474. DOI:10.1002/(SICI)1521-3765(19981204)4:12<2467::AID-CHEM2467>3.0.CO;2-D
38. (a) W. A. Davis, M. P. Cava, *J. Org. Chem.* **1983**, *48*, 2774–2775. DOI:10.1021/jo00164a030  
(b) D. Kahne, D. Collum, *Tetrahedron Lett.* **1981**, *22*, 5011–5014. DOI:10.1016/S0040-4039(01)92406-2
39. K. H. Boltz, H. D. Dell, *Justus Liebig's Ann. Chem.* **1967**, *709*,

- 63–67. DOI:10.1002/jlac.19677090107
40. M. E. Hermes, F. D. Marsh, *J. Org. Chem.* **1972**, *37*, 2969–2979. DOI:10.1021/jo00984a013
41. T. V. Hughes, S. D. Hammond, M. P. Cava, *J. Org. Chem.* **1998**, *63*, 401–402. DOI:10.1021/jo9717548
42. R. C. Wheland, E. L. Martin, *J. Org. Chem.* **1975**, *40*, 3101–3109. DOI:10.1021/jo00909a019
43. Y. Q. Wu, D. C. Limburg, D. E. Wilkinson, G. S. Hamilton, *Org. Lett.* **2000**, *2*, 795–297. DOI:10.1021/ol0055263
44. J. J. Kim, D. J. Kweon, S. D. Cho, K. H. Kim, E. Y. Jung, S. G. Lee, J. R. Falck, Y. J. Yoon, *Tetrahedron* **2005**, *61*, 5889–5894. DOI:10.1016/j.tet.2005.03.138
45. S. A. Bakunov, A. V. Rukavishnikov, A. V. Tkachev, *Synthesis* **2000**, 1148–1159. DOI:10.1055/s-2000-6317
46. K. Shin, J. Tienan, Y. Yoshinori, *J. Am. Chem. Soc.* **2001**, *123*, 9453–9454. DOI:10.1021/ja016355f
47. (a) F. F. Wong, C. Y. Chen, M. Y. Yeh, *Synlett* **2006**, 559–562. DOI:10.1055/s-2006-932470  
(b) C. Y. Chen, F. F. Wong, J. J. Haung, S. K. Lin, M. Y. Yeh, *Tetrahedron Lett.* **2008**, *49*, 6505–6507. DOI:10.1016/j.tetlet.2008.08.106
48. K. H. Chaudhuri, U. S. Mahajan, D. S. Bhalerao, K. G. Akamanchi, *Synlett* **2007**, 2815–2818.
49. J. Nath, B. Patel, L. Jamir, U. B. Sinha, K. V. V. Satyanarayana, *Green Chem.* **2009**, *11*, 1503–1506. DOI:10.1039/b914283p

## Povzetek

Opisujemo zelo učinkovit in enostaven pristop k sintezi izotiocianatov in cianamidov iz ustreznih aminov ob prisotnosti blagega, učinkovitega in nestrupenega reagenta tetrapropilamonijevega tribromida. Dobra okoljska sprejemljivost, stroškovna učinkovitost in visoki izkoristki so glavne odlike te metodologije.

Scientific paper

# Prediction of Physico-chemical Properties of Bacteriostatic N<sup>1</sup>-Substituted Sulfonamides: Theoretical and Experimental Studies

Hossein Nikoofard,<sup>1\*</sup> Mohsen Sargolzaei<sup>1</sup> and Farnosh Faridbod<sup>2</sup><sup>1</sup> Faculty of Chemistry, Shahrood University of Technology, Shahrood 63199-95161, Iran.<sup>2</sup> Center of Excellence in Electrochemistry, Faculty of Chemistry, University of Tehran, Tehran, Iran

\* Corresponding author: E-mail: hnikoofard@shahroodut.ac.ir

Received: 13-03-2017

## Abstract

A computational study at the density functional theory (DFT) as well as electrochemical methods, was carried out on the structural and physico-chemical properties of a series of sulfonamide derivatives (SAs) as WHO essential medications in the treatment of basic health system. The B3LYP/6-311++G(d,p) level of theory carried out on sulfadiazine (SDZ), sulfathiazole (STZ), sulfaquinoxaline (SQX), sulfacetamide (SAA), and the reference unsubstituted sulfonamide (SA) was discussed and rationalized in term of the N<sup>1</sup>-sulfonamide substituent. The geometric structures and the electronic properties related to the bacteriostatic reactivity were revealed to be affected by the steric and “push-pull” characteristics of the substituents. Electrochemical experiments on oxidation of SAs, using cyclic voltammetry are presented. The results obtained showed that the calculated ionization potentials (IPs) could be correlated linearly with the electro-oxidation potentials. From the molecules studied it is evident that SDZ act as the most electro-active agent, possessing the highest biological activity. DFT computations carried out using the standard molar enthalpies of formation in the gas phase predicted improvements in the thermodynamic stabilization of the SDZ, SQX, and SAA molecules and an unstabilization of STZ with respect to the parent molecule SA.

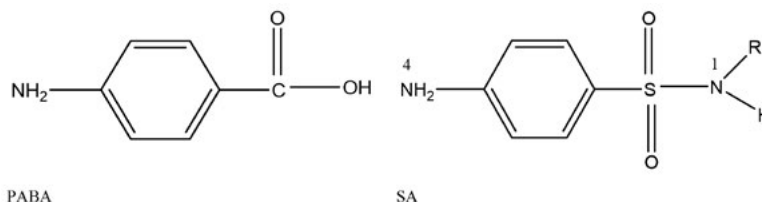
**Keywords:** Sulfonamide, Substituent, Density functional theory, Electrochemical behavior

## 1. Introduction

Sulfa drugs (sulfonamides), characterized by a *p*-aminophenyl group and a sulfonamido one (-SO<sub>2</sub>N-) in their molecular structures, are the basis of some important bacteriostatic agents. These molecules represent a substantial class of pharmaceutical compounds, which are extensively employed as chemotherapeutic agents,<sup>1</sup> and anti-tumor,<sup>2</sup> anti-thyroid,<sup>3</sup> anti-carbonic anhydrase,<sup>4</sup> anti-inflammatory,<sup>5</sup> hypoglycemic,<sup>6</sup> diuretic,<sup>7</sup> COX-inhibitors, and anti-impotence drugs,<sup>8</sup> and also have been used as azo dyes to achieve improved light stability, water solubility, and fixation to fiber. Sulfonamides act as competitive inhibitors of the enzyme dihydropteroate synthase in bacteria, and catalyze changing *p*-aminobenzoic acid into a nutrient necessary for some bacteria.<sup>9</sup> Some sulfonamide derivatives are still extensively used for the treatment of numerous bacterial, fungal infections, protozoal, and the first effective chemotherapeutic agents used in safe therapeutic dosage ranges.<sup>10</sup> Due to their biological and pharmaceuti-

cal ingredients, sulfonamide derivatives find a lot of importance in the literature related to the synthesis of new classes of compounds.<sup>11–15</sup>

Molecular structure of the sulfa drug is analogous to that for *p*-aminobenzoic acid (PABA) (Scheme 1). The similarity between them has been shown by the Wood-fielder theory.<sup>16</sup> According to Bell and Robin,<sup>17</sup> a structure that is comparable to the molecular structure of PABA may interfere within its biological function. The sulfonamide mechanism has been recognized at the enzyme level. In bacteria, anti-bacterial sulfonamides act as the competitive inhibitors of dihydropteroate synthetase. Hence, sulfonamide interferes with the enzyme folic acid synthetase, which is involved in changing PABA to folic acid, which results in the deficiency of folic acid, causing injury to the bacterial cell. Most bacteriostatic SAs have been derivatized basically by variation in the R-substitution linked to the N<sup>1</sup> atom of the sulfonamido group (Scheme 1). Substitution with a heterocyclic structure has



Scheme 1. Sketch map of PABA structure and SA structure with N atom numbering.

produced compounds more active than the parent molecule SA ( $R = H$ ). More widespread experimental studies carried out by Bell,<sup>17</sup> Kumler,<sup>18</sup> Seydel,<sup>19</sup> and others have been devoted to the analysis of the structure-electronic effects that could be related to the pharmaceutical activities, paying special interest to the role of the acidity of the sulfonamido group.<sup>20–22</sup> Sulfonamides are weak acids compared to carboxylic acid amides. Their acidic nature results from the ability of the  $SO_2$  moiety to stabilize the nitrogen anion via resonance. It has been found that their pharmaceutical activity is favored directly by the increased sulfonamide acidity (related to the lower  $pK_a$  values).

The relationship between the chemical structure and pharmaceutical activity of the SA derivatives has prompted the current experimental and theoretical investigations for new sulfa compounds that would possess a greater pharmacological activity.<sup>23–26</sup> In this way, sulfadiazine is one of the substantial sulfonamide antibiotics that are listed as WHO crucial medications in the cure of basic health system.<sup>15</sup> In comparison to the SA derivatives, it has been found that the original SA is at the lowest end of the activity spectrum. Although these drugs are clinically effective in the treatment of various medical disorders, they cause some negative side-effects, which may lead to hepatitis and arthritis. Through relocation, these drugs reach the environment and cause acute toxicity and serious public health hazards.<sup>14</sup>

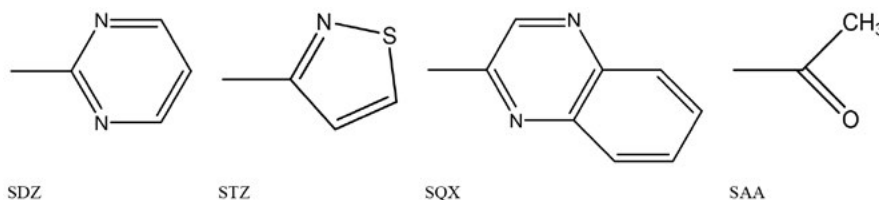
Now we wish to report a theoretical investigation carried out on the SA derivatives including SAA, SDZ, SQX, STZ, and the original sulfonamide SA as the reference molecule, which can be used to evaluate the relevance of the physico-chemical and structural properties toward the steric and electronic influences of the  $N^1$ -substituents. The R groups were chosen by taking into account the structures of some sulfonamide-based drugs. The sketch map of the substituent structures for all the studied SAs is depicted in Scheme 2. Investigations have been carried out to identify the geometric structure, energy disparity be-

tween the lowest unoccupied molecular orbital (LUMO) and the highest occupied molecular orbital (HOMO), atomic and group Mulliken charge distribution, and some appropriate quantum descriptors. Since electrochemical methods are accurate, simple and economical in terms of both time and cost for drug residue monitoring as well as control processes, electro-oxidation behavior of SAs was initially studied on a carbon paste electrode (CPE) using cyclic voltammetry technique.

## 2. Methodology

### 2.1. Computation Method

The ground-state geometry of each sulfonamide was fully optimized using the gradient procedure at the restricted DFT technique, as implemented in the Gaussian 09 program package.<sup>27</sup> A preliminary basis set test carried out for calculations on the electronic ground state for the unsubstituted reference molecule (SA), showed that that 6-311++G(d,p) was the best basis set that can be used within our available hardware/software facilities within a reasonable time. The reports by others<sup>28,29</sup> have also shown that the B3LYP/6-311+G(d,p) level of theory appeared notably adapted to describe sulfonamides to obtain experimental data. The fully-optimized structures by the DFT-B3LYP level<sup>30,31</sup> were confirmed to be the real minima through the zero imaginary frequencies. For all cases, both the radical cation and radical anion were treated as open-shell systems by UB3LYP/6-311++G(d,p). In particular, the values for the electronic chemical potential ( $\mu$ ), global hardness ( $\eta$ ), electrophilicity index ( $\omega$ ), and maximal flow of electrons ( $\Delta N_{Max}$ ) were determined using the Koopman's theorem eigenvalues.<sup>32,33</sup> Furthermore, the standard molar enthalpies of formation in the gas phase at 298.15 K for all the studied species were estimated by the atomization energy route. The detailed description of this calculation procedure has been reported in the literature.<sup>34</sup>



Scheme 2. Sketch map of R group structure for all studied SAs.

## 2. 2. Experimental

All chemical material used for this project were reagent grade from Merck and used as received. A nano-composite modified carbon past electrode consisted of 5% reduced graphene oxide (RGO) decorated CeO<sub>2</sub> nano-particle was employed to study the electro-oxidation of SAs solution using cyclic voltammetry. A homemade ultra-voltammetry system designed in Center of Excellence Electrochemistry (CEE) of University of Tehran was used for the electrochemical measurements at 25.0 ± 0.1 °C. A stock solution (1mM) for each SA derivatives was prepared and kept in refrigerator. Standard solution for measurements was prepared by dilution of stock solution by phosphate buffer (pH 7.4). The external electrode surface was smoothed with a clean and soft paper. A new surface was produced by scraping out the old surface and replacing the carbon paste.

## 3. Results and Discussion

### 3. 1. Geometric Structures of SAs

Full-optimized geometrical structure of each studied sulfonamide obtained at the B3LYP/6-311 ++G(d,p) level of theory are given in Fig. S1 in the Supporting Information. In Table 1, some selected dihedral (*D*) and bond (*A*) angles of the SA derivatives are tabulated. According to this table (column 2), for the dihedral angle *D*<sub>N<sup>4</sup>-ph</sub>, defining the torsion between the amino group (NH<sub>2</sub>) and phenyl ring (ph), a value of 178° is an evidence of complete planarity, and our calculated results indicated that all SAs presented values for *D*<sub>N<sup>4</sup>-ph</sub> close to 180°. It is interesting that introduction of the selected R groups did not affect the planarity of the amino group and phenyl ring present in the parent molecule (SA). It has been found that this planarity in the SA drugs is a necessary condition for a pharmaceutical activity.<sup>23</sup> The dihedral angle between the SO<sub>2</sub> group and the phenyl ring, *D*<sub>ph-SO<sub>2</sub></sub>, was also close to 180° in all SAs (Table 1, column 3). However, for the SAA, SDZ, and SQX species, the C-S-N<sup>1</sup> bond angle (*A*<sub>CSN<sup>1</sup></sub>) displayed a value of nearby 105°, although it was found to be 100° for the STZ molecule. This may be attributed to the different steric effects resulting from the proximity of the substituent R to the sulfonamido group. Our calculated results for all SAs revealed that the bond angle for O-S-O

**Table 1.** Dihedral and bond angles (in degrees) for SA species in neutral state at the B3LYP/6-311++G(d,p) level of theory.

Species	<i>D</i> <sub>N<sup>4</sup>-ph</sub>	<i>D</i> <sub>ph-S</sub>	<i>A</i> <sub>CSN<sup>1</sup></sub>	<i>A</i> <sub>OSO</sub>
SA	178	-180	104	122
SAA	178	179	106	122
SDZ	178	179	105	121
SQX	178	179	105	122
STZ	178	180	100	120

was near 120°, indicating that introduction of the R group did not affect it considerably.

In the case of the optimized structures in the ground state, some selected bond lengths (*d*) of the studied molecules are given in Table 2. As we can see in this table, for all SAs, the bond length for N<sup>4</sup>-ph is 1.38 Å, which is in the order of the C-C bond length in the resonance structure of phenyl ring (on average, 1.39 Å). This means that the amino group is well-conjugated with the phenyl ring, and is not affected by the substituent type. In this way, the N<sup>4</sup>-ph bond distances for both the radical anion and radical cation species, tabulated in Table S1 of the Supporting Information, indicated that the N<sup>4</sup>-ph bond length varied in the following order: anionic (1.40 Å) > neutral (1.38 Å) > cationic (1.34 Å). It is interesting that the ph-S and S-N<sup>1</sup> bond lengths were not varied considerably by the R groups, where the distance between the S atom and R group changed due to the substituent steric hindrance. It has been established<sup>23</sup> that the sulfonamide activity is accompanied by a small distance between the N<sup>1</sup> atom and R group corresponding to the large bond order for *d*<sub>N<sup>1</sup>-R</sub>. According to Table 2 (column 5), the SDZ molecule with a shorter N<sup>1</sup>-R distance possesses a more bacteriostatic activity with respect to the other substituted SAs. It was concluded that the electronic and structural properties of the substituent could contribute to the bacteriostatic activity of a sulfa drug.

**Table 2.** Some selected bond lengths (Å) for SA species in neutral state at the B3LYP/6-311++G(dip) level of theory.

Species	<i>d</i> <sub>N<sup>4</sup>-ph</sub>	<i>d</i> <sub>ph-S</sub>	<i>d</i> <sub>S-N<sup>1</sup></sub>	<i>d</i> <sub>N<sup>1</sup>-R</sub>
SA	1.3851	1.7835	1.7001	-
SAA	1.3803	1.7815	1.7102	1.4022
SDZ	1.3842	1.7773	1.7152	1.3846
SQX	1.3829	1.7758	1.7201	1.3916
STZ	1.3810	1.7787	1.7247	1.4127

### 3. 2. Electronic Properties of SAs

One of the important parameters involved in the bacteriostatic activity of a sulfa drug is the charge distribution of an atom and a group over their molecular structures. We investigated qualitatively the “push-pull” effect of the R substituents on the SA molecules by the Mulliken population analysis. Some atomic and group charge distributions obtained for the neutral and both the radical anion (-) and radical cation (+) of SAs are summarized in Table 3. In all the neutral species, linkage of the R group on the parent molecule SA did not affect the charge on the N<sup>4</sup> atom (Table 3, column 2). This is expected because R group is far from it (see Scheme 1). The calculated results show that the influence of substituent introduction is manifested in the increased negative charge on the N<sup>1</sup> atom in the SAA, SDZ, and SQX species, and an increased positive

charge on it in STZ with respect to the reference molecule SA. These are referred to the electron-withdrawing effect of the R group in the SAA, ADZ, and SQX molecules, and the electron-donating effect of the R group in the STZ molecule, respectively. The same trend was observed for the negative charge on the phenyl ring. Depending on the substituent type, the calculated charge at the SO<sub>2</sub> group shows a large variation. In both the experimental and theoretical works carried out by Bell *et al.*<sup>17</sup> and Soriano-Correa *et al.*,<sup>23</sup> respectively, the increase in the acidity of SAs (which is equivalent to an increase in the bacteriostatic activity) was found to be related to a reduction in the negative charge of the SO<sub>2</sub> group. In other words, the substituent electronegativity is an important parameter that controls the bacteriostatic activity in sulfa drug. Our calculated results showed that SDZ with a more positive charge (or a less negative charge) of the SO<sub>2</sub> group can have a higher reactivity (Table 3, column 5). For the case of radical cation species, the main influence of the injection of one positive charge is manifested in the increased positive charge on the N<sup>4</sup> atom with respect to the N<sup>1</sup> atom. Consequently, the N<sup>4</sup> atom in the *p*-amino group, which is far from the substitution position, was found to be a more reactive zone to the protonation processes than the N<sup>1</sup> atom that is closer to the substituent (see Scheme 1). An inverse trend was observed for the negative charge on the radical anion species. In this regards, the negative charge was distributed mainly on the N<sup>1</sup> atom, which provides that the deprotonation processes were take place most probability at the N<sup>1</sup> atom position with respect to the N<sup>4</sup> atom.

**Table 3.** Some atomic and group charge distributions of SAs in neutral and both radical cation (+) and radical anion (−) states.

Species	N <sup>4</sup>	N <sup>1</sup>	ph	SO <sub>2</sub>
SA	−0.29	−0.34	−0.14	−0.34
SAA	−0.29	−0.40	−0.22	0.03
SDZ	−0.29	−0.49	−0.34	0.36
SQX	−0.31	−0.36	−0.24	0.23
STZ	−0.29	−0.05	−0.07	−0.20
SA(+)	−0.18	−0.38	0.30	−0.08
SAA(+)	−0.18	−0.33	0.27	0.07
SDZ(+)	−0.20	−0.50	−0.01	0.57
SQX(+)	−0.26	−0.41	−0.11	0.53
STZ(+)	−0.25	−0.23	0.16	0.07
SA(−)	−0.23	−0.35	0.12	−0.54
SAA(−)	−0.24	−0.39	−0.22	−0.08
SDZ(−)	−0.25	−0.41	−0.30	−0.07
SQX(−)	−0.30	−0.31	0.00	0.00
STZ(−)	−0.25	−0.33	−0.34	−0.42

It is expected that the presence of a desired R substituent on the sulfonamido group could improve the electron delocalization along the molecular structure. For the case of the SA derivatives, delocalization of the  $\pi$ -electrons onto the molecular backbone led to satisfactory conjuga-

tion systems and improved stabilizations. The extended aromatic structure can correspond to the narrow HOMO-LUMO (H-L) gap energy, which provides a reasonable qualitative indication of the excitation properties and of the ability of electron or hole transport [35–37]. Table 4 displays the H-L gaps for all the SA molecules. According to this data, reduction in the H-L gap values for both the radical anion and radical cation species becomes more considerable with respect to the ones in the neutral state. Thus we may predict that the SA derivatives have the most reactivity in their ionic forms. It is interesting that the H-L gaps for the R substituted species are lower with respect to the reference SA molecule, which is in good agreement with the less bacteriostatic reactivity of the original SA.<sup>23</sup> Among the compounds studied, SDZ and SQX have the lower H-L gaps, indicating that they can be show the higher reactivity. The results obtained revealed that the HOMO-LUMO electronic transitions could be attributed to the tendency of the considered R groups to contribute the  $\pi$ -electrons with the molecular system.

**Table 4.** Calculated values for HOMO-LUMO gaps (eV) for studied species in neutral and ionic states.

Species	Neutral	Cationic	Anionic
SA	0.197	0.074	0.034
SAA	0.192	0.052	0.034
SDZ	0.174	0.050	0.025
SQX	0.166	0.049	0.034
STZ	0.193	0.054	0.034

According to density functional theory, the energy  $E$  can be expressed as a function of the electron number  $N$  and as a functional of the external potential  $v(r)$ . Derivatives of  $E[N; v(r)]$  with respect to  $N$  and  $v(r)$  produce a set of global and local quantities that allow to quantify the concept of reactivity and site selectivity, respectively. The electronic chemical potential  $\mu$ , the molecular hardness  $\eta$ , the electrophilicity index  $\omega$ , and the maximal flow of electrons that a system may accept  $\Delta N_{\text{Max}}$  are defined as:<sup>32,33</sup>

$$\mu = \left(\frac{\partial E}{\partial N}\right)_v \approx \frac{1}{2}(E_L + E_H) \quad (1)$$

$$\eta = \frac{1}{2} \left(\frac{\partial^2 E}{\partial N^2}\right)_v \approx \frac{1}{2}(E_L - E_H) \quad (2)$$

$$\omega = \frac{\mu^2}{2\eta} \quad (3)$$

$$\Delta N_{\text{Max}} = -\frac{\mu}{\eta} \quad (4)$$

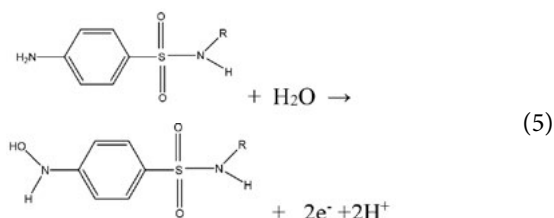
where  $E_H$  and  $E_L$  are the energies of HOMO and LUMO. These electronic that characterize the charge injection and

charge transport properties of such materials are given in Table 5. It was found that the electronic descriptors of SAs are influenced by the electronic and steric properties of the substituent. The values for  $\mu$ ,  $\omega$ , and  $\Delta N_{\text{Max}}$  are related with the escaping tendency of electrons and stabilization energy of the system, and increase with presenting the R group to the parent SA molecule. This indicates that the escaping tendency of electrons in the structures of the SA derivatives, in particular for the deprotonation process, is stabilized by the electron-withdrawing character of the substituent. An inverse trend was observed for the molecular hardness, which points out an obvious substitution effect on the reactivity of the molecules, in particular for the SDZ, SQX, and SAA species. The less change in the electronic properties of the STZ molecule may be referred to the less contribution of its substituent to the conjugated system.

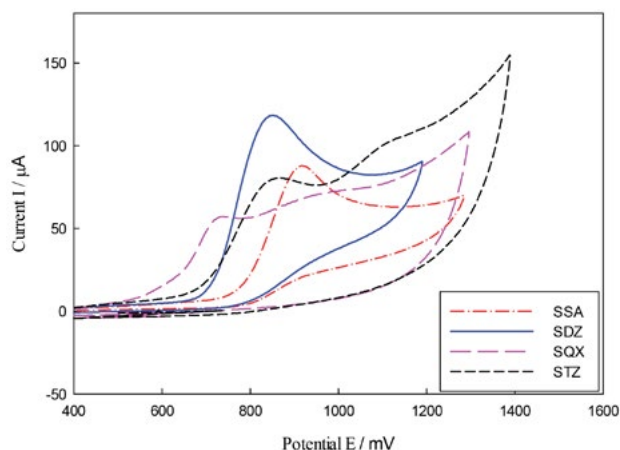
**Table 5.** Calculated values for electronic descriptors  $\mu$ ,  $\eta$ ,  $\omega$ , and  $\Delta N_{\text{Max}}$  for studied SAs.

Species	$\mu$ (eV)	$\eta$ (eV)	$\omega$ (eV)	$\Delta N_{\text{Max}}$
SA	-0.136	0.098	0.187	1.377
SAA	-0.149	0.097	0.230	1.545
SDZ	-0.146	0.087	0.246	1.679
SQX	-0.151	0.084	0.271	1.798
STZ	-0.141	0.097	0.209	1.411

In order to elucidate the electrochemical behavior of the titled SA derivatives, their voltammetric responses obtained at a carbon past electrode. Owing to non-solubility of SAs in acidic rezones, a phosphate buffer solution with pH = 7.4 was used in the cyclic voltammetry measurements. These compounds can be electrochemically oxidized at the amino group ( $\text{NH}_2$ ). Figure 1 shows the cyclic voltammograms of each SAs containing 1.0 mM of sulfacetamide, sulfaquinoxaline, sulfadiazine, and sulfathiazole at the CPE. In all voltammograms, just one oxidation peak was observed which could be expressed as a two-electron, two-proton process via the following reaction:

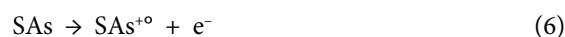


As it can be seen in Figure 1, the anodic peak current and potential at which the oxidation reaction occurs ( $I_{\text{pa}}$  and  $E_{\text{pa}}$ , respectively) are strongly dependent on the characteristic of R group (Scheme 2). Among the SAs, sulfadiazine shows a significant increase in the response current with respect to the other SAs. Under these conditions, it



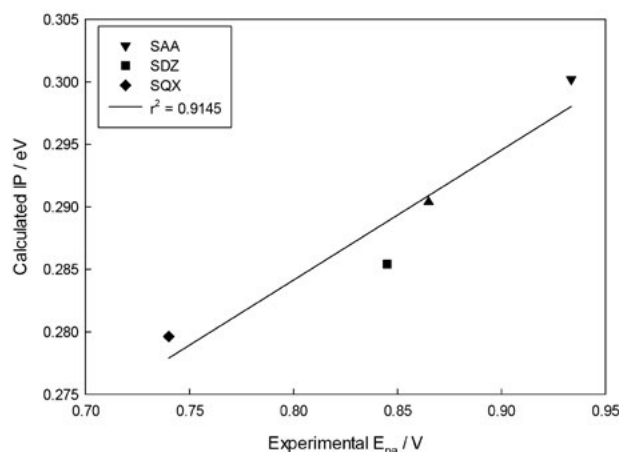
**Figure 1.** Electrochemical behavior of sulfacetamide (SAA), sulfadiazine (SDZ), sulfaquinoxaline (SQX), and sulfathiazole (STZ) at a CPE. All solutions were studied in concentration of 1 mM in a phosphate buffer solution (pH = 7.4) with scan rate of  $0.1 \text{ V s}^{-1}$ .

can be concluded that SDZ possesses a higher electrochemical reactivity, and so it can be considered as a desired pharmaceutical application. Since the anodic peak potential  $E_{\text{pa}}$ , where the oxidation current is maximum, is related to the ionization potential, we calculated the adiabatic IP values for SAs at B3LYP/6-311++G(d,p) level defined as:



where SAs and  $\text{SAs}^{+\bullet}$  stand for the neutral and radical cation states of the sulfonamide derivatives, respectively. In the case of sulfonamide derivatives, the calculated IP is an important parameter for use to estimate the energy barrier for their electro-oxidation reaction.

In Figure 2, the calculated IP values are plotted against the experimental values for  $E_{\text{pa}}$ . According to this figure, one can observe a good correlation between the IP and  $E_{\text{pa}}$  values (the correlation coefficient  $r^2 > 0.90$ ). The observed correlation indicates that a highly delocalized



**Figure 2.** Correlation plot between the calculated IP (eV) and experimental  $E_{\text{pa}}$  (V) for SA derivatives.



system corresponding to a low  $E_{pa}$  value may accept a less barrier energy than a relatively more localized system (with higher  $E_{pa}$ ). This trend is reasonable because a higher electron-conjugation character of the substituent stabilizes the oxidation product (Eq. 2). It can also be observed in Figure 2 that the SAA molecule with a non-cyclic group ( $R = COCH_3$ ) has a large positive shift for  $E_{pa}$ .

### 3. 3. Thermodynamic Stability of SAs

Full-optimized geometrical structure of SAs were used to calculate the vibrational frequencies by means of the B3LYP/6-311 ++G(d,p) level of theory. All vibrational frequency values together some thermochemical quantities of the sulfonamide derivatives including the total energy ( $E$ ), zero-point energy ( $ZPE$ ), enthalpy ( $H$ ), and thermal corrected energy ( $H_{corr}$ ) at 298.15 K were tabulated in Tables S2 and S3. As mentioned in section 2, the gas-phase standard molar enthalpies of formation at 298 K,  $\Delta H_{f,298}^\circ(g)$ , for SAs were calculated through the atomization energy route, and the results obtained were displayed in Figure 3. As it can be seen in this figure, in a comparative study in the gas phase, the improvement in stability (corresponding to  $\Delta H_{f,298}^\circ(g) < 0$ ) was obtained for the SAA, SDZ, and SQX species with respect to the reference molecule SA. Indeed, attachment of an electron-attracting substituent to the sulfonamido group leads to an evident decrease in the standard molar enthalpies of formation and followed by an increase in the thermodynamic stabilization. In agreement with the electronic results obtained in section 3.2, we observed that the thermodynamic stability of the STZ molecule decreased with respect to the unsubstituted parent SA. Since the thermal stability of compounds is an important factor to be considered for the standardization of drugs and pharmaceuticals, it may be concluded that the considered processor helps us to predict the relative thermodynamic stability of new SA derivatives for which the respective experimental determination has not been reported.

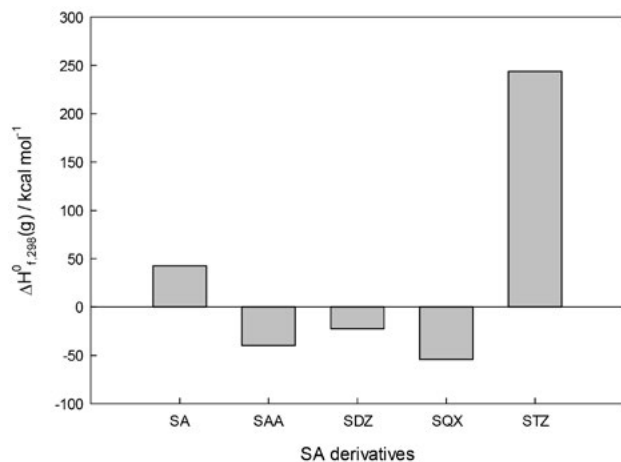


Figure 3. Gas-phase standard molar enthalpy of formation values for SA derivatives at 298 K at the B3LYP/6-311 ++G(d,p) level of theory.

## 4. Conclusion

In the current work, the B3LYP/6-311 ++G(d,p) level of theory was employed to investigate the influence of the  $N^1$ -sulfonamide substituent on the geometrical structure and electronic properties of the SAA, SDZ, SQX, and STZ molecules. Substituting the hydrogen atom of the sulfanamide group by four different substituents played a fine-tune effect on the physico-chemical properties and thermodynamic stabilities of the SA derivatives. In the case of the R substituted species, improvements were obtained in the HOMO-LUMO gap, charge density, and some electronic descriptors with respect to the ones in the reference SA molecule, which were in good agreement with the higher bacteriostatic reactivity of these molecules. Comparison of the cyclic voltammetry experiments for the oxidation potential of SAs obtained in this work, with the calculated ionization potential values shows a linear correlation, which corresponds to the conjugational character of the substituent. The calculations carried out on the neutral and ionic SAs as well as electrochemical measurements showed that the SDZ molecule had a more satisfactory structural and electronic characteristic for the bacteriostatic reactivity. Besides, the calculated results for the standard molar enthalpies of formation in the gas phase revealed an improvement in the thermodynamic stabilization of the SDZ, SQX, and SAA molecules with respect to the unsubstituted parent molecule. Generally, the theoretical data obtained for the efficient injection and transport of the carrier charges involving holes and electrons can be applied for the rational design of a sulfa drug of desired properties.

## 5. Acknowledgment

The authors wish to thank the Shahrood University of Technology for the financial support of this research work.

## 6. References

1. S. Alyar, N. Karacan, J. Enzyme, *Inhib. Med. Chem.* **2009**, *24*, 986–992. DOI:10.1080/14756360802561220
2. T. Owa, T. Nagasu, *Exp. Opin. Ther. Pat.* **2000**, *10*, 1725–1740.
3. R. C. Ogden, C. W. Flexner, *Protease inhibitors in AIDS therapy*, New York, Marcel Dekker, **2001**.
4. I. Nishimori, D. Vullo, A. Innocenti, A. Scozzafava, A. Mastrolorenz, C. T. Supuran, *Bioorg. Med. Chem. Lett.* **2005**, *15*, 3828–3833. DOI:10.1016/j.bmcl.2005.06.055
5. J. J. Li, G. D. Anderson, E. G. Burton, J. N. Cogburn, J. T. Collins, D. J. Garland, S. A. Gregory, H-C. Huang, P. C. Isakson, *J. Med. Chem.* **1995**, *38*, 4570–4578. DOI:10.1021/jm00022a023
6. C. W. Thornbe, *Chem. Soc. Rev.* **1979**, *8*, 563–580. DOI:10.1039/cs9790800563

7. A. E. Boyd, *Diabetes* **1988**, 37, 847–850.  
DOI:10.2337/diab.37.7.847
8. C. T. Supuran, A. Cosini, A. Scozzafave, *Med. Res. Rev.* **2003**, 23, 535–558. DOI:10.1002/med.10047
9. S. Roland, R. Ferone, R. J. Harvey, V. L. Styles, R. W. Morrison, *J. Biol. Chem.* **1979**, 254, 10337–10345.
10. U. Kalidhar, A. Kaur, *Res. J. Pharm., Biol. Chem. Sci.* **2011**, 2, 1116–1135.
11. R. J. Henry, *Bacteriol. Rev.* **1943**, 7, 175–262.
12. S-Y. Won, P. Chandra, T. S. Hee, Y-B. Shim, *Biosens. Bioelectron.* **2013**, 39, 204–209. DOI:10.1016/j.bios.2012.07.043
13. G. Stoev, A. Michailova, *Chromatography* **2000**, 25, 37–42.  
DOI:10.1016/S0021-9673(99)00904-8
14. K. H. Lu, C.Y. Chen, M. R. Lee, *Talanta* **2007**, 72, 1082–1087.  
DOI:10.1016/j.talanta.2007.01.022
15. <http://www.who.int/medicines/publications/essentialmedicines/en/index.html>.
16. W. G. Harter, H. Albrecht, K. Brady, B. Caprathe, J. Dunbar, J. Gilmore, S. Hays, C. R. Kostlan, B. Lunney, N. Walker, *Bioorg. Med. Chem. Lett.* **2004**, 14, 809–813.  
DOI:10.1016/j.bmcl.2003.10.065
17. P. H. Bell, R. O. Roblin, *J. Am. Chem. Soc.* **1942**, 64, 2905–2917. DOI:10.1021/ja01264a055
18. W. D. Kumler, T.C. Daniels, *J. Am. Chem. Soc.* **1943**, 65, 2190–2196. DOI:10.1021/ja01251a053
19. J. K. Seydel, *Pharm. Sci.* **1968**, 57, 1455–1478.  
DOI:10.1002/jps.2600570902
20. Z. H. Chohan, H. A. Shad, L. Toupet, T. B. Hadda, M. Akkurt, *J. Chem. Crystallogr.* **2011**, 41, 159–162.  
DOI:10.1007/s10870-010-9856-x
21. A. M. Mansour, *J. Mol. Struct.* **2013**, 1035, 114–123.  
DOI:10.1016/j.molstruc.2012.09.048
22. A. M. Mansour, N. T. Abdel Ghani, *J. Mol. Struct.* **2013**, 1040, 226–237. DOI:10.1016/j.molstruc.2013.02.028
23. C. Soriano-Correa, R. O. Esquivel, R. P. Sagar, *Int. J. Quant. Chem.* **2003**, 94, 165–172. DOI:10.1002/qua.10597
24. A. Chandran, H.T. Varghese, Y. Sheena Mary, C. Yohannan Panicker, T. K. Manojkumar, C. V. Alsenoy, G. Rajendran, *Spectrochim. Acta A* **2012**, 87, 29–39.  
DOI:10.1016/j.saa.2011.10.073
25. S. Alyar, Ü. Özdemir Özmen, N. Karacan, O. Ş. Şentürk, K. A. Udachin, *J. Mol. Struct.* **2008**, 889, 144–149.  
DOI:10.1016/j.molstruc.2008.01.048
26. H. A. Dabbagh, A. Teimouri, R. Shiasi, A. Najafi Chermahini, *J. Iran. Chem. Soc.* **2008**, 5, 74–82.  
DOI:10.1007/BF03245818
27. M. J. Frisch, G. W. Trucks, H. B. Schlegel, G. E. Scuseria, M. A. Robb, J. R. Cheeseman, V. G. Zakrzewski, J. A. Montgomery Jr., R. E. Stratmann, J. C. Burant, S. Dapprich, J. M. Millam, A. D. Daniels, K. N. Kudin, M. C. Strain, O. Farkas, J. Tomasi, V. Barone, M. Cossi, R. Cammi, B. Mennucci, C. Pomelli, C. Adamo, S. Clifford, J. Ochterski, G. A. Petersson, P. Y. Ayala, Q. Cui, K. Morokuma, D. K. Malick, A. D. Rabuck, K. Raghavachari, J. B. Foresman, J. Cioslowski, J. V. Ortiz, B. B. Stefanov, G. Liu, A. Liashenko, P. Piskorz, I. Komaromi, R. Gomperts, R. L. Martin, D. J. Fox, T. Keith, M. A. Al-Laham, C. Y. Peng, A. Nanayakkara, C. Gonzalez, M. Challacombe, P. M. W. Gill, B. Johnson, W. Chen, M. W. Wong, J. L. Andres, C. Gonzalez, M. Head-Gordon, E. S. Replogle, J. A. Pople, *Gaussian 09W*, Gaussian Inc., Pittsburgh PA, **2009**.
28. M. Karabacak, M. Cinar, M. Kurt, *J. Mol. Struct.* **2010**, 968, 108–114. DOI:10.1016/j.molstruc.2010.01.033
29. J. R. B. Gomes, P. Gomes, *Tetrahedron* **2005**, 61, 27015–2712. DOI:10.1016/j.tet.2005.01.034
30. A. D. Becke, *J. Chem. Phys.* **1993**, 98, 5648–5652.  
DOI:10.1063/1.464913
31. C. T. Lee, W. T. Yang, R.G. Parr, *Phys. Rev. B* **1998**, 37, 785–789. DOI:10.1103/PhysRevB.37.785
32. R. G. Parr, L. V. Szentpaly, S. Liu, *J. Am. Chem. Soc.* **2009**, 121, 1922–1924. DOI:10.1021/ja983494x
33. J. L. Moncada, A. Toro-Labbe, *Chem. Phys. Lett.* **2006**, 429, 161–165. DOI:10.1016/j.cplett.2006.06.087
34. J. W. Ochterski, Gaussian white paper, *Thermochemistry in Gaussian* **2000**, [http://www.gaussian.com/g\\_whitepap/thermo.htm](http://www.gaussian.com/g_whitepap/thermo.htm).
35. H. Cao, J. Ma, G. Zhang, Y. Jiang, *Macromolecules* **2005**, 38, 1123–1130. DOI:10.1021/ma048534y
36. G. Zhang, J. Ma, Y. Jiang, *J. Phys. Chem. B* **2005**, 109, 13499–13509. DOI:10.1021/jp051259c
37. M. A. De Oliveira, H. Duarte, J. Pernaut, W. B. De Almeida, *J. Phys. Chem. A* **2000**, 104, 8256–8265.  
DOI:10.1021/jp001252p

## Povzetek

S teorijo gostotne funkcije (DFT) in z uporabo elektrokemijskih metod smo proučevali strukturne in fizikalno-kemijske lastnosti serije derivatov sulfonamida (SA), ki imajo vlogo nujnih zdravil WHO pri osnovnem zdravljenju. Izračune za sulfadiazin (SDZ), sulfatiazol (STZ), sulfakvinoksalin (SQX), sulfacetamid (SAA) in referenčni nesubstituirani sulfonamid (SA), smo izvedli na B3LYP / 6-311 ++ G (d, p) nivoju. Ugotovili smo, da geometrijske strukture in elektronske lastnosti, povezane z bakteriostatično aktivnostjo, vplivajo na sterične in „push-pull“ značilnosti substituent. Predstavili smo tudi elektrokemijske eksperimente oksidacije SA z uporabo ciklične voltametrije. Izkazalo se je, da med izračunani ionizacijski potenciali (IP) in elektrooksidacijskimi potenciali lahko obstaja linearna zveza. Izmed proučevanih molekul je očitno SDZ najbolj elektroaktiven in izkazuje tudi največjo biološko aktivnost. Izračuni DFT, izvedeni s uporabo standardnih molskih tvorbenih entalpij za tvorbo v plinski fazi, so predvideli možne izboljšave pri termodinamski stabilnosti molekul SDZ, SQX in SAA ter relativno nestabilnost STZ glede na molekulo SA.

Scientific paper

# Methyl Salicylate-Based Vortex-Assisted Surfactant-Enhanced Emulsification Microextraction and HPLC for Determination of Fungicides in Honey Samples

Yanawath Santaladchaiyakit,<sup>1,\*</sup> Jutamas Bunchamnan,<sup>1</sup> Darunee Tongsa<sup>1</sup>  
and Supalax Srijaranai<sup>2</sup>

<sup>1</sup> Department of Chemistry, Faculty of Engineering, Rajamangala University of Technology Isan, Khon Kaen Campus, Khon Kaen 40000, Thailand.

<sup>2</sup> Materials Chemistry Research Center, Department of Chemistry and Center of Excellence for Innovation in Chemistry, Faculty of Science, Khon Kaen University, Khon Kaen 40002, Thailand

\* Corresponding author: E-mail: sanyanawa@gmail.com, yanawath.sa@rmuti.ac.th;  
Tel.: (+66)-4333-8869-70, Fax: (+66)-4333-8869-70

Received: 26-06-2017

## Abstract

Methyl salicylate based vortex-assisted surfactant-enhanced emulsification microextraction (MeSA-VASEME) has been developed and applied for rapid preconcentration of fungicides (i.e., carbendazim, thiabendazole, and fluberidazole) in honey samples followed by high performance liquid chromatographic analysis. MeSA was used as an extraction solvent, while surfactant was used to enhance the extraction performance under the dispersion by vortex agitation. The optimum MeSA-VASEME conditions were 100  $\mu\text{L}$  MeSA, 2.0  $\text{mmol L}^{-1}$  sodium dodecyl sulfate, and vortex agitation at 1200 rpm for 90 s. Preconcentration factors were obtained in the range of 32–40. The limit of detection in the studied honey samples was 0.5  $\mu\text{g L}^{-1}$ . The recovery of the spiked target fungicides at 20, 50, and 100  $\mu\text{g L}^{-1}$  were 81.5–116.8 % with the relative standard deviation below 11%. The proposed method is simple, sensitive, less organic solvent consuming, inexpensive, and a rapid procedure for the residue analysis of fungicides in honey samples.

**Keywords:** Methyl salicylate, VASEME, HPLC, Fungicide, Honey

## 1. Introduction

Bee products including honey are natural products that are rich in minerals, antioxidants, and simple sugars.<sup>1</sup> Honey is found to be used as enzymatic and nonenzymatic antioxidant to prevent deteriorative oxidation reactions in foods such as the browning of fruit and vegetables, lipid oxidation in meat, and to inhibit the growth of food borne pathogens and microorganisms leading to food spoilage.<sup>1</sup> In addition, honey has potential therapeutic properties in infections, wound healing, and cancer.<sup>1</sup> However, bee products can also be a source of toxic substances, such as heavy metals, radioactive isotopes, organic pollutants, and pesticides (e.g., insecticides, fungicides, herbicides, and bactericides) due to environmental pollution and misuse of beekeeping practices.<sup>1,2</sup> Indirect contamination of hon-

ey by pesticides can be found during the pesticide applications in agriculture through soil, water, air, and flowers and then bees come into contact with the pesticides and collect nectar to produce the honey.<sup>3</sup> Pesticide residues (e.g., organohalogenes, organophosphates, organonitrogen, pyrethroids, and carbamates) in honey samples have been reported in the range of 0.05–4310  $\mu\text{g kg}^{-1}$  and were found in many countries.<sup>2</sup> According to the legislations of maximum residue limits (MRLs) set by the European Union (EU) and Official of Brazil, it should be below 50  $\mu\text{g kg}^{-1}$  for most pesticides.<sup>3</sup>

Benzimidazole fungicides are widely used in agriculture for pre- and post-harvest treatment to control and kill fungi or fungal spores in order to prevent the spoilage of crops.<sup>4–6</sup> The active benzimidazole fungicides include benomyl (BN), carbendazim (CBZ), thiabendazole

(TBZ), fuberidazole (FuBZ), thiophanate (TP), and thiophanate-methyl (TPM). Most of the fungicides are normally used to control various diseases in various fruits and vegetables. They are directly applied to soil or sprayed over the crop fields.<sup>4,7</sup> Hence, the studied fungicides may contaminate natural honey after bees come into contact with contaminated plants. From the literature, it was found that CBZ at the level of  $1.62 \mu\text{g kg}^{-1}$  was detected in the honey sample.<sup>8</sup> There are several toxic effects from this fungicide exposure including teratogenicity, congenital malformations, polyploidy, diarrhea, anemia, pulmonary edemas, or necrotic lymphadenopathy.<sup>5,9</sup> Therefore, the development of highly sensitive techniques for trace residue analyses of fungicides in various sample matrices (e.g. food and environmental samples) has been increasingly important for the environment and health protection.

The simultaneous residue determinations of benzimidazole fungicides using micellar electrokinetic chromatography (MEKC),<sup>10</sup> and high performance liquid chromatography (HPLC)<sup>11–14</sup> have been popularly employed. Recently, the solvent-microextraction technique based on the application of vortex agitation, namely vortex-assisted liquid-liquid microextraction (VALLME) has been reviewed.<sup>15</sup> Furthermore, surfactants (as emulsifiers) are used instead of disperser solvents (used in DLLME). This technique is named vortex-assisted surfactant-enhanced emulsification microextraction (VASEME). It was found that VALLME overcomes the disadvantage of DLLME (required disperser solvents), while surfactants used in VASEME assist extraction solvents to better disperse into a sample solution.<sup>16</sup> The combination of vortex agitation and surfactant has also been widely applied to improve the extraction performance and used for the analysis of various compounds.<sup>16–21</sup> In VASEME, extraction solvents/surfactants such as carbon tetrachloride/Triton X-100, toluene/CTAB, 1-octanol/SDS+CTAB, trichloromethane/ammonium perfluorooctanoate, 1-undecanol/Triton X-100, and methyl benzene/Tween 20 can be used.<sup>16–21</sup> As mentioned above,<sup>16–21</sup> it was found that a toxic extraction solvent (e.g. carbon tetrachloride) was used. Meanwhile, the use of lighter density solvents (e.g. toluene, octanol, undecanol) proved difficult to separate and collect the upper extract phase and normally needed special devices to accomplish the phase separation. To overcome these limitations, an alternative extraction solvent such as methyl salicylate (MeSA) seems to be interesting for the extraction and preconcentration of organic compounds, such as fungicides. MeSA has some important characteristics such as (1) high density ( $1.17 \text{ g mL}^{-1}$ ), (2) clear liquid solution at room temperature, (3) low water solubility ( $700 \text{ mg L}^{-1}$ ), and (4) low cost.<sup>22</sup> As our previous work demonstrated, MeSA was used in quite a large volume ( $250 \mu\text{L}$ ) and extraction was carried out in the presence of salt in the extraction solution.<sup>22</sup> However, it seems to be suitable for non-polar compounds, except CBZ. Thus, the further de-

velopment of preconcentration based on MeSA is of interest. The use of MeSA and surfactant (as emulsifier) instead disperser solvent and salt could maybe improve the performance of extraction of target fungicides, especially CBZ. The application of the proposed VASEME using MeSA as an extraction solvent has not been used for the analysis of fungicides in honey samples.

This work is aimed at the development and extension of our previous work using a method named methyl salicylate based vortex-assisted surfactant-enhanced emulsification microextraction (MeSA-VASEME) coupled with HPLC for the simultaneous analysis of target benzimidazole fungicides (e.g. CBZ, TBZ, and FuBZ) in honey samples. The variables affecting MeSA-VASEME procedure were investigated, and analytical performances as well as method validation were also evaluated.

## 2. Experimental

### 2. 1. Chemicals and Reagents

The chemicals and reagents used in this study are of AR grade or higher. The analytical standards of fungicides were purchased from Sigma-Aldrich including CBZ (Munich, Germany), TBZ (Milan, Italy), and FuBZ (Munich, Germany). The stock solutions of each fungicide were prepared at  $1,000 \text{ mg L}^{-1}$  by dissolving an appropriate amount in a small volume ( $\sim 500 \mu\text{L}$ ) of formic acid and further dilution with methanol (MeOH). Methyl salicylate was obtained from Sigma-Aldrich (Shanghai, China). MeOH, ethanol (EtOH), formic acid, and acetonitrile (ACN) were purchased from Merck (Darmstadt, Germany). Sodium dodecyl sulfate (SDS) was purchased from BDH Prolab (Leuven, Belgium). Triton X-100 was purchased from Sigma-Aldrich (MO, USA), while Tergitol® TMN-10 (Sigma-Aldrich, MO, USA) and cetyl trimethylammonium bromide (CTAB) (Sigma-Aldrich, Bangalore, India) were also purchased. The solutions of SDS ( $100 \text{ mmol L}^{-1}$ ), CTAB ( $100 \text{ mmol L}^{-1}$ ), Triton X-100 (25%, w/v), and Tergitol TMN-10 (25%, w/v) were prepared in deionized water before use. Sodium chloride (NaCl) (Ajax Finechem, Auckland, New Zealand), anhydrous sodium sulfate (anh.  $\text{Na}_2\text{SO}_4$ ) (Carlo Erba, Val de Reuil, France), sodium carbonate ( $\text{Na}_2\text{CO}_3$ ) (RFCL Limited, New Delhi, India), and anhydrous sodium acetate (anh. NaOAc) (Carlo Erba, Val de Reuil, France) were used. All aqueous solutions were prepared in deionized water with resistivity of  $18.2 \text{ M}\Omega \text{ cm}$  from  $\text{RiO}_s^{\text{TM}}$  Type I Simplicity 185 (Millipore water, MA, USA).

### 2. 2. Instruments

The HPLC coupled with a photo-diode array detector (PDA) (Shimadzu Corporation, Kyoto, Japan) was used. Data analysis and acquisition of the system were controlled using LCsolution software (Shimadzu). An In-

ertsil C8 column (4.6 × 150 mm, 5.0 μm) connected to a guard C8 column (4.0 × 10 mm, 5.0 μm) (GL Science, Tokyo, Japan) was used as the separation column for target fungicides. Centrifuge NF200 model (Nüve Inc., Ankara, Turkey) and a vortex mixer Genie-2 model (Scientific Industries Inc., NY, USA) were also used.

## 2. 3. HPLC Separation Conditions

The reversed-phase HPLC was used for complete separation of the studied fungicides under the gradient elution of ACN and 0.1% (v/v) formic acid as an optimal mobile phase. A flow rate of 1.0 mL/min was performed throughout the separation process. The chromatographic separation was performed at 25 °C. The detection of the target analytes was performed at 280 nm for CBZ, and at 311 nm for TBZ and FuBZ. The column gradient program<sup>12,22</sup> consisted of 0–2.0 min 15% ACN, 2.0–4.0 min ramped linearly from 15 to 45% ACN, and then 4.0–6.0 min ramped linearly to 75% ACN. After the composition was further kept constant at 75% ACN for 3 min, ACN was linearly decreased to 45% and 15%, respectively. When the pressure reached its initial value, the next separation process could be performed.

## 2. 4. Sample Analysis

Honey samples were purchased from a supermarket in Khon Kaen province, Thailand. Accurate weight (1.00 g) of sample was dissolved in 10 mL water. Then, the 10 mL sample solution was extracted using the MeSA-VASEME procedure and analyzed by HPLC. To evaluate the accuracy, the studied honey samples were fortified with the standard fungicides at various concentration levels of 20, 50, and 100 μg L<sup>-1</sup> prior to the preconcentration.

## 2. 5. MeSA-VASEME Procedure

Methyl salicylate (100 μL) and SDS (2 mmol L<sup>-1</sup>) were injected into the 15 mL conical tube containing a standard or sample solution (10.00 mL). Then, the solution was manually shaken for 15 s before vortex agitation at 1200 rpm for 90 s. After centrifugation at 3000 rpm for 1 min, the extract phase was obtained (at the bottom of the tube). The aqueous phase was then removed by microsyringe. Subsequently, the extract rich phase was mixed with MeOH (100 μL) before subjecting it (20 μL) to HPLC for the analysis.

## 2. 6. Calculation of Preconcentration Factor and Extraction Recovery

Preconcentration factor (PF) and extraction recovery (ER) were used to evaluate the performance of the extraction method and were calculated using the following equations:

$$PF = \frac{C_{\text{ext}}}{C_0} \quad (1)$$

$$ER(\%) = \frac{C_{\text{ext}}}{C_0} \times \frac{V_{\text{ext}}}{V_0} \times 100 = PF \times \frac{V_{\text{ext}}}{V_0} \times 100 \quad (2)$$

where  $C_{\text{ext}}$  is defined as target compound concentration in the collected phase, while  $C_0$  is the initial analyte concentration. The calculation of  $C_{\text{ext}}$  was conducted from the standard calibration curves obtained from the direct analysis (without preconcentration).  $V_{\text{ext}}$  and  $V_0$  are the volume of the collected phase and initial aqueous sample solution (10 mL), respectively.

## 3. Results and Discussion

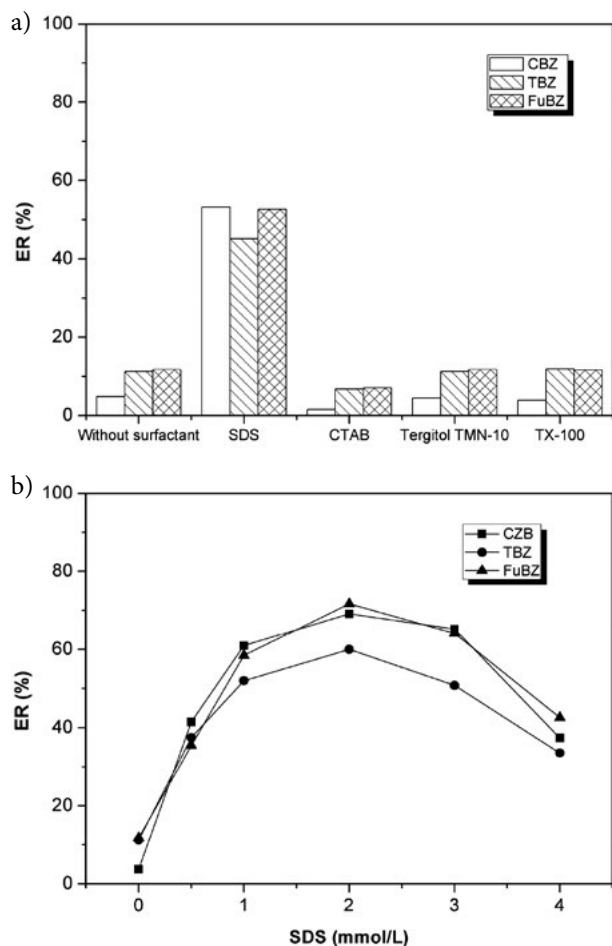
The parameters affecting extraction recovery of target fungicides were investigated including surfactant, extraction solvent, salt additive, solution pH, vortex agitation and centrifugation. One-parameter-at-a-time was used for optimizing extraction conditions, while the other remaining factors were kept constant.

### 3. 1. Effect of Surfactants

By trial and error, three different extraction compositions including (a) MeSA in the presence of sodium acetate, (b) MeSA containing MeOH (as disperser solvent) and sodium acetate, and (c) MeSA in the presence of SDS, were studied. As the results shown in Figure S1 indicate, the chromatograms obtained from the conditions (a) and (b) are similar. This means that the extraction performance of the methods for three studied compounds is insignificantly different under the presence of disperser solvent and/or salt. Meanwhile, MeSA in the presence of SDS gave the highest peak height especially for CBZ. This behavior indicated that SDS can be used as a good emulsifier for improving the extraction of polar analytes. Therefore, the effect of SDS in comparison with other surfactants on the extraction performance of the target fungicides was further investigated.

Theoretically, surfactant was used as an emulsifier in various microextraction methods to accelerate the emulsification of water-immiscible solvent in the aqueous sample solution.<sup>23–25</sup> It has been proven that the addition of surfactant can improve the penetration of different target hydrophobic compounds due to its hydrophobic and hydrophilic groups within the molecule.<sup>26</sup> In this study, surfactants included SDS (at 2.00 mmol L<sup>-1</sup>), CTAB (at 0.50 mmol L<sup>-1</sup>), Tergitol TMN-10 (at 2.71 mmol L<sup>-1</sup>), and Triton X-100 (0.12 mmol L<sup>-1</sup>), while the concentration tested was lower than the critical micelle concentration (CMC) for each surfactant. The CMCs of SDS, CTAB, Tergitol TMN-10, and Triton X-100 were 8, 0.92, 5.7, and 0.24 mmol L<sup>-1</sup>, respectively. The results (Figure 1a) show that SDS (anionic surfactant) provided the highest extraction

recovery in comparison to no surfactant addition, cationic (e.g. CTAB), and non-ionic (e.g. Tergitol TMN-10 and Triton X-100) surfactants. It may be assumed that the target fungicides ( $pK_a \sim 5-6$ ) were in the positive charge<sup>5</sup> under the acidic conditions studied (pH 4) and consequently favorably penetrated and were strongly attracted to SDS molecules. Meanwhile, less interaction between positively charged analytes and cationic or non-ionic surfactant was expected. In addition, it has been reported that good emulsification process was obtained when the concentration of surfactant was lower than CMC.<sup>16</sup> Thus, SDS was then selected for further investigation.



**Figure 1:** Effects of (a) surfactant and (b) SDS on the extraction recovery of the target analytes

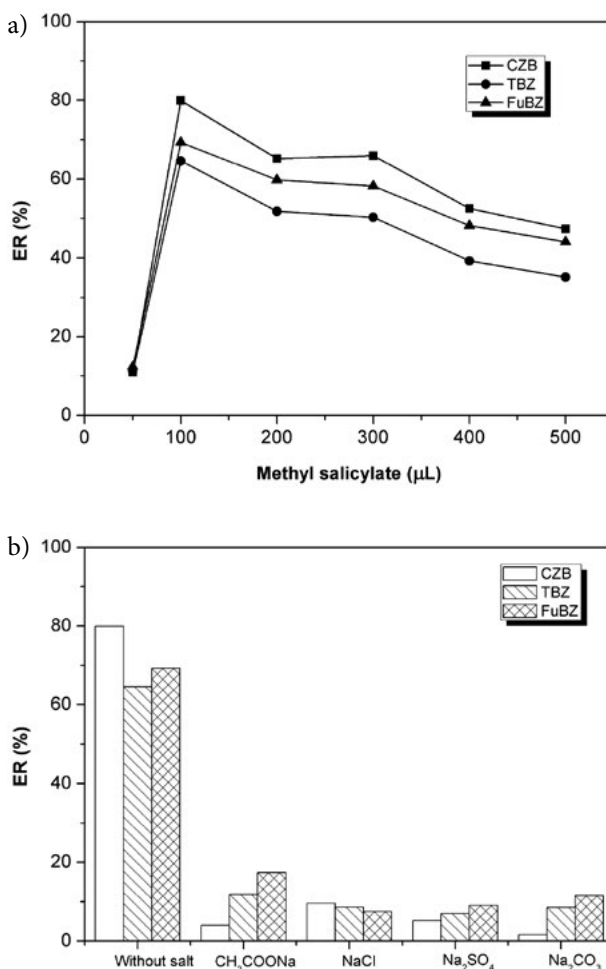
The influence of SDS concentration on the extraction recovery of target fungicides was evaluated in the range of 0–4 mmol L<sup>-1</sup> (see Figure 1b). Increase in the extraction recovery for most target fungicides when concentration of SDS increased was observed up to 2 mmol L<sup>-1</sup>. High concentrations of SDS did not promote better extraction recovery of the target analytes. This behavior may be because of strong self interaction of SDS molecules and the

analytes more favorably dissolve in the aqueous phase resulting in decreased extraction recoveries. In this study, 2 mmol L<sup>-1</sup> SDS was chosen.

### 3. 2. Selection of Extraction Solvent and its Volume

Methyl salicylate was used as an extraction solvent in this study. Based on the  $\log K_{ow}$  (related to hydrophobicity of the analytes) of target fungicides (1.5–2.7) and MeSA (2.55), MeSA seems to be good for extraction of the hydrophobic target fungicides, especially for TBZ and FuBZ. For CZB, the combination of MeSA and SDS could be used for improving the extraction performance of the method. Good characteristics of MeSA as an extraction solvent include (i) the presence of the extract phase at the bottom of the bulk solution (due to its density >1.0 g mL<sup>-1</sup>), (ii) highly solubility in the organic mobile phase, and (iii) no interference of the excess MeSA with the target fungicide peaks.

In this study, the volume of MeSA on the extraction recovery was further studied by varying the volume in the



**Figure 2:** Effects of (a) volume of methyl salicylate and (b) salt addition on the extraction recovery of the target analytes (250 µg L<sup>-1</sup> each).

range of 50–500  $\mu\text{L}$  (Figure 2a). The highest extraction recovery was observed at the MeSA volume of 100  $\mu\text{L}$  and decrease in the extraction performance afterwards. It may be due to the dilution of the target fungicides in higher volume of extract MeSA phase. Thus, 100  $\mu\text{L}$  MeSA was chosen as the optimal value.

### 3. 3. Effect of Salt Addition

In general, the addition of salt into the aqueous sample solution can enhance the extraction recovery of target analytes by decreasing the solubility of the analytes in the aqueous phase and increasing mass transfer toward the organic phase.<sup>15</sup> The decrease in water solubility of target compounds in bulk aqueous phase was expected, resulting in increasing mass transfer of target compounds towards the extract phase. In this investigation,  $\text{CH}_3\text{COONa}$ ,  $\text{NaCl}$ ,  $\text{Na}_2\text{SO}_4$ , and  $\text{Na}_2\text{CO}_3$  were studied at the equal molar concentration ( $\sim 1.71 \text{ mmol L}^{-1}$ ) and compared to with and without salt addition (Figure 2b). It is clearly seen that the addition of salt could not help to improve the extraction recovery of target analytes when compared to the process without salt addition. This may be explained by (i) charge interaction between SDS and counter ions of salts resulting in decreased capability of SDS in the solution, and (ii) salt addition leading to increased viscosity of the bulk aqueous phase. In this study, salt addition was not required throughout the experiments.

### 3. 4. Effect of Solution pH

The effect of sample pH on the extraction recovery of the target fungicides was investigated in the range of 2.0–8.0 (data not shown). It can be found that the pH value strongly affected the extraction efficiency of MsSA-VASEME for fungicide analytes. The highest extraction recovery was found at the pH 4.0 (as the original pH value, without pH adjustment), while higher pHs decreased the extraction efficiency for most analytes. The reason may be the fact that the analytes ( $\text{pK}_{\text{a}1} \sim 4\text{--}5$ ) are in the cationic form (i.e. positive charge) under the acidic pHs and favorably attract SDS molecules (negative charge). On the other hand, the analytes present in the neutral form or negatively charged form result in less interaction between the analytes and SDS. From the investigation, the original pH of the solution of about 4.0 was chosen for the extraction of target fungicides.

### 3. 5. Effect of Vortex Agitation (Extraction Time)

Vortex agitation (speed and time) is one of the important factors in vortex-based microextraction method because it affects the extraction equilibrium (e.g. emulsification and distribution process) of target analytes, and consequently influences the extraction efficiency.<sup>12,17,27</sup> The

vortex agitation time was investigated between 30 and 150 s at speed of 1200 rpm, while the agitation speed was studied in the range of 600–2100 rpm. The results are shown in Figure S2 (a & b), which reveals that appropriate speed and time for the vortex agitation can improve extraction efficiency of the method. In this study, the highest extraction recoveries were found at 90 s at 1200 rpm. A higher speed rate ( $> 1200 \text{ rpm}$ ) and longer time ( $> 90 \text{ s}$ ) decreased the extraction recovery of the target fungicides. Thus, the vortex agitation was chosen at 1200 rpm for 90 s for further evaluation.

### 3. 6. Effect of Centrifugation Time and Speed

Centrifugation speed and time were also investigated in this study because they affect the phase separation of a sample solution. In our previous work,<sup>22</sup> it was reported that a low centrifugation speed (e.g.  $< 2500 \text{ rpm}$ ) could not cause complete phase separation, while the decreased extraction recoveries were observed at high centrifugation speed (i.e. 4000 rpm). In this study, the centrifugation speed (2000–3500 rpm) and time (0–5 min) were investigated (see Figure S3 (a & b)). It is clearly seen that the best extraction recoveries were obtained at a speed of 3000 rpm as the optimum speed for obtaining complete phase separation, and there was a decrease in extraction recoveries afterwards. Meanwhile, the highest extraction recoveries were also observed at the appropriate centrifugation time of 1 min. Therefore, centrifugation at 3000 rpm for 1 min was selected.

### 3. 7. Analytical Performance of the Method

The analytical performance and method validation of the proposed MeSA-VASEME were investigated in two sample matrices (i.e. ultrapure water and honey). The studied parameters were linear dynamic range, coefficient of determination ( $R^2$ ), limits of detection (LODs), limits of quantitation (LOQs) and precision (intra-day and inter-day measurements). LODs were defined as the concentration of the target analytes giving the signal-to-noise ratio of 3 ( $S/N = 3$ ), while LOQs were defined as the  $S/N = 10$ .

In ultrapure water medium, the linearity was found in the range of 0.1–100  $\mu\text{g L}^{-1}$  with  $R^2$  greater than 0.995. LODs were obtained between 0.01 and 0.05  $\mu\text{g L}^{-1}$ , while LOQs were in the range of 0.1–0.2  $\mu\text{g L}^{-1}$ . On the other hand, the LODs obtained from the method without pre-concentration were found to be 3  $\mu\text{g L}^{-1}$  for the studied analytes. The intra-day ( $n = 6$ ) and inter-day ( $n = 6 \times 3$  days) precisions were also investigated by replicate injections of the certain concentration of 100  $\mu\text{g L}^{-1}$  in a day and over several days. The relative standard deviations (RSDs) in terms of peak area and retention time were calculated. It was found that the RSDs below 8.3% for peak area and retention time were obtained. Under the optimal

conditions, preconcentration factors and extraction recoveries were obtained in the range of 32–40, and 64–79%, respectively.

For the investigation in honey samples, the analytical features and method validations were studied in real honey samples. Matrix-matched calibration was performed in this study. The results are summarized in Table 1. The linear dynamic range was in the range of 2–200  $\mu\text{g L}^{-1}$  with  $R^2$  higher than 0.995. The calibrations obtained in each sample are listed in Table 2. LODs and LOQs in honey sample (Brand#1 as a representative sample) were 0.5 and 2  $\mu\text{g L}^{-1}$ , respectively. Precisions in terms of intra-day ( $n = 6$ ) and inter-day ( $n = 3 \times 3$  days) were also studied and expressed as the relative standard deviations (RSDs) of the studied target fungicides at a certain concentration each. High precisions with RSDs below 12% were accepted.

where  $C_{\text{detect}}$  is the detected concentration of analytes after the addition of known amount of standard to real sample,  $C_{\text{real}}$  is the concentration of the target analytes found in real sample, and  $C_{\text{add}}$  is the concentration of the spiked known amount of standard solution in the real sample.

The chromatograms obtained from the spiked samples (see Figure 3) and recovery results (Table 3) are shown. Good relative recoveries of the target fungicides in honey samples were found in the range of 81.5–116.8% with the relative standard deviation below 11%. Intra-day precision ( $n = 6$ ) and intermediate precision ( $n = 3 \times 3$  days) of the proposed method were also studied in the spiked honey sample (Brand#1 as a representative sample) at 100  $\mu\text{g L}^{-1}$  of each fungicide. The studied precisions provided the RSD below 12%. The obtained recoveries and %RSD were in good agreement with the acceptable values of 70–120%

**Table 1:** Figures of merit of the proposed method for the determination of the benzimidazole fungicides in honey samples

Analyte	Linearity ( $\mu\text{g L}^{-1}$ )	LOD ( $\mu\text{g L}^{-1}$ )	LOQ ( $\mu\text{g L}^{-1}$ )	Intra-day precision <sup>a</sup> ( $n = 6$ ), %RSD	Inter-day precision <sup>a</sup> ( $n = 3 \times 3$ days), %RSD
CBZ	2–200	0.5	2	7.7	11.7
TBZ	2–200	0.5	2	8.4	10.0
FuBZ	2–200	0.5	2	8.6	7.2

<sup>a</sup> Precisions were evaluated at the concentration of 100  $\mu\text{g/L}$  for each fungicide spiked in honey brand # 1 (as a representative sample).

**Table 2:** Calibrations obtained by the proposed method for the determination of the benzimidazole fungicides in honey samples

Analyte	Honey Brand#1		Honey Brand#2		Honey Brand#3		Honey Brand#4	
	Linear equation	$R^2$	Linear equation	$R^2$	Linear equation	$R^2$	Linear equation	$R^2$
CBZ	$y = 532x + 3385$	0.996	$y = 805x - 3714$	0.996	$y = 508x - 1717$	0.998	$y = 438x + 1506$	0.997
TBZ	$y = 708x + 8048$	0.995	$y = 1069x - 4201$	0.997	$y = 791x - 537$	0.999	$y = 573x + 3776$	0.999
FuBZ	$y = 1068x + 1600$	0.996	$y = 1865x - 8732$	0.997	$y = 1249x + 796$	0.997	$y = 940x + 6855$	0.997

### 3. 8. Application to Real Samples

The proposed method was then evaluated in different commercial brands of honey samples (4 brands). The matrix-matched calibration was used in this study to avoid endogenous interferences effect on the analysis. The identification and confirmation of the target peaks of the analytes were performed using comparison of retention time of the standard analytes and their absorption spectra data obtained from PDA. An example of honey sample blank is demonstrated in Figure 3. It was found that contamination by the studied fungicides in the studied honey samples was not detected. Accuracy in terms of relative recovery (RR) test at different concentrations spiked (e.g. 20, 50, and 100  $\mu\text{g L}^{-1}$ ) in real honey samples was also investigated. The RR(%) was used for the evaluation of real honey sample analyses. The calculation of RR(%) is as follows:

$$RR(\%) = \frac{C_{\text{detect}} - C_{\text{real}}}{C_{\text{add}}} \times 100 \quad (3)$$

with RSD less than of 20%, at the concentrations spiked in the range of 10–100  $\mu\text{g L}^{-1}$ .<sup>28</sup> According to the results obtained, the proposed method was effective and reliable for the determination of target fungicides in honey samples.

### 3. 9. Comparison of the Proposed Method to Other Relevant Strategies

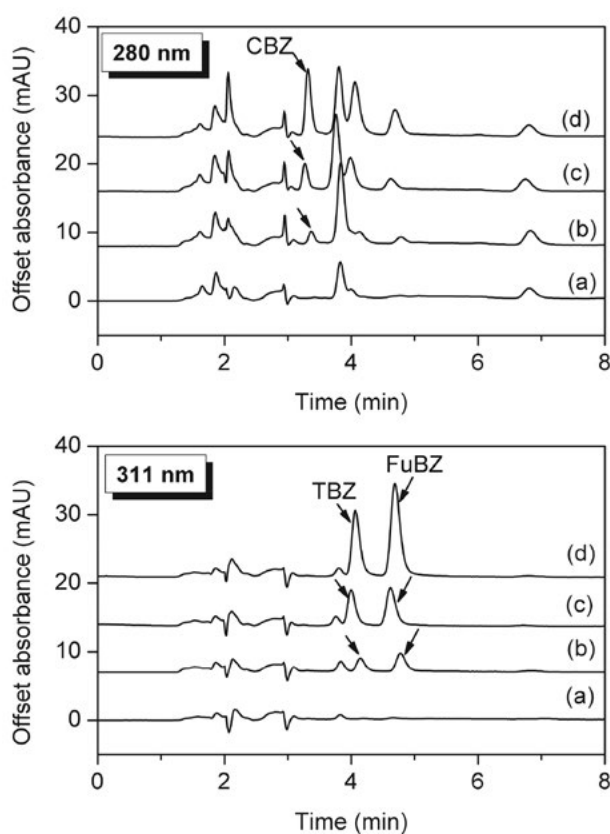
The developed MeSA-VASEME method and other related strategies coupled to HPLC for the analysis of benzimidazole fungicides in various samples (e.g. water) are compared and summarized in Table 4. The SPME<sup>4</sup> and MISPE<sup>6</sup> are promising methods but SPME is expensive and requires a long incubation time (~40 min), high temperature, and high electrolyte salt. Meanwhile, MISPE is a tedious procedure and requires a long synthesis time for the sorbent. Micellar extractions (or cloud-point extractions) using surfactants are normally performed at high incubation temperature (e.g. 90 °C) for a long time.<sup>29</sup> The



**Table 3:** Recovery obtained from the determination of benzimidazole fungicides in honey samples ( $n = 3$ )

Analyte	Spiked ( $\mu\text{g L}^{-1}$ )	Honey brand #1			Honey brand #2			Honey brand #3			Honey brand #4		
		Detected ( $\mu\text{g L}^{-1}$ )	RR (%)	RSD (%)	Detected ( $\mu\text{g L}^{-1}$ )	RR (%)	RSD (%)	Detected ( $\mu\text{g L}^{-1}$ )	RSD (%)	RR (%)	Detected ( $\mu\text{g L}^{-1}$ )	RR (%)	RSD (%)
CBZ	0	ND	–	–	ND	–	–	ND	–	–	ND	–	–
	20	22.97	114.8	3.7	17.47	87.3	4.8	21.15	105.8	5.7	17.99	90.0	1.8
	50	52.81	105.6	1.4	57.55	115.1	7.1	47.60	95.2	3.2	52.88	105.8	9.2
	100	111.62	111.6	10.8	115.05	115.0	3.3	85.56	85.6	4.4	109.89	109.9	9.1
TBZ	0	ND	–	–	ND	–	–	ND	–	–	ND	–	–
	20	16.77	83.8	3.9	17.77	88.9	4.1	19.10	95.5	8.1	16.55	82.7	2.4
	50	46.82	93.6	6.9	53.41	106.8	6.9	50.99	102.0	5.9	44.05	88.1	9.4
	100	89.27	89.3	6.7	115.22	115.2	1.6	90.30	90.3	5.9	111.12	111.1	6.9
FuBZ	0	ND	–	–	ND	–	–	ND	–	–	ND	–	–
	20	19.90	99.5	8.0	16.34	81.7	4.3	20.97	104.9	6.0	16.58	82.9	2.4
	50	50.70	101.4	0.6	55.18	110.4	6.8	47.27	94.5	5.9	40.76	81.5	10.0
	100	103.05	103.0	5.7	116.81	116.8	2.1	90.19	90.2	8.7	107.20	107.2	8.5

ND: Not detected RR: Relative recovery

**Figure 3:** Overlaid chromatograms of honey samples (Brand#1) with (a) honey sample blank and (b–d) spiked at various concentrations of target fungicides (20, 50, and 100  $\mu\text{g L}^{-1}$ , respectively), evaluated at 280 nm and 311 nm.

conventional DLLME uses toxic chlorinated solvent (e.g. chloroform) and needs disperser solvent for emulsification.<sup>30</sup> It was difficult to withdraw the upper extract rich phase and remove the aqueous lower phase in SALLME.<sup>11</sup> It is clearly seen that the proposed MeSA-VASEME provides comparable results such as LODs and recovery. The

developed method is useful for the quantification and qualification of the target fungicides at trace levels in the studied samples. The advantages of the method are a simple procedure, short extraction time, short analysis time, and low cost. The proposed MeSA-VASEME can also be used as an alternative powerful method to the other our previous works demonstrated.<sup>22</sup>

## 4. Conclusions

A simple and fast procedure for preconcentration and analysis using MeSA-VASEME and HPLC-PDA has been successfully developed for target fungicides in honey samples. The preconcentration based MeSA in the presence of surfactant (e.g. SDS) has also been proven to improve the extraction efficiency of target compounds, especially polar analytes. Good extraction efficiency, recovery, and reproducibility were achieved. Low limits of detection at 0.5  $\mu\text{g L}^{-1}$  in honey samples were also obtained. Less consumption of solvents used for the preconcentration step (< 500  $\mu\text{L}$ ), short extraction time (< 10 min), and short separation time (< 5 min) are the advantages of the developed method. The proposed method can be used as an alternative method for trace residue analysis of target fungicides in the studied sample and other related matrices.

## 5. Acknowledgements

This research was financially supported by the Thailand Research Fund (TRF) and Rajamangala University of Technology Isan, through the research grant for new scholars under grant no. TRG5780038. The authors would like to acknowledge Department of Chemistry, Faculty of Science, Khon Kaen University for providing deionized water.

**Table 4:** Comparison of the HPLC technique with different preconcentration methods for the determination of benzimidazole fungicides in various sample matrices

Analyte	Extraction/ clean-up	Extraction condition	Sample matrix	LOD ( $\mu\text{g L}^{-1}$ )	Recovery (%)	Ref.
BN, CBZ, TBZ, FuBZ	SPME	<ul style="list-style-type: none"> <li>• Carboxen-polydimethylsiloxane 75 <math>\mu\text{m}</math> fiber</li> <li>• Heated at 60 <math>^{\circ}\text{C}</math> for 40 min and stirred at 600 rpm</li> <li>• Desorbed by MeOH for 10 min</li> </ul>	Water	0.03–1.30	80.9–119.6	4
BN, CBZ, TBZ, FuBZ	Micellar extraction	<ul style="list-style-type: none"> <li>• Genapol X-080 or POLE (4%, <i>v/v</i>), 4% (<i>w/v</i>) NaCl, 20-min at 90 <math>^{\circ}\text{C}</math></li> </ul>	Water	0.008–6.4 (Genapol X-080), 0.004–5.9 (POLE)	74–92 (Genapol X-080), 72–91 (POLE)	29
CBZ, TBZ	DLLME	<ul style="list-style-type: none"> <li>• Chloroform (extraction solvent) + tetrahydrofuran (disperser solvent) + 10% (<i>w/v</i>) NaCl</li> </ul>	Water	0.5–1.0	84.0–94.0	30
BN, CBZ, TBZ, FuBZ, FluBZ, FBZ, ABZ	MISPE	<ul style="list-style-type: none"> <li>• Molecularly imprinted polymer-divinylbenzene</li> <li>• Eluted by MeOH/acetic acid (50/50, <i>v/v</i>)</li> <li>• Evaporated and re-dissolved in ACN</li> </ul>	Water	0.002– 0.012	90–106	6
CBZ, FuBZ, TPM, TP	SALLE	<ul style="list-style-type: none"> <li>• ACN (2 mL) + <math>\text{NaH}_2\text{PO}_4</math> (0.1 M) + NaCl (5.0 M)</li> <li>• Dried extract phase and re-dissolved with ACN (70%, <i>v/v</i>)</li> </ul>	Water	0.14–0.38	60.4–99.1	11
CBZ, TBZ, FuBZ	VA-DLLME	<ul style="list-style-type: none"> <li>• 250 <math>\mu\text{L}</math> methyl benzoate + 300 <math>\mu\text{L}</math> EtOH + NaOAc (1.0%, <i>w/v</i>)</li> </ul>	Water	0.01–0.05	77.4–110.9	12
CBZ, TBZ, FuBZ	MeSA-DLLME	<ul style="list-style-type: none"> <li>• 250 <math>\mu\text{L}</math> methyl salicylate + NaOAc (1.0%, <i>w/v</i>)</li> </ul>	Water	0.03–0.05	74.1–118.4	22
CBZ, TBZ, FuBZ	MeSA-VASEME	<ul style="list-style-type: none"> <li>• 100 <math>\mu\text{L}</math> methyl salicylate + 0.2 mM SDS</li> </ul>	Honey	0.5	81.5–116.8	Proposed method

## 6. References

- N. Al-Waili, K. Salom, A. Al-Ghamdi, and M. J. Ansari, *Sci. World J.*, **2012**, *2012*, 1–9. DOI:10.1100/2012/930849
- D. R. Lopez, D. A. Ahumada, A. C. Diaz, and J. A. Guerrero, *Food Control*, **2014**, *37*, 33–40. DOI:10.1016/j.foodcont.2013.09.011
- P. A. S. Tette, L. R. Guidi, and M. B. de A. Gloria, *Talanta*, **2016**, *149*, 124–141. DOI:10.1016/j.talanta.2015.11.045
- A. L. Monzón, D. V. Moreno, M. E. T. Padrón, Z. S. Ferrera, and J. J. S. Rodríguez, *Anal. Bioanal. Chem.*, **2007**, *387*, 1957–1963. DOI:10.1007/s00216-006-1083-0
- O. Zamora, E. E. Paniagua, C. Cacho, L. E. Vera-Avila, and C. Perez-Conde, *Anal. Bioanal. Chem.*, **2009**, *393*, 1745–1753. DOI:10.1007/s00216-009-2631-1
- C. Cacho, E. Turiel, and C. Pérez-Conde, *Talanta*, **2009**, *78*, 1029–1035. DOI:10.1016/j.talanta.2009.01.007
- D. P. Zamora, M. M. Galera, A. G. Frenich, J. L. M. Vidal, *Analyst*, **2000**, *125*, 1167–1174. DOI:10.1039/A909886K
- K. M. Kasiotis, C. Anagnostopoulos, P. Anastasiadou, and K. Machera, *Sci. Total Environ.*, **2014**, *485–486*, 633–642. DOI:10.1016/j.scitotenv.2014.03.042
- M. Danaher, H. D. Ruyck, S. R. H. Crooks, G. Dowling, and M. O’Keeffe, *J. Chromatogr. B*, **2007**, *845*, 1–37. DOI:10.1016/j.jchromb.2006.07.046
- R. Rodríguez, Y. Picó, G. Font, and J. Mañes, *J. Chromatogr. A*, **2001**, *924*, 387–396. DOI:10.1016/S0021-9673(01)00716-6
- Y. Wen, J. Li, F. Yang, W. Zhang, W. Li, C. Liao, and L. Chen, *Talanta*, **2013**, *106*, 119–126. DOI:10.1016/j.talanta.2012.12.011
- Y. Santaladchayakit, and S. Srijaranai, *J. Sep. Sci.*, **2014**, *37*, 3354–3361. DOI:10.1002/jssc.201400699
- X. Deng, X. Chen, K. Lin, G. Ding, and P. Yao, *Food Anal. Methods*, **2013**, *6*, 1576–1582. DOI:10.1007/s12161-013-9572-1
- M. Asensio-Ramos, J. Hernández-Borges, T. M. Borges-Miquel, and M. Á. Rodríguez-Delgado, *J. Chromatogr. A*, **2011**, *1218*, 4808–4816. DOI:10.1016/j.chroma.2010.11.030
- V. Andruch, M. Burdel, L. Kocurova, J. Sandrejova, and I. S. Balogh, *Trends Anal. Chem.*, **2013**, *49*, 1–19. DOI:10.1016/j.trac.2013.02.006
- G. Leng, W. Chen, F. Huang, and Q. Cao, *J. Sep. Sci.*, **2014**, *37*, 684–690. DOI:10.1002/jssc.201301033
- Y. Zhang, and H. K. Lee, *J. Chromatogr. A*, **2013**, *1274*, 28–35. DOI:10.1016/j.chroma.2012.12.017
- J. Vichapong, Y. Santaladchayakit, R. Burakham, W. Kanchanamayoon, and S. Srijaranai, *J. Food Compos. Anal.*, **2015**, *37*, 30–37. DOI:10.1016/j.jfca.2014.08.006
- D. Moreno-Gonzalez, J. F. Huertas-Perez, A. M. Garcia-Campana, and L. Gami-Gracia, *Talanta*, **2015**, *139*, 174–180. DOI:10.1016/j.talanta.2015.02.057

20. M. Asadi, A. M. H. Shabani, S. Dadfarnia, and B. Abbasi, *J. Chromatogr. A*, **2015**, *1425*, 17–24. DOI:10.1016/j.chroma.2015.11.005
21. X. Chem, X. You, F. Liu, and X. Zhang, *Anal. Methods*, **2015**, *7*, 9513–9519. DOI:10.1039/c5ay02565f
22. Y. Santaladchaiyakit, N. Phiroonsoontorn, C. Sillapatiwat, K. Kotchalee, and S. Srijaranai, *J. Braz. Chem. Soc.*, **2015**, *26*, 2014–2021. DOI:10.5935/0103-5053.20150181
23. K. Seebunrueng, Y. Santaladchaiyakit, and S. Srijaranai, *Anal. Methods*, **2013**, *5*, 6009–6016. DOI:10.1039/C3AY40096D
24. C. Wu, N. Liu, Q. Wu, C. Wang, and Z. Wang, *Anal. Chim. Acta*, **2010**, *679*, 56–62. DOI:10.1016/j.aca.2010.09.009
25. Z.-H. Yang, P. Wang, W.-T. Zhao, Z.-Q. Zhou, and D.-H. Liu, *J. Chromatogr. A*, **2013**, *1300*, 58–63. DOI:10.1016/j.chroma.2013.02.054
26. Y. Santaladchaiyakit, and S. Srijaranai, *Food Anal. Methods*, **2014**, *7*, 1238–1246. DOI:10.1007/s12161-013-9738-x
27. D. Moreno-González, J. F. Huertas-Pérez, A. M. García-Campaña, and L. Gámiz-Gracia, *Talanta*, **2015**, *139*, 174–180. DOI:10.1016/j.talanta.2015.02.057
28. A. Ambrus, in: J. L. Tadeo (Ed.), *Analysis of pesticides in food and environmental samples*, **2008**, CRC Press, Taylor & Francis Group, New York, 125–152.
29. R. Halko, P. Sanz, S. Ferrera, and J. J. S. Rodríguez, *Chromatographia*, **2004**, *60*, 151–156. DOI:10.1365/s10337-004-0364-z
30. Q. Wu, Y. Li, C. Wang, Z. Liu, X. Zang, X. Zhou, and Z. Wang, *Anal. Chim. Acta*, **2009**, *638*, 139–145. DOI:10.1016/j.aca.2009.02.017

## Povzetek

Za hitro predkoncentracijo fungicidov (karbendazim, tiabendazol, fluberidazol) iz vzorcev medu smo uporabili emulzi-fikacijsko ekstrakcijo s pomočjo surfaktanta in z uporabo vorteksa s topilom metil salicilatom (MeSA-VASEME), ki ji je sledila analiza z visokozmogljivo tekočinsko kromatografijo. Metil salicilat (MeSA) smo uporabili kot ekstrakcijsko topi-lo, medtem ko je surfaktant izboljšal ekstrakcijo ob disperziji z vorteks mešanjem. Optimalni MeSA-VASEME pogoji so bili: 100  $\mu\text{L}$  MeSA, 2,0 mmol  $\text{L}^{-1}$  natrijevega dodecil sulfata in mešanje z vorteksom pri 1200 rpm za 90 s. Dobili smo predkoncentracijske faktorje v območju 32–40. Meja zaznave v preiskovanih vzorcih medu je bila 0,5  $\mu\text{g L}^{-1}$ . Izkoristek dodanih tarčnih fungicidov pri 20, 50 in 100  $\mu\text{g L}^{-1}$  je bil 81,5–116,8 % z relativnim standardnim odklonom pod 11 %. Predlagana metoda je preprosta, občutljiva, porabi manj organskega topila, ni draga, je hiter postopek za analizo preo-stankov fungicidov v vzorcih medu.

Scientific paper

# A One-pot Multicomponent Reaction for the Synthesis of Oligoetherols with Azacyclic Rings

Jacek Lubczak, Renata Lubczak and Iwona Zarzyka

Rzeszów University of Technology, Department of Organic Chemistry, Al. Powstańców Warszawy 6, 35-959 Rzeszów, Poland

\* Corresponding author: E-mail: jml@prz.edu.pl

Received: 04-05-2017

## Abstract

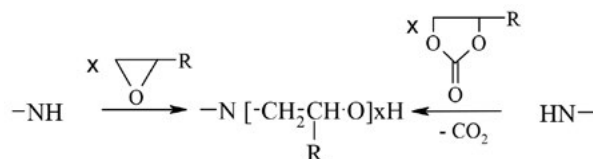
The one-pot multicomponent synthesis of oligoetherols containing azacycles is described. They were obtained by reaction of isocyanuric, barbituric, or uric acid or melamine with glycidol and alkylene carbonates. The isolated products were characterized by physical methods and their properties were compared with the same compounds obtained in two-step protocol. The oligoetherols with 1,3,5-triazine ring obtained by both methods were then used to form polyurethane foams and their properties were compared.

**Keywords:** Azacyclic compounds, glycidol, alkylene carbonates, oligoetherols, one-pot multicomponent reactions, polyurethane foams

## 1. Introduction

The methods of obtaining oligoetherols with azacycles like perhydro-1,3,5-triazine, 1,3,5-triazine, purine or pyrimidine rings, which are present in the structure of isocyanuric acid (IA, I), uric acid (UA, II), barbituric acid (BA, III), and melamine (MEL, IV) (Scheme 1) are described in the literature.<sup>1,2</sup>

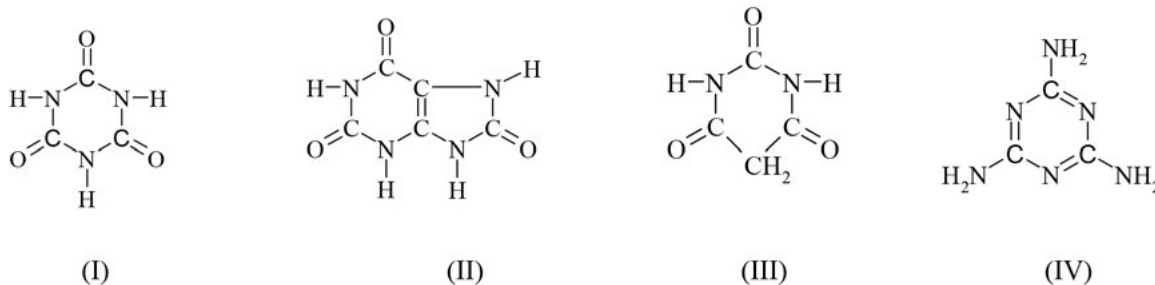
These oligoetherols can be applied to form rigid polyurethane foams (PUFs) of enhanced thermal resistance due to the presence of above mentioned rings. Oligoetherols can be obtained from IA, MEL or adenine and excess oxiranes like ethylene oxide (EO) or propylene oxide (PO)<sup>3-5</sup> or from the reaction of alkylene carbonates (AC) with the mentioned azacyclic compounds.<sup>2</sup> General reaction pathway is shown in Scheme 2.



Scheme 2. Reaction NH groups with oxiranes or alkylene carbonates

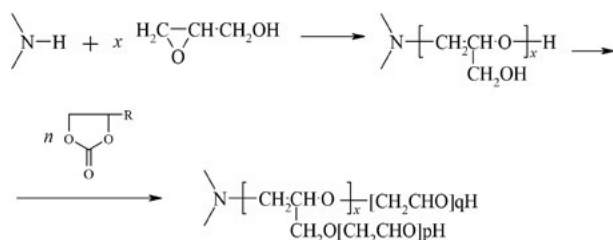
where R = -H, CH<sub>3</sub>

The non-catalytic reactions of IA, UA, BA and MEL with glycidol (GL),<sup>6</sup> and later with AC<sup>7-9</sup> also led to the mentioned oligoetherols. Those syntheses were conducted in two steps; in the first step hydroxyalkyl derivatives of azacycles were obtained as semi-solid resins in reaction of



Scheme 1. Azacyclic compounds used to obtain oligoetherols

azacycles with GL, and then the semiproducts were hydroxyalkylated with excess of ethylene (EC) or propylene (PC) carbonates in the presence of potassium carbonate catalyst according to the Scheme 3.



**Scheme 3.** Obtaining of oligoetherols in two steps: reaction NH groups in azacycles compounds with glycidol and then with alkylene carbonates

where  $R = -H, CH_3, \quad p + q = n$

Those methods have some disadvantages. The derivatization of azacycles with oxiranes is difficult due to low solubility of azacycles in organic solvents suitable for synthesis. Moreover, high boiling solvents like dimethylsulfoxide (DMSO) have to be vacuum distilled from post-reaction mixtures. The DMSO is also unstable at elevated temperatures and its odor originates from the products of its decomposition.<sup>2</sup> On the other hand, the oxiranes are low boiling reagents, therefore the pressure reactors must be used. Also, the oxiranes are toxic, cancerogenic, and form explosive mixtures with air.<sup>10</sup> When AC are used instead oxiranes, the structures of the products are very similar. The reactions with excess AC can be performed at temperatures between 160 °C and 200 °C in the presence of catalysts, like potassium carbonate or diaza[2.2.2]bicyclooctane (DABCO). This protocol results in formation of products with limited functionality and partial decomposition of oligoetherols at synthesis temperature, especially the dehydration of products resulting in the formation of double C=C bonds. That side-reaction also diminishes the functionality of products and finally the PUFs obtained from them have diminished mechanical properties.

Considering the two step synthesis by reaction of azacycle with GL, followed by AC, the exothermic effect observed during the first step causes the temperature increase even above 200 °C (Table 1) which may result in thermal decomposition of oligoetherols. Therefore, the scale-up of this process is technically demanding. Furthermore, the obtained products are semi-solid resins; the high viscosity of the oligoetherols very difficult proper homogenization with isocyanates. Therefore the application of AC for further hydroxyalkylation is necessary to obtain a product of lower viscosity.

Here we describe the results on multicomponent reaction and one-pot reaction (multicomponent one-pot reaction, MOPR) which were optimized in a way to eliminate above mentioned disadvantages. Thus we have ob-

tained one product from at least three substrates introduced at the beginning of the process. In MOPR method the reagents were added consecutively, after the previous step was completed. The products obtained by both methods were isolated and purified in the same way and their properties were compared to those of the products obtained in the two-step protocol. The oligoetherols obtained from MEL were also tested as substrates for polyurethane foams (PUFs). The PUFs obtained here were also compared to those PUFs which were obtained from the oligoetherols synthesized in two-step protocol.

## 2. Experimental Section

### 2.1. Synthesis

To a three-neck round bottom flask equipped with mechanical stirrer, reflux condenser, and thermometer the following reagents were introduced:

- 0.6 mol EC (pure, Fluka, Schwitzland) or PC (pure, Fluka, Schwitzland), 0.6 mol GL (pure, Sigma-Aldrich, Germany), and 0.1 mol IA (pure, Fluka, Switzerland) or
- 0.7 mol EC or PC, 0.6 mol GL, and 0.1 mol UA (pure, Avocado, Germany) or
- 0.8 mol EC or PC, 0.4 mol GL, and 0.1 mol BA (pure, BDH, Laboratory Supplies, UK) or
- 1.6 mol EC or 1.2 mole PC, 0.8 mol GL and 0.1 mol MEL (pure, Fluka, Switzerland).

The mixture was heated at 150 °C until azacyclic compound was dissolved and afterwards the system was kept as such for 1 hour. In the case the system containing MEL the temperature was raised to 120 °C; at that moment the exothermic effect resulted in increase of temperature to 160 °C. The reaction mixture was cooled down to maintain 150 °C until dissolution of MEL was completed and further for 1 hour longer. Then the potassium carbonate (pure, POCH, Poland) as catalyst for the reaction with AC was introduced. The amount of catalyst was the same as previously used for the two-step method;<sup>6–9</sup> the reactions were performed with IA, BA and UA or MEL and EC at 150 °C or with PC at 160 °C until the completed reaction of AC. The progress of reaction was monitored by epoxide number and concentration of AC.

### 2.2. Analytical Methods

The course of the reaction between azacyclic compounds and GL was followed by measuring the content of epoxide groups.<sup>11</sup> The progress of reaction between semi-product and AC was monitored using barium hydroxide method described in the literature.<sup>12</sup> The sample was then treated with 2.5 mL of 0.15 M barium hydroxide, vigorously shaken and the excess of barium hydroxide titrated off with 0.1 M HCl solution. Hydroxyl number of

the obtained oligoetherols was determined with the use of acetic anhydride.<sup>13</sup> Elemental analysis for C, H, N, were done with EA 1108, Carlo-Erba analyzer. IR spectra were registered on PARAGON 1000 FT IR Perkin Elmer spectrometer using ATR technique.

### 2. 3. Properties of Oligoetherols

Density, viscosity, and surface tension of oligoetherols were determined with pycnometer, Höppler viscometer (typ BHZ, prod. Prüfgeratewerk, Germany) and by the detaching ring method, respectively.<sup>14,15</sup>

### 2. 4. Foam Preparation

Into a 500 mL cup 10 g oligoetherol, then 2% water, 2.3% silicon L-6900 (pure, Houdry Hüls, USA) as surfactant, and 2.2% or 3.9% triethylamine (TEA, pure, POCH, Poland) as catalyst were introduced. The mixture was vigorously stirred and then the polymeric methylene diphenyl 4,4'-diisocyanate (pMDI containing 30 mass% of three-functional isocyanates, Merck, Darmstadt, Germany) was added. The mixture was vigorously stirred (1800 rpm) until creaming started.

### 2. 5. Studies of Foams

The apparent density,<sup>16</sup> water uptake,<sup>17</sup> dimensional stability in temperature 150 °C<sup>18</sup> heat conductance coefficient, heat capacity, and compressive strength<sup>19</sup> of polyurethanes foams with flame retardants were measured. Thermal resistance of modified foams was determined both by static methods. In static method the foams were heated at 150, 175 and 200 °C with continuous measurement of mass loss and determination of mechanical properties before and after heat exposure.

## 3. Results and Discussion

### 3. 1. Synthesis of Oligoetherols

The synthesis of oligoetherols was performed as stepwise process in the mixture of all necessary reagents, i.e. azacycle, GL, and AC. This can be considered as multi-components reaction. The first observed reaction was between azacycle and GL. The second step (the reaction with AC) needed addition of catalyst to the reaction mixture. Therefore, the process can also be considered as a one-pot

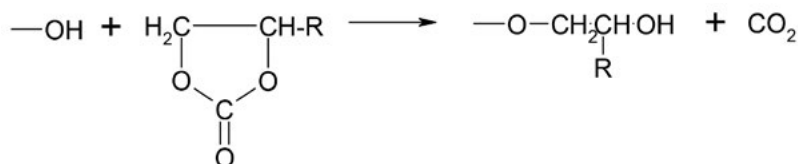
**Table 1.** Exothermic effects accompanying the reaction of azacycles with GL in two-steps synthesis of oligoetherols (the starting amount of azacycle was 0.05 mole)<sup>6–9</sup>

Oligoetherol	Reagents molar ratio	GL-reaction accompanied exothermic effect temp. [°C]	Reaction time [h]
IA:GL:EC <sup>7</sup>	1:6:6	150	1,5
IA:GL:PC <sup>7</sup>	1:6:6	150	1,5
UA: GL:EC <sup>8</sup>	1:6:7	180	0,5
UA: GL:PC <sup>8</sup>	1:6: 7	180	0,5
BA:GL:EC <sup>9</sup>	1:4:8	130	3,0
BA:GL:PC <sup>9</sup>	1:4:7	130	3,0
MEL:GL:EC <sup>6</sup>	1:8:16	230	0,5
MEL:GL:PC <sup>6</sup>	1:8:12	220	0,5

reaction. After heating the reaction mixture up to 150 °C the reaction between azacycle and GL took place. At this stage the AC played the role of a solvent. No exothermic effect was observed in contrary to the two-step method, where after heating of azacycle and GL to 120–130 °C it was found (Table 1). In the case of MEL as azacycle the exothermic effect was observed at 120 °C leading to an increase of temperature to 160 °C (MEL:GL:AC = 1:8:8 system). The temperature of this system was kept at 150 °C by cooling.

The AC are non-flammable, non-toxic, and very polar<sup>10</sup> and they are good solvents for azacycles, therefore in the reaction mixture they are useful as solvents, which are not necessary to be removed after completion of the reaction with GL. They react further after introducing the catalyst (potassium carbonate) at 150 °C or 160 °C to give oligoetherols. On the other hand, the GL enables to obtain oligoetherols with higher functionality in relations to azacycle. The increase of functionality allows to obtain highly crosslinked, rigid PUFs. Moreover, the hydroxyalkyl derivatives obtained from azacycle and GL are better soluble in AC than azacycles, thus homogenization of the mixtures with AC can be reached at lower temperatures than in the case of the azacycle-AC system (temperature needed is 180–230 °C). This allows to avoid thermal decomposition of the semiproducts.

We have obtained oligoetherols in the reaction of azacycles with GL and AC at the same molar ratio of substrates as it has been used earlier in the two-step protocols.<sup>6–9</sup> Analysis of the products obtained from IA, UA, or BA with GL and AC indicated that amount of AC in the



**Scheme 4.** Reaction of alkylene carbonate with hydroxyl group

reaction mixture did not change upon reaction of azacycle with GL, while in the case of MEL, the AC was also consumed at the level of up to 5% of the initial amount. Then,

in the latter system, MEL is hydroxylated also with AC. Generally AC releases CO<sub>2</sub> during the condensation with hydroxyl groups, according to the Scheme 4.

**Table 2.** Elemental analysis and hydroxyl number of oligoetherols obtained in MOPR and two-steps reactions<sup>6-9</sup>

Oligoetherol	Reagents molar ratio	Method of synthesis of oligo-etherol	Elemental analysis [% mas]						Hydroxyl number [mgKOH/g]	
			calculated			found			found	calc.
			C	H	N	C	H	N		
IA:GL:EC	1:6:6	MOPR two-step <sup>7</sup>	47.31	7.53	5.02	47.21 47.51	7.72 7.24	4.95 5.04	592	603
IA:GL:PC	1:6:6	MOPR two-step <sup>7</sup>	50.81	8.14	4.56	50.88 50.69	8.25 8.44	4.48 4.84	534	548
UA:GL:EC	1:6:7	MOPR two-step <sup>8</sup>	48.26	7.39	6.09	48.13 48.51	7.12 7.03	6.25 6.21	571 595	610
UA:GL:PC	1:6:7 1:6:8	MOPR two-step <sup>8</sup>	51.87 52.42	8.06 8.18	5.50 5.20	52.52 51.95	8.25 8.40	5.38 5.83	504 525	551 521
BA:GL:EC	1:4:8	MOPR two-step <sup>9</sup>	49.48	7.73	3.60	49.79	8.03	3.58	560 558	578
BA:GL:PC	1:4:7	MOPR two-step <sup>9</sup>	53.49	8.43	3.37	53.41	8.46	3.51	535 527	540
MEL:GL:EC	1:8:16	MOPR two-step <sup>6</sup>	49.79	8.30	5.90	50.07 49.60	8.21 8.43	5.53 5.44	517 544	552
MEL:GL:PC	1:8:12	MOPR two-step <sup>6</sup>	53.46	8.91	5.94	53.87 53.02	8.81 8.75	6.23 5.70	525 548	476

**Table 3.** The physical properties of oligoetherols at 20 °C obtained various methods in the reaction of azacycles with GL and AC

Oligoetherol	Reagents molar ratio	Method of synthesis of oligo-etherol	Density [g/cm <sup>3</sup> ]	Viscosity [mPa × s]	Surface tension [N/m] × 10 <sup>3</sup>
IA:GL:EC	1:6:6	MOPR two-step <sup>7</sup>	1.28 1.28	17200 17220	50.8 52.6
IA:GL:PC	1:6:6	MOPR two-step <sup>7</sup>	1.24 1.20	16920 16970	48.2 46.9
UA:GL:EC	1:6:7	MOPR two-step <sup>8</sup>	1.27 1.28	30200 (30 °C) 35000 (30 °C)	52.4 57.0
UA:GL:PC	1:6:7 (8)	MOPR two-step <sup>8</sup>	1.21 1.21	42800 47500	45.2 47.0
BA:GL:EC	1:4:8	MOPR two-step <sup>9</sup>	1.26 1.26	93.2 95.6	45.8 46.5
BA:GL:PC	1:4:7	MOPR two-step <sup>9</sup>	1.17 1.18	86.8 86.3	46.8 46.5
MEL:GL:EC	1:8:16	MOPR two-step <sup>6</sup>	1.28 1.26	8445 34260	54.2 46.2
MEL:GL:PC	1:8:12	MOPR two-step <sup>6</sup>	1.20 1.19	25640 65430	46.3 43.5

Elemental analytical data and hydroxyl number measurements indicated that the composition of the obtained oligoetherols is comparable with those of oligoetherols obtained from the two-step reactions (Table 2). Exceptionally the oligoetherol obtained from UA:GL:PC = 1:6:8 system has one equivalent of PC-derived oxyalkylene group more than the oligoetherol obtained in the two-step process. This difference is due to the higher temperature of reaction applied in the two-step protocol, which caused partial decomposition of PC to PO and CO<sub>2</sub> volatiles.

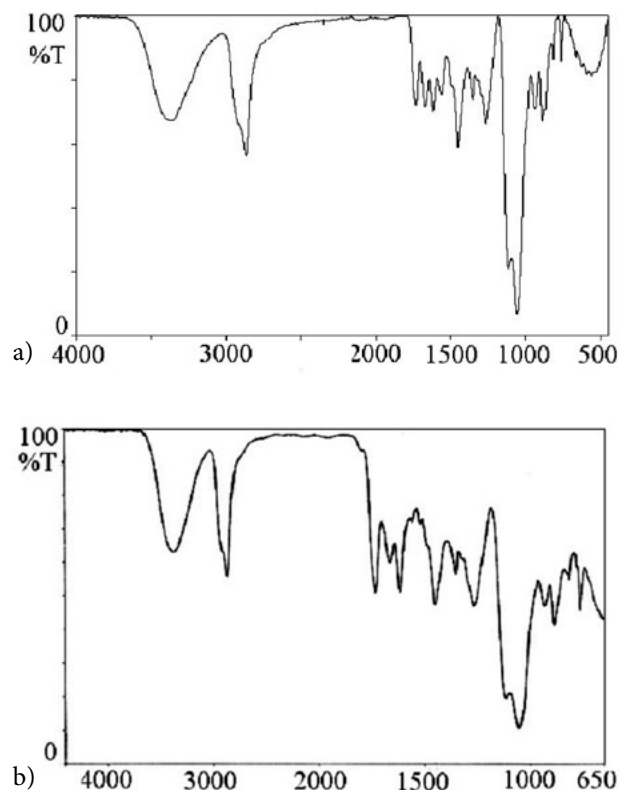


Fig. 1. IR spectrum of oligoetherols obtained in MOPR (a) and in the two-step reaction (b) in molar ratio MEL:GL:EC = 1:8:16

The density, viscosity, surface tension and hydroxyl number of oligoetherols obtained from azacycles, GL, and AC with MOPR method and two-steps method<sup>6-9</sup> are collected in Table 3. The parameters of both series of oligoetherols are comparable except the oligoetherols obtained from MEL. Generally, the oligoetherols obtained in the two-step protocol had higher viscosity, which can be explained by condensation of hydroxyalkyl groups at high temperature and longer reaction time than in the MOPR method.

The IR spectra of oligoetherols obtained from MEL in MOPR method are similar to those obtained in the two-steps method (Fig. 1a versus 1b). In both cases the broad valence hydroxyl group band is centered at 3324 cm<sup>-1</sup>. The ring C=N valence band was observed within 1660–1470 cm<sup>-1</sup> region, while C-OH vibrations were found in the 1350–1450 cm<sup>-1</sup> region. The product of the reaction between MEL and GL and EC had a characteristic band at 2870 cm<sup>-1</sup> attributed to the methylene and methine groups. The band at 813 cm<sup>-1</sup> was related to the 1,3,5-triazine ring, while ether bonds led to the appearance of the band at 1055 cm<sup>-1</sup>. The spectra of the products obtained from PC instead of EC are similar; the additional low-intensity band at 1372 cm<sup>-1</sup> was attributed to the deformation vibration of methyl group. IR spectra of oligoetherols obtained from IA, BA and UA using MOPR and the two-stage method are very similar.

### 3. 2. Obtaining of Polyurethane Foams

The substantial difference of physical properties of the oligoetherols obtained from MEL in MOPR method in comparison with the analogues obtained in the two-steps synthesis prompted us to further study these compounds as substrates to form PUFs. It has been found that amount of isocyanate necessary to form the PUF is independent of the method used (Table 4). However, the optimized amount of catalyst and surfactants are lower in the syntheses by MOPR protocol. Cream times were similar, while rise times are longer and drying times are shorter, which

Table 4. Foaming process

Oligoetherol	Method of synthesis of oligo-etherol	Amount of co-substrate [g/100g oligoetherol]			Foaming Process		
		pMDI	TEA	silicone	Cream time [s]	Rise time [s]	Tack free time [s]
MEL:GL:EC 1:8:16	MOPR	160	2.2	2.3	20	30	immediately
	two-step <sup>6</sup>	160	3.9	3.2	22	13	35
MEL:GL:PC 1:8:12	MOPR	152	3.9	2.3	24	24	immediately
	two-step <sup>6</sup>	152	6.2	3.2	24	11	24

2 mass % of water related to the mass of oligoetherol was used in both methods

Cream time: the time elapsed from the moment of mixing to the start of volume expansion;

Rise time: the time from the start of expansion to the moment of reaching the sample final volume;

Tack free time: the time from reaching by the sample its final volume to the moment of losing its surface adhesion



Table 5. Some properties of polyurethane foams

Foam obtained from oligoetherol	Method of synthesis of oligoetherol	Density [kg/m <sup>3</sup> ]	Absorb. of water [wt %] after		Dimensional stability [%] in temperature 150 °C						Heat conductance coefficient			
					5 min		3 h		24 h			Length change [%] 20 h	Width change [%] 20 h	Height change [%] 20 h
					3 h	24 h	40 h	40 h	40 h					
MEL:GL:EC 1:8:16	MOPR two-step <sup>6</sup>	63.0	1.0	13	1.8	–0.44	–0.59	–0.69	–0.74	–0.46	–0.48	0.0322 ± 0.0005		
MEL:GL:PC 1:8:12	MOPR two-step <sup>6</sup>	42.1	1.2	1.6	1.9	–0.39	–0.41	–0.61	–0.68	–0.80	–0.81	0,0344 ± 0.0006		
		45.6	3.9	6.0	9.0	0.01	0.02	0.01	0.02	0.01	0.02	0.0483		

Table 6. Thermal stability and compressive strength of polyurethane foams

Oligoetherol	Method of synthesis of oligoetherol	Mass loss in % wt. after exposure in month in temperature [°C]			before exposure	Compressive strength [MPa] after exposure in temperature [°C]		
		150	175	200		150	175	200
		MEL:GL:EC	MOPR two-step <sup>6</sup>	12.0		25.7	37.9	0.106
		15.0	23.9	36.8	0.134	0.208	0.245	0.229
MEL:GL:PC	MOPR two-step <sup>6</sup>	11.8	30.0	45.6	0.152	0.404	0.316	0.034
		13.5	23.4	35.1	0.146	0.246	0.205	0.166

Compression strength measured at 10% deformation

could be the result of different reactivity of oligoetherols obtained by the MOPR method. The PUFs obtained from oligoetherols synthesized in MOPR are rigid and have similar apparent density as those obtained from the two-steps derived oligoetherols. They have water uptake value 1.9% in 24 hour test, which is related to domination of closed pores in the structure of PUF (Table 5).

They also showed low polymerization shrinkage. It is noteworthy that generally water uptake of PUFs obtained both from EC and PC in the MOPR is similarly low, while that of PUFs obtained from oligoetherols synthesized in the two-steps method is considerably higher. Also the latter had higher heat conductance coefficient.

The thermal resistance PUFs was studied by static method, *i.e.* by measuring mass loss within one month heat exposure at 150, 175 and 200 °C with concomitant measurements of compression strength (Table 6). Generally, the PUFs obtained from EC show higher thermal resistance than those obtained from PC (Table 6). For comparison the mass losses of PUFs obtained from MEL, GL, and AC in the two-step method are also collected in the Table 6.

The mass loss of PUFs obtained from oligoetherols synthesized by MOPR with EC involved are comparable with the analogues obtained in the two-step procedure, while mass loss of PUFs obtained by MOPR and PC is considerably larger than that of analogous PUFs obtained from corresponding oligoetherols formed in two-step method. Compression strength of PUFs before thermal exposure does not depend on oligoetherol origin. However, the PUFs obtained from oligoetherols synthesized in

MOPR showed considerable increase of compression strength upon annealing at 150 °C, presumable due to additional crosslinking. However annealing at 175 and 200 °C resulted in an important decrease of compression strength compared to the PUFs obtained from oligoetherols synthesized in the two-step processes.

## 4. Conclusions

The one-pot multicomponent reaction (MOPR) of synthesis the oligoetherols with azacyclic rings was established. The substrates were azacycles, glycidol, and alkylene carbonates. The oligoetherols obtained by this method showed similar properties as those obtained from the same reagents used consecutively, with isolation of semiproduct, except for oligoetherols obtained from melamine. The oligoetherols obtained in MOPR are useful substrates to obtain polyurethane foams of enhanced thermal resistance.

## 5. References

1. J. Lubczak, *Polimery*, **2011**, 56, 360–368.
2. J. Lubczak, *Polimery*, **2011**, 56, 452–460.
3. K. Frisch, D. Tummers, A. Nijenhuis, Preparation of tris(b-hydroxypropyl)isocyanurate, US Patent Number 4,198,505, date of patent January 18, 1979.
4. T. Śnieżek, E. Andrysiak, W. Montewski, H. Gniadowska, J.

- Wojciechowski, Method of production of branched polyethers, Polish Patent Number 69168, date of patent December 20, 1973.
5. R. Lubczak, *J. Appl. Polym. Sci.* **2002**, *86*, 489–497. DOI:10.1002/app.11021
  6. K. Cyzio, J. Lubczak, *Polymer Int.*, **2013**, *62*, 1735–1743. DOI:10.1002/pi.4476
  7. K. Cyzio, J. Lubczak, *J. Appl. Polym. Sci.*, **2011**, *122*, 417–426. DOI:10.1002/app.34131
  8. K. Cyzio, J. Lubczak, *Polym. Plast. Technol. Eng.*, **2017**, *56*, 13–21. DOI:10.1080/03602559.2016.1211693
  9. E. Kania, J. Lubczak, *Polimery*, **2014**, *59*, 851–854. DOI:10.14314/polimery.2014.851
  10. D. Kijowska, *Przemysł chemiczny*, **2005**, *84*, 678–683.
  11. Z. Brojer, P. Penczek, Epoxide resins, WNT, Warsaw, Poland, **1972**, pp. 451–452.
  12. D. Kijowska, S. Wołowicz, J. Lubczak, *J. Appl. Polym. Sci.*, **2004**, *93*, 294–300. DOI:10.1002/app.20453
  13. B. Czupryński, Questions of chemistry and technology of polyurethanes, The Publishing House of the Academy of Bydgoszcz, Poland, **2004**, pp.195–196.
  14. T. Broniewski, A. Iwasiewicz, J. Kapko, W. Płaczek, Testing and evaluation of properties of plastics, WNT, Warsaw, Poland **1967**, pp. 129–357.
  15. T. Dryński, Laboratory of Physics, PWN, Warsaw, Poland **1967**, pp. 125–132.
  16. Cellular Plastics and Rubbers. Determination of apparent (bulk) Density, Polish (European) Standards PN-EN ISO 845-2000, Ed. Polish Committee for Standardization.
  17. Cellular Plastics, rigid. Determination of Water Absorption, Polish (European) Standards PN-EN ISO 2896-1986, Ed. Polish Committee for Standardization.
  18. Cellular Plastics, rigid. Test of dimensional Stability, Polish (European) Standards PN-EN ISO 2796-1986, Ed. Polish Committee for Standardization.
  19. Cellular Plastics, Compression Test for rigid Materials, Polish (European) Standards PN- EN ISO 844-1978, Ed. Polish Committee for Standardization.

## Povzetek

Opisujemo enolončno multikomponentno sintezo oligoeterolov, ki vsebujejo azaciklične sisteme. Pripravili smo jih z reakcijami izocianurne, barbiturne ali sečne kisline oz. melamina z glicidolom in alkil karbonati. Izolirane produkte smo karakterizirali s pomočjo fizikalnih metod in pripravljene spojine primerjali s spojinami, ki smo jih pridobili z dvostopenjskim protokolom. Oligoeterole z 1,3,5-triazinskim obročem, dobljene z obema metodama, smo uporabili za pripravo poliuretanskih pen; katerih lastnosti smo tudi primerjali.

Scientific paper

# Synthesis and Structure Activity Relationship of Some Indole Derivatives as Potential Anti-inflammatory Agents

Samar S. Fatahala,<sup>1,\*</sup> Mohammed A. Khedr<sup>2</sup>  
and Mossad S. Mohamed<sup>1</sup>

<sup>1</sup> Pharmaceutical Organic Chemistry Department, Faculty of Pharmacy, Helwan University, Ain-Helwan

<sup>2</sup> Pharmaceutical Chemistry Department, Faculty of Pharmacy, Helwan University, Ain-Helwan  
Postal code: 11795, Helwan, Cairo, Egypt

\* Corresponding author: E-mail: [ssfathatillah@yahoo.com](mailto:ssfathatillah@yahoo.com), [samarradwan1@yahoo.com](mailto:samarradwan1@yahoo.com)

Received: 25-04-2017

## Abstract

A series of fused pyrroles were synthesized and tested for their *in vivo* anti-inflammatory activity. Among 14 examined derivatives, 5 derivatives (**1b–e**, **g** and **5b**), showed a promising anti-inflammatory activity equivalent to reference anti-inflammatory drugs (indomethacin and ibuprofen). A molecular docking study was conducted to interpret the biological activities of the tested compounds. The docking results were complementary with the phase of the biological survey and confirmed the biological effects.

**Keywords:** Fused pyrroles, tetrahydroindoles, Molecular Docking, anti-inflammatory assay

## 1. Introduction

Non-steroid anti-inflammatory drugs (NSAIDs) have been amongst the most widely developed drugs.<sup>1–5</sup> They have provided an alternative to steroid therapy, which has revealed many problems related to parallel endocrine and metabolic activity, induced osteoporosis and hypercalcemia, as shown by Lessigiarska *et al.*<sup>6</sup> The postponement in treatment causes severe side effects including rhinorrhoea, rheumatoid arthritis, and atherosclerosis.<sup>7</sup> With their anti-pyretic and analgesic activities, they represent a choice treatment in various inflammatory diseases such as arthritis and rheumatism.<sup>8–10</sup> 5-dimethyl-3-oxo-2-phenyl-2,3-dihydro-1H-pyrazol-4-yl The NSAIDs have exerted their anti-inflammatory activities through cyclooxygenase (COX) inhibition.<sup>11–13</sup>

Structural variation of the heterocyclic rings through the manipulation of the heterocyclic core influences the activity of the resulting fused systems, among these of pyrroles and their fused derivatives.<sup>14–16</sup> Due to their pharmaceutical importance,<sup>17–22</sup> attention was paid to develop a new synthetic route for pyrroles and their fused forms.<sup>23–28</sup> Pyrrolylacetic acid derivatives such as

tolmetin (Rumatol<sup>®</sup>) and zomepirac (Zomax<sup>®</sup>) were proved to be NSAIDs<sup>6</sup> with strong anti-inflammatory activity.<sup>29,30</sup> Other pyrrole and fused pyrrole compounds have been recently reported as potent COX-1 and COX-2 inhibitors:<sup>31,32</sup> 4-benzodioxine or pyrrole nucleus are described. All the newly synthesized compounds were examined for their *in vitro* and *in vivo* anti-inflammatory activity. Several derivatives, including (S) indomethacin (Indacin<sup>®</sup>), acetaminophen (Emflex<sup>®</sup>) and etodolac (Eto-dine<sup>®</sup>) as indole derivatives, and ketorolac (Ketolac<sup>®</sup>) as a pyrrole derivative.<sup>33–36</sup> These compounds blocked prostaglandin synthesis by non-selective inhibition of COX-1 and COX-2 (indomethacin, acetaminophen, tolmetin and ketorolac) or by selective inhibition of COX-2 (etodolac) (Fig. 1).

Due to the importance of this ring system,<sup>39</sup> we prepared some fused *o*-aminocyanotetrahydrobenzo[*b*]pyrrole derivatives as an essential propagation step in our search for new pyrrole and pyrrolopyrimidine derivatives,<sup>40–43</sup> and evaluated them for the anti-inflammatory activities. In addition, a molecular docking study has been done to explain the activity of the biologically active compounds.

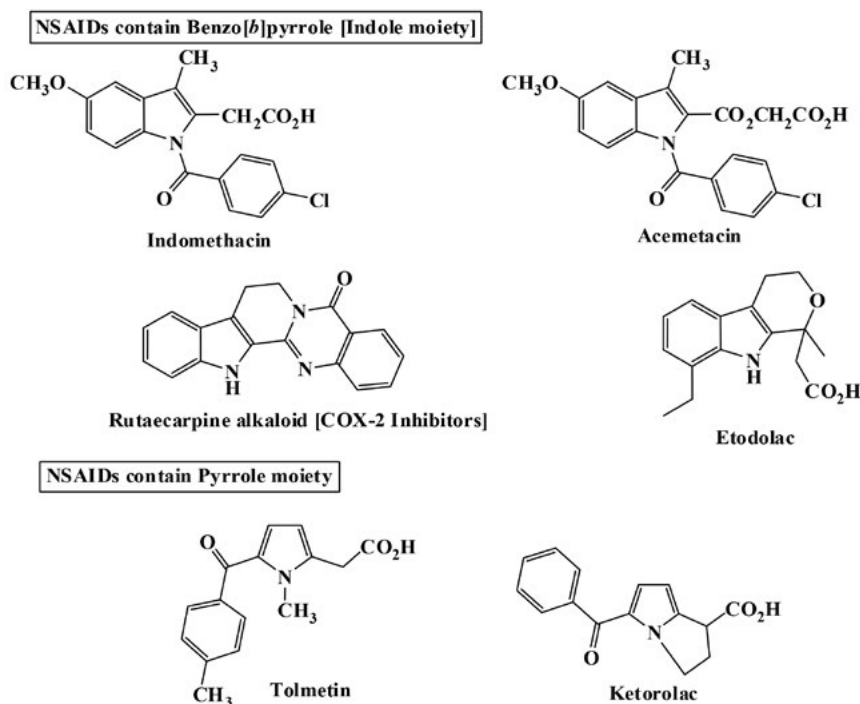


Figure 1: Pyrroles and Indoles derivatives as NSAIDs<sup>37,38</sup> their mechanism of action at the molecular level such as cyclooxygenase (COX)

## 2. Experimental

### 2.1. Chemistry

#### General Information for Chemicals

All melting points were uncorrected and measured using Electro-thermal IA 9100 apparatus (Shimadzu, Japan). IR spectra were recorded as potassium bromide pellets on a Perkin–Elmer 1650 spectrophotometer (USA), Faculty of Science, Cairo University, Cairo, Egypt. <sup>1</sup>H-NMR and <sup>13</sup>C-NMR spectra were performed on Jeol NMR FXQ-300 MHz and Jeol NMR FXQ-500 MHz spectrometers; chemical shifts are expressed as ppm against TMS as the internal reference (Faculty of Science, Cairo University, Cairo, Egypt). Mass spectra were recorded at 70 eV EI Ms-QP 1000 EX (Shimadzu, Japan), Faculty of Science, Cairo University, Cairo, Egypt. Microanalyses were operated using Vario, Elemental apparatus (Shimadzu, Japan), Organic Microanalysis Unit, Faculty of Science, Cairo University, Cairo, Egypt. Column Chromatography was performed on (Merck) Silica gel 60 (particle size 0.06–0.20 mm). Compounds **1a,b**, **3a,b** and **5a** were prepared as reported in the literature.<sup>44</sup> All new compounds yielded spectral data consistent with the proposed structures and microanalysis within ±0.4% of the theoretical values.

#### General methods for the preparation of 2-oxo-substituted malononitriles **I** and **II**

A mixture of 2-chloro-ketone (0.01 mol) and malononitrile (1 g, 0.016 mol) in CHCl<sub>3</sub> (50 mL), was cooled with stirring to 0–5 °C for 30 min. A cold solution of

NaOH (2.5 g in 10 mL of water) was added to the mixture dropwise for 30 min. The stirring was continued for 50 min under ice and the reaction mixture then left for 72 h at room temperature. The precipitate formed was filtered off, recrystallized from appropriate solvent.

#### 2-(2-Oxocyclohexyl)malononitrile (**I**)

It was obtained as a brownish red solid [EtOH/H<sub>2</sub>O]. Yield 64%, m.p. 142–145 °C, FT-IR (KBr)  $\nu_{\max}$  2345, 1690 cm<sup>-1</sup>, EIMS *m/z* (%) 162 [M<sup>+</sup>] (7.5), 106 (100). Anal. Calcd for C<sub>9</sub>H<sub>10</sub>N<sub>2</sub>O: C, 66.65; H, 6.21; N, 17.27. Found: C, 66.98; H, 6.54; N, 17.03.

#### 2-(1-Oxo-2,3-dihydro-1H-inden-2-yl)malononitrile (**II**)

It was obtained as a reddish brown solid [EtOH/H<sub>2</sub>O]. Yield 65%, m.p. 142–147 °C, FT-IR (KBr)  $\nu_{\max}$  2360, 1705 cm<sup>-1</sup>, EIMS *m/z* (%) 196 [M<sup>+</sup>] (4), 144 (100). Anal. Calcd for C<sub>12</sub>H<sub>8</sub>N<sub>2</sub>O: C, 73.46; H, 4.11; N, 14.28. Found: C, 73.78; H, 4.43; N, 14.60.

#### 2-Amino-1-(aryl)-4,5,6,7-tetrahydro-1H-indole-3-carbonitrile **1a-g**

**Method A:** A solution of **I** (1 g, 0.016 mol) in ethanol (30 mL), the appropriate aromatic amine (0.01 mol) and conc HCl (4 mL) were added. The reaction mixture was refluxed for 72 h (TLC monitored), cooled to room temperature, poured onto crushed ice (25 g.), and neutralized with NaOH. The precipitate formed was filtered off, dried and recrystallized from appropriate solvent to give compound **1**.

**Method B:** A solution of **I** (1 g, 0.016 mol) in isopropanol (30 mL), the appropriate aromatic amine (0.01 mol) was added. The reaction mixture was refluxed for 72 h (TLC monitored), then cooled to room temperature, and the solvent was removed under reduce pressure. The residue was dissolved in methanol (10 mL), poured into crushed ice (25 g). The precipitate formed was filtered off, dried and recrystallized from appropriate solvent to give compound **I**

**2-Amino-1-(4-chlorophenyl)-4,5,6,7-tetrahydro-1H-indole-3-carbonitrile (1c)**

It was obtained as a brown solid [EtOH]. Yield for method A) 73% and for B) 52%, m.p. 184–188 °C. FT-IR (KBr)  $\nu_{\max}$  3380–3250, 2315  $\text{cm}^{-1}$ .  $^1\text{H-NMR}$  (DMSO- $d_6$ , 300 MHz)  $\delta$  = 1.63–1.88 (m, 4H, 2  $\times$  CH<sub>2</sub>), 2.5–2.78 (m, 4H, 2  $\times$  CH<sub>2</sub>), 5.78 (br.s, 2H, NH<sub>2</sub>, D<sub>2</sub>O exchangeable), 7.2–7.8 (m, 4H, Ar-H).  $^{13}\text{C NMR}$  (DMSO- $d_6$ ):  $\delta$  34.1 (CH<sub>2</sub>, C-4), 34.9 (CH<sub>2</sub>, C-7), 35.1 (CH<sub>2</sub>, C-5), 36.2 (CH<sub>2</sub>, C-6), 116.1 (N-C=C, C-4a), 116.9 (N-C=C\*, C-7a), 119.8 (C'N), 124.1 (C-2), 125.6 (C-3), 130.9 (CH aromatic, C-2'), 132.2 (CH aromatic, C-3'), 132.8 (CH aromatic, C-5'), 133.4 (CH aromatic, C-6'), 134.1 (C-Cl, C-4'), 145.2 (C-N, C-1') ppm; EIMS  $m/z$  (%) 271 [ $\text{M}^+$ ] (25), 273 [ $\text{M}^+ + 2$ ,  $^{37}\text{Cl}$ ] (8.5), 149 (100). Anal. Calcd for C<sub>15</sub>H<sub>14</sub>ClN<sub>3</sub>; C, 66.30; H, 5.19; N, 15.46. Found: C, 66.68; H, 5.56; N, 15.30.

**2-Amino-1-o-tolyl-4,5,6,7-tetrahydro-1H-indole-3-carbonitrile (1d)**

It was obtained as a brownish red solid [EtOH/H<sub>2</sub>O]. Yield for method A) 80%, B) 52%, m.p. 195–197 °C. FT-IR (KBr)  $\nu_{\max}$  3380–3280, 2285  $\text{cm}^{-1}$ .  $^1\text{H-NMR}$  (DMSO- $d_6$ , 300 MHz)  $\delta$  = 1.53–1.78 (m, 4H, 2  $\times$  CH<sub>2</sub>), 2.12 (s, 3H, CH<sub>3</sub>), 2.5–2.78 (m, 4H, 2  $\times$  CH<sub>2</sub>), 6.18 (br.s, 2H, NH<sub>2</sub>, D<sub>2</sub>O exchangeable), 7.2–7.6 (m, 4H, Ar-H) ppm. EIMS  $m/z$  (%) 251 [ $\text{M}^+$ ] (31), 149 (100). Anal. Calcd for C<sub>16</sub>H<sub>17</sub>N<sub>3</sub>; C, 76.46; H, 6.82; N, 16.72. Found: C, 76.86; H, 6.41; N, 16.77.

**2-Amino-1-p-tolyl-4,5,6,7-tetrahydro-1H-indole-3-carbonitrile (1e)**

It was obtained as a brown solid [EtOH/H<sub>2</sub>O]. Yield for method A) 80%, B) 54%, m.p. 168–172 °C. FT-IR (KBr)  $\nu_{\max}$  3390–3270, 2260  $\text{cm}^{-1}$ .  $^1\text{H-NMR}$  (DMSO- $d_6$ , 300 MHz)  $\delta$  = 1.53–1.78 (m, 4H, 2  $\times$  CH<sub>2</sub>), 1.98 (s, 3H, CH<sub>3</sub>), 2.4–2.78 (m, 4H, 2  $\times$  CH<sub>2</sub>), 5.58 (br.s, 2H, NH<sub>2</sub>, D<sub>2</sub>O exchangeable), 7.2–7.8 (m, 4H, Ar-H) ppm. EIMS  $m/z$  (%) 251 [ $\text{M}^+$ ] (61), 92 (100). Anal. Calcd for C<sub>16</sub>H<sub>17</sub>N<sub>3</sub>; C, 76.46; H, 6.82; N, 16.72. Found: C, 76.43; H, 6.91; N, 16.97.

**2-Amino-1-(1,5-dimethyl-3-oxo-2-phenyl-2,3-dihydro-1H-pyrazol-4-yl)-4,5,6,7-tetrahydro-1H-indole-3-carbonitrile (1f)**

It was obtained as a yellowish brown solid [EtOH/H<sub>2</sub>O]. Yield for method A) 76%, B) 55%, m.p. 234–238 °C. FT-IR (KBr)  $\nu_{\max}$  3350–3270, 2270, 1680  $\text{cm}^{-1}$ .  $^1\text{H-NMR}$  (DMSO- $d_6$ , 300 MHz)  $\delta$  = 1.43–1.68 (m, 4H, 2  $\times$  CH<sub>2</sub>),

2.2–2.45 (m, 4H, 2  $\times$  CH<sub>2</sub>), 2.33 (s, 3H, CH<sub>3</sub>), 3.12 (s, 3H, N-CH<sub>3</sub>), 5.28 (br.s, 2H, NH<sub>2</sub>, D<sub>2</sub>O exchangeable), 7.2–7.6 (m, 5H, Ar-H) ppm. EIMS  $m/z$  (%) 347 [ $\text{M}^+$ ] (38), 173 (100). Anal. Calcd for C<sub>20</sub>H<sub>21</sub>N<sub>5</sub>O: C, 69.14; H, 6.09; N, 20.16; O, 4.61. Found: C, 69.28; H, 6.16; N, 20.30; O, 4.30.

**2-Amino-1-(pyridin-2-yl)-4,5,6,7-tetrahydro-1H-indole-3-carbonitrile (1g)**

It was obtained as a brownish black solid [EtOH]. Yield for method A) 65%, B) 48%, m.p. 194–196 °C. FT-IR (KBr)  $\nu_{\max}$  3370–3290, 2345  $\text{cm}^{-1}$ .  $^1\text{H-NMR}$  (DMSO- $d_6$ , 300 MHz)  $\delta$  = 1.7–1.75 (m, 4H, 2  $\times$  CH<sub>2</sub>), 2.6–2.8 (m, 4H, 2  $\times$  CH<sub>2</sub>), 5.28 (br.s, 2H, NH<sub>2</sub>, D<sub>2</sub>O exchangeable), 7.6–8.4 (m, 4H, Ar-H) ppm. EIMS  $m/z$  (%) 238 [ $\text{M}^+$ ] (100). Anal. Calcd for C<sub>14</sub>H<sub>14</sub>N<sub>4</sub>: C, 70.57; H, 5.92; N, 23.51. Found: C, 70.71; H, 5.83; N, 23.46.

**2-Amino-1-(aryl)-4,5,6,7-tetrahydro-1H-indole-3-carbonitrile 2a,b**

A solution of **II** (1 g, 0.016 mol) in ethanol (30 mL), the appropriate aromatic amine (0.01 mol) and conc HCl (4 mL) were added. The reaction mixture was refluxed for 72 h (TLC monitored), then cooled to room temperature, poured into crushed ice (25 g), and neutralized with NaOH. The precipitate formed was filtered off, dried and recrystallized from appropriate solvent to give compound **2a,b**

**2-Amino-1-phenyl-1,4-dihydroindeno[1,2-b]pyrrole-3-carbonitrile (2a)**

It was obtained as a brownish black solid [EtOH/H<sub>2</sub>O]. Yield 60%, m.p. 218–220 °C. FT-IR (KBr)  $\nu_{\max}$  3410–3240, 2335  $\text{cm}^{-1}$ .  $^1\text{H-NMR}$  (DMSO- $d_6$ , 300 MHz)  $\delta$  = 3.4 (s, 2H, CH<sub>2</sub>), 6.18 (br.s, 2H, NH<sub>2</sub>, D<sub>2</sub>O exchangeable), 6.8–7.4 (m, 9H, Ar-H) ppm. EIMS  $m/z$  (%) 271 [ $\text{M}^+$ ] (100). Anal. Calcd for C<sub>18</sub>H<sub>13</sub>N<sub>3</sub>; C, 79.68; H, 4.83; N, 15.49. Found: C, 79.89; H, 4.97; N, 15.80.

**2-Amino-1-(4-methoxyphenyl)-1,4-dihydroindeno[1,2-b]pyrrole-3-carbonitrile (2b)**

It was obtained as a brown solid [EtOH/H<sub>2</sub>O]. Yield 80%, m.p. 200–205 °C. FT-IR (KBr)  $\nu_{\max}$  3425–3220, 2340  $\text{cm}^{-1}$ .  $^1\text{H-NMR}$  (DMSO- $d_6$ , 300 MHz)  $\delta$  = 3.3 (s, 2H, CH<sub>2</sub>), 3.7 (s, 3H, OCH<sub>3</sub>), 6.23 (br.s, 2H, NH<sub>2</sub>, D<sub>2</sub>O exchangeable), 6.8–7.51 (m, 8H, Ar-H) ppm. EIMS  $m/z$  (%) 301 [ $\text{M}^+$ ] (7.6), 211 (100). Anal. Calcd for C<sub>19</sub>H<sub>15</sub>N<sub>3</sub>O: C, 75.73; H, 5.02; N, 13.94; O, 5.31. Found: C, 75.61; H, 5.39; N, 14.31; O, 5.41.

**N-(3-Cyano-1-(aryl)-pyrrol-2-yl) acetamide 3 and 4**

A suspension of the appropriate compound **1** or **2** (0.01 mol) in acetic anhydride (40 mL) was refluxed for 2 h, cooled, poured onto ice-water, neutralized with ammonia to give a precipitate which was filtered off, dried, and recrystallized from appropriate solvent, to give compounds **3** and **4**.

*N*-(1-(4-Chlorophenyl)-3-cyano-4,5,6,7-tetrahydro-1*H*-indol-2-yl) acetamide (**3c**)

It was obtained as a brownish red solid [MeOH/H<sub>2</sub>O]. Yield 70%, m.p. 184–188 °C. FT-IR (KBr)  $\nu_{\max}$  3300, 2300, 1730 cm<sup>-1</sup>. <sup>1</sup>H-NMR (DMSO-*d*<sub>6</sub>, 300 MHz)  $\delta$  = 1.63–1.88 (m, 4H, 2 × CH<sub>2</sub>), 2.5–2.78 (7H, (4H) 2 × CH<sub>2</sub>, 3H, CH<sub>3</sub>), 7.2–7.8 (m, 4H, Ar-H), 10.15 (s, 1H, NH, D<sub>2</sub>O exchangeable) ppm. EIMS *m/z* (%) 313 [M<sup>+</sup>] (19.7), 315 [M<sup>+</sup>+2, <sup>37</sup>Cl] (6), 149 (100). Anal. Calcd for C<sub>17</sub>H<sub>16</sub>ClN<sub>3</sub>O: C, 65.07; H, 5.14; Cl, 11.30; N, 13.39. Found: C, 65.07; H, 5.14; Cl, 11.30; N, 13.39.

*N*-(3-Cyano-1-*o*-tolyl-4,5,6,7-tetrahydro-1*H*-indol-2-yl) acetamide (**3d**)

It was obtained as a yellowish brown solid [MeOH/H<sub>2</sub>O]. Yield 80%, m.p. 200–205 °C. FT-IR (KBr)  $\nu_{\max}$  3280, 2223, 1703 cm<sup>-1</sup>. <sup>1</sup>H-NMR (DMSO-*d*<sub>6</sub>, 300 MHz)  $\delta$  = 1.53–1.78 (m, 4H, 2 × CH<sub>2</sub>), 2.12 (s, 3H, CH<sub>3</sub>), 2.2–2.58 (m, 7H, (4H) 2 × CH<sub>2</sub>, 3H, CH<sub>3</sub>), 7.2–7.6 (m, 4H, Ar-H), 9.85 (s, 1H, NH, D<sub>2</sub>O exchangeable) ppm. EIMS *m/z* (%) 293 [M<sup>+</sup>] (19.7) 92 (100). Anal. Calcd for C<sub>18</sub>H<sub>19</sub>N<sub>3</sub>O: C, 73.69; H, 6.53; N, 14.32. Found: C, 73.99; H, 6.73; N, 14.67.

*N*-(3-Cyano-1-*p*-tolyl-4,5,6,7-tetrahydro-1*H*-indol-2-yl) acetamide (**3e**)

It was obtained as a reddish black solid [EtOH/H<sub>2</sub>O]. Yield 70%, m.p. 186–190 °C. FT-IR (KBr)  $\nu_{\max}$  3330, 2210, 1690 cm<sup>-1</sup>. <sup>1</sup>H-NMR (DMSO-*d*<sub>6</sub>, 300 MHz)  $\delta$  = 1.53–1.78 (m, 4H, 2 × CH<sub>2</sub>), 1.98 (s, 3H, CH<sub>3</sub>), 2.2–2.68 (m, 7H, (4H) 2 × CH<sub>2</sub>, 3H, CH<sub>3</sub>), 7.2–7.8 (m, 4H, Ar-H), 9.5 (s, 1H, NH, D<sub>2</sub>O exchangeable) ppm. EIMS *m/z* (%) 293 [M<sup>+</sup>] (17.7), 91 (100). Anal. Calcd for C<sub>18</sub>H<sub>19</sub>N<sub>3</sub>O: C, 73.69; H, 6.53; N, 14.32. Found: C, 73.79; H, 6.41; N, 14.39.

*N*-(3-Cyano-1-(1,5-dimethyl-3-oxo-2-phenyl-2,3-dihydro-1*H*-pyrazol-4-yl)-4,5,6,7-tetrahydro-1*H*-indol-2-yl) acetamide (**3f**)

It was obtained as a brownish red solid [MeOH/H<sub>2</sub>O]. m.p. 215–218 °C. FT-IR (KBr)  $\nu_{\max}$  3330, 2230, 1720, 1703 cm<sup>-1</sup>. <sup>1</sup>H-NMR (DMSO-*d*<sub>6</sub>, 300 MHz)  $\delta$  = 1.43–1.68 (m, 4H, 2 × CH<sub>2</sub>), 2.2–2.45 (m, 7H, (4H) 2 × CH<sub>2</sub>), 2.33–2.4 (m, 6H, 2 × CH<sub>3</sub>), 3.12 (s, 3H, N-CH<sub>3</sub>), 7.2–7.6 (m, 5H, Ar-H), 10.3 (s, 1H, NH, D<sub>2</sub>O exchangeable) ppm. EIMS *m/z* (%) 389 [M<sup>+</sup>] (24.1), 159 (100). Anal. Calcd for C<sub>22</sub>H<sub>23</sub>N<sub>5</sub>O<sub>2</sub>: C, 67.85; H, 5.95; N, 17.98. Found: C, 67.78; H, 6.16; N, 17.91.

*N*-(3-Cyano-1-(pyridin-2-yl)-4,5,6,7-tetrahydro-1*H*-indol-2-yl) acetamide (**3g**)

It was obtained as a brown solid [EtOH/H<sub>2</sub>O]. Yield 62%, m.p. 168–170 °C. FT-IR (KBr)  $\nu_{\max}$  3300, 2300, 1730 cm<sup>-1</sup>. <sup>1</sup>H-NMR (DMSO-*d*<sub>6</sub>, 300 MHz)  $\delta$  = 1.7–1.75 (m, 4H, 2 × CH<sub>2</sub>), 2.4–2.6 (m, 7H, (4H) 2 × CH<sub>2</sub>, 3H, CH<sub>3</sub>), 7.6–8.4 (m, 4H, Ar-H), 9.9 (s, 1H, NH, D<sub>2</sub>O exchangeable) ppm. EIMS *m/z* (%) 280 [M<sup>+</sup>] (100). Anal. Calcd for C<sub>16</sub>H<sub>16</sub>N<sub>4</sub>O: C, 68.55; H, 5.75; N, 19.99. Found: C, 68.54; H, 5.42; N, 19.88.

*N*-(3-Cyano-1-phenyl-1,4-dihydroindeno[1,2-*b*]pyrrol-2-yl) acetamide (**4a**)

It was obtained as a brown solid [MeOH/H<sub>2</sub>O]. Yield 64%, m.p. 215–219 °C. FT-IR (KBr)  $\nu_{\max}$  3450 (NH), 2365 (CN), 1710 (C=O) cm<sup>-1</sup>. <sup>1</sup>H-NMR (DMSO-*d*<sub>6</sub>, 300 MHz)  $\delta$  = 2.3 (s, 3H, CH<sub>3</sub>), 3.58 (s, 2H, CH<sub>2</sub>), 7.1–7.67 (m, 9H, Ar-H), 10.47 (br.s, 1H, NH, D<sub>2</sub>O exchangeable) ppm. EIMS *m/z* (%) 313 [M<sup>+</sup>] (8), 146 (100). Anal. Calcd for C<sub>20</sub>H<sub>15</sub>N<sub>3</sub>O: C, 76.66; H, 4.82; N, 13.41. Found: C, 76.69; H, 4.98; N, 13.57.

**General methods for the preparation of aryl-pyrrolo [2,3-*d*]pyrimidin-4-ones 5 and 6**

A suspension of the appropriate compound **1** or **2** (0.01 mol) in formic acid (20 mL, 85%) was refluxed for 3 h, cooled, poured onto ice-water to give a precipitate which was filtered off, dried, and recrystallized from appropriate solvent to afford **5** and **6**.

*9*-(4-Methoxyphenyl)-5,6,7,8-tetrahydro-3*H*-pyrimido [4,5-*b*]indol-4(9*H*)-one (**5b**)

It was obtained as a brown solid [EtOH]. Yield 65%, m.p. 272–276 °C. FT-IR (KBr)  $\nu_{\max}$  3230, 1690, 1560 cm<sup>-1</sup>. <sup>1</sup>H-NMR (DMSO-*d*<sub>6</sub>, 300 MHz)  $\delta$  = 1.33–1.58 (m, 4H, 2 × CH<sub>2</sub>), 2.2–2.48 (m, 4H, 2 × CH<sub>2</sub>), 3.52 (s, 3H, O-CH<sub>3</sub>), 6.9–7.5 (m, 4H, Ar-H), 9.3 (s, 1H, C<sub>2</sub>-H), 12.40 (s, 1H, NH, D<sub>2</sub>O exchangeable) ppm. EIMS *m/z* (%) 295 [M<sup>+</sup>] (18.7), 279 (100). Anal. Calcd for C<sub>17</sub>H<sub>17</sub>N<sub>3</sub>O<sub>2</sub>: C, 69.14; H, 5.80; N, 14.23. Found: C, 69.19; H, 5.98; N, 14.53.

*9*-*o*-Tolyl-5,6,7,8-tetrahydro-3*H*-pyrimido [4,5-*b*]indol-4(9*H*)-one (**5d**)

It was obtained as a yellowish brown solid [MeOH]. Yield 79%, m.p. 228–231 °C. FT-IR (KBr)  $\nu_{\max}$  3230, 1690, 1560 cm<sup>-1</sup>. <sup>1</sup>H-NMR (DMSO-*d*<sub>6</sub>, 300 MHz)  $\delta$  = 1.53–1.78 (m, 4H, 2 × CH<sub>2</sub>), 2.12 (s, 3H, CH<sub>3</sub>), 2.2–2.58 (m, 4H, 2 × CH<sub>2</sub>), 7.2–7.6 (m, 4H, Ar-H), 9.3 (s, 1H, C<sub>2</sub>-H), 12.18 (s, 1H, NH, D<sub>2</sub>O exchangeable) ppm. EIMS *m/z* (%) 279 [M<sup>+</sup>] (17), 118 (100). Anal. Calcd for C<sub>17</sub>H<sub>17</sub>N<sub>3</sub>O: C, 73.10; H, 6.13; N, 15.04; O, 5.73. Found: C, 73.39; H, 6.23; N, 15.34; O, 5.94.

*9*-*p*-Tolyl-5,6,7,8-tetrahydro-3*H*-pyrimido [4,5-*b*]indol-4(9*H*)-one (**5e**)

It was obtained as a brown solid [EtOH]. Yield 71%, m.p. 206–210 °C. FT-IR (KBr)  $\nu_{\max}$  3430, 3330, 1720, 1690, 1560 cm<sup>-1</sup>. <sup>1</sup>H-NMR (DMSO-*d*<sub>6</sub>, 300 MHz)  $\delta$  = 1.53–1.78 (m, 4H, 2 × CH<sub>2</sub>), 1.98 (s, 3H, CH<sub>3</sub>), 2.2–2.68 (m, 4H, 2 × CH<sub>2</sub>), 7.2–7.8 (m, 4H, Ar-H), 9.4 (s, 1H, C<sub>2</sub>-H), 12.15 (s, 1H, NH, D<sub>2</sub>O exchangeable) ppm. EIMS *m/z* (%) 279 [M<sup>+</sup>] (19.3), 188 (100). Anal. Calcd for C<sub>17</sub>H<sub>17</sub>N<sub>3</sub>O: C, 73.69; H, 6.53; N, 14.32. Found: C, 73.79; H, 6.61; N, 14.19.

*9*-(1,5-Dimethyl-3-oxo-2-phenyl-2,3-dihydro-1*H*-pyrazol-4-yl)-5,6,7,8-tetrahydro-3*H*-pyrimido [4,5-*b*]indol-4(9*H*)-one (**5f**)

It was obtained as a yellowish brown solid [EtOH]. Yield 83%, m.p. 260–265 °C. FT-IR (KBr)  $\nu_{\max}$  3430, 3330,

1720, 1690, 1560  $\text{cm}^{-1}$ .  $^1\text{H-NMR}$  ( $\text{DMSO-}d_6$ , 300 MHz)  $\delta$  = 1.43–1.68 (m, 4H,  $2 \times \text{CH}_2$ ), 2.2–2.45 (m, 4H,  $2 \times \text{CH}_2$ ), 2.33 (s, 3H,  $\text{CH}_3$ ), 3.12 (s, 3H,  $\text{N-CH}_3$ ), 7.2–7.6 (m, 5H, Ar-H), 9.1 (s, 1H,  $\text{C}_2\text{-H}$ ), 12.3 (s, 1H, NH,  $\text{D}_2\text{O}$  exchangeable) ppm. EIMS  $m/z$  (%) 375 [ $\text{M}^+$ ] (24.6), 187 (100). Anal. Calcd for  $\text{C}_{21}\text{H}_{21}\text{N}_5\text{O}_2$ : C, 67.18; H, 5.64; N, 18.65. Found: C, 67.28; H, 5.36; N, 18.36.

#### 9-(Pyridin-2-yl)-5,6,7,8-tetrahydro-3H-pyrimido[4,5-b]indol-4(9H)-one (5g)

It was obtained as a brownish red solid [EtOH]. Yield 68%, m.p. 168–170 °C. FT-IR (KBr)  $\nu_{\text{max}}$  3310, 1682, 1587  $\text{cm}^{-1}$ .  $^1\text{H-NMR}$  ( $\text{DMSO-}d_6$ , 300 MHz)  $\delta$  = 1.7–1.75 (m, 4H,  $2 \times \text{CH}_2$ ), 2.4–2.6 (m, 4H,  $2 \times \text{CH}_2$ ), 7.6–8.4 (m, 4H, Ar-H), 9.3 (s, 1H,  $\text{C}_2\text{-H}$ ), 12.21 (s, 1H, NH,  $\text{D}_2\text{O}$  exchangeable) ppm. EIMS  $m/z$  (%) 266 [ $\text{M}^+$ ] (16.4), 132 (100). Anal. Calcd for  $\text{C}_{15}\text{H}_{14}\text{N}_4$ : C, 67.65; H, 5.30; N, 21.04. Found: C, 67.54; H, 5.62; N, 21.88.

#### 10-Phenyl-5,10-dihydro-3H-indeno[2',1':4,5]pyrrolo[2,3-d]pyrimidin-4-one (6a)

It was obtained as an orange solid [MeOH]. Yield 58%, m.p. 215–218 °C. FT-IR (KBr)  $\nu_{\text{max}}$  3330, 1705, 1590  $\text{cm}^{-1}$ .  $^1\text{H-NMR}$  ( $\text{DMSO-}d_6$ , 300 MHz)  $\delta$  = 3.51 (s, 2H,  $\text{CH}_2$ ), 7.3–7.8 (m, 10H, Ar-H + pym H), 12.21 (s, 1H, NH,  $\text{D}_2\text{O}$  exchangeable) ppm. EIMS  $m/z$  (%) 299 [ $\text{M}^+$ ] (18), 221(100).  $\text{C}_{19}\text{H}_{13}\text{N}_3\text{O}$  (299.33). Anal. Calcd for  $\text{C}_{19}\text{H}_{13}\text{N}_3\text{O}$ : C, 76.24; H, 4.38; N, 14.04. Found: C, 76.57; H, 4.61; N, 14.53.

## 3. Biological Assay

### 3.1. Anti-inflammatory Activity

#### Animals

Ninety adult male Sprague-Dawley rats (5 rats per group for 14 tested compounds, control (injected with 1 mL DMSO only, 2 standard drugs), weighing 120–150 g, were housed in cages in a temperature-controlled ( $25 \pm 1$  °C) environment and provided free access to pelleted food and purified drinking water *ad libitum*. The protocol of the study was approved by the animal ethics committee of the Faculty of Pharmacy, Helwan University on 10-01-2012. The study was conducted in accordance with the EC. DFT-IRactive 86/609/EEC for animal experiments.

#### Assessment of Anti-inflammatory Activity

Rat paw oedema assay was carried out according to Winter *et al.*<sup>45</sup> Prepared compounds (equimolar to active dose of the reference drug), control and 2 standard drugs were dissolved in 1 mL DMSO and administrated subcutaneously. One hour later, paw oedema was induced by sub-plantar injection of 0.1 mL of 1% carrageenan (Sigma-Aldrich, St. Louis, USA) into the right paw. Paw volume was measured using a water plethysmometer (Basile, Comerio, Italy). The difference between the right and left paw volu-

me was measured at 1, 2, 3 and 4 h after induction of inflammation. Control group received 1 mL DMSO (as to evaluate the interference of DMSO itself in biological test) subcutaneously and carrageenan in sub-plantar region. Results were expressed as percentage inhibition of inflammation. Ibuprofen (70 mg/kg) and indomethacin (20 mg/kg) were used as the reference drugs.

### Statistical Analysis

Results were expressed as the mean  $\pm$  SEM, and different groups were compared using one way analysis of variance (ANOVA) followed by Tukey–Kramer test for multiple comparisons, using Graph Pad Instant (version 3.05) as the statistical software.

**Calculation:** equimolar doses of tested compounds were calculated in relation to these of reference drug: swel = mean difference in rat paw volume between right and left paw  $\pm$  SE. % inhibition =  $(1 - \text{rt}/\text{rc}) \times 100$  [rt = swel of tested group; rc = swel of control group].

## 3.2. Molecular Docking Study

### MOE 2013.08 Docking

The molecular docking studies were done using MOE 2013.08 and Leadit 2.1.2. All compounds were built and saved as MOE. Rigid receptor was used as a docking protocol. Both receptor-solvent were kept as a »receptor«. Triangle matcher was used as a placement method. Two rescoring were computed, rescoring 1 was selected as London dG. Rescoring 2 was selected as affinity. The force field was used as a refinement.

### Leadit 2.1.2 Docking

All compounds were built and saved as Mol2. The crystal structure of COX-2 enzyme complexes with indomethacin was downloaded from protein data bank (PDB: 4COX). The protein was loaded into Leadit 2.1.2 and the receptor components were chosen by selection of chain A as the main chain when complexes with indomethacin. Binding site was defined by choosing indomethacin as the reference ligand to which all coordinates were computed. Amino acids within radius 6.5 Å were selected in the binding site. All chemical ambiguities of residues were left as default. Ligand binding was driven by enthalpy (classic Triangle matching). For scoring, all default settings were restored. Intra-ligand clashes were computed by using clash factor = 0.6. Maximum number of solutions per iteration = 200. Maximum of solution per fragmentation = 200. The base placement method was used as the docking strategy.

## 4. Result and Discussion

### 4.1. Chemistry

The availability of  $\alpha$ -amino ketones is key to the preparation of *o*-amino-cyanopyrroles.<sup>46–48</sup> Research in-

indicated that  $\alpha$ -amino ketones used for the preparation of *o*-amino-cyanopyrroles were usually obtained *in situ*<sup>49–51</sup> *via* the reaction of  $\alpha$ -hydroxy ketones with amines in acid medium,<sup>52–55</sup> or *via* the reaction of  $\alpha$ -halo ketones with either amines and/or  $\alpha$ -amino acids.<sup>56</sup> As previously mentioned,  $\alpha$ -hydroxy ketones and  $\alpha$ -halo ketones, malononitriles or suitable substituted alkylidenemalonitrile and primary amines constituted essential components for the synthesis of *o*-amino-cyanopyrrole derivatives.<sup>44,57,58</sup>

Regarding fused pyrrole and fused pyrrolopyrimidine derivatives there are few studies reporting the synthesis of *o*-aminocyanotetrahydrobenzo[*b*]pyrrole and *o*-aminocyanooctahydroindeno[2,1-*b*]pyrrole derivatives. Literature also revealed that the reaction of  $\alpha$ -hydroxycyclohexanone (in place of the  $\alpha$ -chloro analogue) with certain amines and malononitrile successfully afforded some *o*-aminocyanotetrahydrobenzo[*b*]pyrroles but in poor yields (20–30%).<sup>44,58,59</sup> These results also indicated that some side reactions happened (Fig. 2a).

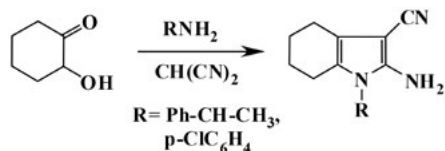


Figure 2a. Typical synthesis of tetrahydrobenzo[*b*]pyrroles

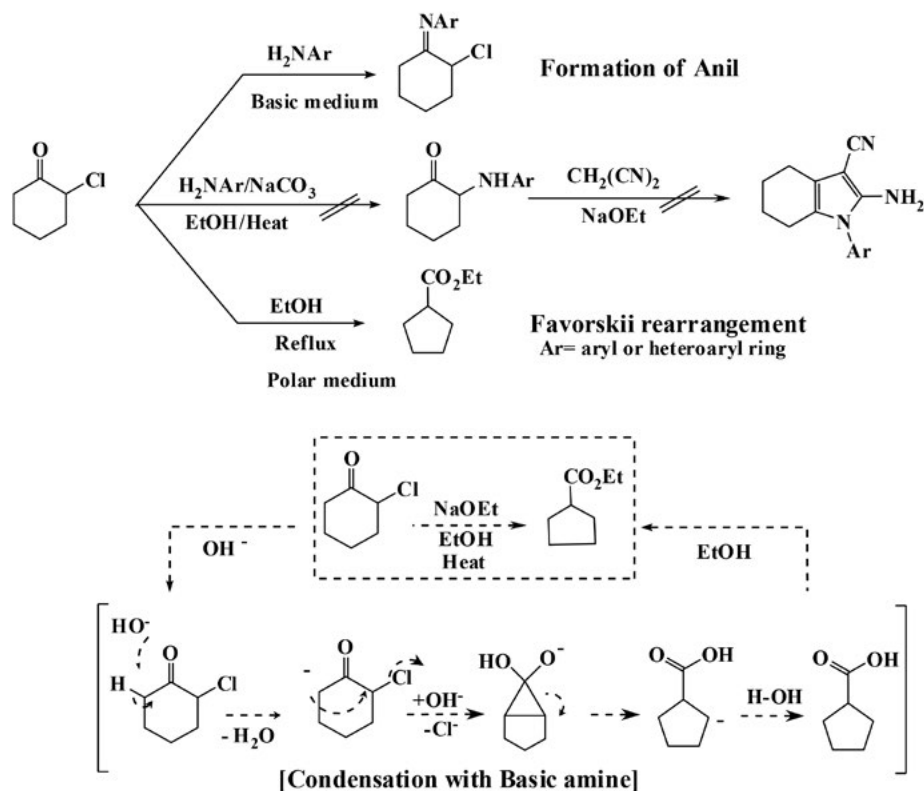


Figure 2b. Favorskii rearrangement (polar basic medium rearrangement),<sup>57</sup> and anil formation<sup>58,59</sup>

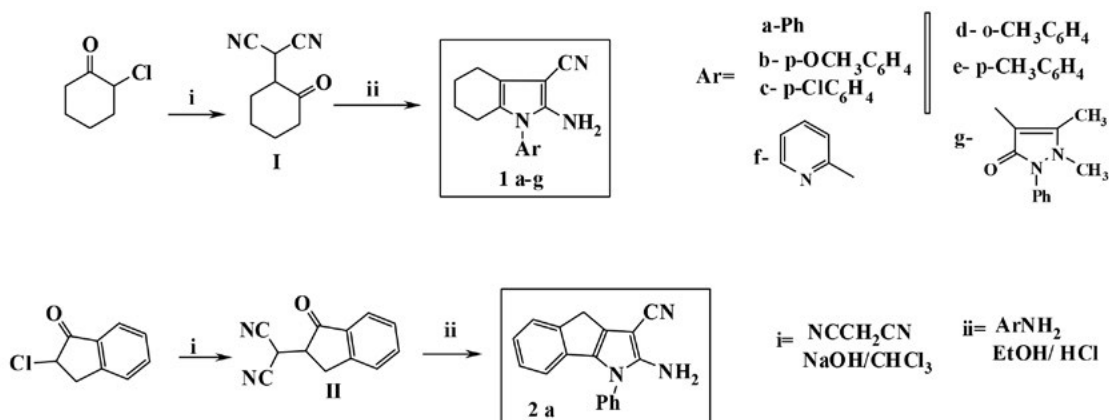
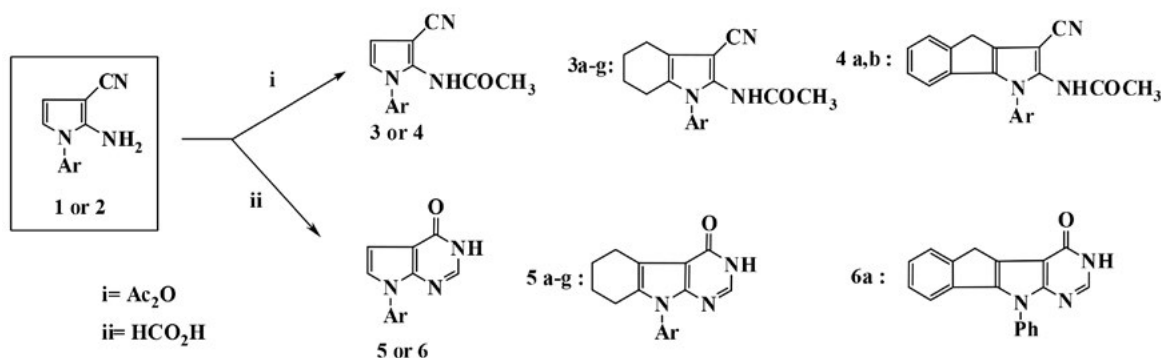
Attempts made to develop such compounds using the regular reactants ( $\alpha$ -chlorocyclohexanone and/or 2-chloroindanone, with certain aromatic amines and malononitrile) were unfruitful.<sup>60</sup> We also found that  $\alpha$ -chlorocyclohexanone under the reaction conditions EtOH/NaOH (polar basic medium) might undergo what is called **Favorskii rearrangement**,<sup>61</sup> rearrangement of an  $\alpha$ -halo ketone upon treatment with a base; the reaction continues through cyclopropanone intermediate formed by nucleophilic attack [EtO<sup>-</sup>]. In addition to the possibility of condensation with amine to give the anil (Fig. 2b).<sup>62,63</sup>

Taking the previous results into consideration, we tried to diminish the potential of such side reactions. Our plan was to prepare the novel intermediate 2-(2-oxocyclohexyl) malononitrile (**I**) from the reaction of 2-chlorocyclohexanone with malononitrile in a nonpolar solvent, followed by condensation with the appropriate aromatic amines.

By applying this method, we successfully set up the required tetrahydrobenzo[*b*]pyrroles **1** with a fair yield. Using the same conditions with 2-chloroindanone it produced **2** (Scheme 1).

On the other hand, aminocyanopyrrole derivatives **1** and **2** were converted to the corresponding acetylated derivatives **3** and **4** *via* condensation with acetic anhydride.<sup>64–66</sup> 3-*d*]pyrimidines were reported to act as potent anti-cancer agents, in this work, a series of novel 2-substituted-



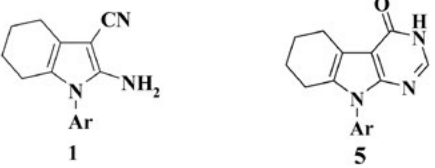
Scheme 1: Synthesis of tetrahydroindoles **1a–g** and **2a**Scheme 2: Synthesis of acetylated pyrroles **3a–g**, **4a,b** and pyrrolopyrimidines **5a–g**, **6a**

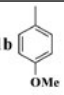
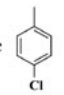
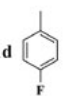
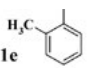
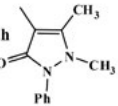
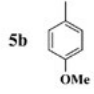
3-cyano-4-phenyl-pyrrole **5**, **6**, 11–18, and 5-phenyl-pyrrolo[2,3-*d*]pyrimidine derivatives **7–10**, 19–24 bearing either sulfathiazole or sulfapyridine were synthesized. The structures of these compounds were confirmed by elemental analysis, IR, (1 Compounds **1** and **2** were converted to pyrrolo[2,3-*d*]pyrimidine-4-ones **5** and **6** *via* condensation with formic acid (Scheme 2).<sup>64</sup>

## 4. 2. Biological Results and Discussion

Fourteen of the synthesized compounds were evaluated for their anti-inflammatory activity, using a method established by Harrk *et al.*<sup>31</sup> 4-benzodioxine or pyrrole nucleus are described. All the newly synthesized compounds were examined for their *in vitro* and *in vivo* anti-inflammatory activity. Several derivatives, including (S Five of the tested compounds induced significant anti-inflammatory activity, compared with that of ibuprofen and indomethacin. Compound **1b** exerted significant activities compared to standard drugs at all time intervals post-carrageenan ( $\cong 78\%$ ,  $\cong 80\%$ ,  $\cong 84\%$  and  $\cong 85\%$  inhibition at 1<sup>st</sup>, 2<sup>nd</sup>, 3<sup>rd</sup> and 4<sup>th</sup> hour interval post-carrageenan). The activity profile was the same as for standard drugs (response increasing with time). Compound **1c** exerted noticeable acti-

vities compared to standard drugs at the 1<sup>st</sup> and 2<sup>nd</sup> hour post-carrageenan ( $\cong 81\%$  and  $\cong 82\%$  inhibition at 1<sup>st</sup> and 2<sup>nd</sup> hour interval post-carrageenan). The activity profile was the same as standard drugs (response increasing with time), yet the activity showed weak, yet significant activities, decreasing at 3<sup>rd</sup> and 4<sup>th</sup> hour post-carrageenan ( $\cong 79\%$  and  $\cong 75\%$  inhibition at 3<sup>rd</sup> and 4<sup>th</sup> hour interval post-carrageenan). Compounds **1d** and **5b** showed a marked anti-inflammatory effect than standard drugs, from the 1<sup>st</sup> hour to 4<sup>th</sup> hour post-carrageenan. Compound **5b** showed a moderate inhibitory action at the 4<sup>th</sup> hour interval: 76% inhibition. Yet, compound **1d** showed the unusual profile compared to standard drugs: it showed  $\cong 79\%$  inhibition at 2<sup>nd</sup> hour post-carrageenan and  $\cong 70\%$  inhibition at 3<sup>rd</sup> hour post-carrageenan and then decreased to 66% inhibition at 4<sup>th</sup> hour post-carrageenan. Compound **1g** exerted a moderate activity compared to standard drugs at the 3<sup>rd</sup> and 4<sup>th</sup> hour post-carrageenan (% inhibition  $\cong 48$  at 3<sup>rd</sup> hour and 61% at 4<sup>th</sup> hour post-carrageenan), it showed no activity at 1<sup>st</sup> and 2<sup>nd</sup> hour intervals post-carrageenan injection. Compounds **1f**, **3c**, **3d**, **3e**, **3f** and **5d,e** were all inactive over all tested periods, showing % inhibition < 12, 21, 25 and 38 at 1<sup>st</sup> to 4<sup>th</sup> hours, respectively, and were indicated as inactive in Table 1.

**Table 1.** *In vivo* anti-inflammatory activity results for active compounds.


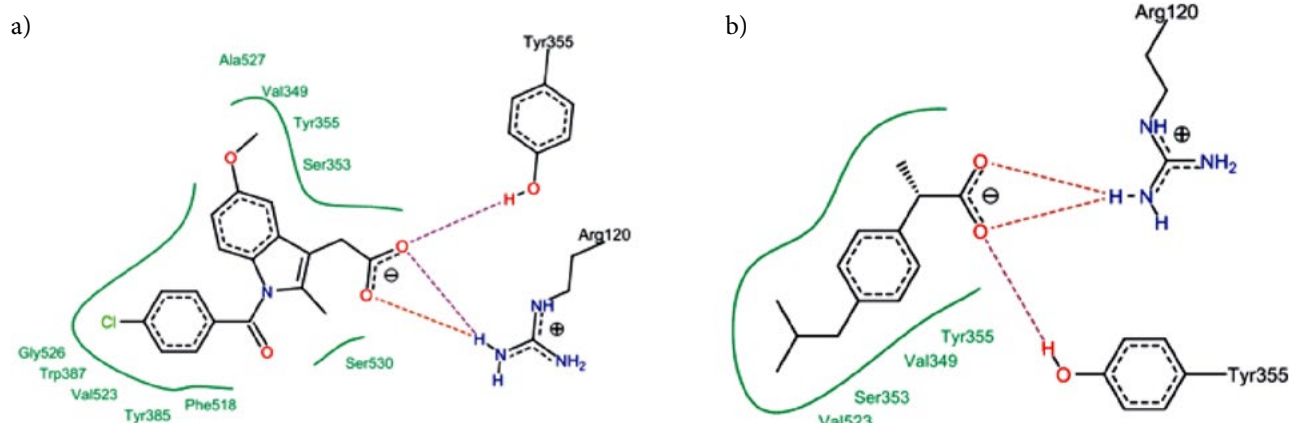
Compounds // (Ar=)	Oedema induced by carrageenan (% Oedema inhibition relative to control)							
	1 Hr		2 Hr		3 Hr		4 Hr	
	Swel ± SE	Swel ± SE	% inh	Swel ± SE	% inh	Swel ± SE	% inh	% inh
	0.048 ± 0.024 <sup>a</sup>	78.7	0.052 ± 0.02 <sup>a</sup>	80	0.086 ± 0.048 <sup>a</sup>	84.3	0.098 ± 0.04 <sup>a</sup>	84.69
	0.042 ± 0.008 <sup>a</sup>	81.37	0.046 ± 0.009 <sup>a</sup>	82.3	0.116 ± 0.048 <sup>a</sup>	79.6	0.159 ± 0.029 <sup>a</sup>	75.06
	0.19 ± 0.036	15.9	0.076 ± 0.038 <sup>a</sup>	70.76	0.022 ± 0.005 <sup>a</sup>	95.98	0.048 ± 0.007 <sup>a</sup>	92
	0.2137 ± 0.03	6.35	0.054 ± 0.01 <sup>a</sup>	78.16	0.086 ± 0.018 <sup>a</sup>	69.43	0.083 ± 0.068 <sup>a</sup>	66.73
	0.2242 ± 0.031	0.79	0.25 ± 0.007	3.65	0.284 ± 0.04	48.17	0.251 ± 0.031 <sup>a</sup>	60.74
	0.152 ± 0.016	32.74	0.15 ± 0.024	42.3	0.234 ± 0.04 <sup>a</sup>	57.29	0.152 ± 0.057 <sup>a</sup>	76.25
Indomethacin	0.224 ± 0.004	0.88	0.764 ± 0.009	20.7	0.286 ± 0.004	44.65	0.084 ± 0.01	*78.58
Ibuprofen	0.216 ± 0.033	4.42	0.158 ± 0.04	39.23	0.286 ± 0.008	48.175	0.193 ± 0.007 <sup>a</sup>	69.84
Control	0.228 ± 0.027		0.26 ± 0.037		0.548 ± 0.08		0.64 ± 0.038	

swel = mean difference in rat paw volume between right and left paw. ± SE a: significantly different from control at the same time interval at  $p < 0.05$  % inhibition =  $(1 - rt/rc) \times 100$  [rt = swel of tested group; rc = swel of control group] swel = swelling SE = standard error %inh = % inhibition

### 4. 3. Molecular Docking Results

Molecular modeling has become very important in the discovery and design of new agents.<sup>67–70</sup> 3D-QSAR and

docking studies were carried out on 23 pyrrole derivatives, to model their HIV-1 gp41 inhibitory activities. The 2D, 3D-QSAR studies were performed using CODESSA software package and comparative molecular field analysis



**Figure 3a.** Binding modes of both A) indomethacin and B) ibuprofen. This was computed with Leadit 2.1.2

(CoMFA It also helps in the interpretation and explanation of the biological results. Molecular docking is one of these approaches and is used to predict the binding mode of organic compounds.<sup>68</sup> A molecular docking study had been done using both MOE 2013.08<sup>71</sup> and Leadit 2.1.2 software.<sup>72,73</sup> Possible binding modes of the active compounds inside the active site of COX-2 were estimated. Indomethacin and ibuprofen were also docked. The presence of a carboxylic group in both indomethacin and ibuprofen was important for the carboxylate anion to form an electrostatic interaction with the cationic guanidine moiety of Arg 120 residue found in the active site of the COX-2 enzyme. The oxygen atom of carbonyl group found in this carboxylic moiety participated with the formation of a hydrogen bond with the hydrogen atom of –OH group of Tyr 355 residue. The binding affinity of indomethacin and ibuprofen was found to be –30.24 kcal/mol and –19.09 kcal/mol, respectively (Fig. 3a).

The clash score was computed with Leadit 2.1.2 software indicating that both drugs have a low clash score (Table 2).

The presence of the *p*-chloro group in the derivative **1c** with higher lipophilic contribution value (–10.90) improving the binding modes and interactions, compared with other tested compounds. All compounds with 2-amino-(substituted)-*1H*-indole-3-carbonitrile shared a hydrogen bond formed between their nitrile groups and the –OH group of Tyr 355. Compound **1g** showed a mode of binding in which three hydrogen bonds with Tyr 355, Arg 120 and Ser 530 were formed. Finally, compound **5b** showed three hydrogen bonds as well with His 90, Tyr 355 and Ser 530 (Fig. 3b).

Compounds **1d** and **1g** had the highest clash penalty score (11.54) which affected their fitting in the binding site and resulted in the lowest affinity values in both MOE 2013.08 and Leadit 2.1.2 docking results. That could explain

Table 2. The clash score for active compounds and standard drugs using Leadit 2.1.2 software.

Compound/ Standard drugs	% of inhibition	MOE docking score	Leadit docking		
			Docking score (kcal/mol)	Lipo score	Clash
<b>1b</b>	84.69	–11.68	–17.03	–13.84	7.11
<b>Indomethacin</b>	78.58	–15.25	–21.24	–12.93	6.06
<b>5b</b>	76.25	–10.38	–15.47	–12.97	6.94
<b>1c</b>	75.06	–10.52	–17.23	–10.90	7.02
<b>Ibuprofen</b>	69.84	–13.35	–19.09	–10.41	5.87
<b>1d</b>	66.73	–10.24	–16.02	–11.42	10.32
<b>1g</b>	60.73	–10.04	–12.54	–14.63	11.54

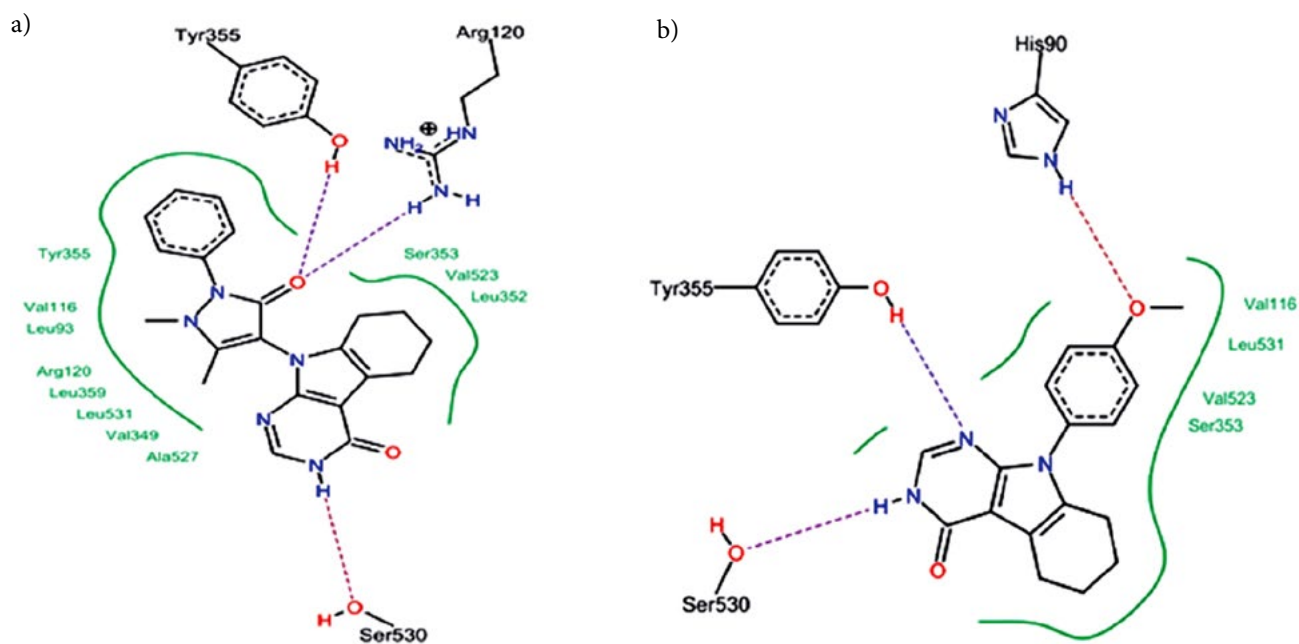


Figure 3b. A) Compound **1g** possible binding mode inside COX-2. B) Compound **5b** predicted interactions.

in their lower inhibition activity compared to the other compounds.

#### 4. 4. Structure–activity Relationships (SAR)

To investigate SAR of any NSAIDs, pathophysiology of inflammation and its treatment have to be well understood. Inflammation represents the response to injury.<sup>74</sup> Many processes are involved in the promotion of the inflammatory process, one of them is the secretion of arachidonic acid (AA) from damaged cells membranes. AA is metabolized by enzyme COX into prostanoids (as prostaglandins) and lipoxygenase (leukotrienes).<sup>75</sup> The major mechanism of action of NSAIDs was found to be the inhibition of PG synthesis, through inhibition of COXs, that is to say preventing the AA from forming PG.<sup>76–78</sup> It has a very short half-life in blood, its oxidation to 15-keto-prostaglandins is catalyzed by 15-hydroxyprostaglandin dehydrogenase (15-PGDH)

In order to design any structure with pyrrole moiety or its fused form indole, vital considerations must be taken to ensure its anti-inflammatory activity.<sup>32,74,79,80</sup>

First, the structure should consist of an acidic moiety (carboxylic acid, enols, ester etc.) attached to a planar, aromatic functional group (appears to correlate with the double bond of AA),<sup>31</sup> benzodioxine or pyrrole nucleus are described. All the newly synthesized compounds were examined for their in vitro and in vivo anti-inflammatory activity. Several derivatives, including (S and a polar linking group (which attaches the aromatic ring to a lipophilic group in AA)).<sup>30</sup> Addition of a second hydrophobic ring, not coplanar with the original aromatic ring, was found to enhance activity,<sup>35</sup> this second heteroaromatic ring or heterocyclic ring was believed to provide the necessary geometry to attach to AA.<sup>81</sup> Taking indomethacin (benzo[*b*]pyrrole) as an example, it was found that *N*-benzoyl moiety seems to play an important role for the COX-1 activity of indomethacin.<sup>32</sup> If the latter moiety is replaced with any other bulkier *N*-substituents, efficient binding to COX-1 pocket is prevented.<sup>12,82–84</sup>

Taking all this into consideration, and to analyze our SAR, two structural components were considered: the nature of the heterocycle nucleus and the character of the side chain (*N*-substitution). First, the influence of the nature of the aromatic heterocyclic system: fused pyrrole **1a**, **1c**, and **1d** showed the highest activity over fused pyrrolopyrimidine **5b**. Regarding the side chain type, addition of bulky heterocyclic ring (anti-pyrine) in compound **1g** causes the activity to decrease over the substituted phenyl in compounds **1a**, **1c**, and **1d**. Also methoxy group at *para*-position in compound **1a** has conferred significantly higher activity during all time intervals than the methyl group at *ortho*-position in compound **1d**. Replacing the antipyrine moiety in compound **1g** with the halogen group at *para*-position in compound **1c** has conferred significantly higher activity during 1<sup>st</sup> and 2<sup>nd</sup> hour

time intervals, with decreased activity in 3<sup>rd</sup> and 4<sup>th</sup> hour post-carrageenan.

## 5. Conclusion

A new strategy was developed to prepare a series of 2-amino-1-(aryl)-4,5,6,7-tetrahydro-1*H*-indole-3-carbonitriles **1a–g** and 2-amino-1-(aryl)-4,5,6,7-tetrahydro-1*H*-indole-3-carbonitriles **2a,b** as potential anti-inflammatory agents. Based on their structure, we can conclude that the best aromatic nucleus was the pyrrole with a *para* substituted phenyl and cyclization to prepare pyrrolopyrimidine derivatives, added some anti-inflammatory activity in the heterocyclic system. The molecular docking study provided the interpretation of the biological activities of the active compounds compared to the two reference drugs indomethacin and ibuprofen.

## 6. Acknowledgements

On the occasion of this, we would like to specify Dr. Rehab Kamel, Assistance professor of pharmacology, Faculty of Pharmacy, Helwan University; and Professor Dr. Aymen Goudah, Professor of Pharmacology, Faculty of Veterinary Medicine, Cairo University; with our sincerest gratitude in appreciation of their great assistance, sincere help, valuable advice and all facilities offered during this study. Our Profuse Thanks and Respects.

## 7. References

1. D.-L. Chen, G.-X. Ma, M.-J. He, Y.-Y. Liu, X.-B. Wang, X.-Q. Yang, *Helv. Chim. Acta* **2016**, *99*, 742–746. DOI:10.1002/hlca.201600159
2. H. Li, S. Fan, J. Cheng, P. Zhang, B. Zhong, W. Shi, *Molecules* **2016**, *21*, 1–8.
3. S. S. Fatahala, S. Hasabelnaby, A. Goudah, G. I. Mahmoud, *Molecules* **2017**, *22*, 1–18.
4. M. Shroff, S. J. Daharwal, *Br. Biomed. Bull.* **2017**, *5*, art. no. 299, 7 pp.
5. M. A. Kale, A. S. Narute, T. M. Kalyankar, *Clin. Anti-inflamm. Anti-Allergy Drugs* **2014**, No. 1, 39–44.
6. I. Lessigiarska, A. Nankov, A. Bocheva, I. Pajeva, A. Bijev, *Farmaco* **2005**, *60*, 209–218. DOI:10.1016/j.farmac.2004.11.008
7. A. Abbas, M. M. Naseer, *Acta Chim. Slov.* **2014**, *61*, 792–802.
8. A. A. Fadda, K. M. Elattar, *J. Biosci. Med.* **2015**, *3*, 114–123.
9. G. M. Cole, S. A. Frautschy, *CNS Neurol. Disord. Drug Targets* **2010**, *9*, 140–148. DOI:10.2174/187152710791011991
10. B. O. Villoutreix, G. Laconde, D. Lagorce, P. Martineau, M. A. Miteva, P. Dariavach, *PLoS One* **2011**, *6*, e21117. DOI:10.1371/journal.pone.0021117
11. J. S. Bang, D. H. Oh, H. M. Choi, B.-J. Sur, S.-J. Lim, J. Y. Kim,

- H.-I. Yang, M. C. Yoo, D.-H. Hahm, K. S. Kim, *Arthritis Res. Ther.* **2009**, *11*, R49. DOI:10.1186/ar2662
12. K. D. Rainsford, *Inflamm. Pathog. Chronic Dis.* **2007**, *42*, 3–27. DOI:10.1007/1-4020-5688-5\_1
13. A. O. H. El-Nezhawy, S. T. Gaballah, M. A. A. Radwan, A. R. B. Abdel-Salam, *Med. Chem. (Los Angeles)*. **2009**, No. 202, 558–569.
14. R. Mohareb, F. Al-Omran, M. Abdelaziz, R. Ibrahim, *Acta Chim. Slov.* **2017**, *64*, 349–364. DOI:10.17344/acsi.2017.3200
15. S. S. Fatahala, M. S. Mohamed, M. Youns, R. H. A.-E. Hameed, *Anticancer. Agents Med. Chem.* **2017**, *17*, 1–12. DOI:10.2174/1871520617666170102152928
16. S. Fatahala, E. Shalaby, S. Kassab, M. Mohamed, *Anticancer. Agents Med. Chem.* **2015**, *15*, 517–526. DOI:10.2174/1871520615666150105113946
17. S. D. Joshi, U. A. More, S. R. Dixit, H. H. Korat, T. M. Aminabhavi, A. M. Badiger, *Med. Chem. Res.* **2013**, *23*, 1123–1147. DOI:10.1007/s00044-013-0709-y
18. J. A. Pfefferkorn, Y. Song, K.-L. Sun, S. R. Miller, B. K. Trivedi, C. Choi, R. J. Sorenson, L. D. Bratton, P. C. Unangst, S. D. Larsen, T.-J. Poel, X.-M. Cheng, C. Lee, N. Erasga, B. Auerbach, V. Askew, L. Dillon, J. C. Hanselman, Z. Lin, G. Lu, A. Robertson, K. Olsen, T. Mertz, C. Sekerke, A. Pavlovsky, M. S. Harris, G. Bainbridge, N. Caspers, H. Chen, M. Eberstadt, *Bioorg. Med. Chem. Lett.* **2007**, *17*, 4538–4544. DOI:10.1016/j.bmcl.2007.05.096
19. S. Y. Kang, E.-J. Park, W.-K. Park, H. J. Kim, D. Jeong, M. E. Jung, K.-S. Song, S. H. Lee, H. J. Seo, M. J. Kim, M. Lee, H.-K. Han, E.-J. Son, A. N. Pae, J. Kim, J. Lee, *Bioorg. Med. Chem. Lett.* **2010**, *20*, 1705–1711. DOI:10.1016/j.bmcl.2010.01.093
20. X. Teng, H. Keys, J. Yuan, A. Degterev, G. D. Cuny, *Bioorg. Med. Chem. Lett.* **2008**, *18*, 3219–3223. DOI:10.1016/j.bmcl.2008.04.048
21. N. Danchev, A. Bijev, D. Yaneva, S. Vladimirova, I. Nikolova, *Arch. Pharm. (Weinheim)* **2006**, *339*, 670–674. DOI:10.1002/ardp.200600116
22. N. Amishiro, A. Okamoto, C. Murakata, T. Tamaoki, M. Okaabe, H. Saito, *J. Med. Chem.* **1999**, *42*, 2946–2960. DOI:10.1021/jm990094r
23. S. B. Almasaudi, N. A. El-Shitany, A. T. Abbas, U. A. Abdel-Dayem, S. S. Ali, S. K. Al Jaouni, S. Harakeh, *Oxid. Med. Cell. Longev.* **2016**, *2016*, 1–10.
24. S. Yang, Y. Kim, D. Jeong, J. H. Kim, S. Kim, Y. Son, B. C. Yoo, E. J. Jeong, T. W. Kim, I. H. Lee, J. Y. Cho, *Biomol. Ther.* **2016**, *24*, 595–603. DOI:10.4062/biomolther.2016.027
25. W. B. Han, A. H. Zhang, X. Z. Deng, X. Lei, R. X. Tan, *Org. Lett.* **2016**, *18*, 1816–1819. DOI:10.1021/acs.orglett.6b00549
26. X. T. Xu, X.-Q. Mou, Q.-M. Xi, W.-T. Liu, W.-F. Liu, Z.-J. Sheng, X. Zheng, K. Zhang, Z.-Y. Du, S.-Q. Zhao, S.-H. Wang, *Bioorg. Med. Chem. Lett.* **2016**, *26*, 5334–5339. DOI:10.1016/j.bmcl.2016.09.034
27. J. L. Amorim, D. L. R. Simas, M. M. G. Pinheiro, D. S. A. Moreno, C. S. Alviano, A. J. R. Da Silva, P. D. Fernandes, *PLoS One* **2016**, *11*, 1–18. DOI:10.1371/journal.pone.0153643
28. M. Malmsten, *Curr. Top. Med. Chem.* **2016**, *16*, 16–24. DOI:10.2174/1568026615666150703121518
29. A. Bocheva, A. Bijev, A. Nankov, *Arch. Pharm. (Weinheim)* **2006**, *339*, 141–144. DOI:10.1002/ardp.200500191
30. M. T. Sarg, M. M. Koraa, A. H. Bayoumi, S. M. Abd El Gilil, *Open J. Med. Chem.* **2015**, *5*, 49–96. DOI:10.4236/ojmc.2015.54005
31. Y. Harrak, G. Rosell, G. Daidone, S. Plescia, D. Schillaci, M. D. Pujol, *Bioorg. Med. Chem.* **2007**, *15*, 4876–4890. DOI:10.1016/j.bmc.2007.04.050
32. G. Dannhardt, W. Kiefer, G. Krämer, S. Maehrlein, U. Nowe, B. Fiebich, *Eur. J. Med. Chem.* **2000**, *35*, 499–510. DOI:10.1016/S0223-5234(00)00150-1
33. S. Ushiyama, T. Yamada, Y. Murakami, S. Kumakura, S. Inoue, K. Suzuki, A. Nakao, A. Kawara, T. Kimura, *Eur. J. Pharmacol.* **2008**, *578*, 76–86. DOI:10.1016/j.ejphar.2007.08.034
34. G. A. Elmegeed, A. R. Baiuomy, O. M. E. Abdel-Salam, *Eur. J. Med. Chem.* **2007**, *42*, 1285–1292. DOI:10.1016/j.ejmech.2007.01.027
35. J. T. Moon, J. Y. Jeon, H. A. Park, Y.-S. Noh, K.-T. Lee, J. Kim, D. J. Choo, J. Y. Lee, *Bioorg. Med. Chem. Lett.* **2010**, *20*, 734–737. DOI:10.1016/j.bmcl.2009.11.067
36. M. S. Mohamed, R. Kamel, R. H. Abd El-hameed, *Med. Chem. Res.* **2012**, *22*, 2244–2252. DOI:10.1007/s00044-012-0217-5
37. P. N. Praveen Rao, E. E. Knaus, *J. Pharm. Pharm. Sci.* **2008**, *11*, 81–110. DOI:10.18433/J3T886
38. L. Gasparini, E. Ongini, G. Wenk, *J. Neurochem.* **2004**, *91*, 521–536. DOI:10.1111/j.1471-4159.2004.02743.x
39. A. Carbone, B. Parrino, P. Barraja, V. Spanò, G. Cirrincione, P. Diana, A. Maier, G. Kelter, H.-H. Fiebig, *Mar. Drugs* **2013**, *11*, 643–654. DOI:10.3390/md11030643
40. M. S. Mohamed, A. E. Rashad, M. E. A. Zaki, S. S. Fatahala, *Acta Pharm.* **2005**, *55*, 237–249.
41. W. M. Hussein, S. S. Fatahala, Z. M. Mohamed, R. P. McGeary, G. Schenk, D. L. Ollis, M. S. Mohamed, *Chem. Biol. Drug Des.* **2012**, *80*, 500–515. DOI:10.1111/j.1747-0285.2012.01440.x
42. M. S. Mohamed, R. Kamel, S. S. Fathallah, *Arch. Pharm. (Weinheim)* **2011**, *344*, 830–839. DOI:10.1002/ardp.201100056
43. M. S. Mohamed, S. Ali, D. H. A. Abdelaziz, S. S. Fathallah, *Biomed. Res. Int.* **2014**, *2014*, 1–13.
44. K. M. H. Hilmy, E. B. Pedersen, *Liebigs Ann. Chem.* **1989**, *1989*, 1145–1146.
45. C. A. Winter, E. A. Risley, G. W. Nuss, *J. Pharmacol. Exp. Ther.* **1963**, *141*, 369–376.
46. E. C. Taylor, R. O. Kan, W. W. Paudler, *J. Am. Chem. Soc.* **1961**, *83*, 4484–4485. DOI:10.1021/ja01482a056
47. E. C. Taylor, R. W. Hendess, *J. Am. Chem. Soc.* **1965**, *87*, 1995–2003. DOI:10.1021/ja01087a025
48. E. C. Taylor, B. Liu, *J. Org. Chem.* **2001**, *66*, 3726–3738. DOI:10.1021/jo001580l
49. E. Fanghänel, K. Gewalt, K. Pütsch, K. Wagner, *J. Prakt. Chem.* **1969**, *311*, 388–394. DOI:10.1002/prac.19693110307
50. T. D. Duffy, D. G. Wibberley, *J. Chem. Soc., Perkin I* **1974**, 1921–1929. DOI:10.1039/p19740001921

51. Z. Puterová, A. Krutošiková, D. Végh, *Arkivoc* **2010**, (i), 209–246.
52. Y. Ding, H. An, Z. Hong, J.-L. Girardet, *Bioorg. Med. Chem. Lett.* **2005**, *15*, 725–727. DOI:10.1016/j.bmcl.2004.11.019
53. T.-C. Chien, E. A. Meade, J. M. Hinkley, L. B. Townsend, *Org. Lett.* **2004**, *6*, 2857–2859. DOI:10.1021/ol049207d
54. M. Qian, R. Glaser, *J. Am. Chem. Soc.* **2004**, *126*, 2274–2275. DOI:10.1021/ja0389523
55. J. U. Jeong, X. Chen, A. Rahman, D. S. Yamashita, J. I. Luengo, *Org. Lett.* **2004**, *6*, 1013–1016. DOI:10.1021/ol049921v
56. R. W. Fischer, M. Misun, *Org. Process Res. Dev.* **2001**, *5*, 581–586. DOI:10.1021/op010041v
57. C. G. Dave, N. D. Desai, *J. Heterocycl. Chem.* **1999**, *36*, 729–733. DOI:10.1002/jhet.5570360325
58. A. O. Abdelhamid, A. M. Negm, I. M. Abbas, *J. Prakt. Chemie* **1989**, *331*, 31–36. DOI:10.1002/prac.19893310106
59. K. M. H. Hilmy, *Arch. Pharm. (Weinheim)* **2004**, *337*, 15–19. DOI:10.1002/ardp.200300773
60. M. S. Mohamed, S. S. Fathallah, *Mini. Rev. Org. Chem.* **2014**, *6*, 477–507.
61. D. W. Goheen, W. R. Vaughan, *Org. Synth.* **1959**, *39*, 37–39. DOI:10.15227/orgsyn.039.0037
62. McNelis, E. kon and E. J. *Chem. Soc., Chem. Comm.* **1973**, 562–563.
63. J. Oh, C. Ziani-Cherif, J.-R. Choi, J. K. Cha, *Org. Synth.* **2002**, *78*, 212–219. DOI:10.15227/orgsyn.078.0212
64. P. M. Traxler, P. Furet, H. Mett, E. Buchdunger, T. Meyer, N. Lydon, *J. Med. Chem.* **1996**, *39*, 2285–2292. DOI:10.1021/jm960118j
65. M. M. Ghorab, F. A. Ragab, H. I. Heiba, H. A. Youssef, M. G. El-Gazzar, *Bioorg. Med. Chem. Lett.* **2010**, *20*, 6316–6320. DOI:10.1016/j.bmcl.2010.08.005
66. C. G. Dave, R. D. Shah, *Molecules* **2002**, *7*, 554–565. DOI:10.3390/70700554
67. C. Teixeira, F. Barbault, J. Rebehmed, K. Liu, L. Xie, H. Lu, S. Jiang, B. Fan, F. Maurel, *Bioorg. Med. Chem.* **2008**, *16*, 3039–3048. DOI:10.1016/j.bmc.2007.12.034
68. M. Martín-Martínez, A. Marty, M. Jourdan, C. Escricut, E. Archer, R. González-Muñiz, M. T. García-López, B. Maignet, R. Herranz, D. Fourmy, M. Marti, *J. Med. Chem.* **2005**, *48*, 4842–4850. DOI:10.1021/jm0501127
69. G. Cristalli, S. Costanzi, C. Lambertucci, S. Taffi, S. Vittori, R. Volpini, *Farmaco* **2003**, *58*, 193–204. DOI:10.1016/S0014-827X(03)00019-3
70. Y.-D. Gao, D. Feng, R. P. Sheridan, G. Scapin, S. B. Patel, J. K. Wu, X. Zhang, R. Sinha-Roy, N. A. Thornberry, A. E. Weber, T. Biftu, *Bioorg. Med. Chem. Lett.* **2007**, *17*, 3877–3879. DOI:10.1016/j.bmcl.2007.04.106
71. Molecular Operating Environment (MOE), 2013.08; Chemical Computing Group Inc.: 1010 Sherbooke St. West, Suite #910, Montreal, QC, Canada, H3A 2R7, 2014. 2014.
72. M. Rarey, B. Kramer, T. Lengauer, G. Klebe, *J. Mol. Biol.* **1996**, *261*, 470–489. DOI:10.1006/jmbi.1996.0477
73. D. M. Lorber, B. K. Shoichet, *Protein Sci.* **1998**, *7*, 938–950. DOI:10.1002/pro.5560070411
74. A. Zarghi, S. Arfaei, *Iran. J. Pharm. Res.* **2011**, *10*, 655–683.
75. J. DeRuiter, In *Principles of Drug Action*; 2002; pp 1–26.
76. D. Choi, Y. L. Piao, Y. Wu, H. Cho, *Bioorg. Med. Chem.* **2013**, *21*, 4477–4484. DOI:10.1016/j.bmc.2013.05.049
77. T. H. Page, J. J. O. Turner, A. C. Brown, E. M. Timms, J. J. Inglis, F. M. Brennan, B. M. J. Foxwell, K. P. Ray, M. Feldmann, *J. Immunol.* **2010**, *185*, 3694–3701. DOI:10.4049/jimmunol.1000906
78. R. Danesi, G. Pasqualetti, E. Giovannetti, F. Crea, G. Altavilla, M. Del Tacca, R. Rosell, *Adv. Drug Deliv. Rev.* **2009**, *61*, 408–417. DOI:10.1016/j.addr.2009.03.001
79. P. P. N. Rao, S. N. Kabir, T. Mohamed, *Pharmaceuticals* **2010**, *3*, 1530–1549. DOI:10.3390/ph3051530
80. S. Ushiyama, T. Yamada, Y. Murakami, S. I. Kumakura, S. I. Inoue, K. Suzuki, A. Nakao, A. Kawara, T. Kimura, *Eur. J. Pharmacol.* **2008**, *578*, 76–86. DOI:10.1016/j.ejphar.2007.08.034
81. W. O. Foye, In *Williams & Wilkins*; 2008.
82. M. R. Shaaban, T. S. Saleh, A. S. Mayhoub, A. Mansour, A. M. Farag, *Bioorg. Med. Chem.* **2008**, *16*, 6344–6352. DOI:10.1016/j.bmc.2008.05.011
83. H. N. Hafez, O. K. Al-duaij, A. B. A. El-gazzar, *International J. Org. Chem.* **2013**, *3*, 110–118. DOI:10.4236/ijoc.2013.32012
84. C. Limban, A. Missir, K. M. S. Fahelbom, M. M. Al-Tabakha, M. T. Caproiu, B. Sadek, *Drug Des. Devel. Ther.* **2013**, *7*, 883–892.

## Povzetek

Sintetizirali smo serijo pripojenih pirollov in jih *in vivo* testirali za njihovo aktivnost proti vnetjem. Med 14 preiskovanimi derivati smo ugotovili, da 5 derivatov (**1b–e**g and **5b**) kaže obetavno aktivnost proti vnetjem. Njihova aktivnost je primerljiva z aktivnostjo referenčnih proti-vnetnih zdravil (indometacin in ibuprofen). Da bi interpretirali rezultate bioloških študij preiskovanih spojin, smo izvedli tudi študije molekulskega sidranja. Rezultati so bili komplementarni tistim, dobljenim z biološkimi testiranj; poleg tega so potrdili biološke učinke preiskovanih spojin.

Scientific paper

# Preparation and Investigation of the Thermal Stability of Phosphate-modified TiO<sub>2</sub> Anatase Powders and Thin Films

Uroš Prah\* and Irena Kozjek Škofic

Faculty of Chemistry and Chemical Technology, University of Ljubljana, Večna pot 113, SI-Ljubljana, Slovenia

\* Corresponding author: E-mail: prah.uros@gmail.com

Received: 04-05-2017

## Abstract

The temperature dependence of the anatase-to-rutile phase transition of TiO<sub>2</sub> powders and thin films was studied. In order to shift the phase transition to higher temperature, samples were doped with a different amount of phosphate ions and their influence on the structure and thermal stability of the anatase phase was investigated. In addition, the effect of the catalyst form (powders or thin films) on the temperature of the anatase-to-rutile phase transition was observed. TiO<sub>2</sub> thin films and powders were prepared using a simple sol-gel method with an alkoxide precursor and citric acid. The thin films were deposited on silicon and aluminum substrates using the dip-coating technique. The content of the anatase phase and the crystallite size at different annealing temperatures were monitored using X-ray diffraction. The course of the thermal decomposition was followed using thermal analyses. The morphology, particle size, shape and elemental makeup of the samples were investigated using scanning electron microscopy and energy-dispersive X-ray spectroscopy. The results showed that the phosphate ions successfully inhibited the growth of the anatase nanoparticles and delayed the phase transition to the rutile phase.

**Keywords:** Anatase, phosphate, sol-gel, thermal stability, thin films

## 1. Introduction

During the past few decades titanium dioxide has been one of the most intensively studied semiconductor materials. It has numerous useful characteristics, such as the unique positions of the valence and conduction bands, a relatively narrow band-gap, chemical and physical stability, favorable electronic and optical properties, non-toxicity and a low price.<sup>1–7</sup> Furthermore, in nanocrystalline form it shows good catalytic and photocatalytic properties. Photons with sufficient energy excite electrons into the conduction band, which leads to the generation of free electrons in the conduction band and positive holes in the valence band. The energy required for the photogeneration of the electron-hole pairs in TiO<sub>2</sub> nanocrystals is 3.0–3.2 eV, which is equivalent to the energy of light in the near-UV region.<sup>8</sup> Some of these pairs react with electron-donor and electron-acceptor species on the semiconductor surface to form reactive radicals, which can be used for the degradation of environmental pollutants, self-cleaning, antifogging and the sterilization of surfaces.<sup>4,5</sup>

TiO<sub>2</sub> naturally occurs in three polymorph crystal modifications: rutile, anatase and brookite.<sup>5,6,9</sup> Of these, the

anatase and rutile phases are the most frequently used, while brookite is less interesting for practical applications due to its lower thermal stability and difficult preparation. Although the band-gap of the anatase phase is wider (3.2 eV) in comparison to rutile (3.0 eV), anatase is considered to exhibit better photocatalytic activity due to its larger surface area and the slower recombination process for the charge carriers.<sup>6,10,11</sup> The anatase is thermodynamically metastable and irreversibly converts to rutile at higher temperatures. This phase transition results in a reduction of the photocatalytic activity (formation of the less-active rutile form) and causes undesirable dimensional changes of the material.<sup>12</sup> Improving the thermal stability of the anatase phase, by increasing the temperature of the anatase-to-rutile phase transition, is particularly important when using TiO<sub>2</sub> in high-temperature applications, such as the degradation of toxic NO<sub>x</sub> and SO<sub>x</sub>, which are usually produced at high temperatures.<sup>13,14</sup>

To achieve a better thermal stability of the anatase phase and thereby inhibit the anatase-to-rutile phase transformation, different ion dopants (F<sup>-</sup>, Si<sup>4+</sup>, Fe<sup>3+</sup>, Al<sup>3+</sup>, etc.) were added to pure TiO<sub>2</sub>. These dopants can occupy both interstitial and substitutional positions in the TiO<sub>2</sub>

crystal lattice or act like a steric barrier (form a layer on the particles' surface) and thus shift the phase transformation to higher temperatures and therefore enhance the thermal stability of the anatase phase.<sup>1,3,6,10,13–16</sup> Phosphate ions react with uncondensed hydroxyl groups on the surface of TiO<sub>2</sub> particles and act as a steric barrier. Thereby phosphate ions effectively hold the anatase particles at certain distance (inhibit the contacts among the particles) and consequently decelerate their growth, because the rutile phase, which is responsible for a drastic increase in the particle size, begins to form at the interface between the anatase particles in the TiO<sub>2</sub> agglomerates.<sup>1,17,18</sup> By keeping the anatase particles separated at a certain distance, the phase transformation can be restricted and at the same time the small particle size can be maintained.<sup>1,3,6,16</sup>

The sol-gel technique is one of the most frequently used methods for the preparation of TiO<sub>2</sub>. The particle size and the morphology of the product can be easily controlled by changing the synthesis parameters. The variety of the prepared products, such as thin films, fibers, xerogels, aerogels, powders and dense ceramics, allows very diverse applications. Different types and amounts of dopants or additives can be easily added during the synthesis. A high degree of homogeneity for the prepared materials can be achieved in a single or even in multicomponent systems.<sup>7,19,20</sup>

Using a powdered catalyst is not favorable for heterogeneous photocatalysis. The problem is its mobility in air and removal from aqueous systems. To avoid these problems, powders are often immobilized on various substrates, for example, thin films can be prepared.<sup>4</sup> The advantages of using thin films are their easy removal from the liquid media and the low consumption of raw materials. In addition, very thin and transparent thin films can be prepared and used for different applications, such as self-cleaning windows and anti-fogging mirrors. Thin films often exhibit different properties compared to powders, such as phase composition, microstructure, reactivity, etc. Therefore, apart from the influence of phosphate ion addition, the influence of the TiO<sub>2</sub> catalyst form (powder or thin film) and the impact of immobilization on the course of the phase conversion of anatase into rutile were studied.

## 2. Experimental

### 2. 1. Chemicals and Materials

Titanium(IV) butoxide (97%), citric acid (≥ 99.5%) and absolute ethanol (≥ 99.8%) were purchased from Sigma Aldrich. Phosphoric acid (85%) was procured from Alfa Aesar. All chemicals were used without further purification. Aluminum foil (thickness 0.01 mm) and pure silicon wafers (1-0-0 single crystal, prepared by Czochralski method, MEMC Elect. Materials Sdn. Bhd.) were used as the substrates for the thin films.

### 2. 2. Synthesis

Sols of TiO<sub>2</sub> and TiO<sub>2</sub> doped with phosphate ions were prepared by dissolving 0.01 mol of citric acid in 20 mL of absolute ethanol. The mixture was stirred on a magnetic stirrer until all the acid was dissolved and then 0.01 mol of titanium butoxide was slowly added to the solution. The beaker with the colloidal solution was closed with parafilm and the stirring was continued for approximately 12 hours. All the sols were stored in a refrigerator (5 °C) until further use.

For the doped sols, the only difference was the addition of a different quantity of phosphoric acid to the homogenous solution of citric acid in ethanol before the addition of the Ti-precursor. Relative to the titanium ions, 5 mol%, 10 mol% and 15 mol% of phosphate ions were added to the solutions.

### 2. 3. Preparation of Powders and Thin Films

For the preparation of the powders, the sols were dried in air at room temperature to produce the xerogels. The films were deposited using the dip-coating technique on aluminum foil and silicon plates, which were first cut to appropriate dimensions and cleaned in an ultrasonic bath in deionized water, followed by absolute ethanol, and then dried. The film thicknesses and their homogeneities were controlled using a constant pulling velocity (20 cm min<sup>-1</sup>). The thin films were dried in air at room temperature. The thin films had good adhesive properties (layers could not be removed by rubbing and cutting) and therefore no additional surfactant was needed. All the prepared xerogels and the dried thin films were then calcined for 1 hour at 400, 500, 600, 700, 800, 900 and 1000 °C. After the calcinations, the powders were thoroughly milled in an agate mortar.

### 2. 4. Characterization

The thermal analyses of the xerogels and thin films were carried out in a dynamic air atmosphere with a flow rate of 100 mL min<sup>-1</sup> on a Mettler Toledo TGA/DSC 1 thermo analyzer, coupled with a Balzers Thermostar quadrupole mass spectrometer. Aluminum foil was used as the supporting material for the thin films. The thin films were cut into small pieces (~2 mm x 2 mm) and analyzed in the temperature range from room temperature up to 600 °C, while the xerogels were measured up to 800 °C. For all the measurements 150-μL platinum crucibles were used. Firstly, the samples were purged with air at 25 °C for 20 min and then heated at 5 K min<sup>-1</sup>. The gas products were transferred to the mass spectrometer through the quartz capillary heated to 190 °C. The baseline was subtracted for all the samples.

The X-ray diffraction (XRD) patterns were recorded on an X PANalytical X'Pert PRO diffractometer using monochromatic Cu-Kα radiation. Measurements of the



heat-treated powders were recorded from  $2\theta = 15^\circ$  to  $60^\circ$  with a step of 0.034 degrees per second and an integration time of 100 s. Thin films were recorded from  $2\theta = 23^\circ$  to  $30^\circ$  with a step of 0.034 degrees per second and an integration time of 500 s. For the XRD analysis, silicon plates were used as a support for the thin films since silicon does not have any peaks in the  $2\theta$  measuring range.

Scanning electron microscope (SEM) images of the samples were taken with a Zeiss Ultra Plus field-emission scanning electron microscope. A small amount of powders and appropriately cut thin films on silicon plates ( $\sim 5 \text{ mm} \times 5 \text{ mm}$ ) were attached to carbon tape on the metal holders. The electrical conductivity of titanium dioxide is sufficient; therefore, sputtering with conductive material was not needed.

The elemental composition and the distribution of the elements in the samples were determined using energy-dispersive X-ray spectroscopy (EDS) coupled to SEM.

### 3. Results and Discussion

#### 3. 1. Thermal Analysis

The thermal decomposition of the xerogels and the thin films was investigated using thermal analysis. The mass losses, exothermic and endothermic changes of the samples during the thermal treatment were measured with thermogravimetric analysis (TG) and differential scanning calorimetry (DSC). For a qualitative analysis of the released gases and for better understanding of the thermal decomposition, mass spectrometry (MS) was also employed. DSC analysis was used to determine the temperature where the anatase-to-rutile phase transition took place. This phenomenon is very hard to detect for at least two reasons. One reason is a very small exothermic effect that accompanies this phase transformation and the other is its position, which is highly dependent on the selected synthesis method and the experimental parameters.<sup>21</sup>

Fig. 1 shows the results of the thermal decomposition of the undoped xerogel sample. Three distinct steps of mass loss were observed. In the first step between room temperature and  $150^\circ\text{C}$ , the weight loss was 7.5%, corresponding to water and ethanol evaporation ( $m/z$  18 and 46). Water evaporation also took place at the beginning of the following step of the mass loss, which is evident from the endothermic minimum on the DSC curve. In the second step, from  $150^\circ\text{C}$  to around  $370^\circ\text{C}$ , the mass decreases by approximately 46% and the third step continued up to  $530^\circ\text{C}$ , with a mass loss of approximately 18%. The last two steps of the mass loss are associated with the decomposition and oxidation of the organic compounds (residues of the citric acid and butoxide groups), which is also supported by the peaks of the alkyl fragments, carbon dioxide and water from the MS signals. The total mass loss of the sample is around 72%. No exothermic peak that could represent the anatase-to-rutile phase transition is observed.

The thermal decomposition of the doped samples is comparable to the undoped sample (Fig. 2). The first and second steps of the thermal decomposition of all the samples occur in the same temperature range and show almost

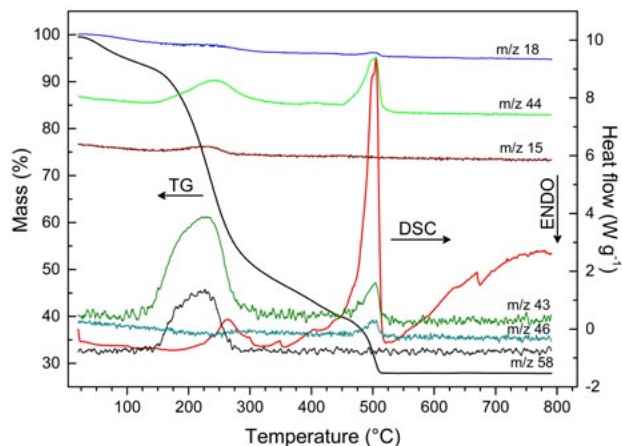


Figure 1. TG, DSC curves and signals from MS of undoped xerogel.

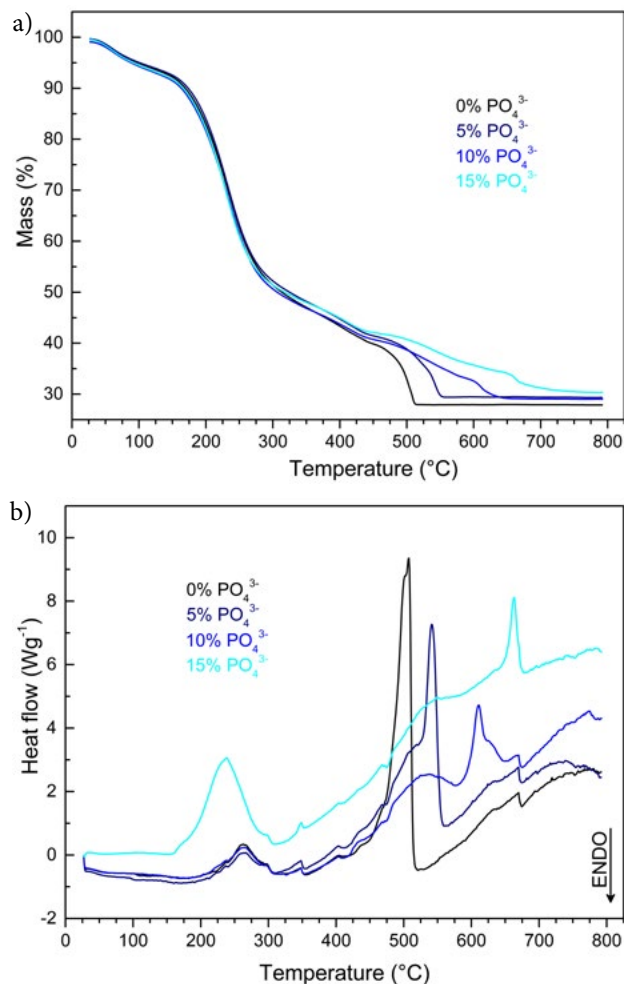


Figure 2. A comparison of (a) TG and (b) DSC curves of doped and undoped xerogels.

identical mass losses, regardless of the quantity of phosphate ions added (overlapping TG curves). The only observed difference is in the last stage of the thermal decomposition, where the temperature of the oxidation of the organic compounds moves to higher temperatures with an increasing amount of added dopant. Therefore, the mass is stabilized at higher values, which have an impact on the selection of the lowest annealing temperature. The same observations were made in the comparison of the DSC curves, wherein the addition of phosphate ions moved the exothermic peak of the last stage of thermal decomposition to higher temperatures, where also instead of one exothermic peak, two smaller one were observed.

Thermal analyses of the thin films deposited on the aluminium foil were also investigated. Due to the much heavier aluminium substrate in comparison to the thin layer, all the effects were much harder to detect. Weight changes during the thermal treatment and also exothermic and endothermic effects were very low and their interpretation was easier in comparison to the results of the xerogels (Fig. 3).<sup>22,23</sup> The total mass loss in the thin films was around 3.5%. However, it should be taken into consideration that the thermal decomposition of the thin films is often carried out differently than in the case of xerogels, because of the

suppressed diffusion of gases on the substrate side, the decomposition steps are not so clear.<sup>24</sup> Despite this difference, the positions of the more intense exothermic and endothermic peaks and the temperature of the total mass loss are positioned in the same temperature ranges.

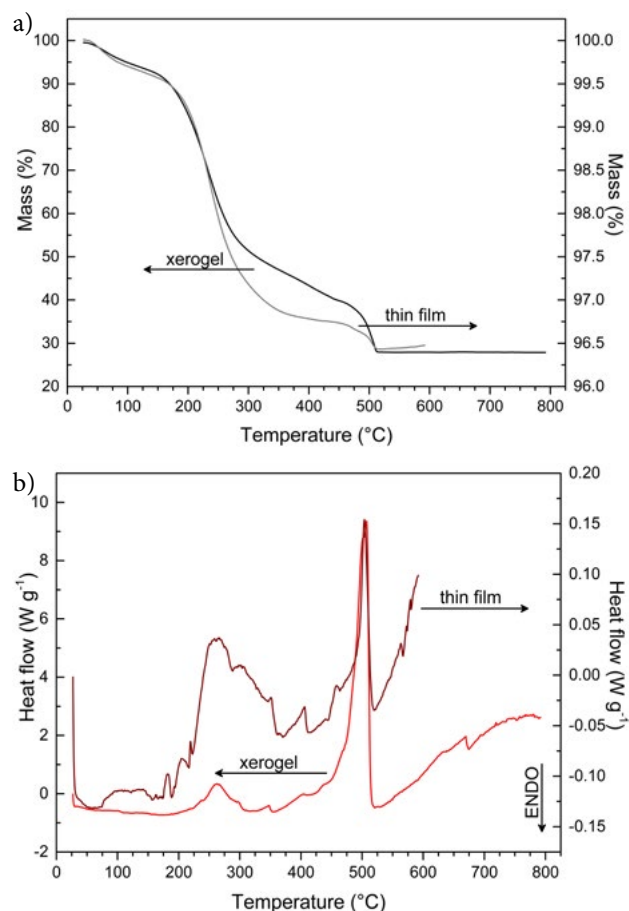
Based on the results of the thermal analysis, a range of annealing temperatures was selected. Because we could not determine the exact temperature where the anatase-to-rutile phase transition occurred, we used a wider range of annealing temperatures. The used temperatures were 400, 500, 600, 700, 800, 900 and 1000 °C.

### 3. 2. XRD Analysis

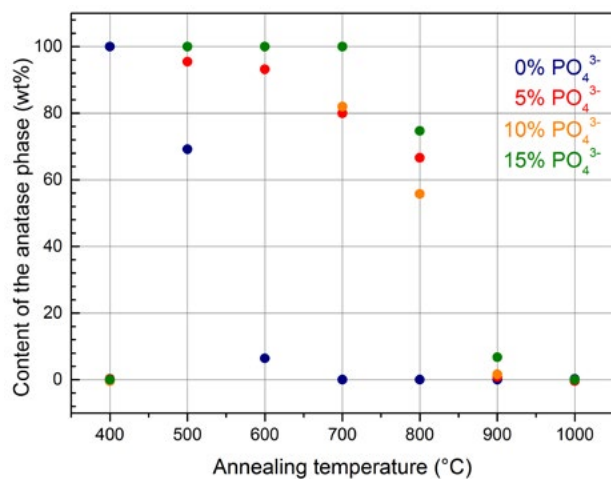
The content of the anatase phase and the particle size were determined by XRD analysis and calculated using the Rietveld analysis and Scherrer formula. The results were calculated from all the peaks in the measuring range and not only from the peaks  $2\theta = 25.28^\circ$  (101) and  $27.40^\circ$  (110), which are often taken as the characteristic peaks of the anatase and rutile phases.<sup>1,25,26</sup>

Firstly, the influence of adding phosphate ions on the average particle size and the thermal stability of the anatase phase in the powders were monitored (Fig. 4). In the undoped samples, the content of the anatase phase quickly dropped with an increasing annealing temperature. At 400 °C amorphous and partially crystallized anatase phase was present, but the content of the anatase phase dropped rapidly to 6.4 wt%, when it was annealed at 600 °C. The particle size increased with the increasing temperature and it was 30 nm at 600 °C (Table 1). When the anatase particles are sufficiently large, they start to interact with each other and the phase transformation occurs at the interfaces between them. With an increasing annealing temperature, more anatase particles were converted to rutile and the phase transformation gradually extends over the entire  $\text{TiO}_2$  agglomerates.

In doped  $\text{TiO}_2$ , the phosphate ions can easily react with the surface hydroxyl groups and form a layer on the surfaces of the anatase nanoparticles. The phosphates act like a steric barrier that prevents any direct contact between the particles, inhibits their growth and the interactions among them. By inhibiting the particle growth and preventing any interaction between the particles, the phase transformation occurs at higher temperatures.<sup>1</sup> The doped powders (with 5, 10 and 15 mol%) showed better thermal stability for the anatase with an increasing proportion of added dopant. The best results were shown by the sample with 15 mol% of added dopant, where only the anatase phase was present up to 700 °C. At 800 °C the anatase content decreased to 74.7% and at 900 °C to 6.8%. At higher dopant ratios (10 and 15 mol%) and high annealing temperatures (900 and 1000 °C) the formation of the new crystal phase, titanyl phosphate, was observed (3–10 wt%), otherwise only the anatase and rutile phases were present (Fig. 5b). All the samples annealed at 1000 °C contained, besides titanyl phosphate, only the rutile phase. The phos-



**Figure 3.** A comparison of (a) TG and (b) DSC curves for the undoped xerogel and the thin film.



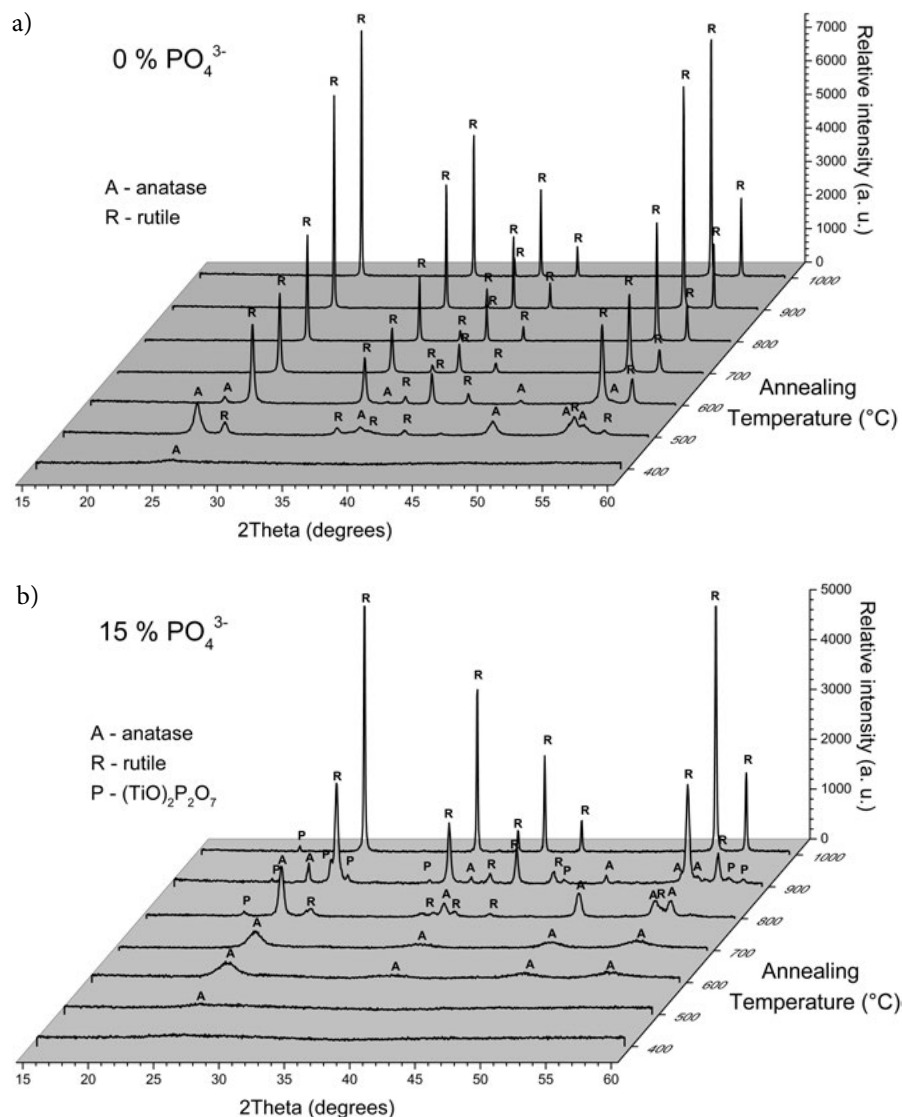
**Figure 4.** Content of anatase phase depending on the dopant ratio at different annealing temperatures in the powders.

**Table 1.** Average size of the anatase particles in powders with different annealing temperatures and dopant ratios.

Annealing temperature (°C)	Dopant ratio (mol%)			
	0	5	10	15
	Average size of the anatase particles (nm)			
400	~8 <sup>c</sup>	0 <sup>a</sup>	0 <sup>a</sup>	0 <sup>a</sup>
500	16.6	~7 <sup>c</sup>	~6 <sup>c</sup>	~10 <sup>c</sup>
600	30.0	8.4	6.6	6.0
700	0 <sup>b</sup>	11.7	8.1	7.8
800	0 <sup>b</sup>	22.9	25.9	28.7
900	0 <sup>b</sup>	26.4	38.8	43.6
1000	0 <sup>b</sup>	0 <sup>b</sup>	0 <sup>b</sup>	0 <sup>b</sup>

a – amorphous phase b – all anatase has been converted to rutile  
c – estimated value based on a partially crystallized anatase

phate ions improved the thermal stability of the anatase phase and raised the temperature of the present anatase



**Figure 5.** Evolution of the recorded powder diffraction patterns with an increasing annealing temperature (a: undoped TiO<sub>2</sub> nanoparticles, b: TiO<sub>2</sub> nanoparticles doped with 15 mol% of phosphate ions).

phase to 900 °C. The average size of the anatase particles was successfully inhibited by the phosphate ions up to 700 °C, where the average particles size remained under 12 nm (Table 1). At temperatures above 800 °C, the steric barrier is no longer able to prevent the particle growth and the phase transformation starts to take place. On the other hand, the addition of phosphate ions also increased the crystallization temperature of the anatase phase, because in doped samples, annealed at temperatures below 500 °C, no crystalline phase was observed (Table 1).

The formation of all the crystalline phases and the particle growth are clear from the series of diffractograms (Fig. 5) that were recorded after the heat treatment at different temperatures for the undoped and (15 mol%) doped powder samples. In the undoped sample, in comparison to the doped sample, the anatase peaks are narrower and have a greater intensity, which is indicative of a larger particle size.

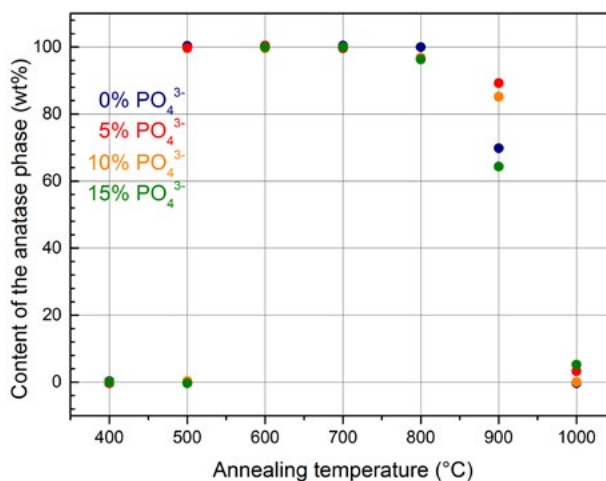


Figure 6. Dependence of the amount of anatase phase on the dopant ratio for different annealing temperatures in thin films.

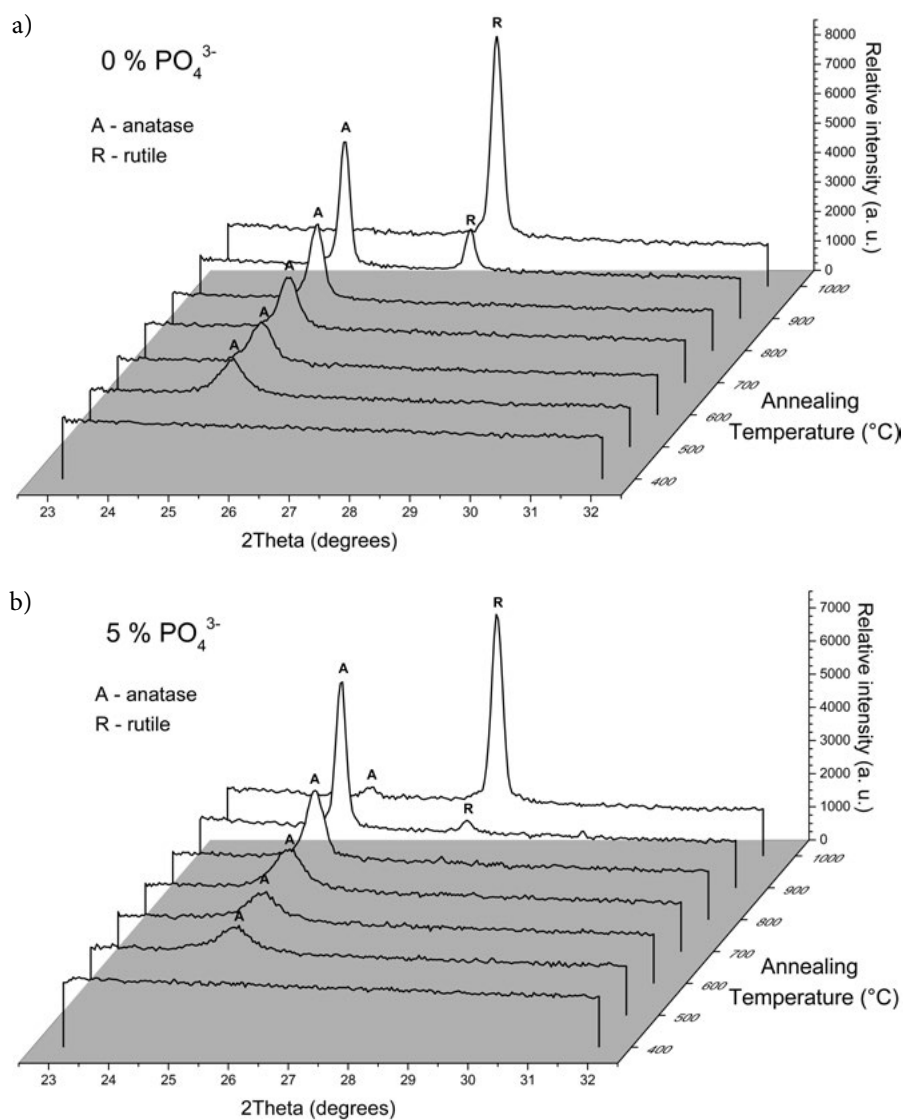


Figure 7. Evolution of the recorded diffraction patterns with an increasing annealing temperature (a: undoped TiO<sub>2</sub> thin films, b: TiO<sub>2</sub> thin films doped with 5 mol% of phosphate ions).

**Table 2.** Average size of the anatase particles in thin films with different annealing temperatures and dopant ratios.

Annealing temperature (°C)	Dopant ratio (mol%)			
	0	5	10	15
	Average size of the anatase particles (nm)			
400	0 <sup>a</sup>	0 <sup>a</sup>	0 <sup>a</sup>	0 <sup>a</sup>
500	18.2	13.7	0 <sup>a</sup>	0 <sup>a</sup>
600	21.6	14.5	9.1	10.7
700	27.7	15.1	8.6	8.6
800	38.3	29.4	29.0	17.0
900	58.6	58.4	64.1	65.2
1000	0 <sup>b</sup>	53.3	0 <sup>b</sup>	52.4

a – amorphous phase b – all anatase has been converted to rutile

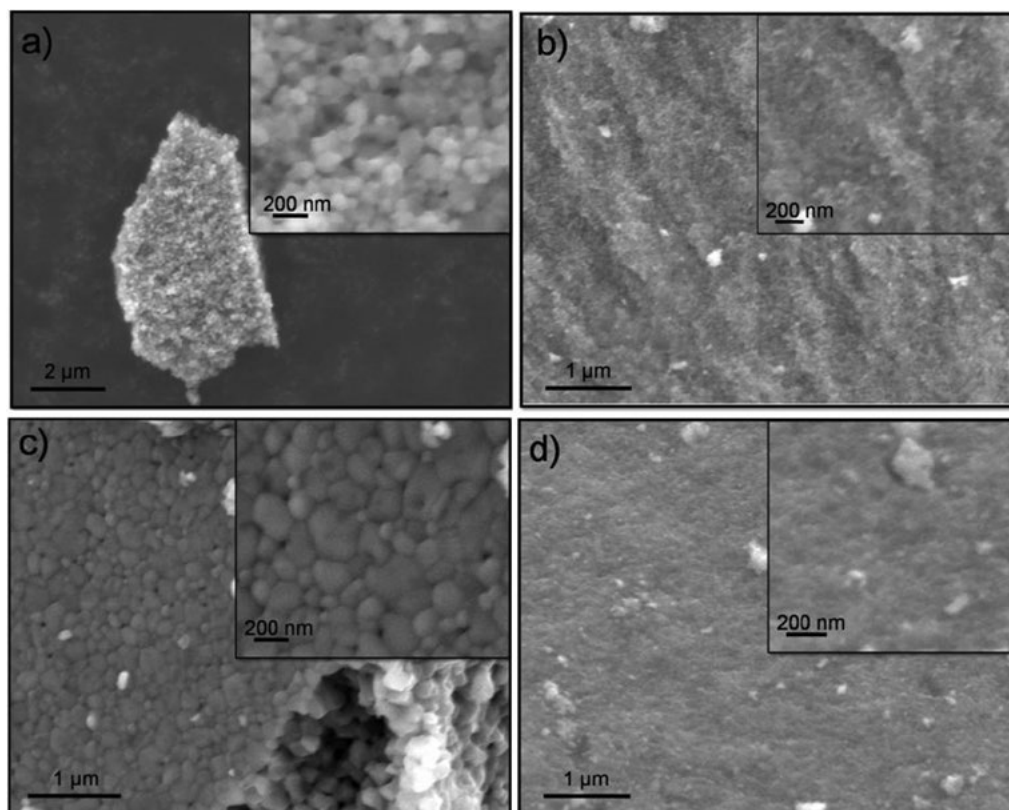
The influence of phosphate ions on the anatase's thermal stability in thin films is illustrated in Fig. 6. In thin films, compared to powders, a much smaller difference between the doped and the undoped samples was detected. In the undoped sample, even at 800 °C, only the anatase phase was present. At higher temperatures, the content of the anatase phase dropped rapidly and at 900 °C it was approximately 70 wt%. At 1000 °C only the rutile phase was detected. The thermal stability of the anatase phase was slightly improved by adding phosphate ions. The best results were shown by the sample with 5 mol% dopant, where at 900 °C there was approximately 90 wt% of anatase phase.

Even at 1000 °C, approximately 5 wt% of anatase phase was detected. In all the samples and at all the annealing temperatures only the anatase and rutile phases were present and no titanyl phosphate was formed. In thin films doped with 5 mol% of phosphate ions, the anatase phase was already crystallized at 500 °C, but in samples with higher content of the added dopant (10 and 15 mol%) the temperature of the anatase crystallization increased to 600 °C.

The reason why the anatase phase in the undoped thin films is more stable than in the powders is in the thickness of the thin films. In thin films, there is a limited amount of TiO<sub>2</sub> because the layer is very thin and is blocked by the substrate on one side. Such a thin layer does not provide enough material for the growth of the anatase particles (Table 2) and the transformation to rutile phase. The formation of the anatase and rutile phases and their particle growth is evidenced by the series of diffractograms of the thin films on silicon (Fig. 7), which were recorded after annealing at different temperatures. In addition, the difference between the undoped sample and the sample doped with 5 mol% of phosphate ions was apparent.

### 3. 3. SEM Analysis

To study the morphology, particle shape and size, SEM images of all the prepared thin films and powders were taken. The nanoparticles in the powders were not iso-

**Figure 8.** SEM micrographs of powders: a) 0% PO<sub>4</sub><sup>3-</sup>, 800 °C b) 15% PO<sub>4</sub><sup>3-</sup>, 800 °C c) 5% PO<sub>4</sub><sup>3-</sup>, 1000 °C and d) 5% PO<sub>4</sub><sup>3-</sup>, 500 °C.

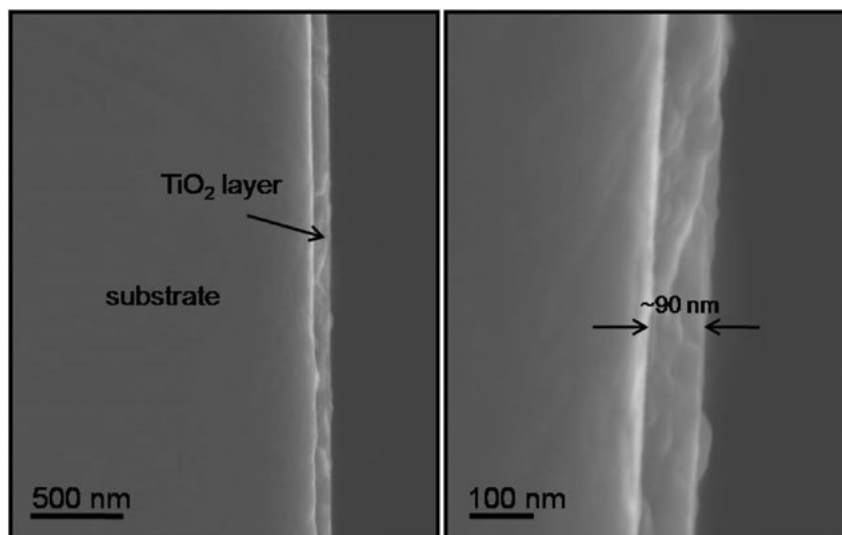


Figure 9. SEM micrographs of a cross-section of undoped thin film, calcined at 600 °C.

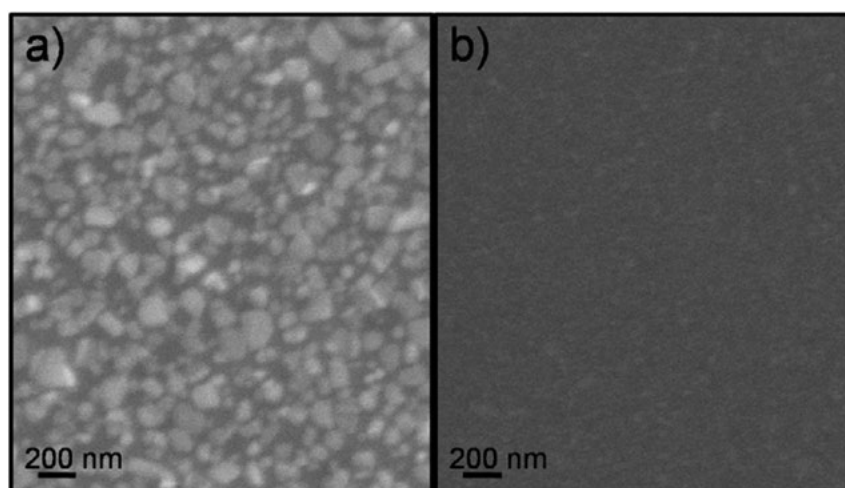


Figure 10. SEM micrographs of thin films: a) 0%  $\text{PO}_4^{3-}$ , 1000 °C and b) 0%  $\text{PO}_4^{3-}$ , 600 °C.

lated, but large agglomerates of several micrometers in size and various shapes were formed. The SEM micrograph in Fig. 8 shows that the phosphate ions strongly inhibited the particle growth. At the same annealing temperature, the average particle size decreased with an increasing amount of dopant. The particle size in the undoped samples increased rapidly with the temperature and at 1000 °C, the particles were larger than 100 nm (Fig. 8c and 8d).

In the thin films, uniformly distributed and homogeneous layer of about 90 nm thickness were observed (Fig. 9). Even though the thin films were prepared by deposition of only one layer, the films covered the whole substrate equally and no areas without thin film were observed. Due to the limited amount of material in the thin films and the presence of a substrate on one side, smaller average particle size in comparison to the powders was observed (Fig. 10).

### 3. 4. EDS Analysis

The elemental makeup of the powders and thin films was investigated with EDS analyses. In the doped samples, the larger areas were mapped to evaluate the homogeneity of the phosphorous distribution. With point analyses the molar ratios between the titanium and the phosphorous were measured (Table 3). The results of the mapping analyses (Fig. 11 and 12) showed a uniform distribution of the elements Ti, O and P on the examined surface of the powders and thin films. In the powders, the quantity of measured dopant varied greatly around the value of the initially added amount during the synthesis. These values were strongly dependent on the size and shape of the agglomerates. For example, the proportion of the measured dopant is higher in the case of smaller agglomerates and non-homogeneous surfaces, and smaller in the case of larger ag-

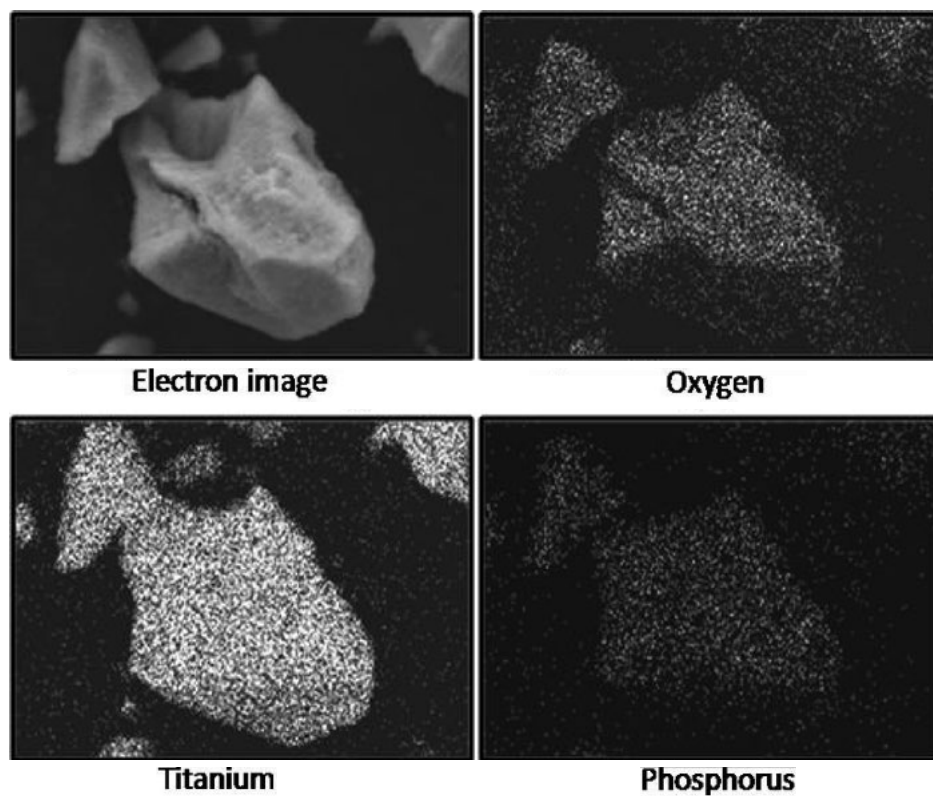


Figure 11. Distribution of the elements Ti, O and P in powder doped with 10 mol% and annealed at 900 °C.

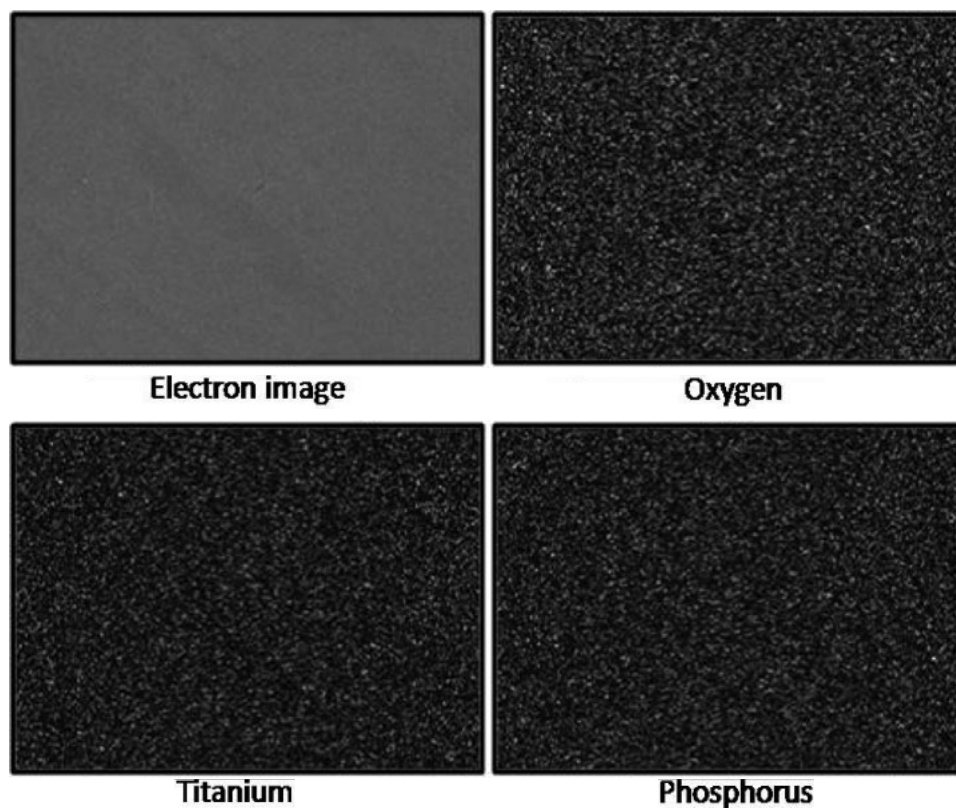


Figure 12. Distribution of the elements Ti, O and P in thin film doped with 15 mol% and annealed at 600 °C.

**Table 3.** The proportion of added and measured dopant in doped TiO<sub>2</sub> powders and thin films.

Form of the samples	The amount of added dopant (mol%)	The amount of measured dopant (mol%)
Powders	5	4.6
	5	4.7
	5	6.2
	10	10.3
	10	11.0
	10	11.8
Thin films	5	20.4
	5	20.6
	5	21.2
	10	33.3
	10	33.7
	10	34.2
	15	44.1
	15	45.2

glomerates. Because EDS is a surface technique, this indicates that phosphate ions are mostly distributed on the surface of the particles. In thin films, the amount of measured dopant was much higher than in powders, which is most likely a consequence of a small thickness of the layer.

#### 4. Conclusion

TiO<sub>2</sub> nanopowders and thin films were prepared by a simple and quick sol-gel method using titanium butoxide as the precursor. The samples were doped with phosphate ions and their influence on the thermal stability of the anatase phase was investigated. Increasing the content of added dopant influenced the last stage of the thermal decomposition, which was shifted to higher temperatures and also impacted on the anatase crystallization temperature. The addition of phosphate ions successfully inhibited the anatase-to-rutile phase transition. In the powders, the temperature of the stable anatase phase rose from 600 °C to 900 °C. On the surface of the nanoparticles, the phosphate ions acted as a steric barrier and inhibited the particle interaction and growth, which shifted the phase transition to higher temperatures. In the undoped thin films, the anatase phase showed a good thermal stability, where at 900 °C there was still around 70 wt% of anatase phase. The addition of the phosphate ions improved the thermal stability of the anatase, and even at 1000 °C some amount of anatase phase was observed. The reasons for such different behaviors of the nanopowders and thin films could be the limited amount of material in the thin layer, which does not provide enough material for the particle growth and phase transformation of the anatase to rutile. The surfaces of all the thin films were homogenous, with uniformly dis-

tributed layers and in the powders, larger agglomerates were formed. The EDS analysis proved that phosphate ions were mainly bound to the particle surface.

#### 5. References

- L. Jing, X. Qin, Y. Luan, Y. Qu, M. Xie, *Appl. Surf. Sci.* **2012**, 258, 3340–3349.
- M. R. Hoffmann, S. T. Martin, W. Choi, D. W. Bahnemann, *Chem. Rev.* **1995**, 95, 69–96. DOI:10.1021/cr00033a004
- L. Korösi, I. Dekany, *Colloids Surf. A: Physicochem. Eng. Asp.* **2006**, 280, 146–154.
- J. Kumar, A. Bansal, *Water Air Soil Pollut.* **2013**, 224, 1–11.
- D. P. Macwan, P. N. Dave, S. Chaturvedi, *J. Mater. Sci.* **2011**, 46, 3669–3686.
- K. Elghniji, J. Soro, S. Rossignol, M. Ksibi, *J. Taiwan Inst. Chem. Eng.* **2012**, 43, 132–139.
- A. Khataee, G. A. Mansoori: Nanostructured Titanium Dioxide Materials. Properties, Preparation and Applications, World Scientific Publishing Co. Pte. Ltd., Singapore, **2012**, pp. 1–97.
- A. Fujishima, T. N. Rao, D. A. Tryk, *J. Photochem. Photobiol. C: Photochem. Rev.* **2000**, 1, 1–21.
- X. Nie, S. Zhuo, G. Maeng, K. Sohlberg, *Int. J. Photoenergy.* **2009**, 1–22. DOI:10.1155/2009/294042
- D. A. Hanaor, M. H. N. Assadi, S. Li, A. Yu, C. C. Sorrell, *Comput. Mech.* **2012**, 50, 185 v194.
- D. A. H. Hanaor, C. C. Sorrell, *J. Mater. Sci.* **2011**, 46, 855–874.
- I. Hagarova, P. Matus, M. Bujdoš, J. Kubova, *Acta Chim. Slov.* **2012**, 59, 102–108.
- J. Chen, Q. Shunchen, Z. Yuexiang, X. Youchang, *Chinese J. Catal.* **2011**, 32, 1173–1179. DOI:10.1016/S1872-2067(10)60229-X
- S. Albonetti, S. Blasioli, M. Bugani, C. Lehaut-Burnouf, S. Augustine, E. Roncari, F. Trifiro, *Environ. Chem. Lett.* **2003**, 1, 197–200. DOI:10.1007/s10311-003-0036-5
- T. A. Sedneva, E. P. Lokshin, A. T. Belyaevskii, T. Kalinnkov, *Inorg. Mater.* **2008**, 44, 726–732. DOI:10.1134/S0020168508070091
- V. Žunič, S. D. Škapin, M. Maček Kržmanc, I. Bračko, A. Sever Škapin, D. Suvorov, *Appl. Catal. A: General.* **2011**, 397, 241–249.
- J. Zhang, M. J. Li, Z. C. Feng, J. Chen, C. Li, *J. Phys. Chem. B.* **2006**, 110, 927–935. DOI:10.1021/jp0552473
- D. J. Reidy, D. J. Holmes, M. A. Morris, *Ceram. Int.* **2006**, 32, 235–239. DOI:10.1016/j.ceramint.2005.02.009
- U. Schubert, N. Hüsing, *Synthesis of Inorganic Materials*, WILEY-VCH Verlag GmbH & Co. KGaA, Weinheim, **2012**, pp. 155–210.
- J. Schneider, M. Matsuoka, M. Takeuchi, J. Zhang, Y. Horiuchi, M. Anpo, D. W. Bahnemann, *Chem. Rev.* **2014**, 114, 9919–9986.
- A. Dassler, A. Feltz, J. Jung, W. Ludwig, E. Kaisersberg, *J. Therm. Anal.* **1988**, 33, 803–809. DOI:10.1007/BF02138591
- R. Cerc Korošec, P. Bukovec, B. Pihlar, J. Padežnik Gomilšek,



- Thermochim. Acta.* **2003**, *402*, 57–67.  
DOI:10.1016/S0040-6031(02)00537-3
23. R. Cerc Korošec, P. Bukovec, in: P. R. Somani (Ed): Chromic materials, phenomena and their technological applications. Multifunctional materials and devices, Applied Science Innovations Pvt. Ltd., Pune, India, **2010**, pp. 241–282.
24. R. Cerc Korošec, I. Kozjek Škofic, N. Bukovec, *Thermochim. Acta*, **2004**, *2*, 211–217. DOI:10.1016/j.tca.2003.08.016
25. L. Q. Jing, B. F. Xin, F. L. Yuan, L. P. Xue, B. Q. Wang, *J. Phys. Chem. B.* **2006**, *110*, 17860–17865.  
DOI:10.1021/jp063148z
26. L. Q. Jing, H. G. Fu, B. Q. Wang, D. J. Wang, B. F. Xin, S. D. Li, J. Z. Sun, *Appl. Catal. B.* **2006**, *62*, 282–291.  
DOI:10.1016/j.apcatb.2005.08.012

## Povzetek

Prahove in tanke plasti TiO<sub>2</sub> smo pripravili po sol-gel sintezni metodi, kjer smo kot prekurzor uporabili titanov butoksid, ki smo mu dodali citronsko kislino. Tanke plasti smo s tehniko potapljanja nanесли na silicijeve in aluminijaste podlage. Plasti in prahove smo dopirali s fosfatnimi ioni ter proučevali njihov vpliv na termično stabilnost anatasne faze. Tanke plasti v primerjavi z nanodelci pogosto prikazujejo različne lastnosti, zato smo analizirali tudi kako oblika pripravljene vzorca vpliva na fazni prehod anatas-rutil. Odvisnost vsebnosti anatasne faze in velikost kristalitov v odvisnosti od temperature termične obdelave smo spremljali z rentgensko praškovo difrakcijo. Potek termičnega razpada smo analizirali s termično analizo. Z vrstičnim elektronskim mikroskopom smo proučevali obliko, velikost delcev in morfologijo pripravljenih tankih plasti ter s pomočjo energijsko disperzijske spektroskopije tudi njihovo elementno sestavo. Rezultati prikazujejo, da fosfatni ioni uspešno zavirajo rast delcev ter s tem posledično pomaknejo fazni prehod anatas-rutil k višjim temperaturam.

Scientific paper

# Recovery of Rutin from *Labisia pumila* Extract Using Solid Phase Extraction

Lee Suan Chua,<sup>1,2,\*</sup> Nur Nabihah Ruzlan<sup>1,2</sup> and Mohamad Roji Sarmidi<sup>1</sup><sup>1</sup>Metabolites Profiling Laboratory, Institute of Bioproduct Development, Universiti Teknologi Malaysia, 81310 UTM Skudai, Johor Bahru, Johor, Malaysia.<sup>2</sup>Department of Bioprocess and Polymer Engineering, Faculty of Chemical and Energy Engineering, Universiti Teknologi Malaysia, 81310 UTM Skudai, Johor Bahru, Johor, Malaysia.\* Corresponding author: E-mail: chualeesuan@utm.my  
Tel.: +6019-7214378; fax: +607-5569706

Received: 05-17-2017

## Abstract

Reflux extraction was used to prepare crude extract from the leaves of *Labisia pumila* var. *Alata* using 60% methanol. The crude extract was subsequently fractionated by C18 solid phase extraction to recover high yield of rutin using 20–100% methanol. The volume of eluent to recover rutin was found to decrease with the increase of methanol concentration. The recovery of rutin was increased from 20 to 80% methanol system, but slightly decreased in the 100% methanol system. Approximately, 70% of rutin could be recovered using the 80% methanol system. This solvent system also appears to have the lowest distance (9.44 MPa<sup>1/2</sup>) for rutin as estimated by Hansen solubility. The recovered rutin rich fraction could achieve up to 3.96 mg/g of fraction which was about 4-fold increment from the crude extract. The increment was also noticed for its antioxidant capacity expressed as scavenging activity which was 2 times higher than crude extract. A portion of water (20%) in the 80% methanol system is important to improve the yield of rutin. Rutin is a glycosylated flavonol, and therefore a small portion of water could enhance its elution compared to the lower performance of 100% methanol in rutin recovery.

**Keywords:** Rutin; *Labisia pumila*; solid phase extraction; aqueous methanol; scavenging activity

## 1. Introduction

Rutin (3',4',5,7-tetrahydroxyflavone-3-rutinoside) is one of the attractive plant-based glycosylated flavonoids because of its remarkable pharmacological activities.<sup>1</sup> This glycoside consists of its aglycone, quercetin and two sugar moieties; glucose and rhamnose. Sometimes, it is called as quercetin-3-O-rutinoside. Quercetin usually coexists with rutin in plants. Quercetin can also be found in intestine after rutin has been hydrolyzed by gastrointestinal microflora.<sup>2</sup> They are excellent sources of pharmaceutical products for phytotherapy nowadays.<sup>3</sup> The medical benefits of rutin can be seen from its wide application in more than 130 therapeutic formulations worldwide.<sup>4–6</sup> Mostly, the formulations are prepared as health supplement and herbal remedy for anti-inflammatory symptoms. Indeed, the demand for natural rutin is on the increase, in line with the increase of scientific evidence on the beneficial effects of rutin.

Numerous studies have been extensively carried out to investigate the extraction methods for high yield of rutin

from plant samples. This includes traditional and advanced technological methods as reviewed by Chua.<sup>1</sup> Recent advancement in extraction technology reveals that ionic liquid and water under subcritical condition could recover polyphenolic compounds from lignocellulosic biomass or plant material. Reflux extraction is a time and cost effective method known for its simple set-up and being easy to operate. It is especially convenient for extraction of phytochemicals from plants because of its temperature and reflux duration control. Sample clean-up process usually follows after extraction for highly complex mixture of samples. Solid phase extraction (SPE) is the commonly employed method for sample clean-up. The principle of SPE strongly depends on the physicochemical properties of its stationary phase, ranging from highly polar to non-polar packing materials. Usually, reversed phase SPE column is used to remove plant impurities such as sugars, proteins and metals prior to analyses, in order to prevent matrix interference and improve data reliability.<sup>7–9</sup> Previous results indicated that rutin could have the highest adsorption capacity in

C18 reversed phase.<sup>10</sup> This long organosilyl ligand phase has higher carbon percentage and lower polarity in chemically bonded packing materials than C8 and C4.

Solvent is the dominant factor not only for extraction, but also for SPE fractionation of plant samples. It acts as a carrier to deliver phytochemicals into medium. The choice of solvent usually follows the principle of “like dissolves like” which explains that solvent with the polarity value near to the polarity of target compound is likely to dissolve the target compound better and *vice versa*. Since 1924, rutin has been extracted using alcoholic solvents such as ethanol and methanol in many studies.<sup>11–13</sup> Mostly, 50–60% of alcoholic solvent could produce the highest yield of rutin from buckwheat.<sup>14,15</sup> A portion of water would enhance the efficiency of extraction by increasing the diffusion of extractable polyphenols through plant tissues.<sup>16</sup> Aqueous solvent can increase the polarity of the solvent system for better separation of rutin from complex pharmaceutical and plant samples.<sup>17–19</sup> Nevertheless, recent advancement of extraction technology revealed that subcritical water or ionic liquid which act as a good hydrogen donor solvent, could effectively recover polyphenolic compounds from lignocellulosic biomass or plant material using hydrothermal treatment.<sup>20–22</sup>

This study was focused on the investigation of rutin recovery from the crude extract of *Labisia pumila* var. *Alata* using different percentages of methanol as the eluent in C18 reversed phase SPE. Rutin is one of the key compounds contributing to the previously reported pharmacological activities of this plant. Therefore, plant extract or fraction rich in rutin is believed can enhance the biological effects. The presence of rutin was detected by highly sensitive and reliable analytical technique, namely multiple reaction monitoring. This target analysis was used to monitor the elution of rutin collected from SPE cartridges, even though rutin was present in trace amount. The rutin-rich fraction was then analyzed for its antioxidant capacity against free radicals using colorimetric method. The finding of this study is important for natural rutin recovery from plant-based samples and wastes, particularly on the effect of methanol concentration in SPE.

## 2. Materials and Methods

### 2. 1. Chemicals and Plant Leaves

The standard chemical of rutin (97%) was purchased from Acros Organics (Pittsburgh, USA). HPLC-grade of methanol, n-hexane, ethyl acetate, hydrochloric acid and formic acid were obtained from Merck (Darmstadt, Germany). Sodium carbonate and aluminium chloride were purchased from Fisher Scientific (Pittsburgh, USA). 1–1 diphenyl-2-picrylhydrazyl (DPPH) and L-ascorbic acid were bought from Sigma-Aldrich (St. Louis, MO). Deionised water was generated from Barnstead NANOpure Diamond water purification system (State of Illinois, USA) at

18.2 MΩ-cm resistivity. C18 ec octadecyl-modified silica cartridges (Chromabond, 1000 mg, 6 mL) were bought from Macherey-Nagel (Hoerd, France). The leaves of *Labisia pumila* var. *Alata* was purchased from Fidea Resources (Selangor, Malaysia). The leaves were rinsed and dried in an oven at 45 °C for 3 days until constant weight. The dried leaves were ground to approximately 2–5 mm for further experimental works.

### 2. 2. Plant Sample Extraction

The dried and ground leaves (150 mg) of the plant were pre-treated with hexane to remove fatty substances by sonication at 30 °C for 15 min. The defatted filtrate was then extracted with 100 mL of 60% methanol in a reflux system at 75 °C for an hour. The boiled solvent was evaporated, condensed and returned to the round bottom flask (500 mL) for rutin extraction. The flask contained plant samples which were immersed by solvent in homogenous condition. This continuous solvent circulation process through vaporization and condensation would enhance the extraction process. The supernatant was collected after extraction and the remaining filtrate was extracted again with new solvent (60% methanol) under the similar extraction conditions in order to ensure complete extraction of rutin from the plant leaves. The supernatant was combined and dried to a constant weight by a rotary evaporator at 55 °C. The plant crude extract (27.3 mg) was stored at –20 °C freezer for the subsequent analysis.

### 2. 3. Solid Phase Extraction of Rutin

A reversed phase SPE was carried out to fractionate rutin from the crude extract of the herb using the principle of column chromatography. The C18 ec cartridge with 14% of carbon content and 45 μm of particle size was used for rutin fractionation. The cartridge was preconditioned before use according to the instruction of manufacturer. A 1 mL crude extract (60 mg/mL) was prepared and loaded onto the preconditioned cartridge, and eluted with different concentrations of methanol (20–100%) at a flow rate of 0.25 mL/min. Each fraction consisted of 1 mL eluent and screened for rutin detection using an Ultra Performance Liquid Chromatography integrated with tandem Mass Spectrometer (UPLC-MS/MS). The fractions containing rutin would be combined and dried *in vacuo* for rutin quantitation. The volume of eluent required for rutin fractionation was monitored until completion. The fraction containing rutin was dried and determined for its concentration.

### 2. 4. UPLC-MS/MS

The analytical UPLC (Waters Acquity, Milford, MA) system was coupled with a triple quadrupole-linear ion trap tandem mass spectrometer (Applied Biosystems 4000 Q TRAP; Life Technologies Corporation, Carlsbad, CA)

with an electrospray ionization source. A C18 reserved phase Acquity column (150 × 4.6 mm, 1.7 μm) protected by a guard column was used throughout this study. The mobile phase was a binary solvent system consisting of solvent A (water with 0.1% formic acid) and solvent B (CH<sub>3</sub>CN). The UPLC gradient was: 0–3 min, 10% B; 3–8 min, 10–90% B; 8–12 min, 90% B; 12–13 min, 90–10% B; 13–15 min, 10% B for final washing and equilibration of the column for the next run. The flow rate was 0.25 mL/min and the injection volume was 5 μL. All samples were filtered with 0.2 μm nylon membrane filter prior to injection. The negative scan mode of multiple reaction monitoring with two transition ions (m/z 609/301 and m/z 609/151) was used for rutin screening and quantitation. The calibration curve was prepared by using a serial of standard rutin solutions with different concentrations from 0.1 to 1.0 ppm. The capillary and voltage of the ion source were maintained at 400 °C and –4.5 kV, respectively. All other parameters were as follows: nitrogen was used as ion source gas for nebulisation, 40 psi; for drying solvent, 40 psi; curtain gas, 10 psi; collision gas, high; declustering potential, –40 V, and collision exit energy, –10 V. The scan rate was 1000 amu/s. Data acquisition and data processing were performed using Analyst 1.4.2.

## 2. 5. Free Radical Scavenging Activity by DPPH Assay

The scavenging activity of the fractions was compared to crude extract, standard rutin, standard ascorbic acid by using DPPH (1,1-diphenyl-2-picrylhydrazyl) assay. A 5 mL DPPH (0.1 mM) in methanol was mixed with 200 μL samples with different concentrations. After 30 minutes of incubation in the dark, the absorbance of the solution was measured by using a UV-Vis spectrophotometer (Shimadzu UV-1800, Tokyo, Japan) at 517 nm. The reagent solution without sample was used as blank. The percentage of inhibition was calculated from Equation (1). The inhibitory activity at 50% (IC<sub>50</sub>) was determined from the curve constructed by Equation (1). The DPPH assay was carried out in triplicate for all samples.

$$\text{Inhibition (\%)} = [(Ac - As)/Ac] \times 100 \quad (1)$$

Where: Ac = absorbance of blank,  
As = absorbance of sample or standard

## 3. Results and Discussion

### 3. 1. Reflux Extraction for Plant Crude Extract

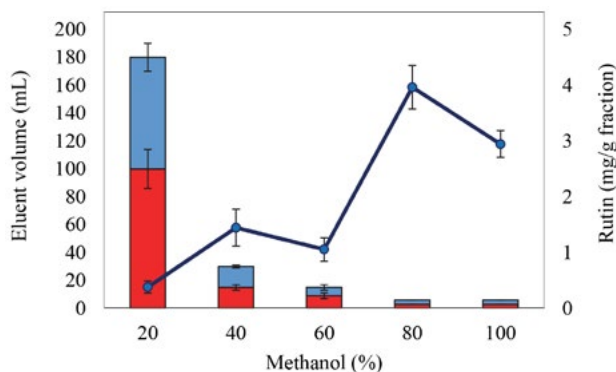
A reflux system was set up to extract phytochemicals from the leaves of *L. pumila* in 60% methanol. This continuous solvent evaporation and condensation process of solid-liquid extraction technique is an effective method for phytochemical extraction because of the ease of operation

at reasonable cost. The solvent system (60% methanol) was chosen based on the finding of previous study conducted by the same group of researchers who did the extraction for *L. pumila*.<sup>23</sup> Alcoholic solvent is well known as the solvent of choice for phytochemical extraction, especially for polyphenols and terpenoids.<sup>24</sup> Since methanol is more polar than ethanol, methanol is likely to be better in penetrating plant cellular membranes than ethanol for phytochemical extraction.<sup>25</sup> However, methanol might not be the solvent of choice for those researchers who would like to perform cell-based assays because of high cytotoxicity of methanol.<sup>26</sup> Pure methanol was also found to be less effective than aqueous methanol.<sup>27</sup> In particular, rutin is a glycosylated quercetin with two sugar moieties. Therefore, a portion of water was necessary to further increase the solvent polarity for the enhancement of extraction efficiency.<sup>28</sup> According to Ammar et al.,<sup>29</sup> the type of solvent and the method of extraction are the most important factors for the extraction of bioactive compounds from plant samples. Approximately, 18.2% of crude extract was obtained in the present study. The result was found to be higher than the extraction yield of the similar herbal plant in 100% ethanol (6.0%) and 100% water (13.4%) reported by Azrie et al..<sup>30</sup>

In comparison with rutin content in the crude extract, the present study produced the extract with rutin concentration of 1.41 mg/g extract which was comparable to the previous results which ranged from 0.46–2.12 mg/g extract<sup>31</sup> and 0.73–2.79 mg/g extract.<sup>32</sup> The result of this study was found to be higher than the findings of Karimi et al..<sup>33–35</sup> Although they are from a similar research group, a broad range of rutin content (4.60–116.85 μg/g extract) was observed. Hence, the variance in rutin content is not only attributed to the solvent system, but also the extraction conditions such as temperature, time and extraction method, as well as the variety and maturity stage of the herb.

### 3. 2. Reversed Phase Column Fractionation for Rutin

A C18 reversed phase column was used for rutin fractionation from the plant crude extract using the eluent system of methanol at different concentrations (20–100% methanol). It was found that the total volume of eluent (line bar) and the volume required (dot bar) for rutin elution were varied from 20–100% of methanol as presented in the primary axis of Figure 1. Similarly, the concentration of rutin eluted from the column also varied at different solvent systems as presented in the secondary axis of Figure 1. The eluent system of 20% methanol required the largest volume of solvent to be discarded before rutin elution, as well as the largest volume of solvent required for rutin elution from the SPE column, but the lowest recovery of rutin (~18%) in the fractionation. As the concentration of methanol was increased, the capacity ratio (*k'*) decreased which resulted in a faster elution on account of a shorter retention time of eluent in the stationary phase.



**Figure 1.** Total volume of eluent (line bar) and volume of eluent containing rutin (dot bar) at the primary axis, and rutin fractionated (line graph) from the methanolic system of solid phase extraction at the secondary axis

Therefore, rutin must be highly soluble in that particular eluent system, so that it can follow the eluent flowing out from the packed column quickly.

As the concentration of methanol was increased, the volume of eluent required for rutin elution was reduced significantly. Rutin was detected at the first 1-mL of elution for the solvent systems of 80 and 100% methanol. Both solvent systems required small volume (3 mL) for complete rutin elution, and 80% methanol produced the highest recovery 69.5% among the solvent systems. This percentage was comparable to the recovery of rutin in the solvent system of 60% methanol. However, 60% methanol was not effective enough because higher volume of eluent was required for rutin elution. Therefore, the affinity of rutin in the 80% methanol system appeared to be the highest among the methanolic systems. This is because rutin could be eluted from the column at the smallest volume of solvent and the highest recovery. A small portion of water (20%) was required for the optimum level of rutin elution. Thus, the 100% methanol system does not seem to be the most effective solvent system for rutin elution. The observation was not in good agreement with the findings of Bulgarian researchers who reported 100% methanol could recover the highest content of rutin, isoquercitrin, narcissin and astragalgin using C18 SPE column for the Euro-

pean *Bupleurum* species, namely *B. baldense* Turra and *B. affine* Sadler.<sup>36</sup> Nevertheless, the recovery of the flavonoids including rutin using 75% methanolic eluent still exhibited the second highest results which were very close to the data attained by elution with 100% methanol.

Based on the Hansen solubility parameters, rutin appears to be well dissolved in the eluent system of 80% methanol. This is because rutin displays the lowest distance (9.44 MPa<sup>1/2</sup>) from the mass center of Hansen sphere in this solvent system (Table 1). The lower distance can provide better miscibility of rutin in the solvent system. The distance is calculated by the solvent blend formulation which is based on the square root of the sum of the difference between partial cohesive energy of solvent and rutin.<sup>37</sup> The energy consists of dispersion, hydrogen bonding and polar bonding which can be estimated from the group contribution method.<sup>38</sup> The Hansen solubility parameters can describe the solubility of solute in solvent better than Hildebrand solubility and log P value.<sup>39</sup> Hildebrand parameter could only describe the solubility of solute in non-polar and non-hydrogen bonding solvent, whereas the one dimensional partition coefficient which is expressed as log P is very limited for ionizable compound like rutin.<sup>38</sup> Rutin has many hydroxyl groups in which their protons are easily released in aqueous based solvents (alcohol and water). In the present study, only half of the rutin content was recovered under the water free eluent. The crucial requirement for a small portion of water has also been highlighted in polyphenol extraction<sup>16</sup> and SPE fractionation in many studies.<sup>17–19</sup> Most probably, the preference of sugar moieties in the molecular structure of rutin is in the aqueous medium, even though its aglycone, quercetin is highly soluble in methanol.

By considering the effectiveness of fractionation, 80% methanol could produce about 60.66 µg rutin in a gram of fraction in a milliliter of eluent which was the highest performance among the other solvent systems (13.84–60.66 µg rutin/g fraction/mL eluent). This information is very important, especially for those researchers who would like to recover rutin by using the minimum level of solvent consumption. The performance of 100% methanol was found

**Table 1.** Rutin solubility in different solvent systems based on Hansen solubility parameters

Methanol (%)	Hansen solubility parameters (MPa <sup>1/2</sup> )				Distance*
	Dispersion (δD)	Polar bonding (δP)	Hydrogen bonding (δH)		
Rutin	19.30	16.10	25.40	–	
Water	15.50	16.00	42.30	18.53	
20	15.34	15.26	38.30	15.16	
40	15.18	14.52	34.30	12.23	
60	15.02	13.78	30.30	10.13	
80	14.86	13.04	26.30	9.44	
100	14.70	12.30	22.30	10.43	

$$* \text{Distance} = \sqrt{4(\delta D_s - \delta D_r)^2 + (\delta P_s - \delta P_r)^2 + (\delta H_s - \delta H_r)^2}$$

Where s denotes for solvent and r denotes for rutin

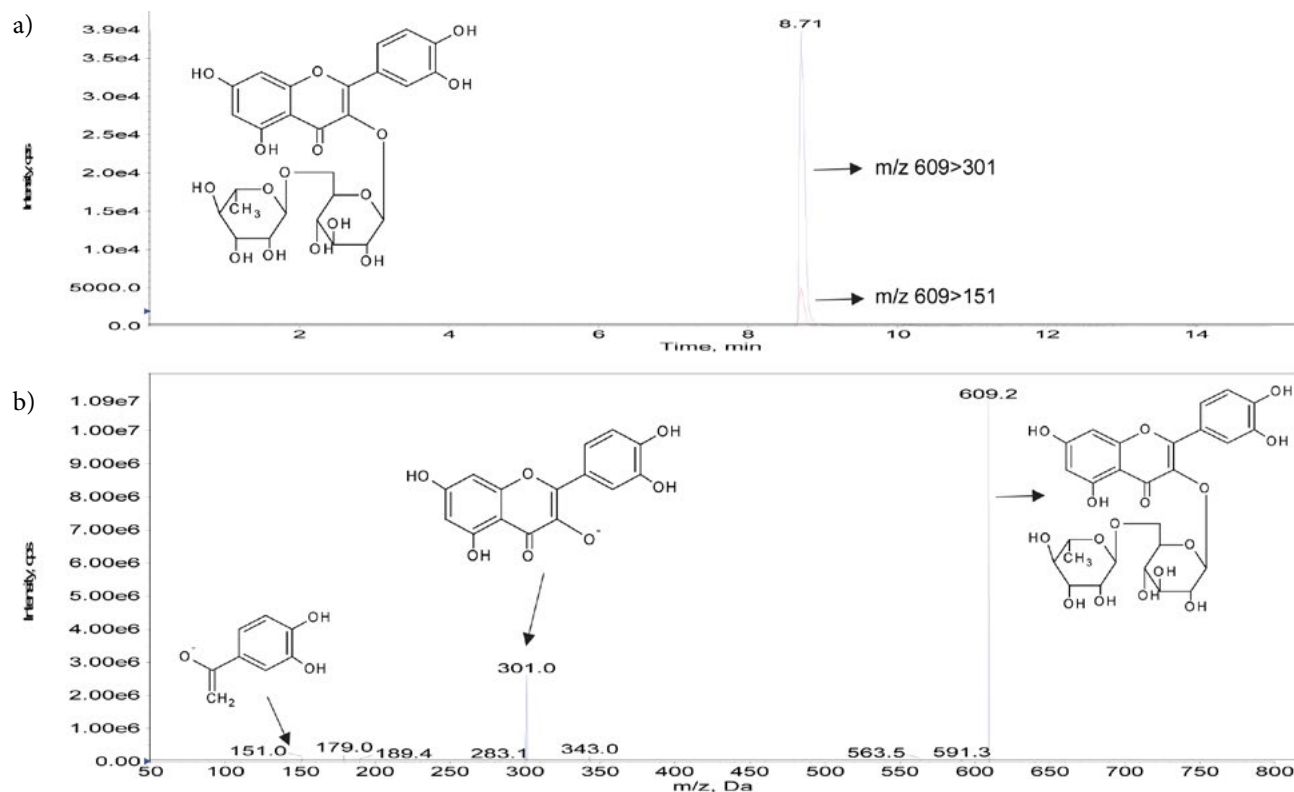


Figure 2. (a) Two transition ions of rutin peaks in multiple reaction monitoring and (b) mass fragmentation of rutin at the negative ion mode

to be the second highest, which was about 52.27  $\mu\text{g}$  rutin in a gram of fraction in a milliliter of eluent. The content of rutin was increased from  $0.85 \pm 0.16$  mg/g plant leaves (0.08%w/w) or  $1.41 \pm 0.54$  mg/g crude extract (0.14%w/w) after reflux extraction, to  $3.96 \pm 0.39$  mg/g fraction (0.40%w/w) after fractionation using 80% methanol as the eluent. The increment was about 2-fold after extraction and 4-fold after fractionation. The quantitation of rutin was measured by UPLC-MS/MS using the multiple reaction monitoring of two transition ions such as  $m/z$  609>301 and  $m/z$  609>151 at negative ion mode as shown in Figure 2.

### 3. 3. Scavenging Activity of Rutin Fraction

The quality of rutin fraction was evaluated based on its scavenging activity using DPPH assay compared to standard chemicals such as rutin and ascorbic acid. The free radicals generated from DPPH were scavenged by antioxidants in a concentration dependent manner. This method measured the colour change based on the reduction of purple-coloured free radical DPPH $^{\bullet}$  to yellow-coloured 2,2-diphenyl-1-picrylhydrazine (DPPH-H). The colour density was recorded by a UV-Vis spectrophotometer at 517 nm. The results showed that  $IC_{50}$  for standard rutin and ascorbic acid was 122 and 84 ppm, respectively. The lower  $IC_{50}$  value indicates the lower amount of sample required to inhibit 50% of free radicals which means the sample has higher scavenging activity. The antioxidant capacity of standard

rutin is comparable to ascorbic acid which is a well-known antioxidant compound. The  $IC_{50}$  of rutin fraction from the 80% methanol eluent system was 800 ppm which was 6 times lower scavenging activity than standard rutin, but almost 2 times higher scavenging activity than its crude extract (Table 2). Therefore, reversed phase fractionation increased the content of rutin in the plant sample, as well as improved its antioxidant capacity. The observation also explains that rutin could be the major radical scavenger. The increase of rutin content in the fractionated sample was found to increase its scavenging activity significantly.

Table 2. Scavenging activity of standard chemicals and plant samples at 50% inhibition

Sample	$IC_{50}$ (ppm)
Standard ascorbic acid	84
Standard rutin	122
Crude extract	1500
80% methanol rutin fraction	800

## 4. Conclusion

The detection of rutin has been reported by many investigators in *L. pumila* recently. It could be the prominent flavonol glycoside in the herbal plant which contributes to the significant pharmacological activities. Therefore, this study investigated the effects of methanol con-

centration for rutin recovery in SPE. A reserved phase SPE system could recover about 70% of rutin from the crude extract of *L. pumila* var. *Alata* using 80% methanol as the eluent. The rutin rich fraction was found to exhibit higher scavenging activity than crude extract, but the value was still lower than standard rutin.

## 5. Acknowledgement

The authors would like to thank Universiti Teknologi Malaysia for internal grant (GUP 05J84), and Ministry of Higher Education Malaysia for HiCoE grant (4J263) to carry out the research activities. We also highly appreciate our internship student, Ms. Lee Si Ning to replicate some experimental works.

## 6. References

- L. S. Chua, *J. Ethnopharmacol.* **2013**, *150*, 805–817. DOI:10.1016/j.jep.2013.10.036
- G. Chen, H. Zhang, J. Ye, *Anal. Chim. Acta* **2000**, *423*, 69–76. DOI:10.1016/S0003-2670(00)01099-0
- Y. Yang, F. Zhang, *Ultrason. Sonochem.* **2008**, *15*, 308–313. DOI:10.1016/j.ultsonch.2007.05.001
- J. E. F. Reynolds, *Martindale-The Extra Pharmacopoeia*, 31<sup>st</sup> ed., The Royal Pharmaceutical Society, Council of the Royal Pharmaceutical Society of Great Britain, London, **1996**, pp. 1679–1680.
- W. Q. Sun, J. F. Sheng, *Handbook of Natural Active Constituents*, Chinese Medicinal Science and Technology Press, Beijing, **1998**, pp. 2240–2316.
- I. Erlund, T. Kosonen, G. Alftan, J. Maenpaa, K. Perttunen, J. Kenraali, J. Parantainen, A. Aro, *Eur. J. Clin. Pharmacol.* **2000**, *56*, 545–553. DOI:10.1007/s002280000197
- S. Y. Yoon, W. J. Choi, J. M. Park, J. W. Yang, *Biotechnol. Tech.* **1997**, *11*, 553–556. DOI:10.1023/A:1018434704902
- E. Aehle, S. R. L. Grandic, R. Ralainirina, S. Baltora-Rosset, F. Mesnard, C. Prouillet, J. C. Maziere, M. A. Fliniaux, *Food Chem.* **2004**, *86*, 579–585. DOI:10.1016/j.foodchem.2003.10.006
- J. Wang, F. A. Wu, H. Zhao, L. Liu, Q. S. Wu, *Afr. J. Biotechnol.* **2008**, *7*, 2147–2155.
- B. Buszewski, S. Kawka, Z. Suprynowicz, T. Wolski, *J. Pharm. Biomed. Anal.* **1993**, *11*, 211–215. DOI:10.1016/0731-7085(93)80199-B
- C. E. Sando, J. U. Lloyd, *J. Biol. Chem.* **1924**, 737–745.
- H. F. Koones, N. J. Clifton, *Extraction of rutin*, United States Patent Office: 2,450,555, 5 Oct 1948.
- F. Fathiazad, A. Delazar, R. Amiri, S. D. Sarker, *Iranian J. Pharm. Res.* **2006**, *5*, 222–227.
- S. Kreft, M. Knapp, I. Kreft, *J. Agr. Food Chem.* **1999**, *47*, 4649–4652. DOI:10.1021/jf990186p
- K. H. Kim, K. W. Lee, D. Y. Kim, H. H. Park, I. B. Kwon, H. J. Lee, *Bioresour. Technol.* **2005**, *96*, 1709–1712. DOI:10.1016/j.biortech.2004.12.025
- E. Altiock, D. Baycin, O. Bayraktar, S. Ulku, *Sep. Purif. Technol.* **2008**, *62*, 342–348. DOI:10.1016/j.seppur.2008.01.022
- J. Dai, R. J. Mumper, *Molecules*, **2010**, *15*, 7313–7352. DOI:10.3390/molecules15107313
- Z. Legnerova, D. Satinsky, P. Solich, *Anal. Chim. Acta* **2003**, *497*, 165–174. DOI:10.1016/j.aca.2003.07.007
- B. Buszewski, S. Kawka, T. Wolski, *Chromatographia* **1993**, *35*, 311–316. DOI:10.1007/BF02277516
- H. Zeng, Y. Wang, J. Kong, C. Nie, Y. Yuan, *Talanta* **2010**, *83*, 582–590. DOI:10.1016/j.talanta.2010.10.006
- M. Grilc, B. Likozar, J. Levec, *ChemCatChem.* **2016**, *8*, 180–191. DOI:10.1002/cctc.201500840
- S. Machmudah, Wahyudiono, H. Kanda, M. Goto, *ARPN J. Eng. App. Sci.* **2016**, *11*, 9509–9518.
- L. S. Chua, N. A. Latiff, S. Y. Lee, C. T. Lee, M. R. Sarmidi, R. A. Aziz, *Food Chem.* **2011**, *127*, 1186–1192. DOI:10.1016/j.foodchem.2011.01.122
- A. Pandey, S. Tripathi, *J. Pharmacog. Phytochem.* **2014**, *2*, 115–119.
- G. X. Wang, *Vet. Parasitol.* **2010**, *171*, 305–313. DOI:10.1016/j.vetpar.2010.03.032
- P. Tiwari, B. Kumar, M. Kaur, G. Kaur, H. Kaur, *Int. Pharm. Sci.* **2011**, *1*, 98–106.
- D. Xiao, P. M. Davidson, D. H. D'Souza, J. Lin, Q. Zhong, *J. Food Eng.* **2010**, *100*, 194–200. DOI:10.1016/j.jfoodeng.2010.03.044
- M. Bimakr, R. A. Rahman, F. S. Taip, A. Ganjloo, L. M. Salleh, J. Selamat, A. Hamid, I. S. M. Zaidul, *Food Bioprod. Process.* **2011**, *89*, 67–72. DOI:10.1016/j.fbp.2010.03.002
- I. Ammar, M. Ennouri, H. Attia, *Ind. Crop. Prod.* **2015**, *64*, 97–104. DOI:10.1016/j.indcrop.2014.11.030
- A. M. Azrie, A. Luqman Chuah, K. Y. Pin, *J. Chem. Pharm. Res.* **2014**, *6*, 172–176.
- M. H. Ibrahim, H. Z. E. Jaafar, E. Karimi, A. Ghasemzadeh, *Sci. World J.* **2014**, *2014*, 360290.
- Z. Ismail, H. K. Beh, M. S. R. Hamil, G. Ghafar, M. A. A. Saeed, A. H. Memon, S. Hashim, Publication number: WO2016093692 A1. 16 June 2016.
- E. Karimi, H. Z. E. Jaafar, S. Ahmad, *Molecules* **2011**, *16*, 4438–4450.
- E. Karimi, H. Z. E. Jaafar, A. Ghasemzadeh, M. H. Ibrahim, *Aus. J. Crop Sci.* **2013**, *7*, 1016–1023.
- E. Karimi, H. Z. E. Jaafar, *Molecules* **2011**, *16*, 6791–6805. DOI:10.3390/molecules16086791
- R. Gevrenova, N. Denkov, D. Zheleva-Dimitrova, *Pharmacia* **2014**, *61*, 17–23.
- The Official Hansen Solubility Parameter Site, [Http://www.Hansen-Solubility.com](http://www.Hansen-Solubility.com) (Accessed: 20 September 2015).
- C. M. Hansen, *Hansen Solubility Parameters*, in *A User's Handbook*, 2<sup>nd</sup> ed. CRC Press, Boca Raton, 2007. DOI:10.1201/9781420006834
- J. Gao, Using Hansen solubility parameters (HSPs) to develop antioxidant-packing film to achieve controlled release. Michigan State University, Thesis for Master of Science, 2014.

## Povzetek

Ekstrakcija z refluksom je bila uporabljena za pripravo osnovnega ekstrakta iz listov *Labisia pumila* var. *Alata*. Za izolacijo rutina z visokim izkoristkom je bil ta v nadaljevanju obdelan s C18 ekstrakcijo v trdni fazi z 20–80 % metanolom. Pri tem je bil z naraščajočo vsebnostjo metanola potreben manjši volumen eluenta, prav tako je naraščal tudi izkoristek, vendar je ta v čistem metanolu rahlo padel. Z 80 % metanolom je bilo izoliranega približno 70 % rutina. Bogata frakcija izolata z rutinom je dosegla 3.96 mg rutina /g frakcije, kar je 4-krat več kot v osnovnem ekstraktu. Tudi antioksidacijska aktivnost se je 2-krat povečala v primerjavi z osnovnim ekstraktom. Na boljši izkoristek rutina lahko vpliva voda (20 %) v 80 % sistemu z metanolom. Rutin je namreč glikoziliran flavonol in majhen delež vode lahko pospeši elucijo v primerjavi s 100 % metanolom.



Scientific paper

# Synthesis and Biological Evaluation of 1,2,4-Triazoles and 1,3,4-Oxadiazoles Derivatives Linked to 1,4-Dihydropyridines Scaffold

Maghsoud Ziaie,<sup>1</sup> Karim Akbari Dilmaghani<sup>1,\*</sup> and Amir Tukmechi<sup>2</sup><sup>1</sup> Department of Organic Chemistry, Faculty of Chemistry, Urmia University, 57159, Urmia, Iran<sup>2</sup> Department of Microbiology, Faculty of Veterinary Medicine, Urmia University, Urmia, Iran

\* Corresponding author: E-mail: kadilmaghani@yahoo.com

Received: 06-05-2017

## Abstract

A series of diethyl-2,6-dimethyl-4-phenyl-1,4-dihydropyridine-3,5-dicarboxylate derivative coupled to 1,3,4-oxadiazole-5-thiones and 1,2,4-triazole-5-thiones moieties at C2,C6 positions of 1,4-dihydropyridine ring system was prepared. This linkage was carried out by the reaction of 1,3,4-oxadiazole-5-thiones and 1,2,4-triazole-5-thiones with 2,6-dibromomethyl-3,5-diethoxycarbonyl-4-phenyl-1,4-dihydropyridine in the presence of potassium carbonate as a weak base and dry acetone as the solvent. The newly synthesized compounds were characterized by FT-IR, <sup>1</sup>H NMR, <sup>13</sup>C NMR spectral data, elemental analysis and FAB-MS. The synthesized compounds were tested for their antimicrobial and antifungal activity against *Escherichia coli* and *Aspergillus fumigatus* *in vitro* in comparison with Enrofloxacin and Amphotericin as the reference drugs which are normally used for treating such infections. The synthetic compounds showed different inhibition zones against tested bacteria and fungi. Compound **8d** showed more antagonistic activity against *E. coli* and *A. fumigatus*.

**Key words:** 1,4-dihydropyridines, 1,3,4-oxadiazoles, 1,2,4-triazoles, antimicrobial activity

## 1. Introduction

Antibiotics are drugs used for treating infection caused by microorganism such as bacteria or fungi and antibiotic resistance is the ability of microorganism to withstand the effect of antibiotics. The resistance of infective bacteria to present antibiotics remains a clinical obstacle in the chemotherapy of many cancers and demands research focused on the discovery of new drugs in the antibiotic drug field. The 1,4-dihydropyridines (1,4-DHPs) were found to be highly effective calcium antagonists and are used in treatment of various cardiovascular activities.<sup>1–4</sup> Apart from CVS activities (1,4-DHPs), they possess a variety of biological activities such as anti-tubercular,<sup>5</sup> antimicrobial,<sup>6–7</sup> anti-inflammatory,<sup>8</sup> anti-tumor,<sup>9–10</sup> analgesic.<sup>11</sup> A substance which has no calcium antagonistic activity but has antibiotic activity would be of value in cancer chemotherapy and has strong ability in overcoming anticancer drug resistance. Among the possible drug resistance modifiers the 1,4-dihydropyridines calcium antagonists such as Verapamil have been extensively studied.<sup>12–13</sup> These examples clearly demonstrate the remarkable potential of

novel DHP derivatives as a source of valuable drug candidates.

In recent years 1,3,4-oxadiazole-5-thiones and 1,2,4-triazole-5-thiones derivatives which belong to an important group of heterocyclic compounds containing five membered ring have received significant attention and numerous reports have highlighted their diverse range of biological activities, such as antimicrobial,<sup>14–15</sup> antifungal,<sup>16–17</sup> antimycobacterial,<sup>18–19</sup> anticancer,<sup>20–21</sup> anti-inflammatory<sup>22–23</sup> and anti convulsant.<sup>24–25</sup> The connection of 1,3,4-oxadiazoles or 1,2,4-triazoles to the 1,4-DHPs core has produced a combination scaffold. 1,4-DHPs can be selectively functionalized at several positions. Synthesis and antibacterial activities of bis(1,3,4-oxadiazole-2-thiol) and bis(4-amino-1,2,4-triazole-3-thiole) derivatives of 1,4-dihydropyridines derivatized at C3, C5 was reported.<sup>26</sup> Synthesis and biological activities of 1,3,4-oxadiazole derivatives linked to N1 of 1,4-dihydropyridines ring system was reported.<sup>27</sup> In spite of the widely developed chemistry of the 1,4-DHPs, much less is known about the synthesis of 1,4-DHPs bearing substituents other than hydrogen atoms or alkyl groups

at C2 and C6. These multicomponent 1,4-DHP derivatives are useful in probing biological activity and might be used as antibiotics and inhibitors of the multidrug-resistant transporters. 1,4-DHP derivatives were prepared by Hantzsch method.<sup>28</sup> Hantzsch dihydropyridine synthesis is a one-pot multicomponent condensation reaction where an aldehyde  $\beta$ -ketoester and a nitrogen donor, such as ammonia or ammonium acetate, under reflux in ethanol forms the final product.<sup>29</sup> In our previous works we reported the synthesis and antibacterial properties of a new series of thioglycoside heterocyclic derivatives of 1,2,4-triazole-5-thiones and 1,3,4-oxadiazole-5-thiones.<sup>30–32</sup> Following our studies on the design of potent antibacterial agents with 1,3,4-oxadiazoles and 1,2,4-triazole moieties, we have reported the connection of 1,2,4-triazole-5-thiones and 1,3,4-oxadiazole-5-thiones moieties to the 2,6-position of 1,4-DHP ring system. These newly synthesized multicomponents 1,4-DHPs are useful in probing biological activity, as they could exhibit antimicrobial effects and could act as inhibitors of the multidrug-resistant transporters.

## 2. Materials and Methods

### 2.1. Bacterial Strain

The antibacterial and antifungal activity of compounds was assayed according to our previously published method.<sup>33</sup> The antibacterial and antifungal activity of compounds was tested against *Escherichia coli* and *Aspergillus fumigatus*.

### 2.2. Bacterium and Fungi Culture

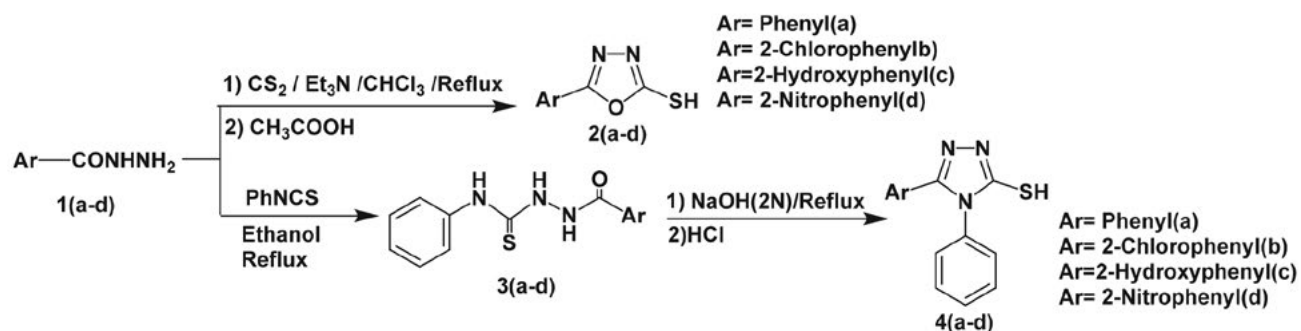
The following microorganisms were used in this study to test antimicrobial activity of compounds: *E. coli* (PTCC 1399) and *Aspergillus fumigatus* (PTCC 5009). All microorganisms were provided by Persian Culture Collections of Microorganism, Iran. Bacteria were cultured for 24 h at 37 °C in brain heart infusion broth (Merck, Darmstadt, Germany) and *A. fumigatus* was cultured for 72 h at 5 °C in Saburo Dextrose broth (Merck, Darmstadt, Germany) and were used as inoculums.

### 2.3. Susceptibility Tests

The following methods were used to evaluate the activity of the compounds. All tests were repeated three times, using distilled water without compounds as a control to test the inhibitory effect of the solvent. Minimum inhibition concentrations (MIC) of compounds against the tested pathological microorganisms were determined using micro broth dilution method.<sup>34</sup> Briefly, serial two-fold dilutions of each compounds (10% w/v) were prepared in 96-well micro titer plate ((from 1:2 to 1:8192) containing cation-adjusted Mueller-Hinton broth (Merck, Darmstadt, Germany). Control micro-titer plates containing medium and distilled water at the same dilutions were also made. Bacteria and fungi suspensions were adjusted to the 0.5 McFarland standards (approximately 1 to 2  $\times$  10<sup>8</sup> CFU/mL). A constant amount of microorganisms were added to all wells and the plates were incubated at 37 and 25 °C for 24–72 hour for *E. coli* and *A. fumigatus*, respectively (final inoculates were adjusted to the 10<sup>5</sup> CFU per each well). Each well was examined for growth, comparing each well to the control. The MIC was defined as the lowest concentration of compounds at which there was no visible growth of the organisms. For each test enrofloxacin and amphotericin were used as the control antimicrobial agents. The minimal bactericidal concentration (MBC; the lowest concentration of compounds that resulted in a 99.9% reduction in CFU of the initial inoculums) was determined by plating count the contents of wells that showed no visible growth of bacteria onto Mueller-Hinton agar and Saburo Dextrose agar plates and incubating at 37 and 25 °C for 24–72 h for *E. coli* and *A. fumigatus*, respectively. The MBC was considered the lowest concentration of compounds that prevented any colony formation.

## 3. Result and Discussion

The main synthetic route for substituted 1,3,4-oxadiazole-5-thiones **2a–d** involves an initial reaction between carboxylic acid hydrazides **1a–d** and carbon disulfide in basic ethanol solution, followed by acidification with di-



Scheme 1. Synthesis of 1,3,4-oxadiazole-5-thione and 1,2,4-triazole-5-thione derivatives

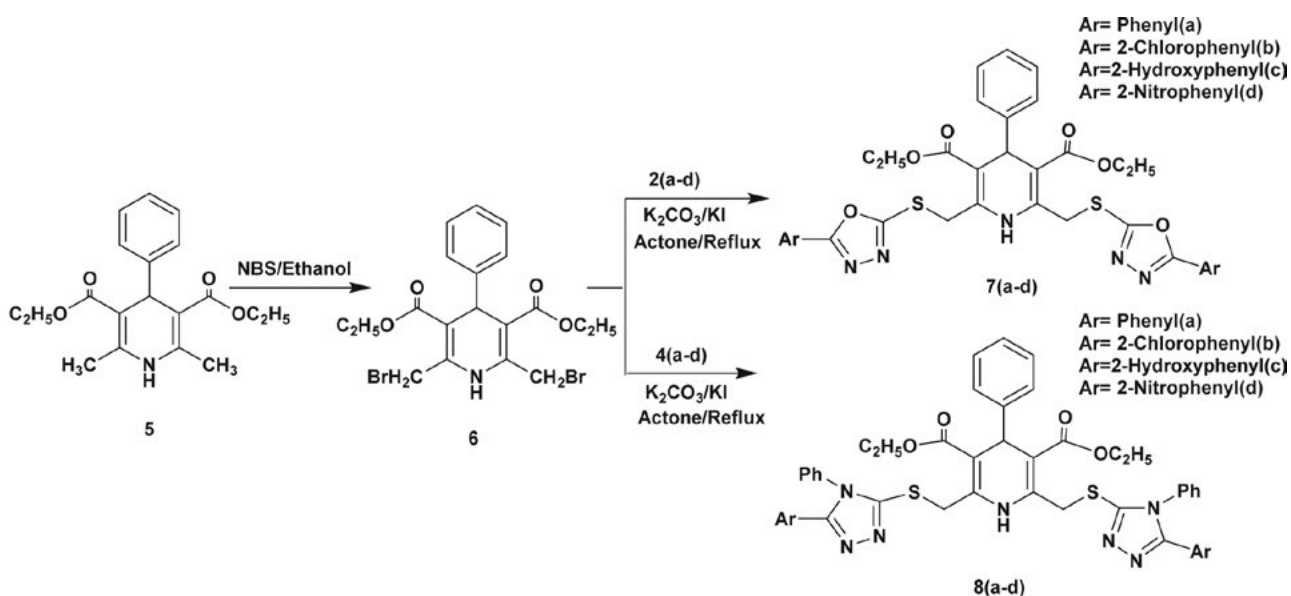
lute hydrochloric acid which resulted in the precipitation of oxadiazole. These compounds were synthesized according to the literature method (Scheme 1).<sup>35–36</sup> 1-Substituted-4-phenylthiosemicarbazides **3a–d** were prepared by the condensation of carboxylic acid hydrazides **1a–d** with phenylisothiocyanate under reflux in absolute ethanol. The cyclodehydration of 1-substituted-4-phenylthiosemicarbazides **3a–d** were carried out in alkaline medium followed by acidification with dilute hydrochloric acid to give 1,2,4-triazole-5-thiones **4a–d** according to the literature method (Scheme 1).<sup>37–39</sup> The existence of thiol-thione tautomerism is known for the compounds **2a–d** and **4a–d** and generally one form is predominant. In the present study, the thione structure was dominated in the solid state. These constitutional isomers were distinguished by IR and <sup>1</sup>H NMR. The appearance of a C=S absorption peak in the region 1248–1278 cm<sup>-1</sup> indicated that the oxadiazoles and triazoles are in their thione form. The <sup>1</sup>H NMR spectra of compounds **2a–d** and **4a–d** exhibited the NH signals (NH function of the oxadiazole and triazole ring) as a singlet in the range  $\delta_{\text{H}}$  12–14 ppm which also supports the proposed thione structure.<sup>35–39</sup>

4-Phenyl-1,4-dihydro-2,6-dimethyl-3,5-pyridine dicarboxylic acid ester (diethyl 2,6-dimethyl-4-phenyl-1,4-dihydropyridine-3,5-dicarboxylate) derivative (compound **5**) was synthesized by condensation of benzaldehyde with two equivalents of  $\beta$ -ketoester in the presence of a nitrogen donor such as ammonia or ammonium acetate according to the procedure reported in the literature.<sup>40</sup> The <sup>1</sup>H NMR spectrum of compound **5** shows a characteristic singlet in the range of  $\delta_{\text{H}}$  5–7 ppm which was due to the NH proton of the 1,4-DHP ring and another important singlet at 5 ppm which was attributed to the CH at C4 of the 1,4-DHP ring. Allylic bromination is the replacement

of a hydrogen on a carbon adjacent to a double bond and *N*-bromosuccinimide (NBS) is a brominating agent that is used as the source of bromine in radical reactions that are used for allylic bromination. The synthesis of 2,6-dibromomethyl-3,5-diethoxycarbonyl-1,4-dihydropyridine (compound **6**) was carried out by bromination of corresponding 2,6-dimethyl-1,4-dihydropyridine (compound **5**) with NBS in methanol according to the procedure reported in the literature.<sup>41</sup> Replacement of the bromines of compound **6** with 1,2,4-triazole-5-thiones **4a–d** or 1,3,4-oxadiazole-5-thiones **2a–d** was carried out in the presence of potassium carbonate as a weak base in dry acetone to afford the corresponding coupled 1,4-dihydropyridines (**7a–d** and **8a–d**) (Scheme 2). The structures identification for compounds **7a–d** and **8a–d** was based on spectroscopic methods. In the IR spectra the disappearance of the C=S absorption peak in the region 1248–1278 cm<sup>-1</sup> and furthermore the absence of NH peak at 12–14 ppm support the connection of oxadiazole and triazoles to 1,4-DHP ring.

The CH<sub>2</sub>X protons at positions C2 and C6 of symmetrically substituted 1,4-dihydropyridine ring become diastereotopic and provide an AB system in the corresponding <sup>1</sup>H NMR spectra. The extent of the observed anisochrony of the methylene protons should be influenced by the spatial conformation of ester groups and the formation of a CH...O=C intramolecular hydrogen bonding.<sup>41</sup>

The *in vitro* antibacterial and antifungal activities of the synthesized compounds against *E. coli* and *A. fumigatus* are shown in Tables 1 and 2. The minimal inhibition concentration for enrofloxacin as the reference antibacterial drug is 36  $\mu\text{g}/\mu\text{L}$  concentration and for amphotericin was 28  $\mu\text{g}/\mu\text{L}$  of drug in the same test conditions.



Scheme 2. Synthesis of 1,4-dihydropyridine compounds bearing 1,3,4-oxadiazole-5-thiones and 1,2,4-triazole-5-thiones

**Table 1.** *In vitro* antibacterial activity of synthetic compounds against *E. coli*.

Compound	MIC (g/mL)	MBC (g/mL)	Compound	MIC (g/mL)	MBC (g/mL)
8a	250	500	7a	500	500
8b	250	500	7b	125	125
8c	125	250	7c	62.5	125
8d	62.5	62.5	7d	62.5	125

**Table 2.** *In vitro* antifungal activity of synthetic compounds against *A. fumigatus*.

Compound	MIC (g/mL)	MFC (g/mL)	Compound	MIC (g/mL)	MFC (g/mL)
8a	500	500	7a	1000	2000
8b	500	500	7b	1000	2000
8c	500	500	7c	1000	2000
8d	250	500	7d	500	1000

From the data presented in Tables 1 and 2 it is clear that compounds **8a–d** showed better antifungal activities than compounds **7a–d** and the compounds **7c,7d,8d** exhibited better and equipotent activity against *E. coli*. The compound **8d** is highly active against *E. coli* and *A. fumigatus*.

## 4. Experimental

### 4.1. General

The melting points of all compounds were recorded on a Philip Harris C4954718 apparatus without calibration. IR spectra were recorded on Thermo Nicolet Nexus 670 FT-IR spectrometer and  $^1\text{H}$  and  $^{13}\text{C}$  NMR spectra measured with Bruker Avance 300 MHz spectrometer. Mass spectra were recorded on a JEOL-JMS 600 (FAB MS) instrument. Thin layer chromatography (TLC) analyses were carried out on silica gel plates. All chemicals were purchased from Merck (Tehran, Iran) and used as received by standard procedures. All of the instruments, chemicals and solvents were dried according to standard methods. Freshly distilled solvents were used throughout, and anhydrous solvents were dried according to the method reported by Perrin and Armarego. Microanalyses were performed on a Leco Analyzer 932.

### 4.2. General Procedure for the Synthesis of 2a–d

Compounds **2a–d** were synthesized by the reaction of  $\text{CS}_2$  (6.7 mL, 0.1 mol) with a suspension of carboxylic acid hydrazides **1a–d** (0.1 mol) in chloroform (100 mL) in the presence of  $\text{Et}_3\text{N}$  (15 mL, 0.1 mol). After refluxing the

reaction mixture for 3 h, the resulting solution was filtered and acidified with acetic acid (20 mL, 20% v/v). On evaporation of the solvent, the solid obtained was washed twice with cold water and finally dried *in vacuo*, then recrystallized from ethanol (yield 80%).<sup>35–36</sup>

### 4.3. General Procedure for the Synthesis of 4a–d

Equimolar quantities of carboxylic acid hydrazides **1a–d** (0.01 mol) and phenylisothiocyanate (1.35 g, 0.01 mol) in appropriate amount of absolute ethanol were refluxed for 6–8 h. The formed precipitate of 1-substituted-4-phenylthiosemicarbazides **3a–d** was filtered, and then a suspension of 0.04 g thiosemicarbazides **3a–d** in sodium hydroxide 0.4 g (0.01 mol, as a 2N solution) was refluxed for 6 h.

The reaction mixture was allowed to cool to the room temperature and was then adjusted to pH 6 with diluted hydrochloric acid. The formed precipitate was then filtered, dried and recrystallized from ethanol, to give 1,2,4-triazole-5-thiones **4a–d** in 75% yields. The following compounds were prepared by an analogous procedure.<sup>37–39</sup>

#### Diethyl 2,6-Dimethyl-4-phenyl-1,4-dihydropyridine-3,5-dicarboxylate (5)<sup>40</sup>

White crystals; 77% (2.535 g), mp 160–162 °C,  $^1\text{H}$  NMR (300 MHz,  $\text{CDCl}_3$ )  $\delta$  1.25 (t,  $J = 7.2$  Hz, 6H,  $-\text{COOCH}_2\text{CH}_3$ ), 2.35 (s, 6H, 2 $\text{CH}_3$ ), 4.10 (q, 4H,  $-\text{COOCH}_2\text{CH}_3$ ), 5.02 (s, 1H, DHP- $\text{C}_4$ -H), 5.72 (br s, 1H, N-H), 7.13–7.32 (m, 5H, Ar-H),  $^{13}\text{C}$  NMR (75 MHz,  $\text{CDCl}_3$ )  $\delta$  14.27, 19.12, 39.66, 59.75, 103.59, 126.11, 127.85, 127.92, 144.76, 147.96, 168.03. IR (KBr)  $\nu$  3340, 3078, 2976, 1651, 1483, 1378, 1100, 1030, 766, 695  $\text{cm}^{-1}$ . Anal. calcd for  $\text{C}_{19}\text{H}_{23}\text{NO}_4$ : C, 69.28; H, 7.04; N, 4.25. Found: C, 69.18; H, 6.98; N, 4.29.

#### Diethyl 2,6-Bis(bromomethyl)-4-phenyl-1,4-dihydropyridine-3,5-dicarboxylate (6)<sup>41</sup>

Lemon crystals; 72% (3.506 g), mp 135 °C,  $^1\text{H}$  NMR (300 MHz,  $\text{CDCl}_3$ )  $\delta$  1.25 (t,  $J = 7.2$  Hz, 6H,  $-\text{COOCH}_2\text{CH}_3$ ), 4.15 (q,  $J = 7.2$  Hz, 4H,  $-\text{COOCH}_2\text{CH}_3$ ), 4.6, 4.9 (dd,  $J_1 = 4.65$ ,  $J_2 = 4.65$  Hz, 4H,  $\text{CH}_2\text{-Br}$ ), 5.03 (s, 1H, DHP- $\text{C}_4$ -H), 6.53 (br s, 1H, N-H), 7.12–7.31 (m, 5H, Ar-H),  $^{13}\text{C}$  NMR (75 MHz,  $\text{CDCl}_3$ )  $\delta$  14.11, 27.15, 40.08, 60.65, 105.79, 126.84, 128.06, 128.19, 142.19, 145.85, 166.31. IR (KBr)  $\nu$  3334, 3084, 2979, 1686, 1508, 1372, 1095, 760, 704, 558  $\text{cm}^{-1}$ . Anal. calcd for  $\text{C}_{19}\text{H}_{21}\text{Br}_2\text{NO}_4$ : C, 46.84; H, 4.34; N, 2.88. Found: C, 46.76; H, 4.31; N, 2.95.

### 4.4. General Procedure for the Synthesis of Compounds 7a–d and 8a–d

A mixture of **2a–d** or **4a–d** (2 mmol),  $\text{K}_2\text{CO}_3$  (0.276 g, 2 mmol) and acetone (20 mL) were stirred at room temperature for 30 minute, and then 0.487 g (1 mmol) com-

pound **6** and KI (cat.) were added and refluxed for 12 h and then evaporated. The residue was extracted with  $\text{CH}_2\text{Cl}_2$  (30 mL) and the organic layer washed with water, dried over  $\text{Na}_2\text{SO}_4$  and evaporated. Recrystallization of crude products from 2-propanol furnished **7a–d** or **8a–d**.

**Diethyl 4-Phenyl-2, 6-bis(((5-phenyl-1,3,4-oxadiazol-2-ylthio)methyl)-1,4-dihydropyridine-3,5-dicarboxylate (7a)**

Pale yellow solid; 73% (0.498 g), m.p. 156–158 °C,  $^1\text{H}$  NMR (300 MHz,  $\text{CDCl}_3$ ):  $\delta$  25 (t,  $J = 7.2$  Hz, 6H,  $-\text{COOCH}_2\text{CH}_3$ ), 4.14 (q,  $J = 7.2$  Hz, 4H,  $-\text{COOCH}_2\text{CH}_3$ ), 4.62 (s, 4H, S- $\text{CH}_2$ ), 5.05 (s, 1H, DHP- $\text{C}_4$ -H), 7.11–7.31 (m, 5H, Ar-H), 7.40–7.52 (m, 6H, Ar-H), 7.90 (d,  $J = 8.1$  Hz, 4H, Ar-H), 8.78 (br s, 1H, N-H),  $^{13}\text{C}$  NMR (75 MHz,  $\text{CDCl}_3$ )  $\delta$  14.13, 32.32, 39.66, 60.37, 104.99, 123.54, 126.62, 126.66, 126.71, 128.11, 128.94, 131.59, 144.17, 147.76, 162.32, 165.38, 166.88. IR (KBr)  $\nu$  3330, 3073, 2979, 1688, 1636, 1483, 1375, 1090, 764, 695, 595  $\text{cm}^{-1}$ . Anal. calcd for  $\text{C}_{35}\text{H}_{31}\text{N}_5\text{O}_6\text{S}_2$ : C 61.66, H 4.58, N 10.27, S 9.40. Found: C, 61.69; H, 4.53; N, 10.24; S, 9.47. HRMS-FAB  $m/z$   $[\text{M}+\text{H}]^+$  calcd for  $\text{C}_{35}\text{H}_{31}\text{N}_5\text{O}_6\text{S}_2$ : 681.17. Found: 681.11.

**Diethyl 2,6-Bis(((5-(2-chlorophenyl)-1,3,4-oxadiazol-2-ylthio)methyl)-4-phenyl-1,4-dihydropyridine-3,5-dicarboxylate (7b)**

Pale yellow solid; 62% (0.465 g), m.p. 156–158 °C,  $^1\text{H}$  NMR (300 MHz,  $\text{DMSO}-d_6$ )  $\delta$  1.25 (t,  $J = 7.2$  Hz, 6H,  $-\text{COOCH}_2\text{CH}_3$ ), 4.15 (q,  $J = 7.2$  Hz, 4H,  $-\text{COOCH}_2\text{CH}_3$ ), 4.65 (dd,  $J_1 = 14.1$  Hz,  $J_2 = 14.1$  Hz, 4H, S- $\text{CH}_2$ ), 5.05 (s, 1H, DHP- $\text{C}_4$ -H), 7.10–7.32 (m, 6H, Ar-H), 7.32–7.51 (m, 5H, Ar-H), 7.86 (d,  $J = 6.6$  Hz, 2H, Ar-H), 8.72 (br s, 1H, N-H);  $^{13}\text{C}$  NMR (75 MHz,  $\text{DMSO}-d_6$ )  $\delta$  14.32, 32.83, 39.60, 60.31, 104.53, 122.53, 126.94, 127.82, 128.19, 128.49, 131.48, 131.58, 132.22, 133.70, 44.16, 146.99, 162.32, 164.22, 166.41. IR (KBr)  $\nu$  3282, 3080, 2978, 1678, 1630, 1488, 1097, 739  $\text{cm}^{-1}$ . HRMS-FAB  $m/z$   $[\text{M}+\text{H}]^+$  calcd for  $\text{C}_{35}\text{H}_{29}\text{Cl}_2\text{N}_5\text{O}_6\text{S}_2$ : 749.09. Found: 749.14. Anal. calcd for  $\text{C}_{35}\text{H}_{29}\text{Cl}_2\text{N}_5\text{O}_6\text{S}_2$ : C, 56.00; H, 3.89; N, 9.33; S, 8.54. Found: C, 56.04; H, 3.84; N, 9.35; S, 8.57.

**Diethyl 2,6-Bis(((5-(2-hydroxyphenyl)-1,3,4-oxadiazol-2-ylthio)methyl)-4-phenyl-1,4-dihydropyridine-3,5-dicarboxylate (7c)**

Pale yellow solid; 69% (0.492 g), m.p. 155–157 °C,  $^1\text{H}$  NMR (300 MHz,  $\text{CDCl}_3$ )  $\delta$  1.26 (t,  $J = 7.2$  Hz, 6H,  $-\text{COOCH}_2\text{CH}_3$ ), 4.14 (q,  $J = 7.2$  Hz, 4H,  $-\text{COOCH}_2\text{CH}_3$ ), 4.63 (dd,  $J_1 = 14.1$  Hz,  $J_2 = 14.1$  Hz, 4H, S- $\text{CH}_2$ ), 5.03 (s, 1H, DHP- $\text{C}_4$ -H), 6.95 (t,  $J = 7.5$  Hz, 2H, Ar-H), 7.05 (d,  $J = 8.4$  Hz, 2H, Ar-H), 7.12–7.32 (m, 5H, Ar-H), 7.42 (t,  $J = 7.5$  Hz, 2H, Ar-H), 7.65 (d,  $J = 7.8$  Hz, 2H, Ar-H), 8.59 (s, 1H, N-H), 9.73 (s, 2H, OH).  $^{13}\text{C}$  NMR (75 MHz,  $\text{CDCl}_3$ )  $\delta$  14.12, 32.43, 39.63, 60.47, 105.41, 107.66, 117.47, 119.92, 126.45, 126.73, 128.02, 128.12, 133.66, 143.66, 146.47, 157.16, 164.75, 165.64, 166.78. IR (KBr)  $\nu$  3302, 2879,

1692, 1620, 1486, 1100, 753, 703  $\text{cm}^{-1}$ . HRMS-FAB  $m/z$   $[\text{M}+\text{H}]^+$  calcd for  $\text{C}_{35}\text{H}_{31}\text{N}_5\text{O}_8\text{S}_2$ : 713.16. Found: 713.23. Anal. calcd for  $\text{C}_{35}\text{H}_{31}\text{N}_5\text{O}_8\text{S}_2$ : C, 58.90; H, 4.38; N, 9.81; S, 8.98. Found: C, 58.86; H, 4.33; N, 9.84; S, 9.02.

**Diethyl 2,6-Bis(((5-(3-nitrophenyl)-1,3,4-oxadiazol-2-ylthio)methyl)-4-phenyl-1,4-dihydropyridine-3,5-dicarboxylate (7d)**

Yellow crystals; 64% (0.493 g), m.p. 150–151 °C,  $^1\text{H}$  NMR (300 MHz,  $\text{CDCl}_3$ )  $\delta$  1.26 (t,  $J = 7.2$  Hz, 6H,  $-\text{COOCH}_2\text{CH}_3$ ), 4.15 (q,  $J = 7.2$  Hz, 4H,  $-\text{COOCH}_2\text{CH}_3$ ), 4.65 (s, 4H, S- $\text{CH}_2$ ), 5.04 (s, 1H, DHP- $\text{C}_4$ -H), 7.10–7.30 (m, 5H, Ar-H, 1H, N-H), 7.69 (t,  $J = 7.8$  Hz, 2H, Ar-H), 8.28 (d,  $J = 7.8$  Hz, 2H, Ar-H), 8.36 (d,  $J = 8.1$  Hz, 2H, Ar-H), 8.72 (d,  $J = 17.1$  Hz, 2H, Ar-H).  $^{13}\text{C}$  NMR (75 MHz,  $\text{CDCl}_3$ )  $\delta$  14.12, 32.35, 39.65, 60.47, 105.25, 121.49, 125.13, 126.04, 126.66, 128.06, 128.09, 130.38, 132.04, 143.81, 146.65, 148.60, 162.32, 164.28, 166.85. IR (KBr)  $\nu$  3333, 3087, 2978, 1693, 1633, 1525, 1479, 1353, 1097, 710  $\text{cm}^{-1}$ . HRMS-FAB  $m/z$   $[\text{M}+\text{H}]^+$  calcd for  $\text{C}_{35}\text{H}_{29}\text{N}_7\text{O}_{10}\text{S}_2$ : 771.14. Found: 771.11. Anal. calcd for  $\text{C}_{35}\text{H}_{29}\text{N}_7\text{O}_{10}\text{S}_2$ : C, 54.47; H, 3.79; N, 12.70; S, 8.31. Found: C, 54.51; H, 3.76; N, 12.67; S, 8.36.

**Diethyl 2,6-Bis(((4,5-diphenyl-4H-1,2,4-triazol-3-ylthio)methyl)-4-phenyl-1,4-dihydropyridine-3,5-dicarboxylate (8a)**

White solid; 76% (0.632 g), m.p. 189–191 °C,  $^1\text{H}$  NMR (300 MHz,  $\text{CDCl}_3$ )  $\delta$  1.22 (t,  $J = 7.2$  Hz, 6H,  $-\text{COOCH}_2\text{CH}_3$ ), 4.08 (q,  $J = 7.2$  Hz, 4H,  $-\text{COOCH}_2\text{CH}_3$ ), 4.49, 4.66 (dd,  $J_1 = 14.1$  Hz,  $J_2 = 14.1$  Hz, 4H, S- $\text{CH}_2$ ), 5.04 (s, 1H, DHP- $\text{C}_4$ -H), 7.10–7.50 (m, 25H, Ar-H), 9.69 (s, 1H, N-H).  $^{13}\text{C}$  NMR (75 MHz,  $\text{CDCl}_3$ )  $\delta$  14.17, 32.35, 39.82, 60.03, 104.42, 126.30, 126.68, 127.49, 127.94, 128.20, 128.33, 129.78, 129.84, 134.25, 145.36, 147.32, 153.61, 155.05, 167.11. IR (KBr)  $\nu$  3292, 3050, 2976, 1688, 1635, 1493, 1095, 766, 695  $\text{cm}^{-1}$ . HRMS-FAB  $m/z$   $[\text{M}+\text{H}]^+$  calcd for  $\text{C}_{47}\text{H}_{41}\text{N}_7\text{O}_4\text{S}_2$ : 831.27. Found: 831.22. Anal. calcd for  $\text{C}_{47}\text{H}_{41}\text{N}_7\text{O}_4\text{S}_2$ : C, 67.85; H, 4.97; N, 11.78; S, 7.71. Found: C, 67.88; H, 4.94; N, 11.79; S, 7.73.

**Diethyl 2,6-Bis(((5-(2-chlorophenyl)-4-phenyl-4H-1,2,4-triazol-3-ylthio)methyl)-4-phenyl-1,4-dihydropyridine-3,5-dicarboxylate (8b)**

White solid; 61% (0.549 g), m.p. 164–165 °C,  $^1\text{H}$  NMR (300 MHz,  $\text{CDCl}_3$ )  $\delta$  1.22 (t,  $J = 7.2$  Hz, 6H,  $-\text{COOCH}_2\text{CH}_3$ ), 4.09 (q,  $J = 7.2$  Hz, 4H,  $-\text{COOCH}_2\text{CH}_3$ ), 4.52, 4.66 (dd,  $J_1 = 14.1$  Hz,  $J_2 = 14.1$  Hz, 4H, S- $\text{CH}_2$ ), 5.04 (s, 1H, DHP- $\text{C}_4$ -H), 7.11–7.36 (m, 21H, Ar-H), 7.48 (d,  $J = 7.2$  Hz, 2H, Ar-H), 9.70 (s, 1H, N-H).  $^{13}\text{C}$  NMR (75 MHz,  $\text{CDCl}_3$ )  $\delta$  14.17, 32.35, 39.83, 60.08, 104.12, 126.32, 126.61, 126.78, 127.95, 128.23, 129.33, 129.62, 131.42, 132.79, 133.34, 134.28, 145.34, 147.25, 152.95, 153.53, 162.32, 167.12. IR (KBr)  $\nu$  3277, 3068, 2978, 1685, 1637, 1499, 1094, 763, 697, 604  $\text{cm}^{-1}$ ; HRMS-FAB  $m/z$   $[\text{M}+\text{H}]^+$  calcd for  $\text{C}_{47}\text{H}_{39}\text{Cl}_2\text{N}_7\text{O}_4\text{S}_2$ : 899.19. Found: 899.25. Anal. calcd

for  $C_{47}H_{39}Cl_2N_7O_4S_2$ : C, 62.66; H, 4.36; N, 10.88; S, 7.12. Found: C, 62.67; H, 4.35; N, 10.90; S, 7.15.

**Diethyl 2,6-Bis((5-(2-hydroxyphenyl)-4-phenyl-4H-1,2,4-triazol-3-ylthio)methyl)-4-phenyl-1,4-dihydropyridine-3,5-dicarboxylate (8c)**

Pale yellow solid; 71% (0.613 g), m.p. 226–228 °C,  $^1H$  NMR (300 MHz,  $CDCl_3$ )  $\delta$  1.22 (t,  $J = 7.2$  Hz, 6H,  $-COOCH_2CH_3$ ), 4.08 (q,  $J = 7.2$  Hz, 4H,  $-COOCH_2CH_3$ ), 4.52, 4.70 (dd,  $J_1 = 14.1$  Hz,  $J_2 = 14.1$  Hz, 4H, S- $CH_2$ ), 5.05 (s, 1H, DHP- $C_4$ -H), 6.40–6.54 (m, 5H, Ar-H), 6.97 (d,  $J = 8.4$  Hz, 2H, Ar-H), 7.12 (t,  $J = 6.9$  Hz, 2H, Ar-H), 7.22 (t,  $J = 7.2$  Hz, 2H, Ar-H), 7.27–7.37 (m, 6H, Ar-H), 7.52–7.63 (m, 6H, Ar-H), 9.25 (s, 1H, N-H), 11.60 (br s, 2H, OH).  $^{13}C$  NMR (75 MHz,  $CDCl_3$ )  $\delta$  14.12, 32.13, 39.74, 60.15, 104.04, 110.04, 117.78, 118.42, 125.48, 126.46, 127.65, 127.97, 128.16, 130.43, 130.67, 131.27, 134.23, 144.61, 147.00, 153.68, 153.83, 157.86, 166.97. IR (KBr)  $\nu$  3303, 2978, 1691, 1618, 1100, 752, 701  $cm^{-1}$ . HRMS-FAB  $m/z$   $[M+H]^+$  calcd for  $C_{47}H_{41}N_7O_6S_2$ : 863.26. Found: 863.30. Anal. calcd for  $C_{47}H_{41}N_7O_6S_2$ : C, 65.34; H, 4.78; N, 11.35; S, 7.42. Found: C, 65.33; H, 4.81; N, 11.32; S, 7.40.

**Diethyl 2,6-Bis((5-(3-nitrophenyl)-4-phenyl-4H-1,2,4-triazol-3-ylthio)methyl)-4-phenyl-1,4-dihydropyridine-3,5-dicarboxylate (8d)**

Pale yellow crystals; 68% (0.627 g), m.p. 189–190 °C,  $^1H$  NMR (300 MHz,  $CDCl_3$ )  $\delta$  1.25 (t,  $J = 7.2$  Hz, 6H,  $-COOCH_2CH_3$ ), 4.08 (q,  $J = 7.2$  Hz, 4H,  $-COOCH_2CH_3$ ), 4.56, 4.66 (dd,  $J_1 = 14.1$  Hz,  $J_2 = 14.1$  Hz, 4H, S- $CH_2$ ), 5.04 (s, 1H, DHP- $C_4$ -H), 7.17–7.58 (m, 19H, Ar-H), 7.68 (d,  $J = 7.8$  Hz, 2H, Ar-H), 8.11 (d,  $J = 9.3$  Hz, 2H, Ar-H), 9.58 (s, 1H, N-H).  $^{13}C$  NMR (75 MHz,  $CDCl_3$ )  $\delta$  14.15, 32.31, 39.76, 60.09, 104.25, 126.39, 127.36, 127.46, 127.95, 128.23, 128.27, 129.52, 130.38, 130.61, 133.37, 133.53, 145.20, 147.28, 147.96, 152.93, 155.05, 162.34, 167.11. IR (KBr)  $\nu$  3304, 3081, 2980, 1687, 1634, 1505, 1353, 1096, 909, 770, 701  $cm^{-1}$ . HRMS-FAB  $m/z$   $[M+H]^+$  calcd for  $C_{47}H_{39}N_9O_8S_2$ : 921.24. Found: 921.17. Anal. calcd for  $C_{47}H_{39}N_9O_8S_2$ : C, 61.23; H, 4.26; N, 13.67; S, 6.95. Found: C, 61.24; H, 4.28; N, 13.65; S, 6.94.

## 5. Conclusion

In this study we demonstrated the synthesis, antibacterial and antifungal activity of new derivatives of 1,4-dihydropyridines bearing 1,2,4-triazole and 1,3,4-oxadiazole moieties at C2 and C6 of 1,4-DHP ring system. It should be noted that compound **8d** exhibited the most potent activity against *E. coli* and *A. fumigates*. The structure-activity relationship of the compounds showed that substitution at the position 2, 6 of the pyridine ring enhances biological activity. Our results will have an impact on further investigation in this field in search of 1,4-dihydropyridine compounds connected with 1,2,4-triazole and 1,3,4-oxadiazole moieties as antibacterial and antifungal agents.

**Acknowledgments.** The authors are grateful to Urmia University for providing a fellowship for the present work and thanks are also given to Prof. Dr. Joachim Thiem from Hamburg University for the ESI-MS measurements.

## 6. References

- D. J. Triggler, *Biochem. Pharmacol.* **2007**, *74*, 1–9. DOI:10.1016/j.bcp.2007.01.016
- D. A. Sica, *J. Hypertens.* **2006**, *8*, 53–56.
- F. Bossert, H. Meyer, E. Wehinger, *Angew. Chem. Int. Ed. Engl.* **1981**, *20*, 762–769. DOI:10.1002/anie.198107621
- J. G. Breitenbucher, G. Figliozzi, *Tetrahedron Lett.* **2000**, *41*, 4311–4315. DOI:10.1016/S0040-4039(00)00660-2
- G. A. Wachter, M. C. Davis, *J. Med. Chem.* **1998**, *41*, 2436–2438. DOI:10.1021/jm9708745
- T. Akbarzadeh, S. Motagian, A. Fallah Tafti, A. Shafiee, A. R. Shahverdi, *Res. Pharm. Sci.* **2008**, *3*, 87–93.
- S. Kalam, B. Darna, A. Garlapati, M. R. Vanga, *Eur. J. Med. Chem.* **2011**, *46*, 1564–71. DOI:10.1016/j.ejmech.2011.02.003
- V. M. Briukhanov, *Exp. Clin. Pharmacol.* **1994**, *57*, 47–49.
- R. Boer, V. Gekeler, *Drugs Future*, **1995**, *20*, 499–509.
- O. Firuzi, K. Javidnia, E. Mansourabadi, L. Saso, A. R. Mehdipour, R. Miri, *Arch. Pharm. Sci. Res.* **2013**, *36*, 1392–1402. DOI:10.1007/s12272-013-0149-8
- S. Ulloora, S. Kumar, R. Shabaraya, A. V. Adhikari, *Med. Chem. Res.* **2013**, *22*, 1549–1562. DOI:10.1007/s00044-012-0156-1
- G. Hamilton, E. P. Cosentini, B. Teleky, T. Koperna, J. Zachari, M. Riegler, W. Feil, R. Schiessel, E. Wenzl, *Anticancer Res.* **1993**, *13*, 2059–2063.
- H. W. van Veen, R. Callaghan, L. Soceneantu, A. Sardini, W. N. Konings, C. F. Higgins, *Nature* **1998**, *391*, 291–295. DOI:10.1038/34669
- N. B. Patel, J. C. Patel, *Sci. Pharm.* **2010**, *78*, 171–193. DOI:10.3797/scipharm.0912-16
- T. Plech, M. Wujec, A. Siwek, U. Kosikowska, A. Malm, *Eur. J. Med. Chem.* **2011**, *46*, 241–248. DOI:10.1016/j.ejmech.2010.11.010
- O. Prakash, M. Kumar, R. Kumar, C. Sharma, K. R. Aneja, *Eur. J. Med. Chem.* **2010**, *45*, 4252–4257. DOI:10.1016/j.ejmech.2010.06.023
- T. Tsukuda, Y. Shiratori, M. Watanabe, H. Ohtsuka, K. Hatatori, M. Shirai, *Bioorg. Med. Chem. Lett.* **1998**, *8*, 1819–1824. DOI:10.1016/S0960-894X(98)00316-3
- M. A. Alia, M. Shaharyar, *Bioorg. Med. Chem. Lett.* **2007**, *17*, 3314–3316. DOI:10.1016/j.bmcl.2007.04.004
- T. A. Kaplancikli, G. Turan-Zitouni, P. Chevallet, *J. Enzyme Inhib. Med. Chem.* **2005**, *20*, 179–182. DOI:10.1080/14756360500043471
- K. Liu, X. Lu, H. J. Zhang, J. Sun, H. L. Zhu, *Eur. J. Med. Chem.* **2012**, *47*, 473–478. DOI:10.1016/j.ejmech.2011.11.015
- A. Kamal, N. Shankaraiah, V. Devaiah, K. L. Reddy, A. Ju-

- vekar S. Sen, N. Kurian, S. Zingde, *Bioorg. Med. Chem. Lett.* **2008**, *18*, 1468–1473. DOI:10.1016/j.bmcl.2007.12.063
22. A. Kumar, C. S. Rajput, *Eur. J. Med. Chem.* **2009**, *44*, 83–90. DOI:10.1016/j.ejmech.2008.03.018
23. H. Kumar, S. A. Javed, S. A. Khan. *Eur. J. Med. Chem.* **2008**, *43*, 2688–2698. DOI:10.1016/j.ejmech.2008.01.039
24. R. R. Somani, G. Kadam, R. Vohra, S. Vijayaraghavan, P. Y. Shirodkar, *Int. J. Pharmacol.* **2010**, *6*, 696–704. DOI:10.3923/ijp.2010.696.704
25. N. Siddiqui, W. Ahsan, *Eur. J. Med. Chem.* **2010**, *45*, 1536–1543. DOI:10.1016/j.ejmech.2009.12.062
26. R. Surendrakumar, A. Manilal, A. J. Abdul Nasser, B. Merdekios, X. Chen, A. Idhayadhulla, *J. Pharmacol. Toxicol.* **2014**, *9*, 119–128. DOI:10.3923/jpt.2014.119.128
27. A. B. Archana, D. R. Dinesh, S. G. Paraag, Y. Shirodkar Prabhakar, *Int. J. Pharm. Chem.* **2014**, *4*, 63–67.
28. A. Hantzsch, *Ber.* **1881**, *14*, 1637–1638. DOI:10.1002/cber.18810140214
29. A. Hantzsch, *Ann. Chem.* **1892**, *215*, 1–81. DOI:10.1002/jlac.18822150102
30. K. Akbari Dilmaghani, F. Nasuhi Pur, N. Hoseini Jazani, A. Alavi, Z. Niknam, F. Mirfakrahrae, *Phosphorus, Sulfur Silicon Relat. Elem.* **2014**, *189*, 81–87. DOI:10.1080/10426507.2013.789877
31. K. Akbari Dilmaghani, F. Nasuhi Pur, M. Hatami Nezhad, *Iran. J. Pharm. Res.* **2015**, *14*, 693–699.
32. K. Akbari Dilmaghani, F. Nasuhi Pur, M. Mohammadpour, J. Mohammadnejad, *Iran. J. Pharm. Res.* **2016**, *15*, 777–782.
33. A. Tukmechi A. M. Ownagh, *Braz. J. Microbiol.* **2010**, *41*, 1086–1092. DOI:10.1590/S1517-83822010000400030
34. H. Katiroglu, Y. Beyatli, B. Aslim, Z. Yüksekdag, T. Atici, *Internet J. Microbiol.* **2006**, *2*, 520–524.
35. N. K. Singh, R. J. Butcher, P. Tripathi, A. K. Srivastava. M. Kumar Bharty, *Acta Cryst.* **2007**, *E63*, 0782–0784.
36. C. H. Lee, H. I. Cho, K. J. Lee, *Bull. Korean Chem. Soc.* **2001**, *22*, 1153–1155.
37. M. Mhasalkar, M. Shah, S. Nikam, K. Anantanarayanan, Deliwala, *J. Med. Chem.* **1970**, *13*, 672–674. DOI:10.1021/jm00298a021
38. I. Khan, S. Ali, S. Hameed, N. Rama, M. Hussain, A. Wadood, R. Uddin, Z. Ul-Haq, A. Khan, S. Ali, M. Choudhary, *Eur. J. Med. Chem.* **2010**, *45*, 5200–5207. DOI:10.1016/j.ejmech.2010.08.034
39. (a) B. V. I. Cohen, *J. Heterocycl. Chem.* **1978**, *15*, 237–240. DOI:10.1002/jhet.5570150211  
(b) K. Sung, A. R. Lee, *J. Heterocycl. Chem.* **1992**, *29*, 1101–1109. DOI:10.1002/jhet.5570290512
40. M. S. Bai, Y. Y. Chen, D. L. Niu, L. Peng, *Acta Cryst.* **2009**, *E65*, 0799.
41. M. Petrova, R. Muhamadejev, B. Vigante, B. Cekavicus, A. Plotniece, G. Duburs, E. Liepinsh, *Molecules* **2011**, *16*, 8041–8052. DOI:10.3390/molecules16098041

## Povzetek

Pripravili smo serijo dietil-2,6-dimetil-4-fenil-1,4-dihidropiridin-3,5-dikarboksilatnih derivatov spojenih z 1,3,4-oksadiazol-5-tionskimi in 1,2,4-triazol-5-tionskimi ostanki na položajih C2,C6 v 1,4-dihidropiridinskem obročnem sistemu. To povezavo smo izvedli z reakcijo med 1,3,4-oksadiazol-5-tioni in 1,2,4-triazol-5-tioni z 2,6-dibromometil-3,5-dietoksikarbonil-4-fenil-1,4-dihidropiridinom ob prisotnosti kalijevega karbonata kot šibke baze in v suhem acetonu kot topilu. Nove pripravljene spojine smo karakterizirali z FT-IR, <sup>1</sup>H NMR in <sup>13</sup>C NMR spektroskopskimi podatki, kot tudi z elementno analizo in FAB-MS. Za sintetizirane spojine smo *in vitro* preverili delovanje proti mikrobom in glivam (proti *Escherichia coli* in *Aspergillus fumigatus*) ter rezultate primerjali z vrednostmi za enofloksacin in amfotericin kot referenčnima zdraviloma, ki se običajno uporabljata za zdravljenje tovrstnih infekcij. Pripravljene spojine so izkazale različne inhibicijske sposobnosti proti testiranim bakterijam in glivam. Spojina **8d** je pokazala največje antagonistične lastnosti proti *E. coli* and *A. fumigatus*.

Scientific paper

# Design, Synthesis and Anti-inflammatory Activity of Derivatives 10-R-3-Aryl-6,7-dihydro-2H-[1,2,4]triazino[2,3-c]quinazolin-2-ones of Spiro-fused Cyclic Frameworks

Oleksandra Kolomoets,<sup>1</sup> Oleksii Voskoboynik,<sup>1</sup> Oleksii Antypenko,<sup>1</sup> Galyna Berest,<sup>1</sup> Inna Nosulenko,<sup>1</sup> Vitaliy Palchikov,<sup>2</sup> Olexandr Karpenko<sup>3</sup> and Sergiy Kovalenko<sup>1,\*</sup>

<sup>1</sup>Organic and Bioorganic Chemistry Department, Zaporizhzhya State Medical University, 26, Mayakovsky Ave., Zaporizhzhya, 69035, Ukraine

<sup>2</sup>Chemistry Department, Oles Honchar Dnipropetrovsk National University, 72, Gagarina Ave., Dnipropetrovsk 49050, Ukraine

<sup>3</sup>Enamine Ltd., Oleksandra Matrosova 23, Kyiv, 01103, Ukraine

\* Corresponding author: E-mail: kovalenkoseriy@gmail.com

Received: 24-05-2017

## Abstract

Present work is devoted to the purposeful search of novel promising anti-inflammatory agents among the insufficiently known 3'-R-10'-R<sub>1</sub>-spiro[hetaryl-3(4),6'-[1,2,4]triazino[2,3-c]quinazolin]-2'(7H)-ones. The virtual combinatorial library of previously unknown spiro-condensed derivatives of [1,2,4]triazino[2,3-c]quinazolines was formed and promising COX-2 inhibitors were identified by molecular docking method. Potential anti-inflammatory agents were synthesized by [5+1]-cyclocondensation of substituted 3-(2-aminophenyl)-6-R-1,2,4-triazin-5(2H)-ones with heterocyclic ketones. The structures of synthesized compounds were verified by complex of physicochemical methods and spectral characteristics features were discussed. Obtained compounds were studied for anti-inflammatory activity using formalin induced paw edema model and highly active compounds were identified. Conducted SAR-analysis showed that combination of triazino[2,3-c]quinazoline moiety with spiro-condensed fragments is a reasonable approach for creating novel anti-inflammatory agents.

**Keywords:** 6,7-dihydro-2H-[1,2,4]triazino[2,3-c]quinazolin-2-ones, spiro-fused cycle, synthesis, molecular docking, anti-inflammatory activity

## 1. Introduction

Inflammation is a chain of complex metabolic and morphological changes, aimed to restore the functions of the damaged tissues or organ in general. Despite the fact that the mentioned process is a natural response to a variety of factors, its role in the pathological states requires the development of drugs for pharmacotherapeutic correction. Thus, the use of drugs such as NSAIDs, may correct as certain stages of inflammation, so exclude the process in general.

At the first stages of the antiphlogistics chemistry formation, the carboxylic acids of various nature (aspirin,

diclofenac, ibuprofen and others) were considered as privileged objects of studies. Whereas recently, the majority of studies focus on substances with a heterocyclic fragment.<sup>1</sup> This signifies considerable side effects of NSAIDs of first generation (COX-1), namely their negative impact on the gastrointestinal tract (gastrotoxicity). Nowadays, new classes of NSAIDs are found, which to some extent do not have mentioned side effect: selective COX-2 inhibitors (nimesulide, meloxicam, piroxicam, lornoxicam) and highly selective (specific) COX-2 inhibitors (celecoxib, rofecoxib, parecoxib, etoricoxib etc.).<sup>2</sup>

The current strategy of creating anti-inflammatory drugs is inextricably associated with further study of



mechanism of inflammation. Advances in molecular biology in the last decades allowed to characterize every stage of this process and made it possible to form a number of approaches of the creation of this drug group.<sup>3,4</sup> Thus, the main trends in the creation of innovational drugs include the development of C5a receptor antagonists, inhibitors of interleukin converting enzyme and tumor necrosis factor inhibitors, p38 MAP kinase inhibitors, inhibitors of matrix metalloproteinase, etc. Undoubtedly, the mentioned strategy with the use of *de novo* methodology (molecular docking) and X-ray analysis of the macromolecules active-site has significantly changed the direction of the synthetic work aimed at creating the drugs for correcting the inflammation. In particular, innovative anti-inflammatory drug of dual inhibition of COX-2/5-LOX – 2-(2,2-dimethyl-6,7-diphenyl-2,3-dihydro-1H-pyrrolizin-5-yl)acetic acid (Licofelone)<sup>5</sup> was found. Moreover, new classes of biologically active substances with the mentioned type of activity were found among triazoles, imidazoles, thiazolidines, 2H-benzo[e][1,2]thiazine-1,1-dioxide, quinolines, quinazolines and other.<sup>1,6–11</sup> Therefore, rational design based on structural similarity to innovative new structures of NSAIDs using the *de novo* methodology and traditional pharmacological screening is important and justified.

So, purposeful search of selective anti-inflammatory agents among original derivatives of 10-R-3-aryl-6,7-dihydro-2H-[1,2,4]triazino[2,3-c]quinazolin-2-ones of spirofused cyclic frameworks was the aim of this work. That is based on rational design, namely structural similarity to a number of innovative and well-known drugs and forecasting the likely biological effects (COX inhibitors) using methods of computer modeling and *in vivo* tests.

## 2. Experimental Section

### 2.1. Chemistry

#### General Methods

Melting points were determined in open capillary tubes in a «Stuart SMP30» apparatus and were uncorrected. Elemental analyses (C, H, N) were performed at the ELEMENTAR vario EL Cube analyzer (USA) and were within  $\pm 0.3\%$  from the theoretical values. IR spectra (4000–600  $\text{cm}^{-1}$ ) were recorded on a Bruker ALPHA FT-IR spectrometer (Bruker Bioscience, Germany) using a module ATR eco ZnSe. <sup>1</sup>H NMR spectra (400 MHz) and <sup>13</sup>C NMR spectra (100 MHz) were recorded on a Varian-Mercury 400 (Varian Inc., Palo Alto, CA, USA) spectrometer with TMS as internal standard in DMSO-*d*<sub>6</sub> solution. LC-MS were recorded using chromatography/mass spectrometric system which consists of a high performance liquid chromatograph «Agilent 1100 Series» (Agilent, Palo Alto, CA, USA) equipped with diode-matrix and mass-selective detector «Agilent LC/MSD SL» (atmospheric pressure chemical ionization – APCI). Electron impact mass spectra (EI-MS) were recorded on a

Varian 1200 L instrument at 70 eV (Varian Inc., Palo Alto, CA, USA).

Substances 1.1–1.5 were synthesized according to the reported procedures.<sup>12</sup> Other starting materials and solvents were obtained from commercially available sources and were used without additional purification.

### 2.2. Molecular Docking

Research was conducted by flexible molecular docking, as an approach of finding molecules with affinity to a specific biological target. Macromolecules from Protein Data Bank (PDB) were used as biological targets, namely COX-1 enzyme in complex with diclofenac (PDB ID – 3N8Y) and COX-2 in association with celecoxib (PDB ID – 3LN1).<sup>13</sup> The choice of biological targets was due to the literature on the mechanism of action of anti-inflammatory drugs.<sup>1</sup>

**Ligand preparation.** Substances were drawn using MarvinSketch 6.3.0 and were saved in mol format.<sup>14</sup> After, they were optimized by program Chem3D using molecular mechanical MM2 algorithm and saved as pdb files. Molecular mechanics has been used to produce more realistic geometry values for the majority of organic molecules owing to the fact of being highly parameterized. Using AutoDockTools-1.5.6 pdb files were converted to PDBQT, number of active torsions was set as default.<sup>15</sup>

**Protein preparation.** Pdb files were downloaded from the protein data bank. Discovery Studio 4.0 was used to delete water molecules and ligand from crystal. Proteins were saved as pdb files. In AutoDockTools-1.5.6 polar hydrogens were added and saved as PDBQT. Grid box was set as following: center\_x = 18.37, center\_y = -52.296, center\_z = 53.949, size\_x = 18, size\_y = 16, size\_z = 16 for COX-2 (3LN1); center\_x = 32.978, center\_y = -44.488, center\_z = -3.76, size\_x = 16, size\_y = 16, size\_z = 16 for COX-1 (3N8Y). Vina was used to carry docking.<sup>15</sup> For visualization Discovery Studio 4.0 was used.

### 2.3. Pharmacology

#### 2.3.1. Anti-inflammatory Activity

Evaluation of anti-inflammatory activity of the synthesized compounds was performed on 84 Wistar white rats of 150–160 g, obtained from the nursery «Institute of Pharmacology and Toxicology of Ukraine» (Kyiv). All experimental procedures and treatments were carried out according to the European Convention and «Regulations on the use of animals in biomedical research».<sup>16</sup> Screening of synthesized compounds with estimated anti-inflammatory activity began with the study of their effect on exudative phase of acute aseptic inflammation (the formalin test). Phlogogen (1% aqueous solution of formaline)<sup>17</sup> was subplantally administered at a dose of 0.1 mL in the back right paw of the rat, the left served as control. The studied compounds stabilized by Tween-80 were intragastric ad-

ministered in a dose of 10 mg/kg 1 h before the administration of phlogogen. Reference drug diclofenac sodium was intragastrically administered to rats at a recommended dose for pre-clinical studies of 8 mg/kg. Measuring paws volume was conducted before the experiment and 3 h after the administration of phlogogen using the described<sup>18</sup> methods.

The activity of these substances was determined by their ability to reduce the extension of swelling compared with control and expressed as a percentage showing how the substance inhibited formalin swelling in relation to control swelling where the value was taken as 100%. The activity of the studied compounds was calculated as follows:

$$A = 100\% - \frac{(V_{se} - V_{he})}{V_{sc} - V_{hc}} \quad (1)$$

where A – antiexudative activity, %;  $V_{se}$  – the volume of swollen paw in the experiment;  $V_{he}$  – the volume of healthy paw in the experiment;  $V_{sc}$  – the volume of swollen paw in control;  $V_{hc}$  – the volume of healthy paw in control.

Statistical data processing was performed using a license program «STATISTICA® for Windows 6.0» (StatSoft Inc., № AXXR712D833214FAN5) and «SPSS 16.0», «Microsoft Office Excell 2003». The results are presented as mean ± standard error of the mean. Arithmetic mean and standard error of the mean were calculated for each of the studied parameters. During verification of statistical hypothesis, null hypothesis was declined if statistical criterion is  $p < 0.05$ .<sup>19</sup>

#### General Procedure for the Synthesis of 3'-R-10'-R<sup>1</sup>-Spiro[hetaryl-3(4),6'-[1,2,4]triazino[2,3-c]quinazolin]-2'(7'H)-ones 2.1–2.11

To a solution of 0.01 M of compounds **1.1–1.5** in 20 mL of glacial acid was added 0.01 M of appropriate heterocyclic carbonyl compound (tetrahydro-4H-pyran-4-one, dihydrothiophen-3(2H)-one, dihydro-2H-thiopyran-3(4H)-one, 1-methylpiperidin-4-one, dihydrothiophen-3(2H)-one 1,1-dioxide, dihydro-2H-thiopyran-3(4H)-one 1,1-dioxide). The reaction mixture was refluxed for 3 h. The solvent was removed by vacuum distillation, the residue was triturated in methanol, the precipitate was filtered and dried. If necessary, crystallized from dioxane.

**3'-Phenyl-2,3,5,6-tetrahydrospiro[pyran-4,6'-[1,2,4]triazino[2,3-c]quinazolin]-2'(7'H)-one (2.1).** Yield: 3.8 g (92.4%); pale yellow crystals; m.p. >300; IR: 3256, 2952, 2856, 1638, 1624, 1611, 1592, 1551, 1514, 1498, 1479, 1435, 1417, 1394, 1334, 1299, 1261, 1214, 1177, 1160, 1150, 1136, 1107, 1097, 1080, 1041, 1027, 1004, 975, 951, 927, 874, 858, 836, 815, 778, 757, 709, 697, 675, 634, 620  $\text{cm}^{-1}$ ; <sup>1</sup>H NMR (DMSO- $d_6$ )  $\delta$  8.18 (d,  $J = 8.4$  Hz, 2H, H-2, 6 Ph), 8.02 (d,  $J = 7.8$  Hz, 1H, H-11), 7.55–7.29 (m, 5H, H-9, H-3, 4, 5 Ph, NH), 7.04 (d,  $J = 8.1$  Hz, 1H, H-8), 6.88 (t,  $J = 7.5$  Hz, 1H, H-10), 3.90–3.80 (m, 2H, H-2, 2', 6, 6' pyrane), 2.56–2.51

(m, 2H, H-3, 5 pyrane), 1.99–1.99 (m, 2H, H-3', 5' pyrane); <sup>13</sup>C NMR (DMSO- $d_6$ )  $\delta$  34.19, 63.26, 75.98, 113.70, 116.81, 118.37, 119.81, 127.36, 128.62, 129.10, 130.27, 130.69, 133.37, 135.46, 144.56, 146.29, 147.28, 161.00. LC-MS:  $m/z = 347$  [M+1]. Anal. Calcd. for  $\text{C}_{20}\text{H}_{18}\text{N}_4\text{O}_2$ : C, 69.35; H, 5.24; N, 16.17. Found: C, 69.38; H, 5.29; N, 16.28.

**1-Methyl-3'-phenylspiro[piperidine-4,6'-[1,2,4]triazino[2,3-c]quinazolin]-2'(7'H)-one (2.2).** Yield: 2.68 g (74.7%); pale yellow crystals; m.p. 269–271 °C; IR: 3274, 1700, 1637, 1623, 1611, 1594, 1550, 1516, 1498, 1484, 1457, 1436, 1416, 1365, 1336, 1266, 1222, 1202, 1186, 1157, 1139, 1108, 1080, 1064, 1031, 1016, 995, 951, 929, 882, 853, 816, 769, 748, 710, 694, 665, 636  $\text{cm}^{-1}$ ; <sup>1</sup>H NMR (DMSO- $d_6$ )  $\delta$  8.21 (d,  $J = 8.0$  Hz, 2H, H-2, 6 Ph), 8.02 (d,  $J = 7.7$  Hz, 1H, H-11), 7.54–7.37 (m, 3H, H-9; H-3, 5 Ph), 7.28 (s, 1H, NH), 7.07 (d,  $J = 7.8$  Hz, 1H, H-8), 6.89 (t,  $J = 7.8$  Hz, 1H, H-10), 2.71 (br.s, 2H, H-2, 6 piperidine), 2.51 (m, 2H, H-2', 6' piperidine), 2.29 (s, 3H,  $\text{CH}_3$ ), 2.08 (d,  $J = 7.3$  Hz, 2H, H-3, 5 piperidine), 1.92 (m, 2H, H-3', 5' piperidine); <sup>13</sup>C NMR (DMSO- $d_6$ )  $\delta$  33.26, 45.79, 50.84, 76.54, 113.61, 116.77, 119.58, 127.28, 128.59, 129.03, 130.66, 133.36, 135.37, 144.57, 147.12, 152.35, 154.20, 156.50, 161.11. LC-MS:  $m/z = 360$  [M+1]. Anal. Calcd. for  $\text{C}_{21}\text{H}_{21}\text{N}_5\text{O}$ : C, 70.17; H, 5.89; N, 19.48. Found: C, 70.21; H, 5.93; N, 19.53.

**1-Methyl-3'-(4-tert-butylphenyl)-spiro[piperidine-4,6'-[1,2,4]triazino[2,3-c]quinazolin]-2'(7'H)-one (2.3).** Yield: 3.30 g (79.4%); pale yellow crystals; m.p. 255–257 °C; <sup>1</sup>H NMR (DMSO- $d_6$ )  $\delta$  8.13 (d, 2H, H-2, 6 Ph), 8.01 (d, 1H, H-11), 7.53–7.35 (m, 3H, H-9, H-3, 5 Ph), 7.30 (s, 1H, NH), 7.08 (d, 1H, H-8), 6.89 (t, 1H, H-10), 2.85–2.68 (m, 2H, H-2, 6 piperidine), 2.61–2.42 (m, 2H, H-2', 6' piperidine), 2.33 (s, 3H,  $-\text{CH}_3$ ), 2.21–2.02 (m, 2H, H-3, 5 piperidine), 2.00–1.81 (m, 2H, H-3', 5' piperidine), 1.37 (s, 9H,  $\text{C}(\text{CH}_3)_3$ ); LC-MS:  $m/z = 416$  [M+1]. Anal. Calcd. for  $\text{C}_{25}\text{H}_{29}\text{N}_5\text{O}$ : C, 72.26; H, 7.03; N, 16.85. Found: C, 72.30; H, 7.11; N, 16.89.

**3'-(4-Fluorophenyl)-1-methylspiro[piperidine-4,6'-[1,2,4]triazino[2,3-c]quinazolin]-2'(7'H)-one (2.4).** Yield: 3.3 g (88.3%); pale yellow crystals; m.p. 260–262 °C; <sup>1</sup>H NMR (DMSO- $d_6$ )  $\delta$  8.32 (t,  $J = 5.8$  Hz, 2H, H-2, 6 Ph), 8.03 (d,  $J = 7.7$  Hz, 1H, H-11), 7.42 (t,  $J = 7.4$  Hz, 1H, H-9), 7.29–7.16 (m, 3H, NH, H-3, 5 Ph), 7.09 (d,  $J = 8.0$  Hz, 1H, H-8), 6.90 (t,  $J = 7.3$  Hz, 1H, H-10), 2.74 (m, 2H, H-2, 6 piperidine), 2.55 (m, 2H, H-2', 6' piperidine), 2.32 (s, 3H,  $-\text{CH}_3$ ), 2.09 (m, 1H, H-3, 5 piperidine), 1.92 (m, 2H, H-3', 5' piperidine); <sup>13</sup>C NMR (DMSO- $d_6$ )  $\delta$  33.15, 45.70, 50.78, 76.55, 113.57, 115.60 (d,  $J = 21.5$  Hz), 116.78, 119.59, 127.30, 129.80 (d,  $J = 2.8$  Hz), 131.49 (d,  $J = 8.6$  Hz), 135.40, 144.56, 146.06, 152.36, 152.49, 161.10, 163.74 (d,  $J = 248.3$  Hz), 172.54. LC-MS:  $m/z = 378$  [M+1]; Anal. Calcd. for  $\text{C}_{21}\text{H}_{20}\text{FN}_5\text{O}$ : C, 66.83; H, 5.34; N, 18.56; Found: C, 66.89; H, 5.41; N, 18.64.

**3'-(4-Methoxyphenyl)-1-methylspiro[piperidine-4,6'-[1,2,4]triazino[2,3-c]quinazolin]-2'(7'H)-one (2.5).** Yield: 3.68 g (94.6%); pale yellow crystals; m.p. 270–272 °C; <sup>1</sup>H NMR (DMSO-*d*<sub>6</sub>) δ 8.25 (d, *J* = 8.6 Hz, 2H, H-2, 6 Ph), 8.01 (d, *J* = 7.4 Hz, 1H, H-11), 7.40 (t, *J* = 6.9 Hz, 1H, H-9), 7.23 (s, 1H, NH), 7.08 (d, *J* = 8.0 Hz, 2H, H-8), 6.97 (d, *J* = 8.7 Hz, 2H, H-3, 5 Ph), 6.89 (t, *J* = 7.3 Hz, 1H, H-10), 3.86 (s, 3H, CH<sub>3</sub>), 2.73 (br.s, 2H, H-2, 6 piperidine), 2.51 (br.s, 2H, H-2', 6' piperidine), 2.31 (s, 3H, -CH<sub>3</sub>), 2.09 (m, 1H, H-3, 5 piperidine), 1.92 (br.s, 2H, H-3', 5' piperidine); <sup>13</sup>C NMR (DMSO-*d*<sub>6</sub>) δ 33.24, 45.78, 50.84, 55.76, 76.43, 113.70, 114.06, 114.27, 116.72, 119.53, 125.65, 127.18, 130.69, 131.65, 144.46, 146.56, 151.98, 161.21, 161.42; LC-MS: *m/z* = 390 [M+1]. Anal. Calcd. for C<sub>22</sub>H<sub>23</sub>N<sub>5</sub>O<sub>2</sub>: C, 67.85; H, 5.95; N, 17.98. Found: C, 67.91; H, 6.02; N, 18.02.

**10'-Bromo-1-methyl-3'-phenylspiro[piperidine-4,6'-[1,2,4]triazino[2,3-c]quinazolin]-2'(7'H)-one (2.6).** Yield: 3.8 g (86.6%); pale yellow crystals; m.p. 270–272 °C; <sup>1</sup>H NMR (DMSO-*d*<sub>6</sub>) δ 8.21 (d, *J* = 7.8 Hz, 2H, H-2, 6 Ph), 8.11 (s, 1H, H-11), 7.56–7.33 (m, 5H, H-9; NH; H-3, 4, 5 Ph), 7.05 (d, *J* = 8.4 Hz, 1H, H-8), 2.73 (m, 2H, H-2, 6 piperidine), 2.51 (m, 2H, H-2', 6' piperidine), 2.30 (s, 3H, -CH<sub>3</sub>), 2.14–1.99 (m, 2H, H-3, 5 piperidine), 1.92 (m, 2H, H-3', 5' piperidine); EI-MS, *m/z* (I<sub>rel</sub>, %) = 292 (6.2), 290 (5.9), 278 (7.5), 276 (6.5), 266 (5), 265 (18), 264 (6.3), 263 (19), 223 (12.1), 155 (5.4), 116 (8.9), 115 (5.3), 109 (11.1), 104 (20.3), 103 (71.9), 102 (6.4), 77 (14.8), 76 (22.6), 75 (5.8), 72 (32.2), 71 (32.5), 70 (100), 69 (6.1), 68 (8.1), 63 (12.3), 58 (17), 57 (41.7), 56 (20.8), 54 (10.3), 53 (6.8), 45 (11.2); LC-MS: *m/z* = 440 [M+2]. Anal. Calcd. for C<sub>21</sub>H<sub>20</sub>BrN<sub>5</sub>O: C, 57.54; H, 4.60; N, 15.98. Found: C, 57.50; H, 4.57; N, 15.93.

**3'-Phenyl-2,3,5,6-tetrahydrospiro[thiopyran-4,6'-[1,2,4]triazino[2,3-c]quinazolin]-2'(7'H)-one (2.7).** Yield: 3.5 g (89.0%); pale yellow crystals; mp >300 °C; <sup>1</sup>H NMR (DMSO-*d*<sub>6</sub>) δ 8.19 (d, *J* = 7.6 Hz, 1H, H-2, 6 Ph), 8.02 (d, *J* = 8.0 Hz, 1H, H-11), 7.51–7.43 (m, 3H, H-3, 4, 5 Ph), 7.40 (t, 1H, H-9), 7.26 (s, 1H, NH), 7.10 (d, *J* = 7.9 Hz, 1H, H-8), 6.89 (t, *J* = 7.3 Hz, 1H, H-10), 3.25–3.12 (m, 2H, H-2, 6 thiopyran), 2.52 (m, 6H, H-2', 3, 3', 5, 5', 6' thiopyran); <sup>13</sup>C NMR (DMSO-*d*<sub>6</sub>) δ 23.71, 35.25, 77.54, 113.41, 116.63, 119.74, 127.24, 128.61, 129.08, 130.71, 133.32, 135.51, 144.36, 147.29, 152.07, 161.05; LC-MS: *m/z* = 363[M+1]. Anal. Calcd. for C<sub>20</sub>H<sub>18</sub>N<sub>4</sub>O<sub>3</sub>: C, 66.28; H, 5.01; N, 15.46. Found: C, 66.31; H, 5.09; N, 15.49.

**3'-Phenyl-4,5-dihydro-2H-spiro[thiophene-3,6'-[1,2,4]triazino[2,3-c]quinazolin]-2'(7'H)-one (2.8).** Yield: 2.8 g (81.6%); m.p. 263–265 °C; pale yellow crystals; IR: 3299, 3076, 2926, 1714, 1640, 1626, 1615, 1598, 1551, 1503, 1486, 1440, 1411, 1338, 1312, 1271, 1249, 1221, 1191, 1170, 1154, 1107, 1080, 1028, 992, 948, 926, 867, 815, 776, 750, 692 cm<sup>-1</sup>; <sup>1</sup>H NMR (DMSO-*d*<sub>6</sub>) δ 8.17 (d, *J* = 4.9 Hz, 2H, H-2, 6 Ph), 8.03 (d, *J* = 7.6 Hz, 1H, H-11), 7.66 (s, 1H, NH), 7.44–

7.34 (m, 3H, H-9, H-3, 5 Ph), 6.95 (d, *J* = 7.9 Hz, 1H, H-8), 6.88 (t, *J* = 7.9 Hz, 1H, H-10), 3.51 (d, *J* = 11.6 Hz, 1H, H-2 thiophene), 3.13 (d, *J* = 11.2 Hz, 1H, H-2' thiophene), 3.10–2.92 (m, 2H, H-5, 5' thiophene), 2.62–2.41 (m, 2H, H-4, 4' thiophene); <sup>13</sup>C NMR (DMSO-*d*<sub>6</sub>) δ 27.85, 39.14, 39.41, 87.60, 113.17, 116.05, 119.72, 127.49, 128.61, 129.16, 130.69, 133.29, 135.48, 145.53, 147.02, 152.34, 161.22. LC-MS: *m/z* = 349 [M+1]. Anal. Calcd. for C<sub>19</sub>H<sub>16</sub>N<sub>4</sub>O<sub>3</sub>: C, 65.50; H, 4.63; N, 16.08. Found: C, 65.61; H, 4.75; N, 16.12.

**3'-Phenyl-5,6-dihydro-2H,4H-spiro[thiopyran-3,6'-[1,2,4]triazino[2,3-c]quinazolin]-2'(7'H)-one (2.9).** Yield: 3.3 g (91.8%); pale yellow crystals; m.p. 274–276 °C; IR: 3272, 2891, 1641, 1626, 1609, 1594, 1553, 1515, 1499, 1483, 1442, 1414, 1333, 1312, 1298, 1273, 1249, 1188, 1153, 1103, 1076, 1030, 1012, 980, 950, 923, 872, 859, 825, 814, 787, 774, 749, 694, 670 cm<sup>-1</sup>; <sup>1</sup>H NMR (DMSO-*d*<sub>6</sub>) δ 8.18 (d, *J* = 5.3 Hz, 2H, H-2, 6 Ph), 8.00 (d, *J* = 7.7 Hz, 1H, H-11), 7.52–7.29 (m, 5H, H-9, H-3, 4, 5 Ph, NH), 7.17 (d, *J* = 8.0 Hz, 1H, H-8), 6.86 (t, *J* = 7.2 Hz, 1H, H-10), 3.38 (d, *J* = 13.4 Hz, 1H, H-2 thiopyran), 2.92 (d, *J* = 13.2 Hz, 1H, H-2' thiopyran), 2.78–2.59 (m, 1H, H-6 thiopyran), 2.55–2.05 (m, 5H, H-4, 4', 5, 5', 6' thiopyran); <sup>13</sup>C NMR (DMSO-*d*<sub>6</sub>) δ 24.37, 27.02, 33.55, 34.76, 75.81, 112.99, 116.56, 116.62, 119.51, 127.27, 128.55, 129.20, 130.68, 133.32, 135.46, 144.45, 144.51, 152.17, 161.04. LC-MS: *m/z* = 363 [M+1]. Anal. Calcd. for C<sub>20</sub>H<sub>18</sub>N<sub>4</sub>O<sub>3</sub>: C, 66.28; H, 5.01; N, 15.46. Found: C, 66.30; H, 5.03; N, 15.49.

**3'-Phenyl-4,5-dihydro-2H-spiro[thiophene-3,6'-[1,2,4]triazino[2,3-c]quinazolin]-2'(7'H)-one 1,1-dioxide (2.10).** Yield: 2.1 g (56.1%); pale yellow crystals; m.p. 266–269 °C; <sup>1</sup>H NMR (DMSO-*d*<sub>6</sub>) δ 8.25 (d, *J* = 5.3 Hz, 1H, H-2, 6 Ph), 8.04 (d, *J* = 7.5 Hz, 1H, H-11), 7.97 (s, 1H, NH), 7.49–7.41 (m, 4H, H-9, H-3, 4, 5 Ph), 7.04–6.84 (m, *J* = 7.7 Hz, 2H, H-8, 10), 4.24 (d, *J* = 14.9 Hz, 1H, H-2 thiophene), 3.50 (d, *J* = 15.0 Hz, 1H, H-2' thiophene), 3.47–3.34 (m, 2H, H-5, 5' thiophene), 3.30–3.03 (m, 1H, H-4 thiophene), 2.74–2.55 (m, 1H, H-4' thiophene); LC-MS: *m/z* = 381 [M+1]. Anal. Calcd. for C<sub>19</sub>H<sub>16</sub>N<sub>4</sub>O<sub>3</sub>S: C, 59.99; H, 4.24; N, 14.73. Found: C, 60.03; H, 4.27; N, 14.77.

**3'-Phenyl-5,6-dihydro-2H,4H-spiro[thiopyran-3,6'-[1,2,4]triazino[2,3-c]quinazolin]-2'(7'H)-one 1,1-dioxide (2.11).** Yield: 4.5 g (91.8%); pale yellow crystals; m.p. 296–299 °C; <sup>1</sup>H NMR (DMSO-*d*<sub>6</sub>) δ 8.25 (d, *J* = 5.1 Hz, 2H, H-2, 6 Ph), 8.05 (d, *J* = 7.7 Hz, 1H, H-11), 7.46 (m, 4H, H-9, H-3, 4, 5 Ph), 7.14 (s, 1H, NH), 7.06 (d, *J* = 8.0 Hz, 1H, H-8), 6.96 (t, *J* = 7.3 Hz, 1H, H-10), 3.97 (d, *J* = 13.9 Hz, 1H, H-2 thiopyran), 3.53 (d, *J* = 15.4 Hz, 1H, H-2' thiopyran), 3.50–3.35 (m, 1H, H-6 thiopyran), 3.23–2.91 (m, 1H, H-6' thiopyran), 2.90–2.63 (m, 1H, H-4 thiopyran), 2.34 (m, 3H, H-4', 5, 5' thiopyran); <sup>13</sup>C NMR (DMSO-*d*<sub>6</sub>) δ 18.09, 31.64, 50.06, 54.57, 77.78, 113.38, 116.95, 120.21, 127.32, 128.50, 129.38, 130.80, 133.18, 135.61, 143.78, 147.26, 151.84, 161.03; LC-MS: *m/z* = 395 [M+1]. Anal. Calcd. for

C<sub>20</sub>H<sub>18</sub>N<sub>4</sub>O<sub>3</sub>S: C, 60.90; H, 4.60; N, 14.20. Found: C, 60.93; H, 4.64; N, 14.26.

## 2. Results and Discussion

Considering the roles of cyclooxygenases (COX-1 and COX-2) as important pharmacological targets and their inhibitors are the basis for the developing of anti-inflammatory drugs, in the first phase of the study the virtual base (80 compounds) of 3'-R-10'-R<sup>1</sup>-spiro [hetaryl-3(4),6'-[1,2,4]triazino[2,3-*c*]quinazolin]-2'(7'*H*)-ones was analyzed using molecular docking. Virtual structural modification of studied compounds, which have heterocyclic fragments at spiro position (position 6) was held by the 3<sup>d</sup> position and at positions 8, 9, 10 and 11 of the aromatic ring. Complexes of COX-1 and COX-2 were downloaded from the Protein Data Bank, to determine the affinity (Table 1), <http://www.rcsb.org/pdb/home/home.do>. As a reference known selective COX-1 and COX-2 inhibitors were used, such as diclofenac sodium and celecoxib. Results of the studies showed that the structures analyzed have a higher affinity to COX-2 and much lower to COX-1. Among 80 tested compound, 7 with the highest affinity, according to the docking, are presented in the Table 1. Compound **2.10** revealed the highest affinity, yet still lower than celecoxib.

The visualization of the interaction of the structures with the active site of COX-2 (Fig. 1) showed, that compound **2.10** revealed the highest affinity (11.5 kcal/mol). There were four hydrogen bonds with the following amino acid residues D:TYR341 (3.08 Å), D:HIS75 (3.37 Å),

D:GLY512 (3.33 Å), D:SER516 (3.63 Å), and besides  $\pi$ -cation electrostatic interaction with D:ARG106 (4.86 Å),  $\pi$ -sigma hydrophobic interactions with D:VAL335 (3.76 Å), D:VAL509 (3.40 Å, 3.65 Å), D:ALA513 (3.82 Å),  $\pi$ -sulfur interaction with D:TRP373 (5.93 Å),  $\pi$ - $\pi$  stacked hydrophobic interaction with D:HIS75 (5.26 Å) and  $\pi$ -alkyl hydrophobic interactions with D:LEU517 (5.14 Å), D:ARG499 (5.27 Å), D:ALA502 (4.31 Å). Analyzing the complex of celecoxib and compound **2.10** with COX-2, similar interactions can be traced, namely with such amino acids D:ARG106, D:ARG499, D:VAL335, D:VAL509, D:LEU517, D:TRP373, D:ALA513. This may indicate that stated class of compound might have the ability to inhibit the COX-2 as celecoxib does.

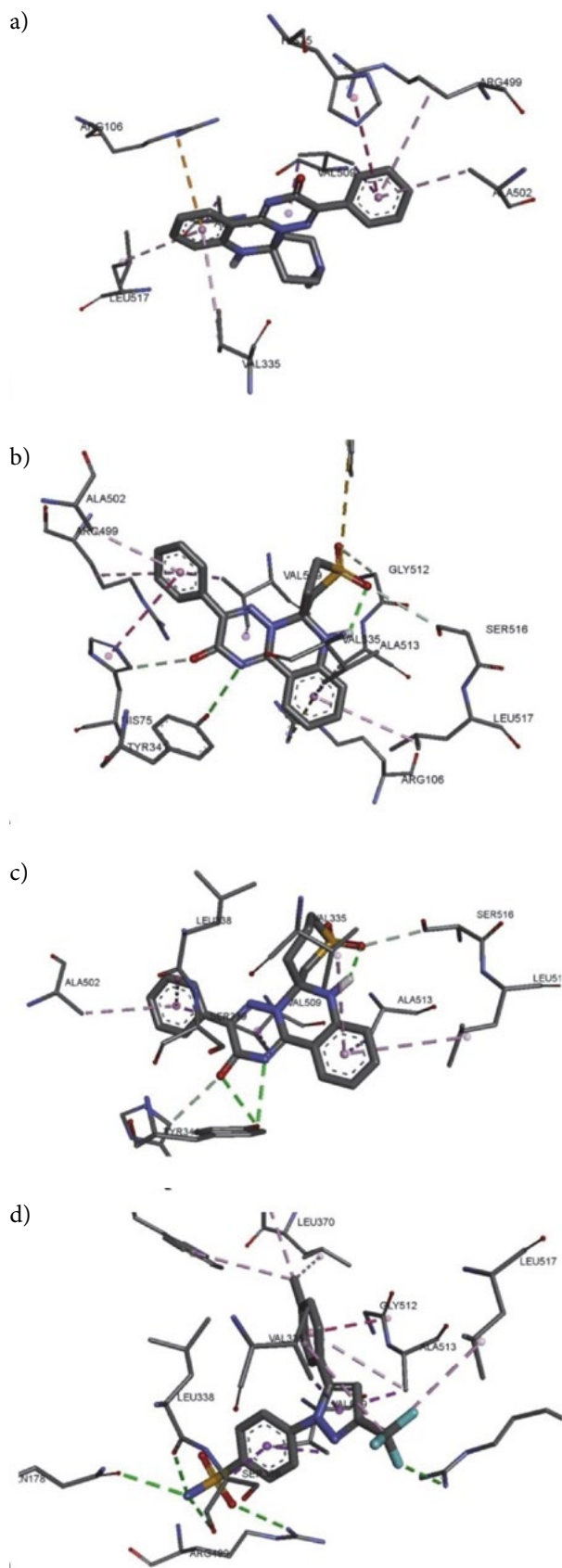
The second stage, namely the synthesis of the corresponding spiro-derivatives **2** provided the interaction of substituted 6-R<sup>1</sup>-3-(2-aminophenyl)-1,2,4-triazine-5(2*H*)-ones **1** and the corresponding heterocyclic ketones (Scheme 1). The heterocyclization was carried out by known method,<sup>20</sup> namely the refluxing in glacial acid.

Synthesized spiro-derivatives **2** are pale yellow crystalline substances, soluble in DMF, slightly soluble in dioxane, insoluble in alcohols and water. The compounds' structures were established with elemental analysis, LC-MS-data, IR and NMR spectra. Thus, triazino[2,3-*c*]quinazoline fragment of compounds **2** in <sup>1</sup>H NMR spectra has the appropriate chemical shifts and multiplicity: 8.11–8.00 ppm (H-11, d), 7.42–7.40 ppm (H-9, t), 7.17–6.95 ppm (H-8, d), and 6.96–6.86 ppm (H-10, t). It is important to note, that H-9 in most cases resonated together with the aromatic protons of substituent at the position 3 and NH proton of position 7 as multiplets. Whereas, protons H-11, H-8 and H-10 have

Table 1. Results of molecular docking of the most active structures

Comp.	Affinity (kcal/mol) to COX-1	Affinity (kcal/mol) to COX-2	Types of interactions with amino acid residues of COX-2
<b>2.1</b>	-7.4	-10.1	D:ARG106 <sup>b</sup> , D:VAL509 <sup>c</sup> , D:ALA513 <sup>c</sup> , D:HIS75 <sup>c</sup> , D:VAL335 <sup>c</sup> , D:LEU517 <sup>c</sup> , D:ARG499 <sup>c</sup> , D:ALA502 <sup>c</sup> .
<b>2.2</b>	-3.6	-10.3	D:ARG106 <sup>b</sup> , D:VAL509 <sup>c</sup> , D:ALA513 <sup>c</sup> , D:HIS75 <sup>c</sup> , D:VAL335 <sup>c</sup> , D:LEU517 <sup>c</sup> , D:ARG499 <sup>c</sup> , D:ALA502 <sup>c</sup> .
<b>2.7</b>	-5.2	-9.0	D:ARG106 <sup>b</sup> , D:VAL509 <sup>c</sup> , D:ALA513 <sup>c</sup> , D:TRP373 <sup>d</sup> , D:HIS75 <sup>c</sup> , D:LEU338 <sup>c</sup> , D:PHE504 <sup>c</sup> , D:VAL335 <sup>c</sup> , D:LEU517 <sup>c</sup> , D:ALA502 <sup>c</sup> .
<b>2.8</b>	-3.3	-10.4	D:HIS75 <sup>a</sup> , D:VAL335 <sup>c</sup> , D:VAL509 <sup>c</sup> , D:ALA513 <sup>c</sup> , D:TRP373 <sup>d</sup> , D:HIS75 <sup>c</sup> , D:LEU338 <sup>c</sup> , D:PHE504 <sup>c</sup> , D:LEU517 <sup>c</sup> , D:ARG499 <sup>c</sup> , D:ALA502 <sup>c</sup> .
<b>2.9</b>	-1.3	-10.6	D:TYR341 <sup>a</sup> , D:HIS75 <sup>a</sup> , D:VAL509 <sup>c</sup> , D:ALA513 <sup>c</sup> , D:SER339 <sup>c</sup> , D:VAL335 <sup>c</sup> , D:LEU338 <sup>c</sup> , D:LEU517 <sup>c</sup> , D:ALA502 <sup>c</sup> .
<b>2.10</b>	-1.4	-11.5	D:TYR341 <sup>a</sup> , D:HIS75 <sup>a</sup> , D:GLY512 <sup>a</sup> , D:SER516 <sup>a</sup> , D:ARG106 <sup>b</sup> , D:VAL335 <sup>c</sup> , D:VAL509 <sup>c</sup> , D:ALA513 <sup>c</sup> , D:TRP373 <sup>d</sup> , D:HIS75 <sup>c</sup> , D:LEU517 <sup>c</sup> , D:ARG499 <sup>c</sup> , D:ALA502 <sup>c</sup> .
<b>2.11</b>	-0.4	-10.9	D:TYR341 <sup>a</sup> , D:HIS75 <sup>a</sup> , D:SER516 <sup>a</sup> , D:VAL509 <sup>c</sup> , D:ALA513 <sup>c</sup> , D:LEU338 <sup>c</sup> , D:SER339 <sup>c</sup> , D:VAL335 <sup>c</sup> , D:LEU517 <sup>c</sup> , D:ALA502 <sup>c</sup> .
Celecoxib	-	-12.1	D:ARG106 <sup>a</sup> , D:ARG499 <sup>a</sup> , D:GLN178 <sup>a</sup> , D:LEU338 <sup>a</sup> , D:SER339 <sup>a</sup> , D:VAL335 <sup>c</sup> , D:CEL682 <sup>c</sup> , D:VAL509 <sup>c</sup> , D:LEU370 <sup>c</sup> , D:VAL335 <sup>c</sup> , D:LEU345 <sup>c</sup> , D:LEU517 <sup>c</sup> , D:TYR371 <sup>c</sup> , D:TRP373 <sup>c</sup> , D:ALA513 <sup>c</sup> .

a – hydrogen, b – electrostatic, c – hydrophobic, d – others.



**Figure 1.** Interaction of compound **2.2** (a), **2.10** (b), **2.11** (c), celastrol (d) with COX-2, PDB ID: 3LN1

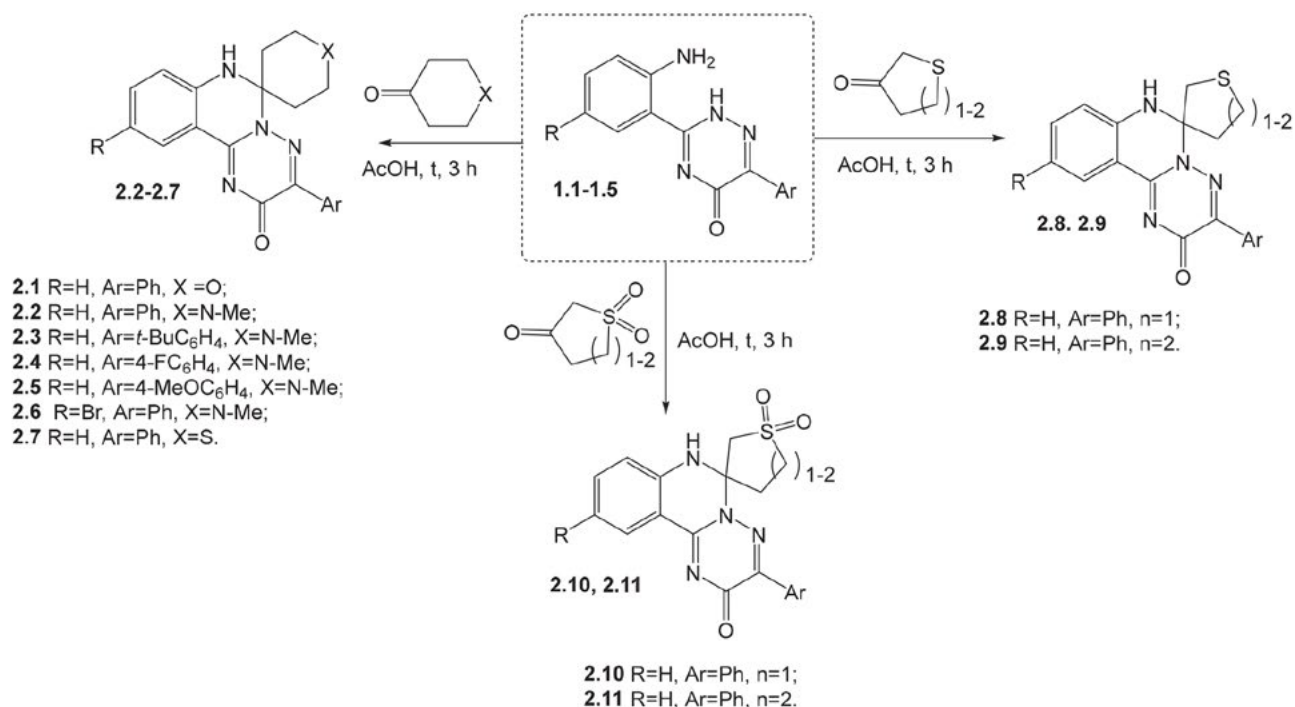
classical multiplicity and  $J$ -coupling ( $J = 8.05\text{--}7.3$  Hz).<sup>21</sup> Phenyl moiety in position 3 of  $^1\text{H}$  NMR spectrum resonated as two proton singlets, H-2,6 at 8.25–8.17 ppm and three proton multiplets of H-3,4,5 at 7.56–7.35 ppm. Signals of  $p$ -substituted phenyl derivatives **2** were registered as  $A_2B_2$ -systems, as two doublets H-2,6 and H-3,5.

The characteristic singlets of NH protons (position 7) in  $^1\text{H}$  NMR spectra of compounds **2** were observed at 7.97–7.14 ppm and their chemical shift depended on the electronic effects of spiro moiety at position 6. Thus, the signal of NH proton of compound **2.1** with spirothiopyran cycle were detected at 7.30 ppm, with spirothiopyran (**2.2–2.6**) at 7.33–7.23 ppm, with spirothiopyran (**2.7, 2.9**) at 7.29–7.26 ppm and with spirothiophene (**2.8**) cycle at 7.66 ppm. In  $^1\text{H}$  NMR spectra of compound **2.11** (oxidized analogue of compound **2.9**) signal of NH proton were shifted to a higher field (7.14 ppm). Whereas, the stated proton of compound **2.10** resonated at a lower field, namely at 7.97 ppm, compared to compound **2.8**, what is likely due to the formation of hydrogen bond between nearby structural fragments.

In the  $^1\text{H}$  NMR spectra of compounds **2.1–2.11** proton signals of position 6 of spiro moiety were recorded as a complex set of multiplets in aliphatic part of spectrum due to the presence of magnetic nonequivalent axial and equatorial protons.<sup>21</sup> Whereas,  $^1\text{H}$  NMR spectra of compounds **2.8, 2.9** have characteristic features, which were associated with the presence in the molecule of a center of asymmetry. Thus, in the spectra of mentioned compounds protons of methylene group of thiophene at position 2 or thiopyran were registered as doublets at 3.13 ppm  $H_{ax}$  ( $J = 11.2$  Hz), 2.92 ppm ( $J = 13.2$  Hz) and  $H_{eq}$  at 3.51 ppm ( $J = 11.6$  Hz), 3.38 ppm ( $J = 13.4$  Hz), respectively. A similar pattern of signals was characteristic for their dioxo analogues (compounds **2.10, 2.11**).

In the  $^{13}\text{C}$  NMR spectra of compounds **2** characteristic signal of  $sp^3$ -hybridized C in spiro position (position 6) was observed at 87.60–75.81 ppm, and its chemical shift was determined by electron withdrawing effect of the spiro cycle. In addition, further structure confirmation was made by the corresponding  $^{13}\text{C}$  signals of hydrogenated pyran cycle (compound **2.1**) at 34.19 and 63.26 ppm,  $N$ -methylpiperidine cycle (**2.2, 2.4, 2.5**) at 33.26–33.15 ppm, 45.79–45.70 ppm and 50.84–50.78 ppm and hydrogenated thiopyran cycle (**2.7**) at 23.71 ppm and 35.28 ppm at 4,6'-spiro position. While other electronic environments of carbon atoms of hydrogenated thiophene (**2.8**) and thiopyran (**2.9**) cycle at 3,6'-spiro position caused a series of four signals at a high field. A similar pattern of signals was characteristic for dioxo analogue compound **2.11**.

Mass spectrometric investigation showed, that compound **2.6** was characterized by a low-intensity molecular ion, that formed high-intensity fragmentation ions  $F_1$  [ $C_6H_5CH=N$ ]<sup>+</sup> ( $m/z$  103, 71.9%),  $F_2$  [ $CH_2N(Me)CH=CH_2$ ]<sup>+</sup> ( $m/z$  70, 100%) and  $F_3$  [ $C_{10}H_6BrN_3O$ ]<sup>+</sup> ( $m/z$  265/263, 18.0/19.0%). The last fragmented ion described



**Scheme 1.** The heterocyclization of 6-R-3-(2-aminophenyl)-1,2,4-triazine-5(2H)-ones

the presence of bromine in the molecule and its isotopic profile. Further carbon-carbon bond breaking and hydrogen rearrangements in F<sub>2</sub> created intense ions [CH<sub>2</sub>NHCH<sub>2</sub>=CH<sub>2</sub>]<sup>+</sup> (*m/z* 57, 41.7%) and [CH<sub>2</sub>NCH<sub>3</sub>]<sup>+</sup> (*m/z* 45, 11.2%), indicating the presence of *N*-methylpiperidine fragment in the molecule.<sup>22</sup>

### 3. Pharmacology

Formalin acute inflammation is characterized by a powerful inflammatory response, which in 3 h of the ex-

periment can be verified by significant swelling of the paw in the control group of animals (average increase in volume of the paw is 47.38%). Administration of compounds **2** to the animals with experimental pathology led to a decrease of exudative reactions and most of compounds exhibited anti-inflammatory action comparable (compounds **2.2**, **2.6**, **2.7**, **2.10**) or higher (**2.3–2.5**, **2.8**, **2.11**) than the effect of the reference diclofenac sodium (Table 2). SAR-analysis (influence of substituents at positions 3 and 6) showed, that 3'-phenyl-2,3,5,6-tetrahydrospiro[pyran-4,6'-[1,2,4]triazino[2,3-*c*]quinazolin]-2'(7'*H*)-one (**2.1**) showed moderate anti-inflammatory effect (higher in the

**Table 2.** Anti-inflammatory activity of synthesized compounds under formalin induced inflammation model

Comp.	Dosage, mg/kg	Increase of the paw volume in 3 h, %	Anti-inflammatory activity, %
Experimental pathology	–	47.38	0
<b>2.1</b>	10.0	24.22	39.39
<b>2.2</b>	10.0	26.28	44.44
<b>2.3</b>	10.0	15.43	69.19
<b>2.4</b>	10.0	20.47	56.57
<b>2.5</b>	10.0	6.74	85.86
<b>2.6</b>	10.0	24.75	48.48
<b>2.7</b>	10.0	22.60	44.44
<b>2.8</b>	10.0	21.61	55.56
<b>2.9</b>	10.0	33.45	29.29
<b>2.10</b>	10.0	23.91	49.49
<b>2.11</b>	10.0	20.04	60.61
Diclofenac sodium	8.0	26.58	45.45

control group to 39.4%). Replacing the hydrogenated spiropyran (**2.1**) by 1-methyl-piperidine (**2.2**) fragment at the spiro position 6 increased activity to 44.44% compared with the control. The intensity of anti-inflammatory activity of compound **2.2** is comparable with diclofenac sodium. The position of sulfur in spirocycle of the isomer hydrogenated spirothiopyranes (**2.7**, **2.9**) determined the anti-inflammatory activity. Thus, the compound **2.7** with 4,6'-spiro position of thiopyran towards triazinoquinazoline cycle exhibited anti-inflammatory activity at the level of diclofenac sodium. Relocation of sulfur in the thiopyran cycle (3,6'-spiro position, compound **2.9**) led to a significant decrease of activity, whereas contraction of thiopyran cycle by a homologous unit (**2.8**) in contrast increased activity to 11.11% (compared with diclofenac). The structural similarity of compounds **2.10** and **2.11** to the celecoxib-like drugs, as we consider led to high anti-inflammatory activity.

Modification of position 3 substituent of triazinoquinazoline cycle via replacing of phenyl substituent by the 4-*tert*-butylphenyl (**2.3**), 4-fluorophenyl (**2.4**) or 4-methoxyphenyl (**2.5**) was substantiated and led to increasing of anti-inflammatory activity at 11.12–40.21%, compared with the reference drug (Tab. 2). While, the introduction of additional bromine (**2.6**) at the 10<sup>th</sup> position of compound **2.2** led to a loss of activity compared to the compounds **2.3–2.5**. Such, this way of modification of the molecule was not promising.

## 4. Conclusions

Based on the methodology of purposeful search of NSAIDs an effective method for the synthesis of 6-spiro-fused 10-R-3-aryl-6,7-dihydro-2*H*-[1,2,4]triazino[2,3-*c*]quinazolin-2-ones (a promising class of anti-inflammatory agents) was proposed. Structural features of the synthesized compounds, as well as their <sup>1</sup>H, <sup>13</sup>C NMR spectroscopy and mass spectrometry data were discussed. It was established that compounds **2.3–2.5**, **2.8** and **2.10** under formaline-induced paw edema model revealed the activity higher comparing to the reference drug – diclofenac sodium. SAR analysis showed that combination of triazine[2,3-*c*]quinazoline cycle with other heterocyclic fragments is reasonable in scope of novel NSAIDs creation and calls for further research.

## 5. References

- J. I. Levin, S. Laufer, Anti-Inflammatory drug discovery. *Royal Society of Chemistry Series No. 26*, Cambridge, **2012**, 528 p. DOI:10.1039/9781849735346.
- G. A. FitzGerald, C. Patrono, *N. Engl. J. Med.* **2001**, 345(6), 433–442. DOI:10.1056/NEJM200108093450607.
- R. G. Kulkarni, G. Achaiah, G. N. R. Sastry, *Curr. Pharm. Des.* **2006**, 12, 2437–2454. DOI:10.2174/138161206777698945.
- B. Botz, K. Bölskei, Z. Helyes, Challenges to develop novel anti-inflammatory and analgesic drugs, *Wiley Interdiscip. Rev.: Nanomed. Nanobiotechnol.* **2017**, 9(3), 1427. DOI:10.1002/wnan.1427.
- S. K. Kulkarni, V. P. Singh, *Curr. Top. Med. Chem.* **2007**, 7, 251–263. DOI:10.2174/156802607779941305.
- R. Paprocka, M. Wiese, A. Eljaszewicz, A. Helmin-Basa, A. Gzella, B. Modzelewska-Banachiewicz, J. Michalkiewicz, *Bioorg. Med. Chem. Lett.* **2015**, 25, 2664–2667. DOI:10.1016/j.bmcl.2015.04.079.
- A. Puratchikody, M. Doble, *Bioorg. Med. Chem.* **2007**, 15, 1083–1090. DOI:10.1016/j.bmc.2006.10.025.
- C. D. Barros, A. A. Amato, T. B. de Oliveira, K. B. R. Iannini, A. L. da Silva, T. G. da Silva, E. S. Leite, M. Z. Hernandez, M. do C. A. de Lima, S. L. Galdino, F. de A. R. Neves, I. da R. Pitta, *Bioorg. Med. Chem.* **2010**, 18, 3805–3811. DOI:https://doi.org/10.1016/j.bmc.2010.04.045.
- Y.-L. Chen, Y.-L. Zhao, C.-M. Lu, C.-C. Tzeng, J.-P. Wang, *Bioorg. Med. Chem.* **2006**, 14, 4373–4378. DOI:10.1016/j.bmc.2006.02.039.
- X. Wen, S.-B. Wang, D.-C. Liu, G.-H. Gong, Z.-S. Quan, *Med. Chem. Res.* **2015**, 24, 2591–2603. DOI:10.1007/s00044-015-1323-y.
- M. A. Hussein, *Med. Chem. Res.* **2013**, 22, 4641–4653. DOI:10.1007/s00044-013-0468-9.
- T. Yu. Sergeieva, O. Yu. Voskoboynik, S. I. Okovytyy, S. I. Kovalenko, S. V. Shishkina, O. V. Shishkin, J. Leszczynski, *J. Phys. Chem. A* **2014**, 118, 1895–1905. DOI:10.1021/jp4052616.
- Protein Data Bank, pdb. Retrieved from <http://www.pdb.org>
- MarvinSketch version: 6.3.0, **2015**, ChemAxon (<http://www.chemaxon.com>).
- O. Trott, A. J. Olson, *J. Comput. Chem.* **2010**, 31, 455–461. DOI:10.1002/jcc.21334.
- European convention for the protection of vertebrate animal used for experimental and other scientific purposes. Council of Europe, Strasbourg, **1986**.
- J. D. J. Liégeois, *Naunyn-Schmiedeberg's Arch. Pharmacol.* **1999**, 359, 220–227. DOI:10.1007/PL00005345.
- N. Shejawal, S. Menon, S. Shailajan, *Hum. Exp. Toxicol.* **2014**, 33, 123–129. DOI:10.1177/0960327113482594.
- M. Pagano, K. Gauvreau, Principles of Biostatistics, Kimberlee Gauvreau Statistics Series, Duxbury Press, **1994**, 524 p.
- S. V. Kholodnyak, K. P. Schabelnyk, O. Yu. Voskoboynik, O. M. Antypenko, S. I. Kovalenko, V. O. Palchykov, S. I. Okovytyy, S. V. Shishkina, *J. Org. Pharm. Chem.* **2016**, 14,3(55), 24–31.
- E. Breitmaier. Structure Elucidation by NMR in Organic Chemistry: A Practical Guide, Third Edition, **2002**, Wiley, 270 p.
- C. Dass. Fundamentals of contemporary mass spectrometry, **2007**, John Wiley & Sons, Inc., 608 p.

## Povzetek

Naše raziskave smo usmerili v načrtno iskanje novih, obetavnih antiinflamatornih spojin, zlasti med relativno neznanimi 3'-R-10'-R<sub>1</sub>-spiro[heteroaril-3(4),6'-[1,2,4]triazino[2,3-c]kinazolin]-2'(7'H)-oni. Pripravili smo virtualno kombinatorialno knjižnico doslej neznanih spiro-pripojenih derivatov [1,2,4]triazino[2,3-c]kinazolinov ter s pomočjo metod molekulskega sidranja identificirali najbolj obetavne inhibitorje COX-2. Nato smo te potencialne spojine, ki bi lahko imele protivnetni učinek, sintetizirali s pomočjo [5+1] ciklokondenzacij substituiranih 3-(2-aminofenil)-6-R-1,2,4-triazin-5(2H)-onov s heterocikličnimi ketoni. Strukture pripravljenih spojin smo določili na osnovi fizikalno-kemijskih metod in spektroskopskih značilnosti. Za dobljene spojine smo določili antiinflamatorno aktivnost z uporabo modela s formalinom inducirane edema šape testnih živali. Na ta način smo identificirali najbolj aktivne spojine. Izvedena analiza primerjave aktivnosti od strukture spojin (SAR analiza) je pokazala, da je kombinacija triazino[2,3-c]kinazolinskega in spiro-pripojenega fragmetna smiselen pristop k pripravi še novih antiinflamatornih zdravil.



Scientific paper

# Green One-pot Synthesis of Novel Polysubstituted Pyrazole Derivatives as Potential Antimicrobial Agents

Hamid Beyzaei,<sup>1,\*</sup> Zahra Motraghi,<sup>1</sup> Reza Aryan,<sup>1</sup> Mohammad Mehdi Zahedi<sup>2</sup>  
and Alireza Samzadeh-Kermani<sup>1</sup>

<sup>1</sup>Department of Chemistry, Faculty of Science, University of Zabol, Zabol, Iran

<sup>2</sup>Department of Chemistry, University of Saskatchewan, 110 Science Place, Saskatoon, SK S7N 5C9, Canada

\* Corresponding author: E-mail: hbeyzaei@yahoo.com and hbeyzaei@uoz.ac.ir

Tel: +98 5431232186 / Fax: +98 5431232180

Received: 05-06-2017

## Abstract

Various biological properties of natural and synthetic pyrazole derivatives such as anti-inflammatory, antimicrobial, neuroprotective, anticonvulsant, antidepressant and anticancer activities encouraged us to propose a new, fast, green and eco-friendly procedure for the preparation of some novel 5-amino-3-(aryl substituted)-1-(2,4-dinitrophenyl)-1*H*-pyrazole-4-carbonitriles. They were efficiently synthesized *via* one-pot two-step process reaction of malononitrile, 2,4-dinitrophenylhydrazine and different benzaldehydes in deep eutectic solvent (DES) glycerol/potassium carbonate. The products yield and reaction times were considerably improved in the presence of applied DES. Antibacterial effects of all newly synthesized pyrazoles in comparison with several common antibiotics were evaluated against a variety of Gram-positive and Gram-negative pathogenic bacteria. In addition to, their inhibitory activities on three fungi were compared to some current antifungal agents. The moderate to good antimicrobial potentials particularly against fungi were observed in the major heterocyclic compounds according to the IZD, MIC, MBC and MFC results.

**Keywords:** Green synthesis; deep eutectic solvent; glycerol/potassium carbonate; polysubstituted pyrazoles; antibacterial and antifungal activities

## 1. Introduction

Pyrazoles are an important class of azoles containing two adjacent nitrogen atoms, which are found as major or minor scaffolds in various medicinal compounds and natural products. L- $\alpha$ -Amino- $\beta$ -(pyrazolyl-*N*)-propanoic acid and withasomnine, which were isolated from *Citrullus vulgaris* (watermelon) juice and from the roots of *Withania somnifera* Dun (Solanaceae), in fact, are two of the few naturally occurring pyrazoles that have found potential use as anti-diabetic and depressant agents in medicinal chemistry.<sup>1,2</sup> Pyrazofurin and formycin are natural C-nucleoside antibiotics that are used to treat viral infections as well as inhibition of tumor cells growth. Stanazolol is a synthetic anabolic steroid that can be applied for treatment of anaemia and hereditary angioedema. In addition to, the pyrazole ring as a part of the chemical structure of drugs such as antipyrine, celecoxib and betazole, plays an essential role in the relief of ear pain and swelling, improvement

of osteoarthritis signs, and treatment of bacterial and fungal infections (Figure 1).

Compounds containing pyrazole moiety exhibit a wide variety of biological and pharmacological activities including analgesic, neuroprotective, anticonvulsant, angiotensin converting enzyme (ACE) inhibitory, anti-angiogenesis, antioxidant and antiviral activities.<sup>3–9</sup> Numerous studies have also focused on antibacterial and antifungal properties of pyrazole derivatives.<sup>10–12</sup> In a research project, inhibitory activities of some heterocyclic Schiff bases derived from thiocarbohydrazide were assessed against various pathogenic bacterial and fungal strains *via* measurement of their inhibition zone diameters. One of the synthesized 1,2,4-triazines could block the growth of all selected microorganism.<sup>13</sup>

Various methods were proposed for the synthesis of pyrazole and their analogues.<sup>14–17</sup> In this regard, a solution of the appropriate triethylamine in 1,4-dioxane efficiently catalysed synthesis of pyridine, thiophene and 4*H*-pyrane

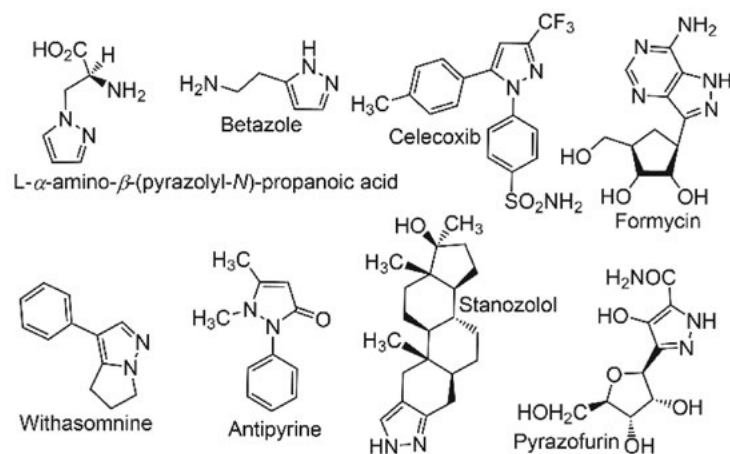


Figure 1. Natural products and drugs containing pyrazole moiety.

derivatives *via* one-pot or multicomponent protocols.<sup>18</sup> Similar procedures were designed to prepare pyrazole derivatives.<sup>19–24</sup> Most of these methods include simultaneous or multistep reaction of aldehyde, hydrazine and active methylene compounds under different conditions.<sup>25–29</sup> Recently, deep eutectic solvents (DESs) were widely applied as eco-friendly media or efficient catalysts in organic synthesis especially for the preparation of pyrazoles.<sup>30–32</sup> Glycerol/potassium carbonate is a new class of DES having its physical properties, such as surface tension, viscosity, density and refractive index, carefully measured.<sup>33</sup> In order to apply glycerol/ $K_2CO_3$  system in organic synthesis, some novel 5-amino-1-(2,4-dinitrophenyl)-1*H*-pyrazole-4-carbonitrile derivatives were prepared *via* the reaction of malononitrile, 2,4-dinitrophenylhydrazine and various benzaldehydes. The *in vitro* antimicrobial activities of synthesized derivatives were studied against a variety of pathogenic bacteria and fungi, as well as structure-activity relationships were expanded.

## 2. Experimental

### 2.1. Chemicals

All reagents, solvents, antibiotics and antifungal agents were purchased from commercial sources (Merck, Sigma and Aldrich), and used without further purification. The bacterial and fungal culture media were obtained from HiMedia. Melting points were determined with Kruss type KSP1N melting point meter and are uncorrected. Reaction progress was monitored by aluminium TLC plates pre-coated by silica gel with fluorescent indicator F254 using  $CH_2Cl_2/CH_3OH$  (9:1, v/v) as the mobile phase, being visualized under UV radiation (254 nm). FT-IR spectra of the products were collected using Bruker Tensor-27 FT-IR spectrometer.  $^1H$  and  $^{13}C$  NMR spectra were recorded at 400 and 100 MHz, respectively, on a Bruker FT-NMR Ultra Shield-400 spectrometer. Elemental analyses were performed for C, H and N on a Thermo Finnigan

Flash EA microanalyzer. DESs were prepared in various ratios of glycerol/ $K_2CO_3$  according to the procedures reported by Naser *et al.*<sup>33</sup> as follows: the mixture of different molar ratios of potassium carbonate and glycerol were vigorously stirred at 80 °C for 2 h to gain homogenous transparent colorless liquids.

### 2.1.1. General Procedure for the Synthesis of Pyrazoles 4a–f

A mixture of  $K_2CO_3$  (0.140 g, 0.001 mol) and glycerol (0.360 g, 0.004 mol) was stirred at 80 °C for 2 h to form a homogenous colorless liquid as DES1. Under the same conditions, the distilled water (0.25 mL), malononitrile (**1**) (0.660 g, 0.001 mol) and benzaldehydes **2a–f** (**2a**: 0.163 g, **2b**: 0.136 g, **2c**: 0.151 g, **2d**: 0.152 g, **2e**: 0.175 g, **2f**: 0.175 g; 0.001 mol) were respectively added to it. The intermediate benzylidene malononitriles **6a–f** were produced in 2 min. 2,4-Dinitrophenylhydrazine (**3**) (0.198 g, 0.001 mol) was added to the mixture. The reaction continued for another 18–28 min. The reaction mixture was cooled to room temperature, and neutralized with glacial acetic acid (0.120 g, 0.002 mol). After adding 1 mL of ethanol, the mixture was poured into ice-cold saturated aqueous NaCl (5 mL). The resulting precipitates were collected by filtration, washed respectively with distilled water (5 mL) and ethanol (5 mL), and recrystallized from methanol to afford pure pyrazoles **4a–f** as colored crystals.

#### 2.1.1.1. *N*-(4-(5-Amino-4-cyano-1-(2,4-dinitrophenyl)-1*H*-pyrazol-3-yl)phenyl)acetamide (**4a**).

Orange crystals; yield: 0.37 g (91%); m.p. 274–275 °C; IR (KBr)  $\nu$  3444, 3281 (NH<sub>2</sub>, NH), 2231 (C≡N), 1540, 1326 (NO<sub>2</sub>) cm<sup>-1</sup>;  $^1H$  NMR (400 MHz, DMSO-*d*<sub>6</sub>)  $\delta$  2.06 (s, 3H, CH<sub>3</sub>), 7.75 (d,  $J$  = 8.7 Hz, 2H, H-3'' and H-5''), 7.87 (d,  $J$  = 8.7 Hz, 2H, H-2'' and H-6''), 7.98 (d,  $J$  = 8.5 Hz, 1H, H-6'), 8.30 (d,  $J$  = 8.5 Hz, 1H, H-5'), 8.55 (s, 2H, NH<sub>2</sub>), 8.79 (s, 1H, H-3'), 10.48 (s, 1H, NH);  $^{13}C$  NMR (100 MHz, DMSO-*d*<sub>6</sub>)  $\delta$  24.67 (CH<sub>3</sub>), 78.00 (C-4), 114.21 (C≡N),

119.20 (C-3'' and C-5''), 123.43 (C-6'), 126.15 (C-1''), 128.60 (C-5'), 130.08 (C-3'), 132.78 (C-2'' and C-6''), 137.17 (C-1'), 141.91 (C-2'), 144.82 (C-4'), 145.38 (C-4''), 149.71 (C-3), 160.67 (C-5), 169.77 (C=O). Anal. Calcd. for  $C_{18}H_{13}N_7O_5$ : C, 53.07; H, 3.22; N, 24.07. Found: C, 53.01; H, 3.18; N, 24.12.

**2. 1. 1. 2. 5-Amino-1-(2,4-dinitrophenyl)-3-(4-methoxyphenyl)-1H-pyrazole-4-carbonitrile (4b).**

Orange crystals; yield: 0.32 g (85%); m.p. 217–219 °C; IR (KBr)  $\nu$  3456, 3326 (NH<sub>2</sub>), 2224 (C≡N), 1538, 1319 (NO<sub>2</sub>) cm<sup>-1</sup>; <sup>1</sup>H NMR (400 MHz, DMSO-*d*<sub>6</sub>)  $\delta$  3.88 (s, 3H, CH<sub>3</sub>), 7.03 (d, *J* = 8.7 Hz, 2H, H-3'' and H-5''), 7.71 (d, *J* = 8.7 Hz, 2H, H-2'' and H-6''), 8.01 (d, *J* = 8.4 Hz, 1H, H-6'), 8.38 (d, *J* = 8.4 Hz, 1H, H-5'), 8.62 (s, 2H, NH<sub>2</sub>), 8.82 (s, 1H, H-3'); <sup>13</sup>C NMR (100 MHz, DMSO-*d*<sub>6</sub>)  $\delta$  56.39 (CH<sub>3</sub>), 77.29 (C-4), 114.40 (C≡N), 115.67 (C-3'' and C-5''), 123.54 (C-6'), 124.59 (C-1''), 127.97 (C-5'), 130.04 (C-3'), 133.84 (C-2'' and C-6''), 137.13 (C-1'), 141.07 (C-2'), 144.93 (C-4'), 149.62 (C-3), 160.91 (C-5), 164.82 (C-4''). Anal. Calcd. for  $C_{17}H_{12}N_6O_5$ : C, 53.69; H, 3.18; N, 22.10. Found: C, 53.64; H, 3.17; N, 22.10.

**2. 1. 1. 3. 5-Amino-1-(2,4-dinitrophenyl)-3-(4-nitrophenyl)-1H-pyrazole-4-carbonitrile (4c).**

Yellow crystals; yield: 0.35 g (89%); m.p. 295–296 °C; IR (KBr)  $\nu$  3445, 3325 (NH<sub>2</sub>), 2228 (C≡N), 1543, 1318 (NO<sub>2</sub>) cm<sup>-1</sup>; <sup>1</sup>H NMR (400 MHz, DMSO-*d*<sub>6</sub>)  $\delta$  8.06 (d, *J* = 9.3 Hz, 1H, H-6'), 8.15 (d, *J* = 7.9 Hz, 2H, H-2'' and H-6''), 8.24 (d, *J* = 7.9 Hz, 2H, H-3'' and H-5''), 8.38 (d, *J* = 9.3 Hz, 1H, H-5'), 8.48 (s, 2H, NH<sub>2</sub>), 8.81 (s, 1H, H-3'); <sup>13</sup>C NMR (100 MHz, DMSO-*d*<sub>6</sub>)  $\delta$  89.02 (C-4), 117.37 (C≡N), 121.69 (C-2'' and C-6''), 123.34 (C-6'), 125.10 (C-3'' and C-5''), 130.35 (C-5'), 131.62 (C-3'), 136.32 (C-1'), 138.05 (C-1''), 142.82 (C-2'), 144.70 (C-4'), 147.29 (C-4''), 148.80 (C-3), 159.75 (C-5). Anal. Calcd. for  $C_{16}H_9N_7O_6$ : C, 48.62; H, 2.30; N, 24.80. Found: C, 48.68; H, 2.25; N, 24.84.

**2. 1. 1. 4. 5-Amino-1-(2,4-dinitrophenyl)-3-(2-hydroxy-3-methoxyphenyl)-1H-pyrazole-4-carbonitrile (4d).**

Brown crystals; yield: 0.33 g (84%); m.p. 198–199 °C; IR (KBr)  $\nu$  3537 (OH), 3428, 3287 (NH<sub>2</sub>), 2206 (C≡N), 1517, 1331 (NO<sub>2</sub>) cm<sup>-1</sup>; <sup>1</sup>H NMR (400 MHz, DMSO-*d*<sub>6</sub>)  $\delta$  3.77 (s, 3H, CH<sub>3</sub>), 6.76 (m, 1H, H-4''), 6.93 (m, 1H, H-5''), 7.31 (m, 1H, H-6''), 7.91 (d, *J* = 8.1 Hz, 1H, H-6'), 8.24 (d, *J* = 8.1 Hz, 1H, H-5'), 8.87 (s, 1H, H-3'), 9.43 (s, 2H, NH<sub>2</sub>), 11.63 (s, 1H, OH); <sup>13</sup>C NMR (100 MHz, DMSO-*d*<sub>6</sub>)  $\delta$  56.23 (CH<sub>3</sub>), 84.75 (C-4), 113.67 (C≡N), 116.95 (C-4''), 118.12 (C-1''), 119.58 (C-5''), 120.71 (C-6''), 123.31 (C-6'), 129.44 (C-5'), 129.99 (C-3'), 137.05 (C-1'), 140.90 (C-2'), 142.15 (C-2''), 144.64 (C-4'), 146.43 (C-3), 148.43 (C-3''), 162.71 (C-5). Anal. Calcd. for  $C_{17}H_{12}N_6O_6$ : C, 51.52; H, 3.05; N, 21.21. Found: C, 51.45; H, 3.11; N, 21.18.

**2. 1. 1. 5. 5-Amino-3-(2,4-dichlorophenyl)-1-(2,4-dinitrophenyl)-1H-pyrazole-4-carbonitrile (4e).**

Yellow crystals; yield: 0.36 g (86%); m.p. 184–186 °C; IR (KBr)  $\nu$  3443, 3287 (NH<sub>2</sub>), 2227 (C≡N), 1514, 1330 (NO<sub>2</sub>) cm<sup>-1</sup>; <sup>1</sup>H NMR (400 MHz, DMSO-*d*<sub>6</sub>)  $\delta$  7.46 (d, *J* = 5.8 Hz, 1H, H-5''), 7.66 (s, 1H, H-3''), 7.86 (d, *J* = 5.8 Hz, 1H, H-6''), 8.01 (d, *J* = 8.0 Hz, 1H, H-6'), 8.29 (d, *J* = 8.0 Hz, 1H, H-5'), 8.77 (s, 1H, H-3'), 8.98 (s, 2H, NH<sub>2</sub>); <sup>13</sup>C NMR (100 MHz, DMSO-*d*<sub>6</sub>)  $\delta$  87.52 (C-4), 113.76 (C≡N), 123.21 (C-6'), 128.39 (C-5'), 128.77 (C-5''), 129.04 (C-1''), 130.06 (C-3'), 130.48 (C-6''), 131.40 (C-3''), 134.55 (C-2''), 135.81 (C-4'), 137.95 (C-1'), 139.16 (C-2'), 144.37 (C-4'), 144.65 (C-3), 157.17 (C-5). Anal. Calcd. for  $C_{16}H_8Cl_2N_6O_4$ : C, 45.85; H, 1.92; N, 20.05. Found: C, 45.90; H, 1.89; N, 19.98.

**2. 1. 1. 6. 5-Amino-3-(2,6-dichlorophenyl)-1-(2,4-dinitrophenyl)-1H-pyrazole-4-carbonitrile (4f).**

Orange crystals; yield: 0.37 g (88%); m.p. 256–257 °C; IR (KBr)  $\nu$  3443, 3287 (NH<sub>2</sub>), 2227 (C≡N), 1514, 1330 (NO<sub>2</sub>) cm<sup>-1</sup>; <sup>1</sup>H NMR (400 MHz, DMSO-*d*<sub>6</sub>)  $\delta$  7.44 (d, *J* = 6.1 Hz, 1H, H-4''), 7.58 (t, *J* = 6.1 Hz, 2H, H-3''), 7.96 (d, *J* = 8.4 Hz, 1H, H-6'), 8.40 (d, *J* = 8.4 Hz, 1H, H-5'), 8.83 (s, 1H, H-3'), 9.01 (s, 2H, NH<sub>2</sub>); <sup>13</sup>C NMR (100 MHz, DMSO-*d*<sub>6</sub>)  $\delta$  84.86 (C-4), 117.36 (C≡N), 123.28 (C-6'), 126.36 (C-1''), 130.48 (C-5'), 130.06 (C-3'' and C-5''), 130.61 (C-4''), 131.41 (C-3'), 131.64 (C-2'' and C-6''), 138.21 (C-1'), 140.90 (C-2'), 144.35 (C-4'), 144.89 (C-3), 158.66 (C-5). Anal. Calcd. for  $C_{16}H_8Cl_2N_6O_4$ : C, 45.85; H, 1.92; N, 20.05. Found: C, 45.81; H, 1.87; N, 20.10.

**2. 2. In vitro Antimicrobial Assay**

Gram-negative bacterial strains including *Pseudomonas aeruginosa* (PTCC 1310), *Shigella flexneri* (PTCC 1234), *Shigella dysenteriae* (PTCC 1188), *Proteus mirabilis* (PTCC 1776), *Proteus vulgaris* (PTCC 1079), *Salmonella enterica subsp. enterica* (PTCC 1709) and *Salmonella typhi* (PTCC 1609); Gram-positive bacterial strains including *Streptococcus pyogenes* (PTCC 1447), *Streptococcus agalactiae* (PTCC 1768), *Streptococcus pneumoniae* (PTCC 1240), *Staphylococcus epidermidis* (PTCC 1435) and *Rhodococcus equi* (PTCC 1633); and fungi including *Aspergillus fumigatus* (PTCC 5009), *Candida albicans* (PTCC 5027) and *Fusarium oxysporum* (PTCC 5115) were prepared from the Persian Type Culture Collection (PTCC), Tehran, Iran. Initial concentrations of 17.6 µg/mL of positive controls were prepared in double-distilled water. Accordingly, heterocyclic compounds were dissolved in 10% DMSO to produce final concentrations of 10240 µg/mL. All the antibiogram assays were repeated at least three times. The results were reported as the mean of three independent experiments. Antibacterial and antifungal activities were determined using both broth microdilution and

disk diffusion methods, according to Clinical and Laboratory Standards Institute (CLSI) guidelines M07-A9, M26-A, M02-A11, M44-A and M27-A2 with a slight modification.<sup>34,35</sup>

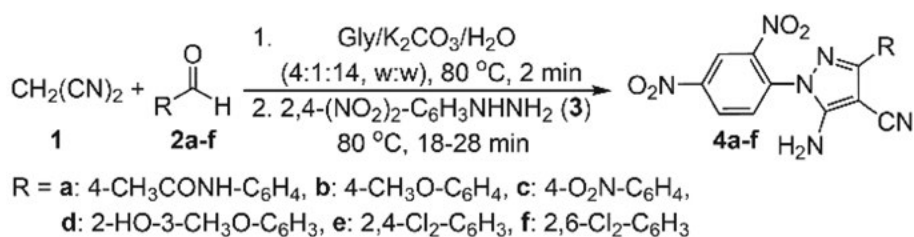
### 3. Results and Discussion

#### 3. 1. Chemistry

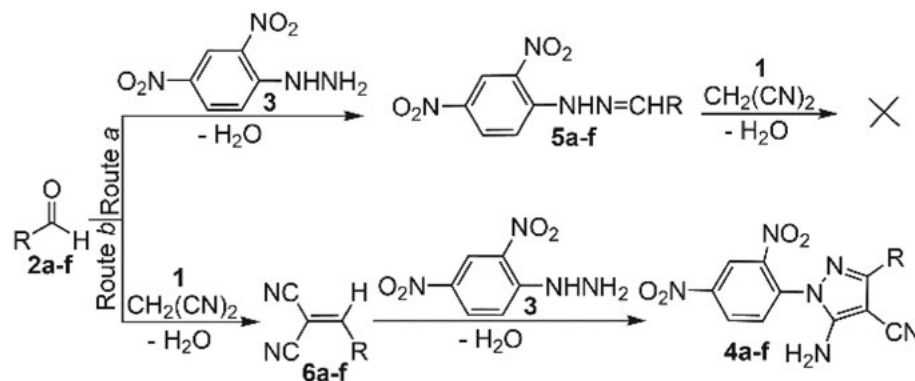
In this project, 5-amino-1*H*-pyrazole-4-carbonitriles were synthesized *via* an efficient, environmentally friendly, cost-effective and fast process. One-pot two-step reaction of malononitrile (**1**), mono or disubstituted benzaldehydes **2a–f** and 2,4-dinitrophenylhydrazine (**3**) produced polyfunctional pyrazoles **4a–f** in high yields (Scheme 1). The best results were obtained with glycerol/ $K_2CO_3$  as the reaction media and catalyst.

The reaction conditions were optimized in terms of solvent, presence or absence of the catalyst and temperature. 1 mmol each of malononitrile (**1**), 4-acetamidobenzaldehyde (**2a**) and 2,4-dinitrophenylhydrazine (**3**) were reacted under different conditions (Table 1). Glycerol as a green, cheap, non-toxic, inflammable and readily available solvent was the component present in all reactions. No target products were obtained when the reaction mixture was stirred at room temperature. The solubility of reagents was improved as the viscosity of glycerol largely decreased with increasing temperature to 80 °C. All efforts to perform three-component reaction in media containing glycerol alone were unsuccessful (Entries 1, 2). The formation of Schiff bases as major products in

glycerol showed that the presence of  $K_2CO_3$  catalyst is required for the synthesis of pyrazoles (Entries 3–6). There are two possible mechanisms to form the products, but it seems that only route *b* will afford the final compounds **4a–f** (Scheme 2). Schiff-base condensation reaction was observed in route *a* under some of the applied conditions. Colorless solutions of various molar ratios of potassium carbonate to glycerol (DES1, 1:4; DES2, 1:5; DES3, 1:6) were selected because their physical properties, including conductivity, surface tension, viscosity, refractive index, density and pH have been evaluated very well in the temperature range of 10–80 °C.<sup>33</sup> Three-component reaction in 0.5 g of each of these three DESs at room temperature have resulted in the Schiff bases and benzyldenemalononitriles as the major products (Entries 7, 9, 11), pyrazoles were obtained in 35–40% yields due to the increase of temperature to 80 °C (Entries 8, 10, 12). One-pot two-step process was screened according to route *b*. Two-step procedure was carried out in all DESs, the increase in molar ratios of glycerol reduced the product yield (Entries 13–18). This can be caused by the higher pH of DES1. The first stage reaction did not proceed completely at room temperature or at higher temperature even after 8 h, due to the lack of appearance of the intermediary benzyldenemalononitriles in the reaction media. Therefore, the next stage reaction of unconsumed reagents especially aldehydes with hydrazine was inevitable under these conditions (Entries 13, 15, 17). Adding water to achieve the final DES1/ $H_2O$  ratios of 1:2, 1:1 and 3:1 (w:w) has improved reaction time and product yield, the condensation reaction of malononitrile with aldehyde



Scheme 1. Total synthesis of polysubstituted pyrazoles **4a–f**.



Scheme 2. Proposed mechanisms for the formation of pyrazole derivatives **4a–f**.

Table 1. Optimization of the model reaction conditions.

Entry	Solvent	Condition	Time (min)	Yield (%)
1	Gly <sup>a</sup>	Three-component, rt	240	–
2	Gly	Three-component, 80 °C	120	Schiff base
3	Gly	One-pot two-step process (route a), rt	240	–
4	Gly	One-pot two-step process (route a), 80 °C	180	Schiff base
5	Gly	One-pot two-step process (route b), rt	240	–
6	Gly	One-pot two-step process (route b), 80 °C	180	Schiff base
7	DES1	Three-component, rt	210	Benzylidene, Schiff base
8	DES1	Three-component, 80 °C	90	40
9	DES2	Three-component, rt	180	Benzylidene, Schiff base
10	DES2	Three-component, 80 °C	90	37
11	DES3	Three-component, rt	150	Benzylidene, Schiff base
12	DES3	Three-component, 80 °C	90	35
13	DES1	One-pot two-step process (route b), rt	180	Benzylidene, Schiff base
14	DES1	One-pot two-step process (route b), 80 °C	120	53
15	DES2	One-pot two-step process (route b), rt	150	Benzylidene, Schiff base
16	DES2	One-pot two-step process (route b), 80 °C	150	47
17	DES3	One-pot two-step process (route b), rt	120	Benzylidene, Schiff base
18	DES3	One-pot two-step process (route b), 80 °C	180	42
19	DES1/H <sub>2</sub> O, 1:2 <sup>b</sup>	One-pot two-step process (route b), 80 °C	50	60
20	DES1/H <sub>2</sub> O, 1:1 <sup>b</sup>	One-pot two-step process (route b), 80 °C	35	75
21	DES1/H <sub>2</sub> O, 2:1 <sup>b</sup>	One-pot two-step process (route b), 80 °C	20	91
22	DES1/H <sub>2</sub> O, 3:1 <sup>b</sup>	One-pot two-step process (route b), 80 °C	40	68

<sup>a</sup> Gly as glycerol; <sup>b</sup> Ratios as w:w; The amount 0.5 g of solvents containing glycerol was used. Under the optimized conditions, mono and disubstituted benzaldehydes **2b–f** were also reacted with malononitrile (**1**) and 2,4-dinitrophenylhydrazine (**3**) to afford pyrazoles **4b–f**. The results are presented in Table 2.

Table 2. Synthesis of polysubstituted pyrazoles **4a–f** under optimized conditions.

Entry	R	Product	Time (min)	Yield <sup>a</sup> (%)
1	4-CH <sub>3</sub> CONH-C <sub>6</sub> H <sub>4</sub>	<b>4a</b>	20	91
2	4-CH <sub>3</sub> O-C <sub>6</sub> H <sub>4</sub>	<b>4b</b>	25	85
3	4-O <sub>2</sub> N-C <sub>6</sub> H <sub>4</sub>	<b>4c</b>	20	89
4	2-HO-3-CH <sub>3</sub> O-C <sub>6</sub> H <sub>3</sub>	<b>4d</b>	30	84
5	2,4-Cl <sub>2</sub> -C <sub>6</sub> H <sub>3</sub>	<b>4e</b>	25	86
6	2,6-Cl <sub>2</sub> -C <sub>6</sub> H <sub>3</sub>	<b>4f</b>	25	88

<sup>a</sup> All yields refer to isolated products

was thus completed within 2 min (Entries 19, 20, 22). The best results were obtained with DES1/H<sub>2</sub>O ratio of 2:1 (w:w), and this was considered as the optimized conditions (Entry 21).

The molecular structures and purity of the newly synthesized compounds were identified by NMR (<sup>1</sup>H and <sup>13</sup>C), FT-IR and elemental analysis (CHN). In FT-IR spectra, absorption bands attributed to symmetric and asymmetric stretching vibrations of amino groups appeared within  $\nu = 3428\text{--}3456$  and  $3281\text{--}3326$  cm<sup>-1</sup>, as well as stretching vibrations of nitro groups were recorded within  $\nu = 1514\text{--}1543$  and  $1318\text{--}1331$  cm<sup>-1</sup>. The presence of nitrile groups was deduced both from IR bonds and <sup>13</sup>C NMR signals appearing at  $\nu = 2206\text{--}2228$  cm<sup>-1</sup> and  $\delta$

113.67–117.37 ppm. In addition to these, <sup>1</sup>H NMR spectra and microanalytical data are in agreement with the chemical structures.

### 3. 2. Antimicrobial Evaluation

The *in vitro* inhibitory activities of the newly synthesized derivatives were evaluated against a variety of pathogenic bacteria and fungi. Amikacin, ceftriaxone and penicillin belonging to aminoglycoside, cephalosporin and penicillin antibiotics, respectively, were used as positive antibacterial controls, as well as antifungal agents including terbinafine, fluconazole and nystatin. The antimicrobial effects were presented as IZD, MIC, MBC and MFC values in Tables 3 and 4.

According to the data reported in Table 3, the derivatives were ordered based on the spread of inhibitory properties and the MIC values as follows: **4b** > **4e** > **4d** > **4c** > **4f** > **4a**. The 3-phenyl ring in pyrazole derivative **4b** was substituted by a methoxy group at *para* position, it was the only compound synthesized effective against *Streptococcus pyogenes* and *Proteus vulgaris*. The pyrazole **4a** containing *p*-acetamidophenyl substituent was effective only against Gram-negative *Salmonella typhi*. The inhibitory effects of derivative **4e** including 2,4-dichlorophenyl substituent were more significant than those of the derivative **4f** with 2,6-dichlorophenyl substituent. Among pyrazoles **4a–f**, the antibacterial properties against *Proteus mirabilis* and

Table 3. Antibacterial effects of synthesized pyrazoles and antibiotics.

Products	Bacteria	4a	4b	4c	4d	4e	4f	AMK <sup>a</sup>	CRO <sup>b</sup>	PEN <sup>c</sup>
1768	IZD <sup>d</sup>	–	9.23	8.53	–	–	–	17.20	–	–
	MIC <sup>e</sup>	–	512	512	–	–	–	2	–	–
	MBC <sup>f</sup>	–	1024	1024	–	–	–	8	–	–
1447	IZD	–	–	–	–	–	15.46	20.17	25.88	22.61
	MIC	–	–	–	–	–	64	1	0.5	0.25
	MBC	–	–	–	–	–	128	4	1	0.5
1709	IZD	–	10.11	–	11.50	10.10	11.51	10.10	32.64	14.03
	MIC	–	256	–	256	512	256	0.5	2	4
	MBC	–	512	–	512	1024	512	1	8	16
1188	IZD	–	15.87	–	–	–	–	20.98	–	–
	MIC	–	256	–	–	–	–	0.063	–	–
	MBC	–	128	–	–	–	–	0.125	–	–
1234	IZD	–	–	–	13.26	–	15.01	7.66	34.08	18.28
	MIC	–	–	–	1024	–	512	0.5	2	8
	MBC	–	–	–	2048	–	1024	4	4	16
1776	IZD	–	–	–	10.74	–	–	14.65	33.91	20.73
	MIC	–	–	–	128	–	–	0.25	0.063	8
	MBC	–	–	–	256	–	–	4	1	32
1609	IZD	12.21	13.89	–	11.67	14.78	–	19.31	30.43	10.95
	MIC	64	64	–	64	32	–	0.063	0.063	4
	MBC	128	128	–	128	64	–	0.25	0.125	16
1435	IZD	–	17.76	12.14	–	13.82	–	20.71	18.54	23.58
	MIC	–	16	64	–	64	–	0.25	0.5	0.5
	MBC	–	32	128	–	256	–	4	2	1
1310	IZD	–	12.10	13.67	–	14.10	–	19.07	16.21	–
	MIC	–	128	16	–	16	–	0.063	0.5	–
	MBC	–	256	32	–	32	–	0.063	1	–
1240	IZD	–	12.16	–	11.55	11.34	–	17.44	–	12.20
	MIC	–	256	–	256	256	–	1	–	8
	MBC	–	512	–	512	512	–	1	–	16
1079	IZD	–	11.78	–	–	–	–	22.42	–	12.82
	MIC	–	16	–	–	–	–	4	–	8
	MBC	–	64	–	–	–	–	4	–	32
1633	IZD	–	19.45	11.92	11.08	15.20	9.52	19.47	21.51	17.29
	MIC	–	32	32	256	128	128	1	2	8
	MBC	–	64	128	512	256	256	2	2	16

–: No noticeable antibacterial effects at selected highest concentration. <sup>a</sup> Amikacin, <sup>b</sup> Ceftriaxone, <sup>c</sup> Penicillin, <sup>d</sup> Inhibition zone diameter in mm, <sup>e</sup> Minimum inhibitory concentration in µg/mL, <sup>f</sup> Minimum bactericidal concentration in µg/mL.

*Shigella dysenteriae* were observed for the compounds **4d** and **4f**, respectively. Amikacin in comparison with two other antibiotics could block the growth of all bacteria.

The *in vitro* antifungal activities of prepared pyrazoles were also evaluated and the results were promising. No inhibitory effect was observed with derivative **4d** containing 2-hydroxy-3-methoxyphenyl substituent at the 3-position of the pyrazole ring. The dichloro compounds **4e** and **4f** had the same antifungal properties despite their different stereochemistry. Data gathered in Table 4 show that terbinafine has more remarkable effects than the others.

## 4. Conclusions

An efficient, one-pot two-step procedure was proposed and the synthesis of polysubstituted pyrazoles has been carried out. Some deep eutectic solvents including different molar ratios of potassium carbonate to glycerol were prepared and applied as reaction media and catalyst in this synthesis. The best results in terms of product yields and reaction times were achieved in molar ratios 1:4:14 of K<sub>2</sub>CO<sub>3</sub>/glycerol/H<sub>2</sub>O. Efficiency of DES K<sub>2</sub>CO<sub>3</sub>/glycerol in organic synthesis is currently under our investigation, and will be in focus of our future research. Furthermore, antimicrobial ac-

**Table 4.** Antifungal effects of synthesized pyrazoles and drugs.

Products	Fungi	4a	4b	4c	4d	4e	4f	TRB <sup>a</sup>	FLC <sup>b</sup>	NYT <sup>c</sup>
5115	IZD <sup>d</sup>	11.56	–	–	–	15.25	15.29	23.94	15.23	20.45
	MIC <sup>e</sup>	64	–	–	–	32	32	32	128	64
	MBC <sup>f</sup>	128	–	–	–	64	64	64	256	128
5027	IZD	21.87	14.77	14.71	–	–	–	36.24	14.81	–
	MIC	64	32	32	–	–	–	32	256	–
	MBC	128	64	64	–	–	–	64	512	–
5009	IZD	–	23.57	–	–	–	–	29.18	21.13	20.52
	MIC	–	512	–	–	–	–	32	32	32
	MBC	–	1024	–	–	–	–	32	64	128

–: No noticeable antibacterial effects at selected highest concentration. <sup>a</sup> Terbinafine, <sup>b</sup> Fluconazole, <sup>c</sup> Nystatin, <sup>d</sup> Inhibition zone diameter in mm, <sup>e</sup> Minimum inhibitory concentration in µg/mL, <sup>f</sup> Minimum fungicidal concentration in µg/mL.

tivities of all synthesized derivatives were evaluated against a broad range of pathogenic bacteria and fungi. Based on the broad-spectrum inhibitory effects of the pyrazole **4b**, including 4-methoxy group on 3-aryl ring, it is suggested that benzaldehydes with small *para* electron donating substituents should be used to synthesize future active analogues.

## 5. Acknowledgements

This work was supported by the University of Zabol under Grant number UOZ-GR-9517-15.

## 6. References

- F. F. Noe, L. Fowden, *Nature* **1959**, *184*, 69–70. DOI:10.1038/184069a0
- A. A. Wube, E. M. Wenzig, S. Gibbons, K. Asres, R. Bauer, F. Bucar, *Phytochemistry* **2008**, *69*, 982–987. DOI:10.1016/j.phytochem.2007.11.001
- S. Domiati, A. El-Mallah, A. Ghoneim, A. Bekhit, H. A. El Razik, *Inflammopharmacology* **2016**, *24*, 163–172. DOI:10.1007/s10787-016-0270-7
- G. Cocconcelli, E. Diodato, A. Caricasole, G. Gaviraghi, E. Genesio, C. Ghiron, L. Magnoni, E. Pecchioli, P. V. Plazzi, G. C. Terstappen, *Bioorg. Med. Chem.* **2008**, *16*, 2043–2052. DOI:10.1016/j.bmc.2007.10.090
- M. J. Ahsan, H. Khalilullah, J. P. Stables, J. Govindasamy, *J. Enzyme Inhib. Med. Chem.* **2013**, *28*, 644–650. DOI:10.3109/14756366.2012.663364
- M. Bonesi, M. R. Loizzo, G. A. Statti, S. Michel, F. Tillequin, F. Menichini, *Bioorg. Med. Chem. Lett.* **2010**, *20*, 1990–1993. DOI:10.1016/j.bmcl.2010.01.113
- K. M. Kasiotis, E. N. Tzanetou, S. A. Haroutounian, *Front. Chem.* **2014**, *2*, 78 (7 pp). DOI:10.3389/fchem.2014.00078
- Y.-F. Li, Z.-Q. Liu, *Free Radic. Biol. Med.* **2011**, *52*, 103–108. DOI:10.1016/j.freeradbiomed.2011.09.032
- D. Swarnkar, R. Ameta, R. Vyas, *European J. Biomed. Pharm. Sci.* **2016**, *3*, 427–431.
- R. E. El-Mekawy, *J. Heterocycl. Chem.* **2017**, *54*, 2367–2374. DOI:10.1002/jhet.2828
- S. Y. Hassan, *Molecules* **2013**, *18*, 2683–2711. DOI:10.3390/molecules18032683
- R. Surendra Kumar, I. A. Arif, A. Ahamed, A. Idhayadhull, *Saudi J. Biol. Sci.* **2016**, *23*, 614–620. DOI:10.1016/j.sjbs.2015.07.005
- K. M. El-Mahdy, A. M. El-Kazak, M. Abdel-Megid, M. Seada, O. Farouk, *Acta Chim. Slov.* **2016**, *63*, 18–25. DOI:10.17344/acsi.2015.1555
- F. Gosselin, P. D. O'Shea, R. A. Webster, R. A. Reamer, R. D. Tillyer, E. J. J. Grabowski, *Synlett* **2006**, *2006*, 3267–3270. DOI:10.1055/s-2006-956487
- Y. Kong, M. Tang, Y. Wang, *Org. Lett.* **2014**, *16*, 576–579. DOI:10.1021/ol403447g
- D. C. Schmitt, A. P. Taylor, A. C. Flick, R. E. Kyne Jr., *Org. Lett.* **2015**, *17*, 1405–1408. DOI:10.1021/acs.orglett.5b00266
- Q. Zhang, L.-G. Meng, K. Wang, L. Wang, *Org. Lett.* **2015**, *17*, 872–875. DOI:10.1021/ol503735c
- R. M. Mohareb, N. Y. M. Abdo, F. O. Al-farouk, *Acta Chim. Slov.* **2017**, *64*, 117–128. DOI:10.17344/acsi.2016.2920
- J.-A. Jiang, C.-Y. Du, C.-H. Gu, Y.-F. Ji, *Synlett* **2012**, *23*, 2965–2968. DOI:10.1055/s-0032-1317668
- A. Kamal, K. N. V. Sastry, D. Chandrasekhar, G. S. Mani, P. R. Adiyala, J. B. Nanubolu, K. J. Singarapu, R. A. Maurya, *J. Org. Chem.* **2015**, *80*, 4325–4335. DOI:10.1021/jo502946g
- N. Panda, A. K. Jena, *J. Org. Chem.* **2012**, *77*, 9401–9406. DOI:10.1021/jo301770k
- G. C. Senadi, W.-P. Hu, T.-Y. Lu, A. M. Garkhedkar, J. K. Vandavasi, J.-J. Wang, *Org. Lett.* **2015**, *17*, 1521–1524. DOI:10.1021/acs.orglett.5b00398
- S. Specklin, E. Decuyppere, L. Plougastel, S. Aliani, F. Taran, *J. Org. Chem.* **2014**, *79*, 7772–7777. DOI:10.1021/jo501420r
- L.-L. Wu, Y.-C. Ge, T. He, L. Zhang, X.-L. Fu, H.-Y. Fu, H. Chen, R.-X. Li, *Synthesis* **2012**, *44*, 1577–1583. DOI:10.1055/s-0031-1290772
- A. Hasaninejad, S. Firoozi, *Mol. Divers.* **2013**, *17*, 459–469. DOI:10.1007/s11030-013-9445-y
- S. Kumari, A. Shekhar, D. D. Pathak, *New J. Chem.* **2016**, *40*, 5053–5060. DOI:10.1039/C5NJ03380B

27. M. O. M'hamed, O. K. Alduaij, *Asian J. Chem.* **2016**, *28*, 543–547. DOI:10.14233/ajchem.2016.19397
28. F. Nemati, S. H. Nikkhah, A. Elhampour, *Chin. Chem. Lett.* **2015**, *26*, 1397–1399. DOI:10.1016/j.ccllet.2015.07.009
29. S. Yadav, P. Rai, M. Srivastava, J. Singh, K. P. Tiwari, J. Singh, *Tetrahedron Lett.* **2015**, *56*, 5831–5835. DOI:10.1016/j.tetlet.2015.07.039
30. M. Capua, S. Perrone, F. M. Perna, P. Vitale, L. Troisi, A. Salomone, V. Capriati, *Molecules* **2016**, *21*, 924 (11 pp). DOI:10.3390/molecules21070924
31. S. B. Katariya, *Asian J. Pharm. Sci. Tech.* **2015**, *5*, 199–201.
32. A. Moshtaghi Zonouz, D. Moghani, *Synth. Commun.* **2016**, *46*, 220–225. DOI:10.1080/00397911.2015.1129668
33. J. Naser, F. Mjalli, B. Jibril, S. Al-Hatmi, Z. Gano, *Int. J. Chem. Eng. Appl.* **2013**, *4*, 114–118. DOI:10.7763/IJCEA.2013.V4.275
34. H. Beyzaei, M. Moghaddam-Manesh, R. Aryan, B. Ghasemi, A. Samzadeh-Kermani, *Chem. Pap.* **2017**, *71*, 1685–1691. DOI:10.1007/s11696-017-0163-2
35. S. Arikan, *Med. Mycol.* **2007**, *45*, 569–587. DOI:10.1080/13693780701436794

## Povzetek

Različne biološke lastnosti naravnih in sintetičnih pirazolskih derivatov, kot so npr. delovanja proti vnetjem in mikrobom, nevrozaščitni učinki, antiepileptični ter antidepresivni učinki in aktivnosti proti rakom, so nas spodbudili, da smo predlagali novo, hitro, zeleno in ekološko sprejemljivo pot za pripravo nekaterih novih 5-amino-3-(aril substituiranih)-1-(2,4-dinitrofenil)-1*H*-pirazol-4-karbonitrilov. Učinkovito smo jih pripravili z enolončno dvostopenjsko reakcijo med malononitrilom, 2,4-dinitrofenilhidrazinom in različnimi benzaldehidi v globoko evtektičnem topilu (DES) glicerol/kalijev karbonat. Uporaba tovrstnega topilnega sistema je opazno povečala izkoristke produktov in skrajšala reakcijske čase. Raziskali smo antibakterijsko delovanje novopripravljenih pirazolov in rezultate primerjali z učinki več običajnih antibiotikov na izbrane Gram-pozitivne in Gram-negativne patogene bakterije. Raziskali smo tudi inhibitorno aktivnost proti trem glivam in jo primerjali z nekaterimi običajnimi učinkovinami proti glivam. Zmerno do dobro antimikrobno delovanje, predvsem pa delovanje proti glivam, smo opazili v nekaterih primerih naših heterocikličnih spojin, kot je bilo razvidno iz izmerjenih IZD, MIC, MBC in MFC vrednosti.



Scientific paper

# Synthesis and Biological Evaluation of Some Novel 1,8-Naphthyridine Derivatives

Sraa Abu-Melha\*

\*Department of Chemistry, Faculty of Science of Girls, King Khaled University, Abha, Saudi Arabia

\* Corresponding author: E-mail: sraa201313@yahoo.com  
Tel: +966504757797

Received: 06-06-2017

## Abstract

A series of substituted 1,8-naphthyridine derivatives was synthesized to be used as cytotoxic and antioxidant agents by applying 1,4-dihydro-4-oxo-1,8-naphthyridine-3-carbohydrazide (**1**) as the starting material. Compound **1** was reacted with different reagents to afford the corresponding 3-heterarylcaryl-1,8-naphthyridine derivatives **3–19** which were tested for their *in vitro* cytotoxicity against Ehrlich Ascites Carcinoma, and antioxidant activity. Compound **15** showed the best cytotoxicity and antioxidant activity.

**Keywords:** 1,8-naphthyridine; quinazolone; pyrazole; cytotoxicity; antioxidant activity

## 1. Introduction

Studies on the synthesis of 1,8-naphthyridines have served as a fertile field of research in the perusal for anti-bacterial agents.<sup>1–3</sup> Nalidixic acid (1-ethyl-3-carboxy-7-methyl-1,8-naphthyridine-4-one) has been found to be effective particularly against gram negative bacteria found in chronic urinary tract infections.<sup>4</sup> 1,8-Naphthyridine derivatives were found to display moderate cytotoxic activity against murine p388 leukemia, when changes were carried out at N-1 and N-7 positions.<sup>5,6</sup> It has been reported that C-3 carboxamide derivatives with a spacer have shown good cytotoxicity along with anti-inflammatory activity.<sup>7</sup>

Pharmacologically, pyrazole and its derivatives represent one of the most important classes of organic heterocyclic compounds, possessing anti-bacterial, anti-fungal,<sup>8</sup> herbicidal<sup>9</sup> and anti-viral activities.<sup>10</sup>

Moreover, the chemistry of carbohydrazoles has gained increased interest in both synthetic organic chemistry and biological fields and has considerable value in many useful applications, such as the assessment process of the three dimensional ultra structure examination techniques of interphase nuclei and tissues, besides their therapeutic importance.<sup>11</sup>

## 2. Experimental

### 2. 1. Materials and Methods

#### 2. 1. 1. Chemicals and Reagents

All the chemicals and solvents used in this study were obtained from Merck (Germany) and Sigma-Aldrich chemical company (Germany).

#### 2. 1. 2. Instruments

All melting points were recorded on Gallenkamp electric melting point apparatus and are uncorrected. The IR spectra  $\nu$  cm<sup>-1</sup> (KBr) were recorded on Perkin-Elmer Infrared Spectrophotometer Model 157, Grating. The <sup>1</sup>H and <sup>13</sup>C NMR spectra were run on Varian Spectrophotometer at 400 MHz and 100 MHz using TMS as the internal reference and DMSO-*d*<sub>6</sub> as the solvent. Chemical shifts ( $\delta$ ) are given in ppm. The mass spectra (EI) were recorded on 70 eV with Kratos MS equipment and/or Varian MAT 311 A Spectrometer at Cairo University, Giza, Egypt, and at Assuit University Central Laboratory. Elemental analyses (C, H, and N) were carried out at the Microanalytical Center of Cairo University, Giza, Egypt (automatic analyzer CHNS, Vario ELIII-elementar, Ger-

many). The results were found to be in good agreement with the calculated values.

## 2. 2. Synthesis

### 2. 2. 1. Synthesis of 1,4-Dihydro-N-(2-methyl-4-oxoquinazolin-3(4H)-yl)-4-oxo-1,8-naphthyridine-3-carboxamide (3)

A mixture of separated or freshly prepared benzoxazine **2**<sup>12</sup> (1.16 g, 10 mmol) and 4-oxo-1,4-dihydro-1,8-naphthyridine-3-carbohydrazide (**1**) (2.04 g, 10 mmol) in ethanol (25 mL) containing glacial acetic acid (5 mL) was refluxed for 4 h. The formed precipitate was filtered off, dried and recrystallized from ethanol to give compound **3**. Yield 63%; White crystal; m.p. 289 °C; IR (KBr):  $\nu_{\max}$  3230–3238 (br, 2 NH), 1668, 1671 (C=O, amidic), 1614 ( $\alpha,\beta$ -unsaturated C=O),<sup>13</sup> 1569 (C=N)  $\text{cm}^{-1}$ ; <sup>1</sup>H NMR (DMSO-*d*<sub>6</sub>)  $\delta$  1.93 (s, 3H, CH<sub>3</sub>), 7.62–8.24 (m, 7H, Ar-H), 9.01 (s, 1H, C<sub>2</sub>-H of naphthyridine ring), 9.21 (s, 1H, NH), 10.66 (s, 1H, NH); <sup>13</sup>C NMR (DMSO-*d*<sub>6</sub>)  $\delta$  21.6, 113.8, 114, 121.1, 122.3, 123.9, 126.6, 127.8, 134.2, 138.1, 141.7, 148.2, 151.4, 152.6, 162.1, 164.4, 165.9, 176.8; MS (EI, 70 eV) *m/z* (%) 347 (M<sup>+</sup>, 4.03), 272 (6.05), 259 (5.26), 230 (10.31), 173 (61.90), 138 (8.82), 123 (8.09), 104 (62.02), 89 (9.44), 77 (100), 75 (17.03), 63 (24.58), 51 (67.43), 49 (13.12); Anal. calcd. for C<sub>18</sub>H<sub>13</sub>N<sub>5</sub>O<sub>3</sub> (347.33): C, 62.24; H, 3.77; N, 20.16. Found: C, 62.36; H, 3.59; N, 20.31.

### 2. 2. 2. Synthesis of Ethyl 3-(2-(4-Oxo-1,4-dihydro-1,8-naphthyridine-3-carbonyl)hydrazono)butanoate (4)

A mixture of compound **1** (2.04 g, 10 mmol) and ethyl acetoacetate (1.3 g, 10 mmol) was refluxed in ethanol (25 mL) containing drops of glacial acetic acid for 2 h. The reaction mixture was cooled to room temperature. The solid product that formed was filtered off, dried, and recrystallized from ethanol to give compound **4**. Yield 95%; pale yellow crystal; m.p. 209 °C; IR (KBr):  $\nu_{\max}$  3237–3255 (br, NH), 1724 (C=O of ester group), 1689 (C=O, amidic), 1625 ( $\alpha,\beta$ -unsaturated C=O), 1567 (C=N)  $\text{cm}^{-1}$ ; <sup>1</sup>H NMR (DMSO-*d*<sub>6</sub>)  $\delta$  0.91 (s, 3H, CH<sub>3</sub>), 1.38 (t, 3H, CH<sub>3</sub>), 2.35 (s, 2H, CH<sub>2</sub>), 4.25 (q, 2H, CH<sub>2</sub>), 7.60–8.24 (m, 3H, CH-pyridine ring), 8.61 (s, 1H, C<sub>2</sub>-H of naphthyridine ring), 10.81 (s, 1H, NH), 11.01 (s, 1H, NH); MS (EI, 70 eV) *m/z* (%) 316 (M<sup>+</sup>, 17.5), 271 (2.8), 245 (0.2), 229 (69.0), 204 (0.5), 202 (1.4), 189 (1.6), 173 (100), 145 (2.3), 104 (12.3), 76 (10.6); Anal. calcd. for C<sub>15</sub>H<sub>16</sub>N<sub>4</sub>O<sub>4</sub> (316.31): C, 56.96; H, 5.10; N, 17.71. Found: C, 56.96; H, 5.12; N, 17.93.

### 2. 2. 3. Synthesis of 3-(3-Methyl-5-oxo-4,5-dihydro-1H-pyrazole-1-carbonyl)-1,8-naphthyridin-4(1H)-one (5)

Compound **4** (3.16 g, 10 mmol) was refluxed in ethanol (30 mL) containing sodium metal (0.23 g, 10 mmol)

for 5 h, cooled to room temperature, and poured into ice cold water. The separated solid was filtered, dried, and recrystallized from ethanol to give **5**. Yield 59%; pale brown powder; m.p. >300 °C; IR (KBr):  $\nu_{\max}$  3134 (NH), 1669, 1674 (C=O, amidic), 1636 ( $\alpha,\beta$ -unsaturated C=O), 1606 (C=N)  $\text{cm}^{-1}$ ; <sup>1</sup>H NMR (DMSO-*d*<sub>6</sub>)  $\delta$  1.22 (s, 3H, CH<sub>3</sub>), 2.07 (s, 2H, CH<sub>2</sub>), 6.76–8.63 (m, 3H, CH-pyridine ring), 8.41 (s, 1H, C<sub>2</sub>-H of naphthyridine ring), 9.83 (s, 1H, NH); <sup>13</sup>C NMR (DMSO-*d*<sub>6</sub>)  $\delta$  26.5, 43.2, 113.8, 114, 122.3, 138, 141.7, 151.4, 152.6, 158.2, 161.4, 167.1, 176.8; MS (EI, 70 eV) *m/z* (%) 270 (M<sup>+</sup>, 0.26), 173 (0.4), 168 (2.07), 125 (0.64), 111 (8.76), 97 (0.63), 84 (13.67), 77 (1.54), 68 (4.23), 52 (100); Anal. calcd. for C<sub>13</sub>H<sub>10</sub>N<sub>4</sub>O<sub>3</sub> (270.24): C, 57.78; H, 3.73; N, 20.73. Found: C, 57.77; H, 3.64; N, 20.71.

### 2. 2. 4. Synthesis of 4-Oxo-N<sup>2</sup>-(4-oxopentan-2-ylidene)-1,4-dihydro-1,8-naphthyridine-3-carbohydrazide (6)

A mixture of **1** (2.04 g, 10 mmol) and acetylacetone (1.0 g, 10 mmol) was refluxed in ethanol (25 mL) containing a few drops of glacial acetic acid for 2 h. The reaction mixture was left to cool, and then poured into ice cold water. The solid product was filtered off, dried, and recrystallized from ethanol to give compound **6**. Yield 41%; dark yellow powder; m.p. >300 °C; IR (KBr):  $\nu_{\max}$  3251 (br, NH), 1743 (C=O, ketonic), 1681 (C=O, amidic), 1627 ( $\alpha,\beta$ -unsaturated C=O), 1569 (C=N), 1548 (C=C)  $\text{cm}^{-1}$ ; <sup>1</sup>H NMR (DMSO-*d*<sub>6</sub>)  $\delta$  1.20 (s, 3H, CH<sub>3</sub>), 2.11 (s, 3H, CH<sub>3</sub>), 2.54 (s, 2H, CH<sub>2</sub>), 8.48 (s, 1H, C<sub>2</sub>-H of naphthyridine ring), 7.62–8.76 (m, 3H, CH-pyridine ring), 10.49 (s, 1H, NH), 11.20 (s, 1H, NH); MS (EI, 70 eV) *m/z* (%) 286 (M<sup>+</sup>, 11.0), 285 (41.57), 148 (38.57), 134 (53.00), 117 (36.02), 77 (78.89), 64 (88.82), 50 (100), 49 (63.92), 45 (64.72); Anal. calcd. for C<sub>14</sub>H<sub>14</sub>N<sub>4</sub>O<sub>3</sub> (286.29): C, 58.73; H, 4.93; N, 19.57. Found: C, 58.72; H, 4.83; N, 19.69.

### 2. 2. 5. Synthesis of 3-(3,5-Dimethyl-1H-pyrazole-1-carbonyl)-1,8-naphthyridin-4(1H)-one (7)

A mixture of **6** (2.86 g, 10 mmol) and acetylacetone (1.0 g, 10 mmol) was refluxed in ethanol (30 mL) containing sodium metal (0.23 g, 10 mmol) for 4 h. The reaction mixture was cooled to room temperature, the separated solid filtered off, washed with a little cold ethanol and recrystallized from ethanol to give **7**. Yield 85%; pale yellow powder; m.p. sharing at 230 °C; IR (KBr):  $\nu_{\max}$  3205 (NH), 1706 (C=O, amidic), 1625 ( $\alpha,\beta$ -unsaturated C=O), 1567 (C=N), 1548 (C=C)  $\text{cm}^{-1}$ ; <sup>1</sup>H NMR (DMSO-*d*<sub>6</sub>)  $\delta$  1.74, 1.79 (2s, 6H, 2 CH<sub>3</sub>), 6.08 (s, 1H, CH), 7.45–8.21 (m, 3H, CH-pyridine ring), 8.47 (s, 1H, C<sub>2</sub>-H of naphthyridine ring), 10.12 (s, 1H, NH); <sup>13</sup>C NMR (DMSO-*d*<sub>6</sub>)  $\delta$  14.2, 19.6, 106.5, 114, 122.3, 125.5, 138, 140.3, 141.7, 151.4, 152.6, 153.1, 176.8, 193.9; MS (EI, 70 eV) *m/z* (%) 271 (M<sup>+</sup>+3,

0.8), 270 ( $M^{+2}$ , 0.5), 204 (9.8), 174 (12.9), 173 (100), 145 (3.3), 120 (0.4), 105 (56.2), 95 (0.2), 90 (4.1), 78 (76.5); Anal. calcd. for  $C_{14}H_{12}N_4O_2$  (268.27): C, 62.68; H, 4.51; N, 20.88. Found: C, 62.81; H, 4.60; N, 20.73.

## 2. 2. 6. Synthesis of *N'*-(2-Hydroxynaphthalen-1-yl)methylene)-4-oxo-1,4-dihydro-1,8-naphthyridine-3-carbohydrazide (8)

A mixture of **1** (2.04 g, 10 mmol) and 2-hydroxy-1-naphthaldehyde (1.72 g, 10 mmol) was refluxed in ethanol containing a catalytic amount of glacial acetic acid (5 drops) for 4 h. The reaction mixture was cooled to room temperature, the separated product filtered off, dried, and recrystallized from ethanol to give the hydrazone derivative **8**. Yield 92%; pale yellow sheets; m.p. 176 °C; IR (KBr):  $\nu_{\max}$  3450 (OH), 3330 (NH), 1702 (C=O, amidic), 1626 ( $\alpha,\beta$ -unsaturated C=O), 1574 (C=N)  $\text{cm}^{-1}$ ;  $^1\text{H}$  NMR (DMSO- $d_6$ )  $\delta$  1.89 (s, 1H, CH), 6.97–8.61 (m, 9H, Ar-H), 9.09 (s, 1H,  $C_2$ -H of naphthyridine ring), 9.21 (s, 1H, NH), 9.68 (s, 1H, NH), 12.24 (s, 1H, NH), 12.95 (s, 1H, OH); Anal. calcd. for  $C_{20}H_{14}N_4O_3$  (358.35): C, 67.03; H, 3.94; N, 15.63. Found: C, 67.29; H, 3.78; N, 15.57.

## 2. 2. 7. Synthesis of 3-(3H-Benzo[e]indazole-3-carbonyl)-1,8-naphthyridin-4(1H)-one (9)

### Pathway 1

Compound **8** (3.58 g, 10 mmol) was refluxed in ethanol containing a few drops of piperidine or triethylamine for 4 h. The reaction mixture was cooled to room temperature, the separated product filtered off, dried, and recrystallized from ethanol to give compound **9**.

### Pathway 2

An equimolar amount of **1** (2.04 g, 10 mmol) and 2-hydroxynaphthaldehyde (1.72 g, 10 mmol) in ethanol (25 mL) in the presence of a catalytic amount of piperidine or triethylamine (4 drops) or sodium ethoxide (10 mmol) was refluxed for 3 h. The reaction mixture was left to cool at room temperature overnight. The formed precipitate was filtered off, dried and recrystallized from ethanol to give compound **9**. Yield 83%; yellow powder; m.p. 291 °C; IR (KBr):  $\nu_{\max}$  3340 (NH), 1710 (C=O, amidic), 1622 ( $\alpha,\beta$ -unsaturated C=O), 1579 (C=N), 1549 (C=C)  $\text{cm}^{-1}$ ;  $^1\text{H}$  NMR (DMSO- $d_6$ )  $\delta$  8.08 (s, 1H,  $C_2$ -H of naphthyridine ring), 8.20 (s, 1H, CH-pyrazole ring), 7.72–8.31 (m, 9H, Ar-H), 11.24 (s, 1H, NH);  $^{13}\text{C}$  NMR(DMSO- $d_6$ )  $\delta$  113.5, 118.0, 121.6, 122.8, 123.6, 124.4, 124.7, 124.9, 125.7, 127.2, 127.3, 127.8, 134.6, 141.9, 151.2, 152.5, 161.7, 164.3, 177.5; MS (EI, 70 eV)  $m/z$  (%) 340 ( $M^+$ , 6.95), 208 (3.42), 170 (26.02), 152 (13.20), 128 (19.71), 115 (72.86), 89 (13.88), 77 (8.22), 62 (13.54), 51 (17.97), 45 (100); Anal. calcd. for  $C_{20}H_{12}N_4O_2$  (340.33): C, 70.58; H, 3.55; N, 16.46. Found: C, 70.67; H, 3.34; N, 16.62.

## 2. 2. 8. Synthesis of 3-(1H-Indazole-1-carbonyl)-1,8-naphthyridin-4(1H)-one(10)

An equimolar amounts of **1** (2.04 g, 10 mmol) and salicylaldehyde (1.22 g, 10 mmol) in ethanol (25 mL) in the presence of a catalytic amount of piperidine (4 drops) was refluxed for 3 h. The reaction mixture was left to cool at room temperature overnight. The formed precipitate was filtered off, dried and recrystallized from ethanol to give compound **10**. Yield 88%; white powder; m.p. 286 °C; IR (KBr):  $\nu_{\max}$  3073 (NH), 1667 (C=O, amidic), 1622 ( $\alpha,\beta$ -unsaturated C=O), 1569 (C=N), 1541 (C=C)  $\text{cm}^{-1}$ ;  $^1\text{H}$  NMR (DMSO- $d_6$ )  $\delta$  8.70 (s, 1H, CH-pyrazole ring), 9.08 (s, 1H,  $C_2$ -H of naphthyridine ring), 6.90–9.24 (m, 5H, Ar-H), 11.28 (s, 1H, NH);  $^{13}\text{C}$  NMR(DMSO- $d_6$ )  $\delta$  114, 115.4, 121.5, 121.9, 122.3, 123.9, 125.5, 127.6, 128.3, 138, 143.2, 151.4, 152.6, 153.1, 176.8, 193.9; Anal. calcd. for  $C_{16}H_{10}N_4O_2$  (290.28): C, 66.20; H, 3.47; N, 19.30. Found: C, 66.15; H, 3.56; N, 19.35.

## 2. 2. 9. Synthesis of 3-(3,4,6-Triamino-2H-pyrazolo[3,4-b]pyridine-2-carbonyl)-1,8-naphthyridin-4(1H)-one (13)

A mixture of **1** (2.04 g, 10 mmol) and 2-amino-prop-1-ene-1,1,3-tricarbonitrile (1.32 g, 10 mmol) in ethanol (25 mL) containing a few drops of glacial acetic acid (5 drops) was refluxed for 4 h. The reaction mixture was then cooled to room temperature and the obtained solid material filtered off, dried and recrystallized from ethanol to give pyrazolopyridine **13**. Yield 51%; pale brown powder; m.p. 288 °C; IR (KBr):  $\nu_{\max}$  3411, 3382 ( $\text{NH}_2$ ), 3228 (br, NH groups), 1671 (C=O, amidic), 1628 ( $\alpha,\beta$ -unsaturated C=O), 1608 (C=N), 1569 (C=C)  $\text{cm}^{-1}$ ;  $^1\text{H}$  NMR (DMSO- $d_6$ )  $\delta$  4.18 (s, 4H,  $\text{NH}_2$ ), 5.90 (s, 1H, CH), 8.08 (s, 1H,  $C_2$ -H of naphthyridine ring), 6.72–8.31 (m, 3H, CH-pyridine ring), 9.81 (s, 1H, NH), 11.60 (s, 2H, 2 C=NH);  $^{13}\text{C}$  NMR (DMSO- $d_6$ )  $\delta$  89.1, 95.1, 118.0, 121.6, 123.6, 134.6, 147.0, 151.2, 152.5, 153.7, 159.8, 161.7, 162.4, 164.3, 177.5; MS (EI, 70 eV)  $m/z$  (%) 336 ( $M^+$ , 38.85), 104 (37.62), 90 (35.08), 84 (33.29), 78 (82.65), 64 (46.06), 54 (40.92), 53 (100), 50 (38.25), 48 (42.52); Anal. calcd. for  $C_{15}H_{12}N_8O_2$  (336.31): C, 53.57; H, 3.60; N, 33.32. Found: C, 53.34; H, 3.53; N, 33.54.

## 2. 2. 10. Synthesis of 3-Amino-5-(methylthio)-1-(4-oxo-1,4-dihydro-1,8-naphthyridine-3-carbonyl)-1H-pyrazole-4-carbonitrile (15)

A mixture of **1** (2.04 g, 10 mmol) and 2-(bis(methylthio)methylene) malononitrile (1.7 g, 10 mmol) in ethanol (25 mL) containing a few drops of glacial acetic acid was refluxed for 4 h. The reaction mixture was then cooled to room temperature and the obtained solid material filtered off, dried and recrystallized from ethanol to give compound **15**. Yield 90%; yellow sheets; m.p. 254 °C; IR (KBr):  $\nu_{\max}$  3413, 3382 ( $\text{NH}_2$ ), 3226 (br, NH groups), 2200

(CN), 1670 (C=O, amidic), 1627 ( $\alpha,\beta$ -unsaturated C=O), 1608 (C=N), 1569 (C=C)  $\text{cm}^{-1}$ ;  $^1\text{H}$  NMR (DMSO- $d_6$ )  $\delta$  1.96 (s, 3H,  $\text{SCH}_3$ ), 4.52 (s, 2H,  $\text{NH}_2$ ), 9.05 (s, 1H,  $\text{C}_2$ -H of naphthyridine ring), 7.60–8.24 (m, 3H, CH-pyridine ring), 9.22 (s, 1H, NH), 10.66 (s, 1H, NH);  $^{13}\text{C}$  NMR (DMSO- $d_6$ )  $\delta$  16.9, 62.2, 113.8, 115.8, 118.0, 121.6, 134.6, 142.5, 152.6, 160.5, 161.7, 165.0, 177.5; MS (EI, 70 eV)  $m/z$  (%) 327 ( $\text{M}^+ + 1$ , 23.92), 294 (31.62), 253 (15.05), 230 (24.34), 173 (31.75), 147 (18.32), 111 (39.36), 105 (28.04), 97 (18.55), 88 (15.66), 71 (29.92), 65 (24.72), 61 (34.46), 56 (100), 50 (26.79); Anal. calcd. for  $\text{C}_{14}\text{H}_{10}\text{N}_6\text{O}_2\text{S}$  (326.33): C, 51.53; H, 3.09; N, 25.75. Found: C, 51.75; H, 3.13; N, 25.66.

### 2. 2. 11. Synthesis of 3-Imino-5-(4-methoxyphenylamino)-1-(4-oxo-1,4-dihydro-1,8-naphthyridine-3-carbonyl)-2,3-dihydro-1H-pyrazole-4-carbonitrile (16)

An equimolar amount of compound **15** (3.26 g, 10 mmol) and *p*-anisidine (1.23 g, 10 mmol) in ethanol (25 mL) in the presence of a few drops of piperidine was refluxed for 4 h. The reaction mixture was left to cool at room temperature overnight. The formed precipitate was filtered off, dried and recrystallized from ethanol to give compound **16**. Yield 65%; dark yellow powder; m.p. 282 °C; IR (KBr):  $\nu_{\text{max}}$  3227 (br, NH), 2200 (CN), 1669 (C=O, amidic), 1625 ( $\alpha,\beta$ -unsaturated C=O), 1600 (C=N), 1571 (C=C)  $\text{cm}^{-1}$ ;  $^1\text{H}$  NMR (DMSO- $d_6$ )  $\delta$  3.52 (s, 2H,  $\text{OCH}_3$ ), 9.05 (s, 1H,  $\text{C}_2$ -H of naphthyridine ring), 7.60–8.24 (m, 3H, CH-pyridine ring), 10.66 (s, 1H, NH), 10.82 (s, 1H, C=NH);  $^{13}\text{C}$  NMR (DMSO- $d_6$ )  $\delta$  48, 54.1, 113.5 (2C), 113.6, 113.8, 114, 115.4 (2C), 122.3, 134.9, 138, 141.7, 149.5, 151.4, 152.6, 159.6, 160, 162, 176.8; MS (EI, 70 eV)  $m/z$  (%) 401 ( $\text{M}^+$ , 9.49), 383 (5.77), 318 (20.98), 308 (15.70), 245 (6.26), 227 (8.00), 211 (5.27), 207 (30.15), 201 (16.45), 186 (14.92), 173 (30.74), 120 (8.80), 108 (13.52), 77 (43.49), 68 (27.50), 52 (100); Anal. calcd. for  $\text{C}_{20}\text{H}_{15}\text{N}_7\text{O}_3$  (401.38): C, 59.85; H, 3.77; N, 24.43. Found: C, 59.95; H, 3.86; N, 24.61.

### 2. 2. 12. Synthesis of 5-Amino-3-(4-nitrophenyl)-1-(4-oxo-1,4-dihydro-1,8-naphthyridine-3-carbonyl)-2,3-dihydro-1H-pyrazole-4-carbonitrile (17)

A mixture of **1** (2.04 g, 10 mmol) in ethanol (25 mL) containing a few drops of glacial acetic acid (5 drops) and 2-(4-nitrobenzylidene)malononitrile (1.99 g, 10 mmol) was refluxed for 3 h, then left to stand at room temperature overnight. The separated solid product was filtered off, dried and recrystallized from ethanol to give **17**. Yield 85%; dark yellow powder; m.p. 350 °C; IR (KBr):  $\nu_{\text{max}}$  3468–3335 ( $\text{NH}_2$ ), 1685 (C=O, amidic), 1629 ( $\alpha,\beta$ -unsaturated C=O), 1582 (C=N), 1550 (C=C), 1552, 1336 ( $\text{NO}_2$ )  $\text{cm}^{-1}$ ;  $^1\text{H}$  NMR (DMSO- $d_6$ )  $\delta$  2.71 (s, 2H,  $\text{NH}_2$ ), 5.29 (s, 1H,

CH), 9.11 (s, 1H,  $\text{C}_2$ -H of naphthyridine ring), 7.57–9.22 (m, 7H, Ar-H), 10.81 (s, 1H, NH), 12.28 (s, 1H, NH);  $^{13}\text{C}$  NMR (DMSO- $d_6$ )  $\delta$  59.7, 63.4, 113.8, 117.3, 118.0, 121.6, 125.1, 128.3, 134.6, 142.5, 145.9, 149.4, 152.5, 158.1, 160.5, 161.7, 177.5; MS (EI, 70 eV)  $m/z$  (%) 403 ( $\text{M}^+$ , 100), 319 (34.34), 266 (44.02), 218 (42.66), 212 (20.30), 204 (21.45), 146 (40.11), 141 (36.01), 105 (28.76), 97 (33.65), 60 (63.03); Anal. calcd. for  $\text{C}_{19}\text{H}_{13}\text{N}_7\text{O}_4$  (403.35): C, 56.58; H, 3.25; N, 24.31. Found: C, 56.71; H, 3.13; N, 24.26.

### 2. 2. 13. Synthesis of 5-Amino-3-(4-chlorophenyl)-1-(4-oxo-1,4-dihydro-1,8-naphthyridine-3-carbonyl)-2,3-dihydro-1H-pyrazole-4-carbonitrile (18)

Equimolar quantities of the starting material **1** (2.04 g, 10 mmol) in ethanol (25 mL) containing a few drops of glacial acetic acid and 2-(4-chlorobenzylidene)malononitrile (1.88 g, 10 mmol) were refluxed for 3 h, then left to stand at room temperature overnight. The separated solid product was filtered off, dried and recrystallized from ethanol to give **18**. Yield 93%; yellow powder; m.p. 307 °C; IR (KBr):  $\nu_{\text{max}}$  3399–3341 ( $\text{NH}_2$ ), 3260 (NH), 1679 (C=O, amidic), 1625 ( $\alpha,\beta$ -unsaturated C=O), 765 (C-Cl)  $\text{cm}^{-1}$ ;  $^1\text{H}$  NMR (DMSO- $d_6$ )  $\delta$  2.83 (s, 2H,  $\text{NH}_2$ ), 5.69 (s, 1H, CH), 9.09 (s, 1H,  $\text{C}_2$ -H of naphthyridine ring), 6.72–8.31 (m, 7H, Ar-H), 10.83 (s, 1H, NH), 11.40 (s, 1H, NH);  $^{13}\text{C}$  NMR (DMSO- $d_6$ )  $\delta$  113.8, 114, 118, 122.4, 125.8 (2C), 126.8 (2C), 131.2, 131.5, 135.5, 138, 141.6, 150, 151.4, 153.1, 161.5, 166.4, 176.2; MS (EI, 70 eV)  $m/z$  (%) 392 ( $\text{M}^+ - 1$ , 0.01), 205 (0.11), 189 (77.30), 173 (100), 144 (21.49), 117 (10.94), 104 (45.37), 77 (47.32), 62 (16.20), 50 (31.49); Anal. calcd. for  $\text{C}_{19}\text{H}_{13}\text{ClN}_6\text{O}_2$  (392.8): C, 58.10; H, 3.34; N, 21.40. Found: C, 58.06; H, 3.12; N, 21.38.

### 2. 2. 14. Synthesis of 3-(3,5-Diamino-1H-pyrazole-1-carbonyl)-1,8-naphthyridin-4(1H)-one (19)

#### Pathway 1

To a solution of **1** (2.04 g, 10 mmol) in ethanol (25 mL) containing a few drops of glacial acetic acid, cyanoacetamide (0.84 g, 10 mmol) was added and the reaction mixture was refluxed for 5 h. The solution was cooled to room temperature, and the formed precipitate was filtered off, dried and recrystallized from ethanol to give pyrazole derivative **19**.

#### Pathway 2

A mixture of **1** (2.04 g, 10 mmol) in ethanol (25 mL) containing a few drops of glacial acetic acid and malononitrile (0.66 g, 10 mmol) were refluxed for 3 h, then left to stand at room temperature overnight. The separated solid product was filtered off, dried and recrystallized from ethanol to give **19**. Yield 71%; gray powder; m.p. 255 °C; IR (KBr):  $\nu_{\text{max}}$  3441 ( $\text{NH}_2$ ), 3232 (br, NH groups), 1668 (amid-

ic C=O), 1634 ( $\alpha,\beta$ -unsaturated C=O), 1612 (C=N), 1570 (C=C)  $\text{cm}^{-1}$ ;  $^1\text{H NMR}$  (DMSO- $d_6$ )  $\delta$  4.01 (s, 4H, 2  $\text{NH}_2$ ), 6.37 (s, 1H, CH-pyrazole ring), 8.07 (s, 1H,  $\text{C}_2$ -H of naphthyridine ring), 7.72–8.31 (m, 3H, CH-pyridine ring), 10.20 (s, 1H, NH);  $^{13}\text{C NMR}$  (DMSO- $d_6$ )  $\delta$  78.6, 118, 121.6, 123.6, 134.6, 148.2, 151.2, 152.5, 161.7, 164.3, 177.5; MS (EI, 70 eV)  $m/z$  (%) 270 ( $\text{M}^+$ , 10), 173 (28.63), 105 (76.12), 95 (0.40), 77 (100), 67 (20.41), 52 (38.72), and 50 (42.40); Anal. calcd. for  $\text{C}_{12}\text{H}_{10}\text{N}_6\text{O}_2$  (270.25): C, 53.33; H, 3.73; N, 31.10. Found: C, 53.46; H, 3.64; N, 31.29.

### 2. 3. Antitumor Activity (or Cytotoxicity) Using *In Vitro* Ehrlich Ascites Assay

The isolated compounds were screened for their antitumor activity. The viability of the cells used in control experiments exceeded 95%. Different concentrations of the tested compounds were prepared (100, 50 and 25  $\mu\text{L}$  from 1 mg/mL in DMSO (< 00.05%, v/v) and complete to 1 mL using RPMI-1640 medium). 5-Fluorouracil (25  $\mu\text{g}/\text{mL}$ ) was prepared in 100  $\mu\text{L}$  DMSO and complete to 1 mL using RPMI-1640 medium. Ehrlich ascites Carcinoma (EAC) were derived from ascetic fluid from diseased mouse (purchased from National Cancer Institute, by National Medical Research Ethics Committee). Ascites fluid from the peritoneal cavity of the diseased mouse (containing Ehrlich cells) was aseptically aspirated. The cells were grown partly floating and partly attached in a suspension culture in RPMI 1640 medium, supplemented with 10% fetal bovine serum. They were maintained at 37  $^\circ\text{C}$  in a humidified atmosphere with 5%  $\text{CO}_2$  for 2 h. The viability of the cells was determined by the microscopical examination using a hemocytometer and using trypan blue stain (that stains only the dead cells).<sup>14</sup>

### 2. 4. Antioxidant Activity Screening Assay 2,2'-Azino-bis-3-ethylbenzthiazoline-6-sulfonic Acid Method

For each of the investigated compounds, 2 mL of ABTS solution (60  $\mu\text{M}$ ) was added to 3 mL  $\text{MnO}_2$  solution (25 mg/mL), all prepared in 5 mL aqueous phosphate buffer solution (pH 7; 0.1 M). The mixture was shaken, centrifuged, filtered, and the absorbance of the resulting green-blue solution (ABTS radical solution) at  $\lambda$  734 nm was adjusted to approximately 0.5. Then, 50  $\mu\text{L}$  of 2 Mm solution of the tested compound in spectroscopic grade

MeOH/phosphate buffer (1:1) was added. The absorbance was measured and the reduction in color intensity was expressed as inhibition percentage. L-Ascorbic acid was used as the standard antioxidant (positive control). Blank sample was run without ABTS and using MeOH/phosphate buffer (1:1) instead of the tested compounds. Negative control was run with ABTS and MeOH/phosphate buffer (1: 1) only.<sup>15,16</sup> The inhibition ratio (%) was calculated using the following formula:

$$(\%)\text{Inhibition} = \frac{A(\text{control}) - A(\text{test})}{A(\text{control})} \times 100 \quad (1)$$

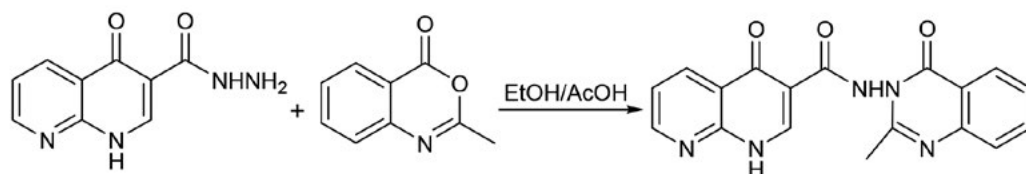
## 3. Results and Discussion

### 3. 1. Chemistry

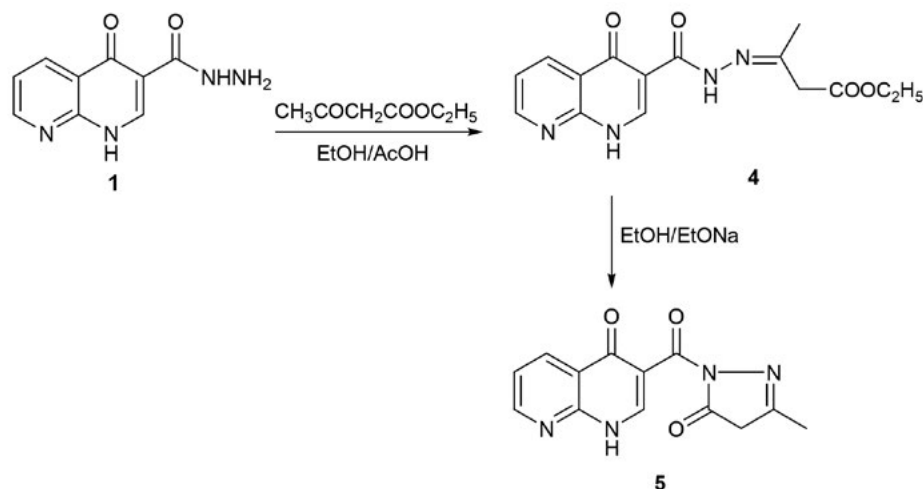
In view of these observations and in continuation of our previous work in quinazoline chemistry,<sup>17,18</sup> we synthesized some new heterocyclic compounds containing quinazoline moiety to evaluate their biological activities. The synthetic procedures adopted to obtain the target compounds are depicted in Schemes 1–10. The starting material, 1,4-dihydro-4-oxo-1,8-naphthyridine-3-carbohydrazide (**1**)<sup>19</sup> when heated with benzoxazine derivative **2**<sup>12</sup> in refluxing ethanol containing a catalytic amount of glacial acetic acid afforded 1,4-dihydro-*N*-(2-methyl-4-oxoquinazolin-3(4*H*)-yl)-4-oxo-1,8-naphthyridine-3-carboxamide (**3**) (Scheme 1).

The IR spectrum showed absorption bands at 3230–3238, 1668, 1671, 1614, and 1569  $\text{cm}^{-1}$  corresponding to stretching vibrations of two NH, amidic carbonyl groups,  $\alpha,\beta$ -unsaturated ketone, and C=N groups.  $^1\text{H NMR}$  spectrum revealed singlet signal at  $\delta$  1.93 ppm due to methyl protons, in addition to the classical pattern of 1,8-naphthyridine protons. The mass spectrum provided more evidence for the correct structure, which showed the molecular ion peak at  $m/z$  347 ( $\text{M}^+$ ).

Compound **1** when reacted with ethyl acetoacetate in refluxing ethanol containing a catalytic amount of glacial acetic acid afforded the acyclic intermediate ethyl 3-(2-(4-oxo-1,4-dihydro-1,8-naphthyridine-3-carbonyl)hydrazono)butanoate (**4**). Heating compound **4** in boiling ethanol containing sodium ethoxide leads to cyclization with the formation of the pyrazolone derivative 3-(3-methyl-5-oxo-4,5-dihydro-1*H*-pyrazole-1-carbonyl)-1,8-naphthyridin-4(1*H*)-one (**5**) (Scheme 2).



Scheme 1

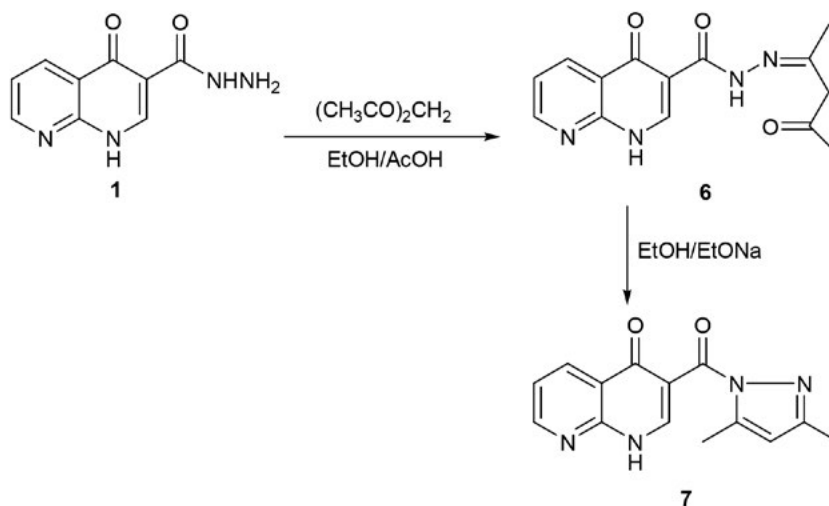


Scheme 2

Similarly, the hydrazide **1** when subjected to react with acetyl acetone in refluxing ethanol containing a catalytic amount of glacial acetic acid afforded the acyclic hydrazone derivative 4-oxo-*N'*-(4-oxopentan-2-ylidene)-1,4-dihydro-1,8-naphthyridine-3-carbohydrazide (**6**) which when refluxed with ethanol containing sodium ethoxide afforded the pyrazole derivative 3-(3,5-dimethyl-1*H*-pyrazole-1-carbonyl)-1,8-naphthyridin-4(1*H*)-one (**7**) (Scheme 3).

Structures **4–7** were proved by elemental and spectral analyses. The IR spectra of compounds **4** and **6** in general showed absorption frequencies at 1567–1569, 1724, and 1689  $\text{cm}^{-1}$  corresponding to C=N and two C=O due to ketonic (ester), and amidic carbonyl functional groups, while the  $^1\text{H}$  NMR spectrum of compound **4** showed a characteristic signal at  $\delta$  0.91 ppm as a singlet signal for  $\text{CH}_3$  protons,  $\delta$  1.38 ppm as a triplet signal for  $\text{CH}_2$  protons,  $\delta$  2.35 ppm as a singlet signal for  $\text{CH}_2$  protons and at  $\delta$  4.25 ppm as a quartet signal for  $\text{CH}_2$  protons besides the

aromatic protons of pyridine ring at  $\delta$  7.60–8.24 ppm, and a singlet signal at 8.61 ppm due to  $\text{C}_2\text{-H}$  of naphthyridine ring. On the other hand, the  $^1\text{H}$  NMR spectrum of compound **6** showed three singlet signals at  $\delta$  1.20, 2.11, 2.54 ppm corresponding to two methyl protons and  $\text{CH}_2$  protons, respectively. In addition, the mass spectrometry measurement gave  $m/z$  316 ( $\text{M}^+$ ) and 286 ( $\text{M}^+$ ) corresponding to the molecular ion peaks of compounds **4** and **6**, respectively. For the pyrazole derivative **5** the IR spectrum showed a new absorption band at 1669  $\text{cm}^{-1}$  corresponding to a new amidic carbonyl and absorption frequency at 1606  $\text{cm}^{-1}$  corresponding to C=N stretching frequency while the IR spectrum of compound **7** showed stretching frequency at 1567  $\text{cm}^{-1}$  due to C=N functional group.  $^1\text{H}$  NMR of compound **5** showed two new singlet signals at  $\delta$  1.22 and 2.07 ppm corresponding to methyl and methylene protons of pyrazolone moiety. On the other hand, the  $^1\text{H}$  NMR spectrum of compound **7** revealed three singlet signals at  $\delta$  1.74, 1.79, and 6.08 ppm attribut-



Scheme 3

able to two methyl groups and methine protons of pyrazole moiety. The mass spectra of compounds **5** and **7** showed their molecular ion peak at  $m/z$  270 ( $M^+$ ) and 270 ( $M^+ + 2$ ), respectively.

In a similar manner, it was found that 2-hydroxy-1-naphthaldehyde when reacted with hydrazide **1** in ethanol containing a catalytic amount of glacial acetic acid afforded the hydrazone derivative **8**. Hydrazone **8** cyclized to the corresponding pyrazole derivative 3-(3*H*-benzo[*e*]indazole-3-carbonyl)-1,8-naphthyridin-4-(1*H*)-one (**9**) when heated in ethanol containing a catalytic amount of piperidine or triethylamine (Scheme 4).

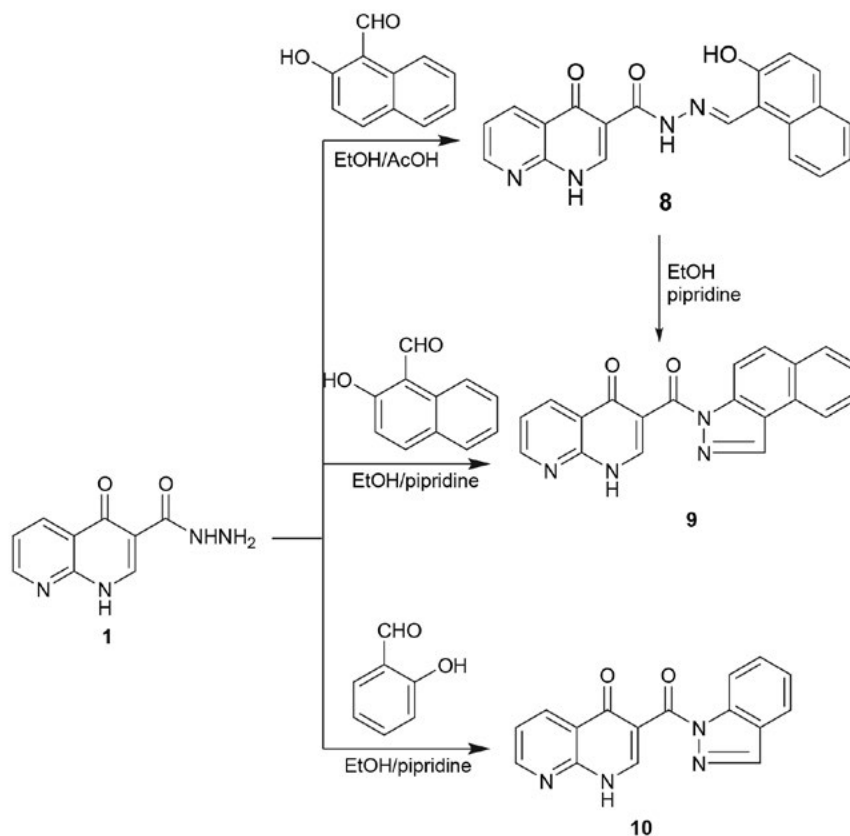
Structures **8** and **9** were proved based on the correct analytical and spectral data. The IR of compound **8** showed bands at 3450 and 1574  $\text{cm}^{-1}$  corresponding to the hydroxyl group and stretching vibration of C=N function. Compound **9** was confirmed by analytical and spectral data, beside it was confirmed chemically by an alternative synthesis. Thus, when hydrazide **1** reacted with 2-hydroxy-1-naphthaldehyde in refluxing ethanol containing a catalytic amount of piperidine or triethylamine or sodium ethoxide afforded directly the corresponding pyrazole derivative **9**. The IR spectrum of compound **9** showed bands at 1579  $\text{cm}^{-1}$  corresponding to C=N function, and the disappearance of the band around 3450  $\text{cm}^{-1}$  corresponding to hydroxyl group which indicates that the hydroxyl group was involved in the cyclization process. The  $^1\text{H}$  NMR spec-

trum showed a characteristic singlet signal at  $\delta$  8.20 ppm due to the pyrazole CH proton plus the classical  $^1\text{H}$  NMR pattern of the rest of 1,8-naphthyridine protons. The mass spectroscopic measurement gives an additional confirmation for compound **9** which showed the molecular ion peak at  $m/z$  340 ( $M^+$ ).

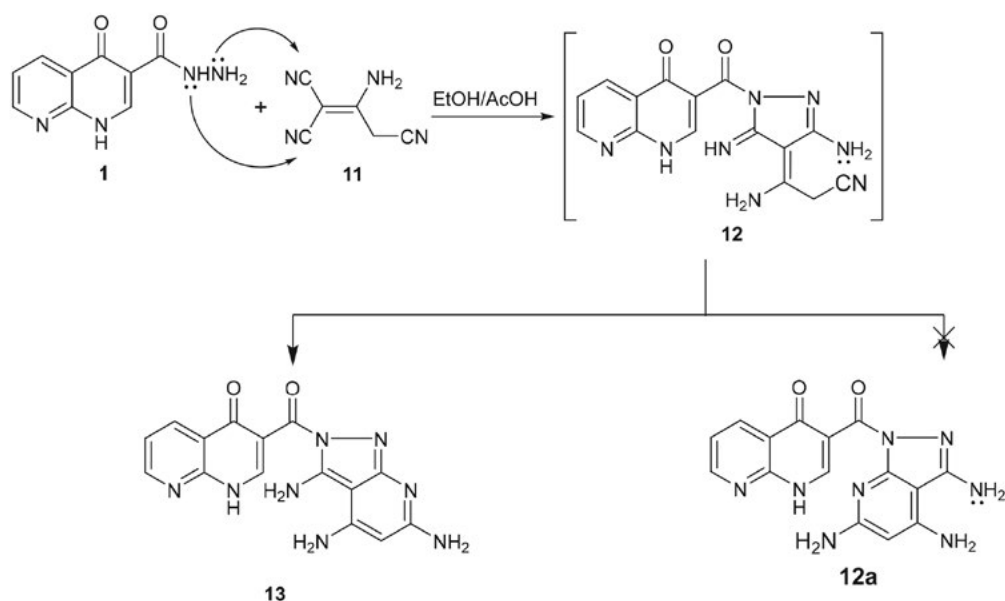
In addition, salicylaldehyde when heated directly with the hydrazide **1** in refluxing ethanol containing a catalytic amount of piperidine or triethylamine afforded the corresponding pyrazole derivative 3-(1*H*-indazole-1-carbonyl)-1,8-naphthyridin-4(1*H*)-one (**10**) (Scheme 4).

The IR spectrum of pyrazole derivative **10** showed a characteristic absorption band at 1569  $\text{cm}^{-1}$  corresponding to C=N function and the disappearance of any band around the region 3400  $\text{cm}^{-1}$  corresponding to hydroxyl group.  $^1\text{H}$  NMR spectrum showed singlet signal at  $\delta$  8.70 ppm attributable to the pyrazole proton. The mass spectroscopic measurement gives an additional confirmation for compound **10** which showed the molecular ion peak at  $m/z$  290 ( $M^+$ ).

An interesting reaction was observed when hydrazide **1** was heated with malononitrile dimmer (**11**) in refluxing ethanol containing a catalytic amount of glacial acetic acid affording the pyrazolopyridine 3-(3,4,6-triamino-2*H*-pyrazolo[3,4-*b*]pyridine-2-carbonyl)-1,8-naphthyridin-4(1*H*)-one (**13**) via the non isolable intermediate **12**. The reaction may be preceded first by addi-



Scheme 4



Scheme 5

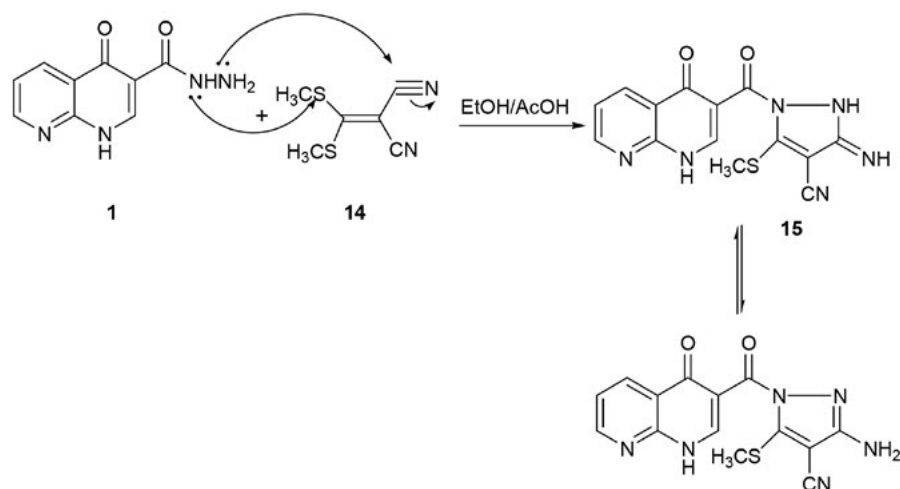
tion of  $\text{NHNH}_2$  moiety to the two cyano groups with the formation of a pyrazole ring. The reaction followed by the attack of the lone pair of electrons of  $\text{NH}_2$  of pyrazole ring to the cyano group as shown in the following mechanism affording the pyrazolopyridine **13** and not the other possibility **12a** because the exocyclic double bond will be more stable in the *Z*-form due to less steric hindrance. This fact confirms that nucleophilic addition occurred from  $\text{NH}_2$  group and not imino group. (Scheme 5).

The IR spectrum of compound **13** showed absorption bands at  $3411$ ,  $3382\text{ cm}^{-1}$  due to  $\text{NH}_2$  functions, besides a broad band at  $3228\text{ cm}^{-1}$  for  $\text{NH}$  groups,  $1671$  and  $1608\text{ cm}^{-1}$  corresponding to amidic  $\text{C}=\text{O}$ ,  $\text{C}=\text{N}$  and the disappearance of any band due to cyano functions at  $2220\text{ cm}^{-1}$  which indicate that the cyano group was involved in the cyclization reaction. The  $^1\text{H NMR}$  showed four singlet

exchangeable signals at  $\delta$  4.18, 9.81, and 11.60 ppm attributable to one amino group and three  $\text{NH}$  protons, respectively. The mass spectrum showed the molecular ion peak at  $m/z$  336 ( $M^+$ ).

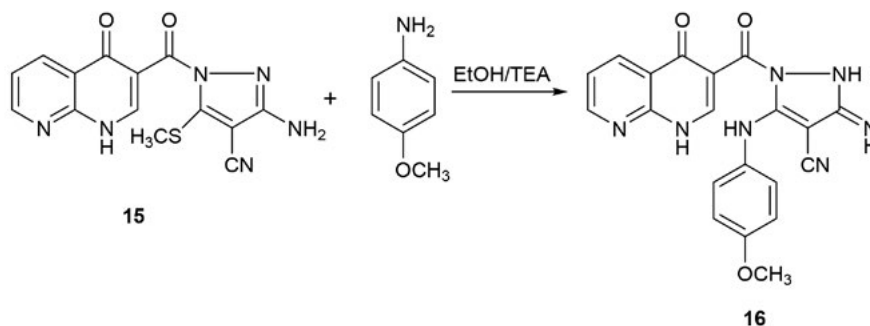
The hydrazide **1** when heated with dimethylthiomethylene malonate (**14**) in the presence of ethanol containing a few drops of glacial acetic acid afforded the pyrazole derivative **15** (Scheme 6). The reaction proceeds according to the proposed following mechanism.

The IR spectrum of compound **15** showed absorption bands at  $3413$ ,  $3382\text{ cm}^{-1}$  corresponding to  $\text{NH}_2$  group,  $3226\text{ cm}^{-1}$  due to  $\text{NH}$  function,  $1670$  and  $1608\text{ cm}^{-1}$  corresponding to amidic  $\text{C}=\text{O}$  and  $\text{C}=\text{N}$  and a characteristic absorption band at  $2220\text{ cm}^{-1}$  corresponding to  $\text{CN}$  group. The  $^1\text{H NMR}$  revealed a characteristic singlet signal of thiomethyl group at  $\delta$  1.96 ppm and three exchangeable



Scheme 6





Scheme 7

singlet signals at  $\delta$  4.52, 9.22, and 10.66 ppm attributable to  $\text{NH}_2$  and NH protons. The mass spectrum showed the molecular ion peak at  $m/z$  327 ( $M^+ + 1$ ).

In addition, when compound **15** was subjected to react with *p*-anisidine in ethanol containing a catalytic amount of triethylamine afforded 3-imino-5-(4-methoxyphenylamino)-1-(4-oxo-1,4-dihydro-1,8-naphthyridine-3-carbonyl)-2,3-dihydro-1*H*-pyrazole-4-carbonitrile (**16**) (Scheme 7).

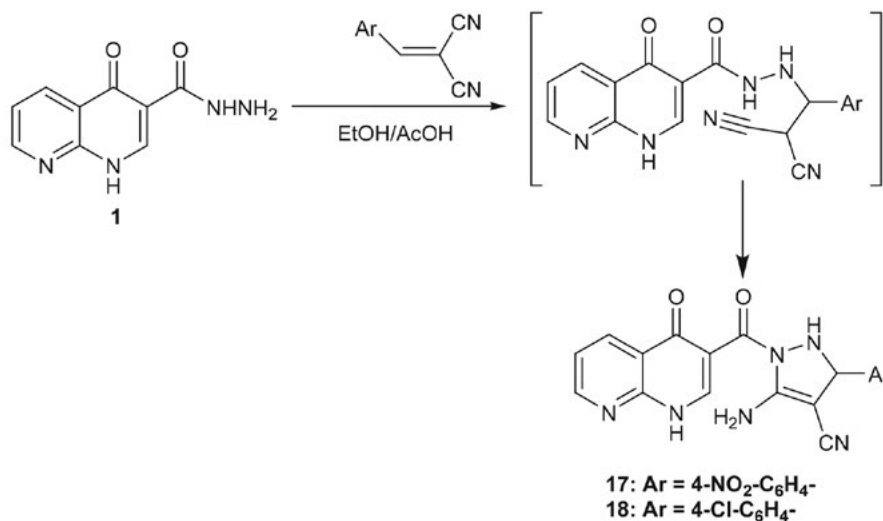
Also, it has been found that when hydrazide **1** reacted with *p*-nitrobenzylidene malononitrile and *p*-chlorobenzylidene malononitrile in ethanol containing a few drops of glacial acetic acid afforded the pyrazole derivatives 5-amino-3-(4-nitrophenyl)-1-(4-oxo-1,4-dihydro-1,8-naphthyridine-3-carbonyl)-2,3-dihydro-1*H*-pyrazole-4-carbonitrile (**17**) or 5-amino-3-(4-chlorophenyl)-1-(4-oxo-1,4-dihydro-1,8-naphthyridine-3-carbonyl)-2,3-dihydro-1*H*-pyrazole-4-carbonitrile (**18**), respectively (Scheme 8).

Structures **17** and **18** were proved based on the analytical and spectral data. The IR spectrum of both compounds showed, in general, characteristic absorption bands at 1582 and 1550  $\text{cm}^{-1}$  corresponding to stretching frequencies of C=N and C=C functions, respectively. The  $^1\text{H}$  NMR of both compounds showed a characteristic sin-

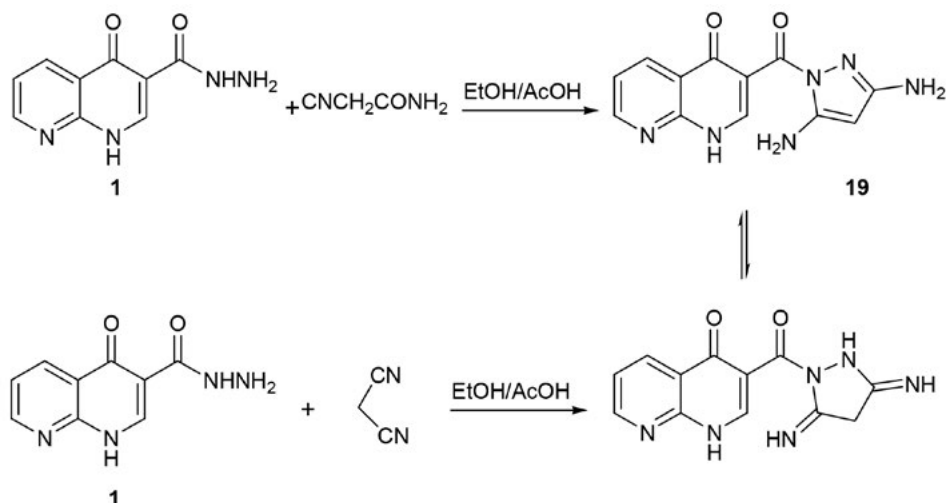
glet signal at  $\delta$  5.29 and 5.69 ppm attributable to methyne protons. The mass spectra of compounds **17** and **18** showed the molecular ion peak at  $m/z$  403 ( $M^+$ ) and 392 ( $M^+ - 1$ ), respectively.

Moreover, when hydrazide **1** reacted with cyanoacetamide in refluxing ethanol in the presence of a catalytic amount of glacial acetic acid afforded the diaminopyrazole derivative 3-(3,5-diamino-1*H*-pyrazole-1-carbonyl)-1,8-naphthyridin-4(1*H*)-one (**19**). The same compound was obtained when the hydrazide **1** was subjected to react with malononitrile under the same reaction conditions (Scheme 9).

Structure **19** was established based on both analytical and spectral data. The IR spectrum showed the classical pattern for carbonyl groups which appear at 1668 and 1634  $\text{cm}^{-1}$ , and showed the stretching vibration of C=N and C=C functions at 1612 and 1570  $\text{cm}^{-1}$ , respectively. On the other hand, the amino groups appeared as a tautomeric equilibrium with amino-imino groups and appeared at 3441 and 3232  $\text{cm}^{-1}$ , respectively.  $^1\text{H}$  NMR of compound **19** revealed two exchangeable signals at  $\delta$  4.01 and 10.20 ppm due to two  $\text{NH}_2$  and NH protons, in addition to two singlet signals at  $\delta$  6.37 and 8.07 ppm for CH-pyrazole and  $\text{C}_2$ -H of naphthyridine ring, besides aromatic protons of pyridine ring at  $\delta$  7.72–8.31 ppm. The mass spectrum gave



Scheme 8



Scheme 9

additional evidence for structure **19** which showed its molecular ion peak at  $m/z$  270 ( $M^+$ ).

## 3. 2. Pharmacology

### 3. 2. 1. Cytotoxicity Against Ehrlich Ascites Carcinoma

#### *Effect of Drugs on the Viability of Ehrlich Ascites Cells In Vitro*

The synthesis, antitumor evaluation and QSAR studies of novel pyrazol derivatives employed against Ehrlich Ascites Carcinoma (EAC, *in vitro*) cells are described. These novel analogues were molecularly designed with the goal of having significant potent cytotoxic effect against EAC cells.

Pyrazoles and related analogues were tested for cytotoxicity against EAC *in vitro*. EAC cells were used because they have a very well known established model of activity.<sup>20</sup> Results for the ED25 value of the active compounds are summarized in Table 1. The data showed clearly that compound **15** showed moderate activity (~45%) compar-

ing with the drug reference (5-FU, 98% activity). The rest of compounds showed weak activity. Thus, it would appear that introducing thiomethyl tautomeric moiety enhanced the cytotoxic properties.

Comparing the obtained cytotoxic activity of tested compounds in this study, the following structure–activity relationships (SAR) were postulated:

1) Compound **15** showed a mild cytotoxic activity (~45%), this may be due to the presence of thiomethyl and cyano groups which have toxic activity in nature.

2) All pyrazole derivatives showed weak activity at ED25. Thus the position and nature of substituents in the structure of pyrazole derivatives seems to modulate cytotoxic activity.

### 3. 2. 2. ABTS Antioxidant Activity Screening

The antioxidant activity assay employed here is one of the several assays that depends on measuring the consumption of stable free radicals, *i.e.* evaluates the free rad-

Table 1. *In vitro* cytotoxicity of pyrazol against Ehrlich Ascites Carcinoma

Compound No.	EAC Assay Dead cells (%) ED25 $\mu$ L (1 mg/mL)		Compound No.	EAC Assay Dead cells (%) ED25 $\mu$ L (1 mg/mL)	
	Control 0	5-FU 98		Control 0	5-FU 98
3	0		15	45	
7	28		16	19	
8	20		17	21	
9	14		18	17	
10	11		19	14	
13				23	

Where ED25 is the effective dose at 25  $\mu$ L of the compounds used.

The dead % refers to the % of the dead tumor cells and 5-Flu is 5-fluorouracil as a well known cytotoxic agent.

ical scavenging activity of the investigated component. The methodology assumes that the consumption of the stable free radical (X') will be determined by the reaction as follows:



The rate and/or the extent of the process measured in terms of the decrease in X' concentration, would be related to the ability of the added compounds to trap free radicals. The decrease in color intensity of the free radical solution due to scavenging of the free radical by the antioxidant material is measured colorimetrically at a specific wavelength. The assay employs the radical cation derived from 2,2'-azino-bis(3-ethyl benzthiazoline-6-sulfonic acid) (ABTS) as a stable free radical to assess antioxidant potential of the isolated compounds and extracts. The advantage of ABTS-derived free radical method over other methods is that the produced color remains stable for more than one hour and the reaction is stoichiometric. The inhibition ratio (%) was calculated using the following formula:

$$\text{(\%Inhibition)} = \frac{A(\text{control}) - A(\text{test})}{A(\text{control})} \times 100 \quad (3)$$

The antioxidant activity of some newly synthesized compounds was evaluated by ABTS method.<sup>21</sup> The data in Table 2 showed clearly that compound **15** demonstrated moderate antioxidant activities. Thus, it would appear that introducing sulfur atoms and the presence of thiomethyl tautomeric equilibrium enhances the antioxidant properties of 1,8-naphthyridine derivatives. By comparing the results obtained of antioxidant of the compound reported in this study to their structures, the following SAR was postulated: compound **15** was nearly in potent to vitamin C which may be attributed to the presence of amino and imino groups which trap the free radical X.

## 4. Conclusion

This work aimed to synthesize a new series of pyrazole derivatives containing 1,8-naphthyridine ring *via* carboxamide linkage. All the structures of the synthesized compounds were confirmed by different spectroscopic data and screened for their *in vitro* cytotoxicity against EAC and antioxidant activity. Results obtained show that compound **15** displayed the best cytotoxicity and antioxidant activity.

## 5. References

- H. Egawa, T. Miyamoto, A. Minamida, Y. Nishimura, H. Okada, H. Uno, T. Motosumoto, *J. Med. Chem.* **1984**, *27*, 1543–1548. DOI:10.1021/jm00378a004
- K. Kohima, M. Motoyoshi, *Japan Kotai Tokyo JP* **1988**, *01*,100,603; *Chem. Abstr.* **1988**, *109*, 189591.
- C. S. Cooper, P. L. Klock, D. T. W. Chu, D. J. Hardy, R. N. Swanson, J. J. Plattner, *J. Med. Chem.* **1992**, *35*, 1392–1398. DOI:10.1021/jm00086a007
- J. Nezval, K. Halocka, *Experientia* **1967**, *23*, 1043–1044. DOI:10.1007/BF02136439
- K. Tomita, Y. Tsuzuki, K. Shibamori, M. Tshima, F. Kajikawa, Y. Sato, S. Kashimoto, K. Chiba, K. Hino, *J. Med. Chem.* **2002**, *45*, 5564–5575. DOI:10.1021/jm010057b
- Y. Tsuzuki, K. Tomita, K. Shibamori, Y. Sato, S. Kashimoto, K. Chiba, *J. Med. Chem.* **2004**, *47*, 2097–2109. DOI:10.1021/jm0304966
- S. K. Srivastava, M. Jaggi, A. T. Singh, A. Madaan, N. Rani, M. Vishnoi, S. K. Agarwal, R. Mukherjee, A. C. Burman, *Bioorg. Med. Chem. Lett.* **2007**, *17*, 6660–6664. DOI:10.1016/j.bmcl.2007.08.006
- M. Lovu, C. Zalaru, F. Dumitrascu, C. Draghici, M. Moraru, E. Criste, *Farmaco.*, **2003**, *58*, 301–307. <http://www.sciencedirect.com/science/article/pii/S0014827X02000149>

Table 2. Antioxidant assay for some prepared new compounds.

Compound No.	Absorbance of samples	(%)Inhibition = $\frac{A(\text{control}) - A(\text{test})}{A(\text{control})} \times 100$ ABTS (% Inhibition)
Control of ABTS	0.47	0%
Ascorbic acid	0.06	87.0%
<b>3</b>	0.42	10.6%
<b>7</b>	0.31	34.0%
<b>8</b>	0.35	25.5%
<b>9</b>	0.36	23.4%
<b>10</b>	0.37	21.3%
<b>13</b>	0.31	34.0%
<b>15</b>	<b>0.19</b>	<b>59.6%</b>
<b>16</b>	0.35	25.5%
<b>17</b>	0.34	27.6%
<b>18</b>	0.35	25.5%
<b>19</b>	0.34	27.6%

9. R. N. Mahajan, F. H. Havaladar, P. S. Fernandes, *Indian J. Chem. Soc.*, **1991**, 68, 245–249.
10. P. G. Baraldi, S. Manfredini, R. Romagnoli, L. Stevanato, A. N. Zaid, R. Manservigi, *Nucleos. Nucleot. Nucleic Acid*, **1998**, 17, 2165–2171. DOI:10.1080/07328319808004307
11. K. M. El-Mahdy, A. M. El-Kazak, M. Abdel-Megid, M. Seada, O. Farouk, *Acta Chim. Slov.*, **2016**, 63, 18–25. DOI:10.17344/acsi.2015.1555
12. C. Párkányi, D. S. Schmidt, *J. Heterocycl. Chem.*, **2000**, 37, 725–729. DOI:10.1002/jhet.5570370409
13. K. Zaima, I. Koga, N. Iwasawa, T. Hosoya, Y. Hirasawa, T. Kaneda, I. S. Ismail, N. H. Lajis, H. Morita, *J. Nat. Med.*, **2013**, 67, 9–16. DOI:10.1007/s11418-012-0638-y
14. A. B. A. El-Gazzar, A. M. S. Youssef, M. M. Youssef, A. A. Abu-Hashem, F. A. Badria, *Eur. J. Med. Chem.* **2009**, 44, 609–624. DOI:10.1016/j.ejmech.2008.03.022
15. F. Badria, M. Ameen, M. Akl, *Z. Naturforschung*, **2007**, 62(9/10), 656–660. DOI:10.1515/znc-2007-9-1005
16. A. A. Fadda, A. El-Shafei, A. M. Khalil, T. A. E. Ameen, F. A. Badria, *Bioorg. Med. Chem.* **2009**, 17, 5096–105. DOI:10.1016/j.bmc.2009.05.053
17. S. S. El-Morsy, A. A. Fadda, M. S. El-Houssini, *Indian J. Chem. Soc.* **1988**, 65, 699–701.
18. A. A. Fadda, H. A. Etman, F. A. Amer, M. Barghout, K. S. Mohamed, *J. Chem. Tech. & Biotech.* **1995**, 62, 170–177. DOI:10.1002/jctb.280620210
19. A. A. Fadda, A. M. El Defrawy, S. A. El-Hadidy, *Amer. J. Org. Chem.* **2012**, 2, 87–96. DOI:10.5923/j.ajoc.20120204.03
20. K. Karrer, J. R. Rtjbini, *Pharmacology*, **1965**, 13, 124–130. DOI:10.1159/000135602
21. E. Lissi, B. Modak, R. Torres, J. Escobar, A. Urzua, *Free Radical Res.* **1999**, 30, 471–477. DOI:10.1080/10715769900300511

## Povzetek

S pomočjo 1,4-dihidro-4-okso-1,8-naftiridin-3-karbohidrazida (**1**) kot izhodne spojine smo pripravili serijo substituiranih 1,8-naftiridinskih derivatov ter jih uporabili kot citotoksične in antioksidativne spojine. Spojino **1** smo reagirali z različnimi reagenti in tako pripravili ustrezne 3-heteroarilkarbonil-1,8-naftiridinske derivative **3–19**, ki smo jih testirali za *in vitro* citotoksičnost proti Ehrlichovim ascitnim karcinomom in za antioksidativno aktivnost. Spojina **15** je pokazala najboljše citotoksične in antioksidativne lastnosti.

Scientific paper

# Preparation and Characterization of Chromium Doped Ni-Cu-Zn Nano Ferrites

Bजारंग लखमन शिंदे,<sup>1</sup> लखमन अप्पा धले,<sup>2</sup> Venkat S. Suryavanshi<sup>3</sup> and Kishan Shankarrao Lohar<sup>2\*</sup>

<sup>1</sup>Department of Chemistry, Waghire College, Saswad Dist: Pune, 412301 (M.S.) India

<sup>2</sup>Department of Chemistry, Shrikrishna Mahavidyalaya, Gunjoti, 413606, Dist: Osmanabad (M.S.) India

<sup>3</sup>Department of Chemistry, Shri Chatrapati Shivaji College, Omerga, Dist: Osmanabad 413 613 (M.S.) India

\* Corresponding author: E-mail: kslohar@rediffmail.com

Received: 07-06-2017

## Abstract

Chromium doped Ni-Cu-Zn nano ferrites with chemical formula  $\text{Ni}_{0.2}\text{Cu}_{0.2}\text{Zn}_{0.6}\text{Fe}_{2-x}\text{Cr}_x\text{O}_4$  ( $x = 0.0, 0.2, 0.4, 0.6, 0.8,$  and  $1.0$ ) were prepared by using sol-gel auto combustion method. The prepared precursors of Chromium substituted Ni-Cu-Zn ferrites were sintered at  $500\text{ }^\circ\text{C}$  for 4h. Compositional stoichiometry were confirmed from EDAX patterns. The XRD data revealed that the all samples possess a single phase cubic spinel structure. The Lattice constant, X-ray density, hopping lengths and crystallite size determined from XRD data decreases with increase in  $\text{Cr}^{3+}$  concentration. The IR spectra show two major absorption bands, high frequency band  $\nu_1 \approx 600\text{ cm}^{-1}$  and low frequency band  $\nu_2 \approx 450\text{ cm}^{-1}$  attributed to the stretching vibration of tetrahedral and octahedral sites respectively. The surface morphology of the prepared samples was studied by Scanning Electron Microscopy and Transmission Electron Morphology.

**Keywords:** Spinel ferrite, Sol-gel auto-combustion; Thermal analysis, Morphology, X-ray diffraction

## 1. Introduction

Nano ferro spinels are of great interest for addressing relationship between physical properties and their crystal structure. Due to their reduced sizes, these nanoparticles may possess novel and/or improved properties in comparison to the bulk materials. This has renewed interest to study different properties of pure and mixed spinel ferrite systems in nanocrystalline regime. Transition metal ferrites both doped and undoped are attractive candidates for a wide range of applications including catalysis,<sup>1-4</sup> and several devices such as antennas, permanent magnets, memory storage devices, microwave devices, telecommunication, computer etc.<sup>5</sup> The polycrystalline ferrites such as Ni-Cu-Zn ferrites have very important structural properties dependent on several factors such as method of preparation, substitution of cations, sintering temperature, sintering time, sintering atmosphere, porosity and microstructure.<sup>6,7</sup> Ni-Cu-Zn ferrites were considered as one of the most versatile magnetic materials to manufacture Multilayer chip inductors (MLCIs) mainly because of their

high electrical resistivity, low sintering temperature and high permeability.<sup>8,9</sup> Recently due to better magnetic properties, controlled shape of nanocrystalline Ni-Cu-Zn ferrites have been the dominant materials for MLIC at high frequency and low sintering temperature.<sup>10-16</sup> These oxides can be sintered at relatively low temperatures with a wide range of compositions. Recently, several methods were used to synthesize highly crystalline and uniformly sized magnetic nanoparticles of Ni-Cu-Zn ferrite.<sup>17-21</sup> Among these methods, the sol-gel method has gained scientific and technological importance during the last three decades.<sup>22-25</sup> The sol-gel auto-combustion synthesis method have many advantages as compared to the conventional methods such as low temperature processing and/or better homogeneity for the synthesis of multi-component materials. Considering the importance of Ni-Cu-Zn ferrite, we investigated the preparation of chromium doped Ni-Cu-Zn nano ferrite by sol-gel auto-combustion method using citric acid as fuel at low temperature with a view to study the influence of the substitution of  $\text{Cr}^{3+}$  ion on the structural properties of the system.

## 2. Experimental

### 2. 1. Materials and Synthetic Procedure

Nanocrystalline chromium substituted Ni-Cu-Zn ferrites, with composition  $\text{Ni}_{0.2}\text{Cu}_{0.2}\text{Zn}_{0.6}\text{Fe}_{2-x}\text{Cr}_x\text{O}_4$  ( $x = 0.0, 0.2, 0.4, 0.6, 0.8$  and  $1.0$ ) were synthesized by the sol-gel auto-combustion method. Analytical reagent grade nickel nitrate ( $\text{Ni}(\text{NO}_3)_2 \cdot 6\text{H}_2\text{O}$ ), copper nitrate ( $\text{Cu}(\text{NO}_3)_2 \cdot 6\text{H}_2\text{O}$ ), zinc nitrate ( $\text{Zn}(\text{NO}_3)_2 \cdot 6\text{H}_2\text{O}$ ), chromium nitrate ( $\text{Cr}(\text{NO}_3)_3 \cdot 9\text{H}_2\text{O}$ ) and iron nitrate ( $\text{Fe}(\text{NO}_3)_3 \cdot 9\text{H}_2\text{O}$ ) were used for synthesis. Citric acid ( $\text{C}_6\text{H}_8\text{O}_7 \cdot \text{H}_2\text{O}$ ) was used as fuel. The reaction procedure was carried out in an air atmosphere without the protection of inert gases. Metal nitrates and citric acid were used in the molar ratio 1:3. The metal nitrates were dissolved in desired stoichiometric proportions together in the minimum amount of double-distilled water to obtain a clear solution. An aqueous solution of citric acid was mixed with the metal-nitrate solution, and ammonia solution was slowly added to adjust the  $\text{pH} \approx 7$ . The mixed solution was placed on a hot plate with continuous stirring at  $90^\circ\text{C}$ . During evaporation, a very viscous brown gel was formed. When all of the water molecules were removed from the mixture, the viscous gel began to froth. After few minutes, the gel was ignited and burnt with glowing flints. The decomposition reaction continued until the entire citrate complex was consumed. The auto-combustion was completed within a minute, yielding brown-colored ash as the precursor. Sintering temperature was determined from TGA / DTA and prepared powders of all the precursor samples were sintered at  $500^\circ\text{C}$  for 4h to obtain the final product.

### 2. 2. Characterization of Samples

Simultaneous thermo gravimetric (TGA) and differential thermal analysis (DTA) of precursors were carried on SDT Q600 V20.9 Build 20 instrument in air atmosphere at heating rate  $10^\circ\text{C} / \text{min}$ , within temperature range  $25^\circ\text{C}$  to  $800^\circ\text{C}$ . The compositional stoichiometry was determined by energy dispersive X-ray spectroscopy (EDAX, Inca Oxford, attached to the SEM). The crystallographic structures were identified by X-ray powder diffraction with  $\text{Cu-K}\alpha$  radiation ( $\lambda = 1.5405 \text{ \AA}$ ) by Phillips X-ray diffractometer (Model 3710). The infrared spectra of all the samples were recorded at room temperature in the range  $300$  to  $800 \text{ cm}^{-1}$  using Perkin Elmer infrared spectrophotometer. Morphology and structure of the powder samples were studied on JEOL-JSM-5600 N Scanning Electron Microscope (SEM) and on Philips (model CM 200) Transmission Electron Microscope (TEM).

## 3. Results and Discussion

### 3. 1. Thermal Analysis (TGA / DTA)

The typical TGA/DTA curves of  $\text{Ni}_{0.2}\text{Cu}_{0.2}\text{Zn}_{0.6}\text{Fe}_{2-x}\text{Cr}_x\text{O}_4$  ( $x = 0.0$ ; Figure 1 and  $x = 1.0$ ; Figure 2), illustrates

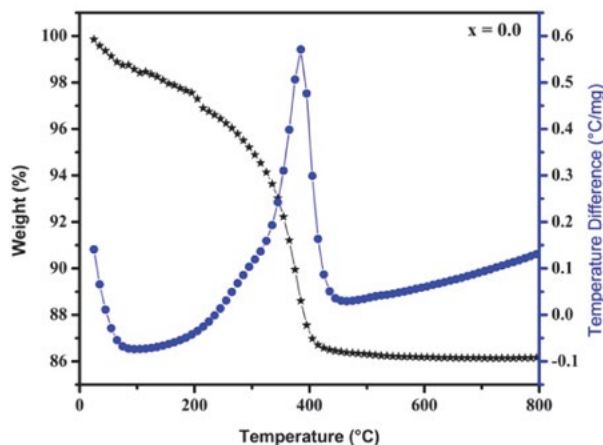


Figure 1: TGA-DTA plot for precursor of  $\text{Ni}_{0.2}\text{Cu}_{0.2}\text{Zn}_{0.6}\text{Fe}_{2-x}\text{Cr}_x\text{O}_4$  ( $x = 0.0$ )

two weight loss steps. The first weight loss step in the temperature range of  $30$ – $100^\circ\text{C}$ , corresponding to endothermic peak around  $80^\circ\text{C}$ , which is due to the loss of coordination water in the precursor. The second weight loss step observed in the temperature range of  $310$ – $425^\circ\text{C}$  corresponding to the exothermic peak around  $380^\circ\text{C}$ , is as a result of the decomposition of unreacted starting citric acid remained after combustion. The released heat in the process of exothermic decomposition has been observed to be sufficient for complete conversion of the metal precursors to metal oxides.<sup>26</sup>

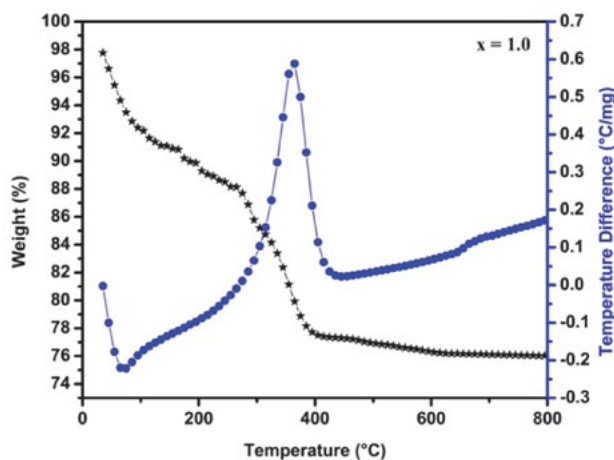


Figure 2: TGA-DTA plot for precursor of  $\text{Ni}_{0.2}\text{Cu}_{0.2}\text{Zn}_{0.6}\text{Fe}_{2-x}\text{Cr}_x\text{O}_4$  ( $x = 1.0$ )

Almost no weight loss was observed above  $425^\circ\text{C}$ , representing the presence of only  $\text{Ni}_{0.2}\text{Cu}_{0.2}\text{Zn}_{0.6}\text{Fe}_{2-x}\text{Cr}_x\text{O}_4$  ferrites in this temperature range.

### 3. 2. Structural Analysis

#### 3. 2. 1. Elemental Analysis

The compositional stoichiometry of  $\text{Ni}_{0.2}\text{Cu}_{0.2}\text{Zn}_{0.6}\text{Fe}_{2-x}\text{Cr}_x\text{O}_4$  ferrite nanoparticles was determined by EDAX.

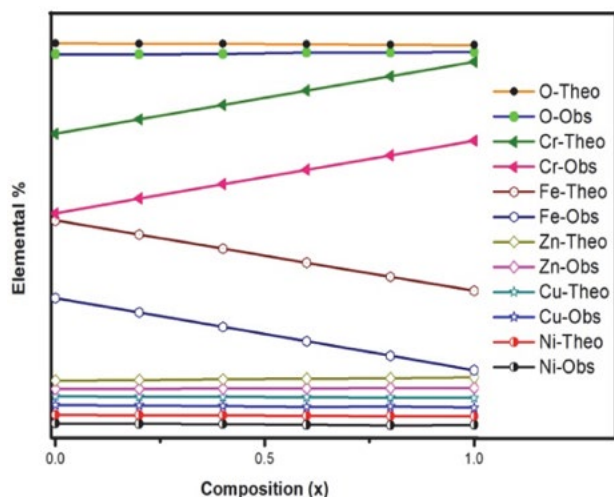


Figure 3. Plots of Observed and Theoretical elemental % versus composition (x)

The EDAX confirmed the homogeneous mixing of the Fe, Ni, Cu, Zn, Cr and O atoms in pure and doped ferrite samples. Figure 3 shows the plots of observed and theoretical percentage of Fe, Ni, Cu, Zn, Cr and O values versus compositions (x). The observed elemental % (obtained from EDAX) values are in close agreement with theoretical % (the starting composition used for the preparation) values. The EDAX analysis is affected by the surface crystalline defects of the nanoparticles. This can also be taken into account to explain the difference between the values of the atomic ratio as determined by EDAX and the expected value.<sup>27,28</sup>

### 3. 2. 2. X-ray Diffraction

X-ray diffraction (XRD) patterns of the  $\text{Ni}_{0.2}\text{Cu}_{0.2}\text{Zn}_{0.6}\text{Fe}_{2-x}\text{Cr}_x\text{O}_4$  ( $x = 0.0, 0.2, 0.4, 0.6, 0.8$  and  $1.0$ ) spinel ferrite system are shown in Figure 4. The XRD patterns confirmed the formation of single phase cubic spinel structure without additional peaks corresponding to any other phases. The crystal structures of Ni-Cu-Zn ferrite are identified as cubic spinel (space group:  $\text{Fd}\bar{3}\text{m}$ ) with the corresponding (220), (311), (222), (400), (422), (333) and (440) planes.

Lattice parameter (a) of all the samples was determined by using the following equation:<sup>29</sup>

$$a = d\sqrt{h^2 + k^2 + l^2} \quad (1)$$

Lattice constant (a) values with an accuracy of  $\pm 0.002 \text{ \AA}$  were calculated for each sample using XRD pattern and are listed in Table 1. It is observed that the lattice constant (a) decreases with increase in  $\text{Cr}^{3+}$  concentration. In the present ferrite system  $\text{Fe}^{3+}$  ions ( $0.67 \text{ \AA}$ ) ions are replaced by the relatively small  $\text{Cr}^{3+}$  ions ( $0.64 \text{ \AA}$ ). The decrease in the lattice constant is related to the difference in ionic radii of  $\text{Fe}^{3+}$  and  $\text{Cr}^{3+}$ .<sup>30-32</sup>

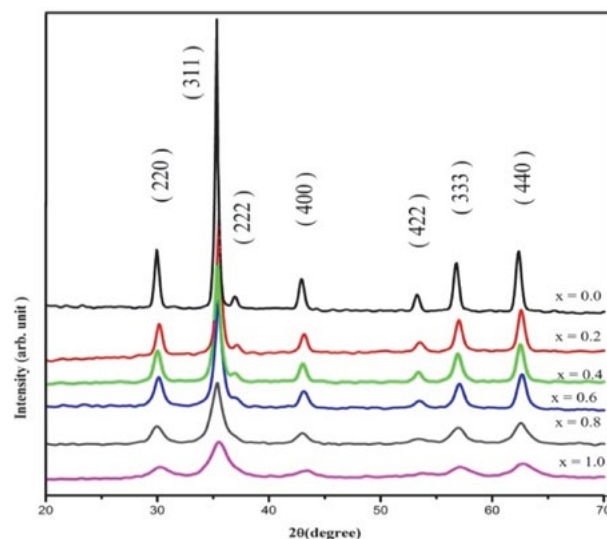


Figure 4. The XRD patterns for  $\text{Ni}_{0.2}\text{Cu}_{0.2}\text{Zn}_{0.6}\text{Fe}_{2-x}\text{Cr}_x\text{O}_4$

The X-ray density of all the samples was obtained by the following relation:

$$d_x = \frac{8M}{Na^3} \quad (2)$$

Where, '8' is formula unit, 'M' is molecular weight, 'N' is Avogadro's number, 'a' is lattice constant. The values of X-ray density are presented in table 1. It is seen from Table I that, like lattice parameter, X-ray density also decreased with increasing  $\text{Cr}^{3+}$  content 'x'. The decrease in X-ray density is attributed to decrease in lattice constant. It is observed that X-ray density increase for  $x = 1.0$ . This is related to the molecular weight of the sample overtakes the volume ( $a^3$ ).

The average crystallite diameter ' $D_{\text{XRD}}$ ' of powder estimated from the most intense (311) peak of XRD and using the Debye-Scherrer method,<sup>29</sup>

$$D_{\text{XRD}} = \frac{C\lambda}{\beta_{1/2} \cos \theta} \quad (3)$$

Where,  $\beta_{1/2}$  is the full width of half maximum in (2 $\theta$ ), ' $\theta$ ' is the corresponding Bragg angle and  $C = 0.9$ . The values of the crystallite size are given in Table 1. The crystallite size is decreases from 30.3 nm to 8.9 nm with increasing  $\text{Cr}^{3+}$  substitution. The decrease in the crystallite size indicates that the addition of the  $\text{Cr}^{3+}$  obstruct the crystal growth.<sup>33</sup> Due to the surface temperature and the molecular concentration at the surface of the crystal results into decrease in the crystal growth.

The percentage porosity 'P' of all the samples was calculated using the values of X-ray density and bulk density:

$$P = 1 - \frac{d_B}{d_x} \times 100\% \quad (4)$$

**Table 1.** Lattice constant ( $a$ ), X-ray density ( $d_x$ ) and hopping lengths ( $L_A$ ) and ( $L_B$ ), particle size ( $D_{\text{xrd}}$ ) and porosity ( $P$ ) of  $\text{Ni}_{0.2}\text{Cu}_{0.2}\text{Zn}_{0.6}\text{Fe}_{2-x}\text{Cr}_x\text{O}_4$

Composition 'x'	'a' (Å)	'd' <sub>x</sub> (g/cm <sup>3</sup> )	L <sub>A</sub> (Å)	L <sub>B</sub> (Å)	P (%)	Particle size (nm)	
						D <sub>xrd</sub>	TEM
0.0	8.418	5.329	3.645	2.976	25.4	30.3	30.6
0.2	8.415	5.316	3.644	2.975	26.1	24.9	25.2
0.4	8.406	5.317	3.640	2.972	27.7	19.1	19.5
0.6	8.394	5.323	3.634	2.967	28.7	16.4	15.9
0.8	8.389	5.314	3.632	2.966	28.4	12.6	12.8
1.0	8.367	5.339	3.623	2.958	32.0	8.9	9.5

Where,  $d_B$  and  $d_x$  are the bulk and X-ray densities respectively.

It is observed that porosity increased from 25.4% ( $x = 0.0$ ) to 32% ( $x = 1.0$ ) with the  $\text{Cr}^{3+}$  substitution. In the present series of  $\text{Ni}_{0.2}\text{Cu}_{0.2}\text{Zn}_{0.6}\text{Fe}_{2-x}\text{Cr}_x\text{O}_4$ , both the molecular weight and the volume of the unit cell decrease with increasing  $\text{Cr}^{3+}$  substitution, but the rate of the decrease of molecular weight is more than that of volume. Therefore, the density decreases with  $\text{Cr}^{3+}$  substitution, this resulted in increase in porosity. Apart from this, the increase in porosity is mainly attributed to decrease in crystallite size, which increases the grain boundaries of the particle and accordingly the porosity.<sup>27</sup>

The distance between the magnetic ions i.e. hopping lengths ( $L_A$  and  $L_B$ ) in the tetrahedral A-site and octahedral B-site was calculated using following relation:<sup>34</sup>

$$L_A = \frac{a\sqrt{3}}{4} \quad (5)$$

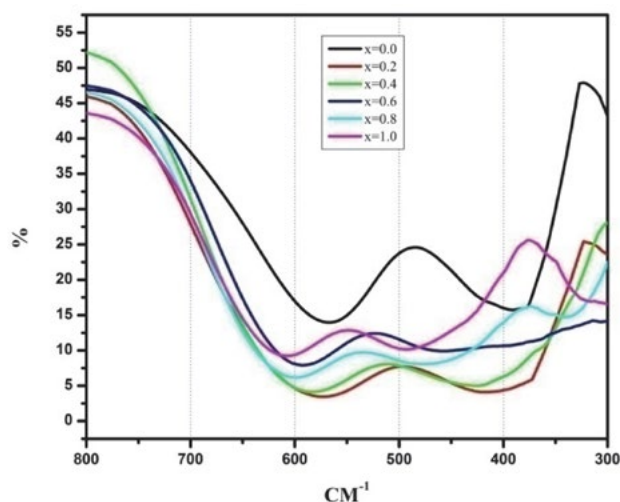
$$L_B = \frac{a\sqrt{2}}{4} \quad (6)$$

It has been observed from Table 1 that the hopping lengths ( $L_A$  and  $L_B$ ) decreased with  $\text{Cr}^{3+}$  substitution. Decrease in both the hopping lengths with  $\text{Cr}^{3+}$  substitution is due to the decrease in lattice constant.

### 3. 2. 3. Infrared Spectroscopy

The infrared spectroscopy is an important tool to probe various ordering phenomena that provide information on the position of ions and vibrational modes of crystals. The substitution of metal ion in ferrites may give rise to structural change within the unit cell without affecting the structure as a whole. Such structural changes brought about by metal ions strongly influence the lattice vibrations.<sup>35</sup> The IR spectra as shown in Figure 5, were recorded at room temperature in the frequency range 300–800  $\text{cm}^{-1}$ . For ferrites, generally it is found two assigned absorption bands appear around 600  $\text{cm}^{-1}$ :  $\nu_1$ , which is attributed to stretching vibration of tetrahedral groups  $\text{Fe}^{3+}-\text{O}^{2-}$  and around 400  $\text{cm}^{-1}$ :  $\nu_2$ , which is attributed to the octahedral groups complex  $\text{Fe}^{3+}-\text{O}^{2-}$ . It is observed

from Table 2 and Figure 6 that the higher frequency band ( $\nu_1$ ) is appeared in the range of 568–610  $\text{cm}^{-1}$  whereas lower frequency band ( $\nu_2$ ) is appeared in the range of 388–491  $\text{cm}^{-1}$ . These bands are characteristics features of spinel structure. It explains that the normal mode of vibration of tetrahedral cluster is higher than that of octahedral cluster. It should be attributed to the shorter bond length of tetrahedral cluster and longer bond length of octahedral cluster.<sup>35</sup>



**Figure 5.** IR spectra for the series  $\text{Ni}_{0.2}\text{Cu}_{0.2}\text{Zn}_{0.6}\text{Fe}_{2-x}\text{Cr}_x\text{O}_4$

The differences in band position and intensity with  $\text{Cr}^{3+}$  substitution may be related to; the decrease in the  $\text{Fe}_B^{3+}-\text{O}_2^{2-}$  intermolecular distance increases the metal-oxygen vibrational energies, which arises from the decrease in the number of  $\text{Fe}^{3+}-\text{O}_2^{2-}$  complexes caused by the increase of the number of  $\text{Cr}^{3+}-\text{O}_2^{2-}$  complexes<sup>35</sup> and, formation of  $\text{Me}^{2+}-\text{O}_2^{2-}$  at A and B sites ( $\text{Me} = \text{Ni}^{2+}, \text{Cu}^{2+}, \text{Zn}^{2+}$ ).

The force constants corresponding to the tetrahedral and octahedral complexes are calculated by using the standard formulae given below:<sup>36</sup>

$$K_t = 7.62 \times M_1 \times \nu_1^2 \times 10^{-2} \quad (7)$$

$$K_o = 10.62 \times \frac{M_2}{2} \times \nu_2^2 \times 10^{-2} \quad (8)$$



**Table 2.** Band position ( $\nu_1$  and  $\nu_2$ ), Force constant ( $K_0$  and  $K_t$ ) and Bond length ( $R_A$  and  $R_B$ ) of system  $\text{Ni}_{0.2}\text{Cu}_{0.2}\text{Zn}_{0.6}\text{Fe}_{2-x}\text{Cr}_x\text{O}_4$ 

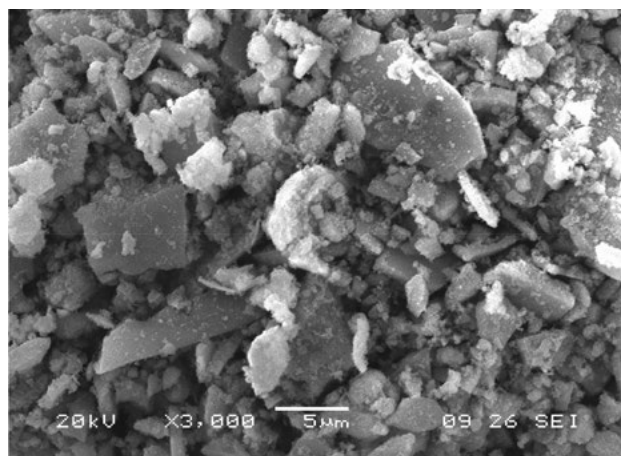
Comp. 'x'	Band positions		Force constants		Bond lengths	
	$\nu_1$ ( $\text{cm}^{-1}$ )	$\nu_2$ ( $\text{cm}^{-1}$ )	$K_0 \times 10^5$ (dyne/cm)	$K_t \times 10^5$ (dyne/cm)	$R_A$ (Å)	$R_B$ (Å)
0.0	568.1	388.9	0.9380	1.6075	3.864	3.065
0.2	574.6	418.1	1.0834	1.8388	3.862	3.064
0.4	585.8	424.7	1.1182	1.8978	3.861	3.063
0.6	597.2	447.2	1.2399	2.0884	3.859	3.063
0.8	603.9	474.2	1.3937	2.3203	3.857	3.062
1.0	610.5	491.9	1.4999	2.4789	3.855	3.061

Where,  $K_0$  is the force constant of octahedral site,  $K_t$  is the force constant of tetrahedral site,  $M_1$  molecular weight of tetrahedral site,  $M_2$  molecular weight of octahedral site,  $\nu_1$  the corresponding center frequency on tetrahedral site, and  $\nu_2$  the corresponding center frequency on octahedral site.

The molecular weights  $M_1$  and  $M_2$  for each sample are calculated from the cation distribution. The force constant is the second derivative of the potential energy with respect to the site radius with the other independent parameters kept constant. The bond lengths  $R_A$  and  $R_B$  have been calculated using the formula given by Gorter.<sup>37</sup> The molecular weights of the tetrahedral  $M_1$  and octahedral  $M_2$  sites have been calculated using the cation. The values of  $R_A$ ,  $R_B$  and the force constants  $K_t$  and  $K_0$  are listed in Table: 2.

### 3. 2. 4. Scanning Electron Microscopy (SEM)

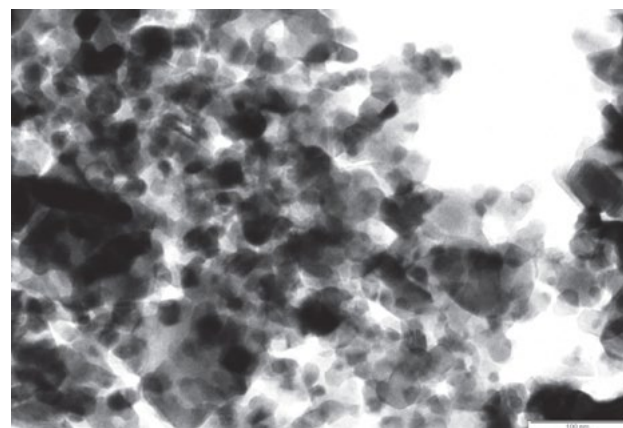
Typical Scanning electron micrograph (SEM) of the sample  $x = 0.6$  is shown in Figure 6. Each composition is characterized by a typical porous structure and small rounded grains. It is observed from SEM images that the structure is affected by the  $\text{Cr}^{3+}$  substitutions. It can be observed from the SEM images that the prepared samples

**Figure 6.** Scanning electron micrograph of  $\text{Ni}_{0.2}\text{Cu}_{0.2}\text{Zn}_{0.6}\text{Fe}_{2-x}\text{Cr}_x\text{O}_4$  ( $x = 0.6$ )

are amorphous and porous in nature. The decrease in the grain size and an increase in porosity are observed with increasing  $\text{Cr}^{3+}$  substitutions. The observed changes in grain size suggest that the substitution of  $\text{Cr}^{3+}$  in Ni-Cu-Zn ferrite solid solution occurs during sol-gel combustion process which enables a better homogeneity in the powders and, hence, a more controlled microstructure is obtained.

### 3. 3. 5. Transmission Electron Microscopy (TEM)

TEM image of the typical sample  $x = 0.4$  is presented in Figure 7.

**Figure 7.** TEM image for  $\text{Ni}_{0.2}\text{Cu}_{0.2}\text{Zn}_{0.6}\text{Fe}_{2-x}\text{Cr}_x\text{O}_4$  ( $x = 0.4$ )

The particles were well distributed and slightly agglomerated. The agglomeration is the indication of high reactivity of the prepared sample with the heat treatment and it may also be come from the magnetostatic interaction between particles. Since  $\text{Cr}^{3+}$  ions provide stability to the Ni-Cu-Zn lattice; it is believed that they also inhibit the process of grain growth through coagulation at the stage where the sol-gel is formed and hence samples of small particle size are produced.<sup>38</sup> Selected area electron diffraction (SAED) patterns of the respective TEM image is also shown in Figure 8.

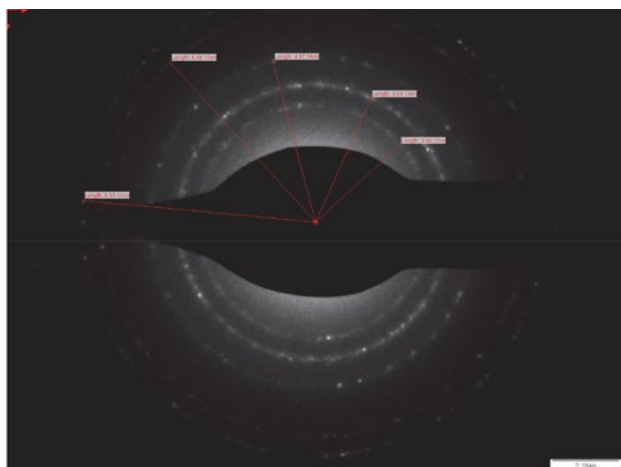


Figure 8. SAED pattern for  $\text{Ni}_{0.2}\text{Cu}_{0.2}\text{Zn}_{0.6}\text{Fe}_{2-x}\text{Cr}_x\text{O}_4$  ( $x = 0.4$ )

The Bragg' rings observed in these SAED patterns corresponding to specific 'd' values, that match perfectly with the 'd' values calculated from XRD. The superimposition of the bright spot with Debye ring pattern indicates polycrystalline nature of the sample which is in accordance with XRD. Like XRD; SAED also confirmed that the sample does not possess any type of impurity or second phase.

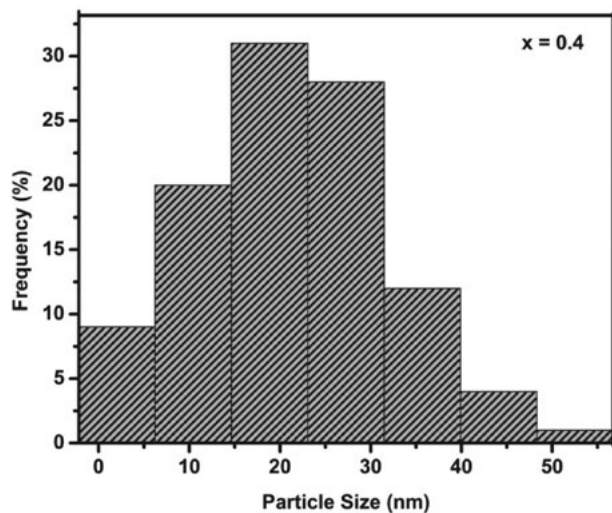


Figure 9. Particles size distribution for  $\text{Ni}_{0.2}\text{Cu}_{0.2}\text{Zn}_{0.6}\text{Fe}_{2-x}\text{Cr}_x\text{O}_4$  ( $x = 0.4$ ) (based on TEM micrograph, Figure 7)

Particles size distributions for  $\text{Ni}_{0.2}\text{Cu}_{0.2}\text{Zn}_{0.6}\text{Fe}_{2-x}\text{Cr}_x\text{O}_4$  ( $x = 0.4$ ) shown in figure 9. Nanocrystalline particles observed were in the range 6–55 nm. Particles with size between 10–30 nm were most abundant (more than 70%). The samples particle size obtained from TEM are in close agreement to the size calculated from the Debye-Scherrer method.

## 4. Conclusion

Nanocrystalline  $\text{Ni}_{0.2}\text{Cu}_{0.2}\text{Zn}_{0.6}\text{Fe}_{2-x}\text{Cr}_x\text{O}_4$  ferrites with  $x = 0.0, 0.2, 0.4, 0.6, 0.8,$  and  $1.0$  were prepared by sol gel auto combustion method using citric acid as a fuel. The EDAX pattern confirmed the homogeneous mixing in pure and doped ferrite samples with desired composition. Structural analysis with XRD reveals that the system confirms the formation of single phase cubic spinel structure of Chromium doped Ni-Cu-Zn Nano Ferrites. Lattice constant and X-ray density decreased with  $\text{Cr}^{3+}$  substitution. The crystallite size is observed in the range of 8.9–30.3 nm, which is in close agreement with crystallite size obtained from TEM. It is concluded from IR spectra that higher frequency band ( $\nu_1$ ) is appeared in the range of 568–610  $\text{cm}^{-1}$  whereas lower frequency band ( $\nu_2$ ) is appeared in the range of 388–491  $\text{cm}^{-1}$  confirming characteristics features of spinel structure. It is observed from SEM that the prepared samples are amorphous and porous in nature. TEM images of the samples confirmed the particle size of obtained ferrite samples is in nm dimensions. The prepared Chromium doped Ni-Cu-Zn Nano Ferrites may be used as catalyst for organic transformations and in several devices such as antennas, memory storage devices, microwave devices etc.

## 5. References

- Mathew, T., Shylesh, S., Devassy, B. M., Vijayaraj, et al., *Applied Catalysis A: General*, **2004**, 273(1), 35–45. DOI:10.1016/j.apcata.2004.06.011
- Lu, H. C., Chang, J. E., Vong, W. W., Chen, et al., *International Journal of Physical Sciences*, **2011**, 6(4), 855–865.
- Lim, C. W., Lee, I. S., *Nano Today*, **2010**, 5(5), 412–434. DOI:10.1016/j.nantod.2010.08.008
- Kooti, M., Afshari, M., *Scientia Iranica*, **2012**, 19(6), 1991–1995. DOI:10.1016/j.scient.2012.05.005
- H. Su, H. Zhang, X. Tang, Z. Zhong, Y. Jing, *Mater. Sci. Eng. B*, **2009**, 162, 22–25. DOI:10.1016/j.mseb.2009.01.030
- Wang, Sea-Fue, et al., *Journal of Magnetism and Magnetic Materials*, **2015**, 394, 470–476. DOI:10.1016/j.jmmm.2015.07.037
- Ahmadpour Ghader, Ali Ghasemi, Ebrahim Paimozd, *Current Nanoscience*, **2012**, 8.4, 598–602. DOI:10.2174/157341312801784393
- T. Nakamura, *J. Magn. Magn. Mater.*, **1997**, 168, 285–291. DOI:10.1016/S0304-8853(96)00709-3
- R. Lebourgeois, S. Duguey, J. P. Ganne, J. M. Heintz, *J. Magn. Magn. Mater.*, **2007**, 312, 328–330. DOI:10.1016/j.jmmm.2006.10.698
- J. H. Jean, C. H. Lee, W. S. Kou, *J. Am. Ceram. Soc.*, **1999**, 82, 343. DOI:10.1111/j.1551-2916.1999.tb20068.x
- V. V. Awati, S. M. Rathod, Sagar E. Shirsath, Maheshkumar L. Mane, *J. Alloys Compds*, **2013**, 553, 157–162. DOI:10.1016/j.jallcom.2012.11.045

12. T. Krishnaveni, B. Rajini Kanth, V. Seetha Rama Raju, S.R. Murthy, *J. Alloys Compds*, **2006**, *414*, 282–286. DOI:10.1016/j.jallcom.2005.07.029
13. T. Krishnaveni, B. Rajini Kanth, et al., *Journal of Alloys and Compounds*, **2006**, *414*, 282–286. DOI:10.1016/j.jallcom.2005.07.029
14. Yen-Pei Fu, Ko-Yin Pan, Cheng-Hsiung Lin, *Materials Letters*, **2002**, *57*, 291–296. DOI:10.1016/S0167-577X(02)00780-2
15. Li, Bo, et al., *Materials Science and Engineering: B*, **2003**, *99*, 1, 252–254. DOI:10.1016/S0921-5107(02)00489-0
16. Zhu, Haikui, et al., *Ceramics International*, **2014**, *40*, 7, 10985–10989. DOI:10.1016/j.ceramint.2014.03.102
17. M. A. Gabal, Y. M. Al Angari, A. Y. Obaid, *Advanced Powder Technology*, **2014**, *25*, 457–461. DOI:10.1016/j.apt.2013.07.009
18. M. Epifani, E. Melissano, G. Pace, M. Schiopa, *J. Europ. Ceram. Soc.*, **2007**, *27*, 115–123. DOI:10.1016/j.jeurceramsoc.2006.04.084
19. N. L. Freitas, J. P. Continho, M. C. Silva, H. L. Lira, et al., *Materials Science Forum*, **2010**, *660*, 943–947. DOI:10.4028/www.scientific.net/MSF.660-661.943
20. Tiago Pinheiro Braga, Bárbara Maria Campos Sales, et al., *Catal. Sci. Technol.*, **2011**, *1*, 1383–1392. DOI:10.1039/c1cy00176k
21. Y. Ahn, E. J. Choi, S. Kim, H. N. Ok, *Mater. Lett.*, **2001**, *50* (1), 47–52. DOI:10.1016/S0167-577X(00)00412-2
22. Lohar K. S., Pachpinde A. M., Langade M. M., et al., *Journal of Alloys and Compounds*, **2014**, *604*, 204–210. DOI:10.1016/j.jallcom.2014.03.141
23. B. G. Toksha, Sagar E. Shirsath, M. L. Mane, S. M. Patange, S. S. Jadhav, K. M. Jadhav, *J. Phys. Chem. C*, **2011**, *115*, 20905–20912 DOI:10.1021/jp205572m
24. Sagrario M. Montemayor, L. A. Garcia-Cerda, J. R. Torres-Lubian, O. S. Rodriguez-Fernandez, *J Sol-Gel Sci Techn*, **2007**, *42*, 181–186
25. J. Azadmanjiri, *Mater. Chem. Phys.*, **2008**, *109*, 109–112 DOI:10.1016/j.matchemphys.2007.11.001
26. A. Mali, A. Ataie, *Ceramics International*, **2004**, *30*, 1979–1983. DOI:10.1016/j.ceramint.2003.12.178
27. Hashim, Mohd, et al., *Powder technology*, **2012**, *229*, 37–44. DOI:10.1016/j.powtec.2012.05.054
28. K. S. Lohar, S. M. Patange, S. E. Shirsath et al., *Int. J. of Modern Phy. B*, **2011**, *25-16*, 2157–2166.
29. B. D. Cullity, “*Elements of X-ray diffraction*”, (Addison-Wesley Publ. Comp. Inc., Reading, Massachusetts, U.S.A.), **1956**, pp. 99.
30. S. M. Patange, Sagar E Shirsath, et al., *Appl. Phys. A: Mater Sci. Proces*, **2009**, *A95*, 429–434. DOI:10.1007/s00339-008-4897-0
31. N. Kumari, V. Kumar, K. Singh, *J. Alloys Compd.*, **2015**, *622*, 628–634. DOI:10.1016/j.jallcom.2014.10.083
32. Yuksel Koseoglu, *Ceramics international*, **2015**, *41*, 6417–6423. DOI:10.1016/j.ceramint.2015.01.079
33. M. Ashtara, A. Munirb, M. Anis-ur-Rehmanb, A. Maqsooda, *Materials Research Bulletin*, **2016**, *79*, 14–21.
34. B. Vishwanathan and V. R. K. Murthy, *Ferrite Material Science and Technology*, New Delhi: Narsoa Publishing House, **1990**, pp. 15–61.
35. S. S. Bellad, R. B. Pujar, B. K. Chougule, *Indian J. Pure Appl. Phys.*, **1998**, *36*, 598–601.
36. A. A. Yousef, M. E. El-Zain, S. A. Mazen, et al., *J. Phys. Condens. Matter*, **1994**, *6*(29), 5717–5724. DOI:10.1088/0953-8984/6/29/014
37. E. W. Gorter, *Philips Res. Rep.*, **1954**, *9*, 295–320.
38. Muhammad Javed Iqbal, Barkat-ul-Ain, *Mater. Sci. Engg. B*, **2009**, *164*, 6–11.

## Povzetek

Nanoferite Ni-Cu-Zn dopirane s kromom in s kemijsko sestavo  $\text{Ni}_{0.2}\text{Cu}_{0.2}\text{Zn}_{0.6}\text{Fe}_{2-x}\text{Cr}_x\text{O}_4$  ( $x = 0.0, 0.2, 0.4, 0.6, 0.8, 1.0$ ) smo pripravili z modificirano sol-gel metodo. Tako pripravljene s kromom substituirane prekurzorje Ni-Cu-Zn feritov smo sintrali štiri ure pri 500 °C. Kemijsko sestavo smo potrdili z energijsko disperzivno rentgensko analizo (EDAX). Podatki rentgenske praškovne analize (XRD) pa razkrivajo, da so imajo vsi vzorci le eno fazo in kubično spinelno strukturo. Konstante osnovne celice, razdalje med magnetnimi ioni in velikost kristalitov, ki smo jih določili z rentgensko praškovno analizo se zmanjšujejo z večanjem koncentracije  $\text{Cr}^{3+}$  ionov. V infrardečih spektrih prevladujeta dva trakova: trak pri visokih frekvencah  $\nu_1 \approx 600 \text{ cm}^{-1}$  in nizkih frekvencah  $\nu_2 \approx 450 \text{ cm}^{-1}$ , ki ju lahko pripišemo valenčnim nihanjem v tetraedričnih in oktaedričnih okoljih. Morfologijo površine pripravljenih vzorcev smo preučevali z uporabo vrstične elektronske mikroskopije (SEM) in presevalne elektronske mikroskopije (TEM).

Scientific paper

# The Impact of a Silane Pigment Treatment on the Properties of Thickness-sensitive Spectrally Selective Paints

Miha Steinbücher,<sup>1</sup> Peter Venturini,<sup>1</sup> Jože Hafner,<sup>2</sup> Matevž Zupančič,<sup>3</sup>  
Peter Gregorčič<sup>3</sup> and Iztok Golobič<sup>3,\*</sup>

<sup>1</sup>Helios Group, Količevo 2, SI-1230 Domžale, Slovenia

<sup>2</sup>Slovenian National Building and Civil Engineering Institute, Dimičeva 12, SI-1000 Ljubljana, Slovenia

<sup>3</sup>University of Ljubljana, Faculty of Mechanical Engineering, Aškerčeva 6, SI-1000 Ljubljana, Slovenia

\* Corresponding author: E-mail: iztok.golobic@fs.uni-lj.si  
phone: +38614771420

Received: 17-06-2017

## Abstract

Thickness-sensitive, spectrally selective paints based on a silane treatment of pigments were prepared with different pigment-volume concentrations. The critical pigment-volume concentration was determined by means of electrochemical impedance spectroscopy, while the pigment particle size distribution was determined with ultrasound spectroscopy. The selectivity versus thickness relation of a paint with a near-critical pigment-volume concentration was studied spectroscopically through performance criteria. Its nonlinearity was shown to be related to the surface topography. This relation was further supported by hydrophobicity measurements. Heat-gathering tests in a simulated solar collector supported the spectroscopic determination of an optimal dry-film thickness.

**Keywords:** TSSS paints, pigment treatment, spectral selectivity, topography, hydrophobicity

## 1. Introduction

Spectrally selective paints play a crucial role in solar collector panels needed for efficient solar-thermal conversion systems.<sup>1</sup> Such systems require spectrally selective absorbers with high absorption of the sunlight and low infrared emittance resulting in little heat loss to environment via convection and radiation. The established measure for the solar irradiation absorptivity as a material property is the solar absorptivity ( $\alpha$ ,  $a_s$ ,  $\alpha_s$ ), defined by the following equation:

$$a_s = \frac{\int_{0.3\mu\text{m}}^{2.5\mu\text{m}} S(\lambda)(1-R(\lambda))d\lambda}{\int_{0.3\mu\text{m}}^{2.5\mu\text{m}} S(\lambda)d\lambda} \quad (1)$$

where  $S(\lambda)$  is the normalized direct solar irradiation distribution function<sup>2</sup> and  $R(\lambda)$  is a hemispheric reflectance spectra of the material surface. On the other hand, the established measure of the fraction of black-body emissivity at a given temperature for a material is the thermal emissivity ( $\epsilon$ ,  $e_p$ ,  $\epsilon_T$ ), defined by the following equation:

$$e_T = \frac{\int_{2.5\mu\text{m}}^{15\mu\text{m}} r(\lambda,T)(1-R(\lambda))d\lambda}{\int_{2.5\mu\text{m}}^{15\mu\text{m}} r(\lambda,T)d\lambda} \quad (2)$$

where  $r(\lambda, T)$  is the black-body radiation distribution function at a given absolute temperature ( $T$ ). Since high solar absorptivity and a low thermal emissivity are desired for solar-energy exploitation, the performance criterion  $PC_C$  was introduced as a measure of the spectral selectivity, combining both  $a_s$  and  $e_T$ :

$$PC_C = -a_s + Ce_T \quad (3)$$

where  $C$  is a constant appropriate for the collector type used. The most commonly used values are  $C = 0.5$  for high-temperature collectors,  $C = 0.25$  for low-temperature collectors and  $C = 0.34$  for unglazed collectors. The  $C$  values as well as classification of collectors are based on experimental work.<sup>3</sup>

Coatings, made from organic spectrally selective materials,<sup>4,5</sup> represent one of efficient options to produce

spectrally selective absorbers. They can be divided into thickness-insensitive, spectrally selective,<sup>6–10</sup> and thickness-sensitive, spectrally selective (TSSS) paints.<sup>11</sup> The development of both types is interlinked in the fields of absorptive pigments and their dispersions,<sup>12</sup> binders,<sup>13</sup> and durability.<sup>14, 15</sup> Typically, black TSSS coatings are based on an interaction between a thin layer of highly absorptive paint applied without a primer and a thermal infrared reflective substrate, such as aluminum, copper or other metals. Their selectivity depends to a large extent on their thickness, as both  $a_s$  and  $e_T$  increase non-linearly with thickness. However, the thickness of the TSSS coatings is seldom measured, as their usual dry-film thicknesses is of the same magnitude as the surface roughness of the commonly used substrates, but thickness measurements commonly used in the paint industry cannot be reliable.<sup>16</sup> The grammage, i.e., the weight of coating per nominal surface, roughness disregarded, is used instead. The other factor influencing selectivity is the substrate. However, its influence on  $a_s$  is not significant with coatings applied in usual thicknesses ( $a_s \geq 0.9$ ). On the other hand,  $e_T$  is very (and almost linearly) dependent on the substrate  $e_T$ .

Since the development of solar selective absorbers with both high conversion efficiency and high-temperature stability remains a challenging issue due to the cost and the materials problems,<sup>17</sup> the main aim of this work is examination of the selectivity of in-situ silane-treated-pigment TSSS (stpTSSS) paints. Therefore, we are focused in study of performance criteria as a function of pigment concentration as well as on the optical properties of the pigment, the binder and the surface topology. Here, the surface-topography study is supported by hydrophobicity analysis performed through measurements of the static contact angle of a water droplet.

## 2. Materials and Methods

The stpTSSS paints were produced according to a previously disclosed procedure.<sup>4</sup> The SUNCOLOR TS S Black Al (Helios Group, SI) paint was used for the particle size determination, topography studies, contact-angle measurements and tests of the heat-gathering properties. Solarect Z (Helios Group, SI) was used as a reference TSSS paint without silane-treated pigments. The paints were applied by spraying, bar or coil coating, diluted with the appropriate Helios SUNCOLOR Thinner (Helios Group, SI) or SUNCOLOR Thinner (Helios Group, SI). The substrates used were acid-pretreated, 0.2-mm-thick, copper ( $e_T = 0.03$ ) sheets and degreased, 0.4-mm-thick aluminum sheets ( $e_T = 0.01–0.02$ ). The coatings were cured in a calibrated Kambič LSP-190 C laboratory oven with  $\pm 5$  °C precision at temperatures  $> 100$  °C.

The coatings' grammage was determined by weighing the difference of uncoated and coated substrates with known surfaces. The masses were determined with a preci-

sion of  $\pm 0.0001$  g. The surfaces of the rectangular samples were determined by measuring their length and width with a precision of  $\pm 0.5$  mm. The resulting grammage measurement error for a substrate of 10.0 cm  $\times$  10.0 cm, typically used in this work, is 0.01 g/m<sup>2</sup>.

The  $a_s$  values were determined by recording the UV-VIS-NIR spectra with a Perkin Elmer Lambda 950 spectrometer with a 150-mm Spectralon integration sphere and processing the spectral data according to equation (1). The error in the measurement of  $a_s \ll 0.01$ .<sup>18</sup>

The  $e_T$  values were determined by recording the IR spectra with a Bruker IFS66/S spectrometer using an OP-TO-SOL integration sphere and processing the spectral data according to equation (2). The error in the measurement is not documented.

The Electrochemical Impedance Spectroscopy (EIS) measurements were performed with a Parstat 2273 potentiostat and a Tait cell. The measuring system has a resolution of 1pA. The EIS<sup>19</sup> data were plotted as a Nyquist chart showing the imaginary impedance ( $Z''$ ) versus the real impedance ( $Z'$ ). The higher arc shows a higher coating capacity and thus better barrier properties and a lower permeability. The EIS data were used for a critical pigment volume concentration (cPVC) determination of the coatings according to the previously described method.<sup>20,21</sup>

The particle sizes were determined with a Dispersion Technology DT-1200 acoustic spectrometer. The method based on acoustic attenuation versus an ultrasound frequency measurement allows for a particle size determination in a realistic, undiluted sample, which is in contrast to the more common dynamic light scattering. The particle size distribution is calculated from the recorded ultrasound spectrum, the dry-matter content, and densities using a unimodal or bimodal model. The uncertainty of the measurement for the sample relevant to this work is below 20 nm.

The substrate and coating topographies were determined with an AFM Park XE100 atomic force microscope with a spatial resolution of 500 pm and 150 pm of background noise. The uncertainty of the measurement for the samples relevant to this work is below 1 nm.

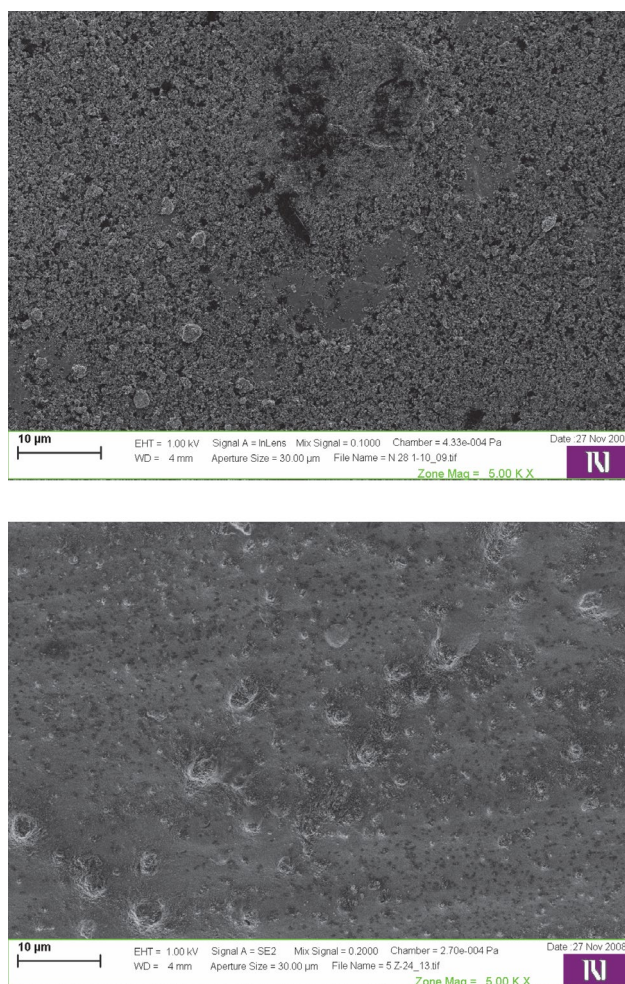
The static contact angles for water were measured with a Krüss DSA 100 drop shape analysis system with the error of the measurement being  $< 1^\circ$ . Three measurements were made for each sample and then averaged.

The thermal response to irradiation was determined with stagnation-temperature measurements of a model absorber in a glazed or unglazed thermally insulated housing. The illumination was provided by filtered Atlas metal halide lamps; the power was regulated by changing the distance between the lamps and the absorber. The light flux was determined with a Kipp & Zonen CM11 pyranometer with a spectral range of 285–2800 nm and a zero offset  $< 7$  W/m<sup>2</sup>. The temperature was measured by means of type-K thermocouples, and a Agilent 34970A and a Windows PC were used for the data acquisition. Low-Fe-content glass with  $T = 0.92$  was used for the glazing.

### 3. Results and Discussion

#### 3.1. PVC Optimization

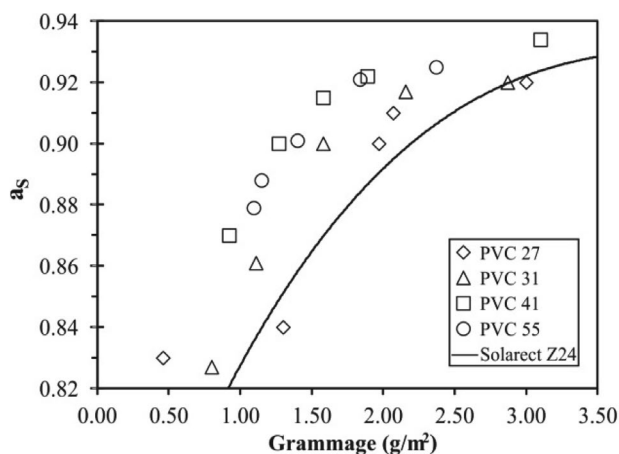
Paints with different pigment volume concentrations (PVCs) were produced according to the already known procedure and applied to a copper substrate by air spraying.<sup>22</sup> The silane coating of pigment in-situ during the dispersion process allows for a better dispersion and smaller particle size, as shown in Fig. 1.



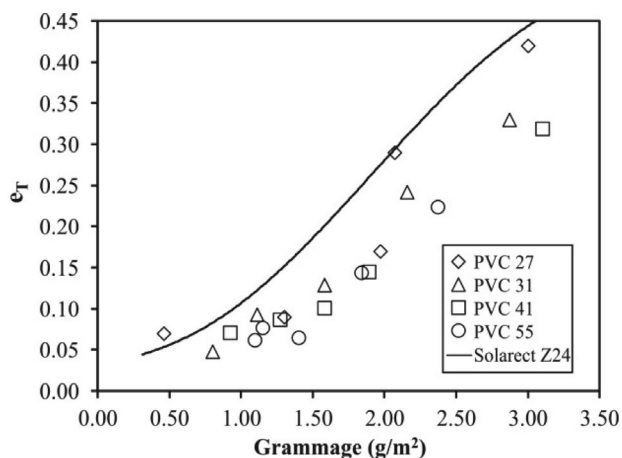
**Figure 1.** SEM analysis of surfaces of TSSS coatings made of silane treated (top) and untreated (bottom) pigments. Samples were made with the same PVC and the same application process.

The  $a_s$  and  $e_T$  values of the resulting coatings are shown in Figs. 2 and 3 with the  $a_s$  and  $e_T$  curves for the Solarect Z24 paint with PVC 27 as a reference. Both paints are based on the same binder and pigment and are formulated with the same PVC. The previously known relationship between the PVC and the spectral selectivity of a TSSS paint is also relevant for the stpTSSS paints. Paints with a higher PVC exhibit higher  $a_s$  and lower  $e_T$  for the same grammage and substrate.

The advantage of the new material is even clearer in a comparison of the PC values. Fig. 4 shows the  $PC_{0.5}$  values derived from the above data.



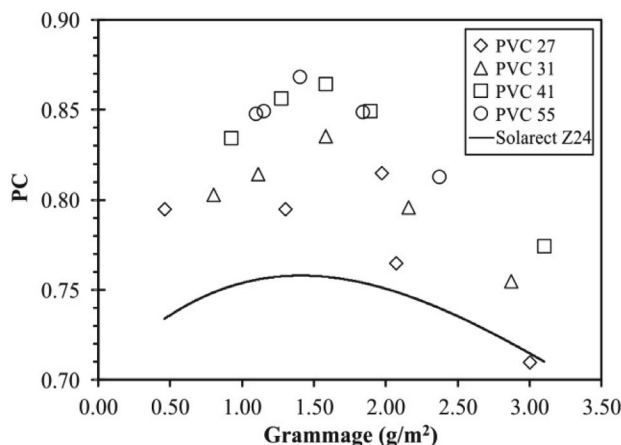
**Figure 2.**  $a_s$  as a function of grammage for stpTSSS at different PVC with a non-silane treated reference, increase of PVC leads to higher  $a_s$  values.



**Figure 3.**  $e_T$  as a function of grammage for stpTSSS at different PVC with a non-silane treated reference, increase of PVC leads to lower  $e_T$  values.

It is clear that the new coatings display better selectivity at a given PVC compared to the reference, but the silane-pigment-treating technology offers a further advance. The reference coating is limited to its PVC with the mechanical properties. The stpTSSS, on the other hand, can be produced at significantly higher PVCs without any apparent loss of adhesion or cohesion. Kunič et al (2009) described simple mechanical tests such as cross-cut adhesion<sup>23</sup> to determine the mechanical stability in organic selective coatings.

However, such simple testing method cannot give a full picture to important properties like film permeability, which significantly influence the coating's durability. It is well known that properties of coating film, including ones

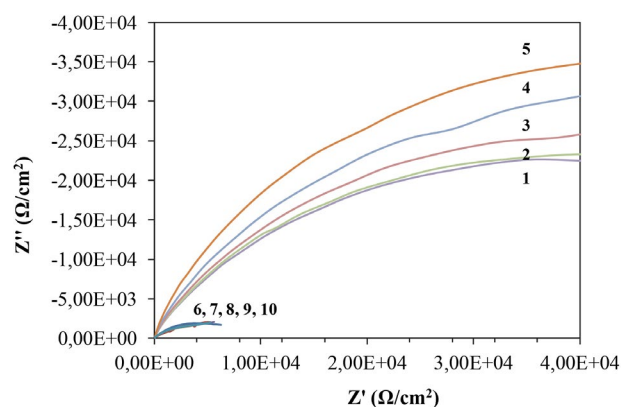


**Figure 4.**  $PC_{0,5}$  values as a function of grammage for stpTSSS at different PVC with a non-silane treated reference. Changes in PVC doesn't significantly influence the optimal grammage, which is about  $1.5 \text{ g/m}^2$ .

tested by cross-cut adhesion test, abruptly changes at cPVC.<sup>24</sup> cPVC is the PVC where there is just enough binder to provide a complete adsorbed layer on the pigment surfaces and to fill the voids between pigment particles in the film. In a film with  $PVC > cPVC$ , pigment particles are not completely wetted and there are voids and/or pores between them.

To determine the cPVC of stpTSSS paints we used electrochemical impedance spectroscopy (EIS) technique. A ladder of coatings with PVCs from 25 to 55 was prepared and applied in a  $20\text{-}\mu\text{m}$  thickness with a bar-coater on a steel substrate. The EIS measurements of the cured coatings were performed and the results are shown as a Nyquist chart in Fig. 5.

The Nyquist chart shows that the film permeability decreases with the PVC until the cPVC is reached, after which it drops significantly. A precise determination of the PVC allowed for the development of the most selective, but still durable, coating. All subsequent experiments were performed with a coating corresponding to the coating 5 in Fig. 5.

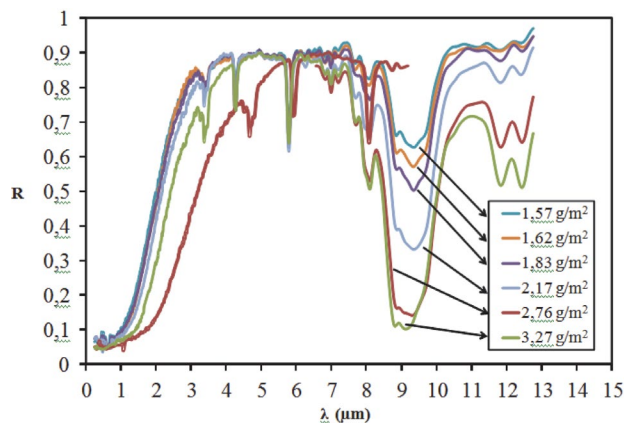


**Figure 5.** Nyquist chart depicting EIS measurement data as  $Z''$  versus  $Z'$  of below (1–5) and above critical (6–10) PVC stpTSSS paints.

### 3. 2. Spectral Selectivity

The questions of the selectivity of the coatings and selectivity optimization were already partially addressed in the PVC dependence. Fig. 4 shows clearly that there is an optimal thickness of the coating from the point of view of selectivity. Fig. 6 shows the combined UV-VIS-NIR and IR spectra of a stpTSSS paint at different thicknesses, expressed as grammages.

The spectral data show strong pigment absorption in the UV and VIS regions, gradually diminishing in the NIR region. In the Thermal Infrared (TIR) region significant absorption bands are visible at  $3\text{--}3.5 \mu\text{m}$  (C-H bond stretching),  $5.8 \mu\text{m}$  (C=O bond stretching),  $7.9 \mu\text{m}$  (Si-C bond stretching),  $9 \mu\text{m}$  (broad, Si-O bond stretching), all corresponding to the paint's binder. The absorption band at  $4.2 \mu\text{m}$  is caused by atmospheric  $\text{CO}_2$  and is numerically subtracted in the  $e_T$  calculations. The increase in the absorptivity with thickness points to well-established light-absorption and scattering phenomena as the reason for the selectivity.<sup>25</sup> The PC data in Fig. 4, on the other hand, show a more distinct nonlinearity compared to the reference coating and point to another mechanism behind the relation between the selectivity and the thickness of the coating. We believe the explanation lies in the surface topography of a thinly applied near cPVC coating.



**Figure 6.** Combined UV-VIS-NIR and IR spectra of a stpTSSS paint applied at different grammages.

### 3. 3. Topography

To interpret the topographies correctly, more data are needed, i.e., the distribution of particle sizes (PSD) in the coating. Fig. 7 shows the particle size distribution obtained by acoustic spectrometry in liquid stpTSSS paint (i.e., before application). Clearly, the bimodal distribution can be explained with pigment particles that have a median particle size of  $300 \text{ nm}$  and a polymer particle dispersion with a median particle size of  $10 \mu\text{m}$ . The latter are dissolved in the curing process and not present in a cured coating.

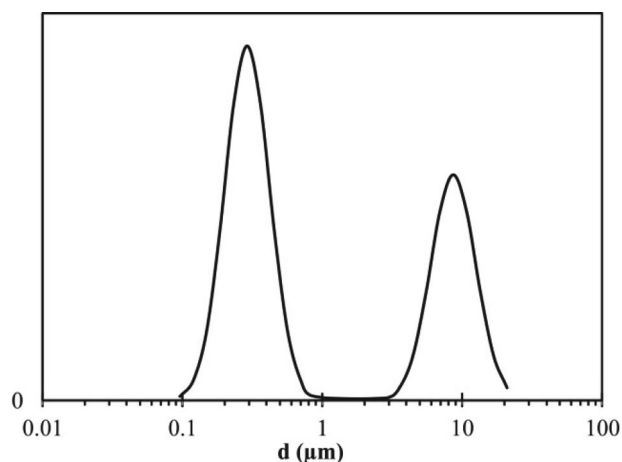


Figure 7. Particle size distribution in liquid TSSS paint.

To study the topography of the TSSS coatings applied at thickness close to the optimal one, optical microscopy is of little help, as the surface roughness of practical substrates approaches or exceeds the thickness of the coating. AFM imaging was used instead. The samples were prepared by air-spraying the paint on an aluminum substrate.

The image of the substrate in Fig. 8 shows a nano-rough surface. From the image of the stpTSSS coating with a grammage of  $1.2 \text{ g/m}^2$  in Fig. 9, a nanostructure with a pattern corresponding to the particle size determined in a liquid coating superimposed on a non-flat substrate can be seen. In some spots a less structured surface due to a larger concentration of the binder can be seen. The AFM image of the surface of the stpTSSS coating with a grammage of  $1.7 \text{ g/m}^2$  in Fig. 10 shows a less structured surface. The uneven surface of the substrate is better filled with the coating and the pigment particles are less obviously exposed. The trend is further evident in Fig. 11, showing an AFM image of the stpTSSS coating with a grammage of  $2.4 \text{ g/m}^2$ . The surface is smoother and the pigment particles are enclosed in a binder, clearly visible below the cPVC coating.

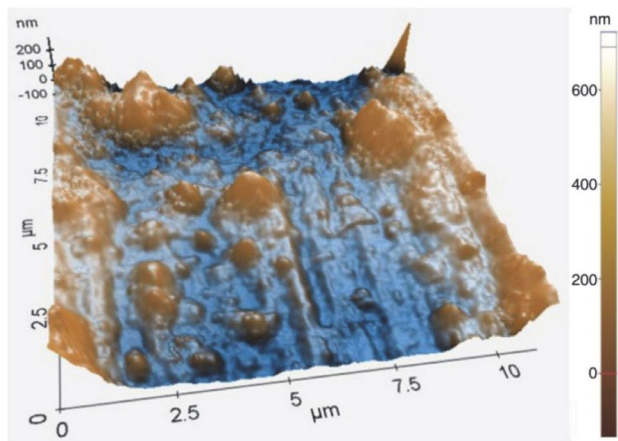


Figure 8. AFM image of aluminum substrate.

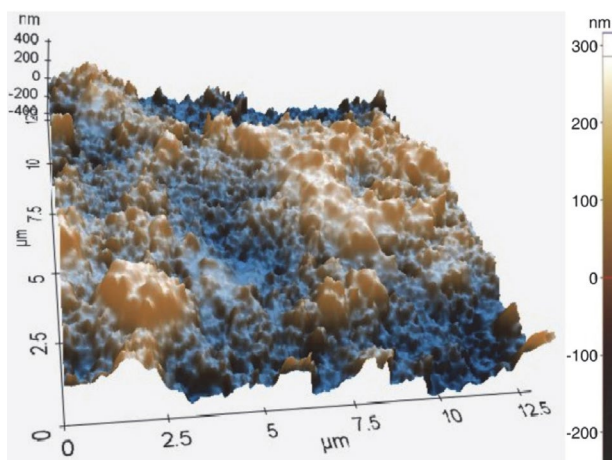


Figure 9. AFM image of stpTSSS coating with  $1.2 \text{ g/m}^2$  grammage on aluminum substrate.

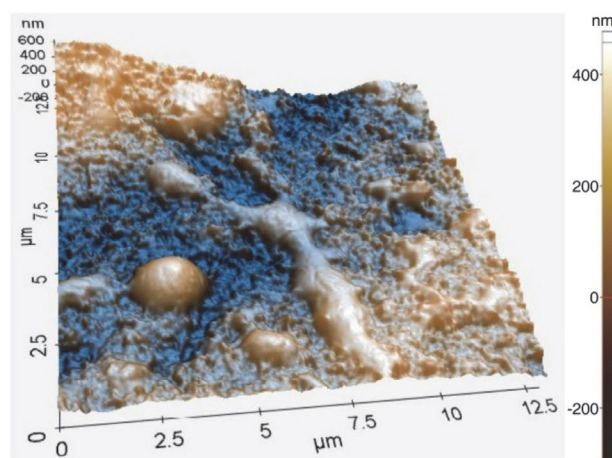


Figure 10. AFM image of stpTSSS coating with  $1.7 \text{ g/m}^2$  grammage on aluminum substrate.

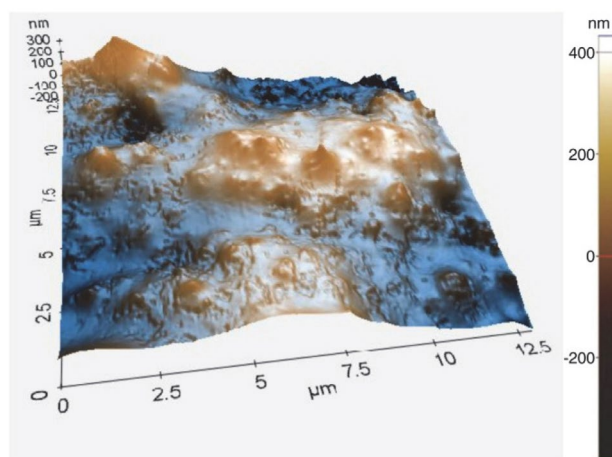


Figure 11. AFM image of stpTSSS coating with  $2.4 \text{ g/m}^2$  grammage on aluminum substrate.

From the above images we can conclude that the PC versus thickness relation for the stpTSSS coatings shown in



Fig. 4 is influenced by the change of the PVC in the top layer of the coating as a significant amount of binder is used for the substrate wetting, thus exposing more pigment particles.

### 3. 4. Hydrophobicity

The nanostructure of the stpTSSS is also evident in its hydrophobicity. We present the contact angles for the water of coatings applied at different grammages in Fig. 12. As the binder has a contact angle for water of  $96^\circ$ , if applied on a thick enough layer to eliminate the influence of a substrate, it is clear from the data that the large contact angles for the stpTSSS coating are the result of structured surfaces. It could also be reasoned that the wetting of the pigment particles in the top layer of the coating is not perfect at lower grammages, resulting in lower contact angles for the more structured surfaces.

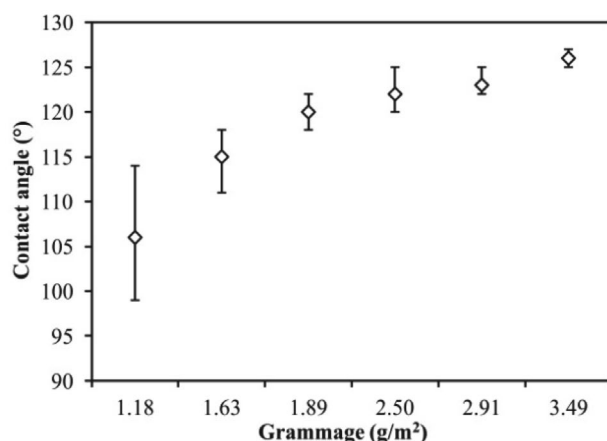


Figure 12. Contact angles for water for stpTSSS coatings applied at different grammages.

### 3. 5. Heat-gathering Properties

The spectroscopic measurements (Fig. 6) and nanotopography (Figs. 8–11) must of course correspond with

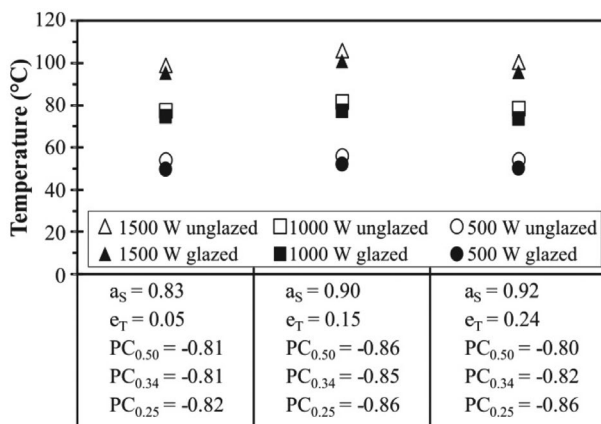


Figure 13. Stagnation temperatures and samples' spectral selectivity in heat gathering tests.

practical results to be of industrial significance. To check the practicability of the stpTSSS coatings the heat-gathering properties were tested. The coatings were prepared with air spraying on an aluminum substrate. Fig. 13 shows the spectral selectivity data of the samples and the stagnation temperatures with glazed and unglazed setups at various illuminations.

The above results clearly show that the best heat-gathering properties are exhibited by the most selective sample, i.e., the one with the lowest  $PC$  value. Relatively low temperatures were achieved in the setups used, which means  $PC_{0.25}$  is the appropriate criteria for coating selection.

## 4. Conclusions

- Silane-treated-pigment TSSS paints (stpTSSS) produced according to a recently disclosed procedure are the first Task-X-certified<sup>26</sup>, organic, spectrally selective coatings. They have now entered industrial production on a major European producer's solar absorber surfaces coil-coating line.
- The selectivity of stpTSSS paints was studied. The performance criteria ( $PC$ ) of the coating were found to decrease with the pigment-volume concentration ( $PVC$ ). The critical  $PVC$  ( $cPVC$ ) was determined by means of EIS.
- The nonlinearity of the  $PC$  versus grammage relation was shown to be related not only to the optical properties of the pigment and the binder used, but also to the surface topography. Thin, near  $cPVC$  coatings exhibit a significantly different surface topography than the thicker coatings. We believe that sub-optimal pigment wetting by the binder in the thinly applied coatings' top layer is caused by a disproportionate amount of binder being used for the substrate wetting, resulting in a  $PVC$  gradient in the coating. This phenomenon, which is not readily observable in thicker coatings, leaves the subject open for further studies.
- Contact-angle measurements for water support the surface-topography findings, i.e., the contact angles increase with the thickness. This can be readily explained by the coatings' compositions and topographies.
- The spectroscopic measurements of the paint's selectivity correlate well with the results obtained with the stagnation temperature built up in a model collector.

## 5. Acknowledgements

Authors wish to thank the staff of Laboratory for the Spectroscopy of Materials at National Institute of Chemistry (of Slovenia) under leadership of Prof. Dr. Boris Orel for spectral selectivity measurements and the staff of Physical Analytical Laboratory at Helios d.d. under leadership

of Dr. Saša Skale for measurements. The work was partially financed through KC-TIGR (Competence Centre sustainable and innovative construction); operation part financed by the European Union, European Regional Development Fund. MS thanks Public Agency for Technology of the Republic of Slovenia (TIA) for financing through MR-08 program, grant number P-MR-08/21; operation part financed by the European Union, European Social Fund. The authors also acknowledge the financial support from the state budgeted by the Slovenian Research Agency (Programme Nos. P2-0223 and P2-0392).

## 6. References

1. F. Cao, K. McEnaney, G. Chen, Z.F. Ren, *Energy Environ. Sci.*, **2014**, *7*, 1615–1627. DOI:10.1039/c3ee43825b
2. ISO 9845-1, Solar energy – Reference solar spectral irradiance at the ground at different receiving conditions – Part 1: Direct normal and hemispherical solar irradiance for air mass 1,5, ISO, Geneve, **1992**.
3. SOLABS, Development of unglazed solar absorbers (resorting to coloured selective coatings on steel material) for building facades, and integration into heating systems, EU project, Contract no. ENK6-CT-2002-00679.
4. M. Koželj, B. Orel, M. Steinbücher, I. Jerman, M. Vodlan, Aminosilane-modified pigments for spectrally selective paints, method for their preparation and application in paints, SI Patent Number 23055, date of patent November 30, **2010**.
5. M. Koželj, B. Orel, M. Steinbücher, I. Jerman, M. Vodlan, Coil-coated spectrally selective coatings on copper or aluminum with pigments modified by aminosilane, EU Patent Number 2432835 B1, date of patent January 27, **2016**.
6. M. Hoeflaak, Optimization of spectrally selective coatings for flat plate solar collectors, in: 8<sup>th</sup> International conference “Optimising paint formulation: preservation, stabilization and care”, Amsterdam, Netherlands, **1988**.
7. B. Orel, H. Spreizer, L. Slemenik Perše, M. Fir, A. Šurca Vuk, D. Merlini, M. Vodlan, *Sol. Energy Mat. Sol. Cells*, **2007**, *91*, 93–107. DOI:10.1016/j.solmat.2006.07.013
8. B. Orel, H. Spreizer, L. Slemenik Perše, M. Fir, A. Šurca Vuk, D. Merlini, M. Vodlan, M. Kohl, *Sol. Energy Mat. Sol. Cells*, **2007**, *91*, 108–119. DOI:10.1016/j.solmat.2006.07.012
9. E. AlShamaileh, *Sol. Energy*, **2010**, *84*, 1637–1643. DOI:10.1016/j.solener.2010.06.003
10. J. Manara, M. Reidinger, M. Rydzek, M. Arduini-Schuster, *Prog. Org. Coat.*, **2011**, *70*, 199–204. DOI:10.1016/j.porgcoat.2010.09.024
11. S. Wijewardane, D.Y. Goswami, *Renewable Sustainable Energy Rev.*, **2012**, *16*, 1863–1873. DOI:10.1016/j.rser.2012.01.046
12. I. Jerman, M. Koželj, B. Orel, *Sol. Energy Mat. Sol. Cells*, **2010**, *94*, 232–245. DOI:10.1016/j.solmat.2009.09.008
13. B. Japelj, A. Šurca Vuk, B. Orel, L. Slemenik Perše, I. Jerman, J. Kovač, *Sol. Energy Mat. Sol. Cells*, **2008**, *92*, 1149–1161. DOI:10.1016/j.solmat.2008.04.003
14. R. Kunič, M. Koželj, B. Orel, A. Šurca Vuk, A. Vilčnik, L. Slemenik Perše, D. Merlini, S. Brunold, *Sol. Energy Mat. Sol. Cells*, **2009**, *93*, 630–640. DOI:10.1016/j.solmat.2008.12.026
15. R. Kunič, M. Mihelčič, B. Orel, L. Slemenik Perše, B. Bizjak, J. Kovač, S. Brunold, *Sol. Energy Mat. Sol. Cells*, **2011**, *95*, 2965–2975. DOI:10.1016/j.solmat.2011.05.014
16. ISO 2808, Paints and varnishes – Determination of film thickness, ISO, Geneve, **2007**.
17. H. D. Liu, T. R. Fu, M. H. Duan, Q. Wan, C. Luo, Y. M. Chen, D. J. Fu, F. Ren, Q. Y. Li, X. D. Cheng, B. Yang, X. J. Hu, *Sol. Energy Mat. Sol. Cells*, **2016**, *157*, 108–116. DOI:10.1016/j.solmat.2016.05.035
18. Measurement of Total Solar Reflectance of Paint Panels using PerkinElmer UV/Vis/NIR Spectrophotometers and UV WinLab Software, Perkin Elmer, Inc., Waltham, USA, **2010**.
19. S. Skale, V. Doleček, M. Slemnik, *Corros. Sci.*, **2007**, *49*, 1045–1055. DOI:10.1016/j.corsci.2006.06.027
20. R. E. Lobnig, W. Villalba, K. Goll, J. Vogelsang, I. Winkels, R. Schmidt, P. Zanger, J. Soetemann, *Prog. Org. Coat.*, **2006**, *55*, 363–374. DOI:10.1016/j.porgcoat.2005.11.015
21. R. E. Lobnig, V. Bonitz, K. Goll, M. Single, W. Villalba, J. Vogelsang, I. Winkels, R. Schmidt, P. Zanger, *Prog. Org. Coat.*, **2007**, *60*, 1–10. DOI:10.1016/j.porgcoat.2007.03.003
22. N. Selvakumar, H. C. Barshilia, *Sol. Energy Mat. Sol. Cells*, **2012**, *98*, 1–23. DOI:10.1016/j.solmat.2011.10.028
23. ISO 2409, Paints and Varnishes – Cross-cut test, ISO, Geneve, **2007**.
24. Z. W. Wicks, F. N. Jones, S. P. Pappas, D. A. Wicks, *Organic Coatings: Science and Technology*, 3<sup>rd</sup> Edition, Wiley, New Jersey, USA, **2007**, pp. 461–471. DOI:10.1002/047007907X
25. M. Klanjšek Gunde, J. Kozar Logar, Z. Cmjak Orel, B. Orel, *Thin Solid Films*, **1996**, *277*, 185–191. DOI:10.1016/0040-6090(95)08023-6
26. B. Carlsson, M. Köhl, Recommended qualification test procedure for solar absorber surface durability, IEA Solar Heating and Cooling Program, Paris, France, **2005**.

## Povzetek

Članek obravnava od debeline odvisne spektralno selektivne premaze, ki so bili pripravljene z različnimi volumnskimi koncentracijami pigmenta temelječih na silansko obdelanih pigmentih. Kritična volumnska koncentracija pigmenta je bila določena s pomočjo elektrokemijske impedančne spektroskopije, porazdelitev velikosti delcev pa z ultrazvočno spektroskopijo. Odvisnost selektivnosti od debeline premaza s skoraj kritično volumnsko koncentracijo pigmenta je bila preučevana spektroskopsko na podlagi zmogljivostnega kriterija. Pokazalo se je, da je nelinearnost slednjega povezana s površinsko topografijo, kar je bilo dodatno potrjeno z meritvami hidrofobnosti. Meritve sposobnosti zbiranja toplote v simuliranem toplotnem zbiralniku so potrdile spektroskopsko določitev optimalne debeline suhega filma.

Scientific paper

# Graphene Oxide/Co<sub>3</sub>O<sub>4</sub> Nanocomposite: Synthesis, Characterization, and Its Adsorption Capacity for the Removal of Organic Dye Pollutants from Water

Kolsoum Pourzare, Saeed Farhadi\* and Yaghoub Mansourpanah

Department of Chemistry, Lorestan University, Khoramabad68151-44316, Iran

\* Corresponding author: E-mail: sfarhadi1348@yahoo.com

Tel: +98 06633120611, fax: +98 06633120618.

Received: 18-06-2017

## Abstract

In this work, graphene oxide/Co<sub>3</sub>O<sub>4</sub> nanocomposite was synthesized via hydrothermal decomposition of [Co(en)<sub>3</sub>](NO<sub>3</sub>)<sub>3</sub> complex onto graphene oxide nanosheets. The as-prepared nanocomposite (denoted as GO/Co<sub>3</sub>O<sub>4</sub>) was structurally characterized by Fourier transform infrared (FT-IR) spectroscopy, X-ray diffraction (XRD), Raman spectroscopy, scanning electron microscopies (TEM and SEM), energy dispersive X-ray (EDX) spectroscopy, magnetic measurements, and N<sub>2</sub> adsorption–desorption analysis. The results demonstrated successful immobilization of Co<sub>3</sub>O<sub>4</sub> nanoparticles with an average diameter size of around 12.5 nm on the surface of graphene oxide nanosheets. The adsorption performance of GO/Co<sub>3</sub>O<sub>4</sub> nanocomposite was investigated towards different organic dyes in aqueous solutions. The results displayed that the adsorption rate of the GO/Co<sub>3</sub>O<sub>4</sub> nanocomposite was 98% for methylene blue (MB) in 12 min, and 66% and 45% for Rhodamine B (RhB) and methyl orange (MO) in 40 min, respectively. The effects of various important parameters including adsorbent dosage, contact time, pH, and temperature on the adsorption process were investigated in detail. The equilibrium adsorption data were better fitted by Langmuir isotherm. Adsorption kinetics is well-modeled using pseudo-second-order model. Different thermodynamic parameters indicated that the adsorption process was physisorption and spontaneous. The findings of the present work highlighted facile fabrication of GO/Co<sub>3</sub>O<sub>4</sub> and its application for rapid and efficient removal of MB from wastewater.

**Keywords:** Graphene oxide nanosheets, Co<sub>3</sub>O<sub>4</sub> nanoparticles, Hydrothermal decomposition, Nanocomposite, Adsorption performance, Organic dyes.

## 1. Introduction

Many chemical industries such as paper, plastics, cosmetics, leather, printing, food, textile, etc. use dyes for coloring their products and release the various types of dyes into water bodies which prevent the penetration of sunlight, retard the photosynthetic reactions, and affect aquatic life.<sup>1–4</sup> Most dye molecules have aromatic rings in their structures, which make them highly toxic, non-biodegradable, carcinogenic, and mutagenic to both human being and aquatic life.<sup>5</sup> Hence, it is essential to remove or minimize dyes to permissible levels, without disturbing the quality of water to be able to use it in diverse industrial and agricultural applications.<sup>6</sup> A wide array of wastewater treatment techniques including membrane filtration, centrifugation, photodegradation, chemical coagulation, and adsorption have been developed for removing dyes from wastewater.

Among these technologies, adsorption is the most widely used method due to its versatility, wide applicability, and economic feasibility.<sup>7</sup> Activated carbon, clays, zeolites, polymeric materials, etc. have been applied to adsorb dyes from wastewater. However, these adsorbents suffer from either low adsorption capacities or separation problem. Hence, the adsorbent having both mentioned characteristics is immensely desired in both science and technology societies.<sup>8</sup> In material science research, a great deal of attention has been focused on graphene, a carbon allotrope with a two-dimensional sheet-like structure with many unique features such as high electrical conductivity, mechanical flexibility, chemical and thermal stability, high surface functionality, and large surface area.<sup>7</sup> Due to strong interplane interactions, graphene and its derivatives tend to aggregate in a layer-by-layer manner which, as a result, a significant part of their surface area is lost. The use of the

dispersion of single-layered GO as an absorbent allows one to utilize the surface area to the utmost extent, but these GO sheets are difficult to collect from water.<sup>9</sup> This problem can be solved via chemical modification of graphene by the process of attaching organic groups or inorganic particles onto graphite oxide (GO) surfaces which can result not only in physical separation of the resultant functionalized graphene sheets but also in the possible formation of a stable dispersed phase of graphene in the synthesis process<sup>10–12</sup> and keep the surface area and pore volume at high levels which is required for applications such as adsorption processes and photocatalysis.<sup>13</sup>

In recent years, various transition metal oxides nanoparticles such as  $\text{Fe}_2\text{O}_3$ ,  $\text{ZnO}$ ,  $\text{Fe}_3\text{O}_4$ ,  $\text{TiO}_2$ , etc., have been deposited on GO nanosheets. For instance, Amino-functionalized  $\text{Fe}_3\text{O}_4$  ( $\text{NH}_2\text{-Fe}_3\text{O}_4$ ) particles were deposited on graphene oxide sheets and were used to adsorb Methylene Blue (MB) and Neutral Red (NR) from aqueous solution by Xie et al.<sup>14</sup> The adsorption test of dyes demonstrated that it only took 30 min for MB and 90 min for NR to reach equilibrium. Luo et al. fabricated magnetic cyclodextrin/graphene oxide (MCGO) materials and investigated their application as excellent adsorbents for methylene blue.<sup>15</sup> MCGO demonstrated extremely fast MB-removal from wastewater with high removal efficiency within 50 min. Li et al. prepared a magnetic  $\text{CoFe}_2\text{O}_4$ -functionalized graphene sheet ( $\text{CoFe}_2\text{O}_4\text{-FGS}$ ) nanocomposite via a facile hydrothermal method and used it to adsorb methyl orange.<sup>16</sup> The observed maximum adsorption capacity at  $10 \text{ mg L}^{-1}$  initial concentration was  $71.54 \text{ mg g}^{-1}$ . In another study, Fan et al. prepared a magnetic chitosan-GO (MCFO) nanocomposite through covalent bonding of chitosan to the surface of  $\text{Fe}_3\text{O}_4$  nanoparticles followed by covalent functionalization of GO with magnetic chitosan which acted as a good adsorbent to adsorb MB from aqueous solutions.<sup>17</sup> Yao et al. also fabricated  $\text{Fe}_3\text{O}_4/\text{SiO}_2/\text{GO}$  nanocomposite through a covalent bonding technique and used it as an adsorbent for the removal of MB from aqueous solution.<sup>18</sup> Maximum MB adsorption capacities were 97, 102.6, and  $111.1 \text{ mg g}^{-1}$  at 25, 45, and  $60 \text{ }^\circ\text{C}$ , respectively.

Spinel-type cobalt oxide ( $\text{Co}_3\text{O}_4$ ) is an important magnetic p-type semiconductor oxide and its synthesis and properties have attracted considerable attention owing to its prominent applications in heterogeneous catalysis, energy storage and conversion, sensors, devices, etc.<sup>19–25</sup> For this reason, various nanostructures of  $\text{Co}_3\text{O}_4$  such as nanoparticles, nanoplates, nanorods, nanotubes, nanodiscs, nanoflowers, nanocubes and hollow microspheres structures have been prepared by using different synthesis methods.<sup>26–33</sup> To the best of our knowledge, the investigation of adsorption properties of  $\text{GO}/\text{Co}_3\text{O}_4$  nanocomposites has not been reported yet. In this study, we presented a solvothermal approach for the production of  $\text{GO}/\text{Co}_3\text{O}_4$  nanocomposite. The resulting products was characterized by FT-IR, XRD, Raman, FE-SEM, EDX,

TEM, and VSM techniques and its adsorption properties in removing dye molecules from aqueous solutions were investigated.

## 2. Experimental

### 2.1. Materials

Methyl orange ( $\text{C}_{14}\text{H}_{14}\text{N}_3\text{NaO}_3\text{S}$ , MO), methylene blue ( $\text{C}_{16}\text{H}_{18}\text{ClN}_3\text{S}$ , MB), Rhodamine B ( $\text{C}_{28}\text{H}_{31}\text{ClN}_2\text{O}_3$ , RhB), Cobalt (II)-chlorid hexahydrate, and all other materials and solvents were purchased from Merck chemical Co (Germany). All chemical materials were of analytical grade and were used as received without further purification.

### 2.2. Synthesis of $\text{Co}_3\text{O}_4$ Nanoparticles

First,  $[\text{Co}(\text{en})_3](\text{NO}_3)_3$  complex was prepared via the simple reaction of an aqueous solution of  $[\text{Co}(\text{en})_3]\text{Cl}_3$  with concentrated nitric acid according to the reported method.<sup>34</sup> To prepare  $\text{Co}_3\text{O}_4$  nanoparticles,  $[\text{Co}(\text{en})_3](\text{NO}_3)_3$  complex was decomposed at  $250 \text{ }^\circ\text{C}$  for 1 h in an electric furnace under ambient air. The decomposition product was collected for characterization.

### 2.3. Synthesis of Graphene Oxide/ $\text{Co}_3\text{O}_4$ Nanocomposite ( $\text{GO}/\text{Co}_3\text{O}_4$ )

Graphene oxide (GO) was prepared by the oxidation of graphite powder under acidic conditions according to modified Hummers method using a mixture of  $\text{H}_2\text{SO}_4$ ,  $\text{NaNO}_3$ , and  $\text{KMnO}_4$ .<sup>35,36</sup> For the synthesis of  $\text{GO}/\text{Co}_3\text{O}_4$  nanocomposite, 50 mg GO was dispersed into 20 mL deionized water by sonication for 1 h to achieve a uniform dispersion of GO. 100 mg as-prepared  $\text{Co}_3\text{O}_4$  nanoparticles were dispersed in deionized water for 15 min and were gradually added into GO suspension. The mixture was sonicated for 30 min and transferred into an autoclave for hydrothermal treatment at  $180 \text{ }^\circ\text{C}$  for 24 h. The resultant product was separated by centrifugation and washed with deionized water, and dried in an oven at  $60 \text{ }^\circ\text{C}$  for 12 h.

### 2.4. Methods of Characterization

Fourier-transform infrared spectra were obtained on Shimadzu FT-IR 8400S (Japan) with temperature controlled high sensitivity detector (DLATGS detector) in the scan range of  $500\text{--}4000 \text{ cm}^{-1}$  using KBr pellet. The XRD patterns were obtained on a Rigaku D-max C III, X-ray diffractometer using Ni-filtered Cu K $\alpha$  radiation ( $\lambda = 1.5406 \text{ \AA}$ ) for phase determination samples. Optical absorption spectra of dyes were obtained on a Cary 100 UV-Vis spectrophotometer in the wavelength range of  $200\text{--}800 \text{ nm}$ . A vibrating sample magnetometer (VSM, Magnetic Daneshpajoh Kasha Co., Iran) was employed to measure magnetic parameter at room temperature. Particle size was ob-

served by a transmission electron microscope (Philips CM120) at the accelerating voltage of 100 kV. SEM images were obtained on MIRA3 TESCAN Field Emission Scanning Electron Microscope equipped with Energy Dispersive X-ray (EDX) analyzer for the elemental analysis of the sample. N<sub>2</sub> adsorption-desorption measurements were performed at 77 K (Micromeritics Tristar ASAP 3000) using Brunauer-Emmett-Teller (BET) method.

## 2. 5. Adsorption Tests

Adsorption experiments were performed by using 30 ml solution with known MB concentration and varying the amount of GO/Co<sub>3</sub>O<sub>4</sub> as the adsorbent from 10 to 30 mg in 40 min. The initial pH of MB solution was adjusted in the range of 4–12 by dropwise adding 0.1 mol/L NaOH or 0.1 mol/L HCl solutions. After adsorption was completed, the solution was separated from the precipitate by centrifugation at 5000 rpm for 5 min. The concentrations of the dye in the solutions after different time intervals were determined with a UV-visible spectrophotometer at the wavelength of 664 nm ( $\lambda_{\max}$ ). The amount of MB adsorbed onto GO/Co<sub>3</sub>O<sub>4</sub> nanocomposite ( $q_t$ ) and its removal rate (R%) were calculated by the following equations:

$$q_t = (C_0 - C_t)V/m, R\% = (C_0 - C_t)100/C_0 = (A_0 - A_t)100/A_0 \quad (1)$$

where  $C_0$  and  $C_t$  (mg/L) are liquid-phase concentrations of dye at initial and at time  $t$ , respectively,  $V$  (L) is the volume of the solution and  $m$  (g) is the mass of the used adsorbent.

$A_0$  and  $A_t$  are the absorbance of MB before and after the adsorption, respectively.

## 3. Results and Discussion

### 3. 1. Characterization of the GO/Co<sub>3</sub>O<sub>4</sub> Nanocomposite

The FT-IR spectra of the samples are shown in Figure 1. For the starting [Co(en)<sub>3</sub>](NO<sub>3</sub>)<sub>3</sub> complex, the characteristic stretching bands of NH<sub>2</sub>, CH<sub>2</sub>, NO<sub>3</sub> were appeared at about 3100–3400, 2951 and 1380 cm<sup>-1</sup>, respectively.<sup>37</sup> As can be seen in the spectrum of Co<sub>3</sub>O<sub>4</sub> (Figure 1(b)), almost all bands associated with the complex obviously disappeared when the complex was decomposed at 250 °C and only two strong bands at 569 and 663 cm<sup>-1</sup> were observed which confirmed the spinel structure of Co<sub>3</sub>O<sub>4</sub>. The former band was attributed to the stretching vibration mode of Co(III)–O and the latter band could be assigned to Co(II)–O bond.<sup>38</sup> The formation of Co<sub>3</sub>O<sub>4</sub> from the [Co(en)<sub>3</sub>](NO<sub>3</sub>)<sub>3</sub> complex can be related to the explosive decomposition of the complex via an intramolecular redox process occurring between the ethylenediamine (en) ligands and NO<sub>3</sub><sup>-</sup> ions as reducing and oxidiz-

ing agents, respectively. This reaction resulted in the formation of solid Co<sub>3</sub>O<sub>4</sub> and gaseous products i.e. CO<sub>2</sub>, H<sub>2</sub>O and NO<sub>x</sub> (NO, N<sub>2</sub>O and NO<sub>2</sub>).<sup>38</sup> Although the exact reaction is unclear and intermediates and gaseous products had not been identified directly, the formation of Co<sub>3</sub>O<sub>4</sub> can be expressed as follows: [Co(en)<sub>3</sub>](NO<sub>3</sub>)<sub>3</sub>(s) → Co<sub>3</sub>O<sub>4</sub>(s) + CO<sub>2</sub>(g) + H<sub>2</sub>O(g) + NO<sub>x</sub> (NO(g) + N<sub>2</sub>O(g) + NO<sub>2</sub>(g)). In FT-IR spectrum of GO (Figure 2(c)) obvious characteristic peaks of GO could be seen, including C=O stretching vibrations of COOH groups (1726 cm<sup>-1</sup>), graphitic C=C stretching vibrations (1618 cm<sup>-1</sup>), O-H deformation vibrations of tertiary C-OH (1398 cm<sup>-1</sup>), C-O stretching vibrations of epoxy/alkoxy groups (1026 cm<sup>-1</sup>) and O-H stretching vibrations (3100–3700 cm<sup>-1</sup>).<sup>39</sup> However, as can be seen in Figure 2(d), after hydrothermal treatment the band of C=O was disappeared and the intensity of O-H and C-O bands were decreased, which indicated the removal of oxygen-containing functional groups and reduction of GO. This finding confirms the formation of reduced graphene oxide (rGO) in the composite and the restoration of a graphitic structure in graphene.<sup>40</sup> Moreover, the two strong absorption peaks in the spectrum of GO/Co<sub>3</sub>O<sub>4</sub> at lower

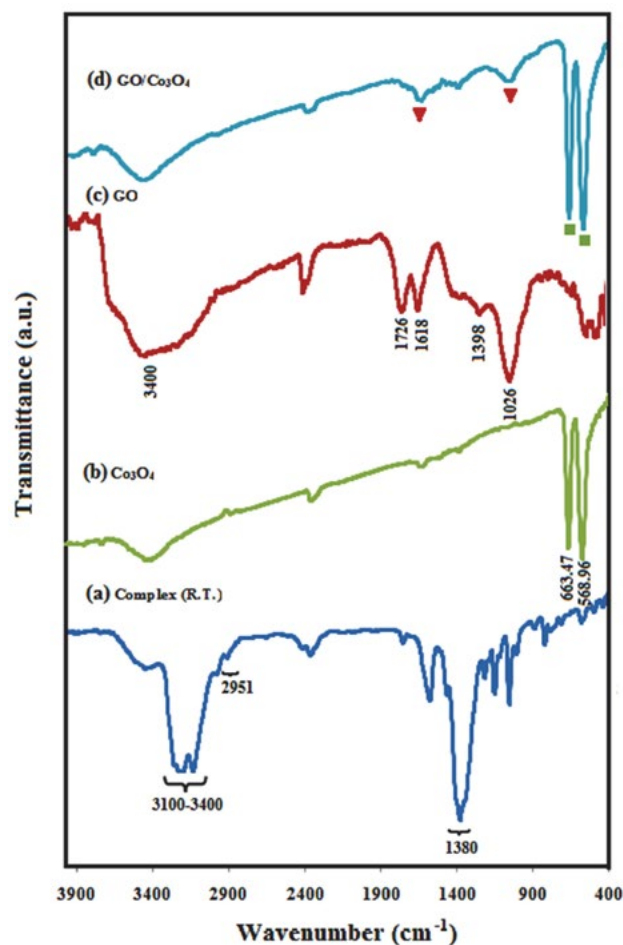
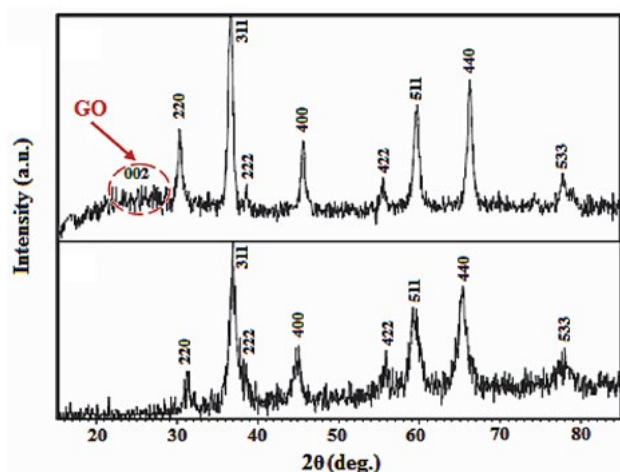


Figure 1. FT-IR spectra of (a) [Co(en)<sub>3</sub>](NO<sub>3</sub>)<sub>3</sub> complex, (b) Co<sub>3</sub>O<sub>4</sub>, (c) GO, and (d) GO/Co<sub>3</sub>O<sub>4</sub>.

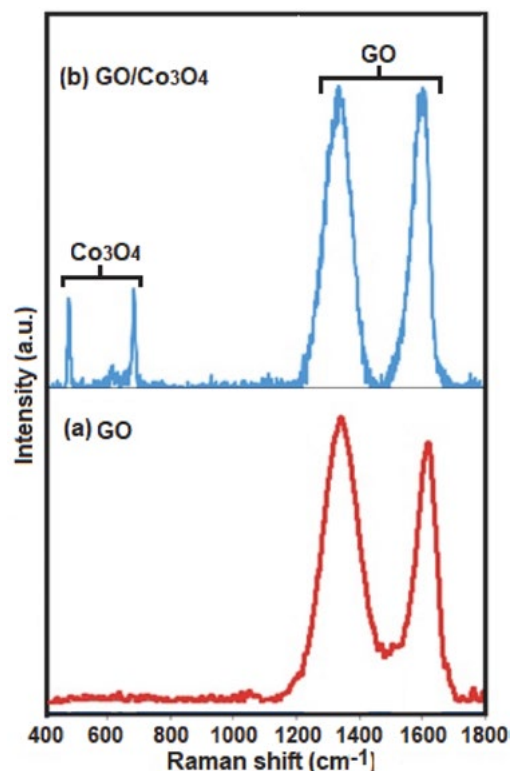
frequencies (in the 400–600  $\text{cm}^{-1}$  range) could be assigned to the stretching vibrations of Co-O bonds of  $\text{Co}_3\text{O}_4$  phase. This result confirmed the formation of  $\text{GO}/\text{Co}_3\text{O}_4$  nanocomposite.

In order to further identify the chemical composition and structure of the prepared samples, powder X-ray diffraction (XRD) was conducted. Figure 2 displays the XRD patterns of  $\text{Co}_3\text{O}_4$  and  $\text{GO}/\text{Co}_3\text{O}_4$  nanocomposite. The diffraction patterns in Figures 2(a) and (b) are similar and can be indexed to the  $\text{Co}_3\text{O}_4$  phase (JCPDS No. 78-1970). Moreover, no characteristic diffraction peaks for GO were observed in the pattern indicating that GO nanosheets were not stacked during the synthesis process. The reason can be attributed to the fact that  $\text{Co}_3\text{O}_4$  nanoparticles anchored on the surfaces of GO prevented the exfoliated GO nanosheets from restacking. However, a broad characteristic peak for graphene nanosheets at about  $2\theta = 23^\circ$  appeared, suggesting that GO was reduced to graphene during the formation of the nanocomposite. The average domain size of  $\text{Co}_3\text{O}_4$  nanoparticles was calculated to be approximately 13 nm by the Scherrer formula:  $D_{\text{XRD}} = 0.9\lambda/(\beta \cos \theta)$ , where  $D_{\text{XRD}}$  is average crystalline size;  $\lambda$ ,  $\beta$ , and  $\theta$  are wavelength of Cu K $\alpha$  radiation, full width at half maximum of the diffraction peak, and Bragg angle, respectively.<sup>41</sup>



**Figure 2.** XRD patterns of (a)  $\text{Co}_3\text{O}_4$  and (b)  $\text{GO}/\text{Co}_3\text{O}_4$  nanocomposite.

Raman spectroscopy is a powerful tool to characterize significant structural changes of GO during the composite synthesis. Figure 3 presents the Raman spectra of GO and  $\text{GO}/\text{Co}_3\text{O}_4$  nanocomposite. According to the Raman spectrum of GO in Figure 3(a), the obvious peaks at 1318 and 1584  $\text{cm}^{-1}$  can be attributed to the disordered structure (D band,  $\text{sp}^3$  carbon atoms of disorders and defects) and graphite structure (G band,  $\text{sp}^2$  carbon atoms in graphitic sheets) of GO, respectively.<sup>42</sup> In the spectrum of  $\text{GO}/\text{Co}_3\text{O}_4$ , D and G peaks still exist, while other two obvious peaks at 477 and 683  $\text{cm}^{-1}$  can be attributed to



**Figure 3.** Raman spectra of (a) GO and (b)  $\text{GO}/\text{Co}_3\text{O}_4$  nanocomposite.

$\text{Co}_3\text{O}_4$ . Compared to GO, it was clear that D and G bands of  $\text{GO}/\text{Co}_3\text{O}_4$  were down shifted by 10  $\text{cm}^{-1}$ . The red shifts of D and G bands for  $\text{GO}/\text{Co}_3\text{O}_4$  provided evidence for charge transfer between GO and  $\text{Co}_3\text{O}_4$ , which indicated a strong interaction between them. Raman spectra further confirmed the successful synthesis of  $\text{GO}/\text{Co}_3\text{O}_4$  composite.

SEM images indicating the microstructural features of GO,  $\text{Co}_3\text{O}_4$ ,  $\text{GO}/\text{Co}_3\text{O}_4$  nanocomposite are shown in Figure 4. SEM image of pure GO in Figure 4(a) shows layered structure of GO having large stacks, possibly consisting of hundreds of graphene oxide nanosheets. It should also be noted that the surfaces of GO sheets were quite flat and smooth. Figure 4(b) shows SEM micrograph of sphere-like  $\text{Co}_3\text{O}_4$  nanoparticles. The SEM images of  $\text{GO}/\text{Co}_3\text{O}_4$  in Figures 4(c) and (d) clearly show graphene oxide nanosheets were successfully decorated with  $\text{Co}_3\text{O}_4$  nanoparticles. It can be clearly seen that the  $\text{Co}_3\text{O}_4$  nanoparticles were well deposited on GO which were a flexible interleaved structure. Some wrinkles are found on the surface, which may be important for preventing aggregation of GO and maintaining high surface area, which could be a great benefit to its adsorption ability. On the contrary with pure GO sheets, the surfaces of GO nanosheets in the nanocomposite were rough, and the edges were highly crumpled.

The morphologies and microstructures of the as-prepared  $\text{Co}_3\text{O}_4$  and  $\text{GO}/\text{Co}_3\text{O}_4$  samples were further

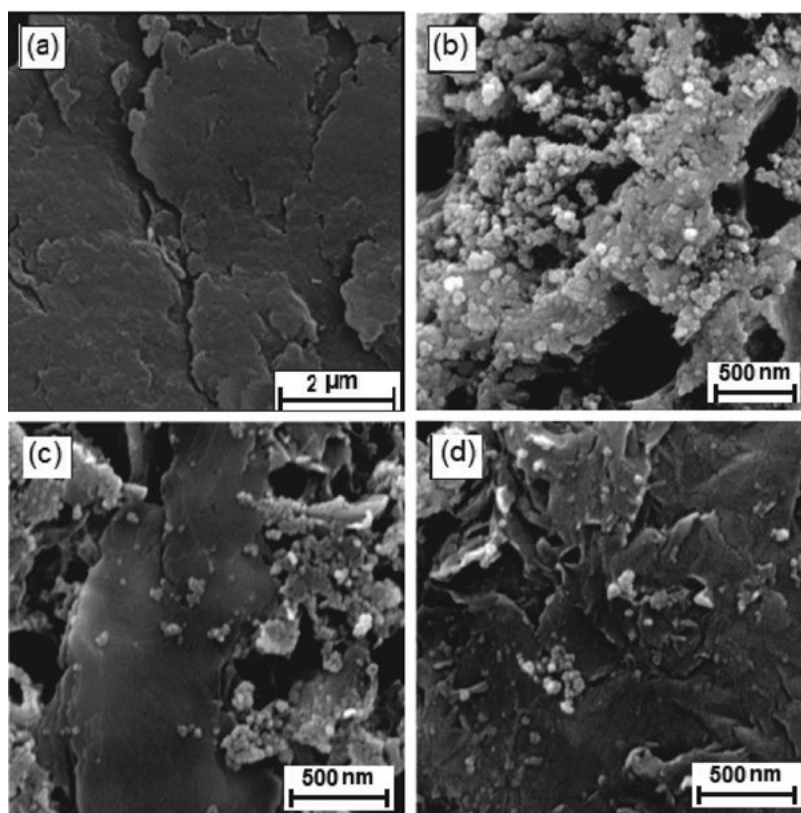


Figure 4. SEM images of (a) GO, (b) Co<sub>3</sub>O<sub>4</sub>, and (c,d) GO/Co<sub>3</sub>O<sub>4</sub>.

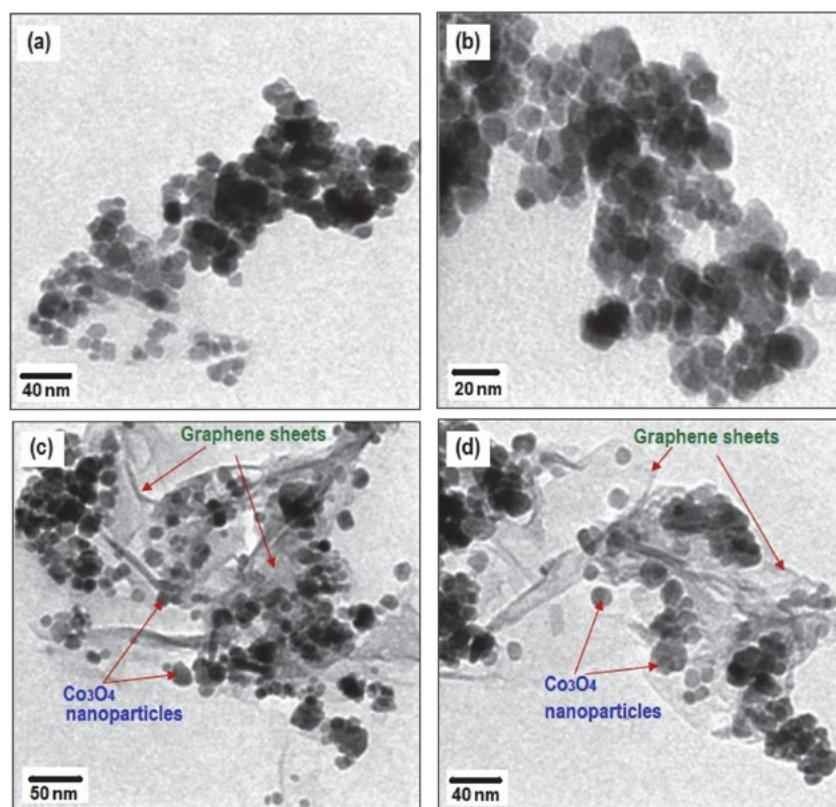
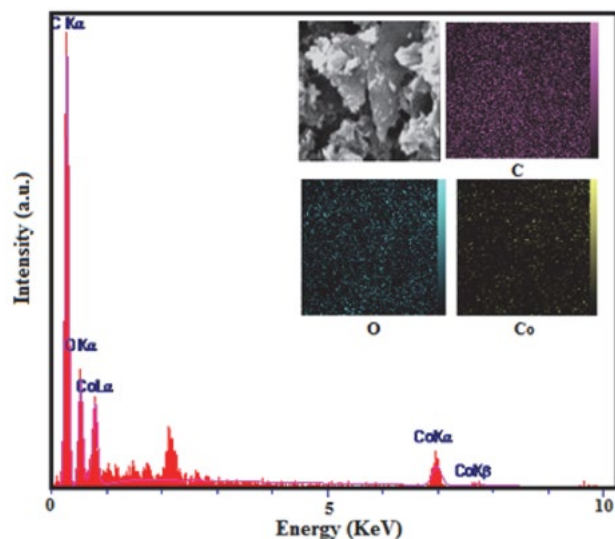


Figure 5. TEM images of (a,b) Co<sub>3</sub>O<sub>4</sub>, and (c,d) GO/Co<sub>3</sub>O<sub>4</sub> nanocomposite.

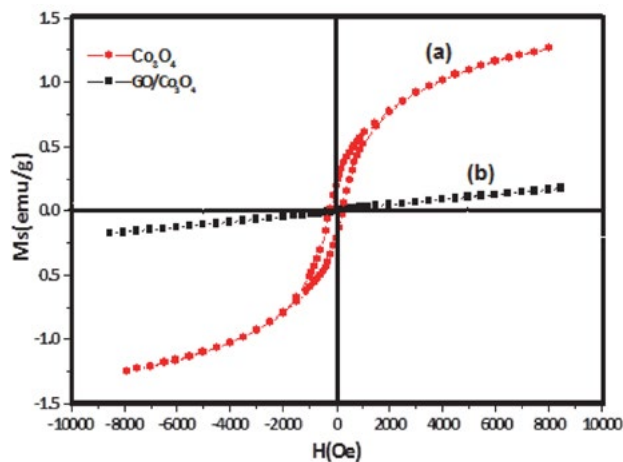
analyzed by TEM. Figures 5(a) and (b) show the typical TEM images of the  $\text{Co}_3\text{O}_4$ , displaying that the product consists of a large quantity of nearly uniform monodispersed spheres with the diameter size in the range of 10–25 nm which loosely aggregated. As can be seen in Figures 5(c) and (d), the almost transparent graphene sheets are fully exfoliated and decorated homogeneously with sphere-like  $\text{Co}_3\text{O}_4$  nanoparticles having an average diameter of 12 nm in consistent with the average particle size calculated from Debye-Scherer formula. No obvious aggregation was seen in Figures 5(c) or 4(d). The GO sheets could not only prevent agglomeration of the  $\text{Co}_3\text{O}_4$  nanoparticles and enable a good dispersion of these spherical particles, but also substantially enhance the specific surface area of the composite.

Further investigation was carried out by energy dispersive X-ray spectroscopy (EDX) to characterize the composition of the as-prepared  $\text{GO}/\text{Co}_3\text{O}_4$  nanocomposite as shown in Figure 6. The presence of C, O and Co elements in the composites could be proven by the EDX elemental spectrum of  $\text{GO}/\text{Co}_3\text{O}_4$ . The inset of Figure 6 shows a representative SEM image of the nanocomposite with corresponding EDX elemental mappings. As presented in the inset of Figure 6, the distribution of corresponding elemental mappings confirmed the existence of C, O, and Co. From the maps, it can be seen that the elements were uniformly distributed over the nanocomposite, confirming the homogeneity of the sample. The results further indicated that  $\text{Co}_3\text{O}_4$  nanocrystals had been successfully loaded on the surface of GO.



**Figure 6.** EDX spectrum of  $\text{GO}/\text{Co}_3\text{O}_4$  nanocomposite. The inset shows the corresponding EDX elemental mappings.

The magnetization curves of  $\text{Co}_3\text{O}_4$  and  $\text{GO}/\text{Co}_3\text{O}_4$  samples were measured at room temperature, as shown in Figure 7. Obviously, the shape of magnetic hysteresis loop



**Figure 7.** Magnetic hysteresis loops of (a)  $\text{Co}_3\text{O}_4$  nanoparticles and (b)  $\text{GO}/\text{Co}_3\text{O}_4$  nanocomposite.

of  $\text{Co}_3\text{O}_4$  sample shows a ferromagnetic behavior. The fine hysteresis loop of  $\text{GO}/\text{Co}_3\text{O}_4$  nanocomposite exhibited a typical weak ferromagnetic behavior at room temperature. The saturation magnetization ( $M_s$ ) of  $\text{Co}_3\text{O}_4$  nanoparticles sample is  $1.3 \text{ emu g}^{-1}$ . In contrast, the  $\text{GO}/\text{Co}_3\text{O}_4$  nanocomposite has smaller  $M_s$  value ( $0.18 \text{ emu g}^{-1}$ ), due to the presence of non-magnetic GO component, weakening its magnetic property.

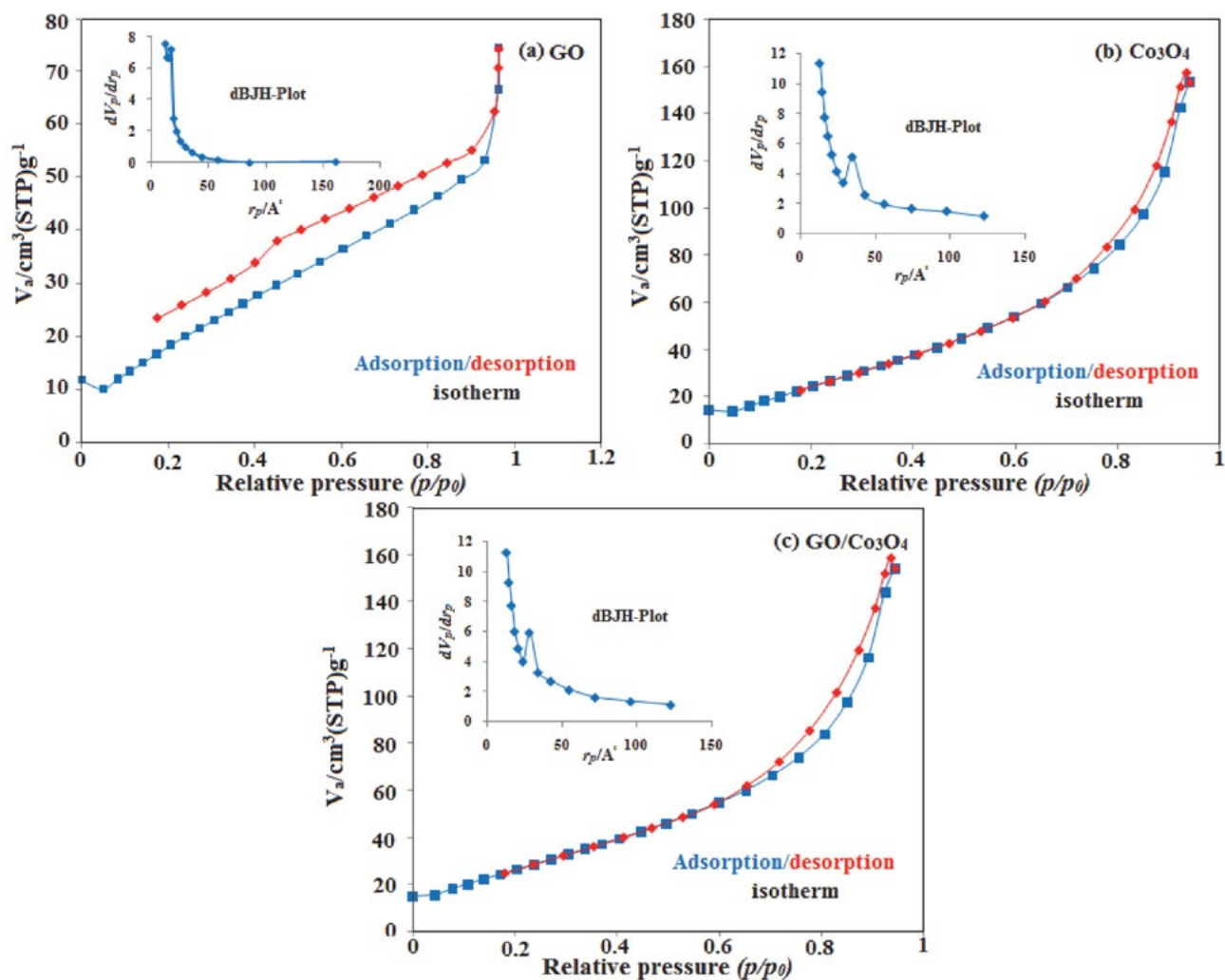
Nitrogen adsorption experiments were used to evaluate the pore size and structure of samples. Figure 8 shows the nitrogen adsorption–desorption isotherms and the corresponding pore size distributions curves (the insets) for GO,  $\text{Co}_3\text{O}_4$  and  $\text{GO}/\text{Co}_3\text{O}_4$  samples. The isotherms in Figure 8(a)–(c) can be classified to type IV with H4 hysteresis loop for GO and H3-hysteresis loops for  $\text{Co}_3\text{O}_4$  and  $\text{GO}/\text{Co}_3\text{O}_4$  samples (according to the IUPAC classification), which indicate the presence of mesopores. The interconnected porous network could mainly contribute to the formation of mesopores of GO and the aggregation of GO nanosheets could result in the formation of the mesopores. Some textural properties of the samples were listed in Table 1. As shown in Table 1, the materials were mesoporous. The BET surface area and pore volume of  $\text{GO}/\text{Co}_3\text{O}_4$  were higher than the values of GO. It can be concluded that the addition of  $\text{Co}_3\text{O}_4$  had a great effect on the structure of GO, greatly increasing the surface area and pore volume, which were all favorable factors for improving the adsorption performance.

**Table 1** Textural properties of GO,  $\text{Co}_3\text{O}_4$  and  $\text{GO}/\text{Co}_3\text{O}_4$  samples.

Entry	Sample	$S_{\text{BET}}$ ( $\text{m}^2/\text{g}$ )	$V_p$ ( $\text{cm}^3/\text{g}$ )	$D_p$ (nm)
1	GO	79.15	0.126	1.26
2	$\text{Co}_3\text{O}_4$	103.67	0.338	1.27
3	$\text{GO}/\text{Co}_3\text{O}_4$	107.27	0.336	1.27

$S_{\text{BET}}$ : BET surface area.  $V_p$ : Total pore volume.  $D_p$ : Average pore diameter calculated using BJH method.





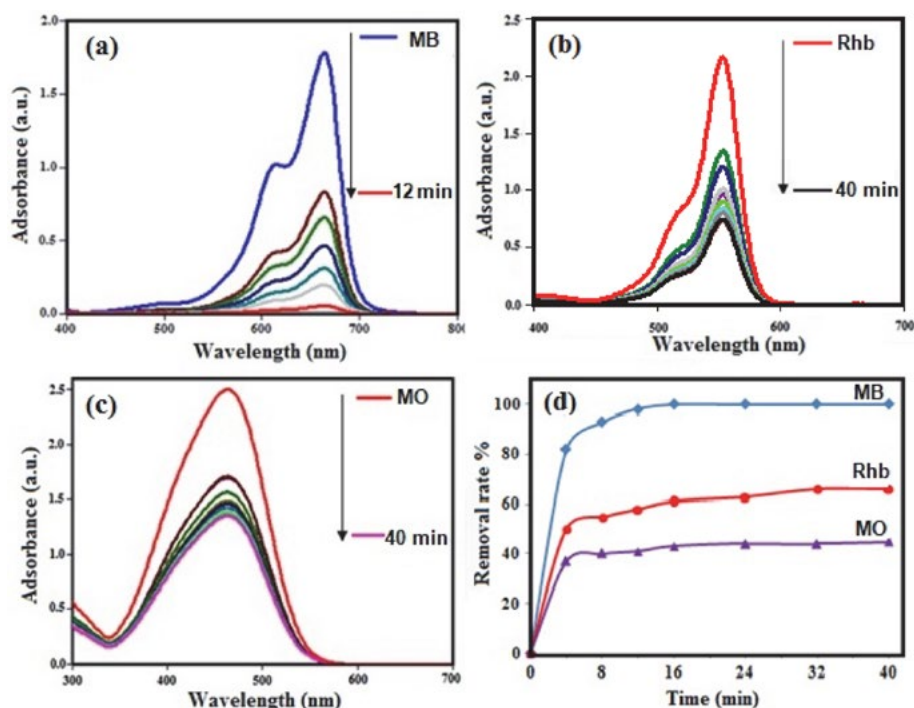
**Figure 8.**  $N_2$  adsorption–desorption isotherms of (a) GO, (b)  $Co_3O_4$  and (c)  $GO/Co_3O_4$  samples. The insets show the corresponding pore size distribution curves.

### 3. 2. Adsorption Studies

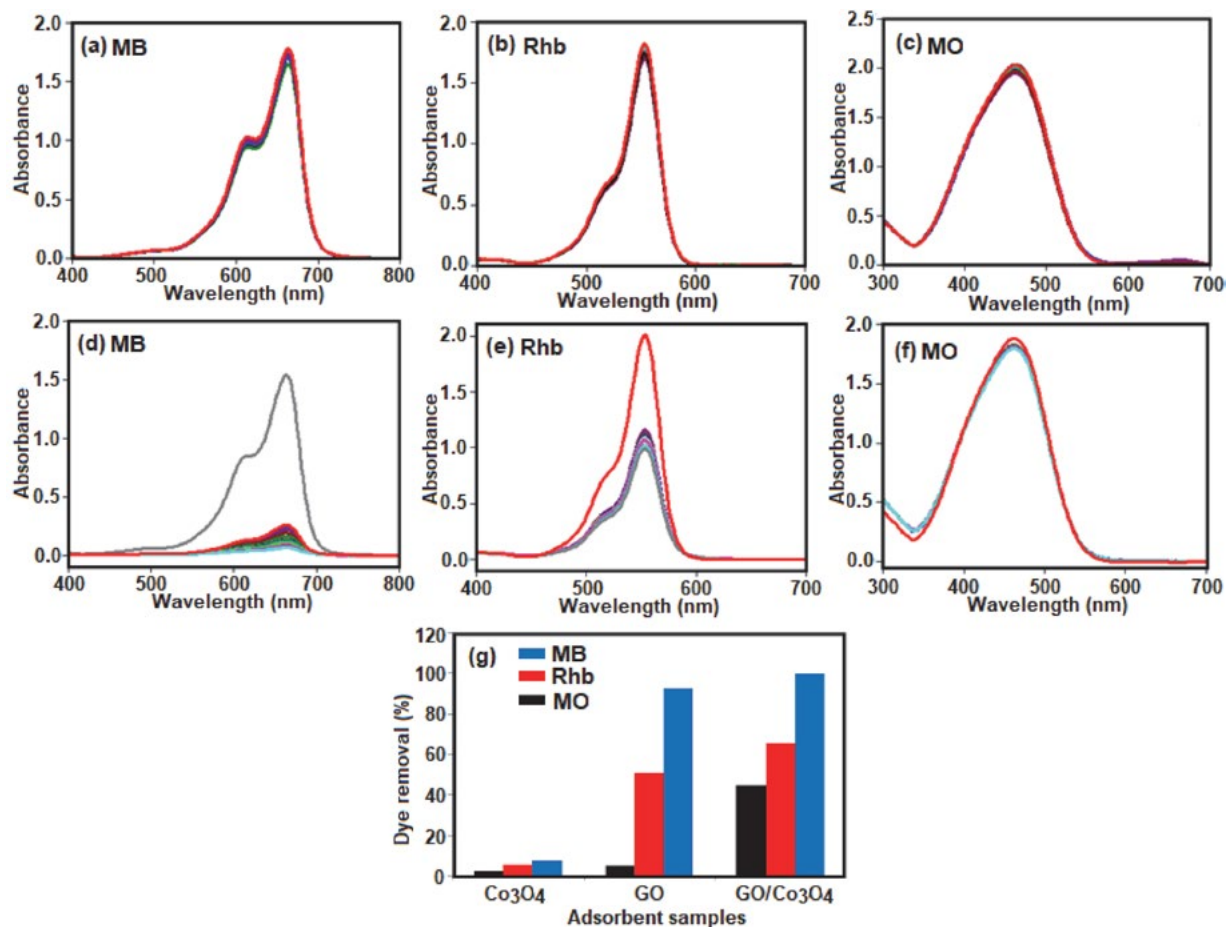
The adsorption activity of  $GO/Co_3O_4$  was examined by dispersing composite powder (30 mg) into an aqueous solution (30 ml,  $25\text{ mg L}^{-1}$ ) of organic dyes (MB, RhB, and MO), and the concentrations of the dye solutions were determined at given intervals by UV-vis absorption spectra. From Figure 9, it can be clearly seen that  $GO/Co_3O_4$  had different adsorption abilities towards MB, RhB, and MO. The removal percentage of MB of up to 98% could be achieved in 12 min, while only 66% and 45% of RhB and MO were removed within 40 min. To better understand adsorption ability of the nanocomposite, MB was chosen as the removal target to study the adsorption performance in more detail, including adsorption kinetic parameters, adsorption isotherms, and thermodynamic parameters.

Figure 10 shows the adsorption abilities of pure  $Co_3O_4$  and GO samples toward MB, RhB, and MO dyes under our reaction conditions. By using  $Co_3O_4$  alone, it is clear from Figure 10(a)–(c) the decrease in intensities of

characteristic UV-Vis absorption bands of these dyes is almost negligible within 40 min, indicating that it has no ability to adsorb dyes even after long contact times. Figure 10(d)–(f) shows that the GO sample has different adsorption ability towards the dyes. It can be seen that the intensity of the absorption bands of MB and RhB decreases with increasing contact time. The adsorption efficiencies of GO nanosheets sample toward these two dyes are about 90% and 50%, respectively, albeit after long adsorption times of 40 min (Figure 10(d) and (e)). On the other hand, as can be seen in Figure 10 (f), the decrease in intensity of characteristic absorption band of MO dye is trace within 40 min. In Figure 10 (g) the adsorption abilities of  $Co_3O_4$ , GO and  $GO/Co_3O_4$  samples toward MB, RhB, and MO dyes were compared. The removal percentages of three dyes in the presence of  $Co_3O_4$  sample as an adsorbent were almost negligible (less than 5%) in 40 min. The removal rates of GO sample for MB and RhB cationic dyes are 90 and 50% after long adsorption time of 40 min and the removal of



**Figure 9.** The adsorption capability of GO/Co<sub>3</sub>O<sub>4</sub> nanocomposite toward different dyes: (a) MB; (b) RhB and (c) MO. (d) The removal efficiency of MB, RhB, and MO dyes.



**Figure 10.** The adsorption capabilities of (a)–(c) Co<sub>3</sub>O<sub>4</sub> nanoparticles and (d)–(f) graphene oxide (GO) nanosheets toward MB, RhB, and MO dyes. (g) Adsorption efficiency (%) of the dyes in the presence of different adsorbent samples.

MO dye is almost negligible at the same time. It is clear that with respect to the removal percentages and adsorption times, the GO/Co<sub>3</sub>O<sub>4</sub> nanocomposite is more suitable and superior. It is suggested that the well dispersed Co<sub>3</sub>O<sub>4</sub> nanoparticles on the graphene surface could act as spacers and thus prohibit the graphene sheets to restack. This directly results in significant increase of the geometry surface area of graphene, which can be of great benefit to adsorption processes. This result is consistent with BET surface area data in Figure 8.

### 3. 3. Kinetic Studies and Effects of Contact

#### Time

Figure 11 shows the effect of GO/Co<sub>3</sub>O<sub>4</sub> adsorbent dosage on the removal of MB. It is obvious that the percentage of dye removed by the adsorbent increased during the initial stage due to the highest amount of available vacant surface sites and was then slow for all samples until a state of equilibrium was reached after 12 min. It is also observed in Figure 11 that the percentage of the adsorbed dye at equilibrium increased sharply from 43% to 98% with increasing adsorbent dosage from 10 to 30 mg that could be attributed to increase of contact area and availability of more adsorption sites.

Meanwhile, to further investigate the adsorption behavior of GO/Co<sub>3</sub>O<sub>4</sub>, pseudo-second-order kinetics model

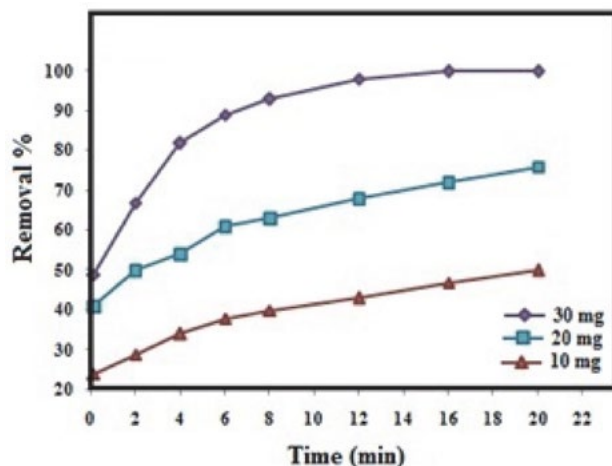


Figure 11. The effect of with different dosages of GO/Co<sub>3</sub>O<sub>4</sub> on the removal of MB

was applied. The pseudo-second-order kinetic model is expressed by the following equation:

$$t/q_t = 1/k_2 q_e^2 + t/q_e \quad (2)$$

where  $k_2$  is rate constant of the pseudo-second-order model ( $\text{g mg}^{-1} \text{min}^{-1}$ ),  $q_e$  and  $q_t$  ( $\text{mg g}^{-1}$ ) are the amounts of the dye adsorbed at equilibrium and at various times  $t$  (min), respectively. The values of  $k_2$  and  $q_e$  at different amount of adsorbent can be determined from the intercept and slope of plots of  $t/q_t$  versus  $t$  (Figure 12), respectively, and the results are given in Table 2. It is observed that the experimental adsorption capacity ( $q_{e,\text{exp}}$ : 24.63) value was close to the calculated adsorption capacity ( $q_{e,\text{cal}}$ : 26.31). Also, large correlation coefficients ( $R^2 = 0.998$ ) suggested that the adsorption kinetic followed the pseudo-second-order model. The values of  $q_{e,\text{cal}}$  were increased from 26.31 to 38.46  $\text{mg g}^{-1}$ , when the initial amount of adsorbent was decreased from 30 mg to 10 mg, due to the affinity for the adsorption surface sites at lower adsorbent concentration.

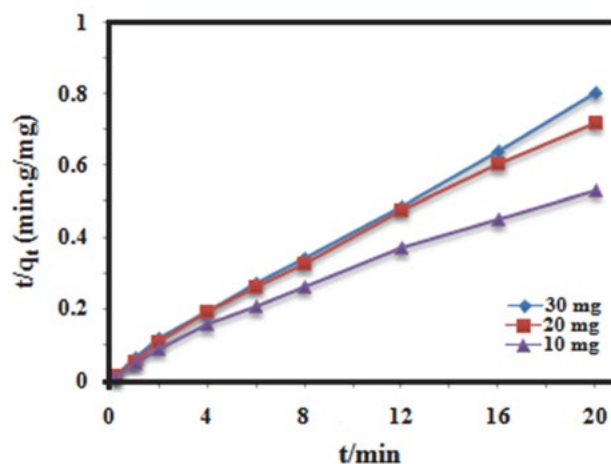


Figure 12. Pseudo-second-order kinetics plot of MB adsorption on GO/Co<sub>3</sub>O<sub>4</sub> nanocomposite.

The comparative removal efficiency of MB with different adsorbents in the aqueous medium is presented in Table 3. It was observed that in term of removal efficiency (%) and contact time, GO/Co<sub>3</sub>O<sub>4</sub> nanocomposite was the most efficient adsorbent (98% adsorption of methylene blue) compared to other reported adsorbents. This may be

Table 2. Adsorption kinetic parameters for the adsorption of MB onto GO/Co<sub>3</sub>O<sub>4</sub>.

Adsorbent dosage (mg)	$q_{e,\text{exp}}$ ( $\text{mg g}^{-1}$ )	$k_2$ ( $\text{g mg}^{-1} \text{min}^{-1}$ ) <sup>a</sup>	$q_{e,\text{cal}}$ ( $\text{mg g}^{-1}$ )	$R^2$
30	24.63	0.05159	26.31	0.998
20	25.15	0.0371	28.57	0.994
10	32.52	0.0193	38.46	0.989

<sup>a</sup>Pseudo-second-order kinetics

**Table 3.** The comparative removal efficiency of MB with different adsorbents.

Entry	Adsorbent material efficiency (%)	Removal	C <sub>MB</sub> (mg L <sup>-1</sup> )	Time (min)	Ref.
1	G-CNT hybrid	97	10	180	[40]
2	H <sub>6</sub> P <sub>2</sub> W <sub>18</sub> O <sub>62</sub> /MOF-5	97	10	10	[49]
3	M-MWCNTs	82	20	120	[51]
4	(4-Hap) <sub>4</sub> [Mo <sub>8</sub> O <sub>26</sub> ]hybrid	100	10	120	[54]
5	H <sub>3</sub> PW <sub>12</sub> O <sub>40</sub> @MIL-101	97.5	20	30	[55]
6	GO/Co <sub>3</sub> O <sub>4</sub> nanocomposite	98	25	12	This work

due to the fact that, in the case of GO/Co<sub>3</sub>O<sub>4</sub> nanocomposite, the main driving force for adsorption was electrostatic forces of attraction between cationic MB molecules and negatively charged oxygen-containing surface groups along with π-π interaction between localized π electrons in the conjugated aromatic rings of the adsorbent and adsorbate which is comparatively stronger than π-π interaction, electrostatic attraction, van der Waals interaction, and hydrogen bonding alone.<sup>43,44</sup>

### 3. 4. Adsorption Isotherm

An adsorption isotherm declares the relationship between the mass of dye adsorbed at a given temperature under equilibrium conditions per unit mass of adsorbent (q<sub>e</sub>, mg g<sup>-1</sup>) and the liquid phase dye concentration (C<sub>e</sub>, mg L<sup>-1</sup>).<sup>45</sup> In this study, to investigate the nature of electrostatic interaction of dye molecules with GO/Co<sub>3</sub>O<sub>4</sub> nanocomposite, Langmuir and Freundlich models were applied, in which the experiments were conducted by varying the amount of adsorbent from 10 to 25 mg at 25 °C while keeping the concentration of methylene blue solution constant (25 mg L<sup>-1</sup>). Langmuir adsorption model supposes that maximum adsorption occurs on a saturated monolayer of solute molecules and all adsorption sites on the ad-

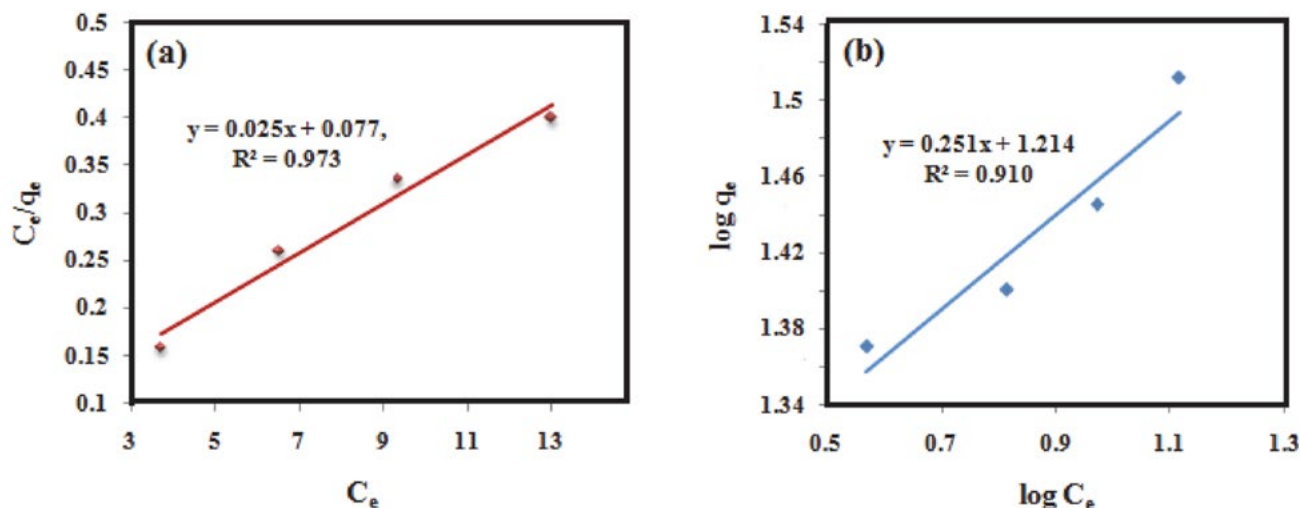
sorbent surface are homogeneous and is given by the following equation:<sup>46</sup>

$$c_e/q_e = 1/k_L q_m + c_e/q_m \tag{3}$$

where k<sub>L</sub> is Langmuir adsorption constant, c<sub>e</sub>, q<sub>e</sub>, and q<sub>m</sub>, are MB concentration at equilibrium (mg L<sup>-1</sup>), the amount of MB adsorbed at equilibrium (mg g<sup>-1</sup>), and the maximum adsorption capacity (mg g<sup>-1</sup>), respectively. The values of q<sub>m</sub> and k<sub>L</sub> are computed from the slope and intercept of the linear plot of c<sub>e</sub>/q<sub>e</sub> versus c<sub>e</sub>. The separation factor (R<sub>L</sub>) is used to evaluate the favorability adsorption on the adsorbent, which is defined by the following equation:<sup>47</sup>

$$R_L = 1/(1 + K_L C_0) \tag{4}$$

The parameter can show that the isotherm is irreversible (R<sub>L</sub> = 0), favorable (0 < R<sub>L</sub> < 1), linear (R<sub>L</sub> = 1) or unfavorable (R<sub>L</sub> > 1). In this work, the value of R<sub>L</sub> calculated for the initial concentrations of MB was 0.11, which illustrated that the adsorption of MB onto GO/Co<sub>3</sub>O<sub>4</sub> was favorable. Freundlich model is based on the assumption that the multilayer of the adsorption process occurs on a heterogeneous surface and is given by the following equation:<sup>47</sup>



**Figure 13.** Adsorption isotherm plots for the adsorption of MB onto GO/Co<sub>3</sub>O<sub>4</sub> nanocomposite: (a) Langmuir isotherm, (b) Freundlich isotherm.

**Table 4.** Isotherm parameters for the adsorption of MB onto GO/Co<sub>3</sub>O<sub>4</sub>.

Langmuir isotherm				Freundlich isotherm		
K <sub>L</sub> (L mg <sup>-1</sup> )	q <sub>m</sub> (mg g <sup>-1</sup> )	R <sub>L</sub>	R <sup>2</sup>	K <sub>F</sub> (mg g <sup>-1</sup> (L mg <sup>-1</sup> ) <sup>1/n</sup> )	n	R <sup>2</sup>
0.32	40	0.11	0.973	16.36	3.98	0.910

$$\log q_e = 1/n \log c_e + \log k_f \quad (5)$$

where  $K_F$  is a Freundlich constant and  $n$  is the heterogeneity factor. The isotherms based on the experimental data are shown in Figures 13(a) and (b), and the parameters obtained from linear regression are summarized in Table 4. According to the obtained data, correlation coefficient  $R^2$  in Langmuir model (0.973) was higher than that of Freundlich model (0.910), which exhibited that Langmuir model was suitable for describing the adsorption equilibrium of MB on GO/Co<sub>3</sub>O<sub>4</sub> nanocomposite.

### 3. 5. Effect of pH

The effect of pH on the adsorption process of dyes is important because industrial dyes are discharged in wastewaters at a pH different from the environmental pH.<sup>48</sup> In general, the solution pH can affect the surface charge of the adsorbent, the degree of ionization/ dissociation of dye molecules as well as dissociation of functional groups on the active sites of the adsorbent.<sup>49,50</sup> Figure 14 shows the effect of initial solution pH on MB adsorption onto GO/Co<sub>3</sub>O<sub>4</sub>. Both, the adsorption capacity and removal rate of MB became significant with increasing solution pH from 4 to 12. This phenomenon can be explained by the fact that at higher pH values, the surface of GO/Co<sub>3</sub>O<sub>4</sub> may become negatively charged, which can attract positively charged MB cations through electrostatic forces. A similar trend was observed for the adsorption of methylene blue onto

magnetic cyclodextrin/graphene oxide,<sup>15</sup> or polydopamine microspheres,<sup>47</sup> magnetite-loaded multi-walled carbon nanotubes,<sup>51</sup> and magnetic graphene oxide.<sup>52</sup>

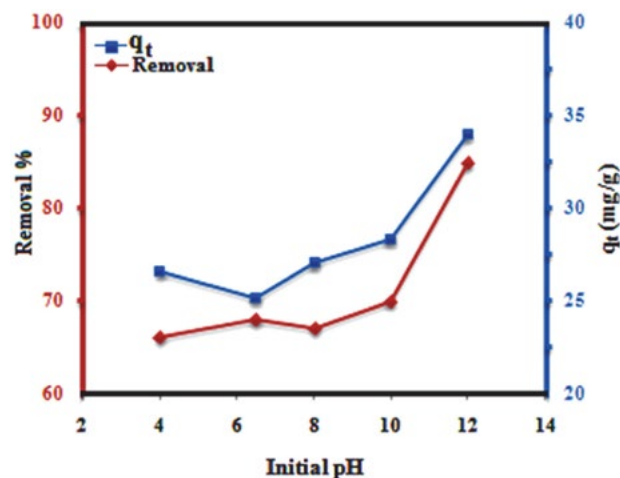
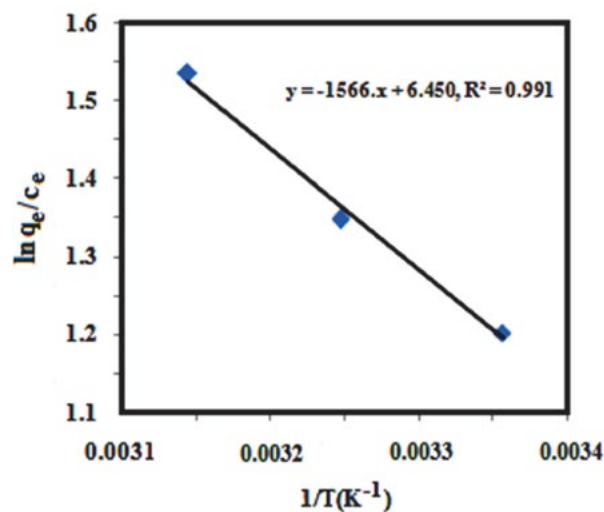
### 3. 6. Thermodynamic Parameters

Thermodynamic studies for the adsorption of MB onto GO/Co<sub>3</sub>O<sub>4</sub> were carried out at different temperatures. Thermodynamic parameters, namely, Gibbs free energy ( $\Delta G^\circ$ ), enthalpy ( $\Delta H^\circ$ ) and entropy ( $\Delta S^\circ$ ) were calculated using following equations:

$$\begin{aligned} \ln K_L &= -\Delta H^\circ/(RT) + \Delta S^\circ/R \\ \Delta G^\circ &= -RT \ln K_L \end{aligned} \quad (6)$$

where  $K_L$  (L/g) is Langmuir constant,  $R$  is universal gas constant (8.314 J mol<sup>-1</sup> K) and  $T$  is absolute temperature (in Kelvin). Plotting  $\ln K_L$  versus  $1/T$  gave a straight line with slope and intercept equal to  $-\Delta H^\circ/R$  and  $\Delta S^\circ/R$ , respectively (Figure 15). The positive value of  $\Delta H^\circ$  (Table 5) showed endothermic nature of adsorption process that it was in accordance with increasing adsorption capacity collaborated with the increase of temperature. The negative value of  $\Delta G^\circ$  for different temperatures showed the feasibility and spontaneous nature of adsorption. The activation energy,  $E_a$ , was calculated by using Arrhenius equation:

$$\ln k = \ln A - E_a/RT \quad (7)$$

**Figure 14.** Effect of initial pH on adsorption capability and removal of MB with GO/Co<sub>3</sub>O<sub>4</sub> nanocomposite.**Figure 15.** Van't Hoff plots for the adsorption of MB onto GO/Co<sub>3</sub>O<sub>4</sub>.

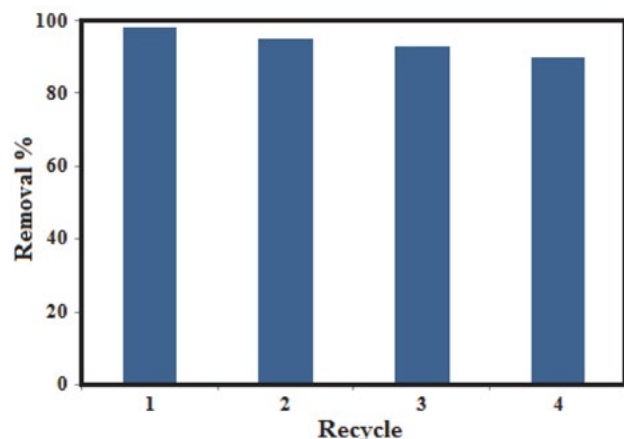
where  $k$  is pseudo-second-order rate constant,  $E_a$ ,  $A$ ,  $R$ , and  $T$  are activation energy, Arrhenius factor, universal gas constant, and temperature in Kelvin, respectively. The linear plot of  $\ln k$  against  $1/T$  provided slope equal to  $-E_a/R$ . The value of  $E_a$  ranging from 5 to 40  $\text{kJ mol}^{-1}$  are characteristic for physisorption while ranging from 40 to 800  $\text{kJ mol}^{-1}$  indicates chemisorptions.<sup>53</sup> The activation energy for the adsorption of MB onto GO/Co<sub>3</sub>O<sub>4</sub> nanocomposite was found to be 7.37  $\text{kJ mol}^{-1}$ , which indicated that the process was governed by physical adsorption.

**Table 5.** Thermodynamic parameters for the adsorption of MB onto GO/Co<sub>3</sub>O<sub>4</sub>.

T (K)	$\Delta G^\circ$ (KJ/mol)	$\Delta H^\circ$ (KJ/mol)	$\Delta S^\circ$ (J/mol k)
298	-2.96	13.01	53.62
308	-3.49	-	-
318	-4.03	-	-

### 3. 7. Recyclability of GO/Co<sub>3</sub>O<sub>4</sub> Nanocomposite

Recovery and regeneration ability of the adsorbent, that can reduce the cost of the treatment process, is crucial for its practical application. For this purpose, the used adsorbent was regenerated with ethanol solution, and the absorption-desorption cycle was repeated four times and the obtained results are shown in Figure 16. In the first three cycles, the removal efficiencies were 98%, 95%, and 93%, respectively, and then remained at 90% at the fourth cycle. These results show that the adsorbent had the potential of reusability.



**Figure 16.** Effect of recycle times of GO/Co<sub>3</sub>O<sub>4</sub> on MB removal rate.

## 4. Conclusion

GO/Co<sub>3</sub>O<sub>4</sub> nanocomposite was synthesized successfully by a hydrothermal route. The results obtained from XRD, FTIR, FESEM, EDS, and TEM techniques showed

that Co<sub>3</sub>O<sub>4</sub> nanoparticles were deposited onto GO nanosheets. Compared with Co<sub>3</sub>O<sub>4</sub> nanoparticles, GO/Co<sub>3</sub>O<sub>4</sub> nanocomposite showed weaker ferromagnetic behavior. The results revealed that GO/Co<sub>3</sub>O<sub>4</sub> nanocomposite demonstrated rapid uptake of cationic methylene blue (MB) and the adsorption process followed pseudo-second-order kinetic model as well as Langmuir isotherms. Rapid adsorption rate was mainly attributed to the electrostatic interaction of oppositely charged adsorbate-adsorbent species along with their  $\pi$ - $\pi$  interaction. Thermodynamic parameters showed that the adsorption was spontaneous. Recyclability tests indicated that GO/Co<sub>3</sub>O<sub>4</sub> nanocomposite could be recycled and utilized several times without losing adsorption capacity.

## 5. Acknowledgements

The authors gratefully acknowledge Lorestan University Research Council and Iran Nanotechnology Initiative Council (INIC) for their financial supports.

## 6. References

- C. A. Demarchi, M. Campos and C. A. Rodrigues, *J. Environ. Chem. Eng.* **2013**, *1*, 1350–1358. DOI:10.1016/j.jece.2013.10.005
- J. Wang, C. Zheng, S. Ding, H. Ma and Y. Ji, *Desalination* **2011**, *273*, 285–291. DOI:10.1016/j.desal.2011.01.042
- F. Marahel, M. A. Khan, E. Marahel, I. Bayesti and S. Hosseini, *Des. Water Treat.* **2015**, *53*, 826–835.
- N. M. Julkapli, S. Bagheri and S. B. A. Hamid, *Scientific World J.* **2014**, 2014. DOI:10.1080/19443994.2013.846240
- H. Hou, R. Zhou, P. Wu and L. Wu, *Chem. Eng. J.* **2012**, *211*, 336–342. DOI:10.1016/j.cej.2012.09.100
- A. K. Sarkar, A. Pal, S. Ghorai, N. Mandre and S. Pal, *Carbohydr. Polym.* **2014**, *111*, 108–115. DOI:10.1016/j.carbpol.2014.04.042
- M. Yusuf, F. Elfighi, S. A. Zaidi, E. Abdullah and M. A. Khan, *RSC Adv.* **2015**, *5*, 50392–50420.
- L. Zhou, C. Gao and W. Xu, *ACS Appl. Mater. Interfaces.* **2010**, *2*, 1483–1491. DOI:10.1021/am100114f
- Y. Chen, L. Chen, H. Bai and L. Li, *J. Mater. Chem. A.* **2013**, *1*, 1992–2001. DOI:10.1039/C2TA00406B
- S. Park and R. S. Ruoff, *Nat. nanotechnol.* **2009**, *4*, 217–224. DOI:10.1038/nnano.2009.58
- X. Wang, X. Li, L. Zhang, Y. Yoon, P. K. Weber, H. Wang, J. Guo and H. Dai, *Sci.* **2009**, *324*, 768–771. DOI:10.1126/science.1170335
- T. Ramanathan, A. Abdala, S. Stankovich, D. Dikin, M. Herrera-Alonso, R. Piner, D. Adamson, H. Schniepp, X. Chen and R. Ruoff, *Nat. Nanotechnol.* **2008**, *3*, 327–331. DOI:10.1038/nnano.2008.96
- B. Li and H. Cao, *J. Mater. Chem.* **2011**, *21*, 3346–3349. DOI:10.1039/C0JM03253K

14. G. Xie, P. Xi, H. Liu, F. Chen, L. Huang, Y. Shi, F. Hou, Z. Zeng, C. Shao and J. Wang, *J. Mater. Chem.* **2012**, *22*, 1033–1039. DOI:10.1039/C1JM13433G
15. L. Li, L. Fan, H. Duan, X. Wang and C. Luo, *RSC Adv.* **2014**, *4*, 37114–37121.
16. N. Li, M. Zheng, X. Chang, G. Ji, H. Lu, L. Xue, L. Pan and J. Cao, *J. Solid State Chem.* **2011**, *184*, 953–958. DOI:10.1016/j.jssc.2011.01.014
17. L. Fan, C. Luo, X. Li, F. Lu, H. Qiu and M. Sun, *J. Hazard. Mater.* **2012**, *215*, 272–279. DOI:10.1016/j.jhazmat.2012.02.068
18. Y. Yao, S. Miao, S. Yu, L. P. Ma, H. Sun and S. Wang, *J. Colloid Interface Sci.* **2012**, *379*, 20–26. DOI:10.1016/j.jcis.2012.04.030
19. F. Jiao and H. Frei, *Angew. Chem.* **2009**, *121*, 1873–1876. DOI:10.1002/ange.200805534
20. H. Sun, H. Tian, Y. Hardjono, C. E. Buckley and S. Wang, *Catal. Today.* **2012**, *186*, 63–68. DOI:10.1016/j.cattod.2011.09.001
21. J. A. Koza, Z. He, A. S. Miller and J. A. Switzer, *Chem. Mater.* **2012**, *24*, 3567–3573. DOI:10.1021/cm3012205
22. Z. Wang and L. Zhou, *Adv. Mater.* **2012**, *24*, 1903–1911. DOI:10.1002/adma.201200469
23. G. Wang, H. Liu, J. Horvat, B. Wang, S. Qiao, J. Park and H. Ahn, *Chem. Eur. J.* **2010**, *16*, 11020–11027. DOI:10.1002/chem.201000562
24. T. Zhu, J. S. Chen and X. W. Lou, *J. Mater. Chem.* **2010**, *20*, 7015–7020. DOI:10.1039/c0jm00867b
25. L. Jin, X. Li, H. Ming, H. Wang, Z. Jia, Y. Fu, J. Adkins, Q. Zhou and J. Zheng, *RSC Adv.* **2014**, *4*, 6083–6089.
26. S. Farhadi and K. Pourzare, *Mater. Res. Bull.* **2012**, *47*, 1550–1556. DOI:10.1016/j.materresbull.2012.02.028
27. S. Farhadi, K. Pourzare and S. Bazgir, *J. Alloys Compd.* **2014**, *587*, 632–637. DOI:10.1016/j.jallcom.2013.10.259
28. L. Wang, J. Deng, Z. Lou and T. Zhang, *Sens. Actuators B Chem.* **2014**, *201*, 1–6. DOI:10.1016/j.snb.2014.04.074
29. J. Xu, L. Gao, J. Cao, W. Wang and Z. Chen, *Electrochim. Acta.* **2010**, *56*, 732–736. DOI:10.1016/j.electacta.2010.09.092
30. D. Vickers, L. Archer and T. Floyd-Smith, *Colloids Surf. A Physicochem. Eng. Aspects*, **2009**, *348*, 39–44. DOI:10.1016/j.colsurfa.2009.06.025
31. J. S. Chen, T. Zhu, Q. H. Hu, J. Gao, F. Su, S. Z. Qiao and X. W. Lou, *ACS appl. mater. interfaces.* **2010**, *2*, 3628–3635. DOI:10.1021/am100787w
32. S. Farhadi, Z. Heydari-Chegeni and M. Mousavi, *J. Alloys Compd.* **2017**, *692*, 923–933. DOI:10.1016/j.jallcom.2016.09.136
33. F. Hong, Y. Ni, Y. Zhong, H. Wu, *J. Alloys Compd.* **2016**, *659*, 112–121. DOI:10.1016/j.jallcom.2015.11.049
34. G. S. Girolami, T. B. Rauchfuss, R.J. Angelici, *Synthesis and technique in inorganic chemistry: a laboratory manual*, University Science Books, Sausalito, CA, **1999**.
35. Y. Yao, Z. Yang, H. Sun and S. Wang, *Ind. Eng. Chem. Res.* **2012**, *51*, 14958–14965. DOI:10.1021/ie301642g
36. P. Bradder, S. K. Ling, S. Wang and S. Liu, *J. Chem. Eng. Data.* **2010**, *56*, 138–141. DOI:10.1021/je101049g
37. K. Nakamoto, *Infrared and Raman spectra of inorganic and coordination compounds*, Wiley Online Library, **1986**.
38. S. Farhadi, M. Javanmard and G. Nadri, *Acta Chim. Slov.* **2016**, *63*, 335–343. DOI:10.17344/acsi.2016.2305
39. B. Pejova, A. Isahi, M. Najdoski and I. Grozdanov, *Mater. Res. Bull.* **2001**, *36*, 161–170. DOI:10.1016/S0025-5408(00)00479-7
40. L. Ai and J. Jiang, *Chem. Eng. J.* **2012**, *192*, 156–163. DOI:10.1016/j.cej.2012.03.056
41. H. P. Klug and L. E. Alexander, *X-ray diffraction procedures*, Wiley New York, **1954**.
42. Y. Zhao, S. Chen, B. Sun, D. Su, X. Huang, H. Liu, Y. Yan, K. Sun and G. Wang, *Sci. Rep.* **2015**, *5*, 7629–7635. DOI:10.1038/srep07629
43. P. Sharma and M. R. Das, *J. Chem. Eng. Data.* **2012**, *58*, 151–158. DOI:10.1021/je301020n
44. Y. Li, Q. Du, T. Liu, X. Peng, J. Wang, J. Sun, Y. Wang, S. Wu, Z. Wang and Y. Xia, *Chem. Eng. Res. Des.* **2013**, *91*, 361–368. DOI:10.1016/j.cherd.2012.07.007
45. L. Sun, S. Hu, H. Sun, H. Guo, H. Zhu, M. Liu and H. Sun, *RSC Adv.* **2015**, *5*, 11837–11844.
46. L. Yao, S. K. Lua, L. Zhang, R. Wang and Z. Dong, *J. Hazard. Mater.* **2014**, *280*, 428–435. DOI:10.1016/j.jhazmat.2014.08.026
47. J. Fu, Z. Chen, M. Wang, S. Liu, J. Zhang, J. Zhang, R. Han and Q. Xu, *Chem. Eng. J.* **2015**, *259*, 53–61. DOI:10.1016/j.cej.2014.07.101
48. X. Rong, F. Qiu, C. Zhang, L. Fu, Y. Wang and D. Yang, *Powder Technol.* **2015**, *275*, 322–328. DOI:10.1016/j.powtec.2015.01.079
49. X. Liu, W. Gong, J. Luo, C. Zou, Y. Yang and S. Yang, *Appl. Surf. Sci.* **2016**, *362*, 517–524. DOI:10.1016/j.apsusc.2015.11.151
50. Z. Chen, J. Zhang, J. Fu, M. Wang, X. Wang, R. Han and Q. Xu, *J. Hazard. Mater.* **2014**, *273*, 263–271. DOI:10.1016/j.jhazmat.2014.03.053
51. L. Ai, C. Zhang, F. Liao, Y. Wang, M. Li, L. Meng and J. Jiang, *J. Hazard. Mater.* **2011**, *198*, 282–290. DOI:10.1016/j.jhazmat.2011.10.041
52. J. H. Deng, X.-R. Zhang, G.-M. Zeng, J.-L. Gong, Q.-Y. Niu and J. Liang, *Chem. Eng. J.* **2013**, *226*, 189–200. DOI:10.1016/j.cej.2013.04.045
53. A. Farghali, M. Bahgat, W. El Roubay and M. Khedr, *J. Alloys Compd.* **2013**, *555*, 193–200. DOI:10.1016/j.jallcom.2012.11.190
54. Y. Q. Zhang, C.-C. Wang, T. Zhu, P. Wang and S.-J. Gao, *RSC Adv.* **2015**, *5*, 45688–45692.
55. T. T. Zhu, Z.-M. Zhang, W.-L. Chen, Z.-J. Liu and E.-B. Wang, *RSC Adv.* **2016**, *6*, 81622–81630.

## Povzetek

Nanokompozit grafenovega oksida (GO)/Co<sub>3</sub>O<sub>4</sub> smo sintetizirali s hidrotermalnim razpadom spojine [Co(en)<sub>3</sub>](NO<sub>3</sub>)<sub>3</sub> na nanoplasteh grafenovega oksida. Tako pripravljen nanokompozit (GO/Co<sub>3</sub>O<sub>4</sub>) smo karakterizirali z infrardečo spektroskopijo (FT-IR), rentgensko praškovno difrakcijo (XRD), ramansko spektroskopijo, vrstično in presevno elektronsko mikroskopijo (TEM, SEM), energijsko disperzivno rentgensko spektroskopijo (EDX), magnetnimi meritvami in N<sub>2</sub> adsorpcijsko – desorpcijsko analizo. Rezultati so pokazali, da so se nanodelci Co<sub>3</sub>O<sub>4</sub>, s povprečnim premerom 12,5 nm pripeli na plasti grafenovega oksida. Adsorpcijsko učinkovitost GO/Co<sub>3</sub>O<sub>4</sub> smo preučevali napram različnim organskim barvilom v vodnih raztopinah. Rezultati adsorpcijske učinkovitosti nanokompozita GO/Co<sub>3</sub>O<sub>4</sub> so: metilen modro: 98 % v 12 minutah; rodamin B 66 % v 40 minutah, metiloranž 45 % v 40 minutah. Podrobno smo preučevali vplive različnih parametrov kot so množina adsorbenta, čas, pH vrednosti in temperatura na adsorpcijski proces. Podatki adsorpcijskega ravnotežja najbolje sledijo Langmuirjevi izotermi, adsorpcijsko kinetiko pa lahko opišemo s psevdo modelom drugega reda. Različni termodinamski parametri kažejo na to, da je proces adsorpcije spontan. Poudarimo lahko tudi lažjo pripravo nanokompozita GO/Co<sub>3</sub>O<sub>4</sub> in njegovo uporabo pri odstranjevanju barvila metilen modro iz odpadnih vod.



Scientific paper

# The Integration of Submicroscopic Representations Used in Chemistry Textbook Sets into Curriculum Topics

Špela Hrast\* and Vesna Ferik Savec

Faculty of Education, University of Ljubljana, Kardeljeva ploščad 16, 1000 Ljubljana, Slovenia

\* Corresponding author: E-mail: spela.hrast@pef.uni-lj.si

Received: 21-06-2017

## Abstract

To support the understanding of chemistry concepts and processes at the particulate level, various representations are included in learning materials. This paper focuses on how submicroscopic representations (SMRs) are integrated into Slovenian chemistry textbook sets with respect to the curriculum topics for 8th and 9th Grade. Textbook set analysis is based on four holistic SMRs descriptors (direct, indirect, combined descriptor, and SMRs without descriptors), which support learners' recognition of SMRs' informational value at different levels by providing different accompanying SMRs add-ons. The textbook sets analysis revealed that the number of SMRs varies significantly with regard to different curriculum topics. The overall proportion of the descriptors that enable the learner a direct recognition of SMRs is low in all curriculum topics. Interestingly, the descriptors that do not enable the learners a direct recognition of SMRs prevail in textbook sets. To obtain more detailed insight into the criteria based on which the textbook authors integrate SMRs with various descriptors into textbook sets, further studies are necessary.

**Keywords:** Chemistry, curriculum, submicroscopic representations, textbook

## 1. Introduction

Textbooks are an important resource in supporting the effective teaching and learning of chemistry, as one school subject in the larger field of science education. They can be used for studying at school as well as at home.<sup>1</sup> In order to be used as teaching materials at schools, the textbook sets for chemistry should be synchronised with the National Curriculum for Chemistry at certain educational levels<sup>2,3</sup> and confirmed by the National Commission for Textbook Approval at the Ministry of Education of the Republic of Slovenia.<sup>4</sup> To support the quality of the textbook sets in chemistry education, significant attention has been paid to textbook analysis. For example, Abraham et al.<sup>5</sup> studied eighth graders' degree of understanding of five selected chemistry concepts found in textbooks and attempted to identify related misconceptions; Sanger and Greenbowe<sup>6</sup> analysed the college chemistry textbooks as sources of misconceptions and errors in electrochemistry; Abd-El-Khalick, Waters, and Le<sup>7</sup> studied representations of nature of science in high school chemistry textbooks over the past four decades; Devetak, Vogrinc, and Glažar<sup>8</sup> studied explanations of states of matter in Slovenian science textbooks from 1th to

8th Grade; and Souza and Porto<sup>9</sup> analysed iconographic and textual aspects of chemistry textbooks which had significant diffusion in the context of Brazilian universities.

Johnstone<sup>10</sup> suggested that representing chemistry concepts and processes is based on representations at three levels: macroscopic (observable phenomena), submicroscopic or particulate (different representations of atomic, molecular, and particle structures), and symbolic (mathematical and chemical symbols). The understanding of chemistry is based on creating mental images for corresponding phenomena on the particulate level. Such mental images are considered to be internal representations that can be visualised through the use of special symbolic systems, so-called external representations of the particulate nature of matter,<sup>11,12</sup> which are referred to as submicroscopic representations (SMRs) in this paper. Few macroscopic observations can be understood without recourse to sub-microscopic representation or models.<sup>13</sup> Various visualisations are used to support students when connecting the three levels of concept representations,<sup>14–16</sup> as the interpretation of the macroscopic phenomenon at the particulate level is perceived to be an important part in contemporary chemistry teaching.<sup>17</sup>

## 2. The Context and the Purpose of the Study

This paper focuses on SMRs in Slovenian chemistry textbook sets with respect to the topics of the National Chemistry Curriculum for 8th and 9th Grade.<sup>3</sup> Previous research has been dealing with misconceptions related with SMRs.<sup>18</sup> The novelty of the present research is in focusing on the descriptors, which accompanying SMRs. Namely, based on their own acceptance of the simultaneous use of SMRs as a part of a triple representation of chemistry concepts (submicroscopic, macroscopic and symbolic levels), chemistry educators, such as authors of textbooks, can assume that students can also easily comprehend and efficiently learn with the use of SMRs.<sup>10</sup> However, the understanding of the kinds of information and inferences that the visualisations in various learning materials provide requires explicit instruction and practice.<sup>19</sup> The research indicates that students' successful learning with SMRs is significantly impacted by their representational competence in chemistry.<sup>20–22</sup> The representational

competence includes a distinct set of skills for constructing, selecting, interpreting, and using disciplinary representations for communicating, learning, or problem solving.<sup>23</sup> Moreover, in the textbook sets the authors can unintentionally devote more emphasis to the implementation of SMRs in particular topics, whereas in others the particular representations can be neglected.

The following research questions (RQ) were stated:

- 1<sup>st</sup> RQ: How does the number of SMRs in Slovenian chemistry textbook sets for 8th and 9th Grade change with respect to curriculum topics?
- 2<sup>nd</sup> RQ: What holistic descriptors of SMR add-ons are used to support learners in the recognition of SMRs' informational value in specific curriculum topics of Slovenian chemistry textbook sets for 8th and 9th Grade?
- 3<sup>rd</sup> RQ: How does the number of specific holistic descriptors of SMR add-ons in Slovenian chemistry textbook sets for 8th and 9th Grade change with respect to curriculum topics?

Table 1. The list of the analysed textbook sets

Textbook set* title	Author(s)	Publisher	Year of publication (Edition) Textbook/ workbook	Number of Pages Textbook/ workbook	Grade/ Learner's age
Kemija danes 1	Gabrič, A., Glažar, S. A., Graunar, M., Slatinek-Žigon, M.	DZS	2014 (1 <sup>st</sup> Ed.)/ 2013 (1 <sup>st</sup> Ed.)	125/106	8/13
Kemija 8, i-učbenik	Sajovic, I., Wissiak Grm, K., Godec, A., Kralj, B., Smrdu, A., Vrtačnik, M., Glažar, S.	Zavod RS za šolstvo	2014	264	8/13
Moja prva kemija	Vrtačnik, M., Wissiak Grm, K. S., Glažar, S. A., Godec, A.	Modrijan	2015 (1 <sup>st</sup> Ed.)/ 2014 (1 <sup>st</sup> Ed.)	240/92, 61	8, 9/13, 14
Peti element 8	Devetak, I., Cvirn Pavlin, T., Jamšek, S.	ROKUS KLETT	2010 (1 <sup>st</sup> Ed.)/ 2010 (1 <sup>st</sup> Ed.)	103/71	8/13
Pogled v kemijo 8	Kornhauser, A., Frazer, M.	MK	2003 (1 <sup>st</sup> Ed.)/ 2004 (1 <sup>st</sup> Ed.)	140/126	8/13
Od atoma do molekule	Smrdu, A.	JUTRO	2012 (2 <sup>nd</sup> Ed.)/ 2012 (2 <sup>nd</sup> Ed.)	128/160	8/13
Kemija danes 2	Graunar, M., Podlipnik, M., Mirnik, J. (textbook) Dolenc, D., Graunar, M., Modec, B. (notebook)	DZS	2016 (1 <sup>st</sup> Ed.)/ 2016 (1 <sup>st</sup> Ed.)	152/96	9/14
Kemija 9, i-učbenik	Jamšek, S., Sajovic, I., Wissiak Grm, K., Godec, A., Boh, B., Vrtačnik, M., Glažar, S.	Zavod RS za šolstvo	2014	271	9/14
Peti element 9	Devetak, I., Cvirn Pavlin, T., Jamšek, S.	ROKUS Klett	2011 (1 <sup>st</sup> Ed.)/ 2011 (1 <sup>st</sup> Ed.)	77/ 79	9/14
Pogled v kemijo 9	Kornhauser, A., Frazer, M.	MK	2005 (1 <sup>st</sup> Ed.)/ 2006 (1 <sup>st</sup> Ed.)	140/115	9/14
Od molekule do makromolekule	Smrdu, A.	Jutro	2013 (2 <sup>nd</sup> Ed.)/ 2013 (2 <sup>nd</sup> Ed.)	128/152	9/14

The term "textbook set (\*)" refers to all materials for students in the written or electronic form.

### 3. Methods

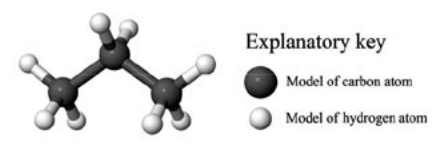
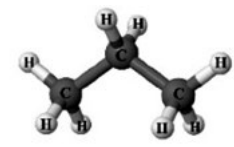
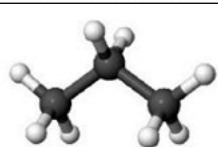
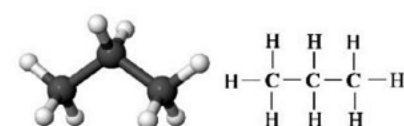

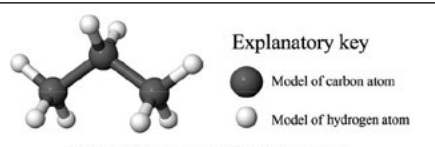
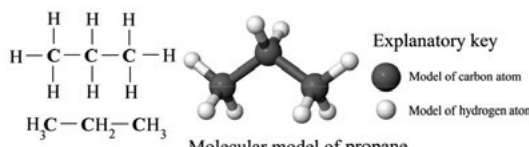
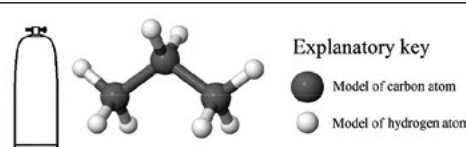
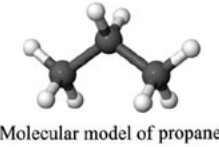
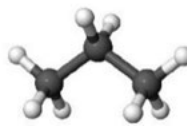
#### 3.1. Sample

In this study, we focused on the chemistry textbook sets in primary school (8th and 9th Grade), which are in Slovenia obligatory written based on the objectives of National Chemistry Curriculum and consequently confirmed by the National Commission for Textbook Approval at the Ministry of Education, Science and Sport in the 2016/17 school year. National Chemistry Curriculum for 8th and 9th Grade<sup>3</sup> for each of the ten topics (Chemistry is a World of Matter, Atom and the Periodic System of Elements,

Compounds and Bonding, Chemical Reactions, The Elements in the Periodic Table, Acids, Bases and Salts, Hydrocarbons and Polymers, Organic Compounds Containing Oxygen, Organic Compounds Containing Nitrogen, The Mole) specifies specific objectives and points out suggested contents how to implement them in chemistry teaching. Teachers are free to distributed the above listed curriculum topics in 70 hours in Grade 8 and 64 hours in Grade 9 with regard to their opinion.

A list of analysed textbook sets is shown in Table 1. As can be derived from the Table 1, in the present study 2826 pages were analysed.

Table 2. Examples of SMR add-ons

Descriptor	Examples of SMR add-ons
Direct (D)	  <p>Hydrogen atoms are represented with white cycles, carbon atoms are represented with black cycles.</p>
Indirect (I)	 <p>Molecular model of propane</p>  <p>Molecular model of propane</p>  <p>Propane is a gas. It consists of C<sub>3</sub>H<sub>8</sub> molecules.</p> <p>Propane (C<sub>3</sub>H<sub>8</sub>)</p>
Combined (C)	 <p>Molecular model of propane (C<sub>3</sub>H<sub>8</sub>)</p>  <p>Molecular model of propane</p>  <p>Molecular model of propane (C<sub>3</sub>H<sub>8</sub>)</p>  <p>Molecular model of propane</p> <p>Hydrogen atoms are represented with white cycles, carbon atoms are represented with black cycles.</p>
Without (W)	

### 3. 2. Instruments

For the purpose of this research, a rubric<sup>24</sup> for the evaluation of SMRs in the textbook sets was used. This rubric was based on the assumption that in practice the learner perceives each SMR as one whole. The four main holistic descriptors accompanying SMRs were used: i.e. direct descriptor (D), indirect descriptor (I), combined descriptor (C), and SMRs without descriptors (W), which support learners' recognition of SMRs' informational value on different levels by providing different accompanying add-ons of SMRs. To ensure the validity of the rubric, 283 pages (10% of all analysed textbook set pages) were analysed by both authors, and the four main types of holistic descriptors were defined. To reduce bias issues related to the use of the rubric for categorisation of SMR descriptors, through discussion and agreement, a 95% inter-rater reliability of the rubric was established. The direct SMR add-ons enable the learner a direct and unambiguous recognition of particles. Thereby, various types of explanatory keys can be used: for example, pictorial, textual, integrated structural, or other symbolic notations used in the explanatory key. Indirect SMR add-ons do not enable the learner a direct recognition of particles. The nature of the particles can be derived based on the compound's name, structure-properties relation or symbolic SMR add-ons, or by other means, but only in cases that the learners have the necessary chemical knowledge, that enables the recognition of its informational value. Combined SMR add-ons enable the learner a direct recognition and provide other information. It is a combination of the direct and the indirect descriptor. Examples of SMR add-ons are presented in Table 2. In order to visualize descriptors explicitly, the type of descriptors represents the only variable and SMR add-ons are accompanying SMR of the same compound (propane molecule).

### 3. 3. Data analysis

The rubric described in the instrument section was used in the analysis of the chemical representations of the

entire sample of chemistry textbook sets, which are presented in Table 1. The textbook sets were analysed individually. The SMRs were categorised with regard to curriculum topics of the National Chemistry Curriculum for 8th and 9th Grade.<sup>3</sup> The core topics in which SMRs were categorised are the following: (1) Chemistry is a World of Matter (orig. *Kemija je svet snovi*); (2) Atom and the Periodic System of Elements (orig. *Atom in periodni sistem elementov*); (3) Compounds and Bonding (orig. *Povezovanje delcev/gradnikov*); (4) Chemical Reactions (orig. *Kemijske reakcije*); (5) The Elements in the Periodic Table (orig. *Elementi v periodnem sistemu*); (6) Acids, Bases and Salts (orig. *Kislina, baze in soli*); (7) Hydrocarbons and Polymers (orig. *Družina ogljikovodikov s polimeri*); (8) Organic Compounds Containing Oxygen (orig. *Kisikova družina organskih snovi*); (9) Organic Compounds Containing Nitrogen (orig. *Dušikova družina organskih spojin*) and (10) The Mole (orig. *Množina snovi*). Eventually, the number of SMRs in each of the topics were counted and the frequencies calculated. Analysed SMRs involved SMRs of molecules, atoms and ions.

## 4. Results and Discussion

The results of the analysis are presented with regard to the research questions.

### 4. 1. The Number of SMRs in Slovenian Chemistry Textbook Sets for 8th and 9th Grade Change With Respect to Curriculum Topics (Related to RQ1)

The number of images about the SMRs in chemistry textbook sets is given in Table 3. Most frequently, the SMRs were used in the topics "Hydrocarbons and Polymers" (28.68%; 407 SMRs) and "Organic Compounds Containing Oxygen" (20.23%; 287 SMRs). The lowest frequencies of the use of SMRs were found in the following

**Table 3.** The proportion of SMRs and curriculum objectives in the particular topics of the textbook sets

The topics of the National Chemistry Curriculum for 8 <sup>th</sup> and 9 <sup>th</sup> Grade	SMRs		Curriculum objectives	
	N	f (%)	N	f (%)
Chemistry is a World of Matter (1)	179	12.61	5	8.62
Atom and the Periodic System of Elements (2)	29	2.04	4	6.90
Compounds and Bonding (3)	150	10.57	5	8.62
Chemical Reactions (4)	69	4.86	6	10.34
The Elements in the Periodic Table (5)	16	1.13	7	12.07
Acids, Bases and Salts (6)	160	11.28	7	12.07
Hydrocarbons and Polymers (7)	407	28.68	9	15.52
Organic Compounds Containing Oxygen (8)	287	20.23	7	12.07
Organic Compounds Containing Nitrogen (9)	116	8.17	5	8.62
The Mole (10)	6	0.42	3	5.17
SUM	1419	100.00	58	100.00

topics: The Mole (0.42%; 6 SMRs), The Elements in the Periodic Table (1.13%; 16 SMRs) and Atom and the Periodic System of Elements (2.04%; 29 SMRs).

It was expected that the change in the number of the SMRs would be proportionally related to the number of objectives in the specific chemistry topics, as the objectives in the Chemistry Curriculum for 8<sup>th</sup> and 9<sup>th</sup> Grade<sup>3</sup> are written operationally and can be interpreted by the use of representations on all three representational levels (macroscopic, submicroscopic, and symbolic). This has been proven true for the topics in which the highest proportion of the SMRs has been used. The highest proportion of SMRs in the chemistry textbook sets for the curriculum topic “Hydrocarbons and Polymers” (28.68%; 407 SMRs) is proportional to the highest proportion of objectives in this topic (15.52%; 9 objectives). Similarly, the proportion of SMRs in the chemistry textbook sets for the curriculum topic “Organic Compounds Containing Oxygen” (20.23%; 287 SMRs) are proportional to the proportion of objectives in this topic (12.07%; 7 objectives). Chemistry concepts and processes of these topics are traditionally explained by combining all three representational levels, which is also encouraged with the notations of the curriculum objectives that directly indicate the relationship between structure, properties, and application of substances. For example, one of the objectives in the curriculum topic “Hydrocarbons and Polymers” states: “Students should know that carbon and hydrogen are the fundamental elements of organic compounds – hydrocarbons, and they can identify the causes for the abundance and the variety of organic compounds”.<sup>24</sup>

Despite the high proportion of associated objectives (10.34%; 6 objectives) in the curriculum, the textbook set analysis revealed surprisingly a low number of SMRs used in the curriculum topic “Chemical Reactions” (4.86%; 69 SMRs). Furthermore, the manner in which notations of the objectives are written indicates the need for their explanation by the combined use of the three levels of their representation. For example, it would be expected that for the achievement of the objectives such as “Students should be able to define reactants and products of chemical reactions”<sup>26</sup> and “Students should get acquainted with chemical equations as notations of chemical reactions”<sup>26</sup> would be to a greater proportion presented in the textbooks, not only with photos of the phenomena and/or examples of experiments with their symbolic notations but also with the underlying SMRs.

More frequent use of the triple-nature representations of chemistry concepts would also be expected in the curriculum topic “The Elements in the Periodic Table”. However, as mentioned before, the number of SMRs in this topic are one of the lowest among the curriculum topics (Table 3). One of the reasons for the lower proportions of SMRs could also be in the nature of some of the objectives. In particular, some objectives explicitly refer to the macroscopic representational level, e.g. “Students should

get to know natural resources of elements and compounds”<sup>27</sup> or to the development of stoichiometric skills, e.g. “Students should know how to calculate a mass percentage of the elements in the compounds”.<sup>27</sup> Consequently, in these cases the use of SMRs could easily be neglected.

#### 4. 2. Holistic descriptors of SMR add-ons used to support learners in the recognition of SMRs’ informational value in specific curriculum topics of Slovenian chemistry textbook sets for 8<sup>th</sup> and 9<sup>th</sup> Grade (related to RQ2)

The analysis revealed that various topics of the Chemistry Curriculum for 8<sup>th</sup> and 9<sup>th</sup> Grade<sup>3</sup> include not only different numbers of SMRs but that those SMRs also include different add-ons. The descriptors of the SMR add-ons have already been presented in Table 2. As expected, the analysis of the textbooks revealed that the authors of the textbook sets used various proportions of different types of descriptors of SMR add-ons in specific topics, which is presented in Table 4 and Table 5.

In the top three topics in which SMRs are most frequently used, i.e. “Hydrocarbons and Polymers”, “Organic Compounds Containing Oxygen” and “Chemistry is a World of Matter”, the use of indirect SMRs add-ons prevail (56.27%, 229 SMRs; 69.69%, 200 SMRs; 36.87%, 66 SMRs, respectively). However, it is interesting that more than one third of SMRs (35.87%, 146 SMRs; 26.13, 75 SMRs; 35.20%, 63 SMRs, respectively) do not include any descriptors. In these cases, the recognition of the informational value of particular SMRs depends entirely on learners’ previous experience, knowledge, and their representational competence. This is surprising for the first curriculum topic “Chemistry is a World of Matter”, as it should introduce some of the examples of simple compounds and the states of matter on the particle level, where students’ development of their representational competence needs to be systematically supported by explicit instruction and practice.<sup>18</sup> In “Hydrocarbons and Polymers” and “Organic Compounds Containing Oxygen” other types of SMR descriptors occur rarely, but in the first topic of the curriculum “Chemistry is a World of Matter”, in addition to the indirect descriptor of SMR add-ons also the significant proportion of the combined descriptors (26.26%; 47 SMRs) were found. In these cases, the recognition of the informational value of a particular SMR is supported by SMR add-ons and the learners’ previous experience, knowledge, and their representational competence.

As mentioned earlier, in the topics of the curriculum “Atom and the Periodic System of Elements”, “The Elements in the Periodic Table”, and “The Mole”, the lowest frequencies of the use of SMRs were found. However, the analysis of different types of SMRs add-ons in the second curriculum topic “Atom and the Periodic System of Ele-

ments” reveals that more than half of the SMRs cases are accompanied by indirect descriptors (55.17%; 16 SMRs) of SMR add-ons, more than one third of SMRs enable the learner a direct recognition of particles (10.34%; 3 SMRs) and provide other information – combined descriptor (31.03%; 9 SMRs). In this case the recognition of the informational value of a particular SMR is substantially supported by SMR add-ons, which greatly enables students easier understanding of the atomic structure, ions formation from the atoms and, consequently, the understanding of the relation between atomic structure and their position in the Periodic Table of Elements with regard to the objectives of the curriculum.<sup>3</sup> In the fifth topic of the curriculum, “The Elements in the Periodic Table”, the SMR cases with indirect descriptors of SMR add-ons (62.50%; 10 SMRs) prevail. The second most frequently used SMRs are SMRs without SMR add-ons (25.00%; 4 SMRs). In the last curriculum topic “The Mole” two thirds of SMRs do not have SMRs add-ons (66.67%; 4 SMRs) and the rest have an indirect descriptor (33.33%; 2 SMRs). For the recognition of SMRs’ informational value learners need to rely on their previous experience, knowledge, and representational competence developed in earlier topics of the curriculum.

In all of the remaining topics “Acids, Bases and Salts”, “Compounds and Bonding”, “Organic Compounds Containing Nitrogen” and “Chemical reactions” the indirect

SMR add-ons prevail (45.63%, 73 SMRs; 58.67%, 88 SMRs; 56.03%, 65 SMRs; 59.42%, 41 SMRs, respectively). Moreover, in these topics, which are placed in different parts of the curriculum, a high proportion of SMRs without any SMR add-ons was found, which do not support recognition of SMRs’ informational value.

#### 4. 3. Holistic descriptors of SMR add-ons used to support learners in the recognition of SMRs’ informational value in particular curriculum topics of Slovenian chemistry textbook sets for 8<sup>th</sup> and 9<sup>th</sup> Grade (related to RQ3)

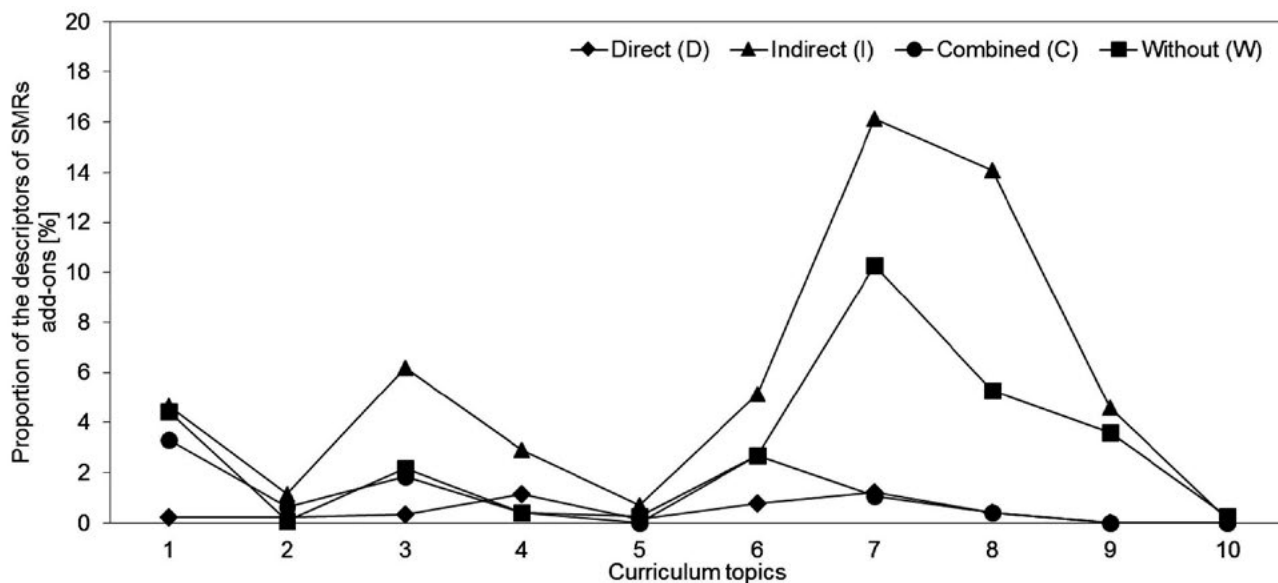
In the textbook set analysis, particular attention has been devoted to studying whether the authors systematically planned the integration of SMS in the textbooks in order to support students’ development of their representational competence. Specifically, in order to do so, Hinze, Rapp, Williamson, et al.,<sup>19</sup> pointed out that explicit instruction for that purpose and practice with the use of particular representations, e.g. SMRs, is necessary. In the context of the textbook sets, it would mean, that particular kinds of SMRs with add-ons would be carefully selected and their integration into the textbook sets continuously upgraded throughout the curriculum.

Table 4. The proportion of SMRs within the particular topics of the textbook sets – part 1

Descriptor of SMR add-ons	The first five topics of the National Chemistry Curriculum for 8 <sup>th</sup> and 9 <sup>th</sup> Grade <sup>3</sup>											
	General		Chemistry is a World of Matter		Atom and the Periodic System of Elements		Compounds and Bonding		Chemical Reactions		The Elements in the Periodic in Table	
	N	f (%)	N	fc (%)	N	fc (%)	N	fc (%)	N	fc (%)	N	fc (%)
Direct (D)	63	4.44	3	1.68	3	10.34	5	3.33	16	23.19	2	12.50
Indirect (I)	790	55.67	66	36.87	16	55.17	88	58.67	41	59.42	10	62.50
Combined (C)	147	10.36	47	26.26	9	31.03	26	17.33	6	8.70	0	0.00
Without (W)	419	29.53	63	35.20	1	3.45	31	20.67	6	8.70	4	25.00
SUM	1419	100.00	179	100.00	29	100.00	150	100.00	69	100.00	16	100.00

Table 5. The proportion of SMRs within the particular topics of the textbook sets – part 2

Descriptor of SMR add-ons	The last five topics of the National Chemistry Curriculum for 8 <sup>th</sup> and 9 <sup>th</sup> Grade <sup>3</sup>									
	Acids, Bases and Salts		Hydrocarbons and Polymers		Organic Compounds Containing Oxygen		Organic Compounds Contenting Nitrogen		The Mole	
	N	fc (%)	N	fc (%)	N	fc (%)	N	fc (%)	N	fc (%)
Direct (D)	11	6.88	17	4.18	6	2.09	0	0.00	0	0.00
Indirect (I)	73	45.63	229	56.27	200	69.69	65	56.03	2	33.33
Combined (C)	38	23.75	15	3.69	6	2.09	0	0.00	0	0.00
Without (W)	38	23.75	146	35.87	75	26.13	51	43.97	4	66.67
SUM	160	100.00	407	100.00	287	100.00	116	100.00	6	100.00



**Figure 1.** The proportion of SMRs with particular descriptors within all of the topics in the textbook sets [Curriculum topics: Chemistry is a World of Matter (1); Atom and the Periodic System of Elements (2); Compounds and Bonding (3); Chemical Reactions (4); The Elements in the Periodic Table (5); Acids, Bases and Salts (6); Hydrocarbons and Polymers (7); Organic Compounds Containing Oxygen (8); Organic Compounds Containing Nitrogen (9); The Mole (10)]

From Figure 1, it can be seen how the overall proportion of different descriptors of SMR add-ons are distributed through the topics of the curriculum. The textbook set analysis revealed that the overall proportion of direct and combined descriptors of SMR add-ons is significantly low through all the curriculum topics (range from 0.00% to 3.31%). That can be connected with the Johnstone's claim<sup>10</sup> that the experienced chemists do the transition between levels of representations very easily and they assumed that learners can do this as easily as they do. These simplified assumptions about learners' easy comprehension and efficient learning with SMRs are reflecting in the low frequency of SMR descriptors, where the informational value of a particular SMR enables the learner a direct recognition of particles, in textbook sets.

It can also be observed from Figure 1, that the overall percentages of SMRs with indirect descriptors or without any add-ons throughout the curriculum are higher than the percentages of SMRs with direct and combined descriptors of SMR add-ons, whereby the figures in the topics "Hydrocarbons and Polymers" and "Organic Compounds Containing Oxygen" stand out (range from 5.29% to 16.14%). From the perspective of the integration of SMRs into the textbook sets based on the assumption about their continuous upgrading throughout the curriculum topics (from the first to last topic), this is a very interesting finding. It can be related to the fact that in these chapters the highest proportion of SMSs is used from all curriculum topics, as proposed earlier, probably as a consequence of the number of curriculum objectives for these topics (Table 3). However, the ratio among the different descriptors of SMR add-ons used in these chapters speaks

in favour of indirect SMR add-ons, which do not enable the learner a direct recognition of particles, as well as SMRs without add-ons, which do not provide any additional information to support the learner's recognition process. The reason for the use of such representations at that point of the textbook sets could either be that the authors assume that the learners are already able to recognise the informational value of SMRs indirectly, because their representational competence has been adequately developed in previous topics, or that the authors integrate SMRs with add-ons into the textbook sets without considering how the correct recognition of the informational value by learners might affect the learning process based on it.

As only a low proportion of direct and combined SMR add-ons was found in the textbook set analysis, it seems worthy to encourage textbook authors to devote special attention to optimally equip the SMRs with add-ons to support students' development of the representational competence across the curriculum. When the learners' perception of SMRs is not a possible initial obstacle for learning, it will be easier to overcome the range of students' misconceptions, related to particle nature of chemical concepts, i.e. in making the distinctions between elements, compounds, and mixtures; appreciations of the reversibility of state changes; seeing atoms and ions as the building blocks of matter; appropriate use of basic chemistry terminology, understanding that Bronsted acids and bases are not substances but molecules and ions etc.<sup>28-31</sup> On the other hand it is important to pay attention to scientific accuracy of SMRs to enable appropriate understanding of chemical concepts and processes.

## 5. Conclusions

When learning chemistry, learners are often challenged by various representations at the submicroscopic level that are included in learning materials, such as textbook sets, to develop understanding of chemistry concepts and processes at the particulate level. Previous research<sup>19,23</sup> has demonstrated that the understanding of visualisations in various learning materials based on recognising the informational value of various representations requires explicit instruction and practice.

This paper presents an analysis of the chemistry textbook sets for 8th and 9th Grade in Slovenia from the perspective of the integration of SMRs into various National Chemistry Curriculum<sup>3</sup> topics. In particular, it was found that the number of SMRs in Slovenian chemistry textbook sets varies significantly with regard to different curriculum topics. In the topics where the highest proportion of the SMRs has been used (“Hydrocarbons and Polymers”, “Organic Compounds Containing Oxygen”), the number of the SMRs is proportionally related to the number of objectives in the specific chemistry topics. Despite the high proportion of objectives in the curriculum, the textbook sets analysis indicates a surprisingly low number of the SMRs used in the curriculum topics “Chemical Reactions” and “The Elements in the Periodic Table”.

Regarding the holistic descriptors of SMR add-ons, that are used to support learners in the recognition of SMRs’ informational value in various curriculum topics, it was found that the descriptors that do not enable the learners a direct recognition of SMRs prevail, especially in the topics “Hydrocarbons and Polymers” and “Organic Compounds Containing Oxygen”, which are in the final part of the curriculum.

In contrast, the textbook set analysis revealed that the overall proportion of the descriptors that enable the learner a direct recognition of the informational value of SMRs is very low through all the curriculum topics. The results can serve as a foundation for a discussion with textbook authors about the role of SMRs with add-ons in supporting students’ development of representational competence across curriculum as well as in the learning process, as it seems valuable that the particular kinds of SMRs with add-ons would be carefully selected and their integration into the textbook sets continuously upgraded throughout the curriculum. Further studies are necessary to obtain more detailed insight into the criteria based on which the authors integrate SMRs with various descriptors into textbook sets.

From the learner’s point of view, in future studies, it would be valuable to focus on research possibilities provided by contemporary technology, such as Eyetracker, for following the learner’s information processing and their use of SMRs in learning with traditional as well as with e-learning materials. Thus far, for example, the importance of various features and notations of visualisations for the learners has been examined with eye trackers by William-

son et al.,<sup>32</sup> who studied students’ use of ball-and-stick images versus electrostatic potential maps when considering electron density, positive charge, proton attack, and hydroxide attack; O’Keefe et al.,<sup>33</sup> who examined how the integration of multiple representations was associated with learning in a multimedia simulation; Ferik Savec et al.<sup>34</sup> examined some of the features of the explanatory key, such as coloured versus black-and-white explanatory keys, and pictorial versus textual explanatory keys, etc.

The results of such studies contribute to the quality of the textbook sets and consequently also to the quality of chemistry teaching and learning, as they can be used for studying in various learning environments.

## 6. References

1. V. Gkitzia, K. Salta, C. Tzougraki, *Chem. Educ. Res. Pract.* **2011**, *12*, 5–14. DOI:10.1039/C1RP90003J
2. A. Bačnik, N. Bukovec, A. Poberžnik, T. Požek Novak, Z. Keuc, H. Popič, M. Vrtačnik, in: N. Purkat (Ed.): Učni načrt. Program gimnazija. Kemija, Ministrstvo za šolstvo in šport, Zavod RS za šolstvo, Ljubljana, **2008**, 59 pp.
3. A. Bačnik, N. Bukovec, M. Vrtačnik, A. Poberžnik, M. Križaj, V. Stefanovik, K. Sotlar, S. Dražumerič, S. Preskar, in: A. Štrukelj (Ed.): Učni načrt. Program osnovna šola. Kemija, Ministrstvo za šolstvo in šport, Zavod RS za šolstvo, Ljubljana, **2011**, 31 pp.
4. Ministrstvo za izobraževanje, znanost in šport, Trubar učbeniški sklad, <https://soca1.mss.edus.si/Trubar/default.aspx>, (assessed: June 9, 2017)
5. M. R. Abraham, E. B. Grzybowski, J. W. Renner, E. A. Marek, *J. Res. Sci. Teach.* **1992**, *29*, 105–120. DOI:10.1002/tea.3660290203
6. M. J. Sanger, T. J. Greenbowe, *J. Chem. Educ.* **1999**, *76*, 853–860. DOI:10.1021/ed076p853
7. F. Abd-El-Khalick, M. Waters, A. P. Le, *J. Res. Sci. Teach.* **2008**, *45*, 835–855. DOI:10.1002/tea.20226
8. I. Devetak, J. Vogrinc, S. A. Glažar, *Int. J. Env. Sci. Ed.* **2010**, *5*, 217–235.
9. K. A. F. Souza, P. A. Porto, *Sci. Educ.* **2012**, *21*, 705–727. DOI:10.1007/s11191-012-9442-z
10. A. H. Johnstone, *J. Comput. Assist. Learn.* **1991**, *7*, 75–83. DOI:10.1111/j.1365-2729.1991.tb00230.x
11. J. K. Gilbert, in: J. K. Gilbert (Ed.): Visualization in Science Education, Springer, Dordrecht, **2005**, pp. 9–27. DOI:10.1007/1-4020-3613-2\_2
12. J. K. Gilbert, M. Reiner, M. Nakhleh. Visualization: Theory and practice in science education. Springer, New York, **2008**, 325 pp. DOI:10.1007/978-1-4020-5267-5
13. J. Oversby, in: J. K. Gilbert, C. J. Boulter (Eds.): Developing models in science education, Kluwer Academic Publishers, Dordrecht, **2000**, pp. 227–251. DOI:10.1007/978-94-010-0876-1\_12
14. H. D. Barke, H. Wirbs, *Chem. Educ. Res. Pract.* **2002**, *3*, 185–200. DOI:10.1039/B2RP90015G



15. V. Ferk Savec, I. Sajovic, K. S. Wissiak Grm, in: J. K. Gilbert (Ed.): *Multiple Representations in Chemical Education*, Springer, Berlin, **2009**, pp. 309–331. DOI:10.1007/978-1-4020-8872-8\_14
16. S. M. Al-Balushi, S. H. Al-Hajri, *Chem. Educ. Res. Pract.* **2014**, *15*, 47–58. DOI:10.1039/C3RP00074E
17. I. Eilks, in: V. G. Tsapalis, H. Sevian (Eds.): *Concepts of Matter in Science Education*, Springer, New York, **2013**, pp. 213–230. DOI:10.1007/978-94-007-5914-5\_10
18. I. Devetak, J. Vogrinc, S. A. Glažar, *Res. Sci. Educ.* **2009**, *4*, 82–94.
19. S. R. Hinze, D. N. Rapp, V. M. Williamson, M. J. Shultz, G. Deslongchamps, K. C. Williamson, *Learn. Instr.* **2013**, *26*, 12–21. DOI:10.1016/j.learninstruc.2012.12.002
20. V. Ferk, M. Vrtacnik, A. Blejec, A. Gril, *Int. J. Sci. Educ.* **2003**, *25*, 1227–1245. DOI:10.1080/0950069022000038231
21. R. Kozma, J. Russell, in: J. Gilbert (Ed.): *Visualization in Science Education*, Kluwer, London, **2005**, pp. 121–146. DOI:10.1007/1-4020-3613-2\_8
22. A. T. Stull, M. Hegarty, B. L. Dixon, M. Stieff, *Cogn. Instr.* **2012**, *30*, 404–434. DOI:10.1080/07370008.2012.719956
23. M. Stieff, S. Scopelitis, M. E. Lira, D. Desutter, *Sci. Educ.* **2016**, *100*, 344–363. DOI:10.1002/sc.21203
24. Š. Hrast, V. Ferk Savec, *J. Balt. Sci. Educ.* **2017**, *16*, in press.
25. A. Bačnik, N. Bukovec, M. Vrtačnik, A. Poberžnik, M. Križaj, V. Stefanovik, K. Sotlar, S. Dražumerič, S. Preskar, in: A. Štrukelj (Ed.): *Učni načrt. Program osnovna šola. Kemija*, Ministrstvo za šolstvo in šport, Zavod RS za šolstvo, Ljubljana, **2011**, pp. 11.
26. A. Bačnik, N. Bukovec, M. Vrtačnik, A. Poberžnik, M. Križaj, V. Stefanovik, K. Sotlar, S. Dražumerič, S. Preskar, in: A. Štrukelj (Ed.): *Učni načrt. Program osnovna šola. Kemija*, Ministrstvo za šolstvo in šport, Zavod RS za šolstvo, Ljubljana, **2011**, pp. 9.
27. A. Bačnik, N. Bukovec, M. Vrtačnik, A. Poberžnik, M. Križaj, V. Stefanovik, K. Sotlar, S. Dražumerič, S. Preskar, in: A. Štrukelj (Ed.): *Učni načrt. Program osnovna šola. Kemija*, Ministrstvo za šolstvo in šport, Zavod RS za šolstvo, Ljubljana, **2011**, pp. 10.
28. K. Taber, *Chemical misconceptions: Prevention, diagnosis and cure (Vol. 1)*, Royal Society of Chemistry, London, **2002**, 246 pp.
29. H. D. Barke, A. Hazari, S. Yitbarek. *Students' misconceptions and how to overcome them*. Springer, Berlin, Heidelberg, **2009**, pp. 21–36. DOI:10.1007/978-3-540-70989-3\_3
30. V. Kind, *Beyond appearances: Students' misconceptions about basic chemical ideas*, School of Education, Durham University, UK, **2009**, 84 pp.
31. H. Barke, N. Harsch, *Afr. J. Chem. Educ.* **2014**, *4*, 82–94.
32. V. M. Williamson, M. Hegarty, G. Deslongchamps, K. C. Williamson III, M. J. Shultz, *J. Chem. Educ.* **2015**, *90*, 159–164. DOI:10.1021/ed200259j
33. P. A. O'Keefe, S. M. Letourneau, B. D. Homer, R. N. Schwartz, J. L. Plass, *Comput. Human. Behav.* **2014**, *35*, 234–242. DOI:10.1016/j.chb.2014.02.040
34. V. Ferk Savec, Š. Hrast, I. Devetak, G. Torkar, *Acta Chim. Slov.* **2016**, *63*, 864–873. DOI:10.17344/acsi.2016.2835

## Povzetek

V podporo razumevanju naravoslovnih pojmov in procesov na ravni delcev so v učna gradiva vključene različne predstavitve (reprezentacije). Članek se osredotoča na preučevanje, kako so submikroskopske reprezentacije (SMR-ji) integrirane v slovenske kemijske učbeniške komplete v povezavi z vsebinami učnega načrta za osnovno šolo. Izhodišče za analizo učbeniškega gradiva so predstavljali štirje holistični deskriptorji SMR-jev (direktni, indirektni, kombinirani deskriptor in SMR-ji brez deskriptorjev), ki glede na specifične opisnike SMR-jev do različne mere podpirajo učenca pri prepoznavanju informacijske vrednosti SMR-jev. Analiza učbeniških kompletov je pokazala, da se število SMR-jev močno spreminja glede na različne vsebine učnega načrta. Delež deskriptorjev, ki učencem omogočajo direktno prepoznavanje SMR-jev, je nizek v vseh vsebinah učnega načrta. Zanimivo je, da deskriptorji, ki ne omogočajo direktne prepoznave SMR-jev, prevladujejo v učbeniških kompletih. Z namenom pridobitve poglobljenega vpogleda v kriterije, na podlagi katerih avtorji učbenikov integrirajo SMR-je z različnimi deskriptorji v učbeniške komplete, so potrebne nadaljnje raziskave.

Scientific paper

# Optimization of UPLC Method for Simultaneous Determination of Rosuvastatin and Rosuvastatin Degradation Products

Jure Zakrajšek,<sup>1,\*</sup> Katarina Bevc-Černilec,<sup>1</sup> Simona Bohanec<sup>1</sup> and Uroš Urleb<sup>2</sup><sup>1</sup> Lek Pharmaceuticals d.d., Development Center Slovenia, Verovškova 57, 1526 Ljubljana, Slovenia<sup>2</sup> Biologics Technical development and Manufacturing, Novartis, Verovškova 57, 1526 Ljubljana, Slovenia

\* Corresponding author: E-mail: jure.zakrajsek@sandoz.com;

Tel.: +386 1 580 26 30, Fax.: +386 1 568 13 93

Received: 23-06-2017

## Abstract

An ultra-performance liquid chromatographic method for simultaneous determination of rosuvastatin and rosuvastatin degradation products was developed and optimized by using fractional factorial experimental design. Optimized method is capable to accurately determine all potential degradation products of rosuvastatin. During the optimization the effect of four chosen chromatographic factors was evaluated. The analytical method operational design region was modeled using Umetrics MODDE software and optimal chromatographic conditions were predicted. The results of the model show that the most important factors to reach good separation between the peaks of rosuvastatin impurities are the pH of buffer solution and the amount of ACN and THF in the mobile phase. The final optimized method using QbD approach was validated for linearity, accuracy and precision for determination of rosuvastatin and rosuvastatin degradation products in rosuvastatin pharmaceutical dosage forms. Limit of detection and quantification were determined for two known specified impurities. The use of experimental designs enabled us to obtain the maximum amount of information about the analytical method design region. Optimization of the method was done without additional experiments, only weighing the responses and rebuilding the statistical model. This approach is very cost-effective when evaluating a variety of different factors and their interactions.

**Keywords:** Fractional factorial design; experimental design; UPLC method optimization; rosuvastatin

## 1. Introduction

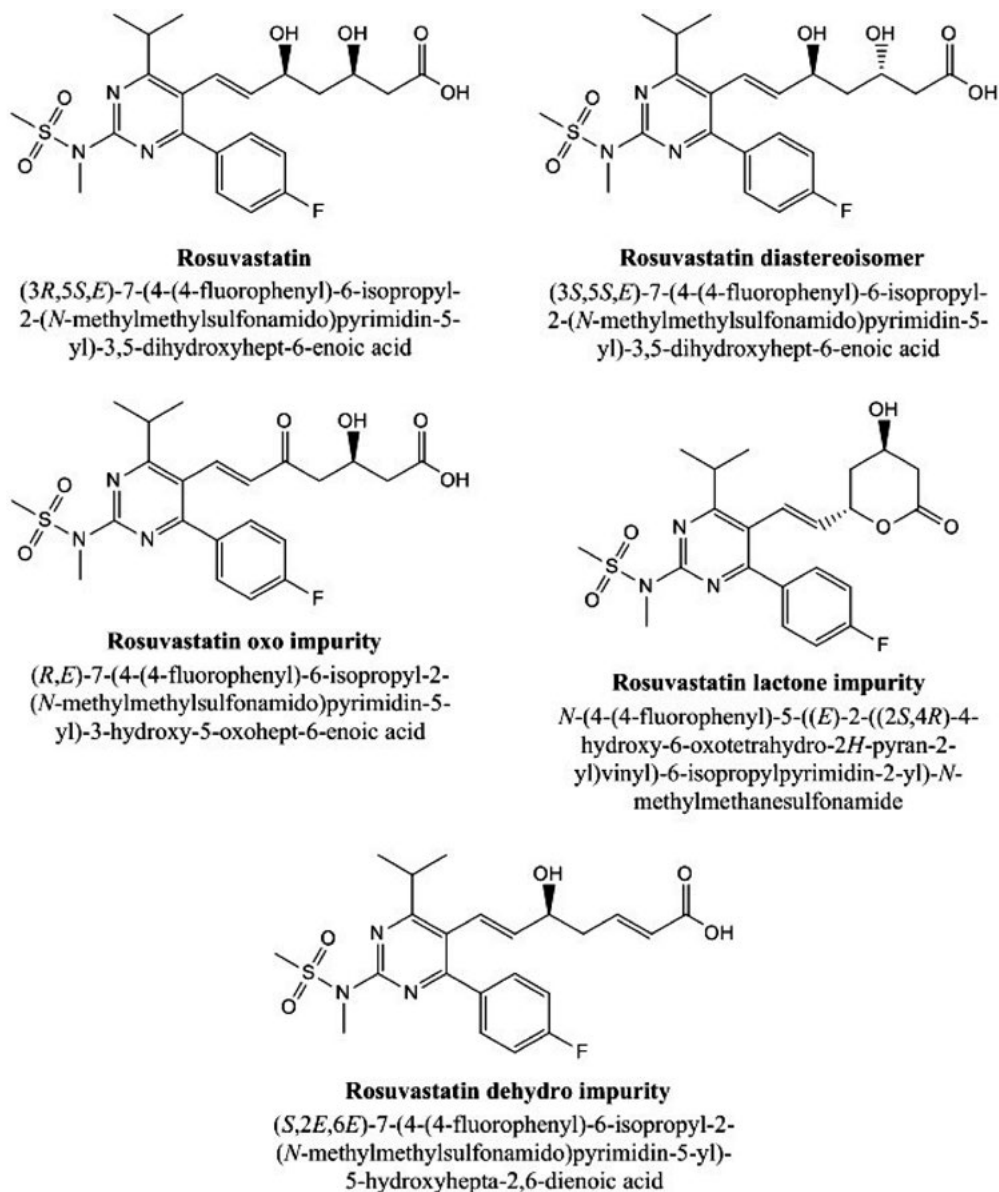
Rosuvastatin belongs to the statin class of pharmaceutical substances that are used for lowering of low-density lipoprotein cholesterol (LDL-C).

Rosuvastatin is mainly administered as a calcium salt of the active hydroxy acid in tablets with 2.5, 5, 10, 20 or 40 mg of rosuvastatin (RSV). Rosuvastatin substance is chemically not stable and degrades into many known and unknown degradation products under different stress conditions (thermal, oxidative, and/or photolytic)<sup>1</sup>. The structural formulas of rosuvastatin and its known impurities are shown in Figure 1.

It is a white amorphous powder only sparingly soluble in water and slightly soluble in ethanol. It contains a polar methane sulphonamide group that interacts with the HMG-CoA reductase.<sup>2,3</sup>

Efforts for applying concepts of quality by design (QbD) principles to analytical method development have increased in recent years in order to achieve more accurate, robust and rugged analytical methods which are used for better control strategy of production processes.<sup>4-6</sup> While quality by design principles are well known and adopted for the development of pharmaceutical products,<sup>7,8</sup> QbD concept has not yet been fully adopted for analytical method development and optimization.

Different experimental designs are used for the evaluation of the effects of different factors and their interactions for process optimization and design space modeling. Compatibility studies between the drug substance and other excipients performed by experimental designs are also described in literature.<sup>9</sup> Maximum amount of obtained information with the smallest possible number of experiments was achieved by this approach.<sup>9</sup> Effect of dif-



**Figure 1.** Structural formula of rosuvastatin (RSV) and its known impurities (RSV diastereoisomer, RSV oxo, RSV lactone, RSV dehydro).

ferent process and formulation parameters on chemical stability of the final drug product was also studied by using fractional factorial designs.<sup>10</sup>

The same principles of QbD can be applied to analytical method development/optimization in order to develop more robust analytical methods and determine the analytical method operation design region.<sup>11,12</sup>

The proposed concept is designed around the analytical target profile (ATP), which predefines the requirements for the analytical method. During the development phase of the analytical method one must show that the analytical method confirms to the criteria set in the ATP.<sup>13</sup>

Use of experimental designs (DoE) in order to assess the multidimensional combination and interactions of factors that could affect the measurements is suggested.<sup>14</sup>

Different experimental designs can be used and are described in the literature to evaluate the effect of different chromatographic parameters such as a buffer pH value, column temperature, percentage of organic modifier in the mobile phase and others.<sup>15–17</sup> The same concepts can be applied not only to chromatographic analytical methods, but also to other analytical techniques such as Karl Fisher titration for water content determination.<sup>18</sup>

To assure the quality of pharmaceutical dosage forms containing rosuvastatin calcium as active ingredient, the assay of rosuvastatin and its degradation products needs to be controlled by a validated analytical method. Various analytical methods have been reported in the literature for determination of rosuvastatin in different pharmaceutical

dosage forms including combinational products. These include HPTLC,<sup>19</sup> HPLC with ultraviolet detection<sup>20–24</sup> and UPLC with ultraviolet detection.<sup>25</sup>

Different HPLC methods with ultraviolet detection have been published for the determination of rosuvastatin degradation products.<sup>25–27</sup> Several methods have also been published for the determination of rosuvastatin in biological fluids using RP-HPLC/UV detection<sup>28</sup> or LC/MS.<sup>29</sup>

The objective of this work was to develop a new analytical method that could simultaneously be used for the determination of rosuvastatin and rosuvastatin degradation products in rosuvastatin pharmaceutical dosage forms. The method has to be stability indicating<sup>30</sup> and capable to detect all changes in product quality during stability testing at various stability conditions according to regulatory requirements (accelerated, long-term or stress stability).<sup>31</sup> Simultaneous determination of rosuvastatin and its degradation products with one analytical method is a great benefit regarding time and resources, taking into account the number of samples that need to be analyzed during the stability studies for regulatory purposes. In addition the method should be accurate, precise and linear with acceptable limit of detection and qualification for all specified impurities (RSV oxo and RSV lactone).<sup>32</sup> The development of the method was done by using QbD principles. The optimization step of the development was performed using experimental designs and analytical method operational design region modeling. A degraded sample from two different stress conditions (photolytic and acidic conditions) was used for the final optimization step.

## 2. Experimental

### 2.1. Chemicals and Reagents

Anhydrous acetic acid ( $\text{CH}_3\text{COOH}$ ), ammonium acetate ( $\text{CH}_3\text{COONH}_4$ ), tetrahydrofuran (THF) purchased from Merck KGaA (Darmstadt, Germany), acetonitrile ( $\text{CH}_3\text{CN}$  – ACN) purchased from J.T. Baker (Avantor Performance Materials, Center Valley, PA) were used for preparation of mobile phases and solvents. Acetonitrile and tetrahydrofuran were of HPLC grade, all other chemicals were of analytical grade.

Milli-Q water purification system (Millipore Corp., Bedford, MA) was used to obtain highly purified water used for all aqueous solutions.

In-house rosuvastatin tert-octylammonium working standard, rosuvastatin oxo tert-octylammonium and rosuvastatin lactone identification standards were used for preparation of standard solutions used for validation and analysis of drug product.

Stock buffer solutions with different pH were prepared by weighing 1.54 g of ammonium acetate and dissolving in 1000 mL of highly purified water. pH of buffer

solution was adjusted to defined pH value using anhydrous acetic acid.

Mixture of stock buffer solution : acetonitrile = 600 : 400 (v/v) was used as solvent for standard and sample preparation.

### 2.2. Equipment

Experiments were performed on a Waters Acquity UPLC separation module, equipped with a quaternary gradient pump, temperature controlled column heater, sampler manager and dual wavelength UV detector (Waters Corporation, Milford, MA). Instrument control was performed using Empower 3 Software for chromatography (Waters Corporation, Milford, MA). Same software was used for data acquisition and processing of results.

Waters Acquity UPLC HSS C18 analytical chromatographic column ( $100 \times 2.1\text{mm}$ ,  $1.8 \mu\text{m}$ ) provided by Waters Corporation (Milford, MA) was used for all optimization experiments.

pH measurements and adjustments were performed with Mettler-Toledo SevenMulti pH meter using a Mettler-Toledo InLab Expert Pro pH electrode (Mettler-Toledo LLC, Columbus, OH).

Mobile phases were vacuum filtered prior the use through Omnipore™ 0.1  $\mu\text{m}$  JV filter, purchased from Millipore (Billerica, MA).

Suntest chamber Atlas SUNTEST XLS+ (Atlas, Mount Prospect, IL) was used to expose sample solutions to artificial sunlight according to ICH guideline for Photostability.<sup>33</sup>

Samples and standard solutions were filtered through Millipore Millex-GV Hydrophilic PVDF 0.22  $\mu\text{m}$  disk filters, purchased from Millipore (Billerica, MA), before the analysis was performed using UPLC method.

### 2.3. Analytical Method

Fast gradient UPLC method was developed for simultaneous determination of rosuvastatin and its degradation products in rosuvastatin formulations with a single injection of the sample and UV detection at two different wavelengths. The initial chromatographic conditions are summarized in Table 1.

The initial method was optimized due to the insufficient resolution between rosuvastatin peak (RSV) and RSV diastereoisomer as presented in the chromatogram of peak identification solutions shown in Figure 2.

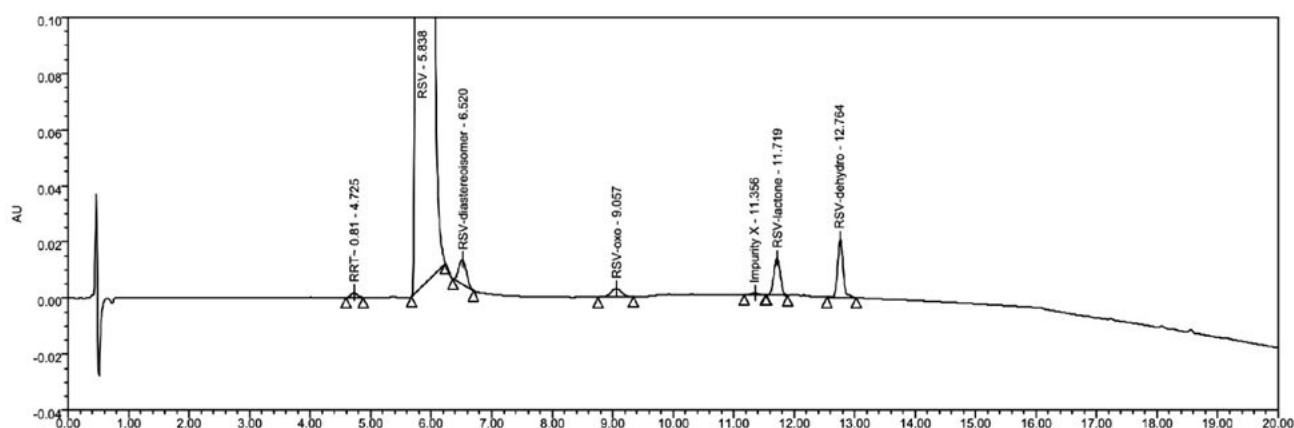
We have optimized the initial chromatographic parameters using a fractional factorial experimental design. The goal of the optimization was to achieve better resolution between rosuvastatin peak and rosuvastatin diastereoisomer and not worsen the resolution between other peaks of degradation products within the chromatogram.

**Table 1.** Chromatographic conditions of the initial UPLC method for assay determination of rosuvastatin.

Mobile phase A	ammonium acetate buffer pH 3.6 : acetonitrile : tetrahydrofuran = 750 : 200 : 40 (v/v/v)
Mobile phase B	ammonium acetate buffer pH 3.6 : acetonitrile : tetrahydrofuran = 250 : 700 : 50 (v/v/v)
Column	Waters Acquity UPLC HSS C18, 100 × 2.1 mm, 1.8 μm
Column temperature	30 °C
Flow rate	0.5 mL/min
Detection wavelength	242 nm (for degradation products) 280 nm (for assay determination)
Injection volume	12 μL

	Time	%A	%B
Gradient parameters	0	88	12
	8.5	88	12
	19.5	30	70
	20	88	12

**Figure 2.** Chromatogram of peak identification solution analyzed with initial chromatographic conditions.

## 2. 4. Standard Solutions

Stock standard solution of rosuvastatin working standard (0.5 mg/mL) was prepared by dissolving appropriate amount of rosuvastatin working standard in solvent.

Working concentrations of rosuvastatin standard solutions were achieved by diluting the stock standard solution with solvent to concentration 2.5 μg/mL (used for the quantitation of degradation products) and concentration 0.25 μg/mL (used for signal-to-noise determination).

Stock standard solution was used for assay determination of rosuvastatin.

Different concentrations of standard solution used in the validation were achieved by diluting the stock standard solution with solvent.

Stock solutions of rosuvastatin oxo (100 μg/mL) and rosuvastatin lactone (100 μg/mL) standards were prepared by dissolving appropriate amount of rosuvastatin oxo or rosuvastatin lactone standard in solvent. Stock solutions were used to prepare spiked samples at appropriate concentration levels used in the validation study.

All standard solutions were filtered through Millipore Millex-GV Hydrophilic PVDF 0.22 μm filter into vials.

## 2. 5. Analysis of Samples

Samples were prepared by dissolving 10 rosuvastatin tablets in appropriate volume of solvent to acquire a concentration 0.5 mg/mL of rosuvastatin. In addition, ultrasonic bath was used to achieve complete disintegration of the tablets.

All sample solutions were filtered through Millipore Millex-GV Hydrophilic PVDF 0.22 μm filter into vials and analyzed with the analytical method.

To evaluate a resolution between unknown impurity X and RSV lactone impurity a degraded sample of rosuvastatin tablets was prepared. Two stock sample solutions were exposed to different degradation conditions. One sample solution was exposed to artificial sunlight under which the unknown impurity X was formed. Hydrochloric acid was added to the second sample solution, as rosuvastatin lactone impurity is known to form under acidic conditions. Both samples were mixed in 1 : 1 (v/v)

ratio to obtain a sample that was used for optimization purposes.

### 3. Results and Discussion

#### 3.1. Chromatographic Condition Optimization

Screening of the influence of four chromatographic factors on different chromatographic responses was performed as the initial step of analytical method optimization. A randomized fractional factorial experimental design ( $2^{4-1}$ ) of resolution IV with central point was used. Buffer pH, amount of acetonitrile in mobile phase A, the amount of organic modifier tetrahydrofuran in mobile phase A and column temperature were selected as factors

**Table 2.** Factors and corresponding levels for  $2^{4-1}$  fractional factorial design used for screening analysis.

Factor name	Abbr.	Settings	Initial
(f1) Buffer pH	pH	3.3 to 3.9	3.6
(f2) Amount of THF	THF	30 to 50 mL	40 mL
(f3) Amount of ACN	ACN	175 to 225 mL*	200 mL
(f4) Column temperature	Temp	25 to 35 °C	30 °C

\*Change in ACN volume was compensated with defined buffer solution volume so that the total volume of buffer solution and ACN was not changed.

of interest, and were used to generate the fractional factorial experimental design. All factors and their corresponding levels are shown in Table 2.

Fractional factorial experimental design was generated using Umetrics MODDE 11.0 software.

Eleven experiments presented in Table 4 were carried out according to the generated experimental design. Three central point experiments (experiment N9, N10 and N11) were also included for the determination of experimental error. All experiments were carried out in a randomized order (run order) in order to eliminate any systematic errors.

Six chromatographic responses presented in Table 3 were selected and measured for all performed experiments: resolution between rosvastatin (RSV) peak and RSV diastereoisomer (Res 1), resolution between impurity X peak and RSV lactone peak (Res 2), resolution between RSV lactone peak and RSV dehydro impurity peak (Res 3), number of theoretical plates of rosvastatin peak (N), symmetry factor for rosvastatin peak (T) and retention time or rosvastatin peak (Rt).

The results of experiments are presented in Table 4.

All obtained and collected response measurements were processed with Umetrics MODDE software. Partial least squares (PLS) multivariate method of simultaneously estimating the models for all the responses was used for fitting and optimizing the statistical model. PLS method

**Table 3.** Responses and used suitability criteria for method optimization and sweet spot analysis.

Response name	Abbr.	Suitability criteria		
		Min	Target	Max
Resolution RSV, RSV diastereoisomer	Res 1	2.5	3.0	–
Resolution impurity X, RSV lactone	Res 2	1.5	2.0	–
Resolution RSV lactone, RSV dehydro	Res 3	6.0	6.5	–
Number of theoretical plates of RSV peak	N	7000	7500	–
Symmetry factor for RSV peak	T	0.8	1.0	1.6
Retention time or RSV peak	Rt	–	6.0	6.5

**Table 4.** Randomized  $2^{4-1}$  fractional factorial design and results of observed responses.

Exp No	Run Order	Factors				Responses					
		f1	f2	f3	f4	Res 1	Res 2	Res 3	N	T	Rt
N1	1	–	–	–	–	3.39	1.39	5.48	7976	1.59	9.432
N2	11	+	–	–	+	2.98	1.26	3.30	8379	1.66	8.907
N3	3	–	+	–	+	2.55	n.a. <sup>†</sup>	7.74	6930	1.51	5.493
N4	4	+	+	–	–	2.66	1.69	5.09	7401	1.53	6.951
N5	8	–	–	+	+	2.30	1.68	6.19	6361	1.45	4.368
N6	2	+	–	+	+	2.07	1.57	3.25	6537	1.45	4.383
N7	7	–	+	+	–	2.22	1.64	6.63	5643	1.37	3.87
N8	10	+	+	+	–	2.07	1.83	4.86	6138	1.37	4.037
N9	9	0	0	0	0	2.63	1.54	5.78	7526	1.51	5.846
N10	5	0	0	0	0	2.64	1.57	5.77	7186	1.54	5.838
N11	6	0	0	0	0	2.63	1.60	5.78	7217	1.54	5.844

<sup>†</sup> Resolution could not be measured due to the coelution of the two peaks.

simultaneously deals with numerous responses, taking their covariances into account. This provides an overview of the relationship between the responses and factors to determine the proper effect on all responses obtained within the statistical model.<sup>34</sup>

This provides an overview of the relationship between the responses and factors to determine the proper effect on all responses obtained within the statistical model.

The main effects of factors were identified for each response using the statistical model and are presented in Figure 3.

Higher amount of ACN and THF in the mobile phase A have negative effect on theoretical plates of RSV peak (N), as presented in Figure 3. In addition, higher level of these two factors also has a negative effect on symmetry factor of RSV peak (T) and retention time of RSV peak (Rt). Higher amount of ACN and THF in the mobile phase A with the combination of higher column temperature also have negative effect on the resolution between RSV peak and RSV diastereoisomer (Res 1).

On the contrary, higher amount of ACN and THF in the mobile phase A have positive effect on resolution between impurity X peak and RSV lactone peak (Res 2), by improving the resolution between these two peaks. The most significant factors affecting the resolution between RSV lactone peak and RSV dehydro peak (Res 3) are buffer

solution pH with negative effect and the amount of THF in the mobile phase A with positive effect.

Reducing the amount of ACN in the mobile phase A and reducing the buffer solution pH would lead to better responses of all measured resolutions.

All non-significant factors were excluded from the statistical model and the model was refitted.

Using MODDE integrated sweet spot analysis tool, the analytical operational design region was modeled. Appropriate suitability criteria were assigned to all the responses measured (see Table 3). Using the analysis tool the optimal chromatographic conditions were predicted (Figure 4).

The analytical method operational design region is presented for all four evaluated factors from the sweet spot diagram in Figure 4. The green area represents the part of the operational design region where all from statistical model calculated responses fulfil the criteria set for individual responses. This area is called the sweet spot. The black cross represents the optimal conditions as predicted by MODDE software tool. The outcome of the sweet spot analysis is in line with our preliminary conclusions obtained from the main effects plot (Figure 3). The sweet spot calculated by MODDE software tool is achieved by lowering buffer solution pH, reducing the amount of ACN in the mobile phase A and raising the column temperature. No additional change was made to the amount of the THF in the mobile

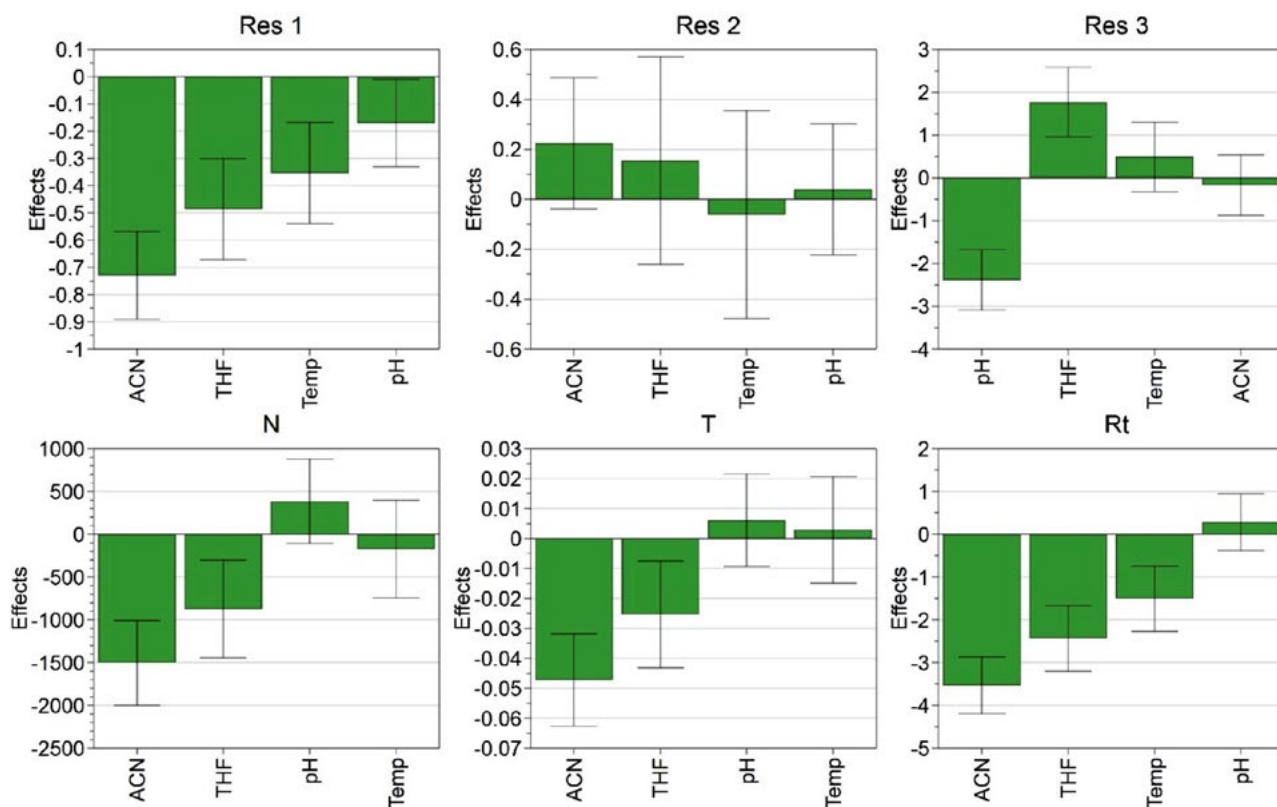
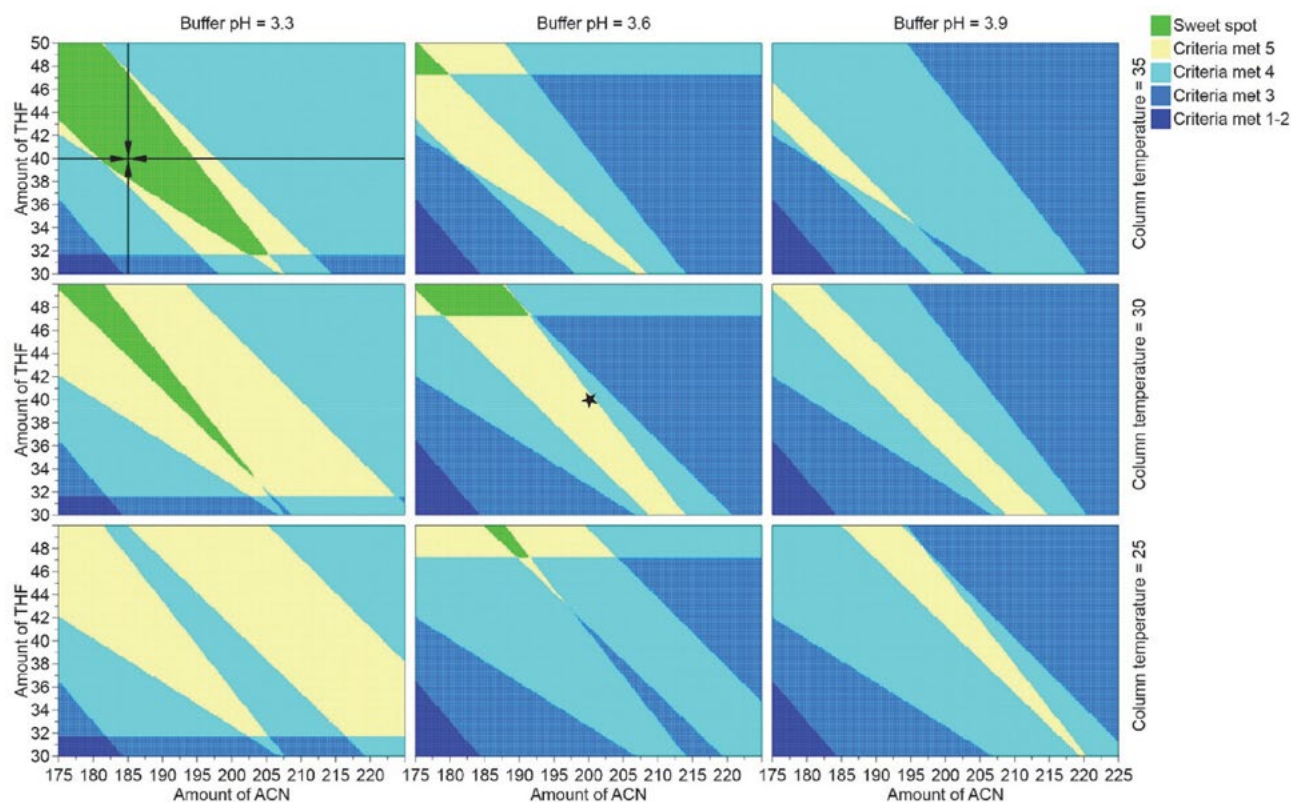
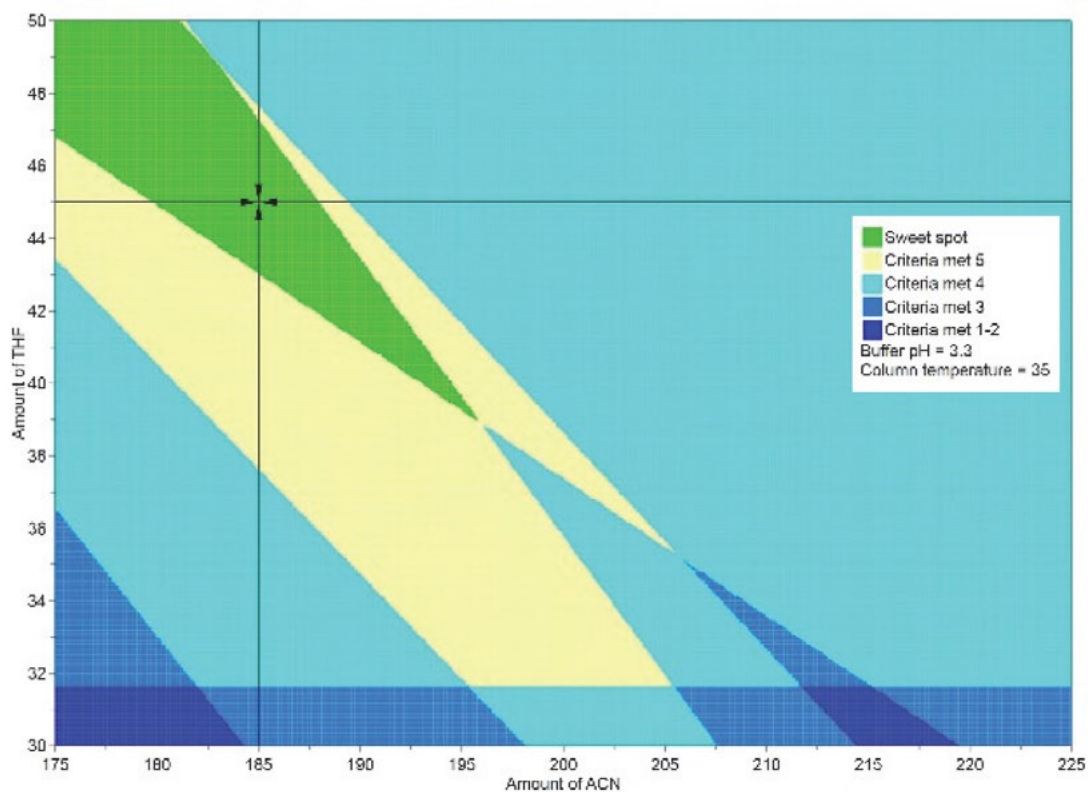


Figure 3. Main effects for all observed responses for UPLC method optimization for the determination of rosuvastatin and rosuvastatin degradation products.



**Figure 4.** Sweet spot diagram for a PLS model of the analytical operational design region. Optimal chromatographic conditions proposed by MODDE are marked with a cross. The initial chromatographic conditions are marked with a star at the center of the figure.



**Figure 5.** Sweet spot diagram for a PLS model of the analytical operational design region with weighted responses.



phase. The chromatographic parameters of the initial sweet spot analysis are presented in Table 5 (initial sweet spot conditions) and in Figure 4 (marked with a star).

Using the suggested sweet spot chromatographic conditions, the degraded sample mixture was analyzed.

Chromatograms of degraded sample mixture (shown as a blue lines) and peak identification solution obtained with chromatographic conditions of the initial sweet spot and final sweet spot conditions (shown as black lines) are presented in Figure 6.

The resolution between impurity X peak and RSV lactone peak was not satisfactory when proposed initial

sweet spot conditions were used while considerably better resolution between RSV and RSV diastereoisomer peak was achieved.

Since we had a statistical model for the analytical method operational design region no additional experiments were performed. MODDE sweet spot analysis was performed once again by weighing the importance of different responses measured. Resolution between RSV peak and RSV diastereoisomer peak (Res 1) and resolution between impurity X peak and RSV lactone peak (Res 2) were assigned with the highest weights, while the weights for all other responses were reduced. This way the sweet spot tool

Table 5. Initial chromatographic conditions compared to initial sweet spot conditions and final sweet spot conditions.

Factor name	Abbr.	Initial chromatographic conditions	Initial sweet spot conditions	Final sweet spot conditions
(f1) Buffer pH	pH	3.6	3.3	3.3
(f2) Amount of THF	THF	40 mL	40 mL	45 mL
(f3) Amount of ACN	ACN	200 mL	185 mL	185 mL
(f4) Column temperature	Temp	30 °C	35 °C	35 °C

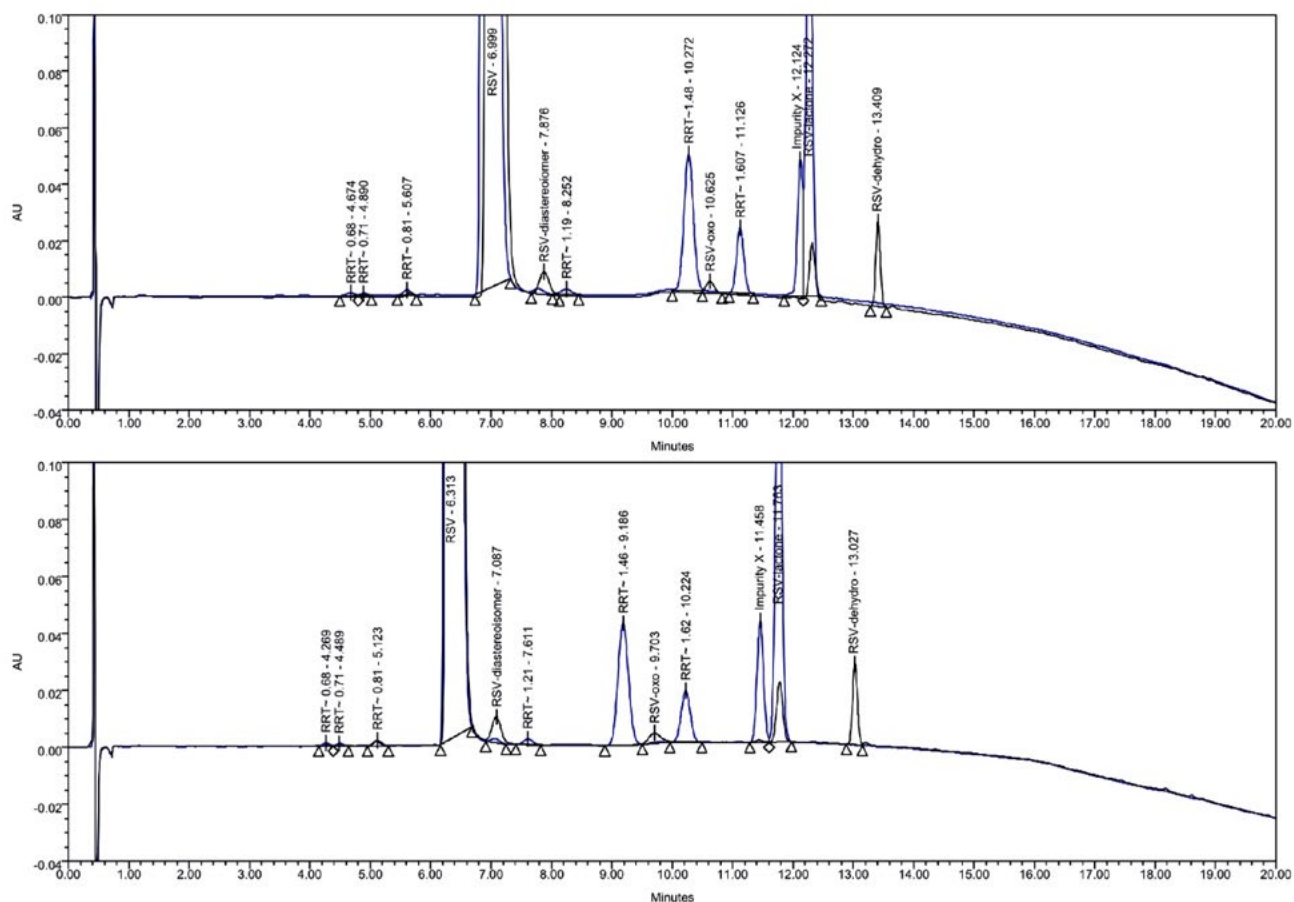


Figure 6. Chromatogram of the peak identification solution (black line) and degraded sample mixture (blue line) analyzed with initial sweet spot conditions (top) and final sweet spot conditions (bottom).

was forced to find a spot with a satisfactory resolution between the critical pairs of impurities and not achieving the acceptance criteria for other responses. Additionally, the criteria for resolution between impurity X peak and RSV lactone peak (Res 2) was also tightened.

After running the sweet spot analysis again with the weighted responses, the new suggested sweet spot was calculated. The analytical method operational design region was modeled again and is presented in Figure 5. pH buffer solution value was fixed to 3.3 and column temperature to 35 °C. New optimal chromatographic conditions proposed by MODDE optimizer are marked with a cross.

The resolution between the unknown impurity X and RSV lactone could be improved with higher amounts of THF in the mobile phase. Suggested chromatographic parameters are presented in Table 5 (final sweet spot conditions).

The chromatogram obtained with the final sweet spot chromatographic conditions (Figure 6 bottom) shows significantly improved resolution between the impurity X peak and RSV lactone peak. The resolution between RSV peak and RSV diastereoisomer is significantly better than with the initial method. Despite all the method changes overall runtime of the analysis method was not prolonged.

### 3. 2. Analytical Method Validation

The optimized analytical method was validated for determination of rosuvastatin and rosuvastatin degradation products in rosuvastatin tablets. Linearity, precision, accuracy, limit of detection and quantification were determined for main compound rosuvastatin and both specified degradation products RSV oxo and RSV lactone. The acceptance criteria for different validation parameters were set in line with ICH requirements.<sup>32</sup>

#### 3. 2. 1. Linearity and Working Range

The linearity of the method for determination of rosuvastatin was determined by using nine different standard solutions of rosuvastatin working standard. All solu-

tions were prepared in three replicates. The covered concentration range was from 0.25 mg/mL to 0.75 mg/mL (50–150% of target concentration). The linearity of rosuvastatin was determined using nine different solutions of rosuvastatin working standard prepared in three replicates for determination of related substances. The concentration range covered was from 0.15 µg/mL to 6.0 µg/mL (0.03– 1.2%). For rosuvastatin lactone and rosuvastatin oxo impurities, the linearity was determined using six different standard solutions prepared in three replicates. The concentration range covered for rosuvastatin lactone was 0.15 µg/mL to 6.0 µg/mL (0.03–1.2 %) and for rosuvastatin oxo 0.25 µg/mL to 3.0 µg/mL (0.05–0.6 %). The obtained linear regression results are presented in Table 6.

The response of all components was found to be linear in the tested concentration range. Good correlation coefficient (> 0.99) was obtained for all components.

#### 3. 2. 2. Precision

Repeatability of the analytical system for determination of rosuvastatin was checked at the target concentration of rosuvastatin (0.5 mg/mL) by six replicate injections of the sample solution.

Repeatability was also validated for known rosuvastatin impurities RSV lactone and RSV oxo. The results of individual impurities are expressed as % (percentage) of RSV lactone and % of RSV oxo. The obtained results and RSD of the measurements are presented in Table 7.

Intermediate precision was performed by injecting six sample solution replicates. The study was done by different analyst that performed the analysis on different days, different chromatographic systems and different UPLC columns. All together six different variations were performed. Assay of rosuvastatin, % of RSV lactone and % of RSV oxo were measured. The results are presented in Table 7.

The results in Table 7 demonstrate good precision of the method for assay determination, RSD value < 1.0%. The precision for individual impurities was found to be acceptable as the criteria for RSD (n = 6 or 36) of the impurities measured at this level was set to < 20 %.

**Table 6.** Average linear regression data for RSV, RSV lactone and RSV oxo obtained for optimized UPLC method.

Component	Target and concentration range [µg/mL]	Slope	Intercept bias in %	Intercept	R <sup>2</sup>
RSV for assay determination	500	2929137	6892266	0.47	0.9998
	250–750				
RSV for degradation products	1.3	7662070	999981	5.05	0.9981
	0.15–6.0				
RSV lactone	2.9	8030538	–14466	–0.06	0.9996
	0.15–5.9				
RSV oxo	2.5	5354275	–51492	–0.71	0.9994
	0.25–3.0				

**Table 7.** Repeatability and intermediate precision results for RSV, RSV lactone and RSV oxo.

Component	Precision		Intermediate precision	
	% content <sup>1</sup>	% RSD <sup>2</sup>	% content <sup>3</sup>	% RSD <sup>4</sup>
<b>RSV for assay determination</b>	99.61	0.96	98.89	0.71
<b>RSV lactone</b>	0.111	2.23	0.105	10.72
<b>RSV oxo</b>	0.091	4.59	0.080	12.30

<sup>1</sup> average of 6 determinations; <sup>2</sup> determined on 6 measurements; <sup>3</sup> average of 36 determinations; <sup>4</sup> determined on 36 measurements

### 3. 2. 3. Accuracy

The accuracy of the proposed analytical method was checked at three concentration levels. For rosuvastatin determination the range was from 70%–130% of the target assay determination concentration. For the determination of degradation products, the accuracy for rosuvastatin was checked in range 0.03 % (0.15 µg/mL)–0.24 % (1.2 µg/mL), for RSV lactone in range 0.03 % (0.15 µg/mL)–1.2 % (6.0 µg/mL) and for RSV oxo in range 0.05 % (0.25 µg/mL)–0.6 % (3.0 µg/mL).

All samples were prepared by spiking the appropriate amount of a component into a placebo solution. Spiked samples were prepared in three replicates and analyzed by the proposed optimized analytical method. The recovery factor was calculated and obtained results are presented in Table 8.

As presented in Table 8 the recovery for the determination of rosuvastatin is acceptable. Individual recovery

values were within  $\leq 100 \pm 3$  % and the  $RSD_{(n=3)}$  of the obtained recovery values was below 2 %, demonstrating good accuracy of the method for determination of rosuvastatin in rosuvastatin drug products.

The accuracy for degradation products determination was also satisfactory for all components. The calculated recovery was within 80–120% for all components and the  $RSD_{(n=3)}$  of the obtained recovery values was below 20%.

### 3. 2. 4. Limit of Detection

The detection limits were determined on the basis of signal-to-noise (S/N) ratio  $\geq 3 : 1$  according to ICH guidelines. The signal-to-noise values and calculated LOD concentrations are presented in Table 9.

The calculated obtained LOD concentration are 0.009 µg/mL for rosuvastatin, 0.009 µg/mL for RSV lac-

**Table 8.** Results of recovery experiments at five concentration levels of RSV, RSV lactone and RSV oxo, obtained with optimized UPLC method.

Component		Level 1	Level 2	Level 3
<b>RSV for assay determination</b>	Concentration range	70 % (350 µg/mL)	100 % (500 µg/mL)	130 % (650 µg/mL)
	Mean recovery <sup>1</sup>	101.31	101.18	101.17
	% RSD <sup>2</sup>	0.16	0.29	0.25
<b>RSV for degradation products determination</b>	Concentration range	0.03 % (0.15 µg/mL)	0.20 % (1.0 µg/mL)	0.24 % (1.2 µg/mL)
	Mean recovery <sup>1</sup>	102.56	101.47	103.88
	% RSD <sup>2</sup>	9.82	4.07	3.25
<b>RSV lactone</b>	Concentration range	0.03 % (0.15 µg/mL)	1.0 % (5.0 µg/mL)	1.2 % (6.0 µg/mL)
	Mean recovery <sup>1</sup>	110.14	105.49	104.84
	% RSD <sup>2</sup>	4.63	0.54	0.75
<b>RSV oxo</b>	Concentration range	0.05 % (0.25 µg/mL)	0.5 % (2.5 µg/mL)	0.6 % (3.0 µg/mL)
	Mean recovery <sup>1</sup>	108.97	99.76	100.01
	% RSD <sup>2</sup>	6.79	0.38	0.51

<sup>1</sup> average of 3 determinations; <sup>2</sup> determined on 3 measurements

**Table 9.** Results of signal-to-noise values and LOD for RSV, RSV lactone and RSV oxo impurities obtained with optimized UPLC method.

Component	Concentration % of RSV	Concentration µg/mL	Average S/N ratio (n = 6)	LOD µg/mL
<b>RSV</b>	0.01	0.05	16.5	0.009
<b>RSV lactone</b>	0.01	0.05	15.9	0.009
<b>RSV oxo</b>	0.02	0.1	10.6	0.028

**Table 10.** Results of signal-to-noise values and LOQ for RSV, RSV lactone and RSV oxo impurities obtained with optimized UPLC method.

Component	Concentration % of RSV	Concentration µg/mL	Average S/N ratio (n = 6)	LOQ µg/mL
RSV	0.03	0.15	51.8	0.029
RSV lactone	0.03	0.15	48.8	0.031
RSV oxo	0.05	0.25	25.9	0.097

tone and 0.028 µg/mL for RSV oxo impurity. The determined S/N ratios are higher than required 3, however lower quantification limits are not needed since the reporting limit for impurities is 0.05% with respect to the concentration of rosuvastatin in the sample.

### 3. 2. 5. Limit of Quantification

The quantitation limits were determined on the basis of signal-to-noise (S/N) ratio  $\geq 10 : 1$  according to ICH guidelines. The signal-to-noise values and calculated LOQ concentrations are presented in Table 10.

The calculated obtained LOQ concentration are 0.029 µg/mL for rosuvastatin, 0.031 µg/mL for RSV lactone and 0.097 µg/mL for RSV oxo impurity. The determined S/N ratios are higher than required 10, but lower quantification limits are not needed as the reporting limit for impurities is 0.05% with respect to the concentration of rosuvastatin in the sample.

## 4. Conclusions

The optimization of a new analytical method capable of simultaneous determination of rosuvastatin assay and its degradation products in rosuvastatin drug products was performed with a single fractional factorial experimental design. Only 11 experiments were needed for the optimization, while at least 16 experiments would be needed to cover the same analytical method operational region of the first optimization step with a traditional one factor at time (OFAT) approach.

During the optimization, it was demonstrated that it is necessary to do the optimization of analytical methods with a sample that contains all possible degradation products. The degradation of the sample in this article was performed by artificial sun-light and acid hydrolysis as this was proven to be the most stability indicating condition for rosuvastatin.

It was shown that with the appropriate statistical model of the analytical method operational region one can also do the optimization with no additional experiments, if the outcome of the first trial is not satisfactory. The responses can be weighted and the sweet-spot analysis run again on the same set of experiments.

The final analytical method optimized with QbD approach was validated according to ICHQ2R1 guideline.<sup>32</sup> The method was found to be linear, accurate and precise

for both rosuvastatin assay determination and determination of rosuvastatin degradation products. The validated method was successfully applied for rosuvastatin drug products.

The final optimized method is stability indicating and is capable to detect all changes in the rosuvastatin product(s) that are stored at different storage and stress stability conditions. It enables to determine the content of rosuvastatin and its degradation products in a single injection run. This optimization reflects in saving of time and resources since one stability study includes hundreds of samples tested during the product's shelf life.

## 5. References

1. R. P. Shah, A. Sahu, S. Singh, *Anal Bioanal Chem* **2013**, *405*, 3215–3231. DOI:10.1007/s00216-013-6760-1
2. A. G. Olsson, F. McTaggart, A. Raza, *Cardiovasc Drug Rev* **2002**, *20*, 303–328. DOI:10.1111/j.1527-3466.2002.tb00099.x
3. K. C. Ferdinand, *Expert opinion on pharmacotherapy* **2005**, *6*, 1897–1910. DOI:10.1517/14656566.6.11.1897
4. F. G. Vogt, A. S. Kord, *J. Pharm. Sci.* **2011**, *100*, 797–812. DOI:10.1002/jps.22325
5. J. Ermer, P. J. Borman, J. Carolan, P. Faulkner, C. Finkler, O. Grosche, M. Hanna-Brown, J. Hoffmann, I. Gill, A. Lenhart, P. W. Nethercote, A. Rignall, T. Sokoliess, G. Wegener, M. Pohl, *Pharmind* **2010**, *72*, 256–264.
6. P. Borman, P. Nethercote, M. Chatfield, D. Thompson, K. Truman, *Pharm. Technol.* **2007**, *31*, 142–152.
7. *ICH Guideline: Pharmaceutical Development Q8(R2)*, CHMP/ICH/167068/04.
8. *Pharmaceutical cGMPs for the 21st Century – A Risk-Based Approach*, U.S. Food and Drug Administration (FDA).
9. S. Bohanec, T. Rozman Peterka, P. Blažič, R. Jurečič, J. Grmaš, A. Krivec, J. Zakrajšek, *Acta Chim. Slov.* **2010**, *57*, 895–903.
10. P. Petelin, M. Homar, A. Bajc, J. Kerč, S. Bohanec, *Acta Chim. Slov.* **2012**, *59*, 156–162.
11. M. Schweitzer, M. Pohl, M. Hanna-Brown, P. Nethercote, P. Borman, G. Hansen, K. Smith, J. Larew, *Pharm. Technol.* **2010**, *34*, 52–59.
12. P. Borman, J. Roberts, C. Jones, M. Hanna-Brown, R. Szucs, S. Bale, *Sep. Sci.* **2010**, *2*, 2–8.
13. T. W. Graul, K. L. Barnett, S. J. Bale, I. Gill, M. Hanna-Brown, in: D. J. am Ende (Ed.): *Chemical Engineering in the Pharmaceutical Industry: R&D to Manufacturing*, Wiley, Hoboken, NJ, US, **2011**, pp. 545–562.

14. M. Moder, S. Bohanec, J. Zupan, *Acta Chim. Slov.* **1997**, *44*, 181–196.
15. S. Karmarkar, R. Garber, Y. Genchanok, S. George, X. Yang, R. Hammond, *J. Chromatogr. Sci.* **2011**, *49*, 439–446. DOI:10.1093/chrscl/49.6.439
16. D. Awotwe-Otoo, C. Agarabi, P. J. Faustino, M. J. Habib, S. Lee, M. A. Khan, R. B. Shah, *J. Pharm. Biomed. Anal.* **2012**, *62*, 61–67. DOI:10.1016/j.jpba.2012.01.002
17. M. Hanna-Brown, P. Borman, S. Bale, R. Szucs, J. Roberts, C. Jones, *Sep. Sci.* **2010**, *2*, 12–20.
18. L. Zhou, J. M. Socha, F. G. Vogt, S. Chen, A. S. Kord, *Am. Pharm. Rev.* **2010**, 74–84.
19. S. J. Varghese, T. K. Ravi, *AOAC Int* **2010**, *93*, 1222–1227.
20. S. Ashour, S. Omar, *Int J Biomed Sci* **2011**, *7*, 283–288.
21. S. K. Banerjee, N. M. Vasava, *Bull. Pharm. Res* **2013**, *3*, 29–33.
22. A. K. Gajjar, V. D. Shah, *Eurasian journal of analytical chemistry* **2010**, *5*, 265–283.
23. M. A. Mukthinuthalapati, V. Bukkapatnam, S. P. Bandaru, *Adv Pharm Bull* **2014**, *4*, 405–411.
24. Z. M. Turabi, O. h. A. Khatatbeh, *International Journal of Pharmaceutical Sciences and Drug Research* **2014**, *6*, 154–159.
25. G. V. R. Reddy, B. V. Reddy, S. W. Haque, H. D. Gautam, P. Kumar, A. P. Kumar, J. H. Park, *Química Nova* **2011**, *34*, 250–255. DOI:10.1590/S0100-40422011000200015
26. T. N. Mehta, A. K. Patel, G. M. Kulkarni, G. Suubbaiah, *J AOAC Int* **2005**, *88*, 1142–1147.
27. S. Palvai, S. C. Seelam, K. Dhanalakshmi, N. Reddy, *International Journal of Pharmacy & Therapeutics* **2013**, *4*, 182–187.
28. Y. Shah, Z. Iqbal, L. Ahmad, A. Khan, M. I. Khan, S. Nazir, F. Nasir, *J Chromatogr B Analyt Technol Biomed Life Sci* **2011**, *879*, 557–563. DOI:10.1016/j.jchromb.2011.01.004
29. S. J. Varghese, T. K. Ravi, *AOAC Int* **2013**, *96*, 307–312. DOI:10.5740/jaoacint.11-117
30. R. Maheswaran, *Pharm. Technol.* **2012**, *36*, 73–80.
31. ICH Guideline: *Stability Testing of New Drug Substances and Products Q1A(R2)*, CPMP/ICH/2736/99.
32. ICH Guideline: *Validation of Analytical Procedures: Text and Methodology Q2(R1)*, CPMP/ICH/381/95.
33. ICH Guideline: *Stability Testing: Photostability Testing of New Drug Substances and Products Q1B*, CPMP/ICH/279/95.
34. L. Eriksson, E. Johansson, N. Kettaneh-Wold, C. Wikstrom, S. Wold: *Design of Experiments – Principles and Applications*, Umetrics AB, Umea, Sweden, 3rd ed., 459, **2008**.

## Povzetek

Z uporabo delnega faktorkega načrta smo ovrednotili vpliv štirih kromatografskih parametrov in izvedli optimizacijo visoko ločljivostne tekočinske kromatografske metode za hkratno določitev rosuvastatina in njegovih razkrojnih produktov. Nova optimizirana metoda omogoča natančno določitev vsebnosti rosuvastatina in vseh razkrojnih produktov rosuvastatina v farmacevtskih pripravkih, ki vsebujejo rosuvastatin.

S pomočjo programa Umetrics MODDE smo izdelali model, ki opisuje delovno območje analitske metode, in napovedali optimalne pogoje kromatografske ločbe. Rezultati statističnega modela so pokazali, da so najpomembnejši parametri, ki zagotavljajo najboljšo ločbo med rosuvastatinom in njegovimi nečistotami, pH puferne raztopine in količina ACN ter THF v mobilni fazi.

Analitsko metodo za določitev rosuvastatina in njegovih razkrojnih produktov, optimizirano s pomočjo QbD pristopa, smo validirali, pri čemer smo ovrednotili njeno linearnost, točnost in natančnost. Za dve znani specificirani nečistoti smo določili mejo določitve in mejo zaznave.

Uporaba programa za statistično načrtovanje poskusov nam je omogočila izvedbo optimizacije le z utežitvijo spremljanih odzivov in ponovnim vrednotenjem delovnega območja analitske metode, brez izvedbe dodatnih poskusov. S statističnim načrtovanjem poskusov smo dobili kar največ informacij o delovnem območju analitske metode z najmanjšim možnim številom izvedenih poskusov. S takšnim pristopom se zmanjšajo tudi stroški razvoja metode, saj nam statistično načrtovanje poskusov omogoča hkratno obravnavo različnih parametrov in njihovih medsebojnih interakcij.

Scientific paper

# Ordering Effects and Percolation in the Structure Formation Process of the Oriented Polyolefin Porous Films

Galina Kazimirovna Elyashevich,<sup>3,\*</sup> Dmitrii Vladimirovich Novikov,<sup>3</sup>  
Ivan Sergeevich Kuryndin,<sup>3</sup> Andreja Jelen<sup>2</sup> and Vili Bukošek<sup>1,\*</sup>

<sup>1</sup> Faculty for Natural Sciences and Engineering, University of Ljubljana, Snežniška c. 5, Ljubljana, 1000 Slovenia

<sup>2</sup> Jožef Stefan Institute, Jamova cesta 39, Ljubljana, 1000 Slovenia

<sup>3</sup> Institute of Macromolecular Compounds, Russian Academy of Sciences, Bolshoi pr. 31, St. Petersburg, 199004 Russia

\* Corresponding author: E-mail: [elya@hq.macro.ru](mailto:elya@hq.macro.ru); [vili.bukosek@ntf.uni-lj.si](mailto:vili.bukosek@ntf.uni-lj.si)

Received: 12-07-2017

## Abstract

Structure transitions and mechanism of the formation of superlattices lamellae in microporous polyolefin (polyethylene and polypropylene) films obtained in the process based on polymer melt extrusion followed by annealing, uniaxial extension and thermal fixation have been studied by statistical analysis of electron microscopy images of the film surface. The structure of the porous films prepared in the multistage process has been studied by SEM, gravimetry and permeability measurements. It has been shown that the pore formation at the stage of uniaxial extension is accompanied by the ordering of lamellae and their self-organization controlled by spin draw ratio and annealing temperature. It was established that an increase of these parameters lead to the transition of disorder–order type. The effect of preparation conditions on the ordering process of regular spatial lattices of lamellae has been discussed.

**Keywords:** Percolation, self-organization, through permeability, porous films, polyethylene, polypropylene

## 1. Introduction

At present time a large number of porous systems containing microscopic pores have been prepared and studied; and among them, polyolefin films are the most promising materials. Owing to high chemical resistance to various media, they are widely used as gas and liquid permeable membrane materials in medical, chemical, and food industries. Microporous polymer films have a number of advantages over porous systems based on inorganic substances, namely: easy manufacturing, small thickness and hence lower resistance to mass transfer, and high elasticity.

Flexible-chain polyolefins such as high density polyethylene<sup>1,2</sup> and polypropylene<sup>3–6</sup> are capable to form the oriented lamellar structures during crystallization of polymer melts under extension. The thermal treatment of these samples at temperatures close to the melting temperature of a polymer leads to an increase in the degree of crystallinity and a decrease in the number of tie chains in amorphous regions between lamellae, and, finally, almost all tie

chains become stressed. In result of such structure formation the materials (films and fibers) acquire so-called “hard elastic” mechanical properties, that is, high elastic modulus and ability to large reversible deformations.<sup>4,7</sup> Due to a very low number of tie chains in amorphous regions the pores appear between lamellae at uniaxial extension of hard elastic samples in air at room temperature. Porous films with well developed networks of through flow channels may be used as microfiltration membranes, separators in galvanic cells, and elastic substrates in composite systems.<sup>8–13</sup>

Up to now, there have been few published papers<sup>5,14</sup> concerning the analysis of the porous film preparation process, at which transition from individual pores to a connected network of through flow channels is observed. In<sup>14</sup> it was shown that the formation of through pores in the samples prepared in the process based on melt extrusion occurs via the percolation mechanism.<sup>15</sup> The task of the work was the investigation of the effect of pore formation process conditions on the percolation transitions and or-

dering effects at the self-organization of lamellar structure in the polyolefin porous films.

## 2. Experimental

The process used to prepare the microporous polyolefin films consists of four stages: (1) melt extrusion, (2) annealing of extruded films, (3) uniaxial extension of the annealed films (pore formation stage), and (4) thermal fixation of the porous structure.<sup>2,5,14</sup> The films are characterized by a multilevel (multifractal) structure.<sup>5</sup> Such structure is formed by stacks of crystalline lamellae arranged normally to the orientation (extension) direction of samples, so that molecular chains in crystallites are oriented in the extension direction. Lamellae stacks are connected by thin “bridges” (stressed ties) and form the framework of the solid-phase percolation cluster.<sup>16</sup> In the process of uniaxial extension, discontinuities (pores) appear in such films as a result of moving apart and bending of lamellae between the bridges of tie chains. It was shown that the number and size of pores grow with an increase in the degree of extension that leads to the coalescence of pores and the formation of through flow channels, i.e., the films become filtration membranes permeable to liquids. It was also found that the overall porosity ( $P$ ) and the permeability ( $G$ ) of the membranes can be controlled by varying the spin draw ratio ( $\lambda$ ) at the polymer melt extrusion, the annealing temperature ( $T_{\text{ann}}$ ) of extruded films and degree of uniaxial extension ( $\epsilon$ ) at the pore formation stage.<sup>17</sup>

Two structure self-ordering types are implemented in the prepared microporous films. The first type includes the cooperative percolation over pores (the formation of through channels) or the geometrical phase transition occurring upon reaching a critical degree of the overall porosity. The second type is associated with the periodic spatial superlattice of lamellae due to the disorder–order transition and ordering of particle aggregates (stacks of lamellae). The percolation transition leads to the formation of a liquid-permeable porous structure and the self-organization of lamellae at increasing the control parameters of the process:  $\lambda$ ,  $T_{\text{ann}}$  and  $\epsilon$ .

Commercial grades of linear PE ( $M_w = 170000$ ,  $M_w/M_n = 4-5$ ) and isotactic PP ( $M_w = 380000$ ,  $M_w/M_n = 4-5$ ) was used for porous films preparation. The melt was crystallized in air. The degree of melt orientation was varied by the spin draw ratio  $\lambda$ . Extruded films were annealed under isometric conditions, i.e. at fixed ends of the film, to prevent their shrinkage at heating. The porous structure of membranes was formed at uniaxial extension of annealed films at room temperature. At the final stage, thermal fixation of the porous samples was performed for relaxation of inner stresses resulting from extension.

The permeability of porous films  $G$  was determined by measuring the liquid (ethanol) flow rate through the film.<sup>8</sup>

An important characteristic of porous systems is overall porosity, i.e., the fraction of the sample volume occupied by pores. In the microporous films under investigation all type of pores, namely, the open-cell, closed and through pores, contribute to the overall porosity  $P$  which was determined by the gravimetric method.

$$P = [(\rho - \rho_p) / \rho] \times 100 \%, \quad (1)$$

Where  $\rho$  is the density of a dense (nonporous) film, being equal to 950 and 900 kg/m<sup>3</sup> for PE and PP films, respectively; and  $\rho_p$  is the density of a porous film determined by weighing.

The images of the surface of membrane samples were obtained on a FE-SEM SUPRA 35 scanning electron microscope (Zeiss, Germany).

Statistic analysis of SEM images was carried out using the cluster two-phase model on a square lattice with the ratio  $r/\xi \approx 0.1$ , where  $r$  is the distance between sites and  $\xi$  is the correlation length of phase clusters. Within this model, we calculated the average lattice density  $\Omega_p$  of porous phase clusters (porous phase fraction in two-dimensional space) and the radial distribution functions  $g(R)$  of the cluster lattice density. The effective size  $d$  and fractal dimension  $D$  of porous phase clusters were determined by the initial region ( $R < d$ ) of the fall of curves  $g(R)$  using the power-law asymptotic,  $g(R) \sim R^{D-2}$ .

The correlation length  $\xi$  was identified with the abscissa of the point at the maximum of the direction averaged radial density distribution function  $g(R)$  of the porous phase clusters. When the point of the maximum was absent, the correlation length was identified with the point at which the function  $g(R)$  reached the asymptote  $g(R) = 1$ .

The angular dependences (indicatrices) of the lattice fractal density  $\rho_s$  of the solid phase clusters were obtained according to the procedure described on the scale of a rectangle with area  $2r\xi$  centered at the occupied lattice site.

The degree of ordering of the lamellae in the films  $\varphi$ , was quantitatively estimated using the coordination order parameter along the extension axis of the films:

$$\varphi = |L_{s\parallel} - L_{p\parallel}| / (L_{s\parallel} L_{p\parallel})^{1/2}, \quad (2)$$

where  $L_{s\parallel}$  and  $L_{p\parallel}$  are the periods of alternation of the lattice densities of the solid phase and the porous phase clusters, respectively, along the  $s$  axis.

The regular spatial lattice of particles corresponds to the parameter  $\varphi = 0$ ; with an increase in the coordination disorder, the parameter  $\varphi$  increases. The periods  $L_{s\parallel}$  and  $L_{p\parallel}$  were determined using the functions  $g(R)_{\parallel}$  calculated in the direction of this axis. The thickness  $l_{\parallel}$  of solid phase particles was calculated as  $l_{\parallel} = 0.8R_{\text{min}}$ , where  $R_{\text{min}}$  is the position of the first minimum of the corresponding function  $g(R)_{\parallel}$ .

### 3. Results and Discussion

The microporous films prepared by the method used in this study are characterized by a relief-like strongly developed surface. This pattern arises at uniaxial extension stage in result of stress release due to the through pores appearance. As can be seen from SEM images, the surface relief of the PE and PP films (Figure 1) is designed by two types of structural elements; namely, extended large comb-like structures arranged perpendicular to the direction of orientation of the film and thin “bridges” aligned parallel to the film orientation direction and connecting the comb-like structures.

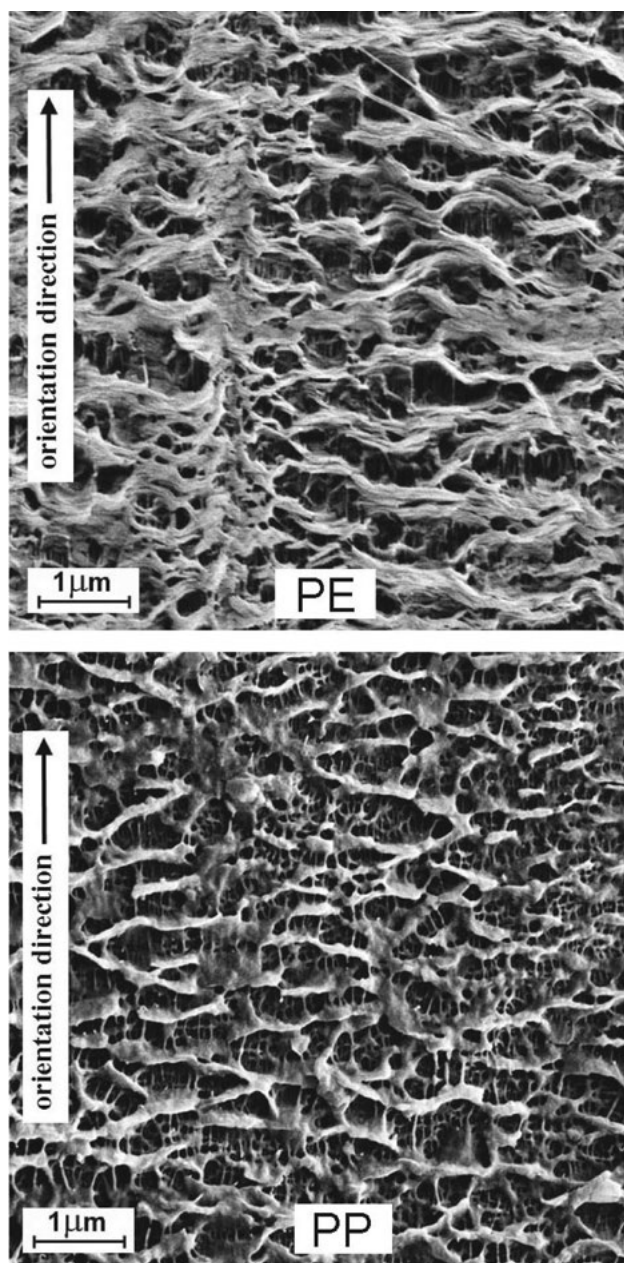


Figure 1. SEM images of the PE and PP porous films surface

Deeper regions (pores) are seen between these structural formations on the sample surface. The PP samples are characterized by smaller sizes of the structural elements of the surface relief and by their considerably larger number as compared to the PE films. These characteristics of the surface structure indicate that the PP films have a more developed surface relief than the PE ones. This is confirmed by the measurements of specific surface, which is equal to 41 and 83 m<sup>2</sup>/g for PE and PP microporous films, respectively.

#### 3. 1. Effect of Spin Draw Ratio on the Ordering Transitions

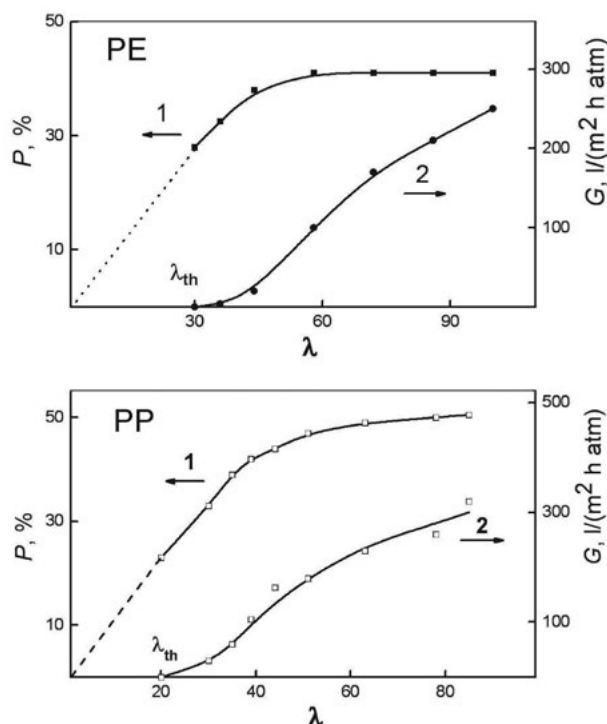
Due to the orientation efforts at the melt extrusion the periodic superlattice of oriented lamellae is formed in the films via the universal mechanism of particle self-ordering, controlled by the spin draw ratio  $\lambda$ . At the stages of extrusion and annealing which is performed at isometric conditions, lamellae are organized in an ensemble of oriented supramolecular structures. Under uniaxial extension of the films prepared at these stages this ensemble transforms to a spatial network of smaller particles, i.e., lamellae stacks (superlattices of lamellae), due to irreversible splitting of structons. The superlattice formation can be considered as the disorder–order transition, which leads to ordering of the multilevel supramolecular polymer structure. At increasing of  $\lambda$  the size and degree of the aggregates ordering increase. The transformation of the microporous films’ surface texture with variations in spin draw ratio is caused by the change in the relative contribution from the stacks of lamellae and stressed ties connecting them to the spatial distribution of the density of the solid phase cluster.

A typical property of the microporous polyolefin films under study is the percolation effects which are associated with the formation of a fractal structure of the surface. The fractal cluster of the solid phase is arisen near the threshold of percolation in result of the coalescence of pores and appearance of through flow channels. Percolation mechanism of the through pores formation is demonstrated by the dependence of the permeability  $G$  (flow rate through the membrane) on  $\lambda$  which exhibits a percolation threshold of  $\lambda$  for permeability at threshold value of the overall porosity  $P$  (the sample volume fraction occupied with pores) (Figure 2).

For PE films the threshold is reached at  $P^* = (30 \pm 2)$  %, for PP ones  $P^* = (23 \pm 2)$  %. The difference between the values of  $P^*$  for PE and PP is connected with the structure details of PE films. This result is in accordance with percolation theory<sup>15</sup> which gives for percolation threshold 2530%.

The transition through the percolation threshold at  $P > P^*$  is accompanied by the formation of a percolation cluster of the porous phase in the material. On the film surface, this transition corresponds to an increase in the correla-





**Figure 2.** Plots of overall porosity  $P$  (1) and permeability  $G$  (2) of porous PE and PP films vs. spin draw ratio  $\lambda$ .

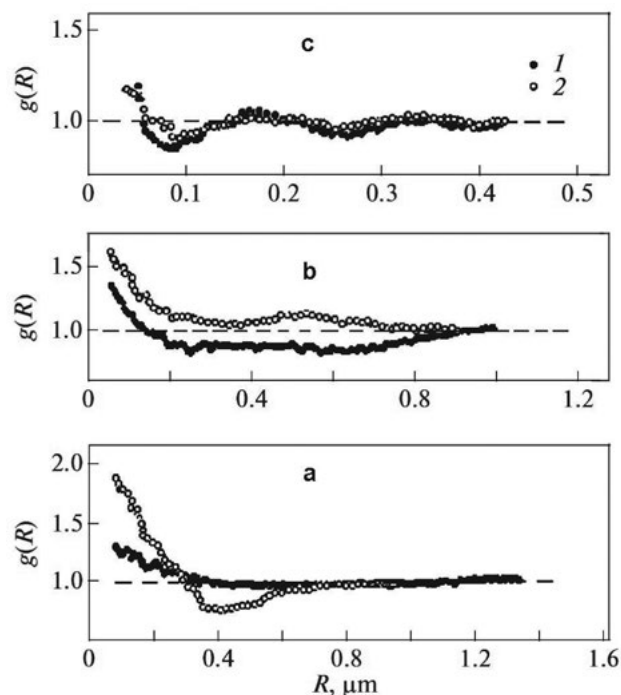
tion length  $\xi$ , a decrease in the total anisotropy of the density distribution  $\rho_s$  of the solid phase clusters, and a disordering of the average density distribution of the porous phase clusters. The above phenomena have a common character and are observed in the computer implementation of the lattice clusters models.

The orientational order of lamellae and the degree of orientation of polymer chains increase with increasing  $\lambda$ . This growth is nonlinear, which is indicated by both the nonmonotonic dependence of the correlation length on  $\lambda$  for investigated samples and a significant scatter of the data on birefringence in PE porous films, obtained by changing the parameter  $\lambda$ .<sup>18</sup> It can be assumed that the nonlinear in  $\lambda$  orientation behavior reflects different conditions of their structure formation depending on parameters of melt extrusion process. In this case, the transition from one mode to another is accompanied by a change in the orientation of molecules and supramolecular structures themselves and also porous phase clusters. Of particular interest is the disorder–order orientation transition on the  $\lambda$  scale, associated with the formation of oriented through channels.

Microporous PE films were prepared at variation of  $\lambda$  in the range 24–69. The structural parameters and porous structure transformation have been investigated by statistical treatment of the SEM images. It was obtained that the lattice density fraction  $\Omega_s$  of the solid phase on the surface of microporous PE films corresponds in two-dimensional mapping to the infinite cluster of the particles at  $\Omega_s \geq \Omega^*$ , where  $\Omega^*$  is the critical value at the percolation threshold ( $0.45 \pm 0.03$ ).<sup>19</sup> In its turn, the porous structure of the films

is transformed upon varying parameter  $\lambda$ , and the transition from discrete pores ( $\Omega_p < \Omega^*$ ) to through channels ( $\Omega_p > \Omega^*$ ) occurs at  $\lambda > 29$ . The existence of the critical value of  $\lambda$ , which provides percolation in PE membranes, was previously found in.<sup>14</sup>

Radial functions  $g(R)$  of the clusters density distribution of the phases in the general case is typical for the structurally nonuniform systems and nonmonotonically approach the straight line  $g(R) = 1$  (Figure 3a) as  $R$  increases. This straight line is reached at  $R = \xi$ , where  $\xi$  is the correlation radius of density fluctuations.<sup>19</sup> It should be expected that the values of  $\xi$  for two mutually complementary percolation clusters coincide (Figures 3b, 3c).



**Figure 3.** Distribution functions  $g(R)$  of the clusters density along the directions: solid phase (1) and porous phase (2) for  $\lambda = 24$  (a), 36 (b) and 69 (c).

At the same time as lattice density  $\Omega_p$  of the cluster of the particles decreases, the value of  $\xi$  increases (Table 1).

For the PE film obtained at  $\lambda = 69$  the periodic oscillation of the functions  $g(R)$  near the value  $g(R) = 1$ , and

**Table 1.** The structural parameters of the porous PE films.

$\lambda$	Solid phase		Pores	
	$\xi$ , $\mu\text{m}$	$d$ , $\mu\text{m}$	$\Omega_p$	$d$ , $\mu\text{m}$
24	0.71	0.6	0.36	0.35
29	0.25	0.13	0.30	0.18
36	0.54	0.28	0.46	0.38
42	0.58	0.80	0.42	0.62
69	–	0.09	0.57	0.09

functions  $g(R)$  almost coincide both for the solid phase and for pores which indicates the formation of the uniform periodic structure of microporous PE films. The infinite cluster is transformed into the two-dimensional quasilattice of oriented particles, and the superlattice is constructed of ordered stacks of lamellae, so that each stack involves  $\sim 2.5$  lamellae. The mean sizes of the particles (stacks of lamellae) and pores in the direction perpendicular to the orientation axis coincide.

The formation of through channels at increasing of  $\lambda$  is associated with ordering the particles in the orientation direction of the samples. Functions  $g(R)$  of clusters of the phases along the orientation direction indicate that the periodicity of alternation of the particles with period  $L_{\parallel}$  appears at the scale of the correlation radius  $\xi$ . It was calculated that the value of  $L_{\parallel}$  substantially exceeds both the thickness of a single lamella (30 nm) and the long period (35 nm).<sup>20</sup> Thus, the anisometric particles that are revealed by SEM on the film surface are the fragments of the solidified polymer material involving the stacks of lamellae. The pattern of the surface is similar to the internal lamellar structure of porous samples; however, they are characterized by a larger scale of structural elements.<sup>20,21</sup> Periods  $L_{\parallel}$  of alternation of the particles and pores in the orientation direction for the porous sample prepared at  $\lambda = 69$  coincide and correspond to the average period  $L = 170$  nm.

Structure transformations in PP porous films were investigated for the samples prepared at  $\lambda = 44$  and 78. In the samples, prepared at  $\lambda = 78$ , the 3D regular lattice of lamellae stacks and also the system of oriented through flow channels providing the highest permeability to the sample are formed. In 2-dimensional images the regular scale lattice of lamellae is characterized by a coincidence of alternation periods of lattice density for solid (s) and porous (p) phases clusters along ( $L_{s\parallel} = L_{p\parallel} = 110$  nm) and perpendicular ( $L_{s\perp} = L_{p\perp} = 110$  nm) to extension direction (axe s), both. In this case overall porosity of the films equal 50%, so solid and porous phases in the lattice may be considered as co-dimensional.

In the film prepared at  $\lambda = 44$  regular 3D lattice of lamellar is absent. Along axes, the condition  $\xi = L_{s\parallel} = L_{p\parallel} = 110$  nm is valid. However, in transverse direction there is no any coordination between radial functions  $g(R)_{s\perp}$  and  $g(R)_{p\perp}$  of a lattice density clusters of phases distribution. In this case the solid and porous phases are non-dimensional ones; the overall porosity is 41%. Non-dimensional character of solid and porous phases is the reason of permeability decreasing of this membrane in 1.5 times in comparison with the film ( $\lambda = 78$ ) which is characterized by regular 3D lattice of lamellae.

The transition “co-dimensional – non-dimensional” solid and porous phases is related to the change of topological structure of the films, namely, to transition from the model of statistical network of pores to model of oriented network of through flow channels.

### 3. 2. The influence of the Annealing Temperature on the Structure Transformation at Pore Formation

The process of the pore formation at uniaxial extension is regulated by self-organization of lamellae and, consequently, strongly depends on the lamellar structure formed at extrusion and annealing stages. Figure 4 shows the relationship of the basic parameters ( $T_{\text{ann}}$  and  $\lambda$ ), ensuring the achievement of percolation values of the overall porosity (23 and 30% for PE and PP films, respectively). This figure shows, under what combination of values  $\lambda$  and  $T_{\text{ann}}$  appears through permeability in porous polyolefin films.

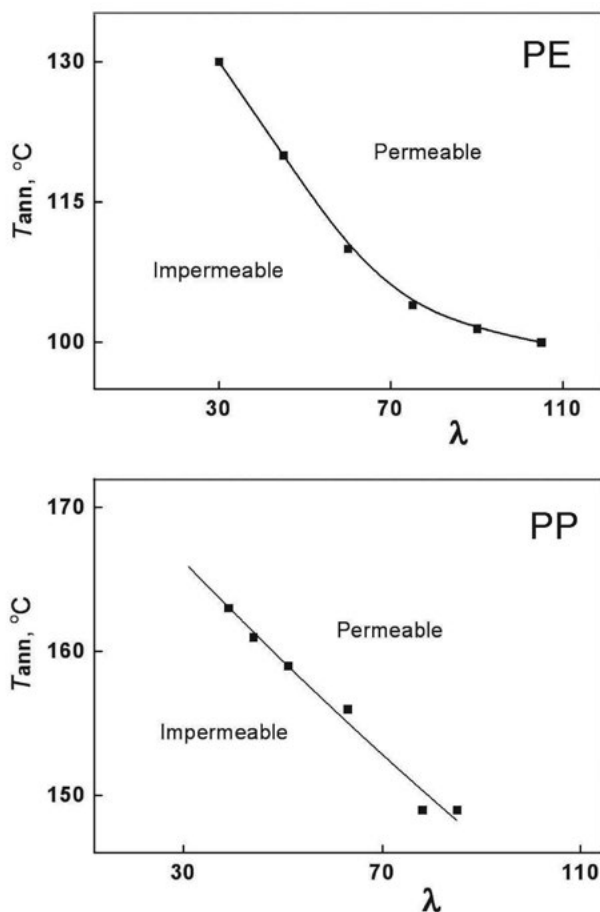


Figure 4. Relation between  $\lambda$  and  $T_{\text{ann}}$  at the threshold values of overall porosity for PE and PP films. Uniaxial extension is 200%.

The figure evidences: when extrusion was performed at lower  $\lambda$ , the percolation value  $P^*$  is achieved at higher  $T_{\text{ann}}$ , and vice versa; if on the extrusion stage greater  $\lambda$  was used, then annealing can be performed at lower temperatures  $T_{\text{ann}}$ . However, this regularity is disrupted for PE. The fact is that structural rearrangement, consisting in increasing the size of lamellae occurs when annealing was carried out at temperatures at which the mobility of the chains in

the PE crystals appears. According to dynamic mechanical analysis (DMA) for obtained PE films, this temperature is in the range 90–100 °C (Figure 5). Annealing of the films at lower temperatures does not permit to realize the perfecting of the lamellar structure and transition to a hard-elastic state, which is a prerequisite for the formation the through channels, upon subsequent uniaxial extension. The weakening of the connection between  $\lambda$  and  $T_{\text{ann}}$  for PE films at  $T_{\text{ann}}$  close to 100 °C shows, that further increase  $\lambda$  does not allows to decrease  $T_{\text{ann}}$  below this temperature. For PP films character of relation between thresholds  $\lambda$  and  $T_{\text{ann}}$  does not change, because in this case used values  $\lambda$  correspond  $T_{\text{ann}}$ , which are higher than appearance of chains mobility in crystals 130–140 °C according to DMA (Figure 5).

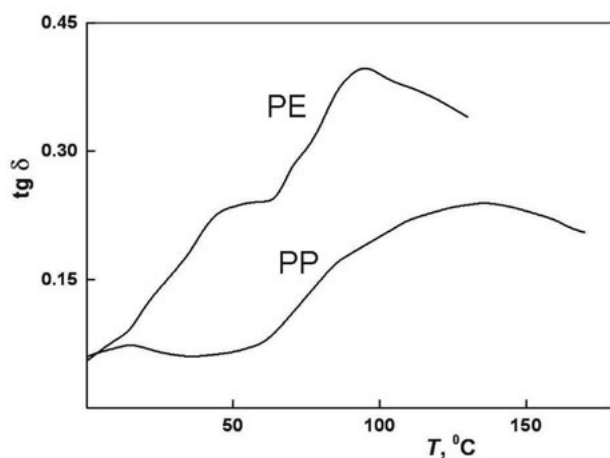


Figure 5. The temperature dependences of  $\text{tg } \delta$ : PE and PP films.

To establish a correlation between the density of the porous phase  $\Omega_p$  (the surface area occupied by all types of pores) and overall porosity  $P$ , the PP films obtained at different  $T_{\text{ann}}$  for which there is a linear relationship between these parameters were selected. In the case of the preva-

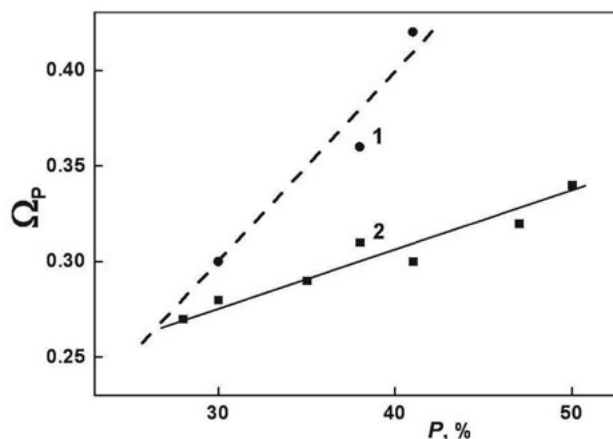


Figure 6. The dependences of the average lattice density  $\Omega_p$  of porous phase clusters on the surface of PE (1) and PP (2) films on overall porosity  $P$ . The dashed line corresponds to  $\Omega_p = P$ .

lence of the through oriented channels (after the percolation threshold) occurs a linear correlation between two and three dimensional porosity (Figure 6).

The dependence of permeability of porous films  $G$  on the parameter  $\tau = (P - P^*)/P^*$  characterizing the degree of deviation of the porosity parameter  $P$  from the percolation threshold  $P^*$  was studied. The parameter  $P$  in the region  $P > P^*$  was varied by changing of  $T_{\text{ann}}$ ;  $P$  linearly increases with  $T_{\text{ann}}$ . It was shown that the dependence  $G(\tau)$  is a power-law function  $G \sim \tau^t$  and is characterized by the critical indices  $t = 1.5$  and  $t = 1.9$  for  $\lambda = 44$  and  $\lambda = 78$ , respectively.

The change of the critical index  $t$  with increasing  $\lambda$  can be associated with the transition from percolation in a random inhomogeneous medium ( $t = 1.5$ ) to anisotropic percolation over oriented through channels ( $t = 1.9$ ). Such a transition should be a consequence of an increase in the cooperativity of the lamellae ordering process at the stage of pore formation and the development of a regular spatial 3D lattice of particles.

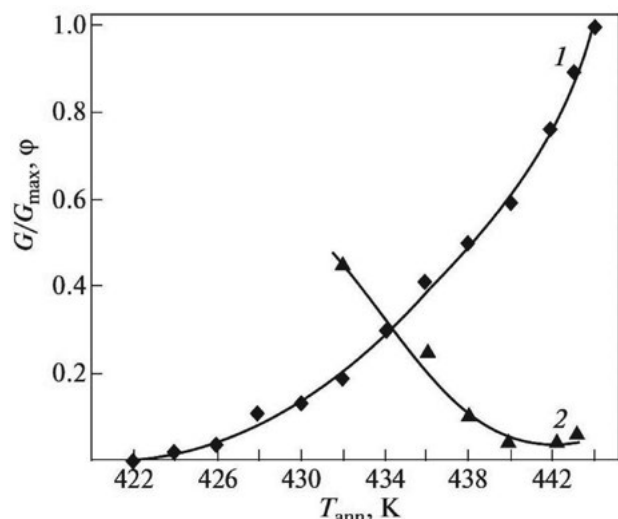
An analysis of the two-dimensional SEM images of the membrane surface makes it possible to clear up the character of pore formation process with increasing porosity  $P$  or the degree of deviation  $\tau$  from the percolation threshold  $P^*$ . The areas occupied by pores increase that corresponds to the pore growth under steady-state conditions at which the lamellar structure of membranes is ordered.

The investigation of correlations between the two-dimensional network density  $\Omega_p$  of porous phase clusters and the volume porosity  $P$  of PP membranes shows that  $\Omega_p$  is independent of  $P$  in the case of  $\lambda = 44$ ; at  $\lambda = 78$  the linear correlation between these parameters is observed. The equality  $\Omega_p = P$  is valid for homogeneous systems. Porous phase clusters in the membranes under study are topologically inhomogeneous due to the presence of three pore types: through, closed, and open cell. The establishment of the linear dependence  $\Omega_p(P)$  in going from  $\lambda = 44$  to  $\lambda = 78$  suggests that, among three pore types, through channels begin to dominate.

With an increase in  $T_{\text{ann}}$ , lamellae undergo ordering: the larger is the value of  $\lambda$ , the higher is the rate of decrease in the degree of ordering the lamellae  $\phi$  which approaches zero at  $T_{\text{ann}} \rightarrow T_m$ . The transition from a less ordered cluster of the solid phase to a more ordered cluster is associated with the convergence of the values of the periods  $L_{\text{p||}}$  and  $L_{\text{p||}}$  and with the formation of a superlattice of lamellae. Similar self-organization of particles in membranes occurs with an increase in the parameter  $\lambda$  at a fixed temperature  $T_{\text{ann}}$ .

The effect of the annealing temperature  $T_{\text{ann}}$  on the degree of ordering the lamellae  $\phi$  in the membranes is illustrated in Figure 7 (curve 2). In the range  $T_{\text{ann}} < 439\text{--}440$  K with an increase in  $T_{\text{ann}}$ , lamellae undergo ordering. In this case, the larger is the value of  $\lambda$ , the higher is the rate of decrease in the parameter  $\phi$ . In the temperature range

$T_{\text{ann}} > 440$  K the parameter  $\varphi$  is calculated for aggregates of lamellae. The permeability  $G$  of the membranes prepared at the parameter  $\lambda = 78$  increases to infinity with an increase in the annealing temperature  $T_{\text{ann}}$  (Figure 7, curve 1). This behavior of the dependence  $G(T_{\text{ann}})$  is explained by the fact that, in the range  $T_{\text{ann}} < 440$  K, the permeability increases as a result of the increase in the degree of ordering of the particle lattice (with a decrease in  $\varphi$ ) at a constant pore size  $d$ , whereas at  $T_{\text{ann}} > 440$  K, it increases due to the increase in the pore size  $d$  when  $\varphi \approx \text{const}$ .

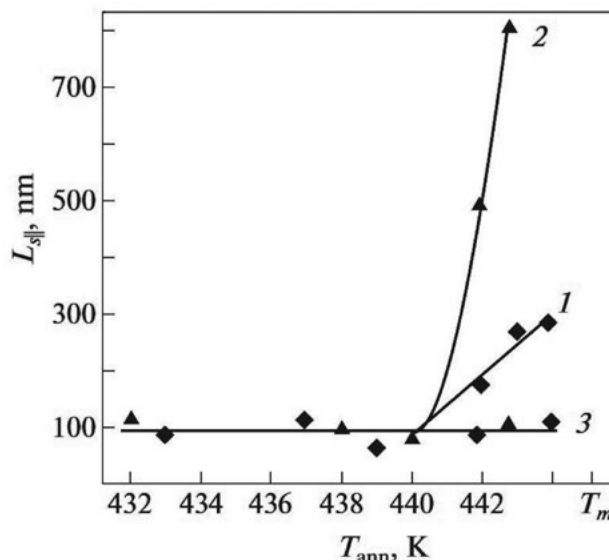


**Figure 7.** The dependences of the ratio  $G/G_{\text{max}}$  for the permeability of porous films (1) and the parameter  $\varphi$  (2) on the temperature  $T_{\text{ann}}$ .

The statistical analysis of SEM images of PP porous films prepared at  $\lambda = 44$  and 78 shows that the films surfaces exhibit polymorphism represented by two regions with different topologies: regularly arranged particles similar to those ones in the films annealed at  $T_{\text{ann}} < 442$  K, and the regions characterized by larger supermolecular structure formed at  $T_{\text{ann}} > 442$  K whose size increases with  $T_{\text{ann}}$ . The transformation of the film surface microrelief from the first type to the second one of regions manifests itself as a sharp increase in the period  $L_{\text{sl}}$  of alternation of the density of the solid phase cluster (Figure 8).

The increase of  $L_{\text{sl}}$  in the films annealed at  $T_{\text{ann}} = 442$ –444 K is associated with the formation of stacks of lamellae constituting the framework of the solid phase percolation cluster.<sup>16</sup> The aggregation of lamellae leads to the separation of the curves  $L_{\text{sl}}(T_{\text{ann}})$  at the point of bifurcation at a temperatures  $T_{\text{ann}} > 440$  K into two branches: for the individual lamellae (curve 3) and for the aggregates of lamellae. It should be noted that the alternation of the solid phase density  $L_{\text{sl}}$  for the individual lamellae, within the error of calculation, does not depend on  $T_{\text{ann}}$  and  $\lambda$ .

Thus, two self-assembly mechanisms with increasing  $T_{\text{ann}}$  were detected: the gradual and bifurcation ones; the latter is characterized by a higher cooperativity of the



**Figure 8.** The dependences of period  $L_{\text{sl}}$  in PP porous films on the annealing temperature  $T_{\text{ann}}$  for the aggregates of lamellae at  $\lambda = 44$  (1), and  $\lambda = 78$  (2), and for the individual lamellae (3).

lamella ordering process. The choice of this or that mechanism by the system depends on the melt spin draw ratio  $\lambda$  during extrusion.

### 3. 3. The Uniaxial Extension Stage

The self-organization of elements forming the the film surface relief, which is similar to the lamellar structure of the polymer, occurs at the stage of uniaxial extension of the films (pore formation). It should be noted that uniaxial extension of the annealed PE and PP films leads to the formation of pores even at small degrees of deformation  $\varepsilon$ , immediately from the beginning of the extension process that may be observed visually in the change of transparent annealed films to opaque milk-white microporous material because of the light scattering on the walls of pores.<sup>22</sup>

Uniaxial extension of the polyolefin samples along the direction of extrusion initiates an ordering process of particles of the solid phase – crystalline lamellae – and the ties connecting them. The self-organization of solid phase particles is accompanied by the increase in anisotropy of mechanical properties of the samples, change in their texture from biaxial to axial, an increasing in the degree of homogeneity of the spatial structure and a significant growth in the permeability, which reaches a value of 250 l/(m<sup>2</sup> h atm) that is characteristic for the membranes with a regular 3D lattice lamellae<sup>2,5,17</sup>.

## 4. Conclusion

The transformations of supermolecular organization in the process of porous structure formation under study

have been analyzed using statistical treatment of the SEM images of the PE and PP films surfaces at variations of their orientation degree. The porous structure of these films is originated at uniaxial extension stage following the extrusion and annealing. Basic characteristics of the porous structure – permeability and overall porosity – are significantly affected by both the degree of orientation  $\lambda$  of the polymer melt at extrusion stage and also the annealing temperature  $T_{\text{ann}}$  of the extruded films. The dependences of permeability on  $T_{\text{ann}}$  and  $\lambda$  are characterized by the percolation threshold for the appearance of through flow channels. At uniaxial extension the permeability increases with degree of extension due to increasing of number and sizes of through pores. This growth is accompanied by a rising of the ordering degree of the structure elements – self-organization and the formation of the superlattice of crystalline lamellae. The sample structure is transformed from biaxial topology of the random network of pores to uniaxial one of the oriented through channels. The self-organization of porous phase is the result of formation the regular spatial lamellar 3D lattice at the pore formation stage. This transformation may be considered as the disorder-order transition which leads to the ordering of the multilevel supermolecular structure of the film.

## 5. Acknowledgments

This study was supported by Joint Research Projects of the Russian Academy of Sciences and the Faculty for Natural Sciences and Engineering, University of Ljubljana (Slovenia), BI-RU/14-15-037 and BI-RU/16-18-017.

## 6. References

1. J. Kim, S. S. Kim, M. Park, M. Jang, *J. Membr. Sci.* **2008**, *318*, 201–209. DOI:10.1016/j.memsci.2008.02.050
2. G. K. Elyashevich, E. Yu. Rozova, E. A. Karpov, RF Patent Number 2,140,936, date of patent April 15, **1997**.
3. J. Loboda-Cackovic, H. Cackovic, R. Hosemann, *Macromol. Sci. Part B. Phys.* **1979**, *16*, 127–144. DOI:10.1080/00222347908212286
4. I. K. Park, H. D. Noether, *Colloid Polym. Sci.* **1975**, *253*, 824–839. DOI:10.1007/BF01452402
5. G. K. Elyashevich, I. S. Kuryndin, V. K. Lavrentyev, A. Yu. Bobrovskii, V. Bukošek, *Phys. Solid State* **2012**, *54*, 1907–1916. DOI:10.1134/S1063783412090090
6. A. V. Yefimov, V. P. Lapshin, V. I. Fartunin, P. V. Kozlov, N. F. Bakeyev, *Polymer Science* **1983**, *25*, 692–700.
7. E. A. Karpov, V. K. Lavrentyev, E. Yu. Rozova, G. K. Elyashevich, *Polymer Science* **1995**, *A.37*, 1247–1253.
8. R. E. Kesting. Synthetic polymer membranes. A structural perspective. 2nd Edn., John Wiley & Sons, New York- Chichester, **1985**.
9. M. Mulder. Basic Principles of Membrane Technology, Kluwer Acad. Publ., Dordrecht, **1991**.
10. S.Y. Lee, S.Y. Park, H.S. Song, *Polymer* **2006**, *47*, 3540–3547. DOI:10.1016/j.polymer.2006.03.070
11. S. S. Zhang, *J. Power Sources* **2007**, *295*, 351–364. DOI:10.1016/j.jpowsour.2006.10.065
12. I. Novák, G. K. Elyashevich, I. Chodák, A. S. Olifirenko, M. Števiar, M. Špírková, N. N. Saprykina, E. N. Vlasova, A. Klei-nová, *Eur. Polym. J.* **2008**, *44*, 2702–2707. DOI:10.1016/j.eurpolymj.2008.05.015
13. A. Bobrovskii, V. Shibaev, G. Elyashevich, E. Rosova, A. Shimkin, V. Shirinyan, A. Bubnov, M. Kaspar, V. Hamplova, M. Glogarova, *Liq. Cryst.* **2008**, *35*, 533–539. DOI:10.1080/02678290802015697
14. G. K. Elyashevich, A. G. Kozlov, E. Yu. Rozova, *Polymer Science, Ser. A.* **1998**, *40*, 567–573.
15. D. Stauffer, A. Aharony, Introduction to percolation theory, Taylor and Francis, London, **1994**.
16. D. V. Novikov, V. K. Lavrentyev, G. K. Elyashevich, V. Bukošek, *Phys. Solid State* **2012**, *54*, 1903–1906. DOI:10.1134/S1063783412090223
17. I. S. Kuryndin, V. K. Lavrentyev, V. Bukošek, G. K. Elyashevich, *Polymer Sci.* **2015**, *A57*, 717–722.
18. A. Bobrovskii, V. Shibaev, G. Elyashevich, E. Rosova, A. Shimkin, V. Shirinyan, K.-L. Cheng, *Polym. Adv. Technol.* **2010**, *21*, 100–112.
19. J. M. Ziman, Models of Disorder, Cambridge University Press, London, **1979**.
20. M. Raab, J. Šcudla, A. G. Kozlov, V. K. Lavrentyev, G. K. Elyashevich, *J. Appl. Polym. Sci.* **2001**, *80*, 214–222.
21. G. K. Elyashevich, I. S. Kuryndin, E. Yu. Rosova, *Polym. Adv. Technol.* **2002**, *13*, 725–736. DOI:10.1002/pat.251
22. A. A. Zinchik, I. S. Kuryndin, K. V. Ezhova, G. K. Elyashevich, *Proc. SPIE* **2016**, 9890, 989016 (1–7). DOI:10.1117/12.2227776.

## Povzetek

Na mikroporoznih poliolefinskih (polietilenskih in polipropilenskih) filmih, pripravljenih v postopku ekstruzije iz taline polimera, čemur je sledilo žarjenje, enoosno raztezanje ter toplotno stabiliziranje, so bili s statistično analizo slik elektronske mikroskopije površja filmov, raziskani strukturni prehodi in mehanizem nastajanja super-rešetk lamel. Strukturo poroznih filmov, pripravljenih v večstopenjskem postopku, smo preučevali z meritvami SEM, gravimetrije in prepustnosti. Pokazano je bilo, da nastajanje por v fazi enoosnega raztezanja spremlja urejanje lamel, njihovo samoorganizacijo nadzira predilno raztezno razmerje ter temperatura žarjenja. Ugotovljeno je bilo, da povečanje teh pokazateljev vodi do prehoda vrste nered – red. Podana je razprava o vplivu pogojev priprave na postopek urejanja pravilne prostorske rešetke lamel.

Scientific paper

# Microwave-assisted One-pot Efficient Synthesis of Functionalized 2-Oxo-2-phenylethylidenes-linked 2-Oxobenzo[1,4]oxazines and 2-Oxoquino[1,4]oxalines: Synthetic Applications, Antioxidant Activity, SAR and Cytotoxic Studies

Vashundhra Sharma,<sup>1,‡</sup> Pradeep K. Jaiswal,<sup>1,‡</sup> Dharmendra K. Yadav,<sup>2,3</sup>  
Mukesh Saran,<sup>4</sup> Jaroslav Prikhodko,<sup>5</sup> Manas Mathur,<sup>4</sup> Ajit K. Swami,<sup>4</sup>  
Irina V. Mashevskaya<sup>5</sup> and Sandeep Chaudhary<sup>1,6,\*</sup>

<sup>1</sup> Department of Chemistry, Malaviya National Institute of Technology, Jawaharlal Nehru Marg, Jaipur-302017, India.

<sup>2</sup> Department of Biochemistry, All India Institute of Medical Sciences (AIIMS), Jodhpur, Rajasthan-342005, India.

<sup>3</sup> College of Pharmacy, Gachon University of Medicine and Science, Room # 502, Hambakmoero 191, Yeonsu-gu, Incheon city, 406-799, Korea.

<sup>4</sup> Department of Advance Molecular Microbiology, Seminal Applied Sciences Pvt. Ltd. Jaipur-302015, India.

<sup>5</sup> Department of Organic Chemistry, Faculty of Chemistry, Perm State University, 15 Bukireva, Perm 614990, Russian Federation.

<sup>6</sup> Materials Research Centre, Malaviya National Institute of Technology, Jawaharlal Nehru Marg, Jaipur-302017, India.

\* Corresponding author: E-mail: E-mail: schaudhary.chy@mnit.ac.in  
Fax: 911412529029; Tel: 911412713319;

‡Both authors have equal contribution.

Received: 21-07-2017

## Abstract

A microwave-assisted, environmentally benign green protocol for the synthesis of functionalized (*Z*)-3-(2-oxo-2-phenylethylidene)-3, 4-dihydro-2*H*-benzo[*b*][1,4]oxazin-2-ones (**11a–n**) in excellent yields (upto 97%) and (*Z*)-3-(2-oxo-2-phenylethylidene)-3,4-dihydroquinoxalin-2(1*H*)-ones (**14a–h**) (upto 96% yield) are reported. The practical applicability of developed methodology were also confirmed by the gram scale synthesis of **11a**, **14c** and **14e**; synthesis of anticancer alkaloid Cephalandole A **16** (89% yield). All the synthesized compounds **11a–n**, **14a–h** and **16** were assessed for their *in vitro* antioxidant activities in DPPH radical scavenging and FRAP assay. In DPPH assay, compounds **11a**, **14c** and **14e**, the most active compounds of the series, were found to show IC<sub>50</sub> value of 10.20 ± 0.08 µg/mL, 9.89 ± 0.15 µg/mL and 8.97 ± 0.13 µg/mL, respectively in comparison with standard reference (ascorbic acid, IC<sub>50</sub> = 4.57 µg/mL). Whereas, in FRAP antioxidant assay seven compounds (**11c**, **11e**, **11i**, **11k**, **11l**, **14d** and **14h**) displayed higher antioxidant activity in comparison to the reference standard BHT (C<sub>0.5</sub>FRAP = 546.2 µM). Moreover, the cytotoxic studies of the compounds **11a**, **14c**, **14e** and **14h** were found to be non-toxic in nature in 3T<sub>3</sub> fibroblast cell lines using MTT assay.

**Keywords:** Benzo[1,4]oxazines; 2-oxobenzo[1,4]oxazines; 2-oxoquino[1,4]oxalines; Antioxidant; Microwave-Assisted Organic Synthesis (MAOS); DPPH; FRAP; Structure-Activity Relationship.

## 1. Introduction

Benzo[1,4]oxazines 1-8, a sub-class of benzo fused heterocycles, are endowed with a wide range of biological activities such as anti-inflammatory,<sup>1</sup> analgesic,<sup>2</sup> antibacterial,<sup>3</sup> neuroprotective,<sup>4</sup> D2 receptor antagonists,<sup>5</sup> antimycobacterial,<sup>6,7</sup> antihypertensive,<sup>8</sup> antifungal,<sup>9</sup> herbicidal,<sup>10</sup> antiarrhythmic,<sup>11</sup> thrombin inhibitor and fibrinogen receptor antagonists,<sup>12</sup> 5-HT receptor antagonists,<sup>13</sup> potent inhibitor of tumor-driven angiogenesis<sup>14a</sup> and selective non-steroidal mineralocorticoid receptor

antagonists<sup>14b</sup> etc. Some marine secondary metabolites such as, Arcticoside 5a (potent antifungal agent) and C-1027 chromophore- III & V 5b (potent antitumor antibiotic),<sup>15</sup> which were isolated from a culture of an arctic marine actinomycete *Streptomyces strain*; possess as benzo[1,4]oxazines substructures in their active scaffolds (figure 1).

Owing to the several biological activities having benzo[1,4]oxazines moieties in their scaffold or in whole molecule, several syntheses of benzo[1,4]oxazines, 2-oxo-

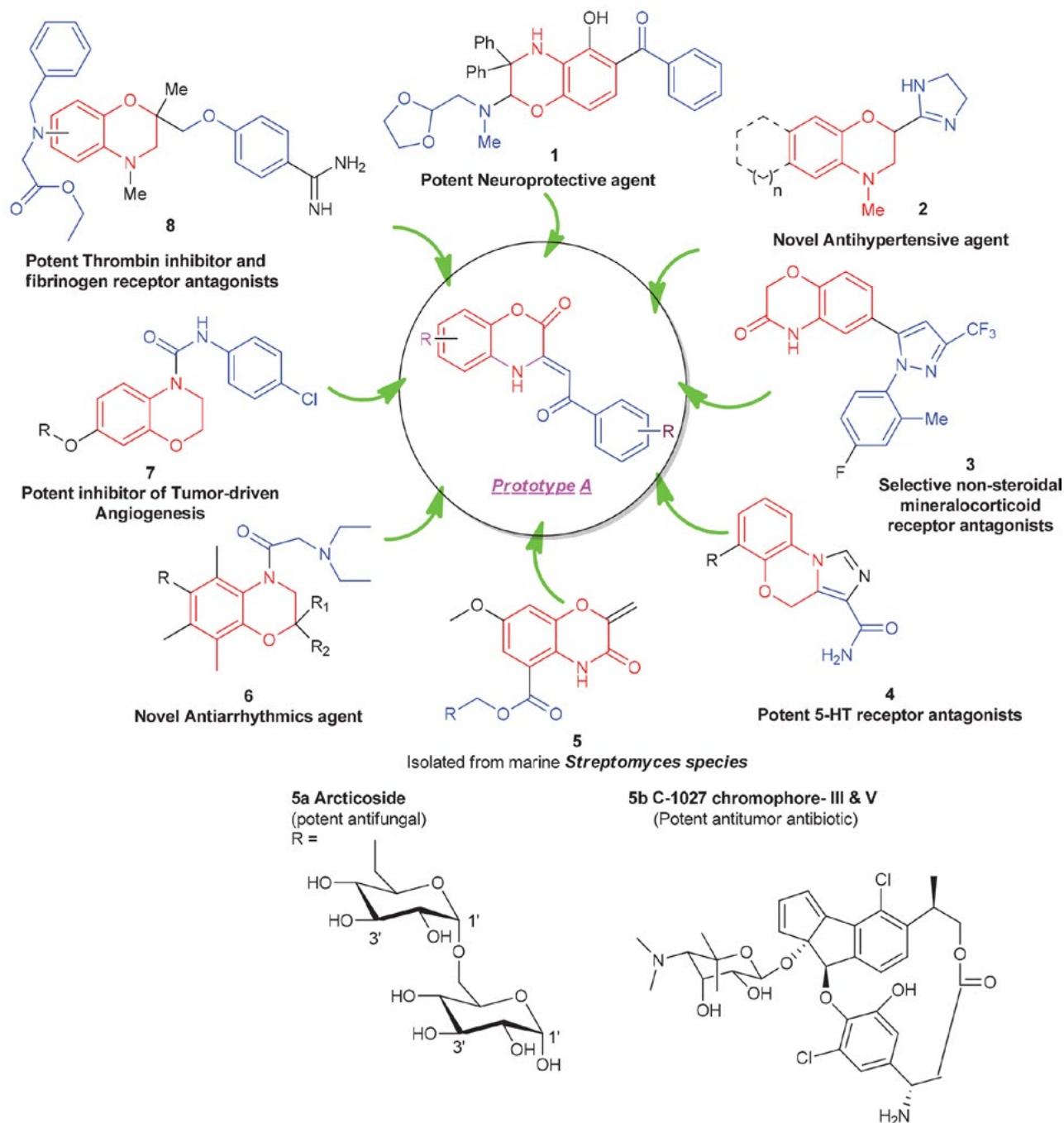


Figure 1. Structures of biologically active benzo[1,4]oxazines 1-8.

benzo[1,4] oxazines and its related structural motifs have been reported in the literature using metal as well as metal-free catalyst.<sup>16–18</sup> Earlier, Kikelj et al. reported the first synthesis of 3-unsubstituted 3,4-dihydro-1,4-benzoxazin-2-ones *via* catalytic hydrogenation of 4-benzyl-3,4-dihydro-1,4-benzoxazin-2-one.<sup>16a</sup> Since then, several metal-catalysed synthesis of substituted benzo[1,4]oxazines have been reported in the literature<sup>16b–d</sup> [figure 2; entry i–iii]. 2-aminophenols or substituted 2-nitrophenols<sup>16f</sup> or 2-halophenols,<sup>16g–j</sup> were most commonly used as starting materials towards the synthesis of benzo[1,4]oxazine derivatives. With 2-aminophenols as the starting substrate, various protection and deprotection steps are required.<sup>16k–l</sup> Xia et al. (2008) reported sulphamic acid as an efficient catalyst for the synthesis of benzo[1,4]oxazines derivatives in one pot reaction condition providing good yield.<sup>16e</sup> In spite of this efficient methodology, sulphamic acid is associated with several drawbacks with respect to its hazardous nature towards animals as well as environment, such as the high toxicity of sulphamic acid in animals ( $LD_{50} = 1312$  mg/kg in mouse via oral route;  $LD_{50} = 3160$  mg/kg in rat via oral route; toxicity value of  $LC_{50} = 70.3$  mg/l in fish *Pimephales promelas* species); acute oral and inhalation toxicity to human etc. Its disposal also induces toxicity to the environment.<sup>16f</sup> Thus, none of the reported methodologies were environmentally benign as these were associated with several drawbacks such as the

use of toxic catalysts, toxic starting materials, hazardous organic solvents, multistep and complicated reaction assembly, limited number of appropriate substrates for diverse synthesis, tedious workup and low yields etc.<sup>19–21</sup> Therefore, an efficient, environmentally benign and more green approach for the synthesis of benzo[1,4]oxazines is still a challenging area of research.

Moreover, it has also been observed that several chalcones and its analogues,<sup>22a–c</sup> quinolines,<sup>22d–f</sup> and coumarin-derived scaffolds,<sup>22g,h</sup> which have 2-oxobenzo[1,4]oxazine-like substructure in their scaffold, were found to be potent antioxidants under several *in vitro* antioxidant assays. So, in our endeavour to search for new class of potent antioxidants we have developed inclinations towards 2-oxo-benzo[1,4]oxazine based analogues (prototype A: figure 1), because it has almost similar substructure as present in coumarins, chalcones and quinolone or its analogues. In this context, we were interested to explore the green synthesis and antioxidant activity of non-naturally occurring 2-oxobenzo[1,4]oxazines derived analogues, because to the best of our knowledge the antioxidant activity of 2-oxobenzo[1,4]oxazine class of molecules have never been studied earlier.

During the past few decades, Microwave-Assisted Organic Synthesis (MAOS) has been identified as an efficient green protocol for accelerating drug discovery process.<sup>23a–d</sup> Moreover, it is well documented that Mi-

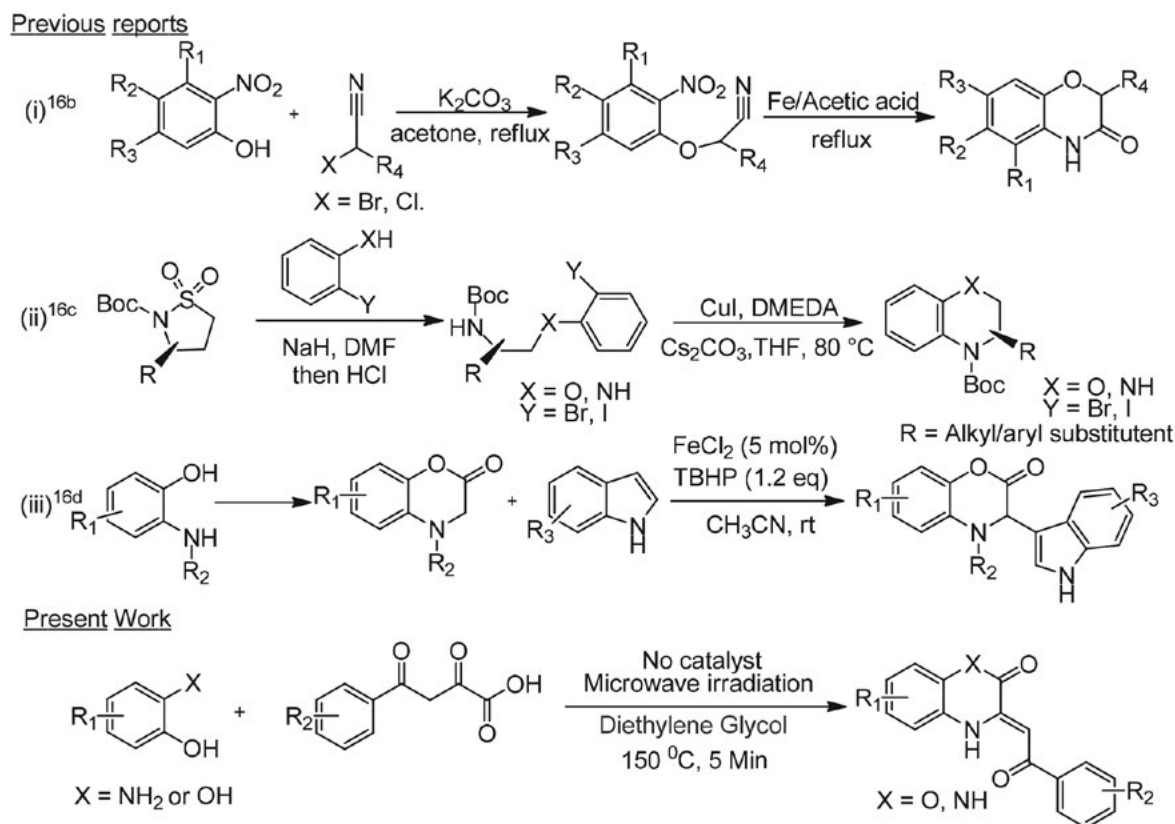


Figure 2. Previous and present reports for the synthesis of substituted benzo[1,4]oxazine derivatives.



crowave irradiation (MW) is a form of electromagnetic energy having lower frequency (300–300000 MHz) and it has several advantages over conventional heating conditions such as: reduction of the reaction times as well as decrease side reactions, increase yields of desired products and improve reproducibility. Therefore, industrial as well as academic research groups are frequently using MAOS for rapid reaction optimization, accelerating the efficient synthesis of new chemical entities and also for the novel methodology development.<sup>23e–g</sup> Hence, utilizing this concept; herein, we report a very simple, mild and highly efficient green protocol for the synthesis of highly functionalized 2-oxobenzo[1,4]oxazines **11a–n** (upto 97% yield) and 2-oxoquino[1,4]oxalines **14a–h** (upto 96% yield) under microwave irradiations using readily available starting materials. The main advantage of this protocol is the avoidance of any toxic reagent, solvent or catalyst. Although, compounds **11a–i** and **14a–h** are already reported in the literature, but they were prepared by other routes,<sup>17</sup> and their antioxidant activities have never been evaluated till now. Therefore, for the first time, we have evaluated the *in vitro* antioxidant activities of all the synthesized compounds **11a–n**, **14a–h** and **16** in DPPH radical scavenging assay using ascorbic acid ( $IC_{50} = 4.57 \mu\text{g/mL}$ ) as standard reference and ferric reducing antioxidant power (FRAP) assay taking BHT ( $546.0 \pm 13.6 \mu\text{M}$ ) as standard reference.

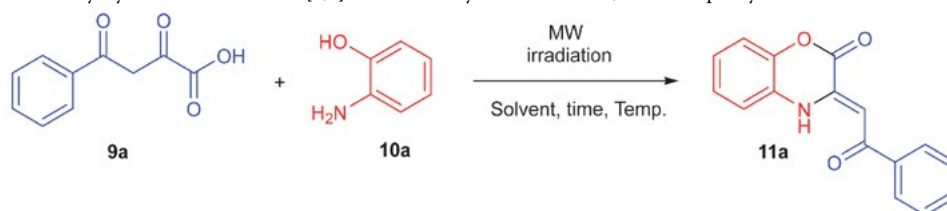
To the best of our knowledge, this is the first report of microwave-assisted synthesis and *in vitro* antioxidant activities of functionalized 2-oxobenzo[1,4]oxazines **11a–n**, 2-oxoquino[1,4]oxalines **14a–h** and **16** in excellent yields having high level of functional group compatibility.

## 2. Results and Discussion

We started our initial investigation towards the development of an environmentally benign, sustainable protocol for the synthesis of 2-oxobenzo[1,4]oxazine with a typical model reaction between 2,4-dioxo-4-phenylbutanoic acid **9a** and 2-aminophenol **10a** in isopropanol (1.0 mL) under nitrogen atmosphere at room temperature for 3 h which furnished the condensation product **11a** in only 18% yield (entry 1, Table 1). Carrying out the above reaction at 90 °C for 3 h afforded **11a** in better yield [(45%), entry 2, Table 1, Method 1]. The product obtained was fully characterized by its spectroscopic data (<sup>1</sup>H and <sup>13</sup>C NMR, HRMS and IR).

Since we observed an increase in the yield of **11a** as we change solvent from isopropanol to DMF and conventional to MW irradiation condition; we switched over to more polar DMSO solvent. Thus, the above reaction was carried out in DMSO solvent, at 150 °C for 10 min under microwave irradiation, which furnished **11a** in 77% yield (entry 7, Table 1, Method B). Decreasing or increasing the

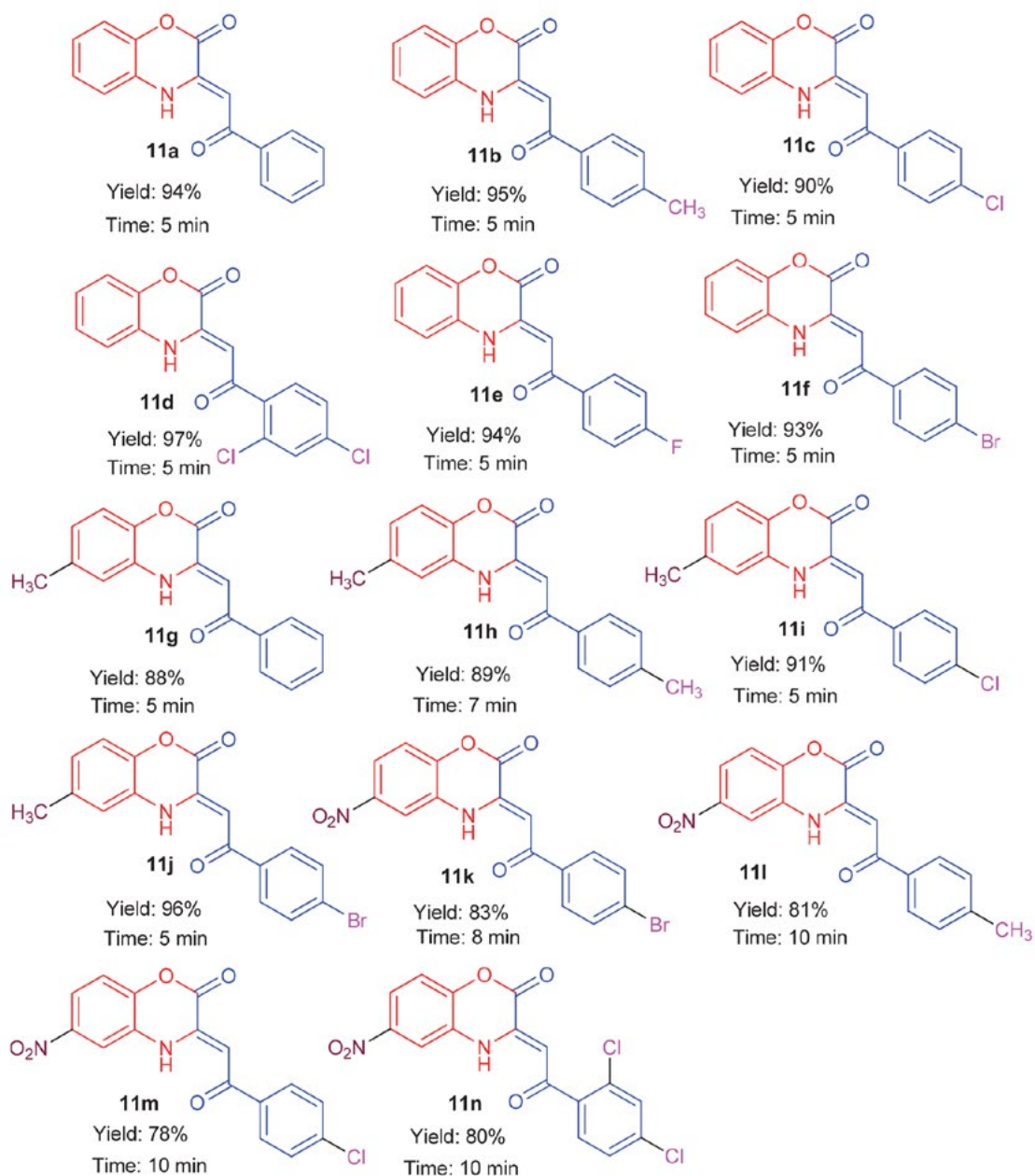
**Table 1.** Optimization study: Synthesis of 2-oxobenzo[1,4]oxazines **11a** by the reaction of 2,4-dioxo-4-phenylbutanoic acid **9a** and 2-aminophenol **10a**.<sup>a</sup>



Entry	Solvent	Temp (°C)	Method A <sup>b</sup>		Method B <sup>c</sup>	
			Time (min)	Yield (%) <sup>d</sup>	Time (min)	Yield (%) <sup>d</sup>
1	Isopropanol	rt	180	18	–	–
2	Isopropanol	90	180	45	10	52
3	Isopropanol	90	300	55	30	58
4	DMF	90	180	51	30	64
5	DMF	120	180	58	20	62
6	DMF	150	120	50	15	69
7	DMSO	150	180	59	10	77
8	DMSO	150	240	61	5	51
9	DMSO	150	300	67	15	72
10	DMSO	180	120	65	2	56
11	<b>Diethylene glycol</b>	<b>150</b>	180	61	<b>5</b>	<b>94</b>
12	Diethylene glycol	150	120	54	3	80
13	Diethylene glycol	150	300	67	7	93
14	Diethylene glycol	170	180	64	2	85
15	Diethylene glycol	160	180	65	2	82
16	Diethylene glycol	170	300	63	5	81

<sup>a</sup> Reaction conditions: **9a** (0.1 mmol), **10a** (0.1 mmol) in solvent (1.0 mL), 5–300 min, N<sub>2</sub> atmosphere. <sup>b</sup> Method A: Conventional heating;

<sup>c</sup> Method B: Microwave Irradiation; <sup>d</sup> Isolated yield after recrystallization/column chromatography.



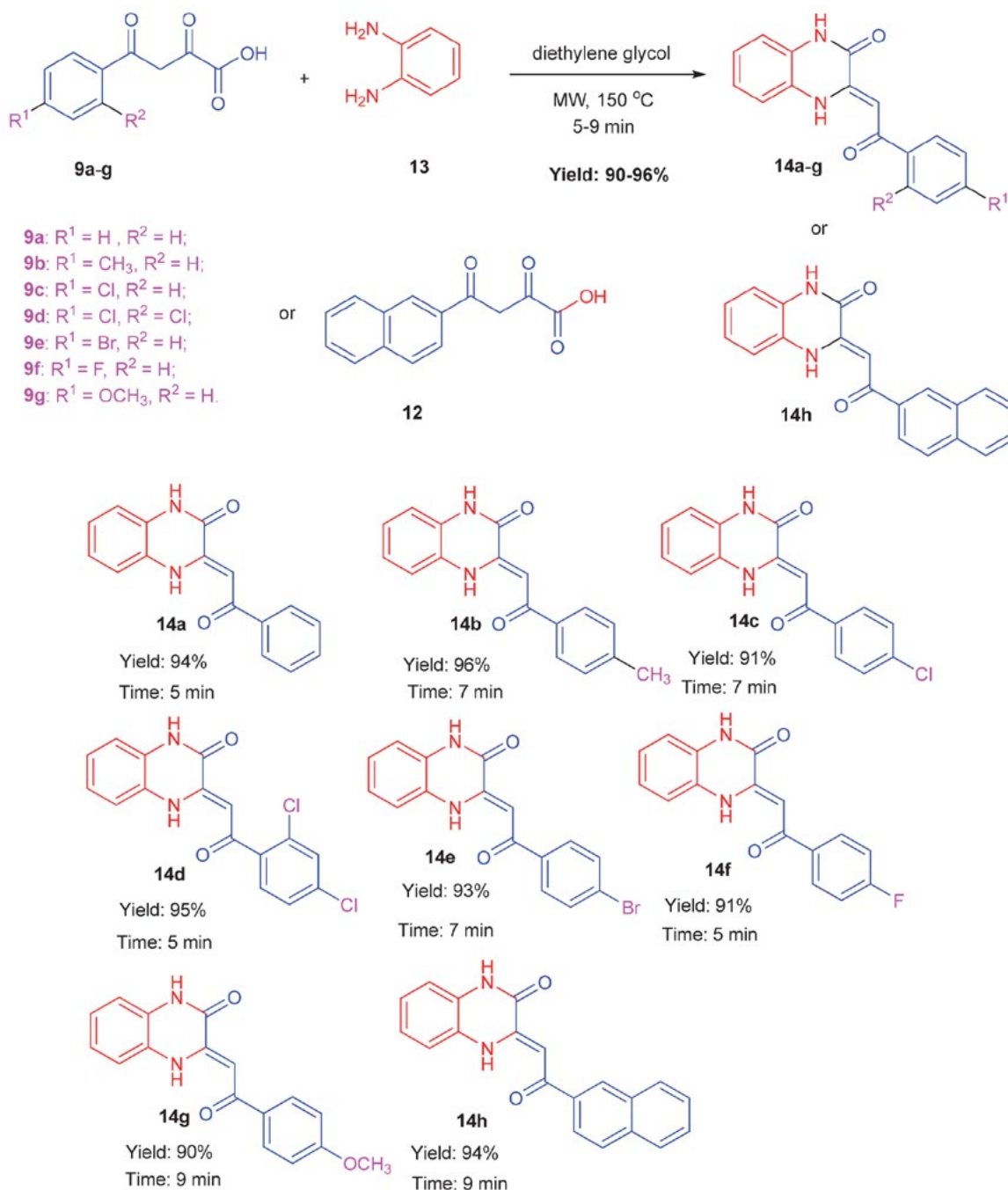
<sup>a</sup> unless otherwise mentioned, all the reactions were carried out with substrates **9a-f** (0.2 mmol), substituted 2-aminophenols **10a-c** (0.2 mmol) in diethylene glycol (2.0 mL) at 150 °C under microwave irradiation. <sup>b</sup> Isolated yield.

**Scheme 1.** Microwave-assisted one-pot green synthesis of 2-oxobenzo[1,4]oxazine analogues (**11a-n**).<sup>a,b</sup>

time for the above reaction in DMSO solvent was not found to be fruitful. (Entries 8–10, Table 1). Then, we planned to perform our model reaction in more polar diethylene glycol as solvent. To our surprise, after 5 min at 150 °C, we obtained **11a** in 94% yield (entry 11, Table 1). Furthermore, in spite of increasing the reaction temperature from 150 °C to 170 °C or increasing/ decreasing the reaction time; we were successful in obtaining **11a** in the yield range of 81–93%

(entries 12–16, Table 1). Finally, based on above screening studies, diethylene glycol as solvent, 150 °C temperature for 5 min was found to be the best optimized reaction condition under microwave irradiations (entry 11, Table 1).

After optimization study, we further investigated the scope and generality of this reaction. Several alkyl/alkoxy/halide/nitro-substituted 2,4-dioxo-4-phenylbutanoic acids **9a–f** were reacted with alkyl/halide/nitro-substitut-



<sup>a</sup> Unless otherwise mentioned, all reactions were carried out with substrates **9a–g** or **12** (0.2 mmol) and 1,2-diamino benzene **13** (0.2 mmol) in diethylene glycol (2.0 mL) at 150 °C under microwave irradiation. <sup>b</sup> Isolated yield.

**Scheme 2.** Microwave-assisted one-pot synthesis of functionalized 2-oxoquino[1,4]oxalines **14a–h**.<sup>a</sup>

ed 2-aminophenol **10a–c** in diethylene glycol under our optimized conditions (Scheme 1). The desired 2-oxobenzo[1,4]oxazines **11a–n** were purified either by flash column chromatography method or by recrystallization (see experimental section).

As evident from scheme 1; substituted 2, 4-dioxo-4-phenylbutanoic acid **9a–f** reacted smoothly with substituted 2-aminophenol **10a–c**, and furnished substituted 2-oxobenzo[1,4]oxazines **11a–n** in 78–97% yield range. It has been observed that nitro-based 2-oxobenzo[1,4]oxazines **11k–n** were obtained in comparatively lesser yields (78–83%) with rest of the compounds **11a–j**. This is due to poor solubility of nitro-based 2-oxobenzo[1,4]oxazines **11k–n** in ethyl acetate which makes the purification of these compounds via column chromatography very tedious and cumbersome. In this study, the most characteristic feature observed was that a broad range of functional groups, like Cl, Br, OMe and NO<sub>2</sub> are well compatible under our optimized reaction conditions. Thus, these groups can further be manipulated to obtain new therapeutic molecules.

After successful implementation of our methodology on **11a–n** series; we extended its synthetic application towards the synthesis of its congener class of bioactive heterocycles i.e. 2-oxoquino[1,4]oxalines **14a–h**; which were synthesized from **9a–g** with phenyl-1,2-diamine **13** using our optimised methodology in the excellent yield (90–96%), as depicted in Scheme 2.

Furthermore, the practicality of this methodology was demonstrated via gram scale synthesis of compounds **11a**, **14c** and **14e**. Thus, the reaction of **9a** (2.00 g, 10.40 mmol), **9c** (2.26 g, 10.00 mmol) or **9e** (2.71 g, 10.00 mmol) with either **10a** (1.13 g, 10.40 mmol) or **13** (1.08 g,

10.00 mmol) in diethylene glycol under MW irradiation at 150 °C for 7–9 min furnished the target compounds, **11a** (2.49 g, 90.41%); **14c** (2.60 g, 87.32%) and **14e** (3.09 g, 90.14%), respectively. (Scheme 3)

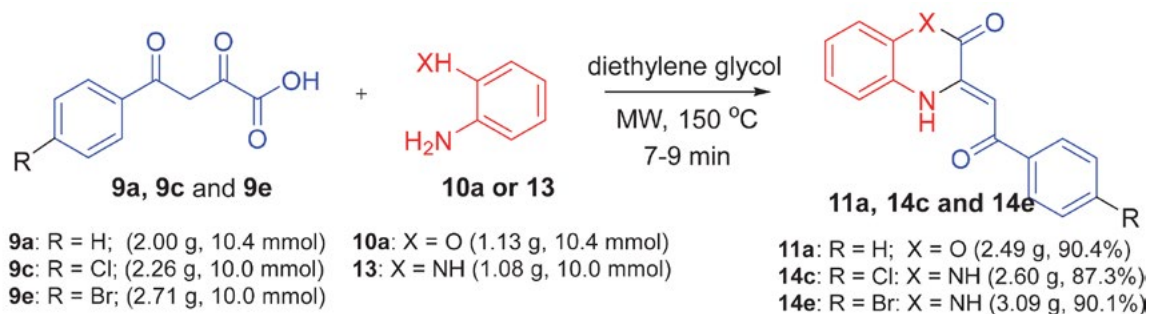
We have further demonstrated practicality of our developed methodology for the synthesis of anticancer indole alkaloid, Cephalandole A, which was isolated from Taiwanese orchid *Cephalanceropsis gracilis* (Orchidaceae). Its crude extract showed good activity against CNS (SF-268; IC<sub>50</sub> = 12.2 μM), breast (MCF-7; IC<sub>50</sub> = 7.57 μM) and lung (NCI-H460; IC<sub>50</sub> = 7.8 μM) carcinoma cell lines.<sup>24</sup> 3-indoleglyoxylic acid (**15**) on reaction with aminophenol (**10a**) in diethylene glycol under MW at 150 °C for 10 min furnished indole alkaloid Cephalandole A (**16**) in 89% yield (Scheme 4). The spectral data was found to be the same as the literature data.

## 2. 1. Material and Methods for Antioxidant Activity

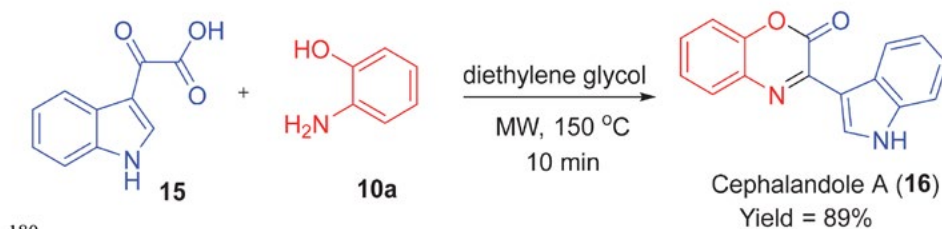
### 2. 1. 1. *In vitro* antioxidant DPPH radical scavenging activity<sup>24a–e</sup>

In DPPH radical scavenging method the synthesized compounds at different concentrations ranging from 10 to 100 μg mL<sup>-1</sup> was mixed with 1.5 mL of a DPPH methanolic solution (20 mg L<sup>-1</sup>). Pure methanol was taken as control and ascorbic acid (vitamin C) was used as a reference compound. The percent of DPPH decoloration of the sample was calculated according to the formula.

$$\text{Decoloration \%} = [1 - (\text{Abs sample} / \text{Abs control})] \times 100$$



Scheme 3. Gram scale synthesis of **11a**, **14c** and **14e**.



Scheme 4. Synthesis of Cephalandole A (**16**)

The decoloration was plotted against the sample concentration and a logarithmic regression curve was established in order to calculate the  $IC_{50}$ . The results are expressed as antiradical efficiency (AE), which is 1000-fold inverse of the  $IC_{50}$  value  $AE = 1000 / IC_{50}$ .

### 2. 1. 2. *In vitro* Ferric Reducing Antioxidant Power (FRAP) Assay<sup>24f</sup>

The FRAP reagent was prepared by mixing freshly prepared 10.0 mM of ferric-tripyridyltriazine (TPTZ) solution, 20.0 mM  $FeCl_3 \times 6H_2O$  solution and 300 mM sodium acetate buffer (pH 3.6) in a ratio of 1:1:10 (v/v/v). Sample was added to 3 mL of FRAP reagent and this reaction mixture was incubated for 30 min at 37 °C temperature. The absorbance of prepared reaction mixture was measured at 593 nm. A freshly prepared solution of  $FeSO_4$  was used for calibration of standard curve. The FRAP antioxidant capacities were expressed in terms of  $C_{0.5FRAP}$  (the concentration of samples with respect to the antioxidant ability equivalent to that of  $FeSO_4$  at 0.5 mmol/L).

### 2. 2. Antioxidant Activity: *In vitro* antioxidant DPPH Radical Scavenging Assay, FRAP Assay and Structure-activity Relationship<sup>25</sup>

The DPPH radical scavenging assay is generally utilised for the screening of antioxidant activity of diverse heterocycles.<sup>25a</sup> DPPH is a stable free radical, which can easily accept an electron or a hydrogen radical to become a stable molecule. Literature reports illustrate that DPPH assay works in two ways; a single electron transfer (SET) or a hydrogen atom transfer (HAT) mechanism.<sup>25b</sup> DPPH in the methanolic medium has odd electron configuration which shows a strong absorption band at 515 nm and the absorbance decreases in the presence of free radical scavengers which results in the colour change from deep purple to yellow.<sup>25c-d</sup> The radical quenching ability strongly depends on the structural accessibility of the radical trapping site. The electron density as well as steric hindrance plays a vital role in the antioxidant activity because they may prevent the test molecule from reaching to the DPPH radical site and thus results in lower activity.<sup>25e</sup>

**Table 2.** Antioxidant activity of synthesized compounds **11a–n**, **14a–h** and **16** by DPPH radical scavenging and FRAP assay.<sup>25</sup>

S. No.	Compound No.	Antioxidant activity <sup>a</sup>	
		DPPH assay ( $IC_{50}$ ) ( $\mu$ g/mL)	FRAP assay ( $C_{0.5FRAP}$ ) ( $\mu$ M)
1	<b>11a</b>	10.20 $\pm$ 0.08	611.5 $\pm$ 23.2
2	<b>11b</b>	19.70 $\pm$ 0.31	763.2 $\pm$ 38.1
3	<b>11c</b>	29.80 $\pm$ 0.17	306.8 $\pm$ 25.8
4	<b>11d</b>	65.32 $\pm$ 0.97	>1000
5	<b>11e</b>	25.02 $\pm$ 0.21	421.7 $\pm$ 37.9
6	<b>11f</b>	23.45 $\pm$ 0.14	845.9 $\pm$ 35.1
7	<b>11g</b>	67.40 $\pm$ 0.28	>1000
8	<b>11h</b>	78.50 $\pm$ 1.41	921.6 $\pm$ 29.6
9	<b>11i</b>	34.42 $\pm$ 0.62	291.7 $\pm$ 23.1
10	<b>11j</b>	42.98 $\pm$ 0.76	>1000
11	<b>11k</b>	21.27 $\pm$ 0.11	489.2 $\pm$ 18.5
12	<b>11l</b>	56.12 $\pm$ 1.03	348.8 $\pm$ 31.4
13	<b>11m</b>	15.70 $\pm$ 0.14	598.5 $\pm$ 23.4
14	<b>11n</b>	78.76 $\pm$ 1.43	>1000
15	<b>14a</b>	27.36 $\pm$ 0.44	638.4 $\pm$ 37.6
16	<b>14b</b>	91.36 $\pm$ 2.04	>1000
17	<b>14c</b>	9.89 $\pm$ 0.15	612.8 $\pm$ 17.8
18	<b>14d</b>	28.24 $\pm$ 0.46	498.4 $\pm$ 22.4
19	<b>14e</b>	8.97 $\pm$ 0.13	689.3 $\pm$ 30.0
20	<b>14f</b>	43.54 $\pm$ 0.88	592.7 $\pm$ 41.6
21	<b>14g</b>	38.97 $\pm$ 0.97	>1000
22	<b>14h</b>	14.27 $\pm$ 0.23	358.3 $\pm$ 17.7
23	<b>16</b>	11.87 $\pm$ 0.14	ND <sup>b</sup>
24	Ascorbic acid	4.57	–
25	BHT	–	546.0 $\pm$ 13.6

<sup>a</sup>Results are expressed as a mean  $\pm$  standard deviation ( $n = 3$ ). DPPH radical scavenging activities are expressed as  $IC_{50}$  concentrations of the compounds ( $\mu$ g/mL) required to inhibit 50 % of the radicals and the maximum inhibition values;

<sup>b</sup>ND means not done.

The FRAP assay was measured using the method as described by Benzie and Strain.<sup>25f</sup> This methodology demonstrates that the antioxidant molecule reacts to a complex of ferric tripyridyltriazine [Fe<sup>3+</sup>-TPTZ] and produces a colored ferrous tripyridyltriazine [Fe<sup>2+</sup>-TPTZ] complex. Generally, the reducing nature of antioxidant molecule is associated with their action by breaking the free radical chain via donating a hydrogen atom.

All the synthesized 2-oxobenzo[1,4]oxazines **11a–n**, 2-oxoquino[1,4]oxalines **14a–h** and Cephalandole A **16** were screened for their *in vitro* antioxidant activities using DPPH radical scavenging activity assay using ascorbic acid as standard reference as well as in FRAP assay using BHT as standard reference (Table 2).<sup>25,26</sup>

The *in vitro* antioxidant screening of compounds **11a–f**, having no substitution at benzoxazine aromatic ring; it had been observed that the compound **11a** was found to be the most active compound having IC<sub>50</sub> value of 10.20 ± 0.08 µg/mL (entry 1, Table 2) in comparison with standard reference ascorbic acid (IC<sub>50</sub> = 4.57 µg/mL). When mono-halo substituents were present at side chain of aromatic ring as in case of **11c**, **11e** and **11f** having –Cl, –F and –Br substituent respectively; these molecules exhibited slightly lesser antioxidant activity in comparison with **11a** (Table 2; entry 3, 5 and 6). Further, 2-oxobenzo[1,4]oxazine having di-halo substituents on side chain of aromatic ring (**11d**) exhibited decrease of antioxidant activity drastically (Table 2; entry 4) in comparison to mono-halo substituted analogues **11c**, **11e** and **11f**. In addition, electron-donating substituents at side chain of aromatic ring in compound **11b** showed better antioxidant activity in comparison to halo-substituted 2-oxobenzo[1,4]oxazine analogues **11c–11f**.

Moreover, in 2-oxobenzo[1,4]oxazines having –CH<sub>3</sub> or –NO<sub>2</sub> substituent at para-position of benzoxazine aromatic nucleus (**11g–11n**); the antioxidant activity was found to be lesser (Table 2; entry 7–14) in comparison with unsubstituted analogues **11a–11f**, except compound **11k** and **11m**; which exhibited better activity profile (Table 2; entry 11 and 13). Whereas, 2-oxobenzo[1,4]oxazine having di-chloro substituents at side chain of aromatic ring (Table 2; entry 14); **11n** was found to be the least active compound among 2-oxobenzo[1,4]oxazine series. Furthermore, the –CH<sub>3</sub> substituent at benzoxazine nucleus along with electron-donating methyl substituent or halo-substituent at side chain of aromatic ring as in compounds **11g–j**; these were found to show moderate to poor antioxidant activities (Table 2; entry 7–10) in comparison to other analogues of the series.

In the case of 2-oxoquino[1,4]oxalines **14a–h** derivatives, compounds **14c** and **14e** were found to be the best compounds of this series and have shown the antioxidant activities having the IC<sub>50</sub> value of 9.89 ± 0.15 µg/mL and 8.97 ± 0.13 µg/mL, respectively, in comparison to ascorbic acid (Table 2; entry 17 and 19). The 2-oxoquino[1,4]oxalines **14f** having fluoro substituent showed lesser antioxidant activity profile (IC<sub>50</sub> value of 43.54 ± 0.88 µg/mL).

It can be speculated that due to larger electronegativity of fluorine atom, which accumulates the electron density, restricts the delocalization of bonds due to which, the free electrons of **14f** are not easily available for quenching of DPPH radical. Furthermore, extending the side chain of phenyl ring to more electron rich naphthyl ring in **14h** (IC<sub>50</sub> = 14.27 ± 0.23 µg/mL) showed promising activity. In addition, the un-substituted 2-oxoquino[1,4]oxaline **14a** and dichloro-substituted side chain of aromatic ring having 2-oxo-quino[1,4]oxaline **14d** showed lesser activity (Table 2; entry 15 and 18) in comparison with **14c** and **14e**. The electron-donating substituents at side chain of aromatic ring (compound **14b** and **14g**) showed poor activity profile (Table 2; entry 16 and 21) in comparison with their corresponding halo-substituted analogues **14c** and **14e**.

All the synthesized compounds were also assessed in the ferric to ferrous reduction assay (FRAP assay) taking BHT as standard reference. (Table 2) In the present study, the trend for ferric ion reducing activities of all the compounds **11a–n** and **14a–h**, with respect to standard reference BHT indicates that the seven compounds (**11c**, **11e**, **11i**, **11k**, **11l**, **14d** and **14h**) were found more potent antioxidant than BHT. The compound which have the mono-halo (such as: F, Cl, Br) substituent at the side chain of aromatic ring in 2-oxobenzo[1,4]oxazine (compound **11c**, **11e**, **11i**, **11k** and **11l**) exhibited higher antioxidants activity than BHT, whereas 2-oxoquino[1,4]oxaline **14d** and **14h**, which have 2,4-dichloro substituent at side chain of aromatic ring or naphthyl substituent displayed better antioxidant activity than standard reference BHT. Compounds **11a**, **11m**, **14c** and **14f** showed comparable FRAP antioxidant activity than standard reference BHT. Rest of the compounds showed moderate to low FRAP antioxidant activity.

Moreover, for the first time the antioxidant activity of Cephalandole A **16** was also evaluated and found to possess moderate antioxidant activity having IC<sub>50</sub> value of 11.87 ± 0.14 µg/mL in comparison to ascorbic acid (Table 2; entry 23) in DPPH radical scavenging assay.

These results showed that the mono-halo substitution at side chain of aromatic ring in nitrogen congener of 2-oxobenzo[1,4]oxazines i.e. 2-oxoquino[1,4]oxalines **14c** and **14e** along with un-substituted 2-oxobenzo[1,4]oxazine **11a** were found to be the most active compounds of the series showing promising antioxidant activities in DPPH radical scavenging. Furthermore, in the FRAP antioxidant assay, seven compounds (**11c**, **11e**, **11i**, **11k**, **11l**, **14d** and **14h**), which have mono-halo substitution at side chain of aromatic ring in 2-oxobenzo[1,4]oxazine (**11c**, **11e**, **11i** and **11k**, **11l**) and dihalo substituent as well as naphthyl substituent at 2-oxoquino[1,4]oxalines (**14d** and **14h**), showed higher antioxidant activity in comparison with BHT, respectively.

### 2. 3. Cytotoxicity

Compounds **11a**, **14c**, **14e** and **14h** (which displayed good antioxidant activity in DPPH radical scavenging as-

say) were also assessed for their cytotoxic studies using MTT assay taking 25–250 µg/mL concentration in 3T<sub>3</sub> fibroblast cell lines.<sup>27</sup> The screening results showed that these compounds were found non-toxic even at 250 µg/mL and displays allowable values of cell viability. (Figure 3)

### 3. Experimental Section

#### 3.1. General

All glass apparatus were oven dried prior to use. Melting points were taken in open capillaries on complab melting point apparatus and are presented uncorrected. Microwave reactor (CEM Discover) was used for operation of reactions. Infrared spectra were recorded on a Perkin-Elmer FT-IR Spectrum 2 spectrophotometer <sup>1</sup>H NMR and <sup>13</sup>C NMR spectra were recorded on ECS 400 MHz (JEOL) NMR spectrometer using CDCl<sub>3</sub>, CD<sub>3</sub>OD and CD<sub>3</sub>SOCD<sub>3</sub> as solvent and tetramethylsilane as internal reference. Electrospray ionization mass spectrometry (ESI-MS) and HRMS were recorded on Xevo G2-S QToF (Waters, USA) Spectrometer. Column chromatography was performed over Merck silica gel (particle size: 60-120 Mesh) procured from Qualigensä (India), flash silica gel (particle size: 230–400 Mesh). All chemicals and reagents were obtained from Sigma Aldrich (USA), Merck (India) or Spectrochem (India) and were used without further purification.

#### 3.2. General Procedure for the Synthesis of (Z)-3-(2-oxo-2-phenylethylidene)-3,4-dihydro-2H-benzo[b][1,4]oxazin-2-one (11a) in optimization study as given in table 1:

##### (1) Method A (conventional heating condition):

A solution of **9a** (19.2 mg, 0.10 mmol) and **10a** (10.9 mg, 0.10 mmol) in given solvent (1.0 mL) was heated at given time and temperature (as shown in Table 1). The

progress of the reaction was monitored by TLC using 9:1 hexane/ethyl acetate as an eluent. After completion of reaction, the reaction mixture was extracted with ethyl acetate (3 × 50 mL) and distilled water. The organic layer was combined and dried over anhydrous Na<sub>2</sub>SO<sub>4</sub> and the organic solvent was removed under reduced pressure to give the crude product. The crude products were purified either by recrystallization using EtOAc/hexane (v/v = 20:80) or by flash column chromatography method over silica gel using 9:1 hexane/ethyl acetate as an eluent which afforded the pure desired 2-oxobenzo[1,4]oxazine **11a** having good yields (18–67%).

##### (2) Method B (microwave irradiation condition):

To a solution of **9a** (19.2 mg, 0.10 mmol) in given solvent (1.0 mL) was added **10a** (10.9 mg, 0.10 mmol), and the reaction mixture was irradiated under microwave at given temperature and time (as shown in Table 1). The progress of the reaction was monitored by TLC using 9:1 hexane/ethyl acetate as an eluent. After completion of the reaction, the reaction mixture was extracted with ethyl acetate (3 × 50 mL) and distilled water. The organic layer was combined and dried over anhydrous Na<sub>2</sub>SO<sub>4</sub> and the organic solvent was removed under reduced pressure to give the crude product. The crude product were purified either by recrystallization using EtOAc/hexane (v/v = 20:80) or by flash column chromatography method over silica gel using 9:1 hexane/ethyl acetate as an eluent which afforded the pure desired 2-oxobenzo[1,4]oxazine **11a** product having good yields (51–94%).

#### 3.3. General Procedure for the synthesis of functionalized (Z)-3-(2-oxo-2-phenylethylidene)-3,4-dihydro-2H-benzo[b][1,4]oxazin-2-ones (11a-n) and (Z)-3-(2-oxophenylethylidene)-3,4-

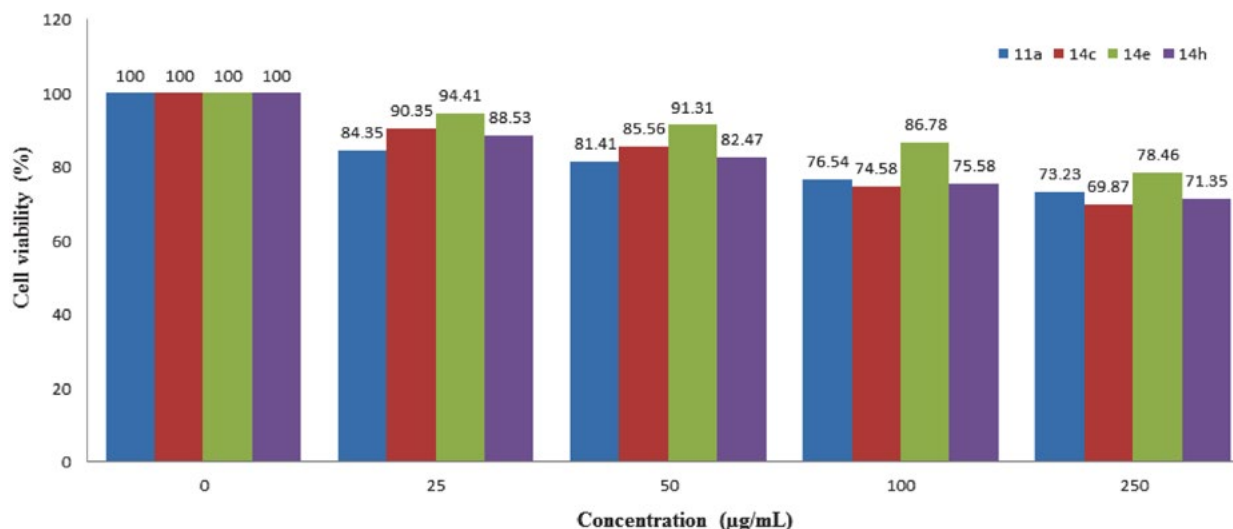
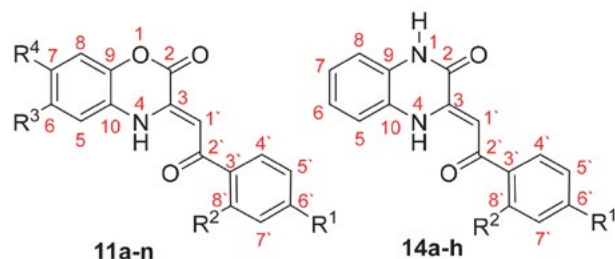


Figure 3. Percentage cell viability test.

### dihydroquinoxalin-2(1H)-ones (14a–h) as given in scheme 1 and scheme 2:

To a solution of compound **9a–f** (0.20 mmol; 1 eq., as given in Scheme 1) or **9a–g** (0.20 mmol; 1 eq. as given in Scheme 2) in diethylene glycol (2.0 mL) was added compound **10a–c** (0.20 mmol; 1 eq., as given in Scheme 1) or **12** and **13** (0.20 mmol; 1 eq., as given in Scheme 2) and the reaction mixture was irradiated under microwave at 150 °C temperature for about 5–10 min depending upon the substrate utilized. The progress of the reaction was monitored by TLC using 9:1 hexane/ethyl acetate as an eluent. After completion of reaction, the reaction mixture was extracted with ethyl acetate (3 × 50 mL) and distilled water. The organic layer was combined and dried over anhydrous Na<sub>2</sub>SO<sub>4</sub> and the organic solvent was removed under reduced pressure to give the crude product. The crude products were purified either by recrystallization using EtOAc/hexane (v/v = 20:80) or by flash column chromatography method over silica gel using 9:1 hexane/ethyl acetate as an eluent which afforded the pure desired (Z)-3-(2-oxo-2-phenylethylidene)-3,4-dihydro-2H-benzo[b][1,4]oxazin-2-ones **11a–n** and (Z)-3-(2-oxo-2-phenylethylidene)-3,4-dihydroquinoxalin-2(1H)-ones **14a–h** having good yields (78–97%).

### 3. 4. Characterization data of (Z)-3-(2-oxo-2-phenylethylidene)-3,4-dihydro-2H-benzo[b][1,4]oxazin-2-ones, (Z)-3-(2-oxo-2-phenylethylidene)-3,4-dihydroquinoxalin-2(1H)-ones (11a–n and 14 a-h) and Cephalandole A



Numbering of atoms in <sup>1</sup>H and <sup>13</sup>C NMR assignment analysis

#### (Z)-3-(2-oxo-2-phenylethylidene)-3,4-dihydro-2H-benzo[b][1,4]oxazin-2-one (11a)<sup>17a-c</sup>

Yellow solid; yield: 94%, R<sub>f</sub> (EtOAc/hexane; 20:80) = 0.85; m.p. 185–186 °C; FT-IR (KBr, ν<sub>max</sub>/cm<sup>-1</sup>) 3434, 1754, 1614, 1594, 1270; <sup>1</sup>H NMR (400 MHz, CDCl<sub>3</sub>) δ 8.00 (d, J = 7.4 Hz, 2H, C4'H, C8'H), 7.55–7.46 (m, 3H, C1'H, C5'H, C7'H), 7.21–7.05 (m, 5H, C5H, C6H, C7H, C8H); <sup>13</sup>C NMR (100 MHz, CDCl<sub>3</sub>) δ 191.6 (>C=O), 156.3 (O=C-O-), 141.3 (C9), 139.1 (C3'), 138.3 (C6'), 132.8 (C3), 128.8 (C10), 127.7 (C4', C8'), 126.0 (C5', C7'), 124.0 (C6), 123.8 (C7), 117.2 (C5), 116.0 (C8), 94.7 (-C=C-); HRMS (ESI) calcd. for C<sub>16</sub>H<sub>11</sub>NO<sub>3</sub> [M+H]<sup>+</sup>: 266.0739; found 266.0734.

#### (Z)-3-(2-oxo-2-(p-tolyl)ethylidene)-3,4-dihydro-2H-benzo[b][1,4]oxazin-2-one (11b)<sup>17b,d</sup>

Yellow solid; yield: 95%, R<sub>f</sub> (EtOAc/hexane; 20:80) = 0.80; m.p. 160–162 °C; FT-IR (KBr, ν<sub>max</sub>/cm<sup>-1</sup>) 3437, 2925, 1759, 1622, 1110; <sup>1</sup>H NMR (400 MHz, CDCl<sub>3</sub>) δ 7.91 (d, J = 7.6 Hz, 2H, C4'H, C8'H), 7.27 (m, 2H, C5'H, C7'H), 7.20–7.16 (m, 2H, C5H, C8H), 7.10–7.06 (m, 2H, C6H, C7H), 7.03 (d, J = 1.2 Hz, 1H, C1'H), 2.41 (s, 3H, -CH<sub>3</sub>); <sup>13</sup>C NMR (100 MHz, CDCl<sub>3</sub>) δ 191.4 (>C=O), 156.5 (O=C-O-), 143.6 (C6'), 141.2 (C9), 138.8 (C3'), 135.7 (C3), 129.5 (C10), 127.9 (C4', 8'), 125.9 (C5', C7'), 123.9 (C6), 123.8 (C7), 117.2 (C5), 115.9 (C8), 94.8 (-C=C-), 21.8 (-CH<sub>3</sub>); HRMS (ESI) calcd. for C<sub>17</sub>H<sub>13</sub>NO<sub>3</sub> [M+H]<sup>+</sup>: 280.0895; found 280.0899.

#### (Z)-3-(2-(4-chlorophenyl)-2-oxoethylidene)-3,4-dihydro-2H-benzo[b][1,4]oxazin-2-one (11c)<sup>17a,d</sup>

Yellow solid; yield: 90%, R<sub>f</sub> (EtOAc/hexane; 20:80) = 0.80; m.p. 155–157 °C; FT-IR (KBr, ν<sub>max</sub>/cm<sup>-1</sup>) 3437, 1759, 1633, 1585, 752; <sup>1</sup>H NMR (400 MHz, CDCl<sub>3</sub>) δ 7.92 (d, J = 8.4 Hz, 2H, C4'H, C8'H), 7.44 (d, J = 8.4 Hz, 2H, C5'H, C7'H), 7.22–7.09 (m, 4H, C5H, C6H, C7H, C8H), 6.98 (s, 1H, C1'H); <sup>13</sup>C NMR (100 MHz, CDCl<sub>3</sub>) δ 190.1 (>C=O), 156.1 (O=C-O-), 141.4 (C6'), 139.4 (C9), 139.1 (C3'), 136.6 (C3), 129.1 (C10), 129.0 (C4', C8'), 126.0 (C5', C7'), 124.3 (C6), 123.6 (C7), 117.3 (C5), 116.1 (C8), 94.2 (-C=C-); HRMS (ESI) calcd. for C<sub>16</sub>H<sub>10</sub>ClNO<sub>3</sub> [M+2H]<sup>+</sup>: 301.0349; found 301.0345.

#### (Z)-3-(2-(2,4-dichlorophenyl)-2-oxoethylidene)-3,4-dihydro-2H-benzo[b][1,4]oxazin-2-one (11d)

Yellow solid; yield: 97%, R<sub>f</sub> (EtOAc/hexane; 20:80) = 0.85; m.p. 160–162 °C; FT-IR (KBr, ν<sub>max</sub>/cm<sup>-1</sup>) 3436, 1758, 1620, 1577, 1101; <sup>1</sup>H NMR (400 MHz, CDCl<sub>3</sub>) δ 12.85 (s, 1H, -NH-), 7.53 (d, J = 7.6 Hz, 1H, C4'H), 7.46 (s, 1H, C8'H), 7.32 (d, J = 8.0 Hz, 1H, C5'H), 7.20–7.12 (m, 5H, C6H, C7H, C8H, C7'H), 6.76 (s, 1H, C1'H); <sup>13</sup>C NMR (100 MHz, CDCl<sub>3</sub>) 191.1 (>C=O), 155.1 (O=C-O-), 140.8 (C9), 138.4 (C6'), 136.8 (C3'), 136.6 (C4'), 131.8 (C10), 130.0 (C3), 129.9 (C8'), 126.7 (C5'), 125.4 (C7'), 123.9 (C6), 122.7 (C7), 116.6 (C5), 115.6 (C8), 97.5 (C1': -C=C-); HRMS (ESI) calcd. for C<sub>16</sub>H<sub>9</sub>Cl<sub>2</sub>NO<sub>3</sub> [M+2H]<sup>+</sup>: 334.9959; found 334.9953.

#### (Z)-3-(2-(4-fluorophenyl)-2-oxoethylidene)-3,4-dihydro-2H-benzo[b][1,4]oxazin-2-one (11e)<sup>17e,i</sup>

Yellow solid; yield: 94%, R<sub>f</sub> (EtOAc/hexane; 20:80) = 0.80; m.p. 152–154 °C; FT-IR (KBr, ν<sub>max</sub>/cm<sup>-1</sup>) 3434, 2925, 1757, 1622, 1596, 1156; <sup>1</sup>H NMR (400 MHz, CDCl<sub>3</sub>) δ 8.03 (dd, J = 5.6, 8.8 Hz, 2H, C4'H, C8'H), 7.22–7.11 (m, 6H, C5H, C6H, C7H, C8H, C5'H, C7'H), 7.00 (s, 1H, C1'H); <sup>13</sup>C NMR (100 MHz, CDCl<sub>3</sub>) δ 190.1 (>C=O), 166.9 (C6'), 156.2 (O=C-O-), 141.3 (C9), 139.2 (C3'), 134.6 (C3), 130.3 (C10), 125.9 (C4', C8'), 124.6 (C6), 123.7 (C7), 117.3 (C5), 116.0 (C5', C7'), 115.8 (C8), 94.3 (C1': -C=C-); HRMS (ESI) calcd. for C<sub>16</sub>H<sub>10</sub>FNO<sub>3</sub> [M+H]<sup>+</sup>: 284.0645; found 284.0649.



**(Z)-3-(2-(4-bromophenyl)-2-oxoethylidene)-3,4-dihydro-2H-benzo[b][1,4]oxazin-2-one (11f)**<sup>17f</sup>

Yellow solid; yield: 93%,  $R_f$  (EtOAc/hexane; 20:80) = 0.85; m.p. 200–202 °C; FT-IR (KBr,  $\nu_{\max}$ /cm<sup>-1</sup>) 3437, 1754, 1624, 1585, 1277, 1111; <sup>1</sup>H NMR (400 MHz, CDCl<sub>3</sub>)  $\delta$  7.85 (d,  $J$  = 8.0 Hz, 2H, C4'H, C8'H), 7.60 (d,  $J$  = 8.0 Hz, 2H, C5'H, C7'H), 7.24–7.09 (m, 4H, C5H, C6H, C7H, C8H), 6.97 (s, 1H, C1'H); <sup>13</sup>C NMR (100 MHz, CDCl<sub>3</sub>)  $\delta$  190.3 (>C=O), 156.1 (O=C-O-), 141.4 (C9), 139.4 (C3'), 137.1 (C3), 132.1 (C5', C7'), 129.2 (C10), 127.8 (C4', C8'), 126.0 (C6'), 124.3 (C6), 123.6 (C7), 117.3 (C5), 116.1 (C8), 94.2 (C1': -C=C-); HRMS (ESI) calcd. for C<sub>16</sub>H<sub>10</sub>BrNO<sub>3</sub> [M+2H]<sup>+</sup>: 344.9844; found 344.9849.

**(Z)-6-methyl-3-(2-oxo-2-phenylethylidene)-3,4-dihydro-2H-benzo[b][1,4]oxazin-2-one (11g)**<sup>17c</sup>

Yellow solid; yield: 88%,  $R_f$  (EtOAc/hexane; 20:80) = 0.90; m.p. 157–158 °C; FT-IR (KBr,  $\nu_{\max}$ /cm<sup>-1</sup>) 3436, 1750, 1618, 1572, 1123, 740; <sup>1</sup>H NMR (400 MHz, CDCl<sub>3</sub>)  $\delta$  8.00–7.98 (m, 2H, C4'H, C8'H), 7.56–7.45 (m, 3H, C1'H, C5'H, C7'H), 7.07–7.02 (m, 2H, C8H, C6'H), 6.88 (d,  $J$  = 8.5 Hz, 2H, C5H, C7H), 2.34 (s, 3H, -CH<sub>3</sub>); <sup>13</sup>C NMR (100 MHz, CDCl<sub>3</sub>)  $\delta$  191.5 (>C=O), 156.5 (O=C-O-), 139.4 (C9), 139.2 (C3'), 138.4 (C6), 136.1 (C3), 132.7 (C6'), 128.8 (C4', C8'), 127.7 (C5', C7'), 124.8 (C7), 123.4 (C10), 116.8 (C5), 116.2 (C8), 94.5 (C1': -C=C-), 21.08 (-CH<sub>3</sub>); HRMS (ESI) calcd. for C<sub>17</sub>H<sub>13</sub>NO<sub>3</sub> [M+H]<sup>+</sup>: 280.0895; found 280.0899.

**(Z)-6-methyl-3-(2-oxo-2-(p-tolyl) ethylidene)-3, 4-dihydro-2H-benzo[b][1,4]oxazin-2-one (11h)**<sup>17e</sup>

Yellow solid; yield: 89%,  $R_f$  (EtOAc/hexane; 20:80) = 0.80; m.p. 162–164 °C; FT-IR (KBr,  $\nu_{\max}$ /cm<sup>-1</sup>) 3434, 1762, 1602, 1313, 1047; <sup>1</sup>H NMR (400 MHz, CDCl<sub>3</sub>)  $\delta$  7.90 (d,  $J$  = 8.1 Hz, 2H, C4'H, C8'H), 7.27 (d,  $J$  = 8.0 Hz, 2H, C5'H, C7'H), 7.06 (d,  $J$  = 8.1 Hz, 1H, C8H), 7.02 (s, 1H, C1'H), 6.88 (d,  $J$  = 9.4 Hz, 2H, C5H, C7H), 2.42 (s, 3H, C6': -CH<sub>3</sub>), 2.35 (s, 3H, C6: -CH<sub>3</sub>); <sup>13</sup>C NMR (100 MHz, CDCl<sub>3</sub>)  $\delta$  191.3 (>C=O), 156.6 (O=C-O-), 143.5 (C6'), 139.3 (C9), 139.0 (C3'), 136.0 (C6), 135.8 (C3), 129.5 (C5', C7'), 127.8 (C4', C8'), 124.6 (C7), 123.5 (C10), 116.8 (C5), 116.1 (C8), 94.6 (C1': -C=C-), 21.7 (C6: -CH<sub>3</sub>), 21.0 (C6': -CH<sub>3</sub>); HRMS (ESI) calcd. for C<sub>18</sub>H<sub>15</sub>NO<sub>3</sub> [M+H]<sup>+</sup>: 294.1052; found 294.1055.

**(Z)-3-(2-(4-chlorophenyl)-2-oxoethylidene)-6-methyl-3,4-dihydro-2H-benzo[b][1,4]oxazin-2-one (11i)**<sup>17h</sup>

Yellow solid; yield: 91%,  $R_f$  (EtOAc/hexane; 20:80) = 0.85; m.p. 145–147 °C; FT-IR (KBr,  $\nu_{\max}$ /cm<sup>-1</sup>) 3437, 1767, 1629, 1582; <sup>1</sup>H NMR (400 MHz, CDCl<sub>3</sub>)  $\delta$  7.94–7.92 (m, 2H, C4'H, C8'H), 7.46–7.43 (m, 2H, C5'H, C7'H), 7.08 (d,  $J$  = 9.2 Hz, 1H, C8H), 6.97 (s, 1H, C1'H), 6.92–6.90 (m, 2H, C5H, C7H), 2.35 (s, 3H, -CH<sub>3</sub>); <sup>13</sup>C NMR (100 MHz, CDCl<sub>3</sub>)  $\delta$  190.1 (>C=O), 156.3 (O=C-O-), 139.5 (C9), 139.4 (C6'), 139.0 (C3'), 136.7 (C6), 136.1 (C3), 129.1 (C4', C8'), 129.0 (C5', C7'), 125.0 (C7), 123.2 (C10), 116.9 (C5), 116.3 (C8),

94.1 (C1': -C=C-), 21.1 (-CH<sub>3</sub>); HRMS (ESI) calcd. for C<sub>17</sub>H<sub>12</sub>ClNO<sub>3</sub> [M+2H]<sup>+</sup>: 315.0506; found 315.0509.

**(Z)-3-(2-(4-bromophenyl)-2-oxoethylidene)-6-methyl-3,4-dihydro-2H-benzo[b][1,4]oxazin-2-one (11j)**

Yellow solid; yield: 96%,  $R_f$  (EtOAc/hexane; 20:80) = 0.85; m.p. 179–181 °C; FT-IR (KBr,  $\nu_{\max}$ /cm<sup>-1</sup>) 3435, 2923, 1763, 1624, 1543, 1052; <sup>1</sup>H NMR (400 MHz, CDCl<sub>3</sub>)  $\delta$  7.87–7.84 (m, 2H, C4'H, C8'H), 7.63–7.59 (m, 2H, C5'H, C7'H), 7.08 (d,  $J$  = 9.2 Hz, 1H, C8H), 6.96 (s, 1H, C1'H), 6.92–6.90 (m, 2H, C5H, C7H), 2.35 (s, 3H, -CH<sub>3</sub>); <sup>13</sup>C NMR (100 MHz, CDCl<sub>3</sub>)  $\delta$  190.2 (>C=O), 156.3 (O=C-O-), 139.5 (C9), 139.4 (C6'), 137.1 (C3'), 136.2 (C6), 132.0 (C3), 129.2 (C5', C7'), 127.7 (C4', C8'), 125.1 (C7), 123.2 (C10), 117.0 (C5), 116.3 (C8), 94.0 (C1': -C=C-), 21.1 (-CH<sub>3</sub>); HRMS (ESI) calcd. for C<sub>17</sub>H<sub>12</sub>BrNO<sub>3</sub> [M+H]<sup>+</sup>: 358.0001; found 358.0007.

**(Z)-3-(2-(4-bromophenyl)-2-oxoethylidene)-6-nitro-3,4-dihydro-2H-benzo[b][1,4]oxazin-2-one (11k)**

Yellow solid; yield: 83%,  $R_f$  (EtOAc/hexane; 20:80) = 0.70; m.p. 195–197 °C; FT-IR (KBr,  $\nu_{\max}$ /cm<sup>-1</sup>) 3435, 2925, 1759, 1525, 1023; <sup>1</sup>H NMR (400 MHz, CDCl<sub>3</sub>)  $\delta$  8.03–7.97 (m, 2H, C4'H, C8'H), 7.89–7.86 (m, 2H, C5'H, C7'H), 7.66–7.63 (m, 2H, C5H, C7H), 7.32 (d,  $J$  = 9.2 Hz, 1H, C8H), 7.07 (s, 1H, C1'H); <sup>13</sup>C NMR (100 MHz, CDCl<sub>3</sub>)  $\delta$  190.8 (>C=O), 154.9 (O=C-O-), 145.3 (C6), 145.0 (C9), 138.0 (C3'), 136.5 (C3), 132.3 (C5', C7'), 129.4 (C4', C8'), 128.6 (C6'), 124.5 (C10), 119.2 (C7), 118.0 (C5), 111.6 (C8), 96.4 (C1': -C=C-); HRMS (ESI) calcd. for C<sub>16</sub>H<sub>9</sub>BrN<sub>2</sub>O<sub>5</sub> [M+2H]<sup>+</sup>: 389.9695; found 389.9699.

**(Z)-6-nitro-3-(2-oxo-2-(p-tolyl) ethylidene)-3, 4-dihydro-2H-benzo[b][1,4]oxazin-2-one (11l)**

Yellow solid; yield: 81%,  $R_f$  (EtOAc/hexane; 20:80) = 0.75; m.p. 220–223 °C; FT-IR (KBr,  $\nu_{\max}$ /cm<sup>-1</sup>) 3433, 1760, 1624, 1524, 1109; <sup>1</sup>H NMR (400 MHz, DMSO-*d*<sub>6</sub>)  $\delta$  8.73 (d,  $J$  = 2.4 Hz, 1H, C4'H), 7.96–7.92 (m, 3H, C5'H, C7'H, C8'H), 7.46–7.37 (m, 3H, C5H, C7H, C8H), 6.95 (s, 1H, C1'H), 2.40 (s, 3H, -CH<sub>3</sub>); <sup>13</sup>C NMR (100 MHz, DMSO-*d*<sub>6</sub>)  $\delta$  189.9 (>C=O), 155.7 (O=C-O-), 145.9 (C6), 143.8 (C9), 139.2 (C6'), 138.5 (C3'), 135.2 (C3), 130.1 (C4', C8'), 128.1 (C5', C7'), 119.5 (C10), 118.9 (C7), 117.7 (C5), 112.6 (C8), 94.8 (C1': -C=C-), 21.7 (-CH<sub>3</sub>); HRMS (ESI) calcd. for C<sub>17</sub>H<sub>12</sub>N<sub>2</sub>O<sub>5</sub> [M+H]<sup>+</sup>: 325.0746; found 325.0741.

**(Z)-3-(2-(4-chlorophenyl)-2-oxoethylidene)-6-nitro-3,4-dihydro-2H-benzo[b][1,4]oxazin-2-one (11m)**

Yellow solid; yield: 78%,  $R_f$  (EtOAc/hexane; 20:80) = 0.70; m.p. 239–240 °C; FT-IR (KBr,  $\nu_{\max}$ /cm<sup>-1</sup>) 3435, 2924, 1622, 1525, 1272; <sup>1</sup>H NMR (400 MHz, DMSO-*d*<sub>6</sub>)  $\delta$  8.73 (s, 1H, C5H), 8.03 (d,  $J$  = 7.2 Hz, 2H, C4'H, C8'H), 7.91 (d,  $J$  = 9.1 Hz, 1H, C7H), 7.59 (d,  $J$  = 7.2 Hz, 2H, C5'H, C7'H), 7.42 (d,  $J$  = 9.0 Hz, 1H, C8H), 6.90 (s, 1H, C1'H); <sup>13</sup>C NMR (100 MHz, DMSO-*d*<sub>6</sub>)  $\delta$  188.9 (>C=O), 156.0 (O=C-O-), 146.0 (C6), 144.7 (C9), 139.8 (C6'), 138.2

(C3'), 137.1 (C3), 129.9 (C4', C8'), 129.6 (C5', C7'), 125.8 (C10), 119.0 (C7), 117.8 (C5), 113.1 (C8), 94.4 (C1': -C=C-); HRMS (ESI) calcd. for C<sub>16</sub>H<sub>9</sub>ClN<sub>2</sub>O<sub>5</sub> [M+2H]<sup>+</sup>: 346.0200; found 346.0204.

**(Z)-3-(2-(2,4-dichlorophenyl)-2-oxoethylidene)-6-nitro-3,4-dihydro-2H-benzo[b][1,4]oxazin-2-one (11n)**

Yellow solid; yield: 80%, R<sub>f</sub> (EtOAc/hexane; 20:80) = 0.75; m.p. 185–187 °C; FT-IR (KBr, ν<sub>max</sub>/cm<sup>-1</sup>) 3588, 2930, 1769, 1585, 1685, 1108; <sup>1</sup>H NMR (400 MHz, CDCl<sub>3</sub>) δ 8.05–7.99 (m, 2H, C7H, C8'H), 7.55(d, J = 8.4 Hz, 1H, C5'H, C7'H), 7.48 (d, J = 2.0 Hz, 1H, C7'H), 7.37–7.33 (m, 2H, C5H, C8H), 6.89 (s, 1H, C1'H); <sup>13</sup>C NMR (100 MHz, CDCl<sub>3</sub>) δ 192.4 (>C=O), 154.5 (O=C-O-), 145.2 (C6), 145.1 (C9), 138.0 (C6'), 137.6 (C3'), 136.9 (C4'), 132.7 (C3), 131.0 (C8'), 130.8 (C5'), 127.6 (C7'), 124.2 (C10), 119.4 (C7), 118.1 (C5), 111.7 (C8), 100.4 (C1': -C=C-); HRMS (ESI) calcd. for C<sub>16</sub>H<sub>8</sub>Cl<sub>2</sub>N<sub>2</sub>O<sub>5</sub> [M+2H]<sup>+</sup>: 379.9810; found 379.9815.

**(Z)-3-(2-oxo-2-phenylethylidene)-3,4-dihydroquinoxalin-2(1H)-one (14a)**<sup>17a,b</sup>

Yellow solid; yield: 94%, R<sub>f</sub> (EtOAc/hexane; 20:80) = 0.85; m.p. 268–269 °C; FT-IR (KBr, ν<sub>max</sub>/cm<sup>-1</sup>) 3060, 1688, 1619; <sup>1</sup>H NMR (400 MHz, DMSO-*d*<sub>6</sub>) δ 10.0 (s, 1H, -NH-), 8.07–8.05 (m, 2H, C4'H, C8'H), 7.55–7.48 (m, 3H, C5'H, C6'H, C7'H), 7.21–7.12 (m, 4H, C5H, C6H, C7H, C8H); 7.03 (s, 1H, C1'H); <sup>13</sup>C NMR (100 MHz, DMSO-*d*<sub>6</sub>) δ 187.9 (>C=O), 155.2 (-NH-C=O), 145.4 (C3), 138.4 (C3'), 131.2 (C6'), 128.2 (C10), 126.5 (C5', C7'), 123.9 (C4', C8'), 123.6 (C9), 123.1 (C6), 116.1 (C7), 115.1 (C5), 114.9 (C8), 89.0 (C1': -C=C-); HRMS (ESI) calcd. for C<sub>16</sub>H<sub>12</sub>N<sub>2</sub>O<sub>2</sub> [M+H]<sup>+</sup>: 265.0899; found 265.0893.

**(Z)-3-(2-oxo-2-(p-tolyl)ethylidene)-3,4-dihydroquinoxalin-2(1H)-one (14b)**<sup>17k</sup>

Yellow solid; yield: 96%, R<sub>f</sub> (EtOAc/hexane; 20:80) = 0.80; m.p. 221–222 °C; FT-IR (KBr, ν<sub>max</sub>/cm<sup>-1</sup>) 3045, 1677, 1615; <sup>1</sup>H NMR (400 MHz, CDCl<sub>3</sub>) δ 10.26 (s, 1H, -NH-), 7.96 (d, J = 8.0 Hz, 2H, C4'H, C8'H), 7.31–7.29 (m, 2H, C5'H, C7'H), 7.21–7.12 (m, 4H, C5H, C6H, C7H, C8H); 7.01 (s, 1H, C1'H), 2.43 (s, 3H, -CH<sub>3</sub>); <sup>13</sup>C NMR (100 MHz, CDCl<sub>3</sub>) δ 190.5 (>C=O), 158.0 (-NH-C=O), 144.6 (C6'), 142.8 (C3), 136.3 (C3'), 130.3 (C10), 129.4 (C5', C7'), 127.7 (C4', C8'), 125.6 (C9), 124.9 (C6), 123.9 (C7), 116.2 (C5), 115.9 (C8), 90.9 (C1': -C=C-), 21.7 (C6': -CH<sub>3</sub>); HRMS (ESI) calcd. for C<sub>17</sub>H<sub>14</sub>N<sub>2</sub>O<sub>2</sub> [M+H]<sup>+</sup>: 279.1055; found 279.1059.

**(Z)-3-(2-(4-chlorophenyl)-2-oxoethylidene)-3,4-dihydroquinoxalin-2(1H)-one (14c)**<sup>17a,k</sup>

Yellow solid; yield: 91%, R<sub>f</sub> (EtOAc/hexane; 20:80) = 0.85; m.p. 267–268 °C; FT-IR (KBr, ν<sub>max</sub>/cm<sup>-1</sup>) 3052, 1686, 1614; <sup>1</sup>H NMR (400 MHz, DMSO-*d*<sub>6</sub>) δ 11.8 (s, 1H, -NH-), 7.98 (d, J = 8.8 Hz, 2H, C4', C8'), 7.57–7.44 (m, 3H, C5'H, C7'H, C8H), 7.19–7.14 (m, 3H, C5H, C6H, C7H); 6.80

(s, 1H, C1'H); <sup>13</sup>C NMR (100 MHz, DMSO-*d*<sub>6</sub>) δ 187.5 (>C=O), 156.1 (-NH-C=O), 146.7 (C3), 138.1 (C6'), 137.3 (C3'), 129.3 (C10), 127.5 (C4', C8'), 124.8 (C5', C7'), 124.2 (C9), 124.1 (C6), 117.3 (C7), 117.2 (C5), 115.9 (C8), 89.9 (C1': -C=C-); HRMS (ESI) calcd. for C<sub>16</sub>H<sub>11</sub>ClN<sub>2</sub>O<sub>2</sub> [M+2H]<sup>+</sup>: 300.0509; found 300.0503.

**(Z)-3-(2-(2,4-dichlorophenyl)-2-oxoethylidene)-3,4-dihydroquinoxalin-2(1H)-one (14d)**<sup>17l</sup>

Yellow solid; yield: 95%, R<sub>f</sub> (EtOAc/hexane; 20:80) = 0.80; m.p. 260–262 °C; FT-IR (KBr, ν<sub>max</sub>/cm<sup>-1</sup>) 3054, 1682, 1618; <sup>1</sup>H NMR (400 MHz, DMSO-*d*<sub>6</sub>) δ 11.84 (s, 1H, -NH-), 7.63–7.49 (m, 4H, C4'H, C5'H, C7'H, C8H), 7.19–7.15 (m, 3H, C5H, C6H, C7H), 6.44 (s, 1H, C1'H); <sup>13</sup>C NMR (100 MHz, DMSO-*d*<sub>6</sub>) δ 187.8 (>C=O), 154.8 (-NH-C=O), 145.2 (C6'), 138.2 (C3), 134.7 (C3'), 130.7 (C8'), 130.3 (C4'), 129.2 (C10), 127.1 (C5'), 126.6 (C9), 123.8 (C7'), 123.5 (C6), 123.1 (C7), 116.3 (C5), 114.9 (C8), 92.8 (C1': -C=C-); HRMS (ESI) calcd. for C<sub>16</sub>H<sub>10</sub>Cl<sub>2</sub>N<sub>2</sub>O<sub>2</sub> [M+2H]<sup>+</sup>: 334.0119; found 334.0113.

**(Z)-3-(2-(4-bromophenyl)-2-oxoethylidene)-3,4-dihydroquinoxalin-2(1H)-one (14e)**<sup>17g</sup>

Yellow solid; yield: 93%, R<sub>f</sub> (EtOAc/hexane; 20:80) = 0.75; m.p. 281–282 °C; FT-IR (KBr, ν<sub>max</sub>/cm<sup>-1</sup>) 3044, 1678, 1606; <sup>1</sup>H NMR (400 MHz, DMSO-*d*<sub>6</sub>) δ 11.81 (s, 1H, -NH-), 7.92–7.89 (m, 2H, C4'H, C8'H), 7.71–7.69 (m, 2H, C5'H, C7'H), 7.44 (s, 1H, C8H), 7.18–7.14 (m, 3H, C5H, C6H, C7H); 6.79 (s, 1H, C1'H); <sup>13</sup>C NMR (100 MHz, DMSO-*d*<sub>6</sub>) δ 186.5 (>C=O), 155.1 (-NH-C=O), 145.7 (C3), 137.5 (C3'), 131.2 (C5', C7'), 128.5 (C10), 126.5 (C4', C8'), 125.1 (C6'), 123.8 (C9), 123.1 (C6), 116.2 (C7), 115.1 (C5), 114.9 (C8), 88.8 (C1': -C=C-); HRMS (ESI) calcd. for C<sub>16</sub>H<sub>11</sub>BrN<sub>2</sub>O<sub>2</sub> [M+2H]<sup>+</sup>: 344.0004; found 344.0009.

**(Z)-3-(2-(4-fluorophenyl)-2-oxoethylidene)-3,4-dihydroquinoxalin-2(1H)-one (14f)**<sup>17g</sup>

Yellow solid; yield: 91%, R<sub>f</sub> (EtOAc/hexane; 20:80) = 0.80; m.p. 252–253 °C; FT-IR (KBr, ν<sub>max</sub>/cm<sup>-1</sup>) 3053, 1680, 1614; <sup>1</sup>H NMR (400 MHz, DMSO-*d*<sub>6</sub>) δ 12.0 (s, 1H, -NH-), 8.02–8.00 (m, 2H, C4'H, C8'H), 7.48 (s, 1H, C8H), 7.33–7.28 (m, 2H, C5'H, C7'H), 7.12–7.11 (m, 3H, C5H, C6H, C7H); 6.76 (s, 1H, C1'H); <sup>13</sup>C NMR (100 MHz, DMSO-*d*<sub>6</sub>) δ 187.1 (>C=O), 164.4 (C6'), 155.7 (-NH-C=O), 145.7 (C3), 135.3 (C3'), 129.9 (C4', 8'), 129.8 (C10), 126.7 (C9), 124.1 (C6), 123.7 (C7), 116.6 (C5), 113.8 (C8), 115.4 (C5', C7'), 88.9 (C1': -C=C-); HRMS (ESI) calcd. for C<sub>16</sub>H<sub>11</sub>FN<sub>2</sub>O<sub>2</sub> [M+H]<sup>+</sup>: 283.0805; found 283.0809.

**(Z)-3-(2-(4-methoxyphenyl)-2-oxoethylidene)-3,4-dihydroquinoxalin-2(1H)-one (14g)**<sup>16e</sup>

Yellow solid; yield: 90%, R<sub>f</sub> (EtOAc/hexane; 20:80) = 0.75; m.p. 241–242 °C; FT-IR (KBr, ν<sub>max</sub>/cm<sup>-1</sup>) 3058, 1689, 1618; <sup>1</sup>H NMR (400 MHz, DMSO-*d*<sub>6</sub>) δ 11.95 (s, 1H, -NH-), 7.95 (d, J = 9.2 Hz, 2H, C4'H, C8'H), 7.45–7.44 (m, 1H, C8H), 7.14–7.03 (m, 5H, C5H, C6H, C7H, C5'H, C7'H);

6.77 (s, 1H, C1'H), 3.83 (s, 3H, -OCH<sub>3</sub>); <sup>13</sup>C NMR (100 MHz, DMSO-*d*<sub>6</sub>) δ 187.7 (>C=O), 162.3 (C6'), 155.9 (-NH-C=O), 144.9 (C3), 131.3 (C4', C8', C10), 129.2 (C3'), 126.5 (C9), 124.3 (C6), 123.7 (C7), 116.3 (C5), 115.3 (C8), 113.9 (C5', C7'), 88.9 (C1': -C=C-), 55.4 (-OCH<sub>3</sub>); HRMS (ESI) calcd. for C<sub>17</sub>H<sub>14</sub>N<sub>2</sub>O<sub>3</sub> [M+H]<sup>+</sup>: 295.1004; found 295.1009.

**(Z)-3-(2-(naphthalen-2-yl)-2-oxoethylidene)-3,4-dihydroquinoxalin-2(1H)-one (14h)**<sup>17m</sup>

Yellow solid; yield: 94%, R<sub>f</sub> (EtOAc/hexane; 20:80) = 0.85; m.p. 263–264 °C, FT-IR (KBr, ν<sub>max</sub>/cm<sup>-1</sup>) 3093, 1694, 1614; <sup>1</sup>H NMR (400 MHz, DMSO-*d*<sub>6</sub>) δ 11.67 (s, 1H, -NH-), 8.17–8.05 (m, 2H, C4'H, C9'H), 7.81–7.72 (m, 3H, C5'H, C6'H, C8'H), 7.52–7.39 (m, 4H, C6H, C8H, C7'H, C10'H); 7.25–7.14 (m, 2H, C5H, C7H), 6.89 (s, 1H, C1'H); <sup>13</sup>C NMR (100 MHz, DMSO-*d*<sub>6</sub>) δ 188.3 (>C=O), 156.3 (-NH-C=O), 146.5 (C3), 144.1 (C3'), 139.9 (C12'), 138.3 (C11'), 129.6 (C9'), 129.4 (C10), 128.5 (C4'), 128.4 (C5'), 127.5 (C9), 127.3 (C8'), 125.3 (C7'), 125.1 (C6'), 124.7 (C6), 124.4 (C7), 117.1 (C10'), 116.3 (C5), 115.9 (C8), 90.1 (C1': -C=C-); HRMS (ESI) calcd. for C<sub>20</sub>H<sub>14</sub>N<sub>2</sub>O<sub>2</sub> [M+H]<sup>+</sup>: 315.1055; found 315.1059.

**Synthesis of Cephalandole A (16):** To a solution of 3-Indoleglyoxylic acid **15** (226.9 mg, 1.20 mmol) in diethylene glycol was added **10a** (130.8 mg, 1.20 mmol) and the reaction mixture was irradiated under MW at 150 °C temperature for 10 min and the progress of reaction was monitored by TLC. After that, the reaction mixture was extracted with ethyl acetate (3 × 50 mL) and distilled water. The organic layer was combined and dried over anhydrous Na<sub>2</sub>SO<sub>4</sub> and the organic solvent was removed under reduced pressure to give the crude product. The crude product was further purified by flash column chromatography method over silica gel using hexane/ethyl acetate (8:2; v/v) as an eluent which afforded the pure desired Cephalandole A **16** having good yield (280.5 mg, 89%). Yellowish solid; m.p. 232–233 °C; <sup>1</sup>H NMR<sup>24c</sup> (400 MHz, DMSO-*d*<sub>6</sub>) δ 11.98 (s, 1H), 8.76–8.74 (m, 1H), 8.69 (s, 1H), 7.85 (d, J = 6.4 Hz, 1H), 7.54–7.39 (m, 4H), 7.27–7.25 (m, 2H); HRMS (ESI) calcd. for C<sub>16</sub>H<sub>10</sub>N<sub>2</sub>O<sub>2</sub> [M+H]<sup>+</sup>: 263.0742; ; found 263.0749.

## 4. Supplementary Data

The characterization spectra of synthesized 2-oxobenzo[1,4]oxazines **11a–n**, 2-oxoquino[1,4]oxalines **14a–h** and Cephalandole A (**16**) are provided in supplementary material via the “Supplementary Content” section of this article’s webpage.

## 5. Conclusions

In summary, we have developed a simple and highly efficient MW-assisted protocol for the synthesis of func-

tionalized 2-oxobenzo[1,4]oxazines **11a–n** and 2-oxoquino[1,4]oxalines **14a–h** in excellent yields. This reaction tolerates a broad range of substrates, and provides a straightforward access to functionalized 2-oxobenzo[1,4]oxazines and 2-oxoquino[1,4]oxalines. The practical applicability of developed methodology was confirmed by the gram scale synthesis of **11a**, **14c** and **14e**, along with the synthesis of Cephalandole A (**16**) (89% yield). All the synthesized compounds were screened for their *in vitro* antioxidant activities using DPPH radical scavenging and FRAP assays. Compounds **11a**, **14c** and **14e**, the most active compounds of the series, were found to show IC<sub>50</sub> value of **10.20 ± 0.08** µg/mL, **9.89 ± 0.15** µg/mL and **8.97 ± 0.13** µg/mL, respectively as compared to standard reference ascorbic acid (IC<sub>50</sub> = 4.57 µg/mL) in DPPH assay, whereas in FRAP assay, seven compounds (**11c**, **11e**, **11i**, **11k**, **11l**, **14d** and **14h**) exhibited higher antioxidant activity in comparison with BHT. Cytotoxic studies revealed that the non-toxic nature of compounds **11a**, **14c**, **14e** and **14h** even at 250 µg/mL concentration. To the best of our knowledge, this is the first report of microwave-assisted synthesis and *in vitro* antioxidant activities of functionalized 2-oxobenzo[1,4]oxazines **11a–n**; and 2-oxoquino[1,4]oxalines **14a–h** and Cephalandole A **16** in excellent yields. The potential *in vitro* antioxidant activity combined with ease of preparation qualifies these compounds as candidates for further lead optimization studies.

## 6. Acknowledgement

S. C. acknowledges SERB, New Delhi for Fast Track young scientist scheme (Grant No. CS-037/2013); DST, New Delhi for DST-RFBR Indo-Russian Joint Research Project (INT/RUS/RFBR/P-169) and CSIR, New Delhi for CSIR-EMR Grant [02 (0189)/14/EMR-II]. V. S. and P. K. J. thanks MNIT, Jaipur and CSIR, New Delhi respectively for providing financial assistance in the form of institute fellowship and RA fellowship, respectively. Materials Research Centre, MNIT, Jaipur is gratefully acknowledged for providing analytical facilities.

## 7. References

- (a) A. Khalaj, M. Abdollahi, A. Kebriaeezadeh, N. Adibpour, Z. Pandi, S. Rasoulamini, *Ind. J. Pharmacol.* **2002**, *34*, 184–188, (b) I. V. Mashevskaya, L. V. Anikina, Yu. B. Vikharev, V. A. Safin, S. V. Kol'tsova, A. N. Maslivets, *Pharm. Chem. J.* **2001**, *35*, 414–417 and references cited therein.  
DOI:10.1023/A:1013724004277
- (a) R. D. Kamble, S. V. Hese, R. J. Meshram, J. R. Kote, R. N. Gacche, B. S. Dawane, *Med. Chem. Res.* **2015**, *24*, 1077–1088; DOI:10.1007/s00044-014-1165-z  
(b) N. Gokhan, H. Erdogan, N. T. Durlu, R. Demirdamar, *Farmaco*, **1999**, *54*, 112–115.

- DOI:10.1016/S0014-827X(98)00111-6
3. M. Beach, R. Frechette, *WO Patent Appl.* 9728167, 1997.
4. (a) P. Lestage, B. Lockhart, M. B. Fleury, M. Largeron, *WO Patent Appl.*, 9962889, 1999.  
(b) E. Blattes, B. Lockhart, P. Lestage, L. Schwendimann, P. Gressens, M. B. Fleury, M. Largeron, *J. Med. Chem.* **2005**, *48*, 1282–1286. DOI:10.1021/jm040874m
5. L. D. Wise, D. J. Wustrow, T. Belliotti, *WO Patent Appl.*, 9745419, 1997.
6. K. Waissner, M. Perina, J. Kunes, V. Klimesova, J. Kaustova, *Farmaco*, **2003**, *58*, 1137–1149.  
DOI:10.1016/j.farmac.2003.07.004
7. S. Konda, S. Raparathi, K. Bhaskar, R. K. Munaganti, V. Guguloth, L. Nagarapu, D. M. Akkewar, *Bioorg. Med. Chem. Lett.* **2015**, *25*, 1643–1646 and references cited therein.  
DOI:10.1016/j.bmcl.2015.01.026
8. F. Touzeau, A. Arrault, G. Guillaumet, E. Scalbert, B. P. Feiffer, M. C. Rettori, P. Renard, J. Y. Méroux, *J. Med. Chem.* **2003**, *46*, 1962–1979. DOI:10.1021/jm021050c
9. K. Waissner, L. Kubicova, V. Buchta, P. Kubanova, K. Bajerova, L. Jiraskova, O. Bednařík, O. Bureš, P. Holý, *Folia Microbiol.* **2002**, *47*, 488–492. DOI:10.1007/BF02818786
10. F. A. Macias, D. Marin, A. Oliveros-Bastidas, J. M. G. Molinillo, *J. Agric. Food. Chem.* **2006**, *54*, 9357–9365.  
DOI:10.1021/jf062168v
11. E. N. Koini, P. Papazafiri, A. Vassilopoulos, M. Koufaki, Z. Horváth, I. Koncz, L. Virág, G. J. Papp, A. Varró, T. Calogeropoulou, *J. Med. Chem.* **2009**, *52*, 2328–2340.  
DOI:10.1021/jm801228h
12. J. Ilaš, Ž. Jakopin, T. Borštnar, M. Stegnar, D. Kikelj, *J. Med. Chem.* **2008**, *51*, 5617–5629. DOI:10.1021/jm8003448
13. S. M. Bromidge, R. Arban, B. Bertani, S. Bison, M. Borriello, P. Cavanni, G. D. Forno, R. Di-Fabio, D. Donati, S. Fontana, M. Gianotti, L. J. Gordon, E. Granci, C. P. Leslie, L. Moccia, A. Pasquarello, I. Sartori, A. Sava, J. M. Watson, A. Worby, L. Zonzini, V. Zucchelli, *J. Med. Chem.* **2010**, *53*, 5827–5843.  
DOI:10.1021/jm100482n
14. (a) D. S. La, J. Belzile, J. V. Bready, A. Coxon, T. De Melfi, N. Doerr, J. Estrada, J. C. Flynn, S. R. Flynn, R. F. Graceffa, S. P. Harriman, J. F. Larrow, A. M. Long, M. W. Martin, M. J. Morrison, V. F. Patel, P. M. Roveto, L. Wang, M. M. Weiss, D. A. Whittington, Y. Teffera, Z. Zhao, A. J. Polverino, J. C. Harmange, *J. Med. Chem.*, **2008**, *51*, 1695–1705;  
DOI:10.1021/jm701129j  
(b) T. Hasui, N. Matsunaga, T. Ora, N. Ohyabu, N. Nishigaki, Y. Imura, Y. Igata, H. Matsui, T. Motoyaji, T. Tanaka, N. Habuka, S. Sogabe, M. Ono, C. S. Siedem, T.P. Tang, C. Gauthier, L. A. De Meese, S. A. Boyd, S. Fukumoto, *J. Med. Chem.* **2011**, *54*, 8616–8631. DOI:10.1021/jm2011645
15. K. Moon, C. H. Ahn, Y. Shin, T. H. Won, K. Ko, S. K. Lee, K. B. Oh, J. Shin, S. Nam, D. C. Oh, *Mar. Drugs* **2014**, *12*, 2526–2538. DOI:10.3390/md12052526
16. (a) N. Zidar, D. Kikelj, *Tetrahedron*, **2008**, *64*, 5756–5761;  
DOI:10.1016/j.tet.2008.04.010  
(b) C. Ramesh, B. R. Raju, V. Kavala, C.-W. Kuo, C.-F. Yao, *Tetrahedron*, **2011**, *67*, 1187–1192;  
DOI:10.1016/j.tet.2010.11.095  
(c) P. Jangili, J. Kashanna, B. Das, *Tetrahedron Lett.*, **2013**, *54*, 3453–3456; DOI:10.1016/j.tetlet.2013.04.090  
(d) C. Huo, J. Dong, Y. Su, J. Tang, F. Chen, *Chem. Commun.* **2016**, *52*, 13341–13344; DOI:10.1039/C6CC05885J  
(e) M. Xia, B. Wu, G.-F. Xiang, *Synthetic Commun.* **2008**, *38*, 1268–1278; DOI:10.1080/00397910701873250  
(f) E. Feng, H. Huang, Y. Zhou, D. Ye, H. Jiang, H. Liu, *J. Org. Chem.* **2009**, *74*, 2846–2849; DOI:10.1021/jo802818s  
(g) G. Feng, J. Wu, W.-M. Dai, *Tetrahedron Lett.* **2007**, *48*, 401–404; DOI:10.1016/j.tetlet.2006.11.084  
(h) Y. Yuan, G. Liu, L. Li, Z. Wang, L. Wang, *J. Comb. Chem.* **2007**, *9*, 158–170; DOI:10.1021/cc060094u  
(i) X. Xing, J. Wu, G. Feng, W.-M. Dai, *Tetrahedron* **2006**, *62*, 6774–6781; DOI:10.1016/j.tet.2006.05.001  
(j) N. G. Kundu, Chaudhuri, G. A. Upadhyay, *J. Org. Chem.* **2001**, *66*, 20–29; DOI:10.1021/jo000826j  
(k) N. Henry, G. Guillaumet, M. D. Pujol, *Tetrahedron Lett.* **2004**, *45*, 1465–1468; DOI:10.1016/j.tetlet.2003.12.030  
(l) E. E. Stepanova, A. V. Babenysheva, A. N. Maslivets, *Russ. J. Org. Chem.* **2011**, *47*, 937–940;  
DOI:10.1134/S1070428011060182  
(m) E. E. Stepanova, Z. G. Aliev, A. N. Maslivets, *Russ. J. Org. Chem.* **2013**, *49*, 1762–1767 and references cited therein;  
DOI:10.1134/S1070428013120105  
(n) Z. G. Aliev, O. P. Krasnykh, A. N. Maslivets, L. O. Atovmyan, *Russ. Chem. Bull.* **2000**, *49*, 2045–2047;  
DOI:10.1023/A:1009532227461  
(o) E. N. Koini, P. Papazafiri, A. Vassilopoulos, M. Koufaki, Z. Horváth, I. Koncz, L. Virág, G. J. Papp, A. Varró, Calogeropoulou, T. *J. Med. Chem.* **2009**, *52*, 2328–2340.  
DOI:10.1021/jm801228h
17. For known compounds, see: (a) M. Xia, *Faming Zhuanli Shenqing Gongkai Shuomingshu*, **2008**, CN 101108860 A; (b) I. V. Mashevskaya, I. A. Tolmacheva, E. V. Voronova, T. F. Odegoeva, G. A. Aleksandrova, A. F. Goleneva, S. V. Koltsova, A. N. Maslivets, *Pharm. Chem. J.* (Translation of *Khimiko-Farmatsevticheskii Zhurnal*), **2002**, *36*, 32–34;  
(c) Y. Iwanami, T. Seki, T. Inagaki, *Bull. Chem. Soc. Jpn.* **1971**, *44*, 1316–1321; DOI:10.1246/bcsj.44.1316  
(d) E. N. Kozminykh, N. M. Igidov, G. A. Shavkunova, V. O. Kozminykh, *Russ. Chem. Bull.* (Translation of *Izvestiya Akademii Nauk, Seriya Khimicheskaya*), **1997**, *46*, 1285–1290;  
(e) V. L. Gein, N. A. Rassudikhina, N. V. Shepelina, M. I. Vakhrin, E. B. Babushkina, E. V. Voronina, *Pharm. Chem. J.* **2008**, *42*, 529–532; DOI:10.1007/s11094-009-0175-5  
(f) M. Xia, B. Wu, G. Xiang, *J. Fluor. Chem.* **2008**, *129*, 402–408; DOI:10.1016/j.jfluchem.2008.01.019  
(g) I. V. Mashevskaya, I. G. Mokrushin; K. S. Bozdyreva, A. N. Maslivets, *Russ. J. Org. Chem.* **2011**, *47*, 253–257;  
DOI:10.1134/S1070428011020151  
(h) J. Reynisson, W. Court, C. O. Neill, J. Day, L. Patterson, E. McDonald, P. Workman, M. Katan, S. A. Eccles, *Bioorg. Med. Chem.* **2009**, *17*, 3169–3176; DOI:10.1016/j.bmc.2009.02.049  
(i) V. A. Maslivets, A. N. Maslivets, *Russ. J. Org. Chem.* **2012**, *48*, 1234–1238 and references cited therein;

- DOI:10.1134/S1070428012090151  
(j) X. Lia, N. Liua, H. Zhanga, S. E. Knudsonb, R. A. Slaydenb, P. J. Tongea, *Bioorg. Med. Chem. Lett.* **2010**, *20*, 6306–6309; DOI:10.1016/j.bmcl.2010.08.076  
(k) V. V. Khalturina, Yu. V. Shklyav, Z. G. Aliev, A. N. Maslives, *Russ. J. Org. Chem.* **2009**, *45*, 1519–1522; DOI:10.1134/S1070428009100169  
(l) R. C. Rastogi, R. H. Khan, K. R. Baruah, C. S. Sarmah, *Ind. J. Hetero. Chem.* **1992**, *1*, 247–248; (m) K. Noriaki, R. Naomi, U. Kimihisa, N. Yuji, T. Kotaro, S. Miho, K. Hideaki, Y. Hiroshi, N. Satoshi, M. Yuzuru, *Jpn. Kokai Tokkyo Koho* 2000, JP 2000154139 A 20000606.
18. (a) G. Choudhary, R. T. Naganaboina, R. K. Peddinti, *RSC Adv.*, **2014**, *4*, 17969–17979, and references cited therein; (b) F. A. Macias, D. Marin, A. Oliveros-Bastidas, J. M. G. Molinillo, *Nat. Prod. Rep.* **2009**, *26*, 478–489; DOI:10.1039/b700682a  
(c) J. Ilas, P. A. Stefanic, M. S. Dolenc, D. Kikelj, *Tetrahedron* **2005**, *61*, 7325–7348, and references therein. DOI:10.1016/j.tet.2005.05.037
19. For selected examples see: (a) K. C. Nicolaou, K. Sugita, P. S. Baran, Y. L. Zhong, *Angew. Chem., Int. Ed.* **2001**, *40*, 207–210; DOI:10.1002/1521-3773(20010105)40:1<207::AID-ANIE207>3.0.CO;2-K  
(b) K. C. Nicolaou, P. S. Baran, Y. L. Zhong, K. Sugita, *J. Am. Chem. Soc.* **2002**, *124*, 2212–2220; DOI:10.1021/ja012124x  
(c) M. Langeron, A. Neudorffer, M. Vuilhorgne, E. Blattes, M. -B. Fleury, *Angew. Chem. Int. Ed.* **2002**, *41*, 824–827. DOI:10.1002/1521-3773(20020301)41:5<824::AID-ANIE824>3.0.CO;2-Z
20. (a) C. Trebaul, J. Roncali, F. Garnier R. Guglielmetti, *Bull. Chem. Soc. Jpn.* **1987**, *60*, 2657; DOI:10.1246/bcsj.60.2657  
(b) R. B. Moffett, *J. Med. Chem.* **1966**, *9*, 475–478; DOI:10.1021/jm00322a006  
(c) A. Chilin, A. Confente, G. Pastorini, A. Guiotto, *Eur. J. Org. Chem.* **2002**, *12*, 1937–1940; DOI:10.1002/1099-0690(200206)2002:12<1937::AID-EJOC1937>3.0.CO;2-W  
(d) D. N. Nicolaides, D. R. Gautam, K. E. Litinas, D. J. Hadji-pavlou-Litina C. A. Kontogiorgis, *J. Heterocycl. Chem.* **2004**, *41*, 605–611; DOI:10.1002/jhet.5570410421  
(e) D. N. Nicolaides, R. W. Awad, E. A. Varella, *J. Heterocycl. Chem.* **1996**, *33*, 633–637; DOI:10.1002/jhet.5570330318  
(f) I. Yavari, S. Sour, M. Sirouspour, H. Djahaniani, *Synthesis*. **2006**, 3243–3249; (h) R. Ballini, A. Palmieri, M. A. K Talaq, S. Gabrielli, *Adv. Synth. Catal.* **2009**, *351*, 2611–2614; (i) D. Albanese, A. Donghi, D. Landini, V. Lupia, M. Penso, *Green Chem.* **2003**, *5*, 367–369; (j) D. Albanese, D. Landini, V. Lupi, M. Penso, *Adv. Synth. Catal.* **2002**, *344*, 299–302.
21. (a) Q. -Y. Zhang, B. -K. Liu, W. -Q. Chen, Q. Wu, Lin, X. -F. A *Green Chem.* **2008**, *10*, 972–977; DOI:10.1039/b806960c  
(b) K. M. H. Nguyen, L. Schwendimann, P. Gressens, M. Langeron, *Org. Biomol. Chem.* **2015**, *13*, 3749–3756.
22. (a) M. R. El Sayed Aly, H. H. Abd, El Razek Fodah, S. Y. Saleh, *Eur. J. Med. Chem.* **2014**, *76*, 517–530; DOI:10.1039/C5OB00049A  
(b) Y. P. Qian, Y. J. Shang, Q. F. Teng, J. Chang, G. J. Fan, X. Wei, R. R. Li, H. P. Li, X. J. Yao, F. Dai, B. Zhou, *Food Chemistry* **2011**, *126*, 241–248; (c) N. A. Shakil, M. K. Singh, M. Sathiyendiran, J. Kumar, J. C. Padaria, *Eur. J. Med. Chem.* **2013**, *59*, 120–131; (d) V. Oliveri, G. I. Grasso, F. Bellia, F. Attanasio, M. Viale, G. Vecchio, *Inorg. Chem.* **2015**, *54*, 2591–2602; (e) L. Savegnago, A. I. Vieira, N. Seus, B. S. Goldani, M. R. Castro, E. J. Lenardão, D. Alves, *Tetrahedron Lett.*, **2013**, *54*, 40–44; (f) A. Detsi, D. Bouloumbasi, K. C. Prousis, M. Koufaki, G. Athanasellis, G. Melagraki, A. Afantitis, O. Iggilsi-Markopoulou, C. Kontogiorgis, D. J. Hadjipavlou Litina, *J. Med. Chem.* **2007**, *50*, 2450–2458; (g) F. Pérez-Cruz, S. Vazquez-Rodriguez, M. J. Matos, A. Herrera-Morales, F. A. Villamena, A. Das, B. Gopalakrishnan, C. Olea-Azar, L. Santana, E. Uriarte, *J. Med. Chem.* **2013**, *56*, 6136–6145; (h) G. Mazzone, A. Galano, J. R. Alvarez-Idaboy, N. Russo, *J. Chem. Inf. Model.*, DOI:10.1021/acs.jcim.6b00006
23. (a) C. O. Kappe, *Angew. Chem. Int. Ed.* **2013**, *52*, 7924–7928; DOI:10.1002/anie.201304368  
(b) A. Sharma, P. Appukkuttan, E. V. Eycken, *Chem. Comm.* **2012**, *48*, 1623–37; DOI:10.1039/C1CC15238F  
(c) C. E. Bell, A. Y. Shaw, F. De Moliner, C. Hulme, *Tetrahedron* **2014**, *70* (1), 54–59; DOI:10.1016/j.tet.2013.11.035  
(d) A. Srinivas, M. Sunitha, K. Raju, B. Ravinder, S. Anusha, T. Rajasri, P. Swapna, D. Sushmitha, D. Swaroopa, G. Nikitha, C. G. Rao, *Acta Chim. Slov.* **2017**, *64*, 319–331; DOI:10.17344/acsi.2016.3153  
(e) L. Moradi, M. A. Sadegh, *Acta Chim. Slov.* **2017**, *64*, 506–512; DOI:10.17344/acsi.2017.3417  
(f) A. Srinivas, M. Santhosh, M. Sunitha, P. Karthik, K. Srinivas, K. V. Reddy, *Acta Chim. Slov.* **2016**, *63*, 827–836. DOI:10.17344/acsi.2015.2124
24. (a) P.-L. Wu, Y.-L. Hsu, C.-W. Jao, *J. Nat. Prod.* **2006**, *69*, 1467–1470; DOI:10.1021/np060395l  
(b) J. Mason, J. Bergman, T. Janosik, *J. Nat. Prod.*, **2008**, *71*, 1447–1450; DOI:10.1021/np800334j  
(c) L. Gross, F. Mohn, N. Moll, G. Meyer, R. Ebel, W. M. Abdel-Mageed, M. Jaspars, *Nat. Chem.* **2010**, *2*, 821–825; DOI:10.1038/nchem.765  
(d) L. Gross, *Nat. Chem.* **2011**, *3*, 273–278. DOI:10.1038/nchem.1008
25. (a) N. G. Baydar, G. Ozkan, S. Yasar, *Food Control*. **2007**, *18*, 113–1136; DOI:10.1016/j.foodcont.2005.09.001  
(b) M. S. Blois, *Nature* **1958**, *181*, 1199–1200; DOI:10.1038/1811199a0  
(c) O. P. Sharma, T. K. Bhat, *Food Chem.* **2009**, *113*, 1202–1205; DOI:10.1016/j.foodchem.2008.08.008  
(d) P. C. Eklund, O. K. Långvik, J. P. Warnå, T. O. Salmi, S. M. Willfor, R. E. Sjöholm, *Org. Biomol. Chem.* **2005**, *3*, 3336–3347; DOI:10.1039/b506739a  
(e) A. Faria, C. Calhau, V. de Freitas, N. Mateus, *J. Agric. Food. Chem.* **2006**, *54*, 2392–2397; DOI:10.1021/jf0526487  
(f) I. F. Benzie, J. J. Strain, *Anal. Biochem.* **1996**, *239*, 70–76. DOI:10.1006/abio.1996.0292
26. (a) W. Brand-Williams, M. E. Cuvelier, C. Berset, *Food Sci.*

Tech. 1995, 28, 25–30;

(b) I. Parejo, F. Viladomat, J. Bastida, A. Rosas-Romero, N. Flerlage, J. Burillo, C. Codina, *J. Agri. Food. Chem.* 2002, 50,

6882. DOI:10.1021/jf020540a

27. M. Danihelová, M. Veverka, E. Šturdík, S. Jantová, *Interdiscip. Toxicol.* 2013, 6, 209–216. DOI:10.2478/intox-2013-0031ww

## Povzetek

V prispevku je opisana okolju prijazna in s pomočjo mikrovalov spodbujena sinteza funkcionaliziranih (*Z*)-3-(2-okso-2-feniletiliden)-3, 4-dihidro-2*H*-benzo[*b*][1,4]oksazin-2-onov (**11a–n**) z odličnimi izkoristki (do 97%) in (*Z*)-3-(2-okso-2-feniletiliden)-3,4-dihidrokinoksalin-2(*1H*)-onov (**14a**) (do 96% izkoristek). Uporabna vrednost razvite metodologije je prikazana na sintezi spojin **11a**, **14c** in **14e** na gramski skali ter na sintezi protitumorskega alkaloida cefalandola A (**16**, 89% izkoristek). Vse sintetizirane spojine, **11a–n**, **14a–h** in **16**, so bile preizkušene na *in vitro* antioksidativno aktivnost, DPPH radikalsko lovljenje in FRAP test. Pri DPPH testiranju so se kot najbolj aktivne pokazale spojine **11a**, **14c** in **14e** z  $IC_{50}$  vrednostmi  $10.20 \pm 0.08$   $\mu\text{g/mL}$ ,  $9.89 \pm 0.15$   $\mu\text{g/mL}$  in  $8.97 \pm 0.13$   $\mu\text{g/mL}$  glede na standardno referenco (askorbinska kislina,  $IC_{50} = 4.57$   $\mu\text{g/mL}$ ), medtem, ko je pri FRAP antioksidativnem testu sedem spojin (**11c**, **11e**, **11i**, **11k**, **11l**, **14d** in **14h**) izkazalo višjo antioksidativno aktivnost kot referenčni standard BHT ( $C_{0.5\text{FRAP}} = 546.2$   $\mu\text{M}$ ). Poleg tega so študije citotoksičnosti spojin **11a**, **14c**, **14e** in **14h** hh pri MTT testiranju pokazale, da so te spojine netoksične do celičnih linij naravnih 3T<sub>3</sub> fibroblastov.

Scientific paper

# Magnetically Recyclable $\text{Fe}_3\text{O}_4/\text{GO-NH}_2/\text{H}_3\text{PMo}_{12}\text{O}_{40}$ Nanocomposite: Synthesis, Characterization, and Application in Selective Adsorption of Cationic Dyes from Water

Saeed Farhadi,<sup>\*,1</sup> Mohammad Hakimi<sup>2</sup> and Mansoureh Maleki<sup>2</sup><sup>1</sup> Chemistry Department, Lorestan University, Khoramabad 68151-44316, Iran.<sup>2</sup> Chemistry Department, Payame Noor University, Tehran 19395-4697, Iran.

\* Corresponding author: E-mail: sfarhadi1348@yahoo.com

Tel.: +986633120611 fax: +986633120618

Received: 03-08-2017

## Abstract

In this study, the  $\text{PMo}_{12}\text{O}_{40}^{3-}$  polyanion was immobilized chemically on amino functionalized magnetic graphene oxide nanosheets. The as-prepared ternary magnetic nanocomposite ( $\text{Fe}_3\text{O}_4/\text{GO-NH}_2/\text{H}_3\text{PMo}_{12}\text{O}_{40}$ ) was characterized by powder X-ray powder diffraction (XRD), fourier transformation infrared spectroscopy (FTIR), Raman spectroscopy, energy dispersive spectroscopy (EDX), field emission scanning electron microscopy (FESEM), BET surface area measurements, magnetic measurements (VSM) and atomic force microscopy (AFM). The results demonstrated the successful loading of  $\text{H}_3\text{PMo}_{12}\text{O}_{40}$  (~36.5 wt.%) on the surface of magnetic graphene oxide. The nanocomposite showed a higher specific surface area ( $77.07 \text{ m}^2/\text{g}$ ) than pure  $\text{H}_3\text{PMo}_{12}\text{O}_{40}$  ( $\leq 10 \text{ m}^2/\text{g}$ ). The adsorption efficiency of this nanocomposite for removing methylene blue (MB), rhodamine B (RhB) and methyl orange (MO) from aqueous solutions was evaluated. The nanocomposite showed rapid and selective adsorption for cationic dyes from mixed dye solutions. The adsorption rate and capacity of  $\text{Fe}_3\text{O}_4/\text{GO-NH}_2/\text{H}_3\text{PMo}_{12}\text{O}_{40}$  were enhanced as compared with GO, GO-NH<sub>2</sub>,  $\text{Fe}_3\text{O}_4/\text{GO-NH}_2$ , and  $\text{H}_3\text{PMo}_{12}\text{O}_{40}$  samples due to enhanced electrostatic attraction and hydrogen-bonding interactions. The nanocomposite is magnetically separated and reused without any change in structure. Thus, it could be a promising green adsorbent for removing organic pollutants in water.

**Keywords:** Graphene oxide nanosheets; Magnetic nanocomposite; Polyoxometalates; Organic dyes; Adsorption;  $\text{Fe}_3\text{O}_4$  nanoparticles.

## 1. Introduction

Industrial activities release an increasing amount of contaminants, such as metal ions, organic dyes, and cleaning agents, which has raised public concern.<sup>1,2</sup> So, wastewater treatment has attracted much attention in the past decades because of grievous effluent discharge of some organic dyes from plating, textile, and printing paper, plastic, cosmetic, pharmaceutical, and food industries that are resistant to biological degradation, making them quite difficult to remove from the wastewater.<sup>3,4</sup> Organic dyes are not only highly visible and, even in a small amount, decrease gas solubility in water, but also toxic, carcinogenic, and mutagenic for human beings.<sup>5-9</sup> Owing to their complex aromatic molecular structures, dyes are generally sta-

ble to light, heat and oxidizing agents.<sup>10</sup> Therefore, effective removal of dyes from dye-wastewater is essential. Among the various technologies such as photocatalytic degradation,<sup>11</sup> electrochemical degradation,<sup>12</sup> and adsorption,<sup>13</sup> adsorption is considered one of the most efficient and economical methods for water purification.<sup>14</sup> Many polymeric and inorganic adsorbents such as carbonaceous nanomaterials,<sup>15</sup> porous metal oxides,<sup>16</sup> clays,<sup>17</sup> chitosan,<sup>18</sup> zeolites,<sup>19</sup> and so on<sup>20,21</sup> were developed for removing pollutants from aqueous solutions. However, such adsorbents are associated with certain problems that limit their practical applications, such as low adsorption capacity, slow adsorption rate, and difficult separation of the adsorbents.<sup>22</sup> Furthermore, some of them are only effective for wastewater including low concentrations of dyes and they

are generally poor at selectively removing the targeted organic dye wastes. Hence, in this regard, it is extremely imperative to find a new desirable adsorption material, which not only is capable of reducing the organic dyes in dye-wastewater with high efficiency and fast adsorption rate but also can achieve selective separation and recovery of raw materials.

Polyoxometalates (POMs), as an outstanding class of anionic metal oxide clusters, have attracted great attention due to their earth-abundant source, rich topology and versatility, controllable shape and size, oxo-enriched surfaces, high electronegativity etc.,<sup>23</sup> which have various applications in many fields, such as catalysis,<sup>24</sup> optics,<sup>25</sup> magnetism,<sup>26</sup> biological medicine,<sup>27</sup> and dye adsorption.<sup>28</sup> The strong attraction of POMs to cationic dyes suggests that they are potential and suitable adsorbents for selectively capturing cationic dyes. However, there are still obvious disadvantages for POMs as adsorbents: (i) their relatively small surface area seriously obstructs the accessibility to the active sites and (ii) their excellent solubility in aqueous solution determines that they cannot be reused and recycled in the process of wastewater treatment. Therefore, plenty of remarkable work has been done to encapsulate POMs into porous solid matrices, such as activated carbon<sup>29</sup> and silica<sup>30</sup> for creating composite materials. Unfortunately, these methods sometimes lead to low POM loading; it is thus of vital significance to search for an applicable solid matrix to immobilize POMs, which might greatly improve their adsorption ability for target dyes.

Among various materials, graphene oxide (GO) has been proven as an effective sorbent for the removal of inorganic and organic pollutants owing to its large theoretical specific surface area (~2630 m<sup>2</sup>/g) and the presence of several active sites on its surface.<sup>31–39</sup> In addition, in comparison with other carbonaceous nanomaterials, GO may be more environmental friendly and have better biocompatibility.<sup>40</sup> However, it is difficult to separate it from aqueous solution because of its small particle size, causing serious health and environmental problems once it is discharged into the environment.<sup>41</sup> The centrifugation method needs a very high rate and the traditional filtration method may cause blockages of filters. Compared with traditional centrifugation and filtration methods, the magnetic separation method is considered as a rapid and effective technique for separating nanomaterials from aqueous solution.<sup>42,43</sup> Hence, magnetite/graphene composites with large specific surface area (enhancing the removal of water pollutants) and magnetic separation (facilitated by the recycling of the composites) have begun to be used in the field of environmental treatment.<sup>44–48</sup>

On the basis of the above discussion, in this work, amino functionalized magnetic graphene oxide (Fe<sub>3</sub>O<sub>4</sub>/GO-NH<sub>2</sub>) was synthesized by a facile method and used as a novel support for immobilizing Keggin-type PMo<sub>12</sub>O<sub>40</sub><sup>3-</sup> anions. This magnetically recoverable ternary nanocomposite material (Fe<sub>3</sub>O<sub>4</sub>/GO-NH<sub>2</sub>/H<sub>3</sub>PMo<sub>12</sub>O<sub>40</sub>) was pre-

pared by a simple acid-base electrostatic interaction between H<sub>3</sub>PMo<sub>12</sub>O<sub>40</sub> and amino groups of Fe<sub>3</sub>O<sub>4</sub>/GO-NH<sub>2</sub>. For one thing, PMo<sub>12</sub>O<sub>40</sub><sup>3-</sup> anion with highly electronegative and hydrophilic properties and structural stability could be utilized as a potential adsorbent for removal of the cationic dyes in dye-wastewater. For another, magnetic GO possesses outstanding porosity and extremely large surface area, and it is insoluble in water, which is an appropriate solid matrix to anchor Keggin-type PMo<sub>12</sub>O<sub>40</sub><sup>3-</sup> anions. The combination of polyoxoanions and Fe<sub>3</sub>O<sub>4</sub>/GO-NH<sub>2</sub> could improve the surface area and avoid the dissolution of POM. The hybrid nanomaterial exhibited superior adsorption rate and selective adsorption ability for the cationic dyes. Remarkably, this material exhibited a large-scale adsorption capacity of 426.7 mg/g for MB. Hence, it is a promising and environmental friendly adsorbent for removing and separating organic pollutants in dye-wastewater.

## 2. Experimental

### 2.1. Materials and Characterization Techniques

Graphite powder (C, 99.95%), 3-aminopropyltriethoxysilane (APTES, 99%), phosphomolybdic acid (H<sub>3</sub>PMo<sub>12</sub>O<sub>40</sub>, 98%), toluene, sulfuric acid (H<sub>2</sub>SO<sub>4</sub>, 98%), and potassium permanganate (KMnO<sub>4</sub>, 98%) were purchased from Merck Chemical Co. All other chemicals were commercially purchased and used without further purification. The infrared spectra were recorded at room temperature using a Shimadzu FT-IR 160 spectrophotometer in the 4000–400 cm<sup>-1</sup> region with KBr pellets. Powder XRD patterns were recorded on a Rigaku D-max C III X-ray diffractometer using Ni-filtered Cu K $\alpha$  radiation ( $\lambda = 1.54184 \text{ \AA}$ ). The morphology of samples was studied using a MIRA3 TESCAN scanning electron microscope equipped with an energy dispersive X-ray analyzer (EDX) for the elemental analysis. AFM images were recorded by multi-mode atomic force microscopy (ARA-AFM, model Full Plus, ARA Research Co., Iran). Magnetic measurements were carried out at room temperature using a vibrating sample magnetometer (VSM, Magnetic Daneshpajoh Kashan Co., Iran) with a maximum magnetic field of 10 kOe. Optical adsorption spectra were obtained using a Cary 100 Varian UV-Vis spectrophotometer in a wavelength range of 200–800 nm. The Brunauer–Emmett–Teller (BET) surface area was measured by N<sub>2</sub> adsorption measurements at 77 K using a Nova 2000 instrument. The concentration of Mo in the composite was determined by inductively coupled plasma atomic emission spectroscopy (ICP-AES, model OEC-730). A controllable Serial-Ultrasonics apparatus (James 6MD, England) operating at an ultrasonic frequency of 100 kHz with a nominal output power of 50 W was used to disperse samples.



## 2. 2. Preparation of Graphene Oxide

Graphene oxide (GO) was prepared by the modified Hummers method through the oxidation of graphite powder.<sup>49,50</sup> Graphite powder (2.0 g) and NaNO<sub>3</sub> (1.0 g) were mixed with 40 mL of concentrated H<sub>2</sub>SO<sub>4</sub> in a 500 mL flask and stirred for 1 h in an ice bath. Then KMnO<sub>4</sub> (6.0 g) was added into the vigorously stirred suspension slowly below 15 °C. The ice bath was then removed, and the mixture was stirred at room temperature until it slowly became brownish slurry. It was diluted with 100 mL of water. The reaction temperature was rapidly increased to 98 °C with effervescence, and the color changed to brown. After that, 200 mL of water and 20 mL of H<sub>2</sub>O<sub>2</sub> (30 wt.%) were added. For purification, the mixture was centrifuged and washed with 10% HCl and then deionized water several times to remove the residual metal ions and acid. After centrifuging and drying at room temperature, GO was obtained as a powder.

## 2. 3. Preparation of Magnetic Graphene Oxide (Fe<sub>3</sub>O<sub>4</sub>/GO)

0.25 g of GO was dispersed in 90 mL of water by sonication for 1 h. Then, 0.84 g of (NH<sub>4</sub>)<sub>2</sub>Fe(SO<sub>4</sub>)<sub>2</sub> and 2.08 g of (NH<sub>4</sub>)Fe(SO<sub>4</sub>)<sub>2</sub> were added to the GO dispersion and its pH was adjusted at 12 by adding 1 mol/L NaOH. The mixture was stirred at 50 °C for 2 h, filtered and washed with water and ethanol three times. The resulting solid was Fe<sub>3</sub>O<sub>4</sub>/GO.

## 2. 4. Preparation of Aminopropyl Functionalized Magnetic Graphene Oxide (Fe<sub>3</sub>O<sub>4</sub>/GO-NH<sub>2</sub>)

To a round bottom flask, 0.40 g of the as-synthesized Fe<sub>3</sub>O<sub>4</sub>/GO dispersed in 50 mL of water, 5 mL of APTES, and 150 mL of ethanol were added. The mixture was stirred for 30 min at room temperature and refluxed at 80 °C for 24 h. After the reaction, the solid was separated by a magnet and washed with ethanol to remove the unreacted APTES. The final product was dried at 80 °C in vacuum for 12 h to obtain Fe<sub>3</sub>O<sub>4</sub>/GO-NH<sub>2</sub>.

## 2. 5. Preparation of the Fe<sub>3</sub>O<sub>4</sub>/GO-NH<sub>2</sub>/H<sub>3</sub>PMo<sub>12</sub>O<sub>40</sub> Hybrid Nanomaterial

1 g of the as-prepared Fe<sub>3</sub>O<sub>4</sub>/GO-NH<sub>2</sub> was dispersed in 80 mL of water and sonicated for 1 h. Then, 1 g of H<sub>3</sub>PMo<sub>12</sub>O<sub>40</sub> in 200 mL of ethanol was added and sonicated for another 1 h. The resulting mixture was stirred at room temperature for 24 h, filtered, and washed with deionized water and ethanol three times to remove the unreacted H<sub>3</sub>PMo<sub>12</sub>O<sub>40</sub>. The final product was dried at 60 °C in open air to obtain magnetic Fe<sub>3</sub>O<sub>4</sub>/GO-NH<sub>2</sub>/H<sub>3</sub>PMo<sub>12</sub>O<sub>40</sub> hybrid nanomaterial. Elemental analysis (ICP-AES) showed that the Mo content in Fe<sub>3</sub>O<sub>4</sub>/GO-NH<sub>2</sub>/H<sub>3</sub>PMo<sub>12</sub>O<sub>40</sub> was

32.55%. According to the elemental analysis results and molecular weight of H<sub>3</sub>PMo<sub>12</sub>O<sub>40</sub>, the loading amount (wt.%) of H<sub>3</sub>PMo<sub>12</sub>O<sub>40</sub> in Fe<sub>3</sub>O<sub>4</sub>/GO-NH<sub>2</sub>/H<sub>3</sub>PMo<sub>12</sub>O<sub>40</sub> was estimated to be 36.5%.

## 2. 6. Dye Adsorption Tests

The aqueous stock solutions of dyes (500 mg/L) were prepared by dissolving solid dyes (MB, RhB, and MO) in deionized water. Working solutions of dyes, when required, were prepared by successive dilution of the stock solution with deionized water. The adsorption experiments of dyes were performed in a 100 mL glass beaker and the adsorption reaction temperature was maintained at 25 °C. In a typical experiment, 25 mg of the as-prepared Fe<sub>3</sub>O<sub>4</sub>/GO-NH<sub>2</sub>/H<sub>3</sub>PMo<sub>12</sub>O<sub>40</sub> hybrid nanomaterial was added into 50 mL of dye aqueous solution (C<sub>0</sub> = 25 mg/L) and stirred in the dark and at predetermined time intervals, a small portion (3 mL) of the dye solution was pipetted out and the solid adsorbent was separated by an external magnet. The concentration (C<sub>t</sub>) of the dye in the clear solution was determined by measuring the absorbance of the solution at fixed wavelengths, 664 nm for MB, 554 nm for RhB, and 463 nm for MO, using a UV-Vis spectrophotometer. A similar experiment was also performed with 50 mL of different concentrations of MB solutions (5, 15, 25, 35, and 50 mg/L). Also, the hybrid nanomaterial was transferred into the mixtures of MB/MO (v:v 1/1, 50 mL, 25 mg/L), MO/RhB, and MB/MO/RhB. UV-Vis spectroscopy was performed to determine the selective adsorption ability of hybrid nanomaterial at given time intervals. Furthermore, the adsorption capability of the Fe<sub>3</sub>O<sub>4</sub>, Fe<sub>3</sub>O<sub>4</sub>/GO, Fe<sub>3</sub>O<sub>4</sub>/GO-NH<sub>2</sub>, and H<sub>3</sub>PMo<sub>12</sub>O<sub>40</sub> samples toward MB dye solution was evaluated under similar conditions as described above. 25 mg of the as-prepared adsorbent was added into 50 mL of 25 mg/L MB solution and stirred in the dark. Dye removal ability (%) was calculated by measuring the dye absorbance at 664 nm before and after adsorption process at room temperature. Finally, Fe<sub>3</sub>O<sub>4</sub>/GO-NH<sub>2</sub>/H<sub>3</sub>PMo<sub>12</sub>O<sub>40</sub> was investigated for its recycling property for the removal of MB after Fe<sub>3</sub>O<sub>4</sub>/GO-NH<sub>2</sub>/H<sub>3</sub>PMo<sub>12</sub>O<sub>40</sub> was separated, washed with ethanol, and dried in a vacuum oven. In all experiments, the adsorption efficiency (η%) and adsorption capacity (q<sub>t</sub>; mg/g) were calculated according to the following equations:

$$\eta\% = [(C_0 - C_t)/C_0] \times 100 = [(A_0 - A_t)/A_0] \times 100 \quad (1)$$

$$q_t = [(C_0 - C_t) \times V]/m$$

Where C<sub>0</sub> (mg/L) and A<sub>0</sub> are the initial dye concentration and absorbance before removal at initial time t = 0, C<sub>t</sub> (mg/L) and A<sub>t</sub> are the concentration and absorbance of dye remaining in the solution after treatment with adsorbent at time t, q<sub>t</sub> is the amount of adsorbed MB molecules on the adsorbent (in mg/g). V (in L) is the initial volume of the MB solution and m (in g) is the mass of the adsorbent.

### 3. Results and Discussion

#### 3. 1. Characterization of the $\text{Fe}_3\text{O}_4/\text{GO}-\text{NH}_2/\text{H}_3\text{PMo}_{12}\text{O}_{40}$ Hybrid Nanomaterial

The GO is an inexpensive, stable, environmentally benign, easily available solid material, and contains rich oxidation functional groups, such as hydroxyl, epoxide, carboxyl, and carbonyl groups. Due to these functional groups, GO can well disperse in polar solvents and forms a homogenous colloidal suspension, which facilitates the contact between reactant and catalytic active site.<sup>51</sup> On the other hand, these rich functional groups can be easily reacted with organic molecules to generate stable covalent functional GO.<sup>19–21</sup> These suggest that attaching organic bases on GO might afford an efficient, reusable and environmentally benign base support for heteropolyacids such as  $\text{PMo}_{12}$ . In this work, Keggin-type  $\text{H}_3\text{PMo}_{12}\text{O}_{40}$  was immobilized onto 3-aminopropyl functionalized GO nanosheets decorated with magnetic  $\text{Fe}_3\text{O}_4$  nanoparticles. The preparation of the  $\text{Fe}_3\text{O}_4/\text{GO}-\text{NH}_2/\text{H}_3\text{PMo}_{12}\text{O}_{40}$  hybrid is illustrated in Figure 1. The surface of  $\text{GO}-\text{NH}_2$  is positively charged by the protonation of  $-\text{NH}_2$ , which helps in anchoring the  $\text{PMo}_{12}\text{O}_{40}^{3-}$  anion due to electrostatic attraction. To confirm the successful construction of the  $\text{Fe}_3\text{O}_4/\text{GO}-\text{NH}_2/\text{H}_3\text{PMo}_{12}\text{O}_{40}$  hybrid, elemental analysis was employed. It revealed that  $\text{Fe}_3\text{O}_4/\text{GO}-\text{NH}_2/\text{H}_3\text{PMo}_{12}\text{O}_{40}$  contains 36.5% Mo, indicating that  $\text{H}_3\text{PMo}_{12}\text{O}_{40}$  molecules were anchored on GO nanosheets. Due to the electrostatic attraction of the absorbed  $\text{PMo}_{12}\text{O}_{40}^{3-}$  and  $-\text{NH}_3^+$  group, the hydrogen bonds between  $-\text{NH}_3^+$  and  $\text{H}_3\text{PMo}_{12}\text{O}_{40}$  molecules are reinforced.<sup>52–54</sup> These are the possible reasons for the significant enhancement of  $\text{Fe}_3\text{O}_4/\text{GO}-\text{NH}_2/\text{H}_3\text{PMo}_{12}\text{O}_{40}$  adsorptivity. Moreover, the structure and composition of the hybrid nanomaterial was characterized by XRD, FT-IR, Raman spectra, EDX, SEM, AFM, VSM, and BET surface area analyses.

Figure 2 displays the XRD patterns for  $\text{Fe}_3\text{O}_4$ ,  $\text{Fe}_3\text{O}_4/\text{GO}-\text{NH}_2$ , and  $\text{Fe}_3\text{O}_4/\text{GO}-\text{NH}_2/\text{H}_3\text{PMo}_{12}\text{O}_{40}$  samples. All

the diffraction patterns in Figure 2(a)–(c) are similar and can be indexed to the  $\text{Fe}_3\text{O}_4$  phase (JCPDS No. 41-1488). No characteristic diffraction peaks of the  $\text{H}_3\text{PMo}_{12}\text{O}_{40}$  appeared which presumably was due to the low content incorporation of  $\text{H}_3\text{PMo}_{12}\text{O}_{40}$ . Also this result implies that the Keggin unit homogeneously disperses into the GO

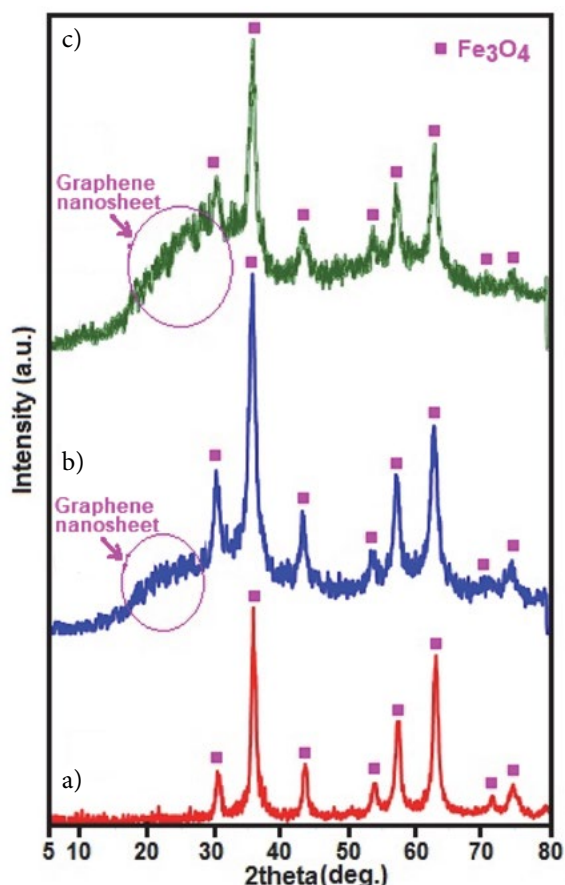


Figure 2. XRD patterns of (a) pure  $\text{Fe}_3\text{O}_4$ , (b)  $\text{Fe}_3\text{O}_4/\text{GO}-\text{NH}_2$  and (c)  $\text{Fe}_3\text{O}_4/\text{GO}-\text{NH}_2/\text{H}_3\text{PMo}_{12}\text{O}_{40}$ .

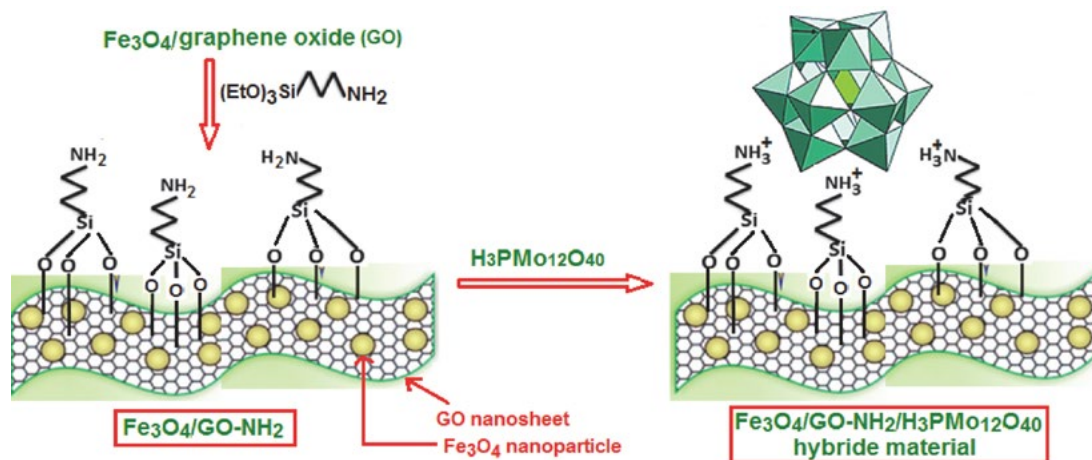


Figure 1. The preparation procedure to attach  $\text{H}_3\text{PMo}_{12}\text{O}_{40}$  on the surface of aminopropyl functionalized magnetic graphene oxide.

nanosheets, which will help to enhance the adsorption activity of the hybrid nanomaterial. Moreover, no characteristic diffraction peaks for GO are observed in the pattern indicating that the GO nanosheets do not stack during the synthesis. The reason can be attributed to the  $\text{Fe}_3\text{O}_4$  and  $\text{H}_3\text{PMo}_{12}\text{O}_{40}$  nanoparticles anchored on the surfaces of GO to prevent the exfoliated GO nanosheets from restacking.<sup>55</sup> However, a broad characteristic peak for graphene nanosheets at about  $2\theta = 23$  appeared, suggesting that the GO was reduced to graphene during the functionalization process.

The FT-IR spectra of synthesized materials are shown in Figure 3. The FT-IR spectrum of the GO in Figure 3(a) shows the C=O and graphitic C=C stretching bands at about 1735 and 1626  $\text{cm}^{-1}$ , respectively.<sup>56</sup> Also, the strong band at 1030  $\text{cm}^{-1}$  is related to the stretching vibrations of the C–OH bonds. In the spectrum of  $\text{Fe}_3\text{O}_4/\text{GO}-\text{Si}(\text{CH}_2)_3\text{NH}_2$  sample (abbreviated as  $\text{Fe}_3\text{O}_4/\text{GO}-\text{NH}_2$ ) in Figure 3(b), the strong band at about 588  $\text{cm}^{-1}$  is assigned to the Fe–O stretching vibration of the spinel-type  $\text{Fe}_3\text{O}_4$  structure.<sup>57</sup> The presence of Si–O bond was confirmed by a strong band at about 1116  $\text{cm}^{-1}$  assigned to the Si–O–C stretching vibration.<sup>58,59</sup> Also, two broad bands at 3430 and 1630  $\text{cm}^{-1}$  can be ascribed to the stretching and bending modes of  $-\text{NH}_2$  groups, respectively. The presence of the anchored propyl chain of APTES was confirmed by C–H stretching vibrations at 2926 and 2850  $\text{cm}^{-1}$ .<sup>59</sup> The FT-IR spectrum of the  $\text{Fe}_3\text{O}_4/\text{GO}-\text{NH}_2$  exhibits peaks at 1223 and 1028  $\text{cm}^{-1}$  corresponding to C–N and C–OH, respectively.<sup>60</sup> These show the successful grafting of APTES onto the magnetic GO sheet through covalent bonds. It is well known that Keggin-type  $\text{PMo}_{12}\text{O}_{40}^{3-}$  polyoxometalate contains a cluster of Mo(VI) ions linked by oxygen atoms with a tetrahedral phosphate group. Oxygen atoms form four physically distinct bonds ( $\text{P}-\text{O}_a$ ,  $\text{Mo}-\text{O}_t$ ,  $\text{Mo}-\text{O}_b$ – $\text{Mo}$ , and  $\text{Mo}-\text{O}_c$ – $\text{Mo}$  bonds), which have distinct infrared signatures as shown in Figure 3(c): 1066  $\text{cm}^{-1}$  for asymmetric stretch vibration of  $\text{P}-\text{O}_a$  ( $\text{O}_a$  corresponds to oxygen atom of tetrahedral phosphate group), 966  $\text{cm}^{-1}$  for asymmetric stretch vibration of  $\text{Mo}=\text{O}_t$  ( $\text{O}_t$  corresponds to the terminal oxygen atoms), 870  $\text{cm}^{-1}$  for bending vibration of  $\text{Mo}-\text{O}_b$ – $\text{Mo}$  ( $\text{O}_b$  corresponds to oxygen atom bridging the two tungsten atoms), and 786  $\text{cm}^{-1}$  for bending vibration of  $\text{Mo}-\text{O}_c$ – $\text{Mo}$  ( $\text{O}_c$  represents oxygen atom at the corners of the Keggin structure).<sup>61</sup> The FT-IR spectrum of the hybrid nanomaterial sample is shown in Figure 3(d), the absorption peaks of  $\text{PMo}_{12}\text{O}_{40}^{3-}$  cluster at 1053, 945, 875, and 798  $\text{cm}^{-1}$  corresponding to the  $\text{P}-\text{O}_a$ ,  $\text{Mo}=\text{O}_t$ ,  $\text{Mo}-\text{O}_b$ – $\text{Mo}$  and  $\text{Mo}-\text{O}_c$ – $\text{Mo}$  band vibrations, and the vibrational bands of  $\text{Fe}_3\text{O}_4/\text{GO}-\text{NH}_2$  located around 1605, 1383, 1042, 746, and 543  $\text{cm}^{-1}$  were all observed in the IR spectrum of the hybrid nanomaterial which demonstrates the coexistence of  $\text{PMo}_{12}\text{O}_{40}^{3-}$ ,  $\text{Fe}_3\text{O}_4$ , and  $\text{GO}-\text{NH}_2$  in the hybrid nanomaterial. The red/blue shift of peaks of the  $\text{Fe}_3\text{O}_4/\text{GO}-\text{NH}_2/\text{H}_3\text{PMo}_{12}\text{O}_{40}$  compared with the parent  $\text{H}_3\text{PMo}_{12}\text{O}_{40}$  can be attributed to strong attraction between

negatively charged  $\text{PMo}_{12}\text{O}_{40}^{3-}$  and positively charged  $\text{Fe}_3\text{O}_4/\text{GO}-\text{NH}_3^+$  surface.<sup>62,63</sup> Raman spectroscopy is a powerful tool to characterize the significant structural changes in GO during the  $\text{Fe}_3\text{O}_4/\text{GO}-\text{NH}_2/\text{H}_3\text{PMo}_{12}\text{O}_{40}$  hybrid synthesis.

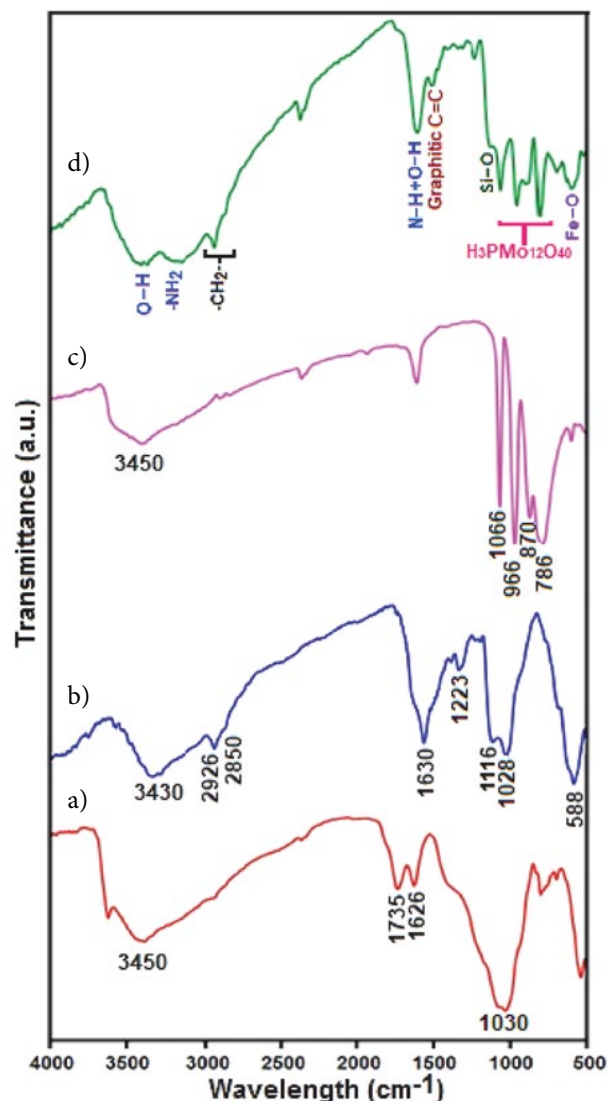
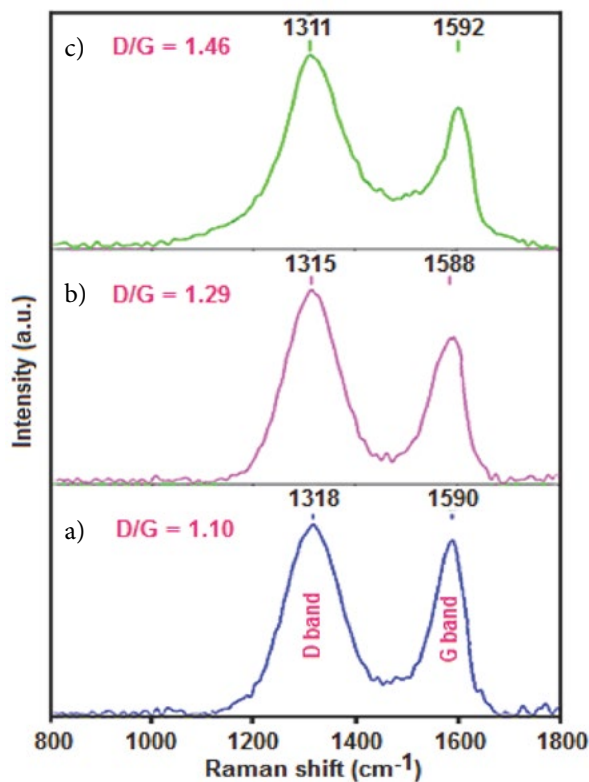


Figure 3. IR spectra of (a) pure GO, (b)  $\text{Fe}_3\text{O}_4/\text{GO}-\text{NH}_2$  and (c)  $\text{H}_3\text{PMo}_{12}\text{O}_{40}$  and (d)  $\text{Fe}_3\text{O}_4/\text{GO}-\text{NH}_2/\text{H}_3\text{PMo}_{12}\text{O}_{40}$ .

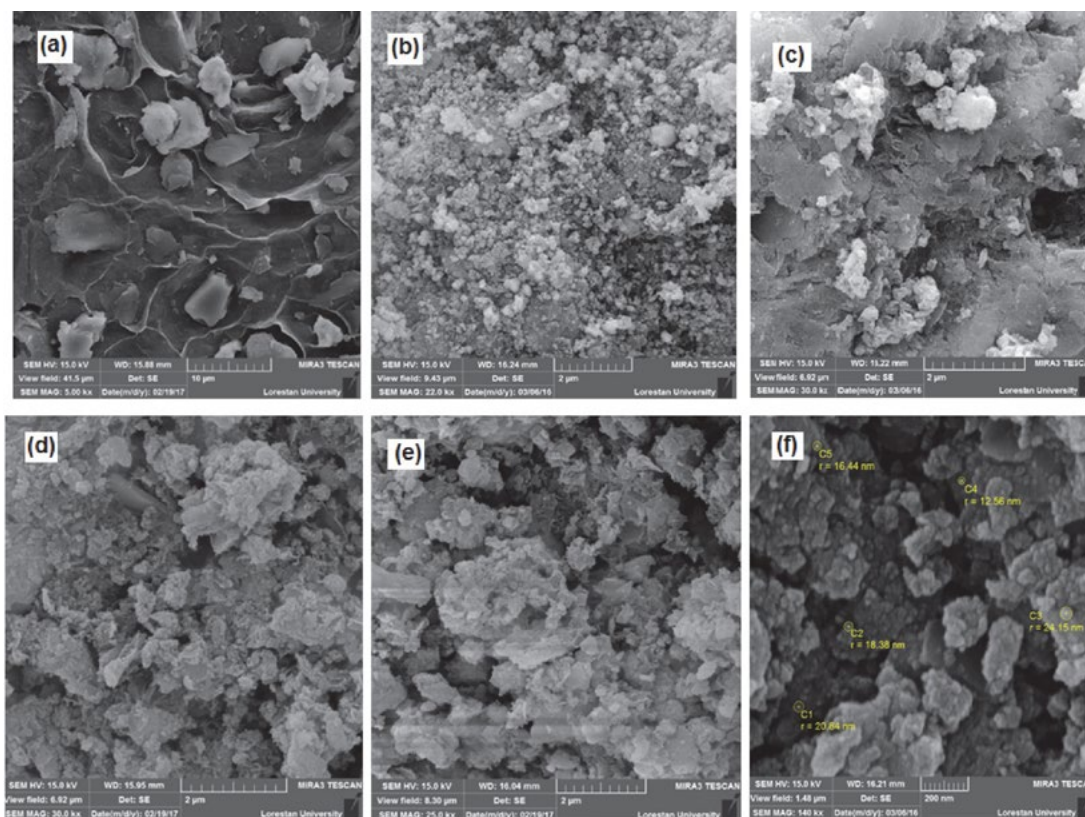
Figure 4 presents the Raman spectra of GO,  $\text{Fe}_3\text{O}_4/\text{GO}-\text{NH}_2$  and  $\text{Fe}_3\text{O}_4/\text{GO}-\text{NH}_2/\text{H}_3\text{PMo}_{12}\text{O}_{40}$ . All the samples display the characteristic D ( $\text{sp}^3$  carbon atoms of disorders and defects) and G bands ( $\text{sp}^2$  carbon atoms in graphitic sheets).<sup>64,65</sup> As compared with the D and G bands of pure GO (D, 1318  $\text{cm}^{-1}$ ; G, 1590  $\text{cm}^{-1}$ ), the two bands of  $\text{Fe}_3\text{O}_4/\text{GO}-\text{NH}_2$  shift to D, 1315  $\text{cm}^{-1}$  and G, 1588  $\text{cm}^{-1}$ , suggesting the successful silylation of GO with APTES. After anchoring the  $\text{H}_3\text{PMo}_{12}\text{O}_{40}$  on the  $\text{Fe}_3\text{O}_4/\text{GO}-\text{NH}_2$ , further shifts in D and G bands are found (D, 1311

$\text{cm}^{-1}$  and G,  $1592 \text{ cm}^{-1}$ ). These shifts in Raman peaks can be attributed to strong interaction between  $\text{PMo}_{12}\text{O}_{40}^{3-}$  anion and positively charged  $\text{Fe}_3\text{O}_4/\text{GO-NH}_3^+$  in  $\text{Fe}_3\text{O}_4/\text{GO-NH}_2/\text{H}_3\text{PMo}_{12}\text{O}_{40}$  hybrid,<sup>66</sup> which is consistent with the FT-IR analysis. In addition, it is shown that the D/G intensity ratios of  $\text{Fe}_3\text{O}_4/\text{GO-NH}_2$  and  $\text{Fe}_3\text{O}_4/\text{GO-NH}_2/\text{H}_3\text{PMo}_{12}\text{O}_{40}$  are higher than that of GO, suggesting a higher level of disorder of the graphene layers during the functionalization process.<sup>67</sup> Also, this is proposed to be caused by the reduction of GO during the syntheses of  $\text{GO-NH}_2$  and  $\text{Fe}_3\text{O}_4/\text{GO-NH}_2/\text{H}_3\text{PMo}_{12}\text{O}_{40}$  hybrid as confirmed by the XRD data.<sup>68</sup> The peaks of Keggin structure did not appear, which indicated that  $\text{H}_3\text{PMo}_{12}\text{O}_{40}$  species on the  $\text{Fe}_3\text{O}_4/\text{GO-NH}_2$  sample were in a high-dispersed state. This result was identical to the XRD results.

SEM images indicating the microstructural features of GO,  $\text{Fe}_3\text{O}_4$ ,  $\text{Fe}_3\text{O}_4/\text{GO-NH}_2$ , and  $\text{Fe}_3\text{O}_4/\text{GO-NH}_2/\text{H}_3\text{PMo}_{12}\text{O}_{40}$  hybrid nanomaterial are shown in Figure 5. The SEM micrograph of pure GO in Figure 5(a) shows the highly porous and layered structure of GO having large stacks, possibly consisting of hundreds of GO nanosheets. It should also be noted that the surfaces of the GO sheets are quite flat and smooth. Figure 5(b) shows the SEM micrograph of sphere-like  $\text{Fe}_3\text{O}_4$  nanoparticles. It is worthy to observe that the lateral size of graphitic nanosheets was not disrupted with the oxidation, The SEM image of  $\text{Fe}_3\text{O}_4/\text{GO-NH}_2$  in Figure 5(c) clearly shows GO nanos-



**Figure 4.** Raman spectra of (a) GO, (b)  $\text{Fe}_3\text{O}_4/\text{GO-NH}_2$  and (c)  $\text{Fe}_3\text{O}_4/\text{GO-NH}_2/\text{H}_3\text{PMo}_{12}\text{O}_{40}$ .



**Figure 5.** SEM images of (a) GO, (b)  $\text{Fe}_3\text{O}_4$ , (c)  $\text{Fe}_3\text{O}_4$ -GO, (d)  $\text{Fe}_3\text{O}_4/\text{GO-NH}_2$ , and (e-f)  $\text{Fe}_3\text{O}_4/\text{GO-NH}_2/\text{H}_3\text{PMo}_{12}\text{O}_{40}$  hybrid nanomaterial.

heets were successfully decorated with the  $\text{Fe}_3\text{O}_4$  nanoparticles consisting of small and elongated grains. It was found that the average size of  $\text{Fe}_3\text{O}_4$  nanoparticles was in the range of 20–30 nm. Figure 5(d)–(f) shows the morphology of the  $\text{Fe}_3\text{O}_4/\text{GO-NH}_2/\text{H}_3\text{PMo}_{12}\text{O}_{40}$  hybrid nanomaterial. As can be seen, agglomerated  $\text{Fe}_3\text{O}_4$  and  $\text{PMo}_{12}$  nanoparticles completely covered the surfaces of large graphene sheets. It should also be noted that the micropores between the graphene sheets were evenly filled up with the  $\text{Fe}_3\text{O}_4$  nanoparticles as clearly seen in the images of stack edges given in Figure 5(d)–(f). All the micrographs of the hybrid nanomaterial clearly indicated that the surface properties of the modified GO product were strongly affected. Opposite to pure GO, the surfaces of GO nanosheets in the hybrid nanomaterial are rough, and the edges are highly crumpled. It can be concluded that microstructural properties of  $\text{Fe}_3\text{O}_4/\text{GO-NH}_2/\text{H}_3\text{PMo}_{12}\text{O}_{40}$  hybrid nanomaterial encourage preparing the highly porous, magnetically active and structurally layered nanomaterials.

AFM is a beneficial tool for studying various morphological features and parameters, since it has the advantage of probing in deep insights of surface topography qualitatively due to its both lateral and vertical nanometer scale spatial resolution. The AFM images in Figure 6 display the surface morphology of the  $\text{Fe}_3\text{O}_4/\text{GO-NH}_2/\text{H}_3\text{PMo}_{12}\text{O}_{40}$ . As observed in Figure 6(a), the AFM image reveals the appearance of sphere-like nanoparticles and their respective particle size and morphology clearly were close to those determined by the SEM images. As can be seen from Figure 6(b), the surface of the composite showed a porous and uniform packed structure with size (height) of particles on the graphene sheet to be approximately 20 nm. Thus, the  $\text{Fe}_3\text{O}_4/\text{GO-NH}_2/\text{H}_3\text{PMo}_{12}\text{O}_{40}$  could provide a rough and coarse surface with porosity for adsorption uses. The results are in good agreement with BET results and SEM images.

Further investigation was carried out by energy dispersive X-ray spectroscopy (EDX) to characterize the composition of the as-prepared  $\text{Fe}_3\text{O}_4/\text{GO-NH}_2/\text{H}_3\text{PMo}_{12}\text{O}_{40}$  hybrid nanomaterial. Figure 7(a)–(i) show the EDX spectrum and a representative SEM image of the hybrid nanomaterial with corresponding EDX elemental mappings. The presence of C, N, Si, O, Fe, P, and Mo elements in the composite can be proved by the EDX elemental spectrum (Figure 7(a)). As presented in Figure 7(b)–(f), the corresponding elemental mapping distribution shows the existence of C, N, Si, O, Fe, P, and Mo. From the maps, it can be seen that the elements are uniformly distributed over the hybrid nanomaterial, confirming the homogeneity of the sample. The P and Mo elements were from  $\text{H}_3\text{PMo}_{12}\text{O}_{40}$  and the results further indicate that the  $\text{H}_3\text{PMo}_{12}\text{O}_{40}$  particles were successfully supported on the surface of the  $\text{Fe}_3\text{O}_4/\text{GO-NH}_2$ .

The magnetic properties of the pure  $\text{Fe}_3\text{O}_4$  and  $\text{Fe}_3\text{O}_4/\text{GO-NH}_2/\text{H}_3\text{PMo}_{12}\text{O}_{40}$  samples were investigated by VSM at room temperature, and the magnetic hysteresis loops are depicted in Figure 8. It is clear that both  $\text{Fe}_3\text{O}_4$  and the  $\text{Fe}_3\text{O}_4/\text{GO-NH}_2/\text{H}_3\text{PMo}_{12}\text{O}_{40}$  composite are soft magnetic materials due to their coercivity ( $H_c$ ) of zero.<sup>69</sup> Moreover, they are also superparamagnetic materials, as their magnetic hysteresis loops passed through the origin of the coordinates. The saturation magnetization values of  $\text{Fe}_3\text{O}_4$  and  $\text{Fe}_3\text{O}_4/\text{GO-NH}_2/\text{H}_3\text{PMo}_{12}\text{O}_{40}$  are 27.50 and 9.16 emu/g, respectively. The saturation magnetization of the magnetic composite decreases by approximately 70% compared with that of pure  $\text{Fe}_3\text{O}_4$ , which can be attributed to the less magnetic source component ( $\text{Fe}_3\text{O}_4$ ) per gram in the composite sample. However, the saturation magnetization of the composite could satisfy the requirements of easy separation in the suspension solution using an extra magnet after reaction as shown in the inset of Figure 8. Thus, the  $\text{Fe}_3\text{O}_4/\text{GO-NH}_2/\text{H}_3\text{PMo}_{12}\text{O}_{40}$  composite can be easily separated using a magnetic separation process after being used for the removal of dye pollutants from aqueous solutions.

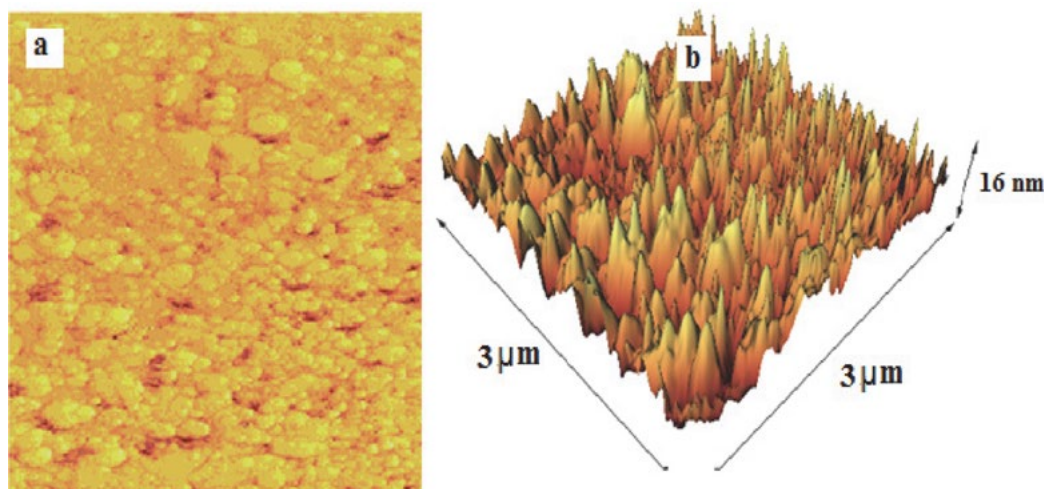
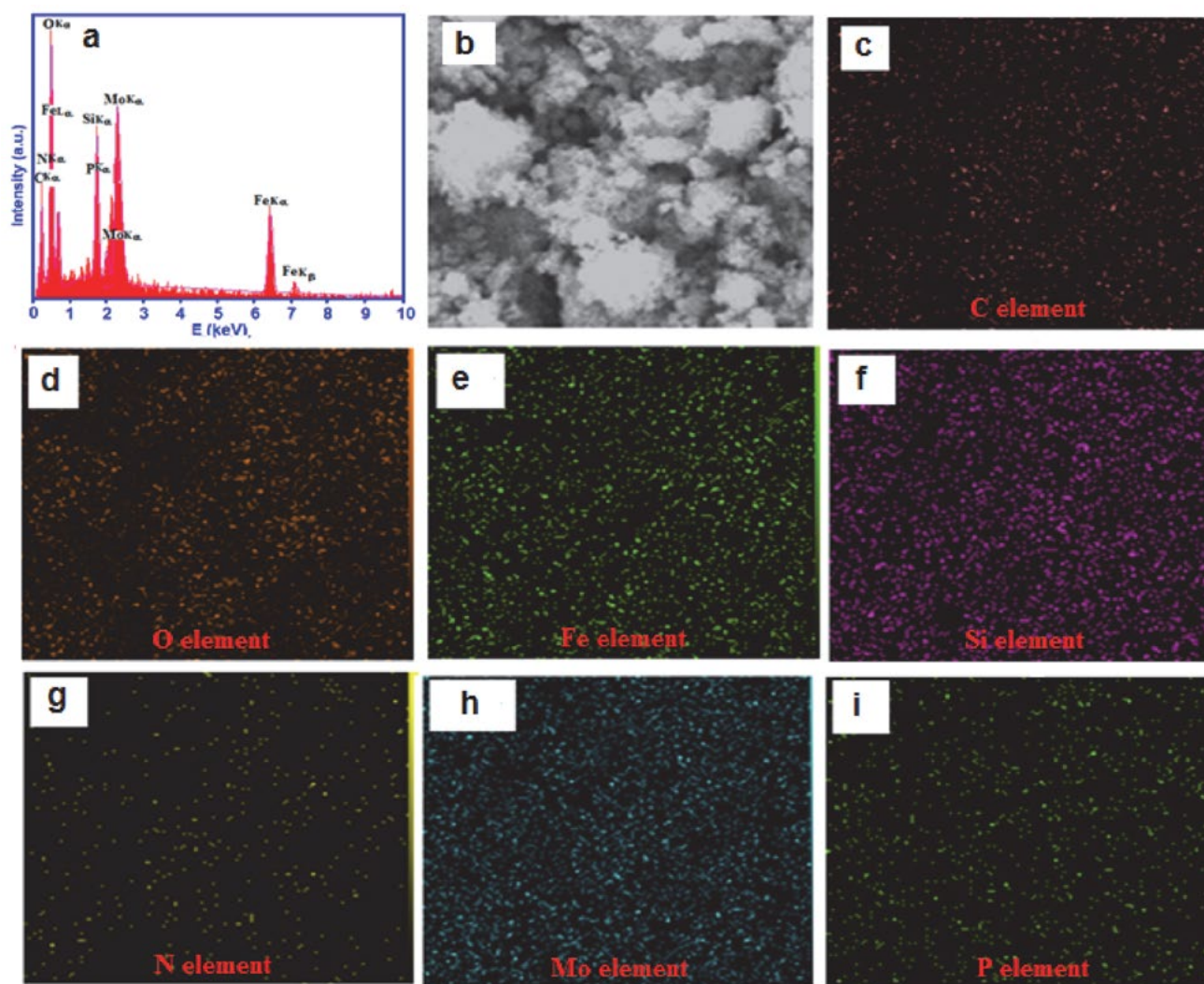
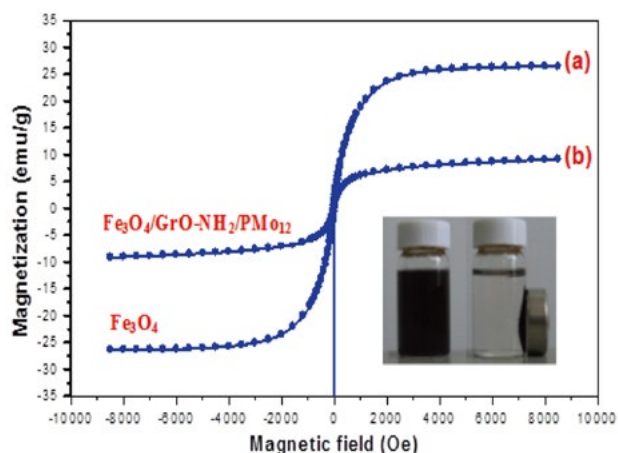


Figure 6. (a) AFM image and (b) height profile of  $\text{Fe}_3\text{O}_4/\text{GO-NH}_2/\text{H}_3\text{PMo}_{12}\text{O}_{40}$  in a three dimensional image.



**Figure 7.** (a) EDX spectrum, and (b)-(i) a representative SEM image of the  $\text{Fe}_3\text{O}_4/\text{GO-NH}_2/\text{H}_3\text{PMo}_{12}\text{O}_{40}$  hybrid nanomaterial with corresponding EDX elemental mappings.



**Figure 8.** Magnetic hysteresis loop of (a)  $\text{Fe}_3\text{O}_4$  and (b)  $\text{Fe}_3\text{O}_4/\text{GrO-NH}_2/\text{PMO}_{12}$  at room temperature. The inset shows the behaviour of the nanocomposite under an external magnetic field.

$\text{N}_2$  adsorption/desorption measurements were performed to investigate specific surface area and the pore size distribution of the  $\text{Fe}_3\text{O}_4/\text{GO-NH}_2/\text{H}_3\text{PMo}_{12}\text{O}_{40}$ . As can be seen in Figure 9(a), the nitrogen adsorption isotherm is a typical type IV curve with a fine H1-type hysteresis loop in the range of ca. 0.8–1.0  $p/p_0$ , indicating the existence of mesoporous structure.<sup>70,71</sup> The BET surface area is measured to be 76.36  $\text{m}^2/\text{g}$  that is much higher than the value of pure POM ( $\leq 10 \text{ m}^2/\text{g}$ ). In addition, the total pore volume is 0.01  $\text{cm}^3/\text{g}$  and according to the corresponding Barrett–Joyner–Halenda (BJH) pore size distribution curve in Figure 9(b), the pore size distribution of the  $\text{Fe}_3\text{O}_4/\text{GO-NH}_2/\text{H}_3\text{PMo}_{12}\text{O}_{40}$  shows a peak centered at around 2.28 nm. Such porosity of  $\text{Fe}_3\text{O}_4/\text{GO-NH}_2/\text{H}_3\text{P-Mo}_{12}\text{O}_{40}$  composite can improve the adsorption performance. It can be concluded that introduction of magnetic  $\text{Fe}_3\text{O}_4/\text{GO-NH}_2$  has a good effect on the structure of  $\text{H}_3\text{P-}$

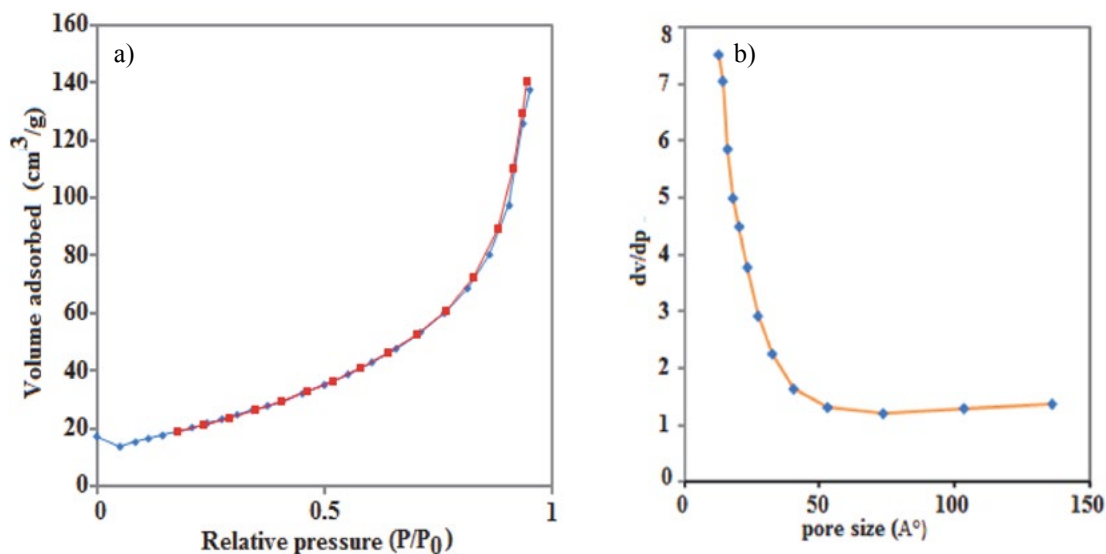


Figure 9. (a)  $N_2$  adsorption–desorption isotherm and (b) pore size distribution of  $Fe_3O_4/GO-NH_2/H_3PMo_{12}O_{40}$ .

$Mo_{12}O_{40}$  and increases the surface area and porosity of POM which are all useful factors for improving the adsorption performance.

### 3. 2. Dye Adsorption Studies

To evaluate the adsorption capability of  $Fe_3O_4/GO-NH_2/H_3PMo_{12}O_{40}$  hybrid nanomaterial for removing or-

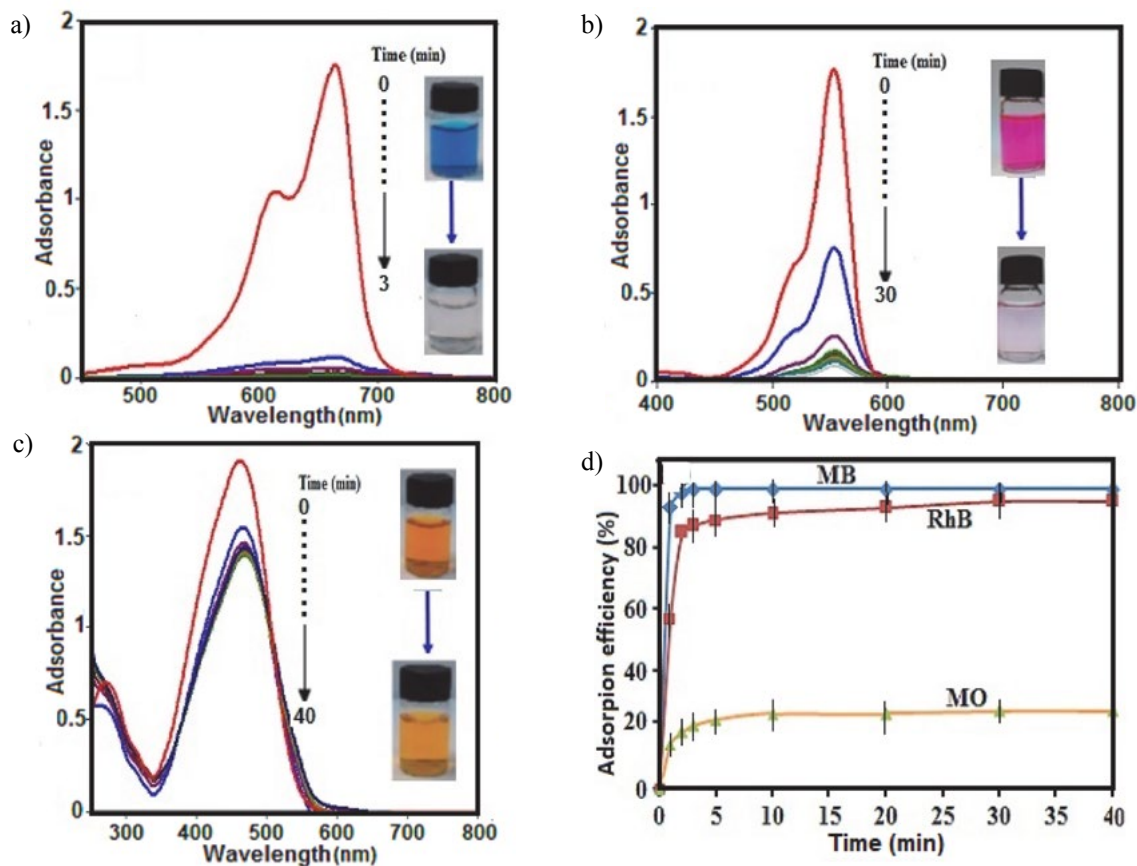


Figure 10. UV-vis spectral changes of dyes aqueous solutions over  $Fe_3O_4/GrO-NH_2/H_3PMo_{12}O_{40}$  at different time intervals: (a) MB dye, (b) RhB dye, (c) MO dye and (d) Comparison of adsorption efficiency (%) of dyes as function of time. Conditions: [dye] = 25 mg/L, 50mL; [Adsorbent] = 25 mg/50 mL at 25 °C.

ganic dyes from contaminated water, three organic pollutants (MB, RhB, and MO) with different sizes and charges were selected for experiments. The adsorption was monitored using the characteristic absorption peak, which is 664, 553 and 463 nm for MB, RhB, and MO, respectively. The decrease in the intensity of these characteristic peaks with adsorption time indicates the decrease in the dye amount in the solution. The time dependent UV-Vis absorption spectra of dyes in the presence of the  $\text{Fe}_3\text{O}_4/\text{GO-NH}_2/\text{H}_3\text{PMo}_{12}\text{O}_{40}$  are shown in Figure 10(a)–(c). The digital images and UV-Vis spectroscopic results show that the characteristic absorption peaks of cationic MB and RhB dyes at 664 and 553 nm almost completely disappeared within 3 and 30 min, respectively. As it can be seen in Figure 10(c), the characteristic absorbance band of MO at 463 nm decreased slightly even after 40 min with negligible fading of the orange color. The results show that the hybrid nanomaterial is a poor adsorbent for anionic MO dye from aqueous solution. As compared in Figure 10(d), it is clear that the  $\text{Fe}_3\text{O}_4/\text{GO-NH}_2/\text{H}_3\text{PMo}_{12}\text{O}_{40}$  has different adsorption abilities toward different organic dyes. The adsorption efficiency for MB is 100% in 3 min and for RhB is 96% in 30 min. The removal of MO dye is less than 25% after 40 min. Particularly, the adsorption rate of 50 mL of 25 mg/L MB and RhB solutions quickly reached 100% and 85%, respectively, in the first three minutes. The different effects on removal of dyes can be related to the structure of the dye molecules and the adsorbent material. Firstly, POMs are a kind of hydrophilic metal-oxo cluster compounds. The hydrophilic/hydrophobic property of the hybrid framework is modulated by loading the  $\text{H}_3\text{PMo}_{12}\text{O}_{40}$  molecules, which allows the ingress and egress of the dye molecules. Secondly, POMs with a large number of negative charges in the hybrid may have a stronger force with the positive charges of dyes. So, the hybrid has demonstrated a good adsorption property toward the cationic dye molecules MB and RhB. However, the removal percent of RhB is relatively low due to the large volume of the RhB molecules, which caused a steric hindrance with the active adsorption sites on the hybrid. Although MO molecules are small enough for ingress and egress, a little uptake capacity of MO was observed as the negative charge of this dye molecule. There are like-charges that repel each other between the POM caged in hybrid and MO.

To further demonstrate the role of anionic  $\text{H}_3\text{PMo}_{12}\text{O}_{40}$  cluster in the hybrid nanomaterial, a series of control experiments were carried out using  $\text{Fe}_3\text{O}_4$ ,  $\text{Fe}_3\text{O}_4/\text{GO}$ ,  $\text{Fe}_3\text{O}_4/\text{GO-NH}_2$ , and pure  $\text{H}_3\text{PMo}_{12}\text{O}_{40}$  samples as adsorbents for removing MB dye. As shown in Figure 11, the adsorption efficiencies of these samples toward the MB dye are 40–78% albeit after long adsorption times of 30–40 min. Apparently, the removal efficiencies and rates of these materials are smaller than those of the  $\text{Fe}_3\text{O}_4/\text{GrO-NH}_2/\text{H}_3\text{PMo}_{12}\text{O}_{40}$  hybrid nanomaterial for cationic MB dye (100% in 3 min). Therefore, there is still merit in exploring the hybrid nanomaterial as efficient adsorbent toward cationic MB dye.

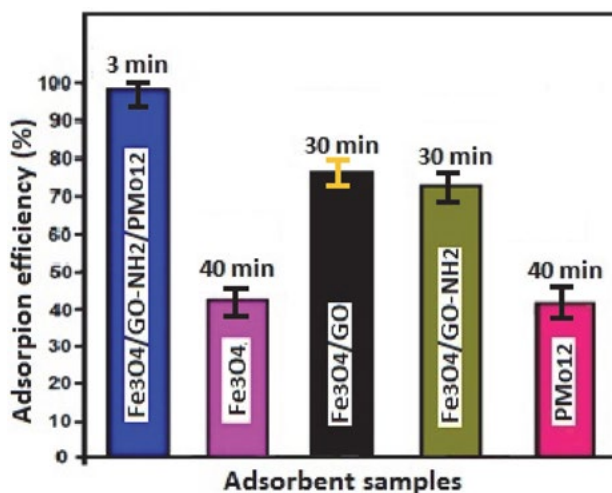
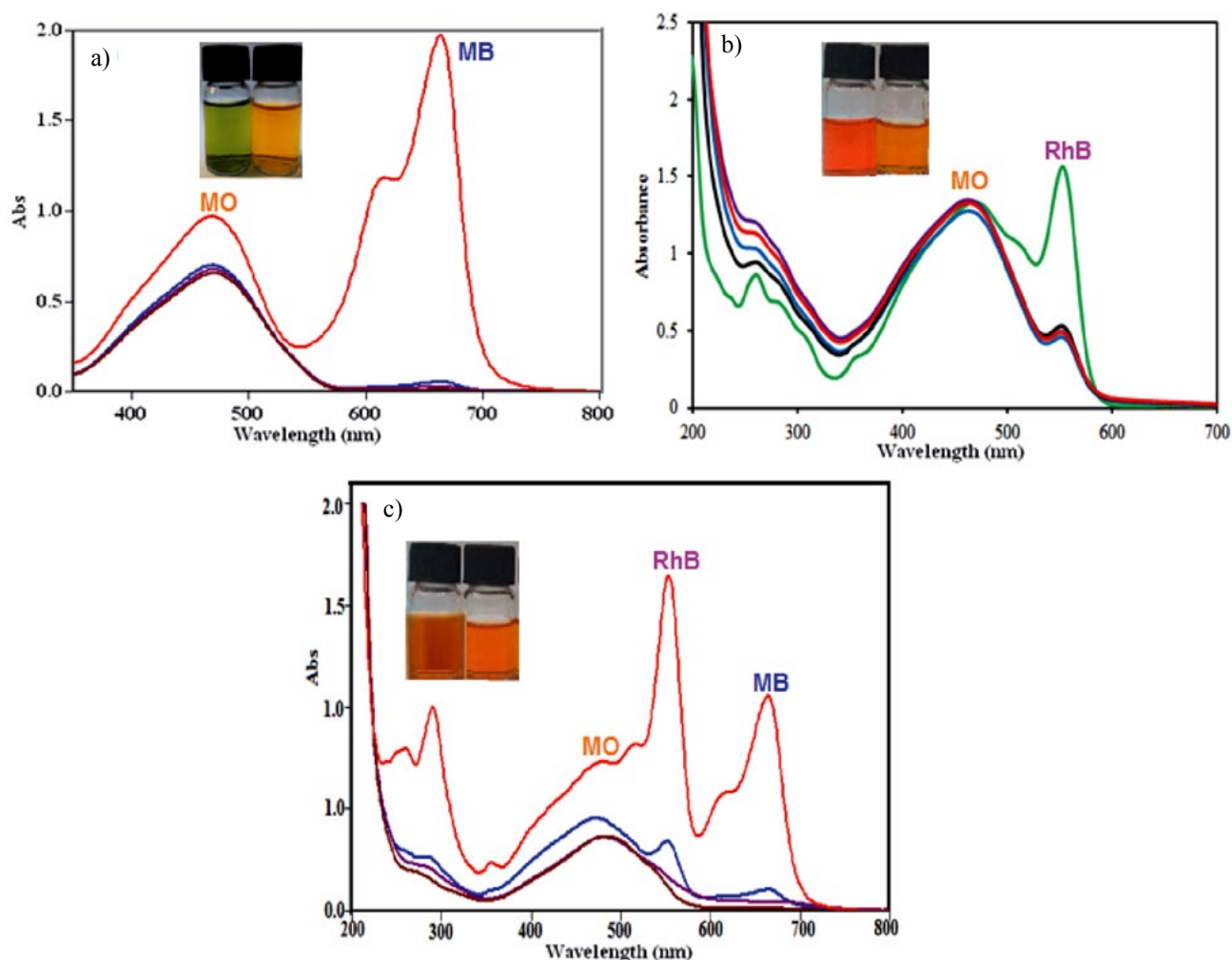


Figure 11. Adsorption efficiency (%) of the MB dye in the presence of different adsorbent samples.

### 3. 3. Selective Adsorption Ability of the Hybrid Nanomaterial for the Mixed Organic Dyes

Selective adsorption and separation of the specific dye are more attractive and challenging in the process of dye-wastewater treatment. In this study, in view of the large uptake capacity of MB and RhB in  $\text{Fe}_3\text{O}_4/\text{GO-NH}_2/\text{H}_3\text{PMo}_{12}\text{O}_{40}$ , it can be anticipated that the composite material may also have an outstanding adsorption and separation behavior in the treatment of mixture of dyes. The selective uptake of dyes was tested using the MB/MO mixture (50 mL,  $C_{0(\text{MB})} = C_{0(\text{MO})} = 25$  mg/L) and MB/RhB mixture (50 mL,  $C_{0(\text{MB})} = C_{0(\text{MO})} = 25$  mg/L) with 25 mg of  $\text{Fe}_3\text{O}_4/\text{GO-NH}_2/\text{H}_3\text{PMo}_{12}\text{O}_{40}$  as adsorbent. The process was monitored by UV-Vis spectroscopy. As MB and MO are similar in molecule size, the preferable uptake of MB from the MB/MO mixture may be assigned to the anionic nature of the composite  $\text{Fe}_3\text{O}_4/\text{GO-NH}_2/\text{H}_3\text{PMo}_{12}\text{O}_{40}$ , as shown in Figure 12(a). For comparison, cationic RhB was selected to mix with anionic MO (50 mL,  $C_{0(\text{MO})} = C_{0(\text{RhB})} = 25$  mg/L). Results revealed that RhB was also preferably adsorbed on the composite material from the MO/RhB mixture as illustrated in Figure 12(b), which may imply that the uptake of dyes is heavily influenced by molecule size along with charges.<sup>72,73</sup> To further validate this point, a ternary mixture of MB, RhB, and MO (50 mL,  $C_{0(\text{MB})} = C_{0(\text{MO})} = C_{0(\text{RhB})} = 25$  mg/L) with 25 mg of the adsorbent was investigated. As exhibited in Figure 12(c), the representative peaks of MB and RhB all disappeared quickly in mixed dyes and only the characteristic absorption peaks of MO were left, suggesting that  $\text{Fe}_3\text{O}_4/\text{GO-NH}_2/\text{H}_3\text{PMo}_{12}\text{O}_{40}$  could selectively capture cationic dyes when utilized in the corresponding ternary mixture. The same conclusion is displayed in the insets of Figure 12(a)–(c) and only the color of MO can be seen in the final solutions of mixed dyes. It can be attributed to the negative charge of this dye mol-





**Figure 12.** Selective adsorption ability of  $\text{Fe}_3\text{O}_4/\text{GO-NH}_2/\text{H}_3\text{PMo}_{12}\text{O}_{40}$  toward mixed dyes solution of (a) MB+MO, (b) RhB+MO, (c) MB+RhB+MO. Conditions :  $C_0$  (MB) =  $C_0$  (RhB) =  $C_0$  (MO) = 25 mg/L and adsorbent dose = 25 mg/50mL

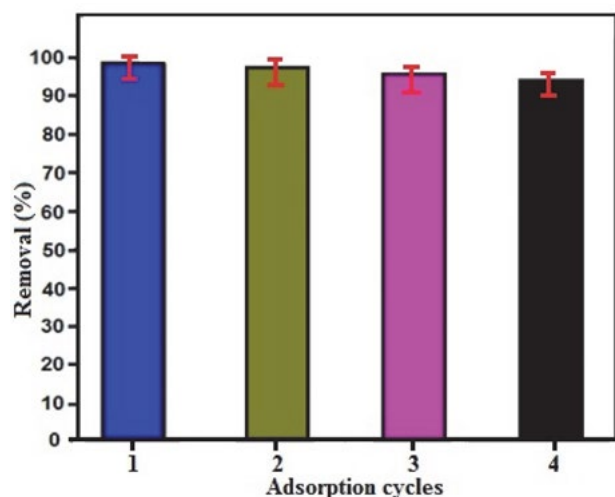
ecule, which repels each other between MO and the  $\text{H}_3\text{P-Mo}_{12}\text{O}_{40}$  cluster in the hybrid nanomaterial. The slightly decreasing absorbance of MO is more likely to be adsorbed on the surface of adsorbent. The results further confirmed that the electrostatic attraction is the key factor for the occurrence of adsorption. Thus,  $\text{Fe}_3\text{O}_4/\text{GO-NH}_2/\text{H}_3\text{PMo}_{12}\text{O}_{40}$  composite nanomaterial is an environmental friendly, active adsorbent for removing different cationic organic pollutants after the immobilization of POM anion.

### 3. 4. The Reusability and Stability of the Hybrid Nanomaterial

The stability and reusability of the adsorbents are an important standard for practical application. To verify whether the composite material is stable and recycled during the adsorption experiments, the cycle tests of  $\text{Fe}_3\text{O}_4/\text{GO-NH}_2/\text{H}_3\text{PMo}_{12}\text{O}_{40}$  on removing MB were explored. After each cycle, the adsorbent was completely separated by a magnet because of the magnetic property in

water. Subsequently, the fast release process of the adsorbed MB was achieved by thoroughly washing the adsorbent with a dilute solution of NaCl and ethanol three times. Then, desorbed adsorbent was added to 50 mL of 25 mg/L MB solution under stirring. As described in Figure 13, the composite nanomaterial showed almost identically rapid adsorption of MB. After four cycles, the regenerated adsorbent was still able to remove 94% MB from the aqueous solution. Thus, we may conclude that the composite nanomaterial can be reusable during the adsorption experiment.

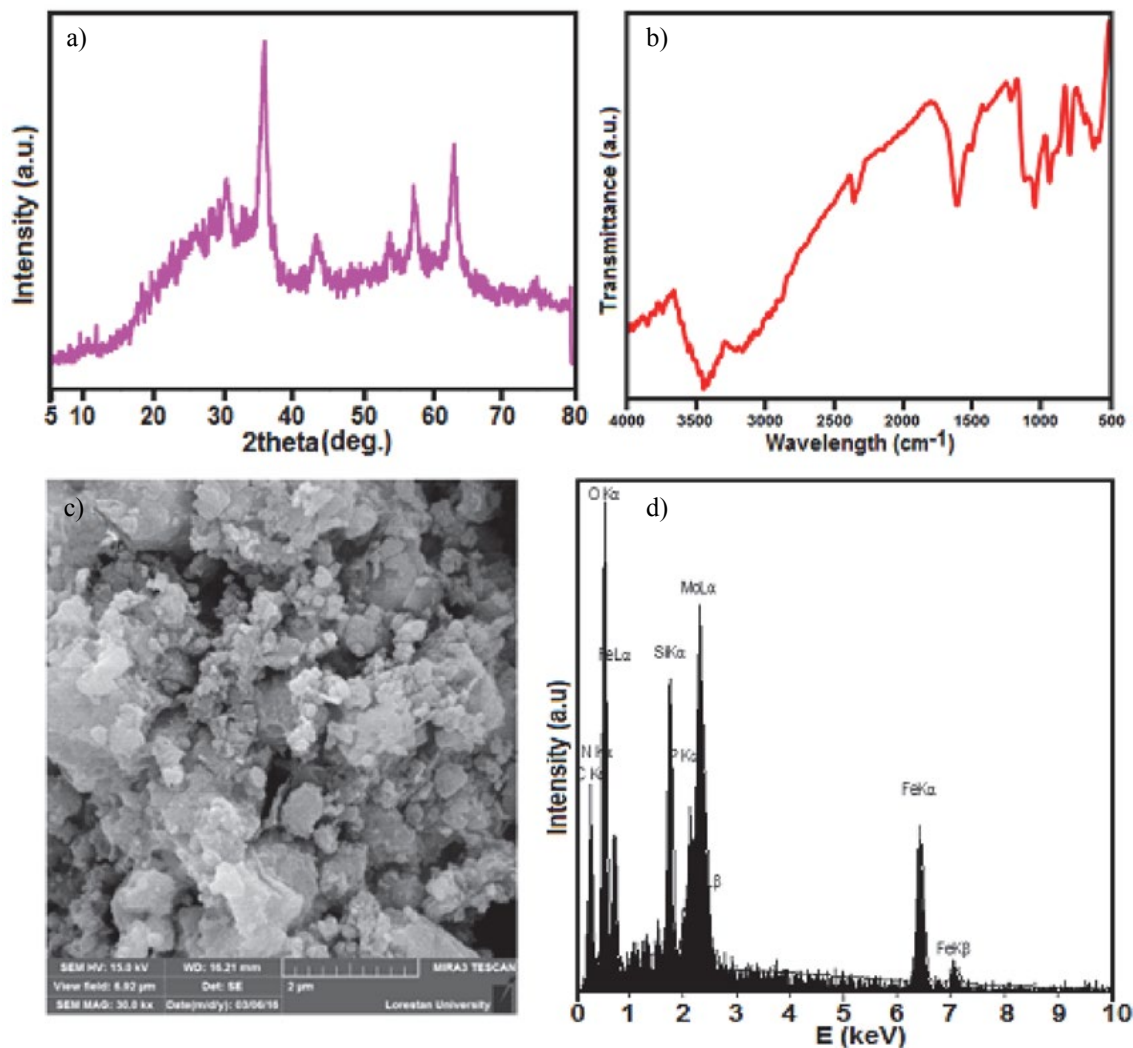
The stability of this material is further discussed. As depicted in Fig. 14(a) and (b), the XRD pattern and FT-IR spectrum of the recovered adsorbent after the fourth run are consistent with those of the as-synthesized composite (see Figures 2(c) and 3(d)). These observations confirmed that the structure of the  $\text{Fe}_3\text{O}_4/\text{GO-NH}_2/\text{H}_3\text{PMo}_{12}\text{O}_{40}$  hybrid nanomaterial is stable under the reaction conditions and is not affected by the reactants. The morphology of the recycled adsorbent particles was also analyzed. Fig. 14(c)



**Figure 13.** Recyclability of the  $\text{Fe}_3\text{O}_4/\text{GO-NH}_2/\text{H}_3\text{PMo}_{12}\text{O}_{40}$  hybrid nanomaterial in the removal of MB dye.

shows a representative SEM image of the adsorbent after four cycles. It could be observed that the recovered adsorbent almost kept its initial size and morphology (see Figure 5(e) and (f)) and the surface of GO nanosheets was still decorated with  $\text{Fe}_3\text{O}_4$  and  $\text{H}_3\text{PMo}_{12}\text{O}_{40}$  particles, revealing the strong binding between the  $\text{Fe}_3\text{O}_4$  nanoparticles and  $\text{H}_3\text{PMo}_{12}\text{O}_{40}$  with GO nanosheets. We can also observe representative peaks of C, N, O, Si, Fe, P, and Mo from the EDX of the recovered  $\text{Fe}_3\text{O}_4/\text{GO-NH}_2/\text{H}_3\text{PMo}_{12}\text{O}_{40}$  (Figure 14(d)). Considering the above mentioned experiment results, we can conclude that the structure of the compound remained intact, which further confirms its excellent stability and recyclability.

The  $\text{Fe}_3\text{O}_4/\text{GO-NH}_2/\text{H}_3\text{PMo}_{12}\text{O}_{40}$  hybrid exhibited the maximum adsorption capacity of 426.7 mg/g when 100 mg of  $\text{Fe}_3\text{O}_4/\text{GO-NH}_2/\text{H}_3\text{PMo}_{12}\text{O}_{40}$  was soaked in 100 mL of 500 mg/L aqueous MB solution for 2 h. As can be seen in Table 1,  $\text{Fe}_3\text{O}_4/\text{GO-NH}_2/\text{H}_3\text{PMo}_{12}\text{O}_{40}$  exhibits



**Figure 14.** (a) XRD pattern, (b) FT-IR spectrum, (c) SEM image, and (d) EDX spectrum of the recovered  $\text{Fe}_3\text{O}_4/\text{GO-NH}_2/\text{H}_3\text{PMo}_{12}\text{O}_{40}$  hybrid nanomaterial after the fourth run.

much higher uptake capacity of MB, compared with the adsorbents that were reported.<sup>74–87</sup> On the basis of the above observations and the characteristics of  $\text{Fe}_3\text{O}_4/\text{GO-NH}_2/\text{H}_3\text{PMo}_{12}\text{O}_{40}$  nanocomposite, we infer that the following factors could contribute to the increased adsorption capacity of this nanocomposite. On the one hand, the anchored aminopropyl groups and the presence of the well dispersed  $\text{Fe}_3\text{O}_4$  and  $\text{H}_3\text{PMo}_{12}\text{O}_{40}$  nanoparticles on the GO nanosheets surface could act as spacers and thus prohibit the graphene sheets to restack. This directly results in significant increase of the specific surface area of graphene structures, which can be of great benefit to adsorption processes. This result is consistent with BET surface area data in Figure 9. On the other hand, the anchored  $\text{PMo}_{12}\text{O}_{40}^{3-}$  polyanions with a large number of negative charges in the ternary hybrid have a stronger attraction force with the positive charges of cationic dyes (e.g. MB). In fact, higher adsorption capacity of the  $\text{Fe}_3\text{O}_4/\text{GO-NH}_2/\text{H}_3\text{PMo}_{12}\text{O}_{40}$  is due to synergistic effect between GO nanosheets and  $\text{PMo}_{12}\text{O}_{40}^{3-}$  polyanions. Thus, this material is a promising adsorbent for the treatment of toxic organic pollutants in the dye-wastewater.

**Table 1.** Comparison of the adsorption capacities of MB onto some typical adsorbents.

Entry	Adsorbent material	Adsorption capacity (mg/g)	Ref.
1	Activated carbon	135	74
2	Nano- ZIF - 8	13.3	74
3	Zeolite	10.86	75
4	$\text{Fe}_3\text{O}_4/\text{graphene}$	33.66	76
5	$\text{H}_3\text{PW}_{12}\text{O}_{40}/\text{ZIF-8}$	810	74
6	$\text{H}_3\text{PW}_{12}\text{O}_{40}/\text{Mn}^{\text{III}}\text{porphyrin}$	10.5	77
7	Graphene	153.83	78
8	$\text{CoFe}_2\text{O}_4/\text{MWCNT}$	14.3	79
9	$\text{H}_6\text{P}_2\text{W}_{18}\text{O}_{62}/\text{MOF-5}$	51.81	80
10	$\text{H}_3\text{PW}_{12}\text{O}_{40}/\text{MIL-101(Fe)}$	473.7	81
11	$\text{H}_4\text{PW}_{11}\text{V}/\text{MIL-101(Cr)}$	371	82
12	$(4\text{-Hap})_4[\text{Mo}_8\text{O}_{26}]$	916.04	83
13	MOF/graphite oxide	18	84
14	Carbon nanotubes	46.2	85
15	MOF-235	187	86
16	Grapheme oxide (GO)	144.92	87
17	Calcium alginate/GO	188.81	87
18	$\text{Fe}_3\text{O}_4/\text{GO-NH}_2/\text{H}_3\text{PMo}_{12}\text{O}_{40}$	426.7	This work

## 4. Conclusions

In summary, the novel ternary hybrid nanomaterial  $\text{Fe}_3\text{O}_4/\text{GO-NH}_2/\text{H}_3\text{PMo}_{12}\text{O}_{40}$  was synthesized by a simple acid-base interaction between aminopropyl functionalized magnetic graphene oxide nanosheets and  $\text{H}_3\text{PMo}_{12}\text{O}_{40}$  and tested as a new adsorbent in the removal of MB, RhB, and MO dyes from aqueous solutions. The results confirmed that this adsorbent displayed much higher adsorp-

tion capacity for cationic dyes and lower adsorption capacity for anionic dyes. This adsorption selectivity is due to the favorable electrostatic interactions between the adsorbents and cationic dyes. High adsorption capacity, compared with other adsorbents, accompanied by the ease of separation by an external magnetic field make the prepared hybrid a powerful separation tool to be utilized in wastewater treatment.

## 5. Acknowledgements

The authors gratefully acknowledge the Lorestan University Research Council and Iran Nanotechnology Initiative Council (INIC) for their financial support.

## 6. References

1. S. Kaur, R. Gopal, W. J. Ng, S. Ramakrishna and T. Matsuura, *MRS Bull.*, **2008**, 33, 21–26. DOI:10.1557/mrs2008.10
2. H. W. Liang, X. Cao, W. J. Zhang, H. T. Lin, F. Zhou, L. F. Chen and S. H. Yu, *Adv. Funct. Mater.*, **2011**, 21, 3851–3858. DOI:10.1002/adfm.201100983
3. L. S. Zhong, J. S. Hu, H. P. Liang, A. M. Cao, W. G. Song and L. J. Wan, *Adv. Mater.*, **2006**, 18, 2426–2431. DOI:10.1002/adma.200600504
4. J. B. Zimmerman, J. R. Mihelcic, S. James, *Environ. Sci. Technol.*, **2008**, 42, 4247–4254. DOI:10.1021/es0871457
5. G. Crini, *Bioresour. Technol.*, **2006**, 97, 1061–1085. DOI:10.1016/j.biortech.2005.05.001
6. R. D. Ambashta and M. Sillanpää, *J. Hazard. Mater.*, **2010**, 180, 38–49. DOI:10.1016/j.jhazmat.2010.04.105
7. S. H. Chen, J. Zhang, C. L. Zhang, Q. Y. Yue, Y. Li and C. Li, *Desalination*, **2010**, 252, 149–156. DOI:10.1016/j.desal.2009.10.010
8. A. Mittal, A. Malviya, D. Kaur, J. Mittal and L. Kurup, *J. Hazard. Mater.* **2007**, 148, 229–240. DOI:10.1016/j.jhazmat.2007.02.028
9. S. B. Wang, Y. Boyjoo, A. Choueib and Z. H. Zhu, *Water Res.* **2005**, 39, 129–138. DOI:10.1016/j.watres.2004.09.011
10. J. B. Zimmerman, J. R. Mihelcic and S. James, *Environ. Sci. Technol.* **2008**, 42, 4247–4254. DOI:10.1021/es0871457
11. Z. Xiong, L. L. Zhang, J. Ma and X. S. Zhao, *Chem. Commun.*, **2010**, 46, 6099–6101. DOI:10.1039/c0cc01259a
12. S. Prakash, A. M. Rajesh and V. K. Shahi, *Chem. Eng. J.*, **2011**, 168, 108–114. DOI:10.1016/j.cej.2010.12.047
13. L. Ai, H. Yue and J. Jiang, *Nanoscale*, **2012**, 4, 5401–5408. DOI:10.1039/C2NR31333B
14. B. Wang, H. Wu, L. Yu, R. Xu, T. T. Lim, and X. W. Lou, *Adv. Mater.*, **2012**, 24, 1111–1116. DOI:10.1002/adma.201104599
15. J. C. Crittenden, R. R. Trussell, D. W. Hand, K. J. Howe and G. Tchobanoglous, *Water Treatment: Principles and Design*, 2nd ed.; Wiley: Chichester, U.K., **2005**.
16. Y. J. Xu, G. Weinberg, X. Liu, O. Timpe, R. Schlogl and D. S.

- Su, *Adv. Funct. Mater.*, **2008**, *18*, 3613–3619.  
DOI:10.1002/adfm.200800726
17. T. Zhu, J. S. Chen and X. W. Lou, *J. Phys. Chem. C*, **2012**, *116*, 6873–6878. DOI:10.1021/jp300224s
18. M. Valix, W. H. Cheung and G. McKay, *Langmuir*, **2006**, *22*, 4574–4582. DOI:10.1021/la051711j
19. N. K. Lazaridis, G. Z. Kyzas, A. A. Vassiliou and D. N. Bikiaris, *Langmuir*, **2007**, *23*, 7634–7643. DOI:10.1021/la700423j
20. E. Alvarez-Ayuso, A. Garcia-Sanchez and X. Querol, *Water Res.*, **2003**, *37*, 4855–4862. DOI:10.1016/j.watres.2003.08.009
21. M. S. Mauter, M. Elimelech, *Environ. Sci. Technol.* **2008**, *42*, 5843–585. DOI:10.1021/es8006904
22. M. Liu, C. Chen, J. Hu, X. Wu and X. Wang, *J. Phys. Chem. C*, **2011**, *115*, 25234–25240. DOI:10.1021/jp208575m
23. J. W. Zhang, J. H. Luo, P. M. Wang, B. Ding, Y. C. Huang, Z. L. Zhao, J. Zhang and Y. G. Wei, *Inorg. Chem.*, **2015**, *54*, 2551–2559. DOI:10.1021/ic502622k
24. S. S. Wang and G. Y. Yang, *Chem. Rev.*, **2015**, *115*, 4893–4962. DOI:10.1021/cr500390v
25. J. S. Li, X. J. Sang, W. L. Chen, L. C. Zhang, Z. M. Zhu, Y. G. Li, Z. M. Su and E. B. Wang, *J. Mater. Chem. A*, **2015**, *3*, 14573–14577. DOI:10.1039/C5TA03259H
26. U. Kortz, A. Muller, J. V. Slagereen, J. Schnack, N. S. Dalal and M. Dressel, *Coord. Chem. Rev.*, **2009**, *253*, 2315–2327. DOI:10.1016/j.ccr.2009.01.014
27. J. T. Rhule, C. L. Hill, D. A. Judd and R. F. Schinazi, *Chem. Rev.*, **1998**, *98*, 327–358. DOI:10.1021/cr960396q
28. A. X. Yan, S. Y. Y. G. Li, Z. M. Zhang, Y. Lu, W. L. Chen and E. B. Wang, *Chem. Eur. J.*, **2014**, *20*, 6927–6933. DOI:10.1002/chem.201400175
29. V. K. Gupta, T. A. Saleh, *Environ. Sci. Pollut. Res.*, **2013**, *20*, 2828–2843. DOI:10.1007/s11356-013-1524-1
30. Y. Chen, S. Zhao and Y. F. Song, *Appl. Catal. A: Gen.*, **2013**, *466*, 307–314. DOI:10.1016/j.apcata.2013.06.030
31. A. Tayyebi and M. Outokesh, *RSC Adv.*, **2016**, *6*, 13898–13913.
32. M. Yusuf, F. Elfghi, S. A. Zaidi, E. Abdullah and M. A. Khan, *RSC Adv.*, **2015**, *5*, 50392–50420.
33. Z. H. Cheng, J. Liao, B. Z. He, F. Zhang, F. A. Zhang, X. H. Huang and L. Zhou, *ACS Sustain. Chem. Eng.* **2015**, *3*, 1677–1685. DOI:10.1021/acssuschemeng.5b00383
34. J. Li, C. L. Chen, R. Zhang and X. K. Wang, *Sci. China Chem.*, **2016**, *59*, 150–158. DOI:10.1007/s11426-015-5452-4
35. G. X. Zhao, L. Jiang, Y. D. He, J. X. Li, H. L. Dong and X. K. Wang, W. P. Hu, *Adv. Mater.*, **2011**, *23*, 3959–3963. DOI:10.1002/adma.201101007
36. J. Wang, Z. M. Chen and B. L. Chen, *Environ. Sci. Technol.*, **2014**, *48*, 4817–4825. DOI:10.1021/es405227u
37. H. Wang, X. Z. Yuan, G. M. Zeng, Y. Wu, Y. Liu, Q. Jiagn and S. S. Gu, *Adv. Colloid Interface Sci.*, **2015**, *221*, 41–59. DOI:10.1016/j.cis.2015.04.005
38. H. Wang, X. Z. Yuan, Y. Wu, H. J. Huang, X. Peng, G. M. Zeng, H. Zhong, J. Liang and M. M. Ren, *Adv. Colloid Interface Sci.*, **2013**, *195–196*, 19–40. DOI:10.1016/j.cis.2013.03.009
39. H. Wang, X. Z. Yuan, Y. Wu, H. J. Huang, G. M. Zeng, Y. Liu, X. L. Wang, N. B. Lin and Y. Qi, *Appl. Surf. Sci.*, **2013**, *279*, 432–440. DOI:10.1016/j.apsusc.2013.04.133
40. H. Chen, B. Gao and H. Li, *J. Hazard. Mater.*, **2015**, *282*, 201–207. DOI:10.1016/j.jhazmat.2014.03.063
41. P. Wang, Q. Shi, Y. Shi, K. K. Clark, G. D. Stucky and A. A. Keller, *J. Am. Chem. Soc.*, **2008**, *131*, 182–188. DOI:10.1021/ja806556a
42. S. Zhang, H. Li, Z. Wang, J. Liu, H. Zhang, B. Wang and Z. Yang, *Nanoscale*, **2015**, *7*, 8495–8502. DOI:10.1039/C5NR00527B
43. X. J. Deng, L. L. Lü, H. W. Li and F. Luo, *J. Hazard. Mater.*, **2010**, *183*, 923–930.
44. M. C. Liu, T. Wen, X. L. Wu, C. L. Chen, J. Hu, J. X. Li and X. K. Wang, *Dalton Trans.*, **2013**, *43*, 14710–14717. DOI:10.1039/c3dt50955a
45. J. Zhu, S. Wei, H. Gu, S. B. Rapole, Q. Wang, Z. Luo, N. Haldolaarachchige, D. P. Young and Z. Guo, *Environ. Sci. Technol.*, **2012**, *46*, 977–98. DOI:10.1021/es2014133
46. Y. Liu, C. Luo, G. Cui and S. Yan, *RSC Adv.*, **2015**, *5*, 54156–54164.
47. X. Bai, R. Feng, Z. Hua, L. Zhou and H. Shi, *Environ. Eng. Sci.*, **2015**, *32*, 370–378. DOI:10.1089/ees.2014.0015
48. F. Gu, M. Liang, D. Han and Z. Wang, *RSC Adv.*, **2015**, *5*, 39964–39972.
49. Y. J. Yao, S. D. Miao, S. Z. Liu, L. P. Ma, H. Q. Sun and S. B. Wang, *Chem. Eng. J.*, **2012**, *184*, 326–332. DOI:10.1016/j.cej.2011.12.017
50. N. I. Kovtyukhova, P. J. Ollivier, B. R. Martin, T. E. Mallouk, S. A. Chizhik, E. V. Buzaneva and A. D. Gorchinskiy, *Chem. Mater.*, **1999**, *11*, 771–778. DOI:10.1021/cm981085u
51. X. Gong, G. Liu, Y. Li, D. Y. W. Yu and W. Y. Teoh, *Chem. Mater.*, **2016**, *28*, 8082–8118. DOI:10.1021/acs.chemmater.6b01447
52. L. Zhao, Y. Chi, Q. Yuan, N. Li, W. Yan and X. Li, *J. Colloid Interface Sci.*, **2013**, *390*, 70–77. DOI:10.1016/j.jcis.2012.08.059
53. Z. Zhang, F. Zhang, Q. Zhu, W. Zhao, B. Ma and Y. Ding, *J. Colloid Interface Sci.*, **2011**, *360*, 189–194. DOI:10.1016/j.jcis.2011.04.045
54. M. Masteri-Farahania, J. Movassagh, F. Taghavi, P. Eghbali and F. Salimi, *Chem. Eng. J.*, **2012**, *184*, 342–346. DOI:10.1016/j.cej.2011.12.094
55. Y. Fu and X. Wang, *Ind. Eng. Chem. Res.*, **2011**, *50*, 7210–7218. DOI:10.1021/ie200162a
56. G. H. Moon, Y. Park, W. Kim and W. Choi, *Carbon*, **2011**, *49*, 3454–3462. DOI:10.1016/j.carbon.2011.04.042
57. L. Q. Guo, P. R. Ye, J. Wang, F. F. Fu and Z. J. Wu, *J. Hazard. Mater.*, **2015**, *298*, 28–35. DOI:10.1016/j.jhazmat.2015.05.011
58. Q. S. Zhao, D. F. Chen, Y. Li, G. L. Zhang, F. B. Zhang and X. B. Fan, *Nanoscale*, **2013**, *5*, 882–885. DOI:10.1039/C2NR33290F
59. M. A. Ghasemzadeh, B. Molaei, M. H. Abdollahi-Basir and F. Zamani, *Acta Chim. Slov.*, **2017**, *64*, 73–82. DOI:10.17344/acsi.2016.2823
60. S. K. Singh, M. K. Singh, P. P. Kulkarni, V. K. Sonkar, J. J. A. Gracio and D. Dash, *ACS Nano*, **2012**, *6*, 2731–2740. DOI:10.1021/nn300172t

61. C. Rocchiccioli-Deltcheff, M. Fournier, R. Franck and R. Thouvenot, *Inorg. Chem.*, **1983**, 22, 207–216. DOI:10.1021/ic00144a006
62. H. Zhang, A. J. Xie, Y. H. Shen, L. G. Qiu and X. Y. Tian, *Phys. Chem. Chem. Phys.*, **2012**, 14, 12757–12763. DOI:10.1039/c2cp41561e
63. D. Zhou and B. H. Han, *Adv. Funct. Mater.*, **2010**, 20, 2717–2722. DOI:10.1002/adfm.200902323
64. Y. B. Sun, D. D. Shao, C. L. Chen, S. B. Yang and X. K. Wang, *Environ. Sci. Technol.* **2013**, 47, 9904–9910. DOI:10.1021/es401174n
65. Y. Sun, D. Shao, C. Chen, S. Yang and X. Wang, *Environ. Sci. Technol.*, **2013**, 47, 9904–9910. DOI:10.1021/es401174n
66. S. Alwarappan, A. Erdem, C. Liu and C.-Z. Li, *J. Phys. Chem. C*, **2009**, 113, 8853–8857. DOI:10.1021/jp9010313
67. Y.-X. Ma, Y.-F. Li, G.-H. Zhao, L.-Q. Yang, J.-Z. Wang, X. Shan and X. Yan, *Carbon*, **2012**, 50, 2976–2986. DOI:10.1016/j.carbon.2012.02.080
68. L. M. Cui, Y. G. Wang, L. Gao, L. H. Hu, L. G. Yan, Q. Wei and B. Du, *Chem. Eng. J.*, **2015**, 281, 1–10. DOI:10.1016/j.ccej.2015.06.043
69. W. Zhang, M. Wang, W. Zhao and B. Wang, *Dalton Trans.*, **2013**, 42, 15464–15474. DOI:10.1039/c3dt52068d
70. X. Q. Tian, C. M. Cheng, L. Qian, B. Z. Zheng, H. Y. Yuan, S. P. Xie, D. Xiao and M. M. F. Choi, *J. Mater. Chem.*, **2012**, 22, 8029–8035. DOI:10.1039/c2jm16057a
71. H. Pang, Y. H. Ma, G. C. Li, J. Chen, J. S. Zhang, H. H. Zheng and W. M. Du, *Dalton Trans.*, **2012**, 41, 13284–13291. DOI:10.1039/c2dt31916k
72. L. Li, X. L. Liu, H. Y. Geng, B. Hu, G. W. Song and Z. S. Xu, *J. Mater. Chem. A*, **2013**, 1, 10292–10299. DOI:10.1039/c3ta11478c
73. X. Zhao, X. Bu, T. Wu, S.-T. Zheng, L. Wang and P. Feng, *Nat. Commun.*, **2013**, 4, 1–9.
74. R. Li, X. Q. Ren, J. S. Zhao, X. Feng, X. Jiang, X. X. Fan, Z. G. Lin, X. G. Li, C. G. Hu and B. Wang, *J. Mater. Chem. A*, **2014**, 2, 2168–2173. DOI:10.1039/C3TA14267A
75. C. D. Woolard, J. Strong and C. R. Erasmus, *Appl. Geochem.*, **2002**, 17, 1159–1164. DOI:10.1016/S0883-2927(02)00057-4
76. Y. Yao, S. Miao, S. Liu, L. P. Ma, H. Sun and S. Wang, *Chem. Eng. J.*, **2012**, 184, 326–332. DOI:10.1016/j.ccej.2011.12.017
77. C. Zou, Z. J. Zhang, X. Xu, Q. H. Gong, J. Li and C. D. Wu, *J. Am. Chem. Soc.*, **2012**, 134, 87–90. DOI:10.1021/ja209196t
78. T. Liu, Y. Li, Q. Du, J. Sun, Y. Jiao, G. Yang, Z. Wang, Y. Xia, W. Zhang and K. Wang, *Colloids Surf., B*, **2012**, 90, 197–203. DOI:10.1016/j.colsurfb.2011.10.019
79. A. A. Farghali, M. Bahgat, W. M. A. El Rouby and M. H. Khe-dr, *J. Solution Chem.* **2012**, 41, 2209–2225. DOI:10.1007/s10953-012-9934-0
80. X. X. Liu, W. P. Gong, J. Luo, C. T. Zou, Y. Yang and S. J. Yang, *Appl. Surf. Sci.*, **2016**, 362, 517–524. DOI:10.1016/j.apsusc.2015.11.151
81. T. T. Zhu, Z.-M. Zhang, W.-L. Chen, Z.-J. Liu and E.-B. Wang, *RSC Adv.*, **2016**, 6, 81622–81630
82. A. X. Yan, S. Y. Y. G. Li, Z. M. Zhang, Y. Lu, W. L. Chen and E. B. Wang, *Chem. Eur. J.*, **2014**, 20, 6927–6933. DOI:10.1002/chem.201400175
83. Y.-Q. Zhang, C.-C. Wang, T. Zhu, P. Wang and S.-J. Gao, *RSC Adv.* **2015**, 5, 45688–45692.
84. L. Li, X. L. Liu, H. Y. Geng, B. Hu, G. W. Song and Z. S. Xu; *J. Mater. Chem., A*, **2013**, 1, 10292–10299. DOI:10.1039/c3ta11478c
85. Y. Yao, F. Xu, M. Chen, Z. Xu and Z. Zhu, *Bioresour. Technol.*, **2010**, 101, 3040–3046. DOI:10.1016/j.biortech.2009.12.042
86. E. Haque, J. W. Jun and S. H. Jhung, *J. Hazard. Mater.*, **2011**, 185, 507–511. DOI:10.1016/j.jhazmat.2010.09.035
87. Y. Li, Q. Du, T. Liu, J. Sun, Y. Wang, S. Wu, Z. Wang, Y. Xia and L. Xia, *Carbohydr. Polym.*, **2013**, 95, 501–507. DOI:10.1016/j.carbpol.2013.01.094

## Povzetek

V raziskavi poročamo o vezavi polianionov  $\text{PMo}_{12}\text{O}_{40}^{3-}$  na amino funkcionalizirane nanoplasti grafenovega oksida (GO). Tako pripravljen ternarni magnetni nanokompozit ( $\text{Fe}_3\text{O}_4/\text{GO-NH}_2/\text{H}_3\text{PMo}_{12}\text{O}_{40}$ ) smo karakterizirali z naslednjimi metodami: rentgensko praškovno difrakcijo (XRD) infrardečo spektroskopijo (FTIR), ramansko spektroskopijo, energijsko disperzivno spektroskopijo (EDS), vrstično elektronsko mikroskopijo z emisijo polja (FE-SEM), meritvami površine (BET), magnetnimi meritvami (VSM) in mikroskopijo na atomsko silo (AFM). Rezultati so pokazali uspešno vezavo  $\text{H}_3\text{PMo}_{12}\text{O}_{40}$  (utežni delež ~36.5 %) na površino magnetnega grafenovega oksida. Specifična površina nanokompozita je bila višja (77.07  $\text{m}^2/\text{g}$ ) od čistega  $\text{H}_3\text{PwMo}_{12}\text{O}_{40}$  ( $\leq 10 \text{ m}^2/\text{g}$ ). Preučevali smo adsorpcijsko učinkovitost nanokompozita v primerih odstranjevanja nekaterih barvil (metilen modro, rodamin B in metiloranž) iz vodnih raztopin. Z uporabo nanokompozita smo prikazali hitro in selektivno adsorpcijo za kationska barvila iz mešanih raztopin barvil. Stopnja in kapaciteta adsorpcije  $\text{Fe}_3\text{O}_4/\text{GO-NH}_2/\text{H}_3\text{PMo}_{12}\text{O}_{40}$  sta bili povečani v primerjavi z GO, GO-NH<sub>2</sub>,  $\text{Fe}_3\text{O}_4/\text{GO-NH}_2$  in  $\text{H}_3\text{P-Mo}_{12}\text{O}_{40}$  zaradi povečane elektrostatske privlačnosti in interakcij preko vodikovih vezi. Nanokompozit lahko ločimo z magneti in ponovno uporabimo, pri čemer v kompozitu ne pride do strukturnih sprememb. Menimo, da nanokompozit  $\text{Fe}_3\text{O}_4/\text{GO-NH}_2/\text{H}_3\text{PMo}_{12}\text{O}_{40}$  predstavlja obetaven "zeleni" adsorbent za odstranjevanje organskih onesnaževal iz voda.

Scientific paper

# Eco-Friendly Multi-Component Synthesis of $\gamma$ -Spiroiminolactones in Water

Hamid Reza Safaei<sup>1,\*</sup> and Mohsen Shekouhy<sup>2</sup>

<sup>1</sup> Department of Applied Chemistry, Shiraz Branch, Islamic Azad University, P.O. Box 71993-5, Shiraz, Iran

<sup>2</sup> Department of Chemistry, College of Sciences, Shiraz University, 71454 Shiraz, Iran

\* Corresponding author: E-mail: safaei@iaushiraz.ac.ir  
Tel.: +98 713 6402715; fax: +98 713 6412488

Received: 20-08-2017

## Abstract

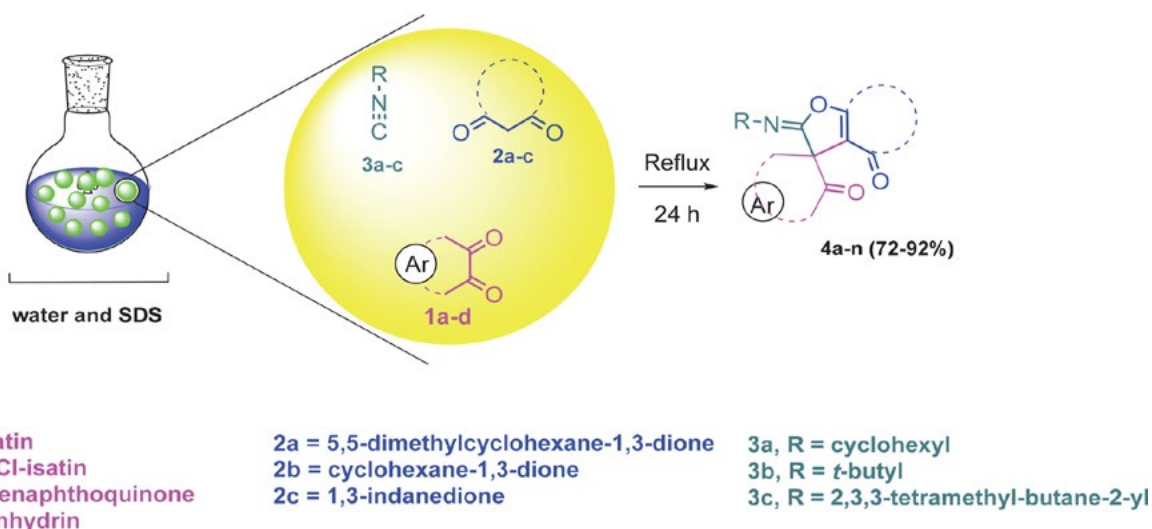
$\gamma$ -Spiroiminolactone derivatives can be synthesized through an one-pot three-component reaction of cyclic carbonyl compounds (isatin, acenaphthoquinone, ninhydrin), activated  $\alpha$ -methylene carbonyl groups and isocyanides in water using sodium dodecyl sulfate (SDS) as a commercially available and cheap surfactant compound. All products were obtained in good to excellent yields without formation of any by-products in water as a green and benign reaction medium. Moreover, presented method was successfully applied for the synthesis of some novel bis(spiroiminolactone) derivatives.

**Keywords:**  $\gamma$ -spiroiminolactone, water, multi-component reaction, isocyanide, surfactant

## 1. Introduction

It is well-known that heterocyclic compounds have played an important role in drug discovery and pharmaceuticals synthesis. Among various kinds of heterocycles, iminolactones have been intensively studied and widely applied as useful intermediates for the synthesis of butenolides.<sup>1</sup> They have been shown wide range of biological ac-

tivities such as antimicrobial,<sup>2</sup> antifungal,<sup>3</sup> anti-inflammatory,<sup>4</sup> anticancer,<sup>5</sup> and antiviral.<sup>6</sup> Moreover, iminolactones have been used for the synthesis of sphingofungin F<sup>7a</sup> that exhibits inhibitory effects toward serine palmitoyl transferase (SPT), which induces apoptosis in both yeast and mammalian cells by blocking the sphingosine biosynthesis pathway.<sup>7b</sup>



Scheme 1. The one-pot multi-component synthesis of  $\gamma$ -spiroiminolactones in water.

For a number of reasons, the development of simple and more benign chemical processes for the synthesis of biologically active compounds in water is one of the major challenges for chemists. Some of these reasons are the fact that water is a safe, inexpensive, readily available, and environmentally benign reaction medium.<sup>8</sup> However, the insolubility of most organic compounds in water is the major drawback of the application of water as a safe reaction medium in organic synthesis. Furthermore, some active sites in organic compounds are either decomposed or deactivated in water. One useful way to overcome this problem is the application of surfactant-combined catalysts that was first introduced by Kobayashi.<sup>9a-c</sup>

As people's concerns about their living environment increases continuously, the design of new multi-component reactions (MCRs) with eco-friendliness, green procedures had drawn significant attention, especially in organic synthesis and drug discovery with environmentally benign solvents (specially water) and reagents.<sup>9b</sup>

In continuation to our recent studies about the synthesis of heterocyclic compounds in water,<sup>10</sup> we wish to report an eco-friendly synthesis of  $\gamma$ -spiroiminolactones (**4a-n**) via a one-pot three component reaction of cyclic 1,2-ketones (**1a-d**), activated  $\alpha$ -methylene carbonyl compounds (**2a-c**), and isocyanide derivatives (**3a-c**) in water. (Scheme 1).

## 2. Results and Discussion

Initially, in order to find the best reaction condition, the one-pot condensation reaction between isatin (**1a**) (1 mmol, 0.147 g), 5,5-dimethylcyclohexane-1,3-dione (**2a**) (1 mmol, 0.140 g) and cyclohexyl isocyanide (**3a**) (1 mmol, 0.109 g) was selected as a model reaction. The reaction yield and duration time were monitored in the presence of sodium dodecyl sulfate (SDS) as a very cheap and readily available surfactant compound under various reaction conditions. The obtained results are summarized in Table 1.

**Table 1.** The one-pot condensation reaction between isatin (**1a**) (1 mmol, 0.147 g), 5,5-dimethylcyclohexane-1,3-dione (**2a**) (1 mmol, 0.140 g) and cyclohexyl isocyanide (**3a**) (1 mmol, 0.109 g) in the presence of SDS as a surfactant in water (5 mL) under various reaction conditions.

Entry	SDS (mol%, g)	Temp. (°C)	Time (h)	Yield (%) <sup>a</sup>
1	5, 0.014	Reflux	48	51
2	10, 0.028	Reflux	36	85
3	15, 0.042	Reflux	24	91
4	20, 0.056	Reflux	24	91
5	25, 0.070	Reflux	24	90
6	15, 0.042	r.t.	48	–
7	15, 0.042	40	48	15
8	15, 0.042	70	48	73
9	–	Reflux	48	–

<sup>a</sup> Isolated yield.

As it is shown in Table 1, the best result was obtained in the presence of 15 mol% of SDS at reflux temperature (Table 1, entry 3). Moreover, the model reaction was studied in the absence of SDS in water at reflux temperature. At this condition the reaction was not proceeded even after a long time (48 h) and a gummy solid was formed (Table 1, entry 9). This observation establishes the crucial role of SDS as a surfactant to produce an appropriate reaction medium. Moreover, the model reaction was investigated in other solvents such as EtOH, MeOH, CH<sub>2</sub>Cl<sub>2</sub>, THF, CH<sub>3</sub>CN, EtOAc and *n*-hexane, and only trace amounts of products were detected (Table 2).

**Table 2.** The one-pot condensation reaction between isatin (**1a**), 5,5-dimethylcyclohexane-1,3-dione (**2a**), and cyclohexyl isocyanide (**3a**) with the presence of SDS in various solvents at reflux conditions.<sup>a</sup>

Entry	Solvent (5 mL)	Time (h)	Yield (%) <sup>b</sup>
1	<i>n</i> -hexane	24	Trace
2	EtOAc	24	Trace
3	CH <sub>3</sub> CN	24	Trace
4	EtOH	24	28
5	MeOH	24	21
6	CH <sub>2</sub> Cl <sub>2</sub>	24	Trace
7	THF	24	Trace

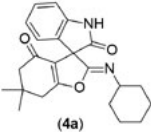
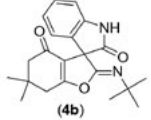
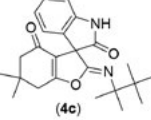
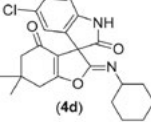
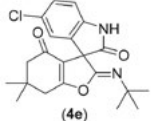
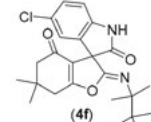
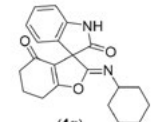
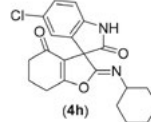
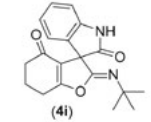
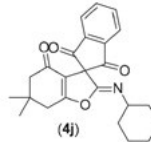
<sup>a</sup> Molar ratio: isatin (1 mmol, 0.147 g), 5,5-dimethylcyclohexane-1,3-dione (1 mmol, 0.140 g), cyclohexyl isocyanide (1 mmol, 0.109 g), and SDS (15 mol%, 0.042 g). <sup>b</sup> Isolated yield.

In the next step, to establish the generality and efficiency of the presented method a variety of starting materials were examined. In this regard a variety of reactive cyclic carbonyl compounds such as isatins, acenaphthoquinone and ninhydrin (**1a-d**), 1,3-dicarbonyl compounds (**2a-c**) and isocyanides (**3a-c**) were examined under optimized conditions (Scheme 1). The obtained results are summarized in Table 3.

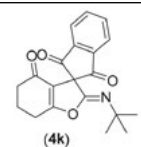
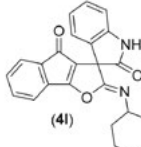
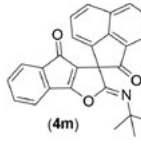
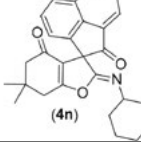
All reactions were completed after 24 h and desired products were obtained in good to excellent yields (72–92%). As it is shown in Table 3, lower yields of products were obtained in the case of ninhydrin (Table 3, entries 10 and 11) that may be due to the higher water solubility of ninhydrin and its lower tendency to diffuse to micelles. We think that two factors play crucial role in this reaction and directly affect the yields and the rates. One is the use of SDS as a surfactant and the other one is water as a solvent.

Recent investigations indicate that water molecules repel small covalent organic molecules and force them to form aggregates in order to decrease the organic surface area.<sup>11a</sup> Forced aggregates of organic reactants are raised in energy more than their unaggregated ground states and are closer in energy to the activated complexes or transition states and this phenomenon significantly leads to the

**Table 3.** The one-pot multi-component synthesis of  $\gamma$ -spiroiminolactone derivatives in the presence of SDS in water after 24 h.

Entry	Reactant 1	Reactant 2	Reactant 3	Product 4	Yield (%) <sup>a</sup>
1	1a	2a	3a	 (4a)	91
2	1a	2a	3b	 (4b)	92
3	1a	2a	3c	 (4c)	89
4	1b	2a	3a	 (4d)	83
5	1b	2a	3b	 (4e)	89
6	1b	2a	3c	 (4f)	82
7	1a	2b	3a	 (4g)	90
8	1b	2b	3a	 (4h)	89
9	1a	2b	3b	 (4i)	91
10	1d	2a	3a	 (4j)	75



Entry	Reactant 1	Reactant 2	Reactant 3	Product 4	Yield (%) <sup>a</sup>
11	1d	2b	3b	 (4k)	72
12	1a	2c	3a	 (4l)	86
13	1c	2c	3b	 (4m)	83
14	1c	2a	3a	 (4n)	83

<sup>a</sup> Isolated yields.

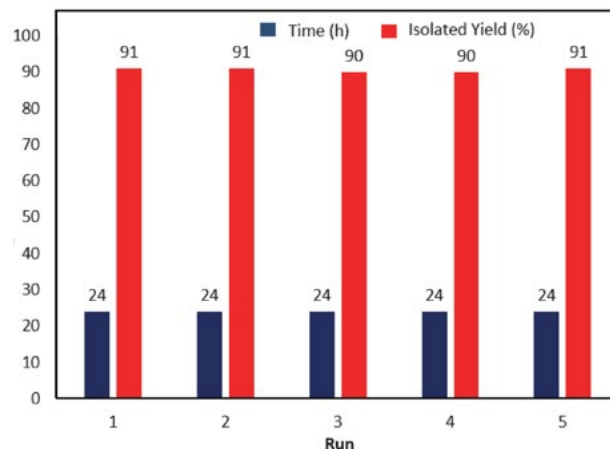
enhancement of the reaction rate. Furthermore, hydrogen bonding between polar transition states and water molecules leads to the stabilization of transition state and decreases the activation gap of the reaction.<sup>11a</sup> Therefore, the use of SDS as a surfactant has major influence on the rate of the reactions. This compound forms many micelles in water with a lipophilic inner site that will act as micro-reactors and prepare appropriate places for organic materials to meet each other. So briefly, SDS makes micelles as nano-reactors for organic reactions in water, therefore organic materials with higher energy states penetrate to these nano-reactors and collide with each other to react.<sup>11b</sup>

In recent years, the synthesis of bis-heterocyclic compounds has been attracted chemists because of unique biological activities such as antibacterial, fungicidal, tuberculostatic, antiamoebic, and plant growth regulation.<sup>12</sup> Therefore, there are numerous reports on the synthesis of various types of these compounds.<sup>13</sup> Considering these facts, we applied our method for the synthesis of some novel bis(spiroiminolactone) derivatives. For this purpose, compound (6) was synthesized as a bis(isatin) compound *via* the reaction of isatin (1a, 2 eq) and 1,4-bis(chloromethyl)benzene (5, 1 eq) in DMF. Then it was condensed with carbonyl compounds processing the  $\alpha$ -methylene group (2a-c) and cyclohexyl isocyanide (3a, 2 eq) in water, and in the presence of SDS (Scheme 2).

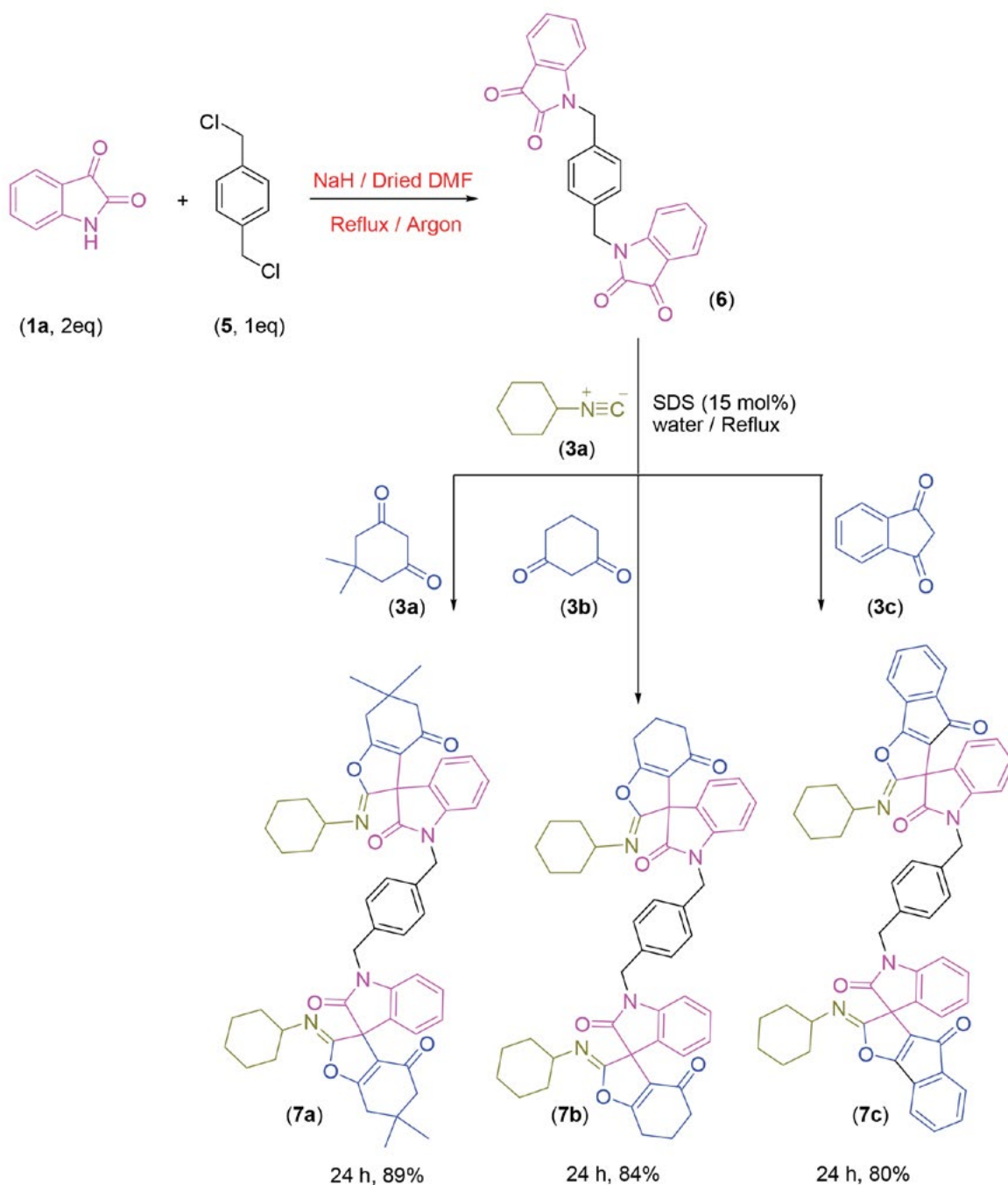
As it is shown in Scheme 3, our proposed mechanism for the synthesis of  $\gamma$ -spiroiminolactones (4a-n) *via* a one-pot three-component reaction between cyclic carbonyl compounds (1a-d), activated  $\alpha$ -methylene carbonyl

groups (2a-c) and isocyanides (3a-c) consists of two steps. In the first step, intermediate (5) forms from the Knoevenagel condensation of cyclic carbonyl compounds (1a-d) and activated  $\alpha$ -methylene carbonyl derivatives (2a-c). In the next step, desired products (4a-n) are obtained *via* the Michael-type addition of isocyanides (3a-c) to the intermediate (5). It is followed by an intermolecular cyclization reaction.

Based on the Jafari report<sup>14</sup> the catalytic effect of micellar SDS in our presented method can be explained as the following. Cyclic carbonyl compounds (1a-d), activat-



**Figure 1.** The one-pot condensation reaction between isatin (1a) (1 mmol, 0.147 g), 5,5-dimethylcyclohexane-1,3-dione (2a) (1 mmol, 0.140 g) and cyclohexyl isocyanide (3a) (1 mmol, 0.109 g) in the presence of recovered SDS in water (5 mL) under reflux condition.

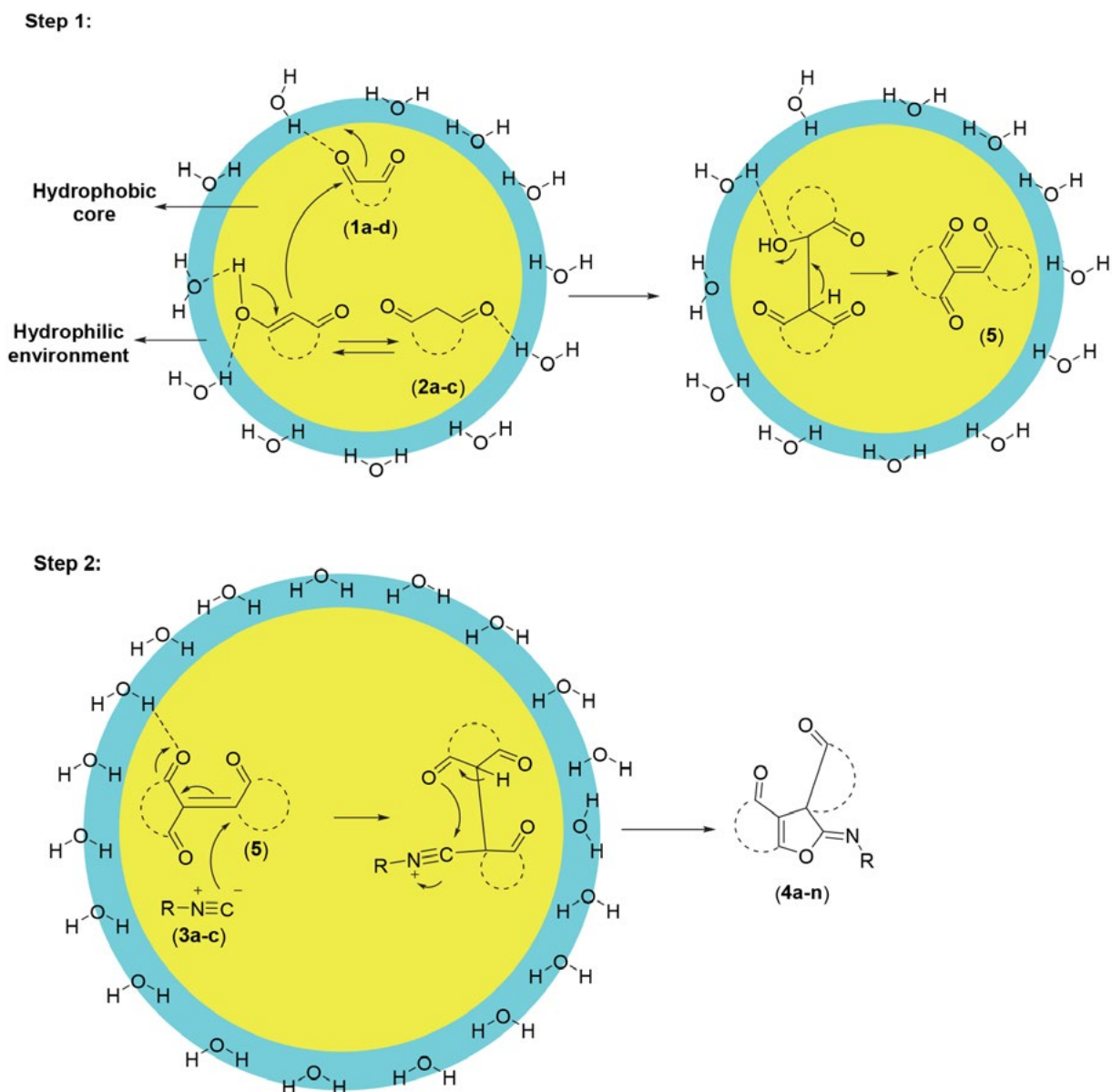


**Scheme 2.** The one-pot three component synthesis of some novel bis(spiroiminolactone) derivatives in water in the presence of SDS.

ed  $\alpha$ -methylene groups (2a-c) and isocyanides (3a-c), which are expected to produce  $\gamma$ -spiroiminolactones (4a-n), are all hydrophobic molecules in aqueous media. In the micellar solution of SDS, the hydrophobic moieties escape from water molecules, which encircle the micelle core of SDS. Therefore, they are activated by hydrogen bonding and are pushed by water molecules into the hydrophobic core of the micellar droplets, where the reactions take place more easily. Water is also a sufficiently polar medium to shift the keto-enol equilibrium to the enol form, which

are highly hydrophilic species. This explanation is also schematically presented by Scheme 3.

The possibility of catalyst recycling was examined by using the model reaction under the optimized conditions. After completion of the reaction, the insoluble products were filtered, water was evaporated under reduced pressure, and the obtained solid was washed with diethyl ether and dried under reduced pressure for 24 h. The recovered SDS was reused five times and no loss of efficiency was observed (Figure 1).



**Scheme 3.** Proposed mechanism for the synthesis of  $\gamma$ -spiroiminolactones (**4a-n**) via a one-pot three-component reaction between cyclic carbonyl compounds (**1a-d**) (isatin, acenaphthoquinone, ninhydrin), activated  $\alpha$ -methylene groups (**2a-c**) and isocyanides (**3a-c**) in the presence of SDS in water.

### 3. Conclusion

In summary, an efficient one-pot procedure for the synthesis of novel  $\gamma$ -spiroiminolactone derivatives is described. This method avoids the use of hazardous catalysts or solvents. The advantages of the presented method are efficiency, generality, high yields of desired products, short reaction times, clean reaction profile, ease of product isolation, simplicity, and agreement with some green chemistry protocols, which all make it a useful and attractive process for the synthesis of  $\gamma$ -spiroiminolactone derivatives. Moreover, the presented method was successfully applied for the synthesis of more complex structures such as novel bis(spiroiminolactone) derivatives.

### 4. Experimental

The chemicals used in this work were obtained from Merck and Sigma-Aldrich companies and were used without purification. Melting points were measured on an Electrothermal 9100 apparatus and are uncorrected.  $^1\text{H}$  and  $^{13}\text{C}$  NMR spectra were recorded on a BRUKER DRX-250 AVANCE spectrometer at 250 and 62.5 MHz respectively. Chemical shifts are given as  $\delta$  values in  $\text{CDCl}_3$  against TMS as an internal standard and  $J$  values are given in Hz. IR spectra were recorded using a Shimadzu FT-IR apparatus. Microanalyses were performed on a Perkin-Elmer 240-B microanalyzer.

**Preparation of 1-(4-((2,3-dioxindolin-1-yl)methyl)benzyl)indoline-2,3-dione (6)**

In a double neck 250 mL round-bottom flask connected to an argon gas inlet, NaH (110 mmol, 2.63 g) was added to a solution of isatin (100 mmol, 14.71 g) in dried DMF 50 mL at 0 °C and resulting mixture was stirred at that temperature under argon atmosphere for 0.5 h, and then warmed to room temperature. Then, 1,4-bis(chloromethyl)benzene (50 mmol, 8.75 g) was added and resulting solution stirred at 80 °C for 8h under argon atmosphere. After this time, the reaction mixture was cooled to room temperature and immediately added to the cold water (500 mL). Resulting precipitates were filtered and dried. Crude products were recrystallized from hot acetic acid and 1-(4-((2,3-dioxindolin-1-yl)methyl)benzyl)indoline-2,3-dione (16.00 g, 81%) was obtained as an orange solid. mp 243–245 °C. IR (KBr)  $\nu$  3050, 2960, 1720, 1670  $\text{cm}^{-1}$ .  $^1\text{H}$  NMR (250 MHz,  $\text{CDCl}_3$ )  $\delta$  (ppm) 5.83 (s, 4H), 7.20 (s, 4H), 7.28 (t,  $J = 7.5$  Hz, 2H), 7.45 (d,  $J = 7.5$  Hz, 2H), 7.64 (t,  $J = 7.5$  Hz, 2H), 7.74 (d,  $J = 7.5$  Hz, 2H).  $^{13}\text{C}$  NMR (62.5 MHz,  $\text{CDCl}_3$ )  $\delta$  (ppm) 46.2, 111.1, 121.3, 123.5, 128.2, 129.3, 133.8, 135.0, 151.3, 166.9, 186.3. Anal. Calcd. for  $\text{C}_{24}\text{H}_{16}\text{N}_2\text{O}_4$ : C, 72.72; H, 4.07; N, 7.07 (%). Found: C, 72.80; H, 4.01; N, 7.11 (%). MS (m/z): 396 ( $\text{M}^+$ ).

**General procedure for the preparation of  $\gamma$ -spiroiminolactones in the presence of SDS in water**

Isocyanide derivative (1 mmol) was added to a mixture of 1,3-dicarbonyl compound (1 mmol), reactive carbonyl compound (isatins, acenaphthoquinone or ninhydrin) (1 mmol) and SDS (0.04 g, 15 mol%) in water (5 mL), and the resulting mixture was refluxed and stirred for 24 h. After this time, the reaction mixture was cooled to room temperature and precipitates were filtered and washed with water (10 mL), and recrystallized from hot ethanol to afford the pure product. For the synthesis of bis(spiroiminolactone) derivatives, 2 mmol of isocyanide and 1,3-dicarbonyl compounds should be applied for each 1 mmol of bis(isatin) compound.

**2-(cyclohexylimino)-6,6-dimethyl-6,7-dihydro-2H-spiro[benzofuran-3,3'-indoline]-2',4(5H)-dione (4a)**

White solid, mp 231–234 °C (dec.) (lit. 230 °C (dec.)).<sup>10a</sup> IR (KBr)  $\nu$  3395, 2858, 1745, 1731, 1654  $\text{cm}^{-1}$ .  $^1\text{H}$  NMR (250 MHz,  $\text{CDCl}_3$ )  $\delta$  (ppm) 0.96 (s, 3H), 0.99 (s, 3H), 1.13–1.28 (m, 10H), 1.92–2.07 (distorted AB system, 2H), 2.32 (d,  $J = 17.5$  Hz, 1H), 2.42 (d,  $J = 17.5$  Hz, 1H), 3.92–4.03 (m, 1H), 6.82–6.97 (m, 3H), 7.24 (t,  $J = 7.5$  Hz, 1H), 8.01 (s, 1H).  $^{13}\text{C}$  NMR (62.5 MHz,  $\text{CDCl}_3$ )  $\delta$  (ppm) 23.1, 23.8, 26.3, 29.6, 31.1, 37.0, 49.7, 55.4, 66.4, 107.6, 121.2, 121.3, 126.1, 126.6, 136.5, 137.9, 140.9, 148.3, 174.2, 191.2. Anal. Calcd. for  $\text{C}_{23}\text{H}_{26}\text{N}_2\text{O}_3$ : C, 72.99; H, 6.92; N, 7.40 (%). Found: C, 73.09; H, 6.98; N, 7.51 (%). MS (m/z): 378 ( $\text{M}^+$ ).

**2-(tert-butylimino)-6,6-dimethyl-6,7-dihydro-2H-spiro[benzofuran-3,3'-indoline]-2',4(5H)-dione (4b)**

White solid, mp 224–226 °C (dec.) (lit. 227 °C (dec.)).<sup>10a</sup> IR (KBr)  $\nu$  3390, 2950, 1750, 1731, 1615  $\text{cm}^{-1}$ .  $^1\text{H}$  NMR (250 MHz,  $\text{CDCl}_3$ )  $\delta$  (ppm) 0.96 (s, 3H), 0.99 (s, 3H), 1.05 (s, 9H), 2.01 (d,  $J = 17.5$  Hz, 1H), 2.13 (d,  $J = 17.5$  Hz, 1H), 2.47 (d,  $J = 17.5$  Hz, 1H), 2.68 (d,  $J = 17.5$  Hz, 1H), 6.44 (d,  $J = 7.5$  Hz, 1H), 6.75 (t,  $J = 7.5$  Hz, 1H), 7.31–7.43 (m, 2H), 8.04 (s, 1H).  $^{13}\text{C}$  NMR (62.5 MHz,  $\text{CDCl}_3$ )  $\delta$  (ppm) 26.7, 29.1, 30.0, 37.4, 50.1, 52.8, 67.4, 108.0, 121.6, 121.7, 126.5, 127.0, 136.9, 138.3, 144.4, 148.7, 174.6, 191.6. Anal. Calcd. for  $\text{C}_{21}\text{H}_{24}\text{N}_2\text{O}_3$ : C, 71.57; H, 6.86; N, 7.95 (%). Found: C, 71.50; H, 6.82; N, 8.02 (%). MS (m/z): 352 ( $\text{M}^+$ ).

**6,6-dimethyl-2-(2,3,3-trimethylbutan-2-ylimino)-6,7-dihydro-2H-spiro[benzofuran-3,3'-indoline]-2',4(5H)-dione (4c)**

White solid, mp 217–220 °C (dec.) (lit. 220 °C (dec.)).<sup>10a</sup> IR (KBr)  $\nu$  3350, 2985, 1724, 1700, 1603  $\text{cm}^{-1}$ .  $^1\text{H}$  NMR (250 MHz,  $\text{CDCl}_3$ )  $\delta$  (ppm) 1.06 (s, 3H), 1.10 (s, 3H), 1.12 (s, 9H), 1.56 (s, 6H), 2.08 (d,  $J = 17.5$  Hz, 1H), 2.18 (d,  $J = 17.5$  Hz, 1H), 2.55 (d,  $J = 18.0$  Hz, 1H), 2.68 (d,  $J = 18.0$  Hz, 1H), 6.75 (d,  $J = 7.5$  Hz, 1H), 6.90 (t,  $J = 7.5$  Hz, 1H), 7.16–7.32 (m, 2H), 8.73 (s, 1H).  $^{13}\text{C}$  NMR (62.5 MHz,  $\text{CDCl}_3$ )  $\delta$  (ppm) 22.9, 24.2, 26.3, 29.6, 33.5, 37.0, 49.7, 67.0, 72.3, 107.6, 121.2, 121.3, 126.1, 126.6, 136.0, 136.5, 137.9, 148.3, 174.2, 191.2. Anal. Calcd. for  $\text{C}_{25}\text{H}_{32}\text{N}_2\text{O}_3$ : C, 73.50; H, 7.90; N, 6.86 (%). Found: C, 73.51; H, 7.93; N, 6.84 (%). MS (m/z): 394 ( $\text{M}^+$ ).

**5'-chloro-2-(cyclohexylimino)-6,6-dimethyl-6,7-dihydro-2H-spiro[benzofuran-3,3'-indoline]-2',4(5H)-dione (4d)**

White solid, mp 256–258 °C (dec.) (lit. 254 °C (dec.)).<sup>10a</sup> IR (KBr)  $\nu$  3400, 2975, 1733, 1710, 1680  $\text{cm}^{-1}$ .  $^1\text{H}$  NMR (250 MHz,  $\text{CDCl}_3$ )  $\delta$  (ppm) 0.97 (s, 3H), 0.99 (s, 3H), 1.12–1.30 (m, 10H), 1.96–2.04 (distorted AB system, 2H), 2.27 (d,  $J = 17.5$  Hz, 1H), 2.40 (d,  $J = 17.5$  Hz, 1H), 3.41–3.50 (m, 1H), 6.78 (d,  $J = 7.5$  Hz, 1H), 7.18 (d,  $J = 7.5$  Hz, 1H), 7.40 (s, 1H), 8.75 (s, 1H).  $^{13}\text{C}$  NMR (62.5 MHz,  $\text{CDCl}_3$ )  $\delta$  (ppm) 23.4, 25.0, 26.5, 29.8, 32.8, 37.2, 49.9, 55.6, 68.9, 109.1, 120.2, 125.5, 129.1, 129.6, 136.8, 137.8, 141.1, 148.5, 174.4, 195.4. Anal. Calcd. for  $\text{C}_{23}\text{H}_{25}\text{ClN}_2\text{O}_3$ : C, 66.90; H, 6.10; N, 6.78 (%). Found: C, 66.93; H, 6.15; N, 6.86 (%). MS (m/z): 412 ( $\text{M}^+$ ).

**2-(tert-butylimino)-5'-chloro-6,6-dimethyl-6,7-dihydro-2H-spiro[benzofuran-3,3'-indoline]-2',4(5H)-dione (4e)**

White solid, m.p. = 234–236 °C (dec.) (lit. 238 °C (dec.)).<sup>10a</sup> IR (KBr)  $\nu$  3250, 2985, 1744, 1632, 1600  $\text{cm}^{-1}$ .  $^1\text{H}$  NMR (250 MHz,  $\text{CDCl}_3$ )  $\delta$  (ppm) 0.97 (s, 3H), 0.99 (s, 3H), 1.11 (s, 9H), 2.05–2.21 (distorted AB system, 2H), 2.53 (d,  $J = 17.5$  Hz, 1H), 2.65 (d,  $J = 17.5$  Hz, 1H), 6.77 (d,  $J = 7.5$  Hz, 1H), 7.13 (d,  $J = 7.5$  Hz, 1H), 7.41 (s, 1H), 8.51 (s, 1H).  $^{13}\text{C}$  NMR (62.5 MHz,  $\text{CDCl}_3$ )  $\delta$  (ppm) 26.3, 28.7, 29.6, 37.0, 49.7, 52.4, 68.9, 105.9, 120.0, 125.3, 128.9, 129.4, 136.5, 137.6, 144.0, 148.3, 176.1, 195.1. Anal. Calcd. for

$C_{21}H_{23}ClN_2O_3$ : C, 65.20; H, 5.99; N, 7.24 (%). Found: C, 65.22; H, 5.91; N, 7.28 (%). MS (m/z): 386 ( $M^+$ ).

**5'-chloro-6,6-dimethyl-2-(2,3,3-trimethylbutan-2-ylimino)-6,7-dihydro-2H-spiro[benzofuran-3,3'-indoline]-2',4(5H)-dione (4f)**

White solid, mp 220–223 °C (dec.) (lit. 224 °C (dec.)).<sup>10a</sup> IR (KBr)  $\nu$  3200, 2970, 1725, 1685, 1600  $cm^{-1}$ . <sup>1</sup>H NMR (250 MHz,  $CDCl_3$ )  $\delta$  (ppm) 0.98 (s, 3H), 1.05 (s, 3H), 1.12 (s, 9H), 1.55 (s, 6H), 2.10–2.27 (distorted AB system, 2H), 2.58 (d,  $J = 17.5$  Hz, 1H), 2.68 (d,  $J = 17.5$  Hz, 1H), 6.74 (d,  $J = 7.5$  Hz, 1H), 7.13 (d,  $J = 7.5$  Hz, 1H), 7.41 (s, 1H), 8.68 (s, 1H). <sup>13</sup>C NMR (62.5 MHz,  $CDCl_3$ )  $\delta$  (ppm) 23.1, 24.4, 26.5, 29.8, 33.7, 37.2, 49.9, 65.9, 71.6, 109.1, 120.2, 125.5, 129.1, 131.3, 134.4, 136.8, 137.8, 148.5, 178.9, 195.5. Anal. Calcd. for  $C_{25}H_{31}ClN_2O_3$ : C, 67.20; H, 6.81; N, 6.53 (%). Found: C, 67.33; H, 6.98; N, 6.36 (%). MS (m/z): 428 ( $M^+$ ).

**2-(cyclohexylimino)-6,7-dihydro-2H-spiro[benzofuran-3,3'-indoline]-2',4(5H)-dione (4g)**

White solid, mp 231–234 °C (dec.) (lit. 235 °C (dec.)).<sup>10a</sup> IR (KBr)  $\nu$  3390, 2855, 1740, 1730, 1655  $cm^{-1}$ . <sup>1</sup>H NMR (250 MHz,  $CDCl_3$ )  $\delta$  (ppm) 1.02–1.31 (m, 10H), 1.93–2.12 (m, 4H), 2.38 (t,  $J = 7.5$  Hz, 2H), 3.98 (m, 1H), 6.74 (d,  $J = 7.5$  Hz, 1H), 6.90 (t,  $J = 7.5$  Hz, 1H), 7.15–7.26 (m, 2H), 8.04 (s, 1H). <sup>13</sup>C NMR (62.5 MHz,  $CDCl_3$ )  $\delta$  (ppm) 19.7, 21.9, 23.4, 26.1, 31.3, 34.5, 55.6, 69.7, 107.8, 117.8, 124.3, 126.8, 128.2, 138.1, 141.1, 146.4, 179.7, 196.3. Anal. Calcd. for  $C_{21}H_{22}N_2O_3$ : C, 71.98; H, 6.33; N, 7.99 (%). Found: C, 71.95; H, 6.38; N, 7.95 (%). MS (m/z): 350 ( $M^+$ ).

**5'-chloro-2-(cyclohexylimino)-6,7-dihydro-2H-spiro[benzofuran-3,3'-indoline]-2',4(5H)-dione (4h)**

White solid, mp 243–245 °C (dec.) (lit. 241 °C (dec.)).<sup>10a</sup> IR (KBr)  $\nu$  3395, 2850, 1746, 1732, 1650  $cm^{-1}$ . <sup>1</sup>H NMR (250 MHz,  $CDCl_3$ )  $\delta$  (ppm) 0.98–1.30 (m, 10H), 1.95–2.34 (m, 4H), 2.31 (t,  $J = 7.5$  Hz, 2H), 3.94 (m, 1H), 6.73 (d,  $J = 7.5$  Hz, 1H), 7.14 (d,  $J = 7.5$  Hz, 1H), 7.40 (s, 1H), 8.04 (s, 1H). <sup>13</sup>C NMR (62.5 MHz,  $CDCl_3$ )  $\delta$  (ppm) 19.7, 21.9, 23.4, 26.6, 31.3, 34.5, 58.3, 69.2, 109.1, 120.2, 125.5, 128.2, 129.1, 133.0, 137.8, 141.1, 144.1, 178.9, 195.9. Anal. Calcd. for  $C_{21}H_{21}ClN_2O_3$ : C, 65.54; H, 5.50; N, 7.28 (%). Found: C, 65.58; H, 5.51; N, 7.34 (%). MS (m/z): 384 ( $M^+$ ).

**2-(tert-butylimino)-6,7-dihydro-2H-spiro[benzofuran-3,3'-indoline]-2',4(5H)-dione (4i)**

White solid, mp 225–228 °C (dec.) (lit. 225 °C (dec.)).<sup>10a</sup> IR (KBr)  $\nu$  3392, 2955, 1752, 1731, 1615  $cm^{-1}$ . <sup>1</sup>H NMR (250 MHz,  $CDCl_3$ )  $\delta$  (ppm) 1.07 (s, 9H), 2.08–2.20 (m, 4H), 2.28 (t,  $J = 7.5$  Hz, 2H), 6.79 (d,  $J = 7.5$  Hz, 1H), 6.91 (t,  $J = 7.5$  Hz, 1H), 7.17 (d,  $J = 7.5$  Hz, 1H), 7.29 (t,  $J = 7.5$  Hz, 1H), 9.01 (s, 1H). <sup>13</sup>C NMR (62.5 MHz,  $CDCl_3$ )  $\delta$  (ppm) 19.3, 21.5, 28.5, 34.1, 52.2, 69.0, 107.4, 121.1, 124.5,

126.4, 127.8, 137.7, 143.8, 145.1, 177.9, 195.5. Anal. Calcd. for  $C_{19}H_{20}N_2O_3$ : C, 70.35; H, 6.21; N, 8.64 (%). Found: C, 70.39; H, 6.27; N, 8.66 (%). MS (m/z): 324 ( $M^+$ ).

**2-(cyclohexylimino)-6,6-dimethyl-6,7-dihydro-2H-spiro[benzofuran-3,2'-indene]-1',3',4(5H)-trione (4j)**

White solid, mp 238–240 °C (dec.) (lit. 242 °C (dec.)).<sup>10a</sup> IR (KBr)  $\nu$  3390, 2855, 1743, 1735, 1730  $cm^{-1}$ . <sup>1</sup>H NMR (250 MHz,  $CDCl_3$ )  $\delta$  (ppm) 0.97 (s, 3H), 0.99 (s, 3H), 1.04–1.38 (m, 10H), 1.98–2.13 (distorted AB system, 2H), 2.47 (d,  $J = 18.0$  Hz, 1H), 2.59 (d,  $J = 17.5$  Hz, 1H), 4.01 (m, 1H), 6.64 (d,  $J = 7.5$  Hz, 2H), 6.98 (d,  $J = 7.5$  Hz, 2H). <sup>13</sup>C NMR (62.5 MHz,  $CDCl_3$ )  $\delta$  (ppm) 22.3, 23.0, 25.5, 28.8, 33.5, 36.2, 48.9, 54.6, 68.5, 115.4, 133.2, 133.5, 136.7, 136.9, 141.7, 157.2, 196.8, 205.1. Anal. Calcd. for  $C_{24}H_{25}NO_4$ : C, 73.64; H, 6.44; N, 3.58 (%). Found: C, 73.66; H, 6.40; N, 3.60 (%). MS (m/z): 391 ( $M^+$ ).

**2-(tert-butylimino)-6,7-dihydro-2H-spiro[benzofuran-3,2'-indene]-1',3',4(5H)-trione (4k)**

White solid, mp 244–246 °C (dec.) (lit. 248 °C (dec.)).<sup>10a</sup> IR (KBr)  $\nu$  3390, 2850, 1745, 1738, 1730  $cm^{-1}$ . <sup>1</sup>H NMR (250 MHz,  $CDCl_3$ )  $\delta$  (ppm) 1.04 (s, 9H), 1.87–2.32 (m, 4H), 2.40 (t,  $J = 7.5$  Hz, 2H), 6.79 (d,  $J = 7.5$  Hz, 2H), 7.01 (d,  $J = 7.5$  Hz, 2H). <sup>13</sup>C NMR (62.5 MHz,  $CDCl_3$ )  $\delta$  (ppm) 20.0, 23.2, 29.2, 34.8, 52.9, 67.8, 115.3, 123.4, 134.5, 137.9, 145.1, 158.3, 196.1, 206.7. Anal. Calcd. for  $C_{20}H_{19}NO_4$ : C, 71.20; H, 5.68; N, 4.15 (%). Found: C, 71.25; H, 5.62; N, 4.20 (%). MS (m/z): 337 ( $M^+$ ).

**2-(cyclohexylimino)spiro[indeno[1,2-b]furan-3,3'-indoline]-2',4(2H)-dione (4l)**

White solid, mp 284–287 °C (dec.) (lit. 284 °C (dec.)).<sup>10a</sup> IR (KBr)  $\nu$  3390, 2855, 1738, 1695  $cm^{-1}$ . <sup>1</sup>H NMR (250 MHz,  $DMSO-d_6$ )  $\delta$  (ppm) 1.01–1.33 (m, 10H), 3.96 (m, 1H), 6.75 (d,  $J = 7.5$  Hz, 1H), 6.90 (t,  $J = 7.5$  Hz, 1H), 7.15–7.26 (m, 4H), 7.64 (t,  $J = 7.5$  Hz, 1H), 7.82 (d,  $J = 7.5$  Hz, 1H), 9.93 (s, 1H). <sup>13</sup>C NMR (62.5 MHz,  $DMSO-d_6$ )  $\delta$  (ppm) 23.1, 23.8, 31.1, 55.4, 64.0, 107.9, 117.2, 121.3, 122.1, 124.4, 125.1, 126.6, 127.0, 128.3, 131.1, 132.5, 139.9, 145.0, 147.8, 152.3, 170.2, 195.7. Anal. Calcd. for  $C_{24}H_{20}N_2O_3$ : C, 74.98; H, 5.24; N, 7.29 (%). Found: C, 74.93; H, 5.26; N, 7.33 (%). MS (m/z): 384 ( $M^+$ ).

**2'-(tert-butylimino)-2H-spiro[acenaphthylene-1,3'-indeno[1,2-b]furan]-2,4'(2'H)-dione (4m)**

White solid, m.p. >300 °C (lit. > 300 °C).<sup>10a</sup> IR (KBr)  $\nu$  3395, 2857, 1730, 1695  $cm^{-1}$ . <sup>1</sup>H NMR (250 MHz,  $CDCl_3$ )  $\delta$  (ppm) 1.05 (m, 9H), 7.12–7.44 (m, 5H), 7.52–7.69 (m, 1H), 7.78–7.91 (m, 1H), 7.98–8.20 (m, 3H). <sup>13</sup>C NMR (62.5 MHz,  $CDCl_3$ )  $\delta$  (ppm) 31.2, 54.5, 76.6, 121.5, 124.0, 125.1, 125.8, 126.5, 127.0, 127.8, 128.8, 129.5, 130.1, 132.0, 132.9, 134.0, 134.1, 134.8, 140.5, 145.3, 147.9, 186.5, 195.8. Anal. Calcd. for  $C_{26}H_{19}NO_3$ : C, 79.37; H, 4.87; N, 3.56 (%). Found: C, 79.39; H, 4.80; N, 3.51 (%). MS (m/z): 393 ( $M^+$ ).

**2'-(cyclohexylimino)-6',6'-dimethyl-6',7'-dihydro-2H, 2'H-spiro[acenaphthylene-1,3'-benzofuran]-2,4'(5'H)-dione (4n)**

White solid, mp 231–233 °C (dec.) (lit. 229 °C (dec.)).<sup>10a</sup> IR (KBr)  $\nu$  2890, 1740, 1620, 1612. <sup>1</sup>H NMR (250 MHz, CDCl<sub>3</sub>)  $\delta$  (ppm) 0.87 (s, 3H), 0.90 (s, 3H), 0.97–1.05 (m, 10H), 1.98–2.14 (distorted AB system, 2H), 2.35–2.44 (distorted AB system, 2H), 4.05 (m, 1H), 7.36–7.42 (m, 1H), 7.65–7.75 (m, 1H), 7.81–7.95 (m, 1H), 7.98–8.23 (m, 3H). <sup>13</sup>C NMR (62.5 MHz, CDCl<sub>3</sub>)  $\delta$  (ppm) 21.4, 26.9, 28.5, 30.2, 35.5, 48.5, 50.1, 54.0, 93.2, 108.6, 112.8, 117.2, 122.0, 124.9, 127.7, 128.4, 130.9, 132.6, 149.0, 153.2, 163.0, 185.7, 191.5, 195.7. Anal. Calcd. for C<sub>27</sub>H<sub>27</sub>NO<sub>3</sub>: C, 78.42; H, 6.58; N, 3.39 (%). Found: C, 78.38; H, 6.61; N, 3.42 (%). MS (*m/z*): 413 (M<sup>+</sup>).

**2'-(cyclohexylimino)-6',6'-dimethyl-6',7'-dihydro-2H, 2'H-spiro[acenaphthylene-1,3'-benzofuran]-2,4'(5'H)-dione (7a)**

White solid, mp >300 °C. IR (KBr)  $\nu$  3050, 2970, 1740, 1730, 1660 cm<sup>-1</sup>. <sup>1</sup>H NMR (250 MHz, DMSO-*d*<sub>6</sub>)  $\delta$  (ppm) 0.96 (s, 6H), 0.99 (s, 6H), 1.07–1.28 (m, 20H), 1.96–2.14 (distorted AB system, 4H), 2.56 (d, *J* = 18.0 Hz, 2H), 2.67 (d, *J* = 18.0 Hz, 2H), 3.92–4.03 (m, 2H), 4.64 (d, *J* = 12.0 Hz, 2H), 4.89 (d, *J* = 12.0 Hz, 2H), 6.76 (d, *J* = 7.5 Hz, 2H), 6.92 (t, *J* = 7.5 Hz, 2H), 7.05 (s, 4H), 7.15–7.26 (m, 4H). <sup>13</sup>C NMR (62.5 MHz, DMSO-*d*<sub>6</sub>)  $\delta$  (ppm) 23.4, 24.0, 26.5, 29.8, 31.3, 37.2, 39.9, 49.9, 55.6, 68.2, 107.9, 116.9, 121.9, 124.0, 127.1, 129.3, 131.6, 136.1, 139.2, 141.0, 147.7, 174.8, 196.1. Anal. Calcd. for C<sub>54</sub>H<sub>58</sub>N<sub>4</sub>O<sub>6</sub>: C, 75.50; H, 6.81; N, 6.52 (%). Found: C, 75.41; H, 6.88; N, 6.43 (%). MS (*m/z*): 859 (M<sup>+</sup>).

**2'-(cyclohexylimino)-6',6'-dimethyl-6',7'-dihydro-2H, 2'H-spiro[acenaphthylene-1,3'-benzofuran]-2,4'(5'H)-dione (7b)**

White solid, mp >300 °C. IR (KBr)  $\nu$  3060, 2950, 1748, 1735, 1665 cm<sup>-1</sup>. <sup>1</sup>H NMR (250 MHz, DMSO-*d*<sub>6</sub>)  $\delta$  (ppm) 0.99–1.29 (m, 20H), 1.96–2.12 (m, 8H), 2.37 (t, *J* = 7.5 Hz, 4H), 3.99 (m, 2H), 4.590 (d, *J* = 12.0 Hz, 2H), 4.73 (d, *J* = 12.0 Hz, 2H), 6.75 (d, *J* = 7.5 Hz, 2H), 6.90 (t, *J* = 7.5 Hz, 2H), 7.06 (s, 4H), 7.15–7.26 (m, 4H). <sup>13</sup>C NMR (62.5 MHz, DMSO-*d*<sub>6</sub>)  $\delta$  (ppm) 19.9, 22.0, 23.5, 26.8, 27.8, 34.7, 46.2, 55.8, 65.6, 108.1, 121.4, 123.3, 126.6, 126.9, 127.3, 129.4, 135.4, 139.3, 141.1, 145.7, 174.1, 196.7. Anal. Calcd. for C<sub>50</sub>H<sub>50</sub>N<sub>4</sub>O<sub>6</sub>: C, 74.79; H, 6.28; N, 6.98 (%). Found: C, 74.74; H, 6.20; N, 7.05 (%). MS (*m/z*): 802 (M<sup>+</sup>).

**2'-(cyclohexylimino)-6',6'-dimethyl-6',7'-dihydro-2H, 2'H-spiro[acenaphthylene-1,3'-benzofuran]-2,4'(5'H)-dione (7c)**

White solid, mp >300 °C. IR (KBr)  $\nu$  3060, 2950, 1748, 1735, 1665 cm<sup>-1</sup>. <sup>1</sup>H NMR (250 MHz, DMSO-*d*<sub>6</sub>)  $\delta$  (ppm) 1.00–1.35 (m, 20H), 3.90 (m, 2H), 4.59 (d, *J* = 12.0 Hz, 2H), 4.74 (d, *J* = 12.0 Hz, 2H), 6.79 (d, *J* = 7.5 Hz, 2H), 6.90 (t, *J* = 7.5 Hz, 2H), 7.11 (s, 4H), 7.14–7.26 (m, 8H),

7.64 (t, *J* = 7.5 Hz, 2H), 7.82 (d, *J* = 7.5 Hz, 2H). <sup>13</sup>C NMR (62.5 MHz, DMSO-*d*<sub>6</sub>)  $\delta$  (ppm) 23.5, 24.2, 31.5, 43.3, 55.8, 66.0, 107.9, 119.2, 121.7, 124.8, 127.2, 127.3, 127.4, 128.7, 129.9, 131.5, 131.8, 132.9, 140.1, 143.6, 146.3, 153.4, 176.0, 193.5. Anal. Calcd. for C<sub>56</sub>H<sub>46</sub>N<sub>4</sub>O<sub>6</sub>: C, 77.22; H, 5.32; N, 6.43 (%). Found: C, 77.13; H, 5.40; N, 6.31 (%). MS (*m/z*): 870 (M<sup>+</sup>).

## 5. Acknowledgements

The research for this paper was financially supported by the Islamic Azad University, Shiraz Branch, Iran, through project entitled Isocyanide-based one-pot three component synthesis of novel spiro-iminolactone derivatives in the presence of SDS in aqueous medium. The authors appreciate the IAU (Shiraz Branch) for its support.

## 6. References

- (a) D. Villemin, L. Liao, *Synth. Commun.* **2003**, *33*, 1575–1585. DOI:10.1081/SCC-120018778  
(b) Y. Tang, C. Li, *Tetrahedron Lett.* **2006**, *47*, 3823–3825. DOI:10.1016/j.tetlet.2006.03.166
- G. Grossmann, M. Poncioni, M. Bornand, B. Jolivet, M. Neuberger, U. Sequin, *Tetrahedron* **2003**, *59*, 3237–4251. DOI:10.1016/S0040-4020(03)00483-6
- (a) S. M. Hein, J. B. Gloer, B. Koster, D. Malloch, *J. Nat. Prod.* **2001**, *64*, 809–812. DOI:10.1021/np000617u  
(b) M. Pour, M. Spulak, V. Balsanek, J. Kunes, P. Kubanova, V. Butcha, *Bioorg. Med. Chem.* **2003**, *11*, 2843–2866. DOI:10.1016/S0968-0896(03)00220-7
- S. Padakanti, M. Pal, K. R. Yeleswarapu, *Tetrahedron* **2003**, *59*, 7915–7920. DOI:10.1016/j.tet.2003.08.021
- (a) S. Takahashi, A. Kubota, T. Nakata, *Tetrahedron Lett.* **2002**, *43*, 8661–8664. DOI:10.1016/S0040-4039(02)02182-2  
(b) F. Bellina, E. Falchi, R. Rossi, *Tetrahedron* **2003**, *59*, 9091–9100. DOI:10.1016/j.tet.2003.09.061
- (a) S. Hanessian, R. Y. Park, R. Y. Yang, *Synlett* **1997**, 351–352. DOI:10.1055/s-1997-803  
(b) A. Choudhury, F. Jin, D. Wang, Z. Wang, G. Xu, D. Nguyen, J. Castoro, M. E. Pierce, P. N. Confalone, *Tetrahedron Lett.* **2003**, *44*, 247–250. DOI:10.1016/S0040-4039(02)02532-7
- (a) F.-F. Gan, Sh.-B. Yang, Y.-Ch. Luo, W.-B. Yang, P.-F. Xu, *J. Org. Chem.* **2010**, *75*, 2737–2740. DOI:10.1021/jo100183d  
(b) M. M. Zweerink, A. M. Edison, G. B. Well, W. Pinto, R. L. Lester, *J. Biol. Chem.* **1992**, *267*, 25032–25038.
- (a) P. A. Grieco, *Organic Synthesis in Water*, Blackie Academic and Professional, London, 1998. DOI:10.1007/978-94-011-4950-1  
(b) P. T. Anastas, T. C. Williamson, *Green Chemistry*, ed., ACS Symposium Series 626, American Chemical Society, Wash-

ington, DC, 1996.

(c) V. J. Li, T. H. Chan, *Organic Reactions in Aqueous Media*, Wiley, New York, 1997.

(d) P. Anastas J. C. Warner, *Green Chemistry: Theory and Practice*, Oxford University Press, Oxford, 1998.

(e) C. J. Li, *Chem. Rev.* **2005**, *105*, 3095–3166.

DOI:10.1021/cr030009u

(f) H. Mehrabi, H. Abusaidi, *J. Iran Chem. Soc.* **2010**, *7*, 890–894. DOI:10.1007/BF03246084

(g) N. Azizi, A. Khajeh Amiri, M. Bolourtchian, M. R. Saidi, *J. Iran Chem. Soc.* **2009**, *6*, 749–753.

DOI:10.1007/BF03246165

(h) Sh. Rostamizadeh, H. Estiri, M. Azad, *J. Iran Chem. Soc.* **2016**, *13*, 1367–1374.

DOI:10.1007/s13738-016-0851-9

(i) M. Riahi, E. Farsani, F. Assady, B. Jalilian Yadollahi, H. Amiri Rudbari, *J. Iran Chem. Soc.* **2015**, *12*, 1207–1212.

DOI:10.1007/s13738-014-0583-7

(j) M. Shiri, *J. Iran Chem. Soc.* **2013**, *10*, 1019–1023.

DOI:10.1007/s13738-013-0239-z

(k) B. Zeynizadeh, M. Zabihzadeh, Z. Shokri, *J. Iran Chem. Soc.* **2016**, *13*, 1487–1492.

DOI:10.1007/s13738-016-0864-4

9. (a) S. Kobayashi, K. Manabe S. Nagayama, in *Modern Carbonyl Chemistry*, ed. J. Otera, Wiley-VCH, Weinheim, 2000.

(b) K. Manabe, Y. Mori, T. Wakabayashi, S. Nagayama, S. Kobayashi, *J. Am. Chem. Soc.* **2000**, *122*, 7202–7207.

DOI:10.1021/ja001420r

(c) S. Kobayashi, S. Nagayama, T. Busujima, *J. Am. Chem. Soc.* **1998**, *120*, 8287–8288. DOI:10.1021/ja980715q

(d) M. Shekouhy, A. Khalafi-Nezhad, *Green Chem.* **2015**, *17*, 4815–4829. DOI:10.1039/C5GC01448D

(e) M. Shekouhy, *Catal. Sci. Tech.* **2012**, *2*, 1010–1020.

DOI:10.1039/c2cy00493c

(f) L. J. Yan, Y. Ch. Wang, *ChemistrySelect* **2016**, *1*, 6948–6960. DOI:10.1002/slct.201601534

(g) A. R. Moosavi-Zare, M. A. Zolfigol, R. Salehi-Moratab, E. Noroozizadeh, *Can. J. Chem.* **2017**, *95*, 194–198.

DOI:10.1139/cjc-2016-0374

(h) A. R. Moosavi-Zare, M. A. Zolfigol, E. Noroozizadeh, R.

Salehi-Moratab, M. Zarei, *J. Mol. Cat. A: Chem.* **2016**, *420*, 246–253. DOI:10.1016/j.molcata.2016.04.021

(i) A. R. Moosavi-Zare, M. A. Zolfigol, E. Noroozizadeh, M. Zarei, R. Karamian, M. Asadbegy, *J. Mol. Cat. A: Chem.* **2016**, *425*, 217–228. DOI:10.1016/j.molcata.2016.10.011

(j) M. A. Ghasemzadeh, M. H. Abdollahi-Basir, *Acta. Chim. Slov.* **2016**, *63*, 627–637.

DOI:10.17344/acsi.2016.2386

(k) F. Moradgholi, J. Lari, M. Vahidi Parsa, M. Mirkarrazi, *Acta Chim. Slov.* **2016**, *63*, 781–789.

DOI:10.17344/acsi.2016.2634

(l) E. Noroozizadeh, A. R. Moosavi-Zare, M. A. Zolfigol, A. Zare, M. Zarei, *Can. J. Chem.* **2017**, *95*, 16–21.

DOI:10.1139/cjc-2016-0258

10. (a) H. R. Safaei, N. Shioukhi, M. Shekouhy, *Monatsh. Chem.* **2013**, *144*, 1855–1863. DOI:10.1007/s00706-013-1060-1

(b) H. R. Safaei, M. Shekouhy, Sh. Khademi, V. Rahmanian, M. Safaei, *J. Ind. Eng. Chem.* **2014**, *20*, 3019–3024.

DOI:10.1016/j.jiec.2013.11.037

11. (a) R. N. Butler, A. G. Coyne, *Chem. Rev.* **2010**, *110*, 6302–6337. DOI:10.1021/cr100162c

(b) B. Samiey, C.-H. Cheng, J. Wu, *J. Chem.* **2014**, 1–14.

DOI:10.1155/2014/908476

12. (a) H. Singh, L. D. S. Yadav, B. K. Bhattacharya, *J. Indian. Chem. Soc.* **1979**, *56*, 1013–1017. (b) N. C. Desai, *Indian J. Chem. Sect. B* **1993**, *32*, 343–346. (c) X. M. Feng, R. Chen, X. C. Liu, Z. Y. Zhang, *Chin. J. Appl. Chem.* **1991**, *8*, 28–33. (d) P. S. Upadhyay, R. N. Vansdadia, A. J. Baxi, *Indian J. Chem. Sect. B* **1990**, *29*, 793–796. (e) Z. Y. Zhang, X. Chen, L. L. Wei, Z. L. Ma, *Chem. Res. Chin. Univ.* **1991**, *7*, 129–135.

(f) A. R. Bhat, F. Athar, A. Azam, *Eur. J. Med. Chem.* **2009**, *44*, 426–431. DOI:10.1016/j.ejmech.2007.11.005

(g) D. B. Reddy, B. Seenaiiah, S. Eswaraiiah, T. Seshamma, M. V. R. Reddy, *J. Indian. Chem. Soc.* **1989**, *66*, 893–899.

(h) P. F. Iqbal, H. Parveen, A. R. Bhat, F. Hayat, A. Azam, *Eur. J. Med. Chem.* **2009**, *44*, 4747–4751.

DOI:10.1016/j.ejmech.2009.06.016

13. R. M. Shaker, *Arkivoc* **2012**, *1*, 1–44.

14. A. A. Jafari, F. Moradgholi, F. Tamaddon, *Eur. J. Org. Chem.* **2009**, *2009*, 1249–1255.

## Povzetek

V prispevku je opisana priprava  $\gamma$ -spiroiminolaktonskih derivatov z enostopenjsko trokomponentno reakcijo cikličnih karbonilnih spojin (kot so: isatin, acetonaftokinon, ninhidrin), spojin z aktivirano  $\alpha$ -metilensko karbonilno skupino in izocianidov v vodi, ob uporabi natrijevega dodecil sulfata (SDS) kot komercialno dostopne in cenene površinsko aktivne snovi. Vsi produkti so bili pridobljeni z dobrimi in nekateri celo z odličnimi izkoristki, brez tvorbe stranskih produktov. Kot reakcijski medij je bila uporabljena voda kot zeleno in nenevarno topilo. Predstavljena metoda je bila tudi uspešno uporabljena za pripravo nekaterih novih bis(spiroiminolaktonskih) derivatov.

Scientific paper

# Synthesis, Nematicidal and Antifungal Properties of Hybrid Heterocyclics

Avula Srinivas,<sup>1,\*</sup> Malladi Sunitha,<sup>1</sup> Pulluri Karthik<sup>1</sup>  
and K. Vasumathi Reddy<sup>2</sup>

<sup>1</sup> Department of Chemistry, Vaagdevi Degree & PG College

<sup>2</sup> Department of Zoology, Vaagdevi Degree & PG College Kishanpura, Warangal, Telangana, India 506001

\* Corresponding author: E-mail: avula.sathwikreddy@gmail.com

Received: 28-08-2017

## Abstract

A new series of 5-((3aR,5S,6S,6aR)-6-((1-(4-chlorophenyl)-1H-1,2,3-triazol-4-yl)methoxy)-2,2-dimethyltetrahydrofuro[2,3-d][1,3]dioxol-5-yl)-3-(4-fluorophenyl)-2,6-diphenyl-3,3a,5,6-tetrahydro-2H-pyrazolo[3,4-d]thiazoles **10a–r** was synthesized by the reaction of chalcone derivatives of 2-((3aR,5S,6S,6aR)-6-((1-(4-chlorophenyl)-1H-1,2,3-triazol-4-yl)methoxy)-2,2-dimethyltetrahydrofuro[2,3-d][1,3]dioxol-5-yl)-3-phenylthiazolidin-4-one **9** with aryl/alkyl hydrazines. The chemical structures of newly synthesized compounds were elucidated by IR, NMR, MS and elemental analysis. The compounds **10a–r** were evaluated for their nematicidal activity against *Dietylenchus myceliophagus* and *Caenorhabditis elegans* by aqueous *in vitro* screening technique. Among them, compounds containing *N*-benzylpyrazole moiety (**10d**, **10j**, **10p**), and *N*-methylpyrazole moiety (**10f**, **10i**, **10r**) showed significant nematicidal activity against both tested nematodes with LD<sub>50</sub> 160–210 ppm, almost equal to oxamyl standard. Further, these compounds **10a–r** were screened for their antifungal (MZI, MIC, and MFC) activity against four fungal organisms *viz.* *Candida albicans* (ATCC 102331), *Aspergillus fumigates* (HIC 6094), *Trichophyton rubrum* (IFO 9185) and *Trichophyton mentagrophytes* (IFO 40996). Most of the new compounds showed appreciable activity against the tested fungi, and emerged as potential molecules for further development.

**Keywords:** Hybrid heterocyclics, click reaction, Knoevenagel condensation, cyclisation, nematicidal activity, antifungal activity

## 1. Introduction

1,2,3-Triazoles are one of the most important classes of heterocyclic organic compounds, which are reported to be present in a plethora of biological activities in diverse therapeutic areas.<sup>1</sup> The 1,2,3-triazole motif is associated with diverse pharmacological activities, such as antibacterial, antifungal, hypoglycemic, antihypertensive and analgesic properties. Polysubstituted five-membered aza heterocycles rank as the most potent glycosidase inhibitors.<sup>2</sup> Further, this nucleus in combination (or linked) with various other classes of compounds, such as amino acids, steroids, aromatic compounds, carbohydrates *etc.*, became prominent in having various pharmacological properties.<sup>3</sup> 1,2,3-Triazole modified carbohydrates have become easily available after the discovery of the Cu(I) catalyzed azide-alkynes 1,3-dipolar cycloaddition reaction<sup>4</sup> and quickly became a pronounced class of non-nat-

ural sugars. The chemistry and biology of triazole modified sugars is dominated by triazole glycosides.<sup>5</sup> Therefore, the synthesis and investigation of biological activity of 1,2,3-triazole glycosides is an important objective, which also received a considerable attention by the medicinal chemists.

Thiazoles are familiar group of heterocyclic compounds possessing a wide variety of biological activities and their utility as medicine is very much established.<sup>6</sup> Thiazole nucleus is also an integral part of all the available penicillins which have revolutionized the therapy of bacterial diseases.<sup>7</sup> Furthermore, there has been considerable interest in the chemistry of thiazolidine-4-one ring system which is the core structure in various synthetic pharmaceuticals displaying a broad spectrum of biological activities.<sup>8–10</sup> The thiazolidine-4-one ring also occurs in nature; thus actithiazic acid isolated from *Streptomycis* strains exhibits highly specific *in vitro* activity against mycobacteri-



um *Tuberculosis*.<sup>11</sup> Thiazolidine-4-ones are known to exhibit diverse bioactivities, such as antiplatelet activating factor,<sup>12</sup> antihistaminic,<sup>13</sup> COX inhibitor,<sup>14</sup> Ca<sup>2+</sup> channel blocking,<sup>15</sup> PAF antagonist,<sup>16</sup> cardioprotective,<sup>17</sup> anti-ischemic<sup>18</sup> and nematocidal activities.<sup>19</sup> Moreover, pyrazoles and their derivatives could be considered as possible antimicrobial agents.<sup>20</sup> The other derivatives display antidepressant,<sup>21</sup> antiarthritic<sup>22</sup> and cerebroprotecting<sup>23</sup> properties. Some aryl pyrazoles were reported to be non-nucleoside human immunodeficiency virus (HIV-1) reverse transcriptase inhibitor,<sup>24</sup> COX-2 inhibitor,<sup>25–27</sup> activator of the nitric oxide receptor and to have soluble guanylate cyclase activity.<sup>28</sup>

Nematodes are tiny worms, some of them are plant parasites, and can play an important role in the predisposition of the host plant to the invasion by secondary pathogens.<sup>29</sup> Plants attacked by nematodes show retarded growth and development, as well as loss in the quality and quantity of the harvest. The nematocides currently still in use are slated for reduction due to the environmental problems, and human and animals health concerns. For example, effective nematocides, such as dibromochloropropane (DBCD) and ethylene dibromide (EDB) have been withdrawn from the market due to their deleterious effects on humans and the environment. Methyl bromide, the most effective and widely used fumigant for soil-borne pests including nematodes, has already been banned.

The use of nonfumigant nematocides, based on organophosphates and carbamates, is expected to increase concomitantly with the withdrawal of methyl bromide, which will bring about new environmental concerns. In fact, the highly toxic Aldicarb used to control insects and nematodes has been detected in ground water.<sup>30</sup> Therefore, alternative nematode control methods or less toxic nematocides need to be developed.<sup>31</sup> One way of searching for such nematocidal compounds is to screen naturally occurring compounds in plants. Several such compounds, e.g. alkaloids, sesquiterpenes, diterpenes, polyacetylenes have nematocidal activity.<sup>32–33</sup> For example, *a*-terthienyl is a highly effective nematocidal compound. Other compounds with nematocidal activity have been isolated from plants, mainly from the family *Asteraceae*.<sup>32–33</sup> However, compounds of plant origin and their analogs have not been developed into commercial nematocides yet; hence there is a need to develop commercial syntheses.

Following the successful introduction of antimicrobial and nematocidal agents, inspired by the biological profile of triazoles, thiazolidinones, pyrazoles and their increasing importance in pharmaceutical and biological fields and in continuation of our work on biologically active molecules<sup>34–48</sup> and in order to enhance the biological activity of triazoles, thiazolidinones and pyrazole moieties, it was thought to be of interest to accommodate triazole, thiazolidinones and pyrazole moieties in single molecular framework. In this article we report the synthesis of a new class of hybrid heterocycles **10a–g** in good yields

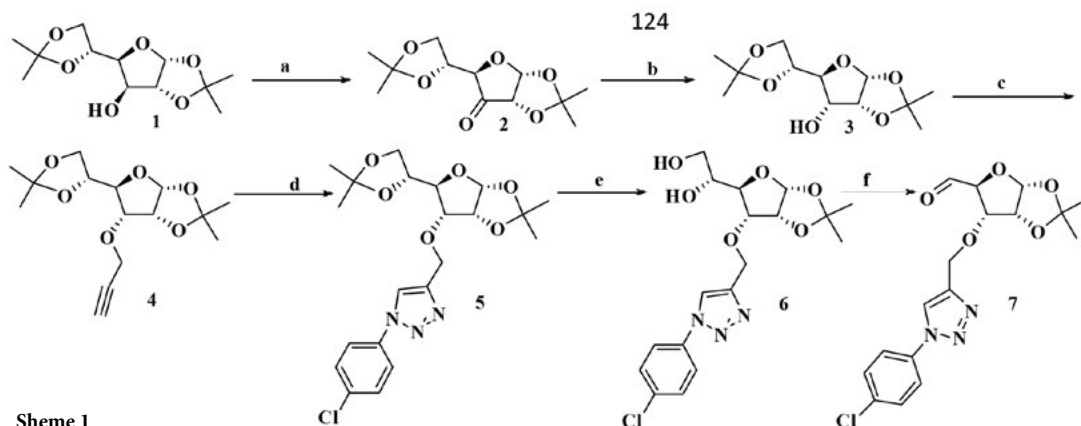
and their evaluation for *in vitro* antifungal and nematocidal activity.

## 2. Results and Discussion

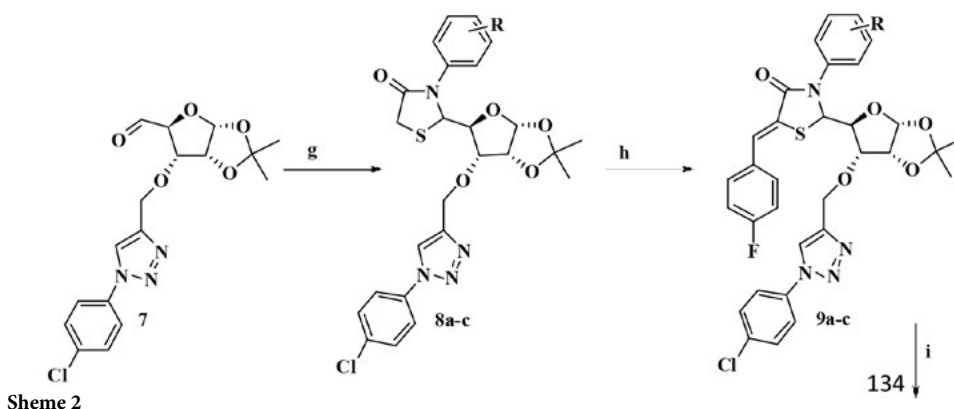
The key intermediate **8** required for the synthesis of title compound was prepared according to the procedure outlined in the Scheme 1. Diacetone D-glucose (**1**) prepared from D-(+)-glucose by treating with acetone in the presence of a catalytic amount of sulphuric acid according to the literature procedure,<sup>49</sup> reduction of **2** (prepared by Swern oxidation of **1**) with NaBH<sub>4</sub> in aq. ethanol at 0 °C for 1 h gave **3** (77%), which on subsequent propargylation in DMF in the presence of NaH for 1 h afforded propargyl ether **4** (80%). Now the propargyl ether converted into triazole **5** (82%) by using 1,3-dipolar cycloaddition with *p*-chlorophenyl azide was carried out at ambient temperature in the presence of CuSO<sub>4</sub> and sodium ascorbate in a mixture of 1:1 *t*-BuOH–H<sub>2</sub>O as reported by Sharpless. Acid hydrolysis of 5,6-acetonide **5** in 60% AcOH furnished the diol **6** (85%), which on oxidative cleavage with NaIO<sub>4</sub> gave the aldehyde **7**. Subsequently one-pot synthesis of triazole linked to thiazolidenone glycosides was carried out by the condensation reaction between **7**, primary aromatic amine and a thioglycolic acid in the presence of ZnCl<sub>2</sub> under microwave irradiation/conventional heating (Scheme 2). In the classical method, the reactions were performed in dry toluene at reflux for a long time (2–4 h), often leading to degradation processes and consequent low yields of isolated products, whereas the application of microwave assisted technology, the reaction is completed in only 5–10 minutes and the compounds, isolated by conventional work-up, are obtained in satisfactory yields, often higher

Table 1. Synthesis of compounds **10a–r**

Compound	R	R <sup>1</sup>	Yield (%)
<b>10a</b>	<i>p</i> -Me-C <sub>6</sub> H <sub>4</sub> -	C <sub>6</sub> H <sub>5</sub> -	69
<b>10b</b>	<i>p</i> -Me-C <sub>6</sub> H <sub>4</sub> -	<i>p</i> -MeOC <sub>6</sub> H <sub>4</sub> -	70
<b>10c</b>	<i>p</i> -Me-C <sub>6</sub> H <sub>4</sub> -	<i>p</i> -Cl-C <sub>6</sub> H <sub>4</sub> -	67
<b>10d</b>	<i>p</i> -Me-C <sub>6</sub> H <sub>4</sub> -	C <sub>6</sub> H <sub>5</sub> -CH <sub>2</sub> -	72
<b>10e</b>	<i>p</i> -Me-C <sub>6</sub> H <sub>4</sub> -	(CH <sub>3</sub> ) <sub>2</sub> -CH-	76
<b>10f</b>	<i>p</i> -Me-C <sub>6</sub> H <sub>4</sub> -	CH <sub>3</sub> -	66
<b>10g</b>	<i>p</i> -Cl-C <sub>6</sub> H <sub>4</sub> -	C <sub>6</sub> H <sub>5</sub> -	68
<b>10h</b>	<i>p</i> -Cl-C <sub>6</sub> H <sub>4</sub> -	<i>p</i> -MeOC <sub>6</sub> H <sub>4</sub> -	70
<b>10i</b>	<i>p</i> -Cl-C <sub>6</sub> H <sub>4</sub> -	<i>p</i> -Cl-C <sub>6</sub> H <sub>4</sub> -	76
<b>10j</b>	<i>p</i> -Cl-C <sub>6</sub> H <sub>4</sub> -	C <sub>6</sub> H <sub>5</sub> -CH <sub>2</sub> -	69
<b>10k</b>	<i>p</i> -Cl-C <sub>6</sub> H <sub>4</sub> -	(CH <sub>3</sub> ) <sub>2</sub> -CH-	67
<b>10l</b>	<i>p</i> -Cl-C <sub>6</sub> H <sub>4</sub> -	CH <sub>3</sub> -	71
<b>10m</b>	<i>p</i> -NO <sub>2</sub> -C <sub>6</sub> H <sub>4</sub> -	C <sub>6</sub> H <sub>5</sub> -	74
<b>10n</b>	<i>p</i> -NO <sub>2</sub> -C <sub>6</sub> H <sub>4</sub> -	<i>p</i> -MeOC <sub>6</sub> H <sub>4</sub> -	76
<b>10o</b>	<i>p</i> -NO <sub>2</sub> -C <sub>6</sub> H <sub>4</sub> -	<i>p</i> -Cl-C <sub>6</sub> H <sub>4</sub> -	72
<b>10p</b>	<i>p</i> -NO <sub>2</sub> -C <sub>6</sub> H <sub>4</sub> -	C <sub>6</sub> H <sub>5</sub> -CH <sub>2</sub> -	74
<b>10q</b>	<i>p</i> -NO <sub>2</sub> -C <sub>6</sub> H <sub>4</sub> -	(CH <sub>3</sub> ) <sub>2</sub> -CH-	71
<b>10r</b>	<i>p</i> -NO <sub>2</sub> -C <sub>6</sub> H <sub>4</sub> -	CH <sub>3</sub> -	67



Scheme 1



Scheme 2

R = a) 4-CH<sub>3</sub>-C<sub>6</sub>H<sub>5</sub>; b) 4-Cl-C<sub>6</sub>H<sub>5</sub>; c) 4-NO<sub>2</sub>-C<sub>6</sub>H<sub>5</sub>

**Reagents and conditions:** a) COCl<sub>2</sub>, CH<sub>2</sub>Cl<sub>2</sub>, Et<sub>3</sub>N, -78 °C → rt, 1.5 h, 83%; b) NaBH<sub>4</sub>, EtOH, H<sub>2</sub>O, (19:1), 0 °C → rt, 78%; c) Propargyl bromide, NaH, DMF, 0 °C → rt; d) *p*-Chlorophenylazide, sodium ascorbate, CuSO<sub>4</sub> · 5H<sub>2</sub>O, *t*-BuOH/H<sub>2</sub>O, 0 °C → rt, 75%; e) 60%, AcOH, rt, 69%; f) NaIO<sub>4</sub>, CH<sub>2</sub>Cl<sub>2</sub>, 0 °C → rt, 75%; g) Ar-NH<sub>2</sub>, SHCH<sub>2</sub>COOH, ZnCl<sub>2</sub>, toluene, 80 °C, 85%; h) 4-F-C<sub>6</sub>H<sub>4</sub>-CHO, AcOH / NaOAc, reflux, 82–88%; i) R'-NHNH<sub>2</sub> · HCl, AcOH / NaOAc reflux, 76–67%.

than those achieved by traditional methods.<sup>35</sup> Compound **8** was then reacted with *p*-fluorobenzaldehyde in the presence of anhydrous NaOAc in glacial AcOH at reflux temperature to give chalcone derivatives of triazole linked thiazolidenone glycosides **9**. Furthermore, the compounds upon cyclocondensation with alkyl/aryl hydrazines in the presence of anhydrous NaOAc in glacial AcOH at reflux temperature gave **10a–r** in good yields. The versatility of the reaction is demonstrated by the fact that both aromatic hydrazines, such as phenyl hydrazines, and aliphatic hydrazines, such as benzylhydrazine, isopropylhydrazine, methylhydrazine, afforded their corresponding **10a–r** in good yields. The structures of synthesized compounds

were confirmed by IR, NMR, MS and elemental analysis. Furthermore, the compounds were subjected to nematocidal and anti bacterial testing.

### 3. Antifungal Activity

The newly prepared compounds **10a–r** were screened for their antifungal activity against four fungal organisms, viz *Candida albicans* (ATCC 10231), *Aspergillus fumigatus* (HIC 6094), *Trichophyton rubrum* (IFO 9185) and *Trichophyton mentagrophytes* (IFO 40996) in dimethyl sulfoxide (DMSO) by agar diffusion method.<sup>50</sup> Amphotericin B was

used as the standard drug and the zones of fungal inhibition values are reported in Table 3. In addition, the MIC and MFC values determined by the broth dilution method<sup>51</sup> are recorded in Table 4.

## 4. Nematicidal Activity

The compounds synthesized **10a–g** in this study were also screened for their nematicidal activity against *Dietylenchus myceliophagus* and *Caenorhabditis elegans* by aqueous *in vitro* screening technique<sup>52</sup> at various concentrations. The nematicidal activity of each tested compound was compared with the standard drug Levamisole. The results have been expressed in terms of LD<sub>50</sub> *i.e.* median le-

thal dose at which 50% of nematodes became immobile (dead). The screened data reveal that compounds **10e** and **10f** are the most effective against *Dietylenchus myceliophagus* and *Caenorhabditis elegans* with LD<sub>50</sub> 190 and 220 × 10<sup>-6</sup> respectively, whereas the other tested compounds showed moderate activity. The LD<sub>50</sub> values of the compounds screened are presented in Table 2.

## 5. Experimental

Commercial grade reagents were used as supplied. Solvents except analytical reagent grade were dried and purified according to literature when necessary. Reaction progress and purity of the compounds were checked by

Table 2. Median lethal dose LD<sub>50</sub> (ppm) of compounds **10a–r**

Compd.	<i>D. myceliophagus</i>	<i>C. elegans</i>	Compd.	<i>D. myceliophagus</i>	<i>C. elegans</i>
<b>10a</b>	850	670	<b>10j</b>	180	200
<b>10b</b>	950	870	<b>10k</b>	520	670
<b>10c</b>	240	360	<b>10l</b>	190	210
<b>10d</b>	190	210	<b>10m</b>	800	620
<b>10e</b>	550	600	<b>10n</b>	920	810
<b>10f</b>	160	200	<b>10o</b>	230	350
<b>10g</b>	810	650	<b>10p</b>	190	190
<b>10h</b>	900	820	<b>10q</b>	510	600
<b>10i</b>	290	380	<b>10r</b>	180	200
<b>Oxamyl</b>	150	180	<b>Oxamyl</b>	150	180

LD<sub>50</sub>: median lethal dose (the concentration at which 50% nematodes became immobile)

Table 3. Inhibitory zone diameters (mm) of **10a–r** against tested fungal strains

Compound	Mean zone of inhibition (MZI) in mm <sup>a</sup>			
	<i>C. albicans</i>	<i>A. fumigatus</i>	<i>T. rubrum</i>	<i>T. mentagrophytes</i>
<b>10a</b>	11	10	–	09
<b>10b</b>	09	15	13	12
<b>10c</b>	13	11	11	10
<b>10d</b>	22	16	15	16
<b>10e</b>	–	13	–	–
<b>10f</b>	20	20	20	18
<b>10g</b>	–	–	17	–
<b>10h</b>	14	–	–	–
<b>10i</b>	–	–	15	–
<b>10j</b>	21	17	14	16
<b>10k</b>	10	–	11	12
<b>10l</b>	18	15	13	16
<b>10m</b>	08	11	10	09
<b>10n</b>	13	–	–	–
<b>10o</b>	15	–	–	–
<b>10p</b>	19	16	11	13
<b>10q</b>	–	–	09	–
<b>10r</b>	21	14	15	14
<b>Amphotericin B</b>	25	20	20	18

Amphotericin B (100 µg/disc) was used as the positive reference; compounds **10a–r** (300 µg/disc).

– indicates no sensitivity or MZI lower than 7 mm. <sup>a</sup> Values are mean (n = 3).

**Table 4.** Minimum inhibitory concentration (MIC) and minimum fungicidal concentration (MFC) in  $\mu\text{g/mL}$  of compounds **10a–r**

Compd.	<i>C. albicans</i>		<i>A. fumigatus</i>		<i>T. rubrum</i>		<i>T. mentagrophytes</i>	
	MIC	MFC	MIC	MFC	MIC	MFC	MIC	MFC
<b>10a</b>	–	–	25.0	25.0	25.0	50.0	25.0	25.0
<b>10b</b>	25.0	25.0	25.0	50.0	12.5	12.5	12.5	25.0
<b>10c</b>	12.5	25.0	6.25	12.5	6.25	12.5	6.25	12.5
<b>10d</b>	3.12	6.25	25.0	25.0	12.5	25.0	25.0	25.0
<b>10e</b>	12.5	25.0	–	–	–	–	–	–
<b>10f</b>	3.12	3.12	3.12	6.25	3.12	6.25	6.25	12.5
<b>10g</b>	6.25	6.25	12.5	25.0	12.5	12.5	6.25	12.5
<b>10h</b>	25.0	50.0	–	–	25.0	50.0	25.0	50.0
<b>10i</b>	12.5	12.5	25.0	25.0	12.5	12.5	25.0	50.0
<b>10j</b>	3.12	6.25	6.25	12.5	6.25	12.5	12.5	25.0
<b>10k</b>	12.5	25.0	25.0	25.0	–	–	25.0	50.0
<b>10l</b>	12.5	25.0	6.25	50.0	6.25	25.0	–	–
<b>10m</b>	12.5	25.0	12.5	50.0	6.25	25.0	12.5	12.5
<b>10n</b>	6.25	12.5	12.5	25.0	12.5	25.0	–	–
<b>10o</b>	25.0	25.0	25.0	50.0	25.0	50.0	6.25	12.5
<b>10p</b>	12.5	25.0	–	–	–	–	–	–
<b>10q</b>	25.0	25.0	25.0	50.0	12.5	25.0	12.5	25.0
<b>10r</b>	12.5	25.0	12.5	25.0	12.5	25.0	12.5	25.0
<b>Amphotericin B</b>	6.25	12.5	3.12	6.25	3.12	12.5	3.12	12.5

– Indicates fungi are resistant to the compound  $>100 \mu\text{g/mL}$  concentration.

thin-layer chromatography (TLC) on pre-coated silica gel F254 plates from Merck and compounds were visualized either by exposure to UV light or dipping in 1% aqueous potassium permanganate solution. Silica gel chromatographic columns (60–120 mesh) were used for separations. Microwave reactions were carried out in mini lab microwave catalytic reactor (ZZKD, WBFY-201). Optical rotations were measured on Perkin–Elmer 141 polarimeter by using a 2 mL cell with a path length of 1 dm with  $\text{CHCl}_3$  or  $\text{CDCl}_3$  as solvent. All melting points are uncorrected and measured using Fisher–Johns apparatus. IR spectra were recorded as KBr disks on a Perkin–Elmer FT IR spectrometer. The  $^1\text{H}$  NMR and  $^{13}\text{C}$  NMR spectra were recorded on a Varian Gemini spectrometer (300 MHz for  $^1\text{H}$  and 75 MHz for  $^{13}\text{C}$ ). Chemical shifts are reported as  $\delta$  on ppm scale against TMS as the internal reference and coupling constants ( $J$ ) are reported in Hz units. Mass spectra were recorded on a VG micro mass 7070H spectrometer. Elemental analyses (C, H, N) were determined by a Perkin–Elmer 240 CHN elemental analyzer and are within  $\pm 0.4\%$  of theoretical values.

**2-((3aR,5S,6S,6aR)-6-((1-(4-Chlorophenyl)-1H-1,2,3-triazol-4-yl)methoxy)-2,2-dimethyltetrahydrofuro[2,3-d][1,3]dioxol-5-yl)-3-phenylthiazolidin-4-ones 8a–c.** To a solution of diol **6** (0.200 g, 0.48 mmol) in  $\text{CH}_2\text{Cl}_2$  (5 mL),  $\text{NaIO}_4$  (0.130 g, 0.61 mmol) was added at  $0^\circ\text{C}$  and stirred at room temperature for 6 h. The reaction mixture was filtered and washed with  $\text{CH}_2\text{Cl}_2$  ( $2 \times 10$  mL). It was dried ( $\text{Na}_2\text{SO}_4$ ) and evaporated to give aldehyde **7** (0.150 g) in quantitative yield as a yellow liquid, which was used as such for the next reaction.

To a stirred mixture of **7** (0.150 g, 0.395 mmol), aromatic amine (0.395 mmol) and anhydrous thioglycolic acid (0.160 g, 0.211 mmol) in dry toluene (5 mL),  $\text{ZnCl}_2$  (0.100g, 0.751 mmol) was added after 2 min and irradiated in microwave bath reactor at 280 W for 4–7 minutes at  $110^\circ\text{C}$ . After cooling, the filtrate was concentrated to dryness under reduced pressure and the residue was taken-up in ethyl acetate. The ethyl acetate layer was washed with 5% sodium bicarbonate solution and finally with brine. The organic layer was dried over  $\text{Na}_2\text{SO}_4$  and evaporated to dryness at reduced pressure. The crude product thus obtained was purified by column chromatography on silica gel (60–120 mesh) with hexane/ethyl acetate as the eluent.

**2-((3aR,5S,6S,6aR)-6-((1-(4-Chlorophenyl)-1H-1,2,3-triazol-4-yl)methoxy)-2,2-dimethyltetrahydrofuro[2,3-d][1,3]dioxol-5-yl)-3-p-tolylthiazolidin-4-one (8a)** m.p.  $191\text{--}193^\circ\text{C}$ ;  $^1\text{H}$  NMR (300 MHz,  $\text{CDCl}_3$ )  $\delta$  8.26 (d,  $J = 8.7$  Hz, 2H, Ar-H), 8.04 (s, 1H, Ar-H), 7.54 (d,  $J = 9.2$  Hz, 2H, Ar-H), 7.39 (d,  $J = 8.33$  Hz, 2H, Ar-H), 7.15 (d,  $J = 8.3$  Hz, 2H, Ar-H), 5.76 (d,  $J = 3.6$  Hz, 1H,  $\text{C}_1\text{H}$ ), 4.96 (d,  $J = 5.2$  Hz, 1H, CH-S), 4.66 (t,  $J = 3.9$  Hz, 1H,  $\text{C}_2\text{H}$ ), 4.54 (s, 2H,  $\text{OCH}_2$ ), 3.96–3.91 (m, 1H,  $\text{C}_4\text{H}$ ), 3.76 (s, 2H,  $\text{CH}_2$ ), 3.26 (dd,  $J_1 = 9.1$  Hz,  $J_2 = 4.2$  Hz, 1H,  $\text{C}_3\text{H}$ ), 2.3 (s, 3H,  $\text{CH}_3$ ), 1.53 (s, 3H,  $\text{CH}_3$ ), 1.36 (m, 3H,  $\text{CH}_3$ );  $^{13}\text{C}$  NMR (75 MHz,  $\text{CDCl}_3$ )  $\delta$  172.6, 143.2, 137.4, 133.6, 132.3, 131.2, 128.4, 127.9, 124.8, 122.9, 119.2, 111.2, 103.8, 81.2, 78.1, 74.1, 65.9, 51.4, 26.1, 16.1; MS:  $m/z$  ( $\text{M}^+ + \text{Na}$ ) 565. Anal. Calcd for  $\text{C}_{26}\text{H}_{27}\text{ClN}_4\text{O}_5\text{S}$ : C, 57.51; H, 5.51; N, 10.32. Found: C, 57.32; H, 5.35; N, 10.09.

**3-(4-Chlorophenyl)-2-((3aR,5S,6S,6aR)-6-((1-(4-chlorophenyl)-1H-imidazol-4-yl)methoxy)-2,2-dimethyltetrahydrofuro[2,3-d][1,3]dioxol-5-yl)thiazolidin-4-one (8b)** m.p. 216–218 °C; <sup>1</sup>H NMR (300 MHz, CDCl<sub>3</sub>) δ 8.02 (s, 1H, Ar-H), 7.50 (d, *J* = 9.2 Hz, 4H, Ar-H), 7.41 (d, *J* = 8.9 Hz, 4H, Ar-H), 5.72 (d, *J* = 3.6 Hz, 1H, C<sub>1</sub>H), 4.94 (d, *J* = 5.2 Hz, CH-S), 4.60 (t, *J* = 3.9 Hz, 1H, C<sub>2</sub>H), 4.51 (s, 2H, OCH<sub>2</sub>), 3.96–3.91 (m, 1H, C<sub>4</sub>H), 3.76 (s, 2H, CH<sub>2</sub>), 3.31 (dd, *J*<sub>1</sub> = 9.1 Hz, *J*<sub>2</sub> = 4.2 Hz, 1H, C<sub>3</sub>H), 1.55 (s, 3H, CH<sub>3</sub>), 1.32 (m, 3H, CH<sub>3</sub>); <sup>13</sup>C NMR (75 MHz, CDCl<sub>3</sub>) δ 170.6, 139.4, 134.8, 133.2, 129.4, 128.6, 125.6, 122.2, 119.4, 111.2, 104.9, 81.5, 74.5, 66.3, 52.6, 34.6, 26.5; MS: *m/z* (M<sup>+</sup>+H) 563. Anal. Calcd for C<sub>25</sub>H<sub>24</sub>Cl<sub>2</sub>N<sub>4</sub>O<sub>5</sub>S: C, 53.29; H, 4.29; N, 9.94. Found: C, 53.21; H, 4.16; N, 9.83.

**2-((3aR,5S,6S,6aR)-6-((1-(4-Chlorophenyl)-1H-1,2,3-triazol-4-yl)methoxy)-2,2-dimethyltetrahydrofuro[2,3-d][1,3]dioxol-5-yl)-3-(4-nitrophenyl)thiazolidin-4-one (8c)** m.p. 201–205 °C; <sup>1</sup>H NMR (300 MHz, CDCl<sub>3</sub>) δ 8.26 (d, *J* = 8.7 Hz, 2H), 8.04 (s, 1H, Ar-H), 7.51 (d, *J* = 9.2 Hz, 2H, Ar-H), 7.42 (d, *J* = 8.5 Hz, 2H, Ar-H), 6.82 (d, *J* = 9.8 Hz, 2H, Ar-H), 5.71 (d, *J* = 3.6 Hz, 1H, C<sub>1</sub>H), 4.96 (d, *J* = 5.2 Hz, CH-S), 4.62 (t, *J* = 3.9 Hz, 1H, C<sub>2</sub>H), 4.53 (s, 2H, OCH<sub>2</sub>), 3.96–3.91 (m, 1H, C<sub>4</sub>H), 3.76 (s, 2H, CH<sub>2</sub>), 3.28 (dd, *J*<sub>1</sub> = 9.1 Hz, *J*<sub>2</sub> = 4.2 Hz, 1H, C<sub>3</sub>H), 1.52 (s, 3H, CH<sub>3</sub>), 1.34 (m, 3H, CH<sub>3</sub>); <sup>13</sup>C NMR (75 MHz, CDCl<sub>3</sub>) δ 170.6, 147.5, 144.4, 143.2, 134.8, 131.2, 128.6, 124.6, 122.4, 119.8, 111.8, 104.9, 81.5, 78.2, 74.8, 66.9, 52.4, 34.6, 26.8; MS: *m/z* (M<sup>+</sup>+H) 574. Anal. Calcd for C<sub>25</sub>H<sub>24</sub>ClN<sub>5</sub>O<sub>7</sub>S: C, 52.31; H, 4.21; N, 12.20. Found: C, 52.26; H, 4.19; N, 12.11.

**(Z)-5-Benzylidene-2-((3aR,5S,6S,6aR)-6-((1-(4-chlorophenyl)-1H-1,2,3-triazol-4-yl)methoxy)-2,2-dimethyltetrahydrofuro[2,3-d][1,3]dioxol-5-yl)-3-phenylthiazolidin-4-ones 9a–c.** A mixture of compound **8** (0.01 mol), *p*-fluorobenzaldehyde (0.02 mol) and sodium acetate (0.01 mol) in anhydrous glacial acetic acid (20 mL), was refluxed for 3 h. The reaction mixture was concentrated and then poured into ice cold water, the solid thus separated was filtered, washed with water and crystallized from glacial acetic acid to afford pure compounds.

**(Z)-2-((3aR,5S,6S,6aR)-6-((1-(4-Chlorophenyl)-1H-1,2,3-triazol-4-yl)methoxy)-2,2-dimethyltetrahydrofuro[2,3-d][1,3]dioxol-5-yl)-5-(4-fluorobenzylidene)-3-*p*-tolylthiazolidin-4-one (9a).** This compound was obtained as brown solid, m.p. 231–235 °C; <sup>1</sup>H NMR (300 MHz, CDCl<sub>3</sub>) δ 8.22 (d, *J* = 8.7 Hz, 2H, Ar-H), 8.06 (s, 1H, Ar-H), 7.84 (s, 1H, CH=C), 7.54 (d, *J* = 9.2 Hz, 2H, Ar-H), 7.39 (d, *J* = 8.33 Hz, 2H, Ar-H), 7.15 (d, *J* = 8.3 Hz, 2H, Ar-H), 6.91–6.87 (m, 5H, Ar-H and CH-S), 5.76 (d, *J* = 3.6 Hz, 1H, C<sub>1</sub>H), 4.66 (t, *J* = 3.9 Hz, 1H, C<sub>2</sub>H), 4.54 (s, 2H, OCH<sub>2</sub>), 3.96–3.91 (m, 1H, C<sub>4</sub>H), 3.26 (dd, *J*<sub>1</sub> = 9.1 Hz, *J*<sub>2</sub> = 4.2 Hz, 1H, C<sub>3</sub>H), 2.3 (s, 3H, CH<sub>3</sub>), 1.53 (s, 3H, CH<sub>3</sub>), 1.36 (m, 3H, CH<sub>3</sub>); <sup>13</sup>C NMR (75 MHz, CDCl<sub>3</sub>) δ 172.6, 143.2, 137.4,

133.6, 132.3, 131.2, 128.4, 127.9, 124.8, 122.9, 119.2, 111.2, 103.8, 81.2, 78.1, 74.1, 65.9, 51.4, 26.1, 16.1; MS: *m/z* (M<sup>+</sup>+H) 649. Anal. Calcd for C<sub>33</sub>H<sub>30</sub>ClFN<sub>4</sub>O<sub>5</sub>S: C, 61.06; H, 4.66; N, 8.63. Found: C, 60.82; H, 4.45; N, 8.43.

**(Z)-3-(4-Chlorophenyl)-2-((3aR,5S,6S,6aR)-6-((1-(4-chlorophenyl)-1H-1,2,3-triazol-4-yl)methoxy)-2,2-dimethyltetrahydrofuro[2,3-d][1,3]dioxol-5-yl)-5-(4-fluorobenzylidene)thiazolidin-4-one (9b).** The compound was obtained as dark yellow solid, m.p. 232–235 °C; <sup>1</sup>H NMR (300 MHz, DMSO-*d*<sub>6</sub>) δ 8.06 (s, 1H, Ar-H), 7.82 (s, 1H, CH=C), 7.52 (d, *J* = 9.2 Hz, 4H, Ar-H), 7.43 (d, *J* = 8.9 Hz, 4H, Ar-H), 6.91–6.87 (m, 5H, Ar-H and CH-S), 5.72 (d, *J* = 3.6 Hz, 1H, C<sub>1</sub>H), 4.60 (t, *J* = 3.9 Hz, 1H, C<sub>2</sub>H), 4.51 (s, 2H, OCH<sub>2</sub>), 3.96–3.91 (m, 1H, C<sub>4</sub>H), 3.31 (dd, *J*<sub>1</sub> = 9.1 Hz, *J*<sub>2</sub> = 4.2 Hz, 1H, C<sub>3</sub>H), 1.55 (s, 3H, CH<sub>3</sub>), 1.32 (m, 3H, CH<sub>3</sub>); <sup>13</sup>C NMR (75 MHz, DMSO-*d*<sub>6</sub>) δ 170.6, 138.4, 134.8, 133.2, 130.8, 129.4, 128.6, 124.6, 122.2, 119.4, 111.2, 104.9, 81.5, 74.5, 66.3, 52.6, 34.6, 26.5; MS: *m/z* (M<sup>+</sup>+H) 669. Anal. Calcd for C<sub>32</sub>H<sub>27</sub>Cl<sub>2</sub>FN<sub>4</sub>O<sub>5</sub>S: C, 57.40; H, 4.06; N, 8.37. Found: C, 57.21; H, 4.01; N, 8.03.

**(Z)-2-((3aR,5S,6S,6aR)-6-((1-(4-Chlorophenyl)-1H-1,2,3-triazol-4-yl)methoxy)-2,2-dimethyltetrahydrofuro[2,3-d][1,3]dioxol-5-yl)-5-(4-fluorobenzylidene)-3-(4-nitrophenyl)thiazolidin-4-one (9c).** The compound was obtained as brown solid, m.p. 216–218 °C; <sup>1</sup>H NMR (300 MHz, DMSO-*d*<sub>6</sub>) δ 8.26 (d, *J* = 8.7 Hz, 2H), 8.04 (s, 1H, Ar-H), 7.84 (s, 1H, CH=C), 7.51 (d, *J* = 9.2 Hz, 2H, Ar-H), 7.42 (d, *J* = 8.5 Hz, 2H, Ar-H), 6.91–6.87 (m, 5H, Ar-H and CH-S), 6.82 (d, *J* = 9.8 Hz, 2H, Ar-H), 5.71 (d, *J* = 3.6 Hz, 1H, C<sub>1</sub>H), 4.62 (t, *J* = 3.9 Hz, 1H, C<sub>2</sub>H), 4.53 (s, 2H, OCH<sub>2</sub>), 3.96–3.91 (m, 1H, C<sub>4</sub>H), 3.76 (s, 2H, CH<sub>2</sub>), 3.28 (dd, *J*<sub>1</sub> = 9.1 Hz, *J*<sub>2</sub> = 4.2 Hz, 1H, C<sub>3</sub>H), 1.52 (s, 3H, CH<sub>3</sub>), 1.34 (m, 3H, CH<sub>3</sub>); <sup>13</sup>C NMR (75 MHz, CDCl<sub>3</sub>) δ 170.6, 147.5, 144.4, 143.2, 138.4, 134.8, 130.6, 131.2, 128.6, 124.6, 122.4, 119.8, 111.8, 104.9, 81.5, 78.2, 74.8, 66.9, 52.4, 26.8; MS: *m/z* (M<sup>+</sup>+Na) 692. Anal. Calcd for C<sub>31</sub>H<sub>29</sub>ClFN<sub>5</sub>O<sub>7</sub>S: C, 55.56; H, 4.36; N, 10.30. Found: C, 55.26; H, 4.29; N, 10.10.

**5-((3aR,5S,6S,6aR)-6-((1-(4-Chlorophenyl)-1H-1,2,3-triazol-4-yl)methoxy)-2,2-dimethyltetrahydrofuro[2,3-d][1,3]dioxol-5-yl)-3-(4-fluorophenyl)-2,6-diphenyl-2-alkyl-6-phenyl-3,3a,5,6-tetrahydro-2H-pyrazolo[3,4-d]thiazoles 10a–r.** A mixture of compound **9** (5 mmol), alkyl/aryl hydrazine (5 mmol) and anhydrous sodium acetate (5 mmol) in glacial acetic acid (20 mL), was refluxed for 7 h. The reaction mixture was concentrated and cooled to room temperature, the solid thus separated was filtered, washed thoroughly with water. The crude product thus obtained was purified by column chromatography on silica gel with hexane/ethyl acetate as eluent to afford pure compounds.

**5-((3aR,5S,6S,6aR)-6-((1-(4-Chlorophenyl)-1H-1,2,3-triazol-4-yl)methoxy)-2,2-dimethyltetrahydrofu-**

**ro[2,3-*d*][1,3]dioxol-5-yl)-3-(4-fluorophenyl)-2-phenyl-6-*p*-tolyl-3,3a,5,6-tetrahydro-2H-pyrazolo[3,4-*d*]thiazole (10a).** This was obtained by reacting compound **9a** (1 g) and phenylhydrazine (0.25 g) as described in the typical procedure and isolated as a brown solid, yield 72%, m.p. 248–250 °C; <sup>1</sup>H NMR (300 MHz, DMSO-*d*<sub>6</sub>) δ 8.20 (d, *J* = 8.7 Hz, 2H, Ar-H), 8.04 (s, 1H, Ar-H), 7.51 (d, *J* = 9.2 Hz, 2H, Ar-H), 7.40 (s, 1H, CH-S), 7.29 (d, *J* = 8.33 Hz, 2H, Ar-H), 7.18–7.15 (m, 5H, Ar-H), 7.05 (d, *J* = 8.3 Hz, 2H, Ar-H), 6.91–6.87 (m, 4H, Ar-H), 5.76 (d, *J* = 3.6 Hz, 1H, C<sub>1</sub>H), 5.62 (d, *J* = 2.2 Hz, 1H, S-CH), 5.25 (d, *J* = 2.2 Hz, 1H, CH-N), 4.66 (t, *J* = 3.9 Hz, 1H, C<sub>2</sub>H), 4.54 (s, 2H, OCH<sub>2</sub>), 3.96–3.91 (m, 1H, C<sub>4</sub>H), 3.26 (dd, *J*<sub>1</sub> = 9.1 Hz, *J*<sub>2</sub> = 4.2 Hz, 1H, C<sub>3</sub>H), 2.3 (s, 3H, CH<sub>3</sub>), 1.53 (s, 3H, CH<sub>3</sub>), 1.36 (m, 3H, CH<sub>3</sub>); <sup>13</sup>C NMR (75 MHz, DMSO-*d*<sub>6</sub>) δ 172.6, 143.2, 141.4, 137.4, 133.6, 132.3, 131.2, 129.3, 125.3, 128.4, 127.9, 124.8, 122.9, 119.2, 111.2, 103.8, 81.2, 78.1, 74.1, 65.9, 51.4, 26.1, 21.3, 16.1; MS: *m/z* (M<sup>+</sup>+H) 773. Anal. Calcd for C<sub>39</sub>H<sub>36</sub>ClFN<sub>6</sub>O<sub>4</sub>S: C, 60.54; H, 4.58; N, 10.86. Found: C, 60.32; H, 4.28; N, 10.47.

**5-((3aR,5S,6S,6aR)-6-((1-(4-Chlorophenyl)-1H-1,2,3-triazol-4-yl)methoxy)-2,2-dimethyltetrahydrofuro[2,3-*d*][1,3]dioxol-5-yl)-3-(4-fluorophenyl)-2-(4-methoxyphenyl)-6-*p*-tolyl-3,3a,5,6-tetrahydro-2H-pyrazolo[3,4-*d*]thiazole (10 b).** This was obtained by reacting compound **9a** (1 g) and *p*-methoxyphenylhydrazine (0.35 g) as described in the typical procedure and isolated as a yellow solid, yield 62%, m.p. 268–272 °C; <sup>1</sup>H NMR (300 MHz, DMSO-*d*<sub>6</sub>) δ 8.18 (d, *J* = 8.7 Hz, 2H, Ar-H), 8.04 (s, 1H, Ar-H), 7.51 (d, *J* = 9.2 Hz, 2H, Ar-H), 7.40 (s, 1H, CH-S), 7.29 (d, *J* = 8.33 Hz, 2H, Ar-H), 7.12–7.10 (m, 4H, Ar-H), 7.05 (d, *J* = 8.3 Hz, 2H, Ar-H), 6.91–6.87 (m, 4H, Ar-H), 5.76 (d, *J* = 3.6 Hz, 1H, C<sub>1</sub>H), 5.62 (d, *J* = 2.2 Hz, 1H, S-CH), 5.25 (d, *J* = 2.2 Hz, 1H, CH-N), 4.66 (t, *J* = 3.9 Hz, 1H, C<sub>2</sub>H), 4.54 (s, 2H, OCH<sub>2</sub>), 3.96–3.94 (m, 1H, C<sub>4</sub>H), 3.91 (s, 3H, OMe), 3.26 (dd, *J*<sub>1</sub> = 9.1 Hz, *J*<sub>2</sub> = 4.2 Hz, 1H, C<sub>3</sub>H), 2.3 (s, 3H, CH<sub>3</sub>), 1.53 (s, 3H, CH<sub>3</sub>), 1.36 (m, 3H, CH<sub>3</sub>); <sup>13</sup>C NMR (75 MHz, DMSO-*d*<sub>6</sub>) δ 172.6, 151.7, 143.2, 141.4, 137.4, 133.6, 132.3, 131.2, 129.3, 125.3, 128.4, 127.9, 124.8, 122.9, 119.2, 111.2, 103.8, 81.2, 78.1, 74.1, 65.9, 55.8, 51.4, 26.1, 21.3, 16.1; MS: *m/z* (M<sup>+</sup>+H) 789. Anal. Calcd for C<sub>40</sub>H<sub>38</sub>ClFN<sub>6</sub>O<sub>5</sub>S: C, 62.46; H, 4.98; N, 10.92. Found: C, 62.12; H, 4.88; N, 10.87.

**2-(4-Chlorophenyl)-5-((3aR,5S,6S,6aR)-6-((1-(4-chlorophenyl)-1H-1,2,3-triazol-4-yl)methoxy)-2,2-dimethyltetrahydrofuro[2,3-*d*][1,3]dioxol-5-yl)-3-(4-fluorophenyl)-6-*p*-tolyl-3,3a,5,6-tetrahydro-2H-pyrazolo[3,4-*d*]thiazole (10c).** This was obtained by reacting compound **9a** (1 g) and *p*-chlorophenylhydrazine (0.45 g) as described in the typical procedure and isolated as a brown solid, yield 76%, m.p. 248–251 °C; <sup>1</sup>H NMR (300 MHz, DMSO-*d*<sub>6</sub>) δ 8.21 (d, *J* = 8.7 Hz, 2H, Ar-H), 8.09 (s, 1H, Ar-H), 7.55 (d, *J* = 9.2 Hz, 2H, Ar-H), 7.42 (s, 1H, CH-S), 7.29 (d, *J* = 8.33 Hz, 2H, Ar-H), 7.10–7.08 (m, 4H,

Ar-H), 7.05 (d, *J* = 8.3 Hz, 2H, Ar-H), 6.91–6.87 (m, 4H, Ar-H), 5.76 (d, *J* = 3.6 Hz, 1H, C<sub>1</sub>H), 5.62 (d, *J* = 2.2 Hz, 1H, S-CH), 5.25 (d, *J* = 2.2 Hz, 1H, CH-N), 4.66 (t, *J* = 3.9 Hz, 1H, C<sub>2</sub>H), 4.54 (s, 2H, OCH<sub>2</sub>), 3.96–3.94 (m, 1H, C<sub>4</sub>H), 3.26 (dd, *J*<sub>1</sub> = 9.1 Hz, *J*<sub>2</sub> = 4.2 Hz, 1H, C<sub>3</sub>H), 2.3 (s, 3H, CH<sub>3</sub>), 1.53 (s, 3H, CH<sub>3</sub>), 1.36 (m, 3H, CH<sub>3</sub>); <sup>13</sup>C NMR (75 MHz, DMSO-*d*<sub>6</sub>) δ 172.6, 151.7, 143.2, 137.4, 133.6, 132.3, 131.2, 129.3, 126.3, 125.3, 128.4, 127.9, 124.8, 122.9, 119.2, 111.2, 103.8, 81.2, 78.1, 74.1, 65.9, 51.4, 26.1, 21.3, 16.1; MS: *m/z* (M<sup>+</sup>+H) 773. Anal. Calcd for C<sub>39</sub>H<sub>35</sub>Cl<sub>2</sub>FN<sub>6</sub>O<sub>4</sub>S: C, 60.54; H, 4.58; N, 10.86. Found: C, 60.32; H, 4.28; N, 10.47.

**2-Benzyl-5-((3aR,5S,6S,6aR)-6-((1-(4-chlorophenyl)-1H-1,2,3-triazol-4-yl)methoxy)-2,2-dimethyltetrahydrofuro[2,3-*d*][1,3]dioxol-5-yl)-3-(4-fluorophenyl)-6-*p*-tolyl-3,3a,5,6-tetrahydro-2H-pyrazolo[3,4-*d*]thiazole (10d).** This was obtained by reacting compound **9a** (1 g) and benzylhydrazine (0.65 g) as described in the typical procedure and isolated as a brown solid, yield 66%. m.p. 288–291 °C; <sup>1</sup>H NMR (300 MHz, DMSO-*d*<sub>6</sub>) δ 8.21 (d, *J* = 8.7 Hz, 2H, Ar-H), 8.09 (s, 1H, Ar-H), 7.55 (d, *J* = 9.2 Hz, 2H, Ar-H), 7.42 (s, 1H, CH-S), 7.29 (d, *J* = 8.33 Hz, 2H, Ar-H), 7.10–7.08 (m, 5H, Ar-H), 7.05 (d, *J* = 8.3 Hz, 2H, Ar-H), 6.91–6.87 (m, 4H, Ar-H), 5.92 (s, 2H, CH<sub>2</sub>Ph), 5.76 (d, *J* = 3.6 Hz, 1H, C<sub>1</sub>H), 5.62 (d, *J* = 2.2 Hz, 1H, S-CH), 5.25 (d, *J* = 2.2 Hz, 1H, CH-N), 4.66 (t, *J* = 3.9 Hz, 1H, C<sub>2</sub>H), 4.54 (s, 2H, OCH<sub>2</sub>), 3.96–3.94 (m, 1H, C<sub>4</sub>H), 3.26 (dd, *J*<sub>1</sub> = 9.1 Hz, *J*<sub>2</sub> = 4.2 Hz, 1H, C<sub>3</sub>H), 2.3 (s, 3H, CH<sub>3</sub>), 1.53 (s, 3H, CH<sub>3</sub>), 1.36 (m, 3H, CH<sub>3</sub>); <sup>13</sup>C NMR (75 MHz, DMSO-*d*<sub>6</sub>) δ 171.6, 151.6, 143.2, 137.4, 133.6, 132.3, 131.2, 129.3, 125.3, 128.4, 127.9, 124.8, 122.9, 119.2, 111.2, 103.8, 81.2, 78.1, 74.1, 65.9, 58.1, 51.4, 26.1, 21.3, 16.1; MS: *m/z* (M<sup>+</sup>+H) 753. Anal. Calcd for C<sub>40</sub>H<sub>38</sub>ClFN<sub>6</sub>O<sub>4</sub>S: C, 63.78; H, 5.08; N, 11.16. Found: C, 63.52; H, 4.96; N, 10.97.

**5-((3aR,5S,6S,6aR)-6-((1-(4-Chlorophenyl)-1H-1,2,3-triazol-4-yl)methoxy)-2,2-dimethyltetrahydrofuro[2,3-*d*][1,3]dioxol-5-yl)-3-(4-fluorophenyl)-2-isopropyl-6-*p*-tolyl-3,3a,5,6-tetrahydro-2H-pyrazolo[3,4-*d*]thiazole (10e).** This was obtained by reacting compound **9a** (1 g) and isopropylhydrazine (0.35 g) as described in the typical procedure and isolated as a yellow solid, yield 76%, m.p. 248–251 °C; <sup>1</sup>H NMR (300 MHz, DMSO-*d*<sub>6</sub>) δ 8.19 (d, *J* = 8.7 Hz, 2H, Ar-H), 8.06 (s, 1H, Ar-H), 7.55 (d, *J* = 9.2 Hz, 2H, Ar-H), 7.42 (s, 1H, CH-S), 7.29 (d, *J* = 8.33 Hz, 2H, Ar-H), 7.05 (d, *J* = 8.3 Hz, 2H, Ar-H), 6.91–6.87 (m, 4H, Ar-H), 5.76 (d, *J* = 3.6 Hz, 1H, C<sub>1</sub>H), 5.62 (d, *J* = 2.2 Hz, 1H, S-CH), 5.25 (d, *J* = 2.2 Hz, 1H, CH-N), 4.66 (t, *J* = 3.9 Hz, 1H, C<sub>2</sub>H), 4.54 (s, 2H, OCH<sub>2</sub>), 3.96–3.94 (m, 1H, C<sub>4</sub>H), 3.26 (dd, *J*<sub>1</sub> = 9.1 Hz, *J*<sub>2</sub> = 4.2 Hz, 1H, C<sub>3</sub>H), 2.80–2.78 (m, 1H, CH), 2.3 (s, 3H, CH<sub>3</sub>), 1.53 (s, 3H, CH<sub>3</sub>), 1.36 (m, 3H, CH<sub>3</sub>), 0.96 (d, *J* = 6.3 Hz, 6H, 2 × CH<sub>3</sub>); <sup>13</sup>C NMR (75 MHz, DMSO-*d*<sub>6</sub>) δ 171.6, 151.6, 143.2, 137.4, 133.6, 132.3, 131.2, 129.3, 128.4, 127.9, 124.8, 122.9, 119.2, 111.2, 103.8, 81.2, 78.1, 74.1, 65.9, 58.1, 51.4, 50.6, 26.1, 21.3, 16.1; MS: *m/z* (M<sup>+</sup>+H) 705. Anal. Calcd for

$C_{36}H_{38}ClFN_6O_4S$ : C, 61.31; H, 5.43; N, 11.92. Found: C, 60.98; H, 5.26; N, 11.77.

**5-((3aR,5S,6S,6aR)-6-((1-(4-Chlorophenyl)-1H-1,2,3-triazol-4-yl)methoxy)-2,2-dimethyltetrahydrofuro[2,3-d][1,3]dioxol-5-yl)-3-(4-fluorophenyl)-2-methyl-6-*p*-tolyl-3,3a,5,6-tetrahydro-2H-pyrazolo[3,4-d]thiazole (10 f).** This was obtained by reacting compound **9a** (1 g) and methylhydrazine (0.25 g) as described in the typical procedure and isolated as a yellow solid, yield 66%, m.p. 228–231 °C;  $^1H$  NMR (300 MHz, DMSO- $d_6$ )  $\delta$  8.19 (d,  $J = 8.7$  Hz, 2H, Ar-H), 8.06 (s, 1H, Ar-H), 7.55 (d,  $J = 9.2$  Hz, 2H, Ar-H), 7.42 (s, 1H, CH-S), 7.29 (d,  $J = 8.33$  Hz, 2H, Ar-H), 7.05 (d,  $J = 8.3$  Hz, 2H, Ar-H), 6.91–6.87 (m, 4H, Ar-H), 5.76 (d,  $J = 3.6$  Hz, 1H, C<sub>1</sub>H), 5.62 (d,  $J = 2.2$  Hz, 1H, S-CH), 5.25 (d,  $J = 2.2$  Hz, 1H, CH-N), 4.66 (t,  $J = 3.9$  Hz, 1H, C<sub>2</sub>H), 4.54 (s, 2H, OCH<sub>2</sub>), 3.96–3.94 (m, 1H, C<sub>4</sub>H), 3.71 (s, 3H, N-CH<sub>3</sub>), 3.26 (dd,  $J_1 = 9.1$  Hz,  $J_2 = 4.2$  Hz, 1H, C<sub>3</sub>H), 2.3 (s, 3H, CH<sub>3</sub>), 1.53 (s, 3H, CH<sub>3</sub>), 1.36 (m, 3H, CH<sub>3</sub>);  $^{13}C$  NMR (75 MHz, DMSO- $d_6$ )  $\delta$  171.6, 151.6, 143.2, 137.4, 133.6, 132.3, 131.2, 129.3, 128.4, 127.9, 124.8, 122.9, 119.2, 111.2, 103.8, 81.2, 78.1, 74.1, 65.9, 58.1, 51.4, 39.3, 26.1, 16.1; MS:  $m/z$  ( $M^+ + Na^+$ ) 689. Anal. Calcd for  $C_{34}H_{34}ClFN_6O_4S$ : C, 60.30; H, 5.06; N, 12.42. Found: C, 60.22; H, 4.96; N, 12.22.

**6-(4-Chlorophenyl)-5-((3aR,5S,6S,6aR)-6-((1-(4-chlorophenyl)-1H-1,2,3-triazol-4-yl)methoxy)-2,2-dimethyltetrahydrofuro[2,3-d][1,3]dioxol-5-yl)-3-(4-fluorophenyl)-2-phenyl-3,3a,5,6-tetrahydro-2H-pyrazolo[3,4-d]thiazole (10g).** This was obtained by reacting compound **9b** (1 g) and phenylhydrazine (0.25 g) as described in the typical procedure and isolated as a brown solid, yield 65%, m.p. 249–251 °C;  $^1H$  NMR (300 MHz, DMSO- $d_6$ )  $\delta$  8.16 (d,  $J = 8.7$  Hz, 2H, Ar-H), 8.02 (s, 1H, Ar-H), 7.49 (d,  $J = 9.2$  Hz, 2H, Ar-H), 7.36 (s, 1H, CH-S), 7.22 (d,  $J = 8.33$  Hz, 2H, Ar-H), 7.13–7.11 (m, 5H, Ar-H), 7.02 (d,  $J = 8.3$  Hz, 2H, Ar-H), 6.81–6.77 (m, 4H, Ar-H), 5.66 (d,  $J = 3.6$  Hz, 1H, C<sub>1</sub>H), 5.58 (d,  $J = 2.2$  Hz, 1H, S-CH), 5.21 (d,  $J = 2.2$  Hz, 1H, CH-N), 4.62 (t,  $J = 3.9$  Hz, 1H, C<sub>2</sub>H), 4.51 (s, 2H, OCH<sub>2</sub>), 3.94–3.91 (m, 1H, C<sub>4</sub>H), 3.26 (dd,  $J_1 = 9.1$  Hz,  $J_2 = 4.2$  Hz, 1H, C<sub>3</sub>H), 1.53 (s, 3H, CH<sub>3</sub>), 1.36 (m, 3H, CH<sub>3</sub>);  $^{13}C$  NMR (75 MHz, DMSO- $d_6$ )  $\delta$  174.6, 143.0, 141.4, 137.4, 133.6, 132.3, 131.2, 129.3, 125.3, 128.4, 127.9, 126.1, 124.8, 122.9, 119.2, 111.2, 103.8, 81.2, 78.1, 74.1, 65.9, 51.4, 26.1, 16.1; MS:  $m/z$  ( $M^+ + H^+$ ) 759. Anal. Calcd for  $C_{39}H_{36}ClFN_6O_4S$ : C, 60.08; H, 4.38; N, 11.07. Found: C, 60.02; H, 4.11; N, 10.95.

**6-(4-Chlorophenyl)-5-((3aR,5S,6S,6aR)-6-((1-(4-chlorophenyl)-1H-1,2,3-triazol-4-yl)methoxy)-2,2-dimethyltetrahydrofuro[2,3-d][1,3]dioxol-5-yl)-3-(4-fluorophenyl)-2-(4-methoxyphenyl)-3,3a,5,6-tetrahydro-2H-pyrazolo[3,4-d]thiazole (10h).** This was obtained by reacting compound **9b** (1 g) and *p*-methoxyphenylhydrazine (0.35 g) as described in the typical procedure

and isolated as a yellow solid, yield 68%, m.p. 274–276 °C;  $^1H$  NMR (300 MHz, DMSO- $d_6$ )  $\delta$  8.18 (d,  $J = 8.7$  Hz, 2H, Ar-H), 8.04 (s, 1H, Ar-H), 7.51 (d,  $J = 9.2$  Hz, 2H, Ar-H), 7.40 (s, 1H, CH-S), 7.29 (d,  $J = 8.33$  Hz, 2H, Ar-H), 7.12–7.10 (m, 4H, Ar-H), 7.05 (d,  $J = 8.3$  Hz, 2H, Ar-H), 6.91–6.87 (m, 4H, Ar-H), 5.76 (d,  $J = 3.6$  Hz, 1H, C<sub>1</sub>H), 5.62 (d,  $J = 2.2$  Hz, 1H, S-CH), 5.25 (d,  $J = 2.2$  Hz, 1H, CH-N), 4.66 (t,  $J = 3.9$  Hz, 1H, C<sub>2</sub>H), 4.54 (s, 2H, OCH<sub>2</sub>), 3.96–3.94 (m, 1H, C<sub>4</sub>H), 3.91 (s, 3H, OMe), 3.26 (dd,  $J_1 = 9.1$  Hz,  $J_2 = 4.2$  Hz, 1H, C<sub>3</sub>H), 1.53 (s, 3H, CH<sub>3</sub>), 1.36 (m, 3H, CH<sub>3</sub>);  $^{13}C$  NMR (75 MHz, DMSO- $d_6$ )  $\delta$  172.6, 151.7, 143.2, 141.4, 137.4, 133.6, 132.3, 131.2, 129.3, 126.1, 125.3, 128.4, 127.9, 124.8, 122.9, 119.2, 111.2, 103.8, 81.2, 78.1, 74.1, 65.9, 55.8, 51.4, 26.1, 16.1; MS:  $m/z$  ( $M^+ + H^+$ ) 789. Anal. Calcd for  $C_{39}H_{35}Cl_2FN_6O_5S$ : C, 59.32; H, 4.47; N, 10.64. Found: C, 58.92; H, 4.18; N, 10.47.

**2,6-Bis(4-chlorophenyl)-5-((3aR,5S,6S,6aR)-6-((1-(4-chlorophenyl)-1H-1,2,3-triazol-4-yl)methoxy)-2,2-dimethyltetrahydrofuro[2,3-d][1,3]dioxol-5-yl)-3-(4-fluorophenyl)-3,3a,5,6-tetrahydro-2H-pyrazolo[3,4-d]thiazole (10i).** This was obtained by reacting compound **9b** (1 g) and *p*-chlorophenylhydrazine (0.45 g) as described in the typical procedure and isolated as a brown solid, yield 76%, m.p. 268–271 °C;  $^1H$  NMR (300 MHz, DMSO- $d_6$ )  $\delta$  8.23 (d,  $J = 8.7$  Hz, 2H, Ar-H), 8.11 (s, 1H, Ar-H), 7.58 (d,  $J = 9.2$  Hz, 2H, Ar-H), 7.46 (s, 1H, CH-S), 7.29 (d,  $J = 8.33$  Hz, 2H, Ar-H), 7.11–7.09 (m, 4H, Ar-H), 7.07 (d,  $J = 8.3$  Hz, 2H, Ar-H), 6.91–6.87 (m, 4H, Ar-H), 5.76 (d,  $J = 3.6$  Hz, 1H, C<sub>1</sub>H), 5.62 (d,  $J = 2.2$  Hz, 1H, S-CH), 5.25 (d,  $J = 2.2$  Hz, 1H, CH-N), 4.66 (t,  $J = 3.9$  Hz, 1H, C<sub>2</sub>H), 4.54 (s, 2H, OCH<sub>2</sub>), 3.96–3.94 (m, 1H, C<sub>4</sub>H), 3.26 (dd,  $J_1 = 9.1$  Hz,  $J_2 = 4.2$  Hz, 1H, C<sub>3</sub>H), 1.53 (s, 3H, CH<sub>3</sub>), 1.36 (m, 3H, CH<sub>3</sub>);  $^{13}C$  NMR (75 MHz, DMSO- $d_6$ )  $\delta$  172.6, 151.7, 143.2, 137.4, 133.6, 132.3, 131.2, 129.3, 126.3, 125.3, 128.4, 127.9, 124.8, 122.9, 119.2, 111.2, 103.8, 81.2, 78.1, 74.1, 65.9, 51.4, 26.1, 16.1; MS:  $m/z$  ( $M^+ + Na^+$ ) 815. Anal. Calcd for  $C_{38}H_{32}Cl_3FN_6O_4S$ : C, 57.47; H, 4.08; N, 10.56. Found: C, 57.22; H, 3.95; N, 10.32.

**2-Benzyl-6-(4-chlorophenyl)-5-((3aR,5S,6S,6aR)-6-((1-(4-chlorophenyl)-1H-1,2,3-triazol-4-yl)methoxy)-2,2-dimethyltetrahydrofuro[2,3-d][1,3]dioxol-5-yl)-3-(4-fluorophenyl)-3,3a,5,6-tetrahydro-2H-pyrazolo[3,4-d]thiazole (10j).** This was obtained by reacting compound **9b** (1 g) and benzylhydrazine (0.65 g) as described in the typical procedure and isolated as a brown solid, yield 71%, m.p. 258–261 °C;  $^1H$  NMR (300 MHz, DMSO- $d_6$ )  $\delta$  8.25 (d,  $J = 8.7$  Hz, 2H, Ar-H), 8.11 (s, 1H, Ar-H), 7.59 (d,  $J = 9.2$  Hz, 2H, Ar-H), 7.46 (s, 1H, CH-S), 7.32 (d,  $J = 8.33$  Hz, 2H, Ar-H), 7.12–7.10 (m, 5H, Ar-H), 7.08 (d,  $J = 8.3$  Hz, 2H, Ar-H), 6.96–6.90 (m, 4H, Ar-H), 5.96 (s, 2H, CH<sub>2</sub>Ph), 5.77 (d,  $J = 3.6$  Hz, 1H, C<sub>1</sub>H), 5.65 (d,  $J = 2.2$  Hz, 1H, S-CH), 5.28 (d,  $J = 2.2$  Hz, 1H, CH-N), 4.66 (t,  $J = 3.9$  Hz, 1H, C<sub>2</sub>H), 4.54 (s, 2H, OCH<sub>2</sub>), 3.96–3.94 (m, 1H, C<sub>4</sub>H), 3.26 (dd,  $J_1 = 9.1$  Hz,  $J_2 = 4.2$  Hz, 1H, C<sub>3</sub>H), 1.53

(s, 3H, CH<sub>3</sub>), 1.36 (m, 3H, CH<sub>3</sub>); <sup>13</sup>C NMR (75 MHz, DMSO-*d*<sub>6</sub>) δ 171.6, 151.6, 143.2, 137.4, 133.6, 132.3, 131.2, 129.3, 125.3, 128.4, 127.9, 124.8, 122.9, 119.2, 111.2, 103.8, 81.2, 78.1, 74.1, 65.9, 58.1, 51.4, 26.1, 16.1; MS: *m/z* (M<sup>+</sup>+H) 773. Anal. Calcd for C<sub>39</sub>H<sub>35</sub>Cl<sub>2</sub>FN<sub>6</sub>O<sub>4</sub>S: C, 60.54; H, 4.56; N, 10.86. Found: C, 60.34; H, 4.36; N, 10.37.

**6-(4-Chlorophenyl)-5-((3aR,5S,6S,6aR)-6-((1-(4-chlorophenyl)-1H-1,2,3-triazol-4-yl)methoxy)-2,2-dimethyltetrahydrofuro[2,3-*d*][1,3]dioxol-5-yl)-3-(4-fluorophenyl)-2-isopropyl-3,3a,5,6-tetrahydro-2H-pyrazolo[3,4-*d*]thiazole (10k).** This was obtained by reacting compound **9b** (1 g) and isopropylhydrazine (0.35 g) as described in the typical procedure and isolated as a yellow solid, yield 69%, m.p. 238–239 °C; <sup>1</sup>H NMR (300 MHz, DMSO-*d*<sub>6</sub>) δ 8.32 (d, *J* = 8.7 Hz, 2H, Ar-H), 8.16 (s, 1H, Ar-H), 7.65 (d, *J* = 9.2 Hz, 2H, Ar-H), 7.52 (s, 1H, CH-S), 7.39 (d, *J* = 8.33 Hz, 2H, Ar-H), 7.09 (d, *J* = 8.3 Hz, 2H, Ar-H), 6.95–6.92 (m, 4H, Ar-H), 5.76 (d, *J* = 3.6 Hz, 1H, C<sub>1</sub>H), 5.62 (d, *J* = 2.2 Hz, 1H, S-CH), 5.25 (d, *J* = 2.2 Hz, 1H, CH-N), 4.66 (t, *J* = 3.9 Hz, 1H, C<sub>2</sub>H), 4.54 (s, 2H, OCH<sub>2</sub>), 3.96–3.94 (m, 1H, C<sub>4</sub>H), 3.26 (dd, *J*<sub>1</sub> = 9.1 Hz, *J*<sub>2</sub> = 4.2 Hz, 1H, C<sub>3</sub>H), 2.80–2.78 (m, 1H, CH), 1.53 (s, 3H, CH<sub>3</sub>), 1.36 (m, 3H, CH<sub>3</sub>), 0.96 (d, *J* = 6.3 Hz, 6H, 2×CH<sub>3</sub>); <sup>13</sup>C NMR (75 MHz, DMSO-*d*<sub>6</sub>) δ 171.6, 151.6, 143.2, 137.4, 133.6, 132.3, 131.2, 129.3, 128.4, 127.9, 124.8, 122.9, 119.2, 111.2, 103.8, 81.2, 78.1, 74.1, 65.9, 58.1, 51.4, 50.6, 26.1, 16.1; MS: *m/z* (M<sup>+</sup>+H) 725. Anal. Calcd for C<sub>35</sub>H<sub>35</sub>Cl<sub>2</sub>FN<sub>6</sub>O<sub>4</sub>S: C, 57.93; H, 4.86; N, 11.58. Found: C, 57.72; H, 4.66; N, 11.46.

**6-(4-Chlorophenyl)-5-((3aR,5S,6S,6aR)-6-((1-(4-chlorophenyl)-1H-1,2,3-triazol-4-yl)methoxy)-2,2-dimethyltetrahydrofuro[2,3-*d*][1,3]dioxol-5-yl)-3-(4-fluorophenyl)-2-methyl-3,3a,5,6-tetrahydro-2H-pyrazolo[3,4-*d*]thiazole (10l).** This was obtained by reacting compound **9b** (1 g) and methylhydrazine (0.25 g) as described in the typical procedure and isolated as a yellow solid, yield 76%, m.p. 241–243 °C; <sup>1</sup>H NMR (300 MHz, DMSO-*d*<sub>6</sub>) δ 8.29 (d, *J* = 8.7 Hz, 2H, Ar-H), 8.16 (s, 1H, Ar-H), 7.59 (d, *J* = 9.2 Hz, 2H, Ar-H), 7.48 (s, 1H, CH-S), 7.39 (d, *J* = 8.33 Hz, 2H, Ar-H), 7.09 (d, *J* = 8.3 Hz, 2H, Ar-H), 6.91–6.88 (m, 4H, Ar-H), 5.76 (d, *J* = 3.6 Hz, 1H, C<sub>1</sub>H), 5.62 (d, *J* = 2.2 Hz, 1H, S-CH), 5.25 (d, *J* = 2.2 Hz, 1H, CH-N), 4.66 (t, *J* = 3.9 Hz, 1H, C<sub>2</sub>H), 4.54 (s, 2H, OCH<sub>2</sub>), 3.96–3.94 (m, 1H, C<sub>4</sub>H), 3.71 (s, 3H, N-CH<sub>3</sub>), 3.26 (dd, *J*<sub>1</sub> = 9.1 Hz, *J*<sub>2</sub> = 4.2 Hz, 1H, C<sub>3</sub>H), 1.53 (s, 3H, CH<sub>3</sub>), 1.36 (m, 3H, CH<sub>3</sub>); <sup>13</sup>C NMR (75 MHz, DMSO-*d*<sub>6</sub>) δ 171.6, 151.6, 143.2, 137.4, 133.6, 132.3, 131.2, 129.3, 128.4, 127.9, 124.8, 122.9, 119.2, 111.2, 103.8, 81.2, 78.1, 74.1, 65.9, 58.1, 51.4, 39.3, 16.1; MS: *m/z* (M<sup>+</sup>+H) 684. Anal. Calcd for C<sub>32</sub>H<sub>30</sub>Cl<sub>2</sub>FN<sub>6</sub>O<sub>4</sub>S: C, 56.14; H, 4.42; N, 12.28. Found: C, 55.92; H, 4.26; N, 12.02.

**5-((3aR,5S,6S,6aR)-6-((1-(4-Chlorophenyl)-1H-1,2,3-triazol-4-yl)methoxy)-2,2-dimethyltetrahydrofu-**

**ro[2,3-*d*][1,3]dioxol-5-yl)-3-(4-fluorophenyl)-6-(4-nitrophenyl)-2-phenyl-3,3a,5,6-tetrahydro-2H-pyrazolo[3,4-*d*]thiazole (10m).** This was obtained by reacting compound **9c** (1 g) and phenylhydrazine (0.25 g) as described in the typical procedure and isolated as a brown solid, yield 75%, m.p. 241–243 °C; <sup>1</sup>H NMR (300 MHz, DMSO-*d*<sub>6</sub>) δ 8.26 (d, *J* = 8.7 Hz, 2H, Ar-H), 8.02 (s, 1H, Ar-H), 7.49 (d, *J* = 9.2 Hz, 2H, Ar-H), 7.22 (d, *J* = 8.33 Hz, 2H, Ar-H), 7.08–7.05 (m, 6H, Ar-H and CH-S), 7.02 (d, *J* = 8.3 Hz, 2H, Ar-H), 6.81–6.77 (m, 4H, Ar-H), 5.66 (d, *J* = 3.6 Hz, 1H, C<sub>1</sub>H), 5.58 (d, *J* = 2.2 Hz, 1H, S-CH), 5.21 (d, *J* = 2.2 Hz, 1H, CH-N), 4.62 (t, *J* = 3.9 Hz, 1H, C<sub>2</sub>H), 4.51 (s, 2H, OCH<sub>2</sub>), 3.94–3.91 (m, 1H, C<sub>4</sub>H), 3.26 (dd, *J*<sub>1</sub> = 9.1 Hz, *J*<sub>2</sub> = 4.2 Hz, 1H, C<sub>3</sub>H), 1.53 (s, 3H, CH<sub>3</sub>), 1.36 (m, 3H, CH<sub>3</sub>); <sup>13</sup>C NMR (75 MHz, DMSO-*d*<sub>6</sub>) δ 174.6, 143.0, 141.4, 137.4, 136.2, 133.6, 132.3, 131.2, 129.3, 128.4, 127.9, 126.1, 124.8, 122.9, 119.2, 111.2, 103.8, 81.2, 78.1, 74.1, 65.9, 51.4, 26.1, 16.1; MS: *m/z* (M<sup>+</sup>+H) 770. Anal. Calcd for C<sub>38</sub>H<sub>33</sub>ClFN<sub>7</sub>O<sub>6</sub>S: C, 59.26; H, 4.32; N, 12.73. Found: C, 59.16; H, 4.10; N, 12.53.

**5-((3aR,5S,6S,6aR)-6-((1-(4-Chlorophenyl)-1H-1,2,3-triazol-4-yl)methoxy)-2,2-dimethyltetrahydrofuro[2,3-*d*][1,3]dioxol-5-yl)-3-(4-fluorophenyl)-2-(4-methoxyphenyl)-6-(4-nitrophenyl)-3,3a,5,6-tetrahydro-2H-pyrazolo[3,4-*d*]thiazole (10n).** This was obtained by reacting compound **9c** (1 g) and *p*-methoxyphenylhydrazine (0.35 g) as described in the typical procedure and isolated as a yellow solid, yield 76%, m.p. 264–266 °C; <sup>1</sup>H NMR (300 MHz, DMSO-*d*<sub>6</sub>) δ 8.28 (d, *J* = 8.7 Hz, 2H, Ar-H), 8.04 (s, 1H, Ar-H), 7.51 (d, *J* = 9.2 Hz, 2H, Ar-H), 7.40–7.35 (m, 5H, Ar-H and CH-S), 7.29 (d, *J* = 8.33 Hz, 2H, Ar-H), 7.05 (d, *J* = 8.3 Hz, 2H, Ar-H), 6.91–6.87 (m, 4H, Ar-H), 5.76 (d, *J* = 3.6 Hz, 1H, C<sub>1</sub>H), 5.62 (d, *J* = 2.2 Hz, 1H, S-CH), 5.25 (d, *J* = 2.2 Hz, 1H, CH-N), 4.66 (t, *J* = 3.9 Hz, 1H, C<sub>2</sub>H), 4.54 (s, 2H, OCH<sub>2</sub>), 3.96–3.94 (m, 1H, C<sub>4</sub>H), 3.91 (s, 3H, OMe), 3.26 (dd, *J*<sub>1</sub> = 9.1 Hz, *J*<sub>2</sub> = 4.2 Hz, 1H, C<sub>3</sub>H), 1.53 (s, 3H, CH<sub>3</sub>), 1.36 (m, 3H, CH<sub>3</sub>); <sup>13</sup>C NMR (75 MHz, DMSO-*d*<sub>6</sub>) δ 172.6, 151.7, 143.2, 141.4, 137.4, 133.6, 132.3, 131.2, 129.3, 126.1, 125.3, 128.4, 127.9, 124.8, 122.9, 119.2, 111.2, 103.8, 81.2, 78.1, 74.1, 65.9, 55.8, 51.4, 26.1, 16.1; MS: *m/z* (M<sup>+</sup>+H) 800. Anal. Calcd for C<sub>39</sub>H<sub>35</sub>ClFN<sub>7</sub>O<sub>7</sub>S: C, 58.53; H, 4.41; N, 12.25. Found: C, 58.22; H, 4.16; N, 12.01.

**2-(4-Chlorophenyl)-5-((3aR,5S,6S,6aR)-6-((1-(4-chlorophenyl)-1H-1,2,3-triazol-4-yl)methoxy)-2,2-dimethyltetrahydrofuro[2,3-*d*][1,3]dioxol-5-yl)-3-(4-fluorophenyl)-6-(4-nitrophenyl)-3,3a,5,6-tetrahydro-2H-pyrazolo[3,4-*d*]thiazole (10 o).** This was obtained by reacting compound **9c** (1 g) and *p*-chlorophenylhydrazine (0.45 g) as described in the typical procedure and isolated as a brown solid, yield 72%, m.p. 285–287 °C; <sup>1</sup>H NMR (300 MHz, DMSO-*d*<sub>6</sub>) δ 8.23 (d, *J* = 8.7 Hz, 2H, Ar-H), 8.11 (s, 1H, Ar-H), 7.58 (d, *J* = 9.2 Hz, 2H, Ar-H), 7.40–7.35 (m, 5H, Ar-H and CH-S), 7.29 (d, *J* = 8.33 Hz, 2H, Ar-H), 7.07 (d, *J* = 8.3 Hz,



2H, Ar-H), 6.91–6.87 (m, 4H, Ar-H), 5.76 (d,  $J = 3.6$  Hz, 1H, C<sub>1</sub>H), 5.62 (d,  $J = 2.2$  Hz, 1H, S-CH), 5.25 (d,  $J = 2.2$  Hz, 1H, CH-N), 4.66 (t,  $J = 3.9$  Hz, 1H, C<sub>2</sub>H), 4.54 (s, 2H, OCH<sub>2</sub>), 3.96–3.94 (m, 1H, C<sub>4</sub>H), 3.26 (dd,  $J_1 = 9.1$  Hz,  $J_2 = 4.2$  Hz, 1H, C<sub>3</sub>H), 1.53 (s, 3H, CH<sub>3</sub>), 1.36 (m, 3H, CH<sub>3</sub>); <sup>13</sup>C NMR (75 MHz, DMSO-*d*<sub>6</sub>)  $\delta$  172.6, 151.7, 143.2, 137.4, 133.6, 132.3, 131.2, 129.3, 126.3, 125.3, 128.4, 127.9, 124.8, 122.9, 119.2, 111.2, 103.8, 81.2, 78.1, 74.1, 65.9, 51.4, 26.1, 16.1; MS:  $m/z$  (M<sup>+</sup> + Na) 815. Anal. Calcd for C<sub>38</sub>H<sub>32</sub>Cl<sub>2</sub>FN<sub>7</sub>O<sub>6</sub>S: C, 56.72; H, 4.01; N, 12.81. Found: C, 56.42; H, 3.95; N, 12.72.

**2-Benzyl-5-((3aR,5S,6S,6aR)-6-((1-(4-chlorophenyl)-1H-1,2,3-triazol-4-yl)methoxy)-2,2-dimethyltetrahydrofuro[2,3-*d*][1,3]dioxol-5-yl)-3-(4-fluorophenyl)-6-(4-nitrophenyl)-3,3a,5,6-tetrahydro-2H-pyrazolo[3,4-*d*]thiazole (10p).** This was obtained by reacting compound **9c** (1 g) and benzylhydrazine (0.65 g) as described in the typical procedure and isolated as a yellow solid, yield 71%, m.p. 275–277 °C; <sup>1</sup>H NMR (300 MHz, DMSO-*d*<sub>6</sub>)  $\delta$  8.35 (d,  $J = 8.7$  Hz, 2H, Ar-H), 8.11 (s, 1H, Ar-H), 7.59 (d,  $J = 9.2$  Hz, 2H, Ar-H), 7.46–7.40 (m, 6H, Ar-H and CH-S), 7.32 (d,  $J = 8.33$  Hz, 2H, Ar-H), 7.08 (d,  $J = 8.3$  Hz, 2H, Ar-H), 6.96–6.90 (m, 4H, Ar-H), 5.96 (s, 2H, CH<sub>2</sub>Ph), 5.77 (d,  $J = 3.6$  Hz, 1H, C<sub>1</sub>H), 5.65 (d,  $J = 2.2$  Hz, 1H, S-CH), 5.28 (d,  $J = 2.2$  Hz, 1H, CH-N), 4.66 (t,  $J = 3.9$  Hz, 1H, C<sub>2</sub>H), 4.54 (s, 2H, OCH<sub>2</sub>), 3.96–3.94 (m, 1H, C<sub>4</sub>H), 3.26 (dd,  $J_1 = 9.1$  Hz,  $J_2 = 4.2$  Hz, 1H, C<sub>3</sub>H), 1.53 (s, 3H, CH<sub>3</sub>), 1.36 (m, 3H, CH<sub>3</sub>); <sup>13</sup>C NMR (75 MHz, DMSO-*d*<sub>6</sub>)  $\delta$  171.6, 151.6, 143.2, 137.4, 133.6, 132.3, 131.2, 129.3, 125.3, 128.4, 127.9, 124.8, 122.9, 119.2, 111.2, 103.8, 81.2, 78.1, 74.1, 65.9, 58.1, 51.4, 26.1, 16.1; MS:  $m/z$  (M<sup>+</sup> + H) 773. Anal. Calcd for C<sub>39</sub>H<sub>35</sub>ClFN<sub>7</sub>O<sub>6</sub>S: C, 59.73; H, 4.50; N, 12.56. Found: C, 59.66; H, 4.41; N, 12.36.

**5-((3aR,5S,6S,6aR)-6-((1-(4-Chlorophenyl)-1H-1,2,3-triazol-4-yl)methoxy)-2,2-dimethyltetrahydrofuro[2,3-*d*][1,3]dioxol-5-yl)-3-(4-fluorophenyl)-2-isopropyl-6-(4-nitrophenyl)-3,3a,5,6-tetrahydro-2H-pyrazolo[3,4-*d*]thiazole (10q).** This was obtained by reacting compound **9c** (1 g) and isopropylhydrazine (0.35 g) as described in the typical procedure and isolated as a brown solid, yield 69%, m.p. 221–223 °C; <sup>1</sup>H NMR (300 MHz, DMSO-*d*<sub>6</sub>)  $\delta$  8.32 (d,  $J = 8.7$  Hz, 2H, Ar-H), 8.16 (s, 1H, Ar-H), 7.65 (d,  $J = 9.2$  Hz, 2H, Ar-H), 7.52–7.48 (m, 5H, Ar-H and CH-S), 7.39 (d,  $J = 8.33$  Hz, 2H, Ar-H), 7.09 (d,  $J = 8.3$  Hz, 2H, Ar-H), 5.76 (d,  $J = 3.6$  Hz, 1H, C<sub>1</sub>H), 5.62 (d,  $J = 2.2$  Hz, 1H, S-CH), 5.25 (d,  $J = 2.2$  Hz, 1H, CH-N), 4.66 (t,  $J = 3.9$  Hz, 1H, C<sub>2</sub>H), 4.54 (s, 2H, OCH<sub>2</sub>), 3.96–3.94 (m, 1H, C<sub>4</sub>H), 3.26 (dd,  $J_1 = 9.1$  Hz,  $J_2 = 4.2$  Hz, 1H, C<sub>3</sub>H), 2.80–2.78 (m, 1H, CH), 1.53 (s, 3H, CH<sub>3</sub>), 1.36 (m, 3H, CH<sub>3</sub>), 0.96 (d,  $J = 6.3$  Hz, 6H, 2×CH<sub>3</sub>); <sup>13</sup>C NMR (75 MHz, DMSO-*d*<sub>6</sub>)  $\delta$  171.6, 151.6, 143.2, 137.4, 133.6, 132.3, 131.2, 129.3, 128.4, 127.9, 124.8, 122.9, 119.2, 111.2, 103.8, 81.2, 78.1, 74.1, 65.9, 58.1, 51.4, 50.6, 26.1, 16.1; MS:  $m/z$  (M<sup>+</sup> + H) 736. Anal. Calcd for C<sub>35</sub>H<sub>35</sub>ClFN<sub>7</sub>O<sub>6</sub>S: C, 57.10; H, 4.79; N, 13.32. Found: C, 56.98; H, 4.56; N, 12.99.

**5-((3aR,5S,6S,6aR)-6-((1-(4-Chlorophenyl)-1H-1,2,3-triazol-4-yl)methoxy)-2,2-dimethyltetrahydrofuro[2,3-*d*][1,3]dioxol-5-yl)-3-(4-fluorophenyl)-2-methyl-6-(4-nitrophenyl)-3,3a,5,6-tetrahydro-2H-pyrazolo[3,4-*d*]thiazole (10r).** This was obtained by reacting compound **9c** (1 g) and methylhydrazine (0.25 g) as described in the typical procedure and isolated as a brown solid, yield 67%, m.p. 251–253 °C; <sup>1</sup>H NMR (300 MHz, DMSO-*d*<sub>6</sub>)  $\delta$  8.29 (d,  $J = 8.7$  Hz, 2H, Ar-H), 8.16 (s, 1H, Ar-H), 7.59 (d,  $J = 9.2$  Hz, 2H, Ar-H), 7.48–7.44 (m, 5H, Ar-H and CH-S), 7.39 (d,  $J = 8.33$  Hz, 2H, Ar-H), 7.09 (d,  $J = 8.3$  Hz, 2H, Ar-H), 5.76 (d,  $J = 3.6$  Hz, 1H, C<sub>1</sub>H), 5.62 (d,  $J = 2.2$  Hz, 1H, S-CH), 5.25 (d,  $J = 2.2$  Hz, 1H, CH-N), 4.66 (t,  $J = 3.9$  Hz, 1H, C<sub>2</sub>H), 4.54 (s, 2H, OCH<sub>2</sub>), 3.96–3.94 (m, 1H, C<sub>4</sub>H), 3.71 (s, 3H, N-CH<sub>3</sub>), 3.26 (dd,  $J_1 = 9.1$  Hz,  $J_2 = 4.2$  Hz, 1H, C<sub>3</sub>H), 1.53 (s, 3H, CH<sub>3</sub>), 1.36 (m, 3H, CH<sub>3</sub>); <sup>13</sup>C NMR (75 MHz, DMSO-*d*<sub>6</sub>)  $\delta$  171.6, 151.6, 143.2, 137.4, 133.6, 132.3, 131.2, 129.3, 128.4, 127.9, 124.8, 122.9, 119.2, 111.2, 103.8, 81.2, 78.1, 74.1, 65.9, 58.1, 51.4, 39.3, 16.1; MS:  $m/z$  (M<sup>+</sup> + H) 684. Anal. Calcd for C<sub>33</sub>H<sub>31</sub>ClFN<sub>7</sub>O<sub>6</sub>S: C, 55.97; H, 4.41; N, 13.85. Found: C, 55.82; H, 4.26; N, 13.72.

## 6. Conclusion

In conclusion, a series of a new class of hybrid heterocycles **10a–r** have been synthesized and evaluated for their nematocidal activity, most of the compounds showed appreciable nematocidal activity. The antifungal activities of these compounds were evaluated against various fungi. Many of the synthesized compounds showed good activity against the tested fungi and therefore have emerged as potential molecules for further development.

## 7. Acknowledgements

The authors are thankful to CSIR-New Delhi for the financial support (Project funding No: 02 (247)15/EMR-II), Director, CSIR- IICT, Hyderabad, India, for NMR and MS spectral analysis and Principal, Vaagdevi Degree & PG College Hanamkonda for his constant encouragement.

## 8. References

- (a) K. D. Hani, D. A. Leigh, *Chem. Soc. Rev.* **2010**, 39, 1240–1251. DOI:10.1039/B901974J
- (b) C. O. Kappe, E. Van der Eycken, *Chem. Soc. Rev.* **2010**, 39, 1280–1290 DOI:10.1039/B901973C
- (c) A. H. El-Sagheer, T. Brown, *Chem. Soc. Rev.* **2010**, 39, 1388–1405 DOI:10.1039/b901971p
- (d) A. Qin, J. W. Y. Lam, B. Z. Tang, *Chem. Soc. Rev.* **2010**, 2522–2544. DOI:10.1039/b909064a
- (e) M. Meldal, C. W. Tornøe, *Chem. Rev.* **2008**, 108, 2952–3015. DOI:10.1021/cr0783479

- (f) H. Nandivada, X. Jiang, J. Lahann, *Adv. Mater.* **2007**, *19*, 2197–2208. DOI:10.1002/adma.200602739
- (g) Y. L. Angell, K. Burgess, *Chem. Soc. Rev.* **2007**, *36*, 1674–1689. DOI:10.1039/b701444a
- (h) D. Fournier, R. Hoogenboom, U. S. Schubert, *Chem. Soc. Rev.* **2007**, *36*, 1369–1380. DOI:10.1039/b700809k
- (i) J. E. Moses, A. D. Moorhouse, *Chem. Soc. Rev.* **2007**, *36*, 1249–1262. DOI:10.1039/B613014N
- (j) J. F. Lutz, *Angew. Chem. Int. Ed.* **2007**, *46*, 1018–1125. DOI:10.1002/anie.200604050
- (k) A. Dondoni, *Chem. – Asian J.* **2007**, *2*, 700–708. DOI:10.1002/asia.200700015
- (l) H. C. Kolb, K. B. Sharpless, *Drug Discovery Today*, **2003**, *8*, 1128–1137. DOI:10.1016/S1359-6446(03)02933-7
2. (a) A. Brick, J. Muldoon, Y.-C. Lin, J. H. Elder, D. S. Goodsell, A. J. Olson, V. V. Fokin, K. B. Sharpless, C.-H. Wong, *Chem-BioChem.* **2003**, *4*, 1246–1248. DOI:10.1002/cbic.200300724
- (b) M. J. Soltis, H. J. Yeh, K. A. Cole, N. Whittaker, R. P. Wersto, E. C. Kohn, *Drug Metab. Dispos.* **1996**, *24*, 799–806.
3. (a) W.-Q. Fan, A. R. Katritzky, 1,2,3-Triazoles, In *Comprehensive Heterocyclic Chemistry II*. Edited by A. R. Katritzky, C. W. Rees, V. Scriven, Elsevier, Oxford. **1996**, *4*, 1–126, pp. 905–1006.
- (b) M. Whiting, J. Muldoon, Y.-C. Lin, S. M. Silverman, W. Lindstrom, A. J. Olson, H. C. Kolb, M. G. Finn, K. B. Sharpless, J. H. Elder, V. V. Fokin, *Angew. Chem. Int. Ed.*, **2006**, *45*, 1435–1439. DOI:10.1002/anie.200502161
- (c) Y. Bourne, H. C. Kolb, Z. Radić, K. B. Sharpless, P. Taylor, P. Marchot, *Proc. Natl. Acad. Sci. U.S.A.* **2004**, *101*, 1449–1454. DOI:10.1073/pnas.0308206100
- (d) W. G. Lewis, G. Green, F. Z. Grynspan, Z. Radić, P. R. Carlier, P. Taylor, M. G. Finn, K. B. Sharpless, *Angew. Chem., Int. Ed.* **2002**, *41*, 1053–1057. DOI:10.1002/1521-3773(20020315)41:6<1053::AID-ANIE1053>3.0.CO;2-4
4. R. Huisgen, A. Padwa, *1,3-Dipolar Cycloaddition Chemistry*, Ed. Wiley, New York, **1984**, *1*, 1–176.
5. (a) N. A. Al-Maoudi, A. Y. Al-Soud, *Tetrahedron Lett.* **2002**, *43*, 4021–4022. DOI:10.1016/S0040-4039(02)00733-5
- (b) B. H. M. Kuijpers, S. Groothuys, A. B. R. Keereweer, P. J. L. M. Quaedflieg, R. H. Blaauw, F. L. van Delft, F. P. J. T. Rutjes, *Org. Lett.* **2004**, *6*, 3123–3126. DOI:10.1021/ol048841o
- (c) C. Srinivas, X. Fang, Q. Wang, *Tetrahedron Lett.* **2005**, *46*, 2331–2334. DOI:10.1016/j.tetlet.2005.01.175
- (d) S. Hotha, R. I. Anegundi, A. A. Natu, *Tetrahedron Lett.* **2005**, *46*, 4585–4588. DOI:10.1016/j.tetlet.2005.05.012
- (e) S. Hotha, S. Kashyap, *J. Org. Chem.* **2006**, *71*, 364–367. DOI:10.1021/jo051731q
6. H. K. Urman, O. Bulay, B. Clayson, P. Shudik, *Cancer Lett.* **1975**, *1*, 69–74. DOI:10.1016/S0304-3835(75)95362-8
7. A. A. Field, A. A. Tyrell, G. P. Lampson, M. R. Hilleman, *Proc. Natl. Acad. Sci. U.S.A.* **1967**, *58*, 1004–1010. DOI:10.1073/pnas.58.3.1004
8. M. G. Vigorita, R. Ottana, F. Monoforte, R. Maccari, A. Trovato, M. T. Monoforte, M. F. Taviano, *Bioorg. Med. Chem. Lett.* **2001**, *11*, 2791–2794. DOI:10.1016/S0960-894X(01)00476-0
9. M. S. Chande, V. J. Suryanarayana, *J. Chem. Res.* **2005**, 345–347. DOI:10.3184/0308234054506749
10. C. V. Kavitha, S. Basappa, N. Swamy, K. Manteling, S. Doreswamy, M. A. Sridhar, S. Prasad, K. S. Rangappa, *Bioorg. Med. Chem. Lett.* **2006**, *14*, 2290–2299. DOI:10.1016/j.bmc.2005.11.017
11. B. A. Sobin, *J. Am. Chem. Soc.* **1952**, *74*, 2947–2948. DOI:10.1021/ja01131a526
12. Y. Tanabe, Y. Kumuro, N. Imanishi, S. Morooka, M. Enomoto, A. Kojima, Y. Sanemistu, M. Mizutani, *Tetrahedron Lett.* **1991**, *32*, 379–382. DOI:10.1016/S0040-4039(00)92633-9
13. T. Previtera, M. G. Vigorita, M. Bisila, F. Orshini, F. Benetolla, G. Bombieri, *Eur. J. Med. Chem.* **1994**, *29*, 317–324. DOI:10.1016/0223-5234(94)90102-3
14. R. Ottana, E. Mazzon, L. Dugo, F. Moforte, R. Maccari, L. Sautebin, G. De Luca, M. G. Vigorita, S. Alcaro, F. Ortuso, *Eur. J. Pharmacol.* **2002**, *448*, 71–80. DOI:10.1016/S0014-2999(02)01888-5
15. T. Kato, T. Ozaki, K. Tamura, *J. Med. Chem.* **1999**, *42*, 3134–3146. DOI:10.1021/jm9900927
16. Y. Tanabe, G. Suzukamo, Y. Komuro, N. Imanishi, S. Morooka, M. Enomoto, A. Kojima, Y. Sanemistu, M. Mizutani, *Tetrahedron Lett.* **1991**, *32*, 379–382. DOI:10.1016/S0040-4039(00)92633-9
17. T. Kato, T. Ozaki, K. Tamura, *Tetrahedron Assym.* **1999**, *10*, 3963–3968. DOI:10.1016/S0957-4166(99)00441-3
18. Y. Adachi, Y. Suzuki, N. Homma, M. Fuzukawa, K. Tamura, I. Nishie, O. Kuromaru, *Eur. J. Pharmacol.* **1999**, *367*, 267–273. DOI:10.1016/S0014-2999(98)00938-8
19. C. S. Reddy, A. Srinivas, A. Nagaraj, *J. Heterocycl. Chem.* **2008**, *45*, 999–1003. DOI:10.1002/jhet.5570450409
20. K. Y. Lee, J. M. Kim, J. N. Kim, *Tetrahedron Lett.* **2003**, *44*, 6737–6740. DOI:10.1016/S0040-4039(03)01648-4
21. P. Erhan, A. Mutlu, U. Tayfun, E. Dilek, *Eur. J. Med. Chem.* **2001**, *36*, 539–543. DOI:10.1016/S0223-5234(01)01243-0
22. R. A. Nugen, M. Meghan, *J. Med. Chem.* **1993**, *36*, 134–139. DOI:10.1021/jm00053a017
23. H. Kawazura, Y. Takahashi, Y. Shiga, F. Shimada, N. Ohta, A. Tamura, *Jpn. J. Pharmacol.* **1997**, *73*, 317–324. DOI:10.1254/jjp.73.317
24. M. J. Genin, C. Bilers, B. J. Kieser, S. M. Poppe, S. M. Swaney, W. G. Tarpley, Y. Yagi, D. L. Romero, *J. Med. Chem.* **2000**, *43*, 1034–1040. DOI:10.1021/jm990383f
25. A. G. Habeb, P. N. P. Rao, E. E. Knaus, *J. Med. Chem.* **2001**, *44*, 3039–3042. DOI:10.1021/jm010153c
26. H. Hashimoto, K. Imamura, J. I. Haruta, K. Wakitani, *J. Med. Chem.* **2002**, *45*, 1511–1517. DOI:10.1021/jm010484p
27. M. Sakya, B. Rast, *Tetrahedron Lett.* **2003**, *44*, 7629–7632. DOI:10.1016/j.tetlet.2003.08.054
28. L. David, D. G. B. Selwood, *J. Med. Chem.* **2001**, *44*, 78–93. DOI:10.1021/jm001034k
29. U. L. B. Jayasinghe, B. M. M. Kumarihamy, A. G. D. Bandara, E. A. Vasquez, W. Kraus, *Nat. Prod. Res.* **2003**, *17*, 259–262. DOI:10.1080/1057563021000060121

30. S. Min, L. Xiaoming, J. Shuishui, L. Lingjie, W. Jiali, W. Shiqiang, *Applied Soil Ecology*. **2016**, *102*, 53–60. DOI:10.1016/j.apsoil.2016.02.011
31. J. W. Noling, J. O. Becker, *J. Nematol.* **1994**, *26*, 573–586.
32. C. In Ho, K. Jun Heon, S. Sang-Chul, P. Il-Kown, *Rus. J. Nematology* **2007**, *15*, 35–40.
33. K. Shigefumi, W. Kojiro, M. Katsura, *Agr. Bio. Chem.* **1976**, *40*, 2085–2089. DOI:10.1080/00021369.1976.10862338
34. J. H. Uhlenbroek, J. D. Bijloo, *Recl. Trav. Chim.* **1958**, *77*, 1004–1008. DOI:10.1002/recl.19580771103
35. (a) A. Srinivas, M. Sunitha, B. Ravinder, S. Anusha, T. Rajasri, P. Swapna, D. Sushmitha, D. Swaroopa, G. Nikitha, C. Govind Rao, *Acta Chim. Slov.* **2017**, *64*, 319–331. DOI:10.17344/acsi.2016.3153  
(b) A. Srinivas, M. Santhosh, M. Sunitha, P. Karthik, K. Srinivas, K. Vasumathi Reddy, *Acta Chim. Slov.* **2016**, *63*, 827–836. DOI:10.17344/acsi.2015.2124
36. A. Srinivas, M. Sunitha, C. Govind Rao, *Acta Chim. Slov.* **2016**, *63*, 344–350. DOI:10.17344/acsi.2015.2124
37. A. Srinivas, *Acta Chim. Soc.* **2016**, *63*, 173–179. DOI:10.17344/acsi.2015.2124
38. A. Srinivas, M. Sunitha, *Indian J. Chem., Sect. B* **2016**, *55B*, 102–109.
39. A. Srinivas, M. Sunitha, *Indian J. Chem., Sect. B* **2016**, *55B*, 231–239.
40. A. Srinivas, M. Sunitha, C. Govind Rao, *Indian J. Chem., Sect. B* **2016**, *55B*, 1239–1242.
41. A. Srinivas, A. Nagaraj, C. S. Reddy, *Eur. J. Med. Chem.* **2010**, *45*, 2353–2358. DOI:10.1016/j.ejmech.2010.02.014
42. C. S. Reddy, A. Srinivas, M. Sunitha, A. Nagaraj, *J. Heterocycl. Chem.* **2010**, *47*, 1303–1309. DOI:10.1002/jhet.474
43. C. S. Reddy, A. Nagaraj, A. Srinivas, G. P. Reddy, *Indian J. Chem., Sect. B*, **2010**, *49B*, 617–622.
44. C. S. Reddy, A. Srinivas, A. Nagaraj, *J. Heterocycl. Chem.* **2009**, *46*, 497–502. DOI:10.1002/jhet.100
45. C. S. Reddy, A. Nagaraj, A. Srinivas, G. P. Reddy, *Indian J. Chem., Sect. B* **2009**, *48B*, 248–254.
46. C. S. Reddy, A. Srinivas, A. Nagaraj, *J. Heterocyclic. Chem.* **2008**, *45*, 1121–1125.
47. C. S. Reddy, G. P. Reddy, A. Nagaraj, A. Srinivas, *Org. Commun.* **2008**, *1*, 84–94.
48. A. Srinivas, A. Nagaraj, C. S. Reddy, *Indian J. Chem., Sect. B* **2008**, *47B*, 787–791.
49. P. A. Levene, G. M. Meyer, *J. Biol. Chem.* **1931**, *92*, 257.
50. National Committee for clinical laboratory standards (NCCLS). Nat. Comm. Lab. Stands. Villanova, 1982, p. 242.
51. Z. K. Khan, Proc. Int. Workshop UNIDO-CDRI, 1997, 210 (1997).
52. C. W. McBeth, G. B. Bergerson, *Phytopathology* **1953**, *43*, 264.

## Povzetek

Z reakcije med halkonskimi derivati 2-((3aR,5S,6S,6aR)-6-((1-(4-klorofenil)-1H-1,2,3-triazol-4-il)metoksi)-2,2-dimetiltetrahydrofuro[2,3-d][1,3]dioksol-5-il)-3-feniltiazolidin-4-onov **9** in aril/alkil hidrazini smo pripravili novo serijo 5-((3aR,5S,6S,6aR)-6-((1-(4-klorofenil)-1H-1,2,3-triazol-4-il)metoksi)-2,2-dimetiltetrahydrofuro[2,3-d][1,3]dioksol-5-il)-3-(4-fluorofenil)-2,6-difenil-3,3a,5,6-tetrahydro-2H-pirazolo[3,4-d]tiazolov **10a–r**. Strukture novih spojin smo določili na osnovi IR, NMR, MS in elementne analize. Za spojine **10a–r** smo tudi določili učinkovanje proti ploskim črvom (nematodam) *Dietylenchus myceliophagus* in *Caenorhabditis elegans* z *in vitro* metodo v vodnih raztopinah. Ugotovili smo, da spojine, ki vsebujejo *N*-benzilpirazolni (**10d**, **10j**, **10p**) ali *N*-metilpirazolni fragment (**10f**, **10i**, **10r**), izkazujejo občutno nematocidno aktivnost proti obema testiranima živalskima vrstama z LD<sub>50</sub> 160–210 ppm, kar je skoraj enako aktivnosti standarda oksamila. Za spojine **10a–r** smo tudi raziskali delovanje proti glivam (izmerili smo MZI, MIC in MFC vrednosti) in sicer: *Candida albicans* (ATCC 102331), *Aspergillus fumigates* (HIC 6094), *Trichophyton rubrum* (IFO 9185) in *Trichophyton mentagrophytes* (IFO 40996). Večina novih spojin je izkazala opazno delovanje proti testiranim glivam, kar daje možnosti nadaljnega razvoja predstavljenih spojin

Scientific paper

# Preparation, Structure, Photoluminescent and Semiconductive Properties, and Theoretical Calculation of a Novel Cadmium Complex with Mixed Ligands

Xiu-Guang Yi,<sup>1,2</sup> Wen-Tong Chen,<sup>1,3,4,\*</sup> Jian-Gen Huang,<sup>1</sup> Ding-Wa Zhang<sup>1</sup>  
and Yin-Feng Wang<sup>1</sup>

<sup>1</sup>Institute of Applied Chemistry, Jiangxi Province Key Laboratory of Coordination Chemistry, School of Chemistry and Chemical Engineering, Jingtangshan University, Ji'an, Jiangxi, 343009, China

<sup>2</sup>Research Center for Rare Earths & Nano/micro Functional Materials, Nanchang University Nanchang, Jiangxi 330031, China

<sup>3</sup>Key Laboratory of Jiangxi Province for Persistent Pollutants Control and Resources Recycle (Nanchang Hangkong University), Nanchang, Jiangxi 330000, China

<sup>4</sup>State Key Laboratory of Structural Chemistry, Fujian Institute of Research on the Structure of Matter, Chinese Academy of Sciences, Fuzhou, Fujian 350002, China

\* Corresponding author: E-mail: wtchen\_2000@aliyun.com  
Tel.: +86(796)8100490; fax +86(796)8100490

Received: 18-09-2017

## Abstract

A novel cadmium complex with mixed ligands  $\{[\text{Cd}(2,2'\text{-biim})(4,4'\text{-bipy})(\text{H}_2\text{O})(\text{ClO}_4)] (\text{ClO}_4)_n\}$  (**1**) (2,2'-biim = 2,2'-biimidazole; 4,4'-bipy = 4,4'-bipyridine) has been synthesized through hydrothermal reaction and its crystal structure was determined by single-crystal X-ray diffraction technique. Single-crystal X-ray diffraction analyses revealed that complex **1** crystallizes in the space group  $Pna2_1$  of the orthorhombic system and exhibits a one-dimensional zig-zag chain structure consisting of  $[\text{Cd}(2,2'\text{-biim})(4,4'\text{-bipy})(\text{H}_2\text{O})(\text{ClO}_4)]_n^{n+}$  cationic chains and isolated  $\text{ClO}_4^-$  anions. Powder photoluminescent characterization reveals that complex **1** has an emission in the green region of the spectrum. Time-dependent density functional theory (TDDFT) calculation showed that the nature of the photoluminescence of complex **1** is originated from the ligand-to-ligand charge transfer (LLCT; from the HOMO of the perchlorate anions to the LUMO of the 4,4'-bipy ligand). A wide optical band gap of 3.25 eV was found by the solid-state UV/vis diffuse reflectance spectrum.

**Keywords:** Cadmium, photoluminescence, semiconductor, TDDFT, LLCT

## 1. Introduction

In recent years, preparation and characterization of coordination complexes have attracted increasing interest not only due to their amazing structural topologies but also their potential applications in the fields of catalyst, sensors, medicine, biology, solar energy conversion, magnetism, photoluminescence materials, and so forth.<sup>1–5</sup> From the perspective of the crystal engineering, the most useful and facile way to construct coordination complexes is to adopt a suitable ligand to connect metal centers. To

this end, the ligand is better to possess as much as donor atoms that enable it to bridge metal centers together to yield extended architectures. N-containing heterocyclic ligands (e.g., 2,2'-biim and 4,4'-bipy namely, 2,2'-biimidazole and 4,4'-bipyridine, respectively), which have several coordination sites and various coordination modes, have been widely applied as such ligands to design novel coordination complexes.<sup>6–12</sup> 2,2'-biim and 4,4'-bipy have been confirmed to be a good chelating or bridging ligand to build coordination complexes. Being very strong N-ligating ligands, 2,2'-biim and 4,4'-bipy are also important to

afford useful supramolecular recognition positions to form interesting supramolecular topologies. Therefore, 2,2'-biim and 4,4'-bipy are important and useful ligands to achieve extended structures or supramolecular geometries. Furthermore, the imidazole or pyridyl rings of the 2,2'-biim or 4,4'-bipy possess delocalized  $\pi$ -electron systems which allow them to become an ideal candidate to prepare photoluminescent materials.

In addition, coordination complexes possessing group 12 (IIB) elements (Zn, Cd, Hg) are attractive due to their photoluminescent and semiconductive properties, various coordination numbers and topologies provided by their  $d^{10}$  configuration of the IIB ions, as well as the important role of zinc played in biological systems.<sup>13–15</sup> For the sake of exploring the metal ions on the structures and properties of the coordination complexes, we often choose the IIB ions as the central ion source. In order to explore novel IIB coordination complexes with attractive structural topologies and interesting properties, we recently focus on the design and preparation of novel IIB coordination complexes with various organic ligands. We report in this work the preparation, crystal structure, photoluminescent and semiconductive properties, and theoretical calculation of a novel cadmium complex with mixed ligands, i.e.  $\{[\text{Cd}(2,2'\text{-biim})(4,4'\text{-bipy})(\text{H}_2\text{O})(\text{ClO}_4)](\text{ClO}_4)\}_n$  (**1**) with a 1-D zigzag chain structure. It should be pointed out that this is the first IIB complex with both 4,4'-bipy and 2,2'-biim ligands.

## 2. Experimental

### 2.1. Materials and Instrumentation.

All chemicals and reagents were of reagent grade, commercially available and directly applied for the reaction. Photoluminescent characterization was measured using solid-state powders of the title complex at room temperature on a JY FluoroMax-3 spectrometer. Time-dependent density functional theory (TDDFT) calculation was performed by virtue of the Gaussian03 suite of program packages. Solid-state UV/vis diffuse reflectance measurement was conducted on a computer-controlled TU1901 UV/vis spectrometer equipped with an integrating sphere attachment. Finely-ground powder sample was coated on barium sulfate which acts as a reference for 100% reflectance.

### 2.2. Synthesis of $\{[\text{Cd}(2,2'\text{-biim})(4,4'\text{-bipy})(\text{H}_2\text{O})(\text{ClO}_4)](\text{ClO}_4)\}_n$ (**1**)

$\text{Cd}(\text{ClO}_4)_2 \cdot 6\text{H}_2\text{O}$  (1.00 mmol, 0.420 g), 2,2'-biim (1.00 mmol, 0.134 g), 4,4'-bipy (1.00 mmol, 0.156 g) and 10 mL distilled water were put into a 25 mL vial of a Teflon-lined stainless steel autoclave. The autoclave was heated around 433 K under autogenous pressure over a period of ten days and powered off, then cooled to room temperature. Finally, light-yellow block crystals were collected, washed with dis-

tilled water, dried in air and used for single-crystal X-ray diffraction as well as property measurements. The yield was 24% (based on cadmium). Caution: perchlorate salts are highly explosive and must be handled with careful!

### 2.3. X-ray Structure Determination

The single-crystal data of the title complex were collected on a SuperNova X-ray diffractometer equipped with a graphite monochromated Mo-K $\alpha$  radiation source ( $\lambda = 0.71073 \text{ \AA}$ ) at 293(2) K. The diffraction was performed by means of a  $\omega$  scan mode. Using the CrystalClear software, we reduced the data set and corrected the empirical absorption.<sup>16</sup> The crystal structure was successfully solved by using the direct methods and Siemens SHELXTLTM Version 5 software package.<sup>17</sup> The non-hydrogen atoms were generated based on the subsequent Fourier difference maps and refined anisotropically. The hydrogen atoms were located theoretically and ride on their parent atoms;

**Table 1.** Crystallographic data and structural analysis for complex **1**

Formula	$\text{C}_{16}\text{H}_{16}\text{CdCl}_2\text{N}_6\text{O}_9$
$M_r$	619.65
Crystal system	orthorhombic
Space group	$Pna2_1$
$a$ (Å)	17.7584(5)
$b$ (Å)	9.8785(3)
$c$ (Å)	12.3847(4)
$V$ (Å <sup>3</sup> )	2172.60(11)
$Z$	4
Reflections collected	6691
Independent, observed reflections ( $R_{int}$ )	3304, 3118 (0.0219)
$d_{calcd.}$ (g/cm <sup>3</sup> )	1.894
$\mu/\text{mm}^{-1}$	1.315
$F(000)$	1232
$R_1, wR_2$	0.0271, 0.0634
$S$	1.027
$\Delta\rho(\text{max, min})$ (e/Å <sup>3</sup> )	0.388, -0.350

**Table 2.** Selected bond lengths (Å) and bond angles (°) for complex **1**

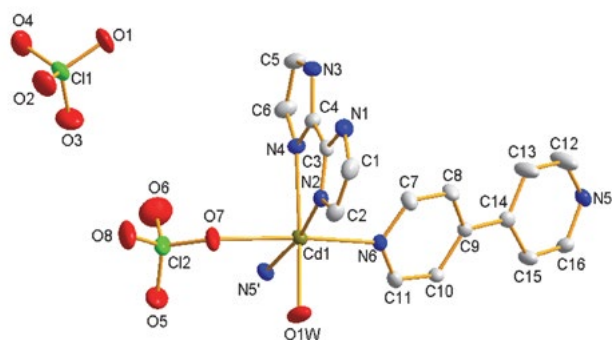
Distance	(Å)	Distance	(Å)
Cd1–N5 <sup>i</sup>	2.290(3)	Cd1–N6	2.355(3)
Cd1–O1W	2.296(3)	Cd1–N4	2.369(4)
Cd1–N2	2.303(3)	Cd1–O7	2.499(4)
Angle	(°)	Angle	(°)
N5 <sup>i</sup> –Cd1–O1W	95.24(14)	N2–Cd1–N4	72.89(11)
N5 <sup>i</sup> –Cd1–N2	170.58(14)	N6–Cd1–N4	91.18(13)
N2–Cd1–O1W	86.63(13)	N5 <sup>i</sup> –Cd1–O7	87.33(12)
N6–Cd1–O1W	99.57(13)	O1W–Cd1–O7	77.90(14)
N2–Cd1–N6	99.89(12)	N2–Cd1–O7	84.04(12)
N5 <sup>i</sup> –Cd1–N4	103.84(12)	N6–Cd1–O7	175.26(12)
N4–Cd1–O1W	158.28(12)	N4–Cd1–O7	92.53(14)

Symmetry code: (i)  $-x - \frac{1}{2}, y + \frac{1}{2}, z - \frac{1}{2}$ .

however, the hydrogen atoms of the coordinated water molecule were not located and are not included into the model. The single-crystal structure was finally refined by using the full-matrix least-squares procedure on  $F^2$ . Crystallographic data and structural refinements for the title complex are summarized in Table 1. Selected bond lengths and bond angles for the crystal structure are displayed in Table 2. The hydrogen bonding interactions are presented in Table 3.

### 3. Results and Discussion

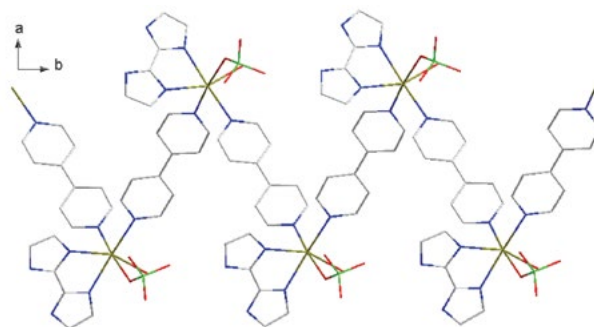
Single-crystal X-ray diffraction measurement revealed that complex **1** crystallizes in the space group  $Pna2_1$  of the orthorhombic system with four formula units in one unit cell and the crystallographically asymmetric unit is comprised of one cadmium ion, one 4,4'-bipy ligand, one 2,2'-biim ligand, one isolated perchlorate anion, one coordinating perchlorate anion and one coordinating water molecule, as presented in Fig. 1. Complex **1** is characterized by a 1-D zigzag chain structure, consisting of  $[\text{Cd}(2,2'\text{-biim})(4,4'\text{-bipy})(\text{H}_2\text{O})(\text{ClO}_4)]_n^{n+}$  cationic chains and isolated  $\text{ClO}_4^-$  anions. The cadmium ion displays a slightly distorted octahedral geometry with the equatorial positions inhabited by three nitrogen atoms from one 2,2'-biim and one 4,4'-bipy ligand as well as one oxygen atom from one coordinating water molecule, and the apical sites are occupied by one oxygen atom from one coordinating perchlorate anion as well as one nitrogen atom from one 4,4'-bipy ligand (Fig. 1).



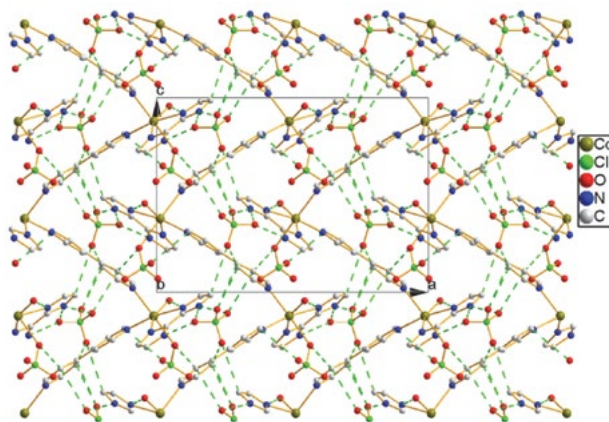
**Figure 1.** An ORTEP diagram of complex **1** with 30% thermal ellipsoids. Hydrogen atoms are omitted for clarity. Symmetry code:  $-x - \frac{1}{2}, y + \frac{1}{2}, z - \frac{1}{2}$ .

The neighboring cadmium ions are interconnected by the 4,4'-bipy ligands through the nitrogen atoms to construct a 1D zigzag chain structure running along the  $b$ -axis, as depicted in Fig. 2. Different from the bridging 4,4'-bipy ligand, the 2,2'-biim molecule acts as a terminal ligand and chelates to one cadmium ion with the chelating angle  $\text{N2}-\text{Cd1}-\text{N4}$  being of  $72.89(11)^\circ$ . In complex **1**, there are two kinds of perchlorate anions, namely, termi-

nally coordinating and isolated. The  $\text{Cd}\cdots\text{Cd}$  distance is  $11.5886(2)$  Å because of the distraction of the long rod-like bridging 4,4'-bipy ligand. The bond lengths of  $\text{Cd}-\text{N}$  are in the range of  $2.290(3)$ – $2.369(4)$  Å with a mean value of  $2.329(4)$  Å. This is in agreement with those found in the literature.<sup>18–20</sup> The bond lengths of  $\text{Cd}-\text{O}$  for water and for perchlorate ligand are  $2.296(3)$  Å and  $2.499(4)$  Å, respectively. This is also comparable with those reported in the literature.<sup>21–24</sup> The bond angle of  $\text{N5}'-\text{Cd1}-\text{N2}$  is  $170.58(14)^\circ$ , close to  $180^\circ$ , while other  $\text{N}-\text{Cd}-\text{N}$  angles locate in a range of  $72.89(11)^\circ$ – $103.84(12)^\circ$ , close to  $90^\circ$ . The bond angles of  $\text{N4}-\text{Cd1}-\text{O1W}$  and  $\text{N6}-\text{Cd1}-\text{O7}$  are  $158.28(12)^\circ$  and  $175.26(12)^\circ$ , respectively, while other  $\text{N}-\text{Cd}-\text{O}$  angles are in a range of  $84.04(12)^\circ$ – $99.57(13)^\circ$ . The bond angle of  $\text{O}-\text{Cd}-\text{O}$  is only  $77.90(14)^\circ$ . The dihedral angle of the pyridyl rings of the 4,4'-bipy ligand is  $14.90(4)^\circ$ . The imidazole rings of the 2,2'-biim ligand is nearly coplanar with a small dihedral angle of  $4.64(2)^\circ$ , which is close to that in another cadmium 2,2'-biim complex ( $3.23^\circ$ ).<sup>25</sup> In complex **1**, there are many hydrogen bonding interactions such as  $\text{N}-\text{H}\cdots\text{O}$  and  $\text{C}-\text{H}\cdots\text{O}$  interactions as listed in Table 3. The 1-D  $[\text{Cd}(2,2'\text{-biim})(4,4'\text{-bipy})(\text{H}_2\text{O})(\text{ClO}_4)]_n^{n+}$  cationic chains and isolated  $\text{ClO}_4^-$  anions are interlinked together through these hydrogen bonding interactions, electrostatic interactions and van der Waals interactions to



**Figure 2.** The 1-D zigzag chain structure of complex **1**.



**Figure 3.** Packing diagram of complex **1** with the dashed lines representing the hydrogen bonding interactions.

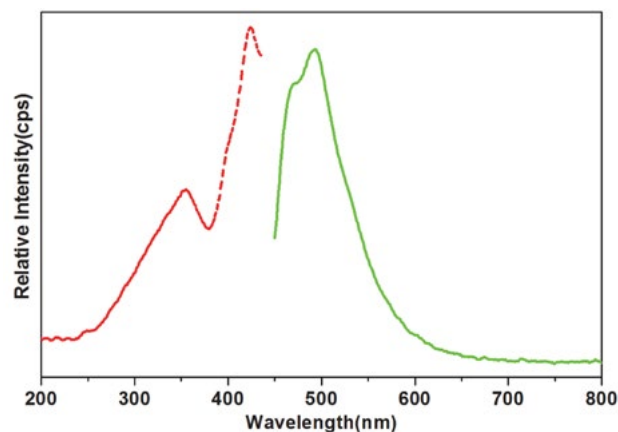
construct a three-dimensional (3-D) supramolecular structure as shown in Fig. 3. To the best of our knowledge, this is the first IIB complex containing both 4,4'-bipy and 2,2'-biim ligands, although a lot of IIB complexes with either 4,4'-bipy or 2,2'-biim as a ligand have been reported thus far.<sup>26–29</sup>

**Table 3.** Hydrogen bonding interactions

<i>D</i> – <i>H</i> ... <i>A</i>	<i>D</i> – <i>H</i> , Å	<i>H</i> ... <i>A</i> , Å	<i>D</i> ... <i>A</i> , Å	<i>D</i> – <i>H</i> ... <i>A</i> , °
N1–H1B...O2 <sup>ii</sup>	0.86	2.38	3.169(6)	153
N1–H1B...O3 <sup>ii</sup>	0.86	2.31	3.058(5)	146
N3–H3A...O2 <sup>ii</sup>	0.86	2.07	2.905(5)	162
C8–H8A...O7 <sup>ii</sup>	0.93	2.54	3.328(6)	142
C10–H10A...O4 <sup>iii</sup>	0.93	2.57	3.298(6)	136

Symmetric codes: (ii)  $-x, -y, \frac{1}{2} + z$ ; (iii)  $x, y, 1 + z$ .

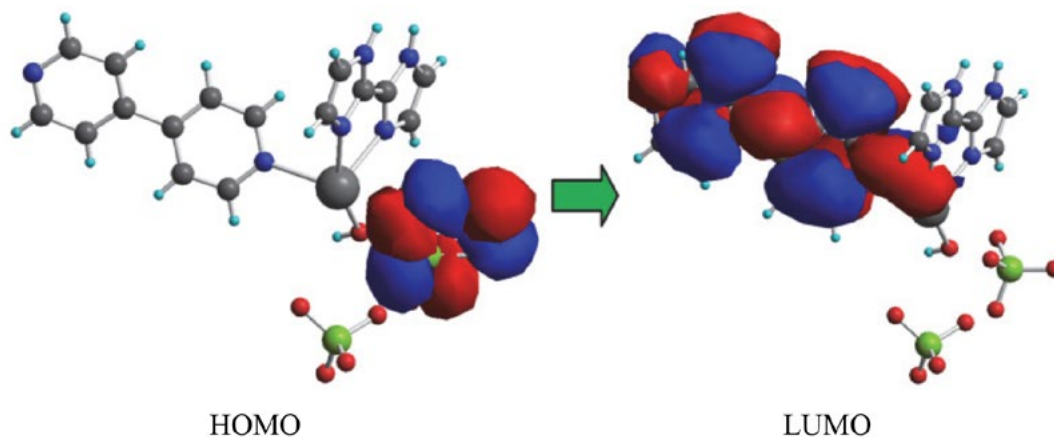
In general, cadmium compounds can exhibit attractive photoluminescent properties and, therefore, they have potential application in the areas of light-emitting diodes, electrochemical displays, photoluminescent materials, sensors.<sup>30,31</sup> Moreover, complexes containing 4,4'-bipy or 2,2'-biim ligands can generally also show good photoluminescence due to the existence of their delocalized  $\pi$  electrons. As a result, the title complex is expected to possess photoluminescent behavior. Based on these considerations, in the present work, we measured the photoluminescent properties of complex **1** using powder-like samples under room temperature. Fig. 4 gives the photoluminescent excitation and emission spectra of complex **1**. As displayed in this figure, the photoluminescent emission spectra of complex **1** show a wide and intensive emission peak, while the photoluminescent excitation spectra show that the effective energy absorption mainly resides in the wavelength span of 250–430 nm. The photoluminescent excitation spectra display a main peak at 424 nm and a shoulder at 355 nm. When it was ex-



**Figure 4.** Photoluminescence spectra of **1** with the red and green lines representing excitation and emission spectra, respectively.

cited by the wavelength of 424 nm, the photoluminescent emission spectra yield a strong emission peak at 493 nm in the green region of the spectrum. As a result, complex **1** could be a candidate material for green photoluminescence.

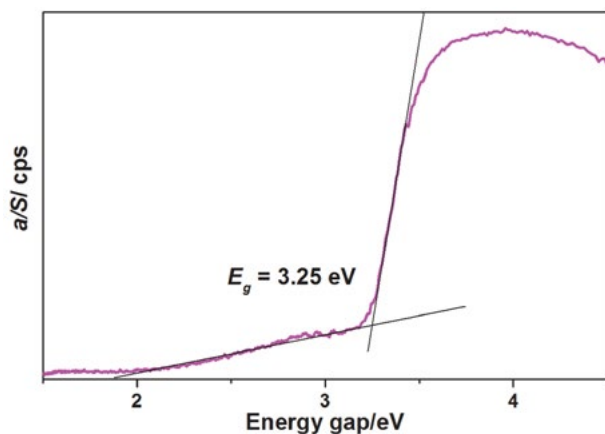
Trying to unveil the nature of the photoluminescence spectra of complex **1**, we truncated ground state geometry from its single-crystal X-ray diffraction data set and carried out its theoretical calculation in light of the time-dependent density functional theory (TDDFT) based on this ground state geometry. The TDDFT investigation was performed with the B3LYP function and by virtue of the Gaussian03 software package. After successfully calculating, the theoretical electron-distribution diagrams were obtained using the ChemOffice Ultra 7.0 graphics program and the results are given in Fig. 5. It is easy to find out that the electron-density distribution of the singlet state of HOMO is totally resided at the coordinating perchlorate anion with an energy being of  $-0.213039$  Hartrees; however, the electron-density population of the singlet state of the LUMO locates at the 4,4'-bipy ligand and the energy of



**Figure 5.** The electron-density population of complex **1**. The isosurfaces correspond to the electronic density differences of  $-10 e \text{ nm}^{-3}$  (blue) and  $+10 e \text{ nm}^{-3}$  (red).

the LUMO is calculated to be  $-0.122838$  Hartrees. The energy difference between LUMO and HOMO is  $0.090201$  Hartrees that is small enough to allow the charge transfer from HOMO to LUMO. Based on these observations, it is proposed that the essence of the photoluminescence of complex **1** could be assigned to the ligand-to-ligand charge transfer (LLCT; from the HOMO of the perchlorate anion to the LUMO of the 4,4'-bipy ligand).

Cadmium compounds are well-known not only for their photoluminescent behaviors but also for their semiconductive properties and the latter enable them to be widely applied in military or civil areas. For example, Hg-CdTe, known as MCT, is one of the most famous military infrared detectors based on the semiconductive properties. Therefore, it could be worthy to measure the semiconductive properties of the title complex. Powder-like barium sulfate acts as a reference for 100% reflectance and finely-ground powder sample was coated on the surface of the barium sulfate. After measuring the solid-state UV/vis diffuse reflectance spectra, the data was treated carefully with the Kubelka-Munk function which is known as  $\alpha/S = (1 - R)^2/2R$ . With regard to this function,  $\alpha$  means the absorption coefficient,  $S$  refers to the scattering coefficient which is actually wavelength independent when the size of the particle is larger than  $5 \mu\text{m}$ , and the  $R$  is related to the reflectance. From the  $\alpha/S$  vs. energy gap diagram, the value of the optical band gap could be determined *via* extrapolating the linear portion of the absorption edges. In this way, the solid-state UV/vis diffuse reflectance spectra showed that complex **1** has a wide energy band gap of  $3.25 \text{ eV}$ , as depicted in Fig. 6. As a result, complex **1** could be a possible candidate for the wide optical band gap semiconductors. The slow slope of the optical absorption edge of complex **1** suggests that it must be an indirect transition.<sup>32</sup> The energy band gap of  $3.25 \text{ eV}$  of complex **1** is obviously larger than those of  $\text{CuInS}_2$  ( $1.55 \text{ eV}$ ),  $\text{CdTe}$  ( $1.5 \text{ eV}$ ) and  $\text{GaAs}$  ( $1.4 \text{ eV}$ ), all of them are broadly applied as efficient photovoltaic materials.<sup>33,34</sup>



**Figure 6.** Solid-state UV/vis diffuse reflectance spectrum for complex **1**.

## 4. Conclusions

In conclusion, a novel cadmium complex with mixed ligands has been synthesized and characterized by single-crystal X-ray diffraction. It exhibits a 1-D zigzag chain structure. It is the first cadmium complex with both 4,4'-bipy and 2,2'-biim ligands. Powder photoluminescent characterization reveals that it displays an emission in the green region. TDDFT calculation revealed that the nature of the photoluminescence is originated from the ligand-to-ligand charge transfer (LLCT; from the HOMO of the perchlorate anions to the LUMO of the 4,4'-bipy ligand). A wide optical band gap of  $3.25 \text{ eV}$  was determined by the solid-state UV/vis diffuse reflectance spectrum.

## 5. Acknowledgements

We gratefully acknowledge the financial support of the NSF of China (21361013, 21362015, 21461013, 51363009), Jiangxi Provincial Science and Technology Support Key Project (20152ACG70021), Jiangxi Provincial Natural Science Foundation (20142BAB205062, 20133ACB20010, 20132BAB203010), Jiangxi Provincial Department of Education's Item of Science and Technology (GJJ150761, GJJ14557, GJJ160745), Jingtangshan University Natural Science Item (JZ0813), the open foundation (ST201522007) of the Key Laboratory of Jiangxi Province for Persistent Pollutants Control and Resources Recycle (Nanchang Hangkong University), and the open foundation (20150019) of the State Key Laboratory of Structural Chemistry, Fujian Institute of Research on the Structure of Matter, Chinese Academy of Sciences.

## 6. Supplementary Material

Crystallographic data for the structure reported in this paper have been deposited with the Cambridge Crystallographic Data Centre as supplementary publication no. CCDC 1569870. Copies of the data can be obtained free of charge on application to CCDC, 12 Union Road, Cambridge CB2 1EZ, UK (fax: (44) 1223 336-033; e-mail: deposit@ccdc.cam.ac.uk).

## 7. References

1. Y.-M. So, W.-H. Leung, *Coord. Chem. Rev.* **2017**, *340*, 172–197. DOI:10.1016/j.ccr.2016.12.009
2. C. C. Mokhtarzadeh, C. E. Moore, A. L. Rheingold, J. S. Figueroa, *Angew. Chem. Int. Ed.* **2017**, *56*, 10894–10899. DOI:10.1002/anie.201705877
3. M. Hoarau, C. Hureau, E. Gras, P. Faller, *Coord. Chem. Rev.* **2016**, *308*, 445–459. DOI:10.1016/j.ccr.2015.05.011
4. P. Zhang, J. M. Suárez, T. Driant, E. Derat, Y. Zhang, M.



- Ménand, S. Roland, M. Sollogoub, *Angew. Chem. Int. Ed.* **2017**, *56*, 10821–10825. DOI:10.1002/anie.201705303
5. A. J. Howarth, M. B. Majewski, M. O. Wolf, *Coord. Chem. Rev.* **2015**, *282–283*, 139–149. DOI:10.1016/j.ccr.2014.03.024
  6. X.-X. Lu, Y.-H. Luo, C. Lu, X. Chen, H. Zhang, *J. Solid State Chem.* **2015**, *232*, 123–130. DOI:10.1016/j.jssc.2015.09.017
  7. X.-F. Yang, M. Liu, H.-B. Zhu, *Inorg. Chem. Commun.* **2017**, *83*, 40–43. DOI:10.1016/j.inoche.2017.06.007
  8. D. P. Malenov, G. V. Janjić, V. B. Medaković, M. B. Hall, S. D. Zarić, *Coord. Chem. Rev.* **2017**, *345*, 318–341. DOI:10.1016/j.ccr.2016.12.020
  9. P. Masłewski, K. Kazimierzczuk, Z. Hnatejko, A. Dołęga, *Inorg. Chim. Acta* **2017**, *459*, 22–28. DOI:10.1016/j.ica.2017.01.014
  10. M.-L. Wei, J.-H. Wang, Y.-X. Wang, *J. Solid State Chem.* **2013**, *198*, 323–329. DOI:10.1016/j.jssc.2012.10.025
  11. M. Zhu, M.-T. Li, L. Zhao, K.-Z. Shao, Z.-M. Su, *Inorg. Chem. Commun.* **2017**, *79*, 69–73. DOI:10.1016/j.inoche.2017.03.020
  12. W.-T. Chen, J.-G. Huang, X.-G. Yi, *Acta Chim. Slov.* **2016**, *63*, 899–904. DOI:10.17344/acsi.2016.2897
  13. L. N. Wang, L. Fu, J. W. Zhu, Y. Xu, M. Zhang, Q. You, P. Wang, J. Qin, *Acta Chim. Slov.* **2017**, *64*, 202–207. DOI:10.17344/acsi.2016.3109
  14. H. S. Mansur, A. A. P. Mansur, A. Soriano-Araújo, Z. I. P. Lobato, *Green Chem.* **2015**, *17*, 1820–1830. DOI:10.1039/C4GC02072C
  15. A. R. D. Voet, H. Noguchi, C. Addy, K. Y. J. Zhang, J. R. H. Tame, *Angew. Chem. Int. Ed.* **2015**, *54*, 9857–9860. DOI:10.1002/anie.201503575
  16. Rigaku, CrystalClear Version 1.3.5, Rigaku Corporation, **2002**.
  17. Siemens, SHELXTL™ Version 5 Reference Manual, Siemens Energy & Automation Inc., Madison, Wisconsin, USA, **1994**.
  18. P. Peng, F.-F. Li, V. S. P. K. Neti, A. J. Metta-Magana, L. Eche-goyen, *Angew. Chem. Int. Ed.* **2014**, *53*, 160–163. DOI:10.1002/anie.201306761
  19. S. Konar, A. Jana, K. Das, S. Ray, J. A. Golen, A. L. Rheingold, S. K. Kar, *Inorg. Chim. Acta* **2013**, *397*, 144–151. DOI:10.1016/j.ica.2012.12.003
  20. J. Jin, X. Han, Q. Meng, D. Li, Y.-X. Chi, S.-Y. Niu, *J. Solid State Chem.* **2013**, *197*, 92–102. DOI:10.1016/j.jssc.2012.09.016
  21. M. Hakimi, Z. Mardani, K. Moeni, F. Mohr, M. A. Fernandes, *Polyhedron* **2014**, *67*, 27–35. DOI:10.1016/j.poly.2013.08.065
  22. J. A. Wilson, P. E. Kraft, R. L. LaDuca, *Inorg. Chim. Acta* **2013**, *404*, 97–104. DOI:10.1016/j.ica.2013.04.027
  23. P.-W. Liu, C.-P. Li, Y. Bi, J. Chen, *J. Coord. Chem.* **2013**, *66*, 2012–2022. DOI:10.1080/00958972.2013.797078
  24. Y.-Y. Liu, J. Liu, J. Yang, B. Liu, J.-F. Ma, *Inorg. Chim. Acta* **2013**, *403*, 85–96. DOI:10.1016/j.ica.2013.03.009
  25. X.-F. Wang, X.-Y. Yu, J.-K. Hu, H. Zhang, *J. Coord. Chem.* **2013**, *66*, 2118–2128. DOI:10.1080/00958972.2013.798654
  26. X. Zhao, F. Liu, L. Zhang, D. Sun, R. Wang, Z. Ju, D. Yuan, D. Sun, *Chem. Eur. J.* **2014**, *20*, 649–652. DOI:10.1002/chem.201304146
  27. S.-N. Zhao, S.-Q. Su, X.-Z. Song, M. Zhu, Z.-M. Hao, X. Meng, S.-Y. Song, H.-J. Zhang, *Cryst. Growth Des.* **2013**, *13*, 2756–2765. DOI:10.1021/cg3018387
  28. W. Xu, J. Jiang, M. Pan, C. Su, *Inorg. Chem. Commun.* **2013**, *31*, 83–86. DOI:10.1016/j.inoche.2013.02.018
  29. X. Zhang, G. Ma, F. Kong, Z. Yu, R. Wang, *Inorg. Chem. Commun.* **2012**, *22*, 44–47. DOI:10.1016/j.inoche.2012.05.020
  30. S. S. M. Rodrigues, D. S. M. Ribeiro, J. X. Soares, M. L. C. Passos, M. L. M. F. S. Saraiva, J. L. M. Santos, *Coord. Chem. Rev.* **2017**, *330*, 127–143. DOI:10.1016/j.ccr.2016.10.001
  31. V. Kumar, K.-H. Kim, P. Kumar, B.-H. Jeon, J.-C. Kim, *Coord. Chem. Rev.* **2017**, *342*, 80–105. DOI:10.1016/j.ccr.2017.04.006
  32. F. Q. Huang, K. Mitchell, J. A. Ibers, *Inorg. Chem.* **2001**, *40*, 5123–5126. DOI:10.1021/ic0104353
  33. P. Dürichen, W. Bensch, *Eur. J. Solid State Inorg. Chem.* **1997**, *34*, 1187–1198.
  34. R. Tillinski, C. Rumpf, C. Näther, P. Duerichen, I. Jess, S. A. Schunk, W. Bensch, *Z. Anorg. Allg. Chem.* **1998**, *624*, 1285–1290. DOI:10.1002/(SICI)1521-3749(199808)624:8<1285::AID-ZAAC1285>3.0.CO;2-5

## Povzetek

S hidrotermalno reakcijo smo sintetizirali nov kadmijev kompleks z različnimi ligandi,  $\{[\text{Cd}(2,2'\text{-biim})(4,4'\text{-bipy})(\text{H}_2\text{O})(\text{ClO}_4)](\text{ClO}_4)\}_n$  (**1**) ( $2,2'\text{-biim} = 2,2'\text{-biimidazol}$ ;  $4,4'\text{-bipy} = 4,4'\text{-bipiridin}$ ), ter določili kristalno strukturo z monokristalno rentgensko difrakcijo. Rentgenska strukturna analiza razkriva, da kompleks **1** kristalizira v prostorski skupini  $Pna2_1$  ortorombskega kristalnega sistema z enodimenzionalnimi cikcak  $[\text{Cd}(2,2'\text{-biim})(4,4'\text{-bipy})(\text{H}_2\text{O})(\text{ClO}_4)]_n^{n+}$  kationskimi verigami in izoliranimi  $\text{ClO}_4^-$  anioni. Analiza fotoluminiscenčnih lastnosti prahu kaže, da kompleks **1** emitira zeleno svetlobo. Izračuni na podlagi teorije časovno odvisnega gostotnostnega funkcionala (TDDFT) kažejo, da je vzrok za pojav fotoluminiscence v kompleksu **1** v prenosu naboja z liganda na ligand (LLCT; od HOMO perkloratnega aniona k LUMO  $4,4'\text{-bipy}$  liganda). S pomočjo UV/Vis difuzne reflektance v trdnem stanju je bil ugotovljen širok prepovedani pas velikosti 3.25 eV.

Short communication

# Geographical Origin Characterization of Slovenian Organic Garlic Using Stable Isotope and Elemental Composition Analyses

Anja Mahne Opatić,<sup>1,2</sup> Marijan Nečemer,<sup>4</sup> David Kocman<sup>1</sup> and Sonja Lojen<sup>1,3</sup><sup>1</sup> Department of Environmental Sciences, "Jožef Stefan" Institute, Jamova cesta 39, Ljubljana, Slovenia<sup>2</sup> Jožef Stefan International Postgraduate School, Jamova cesta 39, Ljubljana, Slovenia<sup>3</sup> Faculty of Environmental Science, University of Nova Gorica, Vipavska 13, Nova Gorica, Slovenia<sup>4</sup> Department of Low and Medium Energy Physics, "Jožef Stefan" Institute, Jamova cesta 39, Ljubljana, Slovenia

\* Corresponding author: E-mail: anja.mahne00@gmail.com

Tel: +038631873994

Received: 25-04-2017

## Abstract

In the present research, the applicability of stable isotope ( $\delta^{13}\text{C}$ ,  $\delta^{15}\text{N}$ ,  $\delta^{34}\text{S}$ ,  $\delta^{18}\text{O}$ ) and multi-element (P, S, Cl, K, Ca, Zn, Br, Rb, Sr) data for determining the geographical origin of garlic (*Allium sativum* L.) at the scale of Slovenia was examined. Slovenia is a rather small country (20273 km<sup>2</sup>) with significant geological and biological diversity. Garlic, valued for its medicinal properties, was collected from Slovenian farms with certified organic production and analyzed by elemental analyzer isotope ratio mass spectrometry combined with energy dispersive X-ray fluorescence spectrometry. Multivariate discriminant analysis (DA) revealed a distinction between four Slovenian macro-regions: the Alpine, Dinaric, Mediterranean and Pannonian. The model was validated through a leave-10%, 20% and 25% out cross validation. The overall success rate of correctly reclassified samples was 77% (on average), indicating that the model and the proposed methodology could be a promising tool for rapid, inexpensive and robust screening to control the provenance of garlic samples.

**Keywords:** Food traceability, Garlic, Geographical origin, Stable isotopes, Elemental composition, Slovenia

## 1. Introduction

Garlic (*Allium sativum* L.), a bulb vegetable widely used in global cuisine, is one of the most investigated food products. It contains approximately 65% water, 28% carbohydrates, 2% proteins, 1.2% free amino acids and 1.5% fiber. A further 2.3% is comprised of organosulfur compounds, which give garlic its characteristic pungent taste and flavor. These compounds are strongly related to garlic's beneficial effects on health,<sup>1</sup> exhibiting antioxidant, antimicrobial, anticarcinogenic and antimutagenic activities as well as containing protective medicinal properties against cardiovascular and respiratory diseases.<sup>1,2</sup>

In recent years, proof of provenance has played an increasingly significant role in food safety and quality surveillance programmes. It also affects consumers' rights in accordance with national legislation, international standards and guidelines. Thus, geographical origin determi-

nation has become another fundamental factor used for evaluating the quality of a product.<sup>3</sup> In Slovenia, the quality of garlic is currently defined by the Rules on the Quality of Vegetables.<sup>4</sup> At larger scale, in Europe, Commission Regulation (EC) No. 2288/97 lays down the marketing standards for garlic.<sup>5</sup> These rules concern the visual appearance of vegetables (size, shape, firmness, cleanliness etc...), packaging and labeling, including the declaration of origin of produce. Nevertheless, rapid, reliable, robust and inexpensive screening methods are still necessary in order to ensure the geographical authenticity and traceability of food products and in addition, the main goal of research in this field has been lately focused on defining the parameters and providing appropriate analytical tools. One of the important techniques, where the scope of geographical assignment of food products can be remarkably extended, relies on a combination of isotopic and elemen-

tal fingerprinting. An important prerequisite is the availability of suitable databases, based on a large number of authentic samples. Moreover, basic knowledge on stable isotope fractionation effects in nature also needs to be increased.<sup>6</sup> For garlic, no databank for tracing its origin at national, continental or global scale has been set up yet, in spite of global utilization of garlic as a condiment in cuisine or for medicinal purposes.<sup>7</sup>

Many authors have attempted to determine the geographical origin of different cereal grains,<sup>8–11</sup> Chinese teas<sup>12</sup> and honey<sup>13</sup> using only stable isotopes of light elements. Samples classification into groups according their geographical origin was relatively successful, indicating that better classification could be achieved by applying not only stable isotope ratios of one or two light elements, but by using multielement stable isotope ratio data. Moreover, the use of stable isotope data in combination with multi-elemental analysis can provide even better discrimination in the case of apple juices,<sup>14</sup> teas,<sup>15</sup> tomatoes,<sup>16</sup> wines<sup>17</sup> and honey.<sup>18</sup> In spite of this, a combination of multielement stable isotopes and multi-element fingerprinting has been rarely used, especially for tracing the geographical origin of vegetables. There has been scarce research on determining the geographical origin of garlic. Smith (2005)<sup>19</sup> proposed trace metal profiling using high-resolution inductively coupled plasma mass spectrometry in order to determine the country of origin of garlic, whilst to authors' very best knowledge there appears to be very little literature data published applying stable isotope ratios or their combination with elemental composition data, e.g. Feher et al., (2017).<sup>20</sup>

The popularity of garlic in Slovenia is increasing extremely. According to the Statistical office of Republic of Slovenia total production of garlic in Slovenia in 2015 was

980 t, hereof 478 t for market production.<sup>21</sup> This was 3 times higher for total production and 35–40 times higher for market production in comparison to 10 years ago. In ten years (*i.e.*, 2005–2015) the garlic import from other countries has decreased for around 20%, and amounted to 1296 t in 2015.<sup>22</sup> Slovenia is a small country (20273 km<sup>2</sup>) characterized by rich geological, climatological and biological diversity. It is situated between the Alps, the Dinaric Mountains, the Pannonian Basin and the Mediterranean Sea, making it ideal for this study. Our primary aim was to examine the possibility of using stable isotope ratio, multielement analyses, and chemometry (specifically, multivariate discriminant analysis (DA)) for characterizing and classifying organically grown Slovenian garlic according to the geographical macro-region in which it was cultivated (Alpine, Dinaric, Pannonian, or Mediterranean). The data gathering at the scale of Slovenia has commenced within the framework of the project "ISO-FOOD- ERA chair for isotope techniques in food quality, safety and traceability" funded by the EU. Furthermore, it is also expected that our findings will initiate the creation of a national database as the proposed methodology could be a promising tool for fast and cheap screening purposes which would allow for seamless implementation into existing food regulations and trade agreements.

## 2. Materials and Methods

### 2.1. Sampling

Samples were collected in autumn 2014 and 2015 from several Slovenian certified organic farms in order to ensure authenticity, traceability and equivalent production regimes. In total, 38 samples of garlic from four different Slovenian macro-regions (Fig. 1) were obtained.

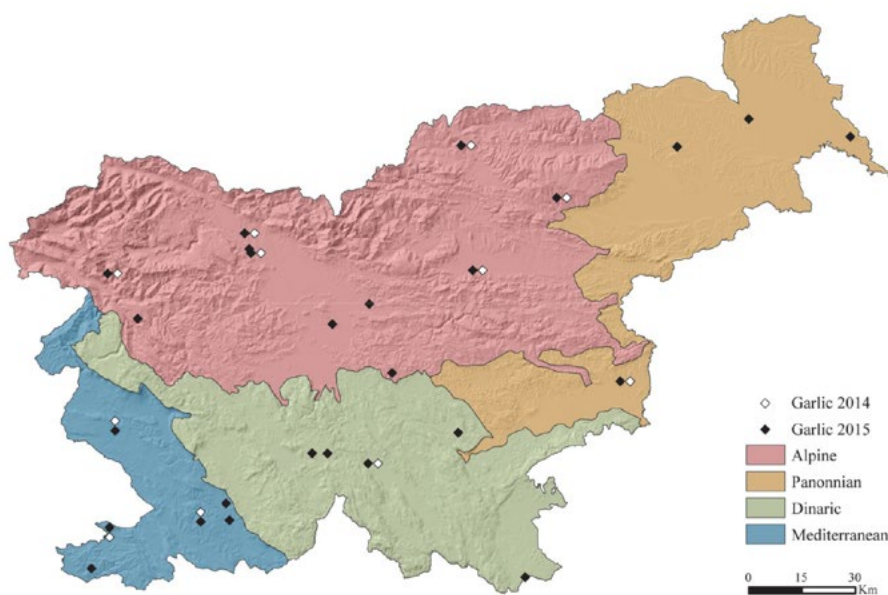


Fig. 1. Regionalization of Slovenia into four macro-regions<sup>23</sup> with sampling sites and years of garlic samples

## 2. 2. Stable Isotope Analysis

Samples for simultaneous carbon, nitrogen and sulfur isotope ratio analysis were dried to constant weight in an oven at 60 °C. The dried samples were then homogenized and ground to a fine powder using a mortar. A known weight (10 mg) of garlic powder was folded and compressed in a tin capsule and introduced into the autosampler. Analysis was carried out using an Elemental vario PYRO cube elemental analyser (OH/CNS Pyrolyser/Elemental Analyser) linked to an IsoPrime100 continuous flow isotope ratio mass spectrometer (IsoPrime, Cheadle, Hulme, UK). Each sample was analyzed in three repetitions. The difference between the replicates for any of the elements did not exceed 0.2‰.

For oxygen stable isotope analysis, liquid samples were obtained by squeezing fresh garlic through a gauze. Isotopic ratios were then measured after equilibration (40 °C, 6h) with 5% CO<sub>2</sub>+ He mixture. Analysis was performed using an IsoPrime100 isotope ratio mass spectrometer and MultiFlow preparation system (IsoPrime, Cheadle, UK) according to the ENV 12141:1996.<sup>24</sup>

The stable isotope compositions are reported according to the IUPAC guidelines<sup>25,26</sup> as relative differences in the isotope ratios (isotope-delta values), as seen in Equation (1)<sup>25</sup>:

$$\delta^{i/j}E = \frac{{}^{i/j}R_p - {}^{i/j}R_{Ref}}{{}^{i/j}R_{Ref}} \quad (1)$$

The superscripts *i* and *j* denote the higher and lower atomic masses of the analysed element E, and *R<sub>p</sub>* and *R<sub>Ref</sub>* denote the heavy-to-light isotope ratios of the element E in the analysed sample and the reported reference material, respectively. A short-hand notation for elements with only two relevant stable isotopes is used in the text, i.e., δ<sup>13</sup>C, δ<sup>15</sup>N, and the δ<sup>34</sup>S; the δ values are expressed in per mil (‰) relative to standards. The δ<sup>13</sup>C values are expressed relative to VPDB (Vienna Peedee belemnite) on a scale normalized by assigning consensus values of -46.6‰ to L-SVEC lithium carbonate and +1.95‰ to NBS 19 calcium carbonate. The δ<sup>18</sup>O values of water are expressed relative to the VSMOW2 (Vienna Standard Mean Ocean Water 2), δ<sup>34</sup>S relative to the VCDT (Vienna Canyon Diablo Troilite), and δ<sup>15</sup>N relative to Air (atmospheric N<sub>2</sub>). By definition, the δ value of the reporting standards is 0‰.

For δ<sup>13</sup>C and δ<sup>15</sup>N measurements, working standards were used, calibrated versus USGS40 (L-glutamic acid; certified δ<sup>13</sup>C<sub>VPDB</sub> value -26.39 ± 0.04‰; recommended δ<sup>15</sup>N value -4.5 ± 0.1‰), USGS41 (L-glutamic acid; certified δ<sup>13</sup>C<sub>VPDB</sub> value +37.63 ± 0.05‰; recommended δ<sup>15</sup>N<sub>Air</sub> value +47.6 ± 0.2‰), IAEA-CH-6 (sucrose with certified δ<sup>13</sup>C value -10.45 ± 0.03‰), IAEA-N-1 (ammonium sulfate with certified δ<sup>15</sup>N<sub>Air</sub> value +0.4 ± 0.2‰) international reference materials, and IAEA-SO-5 (barium sulfate with recommended δ<sup>34</sup>S +0.5 ± 0.2‰) reference material for sulfur. The accuracies of the δ<sup>13</sup>C, δ<sup>15</sup>N, and δ<sup>34</sup>S

analyses were monitored with commercially available isotope standards (Sercon) with recommended δ<sup>13</sup>C and δ<sup>15</sup>N values, and informative δ<sup>34</sup>S values: Wheat Flour Standard Organic Analytical Standard (OAS; -27.21 ± 0.13‰; +2.85 ± 0.17‰; -1.42 ± 0.80‰ for δ<sup>13</sup>C, δ<sup>15</sup>N and δ<sup>34</sup>S, respectively), Sorghum Flour Standard OAS (-13.68 ± 0.19‰; +1.58 ± 0.15‰; +10.11 ± 1.00‰) and Protein (Casein) Standard OAS (-26.98 ± 0.13‰; +5.94 ± 0.08‰; +6.32 ± 0.80‰). All these values were certified by the Elemental Microanalysis Ltd.

The measured δ<sup>18</sup>O values were recalculated using the in-house reference materials (distilled seawater with δ<sup>18</sup>O value +0.34 ± 0.07‰, MilliQ water with δ<sup>18</sup>O value -9.12 ± 0.07‰ and snow with δ<sup>18</sup>O value -19.73 ± 0.09‰). All these working standards were calibrated vs. the IAEA international reference material VSMOW2 with recommended δ<sup>18</sup>O<sub>VSMOW</sub> value 0 ± 0.02‰ and Greenland Ice-Sheet Precipitation (GISP; certified δ<sup>18</sup>O<sub>VSMOW</sub> -24.76 ± 0.09‰). Reproducibility of the measurements was ± 0.1‰ for δ<sup>18</sup>O, ± 0.2‰ for δ<sup>13</sup>C and ± 0.3‰ for δ<sup>15</sup>N and δ<sup>34</sup>S.

## 2. 3. Elemental Analysis

Multielement determination of macro (P, S, Cl, K, Ca) and micro elemental (Zn, Br, Rb, Sr) content was performed in single measurement using non-destructive energy dispersive X-ray fluorescence spectrometry. Pellets were prepared from 0.5 to 1.0 g of powdered sample material using a pellet die and hydraulic press. For excitation, the disc radioisotope excitation source of Fe-55 (25 mCi) and Cd-109 (20 mCi) from Eckert and Ziegler were used. The emitted fluorescence radiation was measured using an energy dispersive X-ray fluorescence spectrometer consisting of a Si(Li) detector (Canberra), a spectroscopy amplifier (Canberra M2024), analogue-to-digital converter (Canberra M8075) and PC-based multichannel analyser (S-100 Canberra). The spectrometer was equipped with a vacuum chamber (Fe-55) for measuring light elements P-Cl. The energy resolution of the spectrometer was 175 eV at 5.9 keV. The complex X-ray spectra were analyzed using AXIL spectral analysis software. Quantification was then performed utilizing the Quantitative Analysis of Environmental Samples (QAES) software, developed in our laboratory.<sup>27,28</sup> The estimated analysis uncertainty was 5% to 10%. The accuracy of the data was checked using the National Institute of Standards and Technology 1573a reference material (tomato leaves).

## 2. 4. Statistical Analysis

Statistical calculations were carried out using the XL-STAT software package (Addinsoft, New York, USA). Simple statistics included analysis of variance by ANOVA with Duncan's tests for comparison of means for normally distributed data, and Kruskal-Wallis one-way analysis of

variance by ranks (Kruskal–Wallis test) for not normally distributed data in order to reveal statistically significant differences, whilst multivariate DA was used for determination of key factors responsible for discrimination of four Slovenian geographical macro-regions.

### 3. Results and Discussion

#### 3.1. Garlic

In Table 1 means and standard deviations of the stable isotope and elemental composition of the 38 garlic samples according to their given macro-region origin are reported, whilst Table 2 gives means, standard deviations and ranges (minimum- maximum) of the stable isotope and elemental composition of the 38 garlic samples, irrespective of geographical origin. The data of  $\delta^{15}\text{N}$ ,  $\delta^{18}\text{O}$ ,  $\delta^{34}\text{S}$ , P, K and Zn were normally distributed and their variances were homoscedastic, while the data of  $\delta^{13}\text{C}$ , S, Cl, Ca, Br, Rb, Sr and Si were not normally distributed. According to ANOVA test three parameters ( $\delta^{18}\text{O}$ , P, K) were statistically significant ( $p < 0.05$ ) for discriminating between the four Slovenian macro-regions. Additionally, the Kruskal–Wallis test revealed that only  $\delta^{13}\text{C}$  is statistically significant for determining the origin of the garlic samples.

#### 3.2. Stable Isotopes

We emphasize that only statistically significant parameters are described below. In this regard, the *post-hoc* Duncan test revealed that it is possible to differentiate the Mediterranean region from all the other regions on the basis of  $\delta^{18}\text{O}$  values. The lowest  $\delta^{18}\text{O}$  values were measured in garlic samples from the Dinaric region (average  $\delta^{18}\text{O} = -2.6\text{‰}$ ), whilst the highest  $\delta^{18}\text{O}$  values were found in samples from the Mediterranean region (average  $\delta^{18}\text{O} = -0.8\text{‰}$ ). The Alpine and Pannonian regions fell in between with average values of  $\delta^{18}\text{O} = -2.1\text{‰}$  and  $\delta^{18}\text{O} = -1.9\text{‰}$ , respectively. The xylem sap of terrestrial plants reflects the integrated isotopic compositions of the water sources, since the water is absorbed through the root system with no isotopic fractionation during uptake. After that, transpiration through the leaf stomata occurs, leading to enrichment of  $\delta^{18}\text{O}$  in the leaf water.<sup>29</sup> The distribution trends of  $\delta^{18}\text{O}$  values in garlic samples is similar to that observed in Slovenian groundwater,<sup>30</sup> when considering the  $\delta^{18}\text{O}$  content of groundwater in the Mediterranean re-

Table 1. Means and standard deviations (SD) of the stable isotope and elemental composition in Slovenian garlic samples, respective to their macro-region origin

Macro-region*	Isotope ratio (mean $\pm$ SD; ‰)			Element analysis (mean $\pm$ SD)									
	$\delta^{13}\text{C}$	$\delta^{15}\text{N}$	$\delta^{18}\text{O}$	$\delta^{34}\text{S}$	Ca (g/kg)	P (g/kg)	K (g/kg)	Cl (g/kg)	S (g/kg)	Zn (mg/kg)	Br (mg/kg)	Rb (mg/kg)	Sr (mg/kg)
A	-27.1 $\pm$ 0.7	6.4 $\pm$ 2.0	-2.1 $\pm$ 1.0	3.5 $\pm$ 1.4	0.47 $\pm$ 0.19	4.09 $\pm$ 1.11	13.0 $\pm$ 2.8	0.26 $\pm$ 0.18	5.17 $\pm$ 1.86	23.1 $\pm$ 6.4	4.11 $\pm$ 2.26	11.1 $\pm$ 6.2	2.00 $\pm$ 0.71
D	-26.4 $\pm$ 0.3	6.9 $\pm$ 2.7	-2.6 $\pm$ 1.1	4.1 $\pm$ 1.0	0.49 $\pm$ 0.13	3.56 $\pm$ 0.57	11.7 $\pm$ 3.0	0.28 $\pm$ 0.23	4.47 $\pm$ 0.98	26.1 $\pm$ 3.3	2.59 $\pm$ 1.27	8.98 $\pm$ 5.70	1.81 $\pm$ 1.13
M	-26.4 $\pm$ 0.5	6.0 $\pm$ 4.1	-0.8 $\pm$ 1.1	1.5 $\pm$ 3.6	0.58 $\pm$ 0.13	5.13 $\pm$ 1.11	15.7 $\pm$ 3.4	0.51 $\pm$ 0.37	7.13 $\pm$ 2.88	25.2 $\pm$ 7.9	32.0 $\pm$ 1.7	5.68 $\pm$ 2.27	2.16 $\pm$ 0.81
P	-27.5 $\pm$ 0.8	7.5 $\pm$ 0.7	-1.9 $\pm$ 1.2	2.3 $\pm$ 1.1	0.50 $\pm$ 0.13	5.11 $\pm$ 0.74	15.2 $\pm$ 2.4	0.22 $\pm$ 0.10	6.01 $\pm$ 1.31	24.5 $\pm$ 5.1	18.8 $\pm$ 0.4	6.96 $\pm$ 3.77	1.49 $\pm$ 1.15
ANOVA**			0.0142			0.0109							
KW test***	0.0115												

\*A- Alpine (n = 18), D- Dinaric (n = 6), M- Mediterranean (n = 9), P- Pannonian (n = 5) \*\*Different letters (a,b,c) in the same column indicate statistically significant differences ( $p < 0.05$ ; Duncan's test). Only p-values lower than 0.05 are reported. \*\*\*According to KW test only p-values lower than 0.05 are reported.

Table 2. Mean, standard deviation (SD) and the range (min-max) of the stable isotope and elemental composition in Slovenian garlic samples

Macro-region*	Isotope ratio (mean $\pm$ SD; ‰)			Element analysis (mean $\pm$ SD)									
	$\delta^{13}\text{C}$	$\delta^{15}\text{N}$	$\delta^{18}\text{O}$	$\delta^{34}\text{S}$	Ca (g/kg)	P (g/kg)	K (g/kg)	Cl (g/kg)	S (g/kg)	Zn (mg/kg)	Br (mg/kg)	Rb (mg/kg)	Sr (mg/kg)
Mean $\pm$ SD	-26.9 $\pm$ 0.7	6.5 $\pm$ 2.6	1.8 $\pm$ 1.2	3.0 $\pm$ 2.2	0.50 $\pm$ 0.16	4.39 $\pm$ 1.14	13.7 $\pm$ 3.2	0.32 $\pm$ 0.26	5.63 $\pm$ 2.14	24.3 $\pm$ 6.1	3.36 $\pm$ 1.97	8.94 $\pm$ 5.50	1.89 $\pm$ 0.85
Range (Min–Max)	-28.5–(-25.6)	0.1–12.3	-4.1–0.6	-4.0–7.1	0.49–1.07	2.25–6.82	7.2–22.1	0.03–1.29	2.62–13.8	11.7–38.7	1.09–9.69	2.2–21.8	0.79–4.10

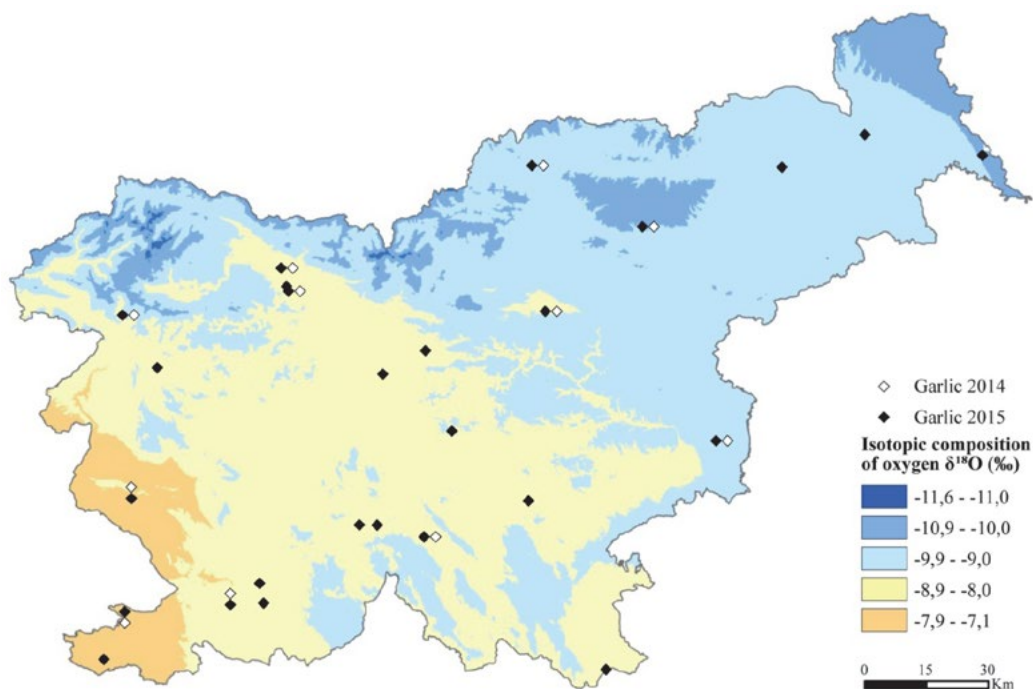


Fig. 2. Assessment of isotopic composition of  $\delta^{18}\text{O}$  in groundwater in Slovenia (multiple linear regression method)<sup>30</sup> and sample sites for garlic samples

gion and in garlic samples from this region (Fig. 2). The lowest values in groundwater were detected in several Alpine areas, which is not in accordance with our results obtained from garlic. Here, it should be taken into account that the distribution of  $\delta^{18}\text{O}$  in precipitation across Slovenia is almost identical to that in groundwater, however, there is no databank for the isotopic composition of precipitation in Slovenia yet. However, our results are in agreement with the literature data,<sup>8,14,31–32</sup> which indicate that the coastal regions have higher  $\delta^{18}\text{O}$  values due to a relatively warm and dry climate (temperature and amount effect, respectively). The factors that most influence the fractionation of  $\delta^{18}\text{O}$  are distance from the sea (continental effect) and altitude and latitude characteristics.<sup>31,32</sup>

### 3. 3. Elements

The elements measured by energy dispersive X-ray fluorescence spectroscopy can be divided into two groups: macro and microelements. In total, 9 elements were determined, 5 macro- (K, P, S, Ca, Cl) and 4 microelements (Zn, Rb, Br, Sr). We emphasize that only the statistically significant parameters are described below and results are depicted as g/kg of dry matter (DM). Based on average values of P, the Mediterranean region (5.13 g/kg) was distinguishable from both the Alpine (4.09 g/kg) and Dinaric regions (3.56 g/kg), but not from the Pannonian (5.11 g/kg). Further, based on the average K values, the Mediterranean region (15.7 g/kg) was found to be statistically different from both the Alpine (13.0 g/kg) and Dinaric (11.7 g/kg) regions, but not from the Pannonian (15.2 g/kg). It was also

not possible to discriminate the Pannonian region from both the Dinaric and Alpine regions.

In order to easier compare the elemental content of Slovenian garlic with literature data, average values can be defined, irrespective to the geographical origin (Table 2). Our results reveal differences in comparison with the literature data. For example, Chekki et al. (2014)<sup>33</sup> reported that concentration of P in Tunisian garlic was 0.14 g/kg, which is lower than in Slovenian garlic (4.39 g/kg), while the opposite is true for Indian (4.60 g/kg) and Turkish (6.01 g/kg) garlic. Contents of K (16.68 g/kg), P (4.78 g/kg), Ca (0.69 g/kg) and Zn (66 mg/kg) in Nigerian garlic were reported by Akinwande and Olatunde (2015).<sup>34</sup> These concentrations are found to be higher than ours. A similar range of concentrations was reported by Gonzálvez A et al. (2008).<sup>35</sup> The present data shows the heterogeneity of the results and the geographical and/or environmental influences on mineral content of garlic, which makes mineral profiling a possible tool for determining the geographical origin of internationally produced garlic.

### 3. 4. Results of Multivariate Discriminant Analysis (DA)

Fig. 3(a) shows discriminant score plots of Slovenian garlic samples in order to verify the possibility to differentiate samples according to the geographical origin using the combination of stable isotope and multi-elemental composition data, while in Fig. 3(b) plot of correlations between initial variables and discriminant factors (F1, F2) is seen. An overlap is observed among garlic samples orig-

inating from both the Alpine and Dinaric geographical regions, whilst samples from both the Pannonian and Mediterranean regions are well separated (Fig. 3a). Overlapping results can occur due to the similar geological characteristics and climate conditions; similar findings of indistinguishable both the Alpine and Dinaric regions were also confirmed by Nečemer et al. (2016)<sup>36</sup> in the case with cow milk. Moreover, the Wilks  $\lambda$  value ranges from 0 to 1, indicating that means of two groups are equal if  $\lambda = 1$ , whereas means are different if  $\lambda = 0$ .<sup>37</sup> In our case, Wilks  $\lambda$  is 0.0289. Further, p-value ( $<0.0001$ ) was lower than the significance level alpha (0.1), which signify that at least one of the means vector is different from another. The discrimination among the garlic samples from the four different macro-regions is distinctly demonstrated along the Function 1 (F1) axis with  $\delta^{13}\text{C}$  (standardized coefficient,  $-0.83$ ),  $\delta^{34}\text{S}$  (0.64), Zn (1.34) and P ( $-1.15$ ). Function 2

(F2) is also linked to the variability within each particular group and the most significant parameters were  $\delta^{13}\text{C}$  ( $-0.80$ ) and  $\delta^{34}\text{S}$  ( $-1.17$ ), P (0.97) and Cl ( $-1.66$ ). Other parameters are less influential. F1 explains 60.48% of the total variance, while F2 accounts for 27.34%. The model was validated through the leave-10%-out cross validation, which gave a success rate of 75%. Additionally, the total prediction ability of leave-20%-out and leave-25%-out was 75% and 80%, respectively. In accordance with the literature data for cereals,<sup>9,10</sup> the results confirm that  $\delta^{13}\text{C}$  is an important parameter for determining geographical origin. The differences in the  $\delta^{13}\text{C}$  values could be attributed to differences in local growth conditions e.g., temperature, relative humidity, drought stress, light intensity, and nutrient availability.<sup>10,38</sup> Conversely,  $\delta^{34}\text{S}$  is rarely used in such investigations, although sulfur isotopes in plants are known to be related to soil geology<sup>13</sup> and are promoted as

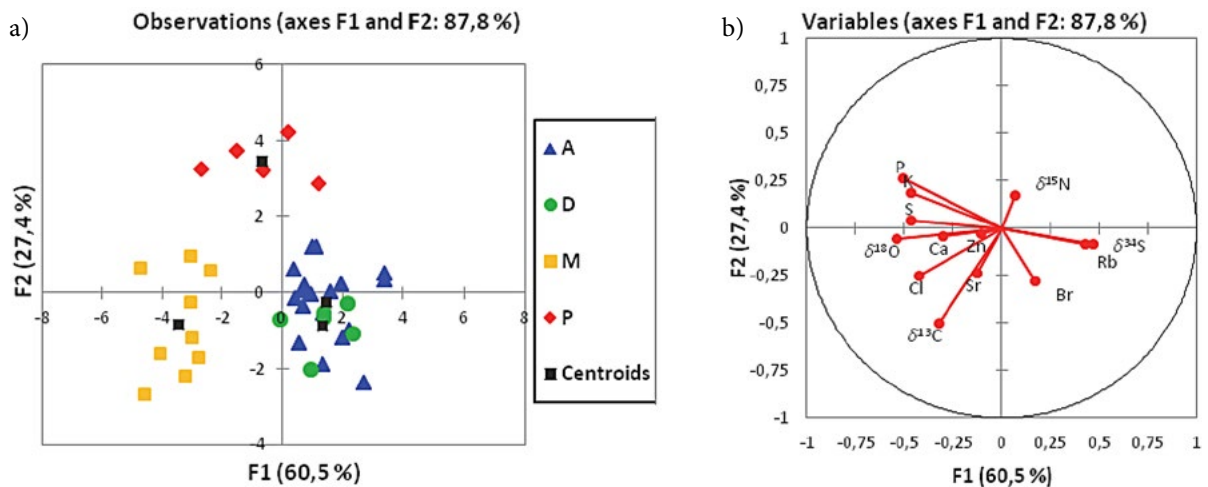


Fig. 3. (a) Discriminant score plots of 38 Slovenian garlic samples from the Alpine (A;  $n = 18$ ), Dinaric (D;  $n = 6$ ), Mediterranean (M;  $n = 9$ ), Pannonian (P;  $n = 5$ ) regions. (b) Plot of correlations between initial variables and discriminant factors (F1, F2)

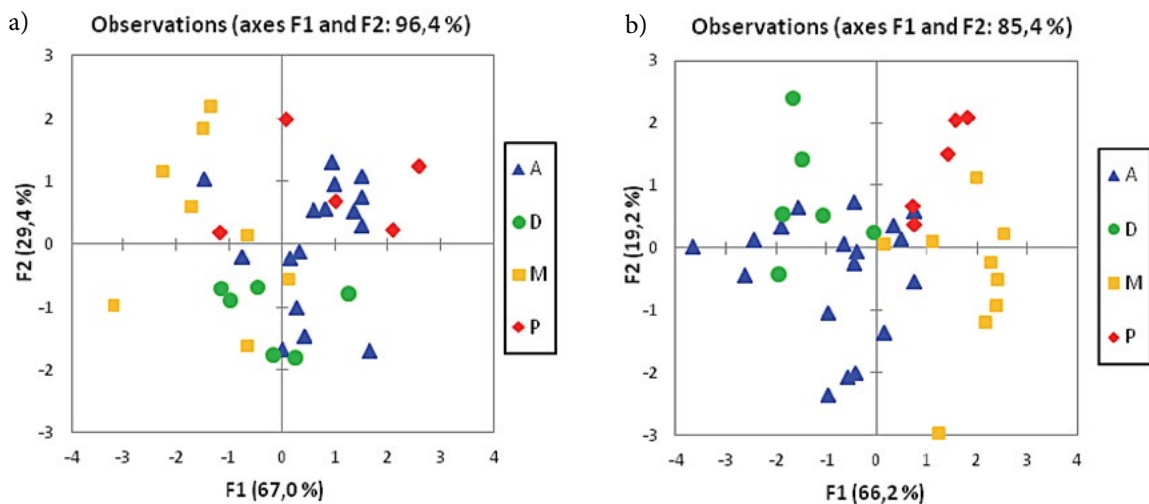


Fig. 4. Discriminant score plots of 38 Slovenian garlic samples from the Alpine (A;  $n = 18$ ), Dinaric (D;  $n = 6$ ), Mediterranean (M;  $n = 9$ ), Pannonian (P;  $n = 5$ ) regions applying (a) stable isotope and (b) elemental parameters

valuable indicators for assigning the origin of plant material.<sup>39</sup> Finally, the elemental fingerprint (especially Zn and P) has an even greater discriminating power than the stable isotope ratios.

Directions and lengths of vectors of initial variables in Fig. 3b indicate that higher mean  $\delta^{13}\text{C}$  values were determined in both the Mediterranean and Dinaric regions compared to the Alpine and Pannonian. Further, the highest mean values of  $\delta^{18}\text{O}$  and contents of K, P, S, Cl and Ca were measured in the Mediterranean region, but the mean Rb and  $\delta^{34}\text{S}$  values were there the lowest. The mean  $\delta^{15}\text{N}$  values were found to be the highest in the garlic samples, originated from the Pannonian region.

Additionally, in order to compare different approaches, stable isotope (Fig. 4a) and multi-elemental (Fig. 4b) data were tested separately. In the case of stable isotope data, the groups were not separated from each other due to overlapping results, while in the case of multi-elemental data the tendency of grouping was noticed. Nonetheless, the groups could not be distinguished according to their macro-regional origin. In first case, the major contributions to separate garlic into groups were  $\delta^{13}\text{C}$  and  $\delta^{18}\text{O}$  in F1 and  $\delta^{13}\text{C}$  and  $\delta^{34}\text{S}$  in F2. Regarding elemental data, garlic differed mostly because of the differences in P and Zn contents in F1, and Zn and Br in F2.

## 4. Conclusions

In conclusion, the stable isotopic compositions of four elements ( $\delta^{13}\text{C}$ ,  $\delta^{15}\text{N}$ ,  $\delta^{34}\text{S}$ ,  $\delta^{18}\text{O}$ ) and elemental composition of nine elements (K, P, S, Ca, Cl, Zn, Br, Rb, Sr) were used to differentiate the geographical origin of organically grown garlic from Slovenian certified farms. The results show a definite tendency towards their respective Slovenian macro-regions, although the slight overlap among some samples is likely due to them having been grown in regions with similar geological and climatic conditions and to the natural variability of the samples. The main parameters that differentiate the origin of the garlic samples were  $\delta^{13}\text{C}$ ,  $\delta^{34}\text{S}$ , Zn, P and Cl. Considering the results obtained, we can conclude that elemental analyser isotope ratio mass spectrometry, when combined with energy dispersive X-ray fluorescence spectrometry, has the potential to be a rapid, simple and powerful method to investigate the origin of a large number of samples. In addition, our preliminary results represented the first model of garlic in Slovenia, regarding the geographical origin of cultivation. Despite these encouraging results, there still remain some limitations and further research based on a larger dataset will be important in establishing databases that are more reliable. The annual differences in the stable isotope ratios and elemental composition of plant materials must also be taken into account, which will mean collecting samples over a number of years. Such expanded databases will require interpretations that are more complex due to the in-

creased number of samples and because of the natural variation in stable isotope ratios and elemental composition.

## 5. Acknowledgements

The authors are very grateful to dr. Peter Kump for kindly providing the QAES (Quantitative Analysis of Environmental Samples) software. Many thanks also to Stojan Žigon for technical support and assistance. This study has received funding from European Union's Seventh Programme for research, technological development and demonstration under grant agreement No. 621329 (ISO-FOOD ERA Chair for isotope techniques in food quality, safety and traceability), Horizon 2020 research and innovation programme under grant agreement No. 692241 (MASSTWIN – Spreading Excellence and widening participation in support of mass spectrometry and related techniques in health, the environment, and food analysis) and the Slovenian Research Agency (research programme P1-0143, Cycling of substances in the environment, mass balances, modelling of environmental processes and risk assessment).

## 6. References

1. S. G. Santhosha, P. Jamuna, S. N. Prabhavathi, *Food Biosci.* **2013**, *3*, 59–74. DOI:10.1016/j.fbio.2013.07.001
2. M. Corzo-Martinez, N. Corzo, M. Villamiel, *Trends Food Sci Technol.* **2007**, *18*, 609–625. DOI:10.1016/j.tifs.2007.07.011
3. Y. Zhao, B. Zhang, G. Chen, *Food Chem.* **2014**, *145*, 300–305. DOI:10.1016/j.foodchem.2013.08.062
4. Rules on the Quality of Vegetables, Official Gazette of the Republic of Slovenia, 86/2000, <https://www.uradni-list.si/glasi-lo-uradni-list-rs/vsebina/2000-01-3815/pravilnik-o-kakovosti-cesna>, (assessed: April 18, 2017)
5. Regulation (EC) No 2288/97, Official Journal L 315, <http://eur-lex.europa.eu/legal-content/EN/TXT/?uri=celex-%3A31997R2288>, (assessed: April 18, 2017)
6. D. M. A. M. Luykx, S.M. van Ruth, *Food Chem.* **2008**, *107*, 897–911. DOI:10.1016/j.foodchem.2007.09.038
7. A. Grégrová, H. Čížková, I. Bulantová, *Czech J Food Sci.* **2013**, *31*, 581–588.
8. M. A. Brescia, G. Di Martino, C. Guillou, F. Reniero, A. Sacco, F. Serra, *Rapid Commun Mass Spectrom.* **2002**, *16*, 2286–2290. DOI:10.1002/rcm.860
9. D. Luo, H. Dong, H. Luo, Y. Xian, J. Wan, X. Guo, Y. Wu, *Food Chem.* **2015**, *174*, 197–201. DOI:10.1016/j.foodchem.2014.11.006
10. Y. Wu, D. Luo, H. Dong, J. Wan, H. Luo, Y. Xian, X. Guo, F. Qin, W. Han, L. Wang, B. Wang, *Food Chem.* **2015**, *174*, 553–557. DOI:10.1016/j.foodchem.2014.11.096
11. Y. Suzuki, Y. Chikaraishi, N.O. Ogawa, *Food Chem.* **2008**, *109*, 470–475. DOI:10.1016/j.foodchem.2007.12.063



12. L. Zhang, J. Pan, C. Zhu, *J Zhejiang Univ.* **2012**, *13*, 824–830. DOI:10.1631/jzus.B1200046
13. A. Schellenberg, S. Chmielus, C. Schlicht, *Food Chem.* **2010**, *121*, 770–777. DOI:10.1016/j.foodchem.2009.12.082
14. K. Bizjak Bat, K. Eler, D. Mazej, B. Mozetič Vodopivec, I. Mulič, P. Kump, N. Ogrinc, *Food Chem.* **2016**, *203*, 86–94. DOI:10.1016/j.foodchem.2016.02.039
15. T. S. Pilgrim, R. J. Watling, K. Grice, *Food Chem.* **2010**, *118*, 921–926. DOI:10.1016/j.foodchem.2008.08.077
16. L. Bontempo, F. Camin F, L. Manzocco, G. Nicolini, R. Wehrens, L. Ziller, R. Larcher, *Rapid Commun Mass Spectrom.* **2011**, *25*, 899–909. DOI:10.1002/rcm.4935
17. S. V. Dutra, L. Adami, A. R. Marcon, *Food Chem.* **2013**, *141*, 2148–2153. DOI:10.1016/j.foodchem.2013.04.106
18. U. Kropf, M. Korošec, J. Bertoneclj, N. Ogrinc, M. Nečemer, P. Kump, T. Golob, *Food Chem.* **2010**, *121*, 839–846. DOI:10.1016/j.foodchem.2009.12.094
19. R. G. Smith, *J Agric Food Chem.* **2005**, *53*, 4041–4045. DOI:10.1021/jf040166+
20. I. Feher, D. A. Magdas, A. Dehelean, G. Cristea, C. Voica, *Rom J Phys.* **2017**, *62*(1-2), 803.
21. Republic of Slovenia, Statistical Office RS, SI- Stat Data Portal, [http://pxweb.stat.si/pxweb/Dialog/varval.asp?lang=2&ma=1502403S&path=../Database/Okolje/15\\_kmetijstvo\\_ribistvo/04\\_rastlinska\\_pridelava/01\\_15024\\_pridelki\\_povrsina/&ti=](http://pxweb.stat.si/pxweb/Dialog/varval.asp?lang=2&ma=1502403S&path=../Database/Okolje/15_kmetijstvo_ribistvo/04_rastlinska_pridelava/01_15024_pridelki_povrsina/&ti=) (assessed: July 18, 2017).
22. Poročilo o stanju kmetijstva, živilstva, gozdarstva in ribištva, Pregled po kmetijskih trgih, [http://www.kis.si/f/docs/Porocila\\_o\\_stanju\\_v\\_kmetijstvu\\_OEK/ZP-2015-trgi-net.pdf](http://www.kis.si/f/docs/Porocila_o_stanju_v_kmetijstvu_OEK/ZP-2015-trgi-net.pdf) (assessed: July 18, 2017).
23. D. Perko, The Regionalization of Slovenia, Geografski inštitut Antona Melika ZRC SAZU, Ljubljana, Slovenija, **2008**, pp. 1–46.
24. SIST ENV 12141:1998 (1998), Fruit and vegetable juices- Determination of the stable oxygen isotope ( $^{18}\text{O}/^{16}\text{O}$ ) of water from fruit juices- Method using isotope ratio mass spectrometry.
25. W. A. Brand, T. B. Coplen, J. Vogl, M. Rosner, T. Prohaska, *Pure and Appl Chem.* **2014**, *86*(3), 425–467. DOI:10.1515/pac-2013-1023
26. T. B. Coplen, Y. Shrestha, *Pure and Appl Chem.* **2016**, *88*(12), 1203–1224. DOI:10.1515/pac-2016-0302
27. M. Nečemer, P. Kump, J. Ščančar, R. Jačimovič, J. Simčič, P. Pelicon, M. Budnar, Z. Jeran, P. Pongrac, M. Regvar, K. Vogel-Mikuš, *Spectrochim Acta, Part B: At Spectrosc.* **2008**, *63*, 1240–1247. DOI:10.1016/j.sab.2008.07.006
28. M. Nečemer M, P. Kump P, Vogel-Mikuš K. in: Golubev IA (Ed.): Use of X-ray fluorescence-based analytical techniques in phytoremediation, Nova Science Publishers, New York, **2010**, pp. 331–358.
29. C. T. Inácio, P. M. Chalk, A. M. T. Magalhães, *Crit Rev Food Sci Nutr.* **2015**, *55*, 1206–1218. DOI:10.1080/10408398.2012.689380
30. S. Cerar, A spatial model of underground water chemical composition in Slovenia in GIS environment, Ph.D.Thesis, Univerza v Ljubljani, Naravoslovno-tehniška fakulteta, Ljubljana, **2016**, pp.
31. C. Kendall, M.G. Sklash, T.D. Bullen. in: Solute model isotope tracers of water and solute sources in catchments, Catchment Syst. J. Wiley & Sons, New York, **1995**, pp. 261–303.
32. W. G. Mook. The global cycle of water. in: Environmental isotopes in the hydrological cycle- Principles and Applications (Vol. 1), International Atomic Energy Agency and United Nations Educational, Scientific and Cultural Organization, Paris, Vienna, **2000**.
33. R. Z. Chekki, A. Snoussi, I. Hamrouni, N. Bouzouita, *Mediterr J Chem.* **2014**, *3*, 947–956.
34. B. A. Akinwande, S.J. Olatunde, *Int Food Researc J.* **2015**, *22*, 332–336.
35. A. González, S. Armenta, M. L. Cervera, M. De La Guardia, *Talanta.* **2008**, *74*, 1085–1095. DOI:10.1016/j.talanta.2007.09.039
36. M. Nečemer, D. Potočnik, N. Ogrinc, *J Food Compos Anal.* **2016**, *52*, 16–23. DOI:10.1016/j.jfca.2016.07.002
37. F. Di Giacomo, A. Del Signore, M. Giaccio, *J Agric Food Chem.* **2007**, *55*, 860–866. DOI:10.1021/jf062690h
38. I. M. Chung, J. K. Kim, Y. I. Jin, Y. T. Oh, M. Prabakaran, K. J. Youn, S. H. Kim, *Food Chem.* **2016**, *212*, 48–57. DOI:10.1016/j.foodchem.2016.05.161
39. N. Krivachy (Tanz), A. Rossmann, H. L. Schmidt, *Food Control.* **2015**, *48*, 143–150.

## Povzetek

V tej študiji smo opisali možnost določanja geografskega porekla organsko pridelanega česna (*Allium sativum* L.) na področju Slovenije z analizo izotopske ( $\delta^{13}\text{C}$ ,  $\delta^{15}\text{N}$ ,  $\delta^{34}\text{S}$ ,  $\delta^{18}\text{O}$ ) ter elementne (P, S, Cl, K, Ca, Si, Zn, Br, Rb, Sr) sestave. Slovenija je razmeroma majhna država (s površino le 20273 km<sup>2</sup>), a z vidika geološke in biološke raznolikosti zelo zanimiva za raziskovanje geografskih vplivov. Rezultate, ki so bili pridobljeni z masno spektrometrijo za analizo izotopskih razmerij in energijsko disperzijsko rentgensko fluorescenčno spektrometrijo, smo statistično ovrednotili z multivariatno diskriminantno analizo. Dobljeni model smo validirali z izpuščanjem objektov, t.j. z 10 %, 20 % in 25 % izpuščenih objektov. V povprečju je bil odstotek pravilne klasifikacije vzorcev česna 77 %, kar nakazuje na to, da sta model ter predlagana metodologija obetajoča za nadaljnje raziskovanje hitre, poceni in robustne kontrole porekla.

Acta Chimica Slovenica Vol. 64 (2017)

## AUTHOR INDEX

Abbasi Muhammad Athar .....	159	Bregar Vladimir Boštjan .....	534
Abbasoglu Rza .....	290	Brudar Sandi .....	564
Abdelaziz Mahmoud A. ....	439	Bukošek Vili.....	980
Abdo Nadia Youssef Megally .....	117	Bukovec Peter .....	577
Abdollahi Najmeh .....	409	Bunchamnan Jutamas.....	849
Abdollahi-Basir Mohammad		Burakham Rodjana .....	590
Hossein .....	73	Burcă Silvia .....	513
Abramović Helena .....	491	Cao Qi .....	95
Abu-Melha Sraa .....	919	Carr Paul D. ....	613
Acharya Manoj .....	45	Cercado-Quezada Bibiana .....	449
Ahmad Irshad .....	159	Cerc-Korošec Romana .....	342
Ahmed Mahmood .....	332	Chaudhary Sandeep .....	988
Ain Qurat-ul.....	159	Chavoshiyan Mahshad .....	613
Ajerloo Bahram .....	129	Chen Guang-Ying .....	633
Akdag Abdurrahman .....	312	Chen Hao-Hua .....	633
Akpinar Merve .....	422	Chen Wen-Tong .....	1042
Al-farouk Fatma Omar .....	117	Cheng Guo-Ping .....	261
Ali Amir .....	332	Cherkezova-Zheleva Zara .....	299
Ali Saqib .....	397	Chua Lee Suan .....	888
Al-Omran Fatima .....	439	Cigić Blaž.....	491
Alyapyshev Mikhail .....	582	Ciuffreda Pierangela .....	603
Amini Mostafa M. ....	479	Contreras-Bustos Roberto .....	449
Antypenko Oleksii .....	902	Čanadanović-Brunet Jasna .....	283
Anusha Siluveru .....	319	Čeh Boris .....	342
Aryan Reza.....	911	Černá Karla .....	598
Ashraf Muhammad .....	159	Černigoj Urh .....	564
Atalay Rengul Cetin .....	621	Četković Gordana .....	283
Athar Muhammad Makshoof .....	332	Dahmann Georg.....	715
Attia Ali Kamal .....	415	Dar'in Dmitriy .....	582
Babain Vasily .....	582	De Lera Garrido Fernando Juan.....	771
Babanly Mahammad Baba .....	221	Deeks Steven G. ....	530
Badiei Alireza .....	701	Dehghani-Firouzabadi Amin .....	686
Balakrishnan Malini .....	83	Demirak Ahmet .....	237
Balati Ali .....	479	Deng Yuanyuan .....	95
Bangal Mukund N. ....	461	Derun Emek Moroydor .....	654
Barani Azam .....	193	Deshmukh Dattatray G. ....	461
Basu Subhankar .....	83	Dhale Laxman Appa .....	931
Bayrakci Mevlut .....	679	Dilmaghani Karim Akbari.....	895
Behzad Sara Karimi .....	479	Divarova Vidka .....	365
Béni Áron .....	248	Dolinar Marko.....	804
Berest Galyna.....	902	Doljak Bojan .....	1
Bevc-Černilec Katarina.....	968	Dolžan Vita .....	530
Beyzaei Hamid.....	911	Drvarič Talian Sara .....	560
Bohanec Simona .....	968	Đilas Sonja .....	283
Boroujeni Kaveh Parvanak .....	692	Đorević Aleksandra .....	603
Botros Samir .....	102	Đurović Dijana .....	276

El-Das Yara S. ....	102	Hussain Ghulam .....	159
Erdani Kreft Mateja .....	534	Ibrahim Rehab A. ....	439
Ertul Seref .....	679	Imamaliyeva Samira Zakir .....	221
Fadavi Abdulhamid .....	692	Imran Muhammad .....	256
Fan Meng .....	55	Indolean Cerasella .....	513
Fanedl Lijana .....	227	Iqbal Muhammad .....	397
Farahani Mohammad Reza .....	256	Islamčević Razboršek Maša .....	537
Farhadi Saeed .....	129, 945, 1005	Ismail Hammad .....	397
Faridbod Farnosh .....	842	Ivanović Milena .....	537
Farooq Umar .....	332	Jaiswal Pradeep K. ....	988
Fatahala Samar S. ....	865	Jamir Latonglila .....	832
Fekry Amany M. ....	415	Janagap Steve .....	818
Ferdin Jana .....	530	Jarc Eva .....	549
Ferk Savec Vesna .....	63, 661, 959	Jelen Andreja .....	980
Fu Lin .....	202	Jereb Marjan .....	747
Gan Hui-Yee .....	144	Jiménez-Becerril Jaime .....	449
Gao Wei .....	256	Jiménez-Reyes Melania .....	449
Gasanly Turan Mirzaly .....	221	Jing Bo .....	95
Gasymov Vagif Akber .....	221	Jukič Marko .....	771
Gazvoda Martin .....	763	Jurca Sabina .....	1
Ghanbari Mohammad .....	479	Juteršek Mojca .....	804
Ghasemzadeh Mohammad Ali .....	73	Južnič Stanislav .....	S67
Glavač Jaka .....	715	Kadić Selmir .....	771
Gobec Stanislav .....	771	Kamel Mona M. ....	102
Godec Andrej .....	S101	Kapitány Sándor .....	248
Golobič Iztok .....	938	Karimi Mohammad Ali .....	193
Golobič Amalija .....	790	Karpenko Olexandr .....	902
Goreshnik Evgeny .....	208, 763	Karthik Pulluri .....	1030
Goričar Katja .....	530	Kaučič Venčeslav .....	381
Grabrijan Katarina .....	771	Kawde Abdel-Nasser .....	267
Gregorčič Peter .....	938	Kazimirovna Elyashevich Galina .....	980
Grethe Thomas .....	373	Keskin Feyyaz .....	237
Grobin Blaž .....	491	Khajuria Heena .....	170
Grošelj Uroš .....	715, 727, 782, 790	Khajuria Ruchi .....	672
Gruden Evelin .....	577	Khalil Omneya M. ....	102
Guštin Ema .....	549	Khan Farman Ali .....	159
Guven Ebru Bilget .....	621	Khedr Mohammed A. ....	865
Hadizadeh Shahla .....	692	Kiani Mahtab .....	707
Hafner Jože .....	938	Kick Thomas .....	373
Hajková Pavlína .....	598	Kinzhybalo Vasyl .....	208
Hakimi Mohammad .....	1005	Kitanovski Nives .....	342
Haleem Muhammad Abdul .....	397	Kocman David .....	1048
Han Xiao-Meng .....	431	Kočevar Marijan .....	737
Han Yong-Jun .....	179, 500	Kolar Mitja .....	537
Hasani Sodabeh .....	692	Kolarević Ana .....	603
Hatefi-Mehrjardi Abdolhamid .....	193	Kolomoets Oleksandra .....	902
He Zeyue .....	95	Kong Lingqian .....	215
Hélix-Nielsen Claus .....	83	Korenak Jasmina .....	83
Hendijani Mehrnoosh .....	707	Košmrlj Janez .....	763
Hetemi Dardan .....	818	Kour Mandeep .....	672
Hidalgo-Herrador José Miguel .....	598	Kovalenko Sergiy .....	902
Hladnik Anžej .....	530	Kozjek Škofic Irena .....	877
Hrast Špela .....	959	Kragelj Lapanja Nevenka .....	1
Hribar-Lee Barbara .....	560	Kranjc Krištof .....	737
Huang Jian-Gen .....	1042	Križaj Igor .....	555
Hundal Geeta .....	672	Kržan Mojca .....	564

Kucukdumlu Asligul .....	621	Mohammadi Abdelnassar .....	129
Kumar Sandeep .....	672	Mohammadipour Mohammad .....	707
Kump Ana .....	549	Mohareb Rafat Milad .....	117, 439
Kuotsu Neivotsonuo Bernadette .....	832	Molaei Bahar .....	73
Ladol Jigmet .....	170	Moradi Leila .....	506
Latinović Zorica .....	555	Motraghi Zahra .....	911
Lazarević Jelena .....	603	Murtaza Ghulam .....	332
Lekova Vanya .....	365	Mushtaq Zahid .....	159
Lenassi Metka .....	530	Mushtaq Afifa .....	397
Leonardi Adrijana .....	555	Mys'kiv Marian Mys'kiv .....	208
Leow Li-Eau .....	144	Nadeem Kashif .....	332
Li Gao-Nan .....	633	Najafi Meysam .....	40
Li Qing-Bin .....	179	Namazian Mansoor .....	613
Li Qing-Bin .....	500	Nečemer Marijan .....	1048
Li Songdong .....	55	Nedović-Vuković Mirjana .....	276
Li Wanjun .....	55	Nidhin Pallipurath Veleelath .....	467
Lodhi Muhammad Arif .....	159	Nikitha Gurala .....	319
Logar Ana .....	661	Nikoofard Hossein .....	842
Lohar Kishan Shankarrao .....	931	Niu Zhi-Gang .....	633
Lojen Sonja .....	1048	Nosulenko Inna .....	902
Lojk Jasna .....	534	Novinec Marko .....	782
Lubczak Jacek .....	858	Obreza Aleš .....	771
Lubczak Renata .....	858	Ong Siew-Teng .....	144
Luk'yanov Mykhailo .....	208	Ozcan Fatih .....	679
Lukić Branislav .....	782	Ozyilmaz Ali Tuncay .....	312
Ma Lihua .....	55	Pajin Biljana .....	283
Ma Chunlei .....	55	Palchikov Vitaliy .....	902
Măicăneanu Andrada .....	513	Pandey Sushil K. .....	672
Mahalingam Umadevi .....	186	Panjičko Mario .....	227
Mahltig Boris .....	373	Paul Arun .....	467
Mahne Opatić Anja .....	1048	Pavlin Mojca .....	534
Makrlík Emanuel .....	582	Peklaj Cirila .....	661
Maleki Mansoureh .....	1005	Peng Xiuxiang .....	95
Mali Anil C. .....	461	Perdih Franc .....	737
Malik Rabia .....	159	Petan Toni .....	549, 555
Mallick Subrata .....	45	Petek Anja .....	537
Manríquez-Reza E. .....	449	Peterlin Boris M. .....	530
Mansourpanah Yaghoub .....	945	Petrinic Irena .....	83
Maraković Nikola .....	15	Petrović Jovana .....	283
Marina Klemenčič .....	804	Pevec Andrej .....	763
Marinšek Logar Romana .....	227	Phucho Tovishe .....	832
Martini Tomaž .....	571	Plemenita Ana .....	530
Mashevskaya Irina V. ....	988	Počkaj Marta .....	342
Mathad Vijayavithal T. ....	461	Podgornik Helena .....	564
Mathur Manas .....	988	Podlipnik Črtomir .....	560
Meden Anton .....	381	Poklar Ulrih Nataša .....	491
Medhane Vijay J. ....	461	Polanc Slovenko .....	763
Medvešček Simona .....	381	Posta József .....	248
Mermer Nevin Karamahmut .....	654	Potkonjak Branislav .....	276
Milanova Maria .....	299	Pourzare Kolsoum .....	945
Milisavljević Branka .....	276	Požgan Franc .....	715, 727
Mirza Bushra .....	397	Prah Uroš .....	877
Mishra Satyaki .....	45	Prek Benjamin .....	798
Mitov Ivan .....	299	Prikhodko Jaroslav .....	988
Mohamed Mossad S. ....	865	Prislan Iztok .....	564
Mohamed Mona A. ....	415		

Qian Shao-Song .....	825	Stojan Jurij .....	571
Qin Jie .....	202, 431, 633	Stojanović Gordana .....	603
Racheva Petya .....	365	Stojnova Kirila .....	365
Rajam Bindhu Muthunadar .....	186	Strojan Klemen .....	534
Rajasri Thallapalli .....	319	Su Wei .....	638
Raju Kammachichu .....	319	Sunitha Malladi .....	319, 1030
Rakuša Temova Žane .....	523	Suryavanshi Venkat S. ....	931
Ramasamy Parimaladevi .....	186	Sushmitha Dupa .....	319
Rao Chakunta Govind .....	319	Svete Jurij .....	534, 715, 727, 782, 790
Ravinder Banothu .....	319	Swami Ajit K. ....	988
Reddy K. Vasumathi .....	1030	Swapna Pothuganti .....	319
Rehman Aziz-ur .....	159	Swaroopu Deva .....	319
Ren Yan-Jie .....	825	Syed Atiya .....	672
Ričko Sebastijan.....	715, 790	Šinko Goran .....	15
Roškar Robert .....	523	Šmelcerović Andrija .....	603
Rozman Damjana .....	571	Štefane Bogdan .....	715, 727
Ruzlan Nur Nabihah .....	888	Tahir Muhammad Nawaz .....	397
Saadiq Muhammad .....	397	Tavaf Elham .....	701
Sadegh Maryam Aghamohammad ....	506	Tišler Zdeněk .....	598
Safaei Hamid Reza.....	1020	Tongsa Darunee .....	849
Sahoo Rudra N. ....	45	Toplak Časar Renata .....	1
Samzadeh-Kermani Alireza .....	911	Tukmechi Amir .....	895
Santaladchaiyakit Yanawath ....	590, 849	Tumbas Šaponjac Vesna .....	283
Santaniello Enzo .....	603	Tuncbilek Meral .....	621
Saran Mukesh.....	988	Turek Bor Lucijan.....	737
Sargolzaei Mohsen.....	842	Tzvetkov Martin .....	299
Sarmidi Mohamad Roji.....	888	Urankar Damijana.....	763
Selucký Pavel .....	582	Urek Raziye Ozturk .....	422
Selvaraj Charles .....	467	Urleb Uroš.....	968
Senberber Fatma Tugce .....	654	Uršula Prosenc Zmrzljak .....	571
Sergeevich Kuryndin Ivan .....	980	Vafazadeh Rasoul .....	409, 613, 686
Shah Syed Adnan Ali .....	159	Vajs Jure.....	763
Shahid Muhammad .....	159	Valcheva Evgenia .....	299
Shahrokh Mansooreh .....	692	Vaňura Petr .....	582
Sharma Vashundhra.....	988	Vavsari Vaezeh Fathi .....	701
Sheikh Haq Nawaz .....	170	Venturini Peter .....	938
Shekouhy Mohsen.....	1020	Veranič Peter .....	534
Shi Jingwen .....	215	Vichapong Jitlada .....	590
Shinde Bajarang Laxman.....	931	Vidmar Beti .....	227
Siddiqui Sabahat Zahra .....	159	Virant Miha .....	560
Singh Rajinder .....	170	Vladimirovich Novikov Dmitrii .....	980
Sinha Upasana Bora.....	832	Voskoboynik Oleksii .....	902
Sóki Erzsébet .....	248	Vražič Dejan.....	747
Soleimani Esmail .....	644	Vrvić Miroslav M. ....	276
Soleymanzadeh Mahdiyeh .....	193	Vulić Jelena .....	283
Sosič Izidor .....	771	Wang Enju .....	638
Soukupová Lenka .....	598	Wang Li .....	179
Spasić Snežana .....	276	Wang Li-Na .....	202
Spassova Ivanka .....	299	Wang Peng .....	202, 431
Srečnik Eva .....	523	Wang Qi .....	55
Srijaranai Supalax .....	590, 849	Wang Xianyou .....	95
Srinivas Avula .....	319, 1030	Wang Xue-You .....	633
Stajčić Slađana .....	283	Wang Xun .....	633
Stanovnik Branko.....	798	Wang Yin-Feng .....	1042
Steinbücher Miha.....	938	Wei Sun .....	633
Stephen Arputharaj David .....	467	Willis Anthony C. ....	409, 613, 686

Wissiak Grm Katarina S. ....	63	Zamani Narges .....	644
Wu Dong-Min .....	633	Zamanian Ali .....	707
Wu Yu-Shan .....	431	Zárybnická Lenka .....	598
Xu Yin-Xiang .....	825	Zarzyka Iwona .....	858
Xu Yu .....	202	Zhang Cai-Xia .....	261
Xue Ling-Wei .....	179	Zhang Daopeng .....	215
Xue Chongchong .....	215	Zhang Ding-Wa .....	1042
Xue Ling-Wei .....	261, 500	Zhang Li-Xin .....	825
Yadav Dharmendra K .....	988	Zhang Meng .....	202
Yi Xiu-Guang .....	1042	Zhao Gan-Qing .....	500
Yildirim Meral .....	654	Zhao Shan-Shan .....	431
Yıldız Dilek .....	237	Zhu Jia-Wei .....	202
Yilmaz Bahar .....	679	Zhu Jin-Long .....	825
You Qi .....	202	Ziaie Maghsoud .....	895
Yuan Shizhuang .....	638	Ziarani Ghodsi Mohammadi .....	701
Zaharieva Joana .....	299	Zupančič Marija .....	577
Zahedi Mohammad Mehdi .....	911	Zupančič Matevž .....	938
Zakrajšek Jure .....	968	Žlajpah Margareta .....	555
Zamani Farzad .....	73		

**DRUŠTVENE VESTI IN DRUGE AKTIVNOSTI**  
**SOCIETY NEWS, ANNOUNCEMENTS, ACTIVITIES**

**Vsebina**

Koledar znanstvenih in strokovnih srečanj .....	S125
Navodila za avtorje .....	S130

**Contents**

Scientific meetings – chemistry, chemical technology and chemical engineering .....	S125
Instructions for authors .....	S130





# KOLENDAR VAŽNEJŠIH ZNANSTVENIH SREČANJ S PODROČJA KEMIJE IN KEMIJSKE TEHNOLOGIJE

## SCIENTIFIC MEETINGS – CHEMISTRY AND CHEMICAL ENGINEERING

### 2018

#### February 2018

---

21 – 23 ChemCYS 2018 – 14<sup>TH</sup> CHEMISTRY CONFERENCE FOR YOUNG SCIENTISTS  
Blankenberge, Belgium  
Information: <http://chemcys.be/>

#### March 2018

---

13 – 15 FILTECH 2018 – INTERNATIONAL CONFERENCE AND EXHIBITION FOR FILTRATION  
AND SEPARATION TECHNOLOGIES  
Cologne, Germany  
Information: <http://www.rsc.org/events/detail/16406/filtech-2018-international-conference-and-exhibition-for-filtration-and-separation-technologies>

21 – 23 POLYMERS: DESIGN, FUNCTION AND APPLICATION  
Barcelona, Spain  
Information: <http://sciforum.net/conference/polymers-2018>

#### April 2018

---

15 – 18 PETROMASS 2018 – XI. INTERNATIONAL MASS SPECTROMETRY CONFERENCE ON  
PETROCHEMISTRY, ENVIRONMENTAL AND FOOD CHEMISTRY  
Bled, Slovenia  
Information: <http://www.petromass2018.com/>

#### May 2018

---

7 – 9 6<sup>TH</sup> INTERNATIONAL CONFERENCE ON POPULATION BALANCE MODELLING  
Ghent, Belgium  
Information: <http://www.pbm2018.ugent.be/>

10 – 12 117<sup>TH</sup> GENERAL ASSEMBLY OF THE BUNSEN SOCIETY FOR PHYSICAL CHEMISTRY  
2018 – KINETICS IN THE REAL WORLD  
Hannover, Germany  
Information: <http://www.bunsen.de/en/veranstaltungen/veranstaltungskalender/bunsentagung-2018/>

20 – 23 ISCRE 25 – 25<sup>TH</sup> INTERNATIONAL SYMPOSIUM ON CHEMICAL REACTION  
ENGINEERING  
Florence, Italy  
Information: <http://www.aidic.it/iscre25/>

20 – 23 5<sup>TH</sup> INTERNATIONAL SCHOOL-CONFERENCE ON CATALYSIS FOR YOUNG  
SCIENTISTS “CATALYST DESIGN: FROM MOLECULAR TO INDUSTRIAL LEVEL”  
Moscow, Russia  
Information: <http://conf.nsc.ru/catdesign2018/en/>

**June 2018**

---

- 3 – 6 6<sup>TH</sup> INTERNATIONAL CONGRESS ON GREEN PROCESS ENGINEERING  
Toulouse, France  
Information: <http://www.gpe2018.org/>
- 3 – 7 POLYMERS AND ORGANIC CHEMISTRY 2018 (POC 2018)  
Palavas Les Flots Palavas, France  
Information: <http://poc2018.enscm.fr>
- 4 – 6 IIS PRAGUE 2018 – 13<sup>TH</sup> INTERNATIONAL SYMPOSIUM ON THE SYNTHESIS AND  
APPLICATIONS OF ISOTOPES AND ISOTOPICALLY LABELLED COMPOUNDS  
Prague, Czech Republic  
Information: <http://www.iis-prague2018.cz/>
- 4 – 7 POLYMERS AND ORGANIC CHEMISTRY 2018 (POC 2018)  
Montpellier, France  
Information: <https://iupac.org/event/polymers-organic-chemistry-2018-poc-2018/>
- 10 – 13 30<sup>TH</sup> EUROPEAN SYMPOSIUM ON APPLIED THERMODYNAMICS  
Prague, Czech Republic  
Information: <http://esat2018.cz/>
- 10 – 13 28<sup>TH</sup> EUROPEAN SYMPOSIUM ON COMPUTER-AIDED PROCESS ENGINEERING  
Graz, Austria  
Information: <https://www.tugraz.at/events/escape28/home/>
- 13 – 15 8<sup>TH</sup> EUROPEAN MEETING ON CHEMICAL INDUSTRY AND ENVIRONMENT  
Nantes, France  
Information: <http://conferences.imt-atlantique.fr/emchie2018/>
- 24 – 28 10<sup>TH</sup> INTERNATIONAL CONFERENCE ON MOLECULAR IMPRINTING, MIP 2018  
Jerusalem, Israel  
Information: <http://www.ortra.com/events/mip2018>
- 30 – Jul 3 3<sup>RD</sup> SOUTH EAST EUROPEAN CONFERENCE ON SUSTAINABLE DEVELOPMENT OF  
ENERGY, WATER AND ENVIRONMENTAL SYSTEMS  
Novi Sad, Serbia  
Information: <http://www.novisad2018.sdewes.org/>

**July 2018**

---

- 1 – 5 WORLD POLYMER CONGRESS MACRO18  
Cairns Queensland, Australia  
Information: <http://www.macro18.org>
- 2 – 6 XVI INTERNATIONAL IUPAC CONFERENCE ON HIGH TEMPERATURE MATERIALS  
CHEMISTRY (HTMC-XVI)  
Ekaterinburg, Russian Federation  
Information: <http://htmc16.ru/>
- 8 – 13 27<sup>TH</sup> IUPAC INTERNATIONAL SYMPOSIUM ON PHOTOCHEMISTRY  
Dublin, Ireland  
Information: <https://iupac.org/event/27th-iupac-international-symposium-photochemistry/>
- 9 – 13 EUROMEMBRANE 2018  
Valencia, Spain  
Information: <http://euromembrane2018.org/>
- 10 – 14 25<sup>TH</sup> INTERNATIONAL CONFERENCE ON CHEMISTRY EDUCATION ICCE 2018)  
Sydney, Australia  
Information: <http://www.icce2018.org/>
- 15 – 20 THE 18<sup>TH</sup> INTERNATIONAL SYMPOSIUM ON SOLUBILITY PHENOMENA AND  
RELATED EQUILIBRIUM PROCESSES (ISSP)  
Tours, France  
Information: <http://issp18.org/>

- 30 – Aug 4      43<sup>RD</sup> INTERNATIONAL CONFERENCE ON COORDINATION CHEMISTRY  
Sendai, Japan  
Information:      <http://iccc2018.jp>
- 
- August 2018**
- 12 – 17      18<sup>TH</sup> INTERNATIONAL BIOTECHNOLOGY SYMPOSIUM  
Montréal, Canada  
Information:      <http://ibs2018montreal.org/>
- 25 – 29      23<sup>RD</sup> INTERNATIONAL CONGRESS OF CHEMICAL AND PROCESS ENGINEERING  
CHISA 2018  
Prague, Czech Republic  
Information:      <http://2018.chisa.cz/>
- 25 – 29      21<sup>ST</sup> CONFERENCE ON PROCESS INTEGRATION, MODELLING AND OPTIMISATION  
FOR ENERGY SAVING AND POLLUTION REDUCTION PRES 2018  
Prague, Czech Republic  
Information:      <http://2018.chisa.cz/>
- 26 – 30      ECC7 – 7<sup>TH</sup> EuCheMS CHEMISTRY CONGRESS  
Liverpool, UK  
Information:      <https://www.euchems2018.org/>
- 26 – 30      35<sup>TH</sup> INTERNATIONAL CONFERENCE ON SOLUTION CHEMISTRY (ICSC)  
Szeged, Hungary  
Information:      <http://www.mke.org.hu/ICSC2018>
- 26 – 31      22<sup>ND</sup> INTERNATIONAL MASS SPECTROMETRY CONFERENCE (IMSC) 2018  
Florence, Italy  
Information:      <http://www.imsc2018.it/>
- 30 – 31      ICOSSE 2018 : 20<sup>TH</sup> INTERNATIONAL CONFERENCE ON OPERATING SYSTEMS AND  
SOFTWARE ENGINEERING  
Bangkok, Thailand  
Information:      <https://www.waset.org/conference/2018/08/bangkok/ICOSSE>
- 
- September 2018**
- 2 – 6      SMARTER 6 meeting  
Ljubljana, Slovenia  
Information:      <https://smarter6.ki.si/>
- 2 – 7      69<sup>TH</sup> ANNUAL MEETING OF THE INTERNATIONAL SOCIETY OF  
ELECTROCHEMISTRY  
Bologna, Italy  
Information:      <http://annual69.ise-online.org/>
- 2 – 7      32<sup>ND</sup> CONFERENCE OF EUROPEAN COLLOID AND INTERFACE SOCIETY (ECIS)  
Ljubljana, Slovenia  
Information:      <http://ecis2018.fkkt.uni-lj.si/index.html>
- 4 – 7      N-LIGANDS2018 – 7<sup>TH</sup> EuCheMS CONFERENCE ON NITROGEN-LIGANDS  
Lisbon, Portugal  
Information:      <http://www.n-ligands2018.com/>
- 9 – 12      12<sup>TH</sup> EUROPEAN SYMPOSIUM ON BIOCHEMICAL ENGINEERING SCIENCES  
Lisbon, Portugal  
Information:      <http://esbes2018.org/>
- 9 – 12      16<sup>TH</sup> EUROPEAN CONFERENCE ON MIXING  
Toulouse, France  
Information:      <http://inpact.inp-toulouse.fr/MIXING16/>

- 9 – 13 EUROPEAN CORROSION CONGRESS  
Prague, Czech Republic  
Information: <http://www.eurocorr2018.org/>
- 9 – 14 8<sup>TH</sup> IUPAC INTERNATIONAL CONFERENCE ON GREEN CHEMISTRY  
Bangkok, Thailand  
Information: <http://www.greeniupac2018.com>
- 10 – 14 9<sup>TH</sup> INTERNATIONAL CONFERENCE FOR CONVEYING AND HANDLING OF PARTICULATE SOLIDS  
London, UK  
Information: <http://www.constableandsmith.com/events/chops-2018/>
- 16 – 19 DISTILLATION & ABSORPTION CONFERENCE 2018  
Firenze, Italy  
Information: <http://www.aidic.it/da2018/>
- 16 – 21 22<sup>ND</sup> INTERNATIONAL CONFERENCE ON ORGANIC SYNTHESIS (22-ICOS)  
Florence, Italy  
Information: <http://www.22-icos-florence.it>
- 16 – 21 13<sup>TH</sup> INTERNATIONAL CONFERENCE ON SOLID STATE CHEMISTRY  
Pardubice, Czech Republic  
Information: <http://www.ssc-conference.com/2018/>
- 18 – 21 11<sup>TH</sup> INTERNATIONAL DRYING SYMPOSIUM  
Valencia, Spain  
Information: <http://www.ids2018.webs.upv.es/>
- 19 – 21 SLOVENIAN CHEMICAL SOCIETY ANNUAL MEETING 2018  
Portorož, Slovenia  
Information: <http://chem-soc.si/scs-annual-meeting-2018>

**October 2018**

---

- 14 – 17 4<sup>TH</sup> INTERNATIONAL CONFERENCE ON BIOINSPIRED AND BIOBASED CHEMISTRY & MATERIALS  
Nice, France  
Information: <http://www.unice.fr/nice-conference/>
- 14 – 18 14<sup>TH</sup> IUPAC INTERNATIONAL CONGRESS OF PESTICIDE CHEMISTRY  
Rio de Janeiro, Brazil  
Information: <https://iupac.org/event/14th-iupac-international-congress-of-pesticide-chemistry/>
- 21 – 24 15<sup>TH</sup> INTERNATIONAL CONFERENCE ON MICROREACTION TECHNOLOGY  
Karlsruhe, Germany  
Information: <http://dechema.de/en/IMRET2018.html>

**November 2018**

---

- 5 – 9 XXIII INTERNATIONAL CONFERENCE ON CHEMICAL REACTORS  
Ghent, Belgium  
Information: [http://conf.nsc.ru/CR\\_23/en/](http://conf.nsc.ru/CR_23/en/)

**2019****May 2019**

---

- 19 – 24 14<sup>TH</sup> IUPAC INTERNATIONAL CONGRESS OF CROP PROTECTION CHEMISTRY  
Ghent, Belgium  
Information: <https://www.iupac2019.be>
-

---

**June 2019**

- 2 – 6                    14<sup>TH</sup> INTERNATIONAL SYMPOSIUM ON MACROCYCLIC AND SUPRAMOLECULAR CHEMISTRY  
Lecce, Italy  
Information:            <https://ismsc2019.eu/>
- 16 – 19                LOSS PREVENTION 2019  
Delft, The Netherlands  
Information:            <http://lossprevention2019.org/>
- 16 – 20                17<sup>TH</sup> INTERNATIONAL CONFERENCE ON CHEMISTRY AND THE ENVIRONMENT – ICCE2019  
Thessaloniki, Greece  
Information:            <http://www.euchems.eu/events/17th-international-conference-chemistry-environment-icce2019/>
- 26 – 30                6<sup>TH</sup> EUROPEAN CONFERENCE ON ENVIRONMENTAL APPLICATIONS OF ADVANCED OXIDATION PROCESSES (EAAOP-6)  
Portorož, Slovenia  
Information:            <http://eaaop6.ki.si/>

---

**July 2019**

- 5 – 12                 IUPAC 2019 PARIS FRANCE  
Paris, France  
Information:            <https://www.iupac2019.org/>
- 21 – 26                THE 18<sup>TH</sup> INTERNATIONAL SYMPOSIUM ON NOVEL AROMATIC COMPOUNDS (ISNA-18)  
Sapporo City, Japan  
Information:            <https://iupac.org/event/18th-international-symposium-novel-aromatic-compounds-isna-18/>

---

**September 2019**

- 15 – 19                11<sup>TH</sup> EUROPEAN CONGRESS OF CHEMICAL ENGINEERING – ECCE11 & 4<sup>TH</sup> EUROPEAN CONGRESS OF APPLIED BIOTECHNOLOGY – ECAB5  
Florence, Italy  
Information:            [http://efce.info/ECCE12\\_ECAB5-p-112545.html](http://efce.info/ECCE12_ECAB5-p-112545.html)

# Acta Chimica Slovenica

## Author Guidelines

### Submissions

Submission to ACSi is made with the implicit understanding that neither the manuscript nor the essence of its content has been published in whole or in part and that it is not being considered for publication elsewhere. All the listed authors should have agreed on the content and the corresponding (submitting) author is responsible for having ensured that this agreement has been reached. The acceptance of an article is based entirely on its scientific merit, as judged by peer review. There are no page charges for publishing articles in ACSi.

### Submission material

Typical submission consists of:

- -full manuscript (Word file, with title, authors, abstract, keywords, figures and tables embedded, and references);
- supplementary files:
  - **Statement of novelty** (Word file),
  - **List of suggested reviewers** (Word file),
  - ZIP file containing **graphics** (figures, illustrations, images, photographs),
  - **Graphical abstract** (single graphics file),
  - **Proposed cover picture** (optional, single graphics file),
  - **Appendices** (optional, Word files, graphics files).

### Submission process

Submission process consists of 5 steps. Before submission, authors should go through the checklist at the bottom of these guidelines page and prepare for submission:

#### Step 1: Starting the submission

- Choose one of the journal sections.
- Confirm all the requirements of the **checklist**.
- Additional plain text comments for the editor can be provided in the relevant text field.

#### Step 2: Upload submission

- Upload full manuscript in the form of a Word file (with title, authors, abstract, keywords, figures and tables embedded, and references).

#### Step 3: Enter metadata

- First name, last name, contact email and affiliation for all authors, in relevant order, must be provided. Corresponding author has to be selected. Full postal address and phone number of the corresponding author has to be provided.
- **Title and abstract** must be provided in plain text.
- Keywords must be provided (max. 6, separated by semicolons).

- Data about contributors and supporting agencies may be entered.
- **References** in plain text must be provided in the relevant text filed.

#### Step 4: Upload supplementary files

- **Statement of novelty** in a Word file must be uploaded
- **List of suggested reviewers** with at least three reviewers must be uploaded as a Word file.
- All **graphics** have to be uploaded in a single ZIP file. Graphics should be named Figure 1.jpg, Figure 2.eps, etc.
- **Graphical abstract image** must be uploaded separately.
- **Proposed cover picture** (optional) should be uploaded separately.
- Any additional **appendices** (optional) to the paper may be uploaded. Appendices may be published as a supplementary material to the paper, if accepted.
- For each uploaded file the author is asked for additional metadata which may be provided. Depending of the type of the file please provide the relevant title (Statement of novelty, List of suggested reviewers, Figures, Graphical abstract, Proposed cover picture, Appendix).

#### Step 5: Confirmation

- -Final confirmation is required.

### Article Types

**Review articles** are welcome in any area of chemistry and may cover a wider or a more specialized area, if a high impact is expected. Manuscripts normally should not exceed 40 pages of one column format (letter size 12, 33 lines per page). Authors should consult the ACSi editor prior to preparation of a review article.

**Scientific articles** should have the following structure:

1. Title (max. 150 characters),
2. Authors and affiliations,
3. Abstract (max. 1000 characters),
4. Keywords (max. 6),
5. Introduction,
6. Experimental (Results and Discussion),
7. Results and Discussion (Experimental),
8. Conclusions,
9. Acknowledgements (if any),
10. References.

The sections should be arranged in the sequence generally accepted for publications in the respective fields. Scientific articles should report significant

and innovative achievements and exhibit a high level of originality.

**Short communications** generally follow the same order of sections, but should be short (max. 2500 words) and report a significant aspect of research work meriting separate publication.

**Technical articles** report applications of an already described innovation. Typically, technical articles are not based on new experiments.

## Preparation of Submissions

**Text** of the submitted articles must be prepared with Word for Windows. Normal style set to single column, 1.5 line spacing, and 12 pt Times New Roman font is recommended. Line numbering (continuous, for the whole document) must be enabled to simplify the reviewing process. For any other format, please consult the editor. Articles should be written preferably in English. Correct spelling and grammar are the sole responsibility of the author(s). Papers should be written in a concise and succinct manner. The authors shall respect the ISO 80000 standard, and IUPAC Green Book rules on the names and symbols of quantities and units. The *Système International d'Unités* (SI) must be used for all dimensional quantities.

**Graphics** (figures, graphs, illustrations, digital images, photographs) should be inserted in the text where appropriate. The captions should be self-explanatory. Lettering should be readable (suggested 8 point Arial font) with equal size in all figures. Use common programs such as Word Excel to prepare figures (graphs) and ChemDraw to prepare structures in their final size (8 cm for single column width or 17 cm for double column width) so that neither reduction nor enlargement is required. In **graphs**, only the graph area determined by both axes should be in the frame, while a frame around the whole graph should be omitted. The graph area should be white. The legend should be inside the graph area. The style of all graphs should be the same. **Figures and illustrations** should be of sufficient quality for the printed version, i.e. 300 dpi minimum. **Digital images and photographs** should be of high quality (minimum 250 dpi resolution). On submission, figures should be of good enough resolution to be assessed by the referees, ideally as JPEGs. High-resolution figures (in JPEG, TIFF, or EPS format) might be required if the paper is accepted for publication.

**Tables** should be prepared in the Word file of the paper as usual Word tables. The captions should be above the table and self-explanatory.

**References** should be numbered and ordered sequentially as they appear in the text, likewise methods, tables, figure captions. When cited in the text, reference numbers should be superscripted, following punctuation marks. It is the sole respon-

sibility of authors to cite articles that have been submitted to a journal or were in print at the time of submission to ACSi. Formatting of references to published work should follow the journal style; please also consult a recent issue:

1. J. W. Smith, A. G. White, *Acta Chim. Slov.* **2008**, *55*, 1055–1059.
2. M. F. Kemmere, T. F. Keurentjes, in: S. P. Nunes, K. V. Peinemann (Ed.): *Membrane Technology in the Chemical Industry*, Wiley-VCH, Weinheim, Germany, **2008**, pp. 229–255.
3. J. Levec, Arrangement and process for oxidizing an aqueous medium, US Patent Number 5,928,521, date of patent July 27, **1999**.
4. L. A. Bursill, J. M. Thomas, in: R. Sersale, C. Collela, R. Aiello (Eds.), *Recent Progress Report and Discussions: 5th International Zeolite Conference*, Naples, Italy, 1980, Gianini, Naples, **1981**, pp. 25–30.
5. J. Szegezdi, F. Csizmadia, Prediction of dissociation constant using microconstants, [http://www.chemaxon.com/conf/Prediction\\_of\\_dissociation\\_constant\\_using\\_microconstants.pdf](http://www.chemaxon.com/conf/Prediction_of_dissociation_constant_using_microconstants.pdf), (assessed: March 31, 2008)

Titles of journals should be abbreviated according to Chemical Abstracts Service Source Index (CASSI).

## Special Notes

- Complete characterization, **including crystal structure**, should be given when the synthesis of new compounds in crystal form is reported.
- Numerical **data should be reported with the number of significant digits corresponding to the magnitude** of experimental uncertainty.
- **The SI system of units and IUPAC recommendations** for nomenclature, symbols and abbreviations should be followed closely. Additionally, the authors should follow the general guidelines when citing spectral and analytical data, and depositing crystallographic data.
- **Characters** should be correctly represented throughout the manuscript: for example, 1 (one) and l (ell), 0 (zero) and O (oh), x (ex), D7 (times sign), B0 (degree sign). Use Symbol font for all Greek letters and mathematical symbols.
- The rules and recommendations of the **IUBMB** and the **International Union of Pure and Applied Chemistry (IUPAC)** should be used for abbreviation of chemical names, nomenclature of chemical compounds, enzyme nomenclature, isotopic compounds, optically active isomers, and spectroscopic data.
- **A conflict of interest** occurs when an individual (author, reviewer, editor) or its organization is involved in multiple interests, one of which could possibly corrupt the motivation for an act in the other. Financial relationships are the most easily identifiable conflicts of interest, while conflicts can occur also as personal relationships, academic competition, etc. **The Edi-**

**tors** will make effort to ensure that conflicts of interest will not compromise the evaluation process; potential editors and reviewers will be asked to exempt themselves from review process when such conflict of interest exists. When the manuscript is submitted for publication, **the authors** are expected to disclose any relationships that might pose potential conflict of interest with respect to results reported in that manuscript. In the Acknowledgement section the source of funding support should be mentioned. The statement of disclosure must be provided as Comments to Editor during the submission process.

- **Published statement of Informed Consent.** Research described in papers submitted to ACSi must adhere to the principles of the Declaration of Helsinki (<http://www.wma.net/e/policy/b3.htm>). These studies must be approved by an appropriate institutional review board or committee, and informed consent must be obtained from subjects. The Methods section of the paper must include: 1) a statement of protocol approval from an institutional review board or committee and 2), a statement that informed consent was obtained from the human subjects or their representatives.
- **Published Statement of Human and Animal Rights.** When reporting experiments on human subjects, authors should indicate whether the procedures followed were in accordance with the ethical standards of the responsible committee on human experimentation (institutional and national) and with the Helsinki Declaration of 1975, as revised in 2008. If doubt exists whether the research was conducted in accordance with the Helsinki Declaration, the authors must explain the rationale for their approach and demonstrate that the institutional review body explicitly approved the doubtful aspects of the study. When reporting experiments on animals, authors should indicate whether the institutional and national guide for the care and use of laboratory animals was followed.
- Contributions authored by **Slovenian scientists** are evaluated by non-Slovenian referees.
- Papers describing **microwave-assisted reactions** performed in domestic microwave ovens are not considered for publication in *Acta Chimica Slovenica*.
- **Manuscripts that are not prepared and submitted in accord with the instructions for authors are not considered for publication.**

## Appendices

Authors are encouraged to make use of supporting information for publication, which is supplementary material (appendices) that is submitted at the same time as the manuscript. It is made available on the Journal's web site and is linked to the article in

the Journal's Web edition. The use of supporting information is particularly appropriate for presenting additional graphs, spectra, tables and discussion and is more likely to be of interest to specialists than to general readers. When preparing supporting information, authors should keep in mind that the supporting information files will not be edited by the editorial staff. In addition, the files should be not too large (upper limit 10 MB) and should be provided in common widely known file formats so as to be accessible to readers without difficulty. All files of supplementary materials are loaded separately during the submission process as supplementary files.

## Proposed Cover Picture and Graphical Abstract Image

Authors are encouraged to submit illustrations as candidates for the journal Cover Picture as well as graphical abstracts. Graphical abstract contains an image that appears as a part of the entry in the table of contents in both online and printed edition. The pictures may be the same. The illustrations must be related to the subject matter of the paper. Usually both proposed cover picture and picture for graphical abstract are the same, but authors may provide different pictures as well.

**Graphical content:** an ideally full-colour illustration of resolution 300 dpi from the manuscript must be proposed with the submission. Graphical abstract pictures are printed in size 6.5 × 4 cm (hence minimal resolution of 770 × 470 pixels). Cover picture is printed in size 11 × 9.5 cm (hence minimal resolution of 1300 × 1130 pixels).

### Statement of novelty

Statement of novelty is provided in a Word file and submitted as a supplementary file in step 4 of submission process. Authors should in no more than 100 words emphasize the scientific novelty of the presented research. Do not repeat for this purpose the content of your abstract.

### List of suggested reviewers

List of suggested reviewers is a Word file submitted as a supplementary file in step 4 of submission process. Authors should propose the names, full affiliation (department, institution, city and country) and e-mail addresses of three potential referees. For each reviewer at least one reference relevant to the scientific field should be provided as well. Appropriate referees should be knowledgeable about the subject but have no close connection with any of the authors. In addition, referees should be from institutions other than (and preferably countries other than) those of any of the authors.

## How to Submit

Users registered in the role of author can start submission by choosing USER HOME link on the top of the page, then choosing the role of the Author and



follow the relevant link for start of submission. Prior to submission we strongly recommend that you familiarize yourself with ACSi style by browsing the journal, either in print or online, particularly if you have not submitted to the ACSi before or recently.

## Correspondence

All correspondence with the ACSi editor regarding the paper goes through this web site and emails. Emails are sent and recorded in the web site database. All emails you receive from the system contain relevant links. **Please do not answer the emails directly but use the embedded links in the emails for carrying out relevant actions.** Alternatively, you can carry out all the actions and correspondence through the online system by logging in and selecting relevant options.

## Proofs

Proofs will be dispatched via e-mail and corrections should be returned to the editor by e-mail as quickly as possible, normally within 48 hours of receipt. Typing errors should be corrected; other changes of contents will be treated as new submissions.

## Submission Preparation Checklist

As part of the submission process, authors are required to check off their submission's compliance with all of the following items, and submissions may be returned to authors that do not adhere to these guidelines.

1. The submission has not been previously published, nor is it under consideration for publication in any other journal (or an explanation has been provided in Comments to the Editor).
2. All the listed authors have agreed on the content and the corresponding (submitting) author is responsible for having ensured that this agreement has been reached.
3. The submission files are in the correct format: manuscript in MS Word; diagrams and graphs are created in Excel and saved in one of the file formats: TIFF, EPS or JPG; illustrations are also saved in one of these formats (See **Author guidelines** for details).
4. The manuscript has been examined for spelling and grammar (spell checked).
5. The **title** (maximum 150 characters) briefly explains the contents of the manuscript.
6. Full names (first and last) of all authors together with the affiliation address are provided. Name of author(s) denoted as the corresponding author(s), together with their e-mail address, full postal address and telephone/fax numbers are given.
7. The **abstract** states the objective and conclusions of the research concisely in no more than 150 words.
8. Keywords (maximum six) are provided.

9. **Statement of novelty** is prepared as a Word file.
10. The text adheres to the stylistic and bibliographic requirements outlined in the **Author guidelines**.
11. Text in normal style is set to single column, 1.5 line spacing, and 12 pt. Times New Roman font is recommended. All tables, figures and illustrations have appropriate captions and are placed within the text at the appropriate points.
12. Mathematical and chemical equations are provided in separate lines and numbered (Arabic numbers) consecutively in parenthesis at the end of the line. All equation numbers are (if necessary) appropriately included in the text. Corresponding numbers are checked.
13. Tables, Figures, illustrations, are prepared in correct format and resolution (see **Author guidelines**).
14. The lettering used in the figures and graphs do not vary greatly in size. The recommended lettering size is 8 point Arial.
15. Separate files for each figure and illustration are prepared. The names (numbers) of the separate files are the same as they appear in the text. All the figure files are packed for uploading in a single ZIP file.
16. Authors have read **special notes** and have accordingly prepared their manuscript (if necessary).
17. References in the text and in the References are correctly cited. (see **Author guidelines**). All references mentioned in the Reference list are cited in the text, and *vice versa*.
18. Permission has been obtained for use of copyrighted material from other sources (including the Web).
19. The names, full affiliation (department, institution, city and country), e-mail addresses and references of three potential referees from institutions other than (and preferably countries other than) those of any of the authors are prepared in the word file.
20. Full-colour illustration or graph from the manuscript is proposed for graphical abstract.
21. **Appendices** (if appropriate) as supplementary material are prepared and will be submitted at the same time as the manuscript.

## Privacy Statement

The names and email addresses entered in this journal site will be used exclusively for the stated purposes of this journal and will not be made available for any other purpose or to any other party.

ISSN: 1580-3155





## KEMIJSKI PRIROČNIK

Opisi posameznih kemikalij so opremljeni tudi s CAS in s številkami carinske tarife, ki je usklajena s kombinirano nomenklaturou EU.

Vsebina knjige je prilagojena dosežkom mednarodnih organizacij (Organizacija za hrano in kmetijstvo – FAO, Organizacija za ekonomsko sodelovanje in razvoj OECD, Svetovna zdravstvena organizacija WHO...), ki so v osemdesetih letih prejšnjega stoletja postavljale temelje nove svetovne politike pri obravnavi kemijskih snovi in njihovega vpliva na človekovo okolje.

Priročnik je rezultat dela strokovnjakov Fakultete za farmacijo in Fakultete za kemijo in kemijsko tehnologijo. Podatki so zbrani iz različnih virov, ki so bili dosegljivi v strokovni literaturi, na spletnih straneh, v uradnih listih in drugih sprejemljivih publikacijah.

Ker je takšen način obravnave nevarnih kemikalij pripravljen v slovenščini, je knjiga pomemben prispevek uresničevanju nacionalnega programa o kemijski varnosti.

Avtorji knjige so Prof. Dr. Aleš Krbavčič, Prof. Dr. Aleš Obreza, Prof. Dr. Marija Sollner-Dolenc, Prof. Dr. Branko Stanovnik in Mag. Milan Škrlić.

Vsebinsko priročnik zajema opise blizu 800 kemikalij, IUPAC kemijski nomenklturni sistem za organske in neorganske spojine, opis svetovnega usklajenega sistema za razvrščanje in označevanje kemikalij (GHS), mednarodni sistem merskih enot, pregled aktivnih snovi in preparatov za zaščito rastlin registriranih v RS in osnovne farmakološko toksikološke lastnosti nekaterih kemijskih funkcionalnih skupin.

Priročnik predstavlja monografije nevarnih kemikalij, opisuje njihove kemijske in fizikalne lastnosti, praktično uporabo ter njihov vpliv na žive organizme in okolje. Namenjena je strokovnjakom, ki delujejo na področju kemije, farmacije, veterine, agronomije pa tudi poslovnim osebam, ki se ukvarjajo s proizvodnjo in prometom z nevarnimi kemikalijami ter nadzirajo njihov promet.

Priročnik nudi veliko koristnih podatkov osebam, ki so pogosto v stiku z naravnim okoljem (lovci, čebelarji, ribiči, ekologi), ki skrbijo za zaščito rastlin (gozdarstvo, poljedelstvo, sadjarstvo) in živali (veterina). V tem pogledu so posebno predstavljene kemikalije, katerih uporaba je dovoljena v Sloveniji na področju kmetijstva, sadjarstva in gozdarstva.

Publikacija je izredno primerena kot učbenik za študente kemije, kemijske tehnologije, farmacije in drugih sorodnih znanosti.

V publikaciji so zajete zakonske določbe glede razvrščanja in označevanja kemikalij v prometu, obenem z uredbo Evropskega parlamenta in Sveta o razvrščanju, označevanju in pakiranju snovi ter zmesi, ki se začne izvajati za snovi s 1. decembrom 2010, za zmesi pa s 1. junijem 2015.



**Cena knjige v elektronski obliki (CD-ROM) znaša 15 EUR**



Izdajo pripravili  
**Neil G. Connolly, Ture Damhus**  
**Richard M. Hartshorn, Alan T. Hutton**

PRIPOROČILA IUPAC 2005  
**NOMENKLATURA**  
**ANORGANSKE**  
**KEMIJE**

ISBN 978-961-90731-8-6

Obseg: 367 str.

Kemijska nomenklatura oz. poimenovanje kemijskih elementov in spojin je potrebno zato, da se vsi, ki jih uporabljajo, med seboj lahko sporazumevajo. Najpomembnejše pri tem je, da je poimenovanje spojin enotno in enoznačno, saj mora biti zagotovljeno, da si pod določenim imenom vsi predstavljajo isto kemijsko spojino.

Z razvojem kemije in celotne splošne znanosti je bilo v preteklosti odkritih ali sintetiziranih ogromno število kemijskih spojin, kar se bo v prihodnosti brez dvoma nadaljevalo s še večjo intenziteto. Vzporedno z odkritji in raziskavami pa se je razvijalo in prilagajalo tudi poimenovanje kemijskih spojin. IUPAC (Mednarodna unija za čisto in uporabno kemijo) skrbi za vsklajeno delovanje na tem področju. V predgovoru k originalu knjige, ki sledi le-temu, je zato natančno opisano, kako je Mednarodna unija poimenovanje kemijskih spojin spremljala, zasledovala in

spreminjala, kadar je bilo to potrebno zaradi jasnosti ali možnosti različnih razumevanj.

Pred nami je tako v letu 2008 prevod »Nomenclature of Inorganic Chemistry, IUPAC Recommendations 2005« v slovenskem jeziku, le tri leta po izidu izvirnika. Zadnja slovenska nomenklatura anorganske kemije je bila izdana leta 1986, njen obseg pa je bil 86 strani (brez preglednic). Nova izdaja prevoda obsega skoraj 400 strani strokovno izjemno zahtevnega teksta. Slovenski prevod je pripravil Andrej Šmalc, z recenzijo in z nekaterimi dodatnimi dejavnostmi v zvezi s pripravo za tisk pa mu je pomagal Primož Šegedin. Za obsežno in strokovno korektno opravljeno delo se obema iskreno zahvaljujem.

**Venčeslav Kaučič**

Častni predsednik Slovensko kemijsko društvo

Slovensko kemijsko društvo  
 Slovenian Chemical Society



Publikacijo lahko kupite v Slovenskem kemijskem društvu,  
 Hajdrihova 19, 1000 Ljubljana

Naročilo oddate preko društvene spletne strani:

<http://www.chem-soc.si/publikacije/nomenklatura-anorganske-kemije>

**Cena: 17,50 EUR**

---

## Koristni naslovi

---

Slovensko kemijsko društvo  
Slovenian Chemical Society



**Slovensko kemijsko društvo**

[www.chem-soc.si](http://www.chem-soc.si)

e-mail: [chem.soc@ki.si](mailto:chem.soc@ki.si)

---



**Wessex Institute of Technology**

[www.wessex.ac.uk](http://www.wessex.ac.uk)

---



**SETAC**

[www.setac.org](http://www.setac.org)

---



**European Water Association**

<http://www.ewa-online.eu/>

---



**European Science Foundation**

[www.esf.org](http://www.esf.org)

---



**European Federation of Chemical Engineering**

<https://efce.info/>

---



INTERNATIONAL UNION OF  
PURE AND APPLIED CHEMISTRY

**International Union of Pure and Applied Chemistry**

<https://iupac.org/>

---

---

## Novice evropske zveze kemijskih društev (EuCheMS) najdete na:

---



**EuCheMS: Brussels News Updates**

<http://www.euchems.eu/newsletters/>

---



# Sistemi za čisto in ultračisto vodo

Kvaliteta vode 1 do 3\*

\*v skladu s standardom ISO 3696 in ustreznimi ASTM ter CLSI



**DONAU LAB** Ljubljana  
Member of LPPgroup

Donau Lab d.o.o., Ljubljana  
Tbilisijska 85  
SI-1000 Ljubljana  
[www.donaulab.si](http://www.donaulab.si)  
[office-si@donaulab.com](mailto:office-si@donaulab.com)



Že od  
**3.214€** +DDV  
(B30 Trace s 25 L Pro rezerv.  
Slika je simbolična.)



# adrona

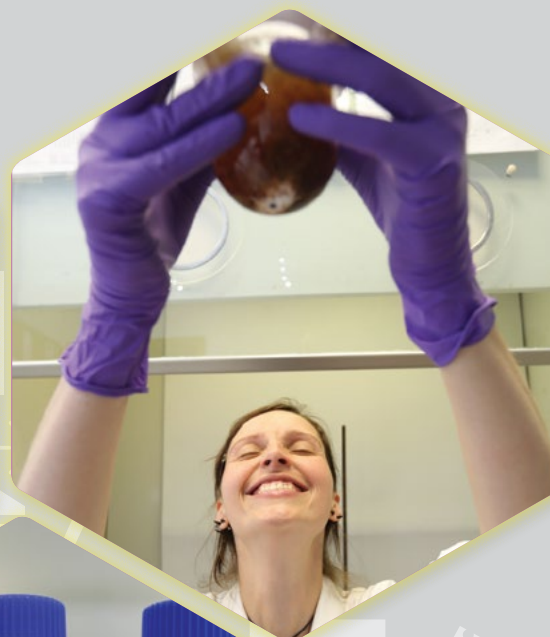
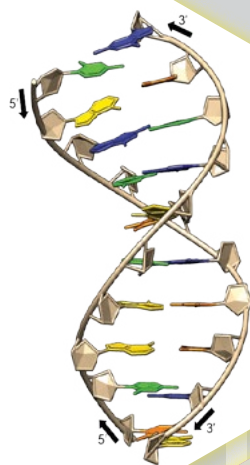


research  
EXCELLENCE



NATIONAL INSTITUTE OF CHEMISTRY

Hajdrihova 19  
1000 Ljubljana  
Slovenia  
www.ki.si



Basic and applied research on materials, life sciences, biotechnology, chemical engineering, structural and theoretical chemistry, analytical chemistry and environmental protection.



In line with the priority areas of the EU Research and Innovation: nanotechnology, genomics and biotechnology for health, sustainable development, climate change, energy efficiency and quality and safety of food.

We expand knowledge and technology transfer to the domestic and foreign pharmaceutical, chemical, automotive and nanobiotechnological industries.



We are aware of the power of youth, so we transfer our knowledge on younger generations with providing many means of collaboration.

contact: mladi@ki.si





# Strast do pametnih premazov

Visoki **standardi, znanje**, strast do **inovacij** ter želja po nenehnih izboljšavah – to je okolje v katerem že več kot 150 let nastajajo Heliosovi **pametni premazi**.

Rešitve, ki zadostijo široki paleti potreb ustvarjajo vez, zaradi katere kupci postanejo naši partnerji in tako rastemo – skupaj.

# BODITE NEUSTAVLJIVI

## MAGNEZIJ Krka 300

edinstvena kombinacija  
Mg+B<sub>2</sub>

Granulat za pripravo napitka vsebuje magnezijev citrat in vitamin B<sub>2</sub>.



Magnezij in vitamin B<sub>2</sub> prispevata k zmanjšanju utrujenosti in izčrpanosti ter normalnemu delovanju živčnega sistema.



Magnezij prispeva tudi k delovanju mišic.



- ✔ Okus po pomaranči in limeti. ✔ Brez konzervansov.
- ✔ Brez umetnih barvil, arom in sladil. ✔ Ena vrečka na dan.

Prehransko dopolnilo ni nadomestilo za uravnoteženo in raznovrstno prehrano. Skrbite tudi za zdrav življenjski slog.

[www.krka.si](http://www.krka.si)

 KRKA

*Naša inovativnost in znanje  
za učinkovite in varne  
izdelke vrhunske kakovosti.*

NOVO



Professor Miha Tišler research was mainly devoted to the syntheses of new heterocyclic compounds and their transformations, development of new reagents, structural studies, tautomerism, etc. Figure shows crystal structure of *N*-[(*Z*)-2-benzoylamino-3-(4,6-dimethyl-2-pyrimidinylamino)propenoyl]-L-proline, one of the numerous compounds prepared in his laboratory in Ljubljana which has become internationally known as the school for heterocyclic chemistry (See Editorial).

